TRANSLATIONAL INSIGHTS INTO MECHANISMS AND THERAPY OF ORGAN DYSFUNCTION IN SEPSIS AND TRAUMA

EDITED BY: Lukas Martin, Christoph Thiemermann, Pietro Ghezzi, Peter Radermacher and Timothy Robert Billiar

PUBLISHED IN: Frontiers in Immunology

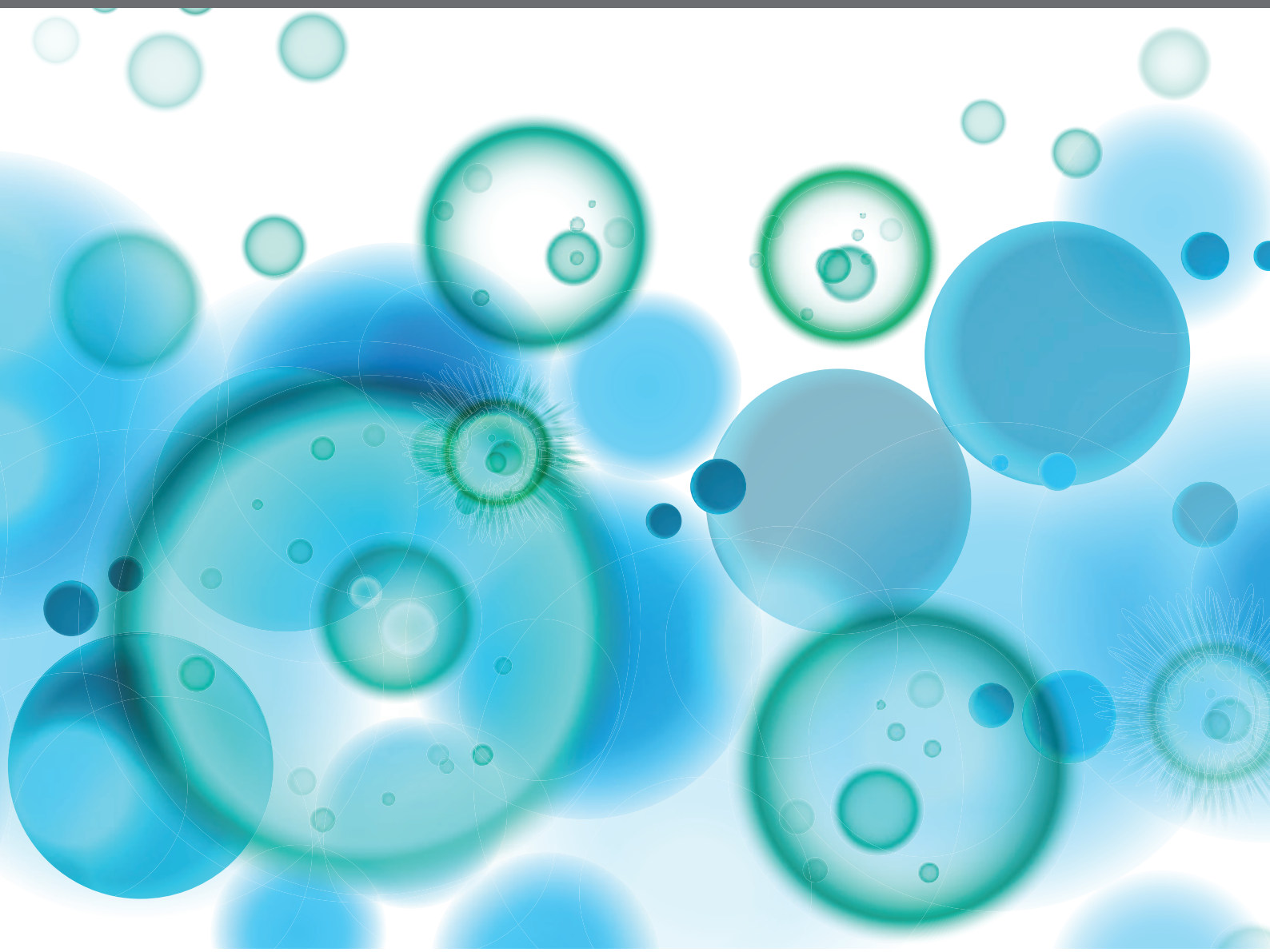

frontiers Research Topics

frontiers

Frontiers eBook Copyright Statement

The copyright in the text of individual articles in this eBook is the property of their respective authors or their respective institutions or funders. The copyright in graphics and images within each article may be subject to copyright of other parties. In both cases this is subject to a license granted to Frontiers.

The compilation of articles constituting this eBook is the property of Frontiers.

Each article within this eBook, and the eBook itself, are published under the most recent version of the Creative Commons CC-BY licence. The version current at the date of publication of this eBook is CC-BY 4.0. If the CC-BY licence is updated, the licence granted by Frontiers is automatically updated to the new version.

When exercising any right under the CC-BY licence, Frontiers must be attributed as the original publisher of the article or eBook, as applicable.

Authors have the responsibility of ensuring that any graphics or other materials which are the property of others may be included in the CC-BY licence, but this should be checked before relying on the CC-BY licence to reproduce those materials. Any copyright notices relating to those materials must be complied with.

Copyright and source acknowledgement notices may not be removed and must be displayed in any copy, derivative work or partial copy which includes the elements in question.

All copyright, and all rights therein, are protected by national and international copyright laws. The above represents a summary only. For further information please read Frontiers' Conditions for Website Use and Copyright Statement, and the applicable CC-BY licence.

ISSN 1664-8714
ISBN 978-2-88966-171-8
DOI 10.3389/978-2-88966-171-8

About Frontiers

Frontiers is more than just an open-access publisher of scholarly articles: it is a pioneering approach to the world of academia, radically improving the way scholarly research is managed. The grand vision of Frontiers is a world where all people have an equal opportunity to seek, share and generate knowledge. Frontiers provides immediate and permanent online open access to all its publications, but this alone is not enough to realize our grand goals.

Frontiers Journal Series

The Frontiers Journal Series is a multi-tier and interdisciplinary set of open-access, online journals, promising a paradigm shift from the current review, selection and dissemination processes in academic publishing. All Frontiers journals are driven by researchers for researchers; therefore, they constitute a service to the scholarly community. At the same time, the Frontiers Journal Series operates on a revolutionary invention, the tiered publishing system, initially addressing specific communities of scholars, and gradually climbing up to broader public understanding, thus serving the interests of the lay society, too.

Dedication to Quality

Each Frontiers article is a landmark of the highest quality, thanks to genuinely collaborative interactions between authors and review editors, who include some of the world's best academicians. Research must be certified by peers before entering a stream of knowledge that may eventually reach the public - and shape society; therefore, Frontiers only applies the most rigorous and unbiased reviews.
Frontiers revolutionizes research publishing by freely delivering the most outstanding research, evaluated with no bias from both the academic and social point of view. By applying the most advanced information technologies, Frontiers is catapulting scholarly publishing into a new generation.

What are Frontiers Research Topics?

Frontiers Research Topics are very popular trademarks of the Frontiers Journals Series: they are collections of at least ten articles, all centered on a particular subject. With their unique mix of varied contributions from Original Research to Review Articles, Frontiers Research Topics unify the most influential researchers, the latest key findings and historical advances in a hot research area! Find out more on how to host your own Frontiers Research Topic or contribute to one as an author by contacting the Frontiers Editorial Office: researchtopics@frontiersin.org

TRANSLATIONAL INSIGHTS INTO MECHANISMS AND THERAPY OF ORGAN DYSFUNCTION IN SEPSIS AND TRAUMA

Topic Editors:
Lukas Martin, University Hospital RWTH Aachen, Germany
Christoph Thiemermann, Queen Mary University of London, United Kingdom
Pietro Ghezzi, Brighton and Sussex Medical School, United Kingdom
Peter Radermacher, University of Ulm, Germany
Timothy Robert Billiar, University of Pittsburgh, United States

Citation: Martin, L., Thiemermann, C., Ghezzi, P., Radermacher, P., Billiar, T. R., eds. (2020). Translational Insights into Mechanisms and Therapy of Organ Dysfunction in Sepsis and Trauma. Lausanne: Frontiers Media SA. doi: 10.3389/978-2-88966-171-8

Table of Contents

06 ***Editorial: Translational Insights Into Mechanisms and Therapy of Organ Dysfunction in Sepsis and Trauma***
Peter Radermacher, Timothy R. Billiar, Pietro Ghezzi, Lukas Martin and Christoph Thiemermann

11 ***Commentary: Arguing for Adaptive Clinical Trials in Sepsis***
Miriam Kesselmeier and André Scherag

14 ***Park 7: A Novel Therapeutic Target for Macrophages in Sepsis-Induced Immunosuppression***
Yanwei Cheng, Tony N. Marion, Xue Cao, Wanting Wang and Yu Cao

22 ***Linagliptin Attenuates the Cardiac Dysfunction Associated With Experimental Sepsis in Mice With Pre-existing Type 2 Diabetes by Inhibiting NF-κB***
Sura Al Zoubi, Jianmin Chen, Catherine Murphy, Lukas Martin, Fausto Chiazza, Debora Collotta, Muhammad M. Yaqoob, Massimo Collino and Christoph Thiemermann

35 ***Effects of Changes in the Levels of Damage-Associated Molecular Patterns Following Continuous Veno–Venous Hemofiltration Therapy on Outcomes in Acute Kidney Injury Patients With Sepsis***
Jie Wu, Jianan Ren, Qinjie Liu, Qiongyuan Hu, Xiuwen Wu, Gefei Wang, Zhiwu Hong, Huajian Ren and Jieshou Li

50 ***Forebrain Cholinergic Signaling Regulates Innate Immune Responses and Inflammation***
Kurt R. Lehner, Harold A. Silverman, Meghan E. Addorisio, Ashbeel Roy, Mohammed A. Al-Onaizi, Yaakov Levine, Peder S. Olofsson, Sangeeta S. Chavan, Robert Gros, Neil M. Nathanson, Yousef Al-Abed, Christine N. Metz, Vania F. Prado, Marco A. M. Prado, Kevin J. Tracey and Valentin A. Pavlov

61 ***TLR3 Ligand Polyl:C Prevents Acute Pancreatitis Through the Interferon-β/Interferon-α/β Receptor Signaling Pathway in a Caerulein-Induced Pancreatitis Mouse Model***
Chaohao Huang, Shengchuan Chen, Tan Zhang, Dapei Li, Zhonglin Huang, Jian Huang, Yanghua Qin, Bicheng Chen, Genhong Cheng, Feng Ma and Mengtao Zhou

76 ***Identification of LPS-Activated Endothelial Subpopulations With Distinct Inflammatory Phenotypes and Regulatory Signaling Mechanisms***
Erna-Zulaikha Dayang, Josée Plantinga, Bram ter Ellen, Matijs van Meurs, Grietje Molema and Jill Moser

88 ***The Fluctuations of Leukocytes and Circulating Cytokines in Septic Humanized Mice Vary With Outcome***
Tomasz Skirecki, Susanne Drechsler, Grazyna Hoser, Mohammad Jafarmadar, Katarzyna Siennicka, Zygmunt Pojda, Jerzy Kawiak and Marcin F. Osuchowski

101 ***Functional Annotation of Genetic Loci Associated With Sepsis Prioritizes Immune and Endothelial Cell Pathways***
Kieu T. T. Le, Vasiliki Matzaraki, Mihai G. Netea, Cisca Wijmenga, Jill Moser and Vinod Kumar

112 ***Midkine is Elevated After Multiple Trauma and Acts Directly on Human Cardiomyocytes by Altering Their Functionality and Metabolism***
Ina Lackner, Birte Weber, Meike Baur, Melanie Haffner-Luntzer, Tim Eiseler, Giorgio Fois, Florian Gebhard, Borna Relja, Ingo Marzi, Roman Pfeifer, Sascha Halvachizadeh, Miriam Lipiski, Nikola Cesarovic, Hans-Christoph Pape, Miriam Kalbitz and TREAT Research Group

125 ***IL-17, IL-27, and IL-33: A Novel Axis Linked to Immunological Dysfunction During Sepsis***
Kristen N. Morrow, Craig M. Coopersmith and Mandy L. Ford

133 ***Bruton's Tyrosine Kinase Inhibition Attenuates the Cardiac Dysfunction Caused by Cecal Ligation and Puncture in Mice***
Caroline E. O'Riordan, Gareth S. D. Purvis, Debora Collotta, Fausto Chiazza, Bianka Wissuwa, Sura Al Zoubi, Lara Stiehler, Lukas Martin, Sina M. Coldewey, Massimo Collino and Christoph Thiemermann

145 ***Endogenous Uteroglobin as Intrinsic Anti-inflammatory Signal Modulates Monocyte and Macrophage Subsets Distribution Upon Sepsis Induced Lung Injury***
Andrea Janicova, Nils Becker, Baolin Xu, Sebastian Wutzler, Jan Tilmann Vollrath, Frank Hildebrand, Sabrina Ehnert, Ingo Marzi, Philipp Störmann and Borna Relja

159 ***Leukocyte-Released Mediators in Response to Both Bacterial and Fungal Infections Trigger IFN Pathways, Independent of IL-1 and TNF-α, in Endothelial Cells***
Kieu T. T. Le, Xiaojing Chu, Martin Jaeger, Josée A. Plantinga, Vasiliki Matzaraki, Sebo Withoff, Leo A. B. Joosten, Mihai G. Netea, Cisca Wijmenga, Yang Li, Jill Moser and Vinod Kumar

172 ***DAMPs and NETs in Sepsis***
Naomi-Liza Denning, Monowar Aziz, Steven D. Gurien and Ping Wang

187 ***Orthopedic Surgery Triggers Attention Deficits in a Delirium-Like Mouse Model***
Ravikanth Velagapudi, Saraswathi Subramaniyan, Chao Xiong, Fiona Porkka, Ramona M. Rodriguiz, William C. Wetsel and Niccolò Terrando

200 ***Diurnal Variation in Systemic Acute Inflammation and Clinical Outcomes Following Severe Blunt Trauma***
Akram M. Zaaqoq, Rami A. Namas, Othman Abdul-Malak, Khalid Almahmoud, Derek Barclay, Jinling Yin, Ruben Zamora, Matthew R. Rosengart, Timothy R. Billiar and Yoram Vodovotz

212 ***Modeling Cardiac Dysfunction Following Traumatic Hemorrhage Injury: Impact on Myocardial Integrity***
Johanna Wall, Sriveena Naganathar, Banjerd Praditsuktavorn, Oscar F. Bugg, Simon McArthur, Christoph Thiemermann, Jordi L. Tremoleda and Karim Brohi

225 ***Trauma Severity and Its Impact on Local Inflammation in Extremity Injury—Insights From a Combined Trauma Model in Pigs***
Klemens Horst, Johannes Greven, Hannah Lüken, Qiao Zhi, Roman Pfeifer, Tim P. Simon, Borna Relja, Ingo Marzi, Hans-Christoph Pape and Frank Hildebrand

235 ***Citrullinated Histone H3 as a Therapeutic Target for Endotoxic Shock in Mice***
Qiufang Deng, Baihong Pan, Hasan B. Alam, Yingjian Liang, Zhenyu Wu, Baoling Liu, Nirit Mor-Vaknin, Xiuzhen Duan, Aaron M. Williams, Yuzi Tian, Justin Zhang and Yongqing Li

246 ***Impaired Glucocorticoid Receptor Dimerization Aggravates LPS-Induced Circulatory and Pulmonary Dysfunction***
Martin Wepler, Jonathan M. Preuss, Tamara Merz, Clair Hartmann, Ulrich Wachter, Oscar McCook, Josef Vogt, Sandra Kress, Michael Gröger, Marina Fink, Angelika Scheuerle, Peter Möller, Enrico Calzia, Ute Burret, Peter Radermacher, Jan P. Tuckermann and Sabine Vettorazzi

260 ***Short-Chain Alcohols Upregulate GILZ Gene Expression and Attenuate LPS-Induced Septic Immune Response***
Hang Pong Ng, Scott Jennings, Steve Nelson and Guoshun Wang

272 ***Hepatocyte-Specific Deletion of AMPKα1 Results in Worse Outcomes in Mice Subjected to Sepsis in a Sex-Specific Manner***
Satoshi Kikuchi, Giovanna Piraino, Michael O'Connor, Vivian Wolfe, Kiana Ridings, Patrick Lahni and Basilia Zingarelli

283 ***Mangiferin Attenuates LPS/D-GalN-Induced Acute Liver Injury by Promoting HO-1 in Kupffer Cells***
Sen Yang, Ge Kuang, Liangke Zhang, Shengwang Wu, Zizuo Zhao, Bin Wang, Xinru Yin, Xia Gong and Jingyuan Wan

295 ***Mesenchymal Stem Cell-Derived Extracellular Vesicles: A Novel Cell-Free Therapy for Sepsis***
Yanwei Cheng, Xue Cao and Lijie Qin

303 ***Non-invasive Assessment of Mitochondrial Oxygen Metabolism in the Critically Ill Patient Using the Protoporphyrin IX-Triplet State Lifetime Technique—A Feasibility Study***
Charles Neu, Philipp Baumbach, Alina K. Plooij, Kornel Skitek, Juliane Götze, Christian von Loeffelholz, Christiane Schmidt-Winter and Sina M. Coldewey

312 ***The Effect of β_2-Adrenoceptor Agonists on Leucocyte-Endothelial Adhesion in a Rodent Model of Laparotomy and Endotoxemia***
Mansoor Nawaz Bangash, Tom E. F. Abbott, Nimesh S. A. Patel, Charles Johnston Hinds, Christoph Thiemermann and Rupert Mark Pearse

322 ***Csf2 Attenuated Sepsis-Induced Acute Kidney Injury by Promoting Alternative Macrophage Transition***
Yiming Li, Pan Zhai, Yawen Zheng, Jing Zhang, John A. Kellum and Zhiyong Peng

frontiers in Immunology

EDITORIAL
published: 25 September 2020
doi: 10.3389/fimmu.2020.01987

Editorial: Translational Insights Into Mechanisms and Therapy of Organ Dysfunction in Sepsis and Trauma

Peter Radermacher[1]*, *Timothy R. Billiar*[2,3], *Pietro Ghezzi*[4], *Lukas Martin*[5] and *Christoph Thiemermann*[6]

[1] Institute for Anesthesiological Pathophysiology and Process Engineering, Ulm University Hospital, Ulm, Germany, [2] Department of Surgery, University of Pittsburgh, Pittsburgh, PA, United States, [3] UPMC International and Commercial Services Division, Pittsburgh, PA, United States, [4] Department of Clinical Medicine, Brighton and Sussex Medical School, Brighton, United Kingdom, [5] Department of Intensive and Intermediate Care, Medical Faculty, University Hospital RWTH, Aachen, Germany, [6] Centre for Translational Medicine and Therapeutics, William Harvey Research Institute, Queen Mary University of London, London, United Kingdom

Keywords: sepsis, trauma, multiple organ failure, SIRS, animal models, translational studies, clinical trials

Editorial on the Research Topic

Translational Insights Into Mechanisms and Therapy of Organ Dysfunction in Sepsis and Trauma

OPEN ACCESS

Edited by:
Rudolf Lucas,
Augusta University, United States

Reviewed by:
Cassiano Felippe GonçAlves-De-Albuquerque,
Rio de Janeiro State Federal University, Brazil

***Correspondence:**
Peter Radermacher
peter.radermacher@uni-ulm.de

Specialty section:
This article was submitted to Inflammation, a section of the journal Frontiers in Immunology

Received: *26 June 2020*
Accepted: *23 July 2020*
Published: *25 September 2020*

Citation:
Radermacher P, Billiar TR, Ghezzi P, Martin L and Thiemermann C (2020) Editorial: Translational Insights Into Mechanisms and Therapy of Organ Dysfunction in Sepsis and Trauma. Front. Immunol. 11:1987. doi: 10.3389/fimmu.2020.01987

Multiple organ dysfunction or even failure after sepsis or trauma is due to a dysregulated host response. Currently, besides (surgical) source control (e.g., control of bleeding or drainage of abscesses) and administration of antimicrobial drugs, therapeutic approaches are limited to supportive care. Advances in our understanding of the key pathophysiological pathways involved in the excessive inflammation triggered by trauma, sepsis and/or ischemia-reperfusion have had limited impact. The 28 article in this Research Topic focus on the molecular mechanisms behind (hyper) inflammation after sepsis or trauma, with special emphasis on preclinical and translational studies that target potential organ-protective and/or -resuscitative therapeutic strategies. Most studies report rodent models of trauma and elective surgery (three articles), non-microbial hyper-inflammation induced with endotoxin exposure (LPS; seven articles) and chemical pancreatitis (one article), and cecal ligation and puncture-induced sepsis (six articles). Additional papers summarize investigations of human material (six articles) or fully-resuscitated large animal models (two articles). These article are complimented by four reviews and a commentary.

RODENT MODELS OF TRAUMA AND (ELECTIVE) SURGERY-RELATED TISSUE INJURY

Velagapudi et al. investigate the pathophysiology of post-traumatic/surgical delirium. The authors investigated the effect of murine limb trauma on post-operative behavior (as assessed using the 5- "choice serial reaction time task" and motor activity) and neuroinflammation and blood-brain barrier integrity (by using light-sheet microscopy). Post-surgery behavior showed impairment, in parallel with reduced microglial ramification and overall cell volume impaired hippocampal astrocytic-tight junctions. Wall et al. characterized the mechanisms underlying post-traumatic cardiac dysfunction in mice undergoing soft tissue trauma and bone fracture

followed by hemorrhage. Despite resuscitation, stroke volume remained at 25% of baseline values, which was associated with leukocyte infiltration and ultrastructural sarcomere and mitochondriadisorganization, leading to increased serum levels of heart fatty acid-binding protein and troponin I. The authors concluded that mitochondria-driven apoptosis may be a target to prevent irreversible post-traumatic cardiac injury. In a rat model of abdominal surgery, Bangash et al. further clarified the anti-inflammatory properties of the β_2-agonist dopexamine. Ileal intravital microscopy demonstrated that attenuated leukocyte-endothelial adhesion in post-capillary venules while neither arteriolar diameter, functional capillary density nor systemic hemodynamics nor lactic acidosis were affected compared to control animals. Interestingly, despite comparable effects on the intestinal microcirculation, high dose dopexamine only, in contrast to the pure β_2-agonist salbutamol, also attenuated surgery-related increase in serum creatinine.

NON-MICROBIAL SYSTEMIC HYPERINFLAMMATION

Although clearly distinct from polymicrobial sepsis, endotoxin (LPS) challenge and chemically-induced pancreatitis are often used to model hyperinflammation, and indeed, sepsis due to their reproducibility and the subsequent organ failure that mimics that of sepsis. Two studies addressed the potential role of the glucocorticoid receptor (GR) in LPS-induced organ dysfunction. Wepler et al. compared wildtype ($GR^{+/+}$) mice with animals with impaired GR dimerization ($GR^{dim/dim}$) under conditions of full intensive care support ("lung-protective" mechanical ventilation, crystalloids, and norepinephrine). $GR^{dim/dim}$ mice presented with more severe shock and aggravated acute lung injury, which coincide with increased tissue osteopontin expression. Ng et al. provided evidence for the anti-inflammatory mechanisms of acute, binge-drinking-like alcohol intoxication: alcohol exposure attenuated the inflammatory response to LPS *in vivo*, ultimately improving survival, which was associated with increased gene expression of the Glucocorticoid-Induced Leucine Zipper (GILZ), a key molecule acting via non-canonical GR activation. Inhibition of ethanol metabolism enhanced this effect, and interestingly, the higher molecular-weight short-chain alcohols propanol and isopropanol were even more potent than ethanol.

Dayang et al. provided new evidence relating to the complex organ- and organ- and microvascular bed-specific LPS-induced expression of the endothelial adhesion molecules E-selectin and VCAM-1. The authors showed in LPS-challenged mice that the renal microvascular endothelium expressed various E-selectin and VCAM-1 subpopulations, i.e., E-selectin$^-$/VCAM-1$^-$, E-selectin$^+$/VCAM-1$^-$, E-selectin$^+$/VCAM-1$^+$, and E-selectin$^-$/VCAM-1$^+$. The formation of subpopulations was a common response of endothelial cells to LPS challenge. FACS analysis demonstrated that the $^{+/+}$ subpopulation expressed the highest cytokine and chemokine response, which was mainly TLR4-mediated. Activation of NF-κB and p38 MAPK were key signaling events in the formation of this $^{+/+}$subpopulation. The translational value of these murine data was highlighted by the recapitulation of these effects in LPS-exposed HUVEC and human lung microvascular endothelial cells.

The role of the forebrain cholinergic system for the systemic immune response was addressed by Lehner et al. The central-acting cholinergic agonist galanthine suppressed the systemic TNFα response to endotoxemia in mice, and this effect was suppressed by both local genetic ablation of acetylcholine release and vagotomy. In contrast, local and selective activation of the M1 muscarinic acetylcholine receptor (M1 mAChR) with the allosteric agonist benzyl quinolone carboxylic acid also suppressed the serum TNFα levels, thereby ultimately improving survival; these beneficial effects were again suppressed in M1 mAChR-ko mice. Overall, these data suggest a bidirectional relationship between brain cholinergic signaling and the systemic inflammatory response.

Two studies focussed on possible therapeutic interventions. Deng et al. investigated the potential of targeting citrullinated histone H3 (CitH3) to neutralize neutrophil extracellular traps. When administered simultaneously with a lethal dose of LPS, anti-CitH3 monoclonal antibodies prevented HUVEC damage *in vitro* and attenuated ALI *in vivo* via inhibition of the inflammatory response, thereby ultimately reducing mortality. The therapeutic potential of the anti-inflammatory xanthone glucoside mangiferin was studied by Yang et al. in mice with LPS/galactosamine-induced acute liver failure. Pre-treatment with magiferin inhibited hepatic TNF-α production, decreased serum aminotransferase activities, and improved survival. This beneficial effect was abolished by Kupffer cell deletion, and at least in part, related to increased heme oxygenase-1 expression.

Models of caerulein-induced acute pancreatitis *in vivo* and taurocholate-induced pancreatic acinar cell line *in vitro* were used to study the roll of the Toll-like receptor 3 (TLR3) ligand polyI:C by Huang et al. PolyI:C is a double-stranded RNA mimic that can act as an immune stimulant by triggering type I interferon (IFN) production and downstream IFN-α/β receptor (IFNAR)-dependent signaling, and pre-treatment inhibited chemotaxis and ROS production. This was abolished in IFN-β- and IFNAR-ko mice.

CECAL LIGATION AND PUNCTURE (CLP)-INDUCED SEPSIS

CLP is one of the most frequently used models of polymicrobial sepsis. While three studies in this special issue were designed to further character molecular pathways of sepsis pathophysiology, others evaluated the efficacy of specific therapeutic interventions. Most of the studies have the merit of integrating the "*Minimum Quality Threshold in Pre-Clinical Sepsis Studies*" (MQTiPSS) guidelines, thus allowing for easier inter-laboratory comparability.

Li et al. addressed the role of the switch of macrophage phenotype from the pro-inflammatory M1 state to the M2 repair (i.e., resolution) state in septic AKI. Coculture of human M1 macrophages with proximal tubular (HK-2) cells revealed that Colony Stimulating Factor 2 (Csf2) was the most up-regulated

protein, and post-CLP injection of a Csf2 antibody attenuated kidney M1-M2 macrophage transition via p-STAT5 signaling, suppressed tubular proliferation, and increased mortality.

The role of AMP-activated protein kinase (AMPK) was investigated in murine CLP-induced sepsis by Kikuchi et al. Mice with genetic deletion of the catalytic α1 isoform (AMPKα1) had higher systemic cytokine levels, liver and lung inflammation and injury, and in particular, more severe hepatic mitochondrial damage and mortality. These deleterious effects were even more pronounced in male animals, suggesting that AMPK-dependent liver metabolic (dys) function is sex-dependent.

Skiretzki et al. further characterized the translational value of an established, "*humanized*" murine model of CLP-induced sepsis. Animals were stratified as "*predicted-to-die (P-DIE)*" or "*predicted-to-survive (P-SUR)*," and blood, bone marrow and spleen were collected for cytokine and chemokines as well as CD-80 and HLA-DR expression. TNFα, IL-6, IL-10, IL-8/KC-, and MCP-1-levels were several-fold higher in the P-DIE group. The study nicely showed that humanized mice reflect human immune responses.

A possible therapeutic potential of the Bruton's tyrosine kinase (BTK) inhibitors ibrutinib and acalabrutinib for septic cardiomyopathy and AKI was investigated by O'Riordan et al. When administered early (1 h) after the CLP-procedure, the BTK inhibitors attenuated sepsis-induced systolic dysfunction and reduced systemic and tissue NF-κB and NLRP3 inflammasome activation. This is clinically relevant as both BTK inhibitors are already approved for the treatment of chronic lymphatic leukemia (CLL), and acalabrutinib has recently been reported to attenuate systemic inflammation in a small cohort of patients with COVID-19 (Roschewski et al.). However, despite promising data on ibrutinib during lipoteichoic acid-induced pulmonary inflammation as well as and ceftriaxone-treated pneumococcal pneumonia (1), a word of caution needs to be mentioned concerning tyrosine kinase inhibitors in general: the RESONATE-17 study on 144 CLL patients treated with ibrutinib reported a 30% incidence of severe infection including pneumonia (2), and in un-resuscitated CLP-induced murine sepsis, the tyrosine kinase inhibitor dasatinib (administered as a pre- and post-treatment) dose-dependently showed a "friend or foe" profile: while low doses attenuated sepsis-related organ dysfunction, and ultimately improved survival, high doses had the opposite effect (3).

Another approved drug, the oral antidiabetic linagliptin, was compared with the selective IkB kinase (IKK) inhibitor (IKK-16), with respect to its effects on septic cardiomyopathy as well as kidney and liver injury in murine high fat diet-induced type 2 diabetes mellitus (T2DM) (Al Zoubi et al.). This study is of particular importance, since it sheds light on one of the most frequently occurring chronic co-morbidities observed in patients with sepsis and/or after trauma, which is well-known to worsen the patient's outcome. In good agreement with these clinical observations, T2DM aggravated sepsis-related (organ) dysfunction associated with sepsis, which was comparably mitigated by both tested drugs. This effect of linagliptin was associated with reductions of NF-κB activation, iNOS expression and serum levels of pro-inflammatory cytokines.

Finally, Janicova et al. characterized the role of uteroglobin in a murine double-hit model of blunt chest trauma and subsequent (24 h) CLP-induced sepsis focussing on dynamic changes in monocyte and macrophage subsets. This double-hit model has the possibility of replicating the frequently occurring similar sequence in critically ill patients, i.e., an initial polytrauma is complicated by consecutive sepsis, and furthermore, allows investigating common "final routes" of these two pathological entities. Both pro-inflammatory monocytes and macrophages significantly increased in blood, lungs and bronchoalveolar lavage fluid (BALF) at the expense of tissue repairing macrophages, which coincided with higher levels of TNF-α, MCP-1, and RAGE. Uteroglobin neutralization further aggravated this pro-inflammatory response, and subsequently, lung damage, thereby highlighting intrinsic anti-inflammatory signaling role of this protein.

LARGE ANIMAL AND HUMAN STUDIES

Despite the substantial demand for personnel, infrastructure and consumables as well as the often lacking test kits for the species involved, large animal (in particular porcine) models have the advantages (i) to allow for integration of standard ICU procedures into the experimental design, and (ii) to study an immunological environment that is closer to the human situation than any other species (except for non-human primates). Horst et al. made use of these facts for the characterization of time-dependent dynamics of the inflammatory response in the blood, the femur fracture hematoma, and muscle samples of polytraumatized ("PT": lung contusion, liver laceration, femur fracture, and controlled hemorrhage) swine in comparison to animals with femur fracture alone (monotrauma). The severity of the polytrauma substantially inhibited the local generation of proinflammatory and angiogenetic mediators, suggesting that these systemic trauma-related changes of the local immunologic milieu might explain the delayed bone repair in PT patients. The same porcine PT model was used by Lackner et al. to address the role of midkine levels for post-traumatic cardiac dysfunction. The porcine data were complemented by (i) the measurement of midkine blood levels in PT patients (ISS $\geq$ 16), and (ii) the functional assessment of human cardiomyocytes incubated with midkine. In PT patients, midkine levels were several-fold higher than in healthy volunteers, while *in vitro* midkine exposure of cardiomyocytes altered cell Ca^{2+} handling and reduced maximum mitochondrial O_2 consumption.

Sophisticated genome/transcriptome analyses were used by Le et al. in two studies (Le, Matzaraki et al.; Le, Chu et al.) that aimed at further characterizing the major determinants of leukocyte and/or endothelium responses to bacterial sepsis. In the first study (Le, Matzaraki et al.) expression quantitative trait loci (eQTL) data from the largest whole-blood eQTL database, cytokine QTLs from pathogen-stimulated peripheral blood mononuclear cells (PBMC), blood transcriptome data from pneumoniae-derived sepsis patients, and transcriptome data from pathogen-stimulated PBMC were integrated and found increased adherence-junction gene expression. The

authors concluded that their approach provided evidence for genetically determined variability in both leucocyte and endothelial responses, which may contribute to explaining sepsis heterogeneity. In their second study (Le, Chu et al.), the authors' group investigated transcriptomic responses of human leukocytes and endothelial cells to Gram negative-bacteria, Gram positive-bacteria, and fungi. While whole pathogen lysates strongly activated leukocytes but not endothelial cells, the mutual leukocyte response to pathogens resulted in endothelial activation. Exposure of endothelial cells to leukocyte mediators activated endothelial cells at both transcription and protein levels, and revealed IL-1, TNF-α, and IFN as important drivers of endothelial activation.

Another study was dedicated to investigate the potential role of circadian rhythm and/or diurnal variations on the systemic inflammatory response, and ultimately outcome in patients with trauma (Zaaqoq et al.). From a total of nearly 500 blunt trauma survivors (ISS > 20) a subgroup of patients injured during daytime ("*mDay*") was compared to patients injured at nighttime ("*mNight*") in order to investigate the impact on 32 inflammatory mediators using Dynamic Network Analysis (DyNA) and Dynamic Bayesian Network (DyBN) inference. Both hospital and ICU length of stay were longer in the mNight patients, which coincided with higher IL-17A but lower MIP-1α, IL-7, IL-15, GM-CSF, and sST2 levels; DyBN yielded cortisol and sST2 as the major upstream determinants upstream of TGF-β1, chemokines, and Th17/protective mediators in both groups, with IL-6 being an additional downstream node in the mNight group only.

In patients with septic AKI undergoing continuous veno–venous hemofiltration (CVVH), Wu et al. investigated the impact of damage-associated molecular pattern (DAMP) (mitochondrial DNA, mtDNA; nuclear DNA, nDNA; heat shock protein 70, HSP70; high mobility group box 1, HMGB1) removal on mortality. Both HSP70 and HMGB1 clearance rates were good predictors of mortality, and high HSP70 clearance coincided with the level of HLA-DR expression. Based on these findings the authors cautioned the use of CVVH in AKI patients with sepsis merely for the removal of inflammatory mediators in the absence of any other indication for this therapeutic measure.

Finally, Neu et al. present a study on the feasibility of a direct, non-invasive, bedside measurement of skin mitochondrial oxygen tension ($mitoPO_2$) with a new commercially available device that makes use of the "*in vivo protoporphyrin IX-triplet state lifetime technique (PpIX-TSLT)*." In 40 patients a three-step measurement was performed after enriching the clavipectoral triangle with 5-aminolevulinic acid, which comprised assessment of baseline values, evaluation of the effect of a local pressure to transitorily stop microcirculatory blood flow, and a second control value. The recorded data allowed calculating average and maximum $mitoVO_2$ at these three time points. The technique was reproducible, easy, and safe; potential tissue edema as assessed by bioimpedance resulted in lower mitochondrial oxygen tension.

REVIEWS AND COMMENTARIES

Two articles reviewed potential new pathways (and consecutive therapeutic targets) of sepsis-related immune paralysis. Cheng et al. discuss the possible role of Parkinson disease protein 7 (Park 7), a well-established regulator of reactive oxygen species (ROS) release through interaction with p47phox, a subunit of NADPH oxidase. Among their various functions, ROS initiate TLR to activate macrophages. Consequently, Park 7 may be a novel therapeutic target to reverse sepsis-related immunosuppression. Morrow et al. discuss septic immune paralysis in the light of the markedly decreased T cell formation of pro-inflammatory cytokines. Since targeting lymphocyte survival did not find its way into clinical practice, cytokines with a more global immune effect may represent alternative therapeutic targets. The authors discuss the possible impact of the interleukin (IL)-17, IL-27, and IL-33 based on data from patient serum and murine models of peritonitis and pneumonia.

Denning et al. review the complex interplay of host response to pathogens *via* interaction of pathogen-associated molecular patterns (PAMPs) and pattern recognition receptors (PRRs) and damage-associated molecular patterns (DAMPs), and Neutrophil extracellular traps (NETs). Examples of DAMPs are extracellular cold-inducible RNA-binding protein (eCIRP), high mobility group box 1 (HMGB1), histones, and adenosine triphosphate (ATP). DAMPs are released by inflammasome activation or passively from dead cells. NETs are mixtures of extracellular DNA with histones, myeloperoxidase, and elastase, all released during inflammation. Although NETs clearly contribute to pathogen clearance, their excessive formation causes tissue damage.

Based on their multiple and ubiquitous properties, Cheng et al. discuss the potential of mesenchymal stem cells (MSCs) in the treatment of sepsis. Highlighting the possible undesired side effects, the authors also emphasize the potential of extracellular vesicles (EVs) derived from MSCs (MSC-EVs). These MSC-EVs appear to exert a therapeutic benefit similar to MSCs in protecting against sepsis-induced organ dysfunction by delivering RNAs and proteins to target cells, while at the same time being devoid of major MSC side effects. In addition, MSC-EVs provide some practical advantages over their parent MSCs.

Finally, Kesselmeier and Scherag comment on the recently popularized "*adaptive clinical trials*" discussing a recent article in this journal by Talisa et al. (4). The authors clearly acknowledge that adaptive trials allow modifying design elements during trial conduct, thereby possibly reducing resources, duration and sample size while simultaneously enhancing the chance of proof for an effective treatment. Nevertheless, the authors discuss the four issues response adaptive randomization (RAR), adaptive enrichment, seamless, and platform designs, which need to be taken into account.

In summary, the Research Topic entitled provides a broad and detailed overview of new molecular and mechanistic avenues for the management of sepsis- and trauma-related multiple organ dysfunction, and represents a major contribution to translational research in the field.

AUTHOR CONTRIBUTIONS

All authors listed have made a substantial, direct and intellectual contribution to the work, and approved it for publication.

FUNDING

This work was supported by the Deutsche Forschungsgemeinschaft (DFG): CRC 1149, MA 7082/3-1.

REFERENCES

1. de Porto AP, Liu Z, de Beer R, Florquin S, de Boer OJ, Hendriks RW, et al. Btk inhibitor ibrutinib reduces inflammatory myeloid cell responses in the lung during murine pneumococcal pneumonia. *Mol Med.* (2019) 25:3.doi: 10.1186/s10020-018-0069-7
2. O'Brien S, Jones JA, Coutre SE, Mato AR, Hillmen P, Tam C, et al. Ibrutinib for patients with relapsed or refractory chronic lymphocytic leukaemia with 17p deletion (RESONATE-17): a phase 2, open-label, multicentre study. *Lancet Oncol.* (2016) 17:1409–18.doi: 10.1016/S1470-2045(16)30212-1
3. Gonçalves-de-Albuquerque CF, Rohwedder I, Ribeiro Silva A, Silveira Ferreira A, Kurz ARM, Cougoule C, et al. The Yin and Yang of tyrosine kinase inhibition during experimental polymicrobial sepsis. *Front Immunol.* (2018) 9:901.doi: 10.3389/fimmu.2018.00901
4. Talisa VB, Yende S, Seymour CW, Angus DC. Arguing for adaptive clinical trials in sepsis. *Front Immunol.* (2018) 9:1502.doi: 10.3389/fimmu.2018.01502

Conflict of Interest: The authors declare that the research was conducted in the absence of any commercial or financial relationships that could be construed as a potential conflict of interest.

Copyright © 2020 Radermacher, Billiar, Ghezzi, Martin and Thiemermann. This is an open-access article distributed under the terms of the Creative Commons Attribution License (CC BY). The use, distribution or reproduction in other forums is permitted, provided the original author(s) and the copyright owner(s) are credited and that the original publication in this journal is cited, in accordance with accepted academic practice. No use, distribution or reproduction is permitted which does not comply with these terms.

frontiers in Immunology

GENERAL COMMENTARY
published: 30 October 2018
doi: 10.3389/fimmu.2018.02507

Commentary: Arguing for Adaptive Clinical Trials in Sepsis

Miriam Kesselmeier[1] *and André Scherag*[1,2]*

[1] Research Group Clinical Epidemiology, Center for Sepsis Control and Care, Jena University Hospital, Jena, Germany,
[2] Institute of Medical Statistics, Computer and Data Sciences, Jena University Hospital, Jena, Germany

Keywords: sepsis, adaptive clinical trials, Bayesian statistics, platform trials, response adaptive randomization

A Commentary on

Arguing for Adaptive Clinical Trials in Sepsis
by Talisa VB, Yende S, Seymour CW, Angus DC. Front. Immunol. (2018) 9:1502. doi: 10.3389/fimmu.2018.01502

OPEN ACCESS

Edited by:
Peter Radermacher, Universität Ulm, Germany

Reviewed by:
Benjamin Mayer, Universität Ulm, Germany
James Russell, University of British Columbia, Canada
Derek C. Angus, University of Pittsburgh, United States

***Correspondence:**
André Scherag
andre.scherag@med.uni-jena.de

Specialty section:
This article was submitted to Inflammation, a section of the journal Frontiers in Immunology

Received: *10 September 2018*
Accepted: *10 October 2018*
Published: *30 October 2018*

Citation:
Kesselmeier M and Scherag A (2018) Commentary: Arguing for Adaptive Clinical Trials in Sepsis. Front. Immunol. 9:2507. doi: 10.3389/fimmu.2018.02507

Adaptive trial designs provide the opportunity to modify design elements during trial conduct. This approach possibly reduces resources, trial duration as well as sample size and may increase the probability of identifying an effective treatment (1). Currently, they are more frequently applied by industrial funders as indicated at clinicaltrials.gov. In a mini-review, Talisa et al. (2) proposed such designs to face the challenges of treatment development in sepsis and underlined their advantages. Finally, they pointed to some challenges in their application. For example, both extensive simulations for the selection of an adequate trial design and statistical models reflecting the trial structure are essential. In general, we completely agree that adaptive designs can be beneficial but they are no magic solutions for all challenges. Moreover, we want to stress that "safety assessments" are not a special topic of adaptive trial designs—data safety monitoring committees will also be in charge here but may require some additional education. With this comment, we would like to initiate a more differentiated view of methodological, statistical and practical challenges related to such designs. We comment on four topics: response adaptive randomization (RAR), adaptive enrichment, seamless, and platform designs.

RAR may be regarded as a kind of futility/inefficiency monitoring because fewer patients are assigned to trial arms in which less efficiency is observed (3). This potentially reduces the total sample size without a considerable loss of precision (1). However, one similarly achieves this aim with adaptive designs without RAR including interim monitoring for futility/inefficiency whose results are easier to comprehend (3). This idea can be extended to flexible multi-arm multi-stage sequential trial designs and, depending on the expected number of effective treatments, applied instead of RAR (4). However, when applying RAR, one must consider further issues. (i) The decision rules for adapting the allocation must be planned upfront of study initiation. Otherwise, introduction of statistical, operational and investigator-driven bias is possible which is difficult to identify and eliminate afterwards (1). (ii) One must pay special attention to the randomization weights update to avoid instable estimates (especially in the trial beginning), extremely unbalanced allocation proportions and erroneous dropping of trial arms (1, 3–6). (iii) Timing plays an important role. First, the outcome might be time-associated, introducing bias if not accounted for (3). Secondly, RAR requires a short-term outcome as otherwise there will be almost no randomization adaptation (1, 7). Short-term outcomes in clinical sepsis research, however, have been questioned (8).

In adaptive enrichment designs, the eligibility criteria are adapted during trial conduct to identify the probably most benefitting patient (sub-) population or the most efficacious dose. This is ideally based on profound understanding of the underlying biology (9). Though, one must decide on the enrichment's primary aim: noise reduction, identification of high-risk patients or of patients most likely showing a positive treatment response (10). Biomarkers are thought to serve as objective indications of biomedical state observed from outside the patient. Roughly one may distinguish prognostic and predictive biomarkers (10, 11). Prognostic enrichment would imply that prognostic biomarker results can be used to increase the selective enrollment of patients having a disease-related endpoint. Predictive enrichment would imply that predictive biomarker results can be used to increase the likelihood of responding to a treatment. Both types of enrichment are of interest for sepsis research but we are facing a "Chicken Egg Problem": For predictive enrichment there is no biomarker to monitor the response to a sepsis treatment given that we are (still) searching for an effective sepsis treatment.

The idea of seamless designs was introduced in drug development in order to move from phase II to phase III without a recruitment stop while using all the information in a joint final analysis (12). Typically, only a limited number of study arms will enter the phase III stage. The optimal time for the transition from phase II to III or the adaptive changes such as the decision on which arm(s) to drop now become crucial determinants of efficiency (13).

Finally, Talisa et al. (2) talked about platform trials. Generally, the platform idea is basically an IT infrastructure that should lead to a more efficient trial conduct by identifying and selecting patients eligible across many trials in parallel. Incorporation of adaptive design features into the platform design will not only require the introduction of Bayesian statistical models but also a big move in terms of trial logistics. Both topics ask for major changes in the way we teach biostatistics in academic medicine, in the way we recruit patients at our trial centers and on the side of some regulators. We want to make sure that clinicians comprehend the results of Bayesian statistical models, see the use of valid—i.e., cleaned—information for adaptations and finally ensure that robust results get accepted by regulators, e.g., as done with the agreement of the U.S. Food and Drug Administration on an adaptive, seamless phase II/III trial with Bayesian interim analysis (14).

In sum, we agree that changes in clinical sepsis research should also consider changes in the way we run clinical trials. In the short-term, however, we see organizational issues to be addressed first, e.g., the implementation of a central IT platform and a better integration of clinical research into the routine infrastructure [e.g., (15)]. Regarding the major methodological changes discussed here, costs and benefits need to be carefully checked. Bias is introduced easily and robustness of findings cannot be expected on the base of just a few observations. Frustrating as clinical sepsis trial results were in the past, we nevertheless learned that some of our ideas were likely too simple, including the way that we ran clinical trials.

AUTHOR CONTRIBUTIONS

Both authors contributed equally to the work, and approved it for publication.

FUNDING

This work was supported by the Integrated Research and Treatment Center, Center for Sepsis Control and Care (CSCC), at the Jena University Hospital funded by the German Ministry of Education and Research (BMBF No. 01EO1502). AS also received funding by BMBF No. 01ZZ1803C.

REFERENCES

1. Park JJ, Thorlund K, Mills EJ. Critical concepts in adaptive clinical trials. *Clin Epidemiol.* (2018) 10:343–51. doi: 10.2147/CLEP.S156708
2. Talisa VB, Yende S, Seymour CW, Angus DC. Arguing for Adaptive Clinical Trials in Sepsis. *Front Immunol.* (2018) 9:1502. doi: 10.3389/fimmu.2018.01502
3. Korn E, Freidling B. Outcome-adaptive randomization in early clinical trials. In: Matsui S, Buyse M and Simon R, editors. *Design and Analysis of Clinical Trials for Predictive Medicine*. Boca Raton, FL: CRC Press (2015) p. 111–28.
4. Lin JC, Bunn V. Comparison of multi-arm multi-stage design and adaptive randomization in platform clinical trials. *Contemp Clin Trials* (2017) 54:48–59. doi: 10.1016/j.cct.2017.01.003
5. Brittain E, Schlesselman JJ. Optimal allocation for the comparison of proportions. *Biometrics* (1982) 38:1003–9. doi: 10.2307/2529880
6. Trippa L, Lee EQ, Wen PY, Batchelor TT, Cloughesy T, Parmigiani G, et al. Bayesian adaptive randomized trial design for patients with recurrent glioblastoma. *J Clin Oncol.* (2012) 30:3258–63. doi: 10.1200/JCO.2011.39.8420
7. Chow SC, Chang M. Adaptive design methods in clinical trials - a review. *Orphanet J Rare Dis.* (2008) 3:11. doi: 10.1186/1750-1172-3-11
8. Cohen J, Vincent JL, Adhikari NK, Machado FR, Angus DC, Calandra T, et al. Sepsis: a roadmap for future research. *Lancet Infect Dis.* (2015) 15:581–614. doi: 10.1016/S1473-3099(15)70112-X
9. Shankar-Hari M, Rubenfeld GD. The use of enrichment to reduce statistically indeterminate or negative trials in critical care. *Anaesthesia* (2017) 72:560–5. doi: 10.1111/anae.13870
10. Prescott HC, Calfee CS, Thompson BT, Angus DC, Liu VX. Toward smarter lumping and smarter splitting: rethinking strategies for sepsis and acute respiratory distress syndrome clinical trial design. *Am J Respir Crit Care Med.* (2016) 194:147–55. doi: 10.1164/rccm.201512-2544CP
11. Buyse M, Michiels S, Sargent DJ, Grothey A, Matheson A, De Gramont A. Integrating biomarkers in clinical trials. *Expert Rev Mol Diagn.* (2011) 11:171–82. doi: 10.1586/erm.10.120
12. Bothwell LE, Avorn J, Khan NF, Kesselheim AS. Adaptive design clinical trials: a review of the literature and clinicaltrials.gov. *BMJ Open* (2018) 8:e018320. doi: 10.1136/bmjopen-2017-018320
13. Jennison C, Turnbull BW. Confirmatory seamless phase II/III clinical trials with hypotheses selection at interim: Opportunities and limitations. *Biometr J.* (2006) 48:650–5. doi: 10.1002/bimj.200610248

14. Lewis RJ, Angus DC, Laterre PF, Kjolbye AL, Van Der Meulen E, Blemings A, et al. Rationale and design of an adaptive phase 2b/3 clinical trial of selepressin for adults in septic shock. Selepressin Evaluation Programme for Sepsis-induced Shock-Adaptive Clinical Trial. *Ann Am Thorac Soc.* (2018) 15:250–7. doi: 10.1513/AnnalsATS.201708-669SD
15. Winter A, Stäubert S, Ammon D, Aiche S, Beyan O, Bischoff V, et al. Smart Medical Information Technology for Healthcare (SMITH). *Methods Inf Med.* (2018) 57:e92–e105. doi: 10.3414/ME18-02-0004

Conflict of Interest Statement: The authors declare that the research was conducted in the absence of any commercial or financial relationships that could be construed as a potential conflict of interest.

Copyright © 2018 Kesselmeier and Scherag. This is an open-access article distributed under the terms of the Creative Commons Attribution License (CC BY). The use, distribution or reproduction in other forums is permitted, provided the original author(s) and the copyright owner(s) are credited and that the original publication in this journal is cited, in accordance with accepted academic practice. No use, distribution or reproduction is permitted which does not comply with these terms.

frontiers in Immunology

MINI REVIEW
published: 13 November 2018
doi: 10.3389/fimmu.2018.02632

Park 7: A Novel Therapeutic Target for Macrophages in Sepsis-Induced Immunosuppression

Yanwei Cheng[1,2], *Tony N. Marion*[3,4], *Xue Cao*[2,3], *Wanting Wang*[1] *and Yu Cao*[1,2]*

[1] *West China Hospital Emergency Department, State Key Laboratory of Biotherapy, West China Hospital, Sichuan University, and Collaborative Innovation Center of Biotherapy, Chengdu, China,* [2] *Disaster Medicine Center, Sichuan University, Chengdu, China,* [3] *Department of Rheumatology and Immunology, West China Hospital, Sichuan University, Chengdu, China,* [4] *Department of Microbiology, Immunology, and Biochemistry, The University of Tennessee Health Science Center, Memphis, TN, United States*

Sepsis remains a serious and life-threatening condition with high morbidity and mortality due to uncontrolled inflammation together with immunosuppression with few therapeutic options. Macrophages are recognized to play essential roles throughout all phases of sepsis and affect both immune homeostasis and inflammatory processes, and macrophage dysfunction is considered to be one of the major causes for sepsis-induced immunosuppression. Currently, Parkinson disease protein 7 (Park 7) is known to play an important role in regulating the production of reactive oxygen species (ROS) through interaction with $p47^{phox}$, a subunit of NADPH oxidase. ROS are key mediators in initiating toll-like receptor (TLR) signaling pathways to activate macrophages. Emerging evidence has strongly implicated Park 7 as an antagonist for sepsis-induced immunosuppression, which suggests that Park 7 may be a novel therapeutic target for reversing immunosuppression compromised by sepsis. Here, we review the main characteristics of sepsis-induced immunosuppression caused by macrophages and provide a detailed mechanism for how Park 7 antagonizes sepsis-induced immunosuppression initiated by the macrophage inflammatory response. Finally, we further discuss the most promising approach to develop innovative drugs that target Park 7 in patients whose initial presentation is at the late stage of sepsis.

Keywords: Park 7, sepsis-induced immunosuppression, inflammation, macrophages, ROS, $p47^{phox}$, NADPH, crystal structure

OPEN ACCESS

Edited by:
Lukas Martin,
Uniklinik RWTH Aachen, Germany

Reviewed by:
Johannes Ehler,
University of Rostock, Germany
Daniel Remick,
Boston University, United States

***Correspondence:**
Yu Cao
yuyuer@126.com

Specialty section:
This article was submitted to Inflammation, a section of the journal Frontiers in Immunology

Received: *11 August 2018*
Accepted: *25 October 2018*
Published: *13 November 2018*

Citation:
Cheng Y, Marion TN, Cao X, Wang W and Cao Y (2018) Park 7: A Novel Therapeutic Target for Macrophages in Sepsis-Induced Immunosuppression. Front. Immunol. 9:2632. doi: 10.3389/fimmu.2018.02632

INTRODUCTION

Sepsis is a common clinical disease with high morbidity and mortality. Annually, ~30 million (1) people are affected by sepsis and more than 6–8 million (2) of those affected die. Despite significant advances in treatment, sepsis is still a major clinical problem and remains the leading cause of death in the critically ill patient population (3, 4) with an associated severe cost burden (5). In 2013, sepsis was responsible for more than $23 billion (6) of hospital costs in the USA alone. Thus, sepsis has been described as "the quintessential medical disorder of the twenty-first century." On 26 May 2017, the World Health Organization listed sepsis as a global health priority by adopting a resolution to improve the prevention, diagnosis and management of this deadly disease (7).

In the recent "sepsis-3" consensus (8), sepsis is defined as a life-threatening, multiorgan dysfunction caused by a dysregulated host response to infection, which is primarily caused by Gram-negative bacteria. However, a global study of 14,000 critically ill patients found that 47% of isolates were Gram-positive, indicating that more patients currently become septic from Gram-positive infections (9). Even after an inciting infection has been resolved, septic patients continue to mount an excessive inflammatory response (10) that leads to tissue damage and organ failure. Key advances have made earlier recognition and treatment of sepsis feasible with the result that some patients can restore immune homeostasis, completely clear infection, and achieve complete recovery (11). Otherwise, patients progress into late stage sepsis and suffer from severe immunosuppression characterized by an impaired activation of the immune response and a hypo-inflammatory response (12), resulting in more difficult recovery and poor long-term outcomes with risk of cognitive and physical impairments, even an increased incidence of delayed death due to the lack of effective treatment for sepsis-induced immunosuppression (13). At present, immunosuppression in septic patients constitutes an important focus of research. Thus far, various interrelated, non-mutually exclusive mechanisms have been proposed to explain sepsis-induced immunosuppression, including cellular apoptosis (14), autophagy (15, 16), regulation by the central nervous system (17, 18), metabolic reprogramming (19), epigenetic regulation (20–22), and endotoxin tolerance (23–25). The immunopathogenesis of sepsis-induced immunosuppression is a very complex process that involves both innate and adaptive immune cells. In fact, it is at least partially caused by the dysfuction of macrophages.

MACROPHAGES AND SEPSIS-INDUCED IMMUNOSUPPRESSION

Macrophages play essential roles throughout all phases of sepsis with their ubiquitous presence and comprehensive effects on immune homeostasis and inflammatory process. After infection, macrophage is activated through Toll-like receptor (TLR) that recognizes pathogen-associated molecular patterns (PAMPs) of the invading pathogen, such as lipopolysaccharide (LPS) in Gram-negative bacteria and lipoteichoic acid (LTA)/peptidoglycan (PGN) in Gram-positive bacteria (26). In the early stage of sepsis, macrophages undergo M1 differentiation and promote host defense by eliminating invading pathogens or damaged tissues and releasing massive amounts of pro-inflammatory cytokines such as tumor necrosis factor alpha (TNF-a), interleukin-1 (IL-1), interleukin-6 (IL-6) and interleukin-8 (IL-8) (27). However, macrophages may be excessively activated during the early phase and produce excessive pro-inflammatory cytokines (28), which have been identified as one of the major causes for the high mortality rate in the early stage of sepsis (29). If macrophage-mediated pro-inflammatory responses cannot be adequately regulated, a cytokine storm may emerge (30) with the pro-inflammatory response becoming pathogenic and eventually immunosuppressive in late stage sepsis (31–33). As activated pro-inflammatory macrophages undergo apoptosis and/or polarize to the M2 phenotype that dampens the pro-inflammatory response, they may contribute to immunosuppression. Due to the cytokine storm, a large number of apoptosis-inducing factors are generated and released, including TNF-a, high mobility group box-1 protein (HMGB1) (34), thereby inducing and promoting macrophage apoptosis (35). Previous studies (36, 37) have determined the presence of an excessive level of macrophages apoptosis in human autopsies and animal models of sepsis. However, escaped M1 macrophages from apoptosis convert into M2 macrophages, showing downregulated inflammatory cytokines but upregulated anti-inflammatory cytokines (38). Certain cytokines (i.e., TNF-a, IL-13, IL-4, IL-10 etc.) can stimulate the polarization of macrophages toward M2 phenotype (39–41). Porta et al. (42) found that LPS-tolerant macrophages have the same characteristics as M2 macrophages. When a gram-negative infection persists, long-term accumulation of LPS can reprogram inflammatory responses (43) from activation to suppression leading to decreased production of inflammatory cytokines (44). The affected host may present a LPS-tolerant state, and macrophages also display the phenomenon of LPS-tolerance (45–47). In addition, M2 phenotype macrophages also accelerate T cell apoptosis and suppress Th1 cell responses (48). Collectively, this "dysfunctional" macrophage plays a key role in the pathogenesis of sepsis-induced immunosuppression because their pro-inflammatory cytokine secretions to support effective immune reactivity against primary or secondary pathogens is compromised. Therefore, modulating homeostasis of pro- and anti-inflammatory responses and functional stabilities of macrophages can be of great benefits for sepsis-induced immunosuppression.

REACTIVE OXYGEN SPECIES (ROS) AND MACROPHAGES

In addition to its cytotoxic function, reactive oxygen species (ROS) can initiate multiple signal transduction cascades to modulate macrophage function and are critical to the regulation of immune responses against pathogens (49). Previous studies have shown that ROS have an established role in regulating TLR signaling pathways, such as TLR/NF-κB and TLR/MARKs pathways (50–52). In LPS-tolerant macrophages, LPS tolerance blunts the TLR4 signaling, inhibiting the activation of the NF-κB signaling pathway downstream of TLR4, resulting in reduced production of inflammatory cytokines in response to LPS challenge (53–55). ROS can modulate the production of pro-inflammatory cytokines from LPS-tolerant macrophages by activating TLR4/NF-κB and TLR/MARKs pathways (49) mainly by accelerating the phosphorylation of IκBα and MAPK phosphatases (56, 57), respectively. In addition, it has been reported that TLR2-deficient macrophages lacked the response to Gram-positive LTA and PGN (58, 59), which can interact with TLR2, leading to NF-κB activation and induction of proinflammatory mediators in macrophages (59, 60). Rajamani (61) also demonstarted that high glucose mediated ROS could

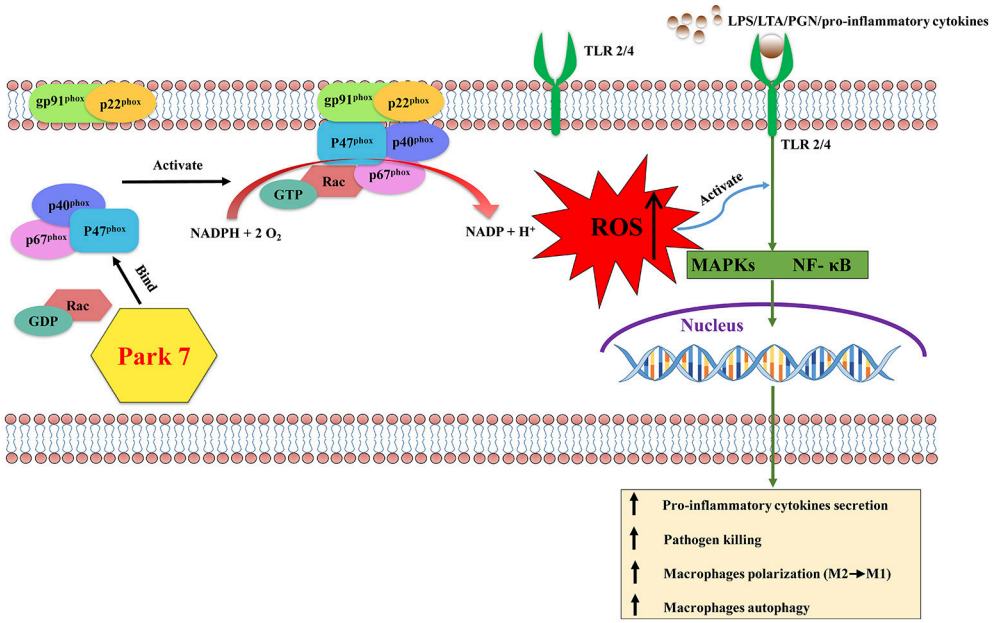

FIGURE 1 | The effects of Park 7 on macrophages in sepsis-induced immunosuppression. During the late stage of sepsis, the activation of macrophages is impaired due to the blunted TLR/NF-κB and/or TLR/MARKs signaling pathways induced with LPS/LTA/PGN/pro-inflammatory cytokines. $p47^{phox}$, a proenzyme subunit of NADPH oxidase, is key to the assembly process of NADPH oxidase. Park 7 can interact with $p47^{phox}$ and promote its phosphorylation and membrane translocation to form the holoenzyme complex. Subsequently the activation of NADPH oxidase produces ROS, which can activate the MAPKs and NF-κB signaling pathways downstream of TLR signaling, resulting in the activation of macrophages. Activated macrophages protect against sepsis-induced immunosuppression by releasing pro-inflammatory cytokines, killing pathogen, polarizing to M1 phenotype and the enhanced capacity of autophagy. Park 7, Parkinson disease 7; LPS, lipopolysaccharide; LTA, lipoteichoic acid; PGN, peptidoglycan; ROS, reactive oxygen species; TLR, Toll-like receptor; NF-κB, nuclear factor kappa-light-chain-enhancer of activated B cells; MAPKs, mitogen-activated protein kinases.

induce TLR-2 activation and downstream NF-κB signaling mediating increased inflammation during diabetic retinopathy. TLR4/NF-κB pathway also plays a central role in the regulation of macrophage polarization (48). M1 macrophage polarization is related to the activation of the TLR4/NF-κB pathway (62), whereas M2 macrophage polarization is associated with the down-regulatation of NF-κB pathway (63). A recent study has confirmed that the p50 subunit of NF-κB inhibits the NF-κB pathway and M1 polarization (42). Kuchler et al. (64) reported that impaired ROS formation contributed to an M2 phenotype shift of macrophages in sepsis by inhibiting NF-κB signaling. Consequently, increased ROS formation may reduce the M2 polarization of macrophages and protect against sepsis-induced immunosuppression.

The TLR4/MARKs pathway is also involved in regulating the LPS/pro-inflammatory cytokines-induced autophagy (65). Autophagy can induce cell death but can also be a cytoprotective process. Deficient autophagy suppresses the immune response in sepsis and increases mortality (15, 16, 66). Macrophage autophagy is considered an important part of the host immune defense, eliminating intracellular pathogens through heterophagy. It has been reported that ROS can influence the MAPK pathways to activate macrophage autophagy. In hepatoma cells, migration inhibitory factor, produced by many cells including macrophages, induced autophagy via ROS generation (67). Likewise, autophagy also participates in regulating functions of macrophages and affects their ability to defend and clear pathogens through activating NF-κB pathway (68) and enhancing phagocytic capacity of macrophages (69). All of this suggests that ROS can activate macrophages to improve bactericidal and autophagy and increase production of pro-inflammatory cytokines, thereby helping to maintain immune homeostasis. Thus, a novel approach to improve ROS production in macrophages may be a useful therapy for sepsis-induced immunosuppression.

PARKINSON DISEASE 7

Parkinson disease 7 (Park 7), also known as DJ-1 (70), is highly conserved in almost all organisms and is ubiquitously expressed in all tissues and organs (71). Park 7 was initially discovered as a novel oncogene product (72) and is considered as a major causal factor for the early onset of Parkinson's disease (73). In the past two decades, Park 7 has been intensely studied in many diseases including cancer (74), neurodegenerative disorderes (75) and stroke (76). Among these diseases, Park 7 not only serves as a reliable predictor of auxiliary diagnosis, but also is a useful therapeutic target. Park 7 is a multi-functional protein with transcriptional regulation, protein chaperone, protease, and antioxidative stress functions (77). At present, increasing evidence has demonstrated that Park 7 plays

important functions in protecting neurons (78), astrocytes (79), cardiomyocytes (80, 81), and renal proximal tubule cells (82) against oxidative stress-induced cell injury. In addition, Park 7 played an important role in restoring impaired autophagy and ameliorated phenylephrine-induced cardiac hypertrophy in a repression of cardiac hypertrophy model (83). Oxidative stress is strongly related to inflammation and is thought to be involved in the processes of many diseases, including sepsis (84). Recently, accumulating lines of evidence for Park 7 in activating the inflammatory response through modulating ROS regulating oxidative stress have also been reported (53, 85). As an antioxidant, Park 7 helps to limit to cell and tissue injury in a number of diseases by removing accumulated ROS (82, 86–89). However, studies had shown that Park 7 surprisingly seems to be required for high intracellular ROS production (85, 90). Therefore, Park 7 plays a dual role in buffering cellular ROS levels: functions as a scavenger in high ROS levels, whereas helps ROS production when essential ROS are required. In view of the hypo-inflammation characteristics of sepsis-induced immunosuppression and the critical role of Park 7 in modulating ROS production and initiating an inflammatory response, recently it has been reported that Park 7 can protect against sepsis-induced immunosuppression.

PARK 7 PROTECTS AGAINST SEPSIS-INDUCED IMMUNOSUPPRESSION (FIGURE 1)

In a park 7 knock-out (KO) mouse injected with LPS, Liu et al. (53) found that park 7 KO mice present immunosuppression phenotypes similar to the late stage of sepsis but not acute inflammation state, suggesting that park7 KO mice could serve as an animal model of sepsis-induced immunosuppression. In this model, Park 7 absence led to macrophage paralysis that resulted in increased abdominal bacterial burdens, reduced local and systemic inflammation, and impaired pro-inflammatory cytokines induction, eventually leading to high susceptibility to LPS. Neutrophil paralysis, similar to macrophage paralysis described above, was described in experimental studies of patients and sepsis animal models and was associated with decreased production of ROS in neutrophils (91, 92). In a liver fibrosis model, Park 7 deficiency inhibited ROS production in macrophages (93). Similarly, Liu et al. also observed greatly reduced ROS production in macrophages from park 7 KO mice (53). Macrophages with Park 7 deficiency showed downregulation of NF-κB and MAPK signaling pathways downstream of TLR suggesting that Park 7 deficiency can reduce the ROS production to limit TLR signaling and impair the activation of macrophages. Restoration of Park 7 expression with an inducible Park7 transgene restored the production of ROS in Park 7 KO macrophages to subsequently restore TLR signaling, pro-inflammatory cytokine production, bactericidal function, and eventually improve survival of the Park 7 KO mice in the late stage of sepsis. However, immunosuppressive IL-10 was not simultaneously enhanced after restoration of Park7 expression. During the late stage of sepsis, Park 7 may also enhance the macrophage functions by restoring impaired macrophages autophay through increased ROS and TLR/MARK signaling. Macrophage autophagy can affect cell death via complex pathways involving crosstalk with apoptosis, which may also partly attenuate immunosuppression (94). Moreover, Park 7 may contribute to the M1 macrophages polarization and inhibit the M2 macrophages polarization by the increased ROS.

Although there are many sources of ROS within macrophages, NADPH oxidase-derived ROS are critical in host defense. When macrophages are stimulated by an extracellular stimulus such as hormones, cytokines, and other inflammatory factors, the six proenzyme subunits of NADPH oxidase (95), including $p22^{phox}$, $gp91^{phox}$, GTPase Rac, $p40^{phox}$, $p47^{phox}$, and $p67^{phox}$, form the holoenzyme complex that catalyzes the transfer of NADPH electrons to oxygen molecules to produce ROS (96). Key to the assembly process of the holoenzyme complex is $p47^{phox}$ (97, 98). After macrophages are stimulated extracellularly, $p47^{phox}$, which resides in the cytosol during the resting state (95), is phosphorylated and translocated to the plasma membrane together with the remaining proenzyme subunits and activation of NADPH oxidase (99, 100). Consistent with Liu's study (53), by interacting with $p47^{phox}$ and modulating phosphorylation and membrane translocation of $p47^{phox}$, Park7 promoted NADPH oxidase assembly and induced the production of ROS in macrophages. This mechanism supports the hypothesis that Park 7-targeted therapy maybe useful in the future in the treatment of sepsis-induced immunosuppression.

IS PARK 7 A POTENTIAL TARGET FOR DRUG TREATMENT IN THE FUTURE?

In this decade, many reports have shown the therapeutic potency of Park 7 and Park 7-targeting molecules/compounds in treating several neurodegenerative disorders (101–103). Can Park 7 be a potential target for drug treatment for sepsis-induced immunosuppression in the future? Structure-based drug design (SBDD) (104), as a valuable pharmaceutical lead discovery tool, opens up new opportunities for drug design for the patient with sepsis-induced immunosuppression. A typical example is the successful design of many valuable drugs by SBDD based on the crystal structure of Class B G-protein-coupled receptors (105). As noted above, the interaction of Park 7 and $p47^{phox}$ is a decisive factor in activating macrophages to ameliorate sepsis-induced immunosuppression, suggesting that the interaction between Park 7 and $p47^{phox}$ may be an ideal target for drug design. Single crystal structures of Park 7 and $p47^{phox}$ have been determined. Human Park 7 consists of 189 amino acids from N-terminus to C-terminus, which folds into a helix-strand-helix sandwich structure (106). The C-terminal domain (CTD) of Park 7 physically interacts with $p47^{phox}$ *in vitro* (53). In addition, the C106 and L166 residues in the CTD of Park 7 are important for its functions (107, 108), suggesting the two residues might play a key role in Park 7 interacting with $p47^{phox}$. However, the details of the interaction depend on the crystal structure of the Park7-$p47^{phox}$ complex. Therefore, determing Park7-$p47^{phox}$ complex structure should be an urgent issue for future research.

With regard to a potential drug treatment based on Park 7 in the future it might be important to discuss three relevant points here. (1) It would be necessary to detect/diagnose the immune status of the patient in sepsis-induced immunosuppression. (2) In line with this it would be crucial to find the right timing to start drug treatment to overcome sepsis-induced immunosuppression. (3) Considering the complexity of the host response during sepsis and the variety of pathophysiological pathways involved, it is unlikely that the current "one-target" and "one-size-fits-all" approach will ever be successful. To date, absolute lymphocyte count and decreased expression of HLA-DR by monocytes seem to be the most robust markers for patient stratification in multicenter clinical trials (109–112). Measurement of soluble mediators such as IL-6, IL-10, and TNF-a can also help detect immune status. However, a convenient, faster detection protocol and other effective drugs are extremely necessary. These are interesting issues that are worth pursuing in the future.

CONCLUSION

In summary, macrophages, as one of the most important cells of the innate immune system, play an important role in inflammatory and immune processes. In the early stage of sepsis, macrophages usually have a pro-inflammatory phenotype, whereas the excessive inflammatory macrophage response can lead to macrophages apoptosis and change macrophage polarization contributing to the immunosuppression. ROS have the capacity to initiate many TLR signaling pathways and in turn modulate macrophage functions and are produced by the activation of NADPH oxidase. Park 7 has been extensively studied in many diseases and can serve as an effective therapeutic target. For research on sepsis in the late stage, Park7 KO mice can be an ideal model. The interaction of Park7 and $p47^{phox}$ can activate NADPH oxidase and subsequently increase ROS in macrophages to initiate TRL signaling to in turn, reinforce macrophage functions to protect against sepsis–induced immunosuppression. In light of this understanding, the Park 7/$p47^{phox}$/ROS axis may become an effective therapeutic target for sepsis induced immunosuppression.

AUTHOR CONTRIBUTIONS

YaC wrote the first draft of this article. XC and WW designed the figure. YC and TM critically revised the manuscript for important intellectual content. All authors approved the final version.

FUNDING

The present work was supported by the National Natural Science Foundation of China (Grant Nos. 81471836 and 81772037), the Chengdu Science and Technology Huimin Project (Grant No. 2016-HM0M2-00099-SF).

REFERENCES

1. Fleischmann C, Scherag A, Adhikari NK, Hartog CS, Tsaganos T, Schlattmann P, et al. Assessment of Global Incidence and Mortality of Hospital-treated Sepsis. Current estimates and limitations. *Am J Respir Crit Care Med.* (2016) 193:259–72. doi: 10.1164/rccm.201504-0781OC
2. Seymour CW, Rea TD, Kahn JM, Walkey AJ, Yealy DM, Angus DC. Severe sepsis in pre-hospital emergency care: analysis of incidence, care, and outcome. *Am J Respir Crit Care Med.* (2012) 186:1264–71. doi: 10.1164/rccm.201204-0713OC
3. Dombrovskiy VY, Martin AA, Sunderram J, Paz HL. Rapid increase in hospitalization and mortality rates for severe sepsis in the United States: a trend analysis from 1993 to 2003. *Crit Care Med.* (2007) 35:1244–50. doi: 10.1097/01.ccm.0000261890.41311.e9
4. Melamed A, Sorvillo FJ. The burden of sepsis-associated mortality in the United States from 1999 to 2005: an analysis of multiple-cause-of-death data. *Crit Care* (2009) 13:R28. doi: 10.1186/cc7733
5. Tiru B, DiNino EK, Orenstein A, Mailloux PT, Pesaturo A, Gupta A, et al. The Economic and Humanistic burden of severe sepsis. *Pharmacoeconomics* (2015) 33:925–37. doi: 10.1007/s40273-015-0282-y
6. Torio CM, Moore BJ. *National Inpatient Hospital Costs: The Most Expensive Conditions by Payer, 2013: Statistical Brief #204*, in *Healthcare Cost and Utilization Project (HCUP) Statistical Briefs*. (2006). Rockville, MD: Agency for Healthcare Research and Quality (US).
7. Reinhart K, Daniels R, Kissoon N, Machado FR, Schachter RD, Finfer S. Recognizing sepsis as a global health priority - A WHO resolution. *N Engl J Med.* (2017) 377:414–7. doi: 10.1056/NEJMp1707170
8. Singer M, Deutschman CS, Seymour CW, Shankar-Hari M, Annane D, Bauer M, et al. The third international consensus definitions for sepsis and septic shock (Sepsis-3). *JAMA* (2016) 315:801–10. doi: 10.1001/jama.2016.0287
9. Vincent JL, Rello J, Marshall J, Silva E, Anzueto A, Martin CD, et al. International study of the prevalence and outcomes of infection in intensive care units. *JAMA* (2009) 302:2323–9. doi: 10.1001/jama.2009.1754
10. van der Poll T, van de Veerdonk FL, Scicluna BP, Netea MG. The immunopathology of sepsis and potential therapeutic targets. *Nat Rev Immunol.* (2017) 17:407–20. doi: 10.1038/nri.2017.36
11. Kumar A, Kethireddy S. Emerging concepts in optimizing antimicrobial therapy of septic shock: speed is life but a hammer helps too. *Crit Care* (2013) 17:104. doi: 10.1186/cc11890
12. Hotchkiss RS, Monneret G, Payen D. Immunosuppression in sepsis: a novel understanding of the disorder and a new therapeutic approach. *Lancet Infect Dis.* (2013) 13:260–8. doi: 10.1016/s1473-3099(13)70001-x
13. Iwashyna TJ, Ely EW, Smith DM, Langa KM. Long-term cognitive impairment and functional disability among survivors of severe sepsis. *JAMA* (2010) 304:1787–94. doi: 10.1001/jama.2010.1553
14. Hotchkiss RS, Swanson PE, Freeman BD, Tinsley KW, Cobb JP, Matuschak GM, et al. Apoptotic cell death in patients with sepsis, shock, and multiple organ dysfunction. *Crit Care Med.* (1999) 27:1230–51.
15. Lin CW, Lo S, Hsu C, Hsieh CH, Chang YF, Hou BS, et al. T-cell autophagy deficiency increases mortality and suppresses immune responses after sepsis. *PLoS ONE* (2014) 9:e102066. doi: 10.1371/journal.pone.0102066
16. Oami T, Watanabe E, Hatano M, Sunahara S, Fujimura L, Sakamoto A, et al. Suppression of T cell autophagy results in decreased viability and function of T cells through accelerated apoptosis in a murine sepsis model. *Crit Care Med.* (2017) 45:e77–85. doi: 10.1097/ccm.0000000000002016
17. Singer BH, Newstead MW, Zeng X, Cooke CL, Thompson RC, Singer K, et al. Cecal ligation and puncture results in long-term central nervous system myeloid inflammation. *PLoS ONE* (2016) 11:e0149136. doi: 10.1371/journal.pone.0149136
18. Martelli D, Yao ST, McKinley MJ, McAllen RM. Reflex control of inflammation by sympathetic nerves, not the vagus. *J Physiol.* (2014) 592:1677–86. doi: 10.1113/jphysiol.2013.268573

19. Arts RJ, Gresnigt MS, Joosten LA, Netea MG. Cellular metabolism of myeloid cells in sepsis. *J Leukoc Biol.* (2017) 101:151–164. doi: 10.1189/jlb.4MR0216-066R
20. Cazalis MA, Lepape A, Venet F, Frager F, Mougin B, Vallin H, et al. Early and dynamic changes in gene expression in septic shock patients: a genome-wide approach. *Intensive Care Med Exp.* (2014) 2:20. doi: 10.1186/s40635-014-0020-3
21. Xiao W, Mindrinos MN, Seok J, Cuschieri J, Cuenca AG, Gao H, et al. A genomic storm in critically injured humans. *J Exp Med.* (2011) 208:2581–90. doi: 10.1084/jem.20111354
22. Davenport EE, Burnham KL, Radhakrishnan J, Humburg P, Hutton P, Mills TC, et al. Genomic landscape of the individual host response and outcomes in sepsis: a prospective cohort study. *Lancet Respir Med.* (2016) 4:259–71. doi: 10.1016/s2213-2600(16)00046-1
23. Allantaz-Frager F, Turrel-Davin F, Venet F, Monnin C. De Saint Jean A, Barbalat V, et al. Identification of biomarkers of response to IFNg during endotoxin tolerance: application to septic shock. *PLoS ONE* (2013) 8:e68218. doi: 10.1371/journal.pone.0068218
24. Giza DE, Vasilescu C. [MicroRNA's role in sepsis and endotoxin tolerance. More players on the stage]. *Chirurgia* (2010) 105:625–30. doi: 10.3109/19401736.2015.1060434
25. Andrades ME, Morina A, Spasic S, Spasojevic I. Bench-to-bedside review: sepsis - from the redox point of view. *Crit Care* (2011) 15:230. doi: 10.1186/cc10334
26. Kumar H, Kawai T, Akira S. Pathogen recognition by the innate immune system. *Int Rev Immunol* (2011) 30:16–34. doi: 10.3109/08830185.2010.529976
27. Murray PJ, Wynn TA, Protective and pathogenic functions of macrophage subsets. *Nat Rev Immunol.* (2011) 11:723–37. doi: 10.1038/nri3073
28. Wang TS, Deng JC. Molecular and cellular aspects of sepsis-induced immunosuppression. *J Mol Med.* (2008) 86:495–506. doi: 10.1007/s00109-007-0300-4
29. Angus DC, van der Poll T. Severe sepsis and septic shock. *N Engl J Med.* (2013) 369:840–51. doi: 10.1056/NEJMra1208623
30. Rittirsch D, Flierl MA, Ward PA. Harmful molecular mechanisms in sepsis. *Nat Rev Immunol.* (2008) 8:776–87. doi: 10.1038/nri2402
31. Nathan C, Ding A. Nonresolving inflammation. *Cell* (2010) 140:871–82. doi: 10.1016/j.cell.2010.02.029
32. Sindrilaru A, Peters T, Wieschalka S, Baican C, Baican A, Peter H, et al. An unrestrained proinflammatory M1 macrophage population induced by iron impairs wound healing in humans and mice. *J Clin Invest.* (2011) 121:985–97. doi: 10.1172/jci44490
33. Krausgruber T, Blazek K, Smallie T, Alzabin S, Lockstone H, Sahgal N, et al. IRF5 promotes inflammatory macrophage polarization and TH1-TH17 responses. *Nat Immunol.* (2011) 12:231–8. doi: 10.1038/ni.1990
34. Zhu XM, Yao YM, Liang HP, Liu F, Dong N, Yu Y, et al. Effect of high mobility group box-1 protein on apoptosis of peritoneal macrophages. *Arch Biochem Biophys.* (2009) 492:54–61. doi: 10.1016/j.abb.2009.09.016
35. Luan YY, Yao YM, Xiao XZ, Sheng ZY. Insights into the apoptotic death of immune cells in sepsis. *J Interferon Cytokine Res.* (2015) 35:17–22. doi: 10.1089/jir.2014.0069
36. Rimmele T, Payen D, Cantaluppi V, Marshall J, Gomez H, Gomez A, et al. Immune cell phenotype and function in sepsis. *Shock* (2016) 45:282–91. doi: 10.1097/shk.0000000000000495
37. Luan YY, Dong N, Xie M, Xiao XZ, Yao YM. The significance and regulatory mechanisms of innate immune cells in the development of sepsis. *J Interferon Cytokine Res.* (2014) 34:2–15. doi: 10.1089/jir.2013.0042
38. Mantovani A, Sica A, Locati M. Macrophage polarization comes of age. *Immunity* (2005) 23:344–6. doi: 10.1016/j.immuni.2005.10.001
39. Gordon S, Martinez FO. Alternative activation of macrophages: mechanism and functions. *Immunity* (2010) 32:593–604. doi: 10.1016/j.immuni.2010.05.007
40. Sica A, Mantovani A. Macrophage plasticity and polarization: in vivo veritas. *J Clin Invest.* (2012) 122:787–95. doi: 10.1172/jci59643
41. Ip WKE, Hoshi N, Shouval DS, Snapper S, Medzhitov R. Anti-inflammatory effect of IL-10 mediated by metabolic reprogramming of macrophages. *Science* (2017) 356:513–9. doi: 10.1126/science.aal3535
42. Porta C, Rimoldi M, Raes G, Brys L, Ghezzi P, Di Liberto D, et al. Tolerance and M2 (alternative) macrophage polarization are related processes orchestrated by p50 nuclear factor kappaB. *Proc Natl Acad Sci USA.* (2009) 106:14978–83. doi: 10.1073/pnas.0809784106
43. Seeley JJ, Ghosh S. Molecular mechanisms of innate memory and tolerance to LPS. *J Leukoc Biol.* (2017) 101:107–119. doi: 10.1189/jlb.3MR0316-118RR
44. Biswas SK, Lopez-Collazo E. Endotoxin tolerance: new mechanisms, molecules and clinical significance. *Trends Immunol.* (2009) 30:475–87. doi: 10.1016/j.it.2009.07.009
45. Sato S, Takeuchi O, Fujita T, Tomizawa H, Takeda K, Akira S. A variety of microbial components induce tolerance to lipopolysaccharide by differentially affecting MyD88-dependent and -independent pathways. *Int Immunol.* (2002) 14:783–91. doi: 10.1093/intimm/dxf046
46. Medvedev AE, Kopydlowski KM, Vogel SN. Inhibition of lipopolysaccharide-induced signal transduction in endotoxin-tolerized mouse macrophages: dysregulation of cytokine, chemokine, and toll-like receptor 2 and 4 gene expression. *J Immunol.* (2000) 164:5564–74. doi: 10.4049/jimmunol.164.11.5564
47. Dobrovolskaia MA, Medvedev AE, Thomas KE, Cuesta N, Toshchakov V, Ren T, et al. Induction of in vitro reprogramming by Toll-like receptor (TLR)2 and TLR4 agonists in murine macrophages: effects of TLR "homotolerance" versus "heterotolerance" on NF-kappa B signaling pathway components. *J Immunol.* (2003) 170:508–19. doi: 10.4049/jimmunol.170.1.508
48. Liu YC, Zou XB, Chai YF, Yao YM. Macrophage polarization in inflammatory diseases. *Int J Biol Sci.* (2014) 10:520–9. doi: 10.7150/ijbs.8879
49. West AP, Brodsky IE, Rahner C, Woo DK, Erdjument-Bromage H, Tempst P, et al. TLR signalling augments macrophage bactericidal activity through mitochondrial ROS. *Nature* (2011) 472:476–80. doi: 10.1038/nature09973
50. Lee CC, Avalos AM, Ploegh HL. Accessory molecules for Toll-like receptors and their function. *Nat Rev Immunol.* (2012) 12:168–79. doi: 10.1038/nri3151
51. Gallego C, Golenbock D, Gomez MA, Saravia NG. Toll-like receptors participate in macrophage activation and intracellular control of Leishmania (Viannia) panamensis. *Infect Immun.* (2011) 79:2871–9. doi: 10.1128/iai.01388-10
52. Kamata H, Honda S, Maeda S, Chang L, Hirata H, Karin M. Reactive oxygen species promote TNFalpha-induced death and sustained JNK activation by inhibiting MAP kinase phosphatases. *Cell* (2005) 120:649–61. doi: 10.1016/j.cell.2004.12.041
53. Liu W, Wu H, Chen L, Wen Y, Kong X, Gao WQ. Park7 interacts with p47(phox) to direct NADPH oxidase-dependent ROS production and protect against sepsis. *Cell Res.* (2015) 25:691–706. doi: 10.1038/cr.2015.63
54. Hoogendijk AJ, Garcia-Laorden MI, van Vught LA, Wiewel MA, Belkasim-Bohoudi H, Duitman J, et al. Sepsis patients display a reduced capacity to activate nuclear factor-kappaB in multiple cell types. *Crit Care Med.* (2017) 45:e524–31. doi: 10.1097/ccm.0000000000002294
55. Nomura F, Akashi S, Sakao Y, Sato S, Kawai T, Matsumoto M, et al. Cutting edge: endotoxin tolerance in mouse peritoneal macrophages correlates with down-regulation of surface toll-like receptor 4 expression. *J Immunol.* (2000) 164:3476–9. doi: 10.4049/jimmunol.164.7.3476
56. Zhang J, Wang X, Vikash V, Ye Q, Wu D, Liu Y, et al. ROS and ROS-Mediated Cellular Signaling. *Oxid Med Cell Longev.* (2016) 2016:4350965. doi: 10.1155/2016/4350965
57. Park J, Min JS, Kim B, Chae UB, Yun JW, Choi MS, et al. Mitochondrial ROS govern the LPS-induced pro-inflammatory response in microglia cells by regulating MAPK and NF-kappaB pathways. *Neurosci Lett.* (2015) 584:191–6. doi: 10.1016/j.neulet.2014.10.016
58. Park OJ, Han JY, Baik JE, Jeon JH, Kang SS, Yun CH, et al. Lipoteichoic acid of *Enterococcus faecalis* induces the expression of chemokines via TLR2 and PAFR signaling pathways. *J Leukoc Biol.* (2013) 94:1275–84. doi: 10.1189/jlb.1012522
59. Hong SW, Baik JE, Kang SS, Yun CH, Seo DG, Han SH. Lipoteichoic acid of *Streptococcus mutans* interacts with Toll-like receptor 2 through the lipid moiety for induction of inflammatory mediators in murine macrophages. *Mol Immunol.* (2014) 57:284–91. doi: 10.1016/j.molimm.2013.10.004
60. Paul-Clark MJ, McMaster SK, Belcher E, Sorrentino R, Anandarajah J, Fleet M, et al. Differential effects of Gram-positive versus Gram-negative

bacteria on NOSII and TNFalpha in macrophages: role of TLRs in synergy between the two. *Br J Pharmacol.* (2006) 148:1067–75. doi: 10.1038/sj.bjp.0706815
61. Rajamani U, Jialal I. Hyperglycemia induces Toll-like receptor-2 and−4 expression and activity in human microvascular retinal endothelial cells: implications for diabetic retinopathy. *J Diabetes Res.* (2014) 2014:790902. doi: 10.1155/2014/790902
62. Odegaard JI, Chawla A. Mechanisms of macrophage activation in obesity-induced insulin resistance. *Nat Clin Pract Endocrinol Metab.* (2008) 4:619–26. doi: 10.1038/ncpendmet0976
63. Pollard JW, Trophic macrophages in development and disease. *Nat Rev Immunol.* (2009) 9:259–70. doi: 10.1038/nri2528
64. Kuchler L, Giegerich AK, Sha LK, Knape T, Wong MS, Schroder K, et al. SYNCRIP-dependent Nox2 mRNA destabilization impairs ROS formation in M2-polarized macrophages. *Antioxid Redox Signal.* (2014) 21:2483–97. doi: 10.1089/ars.2013.5760
65. Xu Y, Jagannath C, Liu XD, Sharafkhaneh A, Kolodziejska KE, Eissa NT. Toll-like receptor 4 is a sensor for autophagy associated with innate immunity. *Immunity* (2007) 27:135–44. doi: 10.1016/j.immuni.2007.05.022
66. Nakahira K, Haspel JA, Rathinam VA, Lee SJ, Dolinay T, Lam HC, et al. Autophagy proteins regulate innate immune responses by inhibiting the release of mitochondrial DNA mediated by the NALP3 inflammasome. *Nat Immunol.* (2011) 12:222–30. doi: 10.1038/ni.1980
67. Chuang YC, Su WH, Lei HY, Lin YS, Liu HS, Chang CP, et al. Macrophage migration inhibitory factor induces autophagy via reactive oxygen species generation. *PLoS ONE* (2012) 7:e37613. doi: 10.1371/journal.pone.0037613
68. Ren C, Zhang H, Wu TT, Yao YM. Autophagy: a potential therapeutic target for reversing sepsis-induced immunosuppression. *Front Immunol.* (2017) 8:1832. doi: 10.3389/fimmu.2017.01832
69. Lee S, Lee SJ, Coronata AA, Fredenburgh LE, Chung SW, Perrella MA, et al. Carbon monoxide confers protection in sepsis by enhancing beclin 1-dependent autophagy and phagocytosis. *Antioxid Redox Signal.* (2014) 20:432–42. doi: 10.1089/ars.2013.5368
70. Bandyopadhyay S, Cookson MR. Evolutionary and functional relationships within the DJ1 superfamily. *BMC Evol Biol.* (2004) 4:6. doi: 10.1186/1471-2148-4-6
71. Shen ZY, Sun Q, Xia ZY, Meng QT, Lei SQ, Zhao B, et al. Overexpression of DJ-1 reduces oxidative stress and attenuates hypoxia/reoxygenation injury in NRK-52E cells exposed to high glucose. *Int J Mol Med.* (2016) 38:729–36. doi: 10.3892/ijmm.2016.2680
72. Nagakubo D, Taira T, Kitaura H, Ikeda M, Tamai K, SM Iguchi-Ariga, et al. DJ-1, a novel oncogene which transforms mouse NIH3T3 cells in cooperation with ras. *Biochem Biophys Res Commun.* (1997) 231:509–13. doi: 10.1006/bbrc.1997.6132
73. Bonifati V, Rizzu P, van Baren MJ, Schaap O, Breedveld GJ, Krieger E, et al. Mutations in the DJ-1 gene associated with autosomal recessive early-onset parkinsonism. *Science* (2003) 299:256–9. doi: 10.1126/science.1077209
74. Clements CM, McNally RS, Conti BJ, Mak TW, Ting JP. DJ-1, a cancer- and Parkinson's disease-associated protein, stabilizes the antioxidant transcriptional master regulator Nrf2. *Proc Natl Acad Sci USA.* (2006) 103:15091–6. doi: 10.1073/pnas.0607260103
75. Honbou K, Suzuki NN, Horiuchi M, Niki T, Taira T, Ariga H, et al. The crystal structure of DJ-1, a protein related to male fertility and Parkinson's disease. *J Biol Chem.* (2003) 278:31380–4. doi: 10.1074/jbc.M305878200
76. Dongworth RK, Mukherjee UA, Hall AR, Astin R, Ong SB, Yao Z, et al. DJ-1 protects against cell death following acute cardiac ischemia-reperfusion injury. *Cell Death Dis.* (2014) 5:e1082. doi: 10.1038/cddis.2014.41
77. Hijioka M, Inden M, Yanagisawa D, Kitamura Y. DJ-1/PARK7: a new therapeutic target for Neurodegenerative disorders. *Biol Pharm Bull.* (2017) 40:548–52. doi: 10.1248/bpb.b16-01006
78. Kim W, Kim DW, Jeong HJ, Yoo DY, Jung HY, Nam SM, et al. Tat-DJ-1 protects neurons from ischemic damage in the ventral horn of rabbit spinal cord via increasing antioxidant levels. *Neurochem Res.* (2014) 39:187–93. doi: 10.1007/s11064-013-1205-y
79. Yanagida T, Tsushima J, Kitamura Y, YanagisawaD, Takata K, Shibaike T, et al. Oxidative stress induction of DJ-1 protein in reactive astrocytes scavenges free radicals and reduces cell injury. *Oxid Med Cell Longev.* (2009) 2:36–42. doi: 10.4161/oxim.2.1.7985
80. Yu HH, Xu Q, Chen HP, Wang S, Huang XS, Huang QR, et al. Stable overexpression of DJ-1 protects H9c2 cells against oxidative stress under a hypoxia condition. *Cell Biochem Funct.* (2013) 31:643–51. doi: 10.1002/cbf.2949
81. Billia F, Hauck L, Grothe D, Konecny F, Rao V, Kim RH, et al. Parkinson-susceptibility gene DJ-1/PARK7 protects the murine heart from oxidative damage in vivo. *Proc Natl Acad Sci USA.* (2013) 110:6085–90. doi: 10.1073/pnas.1303444110
82. Cuevas S, Zhang Y, Yang Y, Escano C, Asico L, Jones JE, et al. Role of renal DJ-1 in the pathogenesis of hypertension associated with increased reactive oxygen species production. *Hypertension* (2012) 59:446–52. doi: 10.1161/hypertensionaha.111.185744
83. Xue R, Jiang J, Dong B, Tan W, Sun Y, Zhao J, et al. DJ-1 activates autophagy in the repression of cardiac hypertrophy. *Arch Biochem Biophys.* (2017) 633:124–32. doi: 10.1016/j.abb.2017.09.012
84. Galley HF. Oxidative stress and mitochondrial dysfunction in sepsis. *Br J Anaesth.* (2011) 107:57–64. doi: 10.1093/bja/aer093
85. Chen L, Luo M, Sun X, Qin J, Yu C, Wen Y, et al. DJ-1 deficiency attenuates expansion of liver progenitor cells through modulating the inflammatory and fibrogenic niches. *Cell Death Dis.* (2016) 7:e2257. doi: 10.1038/cddis.2016.161
86. Xu X, Martin F, Friedman JS. The familial Parkinson's disease gene DJ-1 (PARK7) is expressed in red cells and plays a role in protection against oxidative damage. *Blood Cells Mol Dis.* (2010) 45:227–32. doi: 10.1016/j.bcmd.2010.07.014
87. Zhang XL, Yuan YH, Shao QH, Wang ZZ, Zhu CG, Shi JG, et al. DJ-1 regulating PI3K-Nrf2 signaling plays a significant role in bibenzyl compound 20C-mediated neuroprotection against rotenone-induced oxidative insult. *Toxicol Lett.* (2017) 271:74–83. doi: 10.1016/j.toxlet.2017.02.022
88. Taira T, Saito Y, Niki T, SM Iguchi-Ariga, Takahashi K, Ariga H. DJ-1 has a role in antioxidative stress to prevent cell death. *EMBO Rep.* (2004) 5:213–8. doi: 10.1038/sj.embor.7400074
89. Amatullah H, Shan Y, Beauchamp BL, Gali PL, Gupta S, T Maron-Gutierrez, et al. DJ-1/PARK7 impairs bacterial clearance in sepsis. *Am J Respir Crit Care Med.* (2017) 195:889–905. doi: 10.1164/rccm.201604-0730OC
90. Vasseur S, Afzal S, Tomasini R, Guillaumond F, Tardivel-Lacombe J, Mak TW, et al. Consequences of DJ-1 upregulation following p53 loss and cell transformation. *Oncogene* (2012) 31:664–70. doi: 10.1038/onc.2011.268
91. Alves-Filho JC, Spiller F, Cunha FQ. Neutrophil paralysis in sepsis. *Shock* (2010) 34(Suppl. 1):15–21. doi: 10.1097/SHK.0b013e3181e7e61b
92. Kovach MA, Standiford TJ. The function of neutrophils in sepsis. *Curr Opin Infect Dis.* (2012) 25:321–7. doi: 10.1097/QCO.0b013e3283528c9b
93. Yu Y, Sun X, Gu J, Yu C, Wen Y, Gao Y, et al. Deficiency of DJ-1 Ameliorates liver Fibrosis through inhibition of Hepatic ROS production and inflammation. *Int J Biol Sci.* (2016) 12:1225–35. doi: 10.7150/ijbs.15154
94. Qiu P, Liu Y, Zhang J. Review: the role and mechanisms of macrophage autophagy in sepsis. *Inflammation* (2018) 1–14. doi: 10.1007/s10753-018-0890-8
95. Groemping Y, Lapouge K, Smerdon SJ, Rittinger K. Molecular basis of phosphorylation-induced activation of the NADPH oxidase. *Cell* (2003) 113:343–55. doi: 10.1016/S0092-8674(03)00314-3
96. Babior BM. NADPH oxidase: an update. *Blood* (1999) 93:1464–76.
97. de Mendez I, Homayounpour N, Leto TL. Specificity of p47phox SH3 domain interactions in NADPH oxidase assembly and activation. *Mol Cell Biol.* (1997) 17:2177–85.
98. Lambeth JD. NOX enzymes and the biology of reactive oxygen. *Nat Rev Immunol.* (2004) 4:181–9. doi: 10.1038/nri1312
99. El-Benna J, Dang PM, Gougerot-Pocidalo MA, Marie JC, Braut-Boucher F. p47phox, the phagocyte NADPH oxidase/NOX2 organizer: structure, phosphorylation and implication in diseases. *Exp Mol Med.* (2009) 41:217–25. doi: 10.3858/emm.2009.41.4.058
100. Gao XP, Standiford TJ, Rahman A, Newstead M, Holland SM, Dinauer MC, et al. Role of NADPH oxidase in the mechanism of lung neutrophil sequestration and microvessel injury induced by Gram-negative sepsis: studies in p47phox$^{-/-}$ and gp91phox$^{-/-}$ mice. *J Immunol.* (2002) 168:3974–82. doi: 10.4049/jimmunol.168.8.3974
101. Kitamura Y, Watanabe S, Taguchi M, Takagi K, Kawata T, Takahashi-Niki K, et al. Neuroprotective effect of a new DJ-1-binding compound

against neurodegeneration in Parkinson's disease and stroke model rats. *Mol Neurodegener.* (2011) 6:48. doi: 10.1186/1750-1326-6-48
102. Lev N, Barhum Y, Ben-Zur T, Aharony I, Trifonov L, Regev N, et al. A DJ-1 based Peptide attenuates dopaminergic degeneration in mice models of Parkinson's disease via enhancing Nrf2. *PLoS ONE* (2015) 10:e0127549. doi: 10.1371/journal.pone.0127549
103. Kitamura Y, Inden M, Kimoto Y, Takata K, Yanagisawa D, Hijioka M, et al. Effects of a DJ-1-binding compound on spatial learning and memory impairment in a mouse model of Alzheimer's Disease. *J Alzheimers Dis.* (2017) 55:67–72. doi: 10.3233/jad-160574
104. Grey JL, Thompson DH. Challenges and opportunities for new protein crystallization strategies in structure-based drug design. *Expert Opin Drug Discov.* (2010) 5:1039–45. doi: 10.1517/17460441.2010.515583
105. Zhang H, Qiao A, Yang D, Yang L, Dai A, de Graaf C, et al. Structure of the full-length glucagon class B G-protein-coupled receptor. *Nature* (2017) 546:259–64. doi: 10.1038/nature22363
106. Wilson MA, Collins JL, Hod Y, Ringe D, Petsko GA. The 1.1-A resolution crystal structure of DJ-1, the protein mutated in autosomal recessive early onset Parkinson's disease. *Proc Natl Acad Sci USA.* (2003) 100:9256–61. doi: 10.1073/pnas.1133288100
107. Olzmann JA, Brown K, Wilkinson KD, Rees HD, Huai Q, Ke H, et al. Familial Parkinson's disease-associated L166P mutation disrupts DJ-1 protein folding and function. *J Biol Chem.* (2004) 279:8506–15. doi: 10.1074/jbc.M311017200
108. Wilson MA. The role of cysteine oxidation in DJ-1 function and dysfunction. *Antioxid Redox Signal.* (2011) 15:111–22. doi: 10.1089/ars.2010.3481
109. Schefold JC. Measurement of monocytic HLA-DR (mHLA-DR) expression in patients with severe sepsis and septic shock: assessment of immune organ failure. *Intensive Care Med.* (2010) 36:1810–2. doi: 10.1007/s00134-010-1965-7
110. Cheron A, Monneret G, Landelle C, Floccard B, Allaouchiche B. [Low monocytic HLA-DR expression and risk of secondary infection]. *Ann Fr Anesth Reanim.* (2010) 29:368–76. doi: 10.1016/j.annfar.2010.02.015
111. Monneret G, Venet F. Sepsis-induced immune alterations monitoring by flow cytometry as a promising tool for individualized therapy. *Cytometry B Clin Cytom.* (2016) 90:376–86. doi: 10.1002/cyto.b.21270
112. Monneret G, Venet F, Pachot A, Lepape A. Monitoring immune dysfunctions in the septic patient: a new skin for the old ceremony. *Mol Med.* (2008) 14:64–78. doi: 10.2119/2007-00102.Monneret

Conflict of Interest Statement: The authors declare that the research was conducted in the absence of any commercial or financial relationships that could be construed as a potential conflict of interest.

Copyright © 2018 Cheng, Marion, Cao, Wang and Cao. This is an open-access article distributed under the terms of the Creative Commons Attribution License (CC BY). The use, distribution or reproduction in other forums is permitted, provided the original author(s) and the copyright owner(s) are credited and that the original publication in this journal is cited, in accordance with accepted academic practice. No use, distribution or reproduction is permitted which does not comply with these terms.

frontiers in Immunology

ORIGINAL RESEARCH
published: 18 December 2018
doi: 10.3389/fimmu.2018.02996

Linagliptin Attenuates the Cardiac Dysfunction Associated With Experimental Sepsis in Mice With Pre-existing Type 2 Diabetes by Inhibiting NF-κB

Sura Al Zoubi[1], Jianmin Chen[1], Catherine Murphy[1], Lukas Martin[1], Fausto Chiazza[2], Debora Collotta[2], Muhammad M. Yaqoob[1], Massimo Collino[2†] and Christoph Thiemermann[1*†]*

[1] Centre for Translational Medicine and Therapeutics, William Harvey Research Institute, Queen Mary University of London, London, United Kingdom, [2] Department of Drug Science and Technology, University of Turin, Turin, Italy

OPEN ACCESS

Edited by:
Rudolf Lucas,
Augusta University, United States

Reviewed by:
Hugo Caire Castro-Faria-Neto,
Fundação Oswaldo Cruz (Fiocruz), Brazil
Markus Bosmann,
Boston University, United States

***Correspondence:**
Sura Al Zoubi
s.y.y.alzoubi@qmul.ac.uk
Christoph Thiemermann
c.thiemermann@qmul.ac.uk

[†] These authors have contributed equally to this work and are joint last author

Specialty section:
This article was submitted to Inflammation, a section of the journal Frontiers in Immunology

Received: 04 September 2018
Accepted: 04 December 2018
Published: 18 December 2018

Citation:
Al Zoubi S, Chen J, Murphy C, Martin L, Chiazza F, Collotta D, Yaqoob MM, Collino M and Thiemermann C (2018) Linagliptin Attenuates the Cardiac Dysfunction Associated With Experimental Sepsis in Mice With Pre-existing Type 2 Diabetes by Inhibiting NF-κB. Front. Immunol. 9:2996. doi: 10.3389/fimmu.2018.02996

The mortality rate of patients who develop sepsis-related cardiac dysfunction is high. Many disease conditions (e.g., diabetes) increase the susceptibility to infections and subsequently sepsis. Activation of the NF-κB pathway plays a crucial role in the pathophysiology of sepsis-associated cardiac dysfunction and diabetic cardiomyopathy. The effect of diabetes on outcomes in patients with sepsis is still highly controversial. We here hypothesized that type 2 diabetes (T2DM) augments the cardiac (organ) dysfunction associated with sepsis, and that inhibition of the NF-κB pathway with linagliptin attenuates the cardiac (organ) dysfunction in mice with T2DM/sepsis. To investigate this, 10-week old male C57BL/6 mice were randomized to receive normal chow or high fat diet (HFD), 60% of calories derived from fat). After 12 weeks, mice were subjected to sham surgery or cecal ligation and puncture (CLP) for 24 h. At 1 hour after surgery, mice were treated with linagliptin (10 mg/kg, i.v.), IKK-16 (1 mg/kg, i.v.), or vehicle (2% DMSO, 3 ml/kg, i.v.). Mice also received analgesia, fluids and antibiotics at 6 and 18 h after surgery. Mice that received HFD showed a significant increase in body weight, impairment in glucose tolerance, reduction in ejection fraction (%EF), and increase in alanine aminotransferase (ALT). Mice on HFD subjected to CLP showed further reduction in %EF, increase in ALT, developed acute kidney dysfunction and lung injury. They also showed significant increase in NF-κB pathway, iNOS expression, and serum inflammatory cytokines compared to sham surgery group. Treatment of HFD-CLP mice with linagliptin or IKK-16 resulted in significant reductions in (i) cardiac, liver, kidney, and lung injury associated with CLP-sepsis, (ii) NF-κB activation and iNOS expression in the heart, and (iii) serum inflammatory cytokine levels compared to HFD-CLP mice treated with vehicle. Our data show that pre-existing type 2 diabetes phenotype worsens the organ dysfunction/injury associated with CLP-sepsis in mice. Most notably, inhibition of NF-κB reduces the organ dysfunction/injury associated with sepsis in mice with pre-existing T2DM.

Keywords: sepsis, septic cardiomyopathy, NF-κB, IKK-16, DPP-4, linagliptin, type 2 diabetes mellitus, mice

INTRODUCTION

Sepsis is a dysregulated body response to infection that results in life-threatening organ dysfunction (1). The cardiovascular system is one of the important systems affected by sepsis. Most septic patients, and all patients with septic shock, develop sepsis-related cardiovascular dysfunction (2, 3), which is a key driver of in-hospital mortality in these patients (4). Both the incidence of sepsis and sepsis-related mortality increase with age due to the presence of significant comorbidities including chronic kidney disease and type 2 diabetes in the elderly (5). The prevalence of diabetes is increasing worldwide (6). Patients with diabetes are at high risk of developing diabetic cardiomyopathy, left ventricular (LV) hypertrophy, ischemic cardiac injury, and heart failure (6–9). Diabetic patients are more susceptible to both common and rare infections and have a higher incidence of sepsis than patients that do not suffer from the disease (10, 11). However, the effect of diabetes on outcome in patients with infections is controversial with some studies showing increased hospitalization, organ dysfunction/injury, and mortality in diabetic patients with e.g., pneumonia (12–14), while other studies report either no effect (15–17) or even protective effects (18–21). Hence, this study was undertaken to investigate the effects of pre-existing type 2 diabetes mellitus (T2DM) caused by high fat diet (HFD) on cardiac dysfunction in mice with sepsis.

Dipeptidyl peptidase-4 (DPP-4) inhibitors (gliptins) are among the most recently approved drugs for the treatment of hyperglycemia in patients with T2DM. Gliptins mediate their anti-diabetic effects by primarily inhibiting degradation of endogenous glucagon-like peptide 1 (GLP-1) and glucose-dependent insulinotropic peptide (GIP), resulting in prolongation of postprandial insulin secretion. Given the numerous and varied substrates enzymatically cleaved or bound by DPP-4, DPP-4 inhibitors may have the potential to exhibit a broader range of salutary pleiotropic effects in the heart and vasculature, increasing the concentration of peptides with potential vasoactive and cardioprotective effects, which may be independent of GLP-1 and its receptor. DPP-4 signaling cascade has been recently demonstrated to be involved also in the pathologic features of sepsis, mainly due to a selective cross-talk between DPP-4 and nuclear factor- kappa B (NF-κB) signaling pathways (22–25). In sepsis, microbial components activate different antigen presenting cells (APCs) after binding to their Toll like receptor (TLR) 4 and 2. Exposed caveolin-1 from the activated APC interacts with DDP-4 in T cells which results in strong NF-κB activation in both the APCs and the T cells (23). Adenosine deaminase (ADA) is another activator of DPP-4. The activity of ADA in the serum is increased during inflammatory diseases (e.g., sepsis) as a result of increased macrophages activity (26) and the interaction of ADA with DPP-4 leads to NF-κB activation in T cells (22). The expression of DPP-4 is increased in diabetic patients (27–29).

Activation of NF-κB plays a crucial role in the pathophysiology of both septic (30–32) and diabetic cardiomyopathy (33). In sepsis, activation of NF-κB is secondary to activation of TLR 2 and 4 by e.g., by wall fragments of Gram-negative (e.g., lipopolysaccharide; LPS) or Gram-positive bacteria (e.g., peptidoglycan; PepG) and/or pro-inflammatory cytokines including tumor-necrosis factor-α (TNF-α) or interleukin-1 (IL-1). In addition to pro-inflammatory cytokines, the activation of NF-κB in diabetes is also driven by free fatty acids (34) (which activate TLR4) and advanced glycation end products (which activate RAGE) (35). We have recently demonstrated that inhibition of the activation of NF-κB by a selective IκB kinase (IKK) inhibitor (IKK-16) attenuates the cardiac dysfunction caused by sepsis in mice without co-morbidities (32) and in mice with pre-existing chronic kidney disease (36). However, the potential protective effects of the impairment of the cross-talk between DDP-4 and NF-κB activation in sepsis-induced multiorgan dysfunction have never been tested in animal models of diet-induced diabetes, which is known to be characterized by an increase in baseline NF-κB activity. Here we investigate (a) the role of NF-κB activation in the cardiac dysfunction caused by HFD with or without sepsis, (b) the effect of linagliptin treatment on cardiac performance in the model of sepsis and T2DM. To investigate the relative contribution of NF-κB inhibition in the observed effects of linagliptin, IKK-16, a potent and selective IKK inhibitor, was used as a comparative pharmacological tool.

MATERIALS AND METHODS

Ethical Statement

The animal protocols followed in this study were approved by the local Animal Use and Care Committee in accordance with the derivatives of both, the Home Office Guidance in the Operation of Animals (Scientific Procedure Act 1986) published by Her Majesty's Stationary Office, the Guide for the Care and Use of Laboratory Animals of the National Research Council (home office project license, PPL: 70/8350) and by the local ethical committee (DGSAF 0021573-P-12/11/2013) and are in keeping with the European Directive 2010/63/EU as well as the 2011 Guide for the Care and Use of Laboratory Animals.

Animals

This study was conducted on 56 male C57BL/6 mice aged 10 weeks (Charles River, Kent, UK) weighing 25–30 g, receiving a standard diet and water *ad libitum* (before starting the experiments). Mice were housed 5 per cage in a temperature-controlled room with a 12-h light/dark cycle.

High Fat Diet Model of Type 2 Diabetes Mellitus

In this model of diet-induced obesity and insulin resistance, mice (Charles River UK, Kent) were randomized to receive standard chow diet [LabDiet®, St. Louis (5053: protein provides 25%, fat 13%, and carbohydrate 62% of the total calories)] or high fat diet [TestDiet®, St. Louis (58Y1: Blue diet; protein provides 18.1%, fat 61.6%, and carbohydrate 20.3% of the total calories)] with free access to water for 12 weeks. Body weight, food intake, and calories intake were measured weekly through the experiment to monitor feeding behavior.

Oral Glucose Tolerance Test (OGTT)

Mice were fasted for 6 h with free access to water. At the end of the 6 h fasting, the body weight and fasting blood glucose were measured using tail vein blood. Mice then received a bolus dose of glucose (2 g/kg, dissolved in drinking water) via oral gavage. Blood glucose levels were then measured at 15, 30, 45, 60, 90, and 120 min post glucose administration using blood glucose meter Accu-Chek® (Accu-Chek Compact System; Roche Diagnostics, Basel, Switzerland).

Insulin Tolerance Test (ITT)

Mice were fasted for 4 h with free access to water. At the end of the 4 h fasting, the body weight and fasting blood glucose were measured using tail vein blood. Mice then received a dose of insulin aspart (NovoRapid®) (0.75 U/kg, i.p.). Blood glucose level was then measured at 15, 30, 45, 60, 90, and 120 min post insulin administration using blood glucose meter Accu-Chek® (Accu-Chek Compact System; Roche Diagnostics, Basel, Switzerland).

Measuring Fasting Plasma Insulin

Mice were fasted for 6 h with free access to water. At the end of the 6 h fasting period, blood samples were collected from the tail vein. Fasting plasma insulin levels were then measured using human insulin ELISA kit following the manufacturer's instructions (Abcam®, Cambridge, UK).

Assessment of Baseline Kidney Function

During the last week of the experiment, mice were housed in the metabolic cages to collect urine. They were housed (one mouse per cage) for 24 h with free access to food and water. Urine biochemistry (creatinine and sodium levels) was assessed blindly by IDEXX the commercial veterinary testing laboratory (IDEXX Ltd; West Sussex, UK). Urine albumin was measured using a mouse albumin ELISA kit following manufacturer instructions (Cambridge Bioscience®, Cambridge, UK). Then creatinine clearance (CrCl) and urine albumin to creatinine ratio (ACR) were calculated using the following equations:

$$\mathrm{CrCl} = \frac{\mathrm{Urine\ \ Creatinine}}{\mathrm{Serum\ \ Creatinine}} \times \frac{\mathrm{Urine\ \ Volume}}{\mathrm{Time}}$$

Equation 1: Creatinine clearance (ml/min) is calculated using four measurements (a) urine creatinine (μmol/L), (b) serum creatinine (μmol/L), (c) urine volume (ml), and (d) time (minutes).

$$\mathrm{ACR} = \frac{\mathrm{Urine\ \ Albumin}}{\mathrm{Urine\ \ Creatinine}}$$

Equation 2: Urine albumin to creatinine ratio is calculated using 2 (a) urine albumin (μg/L) and (b) urine creatinine (mg/L).

Assessment of Cardiac Function *in vivo* (Echocardiography)

Echocardiography was conducted *in vivo* at baseline (before sepsis challenge) then at 24 h after CLP to measure cardiac function using a 30 MHz RMV707B scan head and a Vevo-770 imaging system (VisualSonics, Toronto, Ontario, Canada).

Animals were anesthetized using 3% isoflurane delivered with 0.4 l/min oxygen in the anesthesia chamber. After being sedated, mice were then transferred to the echo table and taped from the limbs in a supine position onto the metal ECG leads on the Echo platform. Anesthesia was maintained during the whole imaging process using 0.5–2% isoflurane delivered with 0.4 l/min oxygen via nosecone under spontaneous breathing. The handling platform was warmed to 40°C in order to keep the core body temperature of the mice. After being placed on the platform, the fur on the chest was then removed carefully using Veet® hair removing cream. A pre-warmed echo gel is then applied to the chest to start the measurement. At least 10 min were left for the animals to stabilize before any measurement was taken. The body temperature was monitored using a rectal probe and the heart rate was obtained from ECG tracing during the whole procedure.

Measurements from both two-dimensional (brightness mode, B-mode) and one-dimensional (motion mode, M-mode) were obtained. Measurements of the left ventricle internal dimension (LVID) in both systole and diastole from the M-mode at the level of the papillary muscles were used to calculate the percentage ejection fraction (% EF), fractional shortening (% FS), and the measurements of LV end-systolic and end-diastolic areas from the B-mode were used to calculate the percentage functional area change (% FAC) using the following equations:

$$\%\ \mathrm{EF} = \frac{(\mathrm{LVID;\ d}^3 - \mathrm{LVID;\ s}^3)}{\mathrm{LVID;\ d}^3} \times 100$$

Equation 3: Ejection fraction (%) is calculated using 2 measurements (a) left ventricle internal dimension during diastole (LVID;d, mm) and (b) left ventricle internal dimension during systole (LVID;s, mm).

$$\%\ \mathrm{FS} = \frac{(\mathrm{LVID;\ d} - \mathrm{LVID;\ s})}{\mathrm{LVID;\ d}} \times 100$$

Equation 4: Fractional shortening (%) is calculated using 2 measurements (a) left ventricle internal dimension during diastole (LVID;d, mm) and (b) left ventricle internal dimension during systole (LVID;s, mm).

$$\%\ \mathrm{FAC} = \frac{(\mathrm{LVarea;\ d} - \mathrm{LVarea;\ s})}{\mathrm{LVarea;\ d}} \times 100$$

Equation 5: Fractional area change (%) is calculated using 2 measurements (a) left ventricle end-diastolic area (LV area;d, mm^2) and (b) left ventricle end-systolic area (LV area;s, mm^2).

Model of Cecal Ligation and Puncture (CLP) Induced Polymicrobial Sepsis

At 12 weeks after starting the HFD, mice fed either chow or HFD were randomized to undergo either sham operation or CLP surgery. Before surgery, mice were anesthetized using (1.5 ml/kg, i.p.) of 2:1 ketamine (100 mg/ml): xylazine (20 mg/ml) solution. To obtain adequate analgesia, buprenorphine (0.05 mg/kg, i.p.) was administered just before starting the surgery. The fur of the abdomen was removed using Veet®

hair removing cream and the area cleaned with 70% ethanol. A 1.5 cm midline incision of the abdomen was made and the caecum was exposed. The caecum then was ligated below the ileocecal valve and two punctures were made one at each end using an 18-G needle. A small amount of fecal matter was then squeezed from both punctures before the caecum was returned to its anatomical position and the cut in the abdomen was then sutured. Each mouse then received a resuscitation fluid (1 ml 0.9% NaCl, s.c.). Mice were left on a homeothermic blanket to recover then placed back into fresh clean cages. At 1 h after CLP surgery, mice from the HFD group were randomized to receive linagliptin (10 mg/kg, i.v), IKK-16 (1 mg/kg i.v.) or vehicle (2% DMSO; 3 ml/kg, i.v.). At 6 and 18 h after surgery, antibiotic (imipenem/cilastatin, 20 mg/kg) dissolved in resuscitation fluid (15 ml/kg 0.9% NaCl, s.c.) was administered along with analgesia (buprenorphine, 0.05 mg/kg, i.p.). At 24 h, mice were anesthetized for assessment of cardiac function *in vivo*. As a terminal procedure, mice were anesthetized using high dose isoflurane (3% delivered in 0.9 l/min O_2) before being sacrificed. Blood samples were collected by cardiac puncture and vital organs were collected and snap frozen using liquid nitrogen then stored for further analysis at −80°C freezer. Mice that underwent sham surgery were anesthetized and handled in the same manner as CLP mice during surgery. However, in animals undergoing sham surgery, the cecum (although exposed) was not subjected to perforation. At 1 h after surgery, sham mice were treated with vehicle (2% DMSO, 3 ml/kg, i.v.) and they were also treated with antibiotic (imipenem/cilastatin, 20 mg/kg) dissolved in resuscitation fluid (15 ml/kg 0.9% NaCl, s.c.) along with analgesia (buprenorphine, 0.05 mg/kg, i.p.) at 6 and 18 h after surgery. Surgery, treatments and assessment of cardiac function were performed by different member of the research team to minimize subjective errors. The investigator assessing the cardiac function was blinded as to the intervention that was used in the study.

Western Blot Analysis

Immunoblot analyses of heart biopsies were carried out using a semi-quantitative western blotting. We measured the degree of phosphorylation of IKK, IκBα, and Akt, nuclear translocation of p65 NF-κB subunit to the nucleus and inducible nitric oxide synthase (iNOS) expression. For sample handling, blood was withdrawn from mice at the time of euthanasia, heart tissue was then washed with saline solution prior to homogenisation. For sample preparation, a piece of heart tissue was taken and diluted (1:10) with homogenisation buffer (HB) at 4°C to obtain a whole tissue lysate, that contains endothelium, cardiomyocytes and leucocytes, for protein extraction. Cytosolic and nuclear extracts from hearts were prepared as previously described (37). Succinctly, hearts were homogenized at 10% (wt/vol) with a Potter Elvehjem homogenizer (Wheaton, Millville, NJ) using a homogenization buffer containing 20 mM HEPES (pH 7.9), 1 mM $MgCl_2$, 0.5 mM EDTA, 1% Nonidet P-40, 1 mM EGTA, 1 mM DTT, 0.5 mM PMSF, 1 μl/ml of PIC. Homogenates were centrifuged at 1,300 g for 5 min at 4°C. Supernatants were removed and centrifuged at 16,000 g at 4°C for 40 min to obtain supernatant containing the cytosolic fraction. The pelleted nuclei were resuspended in extraction buffer (1/3 volume of the homogenation buffer) containing 20 mM HEPES (pH 7.9), 1.5 mM MgCl2, 300 mM NaCl, 0.2 mM EDTA, 20% glycerol, 1 mM EGTA, 1 mM DTT, 0.5 mM PMSF, 1 μl/ml of PIC, and incubated in ice for 30 min, followed by centrifugation at 16,000 g for 20 min at 4°C. The resulting supernatants containing nuclear proteins were carefully removed. Both cytosolic and nuclear proteins were measured using bicinchoninic acid (BCA) protein assay following manufacturer's directions (Therma Fisher Scientific, Rockford, IL). Proteins were separated by gel electrophoresis using sodium dodecyl sulfate polyacrylamide (SDS-PAGE) then transferred into a Polyvinylidene difluoride (PVDF) membrane. The membrane then was blocked 1 h in 5% dry milk solution in TBS-tween). Incubation of the membrane was conducted overnight at 4°C with primary antibody in 5% blocking solution then incubated the next day with the appropriated HRP-conjugated secondary antibody at room temperature for 30 min and then detected with enhanced chemilumescent (ECL) detection system and quantified by densitometry using BioRad Image Lab Software™ 6.0. Results were normalized with respect to densitometric value of mouse anti-tubulin for cytosolic and total proteins, and mouse anti-histone H3 for nuclear proteins.

Cytokine Measurements

Serum cytokines levels (TNF-α, IL-6, KC, and IL-10) were measured using a bead-based immunoassay method. Serum samples were prepared and handled following manufacturer instructions (Biolegend®, San Diego, USA). Data was obtained using a LSR Fortessa (Biociences®, Berkshire, UK) and analyzed using the Legendplex™ 7.1.0.0 software.

Measuring Myeloperoxidase (MPO) Activity in the Lung

MPO was extracted from the tissues according to the methods described by Barone et al. (38) with slight modifications to measure neutrophil accumulation in the lungs. For samples preparation, a piece of lung was diluted (1:20) with 5 mM potassium phosphate buffer to homogenize the sample (at 4°C). For measurements of MPO activity, the homogenate was centrifuged (at 13,000 RPM, 30 min, 4°C). The resulted supernatant was discarded. A 5-time dilution with 0.5% hexadecyl-trimethyl-ammonium bromide in 50 mM potassium phosphate buffer was used to suspend and homogenize the pellet. The resulted solution was then frozen and thawed three times followed by 10 s sonication at room temperature and then incubated at 4°C for 30 min then centrifuged (at 12,500 RPM, 15 min, 4°C). MPO activity was measured in the supernatant by mixing 100 μl of the supernatant with 0.167 mg/ml o-dianiside dihydrochloride and 0.0005% hydrogen peroxide in 2.9 ml 50 mM potassium phosphate buffer. UV-visible spectrophotometer was used to measure the change in absorbance at 460 nm for 1.5 min. MPO activity was presented as the quantity of the enzyme degraded 1 μmol of peroxide/min at 25°C and expressed as μU/gram of the lung tissue.

Measuring N-acetyl-β-D-glucosaminidase (NAG) Activity in the Lung

NAG activity was analyzed to measure macrophage accumulation in the lung. For samples preparation, a piece of lung was diluted with 0.01 M phosphate buffer saline and homogenized (at 4°C). The resulted solutions were then frozen and thawed three times followed by 10 s sonication at room temperature to break the cells. For measurements of NAG activity, the homogenate was centrifuged (at 5,000 RPM, 30 min, 4°C). The resulted supernatants were then used to measure NAG activity using a NAGase ELISA kit following manufacturer instructions (Elabscience®, Houston, Texas, USA).

Statistical Analysis

Data was analyzed using GraphPad Prism 7.0 (GraphPad Software, San Diego, California, USA). Values stated in the text and figures are presented as a mean ± standard error of the mean (SEM) of n observations, where n is the number of animals used. Data was tested for normality using D'Agostino-Pearon normality test and then assessed using One-way ANOVA test followed by Bonferroni's *post-hoc* test or unpaired Student *t*-test where appropriate. *P*-values of less than 0.05 were considered to be statically significant.

Materials

Unless otherwise stated, all materials, reagents, and solutions were purchased from Sigma-Aldrich Ltd (Poole, Dorset, UK).

RESULTS

Diabetic Phenotype and Characterization of Organ Dysfunction in Mice With Experimental T2DM Caused by HFD

When compared to chow fed mice, mice fed a HFD showed a significant increase in fasting blood glucose, impairment in glucose tolerance after being challenged with an oral dose of glucose, impairment in insulin tolerance after challenge with i.p. insulin, an increase in fasting plasma insulin as well as an increase in total cholesterol. Mice fed a HFD also showed significant increases in (i) total body weight secondary to an increase in fat mass, but not lean mass; (ii) an increase in the serum levels of alanine aminotransferase (ALT) indicating the development of liver injury; (iii) increase in urine albumin to creatinine ratio (ACR) as well as a (iv) a decrease in creatinine clearance (CrCl) indicating the development of diabetic nephropathy (proteinuria) and glomerular dysfunction ($P < 0.05$). Mice also showed mild cardiomyopathy as evidence by a small, but significant, reduction in ejection fraction (EF%), fractional shortening (FS%), and fractional area change (FAC%) ($P < 0.05$; **Table 1**).

TABLE 1 | Baseline data for both chow and HFD groups before interventions (CLP or sham surgeries).

Parameter	Chow	HFD
Net weight gain from baseline *(grams)*	5.34 ± 0.47, $n = 18$	15.92 ± 1.19, $n = 18$*
Food intake$ *(grams/mouse/week)*	3.38 ± 0.02, $n = 12$ (weeks)	2.82 ± 0.03, $n = 12$ (weeks)*
Calorie intake$ *(Kcal/mouse/week)*	17.29 ± 0.12, $n = 12$ (weeks)	19.99 ± 0.24, $n = 12$ (weeks)*
AUC for OGTT *(g.min/dl)*	29.65 ± 0.55, $n = 18$	47.73 ± 2.96, $n = 18$*
AUC for ITT *(g.min/dl)*	6.57 ± 0.14, $n = 5$	9.63 ± 0.44, $n = 10$*
Fasting blood glucose *(mg/dl)*	183.9 ± 4.68, $n = 18$	294.9 ± 13.9, $n = 18$*
Fasting plasma insulin *(μIU/ml)*	20.16 ± 0.86, $n = 10$	71.80 ± 7.75, $n = 9$*
Ejection fraction *(%)*	71.92 ± 0.81, $n = 18$	64.26 ± 0.95, $n = 18$*
Fractional shortening *(%)*	40.73 ± 0.67, $n = 18$	34.73 ± 0.68, $n = 18$*
Fractional area change *(%)*	51.37 ± 0.41, $n = 18$	45.8 ± 1.14, $n = 18$*
Left ventricle mass *(mg)*	127.2 ± 2.92, $n = 18$	131.6 ± 4.04, $n = 18$
Urea *(mmol/L)*	9.47 ± 0.32, $n = 18$	9.45 ± 0.24, $n = 18$
Creatinine *(μmol/L)*	28.49 ± 1.71, $n = 18$	32 ± 1.25, $n = 18$
Alanine aminotransferase *(U/L)*	32.9 ± 4.05, $n = 18$	68.26 ± 9.54, $n = 18$*
Creatinine Clearance *(ml/min)*	154.1 ± 17.56, $n = 14$	96.55 ± 8.79, $n = 18$*
Urine Albumin to Creatinine Ratio *(μg/mg)*	0.19 ± 0.02, $n = 10$	0.72 ± 0.07, $n = 10$*
Triglyceride *(mg/dl)*	183.6 ± 9.65, $n = 18$	175.4 ± 8.53, $n = 18$
Total cholesterol *(mg/dl)*	147.3 ± 2.24, $n = 18$	183.7 ± 3.56, $n = 18$*

*Mice fed a HFD were compared to age-matched mice fed a chow diet. Data is presented as mean ± SEM for n number of observations. Data was analyzed by unpaired t-test. *$P < 0.05$ vs. the chow-fed group. $: mean food intake of 18 mice in each group during the study period 12 weeks ($n = 12$). AUC, area under the curve; OGTT, oral glucose tolerance test; ITT, insulin tolerance test*

Pre-existing T2DM Augments the Multiple Organ Dysfunction and Systemic Inflammation Associated With Sepsis in Mice

Subjecting mice on chow diet to CLP resulted in a small (but not significant) effect on systolic cardiac function compared to sham surgery ($P > 0.05$; **Figure 1**). However, mice fed a HFD and subjected to CLP exhibited a large and significant reduction in systolic cardiac function compared to sham surgery ($P < 0.05$; **Figure 1**).

To understand the signaling mechanism associated with cardiac dysfunction, we investigated the effect of HFD on the activation of key signaling pathways of inflammation and cell survival including pathways leading to the activation of NF-κB with or without sepsis. Mice fed a HFD exhibited significant increases in the phosphorylation of IKKα/β on $Ser^{178/180}$, the phosphorylation of IκBα on $Ser^{32/36}$, the translocation of p65 NF-κB to the nucleus, the expression of iNOS, and a significant decrease in the phosphorylation of Akt on Ser^{473} ($P < 0.05$; **Figures 2**, **3**). Exposing mice on chow diet to CLP resulted in a similar degree of activation of NF-κB and, indeed, iNOS expression (in the heart) as observed in mice with HFD alone. CLP-sepsis in mice on HFD resulted in a further increase in the phosphorylation of IKKα/β and IκBα, the translocation of p65, and iNOS expression ($P < 0.05$; **Figure 2**) with no significant effect on Akt phosphorylation ($P > 0.05$; **Figure 3**).

We also studied the effect of HFD on the systematic synthesis of key, NF-κB-dependent cytokines including TNF-α, IL-6, KC, and IL-10. When compared to mice on chow diet, mice on HFD for 12 weeks showed no significant changes in cytokines levels ($P > 0.05$; **Figure 2**). When compared to mice on regular chow

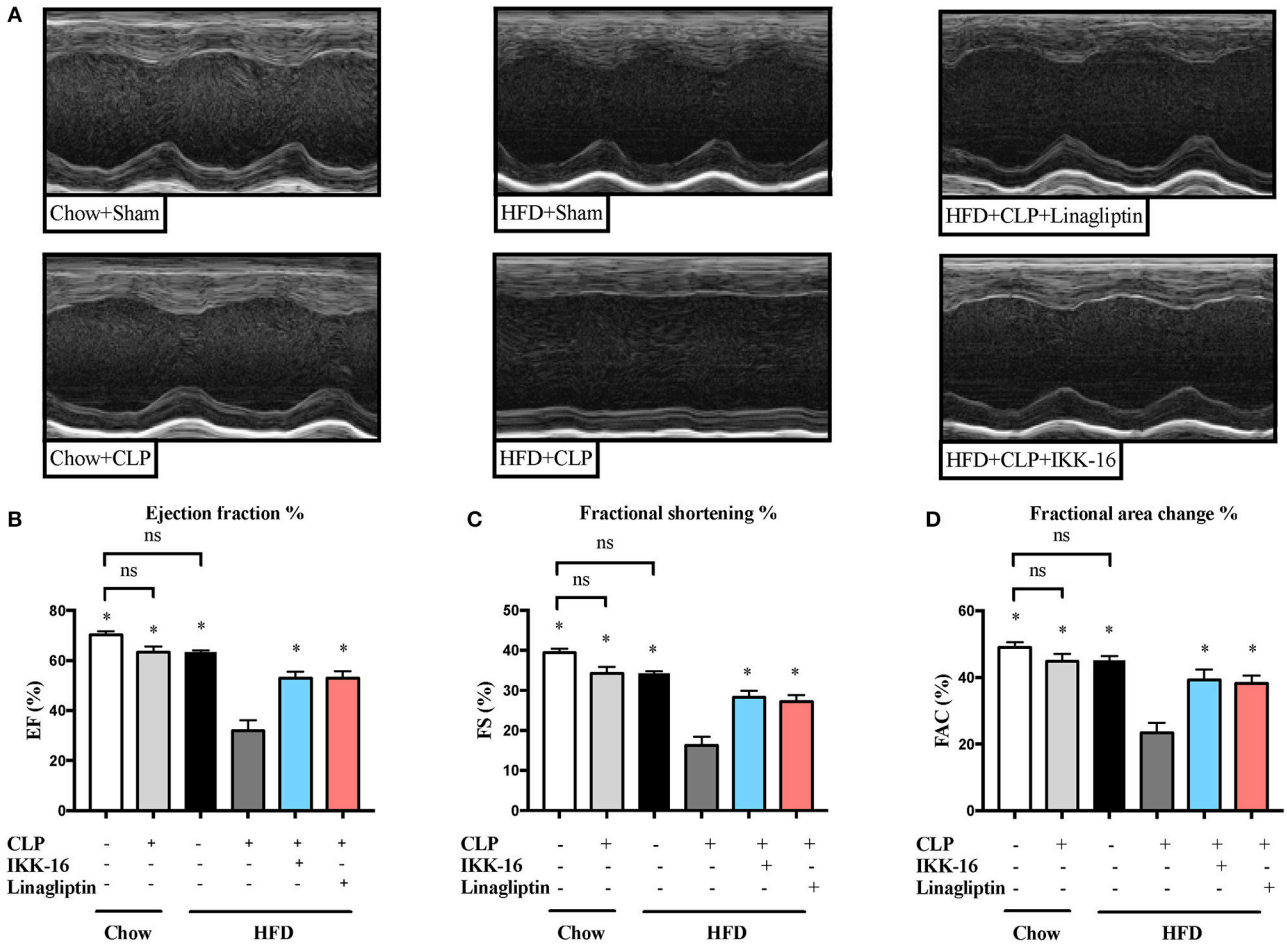

FIGURE 1 | Effects of CLP challenge and linagliptin or IKK-16 post treatment on cardiac function in mice with T2DM**.** Mice from chow and HFD groups were randomized to undergo CLP or sham surgery. At 1 h after CLP, mice on HFD were randomized to receive linagliptin (10 mg/kg, i.v.), IKK-16 (1 mg/kg, i.v.), or vehicle (2% DMSO, 3 ml/kg). Cardiac function was assessed at 24 h after CLP or sham surgery in mice fed a chow diet or a HFD. **(A)** Representative M-mode echocardiograms; percentage % **(B)** EF, **(C)** FS, and **(D)** FAC. Data was analyzed using one-way ANOVA followed by Bonferroni's *post-hoc* test and expressed as mean ± SEM. *$P < 0.05$ compared to HFD+CLP group. ($n = 8$ for sham surgery groups and 10 for CLP groups).

diet subjected to sham surgery, mice on chow diet subjected to CLP (in the presence of antibiotics) showed no significant changes in cytokines levels in the serum ($P > 0.05$; **Figure 4**). CLP-sepsis in mice on HFD resulted in large increases in the serum levels of TNF-α, IL-6, KC, and IL-10 when compared to mice on HFD subjected to sham surgery and mice on chow diet subjected to CLP ($P < 0.05$; **Figure 4**).

Markers for lung inflammation were also measured to study the effect of pre-existing diabetes on lung injury associated with sepsis. When compared to micev on chow diet, mice on HFD showed no significantv changes in MPO or NAG activities in the lungs after sham surgery ($P > 0.05$; **Figure 5**). Whenv compared to mice on regular chow diet subjected to sham surgery, mice on chow diet subjected to CLP showed a significant increase in NAG activity in the lung ($P < 0.05$; **Figure 5**) with no change in MPO activity ($P > 0.05$; **Figure 6**). Subjecting mice on HFD to CLP surgery resulted in big increases in both MPO and NAG activities when compared to mice on HFD subjected to sham surgery and mice on chow diet subjected to the same CLP ($P < 0.05$; **Figure 5**).

Our CLP-sepsis model with moderate severity had (in the presence of antibiotics and fluid resuscitation) no effect on serum creatinine, urea, or ALT compared to sham surgery ($P > 0.05$; **Figure 6**). However, challenge of mice on HFD with CLP resulted (despite the presence of antibiotics and fluid resuscitation) in significant increases in serum creatinine, urea, and ALT levels ($P < 0.05$; **Figure 6**). These results indicate that pre-existing T2DM increases the severity of both renal dysfunction and hepatocellular injury.

Effect of Linagliptin Post Treatment on the Multiple Organ Dysfunction Associated With Sepsis in Mice With Pre-existing T2DM

When compared to mice on HFD subjected to sham surgery, mice on HFD subjected to CLP and treated with vehicle

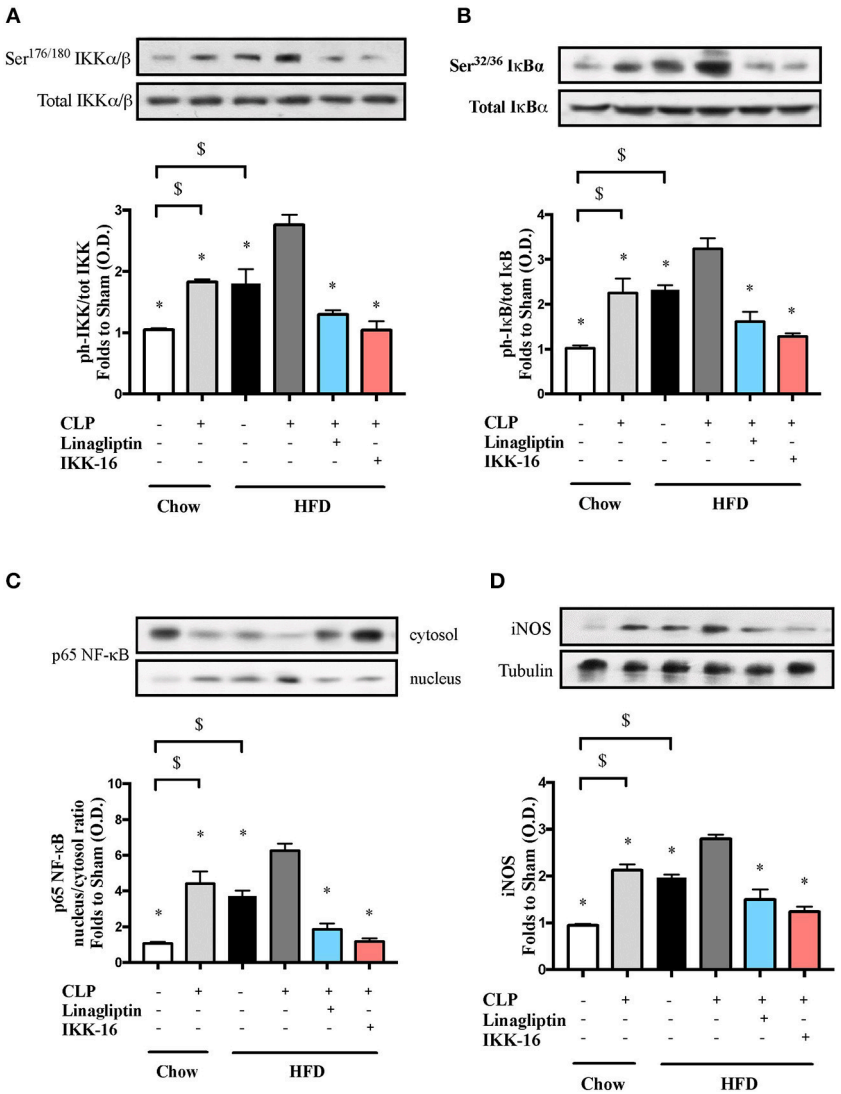

FIGURE 2 | Effects of CLP and linagliptin or IKK-16 post treatment on NF-κB signaling pathway in the heart of mice with pre-existing T2DM**.** Mice from chow and HFD groups were randomized to undergo CLP or sham surgery. At 1 h after CLP, mice on HFD were randomized to receive linagliptin (10 mg/kg i.v.), IKK-16 (1 mg/kg i.v.), or vehicle (2% DMSO, 3 ml/kg). At 24 h heart samples were collected and signaling events were assessed. Densitometry analysis of the bands is expressed as relative optical density (O.D.) of **(A)** IKKα/β phosphorylation on $Ser^{178/180}$ corrected to the corresponding total IKKα/β content and normalized using the related sham band; **(B)** IκBα phosphorylation on $Ser^{32/36}$ corrected to the corresponding total IκBα content and normalized using the related sham band; **(C)** NF-κB p65 subunit levels in both, cytosolic and nuclear fractions expressed as a nucleus/cytosol ratio normalized using the related sham bands; **(D)** inducible nitric oxide synthase (iNOS) expression corrected for the corresponding tubulin band and normalized using the related sham band. Data was analyzed using one-way ANOVA followed by Bonferroni's *post-hoc* test and expressed as mean ± SEM.*$P < 0.05$ compared to HFD+CLP group, $\$P < 0.05$. ($n = 4$–6 per group).

developed significant systolic cardiac dysfunction. Treatment of mice on HFD with linagliptin, at 1 h after CLP, attenuated the systolic cardiac dysfunction caused by CLP ($P < 0.05$; **Figure 1**).

Having found that linagliptin attenuates the cardiac dysfunction associated with CLP-sepsis in diabetic mice, we then investigated the potential mechanism(s) of this beneficial effect. Treatment of mice on HFD with linagliptin, at 1 h after CLP, also resulted in significant reduction in IKKα/β and IκBα phosphorylation, p65 translocation, and iNOS expression when compared to mice on HFD subjected to CLP and treated with vehicle ($P < 0.05$; **Figure 2**). Moreover, linagliptin treatment of HFD/CLP mice restored the degree of Akt phosphorylation to almost that seen in sham mice ($P < 0.05$; **Figure 3**).

Systemic inflammation was also attenuated after linagliptin treatment. When compared to mice on HFD challenged CLP and treated with vehicle, delayed treatment with linagliptin at 1 h after CLP resulted in significant reduction in IL-6, KC, and IL-10 synthesis ($P < 0.05$; **Figure 4**) and in a reduction in TNF-α that did not, however, reached statistical significance when compared to mice treated with vehicle ($P > 0.05$, **Figure 4**).

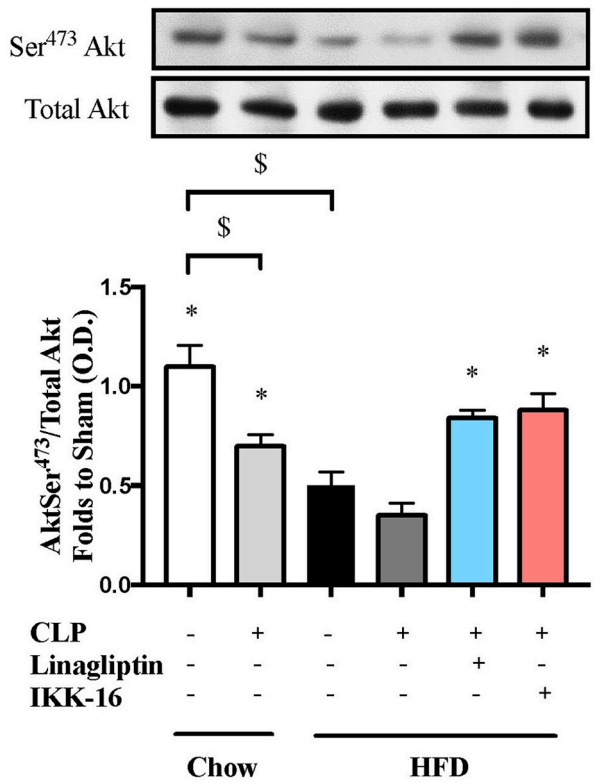

FIGURE 3 | Effects of CLP and linagliptin or IKK-16 post treatment on Akt pro-survival pathway in the heart of mice with pre-existing T2DM. Mice from chow and HFD groups were randomized to undergo CLP or sham surgery. At 1 h after CLP, mice on HFD were randomized to receive linagliptin (10 mg/kg i.v.), IKK-16 (1 mg/kg i.v.), or vehicle (2% DMSO, 3 ml/kg). At 24 h, heart samples were collected and signaling events were assessed. Densitometry analysis of the bands is expressed as relative optical density (O.D.) of phosphorylated Akt on Ser^{473} corrected for the corresponding total Akt content and normalized using the related sham band. Data was analyzed using one-way ANOVA followed by Bonferroni's *post hoc* test and expressed as mean ± SEM.*$P < 0.05$ compared to HFD+CLP group, $\$P < 0.05$. ($n = 4$–6 per group).

Accordingly, a significant reduction in markers of lung inflammation, specifically the MPO and NAG activities, was observed in the lungs of mice exposed to linagliptin post-treatment when compared to mice on HFD subjected to CLP and treated with vehicle only ($P < 0.05$, **Figure 5**).

When compared to mice on HFD subjected to CLP and treated with vehicle, mice on HFD and treated with linagliptin, at 1 h after CLP, showed significant reduction in serum creatinine, urea, and ALT levels indicating that linagliptin attenuated the renal dysfunction and liver injury caused by CLP ($P < 0.05$; **Figure 6**).

Effect of IKK-16 Post Treatment on the Multiple Organ Dysfunction Associated With Sepsis in Mice With Pre-existing T2DM

In order to investigate whether inhibition of NF-κB was the main reason of the attenuated organ injury caused by sepsis in diabetic mice after linagliptin treatment, we have investigated the effects of the specific IKK-inhibitor IKK-16 in these animals. When compared to mice on HFD subjected to sham surgery, mice on HFD subjected to CLP and treated with vehicle developed significant systolic cardiac dysfunction. Delayed treatment of HFD mice with IKK-16 at 1 h after CLP attenuated the systolic cardiac dysfunction ($P < 0.05$; **Figure 1**) caused by sepsis.

The restoration of cardiac function afforded by IKK-16 in diabetic CLP-mice was accompanied by significant reduction in IKKα/β and IκBα phosphorylation, p65 translocation, and iNOS expression in mice treated with IKK-16 when compared to mice on HFD challenged with CLP and treated with vehicle ($P < 0.05$; **Figure 2**). Moreover, IKK-16 treatment restored the Akt phosphorylation ($P < 0.05$; **Figure 3**) caused by HFD with or without sepsis.

When compared to mice on HFD subjected to CLP and treated with vehicle, delayed treatment with IKK-16 at 1 h after CLP resulted in significant reduction of both the systemic levels TNF-α, IL-6, KC, and IL-10 ($P < 0.05$; **Figure 4**) and local (lung) MPO and NAG activities ($P < 0.05$, **Figure 5**). They also showed significant reduction of serum creatinine, urea, and ALT levels indicating that IKK-16 reduced both the renal dysfunction and the liver injury caused by sepsis in mice fed with a HFD ($P < 0.05$; **Figure 6**).

Interestingly, no statistically significant differences between the two post-treatment groups were recorded for any of the measured markers.

DISCUSSION

Although the mortality rate among septic patients has declined due to improved supportive care for patients in the ICU (39), the incidence of sepsis has increased as a result of the aging of the population (40) which is associated with the presence of significant comorbidities such as T2DM (5). Patients with T2DM are more likely to develop infections and subsequently sepsis (10, 11). The cardiovascular system is one of the most important systems affected by sepsis and the development of cardiovascular dysfunction in sepsis has been linked to several pathophysiological driver including inflammatory cytokines and NO (32, 36). Many studies of the pathophysiology of sepsis have shown beneficial effects in pre-clinical models of sepsis. However, clinical studies that tested the efficacy of drugs targeted at identical aspects of the pathophysiology (often by using identical interventions) have failed to improve survival in septic patients (as a result of the limitations in both animal models and experimental designs) (41).

In this study, a clinically relevant model of T2DM caused by prolonged administration of HFD (for 12 weeks) was established in C57BL/6 male mice. As the consumption of a western diet is a key driver underlying the development of T2DM, our model of feeding a HFD for longer periods recapitulates the main cause of T2DM in humans and is considered to be one of the most clinically, relevant model of T2DM to date. Indeed,

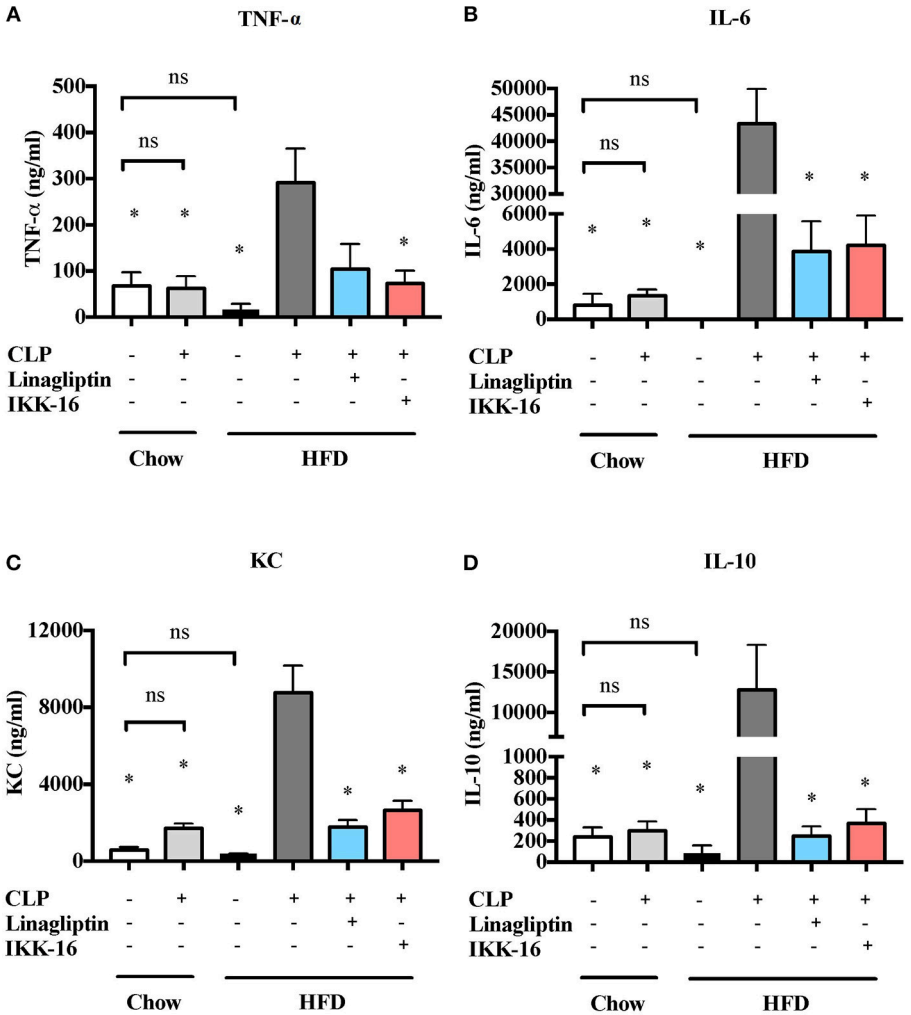

FIGURE 4 | Effects of CLP challenge and linagliptin or IKK-16 post treatment on systemic inflammation in mice with T2DM**.** Mice from chow and HFD groups were randomized to undergo CLP or sham surgery. At 1 h after CLP, mice on HFD were randomized to receive linagliptin (10 mg/kg, i.v.), IKK-16 (1 mg/kg, i.v.), or vehicle (2% DMSO, 3 ml/kg). At 24 h after CLP, blood samples were collected and inflammatory cytokines concentrations were measured in the serum. **(A)** TNF-α, **(B)** IL-6, **(C)** KC, and **(D)** IL-10. Data was analyzed using one-way ANOVA followed by Bonferroni's *post-hoc* test and expressed as mean ± SEM. *$P < 0.05$ compared to HFD+CLP group. ($n = 4$ per sham surgery group and $n =$ 6–8 per CLP group).

feeding of mice with HFD resulted, within 12 weeks, in the development of a diabetic phenotype (significant weight gain, impaired glucose tolerance, increased fasting blood glucose and increased fasting plasma insulin) and diabetic cardiomyopathy (reduction in %EF) as a result of NF-κB activation in the heart (see below).

A "two-hit" model of pre-existing T2DM (secondary to HFD administration) followed by a mild CLP surgery (which did not cause significant organ dysfunction in young and healthy mice, but which we have reported to cause substantial organ dysfunctions in old mice or mice with CKD) was used to study (a) the effect of pre-existing T2DM on the cardiac dysfunction associated with sepsis and (b) to test novel therapeutic interventions aimed at reducing cardiac dysfunction in T2DM/sepsis mice. We show here, for the first time, that pre-existing T2DM augments the cardiac dysfunction associated with sepsis. T2DM alone resulted in a small degree of NF-κB activation and iNOS expression in the heart. However, sepsis (second hit) in diabetic mice resulted in a dramatic increase in the serum concentrations of proinflammatory cytokines and a further increase in both NF-κB activation and iNOS expression in the heart. Diabetes also resulted in reduction in the activation (phosphorylation) of the Akt pro-survival pathway, while sepsis resulted in further reduction of Akt phosphorylation in the heart. These two findings suggest that the cardiac dysfunction associated with T2DM/sepsis is most likely a result of the activation of the NF-κB pro-inflammatory signaling pathway (with subsequent increase in iNOS expression and serum inflammatory cytokines levels) and the concomitant inhibition of Akt pro-survival pathways.

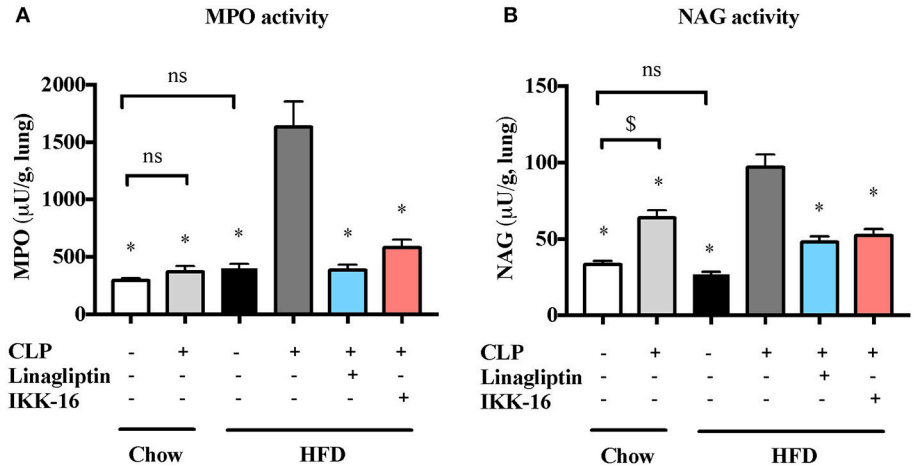

FIGURE 5 | Effects of CLP and linagliptin or IKK-16 post treatment on neutrophil/macrophage infiltration in the lung in mice with pre-existing T2DM. Mice from chow and HFD groups were randomized to undergo CLP or sham surgery. At 1 h after CLP, mice on HFD were randomized to receive linagliptin (10 mg/kg, i.v.), IKK-16 (1 mg/kg, i.v.), or vehicle (2% DMSO, 3 ml/kg). At 24 h after CLP, lung samples were collected and neutrophil and macrophages infiltration were measured as the **(A)** MPO and **(B)** NAG activities. Data was analyzed using one-way ANOVA followed by Bonferroni's *post-hoc* test and expressed as mean ± SEM for n number of observations. *$P < 0.05$ compared HFD+CLP group. $\$P < 0.05$ ($n = 6$ per group).

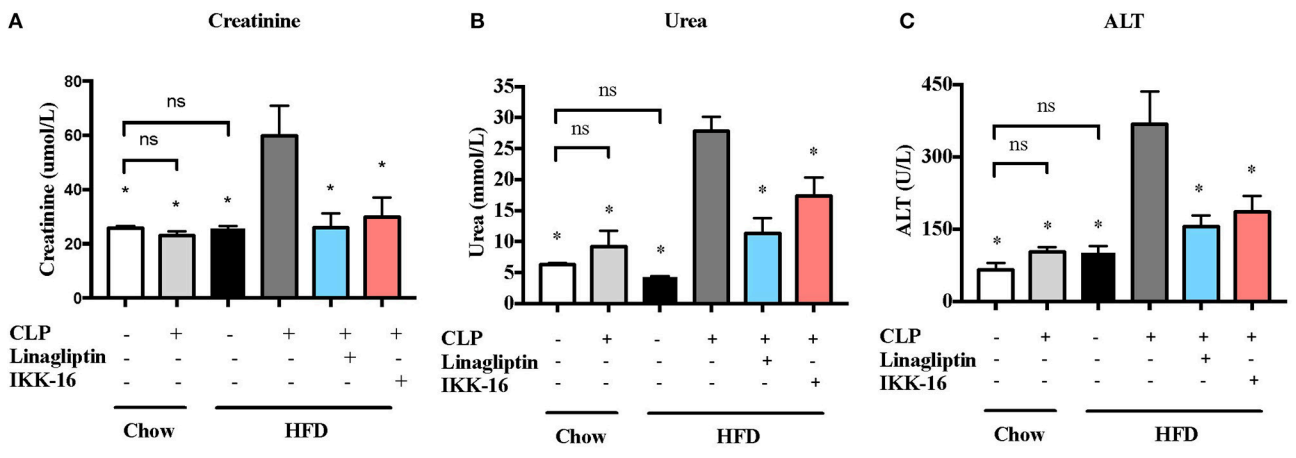

FIGURE 6 | Effects of CLP and linagliptin or IKK-16 post treatment on renal dysfenction and hepatocelleular injury in mice with pre-existing T2DM. Mice from chow and HFD groups were randomized to undergo CLP or sham surgery. At 1 h after CLP, mice on HFD were randomized to receive linagliptin (10 mg/kg, i.v.), IKK-16 (1 mg/kg, i.v.), or vehicle (2% DMSO, 3 ml/kg). At 24 h after CLP, blood samples were collected and serum **(A)** urea, **(B)** creatinine, and **(C)** ALT levels were measured. Data was analyzed using one-way ANOVA followed by Bonferroni's *post-hoc* test and expressed as mean ± SEM. *$P < 0.05$ compared to HFD+CLP group. ($n = 8$ per sham surgery group, $n = 10$ per CLP groups).

The DPP-4 inhibitors gliptins (e.g., linagliptin and sitagliptin) have been used as anti-diabetic drugs that exert their catalytic effect by increasing the incretin levels. However, recent evidence indicates that DPP-4 inhibitors, as well as glucagon like peptide-1 (GLP-1) receptors agonists (e.g., liraglutide), also have anti-inflammatory effects. The (off-target) non-catalytic effects of DPP-4 inhibitors have recently been discussed in the literature as a potential new therapeutic strategy for the treatment of diseases associated with local or systemic inflammation. Indeed, some preclinical studies suggest that inhibition of DPP-4 by different gliptins results in less cardiac dysfunction in a murine model of HFD-induced fibrosis and inflammation (42) and in a rat model of heart failure (43) by inhibiting NF-κB and by reducing the formation of pro-inflammatory cytokines. The effect of some gliptins and GLP-1 receptor agonists on survival and inflammation was also studied in animal models of endotoxaemia. Rodents subjected to endotoxaemia and treated with linagliptin or liraglutide (or their respective vehicles) showed an increase in survival rate (44, 45), and decreased formation of reactive oxygen species (ROS) (46). Treatment of cardiomyocytes with sitagliptin decreased the inflammatory response triggered by LPS (47). In contrast, pre-treatment with sitagliptin had no effect on survival in endotoxaemic animals (44, 45). Furthermore, treatment of

endotoxaemic mice with vildagliptin ameliorated the degree of pulmonary fibrosis (48). However, the effect of DPP-4 inhibitors on the cardiac (organ) dysfunction associated with sepsis (in the absence or presence of diabetes) has not yet been investigated.

Based on previous work in animals with sepsis (without T2DM), we have hypothesized that the activation of NF-κB (pro-inflammatory) and the inhibition of Akt (pro-survival) pathways are the reasons for the cardiac dysfunction in T2DM/sepsis and, hence, studied the effect of linagliptin (repurposing of linagliptin) on NF-κB inhibition and Akt activation and their impact on cardiac performance. Indeed, the results of this study highlighted, for the first time, that inhibition of DPP-4 using linagliptin (at 1 h after CLP) attenuates the cardiac dysfunction associated with T2DM/CLP-sepsis and this was associated with, or occurred as a result of, an inhibition of NF-κB activation and preservation of Akt pathway activation in the heart. Treatment with linagliptin also resulted in attenuation of the multiple organ dysfunction associated with T2DM/CLP-sepsis.

To confirm the potential key role of the activation of NF-κB in the pathophysiology of septic cardiomyopathy in animals with T2DM, we investigated the effect of NF-κB pathway inhibition using a selective IKK inhibitor (IKK-16) on cardiac (organ) dysfunction associated with sepsis. Treatment with IKK-16 ameliorated the cardiac dysfunction in mice with T2DM/sepsis. This enhanced cardiac function was a result of the decreased NF-κB activation (and iNOS expression) and inflammatory cytokines synthesis and the restored Akt phosphorylation. This restoration of Akt phosphorylation can be a result of heat shock protein 90 (Hsp 90) binding to the α and β subunits of IKK as well as to endothelial nitric oxide synthase (eNOS) (49, 50). The interaction of Hsp90 and eNOS creates a complex with Akt which allows eNOS and Akt to function on the same domain of Hsp90 (51). This interaction is increased when IKK is inhibited, resulting in increased Akt-eNOS pathway activation (52). Many other studies showed that pharmacological interventions that inhibit NF-κB reduced the multiple organ dysfunction associated with sepsis (32, 36, 53). Indeed, in this study a single dose of IKK-16 at 1 h after CLP resulted in attenuation of the multiple organ dysfunction associated with T2DM/sepsis.

Although we cannot exclude that other effects associated with DPP-4 inhibition (that do not involve NF-κB inhibition) may have contributed to the observed beneficial effects of linagliptin, our data demonstrating that the magnitude of the effect of the inhibition of NF-κB with IKK-16 is similar to the one observed with linagliptin supports the view that inhibition of the activation of NF-κB is at the heart of the observed beneficial effects of both linagliptin and IKK-16. Our data also indicate (and indeed support the view of other publications) that linagliptin may be "repurposed" for the use in sepsis and/or other conditions that are associated with local or systemic inflammation driven by the excessive activation of NF-κB.

CONCLUSIONS AND LIMITATIONS

Our data shows that a pre-existing, diabetic phenotype worsens the cardiac (organ) dysfunction associated with CLP-sepsis in mice. It also shows that activation of the NF-κB pathway is a key driver of cardiac dysfunction in mice with T2DM/sepsis. Most notably, it shows, for the first time, that inhibition of NF-κB using linagliptin or IKK-16 attenuates this cardiac (organ) dysfunction even in mice with pre-existing T2DM. Therefore, targeting NF-κB activation may be a potential strategy to treat the excessive inflammation and cardiac (organ) dysfunction in patients with T2DM and sepsis. However, our study was conducted in relatively young mice (22-week old) and treatment of septic mice was introduced relatively early in the disease course (at 1 h of the induction of sepsis) in mice treated with antibiotics and fluids to mimic "standard care" in humans with sepsis. Clearly, more studies are needed to elucidate how late after the onset of sepsis linagliptin or IKK-16 can be administered to attenuate the cardiac (organ) dysfunction, especially in older mice (ideally 12 to 18-month old). The latter studies are often limited by either the availability of mice of a relevant age or cost of these animals (and often both). This is of particular importance as most cases of sepsis occur in elderly and they are usually diagnosed later in the disease when patients either have already developed multiple organ dysfunctions or, at least, significant cardiovascular abnormalities. Further studies using other DPP-4 inhibitors and/or GLP-1 receptor agonists are needed to investigate whether any of the observed beneficial effects of linagliptin are secondary to the increased incretin levels or are, indeed, a direct effect of DPP-4 inhibition and to determine whether the inhibition of NF-κB reported with linagliptin in our study is, indeed, a unique class-specific effect or an off-target effect of linagliptin.

AUTHOR CONTRIBUTIONS

SA, JC, MC, MY, and CT conceived and designed the experiment. SA, JC, CM, LM, FC, and DC performed the experiments. SA, MC, CT analyzed the data. SA, MC, and CT contributed to the writing of the manuscript.

FUNDING

SA is sponsored by Al-Balqa Applied University, Jordan. This work was, in part, funded by the William Harvey Research Foundation and the University of Turin (Ricerca Locale 2017 and 2018).

ACKNOWLEDGMENTS

Part of this work was presented at the 78th scientific session of the American Diabetes Association (ADA).

REFERENCES

1. Singer M, Deutschman CS, Seymour CW, Shankar-Hari M, Annane D, Bauer M, et al. The third international consensus definitions for sepsis and septic shock (Sepsis-3). *JAMA* (2016) 315:801–10. doi: 10.1001/jama.2016.0287
2. Martin L, Derwall M, Al Zoubi S, Zechendorf E, Reuter DA, Thiemermann C, et al. The septic heart current understanding of molecular mechanisms and clinical implications. *Chest* (in press) 18. doi: 10.1016/j.chest.2018.08.1037
3. Merx MW, Weber CD. Sepsis and the heart. *Circulation* (2007) 116:793–802. doi: 10.1161/CIRCULATIONAHA.106.678359
4. Blanco J, Muriel-Bombín A, Sagredo V, Taboada F, Gandía F, Tamayo L, et al. Incidence, organ dysfunction and mortality in severe sepsis: a Spanish multicentre study. *Crit Care* (2008) 12:1–14. doi: 10.1186/cc7157
5. Angus DC, Linde-Zwirble WT, Lidicker J, Clermont G, Carcillo J, Pinsky MR. Epidemiology of severe sepsis in the United States: analysis of incidence, outcome, and associated costs of care. *Crit Care Med*. (2001) 29:1303–1310. doi: 10.1097/00003246-200107000-00002
6. World Health Orgaization. *Global Report on Diabetes* (2016).
7. Amirican diabetes association. Standards of medical care in diabetes-−2016 abridged for primary care providers. *Clin Diabetes* (2016) 34:3–21. doi: 10.2337/diaclin.34.1.3
8. Rubler S, Dlugash J, Yuceoglu YZ, Kumral T, Branwood AW, Grishman A. New type of cardiomyopathy associated with diabetic glomerulosclerosis. *Am J Cardiol*. (1972) 30:595–602. doi: 10.1016/0002-9149(72)90595-4
9. Rerkpattanapipat P, Agostino RBD, Link KM, Shahar E, Lima JA, Bluemke DA, et al. Location of arterial stif fening differs in those with impaired fasting glucose versus diabetes: implications for left ventricular hypertrophy from the multi-ethnic study of Atherosclerosis. *Diabetes* (2009) 58:946–53. doi: 10.2337/db08-1192
10. Casqueiro J, Casqueiro J, Alves C. Infections in patients with diabetes mellitus : a review of pathogenesis. *Indian J Endocrinol Metab*. (2012) 16:27–36. doi: 10.4103/2230-8210.94253
11. Schuetz P, Castro P, Shapiro NI. Diabetes and sepsis: preclinical findings and clinical relevance. *Diabetes Care* (2011) 34:771–8. doi: 10.2337/dc10-1185
12. Kornum J, Thomsen R, Riis A, Lervang H, Schønheyder H, Sørensen H. Type 2 diabetes and pneumonia outcomes: a population-based cohort study. *Diabetes Care* (2007) 30:2251–7. doi: 10.2337/dc06-2417
13. Benfield T, Jensen J, Nordestgaard B. Influence of diabetes and hyperglycaemia on infectious disease hospitalisation and outcome. *Diabetol* (2007) 50:549–54. doi: 10.1007/s00125-006-0570-3
14. Thomsen RW, Hundborg HH, Lervang H, Johnsen SP, Schønheyder HC, Sørensen HT. Diabetes mellitus as a risk and prognostic factor for community-acquired bacteremia due to enterobacteria : a 10-year, population-based study among adults. *Clin Infect Dis*. (2005) 40:628–31. doi: 10.1086/427699
15. Vincent J, Preiser J, Sprung CL, Moreno R, Sakr Y. Insulin-treated diabetes is not associated with increased mortality in critically ill patients. *Crit Care* (2010) 14:R12. doi: 10.1186/cc8866
16. Esper AM, Moss M, Martin GS. The effect of diabetes mellitus on organ dysfunction with sepsis : an epidemiological study. *Crit Care* (2009) 13:9–14. doi: 10.1186/cc7717
17. van Vught LA, Holman R, de Jonge E, de Keizer NF, van der Poll T. Diabetes is not associated with increased 90-day mortality risk in critically ill patients with sepsis. *Crit Care Med*. (2017) 45:e1026–e1035. doi: 10.1097/CCM.0000000000002590
18. McAlister F, Majumdar S, Blitz S, Rowe B, Romney J, Marrie TJ. The relation between hyperglycemia and outcomes in 2,471 patients admitted to the hospital with community-acquired pneumonia. *Diabetes Care* (2005) 28:810–5. doi: 10.2337/diacare.28.4.810
19. Moss M, Guidot D, Steinberg K, Duhon GF, Treece P, Wolken R, et al. Diabetic patients have a decreased incidence of acute respiratory distress syndrome. *Crit Care Med*. (2000) 28:2187–92. doi: 10.1097/00003246-200007000-00001
20. Siegl D, Annecke T, Johnson BL III Schlag C, Martignoni A, Huber N, et al. Obesity-induced hyperleptinemia improves survival and immune response in a murine model of sepsis. *Anesthesiology* (2014) 121:98–114. doi: 10.1097/ALN.0000000000000192
21. Rawlings ND, Barrett AJ, Finn R. Twenty years of the MEROPS database of proteolytic enzymes, their substrates and inhibitors. *Nucleic Acids Res*. (2016) 44:343–50. doi: 10.1093/nar/gkv1118
22. Jhajharia S, Pradhan T, Ekka A, Das AK. Effect of Dipeptidyl Peptidase-4 inhibitors on adenosine deaminase Ac- tivity in Type-2 Diabetes Mellitus. *Biomed Res*. (2014) 25:489–93. Available online at: www.biomedres.info
23. Ohnuma K, Inoue H, Uchiyama M, Yamochi T, Hosono O, Dang NH. T-cell activation via CD26 and caveolin-1 in rheumatoid synovium. *Mod Rheumatol*. (2006) 16:3–13. doi: 10.3109/s10165-005-0452-4
24. Klemann C, Wagner L, Stephan M, von Hörsten S. Cut to the chase : a review of CD26 / dipeptidyl peptidase-4' s (DPP4) entanglement in the immune system. *Clin Exp Immunol*. (2016) 185:1–21. doi: 10.1111/cei.12781
25. Ohnuma K, Uchiyama M, Yamochi T, Nishibashi K, Hosono O. Caveolin-1 Triggers T-cell Activation via CD26 in Association. *J Biol Chem*. (2007) 282:10117–31. doi: 10.1074/jbc.M609157200
26. Conlon BA, Law WR. Macrophages are a source of extracellular adenosine deaminase-2 during inflammatory responses. *Clin Exp Immunol*. (2004) 138:14–20. doi: 10.1111/j.1365-2249.2004.02591.x
27. Lamers D, Famulla S, Wronkowitz N, Hartwig S, Lehr S, Ouwens DM, et al. Dipeptidyl peptidase 4 is a novel adipokine potentially linking obesity to the metabolic syndrome. *Diabetes* (2011) 60:1917–25. doi: 10.2337/db10-1707
28. Kang SH, Park DB, Oh B, Kim J, Heo ST. CD26/DPP4 Levels in peripheral blood and T Cells in patients with Type 2 diabetes mellitus. *J Clin Endocrinol Metab*. (2013) 98:2553–61. doi: 10.1210/jc.2012-4288
29. Miyazaki M, Kato M, Tanaka K, Tanaka M, Kohjima M, Nakamura K, et al. Increased hepatic expression of dipeptidyl peptidase-4 in non-alcoholic fatty liver disease and its association with insulin resistance and glucose metabolism. *Mol Med Rep*. (2012) 5:729–33. doi: 10.3892/mmr.2011.707
30. Kapoor A, Shintani Y, Collino M, Osuchowski MF, Busch D, Patel NS, et al. Protective role of peroxisome proliferator-activated receptor-β/δ in septic shock. *Am J Respir Crit Care Med*. (2010) 182:1506–15. doi: 10.1164/rccm.201002-0240OC
31. Khan A, Coldewey S, Patel N, Rogazzo M, Collino M, Yaqoob MM, et al. Erythropoietin attenuates cardiac dysfunction in experimental sepsis in mice via activation of the β-common receptor. *Dis Model Mech*. (2013) 6:1021–30. doi: 10.1242/dmm.011908
32. Coldewey SM, Rogazzo M, Collino M, Patel NSA, Thiemermann C. Inhibition of I B kinase reduces the multiple organ dysfunction caused by sepsis in the mouse. *Dis Model Mech*. (2013) 6:1031–42. doi: 10.1242/dmm.012435
33. Thomas CM, Yong QC, Rosa RM, Seqqat R, Gopal S, Casarini DE, et al. Cardiac-specific suppression of NF-κB signaling prevents diabetic cardiomyopathy via inhibition of the renin-angiotensin system. *Am J Physiol Circ Physiol*. (2014) 307:H1036–45. doi: 10.1152/ajpheart.00340.2014
34. Kim F, Pham M, Luttrell I, Bannerman DD, Tupper J, Thaler J, et al. Toll-like receptor-4 mediates vascular inflammation and insulin resistance in diet-induced obesity. *Circ Res*. (2007) 100:1589–96. doi: 10.1161/CIRCRESAHA.106.142851
35. Yao D, Brownlee M. Hyperglycemia-induced reactive oxygen species increase expression of the receptor for advanced glycation end products (RAGE) and RAGE ligands. *Diabetes* (2010) 59:249–55. doi: 10.2337/db09-0801
36. Chen J, Kieswich JE, Chiazza F, Moyes AJ, Gobbetti T, Purvis GS, et al. IκB Kinase inhibitor attenuates sepsis-induced cardiac dysfunction in CKD. *J Am Soc Nephrol*. (2017) 28:94–105. doi: 10.1681/ASN.2015060670
37. Mastrocola R, Collino M, Penna C, Nigro D, Chiazza F, Fracasso V, et al. Maladaptive modulations of nlrp3 inflammasome and cardioprotective pathways are involved in diet-induced exacerbation of myocardial ischemia/reperfusion injury in mice. *Oxid Med Cell Longev*. (2016) 2016:1–12. doi: 10.1155/2016/3480637
38. Barone FC, Hillegass LM, Price WJ, White RF, Lee EV, Feuerstein GZ, et al. Polymorphonuclear leukocyte infiltration into cerebral focal ischemic tissue: myeloperoxidase activity assay and histologic verification. *J Neurosci Res Cell Sci*. (1991) 29:336–45. doi: 10.1002/jnr.490290309
39. Gavazzi G, Krause K. Ageing and infection. *Lancet Infect Dis*. (2002) 2:659–66. doi: 10.1016/S1473-3099(02)00437-1
40. Mayr FB, Yende S, Angus DC, Mayr FB, Yende S, Angus DC. Epidemiology of severe sepsis epidemiology of severe sepsis. *Virulence* (2014) 5594:4–11. doi: 10.4161/viru.27372
41. Lewis AJ, Lee JS, Rosengart MR. Translational sepsis research. *Crit Care Med*. (2018) 46:1497–505. doi: 10.1097/CCM.0000000000003271

42. Aroor AR, Habibi J, Kandikattu HK, Garro-Kacher M, Barron B, Chen D, et al. Dipeptidyl peptidase - 4 (DPP - 4) inhibition with linagliptin reduces western diet - induced myocardial TRAF3IP2 expression, inflammation and fibrosis in female mice. *Cardiovasc Diabetol*. (2017) 16:1–15. doi: 10.1186/s12933-017-0544-4
43. Esposito G, Cappetta D, Russo R, Rivellino A, Ciuffreda LP, Roviezzo F, et al. Sitagliptin reduces inflammation, fibrosis and preserves diastolic function in a rat model of heart failure with preserved ejection fraction. *Br J Pharmacol*. (2017) 174:4070–86. doi: 10.1111/bph.13686
44. Steven S, Hausding M, Kröller-Schön S, Mader M, Mikhed Y, Stamm P, et al. Gliptin and GLP-1 analog treatment improves survival and vascular inflammation/dysfunction in animals with lipopolysaccharide-induced endotoxemia. *Basic Res Cardiol*. (2015) 110:6. doi: 10.1007/s00395-015-0465-x
45. Steven S, Jurk K, Kopp M, Kröller-Schön S, Mikhed Y, Schwierczek K, et al. Glucagon-like peptide-1 receptor signalling reduces microvascular thrombosis, nitro-oxidative stress and platelet activation in endotoxaemic mice. *Br J Pharm*. (2017) 174:1620–32. doi: 10.1111/bph.13549
46. Kröller-Schön S, Knorr M, Hausding M, Oelze M, Schuff A, Schell R, et al. Glucose-independent improvement of vascular dysfunction in experimental sepsis by dipeptidyl-peptidase 4 inhibition. *Cardiovasc Res*. (2012) 96:140–9. doi: 10.1093/cvr/cvs246
47. Lin C, Lin C. Sitagliptin attenuates inflammatory responses in lipopolysaccharide - stimulated cardiomyocytes via nuclear factor-κB pathway inhibition. *Exp Ther Med*. (2016) 11:2609–15. doi: 10.3892/etm.2016.3255
48. Suzuki T, Tada Y, Gladson S, Nishimura R, Shimomura I, Karasawa S. Vildagliptin ameliorates pulmonary fibrosis in lipopolysaccharide-induced lung injury by inhibiting endothelial-to-mesenchymal transition. *Respir Res*. (2017) 18:1–11. doi: 10.1186/s12931-017-0660-4
49. Chen G, Cao P, Goeddel DV, Francisco SS. TNF-Induced recruitment and activation of the ikk complex require Cdc37 and Hsp90. *Mol Cell* (2002) 9:401–10. doi: 10.1016/S1097-2765(02)00450-1
50. Fleming I, Busse R. Molecular mechanisms involved in the regulation of the endothelial nitric oxide synthase. *Am J Physiol Regul Integr Comp Physiol*. (2003) 284:R1–12. doi: 10.1152/ajpregu.00323.2002
51. Fontana J, Fulton D, Chen Y, Fairchild TA, McCabe TJ, Fujita N, et al. Domain mapping studies reveal that the M domain of hsp90 serves as a molecular scaffold to regulate Akt-dependent phosphorylation of endothelial nitric oxide synthase and NO release. *Circ Res*. (2002) 90:866–73. doi: 10.1161/01.RES.0000016837.26733.BE
52. Mohan S, Konopinski R, Yan B, Centonze VE, Natarajan M. High glucose-induced IKK-Hsp-90 interaction contributes to endothelial dysfunction. *Am J Physiol Cell Physiol*. (2009) 296:182–92. doi: 10.1152/ajpcell.00575.2007
53. Martin L, Horst K, Chiazza F, Oggero S, Collino M, Brandenburg K, et al. The synthetic antimicrobial peptide 19-2.5 attenuates septic cardiomyopathy and prevents down-regulation of SERCA2 in polymicrobial sepsis. *Sci Rep*. (2016) 6:37277. doi: 10.1038/srep37277

Conflict of Interest Statement: The authors declare that the research was conducted in the absence of any commercial or financial relationships that could be construed as a potential conflict of interest.

Copyright © 2018 Al Zoubi, Chen, Murphy, Martin, Chiazza, Collotta, Yaqoob, Collino and Thiemermann. This is an open-access article distributed under the terms of the Creative Commons Attribution License (CC BY). The use, distribution or reproduction in other forums is permitted, provided the original author(s) and the copyright owner(s) are credited and that the original publication in this journal is cited, in accordance with accepted academic practice. No use, distribution or reproduction is permitted which does not comply with these terms.

frontiers in Immunology

ORIGINAL RESEARCH
published: 07 January 2019
doi: 10.3389/fimmu.2018.03052

Effects of Changes in the Levels of Damage-Associated Molecular Patterns Following Continuous Veno–Venous Hemofiltration Therapy on Outcomes in Acute Kidney Injury Patients With Sepsis

Jie Wu[1], Jianan Ren[1], Qinjie Liu[1], Qiongyuan Hu[1], Xiuwen Wu[1]*, Gefei Wang[1], Zhiwu Hong[1], Huajian Ren[2] and Jieshou Li[1]*

[1] Department of Surgery, Affiliated Jinling Hospital, Medical School of Nanjing University, Nanjing, China, [2] Department of Surgery, Jinling Hospital, Nanjing Medical University, Nanjing, China

OPEN ACCESS

Edited by:
Timothy Robert Billiar, University of Pittsburgh, United States

Reviewed by:
Sergio Iván Valdés-Ferrer, Instituto Nacional de Ciencias Médicas y Nutrición Salvador Zubirán (INCMNSZ), Mexico
Ben Lu, Central South University, China

***Correspondence:**
Jianan Ren
jiananr@gmail.com
Xiuwen Wu
lygwxw@163.com

Specialty section:
This article was submitted to Inflammation, a section of the journal Frontiers in Immunology

Received: *08 August 2018*
Accepted: *10 December 2018*
Published: *07 January 2019*

Citation:
Wu J, Ren J, Liu Q, Hu Q, Wu X, Wang G, Hong Z, Ren H and Li J (2019) Effects of Changes in the Levels of Damage-Associated Molecular Patterns Following Continuous Veno–Venous Hemofiltration Therapy on Outcomes in Acute Kidney Injury Patients With Sepsis. Front. Immunol. 9:3052. doi: 10.3389/fimmu.2018.03052

Background: We investigated the association of damage-associated molecular pattern (DAMP) removal with mortality in sepsis patients undergoing continuous veno–venous hemofiltration (CVVH).

Methods: Circulating levels of DAMPs [mitochondrial DNA (mtDNA); nuclear DNA (nDNA); heat shock protein 70 (HSP70); and high mobility group box 1 (HMGB1)] and cytokines were measured at baseline, 6 and 12 h after initiation of CVVH. Urinary DNA levels were analyzed at baseline and end of CVVH. The expression of human leukocyte antigen (HLA)-DR was assayed at 0, 3, and 7 days after initiation of CVVH. Moreover, the effects of HSP70 and HMGB1 clearance on survival were analyzed.

Results: We evaluated 43 patients with acute kidney injury (AKI) (33 sepsis patients). Twenty-two sepsis patients (67%) and three non-sepsis patients (30%) expired ($P = 0.046$). Significant reductions in the levels of circulating interleukin-6 ($P = 0.046$) and tumor necrosis factor-α ($P = 0.008$) were found in the sepsis group. The levels of mtDNA were increased (*ND2*, $P = 0.035$; *D-loop*, $P = 0.003$), whereas that of HSP70 was reduced ($P = 0.000$) in all patients during the first 12 h. The levels of DAMPs in the plasma were markedly increased after blood passage from the inlet through the dialyzer in survivor sepsis patients. The clearance rates of HSP70 and HMGB1 were good predictors of mortality [area under the curve (AUC) = 0.937, $P = 0.000$; AUC = 0.90, $P = 0.001$, respectively]. The level of HLA-DR was increased in response to higher HSP70 clearance ($P = 0.006$). Survival was significantly worse in groups with higher clearance rates of HSP70 and HMGB1 than the cut-off value (log-rank test: $P = 0.000$ for both). Higher HSP70 clearance was a significant independent predictor of mortality (odds ratio = 1.025, 95% confidence interval [CI]: 1.012–1.039, $P = 0.000$). The urinary nDNA (*β-globin*) level before CVVH was an independent risk factor for the duration of CVVH in patients with sepsis (sRE = 0.460, 95% CI: 1.720–8.857, $P = 0.005$).

Conclusion: CVVH removes inflammatory factors, reduces urinary DAMPs, and removes plasma DAMPs. However, survival decreases in response to higher HSP70 clearance.

Keywords: continuous veno–venous hemofiltration, damage-associated molecular patterns, acute kidney injury, heat shock protein 70, high mobility group box 1, urinary nuclear DNA

INTRODUCTION

Sepsis is a life-threatening disease caused by a dysregulated host response to infection (1). In particular, acute kidney injury (AKI) is one of the most common types of organ dysfunction, appearing early in the course of sepsis. Nearly half of patients develop AKI in the intensive care unit and account for approximately half of sepsis-related deaths (2, 3). The high mortality associated with septic AKI may be at least partly explained by an incomplete understanding of its pathophysiology and a delay in diagnosis.

The levels of pro-inflammatory mediators in the serum are increased in patients with AKI, regardless of its cause (4, 5). Pro- and anti-inflammatory mediators, as well as damage-associated molecular patterns (DAMPs), play important roles in regulating the immunological response that mediates the severity and complications of sepsis (6, 7). DAMPs, also known as alarmins, are constitutively available endogenous molecules released in response to tissue damage and involved in the activation of the immune system. A subset of DAMPs are nuclear or cytosolic molecules, such as mitochondrial DNA (mtDNA), nuclear DNA (nDNA), high mobility group box 1 (HMGB1), and heat shock protein 70 (HSP70). In recent years, Rajaee et al. stated that the definition of interleukin (IL)-1 and IL-33 as DAMPs or cytokines remains controversial (8).

Recently, an increased level of mtDNA in the urine has emerged as a novel non-invasive biomarker for the detection of AKI (9). Moreover, our research has demonstrated the effectiveness of using urinary levels of mtDNA as evidence of renal mitochondrial injury induced by AKI after sepsis (10). However, the role of circulating DAMPs in AKI is controversial (11, 12).

Currently, continuous renal replacement therapy (CRRT) is the main support strategy for AKI, involving several types of treatment. Considerable evidence has suggested that CRRT controls azotemia and fluid balance (13, 14). It has been reported that continuous veno–venous hemofiltration (CVVH) may assist in reducing acute inflammation through the removal of pro-inflammatory cytokines and signaling molecules, such as the tumor necrosis factor (TNF)-α and various ILs (4, 15). However, the effectiveness of pro-inflammatory molecule clearance is controversial. Several clinical studies have shown that changes in the type of CRRT modes did not reduce mortality compared with the standard mode, even after extensive removal of pro-inflammatory cytokines in the new mode groups (16, 17).

Studies investigating DAMPs and CRRT are limited to a particular molecule and the relationship between levels of DAMPs in the plasma and complications at a certain point in time (18). Thus far, there is no study reporting the effect of CVVH on the levels of DAMPs and the effects of these changes on the prognosis of patients. Therefore, the present study investigated the effects of CVVH on the circulating and urinary levels of DAMPs in AKI patients and the roles of DAMP clearance on patient outcome.

Abbreviations: CVVH, Continuous veno-venous hemofiltration; DAMPs, Damage-Associated Molecular Patterns; mtDNA, mitochondrial DNA; nDNA, nuclear DNA; HSP70, Heat Shock Protein 70; HMGB1, High Mobility Group Box 1; cf-DNA, Cell-free DNA; TNF-α, tumor necrosis factor alpha; IFN-γ, interferon gamma; mHLA-DR, mononuclear human leukocyte antigen-DR; APACHE II, Acute Physiology and Chronic Health Evaluation II; SOFA, Sequential Organ Failure Assessment; ICU, Intensive care unit; NGAL, neutrophil gelatinase-associated lipocalin; ABC, antibodies bound per cell; IQR, interquartile range; KDIGO, Kidney Disease, Improving Global Outcomes; mCLcytokines, mean of cytokines clearance rate; mCLDAMPs, mean of DAMPs clearance rate; mCDAMPs, mean of circulating DAMPs levels.

MATERIALS AND METHODS

Study Population

The population of this prospective study consisted of 43 patients with AKI requiring CVVH who were admitted to the surgical intensive care unit (SICU) of Jinling Hospital (Nanjing, China). The study was approved by the Ethics Committee of Jinling Hospital, Nanjing and conducted from November 2016–August 2017. Written informed consent was provided by all enrolled patients prior to their participation in the study.

The inclusion criteria were: age >18 years; presence of AKI requiring CVVH; presence of sepsis. The exclusion criteria were: refusal to provide consent; history of chronic kidney disease; expected duration of CVVH <12 h; death within 24 h from initiation of CVVH; ongoing CRRT; and previous renal transplantation. Baseline demographic and clinical data were automatically recorded using a software (Nanjing Haitai Medical Information System, Nanjing, China) or by physicians. For comparison, 10 age- or sex- matched AKI patients without sepsis receiving CVVH were included.

Definitions

We defined AKI according to the Kidney Disease: Improving Global Outcomes (KDIGO) criteria (19), corresponding to stage 1 of the KDIGO classification with increased serum creatinine level ≥0.3 mg/dL (≥26.5 μmol/L) within 48 h or increased serum creatinine ≥1.5-fold compared with baseline within 7 days. Sepsis and septic shock were defined according to the Third International Consensus Definitions for Sepsis and Septic Shock (1). Indication of CVVH required at least one of the following criteria: oliguria (urine output <100 mL continued for 6 h after adequate fluid resuscitation), serum creatinine (Scr) >250 μmol/L (2.8 mg/dL), serum potassium concentration >6.5

mmol/L, severe acidemia (pH < 7.2), and presence of severe fluid overload.

CVVH Procedure

All patients were treated with CVVH using the Aquarius hemodialysis system (Baxter International Inc., Chicago, IL, USA). Central venous catheterizations (Quinton-Mahurkar dual-lumen hemodialysis catheters, Kendall, Tyco Healthcare Group LP, USA) through femoral vein sites were used for vascular access. Administration of CVVH was similar for all patients under the following parameters: blood flow, 100–200 mL/minnum; filter, high flux AV600S (polysulfone, 1.4 m^2, Fresenius Medical Care); replacement fluid infused at 4 L/h through the pre-dilution route. The daily net ultrafiltration volume was decided by the attending physician. Safety monitoring, including serum electrolyte balance, acid base status, and fluid balance was performed twice daily. Anticoagulation treatment was performed according to the patient's condition. In general, citrate anticoagulation was combined with low-dose heparin to maintain the activated clotting time within the extracorporeal circuit within a desired range (200–250 s). In addition, mechanical ventilation, vasopressor therapy, or any other standard treatment was used regardless of the presence of sepsis, as long as the treatment indications were met.

Sample Collection and Processing

Collection of blood samples (12 mL) was performed from both the inlet and outlet of the dialyzer at baseline and 6 and 12 h after initiation of CVVH. Of this sample volume, 4 mL were collected in ethylenediamine tetracetate tubes, whereas the remaining 8 mL were stored in promoting coagulating tubes. Ultrafiltrate collections (10 mL) were drawn within the first 2 h. Urine samples were collected at baseline and end of CVVH. All samples were immediately transported to the laboratory and placed on ice. Blood samples were centrifuged at 3,000 × g at 4°C for 10 min, whereas the ultrafiltrate collections and urine samples were centrifuged at 1,000 × g at 4°C for 5 min. Supernatants were collected and stored at −80°C until further analysis. Samples were collected in the first 12 h of CVVH.

Isolation and Quantification of mtDNA and nDNA

Free DNA was isolated from 200 μL plasma samples using the QIAamp DNA Blood Mini Kit (Qiagen, Valencia, CA, USA), and 1.75 mL urine samples using an urine DNA isolation kit (NorgenBiotek, Ontario, Canada), DNA was eluted in 100 μL of supplied buffer as previously described (10, 20). Quantitative polymerase chain reaction [qPCR; real-time polymerase chain reaction (PCR)] targeting mitochondrial genes (*D-loop* and *ND2*) and nuclear genes (*GAPDH* and *β-globin*) was performed to quantify cell-free DNA (cf-DNA) content. The efficiency of all reactions was >98%. All samples were analyzed in triplicate. The standard curve of the quantitative assay was produced through the serially diluted template cloned into a plasmid DNA.

Analysis of Cytokines and DAMPs

The different cytokines (IL-1β, IL-6, TNF-α, IFN-γ, IL-10) and HSP70 and urinary neutrophil gelatinase-associated lipocalin (NGAL) were quantified using an enzyme-linked immunosorbent assay (ELISA) kit (R&D System, USA), while the levels of HMGB1 were quantified using a different ELISA kit (SAB, USA), according to the instructions provided by the manufacturer.

Based on the mass conservation principle, the removal rate of cytokines during CVVH was calculated as follows (without considering the concentration of cytokines at baseline):

$$Ctr = (Ci–Co)/Ci$$
$$Clr = Ctr \times Qb$$

Ctr, Total concentration removal rate
Ci, Concentration in the inlet plasma prior to the addition of replacement fluid
Co, Concentration in the outlet plasma
Clr, Clearance rate
Qb, Inlet blood flow rate (mL/min).

Quantification of Monocyte Human Leukocyte Antigen-DR (mHLA-DR)

Quantification of mHLA-DR was performed according to the description by Döcke et al. (21). In brief, whole blood was acquired at 0, 3, and 7 days after initiation of CVVH and lysed using red blood cell lysis buffer (KeyGEN BioTECH, Jiangsu, China). Subsequently, they were fixed in 4% paraformaldehyde and incubated with Anti-HLA-DR/Anti-Monocyte Stain (Becton Dickinson, San Jose, CA, USA). Samples were analyzed using a FACScan (Becton Dickinson, San Jose, CA, USA) with a five-color upgrade (CyTech, Fremont, CA, USA). Flow files were analyzed in CellQuest Pro (Becton Dickinson, San Jose, CA, USA). Antibodies bound per cell (ABC) were calculated by standardizing HLA-DR geometric mean fluorescence intensity (GMFI) of monocytes to BD Quantibrite-phycoerythrin (PE) beads (Becton Dickinson, San Jose, CA, USA).

Statistical Analyses

Results are expressed as the mean ± standard deviation (SD) or median with interquartile range (IQR), as appropriate. Comparison of continuous variables between the two groups was conducted using the Student's *t*-test or Mann–Whitney *U*-test depending on Gaussian distribution. Categorical variables were compared between the two groups using the chi-square test and Fisher's exact test, as appropriate. We analyzed all datasets using a two-way repeated-measure ANOVA to examine the effects of CVVH duration. Analyses of receiver operating characteristic (ROC) curves were conducted to test the effectiveness for the prediction of certain outcomes. The optimal cut-off value was defined as the value closest to the Youden Index. Correlation analyses were performed on multiple variables, and the degree of correlation was determined by calculation of the Spearman rank-order coefficients. The Kaplan–Meier method and binary logistic regression analysis was used to determine predictors of mortality. Linear logistic regression analysis was performed to determine independent predictors of CVVH duration. The

criterion for statistical significance in all comparisons was $P < 0.05$. All analyses were performed using the SPSS v21.0 software (IBM, Armonk, NY, USA).

RESULTS

Demographic and Outcome Parameters of AKI Patients With or Without Sepsis

The study flowchart is shown in **Figure 1**. The samples and clinical data were collected at the specified time points as shown in **Figure 1B**. The consecutive case series included AKI patients who met the criteria for CVVH indication, excluding those with chronic kidney disease. According to the hospital records and laboratory examination, the patients were classified as sepsis-associated AKI or non-sepsis-associated AKI. A total of 43 patients were enrolled in the study. Among them, 33 patients presented with sepsis, whereas 10 AKI patients presented without sepsis (control group). The aim of this classification was to investigate differences in the clearance rate of cytokines or DAMPs during CVVH between different diseases. All patients conformed to the criteria of CVVH and the characteristics of patients are shown in **Table 1**.

AKI patients with sepsis were significantly older compared with those without sepsis (48.9 ± 13.9 vs. 37.3 ± 9.4 years, respectively; $P = 0.042$) and had markedly lower 24-h urinary output (280 vs. 750 mL, respectively; $P = 0.009$) at the time of enrollment. At baseline, clinical indices [i.e., Acute Physiology and Chronic Health Evaluation (APACHE) II score, Sequential Organ Failure Assessment (SOFA) score, cytokine levels, and DAMPs levels] were comparable between the two groups.

However, the outcomes were distinct between the two groups. The median duration of CVVH for the treatment of AKI patients with sepsis was longer than that for non-sepsis patients (8 vs. 5 days, respectively; $P = 0.042$). The median duration of mechanical ventilation was significantly longer in the AKI with sepsis group (12.5 vs. 0 days, respectively; $P = 0.005$). Moreover, in-hospital mortality was significantly higher in the AKI with sepsis group vs. the AKI without sepsis group (66.7 vs. 30.0%, respectively; $P = 0.042$) (**Table 1**). Of note, CVVH parameters were similar between the two groups, except for treatment duration.

Clinical Indicators and Cytokine Levels During CVVH

We classified the AKI patients with sepsis into two groups, namely "survivors" and "non-survivors" to evaluate clinical data trends (**Figure S1**). As expected, most of the indices of liver and kidney function (e.g., levels of liver enzymes, serum creatinine, and blood urea) were improved during the first 7 days after initiation of CVVH, irrespectively of patient survival. However, in non-survivors, the level of total bilirubin temporarily returned within the normal range but rapidly increased after termination of CVVH. In contrast, the urine output did not recover during CVVH.

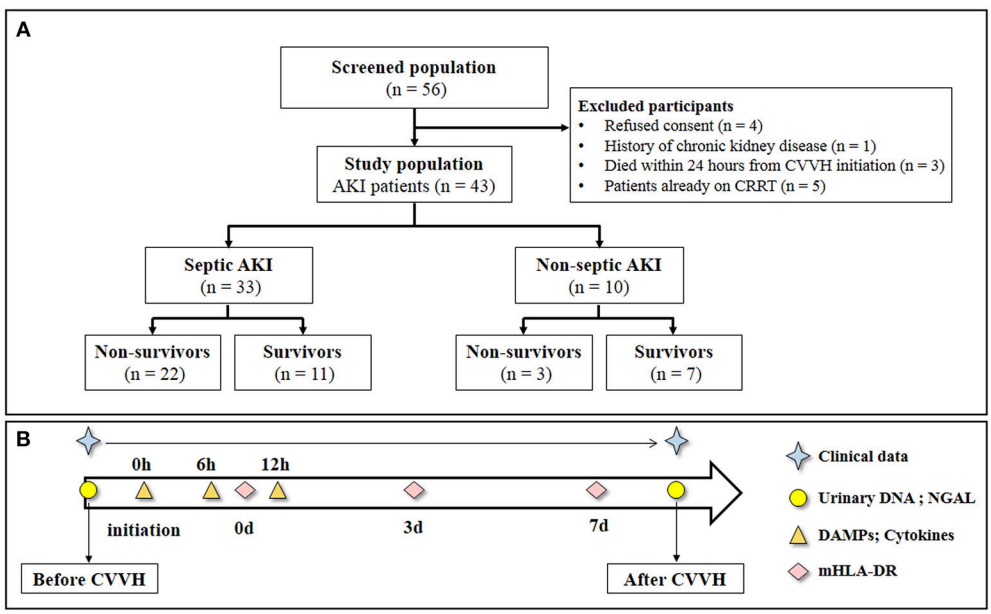

FIGURE 1 | Study flow and schedule for samples collection. **(A)** Study flow. **(B)** Clinical data was obtained every day during the study period. Urinary DNA (mitochondrial DNA and nuclear DNA) and urinary NGAL were measured at baseline and end of CVVH. The level of Circulatory cytokines and DAMPs were measured from the inlet and outlet of the dialyzer at baseline, 6 and 12 h after CVVH initiation. Levels of mHLA-DR were measured at 0, 3, and 7 days after CVVH initiation. CVVH, continuous veno-venous hemofiltration; NGAL, neutrophil gelatinase-associated lipocalin; DAMPs, damage-associated molecular patterns; mHLA-DR, mononuclear human leukocyte antigen-DR.

TABLE 1 | Clinical characteristics and biochemical variables of the study population.

Characteristics	CVVH patients			*P*-value
	Total ($n = 43$)	Sepsis ($n = 33$)	Non-sepsis ($n = 10$)	
DEMOGRAPHIC DATA				
Age, mean (SD), y	46.5 ± 13.8	48.9 ± 13.9	37.3 ± 9.4	**0.046**
Male, *n* (%)	31 (72.1)	23 (69.7)	8 (80.0)	0.642
BMI, mean (SD)	25.7 ± 4.3	25.3 ± 4.0	49.0 ± 14.0	0.237
SOFA score, mean (SD)	10.6 ± 5.1	11.3 ± 5.2	8.0 ± 4.1	0.132
APACHE II score, mean (SD)	13.5 ± 6.4	14.5 ± 6.2	9.9 ± 6.0	0.089
CVVH PARAMETERS				
Duration of CVVH, median (IQR), d	6.0 [3.5–13.0]	8.0 [2.8–19.3]	5.0 [4.0–7.0]	**0.046**
Blood flow, median (IQR), mL/min	140 [120–160]	155.0 [120.0–165.0]	140 [130–160]	0.071
Replacement fluid dose, median (IQR), mL/h	130 [130–145]	130.0 [130.0–142.5]	145 [130–260]	0.357
Observed effluent rate, mL/h	4,000	4,000	4,000	
ICU ADMISSION				
Biochemical parameters				
24h Urine output, median (IQR), ml	470 [91–1013]	280.5 [87.5–925.0]	750.0 [348.0–1740.0]	**0.009**
Creatinine, mean (SD),μmol/L	339.3 ± 252.5	323.7 ± 220.0	397.1 ± 365.2	0.503
BUN, mean (SD), mmol/L	20.1 ± 14.2	18.9 ± 10.6	24.9 ± 3.9	0.321
eGFR, median (IQR), mL/min/1.73 m^2	17.8 [11.1–52.9]	16.9 [11.1–49.1]	21.0 [5.2–59.8]	0.418
Urinary NGAL, median (IQR), ng/mL	8.9 [4.7–10.6]	9.4 [6.0–10.5]	4.5 [0.4–16.3]	0.750
ALT, median (IQR), U/L	47.0 [22.0–84.0]	55.0 [23.0–89.0]	32.0 [19.0–69.0]	0.186
AST, median (IQR), U/L	68.5 [37.8–152.0]	67.0 [39.5–55.0]	70.0 [33.0–89.0]	**0.022**
CRP, mean (SD), mg/L	194.6 ± 92.3	191.4 ± 96.3	206.5 ± 81.1	0.705
PCT, median (IQR), ng/mL	8.8 [2.8–26.3]	7.8 [2.8–24.5]	14.4 [2.8–70.3]	0.232
Leukocyte count, mean (SD), $\times 10^9$/L	13.8 ± 7.4	13.38 ± 7.23	15.24 ± 8.65	0.565
RBC, mean (SD), $\times 10^9$/L	3.5 ± 1.1	3.37 ± 1.12	3.85 ± 1.06	0.312
PLT count, median (IQR), $\times 10^9$/L	129.0 [86.5–288.0]	134.5 [87.3–224.5]	117.0 [67.0–239.0]	0.163
APTT, mean (SD), s	42.4 ± 20.5	43.7 ± 22.3	37.6 ± 11.5	0.492
PT, mean (SD), s	15.3 ± 1.7	15.2 ± 1.6	15.5 ± 2.1	0.650
INR, median (IQR)	1.3 [1.2–1.5]	1.3 [1.2–1.5]	1.4 [1.2–1.5]	0.653
Serum albumin, mean (SD), g/L	56.7 ± 12.0	29.0 ± 5.0	33.1 ± 8.6	0.111
Total Bilirubin, median (IQR), μmol/L	34.0 [24.3–121.0]	32.5 [23.7–114.3]	37.9 [24.1–135.9]	0.055
Serum sodium, mean (SD), mmol/L	139.4 ± 6.1	139.8 ± 5.3	137.7 ± 8.6	0.439
Serum potassium, mean (SD), mmol/L	4.7 ± 1.0	4.7 ± 1.1	4.4 ± 0.8	0.476
Serum calcium, mean (SD), mmol/L	1.9 ± 0.5	1.9 ± 0.5	2.0 ± 0.3	0.776
Serum phosphorus, mean (SD), mmol/L	1.5 ± 0.8	1.5 ± 0.7	1.5 ± 1.1	0.983
Serum cytokine levels				
IL-1b, median (IQR), pg/mL	14.9 [7.9–18.3]	15.3 [8.4–19.7]	11.3 [3.0–16.7]	0.199
IL-6, median (IQR), pg/mL	72.9 [17.5–142.7]	95.6 [17.6–191.7]	33.9 [10.0–79.8]	0.503
IFN-γ, median (IQR), pg/mL	149.4 [79.0–272.8]	203.6 [99.7–268.8]	80.9 [27.1–445.6]	0.423
TNF-α, median (IQR), pg/mL	17.9 [4.5–155.6]	16.2 [4.6–112.8]	54.4 [2.1–205.6]	1.000
IL-10, median (IQR), pg/mL	4.2 [1.2–13.7]	4.3 [1.2–13.1]	4.2 [0.9–15.9]	0.682
Serum or plasma DAMPs levels				
HSP70, median (IQR), ng/mL	34.4 [14.2–124.4]	34.7 [14.7–128.2]	32.6 [9.6–129.6]	0.110
HMGB1, median (IQR), pg/mL	838.5 [666.2–1013.1]	836.1[653.8–1001.8]	902.0 [678.7–1160.9]	0.607
MtDNA, mean (SD), $\log_{10}$ copies/mL				
ND2	6.9 ± 0.5	7.0 ± 0.4	6.8 ± 0.5	0.212
D-loop	6.5 ± 0.7	6.5 ± 0.7	6.5 ± 0.7	0.927
NDNA, mean (SD), log10 copies/mL				
GAPDH	4.2 ± 0.5	4.2 ± 0.4	4.1 ± 0.6	0.483
β-globin	3.8 ± 0.5	3.8 ± 0.5	3.7 ± 0.6	0.746

(Continued)

TABLE 1 | Continued

Characteristics	CVVH patients			*P*-value
	Total ($n = 43$)	Sepsis ($n = 33$)	Non-sepsis ($n = 10$)	
Urinary DAMPs levels, mean (SD), log_{10} copies/mL				
ND2	7.9 ± 0.5	7.9 ± 0.5	7.8 ± 0.6	0.663
D-loop	7.8 ± 0.8	7.9 ± 0.5	7.4 ± 1.4	0.384
GAPDH	4.5 ± 0.9	4.6 ± 1.0	4.2 ± 0.8	0.389
β-globin	4.5 ± 1.0	4.6 ± 1.1	4.1 ± 0.9	0.262
OUTCOMES				
Hospital LOS, median (IQR), d	24.0 [13.5–41.0]	24.0 [13.8–46.5]	24.0 [12.0–32.0]	0.321
ICU LOS, median (IQR), d	15.0 [10.0–25.5]	20.5 [11.5–27.8]	12.0 [7.0–11.0]	0.418
Duration of mechanical ventilation, median (IQR), d	9.0 [0.0–23.5]	12.5 [2.5–32.0]	0.0 [0.0–9.0]	**0.005**
Duration of non-CVVH, median (IQR), d	16.0 [5.5–25.5]	16.0 [4.0–28.3]	8.0 [17.0–23.0]	**0.006**
Duration of (any) vasopressor, median (IQR), d	1.0 [0.0–8.0]	2.0 [0.0–10.5]	0.0 [0.0–5.0]	**0.000**
Hospital mortality, *n* (%)	25 (58.1)	22 (66.7)	3 (30.0)	**0.046**
28-day mortality, *n* (%)	16 (37.2)	14 (42.4)	2 (20.0)	0.233
SITE OF INFECTION, *n* (%)				
Lung		14 (42.4)		
Abdomen		15 (45.5)		
Catheter		3 (9.1)		
Unknown		1 (3.0)		

BMI, body mass index; APACHE, Acute Physiology and Chronic Health Evaluation; SOFA, Sepsis-related Organ Failure; CVVH, continuous veno–venous hemofiltration; BUN, blood urea nitrogen; eGFR, estimated glomerular filtration; NGAL, neutrophil gelatinase-associated lipocalin; ALT, Alanine aminotransferase; AST, Aspartate amino transferase; CRP, C-reaction protein; PCT, procalcitonin; RBC, red blood cell; PLT, platelet; APTT, activated partial thromboplastin time; PT, prothrombin time; DAMPs, Damage-Associated Molecular Patterns; mtDNA, mitochondrial DNA; nDNA, nuclear DNA; HSP70, Heat Shock Protein 70; HMGB1, high-mobility group box 1 protein; INR, International Normalized Ratio; LOS, length of stay; ICU, Intensive care unit; IQR, interquartile range; SD, standard deviation.

Normally distributed data are presented as the mean (SD) (analysis of variance); non-normally distributed data are presented as median (IQR) (nonparametric Mann–Whitney U-tests); and categorical variables are presented as n (%) (chi-square test). Data in bold reflected P values < 0.05.

The levels of cytokines were measured from the inlet and outlet of the CVVH dialyzer at baseline, 6, and 12 h after initiation of CVVH to evaluate the effect of CVVH on cytokine removal. Only the levels of IL-6 and TNF-α were decreased in the AKI with sepsis group ($P = 0.046$ and $P = 0.008$, respectively) (**Figure 2A**). There was no difference in the levels of all measured cytokines between the inlet and outlet, regardless of the presence or absence of sepsis in AKI patients (**Figure 2B**). Furthermore, the levels of circulating cytokines were similar between the surviving and non-surviving AKI patients with sepsis (**Figure 2C**).

Circulating and Urinary Levels of DAMPs During CVVH

The circulating levels of DAMPs, including mtDNA (*ND2, D-loop*), nDNA [*glyceraldehyde 3-phosphate dehydrogenase (GAPDH), β-globin]*, HSP70, and HMGB1, were measured at the same time points as those used for the measurement of cytokine levels. All plasma samples exhibited detectable levels of DAMPs. In the first 12 h after initiation of CVVH, the levels of mtDNA were increased in all AKI patients, regardless of the presence or absence of sepsis (*ND2*: $P = 0.035$; *D-loop*: $P = 0.003$; **Figure 3A**, **Figure S2**). The level of HSP70 in the plasma was reduced in both AKI patients with sepsis ($P = 0.000$) and without sepsis ($P = 0.001$). However, this trend was particularly apparent in the former group. The levels of nDNA in the plasma, including *GAPDH*, *β-globin*, and HMGB1 were unaltered during the first 12 h (**Figure 3A**, **Figure S2**). In brief, the tendency of change in the levels of DAMPs during CVVH was similar between the sepsis and non-sepsis group.

In addition, we compared the levels of DAMPs between the inlet and outlet of the dialyzer at the same time points to determine the effect of CVVH on the rates of DAMP clearance. We did not find differences between the inlet and outlet data in the sepsis or non-sepsis group, except an increase in the level of *ND2* after blood passage through the filter in non-sepsis group (inlet: 7.08 ± 0.40 log_{10} copies/mL; outlet: 7.24 ± 0.41 log_{10} copies/mL; $P = 0.008$) (**Figure 3B**). We further divided the patients with sepsis into a survivor and non-survivor group. The circulating concentrations of DAMPs, including mtDNA, nDNA, HSP70, and HMGB1, were increased in the survivor group after blood passage through the dialyzer (**Figure 3C**, **Figure S2**). Notably, the levels of HMGB1 were decreased significantly in the non-survivor group (**Figure 3C**).

In our previous study, we demonstrated the effectiveness of using the urinary levels of mtDNA as evidence of renal mitochondrial injury induced by AKI after sepsis. Thus, we measured the urinary levels of NGAL and cf-DNA at baseline and end of CVVH to evaluate renal function. The urinary levels of nDNA and mtDNA were reduced after CVVH (**Figure 4**), unlike that of NGAL (despite an observed increasing trend, *P*

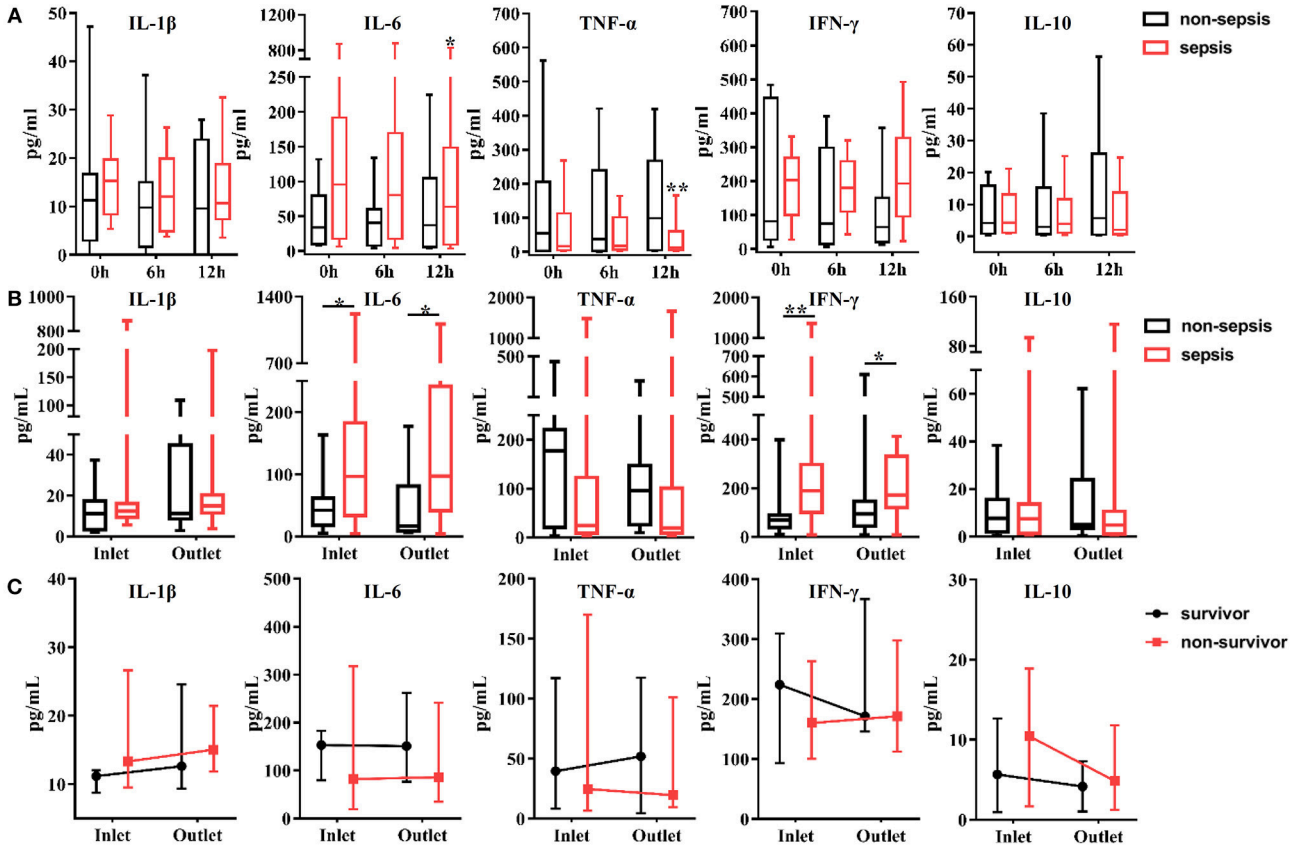

FIGURE 2 | Effects of continuous veno-venous hemofiltration (CVVH) on levels of circulating cytokines. Cytokines, including IL-1b, IL-6, IFN-γ, TNF-α, and IL-10 were measured at baseline, 6, 12 h of CVVH from inlet and outlet of the filter. **(A)** Tendency of cytokines levels during the first 12 h was analyzed by repeated measure ANOVA in sepsis and non-sepsis groups, respectively. **(B)** Serum levels of cytokines at inlet and outlet in sepsis and non-sepsis groups (Median, IQR). **(C)** Comparisons of serum levels of cytokines between inlet and outlet in survived or non-survived septic patients. Data are presented as median and interquartile range. Error bars of the line chart denote the median with IQR. *P*-values indicating differences between the patients of two groups were calculated using Mann–Whitney *U*-tests. $^{*}P < 0.05$, $^{**}P < 0.01$. IFN, interferon; IL, interleukin; TNF, tumor necrosis factor; CVVH, continuous veno-venous hemofiltration; IQR, interquartile range.

= 0.257), regardless of the presence or absence of sepsis in AKI patients. Consistently, clinical indicators for the evaluation of renal function (i.e., serum creatinine, blood urea nitrogen, and estimated glomerular filtration) were also reduced following treatment with CVVH (**Figure S1**). Therefore, CVVH may (at least partly) improve renal function.

Relationship Between the Clearance Rate of DAMPs, Level of mHLA-DR, and Outcomes

To further investigate the effect of DAMP removal in AKI patients with sepsis, we calculated their clearance rate and assessed its association with the outcome and immune state. The clearance rate is similar to the meaning of the creatinine clearance rate in the kidney, which represents the net result of the production and clearance rates of the molecules. Thus, its value depends on the integrated effects of production by the cells and clearance by the filter. Higher values indicate high clearance rates vs. production rates.

In the present study, the clearance rates of *β-globin*, HSP70, and HMGB1 were higher in all non-surviving AKI patients with sepsis ($P = 0.006$, $P = 0.005$, and $P = 0.000$, respectively) (**Figure 5**). Furthermore, we performed analyses of ROC curves to determine predictors of mortality (**Table S1**), including the circulating levels of DAMPs as well as the clearance rates of cytokines and DAMPs. The clearance rates of HSP70, HMGB1, and *β-globin* were good predictors of mortality (**Figure 6**). Analyses of the area under the curve (AUC) of ROC curves showed that the clearance rate of *β-globin* was similar to that of the APACHE II score at baseline. Notably, the clearance rates of HSP70 and HMGB1 exhibited a similar prediction efficiency to that of the SOFA score at baseline. Consistent with these findings, the Kaplan–Meier survival analysis revealed that patients with higher HSP70 or HMGB1 clearance rate were associated with significantly higher risk of mortality than those with lower clearance rate (log-rank test: $P = 0.000$ for both) (**Figure 7**).

In addition, we measured the level of mHLA-DR—an indicator of the immune state—at 0, 3, and 7 days after initiation of CVVH to evaluate the immune state of the patients. We found

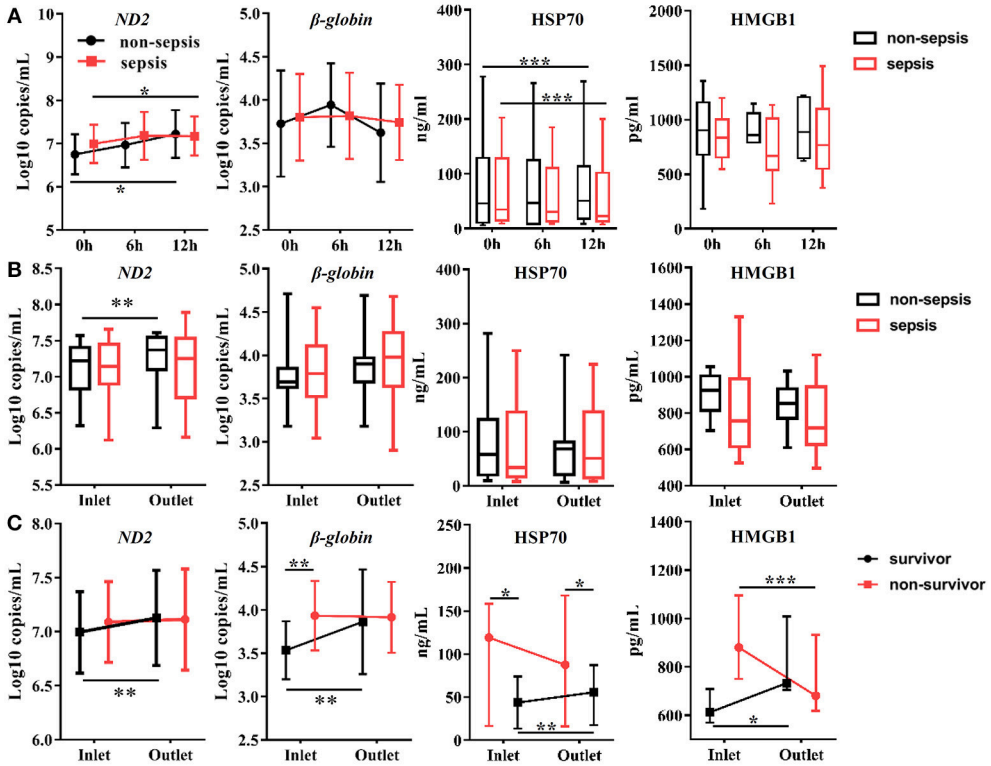

FIGURE 3 | Effects of CVVH on levels of circulating Damage-Associated Molecular Patterns (DAMPs). DAMPs, including mitochondrial DNA (*ND2*), nuclear DNA (*β-globin*), HSP70, and HMGB1, were measured at baseline, 6, 12 h of CVVH from inlet and outlet of filter. **(A)** Tendency of DAMPs levels during the first 12 h was analyzed by repeated measure ANOVA in sepsis and non-sepsis groups, respectively. Error bars of the line chart denote the mean with SD. **(B)** Box plots shown the levels of DAMPs at inlet and outlet in sepsis and non-sepsis groups. **(C)** Comparisons of mean levels of mtDNA and nDNA, and levels of HSP70 and HMGB1 (median ± IQR) between inlet and outlet in survived or non-survived septic patients. Comparison of continuous variables between the two groups was conducted with the Student's *t*-test or Mann–Whitney *U*-test depending on Gaussian distribution. $^{*}P < 0.05$, $^{**}P < 0.01$, $^{***}P < 0.001$. DAMPs, damage-associated molecular patterns; mtDNA, mitochondrial DNA; nDNA, nuclear DNA; HSP70, heat shock protein 70; HMGB1, high-mobility group box 1 protein; CVVH, continuous veno-venous hemofiltration.

no difference in the level of mHLA-DR expression between AKI patients with sepsis and those without sepsis (median ± IQR) (**Figure 8A**). However, the level of mHLA-DR was increased in AKI patients with sepsis who expired ($P = 0.05$) (**Figure 8B**). To ascertain the relationship between the clearance rate of DAMPs and the change in the level of mHLA-DR in AKI patients with sepsis, we classified patients into two groups based on the cut-off value of DAMPs (**Figures 8C–E**). Interestingly, the level of mHLA-DR was significantly increased in patients with higher *β-globin* and HSP70 clearance rates than the cut-off value ($P = 0.02$ and $P = 0.006$, respectively). Similarly, there was a tendency toward increase in the level of mHLA-DF in patients with higher HMGB1 clearance rate than the cut-off value ($P = 0.074$). In addition, the level of HMGB1 at the outlet was negatively related with the level of mHLA-DR (Spearman rank correlation coefficient $= -0.512$, $P = 0.013$) (**Figure 8F**).

Multivariate Logistic Regression Analysis

We performed univariate and multivariate logistic regression analyses to examine other baseline or disease-related factors and evaluate the contribution of the clearance rates of *β-globin*, HSP70, or HMGB1 to mortality. These analyses revealed that only the clearance rate of HSP70 remained independently associated with high mortality after adjustment for age, APACHE II score, SOFA score, urine output, level of total bilirubin, and coagulation indicators [odds ratio (OR): 1.025; 95% confidence interval (CI): 1.012–1.039; $P = 0.000$] (**Table 2**).

In addition, we analyzed the contribution of the urinary levels of DAMPs to the duration of CVVH. The urinary level of *β-globin* was an independent factor for the duration of CVVH even after adjustment for age, APACHE II score, SOFA score, urine output, level of creatinine in the serum, estimated glomerular filtration rate, and level of blood urea (standardization regression coefficient: 0.460; 95% CI: 1.720–8.857, $P = 0.005$) (**Table 3**).

DISCUSSION

This was the first study to evaluate the efficiency of CVVH for the removal of DAMPs and the effects of this removal. Our study demonstrated three key findings. Firstly, the newly identified urinary indicators of renal injury (i.e., mtDNA and

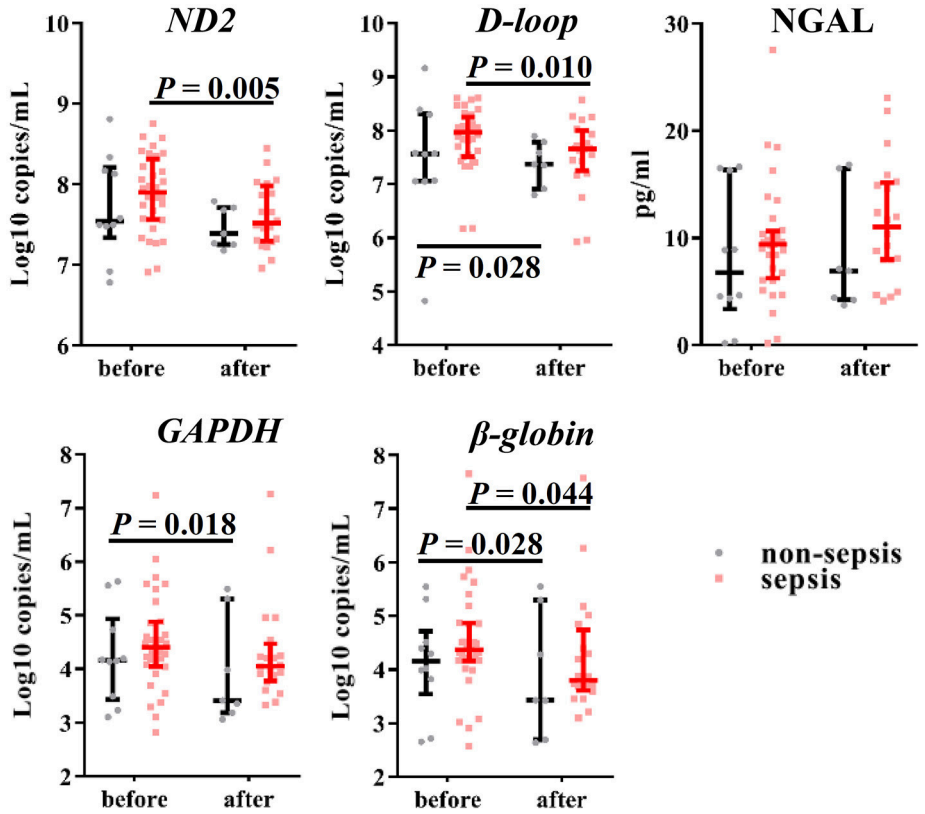

FIGURE 4 | Effects of CVVH on levels of urinary mtDNA, nDNA and NGAL. Mitochondrial DNA (*ND2, D-loop*), nuclear DNA (*GAPDH, β-globin*) and NGAL in urine were measured at baseline and end of CVVH. Error bars denote the median and interquartile range. *P*-values indicating differences between the patients of two groups were calculated using Mann–Whitney *U*-tests. mtDNA, mitochondrial DNA; nDNA nuclear DNA; NGAL, neutrophil gelatinase-associated lipocalin; CVVH, continuous veno-venous hemofiltration.

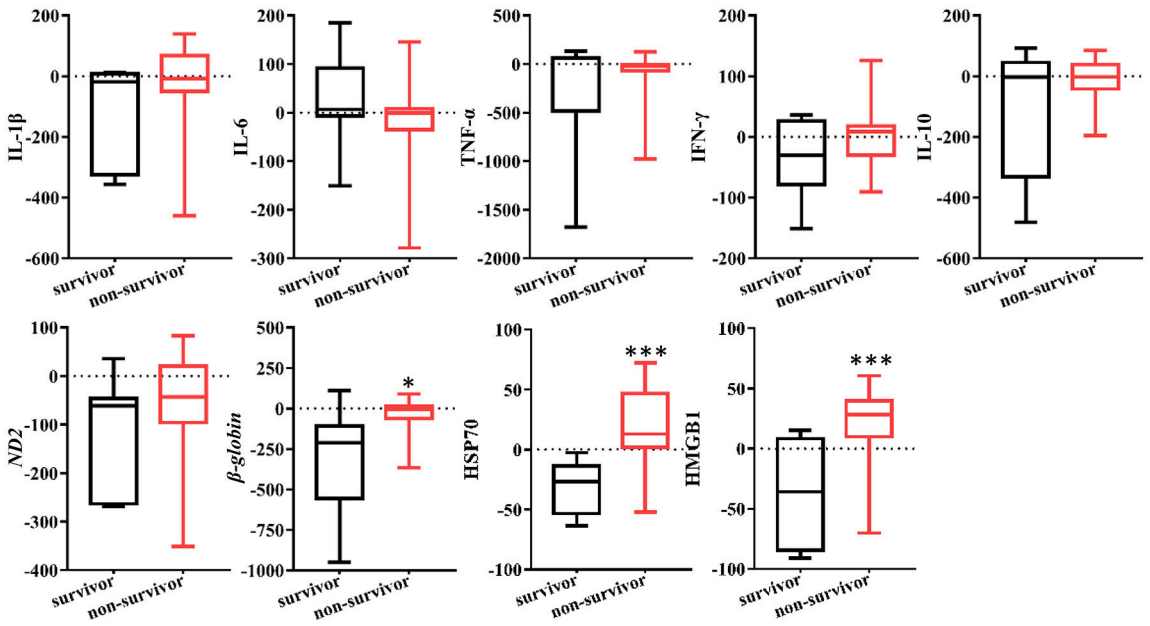

FIGURE 5 | Clearance rate of cytokines and DAMPs in survived or non-survived septic patients. Box plots showed the levels of cytokines and DAMPs clearance rate AKI patients with sepsis. *P*-values indicating differences between the patients of two groups were calculated using Mann–Whitney *U*-tests. $^{*}P < 0.05$, $^{***}P < 0.001$. IFN, interferon; IL, interleukin; TNF, tumor necrosis factor; HSP70, heat shock protein 70; HMGB1, high-mobility group box 1 protein.

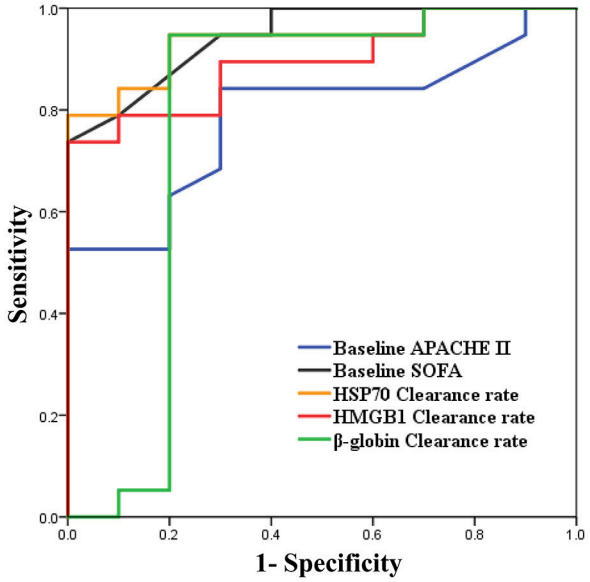

Variables	AUC	*P* value	95% CI
***β-globin* clearance rate**	0.78	0.015	0.54-1.00
Baseline APACHE II	0.79	0.012	0.62-0.95
Baseline SOFA	**0.95**	0.000	0.87-1.00
HSP70 clearance rate	**0.94**	0.000	0.85-1.00
HMGB1 clearance rate	**0.90**	0.001	0.78-1.00

FIGURE 6 | Receiver Operating Characteristic curves (ROC) of the HSP70, HMGB1, and *β-globin* clearance to predict hospital mortality. ROC curve of the mean of *β-globin* clearance rate and HMGB1 clearance rate, and HSP70 clearance rate, and baseline APCHE II, SOFA score. AUC, area under curve; CI, confidence interval; APACHE, Acute Physiology and Chronic Health Evaluation; SOFA, Sepsis-related Organ Failure; CVVH, continuous veno-venous hemofiltration; HSP70, heat shock protein 70; HMGB1, high-mobility group box 1 protein.

nDNA) recovered after CVVH and the level of urinary nDNA was an independent prognostic factor for the duration of CVVH. Secondly, the efficiency of CVVH for the removal of cytokines and DAMPs was variable. The levels of IL-6, TNF-α, and HSP70 decreased within the first 12 h of CVVH in AKI patients with sepsis, whereas the levels of DAMPs at the outlet were temporarily increased after blood passage from the inlet through the dialyzer in survivor AKI patients with sepsis. Finally, the higher clearance rate of DAMPs (especially HSP70) was significantly associated with poor outcomes and immune disorders.

CRRT is undoubtedly beneficial for patients with lethal electrolyte abnormalities, renal dysfunction, or liver dysfunction (15). In our previous study, we demonstrated that the urinary levels of nDNA and mtDNA are novel biomarkers of AKI, and may be used as evidence of renal mitochondrial injury induced by AKI after sepsis (10). Our results revealed that the urinary levels of nDNA and mtDNA decreased after CVVH in all patients, and urinary nDNA (*β-globin*) was an independent prognostic factor for the duration of CVVH. Furthermore, we observed improvement in the indices of renal and liver function, especially the levels of creatinine in the serum, blood urea, and liver enzymes. Therefore, we infer that CVVH may (at least partly) improve kidney injury in terms of histopathology. Nevertheless, the 24-h urinary volume did not recover during CVVH in patients who eventually expired. Perez-Fernandez et al. also emphasized that a low urine output was associated with poor outcome in AKI patients with sepsis (22). Considering that the urine output was also dependent on the circulatory function, persistently low urine output may be mainly due to disease progression-induced disturbances in microcirculation.

Our previous research revealed that the concentration of cf-DNA increased in patients with severe disease (20). Accordingly, we found that the level of nDNA correlated with prognosis. In addition, in surviving AKI patients with sepsis, the concentrations of DAMPs were markedly increased after blood passage through the inlet of the dialyzer, but declined or recovered prior to the subsequent sampling time point. DAMPs were detected in the filtrate (data not shown), suggesting that clearance through CVVH was reliable. However, in non-survivors, the level of DAMPs remained high. These results suggest defects in the elimination of DAMPs in non-survivors.

Although studies reported that the levels of IL-6 and TNF-α decreased with time (6), there is currently no consensus to guide clinicians in terms of controlling the levels of inflammation and DAMPs in AKI patients with sepsis managed through CRRT. This may be attributed to a lack of evidence and deep insight into the effects of CRRT on the human body (23).

In this study, there was no correlation between cytokine clearance and mortality. Chung et al. also showed that high-volume hemofiltration did not reduce mortality compared with standard treatment, despite the extensive removal of pro-inflammatory cytokines in patients treated with high-volume hemofiltration (17). Park et al. also performed a randomized controlled trial, demonstrating that a high dose of CVVH (80 mL/kg/h) did not improve outcomes in sepsis-associated AKI patients despite its considerable effect on the removal of pro-inflammatory cytokines (16). Thus, CRRT-induced changes in the levels of cytokines may not be sufficient to influence clinical endpoints. Moreover, in recent years, a new concept termed "dialysis trauma" suggests that dialysis involves microcirculation (24). Our findings suggest that elimination of DAMPs worsened the outcome in AKI patients with sepsis undergoing CVVH. The net outcome is dependent on a balance of the detrimental effects vs. the protective effects of CVVH. This may explain the inadequacy of CRRT-induced changes in the levels of pro-inflammatory factors to influence clinical outcomes.

Several studies have investigated the roles of DAMPs in critical-care illness and sepsis (6, 25, 26). However, there are no studies addressing the clearance rate of DAMPs in CVVH and its effects on the outcomes and immune homeostasis. In this study, data revealed that there was no difference between patients with or without sepsis. Thus, we excluded the effect of

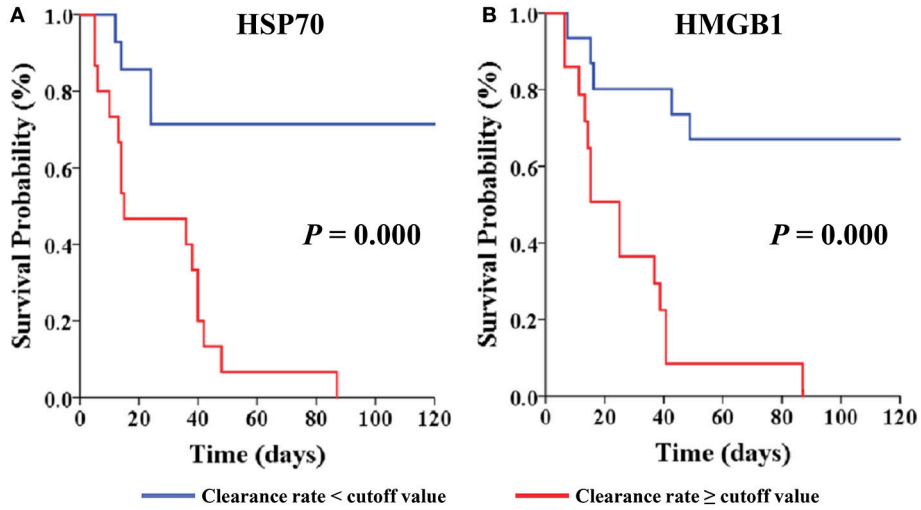

FIGURE 7 | Kaplan-Meier Survival by cut-off value of clearance rate for the AKI with septic patients. Patients are stratified by cut-off value of HSP70 clearance rate **(A)** and HMGB1 clearance rate **(B)**. Patients were censored from survival analysis after discharge. HSP70, heat shock protein 70; HMGB1, high-mobility group box 1 protein.

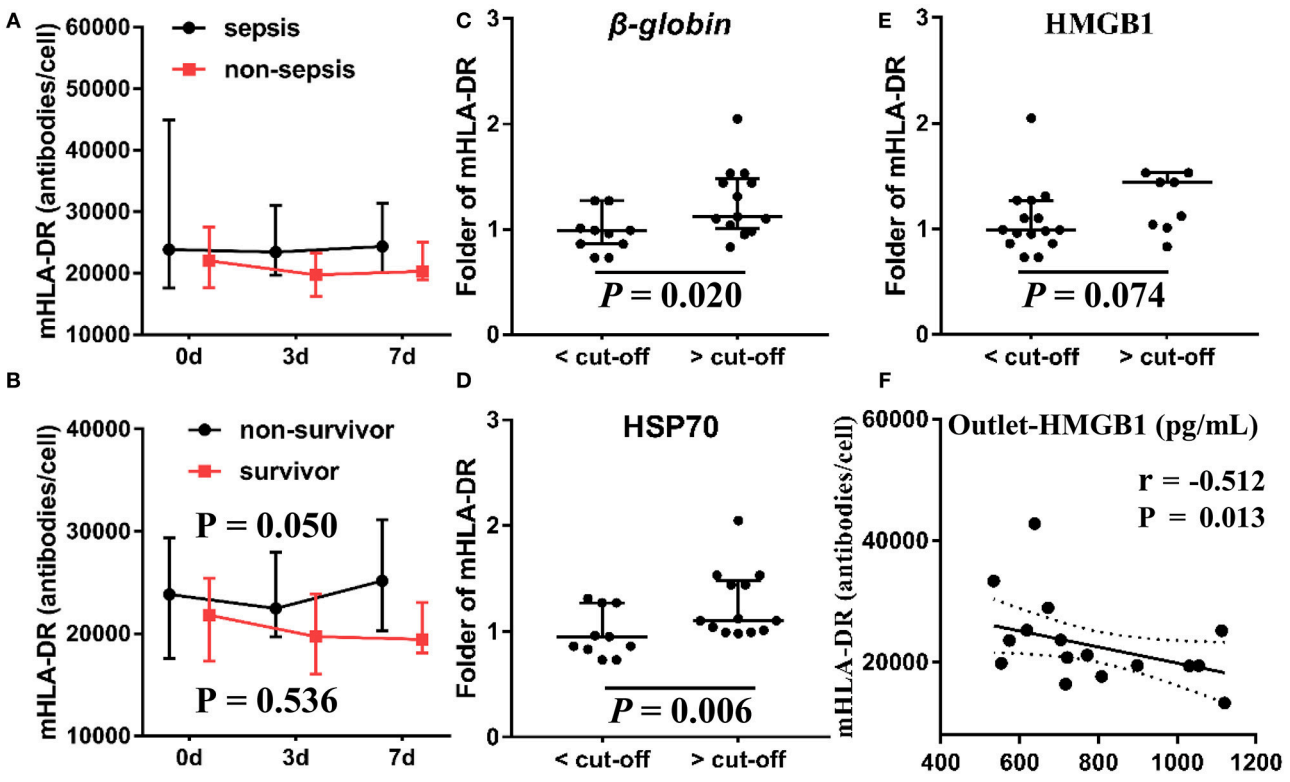

FIGURE 8 | Association between mHLA-DR, outcome and DAMPs clearance. The levels of mHLA-DR were inspected at baseline, 3, 7 day after the CVVH initiation. Tendency of mHLA-DR changes (median ± IQR) was analyzed by repeated measure ANOVA in sepsis and non-sepsis groups **(A)** or survived and non-survived septic patients **(B)** The subjects were divided into two groups based on the cut-off value of the clearance rates of *β-globin* **(C)**, HSP70 **(D)**, and HMGB1 **(E)** to compare the difference of mHLA-DR fold change on day 7 after CVVH initiation, *P*-values indicating differences between the patients of two groups were calculated using Mann–Whitney *U*-tests. **(F)** Correlations between the levels of mHLA-DR on 7 day and the level of HMGB1 at outlet were determined using Spearman correlation test. CVVH, continuous veno-venous hemofiltration; DAMPs, damage-associated molecular patterns; mHLA-DR, mononuclear human leukocyte antigen-DR; HSP70, heat shock protein 70; HMGB1, high-mobility group box 1 protein.

TABLE 2 | Mortality prediction and HSP70 removed amount rate on CVVH.

	Logistic regression		
	***P*-value**	**Odds ratio**	**95% CI**
Clearance of HSP70 unadjusted	0.000	1.067	1.032–1.103
Adjusted for age and APACHE II score	0.001	1.068	1.027–1.110
Adjusted for age, APACHE II score, SOFA score, 24h urine output, eGFR and PLT count	0.000	1.028	1.014–1.042
Adjusted for age, APACHE II score, SOFA score, 24h urine output, CRP, eGFR, PLT count, APTT and total bilirubin	0.000	1.025	1.012–1.039

APACHE, Acute Physiology and Chronic Health Evaluation; SOFA, Sepsis-related Organ Failure; eGFR, estimated glomerular filtration; CRP C, reaction protein; PLT, platelet; APTT, activated partial thromboplastin time.

TABLE 3 | Prediction for duration of CVVH.

	Linear regression		
	***P*-value**	**sRE**	**95% CI**
Urinary *β-globin* level before the CVVH initiation unadjusted	0.005	0.481	1.774–9.291
Adjusted for age and APACHE II score	0.005	0.481	1.774–9.421
Adjusted for age, APACHE II score, SOFA score, 24h urine output	0.005	0.460	1.720–8.857
Adjusted for age, APACHE II score, SOFA score, 24h urine output, serum creatinine, eGFR and blood urea	0.005	0.460	1.720–8.857

sRE, standardization regression coefficient; CVVH, continuous veno–venous hemofiltration; APACHE, Acute Physiology and Chronic Health Evaluation; SOFA, Sepsis-related Organ Failure; eGFR, estimated glomerular filtration.

the disease on DAMPs and cytokines during the first 12 h of CVVH. Furthermore, we compared the difference between the non-survivors and survivors in the sepsis group. A higher level of mHLA-DR was linked to higher mortality. In our study, AKI patients with sepsis who expired had markedly higher levels of mHLA-DR than patients in other studies (27, 28). The mHLA-DR is currently the "gold standard" for the identification of immunosuppression and participates in antigen presentation and perpetuation of the inflammatory reaction (29, 30). Hence, a higher level of mHLA-DR may reflect excessive immune activation. Accordingly, we demonstrated that the clearance rates of HSP70 and HMGB1 were higher in AKI patients with sepsis who expired. The clearance rates of HSP70 and HMGB1 increase in parallel with the level of mHLA-DR, indicating that the levels of DAMPs may play an anti-inflammatory role. Consistently, several studies have demonstrated that DAMPs may induce immune suppression and regulate immune response. This has been specifically described for HMGB1 (31, 32) and HSP70 (33, 34). Scholars have demonstrated that the extracellular levels of HSP70 activate and suppress the immune response *via* the paired receptors sialic acid-binding immunoglobulin-like lectins Siglec-5 and Siglec-14 (34–36). Thus, excessive removal of HSP70 during CVVH may amplify the inflammatory process, disrupt immune homeostasis, and exacerbate disease.

Timmermans et al. reported that, in trauma patients, released DAMPs are associated with an acute, predominantly anti-inflammatory response, and a suppressed state of the immune system (28). Schafer et al. also demonstrated that mtDNA may be a link between initial inflammation and subsequent immunosuppression in critically ill patients, probably through a Toll-like receptor-9 pathway (37). Leijte et al. (38) have shown that increased levels of plasma DAMPs were associated with immune suppression and post-operative infections in patients undergoing cytoreductive surgery and hyperthermic intraperitoneal chemotherapy. Our results showed that extensive clearance of DAMPs was associated with an extremely high level of mHLA-DR expression and higher mortality. Collectively, these results imply that DAMPs, especially HSP70 and HMGB1, may act as anti-inflammatory molecules involved in the modulation of the immune system. Excessive removal of these molecules during CVVH may exacerbate disease and amplify the inflammatory process. Consequently, patients may expire due to an exaggerated inflammatory response at the early stage of sepsis.

This study had several shortcomings. Firstly, the patient population was small. Further, studies with larger samples are warranted to confirm the present results. Although the sample size of this study was small, our novel findings are important for the management of AKI patients with sepsis in the clinical setting. Secondly, we did not compare the different modes of RRT (e.g., high dose vs. conventional dose) or the types of filtration membrane. Hence, we were unable to reach a conclusion regarding the preferred type of membrane or mode of CRRT. Nevertheless, the process of CVVH was consistent throughout the study period, avoiding potential confounders. In addition, we did not investigate sepsis patients who were not treated with CVVH. It is not possible to calculate the clearance rate in a non-CVVH group. Moreover, the pathophysiological mechanisms of sepsis in the absence of CVVH are different from those involved in the population of the present study, regardless of disease severity. Consequently, an investigation of differences between the outcomes of sepsis patients with or without CVVH would be meaningless. Thirdly, there were

confounders (e.g., early initiation of antibiotic therapy, source control, and vasopressor support) in our study during CVVH. However, we collected the samples during the first 12 h to avoid the influence of other long-term treatments on the clearance rate. Continuous monitoring of clinical data showed that disease severity was similar during the first day of CVVH. In addition, several studies have suggested that the nDNA level is linked to disease severity (39) and our data showed that the circulating levels of nDNA during the first 12 h of CVVH were almost constant. Thus, these clinical confounders did not influence the conclusions of this study. Fourthly, there was a lack of data regarding the long-term impact of changes in the levels of DAMPs on the levels of mHLA-DR and prognosis.

Despite the aforementioned limitations, our study has important implications for clinicians. Mortality among patients in the intensive care unit remains high, despite the latest advances and innovations in CRRT (17). Most of the researchers and physicians are focused on the role of CRRT in reducing the levels of cytokines. However, despite the extensive removal of pro-inflammatory cytokines in the high-volume hemofiltration (HVHF) groups, CRRT did not reduce mortality compared with standard treatment (16). Our results indicated that extensive removal of DAMPs during CVVH was associated with poor prognosis, which may neutralize the beneficial effect of this treatment. Therefore, it is imperative to develop new filtration membranes–with improved biocompatibility to reduce the stress of circulatory cells–and individualized hemofiltration strategies by monitoring the change in the levels of DAMPs. Collectively, we do not recommend the use of CVVH merely for the removal of pro-inflammatory factors in the treatment of sepsis due to the complex effects of CVVH on DAMPs. In addition, extensive elimination of DAMPs may intensify the immune imbalance in patients with sepsis. This hypothesis is consistent with the recommendations included in the guidelines of the 2016 Surviving Sepsis Campaign (23). An advanced understanding of the host response during CVVH is necessary to optimize hemofiltration, shorten the course of AKI, reduce injury to distant organs, and improve survival.

CONCLUSIONS

The urinary levels of mtDNA and nDNA recovered after CVVH, and the level of nDNA was an independent prognostic factor for the duration of CVVH. These findings indicated that CVVH can alleviate kidney injury. However, the efficiency of CVVH for the removal of cytokines and DAMPs was variable and complex. The circulating levels of DAMPs were rapidly and temporarily increased after blood–obtained from surviving AKI patients with sepsis–passaging through the dialyzer. The levels of HSP70 and HMGB1 decreased in AKI patients with sepsis who expired. Moreover, the higher clearance rate of DAMPs, especially HSP70 and HMGB1, was significantly associated with immune disorders and poor prognosis. Thus, we do not recommend the use of CVVH in AKI patients with sepsis merely for the removal of inflammatory mediators without other definitive indications for CVVH.

DATA AVAILABILITY

The datasets analyzed during the present study are available from the corresponding author on reasonable request.

AUTHOR'S NOTE

All authors are employees of the Department of Surgery, Jinling Hospital, 305 East Zhongshan Road, Nanjing, 210002, China. An abstract of these data has been accepted as an oral presentation at the 38th Annual Meeting of the Surgical Infection Society.

AUTHOR CONTRIBUTIONS

JW, JR, and XW conceived the study and interpreted the results. JR designed the study. JW, QL, QH, and ZH acquired the data. JW wrote the manuscript. All authors contributed to the study design and manuscript preparation, and read and approved the final manuscript.

FUNDING

The study was supported by the National Natural Science Foundation of China (81571881, 81772052) and Key Project of Jiangsu Social Development (BE2016752). Youth Project of the Natural Science Foundation of Jiangsu Province (BK20150559). The funding bodies did not play a role in the design, analysis, or interpretation of data in this study.

ACKNOWLEDGMENTS

We thank The Charlesworth Group for editorial assistance.

SUPPLEMENTARY MATERIAL

The Supplementary Material for this article can be found online at: https://www.frontiersin.org/articles/10.3389/fimmu.2018.03052/full#supplementary-material

Figure S1 | Tendency of change in clinical data under CVVH in survived and non-survived septic AKI patients. Twenty-four clinical indexes, including blood routine, liver function, renal function, electrolyte concentration, and coagulation function, etc. were collected every day during the first 7 days after CVVH initiation to form the line chart. The values at "After" denotes the indexes were acquired within 1 day of termination of CVVH treatment. [a]Tendency of change was significant in total patients ($P < 0.05$). [#]Tendency was significant different between survived and non-survived sepsis patients ($P < 0.05$). [Δ]The difference between before and after CVVH were significant distinct between survived and non-survived groups ($P < 0.05$). *The values were significant different between survived and non-survived groups after finished CVVH treatment ($P < 0.05$). BUN, blood urea nitrogen; eGFR, estimated glomerular filtration; ALT, Alanine aminotransferase; AST, Aspartate amino transferase; CRP, C-reaction protein; PCT, procalcitonin; RBC, red blood cell; PLT, platelet; APTT, activated partial thromboplastin time; PT, prothrombin time; INR, International Normalized Ratio.

Figure S2 | Effects of CVVH on *D-loop* (mtDNA) and *GAPDH* (nDNA) level and the clearance rate of them. Mitochondrial DNA (*D-loop*), nuclear DNA (*GAPDH*) were measured at baseline, 6, 12 h of CVVH at inlet and outlet. **(A)** Tendency of their levels during the first 12 h was analyzed by repeated measure ANOVA in sepsis and non-sepsis groups, respectively. Error bars of the line chart denote the mean with SD. **(B)** Box plots shown the levels of DAMPs at inlet and outlet in sepsis and non-sepsis groups. **(C)** Comparisons of mean levels of mtDNA and nDNA in survived or non-survived septic patients. **(D)** Box plots shown the levels of clearance rate (median ± IQR) in survived or non-survived septic patients. $*P < 0.05$, $**P < 0.01$, $P < 0.001$. DAMPs, damage-associated molecular patterns; mtDNA, mitochondrial DNA; nDNA, nuclear DNA; CVVH, continuous veno-venous hemofiltration; IQR, interquartile range.

Table S1 | Receiver Operating Characteristic curves (ROC) of the clearance of DAMPs and cytokines to predict hospital mortality. Fold front denotes the significance of ROC analysis was <0.05. The cut-off values and corresponding sensitivity and specificity were calculated based on Youden index. IFN, interferon; IL, interleukin; TNF, tumor necrosis factor; DAMPs, Damage-Associated Molecular Patterns; mtDNA, mitochondrial DNA; nDNA, nuclear DNA; HSP70, Heat Shock Protein 70; HMGB1, high-mobility group box 1.

REFERENCES

1. Singer M, Deutschman CS, Seymour CW, Shankar-Hari M, Annane D, Bauer M, et al. The third international consensus definitions for sepsis and septic shock (Sepsis-3). *J Am Med Assoc*. (2016) 315:801–10. doi: 10.1001/jama.2016.0287
2. Bagshaw SM, George C, Bellomo R, Committee ADM. Early acute kidney injury and sepsis: a multicentre evaluation. *Crit Care* (2008) 12:R47. doi: 10.1186/cc6863
3. Kolhe NV, Stevens PE, Crowe AV, Lipkin GW, Harrison DA. Case mix, outcome and activity for patients with severe acute kidney injury during the first 24 hours after admission to an adult, general critical care unit: application of predictive models from a secondary analysis of the ICNARC Case Mix Programme database. *Crit Care* (2008) 12 (Suppl. 1):S2. doi: 10.1186/cc7003
4. Quinto BM, Iizuka IJ, Monte JC, Santos BF, Pereira V, Durao MS, et al. TNF-alpha depuration is a predictor of mortality in critically ill patients under continuous veno-venous hemodiafiltration treatment. *Cytokine* (2015) 71:255–60. doi: 10.1016/j.cyto.2014.10.024
5. Marx D, Metzger J, Pejchinovski M, Gail RB, Frantzi M, Latosinska A, et al. Proteomics and metabolomics for AKI diagnosis. *Semin Nephrol*. (2018) 38:63–87. doi: 10.1016/j.semnephrol.2017.09.007
6. Simmons JD, Lee YL, Mulekar S, Kuck JL, Brevard SB, Gonzalez RP, et al. Elevated levels of plasma mitochondrial DNA DAMPs are linked to clinical outcome in severely injured human subjects. *Ann Surg.* (2013) 258:591–6. doi: 10.1097/SLA.0b013e3182a4ea46
7. Jaber BL, Pereira BJ. Extracorporeal adsorbent-based strategies in sepsis. *Am J Kidney Dis.* (1997) 30 (5 Suppl. 4), S44–56.
8. Rajaee A, Barnett R, Cheadle WG. Pathogen- and danger-associated molecular patterns and the cytokine response in sepsis. *Surg Infect.* (2018) 19:107–16. doi: 10.1089/sur.2017.264
9. Jansen MPB, Pulskens WP, Butter LM, Florquin S, Juffermans NP, Roelofs J, et al. Mitochondrial DNA is released in urine of SIRS patients with acute kidney injury and correlates with severity of renal dysfunction. *Shock* (2018) 49:301–10. doi: 10.1097/SHK.0000000000000967
10. Hu Q, Ren J, Ren H, Wu J, Wu X, Liu S, et al. Urinary mitochondrial DNA identifies renal dysfunction and mitochondrial damage in sepsis-induced acute kidney injury. *Oxid Med Cell Longev*. (2018) 2018:8074936. doi: 10.1155/2018/8074936.
11. He J, Lu Y, Xia H, Liang Y, Wang X, Bao W, et al. Circulating mitochondrial DAMPs are not effective inducers of proteinuria and kidney injury in rodents. *PLoS ONE* (2015) 10:e0124469. doi: 10.1371/journal.pone.0124469
12. Tsuji N, Tsuji T, Ohashi N, Kato A, Fujigaki Y, Yasuda H. Role of mitochondrial DNA in septic AKI via toll-like receptor 9. *J Am Soc Nephrol*. (2016) 27:2009–20. doi: 10.1681/ASN.2015040376
13. Bellomo R, Tipping P, Boyce N. Continuous veno-venous hemofiltration with dialysis removes cytokines from the circulation of septic patients. *Crit Care Med*. (1993) 21:522–6.
14. Piccinni P, Dan M, Barbacini S, Carraro R, Lieta E, Marafon S, et al. Early isovolaemic haemofiltration in oliguric patients with septic shock. *Intensive Care Med*. (2006) 32:80–6. doi: 10.1007/s00134-005-2815-x
15. Villa G, Neri M, Bellomo R, Cerda J, De Gaudio AR, De Rosa S, et al. Nomenclature for renal replacement therapy and blood purification techniques in critically ill patients: practical applications. *Crit Care* (2016) 20:283. doi: 10.1186/s13054-016-1456-5
16. Park JT, Lee H, Kee YK, Park S, Oh HJ, Han SH, et al. High-dose versus conventional-dose continuous venovenous hemodiafiltration and patient and kidney survival and cytokine removal in sepsis-associated acute kidney injury: a randomized controlled trial. *Am J Kidney Dis*. (2016) 68:599–608. doi: 10.1053/j.ajkd.2016.02.049
17. Chung KK, Coates EC, Smith DJ Jr, Karlnoski RA, Hickerson WL, Arnold-Ross AL, et al. High-volume hemofiltration in adult burn patients with septic shock and acute kidney injury: a multicenter randomized controlled trial. *Crit Care* (2017) 21:289. doi: 10.1186/s13054-017-1878-8
18. Ueno T, Ikeda T, Yokoyama T, Kihara Y, Konno O, Nakamura Y, et al. Reduction in circulating level of HMGB-1 following continuous renal replacement therapy in sepsis. *Cytokine* (2016) 83:206–9. doi: 10.1016/j.cyto.2016.05.004
19. Kellum JA, Lameire N, Group KAGW. Diagnosis, evaluation, and management of acute kidney injury: a KDIGO summary (Part 1). *Crit Care* (2013) 17:204. doi: 10.1186/cc11454
20. Hu Q, Ren J, Wu J, Li G, Wu X, Liu S, et al. Elevated levels of plasma mitochondrial DNA are associated with clinical outcome in intra-abdominal infections caused by severe trauma. *Surg Infect.* (2017) 18:610–8. doi: 10.1089/sur.2016.276
21. Döcke WD, Hoflich C, Davis KA, Rottgers K, Meisel C, Kiefer P, et al. Monitoring temporary immunodepression by flow cytometric measurement of monocytic HLA-DR expression: a multicenter standardized study. *Clin Chem*. (2005) 51:2341–7. doi: 10.1373/clinchem.2005.052639
22. Perez-Fernandez X, Sabater-Riera J, Sileanu FE, Vazquez-Reveron J, Ballus-Noguera J, Cardenas-Campos P, et al. Clinical variables associated with poor outcome from sepsis-associated acute kidney injury and the relationship with timing of initiation of renal replacement therapy. *J Crit Care* (2017) 40:154–60. doi: 10.1016/j.jcrc.2017.03.022
23. Rhodes A, Evans LE, Alhazzani W, Levy MM, Antonelli M, Ferrer R, et al. Surviving sepsis campaign: international guidelines for management of sepsis and septic shock: 2016. *Crit Care Med*. (2017) 45:486–552. doi: 10.1097/CCM.0000000000002255
24. Pipili C, Vasileiadis I, Grapsa E, Tripodaki ES, Ioannidou S, Papastylianou A, et al. Microcirculatory alterations during continuous renal replacement therapy in ICU: a novel view on the 'dialysis trauma' concept. *Microvasc Res*. (2016) 103:14–8. doi: 10.1016/j.mvr.2015.09.004
25. Rosin DL, Okusa MD. Dangers within: DAMP responses to damage and cell death in kidney disease. *J Am Soc Nephrol*. (2011) 22:416–25. doi: 10.1681/ASN.2010040430
26. Xie L, Liu S, Cheng J, Wang L, Liu J, Gong J. Exogenous administration of mitochondrial DNA promotes ischemia reperfusion injury via TLR9-p38 MAPK pathway. *Regul Toxicol Pharmacol*. (2017) 89:148–54. doi: 10.1016/j.yrtph.2017.07.028
27. Gouel-Cheron A, Allaouchiche B, Floccard B, Rimmele T, Monneret G. Early daily mHLA-DR monitoring predicts forthcoming sepsis in severe trauma patients. *Intensive Care Med*. (2015) 41:2229–30. doi: 10.1007/s00134-015-4045-1
28. Timmermans K, Kox M, Vaneker M, van den Berg M, John A, van Laarhoven A, et al. Plasma levels of danger-associated molecular patterns are associated with immune suppression in trauma patients. *Intensive Care Med*. (2016)42:551–61. doi: 10.1007/s00134-015-4205-3
29. Monneret G, Venet F. Sepsis-induced immune alterations monitoring by flow cytometry as a promising tool for individualized therapy. *Cytometry B Clin Cytom*. (2016) 90:376–86. doi: 10.1002/cyto.b.21270

30. Gainaru G, Papadopoulos A, Tsangaris I, Lada M, Giamarellos-Bourboulis EJ, Pistiki A. Increases in inflammatory and CD14(dim)/CD16(pos)/CD45(pos) patrolling monocytes in sepsis: correlation with final outcome. *Crit Care* (2018) 22:56. doi: 10.1186/s13054-018-1977-1
31. Li S, Luo C, Yin C, Peng C, Han R, Zhou J, et al. Endogenous HMGB1 is required in endotoxin tolerance. *J Surg Res*. (2013) 185:319–28. doi: 10.1016/j.jss.2013.05.062
32. Parker KH, Sinha P, Horn LA, Clements VK, Yang H, Li J, et al. HMGB1 enhances immune suppression by facilitating the differentiation and suppressive activity of myeloid-derived suppressor cells. *Cancer Res*. (2014) 74:5723–33. doi: 10.1158/0008-5472.CAN-13-2347
33. Aneja R, Odoms K, Dunsmore K, Shanley TP, Wong HR. Extracellular heat shock protein-70 induces endotoxin tolerance in THP-1 cells. *J Immunol*. (2006) 177:7184–92. doi: 10.4049/jimmunol.177.10.7184
34. Borges TJ, Wieten L, van Herwijnen MJ, Broere F, van der Zee R, Bonorino C, et al. The anti-inflammatory mechanisms of Hsp70. *Front Immunol*. (2012) 3:95. doi: 10.3389/fimmu.2012.00095
35. Asea A, Kraeft SK, Kurt-Jones EA, Stevenson MA, Chen LB, Finberg RW, et al. HSP70 stimulates cytokine production through a CD14-dependant pathway, demonstrating its dual role as a chaperone and cytokine. *Nat Med*. (2000) 6:435–42. doi: 10.1038/74697
36. Fong JJ, Sreedhara K, Deng L, Varki NM, Angata T, Liu Q, et al. Immunomodulatory activity of extracellular Hsp70 mediated via paired receptors Siglec-5 and Siglec-14. *EMBO J*. (2015) 34:2775–88. doi: 10.15252/embj.201591407
37. Schafer ST, Franken L, Adamzik M, Schumak B, Scherag A, Engler A, et al. Mitochondrial DNA: an endogenous trigger for immune paralysis. *Anesthesiology* (2016) 124:923–33. doi: 10.1097/ALN.0000000000001008
38. Leijte GP, Custers H, Gerretsen J, Heijne A, Roth J, Vogl T, et al. Increased plasma levels of danger-associated molecular patterns are associated with immune suppression and postoperative infections in patients undergoing cytoreductive surgery and hyperthermic intraperitoneal chemotherapy. *Front Immunol*. (2018) 9:663. doi: 10.3389/fimmu.2018.00663
39. Timmermans K, Kox M, Scheffer GJ, Pickkers P. Plasma nuclear and mitochondrial DNA levels, and markers of inflammation, shock, and organ damage in patients with septic shock. *Shock* (2016) 45:607–12. doi: 10.1097/SHK.0000000000000549

Conflict of Interest Statement: The authors declare that the research was conducted in the absence of any commercial or financial relationships that could be construed as a potential conflict of interest.

Copyright © 2019 Wu, Ren, Liu, Hu, Wu, Wang, Hong, Ren and Li. This is an open-access article distributed under the terms of the Creative Commons Attribution License (CC BY). The use, distribution or reproduction in other forums is permitted, provided the original author(s) and the copyright owner(s) are credited and that the original publication in this journal is cited, in accordance with accepted academic practice. No use, distribution or reproduction is permitted which does not comply with these terms.

frontiers in Immunology

ORIGINAL RESEARCH
published: 02 April 2019
doi: 10.3389/fimmu.2019.00585

Forebrain Cholinergic Signaling Regulates Innate Immune Responses and Inflammation

Kurt R. Lehner[1], Harold A. Silverman[1,2], Meghan E. Addorisio[2], Ashbeel Roy[3,4], Mohammed A. Al-Onaizi[3,5], Yaakov Levine[6], Peder S. Olofsson[2,7], Sangeeta S. Chavan[1,2], Robert Gros[3,4,8], Neil M. Nathanson[9], Yousef Al-Abed[2,10], Christine N. Metz[1,2], Vania F. Prado[3,4,11,12], Marco A. M. Prado[3,4,11,12], Kevin J. Tracey[1,2†] and Valentin A. Pavlov[1,2†]*

[1] Zucker School of Medicine at Hofstra/Northwell, Hempstead, NY, United States, [2] Center for Biomedical Science and Bioelectronic Medicine, The Feinstein Institute for Medical Research, Northwell Health, Manhasset, NY, United States, [3] Schulich School of Medicine and Dentistry, Robarts Research Institute, University of Western Ontario, London, ON, Canada, [4] Department of Physiology and Pharmacology, Schulich School of Medicine and Dentistry, University of Western Ontario, London, ON, Canada, [5] Department of Anatomy, Faculty of Medicine, Kuwait University, Kuwait City, Kuwait, [6] SetPoint Medical Corporation, Valencia, CA, United States, [7] Department of Medicine, Center for Bioelectronic Medicine, Center for Molecular Medicine, Karolinska Institutet, Karolinska University Hospital, Stockholm, Sweden, [8] Department of Medicine, Schulich School of Medicine and Dentistry, University of Western Ontario, London, ON, Canada, [9] Department of Pharmacology, University of Washington, Seattle, WA, United States, [10] Department of Medicinal Chemistry, Center for Molecular Innovation, The Feinstein Institute for Medical Research, Northwell Health, Manhasset, NY, United States, [11] Department of Anatomy and Cell Biology, Schulich School of Medicine and Dentistry, University of Western Ontario, London, ON, Canada, [12] Graduate Program in Neuroscience, Schulich School of Medicine and Dentistry, University of Western Ontario, London, ON, Canada

OPEN ACCESS

Edited by:
Pietro Ghezzi, Brighton and Sussex Medical School, United Kingdom

Reviewed by:
Bruno Bonaz, Centre Hospitalier Universitaire de Grenoble, France
Egle Solito, Queen Mary University of London, United Kingdom

***Correspondence:**
Valentin A. Pavlov
vpavlov@northwell.edu

[†] These authors have contributed equally to this work

Specialty section:
This article was submitted to Inflammation, a section of the journal Frontiers in Immunology

Received: *14 December 2018*
Accepted: *05 March 2019*
Published: *02 April 2019*

Citation:
Lehner KR, Silverman HA, Addorisio ME, Roy A, Al-Onaizi MA, Levine Y, Olofsson PS, Chavan SS, Gros R, Nathanson NM, Al-Abed Y, Metz CN, Prado VF, Prado MAM, Tracey KJ and Pavlov VA (2019) Forebrain Cholinergic Signaling Regulates Innate Immune Responses and Inflammation. Front. Immunol. 10:585. doi: 10.3389/fimmu.2019.00585

The brain regulates physiological functions integral to survival. However, the insight into brain neuronal regulation of peripheral immune function and the neuromediator systems and pathways involved remains limited. Here, utilizing selective genetic and pharmacological approaches, we studied the role of forebrain cholinergic signaling in the regulation of peripheral immune function and inflammation. Forebrain-selective genetic ablation of acetylcholine release and vagotomy abolished the suppression of serum TNF by the centrally-acting cholinergic drug galantamine in murine endotoxemia. Selective stimulation of acetylcholine action on the M1 muscarinic acetylcholine receptor (M1 mAChR) by central administration of the positive allosteric modulator benzyl quinolone carboxylic acid (BQCA) suppressed serum TNF (TNFα) levels in murine endotoxemia. This effect was recapitulated by peripheral administration of the compound. BQCA also improved survival in murine endotoxemia and these effects were abolished in M1 mAChR knockout (KO) mice. Selective optogenetic stimulation of basal forebrain cholinergic neurons innervating brain regions with abundant M1 mAChR localization reduced serum TNF in endotoxemic mice. These findings reveal that forebrain cholinergic neurons regulate innate immune responses and inflammation, suggesting the

possibility that in diseases associated with cholinergic dysfunction, including Alzheimer's disease this anti-inflammatory regulation can be impaired. These results also suggest novel anti-inflammatory approaches based on targeting forebrain cholinergic signaling in sepsis and other disorders characterized by immune dysregulation.

Keywords: forebrain cholinergic, cytokines, inflammation, vagus nerve, endotoxemia, sepsis, neural regulation

INTRODUCTION

The nervous system regulates and coordinates physiological functions and defense mechanisms. A major defense mechanism against pathogen invasion and tissue injury is provided by the innate immune system through inflammation (1). However, dysregulated immune responses and aberrant inflammation are implicated in the etiology of sepsis, inflammatory bowel disease, and many other life-threatening and debilitating disorders (1–6). While accumulating evidence reveals that the nervous system and specifically the vagus nerve regulate immune function and inflammation, the role of brain pathways in this context remains poorly understood (2, 7, 8). The brain regulation of peripheral inflammation and the mediating role of the vagus nerve have been indicated in studies with the experimental anti-inflammatory compound CNI-1493 (Semapimod). Administration of this molecule in the brain suppresses serum TNF (TNF-α) in murine endotoxemia and this effect is abrogated by surgical transection of the vagus nerve (vagotomy) (9). CNI-1493 binds to muscarinic acetylcholine receptors (mAChRs) (10) and administration of compounds that mimic the action of acetylcholine on mAChRs in the brain also suppresses circulating TNF and other pro-inflammatory cytokines (10–12). In addition, galantamine, an acetylcholinesterase inhibitor, which increases acetylcholine levels suppresses peripheral pro-inflammatory cytokine levels acting through a brain mAChR-mediated mechanism (13–15). These cholinergic effects in the brain are linked with activation of the vagus nerve-based inflammatory reflex (11, 13, 14, 16, 17), a physiological immunoregulatory circuit (18, 19) with recently demonstrated utility in treating human inflammatory diseases (20, 21). These studies have implicated brain cholinergic signaling in the regulation of pro-inflammatory cytokine release and inflammation. The cholinergic system in the brain has a diverse topographic neuronal organization and projection patterns (22, 23), and specific insight into the role of cholinergic pathways and receptors in the brain in peripheral immunoregulation is presently lacking.

A major collection of cholinergic neurons is localized in the basal forebrain (22, 24). These neurons project to forebrain regions with abundant expression of M1 mAChRs, including neocortical areas and the hippocampus (23), and regulate neuroplasticity, cognition, and other processes (22, 23, 25). Here, utilizing mice with selective genetic forebrain ablation of acetylcholine release, positive allosteric M1 mAChR modulation, and optogenetic stimulation of basal forebrain cholinergic neurons, we indicate a role for forebrain cholinergic signaling via M1 mAChRs in the physiological regulation of inflammation.

RESULTS

Acetylcholine in Forebrain Mediates Cholinergic Suppression of Peripheral Pro-inflammatory Cytokine Release via a Vagus Nerve-Dependent Signaling

To investigate the role of forebrain neuronal acetylcholine in regulating peripheral inflammation, we utilized mice with selective forebrain deprivation of acetylcholine release and galantamine, a centrally-acting cholinergic drug (an acetylcholinesterase inhibitor) with anti-inflammatory properties (13, 14). A major molecular determinant of acetylcholine release is the vesicular acetylcholine transporter (VAChT), which loads acetylcholine in vesicles prior to its release in the synaptic cleft (26, 27). We used mice with Cre-*lox*P-based forebrain VAChT ablation, a genetic manipulation that provides a non-invasive means of selective elimination of forebrain acetylcholine release and cholinergic activity without loss of neurons (27). This is important as cholinergic neurons can also secrete GABA with ACh and targeting VAChT allows for selective manipulation of ACh release (28–31). As shown in **Figure 1A**, no VAChT immunoreactivity in the forebrain (hippocampus, CA3 area shown) was detected in these $VAChT^{Nkx2.1-Cre-flox/flox}$ ($VAChT^{-/-}$) mice as compared with $VAChT^{flox/flox}$ ($VAChT^{+/+}$) control mice. This observation was consistent with the previously reported lack of VAChT immunoreactivity in several forebrain areas of $VAChT^{-/-}$ mice and no significant alterations in VAChT protein expression in brainstem regions as a result of genetic deletion (27). The selective forebrain VAChT ablation was not associated with differences in VAChT protein levels (immunofluorescence) in the spinal cord and peripheral neuronal varicosities in the heart (**Figures 1B,C**). These observations indicated that VAChT ablation was limited to the basal forebrain cholinergic system. Furthermore, no differences were observed between $VAChT^{-/-}$ and $VAChT^{+/+}$ mice on 24 h heart rate recording (**Figure 1D**). There were no differences between the two groups of mice in heart rate responses to atropine (mAChR blocker) and propranolol (beta adrenergic receptor blocker) i.p. administrations (**Figures 1E–G**). In addition, sensitivity to post-handling stress was similar between genotypes, because heart rate responses to saline administration did not differ between the two groups of mice (**Figure S1**).

The effects of acetylcholine in the brain can be modulated (enhanced) through inhibiting its degradation using centrally-acting acetylcholinesterase inhibitors, including galantamine. Administration (i.p.) of galantamine in $VAChT^{+/+}$ mice prior to endotoxin significantly reduced serum TNF levels as compared to vehicle administration ($P = 0.017$) (**Figure 2A**). However,

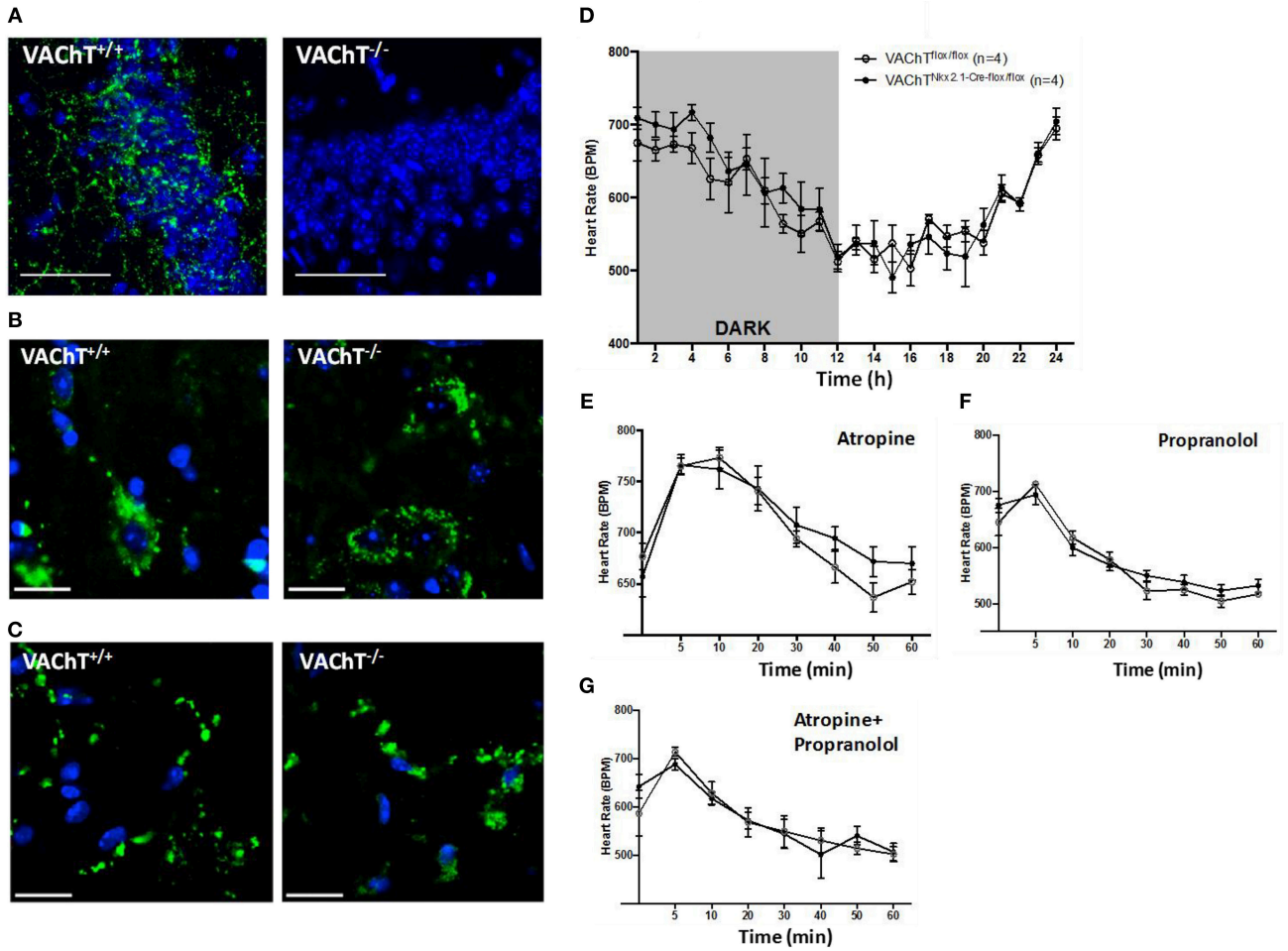

FIGURE 1 | Morphological and functional evaluation of forebrain VAChT KO mice. **(A)** VAChT protein immunostaining (in green) shown in a hippocampal region of VAChT$^{+/+}$ mice is not detected in VAChT$^{-/-}$ mice (scale bar = 100 μm). **(B)** VAChT protein immunostaining (in green) in spinal cord of VAChT$^{+/+}$ and VAChT$^{-/-}$ mice (scale bar = 20 μm). **(C)** VAChT protein immunostaining (in green) in the heart right atrium of VAChT$^{+/+}$ and VAChT$^{-/-}$ mice (scale bar = 20 μm). **(D)** Freely moving VAChT$^{flox/flox}$ (VAChT$^{+/+}$) mice and VAChT $^{Nkx2.1-Cre-flox/flox}$ (VAChT$^{-/-}$) mice exhibit no differences in heart rate during 24 h recording using radio-frequency telemeters. Freely moving VAChT$^{+/+}$ (open circles) and VAChT$^{-/-}$ mice (black circles) exhibit no difference in heart rate responses to atropine **(E)**, propranolol **(F)**, or atropine and propranolol **(G)** i.p. administration (n = 4 mice/genotype).

galantamine failed to significantly alter serum TNF levels in VAChT$^{-/-}$ mice (**Figure 2A**). In addition, serum TNF levels in VAChT$^{-/-}$ mice were significantly higher than in VAChT$^{+/+}$ mice during endotoxemia ($P = 0.009$) (**Figure 2A**), suggesting that physiological cholinergic transmission in the forebrain regulates peripheral innate immune responses. Galantamine was previously shown to stimulate vagus nerve activity (17, 32). We next examined the role of the vagus nerve in mediating galantamine forebrain-triggered anti-inflammatory effect in endotoxemic C57BL/6 mice. Galantamine administration significantly decreased serum TNF levels as compared with vehicle during endotoxemia in sham-operated (control) mice ($P = 0.019$) (**Figure 2B**). This effect was markedly diminished in mice with cervical unilateral vagotomy (**Figure 2B**), thus indicating a role of the efferent vagus nerve. Collectively, these data indicate that acetylcholine derived from cholinergic neurons in forebrain plays a role in mediating the suppressive effect of galantamine on peripheral TNF levels in a vagus nerve-dependent manner during murine endotoxemia.

Stimulation of Acetylcholine Action on the M1 mAChR by Allosteric Modulation Suppresses Lethal Peripheral Inflammation

Basal forebrain cholinergic neurons project to regions with high expression of M1 mAChR, including several neocortical areas and the hippocampus. Acetylcholine released from these neurons stimulates the postsynaptically located M1 mAChR that processes cholinergic transmission (33). Positive allosteric modulation of the M1 mAChR is a selective approach of increasing endogenous acetylcholine activity at the receptor (34, 35). To study the effect of acetylcholine on brain M1 mAChR in the regulation of

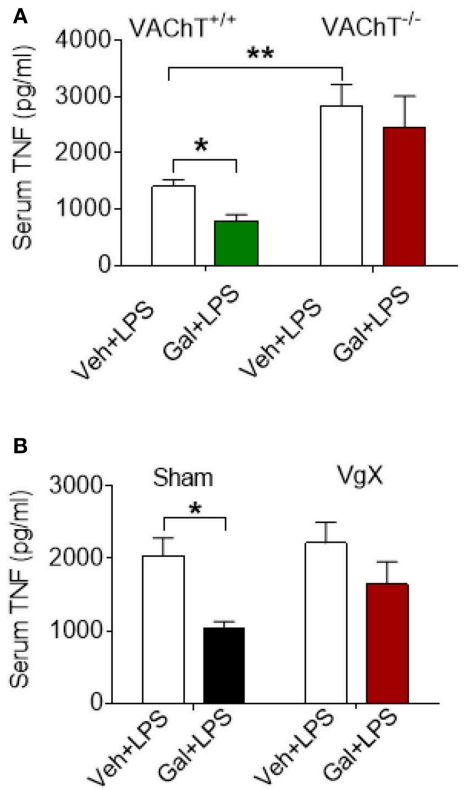

FIGURE 2 | Selective forebrain cholinergic deficit and vagotomy alter cholinergic suppression of peripheral pro-inflammatory cytokine levels. **(A)** Galantamine (Gal, i.p.) as compared to vehicle (Veh), suppresses serum TNF in VAChT$^{+/+}$ control mice, but not in VAChT$^{-/-}$ mice during endotoxemia, and serum TNF in vehicle injected VAChT$^{-/-}$ mice are higher as compared to VAChT$^{+/+}$ control mice (*$P = 0.017$, **$P = 0.007$, two-way ANOVA, Sidak's multiple comparisons test), $n = 6$–7 per group. **(B)** Vagotomy (VgX) abolishes the suppression of serum TNF in endotoxemic mice (*$P = 0.019$, two-way ANOVA, Sidak's multiple comparisons test), $n = 6$–8 per group. See Methods for details.

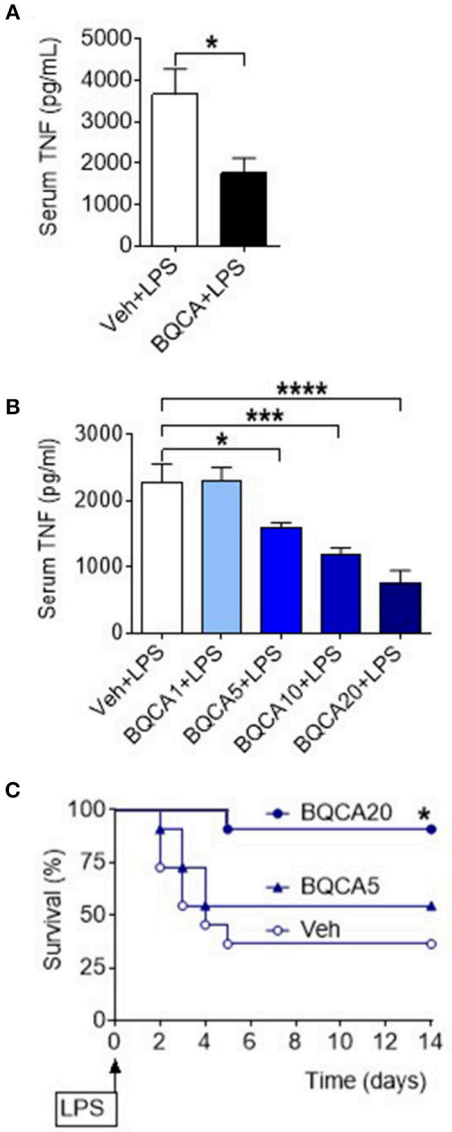

FIGURE 3 | Activation of acetylcholine action on the M1 mAChR using a positive allosteric modulator (BQCA) suppresses serum TNF levels and improves survival in endotoxemia. **(A)** BQCA (5 μ/kg, i.c.v.) suppresses serum TNF (*$P = 0.018$, unpaired two-tailed Student's t test), $n = 6$–7 per group. **(B)** Peripheral i.p. administration of BQCA 1–20 (1–20 mg/kg) in endotoxemic mice suppresses serum TNF levels (*$P = 0.027$, ***$P = 0.0005$, ****$P < 0.0001$, one-way ANOVA, Dunnett's multiple comparisons test), $n = 7$–8 per group. **(C)** Peripheral i.p. administration of BQCA 20 (20 mg/kg) in endotoxemic mice improves survival in endotoxemia (*$P = 0.035$, Log-rank test), $n = 11$–12 per group.

peripheral inflammation, we used benzyl quinolone carboxylic acid (BQCA), a positive allosteric modulator of M1 mAChR (34, 35). BQCA has previously been shown to selectively increase (up to 129-fold) the functional affinity of endogenous acetylcholine for M1 mAChR (35). Intracerebroventricular (i.c.v.) injection of BQCA (5 μg/kg) resulted in significant suppression of serum TNF as compared with vehicle administration following endotoxin challenge ($P = 0.018$) (**Figure 3A**). This observation indicated that selective activation of acetylcholine action on the M1 mAChR in the brain suppresses peripheral inflammation in murine endotoxemia. To facilitate subsequent studies with BQCA, we examined whether peripheral administration of BQCA, which is known to cross the blood brain barrier (34, 35), recapitulates anti-inflammatory effects. Intraperitoneal (i.p.) treatment of mice with BQCA (1–20 mg/kg) resulted in a dose-dependent decrease in serum TNF following endotoxin as compared to vehicle injection ($P < 0.001$, when 20 mg/kg BQCA was used) (**Figure 3B**). I.p. administration of BQCA also dose-dependently improved the survival rate in this lethal murine endotoxemia model as compared to vehicle administration ($P = 0.035$ when 20 mg/kg BQCA was used) (**Figure 3C**).

BQCA treatment (20 mg/kg, i.p.) did not significantly alter serum TNF in M1 mAChR KO mice (as compared to vehicle treatment), while in wild type (WT) mice this drug effect was significant ($P = 0.028$) (**Figure 4A**). Previous studies have shown that activation of brain mAChR-mediated cholinergic signaling results in suppression of TNF in spleen, a major

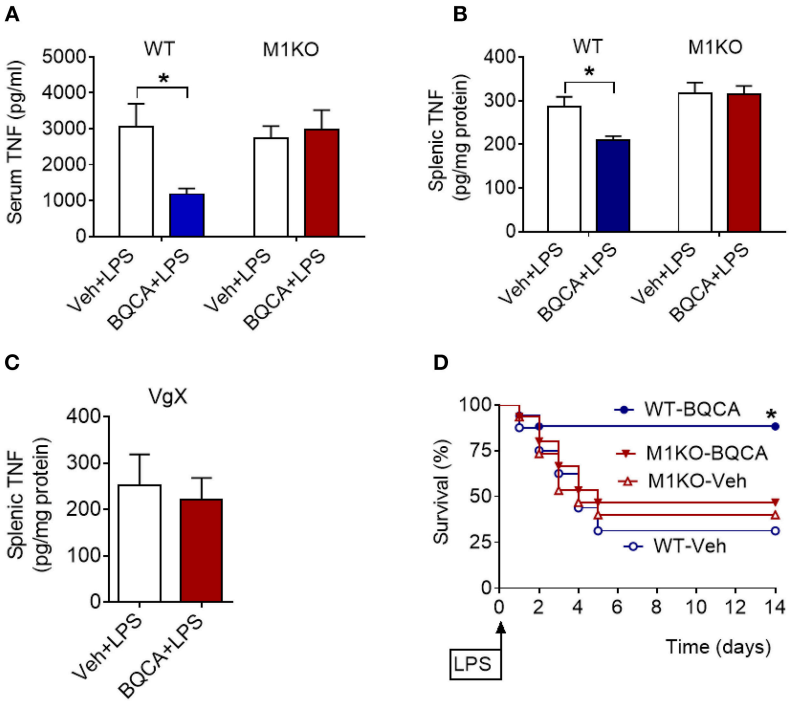

FIGURE 4 | Anti-inflammatory effects of BQCA in endotoxemia are mediated by M1 mAChRs. **(A)** Peripheral (i.p.) administration of BQCA (20 mg/kg, i.p.) suppresses serum TNF in wild type (WT) mice and does not alter serum TNF in M1 mAChR KO mice during endotoxemia (*$P = 0.01$, two-way ANOVA, Sidak's multiple comparisons test), $n = 8$–10. **(B)** Peripheral (i.p.) administration of BQCA (20 mg/kg, i.p.) suppresses splenic TNF in WT mice and does not alter splenic TNF in M1 mAChR KO mice (*$P = 0.017$, two-way ANOVA, Sidak's multiple comparisons test), $n = 7$–10. **(C)** Vagotomy (VgX) abolishes the effect of BQCA on splenic TNF during endotoxemia (unpaired two-tailed Student's *t* test), $n = 7, 8$. **(D)** Peripheral (i.p.) administration of BQCA (20 mg/kg, i.p.) improves survival in endotoxemic WT mice and does not alter the survival rate in M1 mAChR KO mice during endotoxemia (*$P = 0.028$, Log-rank test), $n = 15$–18 per group. See Methods for details.

source of pro-inflammatory cytokines and an organ target of the vagus-nerve-based inflammatory reflex (36–38). BQCA (i.p.) administration 1 h prior to endotoxin significantly suppressed splenic TNF in WT mice ($P = 0.047$) and did not alter splenic TNF in M1 mAChR KO mice (**Figure 4B**). BQCA also failed to significantly alter splenic TNF in endotoxemic WT mice with unilateral cervical vagotomy (**Figure 4C**). In addition, BQCA (20 mg/kg, i.p.) injected 1 h prior to endotoxin was sufficient to significantly improve survival in WT mice ($P = 0.028$), but failed to significantly alter survival in endotoxemic M1 mAChR KO mice (**Figure 4D**). Together these results show that enhancement of acetylcholine activity on the M1 mAChR is sufficient to suppress inflammation in murine endotoxemia and that the efferent vagus nerve is necessary for this anti-inflammatory effect.

Selective Optogenetic Stimulation of Basal Forebrain Medial Septum Cholinergic Neurons Suppresses Serum TNF Levels

We next examined whether the anti-inflammatory effect of acetylcholine acting on M1 mAChR (achieved by allosteric modulation with BQCA) could be replicated by direct stimulation of basal forebrain cholinergic neurons *in vivo*. The medial septum (medial septal nucleus) is a major nucleus in the basal forebrain cholinergic system (22, 23). The medial septum also plays an important role as a relay of afferent vagus nerve signaling in the forebrain as recently demonstrated (39). Accordingly, we stimulated basal forebrain medial septum cholinergic neurons using a selective optogenetic approach in transgenic mice. These mice express channelrhodopsin-2 coupled to a yellow fluorescent protein (ChR2-YFP) under the control of the choline acetyltransferase (ChAT) promoter. Immunofluorescent staining of brain slices confirmed the neuronal colocalization of ChAT and ChR2-YFP in the medial septum (**Figure 5A**) and the abundant expression of ChR2-YFP in the medial septum and the adjacent vertical limb of the diagonal band of Broca (**Figure S2**). Photoactivation of medial septum neurons by laser light (473 nm) significantly suppressed serum TNF levels compared with sham stimulation ($P = 0.039$) (**Figure 5B**) in mice with confirmed (by microscopic histochemical evaluation) location of the fiber tip in the medial septum (**Figure S3**; **Supplementary Methods**). Laser light exposure of medial septum neurons in C57BL/6 mice not expressing ChR2-YFP on cholinergic neurons (non-carriers) was performed to control for possible confounding effects of heat and other non-thermal effects of light. This manipulation failed to alter serum TNF levels (**Figure 5C**) thus confirming the specific cholinergic nature of the mechanism. As ChAT-ChR2-YFP mice have been shown to overexpress VAChT (40, 41) and present increased cholinergic tone, LPS was administered

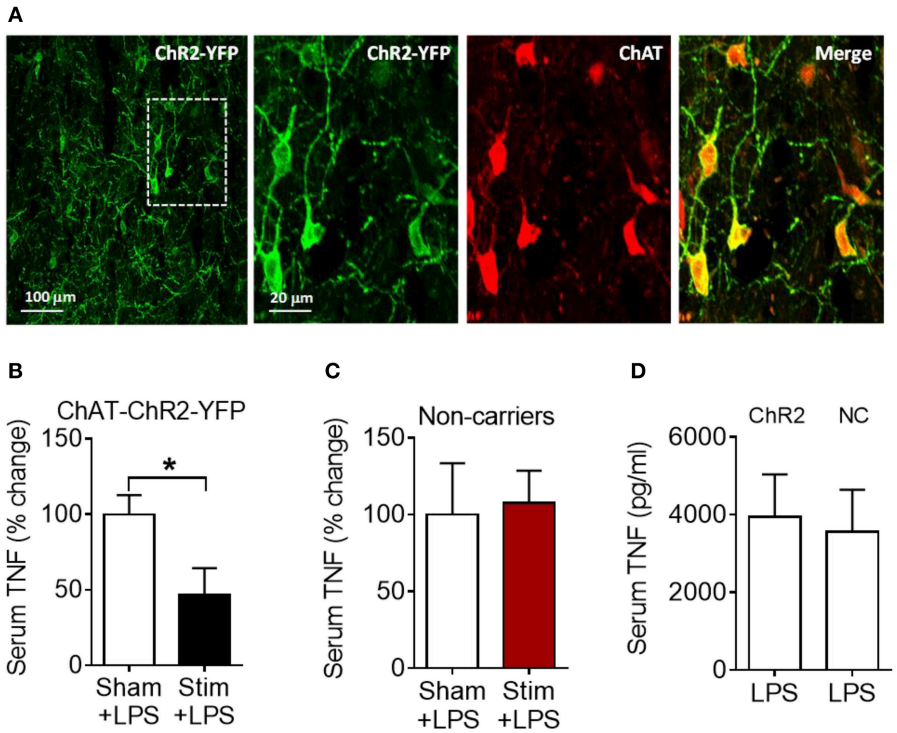

FIGURE 5 | Optogenetic stimulation of basal forebrain cholinergic neurons in the medial septum suppresses serum TNF in endotoxemic mice. **(A)** Immunostaining of medial septum neurons in a brain section of a ChAT-ChR2-EYFP mouse: EYFP immunostaining (first and second panel); ChAT immunostaining of the same area (third panel); and double immunostaining (fourth panel). **(B)** Optogenetic stimulation suppresses serum TNF during endotoxemia (*$P = 0.039$, unpaired two-tailed Student's *t* test), $n = 5$–6 per group. **(C)** Laser light exposure of medial septum neurons in control (non-carrier) mice does not significantly alter serum TNF levels during endotoxemia (unpaired two-tailed Student's *t* test), $n = 6$–7 per group. **(D)** LPS (i.p.) administration to ChAT-ChR2-EYFP (ChR2) and control (non-carrier, NC) mice does not result in statistically different serum TNF levels, (unpaired two-tailed Student's *t* test), $n = 9$ per group. See Methods for details.

to ChAT-ChR2-YFP and non-carrier mice not subjected to anesthesia and surgical manipulation. No differences in serum TNF levels upon LPS administration were observed between the two groups of mice (**Figure 5D**), indicating that the genetic modification by itself did not alter the inflammatory response. These results show that selective activation of basal forebrain medial septum cholinergic neurons decreases peripheral inflammation in endotoxemia.

DISCUSSION

Here, we show a role for forebrain cholinergic signaling and the M1 mAChR in the brain neuronal regulation of inflammation through vagus nerve-mediated signaling.

Genetic ablation of VAChT, which eliminates synaptic acetylcholine release from basal forebrain cholinergic neurons (27), abolished the anti-inflammatory effect of the centrally-acting acetylcholinesterase inhibitor galantamine. These findings point to forebrain acetylcholine as a major mediator of galantamine anti-inflammatory effects in endotoxemia. The selective forebrain cholinergic deficit (in VAChT$^{-/-}$ mice) also resulted in increased circulatory TNF levels in endotoxemic mice, thus suggesting a tonic anti-inflammatory role of acetylcholine in forebrain.

Forebrain areas, including the cortex (neocortex) and the hippocampus have abundant (predominantly post-synaptic) localizations of the M1 mAChR, which plays a major role in processing the effects of acetylcholine released from basal forebrain cholinergic neurons (22). Positive allosteric modulation of the M1 mAChR by BQCA is a selective approach of increasing the activity of the endogenous acetylcholine on the receptor (34, 35). The anti-inflammatory effects of the centrally-acting BQCA demonstrated here indicate a role of acetylcholine acting on the M1 mAChR in controlling peripheral inflammatory responses. Unilateral vagotomy attenuated the anti-inflammatory effects of galantamine and BQCA, thus indicating a brain-to periphery mediating role for the vagus nerve. The vagus nerve is an important neuroanatomical component of the inflammatory reflex (18) in which sensory and motor vagus nerve signaling regulates cytokine production by immune cells in the spleen, and alleviates inflammation (2, 19). Importantly, recent studies demonstrated that afferent vagus nerve signaling reaches the forebrain (hippocampus and cortex), and identified basal forebrain cholinergic nuclei, including the medial septum as major relay components (39, 42, 43). Together with these findings, our observations suggest a role for the medial septum in a forebrain regulatory hub of the inflammatory reflex. This regulation possibly involves other brain regions

through multisynaptic pathways with brainstem nuclei providing peripheral vagus nerve projections. These brain networks remain to be further elucidated.

In addition to positive allosteric modulation of acetylcholine action on M1 mAChR, suppression of serum TNF levels during endotoxemia was also achieved by selective optogenetic stimulation of a subset of basal forebrain cholinergic neurons in the medial septum. Although optogenetic stimulation was performed in animals under isoflurane anesthesia and there is some evidence that relatively high doses of isoflurane can increase blood-brain barrier permeability (44), the proper sham stimulation pointed to the specificity of the effect. Medial septum cholinergic neurons innervate the hippocampus and the parahippocampal region, which are interconnected with several neocortical and subcortical areas (23, 24, 39). Multisynaptic connections between the hippocampus and the hypothalamus have also been described. Although we stereotactically targeted optogenetic stimulation of the medial septum, a spread of stimulation to adjacent cholinergic neurons in the diagonal band of Broca cannot be excluded. Cholinergic neurons in the diagonal band of Broca project to cortical areas and the amygdala (22–24). These neural networks involving cholinergic circuits suggest that multiple points of regulation can be further explored in studying the brain control of peripheral inflammation. Some of these networks have been previously associated with the regulation of autonomic responses, including modulation of vagus nerve activity (2). These previous observations are consistent with our findings that signaling through the vagus nerve mediates brain cholinergic modulation of peripheral inflammation. Our findings have clinical relevance. Galantamine is in clinical use for alleviation of cognitive deterioration in patients with Alzheimer's disease. We have also recently shown that treatment with galantamine alleviates inflammation and insulin resistance in patients with the metabolic syndrome (45). BQCA and other centrally-acting positive allosteric modulators of the M1 mAChR have also been preclinically developed in the search of efficient treatments of Alzheimer's disease and other neurological conditions (34, 35). Our results suggest considering these two types of therapeutics as anti-inflammatory agents. While optogenetics provide a very selective approach for spatiotemporal neuronal control in studying neural circuitries (46), this technology currently has limited therapeutic implications (47–49). However, medial septum deep brain (electrical) stimulation has been successfully used for improving spatial working memory and cognition in experimental settings of traumatic brain injury (50, 51). Future insights into brain networks triggered by medial septum neuronal stimulation and possibly other regions may further inform implications of deep brain stimulation and non-invasive approaches, including transcranial magnetic stimulation and transcranial direct current stimulation (52–54) in therapeutic anti-inflammatory strategies.

Basal forebrain cholinergic signaling has a documented role in attention, learning and memory, and degeneration of basal forebrain cholinergic neurons, which results in diminished release of acetylcholine in the forebrain, is one of the hallmarks of Alzheimer's disease (23). Intriguingly, increased peripheral TNF and other pro-inflammatory cytokine levels have been found in Alzheimer's disease (55), and peripheral inflammation has been linked to exacerbation of brain pathogenesis and neurodegeneration, affecting cholinergic neurons (56, 57). This may be of importance given that cholinergic neurotransmission is dysfunctional in different types of dementia (58), suggesting a potential mechanism by which patients with Alzheimer's disease and other types of dementia may be more susceptible to distinct types of infection (59).

Peripheral inflammation in sepsis, liver disease, and other inflammatory conditions also is linked with brain inflammation (2, 60) and deterioration in brain function and delirium within the scope of characteristic encephalopathies (2, 61–64). Dysregulation in cholinergic signaling has a documented role in brain derangements, including delirium and encephalopathies in sepsis and other inflammatory conditions (60, 65–67). Together with these previously published findings, our observations suggest a bidirectional relationship between brain cholinergic signaling and peripheral inflammation. In this context targeted pharmacological or device-generated modulation of forebrain cholinergic signaling may have broader therapeutic implications.

MATERIALS AND METHODS

Animals

Male mice were used in all experiments. BALB/c mice (24–28 g) were purchased from Taconic. Mice with genetic deletion of VAChT in the forebrain ($VAChT^{-/-}$ mice) were generated as previously described (27). Briefly, $VAChT^{flox/flox}$ mouse line (crossed for five generations with C57BL/6J) was crossed with the Nkx2.1-Cre mouse line (C57BL/6J-Tg(Nkx2-1-cre)2Sand/J) (Jackson Laboratory, stock No: 008661). Control $VAChT^{+/+}$ mice were $VAChT^{flox/flox}$ littermates. ChAT-ChR2-YFP BAC transgenic mice (Jackson Laboratory, stock No: 014546) (68) and non-carrier wild type mice (on the C57BL/6 background) were used in experiments with laser light exposure of the medial septum neurons. M1 mAChR ($Chrm1^{-/-}$) KO mice (69) were generated on the C57Bl/6 background as previously described (70). M1 mAChR KO and wild type (WT) littermates were received from Charles River. Animals were allowed to acclimate for at least 2 weeks prior to the corresponding experiment. All animals were housed in standard conditions (a 12 h light–dark cycle) with access to regular chow and water.

Chemicals

Galantamine (Galantamine hydrobromide) (purity ≥95% by HPLC) was purchased from Calbiochem. Galantamine working solutions were prepared in sterile saline. Benzyl quinolone carboxylic acid (BQCA) (purity: ≥97% (HPLC) was purchased from Enzo Life Sciences. BQCA working solutions were prepared in betacyclodextrin and contained 5% betacyclodextrin in sterile saline (35). Atropine (purity: ≥99% (TLC) and propranolol (purity: ≥98% (TLC) were purchased from Sigma and working solutions prepared in sterile saline.

Endotoxemia and Drug Treatment

Endotoxemia in mice was induced by administering LPS (endotoxin, Sigma L4130 O111:B4 for consistency with our

previous studies (13, 36, 71, 72) in doses as indicated, injected i.p.) Groups of animals were treated i.p. with galantamine (3 mg/kg) or different doses of BQCA or vehicle (sterile saline as a vehicle in galantamine treatments or 5% betacyclodextrin containing sterile saline as a vehicle in BQCA treatments) 1 h prior to endotoxin administration. Vehicle or BQCA (5 μg/kg) [based on the information available about the effect of the compound on M1 mAChR (34, 35)] was also administered i.c.v. 1 h prior to endotoxin (8 mg/kg, i.p.). In experiments with optogenetic stimulation LPS was injected i.p. 1 h after the end of stimulation or sham stimulation. Animals were euthanized by CO_2 asphyxiation 1.5 h after endotoxin administration, and blood was collected via cardiac puncture (from the right ventricle) for cytokine (TNF) determination. In other sets of survival experiments, groups of mice were treated with BQCA or vehicle (i.p.) 1 h prior to endotoxin (8 mg/kg, i.p.) injection. Mice were monitored for survival twice daily for the first 5 days, and then daily for the remainder of the 14 day experiments.

Vagotomy

To avoid potential high lethality associated with bilateral cervical vagotomy, a unilateral cervical vagotomy was performed. Mice were anesthetized by isoflurane inhalation and the right cervical vagus nerve was exposed, ligated with a 4–0 silk suture, and divided. In sham-operated animals, the cervical vagus nerve was visualized, but was neither isolated from the surrounding tissues nor transected. All animals were permitted to recover for 7 days following the surgical procedure and before their inclusion in endotoxemia experiments.

Brain Surgical Manipulations and Optogenetic Stimulation

In experiments with optogenetic stimulation, mice were anesthetized with isoflurane and placed on a stereotactic frame (Kopf Instruments). Body temperature was maintained between 36.5 and 37°C using a feedback controlled rectal thermometer and heating pad. Using aseptic technique, the scalp was incised to expose the skull and the overlying connective tissue was removed. A small (∼500 μm) craniotomy was performed on the desired locations for fiber insertion. Mice expressing light-activated cation ChR2 tagged with a fluorescent protein (ChR2-YFP) under the control of the choline acetyltransferase (ChAT) promoter were used in optogenetic experiments. The optic fiber was inserted slowly over 3 min, targeting the dorsal cholinergic neurons in the medial septum at a location 0.8 mm anterior to Bregma and 0.7 mm lateral to a depth of 3.5 mm at a 10 degree angle below dura, which was opened with a 27 gauge needle. Laser light was delivered via a 200 μm diameter fiber (Thorlabs) inserted into the craniotomy. For ChR2 activation, a 473 nm laser (Optoengine, LLC) was used at a power of 10 mW at the tip. The laser was controlled by a waveform generator (Agilent). Stimulation was performed by using square pulses at 20 Hz for 10 min. Sham stimulation was carried out the same way with the exception that following optic fiber insertion, no laser stimulation was performed. Following optogenetic stimulation or sham stimulation, the fiber was removed over 3 min, the craniotomy was covered using paraffin wax, and the animal recovered for 1 h on a heating pad at 37°C prior to LPS injection. Laser light exposure of medial septum neurons or sham laser light exposure was performed following the same protocol in non-carrier mice.

Brain Surgical Manipulations and I.C.V. Drug Administration

Craniotomies were performed as described above at a location 0.6 mm posterior and 1.2 mm lateral to Bregma targeting the right lateral ventricle. A 10 μL Hamilton microsyringe in a microinjector pump (UMP3-1, World Precision Instruments) was lowered into the right lateral ventricle over 3 min to a depth of 2.1 mm. Following 5 min of equilibration, BQCA (5 ug/kg) or vehicle was delivered over 3 min. Following injection, the syringe remained in place for 5 min to prevent backflow. Then the needle was slowly removed over 3 min. The craniotomy was covered using paraffin wax and the animal recovered for 1 h on a heating pad at 37° C prior to LPS injection.

Immunohistochemistry and Immunofluorescent Microscopy

Expression of ChR2-EYFP in cholinergic neurons of the medial septum was confirmed with immunofluorescent staining for choline acetyltransferase (ChAT) and ChR2-YFP. Mice underwent intracardiac perfusion with 1 × PBS followed by 4% paraformaldehyde. Brains were harvested and cryoprotected with subsequent incubations of 15% and 30% sucrose. They were then stored in O.C.T. at −20°C. 20 μm sections were collected on gelatin subbed slides (SouthernBiotech) using a cryostat (Leica Microsystems). Slides were rinsed in 1 × PBS followed by washing with 0.25% Triton X-100/1 × PBS (PBT). Blocking was performed with a solution of 10% MeOH, 0.1% bovine serum albumin (BSA), 3% normal donkey serum (NDS), and 0.05% hydrogen peroxide. Slides were then washed in PBT. Cholinergic neurons were visualized using goat anti-ChAT (Millipore, AB144 1:200, dilution) as a primary antibody and specific ChR2-EYFP expression was visualized using rabbit anti-GFP Alexa Fluor 488 (ThermoFisher Scientific, A21311, 1:400 dilution) in a solution of PBT containing 1% NDS. Donkey anti-goat Alexafluor 555 (Thermo Fisher Scientific, A21432, 1:200 dilution) in a solution of 1% NDS/PBT was used to visualize Goat anti-ChAT, and slides were mounted and coverslipped with DAPI-Fluoromount G (Southern BioTech). Images were taken using an Olympus FluoView FV300 Confocal Laser Scanning Microscope.

In experiments with $VAChT^{-/-}$ and $VAChT^{+/+}$ animals, mice were anesthetized with ketamine (100 mg/kg) and xylazine (25 mg/kg) in 0.9% sodium chloride, and then sacrificed by trans-cardial perfusion. Brains were harvested and placed in 4% paraformaldehyde in 1 × PBS overnight at 4°C. The brains were isolated and 40 μm sections of the tissue were obtained using a vibratome. Brain sections were incubated in a blocking solution of 1 × PBS/0.4% Triton X-100 containing 0.1% glycine (wt/vol), 0.1% lysine (wt/vol), 1% BSA (wt/vol), and 1% normal

donkey serum (wt/vol). Sections were incubated with anti-VAChT primary antibody (catalog no. 139103; Synaptic Systems) overnight. Sections were then incubated with the Alexa Fluor 488 anti-rabbit secondary antibody (1:1,000; Life Technologies) for 1 h. The nuclei were labeled with Hoechst. Images were acquired using the Zeiss LSM 510 Meta confocal system as previously described (27).

Serum Isolation and Cytokine Determination

The blood was allowed to clot for 80 min following collection. It was then centrifuged at 5,000 rpm (1,500 × g) for 10 min, and the supernatant (serum) was collected and stored at −20°C until analysis. Serum TNF was quantified by using ELISA per the manufacturer's instructions (eBioscience).

Electrocardiography (ECG)

Electrocardiograms were recorded using radiotelemeters. The radio frequency transmitters were implanted subcutaneously under anesthesia and ECG recordings were initiated following a minimum recovery period of 7 days post-implantation. Heart rate was continuously measured in awake, freely moving mice over 24 h to obtain baseline recordings. To determine the effect of autonomic blockade, heart rate was recorded for 60 min following administration of atropine (1 mg/kg, i.p.), propranolol (1 mg/kg, i.p.), or atropine + propranolol. All data were collected using the Dataquest A.R.T. software (Transoma Medical). Experiments were performed as previously described (73, 74).

Statistical Analysis

GraphPad Prism 6.0 software was used for all statistical analysis. Values are presented as mean ± SEM. One-way or two-way ANOVA, followed by appropriate *post-hoc* tests for multiple comparisons, and a two-tailed two-sample equal variance Student's *t*-test were performed to determine statistical significance. The statistical significance of differences between groups of animals in survival experiments was analyzed by Log-rank test. *P* values equal to or below 0.05 were considered significant.

DATA AVAILABILITY

All datasets generated for this study are included in the manuscript and/or the **Supplementary Files**.

ETHICS STATEMENT

All animal experiments were performed in accordance with the National Institutes of Health Guidelines under protocols approved by the Institutional Animal Care and Use Committee and the Institutional Biosafety Committee of the Feinstein Institute for Medical Research, Northwell Health, Manhasset, NY and the Institutional Animal Care and Use Committee at the University of Western Ontario (Protocols 2018-103 and 2018-104).

AUTHOR CONTRIBUTIONS

KRL, MAMP, KJT, and VAP designed research. KRL, MEA, HAS, MA-O, AR, YL, PSO, SSC, RG, VFP, and VAP performed research. NMN, YA-A, RG, VFP, and MAMP contributed reagents, analytic tools and knockout and transgenic mice. KRL, HAS, RG, YA-A, CNM, VFP, MAMP, KJT, and VAP analyzed and interpreted data. KRL, KJT, and VAP wrote the manuscript. NMN, CNM, PSO, YA-A, and MAMP provided additional comments to finalize the paper.

ACKNOWLEDGMENTS

This work was supported by the following grants from the National Institute of General Medical Sciences, NIH: RO1GM089807 (to VAP and KJT), and RO1GM057226 (to KJT) and CIHR (MP 93651, 12600, 89919) (to VFP and MAMP).

SUPPLEMENTARY MATERIAL

The Supplementary Material for this article can be found online at: https://www.frontiersin.org/articles/10.3389/fimmu.2019.00585/full#supplementary-material

REFERENCES

1. Medzhitov R. Origin and physiological roles of inflammation. *Nature*. (2008) 454:428–35. doi: 10.1038/nature07201
2. Pavlov VA, Chavan SS, Tracey KJ. Molecular and functional neuroscience in immunity. *Annu. Rev. Immunol*. (2018) 36:783–812. doi: 10.1146/annurev-immunol-042617-053158
3. Salzano S, Checconi P, Hanschmann EM, Lillig CH, Bowler LD, Chan P, et al. Linkage of inflammation and oxidative stress via release of glutathionylated peroxiredoxin-2, which acts as a danger signal. *Proc Natl Acad Sci USA*. (2014) 111:12157–62. doi: 10.1073/pnas.1401712111
4. Xu H, Turnquist HR, Hoffman R, Billiar TR. Role of the IL-33-ST2 axis in sepsis. *Mil Med Res*. (2017) 4:3. doi: 10.1186/s40779-017-0115-8
5. Chen J, Kieswich JE, Chiazza F, Moyes AJ, Gobbetti T, Purvis GS, et al. IkappaB kinase inhibitor attenuates sepsis-induced cardiac dysfunction in CKD. *J Am Soc Nephrol*. (2017) 28:94–105. doi: 10.1681/ASN.2015060670
6. Rothbard JB, Rothbard JJ, Soares L, Fathman CG, Steinman L. Identification of a common immune regulatory pathway induced by small heat shock proteins, amyloid fibrils, and nicotine. *Proc Natl. Acad Sci USA*. (2018) 115:7081–6. doi: 10.1073/pnas.1804599115
7. Hoover DB. Cholinergic modulation of the immune system presents new approaches for treating inflammation. *Pharmacol. Ther*. (2017) 179:1–16. doi: 10.1016/j.pharmthera.2017.05.002
8. Yuan PQ, Tache Y. Abdominal surgery induced gastric ileus and activation of M1-like macrophages in the gastric myenteric plexus: prevention by central vagal activation in rats. *Am J Physiol Gastrointest Liver Physiol*. (2017) 313:G320–9. doi: 10.1152/ajpgi.00121.2017
9. Bernik TR, Friedman SG, Ochani M, DiRaimo R, Ulloa L, Yang H, et al. Pharmacological stimulation of the cholinergic antiinflammatory pathway. *J Exp Med*. (2002) 195:781–8. doi: 10.1084/jem.20011714
10. Pavlov VA, Ochani M, Gallowitsch-Puerta M, Ochani K, Huston JM, Czura CJ, et al. Central muscarinic cholinergic regulation of the systemic inflammatory

response during endotoxemia. *Proc Natl Acad Sci USA*. (2006) 103:5219–23. doi: 10.1073/pnas.0600506103
11. Munyaka P, Rabbi MF, Pavlov VA, Tracey KJ, Khafipour E, Ghia JE. Central muscarinic cholinergic activation alters interaction between splenic dendritic cell and CD4+CD25- T cells in experimental colitis. *PLoS ONE*. (2014) 9:e109272. doi: 10.1371/journal.pone.0109272
12. Lee ST, Chu K, Jung KH, Kang KM, Kim JH, Bahn JJ, et al. Cholinergic anti-inflammatory pathway in intracerebral hemorrhage. *Brain Res*. (2010) 1309:164–71. doi: 10.1016/j.brainres.2009.10.076
13. Pavlov VA, Parrish WR, Rosas-Ballina M, Ochani M, Puerta M, Ochani K, et al. Brain acetylcholinesterase activity controls systemic cytokine levels through the cholinergic anti-inflammatory pathway. *Brain Behav Immun*. (2009) 23:41–5. doi: 10.1016/j.bbi.2008.06.011
14. Ji H, Rabbi MF, Labis B, Pavlov VA, Tracey KJ, Ghia JE. Central cholinergic activation of a vagus nerve-to-spleen circuit alleviates experimental colitis. *Mucosal Immunol*. (2014) 7:335–47. doi: 10.1038/mi.2013.52
15. Yang Y, Peng Y, Yang J. Galantamine protects against hydrochloric acid aspiration-induced acute respiratory distress syndrome in rabbits. *Trop J Pharm Res*. (2018) 17:669–73. doi: 10.4314/tjpr.v17i4.15
16. Song JG, Li HH, Cao YF, Lv X, Zhang P, Li YS, et al. Electroacupuncture improves survival in rats with lethal endotoxemia via the autonomic nervous system. *Anesthesiology*. (2012) 116:406–14. doi: 10.1097/ALN.0b013e3182426ebd
17. Pham GS, Wang LA, Mathis KW. Pharmacological potentiation of the efferent vagus nerve attenuates blood pressure and renal injury in a murine model of systemic lupus erythematosus. *Am J Physiol Regul Integr Comp Physiol*. (2018) 315:R1261–71. doi: 10.1152/ajpregu.00362.2017
18. Tracey KJ. The inflammatory reflex. *Nature*. (2002) 420:853–9. doi: 10.1038/nature01321
19. Rosas-Ballina M, Olofsson PS, Ochani M, Valdes-Ferrer SI, Levine YA, Reardon C, et al. Acetylcholine-synthesizing T cells relay neural signals in a vagus nerve circuit. *Science*. (2011) 334:98–101. doi: 10.1126/science.1209985
20. Koopman FA, Chavan SS, Miljko S, Grazio S, Sokolovic S, Schuurman PR, et al. Vagus nerve stimulation inhibits cytokine production and attenuates disease severity in rheumatoid arthritis. *Proc Natl Acad Sci USA*. (2016) 113:8284–9. doi: 10.1073/pnas.1605635113
21. Bonaz B, Sinniger V, Hoffmann D, Clarencon D, Mathieu N, Dantzer C, et al. Chronic vagus nerve stimulation in Crohn's disease: a 6-month follow-up pilot study. *Neurogastroenterol Motility*. (2016) 28:948–53. doi: 10.1111/nmo.12792
22. Mesulam MM, Mufson EJ, Wainer BH, Levey AI. Central cholinergic pathways in the rat: an overview based on an alternative nomenclature (Ch1-Ch6). *Neuroscience*. (1983) 10:1185–201. doi: 10.1016/0306-4522(83)90108-2
23. Ballinger EC, Ananth M, Talmage DA, Role LW. Basal forebrain cholinergic circuits and signaling in cognition and cognitive decline. *Neuron*. (2016) 91:1199–218. doi: 10.1016/j.neuron.2016.09.006
24. Gielow MR, Zaborszky L. The Input-Output Relationship of the Cholinergic Basal Forebrain. *Cell Rep*. (2017) 18:1817–30. doi: 10.1016/j.celrep.2017.01.060
25. Picciotto MR, Higley MJ, Mineur YS. Acetylcholine as a neuromodulator: cholinergic signaling shapes nervous system function and behavior. *Neuron*. (2012) 76:116–29. doi: 10.1016/j.neuron.2012.08.036
26. Prado MA, Reis RA, Prado VF, de Mello MC, Gomez MV, de Mello FG. Regulation of acetylcholine synthesis and storage. *Neurochem Int*. (2002) 41:291–9. doi: 10.1016/S0197-0186(02)00044-X
27. Al-Onaizi MA, Parfitt GM, Kolisnyk B, Law CS, Guzman MS, Barros DM, et al. Regulation of cognitive processing by hippocampal cholinergic tone. *Cereb. Cortex*. (2017) 27:1615–28. doi: 10.1093/cercor/bhv349
28. Takacs VT, Cserep C, Schlingloff D, Posfai B, Szonyi A, Sos KE, et al. Co-transmission of acetylcholine and GABA regulates hippocampal states. *Nat. Commun*. (2018) 9:2848. doi: 10.1038/s41467-018-05136-1
29. Case DT, Burton SD, Gedeon JY, Williams SG, Urban NN, Seal RP. Layer- and cell type-selective co-transmission by a basal forebrain cholinergic projection to the olfactory bulb. *Nat Commun*. (2017) 8:652. doi: 10.1038/s41467-017-00765-4
30. Kljakic O, Janickova H, Prado VF, Prado MAM. Cholinergic/glutamatergic co-transmission in striatal cholinergic interneurons: new mechanisms regulating striatal computation. *J Neurochem*. (2017) 142(Suppl. 2):90–102. doi: 10.1111/jnc.14003
31. Saunders A, Granger AJ, Sabatini BL. Corelease of acetylcholine and GABA from cholinergic forebrain neurons. *eLife*. (2015) 4:e06412. doi: 10.7554/eLife.06412
32. Waldburger JM, Boyle DL, Edgar M, Sorkin LS, Levine YA, Pavlov VA, et al. Spinal p38 MAP kinase regulates peripheral cholinergic outflow. *Arthritis Rheum*. (2008) 58:2919–21. doi: 10.1002/art.23807
33. Volpicelli LA, Levey AI. Muscarinic acetylcholine receptor subtypes in cerebral cortex and hippocampus. *Progr Brain Res*. (2004) 145:59–66. doi: 10.1016/S0079-6123(03)45003-6
34. Shirey JK, Brady AE, Jones PJ, Davis AA, Bridges TM, Kennedy JP, et al. A selective allosteric potentiator of the M1 muscarinic acetylcholine receptor increases activity of medial prefrontal cortical neurons and restores impairments in reversal learning. *J Neurosci*. (2009) 29:14271–86. doi: 10.1523/JNEUROSCI.3930-09.2009
35. Ma L, Seager MA, Wittmann M, Jacobson M, Bickel D, Burno M, et al. Selective activation of the M1 muscarinic acetylcholine receptor achieved by allosteric potentiation. *Proc Natl Acad Sci USA*. (2009) 106:15950–5. doi: 10.1073/pnas.0900903106
36. Rosas-Ballina M, Valdes-Ferrer SI, Dancho ME, Ochani M, Katz D, Cheng KF, et al. Xanomeline suppresses excessive pro-inflammatory cytokine responses through neural signal-mediated pathways and improves survival in lethal inflammation. *Brain Behav Immun*. (2015) 44:19–27. doi: 10.1016/j.bbi.2014.07.010
37. Huston JM, Ochani M, Rosas-Ballina M, Liao H, Ochani K, Pavlov VA, et al. Splenectomy inactivates the cholinergic antiinflammatory pathway during lethal endotoxemia and polymicrobial sepsis. *J Exp Med*. (2006) 203:1623–8. doi: 10.1084/jem.20052362
38. Rosas-Ballina M, Ochani M, Parrish WR, Ochani K, Harris YT, Huston JM, et al. Splenic nerve is required for cholinergic antiinflammatory pathway control of TNF in endotoxemia. *Proc Natl Acad Sci USA*. (2008) 105:11008–13. doi: 10.1073/pnas.0803237105
39. Suarez AN, Hsu TM, Liu CM, Noble EE, Cortella AM, Nakamoto EM, et al. Gut vagal sensory signaling regulates hippocampus function through multi-order pathways. *Nat Commun*. (2018) 9:2181. doi: 10.1038/s41467-018-04639-1
40. Kolisnyk B, Guzman MS, Raulic S, Fan J, Magalhaes AC, Feng G, et al. (2013). ChAT-ChR2-EYFP mice have enhanced motor endurance but show deficits in attention and several additional cognitive domains. *J Neurosci*. 33: 10427–38. doi: 10.1523/JNEUROSCI.0395-13.2013
41. Janickova H, Rosborough K, Al-Onaizi M, Kljakic O, Guzman MS, Gros R, et al. (2017). Deletion of the vesicular acetylcholine transporter from pedunculopontine/laterodorsal tegmental neurons modifies gait. *J Neurochem*. 140:787–98. doi: 10.1111/jnc.13910
42. Broncel A, Bocian R, Klos-Wojtczak P, Konopacki J. Medial septal cholinergic mediation of hippocampal theta rhythm induced by vagal nerve stimulation. *PLoS ONE*. (2018) 13:e0206532. doi: 10.1371/journal.pone.0206532
43. Hickman JL PX, Donegan D, Welle CG. Temporally precise vagus nerve stimulation (VNS) enhances motor learning and performance of a skilled forelimb reach task. In: *Neuroscience Meeting Planner*. San Diego, CA: Society for Neuroscience Online, Society for Neuroscience (2018).
44. Tetrault S, Chever O, Sik A, Amzica F. Opening of the blood-brain barrier during isoflurane anaesthesia. *Eur J Neurosci*. (2008) 28:1330–41. doi: 10.1111/j.1460-9568.2008.06443.x
45. Consolim-Colombo FM, Sangaleti CT, Costa FO, Morais TL, Lopes HF, Motta JM, et al. Galantamine alleviates inflammation and insulin resistance in patients with metabolic syndrome in a randomized trial. *JCI Insight*. (2017) 2:93340. doi: 10.1172/jci.insight.93340
46. Ye H, Fussenegger M. Optogenetic medicine: synthetic therapeutic solutions precision-guided by light. *Cold Spring Harb Perspect Med*. (2018). doi: 10.1101/cshperspect.a034371
47. Boyden ES. Optogenetics and the future of neuroscience. *Nat Neurosci*. (2015) 18:1200–1. doi: 10.1038/nn.4094
48. Deisseroth K. Optogenetics: 10 years of microbial opsins in neuroscience. *Nat Neurosci*. (2015) 18:1213–25. doi: 10.1038/nn.4091
49. Montgomery KL, Iyer SM, Christensen AJ, Deisseroth K, Delp SL. Beyond the brain: Optogenetic control in the spinal cord and peripheral nervous system. *Sci Transl Med*. (2016) 8:337rv335. doi: 10.1126/scitranslmed.aad7577

50. Lee DJ, Gurkoff GG, Izadi A, Berman RF, Ekstrom AD, Muizelaar JP, et al. Medial septal nucleus theta frequency deep brain stimulation improves spatial working memory after traumatic brain injury. *J Neurotrauma*. (2013) 30:131–9. doi: 10.1089/neu.2012.2646
51. Lee DJ, Gurkoff GG, Izadi A, Seidl SE, Echeverri A, Melnik M, et al. Septohippocampal neuromodulation improves cognition after traumatic brain injury. *J Neurotrauma*. (2015) 32:1822–32. doi: 10.1089/neu.2014.3744
52. Zimerman M, Hummel FC. Non-invasive brain stimulation: enhancing motor and cognitive functions in healthy old subjects. *Front Aging Neurosci*. (2010) 2:149. doi: 10.3389/fnagi.2010.00149
53. Cabrera LY, Evans EL, Hamilton RH. Ethics of the electrified mind: defining issues and perspectives on the principled use of brain stimulation in medical research and clinical care. *Brain Topogr*. (2014) 27:33–45. doi: 10.1007/s10548-013-0296-8
54. Fregni F, Pascual-Leone A. Technology insight: noninvasive brain stimulation in neurology-perspectives on the therapeutic potential of rTMS and tDCS. *Nat Clin Pract Neurol*. (2007) 3:383–93. doi: 10.1038/ncpneuro0530
55. Kokras N, Stamouli E, Sotiropoulos I, Katirtzoglou EA, Siarkos KT, Dalagiorgou G, et al. Acetyl cholinesterase inhibitors and cell-derived peripheral inflammatory cytokines in early stages of alzheimer's disease. *J Clin Psychopharmacol*. (2018) 38:138–43. doi: 10.1097/JCP.0000000000000840
56. Perry VH, Cunningham C, Holmes C. Systemic infections and inflammation affect chronic neurodegeneration. *Nat Rev Immunol*. (2007) 7:161–7. doi: 10.1038/nri2015
57. Holmes C, Cunningham C, Zotova E, Woolford J, Dean C, Kerr S, et al. Systemic inflammation and disease progression in Alzheimer disease. *Neurology*. (2009) 73:768–74. doi: 10.1212/WNL.0b013e3181b6bb95
58. Hampel H, Mesulam MM, Cuello AC, Farlow MR, Giacobini E, Grossberg GT, et al. The cholinergic system in the pathophysiology and treatment of Alzheimer's disease. *Brain*. (2018) 141:1917–33. doi: 10.1093/brain/awy132
59. McManus RM, Heneka MT. Role of neuroinflammation in neurodegeneration: new insights. *Alzheimers Res Ther*. (2017) 9:14. doi: 10.1186/s13195-017-0241-2
60. Zaghloul N, Addorisio ME, Silverman HA, Patel HL, Valdes-Ferrer SI, Ayasolla KR, et al. Forebrain cholinergic dysfunction and systemic and brain inflammation in murine sepsis survivors. *Front Immunol*. (2017) 8:1673. doi: 10.3389/fimmu.2017.01673
61. Dantzer R, O'Connor JC, Freund GG, Johnson RW, Kelley KW. From inflammation to sickness and depression: when the immune system subjugates the brain. *Nat Rev Neurosci*. (2008) 9:46–56. doi: 10.1038/nrn2297
62. Coltart I, Tranah TH, Shawcross DL. Inflammation and hepatic encephalopathy. *Arch Biochem Biophys*. (2013) 536:189–96. doi: 10.1016/j.abb.2013.03.016
63. Felipo V. Hepatic encephalopathy: effects of liver failure on brain function. *Nat Rev Neurosci*. (2013) 14:851–8. doi: 10.1038/nrn3587
64. Metz CN, Pavlov VA. Vagus nerve cholinergic circuitry to the liver and the gastrointestinal tract in the neuroimmune communicatome. *Am J Physiol Gastrointest Liver Physiol*. (2018) 315:G651–8. doi: 10.1152/ajpgi.00195.2018
65. Garcia-Ayllon MS, Cauli O, Silveyra MX, Rodrigo R, Candela A, Compan A, et al. Brain cholinergic impairment in liver failure. *Brain*. (2008) 131:2946–56. doi: 10.1093/brain/awn209
66. Maldonado JR. Neuropathogenesis of delirium: review of current etiologic theories and common pathways. *Am J Geriatr Psychiatry*. (2013) 21:1190–222. doi: 10.1016/j.jagp.2013.09.005
67. Hshieh TT, Fong TG, Marcantonio ER, Inouye SK. Cholinergic deficiency hypothesis in delirium: a synthesis of current evidence. *J Gerontol Ser A Biol Sci Med Sci*. (2008) 63:764–72. doi: 10.1093/gerona/63.7.764
68. Zhao S, Ting JT, Atallah HE, Qiu L, Tan J, Gloss B, et al. Cell type-specific channelrhodopsin-2 transgenic mice for optogenetic dissection of neural circuitry function. *Nat Methods*. (2011) 8:745–52. doi: 10.1038/nmeth.1668
69. Hamilton SE, Loose MD, Qi M, Levey AI, Hille B, McKnight GS, et al. Disruption of the m1 receptor gene ablates muscarinic receptor-dependent M current regulation and seizure activity in mice. *Proc Natl Acad Sci USA*. (1997) 94:13311–6. doi: 10.1073/pnas.94.24.13311
70. Kow RL, Cheng EM, Jiang K, Le JH, Stella N, Nathanson NM. (2015). Muscarinic M1 receptor and cannabinoid CB1 receptor do not modulate paraoxon-induced seizures. *Pharmacol Res Perspect*. 3:e00100. doi: 10.1002/prp2.100
71. Parrish WR, Rosas-Ballina M, Gallowitsch-Puerta M, Ochani M, Ochani K, Yang LH, et al. Modulation of TNF release by choline requires alpha7 subunit nicotinic acetylcholine receptor-mediated signaling. *Mol Med*. (2008) 14:567–74. doi: 10.2119/2008-00079.Parrish
72. Tarnawski L, Reardon C, Caravaca AS, Rosas-Ballina M, Tusche MW, Drake AR, et al. Adenylyl cyclase 6 mediates inhibition of TNF in the inflammatory reflex. *Front Immunol*. (2018) 9:2648. doi: 10.3389/fimmu.2018.02648
73. Roy A, Dakroub M, Tezini GC, Liu Y, Guatimosim S, Feng Q, et al. Cardiac acetylcholine inhibits ventricular remodeling and dysfunction under pathologic conditions. *FASEB J*. (2016) 30:688–701. doi: 10.1096/fj.15-277046
74. Roy A, Fields WC, Rocha-Resende C, Resende RR, Guatimosim S, Prado VF, et al. Cardiomyocyte-secreted acetylcholine is required for maintenance of homeostasis in the heart. *FASEB J*. (2013) 27:5072–82. doi: 10.1096/fj.13-238279

Conflict of Interest Statement: VAP, SSC, and KJT are inventors on patents broadly related to the topic of this paper and have assigned their rights to the Feinstein Institute for Medical Research. YL was employed by SetPoint Medical Corporation (Valencia, CA 91355, USA).

The remaining authors declare that the research was conducted in the absence of any commercial or financial relationships that could be construed as a potential conflict of interest.

Copyright © 2019 Lehner, Silverman, Addorisio, Roy, Al-Onaizi, Levine, Olofsson, Chavan, Gros, Nathanson, Al-Abed, Metz, Prado, Prado, Tracey and Pavlov. This is an open-access article distributed under the terms of the Creative Commons Attribution License (CC BY). The use, distribution or reproduction in other forums is permitted, provided the original author(s) and the copyright owner(s) are credited and that the original publication in this journal is cited, in accordance with accepted academic practice. No use, distribution or reproduction is permitted which does not comply with these terms.

frontiers in Immunology

ORIGINAL RESEARCH
published: 03 May 2019
doi: 10.3389/fimmu.2019.00980

TLR3 Ligand PolyI:C Prevents Acute Pancreatitis Through the Interferon-β/Interferon-α/β Receptor Signaling Pathway in a Caerulein-Induced Pancreatitis Mouse Model

Chaohao Huang[1,2,3], Shengchuan Chen[1,2,3], Tan Zhang[1,2,3], Dapei Li[2,3], Zhonglin Huang[2,3], Jian Huang[4], Yanghua Qin[5], Bicheng Chen[1], Genhong Cheng[2,3], Feng Ma[1,2,3] and Mengtao Zhou[1]**

[1] Key Laboratory of Diagnosis and Treatment of Severe Hepato-Pancreatic Diseases of Zhejiang Province, Department of Surgery, First Affiliated Hospital of Wenzhou Medical University, Wenzhou, China, [2] Suzhou Institute of Systems Medicine, Peking Union Medical College, Chinese Academy of Medical Sciences, Suzhou, China, [3] Center for Systems Medicine, Institute of Basic Medical Sciences, Peking Union Medical College, Chinese Academy of Medical Sciences, Beijing, China, [4] Department of Emergency, First Affiliated Hospital of Soochow University, Suzhou, China, [5] Department of Laboratory Diagnosis, Changhai Hospital, The Second Military Medical University, Shanghai, China

Acute pancreatitis (AP) is a common and devastating inflammatory disorder of the pancreas. However, there are still no effective treatments available for the disease. Therefore, it is important to discover new therapeutic targets and strategies for better treatment and prognosis of AP patients. Toll-like receptor 3 (TLR3) ligand polyI:C is a double-stranded RNA mimic that can be used as an immune stimulant. Our current study indicates that polyI:C exerted excellent anti-inflammatory effects in a caerulein-induced AP mouse model and taurocholate-induced pancreatic acinar cell line injury model. We found that polyI:C triggers type I interferon (IFN) production and downstream IFN-α/β receptor (IFNAR)-dependent signaling, which play key roles in protecting the pancreas from inflammatory injury. Knockout of IFN-β and IFNAR in mice abolished the preventive effects of polyI:C on caerulein-induced AP symptoms, which include pancreatic edema, neutrophil infiltration, the accumulation of reactive oxygen species (ROS), and inflammatory gene expression. Treating pancreatic acinar 266-6 cells with an IFNAR inhibitor, which blocks the interaction between type I IFN and IFNAR, diminishes the downregulation of oxidative stress by polyI:C. Additionally, a subsequent transcriptome analysis on the role of polyI:C in treating pancreatitis suggested that chemotaxis of neutrophils and the production of ROS were inhibited by polyI:C in the pancreases damaged by caerulein injection. Thus, polyI:C may act as a type I IFN inducer to alleviate AP, and it has the potential to be a promising therapeutic agent used at the early stages of AP.

Keywords: acute pancreatitis, TLR3 ligands, polyI:C, reactive oxygen species, type I interferon, IFN-β, neutrophil infiltration

OPEN ACCESS

Edited by:
Timothy Robert Billiar, University of Pittsburgh, United States

Reviewed by:
Hansjörg Hauser, Helmholtz Association of German Research Centers (HZ), Germany
Kaifeng Shao, Harvard Medical School, United States

***Correspondence:**
Mengtao Zhou
zhoumengtao@wmu.edu.cn
Feng Ma
mf@ism.cams.cn

Specialty section:
This article was submitted to Inflammation, a section of the journal Frontiers in Immunology

Received: *23 October 2018*
Accepted: *16 April 2019*
Published: *03 May 2019*

Citation:
Huang C, Chen S, Zhang T, Li D, Huang Z, Huang J, Qin Y, Chen B, Cheng G, Ma F and Zhou M (2019) TLR3 Ligand PolyI:C Prevents Acute Pancreatitis Through the Interferon-β/Interferon-α/β Receptor Signaling Pathway in a Caerulein-Induced Pancreatitis Mouse Model. Front. Immunol. 10:980. doi: 10.3389/fimmu.2019.00980

HIGHLIGHTS

- PolyI:C significantly alleviates caerulein-induced acute pancreatitis;
- PolyI:C attenuates acute pancreatitis-related oxidative stress;
- PolyI:C protects mice from pancreatic injuries in an IFN-β-dependent manner;
- TLR3 agonists would be promising therapeutic agents for acute pancreatitis.

INTRODUCTION

Acute pancreatitis (AP) is an inflammatory condition of the pancreas, that frequently leads to systemic inflammatory response syndrome (SIRS), multiple organ dysfunction syndromes (MODS), and even death without early intervention (1). The mortality of individuals with AP-MODS exceeds 20%, and the quality of life of those who experience the devastating inflammatory disease is significantly worse than that of the general population (2). Research from many groups including our own have shown that pancreatitis involves pancreas edema, inflammatory cell infiltration, and high levels of serum amylase and lipase (3, 4). Meanwhile, reactive oxygen species (ROS) generated by injured pancreatic acinar cells and infiltrated immune cells are key factors in the progression of pancreatitis (5). Therefore, novel therapeutic strategies or pharmaceutical interventions to decrease the accumulation of ROS, limit local inflammatory damage, and accelerate the recovery of the injured pancreas are needed urgently.

Previous studies on AP have suggested that damage of pancreatic acinar cells results in the upregulation of inflammatory cytokines and chemokines (6). They initiate the inflammatory response and the recruitment of inflammatory cells, which leads to pancreatitis (7). Activated inflammatory cells contribute to subsequent pancreatic injury through the generation of ROS (8). As the ROS accumulate, so does the demand for the anti-superoxide response (9). Heme Oxygenase-1 (HO-1), a well-known anti-oxidant molecule, is always highly expressed during the inflammatory response (10). High levels of HO-1 are an indicator of severe tissue damage and oxidative stress, which require a stronger anti-oxidant reaction (10). Thus, HO-1 could be used as an indicator for measuring the severity of damage and inflammation in AP.

PolyI:C is synthetic double-stranded RNA, which is used as a viral RNA mimic to induce type I IFN and trigger antiviral immunity-based pathways in the host. PolyI:C is considered to be a pathogen-associated molecular pattern (PAMP) because it interacts with Toll-like receptor 3 (TLR3) and activates TLR3-dependent downstream signaling (11, 12). Pattern recognition receptors (PRRs) such as TLR9 and NLRP3 are required for the development of inflammation in AP, and their antagonism could provide a new therapeutic strategy for treating AP (13). Moreover, TLR3 ligand polyI:C treatment significantly decreases the mortality and liver injury caused by injection of lipopolysaccharide (LPS) in the presence of D-galactosamine (D-GalN) in C57BL/6 mice (14), which has driven us to test the anti-inflammatory role of polyI:C during AP progression. As a downstream product of the TLR3-TRIF-TBK1-IRF3 signaling axis, type I IFN has been demonstrated as an immune mediator that also exerts an anti-inflammatory function as well as its antiviral activity (15). IFN-α and IFN-β are key members of the type I IFN family in combating virus infection and regulating immune function, and IFN-β is the initial response of type I IFN produced at the early stages of infection or following PAMP stimulation (16, 17). Subsequently, more IFN-β and IFN-α is produced at the later stages of infection via a positive feedback loop (16–18). It was demonstrated that IFN-β counteracts the overexpressed ICAM-1 in cultured brain-derived microvascular endothelial cells (BMEC) incubated with TNF-α, which leads to a reduction in the adhesion of leukocytes to blood vessels and thus a reduced inflammatory reaction (19). Many other similar observations support the conclusion that IFN-β participates in attenuating the acute inflammatory response because of its regulatory effect (20, 21). It is interesting to investigate whether polyI:C has the potential to limit detrimental and pathological immune responses which lead to tissue damage in a caerulein-induced pancreatitis mouse model, via the IFN-β/IFNAR signaling pathway.

In this study, we have found that polyI:C pretreatment prevents caerulein-induced pancreas edema, neutrophil infiltration, the accumulation of ROS, and inflammatory gene expression in the AP mice models. PolyI:C-triggered IFN-β production and downstream IFNAR signaling activation are required for the suppressive effect of polyI:C in the caerulein-induced AP model. Our study has not only demonstrated the protective role of polyI:C in limiting AP, but has also suggested a potential application of TLR3 ligands in the treatment of AP.

MATERIALS AND METHODS

Mice and Reagents

Ifnb$^{-/-}$ mice and *Ifnar1*$^{-/-}$ mice were gifted from Genhong Cheng Laboratory (University of California, CA, USA). *Tlr4*$^{-/-}$ mice were purchased from Model Animal Research Center (Nanjing, China). Wild-type (WT) C57BL/6 mice were acquired from Vital River Laboratory Animal Technology (Beijing, China). All the mice were maintained in the specific pathogen-free (SPF) environment at Suzhou Institute of Systems Medicine (ISM) under a controlled temperature (25°C) and a 12-h day/night cycle. Male 8–10-week-old mice were used in all the experimental AP mice models. All mice experiments were undertaken in accordance with the US National Institutes of Health Guide for the Care and Use of Laboratory Animals, with the approval of the Scientific Investigation Board of ISM, Suzhou. Antibodies against HO-1 (#70081) and GAPDH (#5174) were from Cell Signaling Technology (Danvers, MA). NQO1 antibody (#ab2346) and KEAP1 antibody (#ab119403) were from Abcam (Cambridge, MA). Caerulein and IFNAR inhibitor were from MCE (Monmouth Junction, NJ). L-Arginine was from Sigma-Aldrich (St. Louis, MO). PolyI:C was from Thermo Fisher Scientific (Waltham, MA). Recombinant mouse IFN-β was from R&D Systems (Minneapolis, MN). Taurocholate was from SolarBio (Beijing, China).

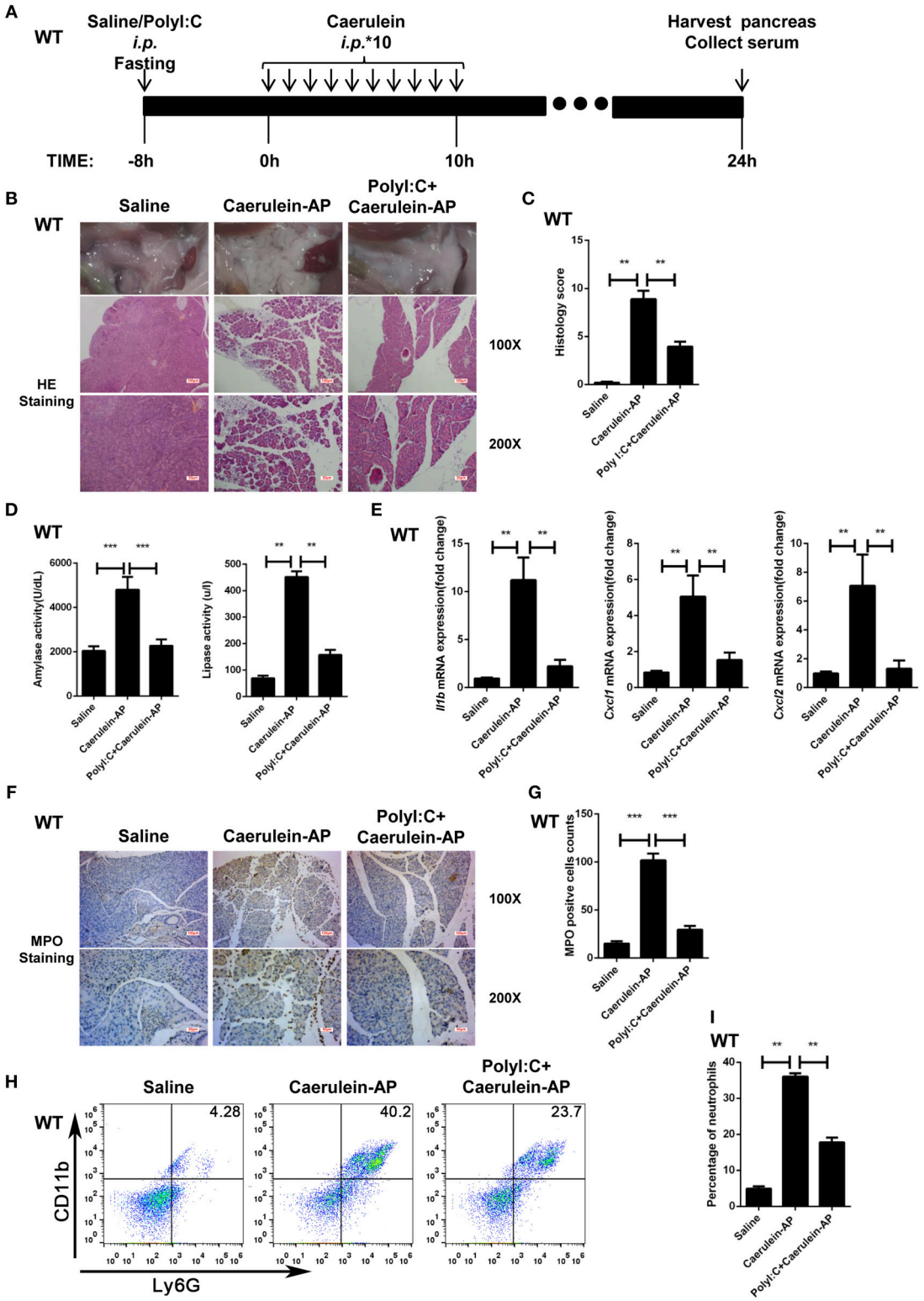

FIGURE 1 | Polyl:C prevents caerulein-induced AP in the WT mice. **(A)** Schematic diagram of the caerulein-induced experimental AP mouse model. Saline or polyl:C (10 mg/kg) was intraperitoneally administrated 8 h prior to the induction of AP. **(B)** Histopathological examination of the effect of polyl:C on WT caerulein-induced experimental AP mouse models. Top panel: gross observation; middle panel: H&E staining, 100X magnification; bottom panel: H&E staining, 200X magnification.

(Continued)

FIGURE 1 | (C) Histology scores of pancreatitis were evaluated and compared after observing five separate fields. **(D)** Activities of the serum amylase (left) and lipase (right) from Saline, Caerulein-AP, and PolyI:C+Caerulein-AP WT mice were compared via enzymatic methods. **(E)** mRNA expression levels of *Il1b*, *Cxcl1*, and *Cxcl2* genes in the pancreatic tissue from Saline, Caerulein-AP, and PolyI:C+Caerulein-AP WT mice were detected by RT-qPCR and normalized to *Rpl32*. **(F)** Neutrophil infiltrations in the pancreases from WT caerulein-induced experimental AP mouse models were measured and compared by MPO staining. Top panel: 100X magnification; bottom panel: 200X magnification. **(G)** MPO^+ cells were counted and compared after observing five separate fields. **(H)** Pancreases neutrophils from the Saline, Caerulein-AP, and PolyI:C+Caerulein-AP WT mice were analyzed by flow cytometry. $CD11b^+Ly6G^+$ cells were considered as neutrophils. **(I)** The percentage of neutrophils from indicated groups were calculated and compared. Data of **(B,F,H)** are representative of three independent experiments. Data of **(C,G)** are shown as mean ± SD ($n = 5$) from one representative experiment. Data of **(D,E,I)** are shown as mean ± SEM from at least three independent experiments. $^*p < 0.05$, $^{**}p < 0.01$, $^{***}p < 0.001$, one-way ANOVA test.

Experimental AP Mice Models

Before the induction of experimental AP, the mice fasted for 8 h and were intraperitoneally injected with 100 μl polyI:C (10 mg/kg) or saline as a control. After 1 or 8 h of polyI:C/saline injection, the mice were intraperitoneally administered 200 μl caerulein (200 μg/kg) 10 times or L-Arginine (2.5 g/kg) twice, 1 h apart. Mice were sacrificed at 24 h post the initial induction of the AP, and the serum and pancreas were collected for further analysis. The pancreases were placed in 4% paraformaldehyde for histological analysis or stored in RNAlater (QIAGEN, Düsseldorf, Germany) for RNA extraction. In addition, fresh pancreases were isolated for analyzing inflammatory immune cell infiltration via flow cytometry or snap-frozen for protein extraction for western blotting analysis.

Cell Culture and Flow Cytometry Analysis

The mouse pancreatic acinar 266-6 cell line was purchased from ATCC (Manassas, VA) and cultured in RPMI-1640 medium supplemented with 10% FBS (Gibco, ThermoFisher Scientific) 100 IU/ml penicillin and 100 μg/ml streptomycin under the conditions of 37°C and 5% CO_2. To induce pancreatitis *in vitro*, the 266-6 cells were stimulated with 0.5 mM taurocholate in the presence of polyI:C (1 μg/ml) or IFN-β (200 U/ml). Twenty-four hours later, cells were collected for the following Western blot assay, DCFH-DA staining, and flow cytometry analysis. To analyze the infiltrated innate immune cells during caerulein-induced AP, pancreases of mice were immediately harvested and incubated with 1 mg/ml collagenase D (ThermoFisher Scientific, Waltham, MA), and minced into small pieces on ice. Single pancreatic cell suspensions were first stained with Fc blocking antibody, then immune-labeled with fluorochrome-conjugated antibodies in PBS supplemented with 2% heat-inactivated FBS (Gibco, Thermo Fisher Scientific); isotype controls were also included. Antibodies Alexa Fluor 647-conjugated anti-CD11b, PE-conjugated anti-F4/80, and PerCP/Cy5.5-conjugated anti-Ly6G were purchased from BioLegend (San Diego, CA). Flow cytometry analysis was performed on a Life Launch Attune NxT Flow Cytometer (ThermoFisher Scientific, Waltham, MA) after gating the living cells. Data were analyzed using FlowJo software (version 10.0).

Pancreas Histological Examination and Neutrophil Immunohistochemistry

Pancreatic tissues were collected 24 h after the induction of AP by caerulein and were fixed in 4% paraformaldehyde in PBS. Paraffin embedded tissues from each mouse were sectioned at 5 μm and these were followed by H&E staining. Immunohistochemistry for neutrophil marker MPO (#ab9535, Abcam, San Francisco, CA) was performed on saline or caerulein-induced AP tissues. Briefly, 5 μm thick paraffin sections of formalin-fixed paraffin-embedded pancreatic tissue were fixed in dimethylbenzene, quenched with 3% H_2O_2, and blocked with goat serum. After three washes with PBS, the sections were treated with anti-MPO primary antibody (1:50) overnight. Then, the sections were incubated with horseradish-peroxidase–conjugated secondary antibody for 1 h. Finally, color was developed using DAB as peroxidase substrate, and the slides were counterstained with hematoxylin for bright field microscopy. The degree of pancreatic injury was evaluated by light microscopy in 200X magnification over five separate fields. The severity of pancreatitis was scored mainly based on the description in the previous study (22), and is listed in **Supplementary Table 2**.

Enzymatic Method Measurement of Serum Amylase and Lipase

Blood from experimental AP mouse models was centrifuged at 4,000 rpm, 1,500 g for 10 min at 4°C to separate the serum. Serum samples were diluted to the appropriate concentration and incubated with corresponding reagents in kit, then amylase and lipase activities were measured by commercial α-Amylase Assay Kit (C016-1) and Lipase Activity Kit (A054-2), respectively, according to the manufacturer's instructions (Nanjing Jiancheng Bioengineering Institute, Nanjing, China).

Intracellular ROS Detection

Intracellular ROS intensity was measured by Reactive Oxygen Species Assay Kit (Beyotime, Shanghai) as described in the manufacturer's instructions. DCFH-DA fluorescence was measured by using Life Launch Attune NxT Flow Cytometer (Thermo Fisher Scientific, Waltham, MA, USA). Images were taken using Nikon Eclipse TI fluorescence microscope (Nikon Corporation, Tokyo). Data were analyzed using FlowJo software (version 10).

Protein Extraction and Western Blotting

Snap-frozen pancreatic tissues were homogenized and resuspended in the buffer containing 4% sodium dodecyl sulfate (SDS) and 100 mM Tris-HCl. For immunoblot analysis, pancreatic tissue and 266-6 cells were collected in Triton lysis buffer (50 mM Tris-Cl, pH 7.5, 150 mM NaCl, 1 mM EDTA, 1% Triton X-100, and 5% glycerol) containing complete protease

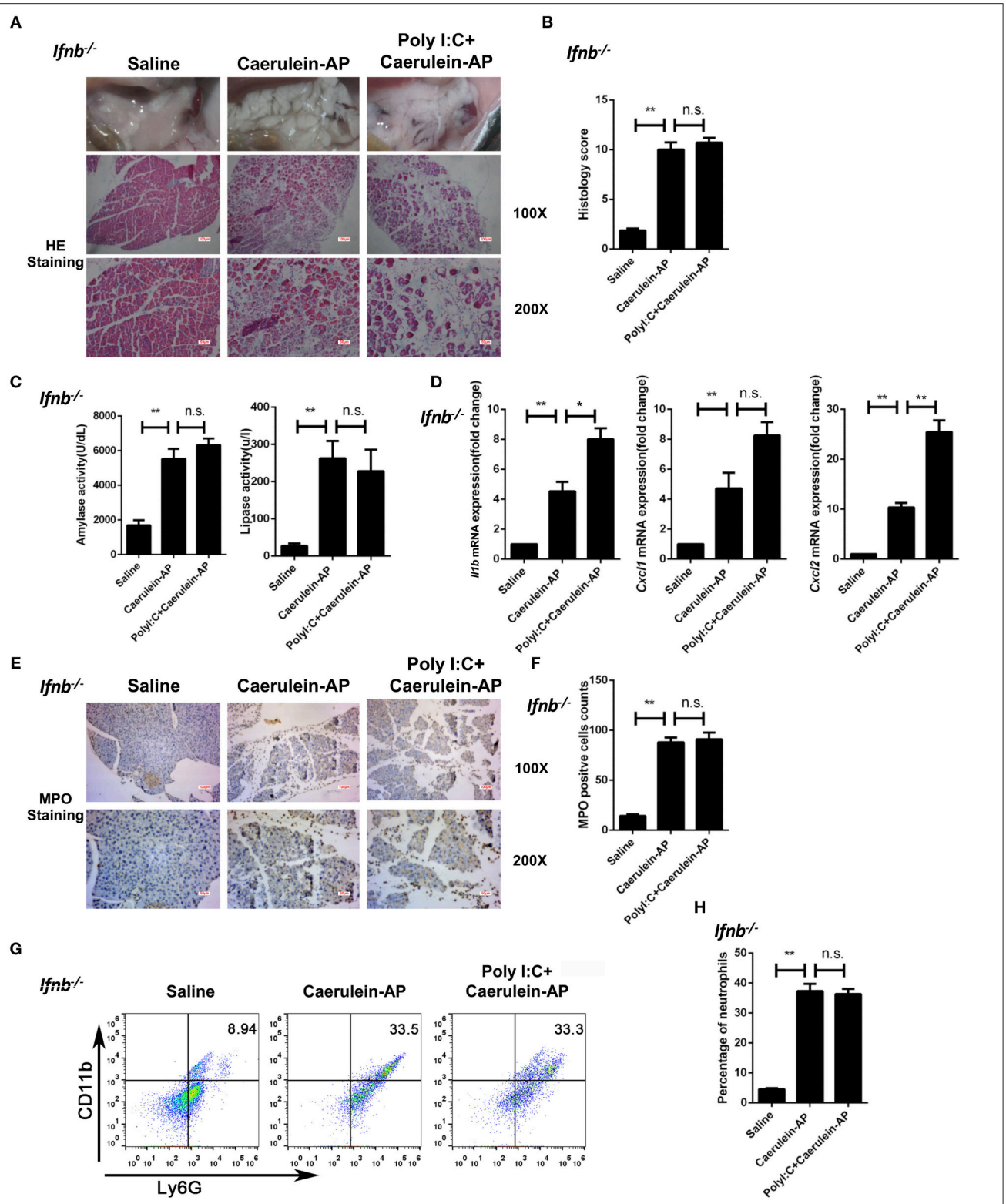

FIGURE 2 | Knockout of Ifnb abolishes the protective effects of polyI:C on the caerulein-induced AP mouse model. **(A)** Histopathological examination of the effect of polyI:C on *Ifnb*$^{-/-}$ caerulein-induced experimental AP mouse models. Top panel: gross observation; middle panel: H&E staining, 100X magnification; bottom panel: H&E staining, 200X magnification. **(B)** Histology scores of pancreatitis were evaluated and compared after observing five separate fields. **(C)** Activities of the serum amylase (left) and lipase (right) from Saline, Caerulein-AP, and PolyI:C+Caerulein-AP *Ifnb*$^{-/-}$ mice were compared via enzymatic methods.

(Continued)

FIGURE 2 | (D) mRNA expression levels of *Il1b*, *Cxcl1*, and *Cxcl2* genes in the pancreatic tissue from Saline, Caerulein-AP, and PolyI:C+Caerulein-AP *Ifnb*$^{-/-}$ mice were detected by RT-qPCR and normalized to *Rpl32*. **(E)** Neutrophil infiltrations in the pancreases from *Ifnb*$^{-/-}$ caerulein-induced experimental AP mouse models were measured and compared by MPO staining. Top panel: 100X magnification; bottom panel: 200X magnification. **(F)** MPO^{+} cells were counted and compared after observing five separate fields. **(G)** Pancreases neutrophils from the Saline, Caerulein-AP, and PolyI:C+Caerulein-AP *Ifnb*$^{-/-}$ mice were analyzed by flow cytometry. CD11b^{+}Ly6G^{+} cells were considered as neutrophils. **(H)** The percentage of neutrophils from indicated groups were calculated and compared. Data of **(A,E,G)** are representative of three independent experiments. Data of **(B,F)** are shown as mean ± SD ($n = 5$) from one representative experiment. Data of **(C,D,H)** are shown as mean ± SEM from at least three independent experiments. *$p < 0.05$, **$p < 0.01$, n.s., not significant, one-way ANOVA test.

inhibitors (Roche). Protein concentrations of the extracts were measured with a BCA assay (ThermoFisher Scientific) and equalized with the lysis buffer. Equal amounts of the extracts were loaded and subjected to SDS-PAGE, transferred onto PVDF membranes (Millipore), and then blotted with enhanced chemiluminescence (Pierce) or Odyssey Imaging Systems (LI-COR Biosciences).

RNA Isolation and Quantitative PCR (qPCR)

RNA was isolated from pancreatic tissue which was stored in RNAlater or 266-6 cells using TRIzol (ThermoFisher Scientific) according to the manufacturer's instructions. Following RNA concentration, quantitation of 1 μg of RNA was used to make cDNA using PrimeScript™ RT Reagent Kit for RT-PCR (Takara Shuzo Co., Tokyo) according to the manufacturer's instructions. Real time PCR analysis was performed using cDNA in the Roche 480 instrument using SYBR from Toneker Biotech (Suzhou, Jiangsu). The relative mRNA expression level of genes was normalized to the internal control ribosomal protein gene *Rpl32* by using $2^{-\Delta\Delta Ct}$ cycle threshold method (23). The primer sequences for qPCR were from the primer bank (24), and sequences are listed in **Supplementary Table 1**.

RNA-Sequencing Data Acquisition, Quality Control, and Processing

Total pancreas RNA was extracted from caerulein-induced experimental AP mice models. RNA concentration was quantified using a Qubit 2.0 Fluorometer (Thermo Fisher). The quality of extracted RNA was evaluated using an Agilent Technology 2100 Bioanalyzer. RNA libraries were constructed using a TruSeq Stranded mRNA Sample Prep Kit (Illumina) according to the manufacturer's guidelines. The quantity and quality of the libraries were also assessed by Qubit and Agilent 2100 Bioanalyzer, respectively; their molar concentration was validated by qPCR for library pooling. Libraries were sequenced on the HiSeq X10 using the paired end 2*150 bp, dual-index format. For RNA-Seq data analysis, Trimmomatic was used to remove Illumina sequencing adapters within raw reads of every sample, trim low quality bases of both read ends (with parameters LEADING:3 TRAILING:3 SLIDINGWINDOW:4:15) and drop one read if its length is <36 bp. Secondly, the clean reads were mapped to mouse mm 10 reference genome with STAR, and the alignment bam files were used as htseq-count (command of python package HTSeq) input to get read counts of genes. Finally, DESeq2 was used to identify DEGs ($p \leq 0.05$, FC ≥ 2) based on raw read counts. For DEGs, Ingenuity Pathway Analysis (IPA) and GO biological process were performed by Fisher's exact test, the enrichment *p*-values of which were corrected by the Bonferroni method. RNA-Seq data have been deposited to Gene Expression Omnibus (GSE119844).

Statistical Analysis

The data represent the mean of at least three independent experiments, and error bars represent standard error or standard deviation of the mean. Statistical analysis was performed by unpaired 2-tailed student *t* test or one-way analysis of variance (ANOVA) followed by Tukey's multiple-comparison tests using GraphPad Prism (version 5; GraphPad Sofware Inc.). $p < 0.05$ was considered as a statistically significant difference.

RESULTS

PolyI:C Prevents AP in WT Mice

The protective effect of polyI:C on pancreatitis was evaluated in the caerulein-AP experimental mouse model at 24 h after the first injection of caerulein (**Figure 1A**). Administration with caerulein led to dramatic pathological changes including pancreas edema, inflammatory cell infiltration, and tissue necrosis. However, polyI:C pretreatment prevents these pancreatitis symptoms induced by caerulein injection (**Figures 1B,C**). Consistently, polyI:C pretreatment inhibited the elevation of serum amylase and lipase in the caerulein-AP mouse model (**Figure 1D**). PolyI:C also suppressed the induction of inflammatory cytokine and chemokine gene expression including IL-1β, CXCL1, and CXCL2 in the injured pancreases from caerulein-AP mice (**Figure 1E**). Neutrophils were recruited into the injured pancreases during pancreatitis progression, whereas notably fewer MPO^{+} cells were observed in the injured pancreases from caerulein-AP mice pretreated with polyI:C. This suggests polyI:C pretreatment inhibited neutrophil infiltration, a key cause of AP (**Figures 1F,G**). These immunohistochemistry results were verified by flow cytometry assay. Significantly fewer infiltrated CD11b^{+}Ly6G^{+} cells (neutrophils) were detected in the pancreases from polyI:C-pretreated AP models (**Figures 1H,I**), while the infiltrated CD11b^{+}F4/80^{+} cells (macrophages) were not affected (**Supplementary Figure 1**). These data indicate that polyI:C pretreatment specifically inhibits neutrophil infiltration rather than other immune cells such as macrophages.

Additionally, we checked whether polyI:C pretreatment affects pancreas homeostasis in a non-pathogenic saline-injected mouse model instead of in the AP model (**Supplementary Figure 2A**). No significant differences to pancreas edema, serum amylase and lipase levels, inflammatory cytokine and chemokine gene expression or neutrophil and macrophage infiltration were observed between the saline-pretreated and polyI:C-pretreated groups

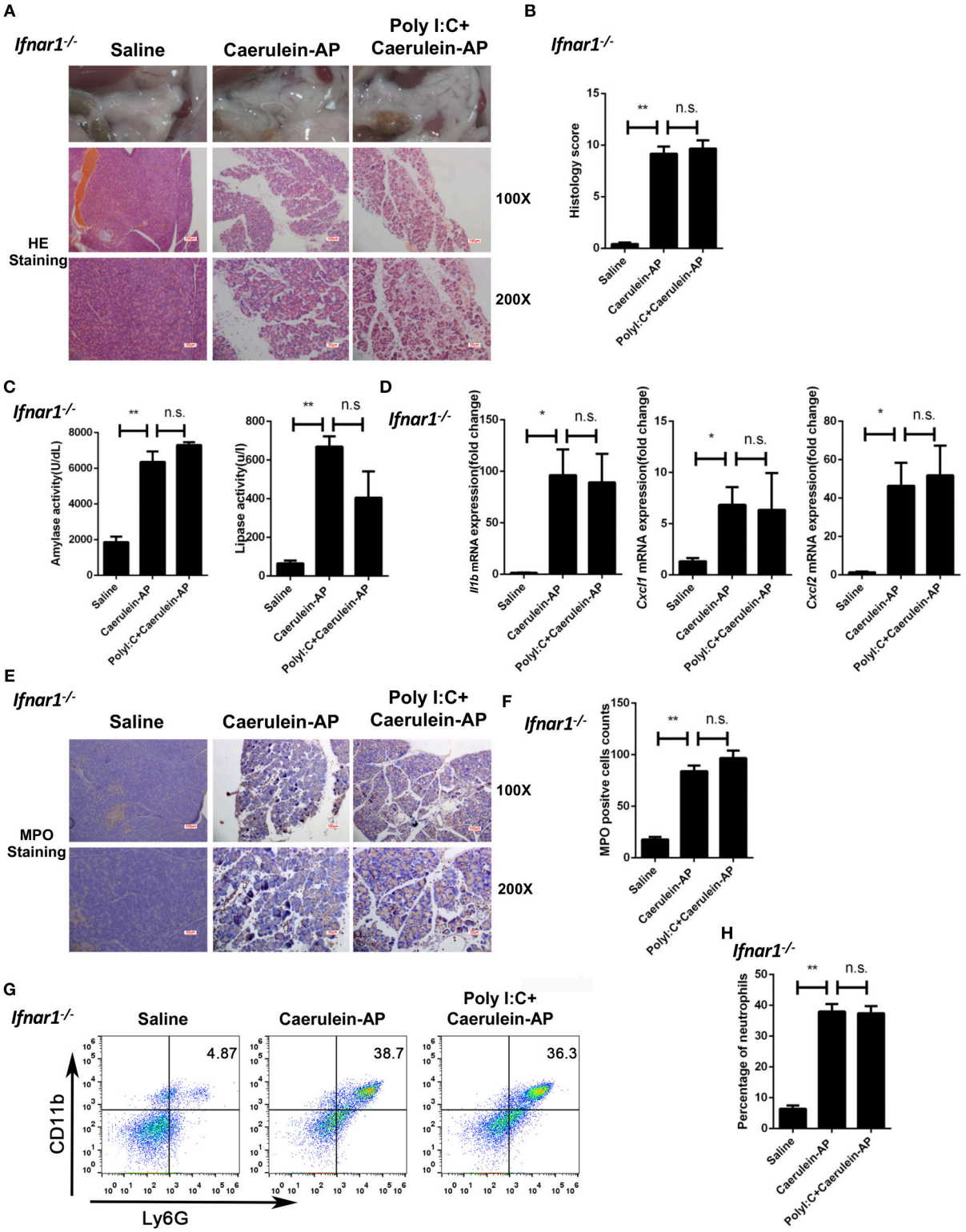

FIGURE 3 | Knockout of Ifnar1 also abolishes the protective effects of polyI:C on the caerulein-induced AP mouse model. **(A)** Histopathological examination of the effect of polyI:C on *Ifnar1*$^{-/-}$ caerulein-induced experimental AP mouse models. Top panel: gross observation; middle panel: H&E staining, 100X magnification; bottom panel: H&E staining, 200X magnification. **(B)** Histology scores of pancreatitis were evaluated and compared after observing five separate fields. **(C)** Activities of the serum amylase (left) and lipase (right) from Saline, Caerulein-AP, and PolyI:C+Caerulein-AP *Ifnar1*$^{-/-}$ mice were compared via enzymatic methods.

(Continued)

FIGURE 3 | (D) mRNA expression levels of *Il1b*, *Cxcl1*, and *Cxcl2* genes in the pancreatic tissue from Saline, Caerulein-AP, and PolyI:C+Caerulein-AP *Ifnar1*$^{-/-}$ mice were detected by RT-qPCR and normalized to *Rpl32*. **(E)** Neutrophil infiltrations in the pancreases from *Ifnar1*$^{-/-}$ caerulein-induced experimental AP mouse models were measured and compared by MPO staining. Top panel: 100X magnification; bottom panel: 200X magnification. **(F)** MPO^{+} cells were counted and compared after observing five separate fields. **(G)** Pancreases neutrophils from the Saline, Caerulein-AP, and PolyI:C+Caerulein-AP *Ifnar1*$^{-/-}$ mice were analyzed by flow cytometry. CD11b^{+}Ly6G^{+} cells were considered as neutrophils. **(H)** The percentage of neutrophils from indicated groups was calculated and compared. Data of **(A,E,G)** are representative of three independent experiments. Data of **(B,F)** are shown as mean ± SD ($n = 5$) from one representative experiment. Data of **(C,D,H)** are shown as mean ± SEM from at least three independent experiments. *$p < 0.05$, **$p < 0.01$, n.s., not significant, one-way ANOVA test.

(**Supplementary Figures 2B–G**). These results suggest that polyI:C administration to pancreases is potentially safe.

We also tested the protective effect of polyI:C in L-arginine-induced AP mouse models (**Supplementary Figure 3A**). PolyI:C pretreatment significantly reduced the pancreatic injury caused by L-Arginine injection (**Supplementary Figure 3B**). Consistently, induction of serum amylase and lipase by L-Arginine was also attenuated in the polyI:C-pretreated group (**Supplementary Figure 3C**).

To verify the preventive or therapeutic effect of polyI:C in AP, we tested multiple time windows of polyI:C injection. PolyI:C administration 1 h prior to the induction of AP by caerulein effectively inhibited pancreatic injury (**Supplementary Figures 4A,B**), and also suppressed serum amylase and lipase induction by caerulein (**Supplementary Figure 4C**). However, polyI:C administration after induction of AP by caerulein in WT mice did not show a significant protective effect (data not shown).

Thus, we have found that the TLR3 ligand polyI:C effectively and safely prevents caerulein-induced AP and L-Arginine-induced AP in WT mice.

IFN-β/IFNAR Signaling Is Required for the Preventive Effect of PolyI:C on AP

To confirm whether polyI:C-triggered type I IFN production mediated the protective effect of polyI:C in AP mice, we pretreated *Ifnb*$^{-/-}$ mice with polyI:C in the caerulein-induced AP mouse model. PolyI:C did not alleviate the AP symptoms such as pancreas edema, inflammatory cell infiltration, and tissue necrosis in the *Ifnb*$^{-/-}$ mice (**Figures 2A,B**). Consistently, polyI:C did not inhibit the elevation of serum amylase and lipase in the *Ifnb*$^{-/-}$ experimental AP mice (**Figure 2C**). In addition, we found even higher inflammatory cytokine and chemokine gene expression (such as IL-1β and CXCL2) in the polyI:C-pretreated *Ifnb*$^{-/-}$ AP mice, whereas polyI:C inhibited those inflammatory genes significantly in the WT AP mice (**Figures 1E**, **2D**). The number of infiltrated neutrophils in *Ifnb*$^{-/-}$ AP mice was indistinguishable between the saline and polyI:C pretreated groups (**Figures 2E–H**). These results indicate that polyI:C-triggered IFN-β production potentially meditates the preventive effect of polyI:C on AP.

Next, we used the *Ifnar1*$^{-/-}$ mice to confirm the above conclusion. The protective function of polyI:C was not seen in *Ifnar1*$^{-/-}$ AP mice. Similar to the phenotypes observed in the *Ifnb*$^{-/-}$ AP mice, there was no significant changes in pancreas histopathological results (**Figures 3A,B**), serum amylase and lipase activity levels (**Figure 3C**), pancreas inflammatory genes (**Figure 3D**), and neutrophil infiltration (**Figures 3E–H**) between the saline and polyI:C pretreated groups. In summary, these experiments suggest that IFN-β/IFNAR signaling is necessary for the preventive effect of polyI:C on caerulein-induced AP.

PolyI:C Inhibits Oxidative Stress in AP in an IFN-β/IFNAR-Dependent Manner

The accumulation of ROS drives persistent tissue damage, resulting in the death of acinar cells, edema formation, and infiltration of inflammatory cells into the pancreas (25). Therefore, we tested whether polyI:C could inhibit the generation of ROS in oxidative injury-induced pancreatitis. As shown in **Figure 4A**, polyI:C treatment significantly suppressed the induction of anti-oxidant protein HO-1 by taurocholate in the 266-6 cells, however it did not suppress other anti-oxidant proteins such as KEAP1 and NQO1 (**Supplementary Figure 5**). Further experiments confirmed the role of the IFN-β/IFNAR signaling pathway in modulating ROS generation. PolyI:C or IFN-β treatment downregulated the induction of HO-1 protein by taurocholate, and blocking IFN-β and IFNAR interaction using an IFNAR inhibitor reversed the effect of polyI:C and IFN-β on HO-1 induction (**Figure 4B**).

HO-1 is not only an anti-oxidant protein for reducing ROS but can also be used as an indicator for measuring the severity of damage and inflammation in AP. Downregulation of HO-1 by polyI:C suggests the inhibition of oxidative stress. As we expected, polyI:C or IFN-β treatment significantly reduced the ROS level in taurocholate-stimulated 266-6 cells according to the fluorescence microscopy and flow cytometry results (**Figures 4C,D**).

Furthermore, we confirmed that polyI:C inhibited the generation of ROS in the pancreases of AP mice via the IFN-β/IFNAR signaling pathway. Homogenates of pancreases resected from experimental AP models with or without polyI:C in WT, *Ifnb*$^{-/-}$, and *Ifnar1*$^{-/-}$ mice were analyzed by immunoblotting for HO-1 protein levels. PolyI:C pretreatment suppressed HO-1 induction in the WT AP mice (**Figure 4E**). However, even higher HO-1 protein levels were detected in the polyI:C-pretreated *Ifnb*$^{-/-}$ and *Ifnar*$^{-/-}$ AP mice (**Figures 4F,G**). These data suggest that IFN-β and IFNAR downstream signaling inhibits oxidative stress during AP progression, which could be indicated by higher HO-1 production. Our results suggest that polyI:C inhibits ROS generation independently of HO-1. Without IFN-β/IFNAR signaling, polyI:C cannot facilitate the clearance of ROS, and thus, the pancreas requires more HO-1 anti-oxidant protein. TLR4 was reported to be suppressed by the TLR3 ligand polyI:C and thus, alleviates liver injury induced by LPS and D-GalN (14).

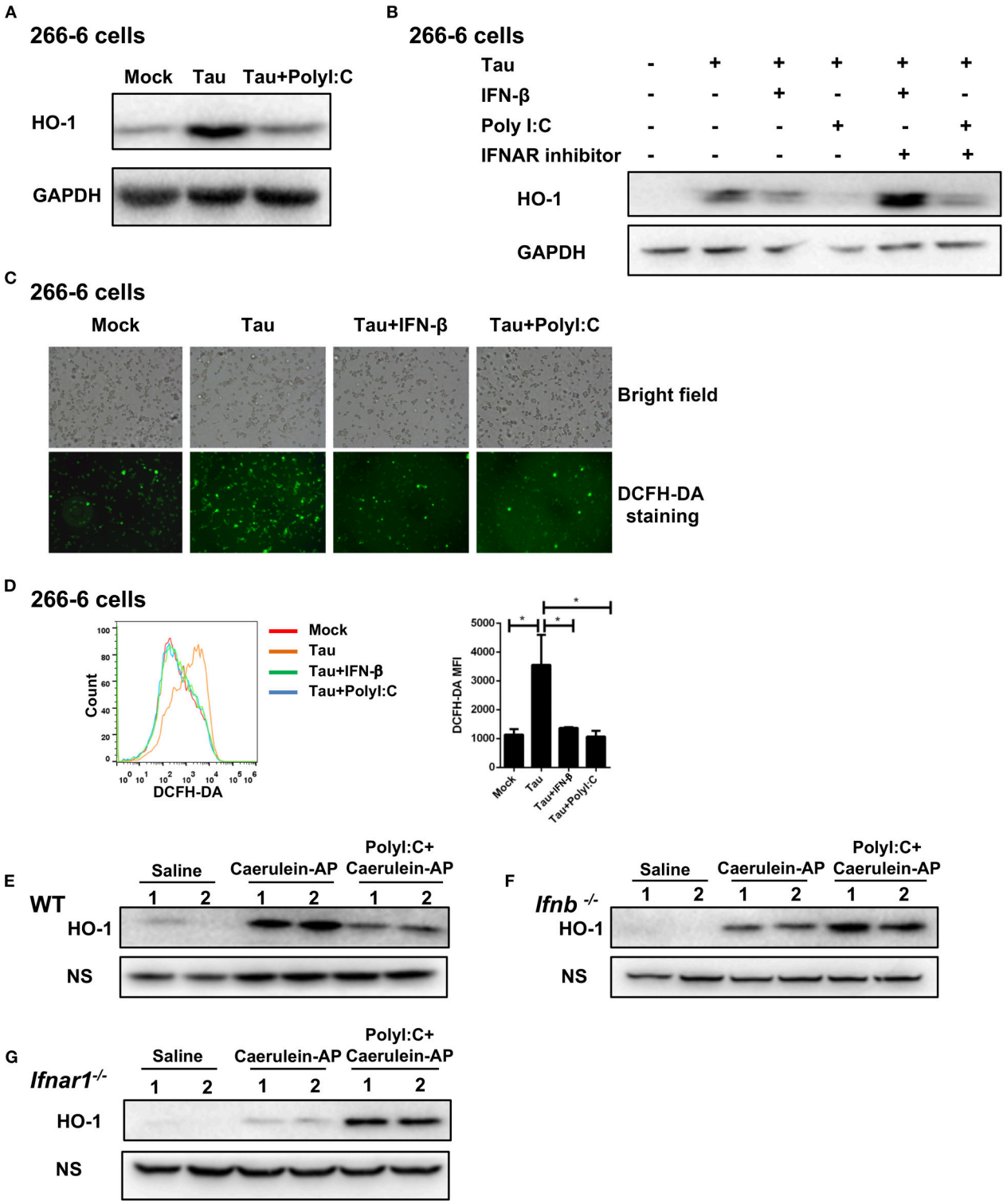

FIGURE 4 | Polyl:C inhibits ROS production in AP via the IFN-β/IFNAR-dependent signaling pathway. **(A)** 266-6 cells were stimulated with 0.5 mM taurocholate in the absence or presence of polyI:C (1 μg/ml), 24 h later, HO-1 protein levels in the cells were measured by western blotting; GAPDH was used as a loading control. **(B)** 266-6 cells were stimulated with 0.5 mM taurocholate in the absence or presence of IFN-β (200 U/ml), polyI:C (1 μg/ml), or IFNAR inhibitor (1 μM). Twenty-four hours later, HO-1 protein levels in the cells were measured by western blotting; GAPDH was used as a loading control. **(C,D)** 266-6 cells were stimulated with 0.5 mM taurocholate in the absence or presence of polyI:C (1 μg/ml) or IFN-β (200 U/ml), intracellular ROS was stained by DCFH-DA, and detected by fluorescence microscopy **(C)** and flow cytometry **(D)**. Median fluorescence intensity (MFI) of stained DCFH-DA was calculated (**D**, right panel).

(Continued)

FIGURE 4 | (E–G) HO-1 protein expression levels in the pancreases from Saline, Caerulein-AP, and PolyI:C+Caerulein-A WT **(E)**, *Ifnb*$^{-/-}$ **(F)**, and *Ifnar1*$^{-/-}$ mice **(G)** were measured by western blotting; a non-specific (NS) band was shown as a loading control. Data of **(A–C,E–G)** are representative of three independent experiments. Data of **(D)**, right panel are shown as mean ± SEM ($n = 3$). *$p < 0.05$, one-way ANOVA test.

However, in the caerulein-induced AP model, polyI:C protected the pancreas of AP mice from injury and inhibited the induction of amylase and lipase, although it was not as effective as in WT mice (**Supplementary Figure 6**).

By analyzing ROS levels and the amount of the oxidative stress indicator protein *in vitro* and *in vivo*, we have confirmed that polyI:C inhibits oxidative stress during AP progression in an IFN-β/IFNAR-dependent manner.

PolyI:C Inhibits Multiple Genes Which Positively Correlated With AP Progression

To explore the mechanism of action of polyI:C in preventing AP, we performed RNA-sequencing and analyzed the pancreas' transcriptomes from the saline-pretreated, AP, and polyI:C-pretreated AP mice. We focused on the genes that were significantly induced during AP and suppressed by polyI:C pretreatment. Among them were the inflammatory cytokine gene *Il1β*, the inflammatory chemokine genes *Cxcl1* and *Cxcl2*, and other genes, such as *Ccl2*, *Ccr2*, *C5a1*, *Mrc1*, *Ccr5*, *Hck*, *Tyrobp*, *Procr*, and *Fgr*, related to neutrophil recruitment, neutrophil movement, the immune response of neutrophils, and ROS production (**Figure 5A**). We verified some of the genes we were interested in and further analyzed all the differently expressed genes using IPA software (**Figures 5B**, **6**). Key pathways and related genes that facilitated AP progression and were suppressed by polyI:C are shown in heatmaps (**Figure 6**).

In summary, our study has shown that polyI:C triggers IFN-β production by activating the master transcription factor IRF3, and IFN-β inhibits neutrophil infiltration, thus, alleviating AP symptoms such as edema, release of amylase and lipase, generation of ROS, and the induction of inflammatory genes by activating downstream IFNAR signaling (**Figure 7**).

DISCUSSION

It has been well-established that type I IFN has a protective effect against viral infections by activating IFNAR downstream signaling and inducing IFN-stimulated genes (ISGs) (26). However, it is debated whether type I IFN plays beneficial or detrimental roles in inflammatory diseases (22). Unlike other TLRs such as TLR2, TLR4, and TLR9 usually promote inflammation (24), and TLR3 seems to act as the "peacemaker" in the maintenance of a healthy internal environment. It has been shown that TLR3 or TLR7 sense viral infection in the gut and trigger the production of IFN-β that dampens DSS-induced experimental colitis (27). Here, we have described an anti-inflammatory role of TLR3 in AP. We have found that pretreatment with TLR3 ligand polyI:C protects the caerulein-induced AP mice in an IFN-β/IFNAR-dependent manner.

Compared to the recombinant type I IFN, viral dsRNA mimic polyI:C is much more stable, easier to deliver, and has a lower cost. The use of TLR3 agonists as immunotherapeutic agents has been employed in cancer therapy to induce tumor cell apoptosis in type I IFN-dependent and independent pathways (28, 29). Pretreatment of polyI:C is very effective in preventing caerulein-induced AP and L-arginine-induced AP. In addition, polyI:C is safe for use in mice pancreases according to the non-pathogenic saline-injected mouse model. Given the efficacy and safety of polyI:C in protecting AP mice, it has shown the great potential of the application of TLR3 agonists to prevent AP.

In the AP models we used in this study, IFN-β was found to be responsible for most of the preventive effects of polyI:C on AP, whereas IFN-α seems to play a minor role in this process. Type I IFN is secreted from macrophages during AP progression, and IFN-β is predominantly secreted from macrophages, endothelial cells, and epithelial cells (30). Large amounts of IFN-α protein is produced by plasmacytoid dendritic cells under certain conditions (26). IFN-β is primarily produced during AP and induces the secondary wave of IFN-α via the well-established type I IFN positive feedback regulation loop (16–18). Most IFN-α genes are ISGs (31). Both IFN-β and IFN-α activate downstream signaling via the same receptor, IFNAR. However, the affinities of IFN-β and IFN-α for the receptor are different. IFN-β and IFN-α also induce the expression of different genes, which are expressed in macrophages stimulated with the same concentration of IFN-β and IFN-α (32, 33). In this study, we identified that IFN-β-induced genes play key roles in preventing AP.

Between 8 h and at least 1-h pretreatment of polyI:C before infection with caerulein or L-arginine is required for effective prevention of AP in the experimental mouse models. PolyI:C did not exert a good therapeutic effect on AP mice if polyI:C is injected post AP induction, since it takes over 6 h for polyI:C to induce the production of type I IFN. However, the level of serum amylase in human AP patients usually reaches its peak at around 48 h and returns to normal levels over the next 5–7 days (34), which is a much wider time window to administer polyI:C to human AP patients. Therefore, it is possible to use TLR3 agonists such as polyI:C as novel AP therapeutic agents if we treat AP patients with polyI:C at the early stages of disease.

It has previously been reported that polyI:C treatment significantly decreases mortality and liver injury caused by injection of LPS in the presence of D-GalN (14). PolyI:C also shows therapeutic effect against cerebral ischemia/reperfusion injury through the downregulation of TLR4 signaling (35). However, our results show that polyI:C protects *Tlr4*$^{-/-}$ AP mice from pancreatic injury and inhibits the induction of amylase and lipase, although it is most effective in WT mice. In addition to IFN-β and downstream IFNAR signaling, it is possible that other polyI:C-responsive genes such as TLR4 also partially mediate the preventive effect of polyI:C on AP. Our future studies will aim to identify the ISGs stimulated by polyI:C that prevent AP.

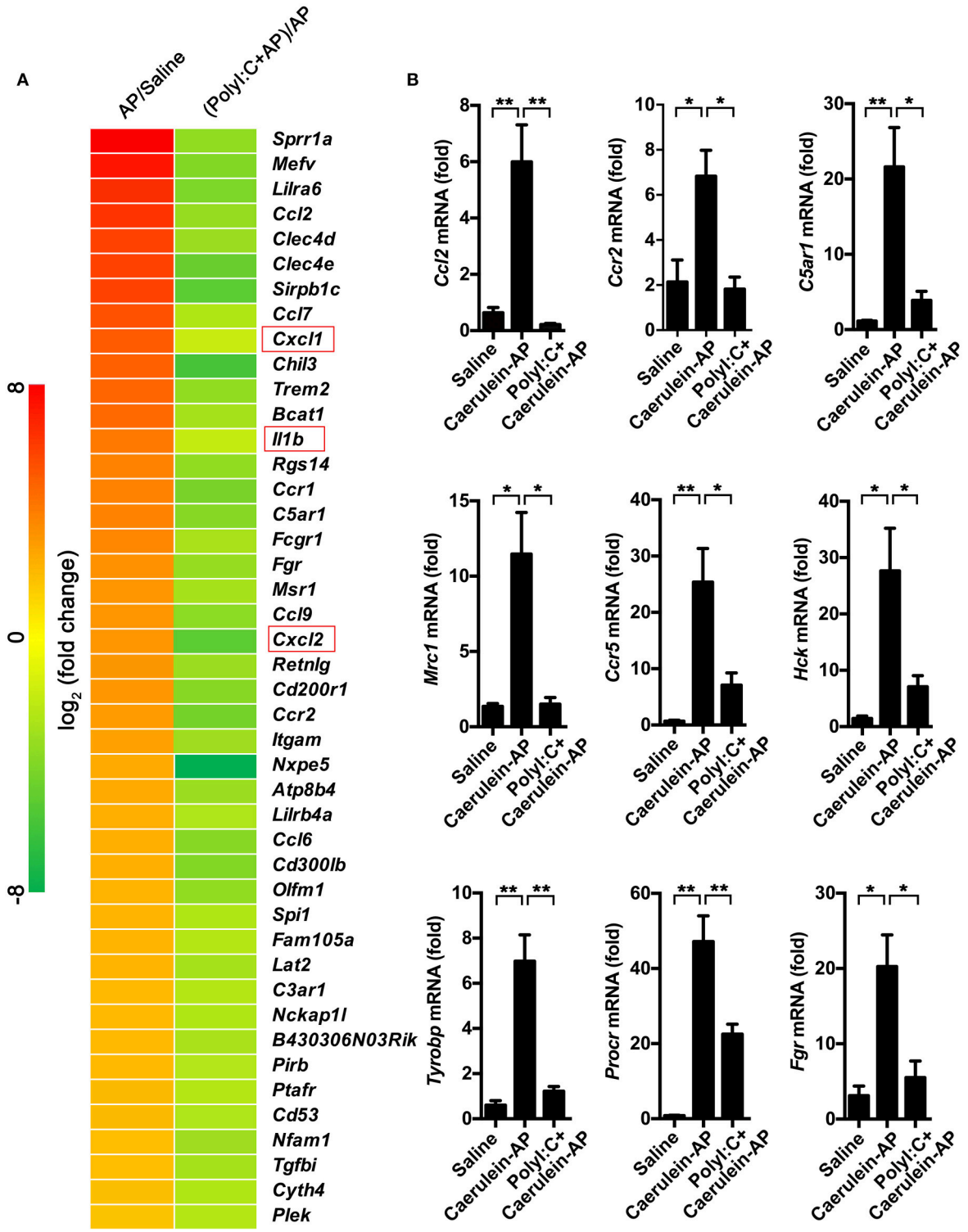

FIGURE 5 | Polyl:C suppresses multiple genes related to the progression of AP. **(A)** Gene expression profiles of the pancreases from Saline, Caerulein-AP, and Polyl:C+Caerulein-AP WT mice were detected by RNA-Seq. Top polyl:C-suppressed and caerulein-inducible DEGs (differentially expressed genes) are shown in the heatmap. **(B)** Samples are treated as described in **(A)**, and mRNA expression level of the genes related to the progression of AP such as *Ccl2, Ccr2, C5ar1, Mrc1, Ccr5, Hck, Tyrobp, Procr,* and *Fgr* were verified by qPCR. Data of **(A)** are representative of three independent experiments. Data of **(B)** are shown as mean ± SEM ($n = 3$). $^{*}p < 0.05$, $^{**}p < 0.01$, one-way ANOVA test.

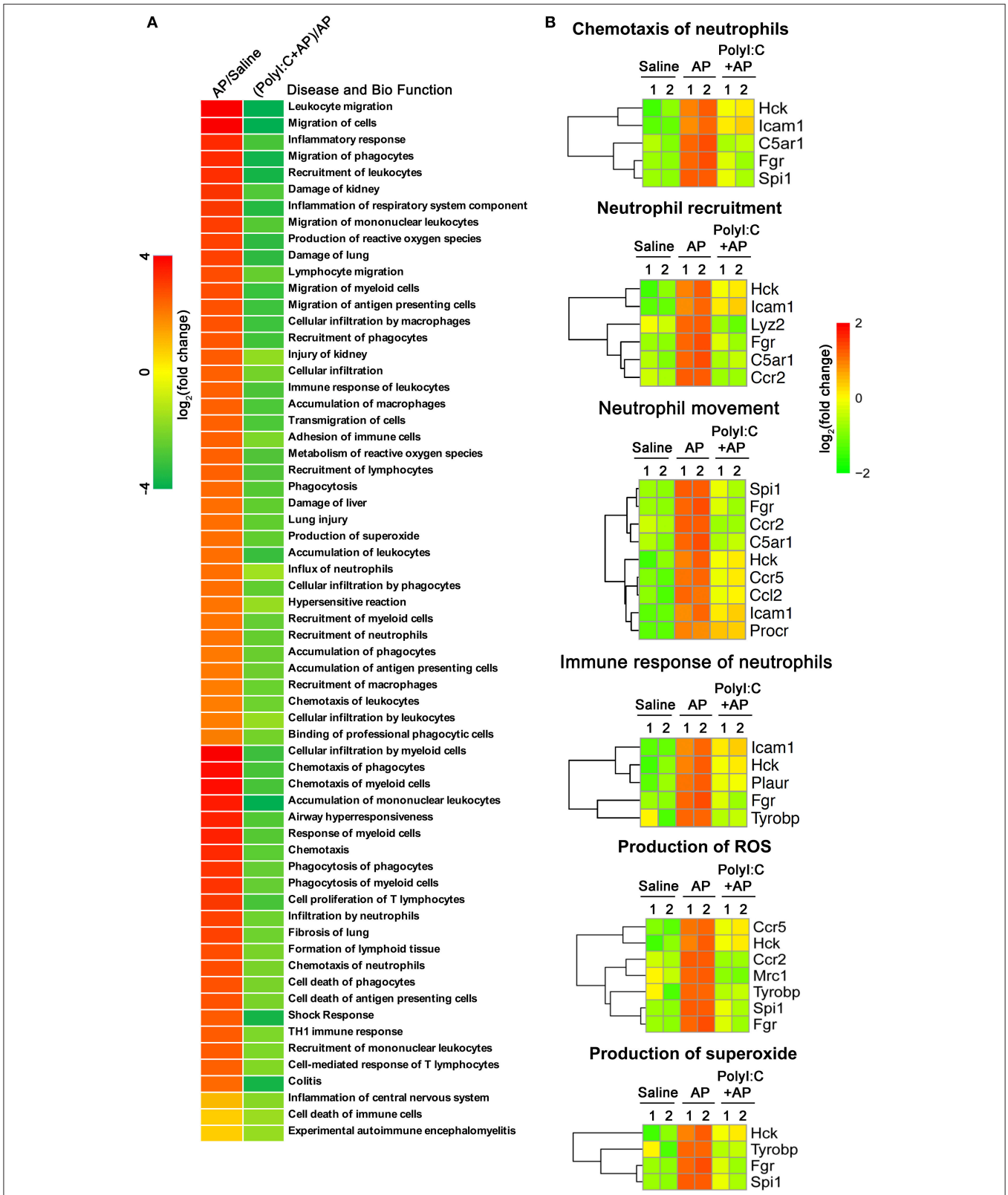

FIGURE 6 | PolyI:C suppresses ROS production and neutrophil functions. **(A)** Gene expression profile of the pancreases from Saline, Caerulein-AP, and PolyI:C+Caerulein-AP WT mice was detected by RNA-Seq. DEGs were analyzed by the IPA and GO, and clustered into the pathways related to the disease and bio functions. **(B)** Genes related to the six pathways on ROS production and neutrophil functions are shown.

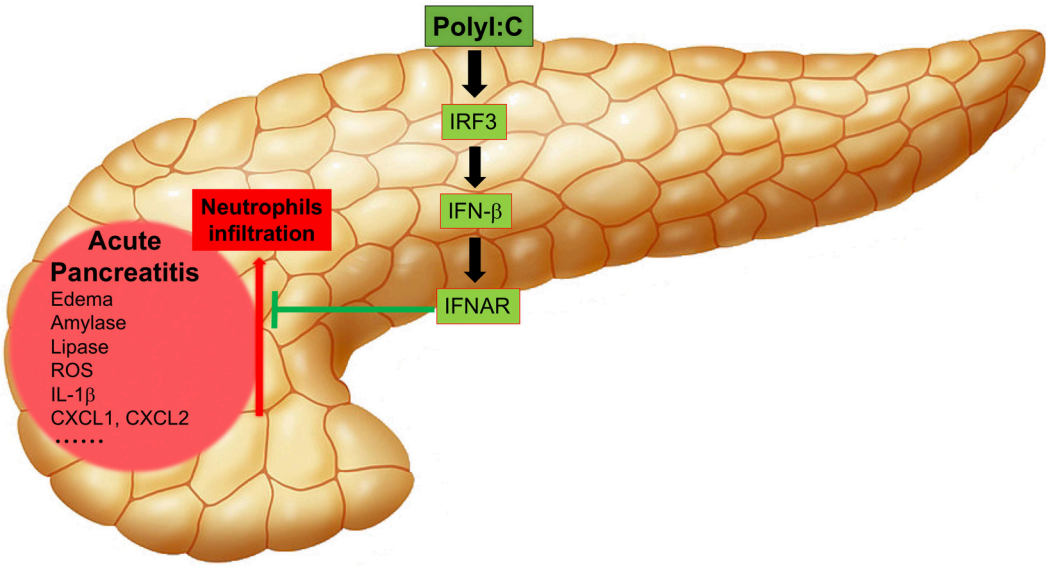

FIGURE 7 | Working model of polyI:C-mediated protection on pancreases from inflammatory injuries. PolyI:C triggers the IFN-β production by activating the master transcription factor IRF3, and IFN-β inhibits neutrophil infiltration, and thus alleviates the AP symptoms such as edema, release of amylase and lipase, production of ROS, expression of the inflammatory genes by activating the downstream IFNAR signaling.

PolyI:C treatment inhibited the induction of the inflammatory cytokine IL-1β as well as the chemokine genes including CXCL1 and CXCL2 in pancreases from AP mice. The infiltration of neutrophils but not of macrophages to the injured pancreases of AP mice was suppressed. In addition, a lower production of ROS was detected in both the acinar cell line and the injured pancreases of AP mice pretreated with polyI:C. This is consistent with the reduced induction of anti-oxidant protein HO-1 during AP progression. HO-1 usually acts as a protective effector to clear the elevated ROS in inflammatory cells (36). Suppressed generation of ROS by polyI:C leads to a weak induction of HO-1, which suggests polyI:C-triggered type I IFN production protects acinar cells and mice pancreases in a HO-1-independent manner. Pretreatment with polyI:C enhanced the induction of HO-1 protein production in pancreases from *Ifnb*$^{-/-}$ and *Ifnar1*$^{-/-}$ AP mice. This is consistent with the results that polyI:C did not protect the *Ifnb*$^{-/-}$ and *Ifnar1*$^{-/-}$ AP mice. ROS drives cytochrome C release, leading to ATP-dependent caspase activation and apoptosis which occurs in many cell types (37). Thus, there is a need to identify strategies to clear accumulated ROS during oxidative stress in AP. For example, type III IFN member IFN-λ regulated the activation of AKT in a non-translational manner independent of the STAT pathway to diminish ROS production (10). We have outlined a novel HO-1 independent pathway to clear ROS using type I IFN during AP progression.

AP is characterized by the activation of exocrine zymogen granules, which contain digestive enzymes (38), the infiltration of macrophage and neutrophils (39), and necrosis or apoptosis of pancreatic cells (40). Despite damaged primary pancreatic acinar cells, neutrophils isolated from patients with pancreatitis produce ROS to a greater extent (8, 41). Crosstalk among damaged cells, neutrophils, and ROS appears to synergistically promote the process of pancreatitis. According to the transcriptomic profiles of polyI:C-induced genes, we found that these genes were involved in the recruitment of inflammatory cells, production of ROS, and regulation of the inflammatory response. PolyI:C attenuated the positive feedback regulatory loop between ROS and proinflammatory cytokines in AP.

Inflammation occurring in the pancreas triggers multiple processes by recruiting inflammatory neutrophils and increasing ROS production, which leads to a homeostatic imbalance and sequentially promotes increasingly severe inflammatory injury. Regarding the protective role of polyI:C in preventing AP, TLR3 agonists are promising therapeutic agents to safely and effectively prevent AP at the early stages of pancreatitis.

ETHICS STATEMENT

All animal procedures were approved by the Institutional Animal Care and Use Committee of Suzhou Institute of Systems Medicine.

AUTHOR CONTRIBUTIONS

FM and MZ conceived the idea. FM and CH designed the experiments. CH, SC, TZ, DL, ZH, JH, YQ, and BC finished all the experiments and data analysis. FM and CH wrote the manuscript. All authors contributed to the interpretation of the experiments, critically reviewed the manuscript, and gave the final approval of the manuscript submission.

FUNDING

This work was supported by the NFSC (81570583, 81770630, 81471606, 31670883, 31771560, 31800760, and 31870912), National Thousand Youths Talents Program to FM, CAMS Initiative for Innovative Medicine (2016-I2M-1-005), Non-profit Central Research Institute Fund of CAMS (2016ZX310189, 2016ZX310194, and 2017NL31004), NSF of Jiangsu Province (BK20170408), and the Shanghai Pujiang Program (16PJD001), Key Laboratory of Diagnosis and Treatment of Severe Hepato-Pancreatic Diseases of Zhejiang Province, Province and Ministry (WKJ-ZJ-1706), New Century Talents Project to MZ, Zhejiang Medical Support Discipline-General Surgery and the Technology Innovation Team of Diagnosis and Innovative Research Groups of the General Surgery of Wenzhou (No. C20150003).

ACKNOWLEDGMENTS

We appreciate the technical support from the RNA technology platform of Suzhou Institute of Systems Medicine.

SUPPLEMENTARY MATERIAL

The Supplementary Material for this article can be found online at: https://www.frontiersin.org/articles/10.3389/fimmu.2019.00980/full#supplementary-material

REFERENCES

1. Lankisch PG, Apte M, Banks PA. Acute pancreatitis. *Lancet*. (2015) 386:85–96. doi: 10.1016/S0140-6736(14)60649-8
2. Mole DJ, Webster SP, Uings I, Zheng X, Binnie M, Wilson K, et al. Kynurenine-3-monooxygenase inhibition prevents multiple organ failure in rodent models of acute pancreatitis. *Nat Med*. (2016) 22:202–9. doi: 10.1038/nm.4020
3. Awla D, Zetterqvist AV, Abdulla A, Camello C, Berglund LM, Spegel P, et al. NFATc3 regulates trypsinogen activation, neutrophil recruitment, and tissue damage in acute pancreatitis in mice. *Gastroenterology*. (2012) 143:1352–60 e7. doi: 10.1053/j.gastro.2012.07.098
4. Jin Y, Bai Y, Li Q, Bhugul PA, Huang X, Liu L, et al. Reduced pancreatic exocrine function and organellar disarray in a canine model of acute pancreatitis. *PLoS ONE*. (2016) 11:e0148458. doi: 10.1371/journal.pone.0148458
5. Yu JH, Kim H. Oxidative stress and inflammatory signaling in cerulein pancreatitis. *World J Gastroenterol*. (2014) 20:17324–9. doi: 10.3748/wjg.v20.i46.17324
6. Kang R, Zhang Q, Hou W, Yan Z, Chen R, Bonaroti J, et al. Intracellular Hmgb1 inhibits inflammatory nucleosome release and limits acute pancreatitis in mice. *Gastroenterology*. (2014) 146:1097–107. doi: 10.1053/j.gastro.2013.12.015
7. Gravante G, Garcea G, Ong SL, Metcalfe MS, Berry DP, Lloyd DM, et al. Prediction of mortality in acute pancreatitis: a systematic review of the published evidence. *Pancreatology*. (2009) 9:601–14. doi: 10.1159/000212097
8. Gukovskaya AS, Vaquero E, Zaninovic V, Gorelick FS, Lusis AJ, Brennan ML, et al. Neutrophils and NADPH oxidase mediate intrapancreatic trypsin activation in murine experimental acute pancreatitis. *Gastroenterology*. (2002) 122:974–84. doi: 10.1053/gast.2002.32409
9. Merry TL, Ristow M. Nuclear factor erythroid-derived 2-like 2 (NFE2L2, Nrf2) mediates exercise-induced mitochondrial biogenesis and the anti-oxidant response in mice. *J Physiol*. (2016) 594:5195–207. doi: 10.1113/JP271957
10. Broggi A, Tan Y, Granucci F, Zanoni I. IFN-lambda suppresses intestinal inflammation by non-translational regulation of neutrophil function. *Nat Immunol*. (2017) 18:1084–1093. doi: 10.1038/ni.3821
11. Fortier ME, Kent S, Ashdown H, Poole S, Boksa P, Luheshi GN. The viral mimic, polyinosinic:polycytidylic acid, induces fever in rats via an interleukin-1-dependent mechanism. *Am J Physiol Regul Integr Comp Physiol*. (2004) 287:R759–66. doi: 10.1152/ajpregu.00293.2004
12. Li Y, Xu XL, Zhao D, Pan LN, Huang CW, Guo LJ, et al. TLR3 ligand Poly IC attenuates reactive astrogliosis and improves recovery of rats after focal cerebral ischemia. *CNS Neurosci Ther*. (2015) 21:905–13. doi: 10.1111/cns.12469
13. Hoque R, Sohail M, Malik A, Sarwar S, Luo Y, Shah A, et al. TLR9 and the NLRP3 inflammasome link acinar cell death with inflammation in acute pancreatitis. *Gastroenterology*. (2011) 141:358–69. doi: 10.1053/j.gastro.2011.03.041
14. Jiang W, Sun R, Wei H, Tian Z. Toll-like receptor 3 ligand attenuates LPS-induced liver injury by down-regulation of toll-like receptor 4 expression on macrophages. *Proc Natl Acad Sci USA*. (2005) 102:17077–82. doi: 10.1073/pnas.0504570102
15. Billiau A. Anti-inflammatory properties of Type I interferons. *Antiviral Res*. (2006) 71:108–16. doi: 10.1016/j.antiviral.2006.03.006
16. Sato M, Suemori H, Hata N, Asagiri M, Ogasawara K, Nakao K, et al. Distinct and essential roles of transcription factors IRF-3 and IRF-7 in response to viruses for IFN-alpha/beta gene induction. *Immunity*. (2000) 13:539–48. doi: 10.1016/S1074-7613(00)00053-4
17. Marie I, Durbin JE, Levy DE. Differential viral induction of distinct interferon-alpha genes by positive feedback through interferon regulatory factor-7. *EMBO J*. (1998) 17:6660–9. doi: 10.1093/emboj/17.22.6660
18. Sato M, Hata N, Asagiri M, Nakaya T, Taniguchi T, Tanaka N. Positive feedback regulation of type I IFN genes by the IFN-inducible transcription factor IRF-7. *FEBS Lett*. (1998) 441:106–10.
19. Trojano M, Avolio C, Liuzzi GM, Ruggieri M, Defazio G, Liguori M, et al. Changes of serum sICAM-1 and MMP-9 induced by rIFNbeta-1b treatment in relapsing-remitting MS. *Neurology*. (1999) 53:1402–8.
20. Zhang LN, Velichko S, Vincelette J, Fitch RM, Vergona R, Sullivan ME, et al. Interferon-beta attenuates angiotensin II-accelerated atherosclerosis and vascular remodeling in apolipoprotein E deficient mice. *Atherosclerosis*. (2008) 197:204–11. doi: 10.1016/j.atherosclerosis.2007.03.019
21. Triantaphyllopoulos KA, Williams RO, Tailor H, Chernajovsky Y. Amelioration of collagen-induced arthritis and suppression of interferon-gamma, interleukin-12, and tumor necrosis factor alpha production by interferon-beta gene therapy. *Arthritis Rheum*. (1999) 42:90–9. doi: 10.1002/1529-0131(199901)42:1<90::AID-ANR12>3.0.CO;2-A
22. Wang Y, Kayoumu A, Lu G, Xu P, Qiu X, Chen L, et al. Experimental models in syrian golden hamster replicate human acute pancreatitis. *Sci Rep*. (2016) 6:28014. doi: 10.1038/srep28014
23. Schmittgen TD, Livak KJ. Analyzing real-time PCR data by the comparative C(T) method. *Nat Protoc*. (2008) 3:1101–8. doi: 10.1038/nprot.2008.73
24. Wang X, Spandidos A, Wang H, Seed B. PrimerBank: a PCR primer database for quantitative gene expression analysis, 2012 update. *Nucleic Acids Res*. (2012) 40:D1144–9. doi: 10.1093/nar/gkr1013
25. Booth DM, Murphy JA, Mukherjee R, Awais M, Neoptolemos JP, Gerasimenko OV, et al. Reactive oxygen species induced by bile acid induce apoptosis and protect against necrosis in pancreatic acinar cells. *Gastroenterology*. (2011) 140:2116–25. doi: 10.1053/j.gastro.2011.02.054
26. Ivashkiv LB, Donlin LT. Regulation of type I interferon responses. *Nat Rev Immunol*. (2014) 14:36–49. doi: 10.1038/nri3581
27. Yang JY, Kim MS, Kim E, Cheon JH, Lee YS, Kim Y, et al. Enteric viruses ameliorate gut inflammation via toll-like receptor 3 and toll-like receptor 7-mediated interferon-beta production. *Immunity*. (2016) 44:889–900. doi: 10.1016/j.immuni.2016.03.009
28. Bianchi F, Pretto S, Tagliabue E, Balsari A, Sfondrini L. Exploiting poly(I:C) to induce cancer cell apoptosis. *Cancer Biol Ther*. (2017) 18:747–756. doi: 10.1080/15384047.2017.1373220

29. Zhao X, Ai M, Guo Y, Zhou X, Wang L, Li X, et al. Poly I:C-induced tumor cell apoptosis mediated by pattern-recognition receptors. *Cancer Biother Radiopharm*. (2012) 27:530–4. doi: 10.1089/cbr.2012.1226
30. Raymond SL, Holden DC, Mira JC, Stortz JA, Loftus TJ, Mohr AM, et al. Microbial recognition and danger signals in sepsis and trauma. *Biochim Biophys Acta Mol Basis Dis*. (2017) 1863(10 Pt B):2564–73. doi: 10.1016/j.bbadis.2017.01.013
31. Erlandsson L, Blumenthal R, Eloranta ML, Engel H, Alm G, Weiss S, et al. Interferon-beta is required for interferon-alpha production in mouse fibroblasts. *Curr Biol*. (1998) 8:223–6.
32. Jaitin DA, Roisman LC, Jaks E, Gavutis M, Piehler J, Van der Heyden J, et al. Inquiring into the differential action of interferons (IFNs): an IFN-alpha2 mutant with enhanced affinity to IFNAR1 is functionally similar to IFN-beta. *Mol Cell Biol*. (2006) 26:1888–97. doi: 10.1128/MCB.26.5.1888-1897.2006
33. Gavutis M, Lata S, Lamken P, Muller P, Piehler J. Lateral ligand-receptor interactions on membranes probed by simultaneous fluorescence-interference detection. *Biophys J*. (2005) 88:4289–302. doi: 10.1529/biophysj.104.055855
34. Rompianesi G, Hann A, Komolafe O, Pereira SP, Davidson BR, Gurusamy KS. Serum amylase and lipase and urinary trypsinogen and amylase for diagnosis of acute pancreatitis. *Cochrane Database Syst Rev*. (2017) 4:CD012010. doi: 10.1002/14651858.CD012010.pub2
35. Wang PF, Fang H, Chen J, Lin S, Liu Y, Xiong XY, et al. Polyinosinic-polycytidylic acid has therapeutic effects against cerebral ischemia/reperfusion injury through the downregulation of TLR4 signaling via TLR3. *J Immunol*. (2014) 192:4783–94. doi: 10.4049/jimmunol.1303108
36. Orozco LD, Kapturczak MH, Barajas B, Wang X, Weinstein MM, Wong J, et al. Heme oxygenase-1 expression in macrophages plays a beneficial role in atherosclerosis. *Circ Res*. (2007) 100:1703–11. doi: 10.1161/CIRCRESAHA.107.151720
37. Orrenius S, Gogvadze V, Zhivotovsky B. Mitochondrial oxidative stress: implications for cell death. *Annu Rev Pharmacol Toxicol*. (2007) 47:143–83. doi: 10.1146/annurev.pharmtox.47.120505.105122
38. Gukovsky I, Pandol SJ, Mareninova OA, Shalbueva N, Jia W, Gukovskaya AS. Impaired autophagy and organellar dysfunction in pancreatitis. *J Gastroenterol Hepatol*. (2012) 27(Suppl. 2):27–32. doi: 10.1111/j.1440-1746.2011.07004.x
39. Dawra R, Sah RP, Dudeja V, Rishi L, Talukdar R, Garg P, et al. Intra-acinar trypsinogen activation mediates early stages of pancreatic injury but not inflammation in mice with acute pancreatitis. *Gastroenterology*. (2011) 141:2210–7 e2. doi: 10.1053/j.gastro.2011.08.033
40. Bradley EL III. A clinically based classification system for acute pancreatitis. Summary of the International Symposium on Acute Pancreatitis, Atlanta, Ga, September 11 through 13, 1992. *Arch Surg*. (1993) 128:586–90.
41. Peake J, Suzuki K. Neutrophil activation, antioxidant supplements and exercise-induced oxidative stress. *Exerc Immunol Rev*. (2004) 10:129–41.

Conflict of Interest Statement: The authors declare that the research was conducted in the absence of any commercial or financial relationships that could be construed as a potential conflict of interest.

Copyright © 2019 Huang, Chen, Zhang, Li, Huang, Huang, Qin, Chen, Cheng, Ma and Zhou. This is an open-access article distributed under the terms of the Creative Commons Attribution License (CC BY). The use, distribution or reproduction in other forums is permitted, provided the original author(s) and the copyright owner(s) are credited and that the original publication in this journal is cited, in accordance with accepted academic practice. No use, distribution or reproduction is permitted which does not comply with these terms.

frontiers in Immunology

ORIGINAL RESEARCH
published: 24 May 2019
doi: 10.3389/fimmu.2019.01169

Identification of LPS-Activated Endothelial Subpopulations With Distinct Inflammatory Phenotypes and Regulatory Signaling Mechanisms

Erna-Zulaikha Dayang[1], Josée Plantinga[1], Bram ter Ellen[1], Matijs van Meurs[1,2], Grietje Molema[1†] and Jill Moser[1,2†]*

[1] Medical Biology Section, Department of Pathology and Medical Biology, University Medical Center Groningen, University of Groningen, Groningen, Netherlands, [2] Department of Critical Care, University Medical Center Groningen, University of Groningen, Groningen, Netherlands

OPEN ACCESS

Edited by:
Timothy Robert Billiar, University of Pittsburgh, United States

Reviewed by:
Michael Hickey, Monash University, Australia
Jaya Talreja, Wayne State University, United States

***Correspondence:**
Jill Moser
j.moser@umcg.nl

[†]These authors share senior authorship

Specialty section:
This article was submitted to Inflammation, a section of the journal Frontiers in Immunology

Received: *28 January 2019*
Accepted: *08 May 2019*
Published: *24 May 2019*

Citation:
Dayang E-Z, Plantinga J, ter Ellen B, van Meurs M, Molema G and Moser J (2019) Identification of LPS-Activated Endothelial Subpopulations With Distinct Inflammatory Phenotypes and Regulatory Signaling Mechanisms. Front. Immunol. 10:1169. doi: 10.3389/fimmu.2019.01169

Sepsis is a life-threatening condition caused by a dysregulated host response to infection. Endothelial cells (EC) are actively involved in sepsis-associated (micro)vascular disturbances and subsequent organ dysfunction. Lipopolysaccharide (LPS), a Gram-negative bacterial product, can activate EC leading to the expression of pro-inflammatory molecules. This process is molecularly regulated by specific receptors and distinct, yet poorly understood intracellular signaling pathways. LPS-induced expression of endothelial adhesion molecules E-selectin and VCAM-1 in mice was previously shown to be organ- and microvascular-specific. Here we report that also within renal microvascular beds the endothelium expresses different extents of E-selectin and VCAM-1. This heterogeneity was recapitulated *in vitro* in LPS-activated human umbilical vein EC (HUVEC). Within 2 h after LPS exposure, four distinct HUVEC subpopulations were visible by flow cytometric analysis detecting E-selectin and VCAM-1 protein. These encompassed E-selectin$^-$/VCAM-1$^-$ (–/–), E-selectin$^+$/VCAM-1$^-$ (E-sel+), E-selectin$^+$/VCAM-1$^+$ (+/+), and E-selectin$^-$/VCAM-1$^+$ (VCAM-1+) subpopulations. The formation of subpopulations was a common response of endothelial cells to LPS challenge. Using fluorescence-activated cell sorting (FACS) we demonstrated that the +/+ subpopulation also expressed the highest levels of inflammatory cytokines and chemokines. The differences in responsiveness of EC subpopulations could not be explained by differential expression of LPS receptors TLR4 and RIG-I. Functional studies, however, demonstrated that the formation of the E-sel+ subpopulation was mainly TLR4-mediated, while the formation of the +/+ subpopulation was mediated by both TLR4 and RIG-I. Pharmacological blockade of NF-κB and p38 MAPK furthermore revealed a prominent role of their signaling cascades in E-sel+ and +/+ subpopulation formation. In contrast, the VCAM-1+ subpopulation was not controlled by any of these signaling pathways. Noteworthy is the existence of a "quiescent" subpopulation that was devoid of the two adhesion molecules and did not express cytokines or chemokines despite LPS exposure. Summarizing, our findings suggest that LPS activates different

signaling mechanisms in EC that drive heterogeneous expression of EC inflammatory molecules. Further characterization of the signaling pathways involved will enhance our understanding of endothelial heterogeneous responses to sepsis related stimuli and enable the future design of effective therapeutic strategies to interfere in these processes to counteract sepsis-associated organ dysfunction.

Keywords: endothelial cells, HUVEC, lipopolysaccharide (LPS), adhesion molecules, endothelial heterogeneity, intracellular signaling

INTRODUCTION

Sepsis is defined as a life-threatening organ dysfunction caused by a dysregulated host response to infection (1). Despite diagnostic advances in early recognition, sepsis often escalates to multiple organ dysfunction syndrome (MODS), leading to poor outcome. Sepsis affects around 30 million people yearly worldwide, resulting in 6 million deaths (2). Although several mechanisms have been suggested to contribute to the pathophysiology of sepsis, it is still incompletely understood, thereby hindering the development of successful treatment options for patients with sepsis and sepsis-induced multiple organ dysfunction syndrome.

Endothelial cells (EC) line all blood vessels and are one of the first cells to respond to microbial product such as Lipopolysaccharide (LPS) (3). During sepsis, EC respond to LPS via the activation of pattern recognition receptors (PRRs), producing pro-inflammatory cytokines, chemokines, and adhesion molecules (4). Adhesion molecules such as E-selectin, VCAM-1, and ICAM-1 facilitate endothelial cell—leukocyte interactions, resulting in leukocyte recruitment into inflamed tissues leading to subsequent impairment of organ function (5). Therapeutic strategies designed to attenuate EC production of these inflammation associated molecules to prevent leukocyte adhesion and transmigration, may lead to diminished organ failure in patients with sepsis.

Previous studies from our laboratory have shown that in mice, LPS or TNF-α exposure results in organ and microvascular compartment specific expression of adhesion molecules (6–8). Within the kidney, at the microvascular compartment level, TNF-α induced expression of E-selectin is abundant in glomeruli, but low in the arterioles. In contrast, VCAM-1 is highly expressed in the arterioles, while expressed to a lesser extent in the glomeruli (6, 7). Our knowledge on inter- and intra-organ endothelial heterogeneity has expanded in recent years, yet how these heterogeneous responses are molecularly controlled following LPS challenge still remains elusive.

Toll-Like Receptor 4 (TLR4) (9) and the more recently identified retinoic acid inducible gene-I (RIG-I) (10) are pattern recognition receptors which have been shown to drive endothelial responses to LPS. The recognition of LPS via these receptors results in the induction of endothelial adhesion molecules, cytokines, and chemokines via several downstream signaling pathways, that include NF-κB (10–12), and p38 MAPK (12, 13). Although both NF-κB and p38 MAPK have been implicated in controlling LPS-mediated inflammatory responses, it is unknown whether one, the other, both, or other signaling pathways regulate individual EC responses at a cellular level. Likewise, and of interest in relation to the microvascular compartment specific responses of the endothelium to LPS challenge *in vivo*, whether all EC are equipped with similar downstream signaling machinery remains to be elucidated.

Here, we investigate the molecular control of the early stages of EC activation by LPS in relation to the previously reported heterogeneous EC responses found *in vivo*. We focused on LPS induced expression patterns of E-selectin and VCAM-1 within mouse renal microvascular compartments *in vivo* and their patterns in HUVEC *in vitro* using immunofluorescent staining and flow cytometry, respectively. Based on the outcome we next investigated *in vitro* whether different stages of cell division could explain the observed heterogeneous subpopulations formed, and whether these subpopulations behaved differently because of differential expression of LPS signaling machinery components. Additionally, we used pharmacological tools to examine the activity of different kinase signaling pathways to explain heterogeneous subpopulation formation in HUVEC upon LPS exposure.

MATERIALS AND METHODS

Mice

Male C57BL/6 mice purchased from Envigo (Horst, The Netherlands) and housed in a specific pathogen-free facility, maintained on chow and water *ad libitum*, and housed in temperature-controlled chambers (24°C) with a 12 h light/dark cycle. Mice were challenged with intraperitoneal (i.p) injection of 1 mg/kg LPS [*E. coli*, serotype O26:B6 (15,000 EU/g), Sigma-Aldrich, St. Louis, MO, USA] as described elsewhere (14). Control mice were i.p administered with the same volume of 0.9% NaCl. Mice were terminated under isoflurane anesthesia 4 h after LPS challenge. Blood was subsequently drawn via cardiac puncture and the organs harvested, snap-frozen on liquid nitrogen and stored at −80°C until further analysis. All experiments were performed in compliance with the animal ethics committee of the University of Groningen.

Endothelial Cell Culture and Stimulation

Human umbilical vein endothelial cells (HUVEC) and human lung microvascular endothelial cells (HMVEC-L) were purchased from Lonza (Lonza, Breda, the Netherlands) and cultured in EBM-2 medium supplemented with EGM-2 MV Single Quot Kit Supplements and Growth factors (Lonza) at 37°C with 5% CO_2/95% air conditions until passage 5 at

the UMCG Endothelial Cell Facility. Additionally, HUVEC were isolated from umbilical cords and cultured on 1% gelatin coated plates with RPMI 1640 medium (Lonza) supplemented with 20% heat inactivated FCS, 2 mM L-glutamine, 5 U/ml heparin, 50 μg/ml endothelial growth factor, and antibiotics (100IE/penicillin and 50 μg/ml streptomycin). HUVEC and HMVEC-L were seeded in 6 or 12 well plates. HUVEC were 70% confluent on the day of siRNA transfection while they were confluent when treated with LPS (E. coli, serotype O26:B6; E. coli, serotype O111:B4, Sigma Aldrich, St. Louis, MO) at 1 μg/mL for 4 h unless indicated otherwise.

Cryosection Immunofluorescence Staining

Five-micrometer cryosections from snap-frozen mouse kidneys were fixed in acetone for 10 min. The sections were blocked with 0.00125% H_20_2 (Merck, Darmstadt, Germany) in demineralized H_20 for 10 min, and subsequently blocked with 3% bovine serum albumin (BSA) in phosphate buffered saline (PBS) (w/v) for 30 min. Kidney sections were incubated at room temperature (RT) for 1 h with primary rat-anti-mouse E-selectin antibody (10 μg/mL, clone MES-1, kindly provided by Dr. D Brown, UCB Celltech, Brussels, Belgium) diluted in 5% fetal calf serum (FCS) (Sigma, St. Louis, Missouri, USA) in PBS. After washing, sections were incubated with rabbit anti-rat IgG (Vector Laboratories Inc, Burlingame, CA, USA) in 1% normal mouse serum (NMS) (Sanquin, Amsterdam, NL)/5% FCS in PBS for 45 min. The sections were then washed and incubated with anti-rabbit HRP polymer (Dako, Carpentaria, CA, USA) for 30 min. After washing, the sections were exposed to Alexa Fluor®555 Tyramide reagent prepared according to the manufacturer's instructions (#B40955, Thermo Fisher Scientific, Carlsbad, CA, USA). For the sequential second primary antibody incubation, the sections were washed and blocked again with 3% (w/v) BSA in PBS for 30 min. The second primary antibody, rat anti-mouse VCAM-1 (hybridoma supernatant of clone M/K-1.9, ATCC, Manassas VA, USA) was added to the sections for 1 h at RT. After washing, the sections were incubated with 20 μg/mL of goat anti-rat antibody conjugated with Alexa Fluor®488 (Thermo Fisher Scientific) / DAPI (1.5 μg/mL; Thermo Fisher Scientific) in 5% FCS in PBS for 45 min, washed, and mounted with Aqua/polymount (Polysciences Inc, Warrington, PA, USA). Isotype controls included rat IgG2a and rat IgG1 (10 μg/mL; both from Antigenix America Inc., Huntington Station, NY, USA). Images were taken using a Leica SP8 confocal laser scanning microscope (Leica Microsystems Ltd., Germany) with objective and numerical apertures of 40X and 1.3, respectively. Image cubes were recorded with appropriate filters using Leica application suite X software. Peak emission for Alexa Fluor 488 (VCAM-1) was at 550 nm and for Alexa Fluor 555 (E-selectin) at 610 nm. All images were captured with equal exposure times and then analyzed using Imaris image analysis software (Bitplane AG, Zurich, Switzerland).

For CD31/E-selectin respectively CD31/VCAM-1 double staining, the kidney cryosections were blocked with peroxidase and 3% BSA as described above, incubated with rat-anti mouse CD31 antibody (0.15 μg/mL, # 550274 BD Pharmingen, Franklin Lakes, NJ, USA) diluted in 5% FCS in PBS for 1 h, and subsequently stained with rat anti-mouse antibody E-selectin, or rat anti-mouse VCAM-1 according to the above-described protocols. The images were taken with a Leica DM4000B fluorescence microscope equipped with a Leica DFC345FX digital camera (Leica Microsystems Ltd., Germany) and Leica LAS V4.5 Image Software at 100X magnification with equal exposure times.

Flow Cytometry

We employed flow cytometry to determine the expression of endothelial adhesion molecules. HUVEC or HMVEC-L were briefly washed with sterile PBS, trypsinized with trypsin-EDTA (0.025%) and washed with ice-cold wash buffer (5% FCS in PBS). Cells were then transferred to FACS tubes, washed and resuspended in 3% v/v PE-conjugated mouse anti-human E-selectin (Cat. No #322606, BioLegend, San Diego, CA, USA) and APC-conjugated mouse anti-human VCAM-1 (Cat. No #305810, BioLegend) antibodies in wash buffer for 30 min on ice in the dark. For intracellular staining, HUVEC were fixed with Fixation Reagent A (#GAS004, Thermo Fisher Scientific) for 15 min, washed, and subsequently incubated with perm buffer Reagent B (Thermo Fisher Scientific) and 3% (v/v) Brilliant Violet 421-conjugated anti-Ki67 (#330505, Biolegend, San Diego, CA, USA) antibody in wash buffer for 30 min, on ice in the dark. The cells were then washed and resuspended in wash buffer and analyzed using a MACSQuant Analyzer 10 flow cytometer (Miltenyi Biotech, San Diego, CA, USA). Data analysis was performed using Kaluza Flow analysis software (v.2.1) (Beckman Coulter, Brea, CA, USA) or FlowJo software (v.10) (Ashland, OR, USA). Isotype control antibodies mouse IgG1κ-BV421 (Cat No #400157, Biolegend), IgG2aκ-PE (Cat No #2-4724-42, eBioscience, San Diego, CA, USA), and mouse IgG1 (Cat No # IC002A, R&D System, Minneapolis, MN, USA) were used to correct for signals from non-specific binding.

Fluorescence-Activated Cell Sorting (FACS)

HUVEC treated with LPS for 4 h were trypsinized**,** washed and subsequently incubated with PE-conjugated mouse anti-human E-selectin and APC-conjugated mouse anti-human VCAM-1 antibodies as described above. After the staining procedure, the cells were sorted into 4 subpopulations based on the staining pattern of E-selectin and VCAM-1 using a MoFlo Astrios FACS machine (Beckman Coulter, Brea, CA, USA): "quiescent" E-sel$^-$/VCAM-1$^-$ (-/-), E-sel$^+$/VCAM$^-$1- (E-sel+), E-sel$^+$/VCAM-1$^+$ (+/+), and E-sel$^-$/VCAM-1$^+$ (VCAM-1+) subpopulations (see **Figure 4A)**. After sorting, the purity of each collected population of cells was verified by flow cytometry before subsequent analyses were performed (data not shown).

Trypsinization *per se* did not alter detection of membrane expression of the adhesion molecules in flow cytometry, as detachment of endothelial cells with versene, a gentle non-enzymatic cell dissociation reagent, showed similar patterns of endothelial surface protein expression (data not shown).

Gene Expression Analysis by RT-qPCR

Total RNA from the cells was isolated using the RNeasy® mini kit (Qiagen, Venlo, The Netherlands) according to the manufacturer's protocols. RNA concentration (OD 260) and purity (OD260/OD280) was determined using a NanoDrop® ND-1000 UV-Vis spectrophotometer (NanoDrop Technologies, Rockland, ME, USA). Samples with an OD260/OD280 ratio of ≥1.8 were included in the analysis. cDNA synthesis was performed as previously described (15). Quantitative (q)PCR was performed in a ViiA 7 PCR System (Applied Biosystems Nieuwerkerk aan den IJssel, The Netherlands) using the following assay-on-Demand primers (Applied Biosystems,): GAPDH (assay ID Hs99999905_m1), E-selectin (assay ID Hs00174057_m1), VCAM-1 (assay ID Hs00365486_m1), TLR4 (assay ID Hs00152939_m1), RIG-I (assay ID Hs00204833_m1), MAVS (assay ID Hs00920075), IL-6 (assay ID Hs00174131_m1), IL-8 (assay ID Hs00174103_m1), MCP-1 (assay ID Hs00234140_m1), CXCL10 (assay ID Hs01124251_g1), and CXCL6 (assay ID Hs00605742_g1). Duplicate analyses were performed for each sample and the obtained threshold cycle values (C_T) averaged. All genes were normalized to the expression of housekeeping gene GAPDH, yielding the ΔC_T value. The relative mRNA level was calculated by $2^{-\Delta CT}$.

siRNA–Mediated Gene Silencing

TLR4, RIG-I, and MAVS were knocked down in HUVEC using FlexiTube siRNA (Qiagen). AllStars negative control siRNA (Qiagen) was used as a negative control for all RNA interference experiments. Transient transfection was performed using Lipofectamine 2000 (Life Technologies, Carlsbad, CA, USA) according to the manufacturer's instructions. Knockdown of these genes did not diminish endothelial cell viability as described previously (10).

Pharmacological Inhibition of Signaling Pathways

BAY11-7082 (BAY) (Alexis Biochemicals, San Diego, CA, USA) was dissolved in DMSO as a 20mM stock solution, while LY2228820 (LY) (MedChemExpress, Monmouth Junction, NJ, USA) was dissolved in DMSO as a 10 mM stock solution according to manufacturers' instructions. Stocks were stored at −80°C until needed. Prior to the experiment, BAY and LY stock solutions were diluted in HUVEC culture medium. HUVEC were pre-treated with 10 μM of BAY 30 min before, and/or 10 μM of LY 1 h before LPS stimulation. The viability and morphology of HUVEC were assessed microscopically before and after pre-treatment with either BAY or LY, and they were found to be of normal cobble-stone morphology throughout the experiments.

Statistical Analysis

Statistical analysis of results was performed by two-tailed unpaired Student *t*-test, or one-way ANOVA followed by Bonferroni *post hoc* analysis to compare multiple replicate means. All statistical data were analyzed using GraphPad Prism software v.7 (GraphPad Prism Software Inc., San Diego, CA, USA). Differences were considered significant when $p < 0.05$.

RESULTS

Distinct Expression Patterns of E-Selectin and VCAM-1 Are Found Within Kidney Microvascular Compartments of LPS-Treated Mice

Heterogeneous expression of E-selectin and VCAM-1 between different renal microvascular compartments has been previously reported. Intravascular heterogeneity in expression of endothelial adhesion molecules within specific renal microvascular beds, on the other hand, is not extensively described. To investigate the expression patterns of E-selectin and VCAM-1 in the different kidney microvascular segments, we performed immunofluorescent double staining to detect these two adhesion molecules at the same time. In control kidney, E-selectin protein was absent from all microvascular compartments, while arterioles expressed basal VCAM-1 protein **Figure 1**, confirming previous data from our laboratory (7, 16). Following LPS challenge, E-selectin and VCAM-1 became visible in all kidney microvascular segments. However, E-selectin was mainly expressed in the glomeruli, whereas the arterioles predominantly expressed VCAM-1, with scattered co-expression of E-selectin. The peritubular capillaries and post-capillary venules mainly co-expressed E-selectin and VCAM-1, while occasional single E-selectin or VCAM-1 positive cells were found **Figure 1**. Double immunostaining of CD31, a pan-endothelial marker and E-selectin respectively VCAM-1 confirmed their expression by endothelial cells in the microvascular segments **(Supplementary Figure 1).** These data demonstrate that EC in different microvascular compartments, and also within the same microvascular compartment, exert a heterogeneous phenotype which can be identified by different patterns of E-selectin and VCAM-1 protein expression following LPS challenge.

LPS Stimulation of Endothelial Cells *in vitro* Uncover Cell Subpopulations Based on E-Selectin and VCAM-1 Expression

To investigate whether EC *in vitro* can also express E-selectin and VCAM-1 in varying patterns, we stimulated HUVEC with 1 μg/mL LPS for 4 h, after which we flow cytometrically determined E-selectin and VCAM-1 protein levels. In control cells, E-selectin and VCAM-1 expression levels were low **(Figure 2A)**. After 4 h of LPS stimulation, the expression of both E-selectin and VCAM-1 was increased, as evidenced by the shift in the Mean Fluorescent Intensity (MFI) relative to non-stimulated controls **(Figure 2A).** At the cell population level, 4 h of LPS exposure surprisingly revealed the formation of EC subpopulations **Figure 2B**; **Supplementary Figure 2A** which bear similarities with the subpopulations observed in the microvasculature in the kidney. A large subpopulation of EC (approximately 50%) expressed both E-selectin and VCAM-1, while at the same time a significant subset of cells (approximately 20%) remained "quiescent" despite exposure to LPS **Figure 2B**; **Supplementary Figure 2A**. Moreover, two additional EC subpopulations were identified that expressed either E-selectin or VCAM-1 **Figure 2B**; **Supplementary Figure 2A**. Similar

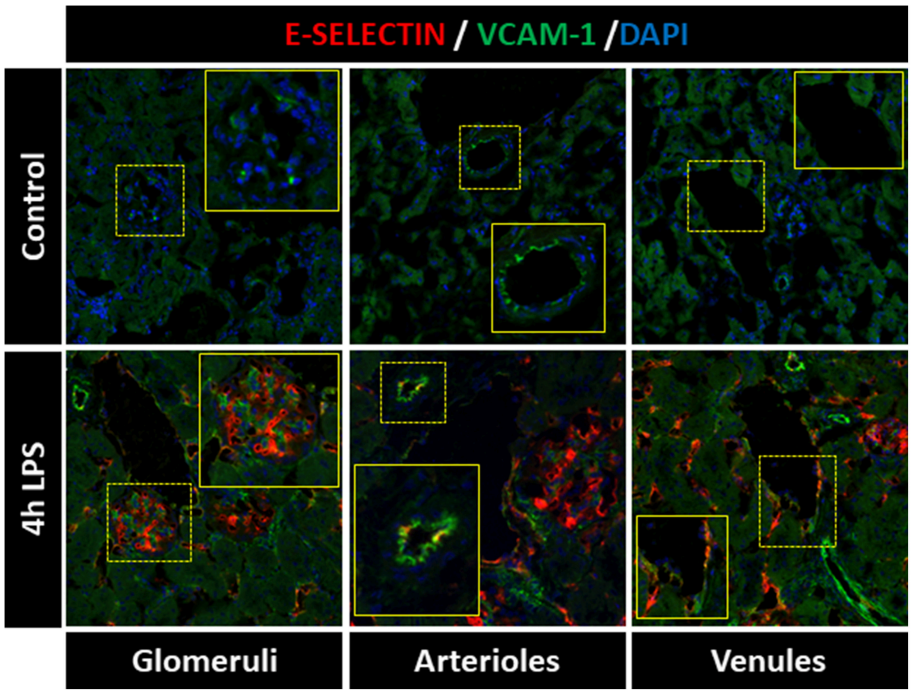

FIGURE 1 | Distinct expression patterns of E-selectin and VCAM-1 are found within kidney microvascular compartments of LPS-treated mice. E-selectin and VCAM-1 expression varied between and within the renal microvascular segments of LPS-treated mice. The images show immunofluorescence staining of E-selectin (red), VCAM-1 (green), and DAPI nuclear staining (blue) in the kidney of control mice (vehicle treated) and mice challenged with LPS (1 mg/kg, i.p.) and sacrificed 4 h later. All images were captured with equal exposure times. Original magnification x400.

results were found when exposing HUVEC isolated from single donors to 4 h LPS **(Figure 2B)**, and also human lung microvascular endothelial cells (HMVEC-L) exposed to LPS revealed the formation of these four subpopulations **Figure 2B**. Endothelial subpopulations identified by heterogeneous expression of E-selectin and VCAM-1 and combinations thereof after LPS exposure is therefore not restricted to HUVEC and not donor related but a common response of endothelial cells.

We next studied the kinetics of E-selectin and VCAM-1 expression in HUVEC. Upon LPS exposure, some EC started to express E-selectin as early as 1 h after start of activation by LPS, while at 2 h, VCAM-1 expression became apparent **Figure 2C**; **Supplementary Figure 2B**. Moreover, at this early timepoint, four EC subpopulations already had started to form, i.c., "quiescent" E-selectin$^-$/VCAM-1$^-$ (-/-), E-selectin$^+$/VCAM-1$^-$ (E-sel+), E-selectin$^+$/VCAM-1$^+$ (+/+), and E-selectin$^-$/VCAM-1$^+$ (VCAM-1+). These expression profiles were retained until 6 h of LPS exposure, after which the E-selectin positive subpopulation diminished in cell number, while the VCAM-1+ subset and quiescent subpopulations increased. At 24 h, most EC had returned to a quiescent state, with only a small VCAM-1+ subset (7% of all cells) still being present **(Figure 2C)**. A quiescent endothelial cell subpopulation was constantly present at all times **Figure 2C**; **Supplementary Figure 2B**. Furthermore, these patterns of E-selectin and VCAM-1 expression were similar when exposed to different LPS concentrations, except for the lowest LPS concentration (0.1 μg/mL) which did not seem to activate the endothelial cells (**Supplementary Figure 2C**). Taken together, our data demonstrate that activation of endothelial cells by LPS leads to E-selectin and VCAM-1 (co)expression patterns that are dynamically changing depending on the time of exposure to LPS and which are not affected by the concentration of LPS used.

Cell Division Is Not a Major Factor in Controlling the Ability of EC to Express E-Selectin and/or VCAM-1 When Exposed to LPS

HeLa cells were reported to repress NF-κB activity following inflammatory stimulation while dividing as cell division appeared to have a higher cellular priority (17). Whether this also occurs in dividing endothelial cells is currently unknown. We hypothesized that the quiescent EC subpopulation was unable to express E-selectin and VCAM-1 because these cells are actively dividing. Staining for Ki67, a marker of actively dividing cells, however, revealed that the total number of Ki67 cells in the HUVEC population as a whole was only approximately 7% **Figure 3**. This is much less than the 25% of cells in the quiescent cell population after LPS stimulation. Moreover, when gating the Ki67 positive cells we found that they were present in all four flow cytometric quadrants **Figure 3**. Hence, cell division *per se* does not seem to be a major factor influencing the ability of EC to express E-selectin and/or VCAM-1 and is therefore not a likely factor

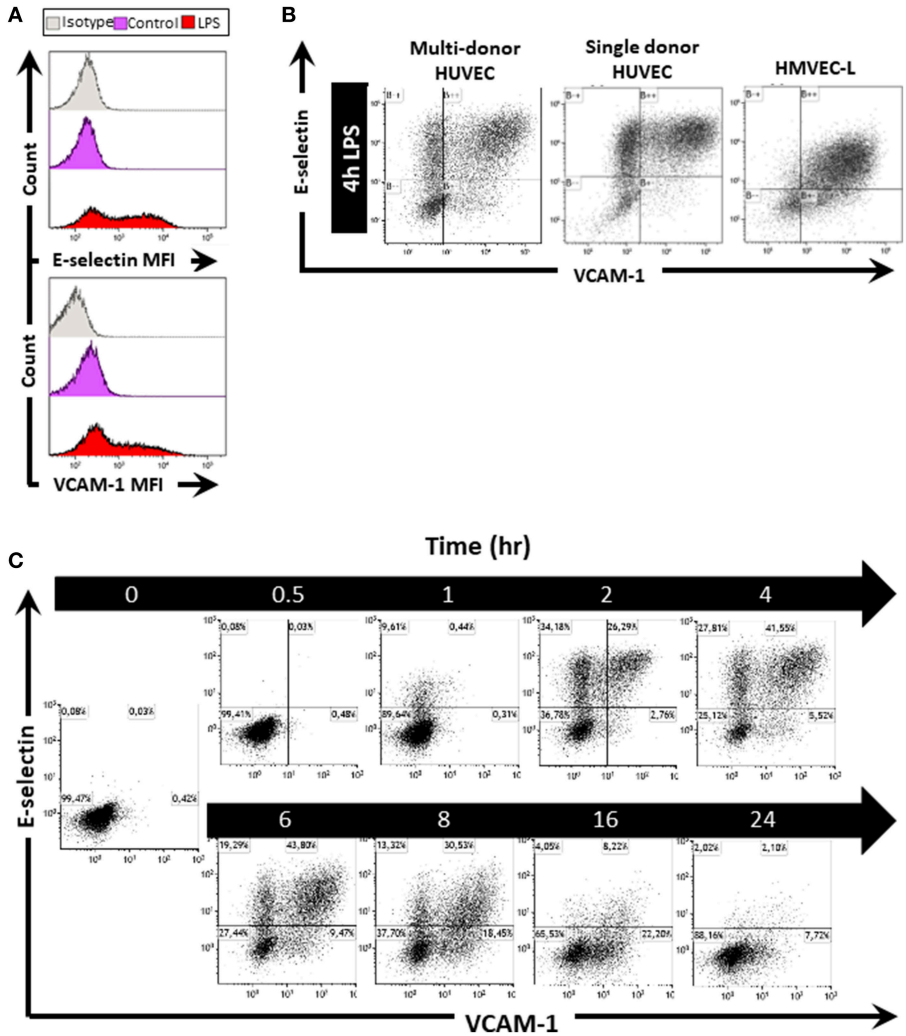

FIGURE 2 | LPS stimulation of endothelial cells *in vitro* induces the formation of EC subpopulations based on E-selectin and VCAM-1 expression. **(A)** Histograms of HUVEC as one whole population show the mean fluorescent intensity (MFI) of E-selectin and VCAM-1 in untreated control and EC treated with LPS for 4 h. Isotype controls were also included. **(B)** Scatterplots of EC subpopulations based on E-selectin and VCAM-1 expression in multi-donor HUVEC, single donor HUVEC, and lung microvascular endothelium (HMVEC-L), 4 h after LPS exposure. The data shown is representative of at least four independent experiments. **(C)** Kinetics of EC subpopulation formation based on E-selectin and VCAM-1 expression in HUVEC stimulated with LPS for the indicated time periods. The data shown is representative of two independent experiments.

contributing to the "quiescence status" of EC that do not express the adhesion molecules upon exposure to LPS.

Endothelial Subpopulations Have Distinct mRNA Expression Levels of LPS Signaling Pathway Components and Inflammatory Genes

LPS induced adhesion molecule expression in EC is known to be mediated by at least two pattern recognition receptors, TLR4 and RIG-I (10, 18). We therefore hypothesized that the subpopulation distribution of EC after LPS exposure identified by E-selectin and VCAM-1 patterns was due to different subpopulations expressing LPS signaling components to different extents. To investigate this, we incubated HUVEC with LPS for 4 h and then separated the quiescent -/-, E-sel+, +/+ and VCAM-1+ subpopulations by fluorescence activated cell sorting (FACS). After sorting and confirmation of subpopulation purity (data not shown), we first determined the E-selectin and VCAM-1 mRNA expression levels **Figure 4B**. E-selectin and VCAM-1 mRNA levels were close to absent in the quiescent -/- subpopulation, while E-selectin mRNA was high in E-sel+ and +/+ subpopulations, and VCAM-1 mRNA was high in +/+ and VCAM-1+ subpopulations thereby corroborating the protein data. We proceeded to determine the mRNA expression levels of TLR4 and RIG-I within the different EC subpopulations. TLR4 mRNA levels were similar in all EC subpopulations including the quiescent one **Figure 4B**. RIG-I mRNA levels were highest in the E-sel^{+}/VCAM-1^{+} cell population and expressed at a slightly lower level in the other EC subpopulations

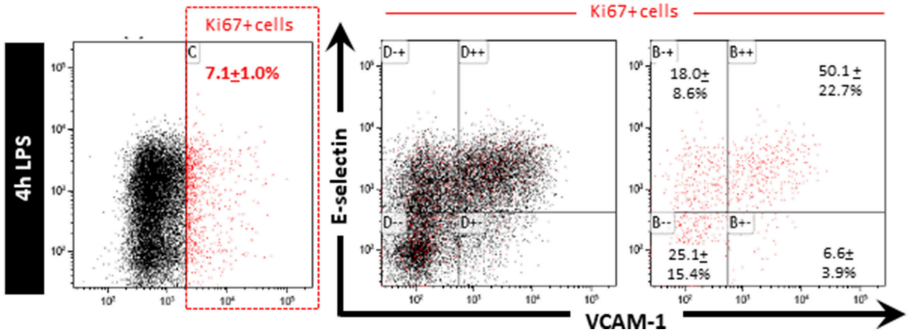

FIGURE 3 | Cell division is not a major factor controlling the ability of EC to express E-selectin and/or VCAM-1 when exposed to LPS. HUVEC exposed to LPS for 4 h were stained for Ki67 after which Ki67 positive cells were gated and the extent of E-selectin and VCAM-1 expression on those cells determined. Ki67 positive cells are indicated in red. The percentage of Ki67 positive cells expressing different extents of E-selectin and VCAM-1 is reported as the mean ± SD of three independent experiments.

Figure 4B, while mRNA levels of MAVS, a downstream protein adaptor of RIG-I, were similar in all four EC subpopulations **Figure 4B**. To further investigate the inflammatory status of the four subpopulations, we analyzed the expression levels of a series of cytokines/chemokines known to be produced by endothelial cells in inflammatory conditions. While both the quiescent and the VCAM-1+ subpopulations expressed the lowest levels of these genes, the +/+ subpopulation exerted the most pronounced inflammatory phenotype **Figure 4C**. These results demonstrate that upon LPS exposure, there are distinct endothelial subpopulations with varying LPS signaling components and inflammatory phenotypes within a HUVEC cell population.

TLR4 and RIG-I Differentially Regulate LPS-Mediated E-Selectin/VCAM-1 Expressing Subpopulations

Since both receptors are expressed in all EC subpopulations, we proceeded to examine the effect of TLR4 and RIG-I siRNA knockdown on the formation of E-selectin and VCAM-1 expressing subpopulations in HUVEC upon LPS exposure. Knockdown of both TLR4 and RIG-I resulted in diminished protein levels of both E-selectin and VCAM-1 when analyzing the HUVEC population as a whole (data not shown) corroborating previous findings (10). While only TLR4 knockdown resulted in inhibition of the E-sel+ subpopulation formation, knockdown of either TLR4 or RIG-I resulted in a major inhibition of +/+ subpopulation formation **Figure 5A**. As a consequence, the -/- "quiescent" subpopulation increased **Figure 5A**. In contrast to the inhibitory effect observed on the E-sel+ or +/+ subpopulations, knockdown of TLR4 or RIG-I did not inhibit the VCAM-1+ subpopulation from forming **Figure 5A**. Similar to the effects of RIG-I knockdown, MAVS knockdown inhibited the formation of the +/+ subpopulation with no effect on E-sel+ or VCAM-1+ subpopulation formation **Figure 5B**. These results suggest that TLR4 predominantly controls the formation of E-sel+ cells and that both TLR4 and RIG-I control the formation of the E-sel+/VCAM-1+ population.

LPS-Mediated E-Selectin/VCAM-1 Expressing HUVEC Subpopulations Are Regulated by Different Downstream Signaling Mechanisms

We previously found that the absence of RIG-I or MAVS inhibited nuclear translocation of the NF-κB p65 subunit (10). Moreover, the NF-κB p65 subunit translocated from the cytoplasm to the nucleus in only 26% of EC 30 min after LPS stimulation (**Supplementary Figure 3**). Apart from NF-κB signaling, activation of p38 MAPK signaling in LPS exposed endothelial cells has previously been reported (19, 20). We therefore investigated whether one or both of these two signaling pathways were affecting the formation of one or more subpopulations employing pharmacological tools and if so, to what extent the subpopulations were affected.

When examining the subpopulation distribution after 2 h exposure to LPS we found that p38 MAPK inhibition using LY exerted a major inhibitory effect on the formation of the E-sel+ subpopulation **Figure 6A**. In contrast, NF-κB inhibition using BAY did not significantly influence the formation of any of the subpopulations at this early time point. At 4 h LPS exposure however, blockade of NF-κB and p38 MAPK had inhibited the formation of the +/+ subpopulation (**Figure 6B**). In addition, the combination of NF-κB and p38 MAPK inhibition strongly diminished the formation of the E-selectin+/VCAM-1+ expressing subpopulation **Figure 6B**. Formation of the VCAM-1+ subpopulation was not affected by inhibition of NF-κB and/or p38 MAPK. Also, inhibition of both NF-κB and p38 MAPK did not fully block the formation of the subpopulations, suggesting that other signaling pathways contribute to their formation.

DISCUSSION

Sepsis is a life-threatening condition which is characterized by progressive host dysregulation, following a known or suspected infection (1). Sepsis pathophysiology is still not fully understood which has hampered the development of therapeutic options

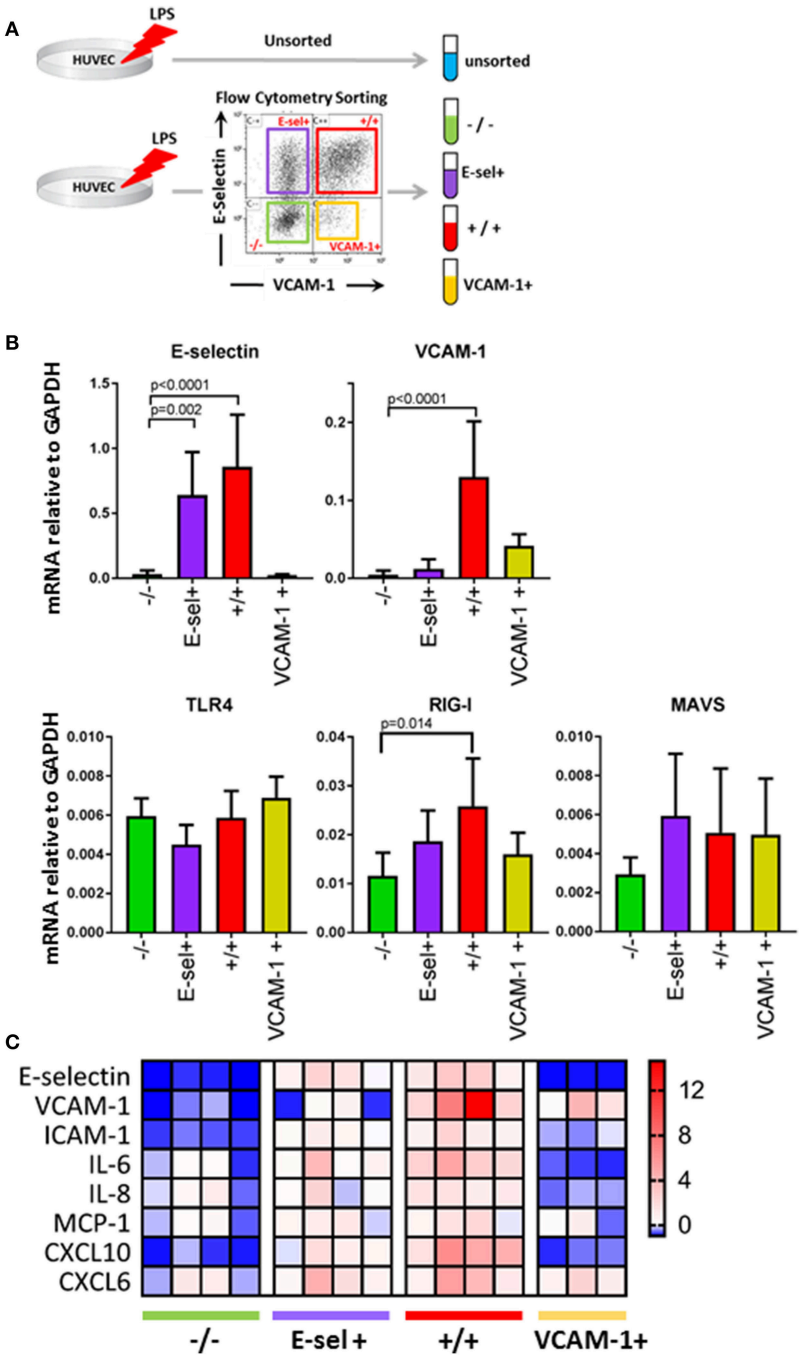

FIGURE 4 | Endothelial subpopulations have distinct mRNA expression levels of LPS signaling pathway components and inflammatory genes. **(A)** Experimental design for EC sorting using FACS. **(B)** mRNA expression levels of E-selectin, VCAM-1, TLR4, RIG-I, and MAVS in sorted EC subpopulations as determined by RT-qPCR using GAPDH as the housekeeping gene. Bars represent the mean ± SD of 5 independent experiments. $p < 0.05$ is considered statistically significant. **(C)** Heatmap displaying pro-inflammatory adhesion molecule, cytokine, and chemokine mRNA levels in sorted EC subpopulations compared to unsorted LPS control EC. The data shown is from four independent experiments.

counteracting organ failure in patients with sepsis. Due to their location, endothelial cells are among the first cells to respond to systemic pathogens or bacterial products (3). A hallmark of sepsis-related organ dysfunction is (micro)vascular dysfunction which include endothelial activation. This results in immune cell infiltration which can be detrimental for organ function (5). The current study aimed to explore the molecular control of early LPS mediated endothelial activation in relation to

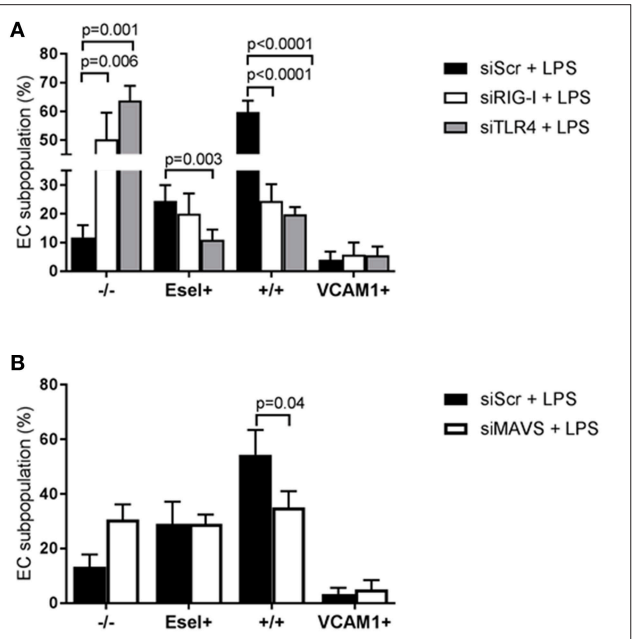

FIGURE 5 | TLR4 and RIG-I-MAVS differentially regulate LPS-mediated E-selectin/VCAM-1 subpopulation formation. **(A)** The effect of small interfering RNA (siRNA)-based RIG-I and TLR4 knockdown on the formation of LPS-induced EC subpopulations based on E-selectin and VCAM-1 expression after 4 h of LPS exposure compared to scramble siRNA (siScr) controls. Bars represent the mean ± SD of 4 independent experiments. **(B)** The consequence of MAVS knockdown on the formation of the EC subpopulations. Bars represent the mean ± SD of 3 independent experiments. $p < 0.05$ is considered statistically significant.

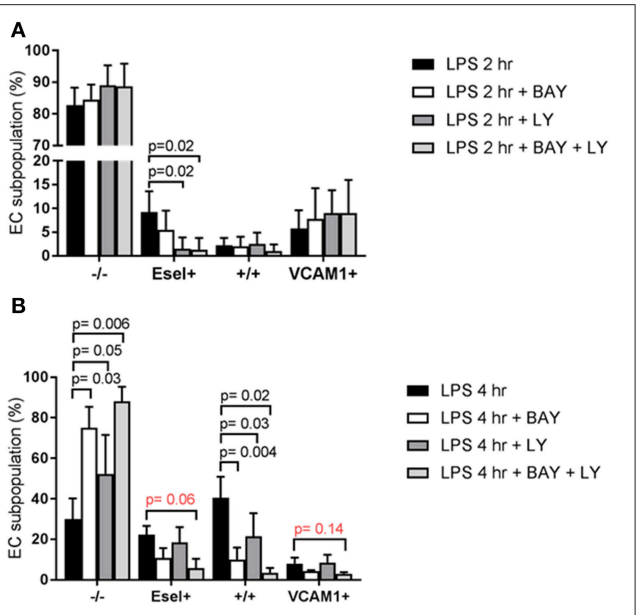

FIGURE 6 | LPS-mediated E-selectin/VCAM-1 HUVEC subpopulations are regulated by different downstream signaling mechanisms. **(A)** The effect of pharmacologically inhibiting NF-κB with BAY 11-7082 (BAY) and p38 MAPK with LY2228820 (LY) pre-treatment on the formation of the LPS-induced EC subpopulations based on E-selectin and VCAM-1 expression, after 2 h of LPS exposure; and **(B)** after 4 h of LPS exposure. Bars represent the mean ± SD of 4 independent experiments. $p < 0.05$ is considered statistically significant.

previously reported heterogeneous EC responses found *in vivo*. Our findings reveal that in the kidneys of mice challenged with LPS, EC between different microvascular compartments and also within the same microvascular bed, exert a heterogeneous phenotype as identified by different patterns of E-selectin and VCAM-1 protein expression. Moreover, we observed that *in vitro* in endothelial cell cultures, subpopulations appear shortly after the start of LPS exposure that exert a phenotypic E-selectin/VCAM-1 heterogeneity similar to that observed in the mouse kidney. These endothelial subpopulations have distinct inflammatory phenotypes, with the E-selectin/VCAM-1 double positive subset showing the highest level of activation. The formation of the subpopulations is differentially regulated by distinct signaling mechanisms, both at the level of TLR4 and RIG-I, and at the level of the NF-κB and p38 MAPK pathways. Strikingly, we found a quiescent population of cells that was not only devoid of E-selectin and VCAM-1 expression but was also lacking the expression of other proinflammatory cytokines and chemokines despite exposure to LPS.

It is well known that EC acquire organ- and tissue-specific identities to support the unique requirements of various organs in the body (21). The differential expression of E-selectin and VCAM-1 in different renal microvascular compartments of LPS-treated mice reported in this study corroborates previous observations from our group (6, 7). In addition, we revealed that within the same microvascular compartment, endothelial cells heterogenically express E-selectin and VCAM-1 following LPS challenge. While phenotypic differences between adjacent EC conditioned in the same environment were previously shown for endothelial barrier antigen in capillaries of the brain of rats (22) and for Tie-2 in mouse xenografts associated tumor neovessels (23), heterogeneous expression of cell adhesion molecules within individual microvascular segments has to our knowledge not been reported before. Interestingly, endothelial cells *in vitro* exhibited a similar phenotypic heterogeneity in E-selectin and VCAM-1 (co)expression patterns. The four subpopulations of EC, each with a different composition of E-selectin / VCAM-1 (co)expression, did not only appear in multi-donor HUVEC, but also in single-donor HUVEC and in human lung microvascular endothelial cells (HMVEC-L) exposed to LPS. From this we conclude that the observed heterogenous responsiveness is not a specific attribute of HUVEC but rather a common response of endothelial cells exposed to LPS. Of notice, HMVEC-L displayed a different composition of EC subpopulations, which could be attributed to a specific lung-microvascular phenotypical characteristic to support dedicated biological functions in the lungs. The E-sel^{+}/VCAM-1^{+} subpopulation also expressed the highest levels of inflammatory mediators IL-6, IL-8, MCP-1, CXCL6, and CXCL10, implying that this subpopulation has a more generalized higher activation status than the other three subpopulations. This finding is in line with a previous study that showed that high IL-8-secreting EC produced higher levels of endothelial adhesion molecules,

chemokines, and cytokines compared to their low IL-8-secreting EC counterparts (24). Why CXCL6, a chemoattractant for neutrophils, was specifically expressed in the VCAM-1+ subpopulation remains to be clarified. Follow up studies will determine the full nature and extent of activation of the cells in these subpopulations.

Intriguingly, we found a subpopulation of EC that did not express E-selectin or VCAM-1 despite prolonged exposure to LPS. Gene expression analysis of this sorted subpopulation of cells showed that these cells had a broader "quiescent" phenotype since they also did not express inflammatory cytokines and chemokines upon LPS exposure. One possible explanation for these findings could have been that these cells lack LPS-signaling machinery, but we showed that that was not the case as this population was expressing both TLR4 and RIG-I, two of the main LPS-signaling molecules in endothelial cells. Another explanation for these findings might have been that the cells in the "quiescent" phenotype subpopulation were dividing and thereby subjected to repression of NF-κB–driven inflammation as was previously reported in HeLa cells (17). However, we found only 7% of the total HUVEC population to be proliferating, while the quiescent population represented around 20% of cells. Moreover, Ki67 positive, proliferating cells were also able to express E-selectin, which confirmed previous observations (25, 26) and VCAM-1. Hence, cell proliferation does not appear to be a major contributing factor leading to the "quiescent" status of these cells. Since exaggerated and prolonged inflammatory responses can be detrimental to cells, a negative feedback loop mechanism exists that regulates the magnitude and duration of inflammation (27). An example of such is the activation of the zinc finger protein A20 which limits inflammation downstream of the NF-κB pathway. A20 mRNA levels were, however, comparable in all EC subpopulations (data not shown) including the quiescent EC subpopulation which suggests that an A20-dependent inhibitory feedback mechanism is not controlling the quiescent status of these E-selectin$^-$/VCAM-1$^-$ cells. Why these cells remain quiescent despite LPS exposure is currently unknown. We will investigate this further since understanding the molecular mechanisms associated with this quiescent phenotype may eventually be exploited for therapeutic strategies to inhibit endothelial activation in the setting of sepsis.

We explored the possibility that the heterogeneous responses by the EC subpopulations were attributed to intrinsic cellular differences in the functionality of the LPS signaling components. Using siRNA-based knock down we investigated the role of TLR4 and RIG-I in this process. While TLR4 mediated both E-sel+ and E-sel$^+$/VCAM-1$^+$ subpopulation formation, RIG-I mainly had a role in E-sel$^+$/VCAM-1$^+$ subpopulation formation. Knocking down MAVS, a RIG-I adaptor protein, did not

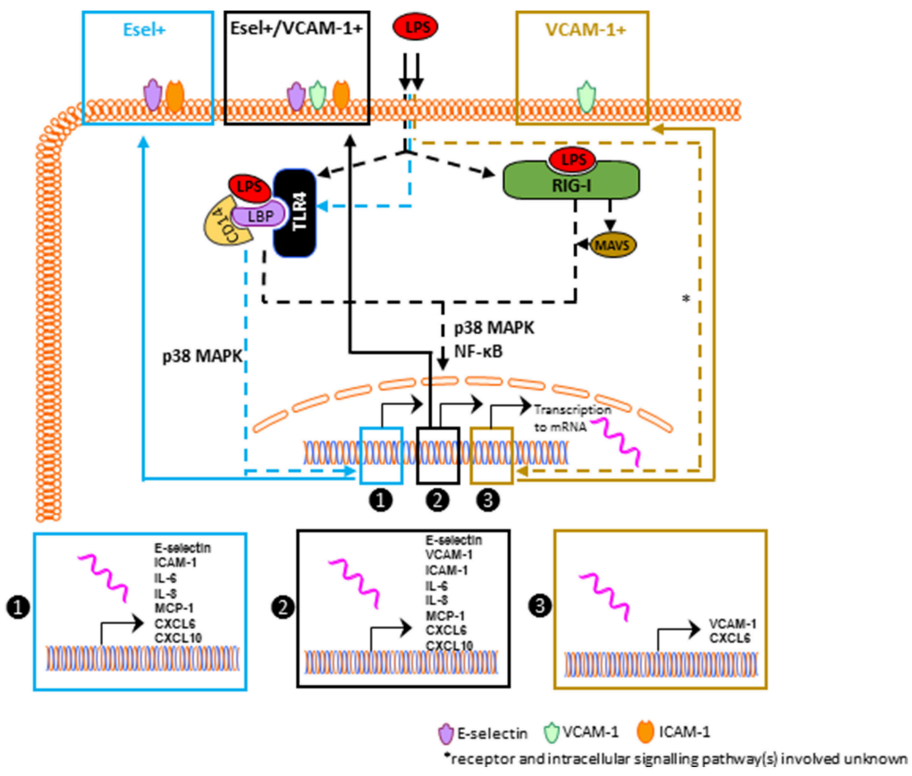

FIGURE 7 | Proposed cellular regulatory mechanisms that control the formation of LPS-mediated EC subpopulations. Dashed lines represent pathways involved in transcriptional control of pro-inflammatory molecules, and solid lines represent pro-inflammatory proteins on EC. The blue, black, and brown lines represent intracellular signaling pathways that determine E-sel+, E-sel+/VCAM-1+, and VCAM-1+ subpopulation formation.

affect the formation of E-sel+ and VCAM-1+ subpopulations. Pharmacological inhibition studies showed that NF-κB and p38 MAPK were the predominant controlling pathways for the formation of the E-sel+ and E-sel^{+}/VCAM-1^{+} subpopulations (see **Figure 7**). The fact that the VCAM-1+ population at early time points of LPS stimulation was not affected by any of the pathways investigated raises the question how this subpopulation is being formed when endothelial cells are exposed to LPS. One way to establish a clear role of LPS signaling in VCAM-1+ subpopulation formation is by performing knockdown experiments and examining the activation status when the VCAM-1+ subpopulation is at its peak (16 h after LPS stimulation, **Supplementary Figure 2B**). At 16 h of LPS exposure, it is highly likely that secondary or tertiary responses have become part of the equation following the release of pro-inflammatory cytokines, such as IL-6 and IL-8. Exposing naïve HUVEC to cytokines (e.g., IL-6) has been shown to increase E-selectin, VCAM-1, and ICAM-1 (28). Considering the pharmacological importance of the findings reported here, we will investigate this issue in more detail in HUVEC subpopulations using kinase activity platform technology.

In conclusion, renal endothelial cells exert a heterogeneous pattern of E-selectin and VCAM-1 expression following LPS challenge, in different as well as within the same microvascular segments. Such a heterogeneous response was recapitulated *in vitro* when HUVEC and human lung microvascular endothelial cells were exposed to LPS. The here identified and described endothelial subpopulations have distinct inflammatory phenotypes and are regulated by different signaling mechanisms. At this point, it is not known whether signaling differences contributing to the heterogeneous expression of E-selectin and VCAM-1 has biological relevance, nor what the pharmacological ramifications are. Such biological relevance should be investigated in *in vivo* settings, as the molecular signatures of endothelial cells differ depending on their specialized functions and microenvironment both in homeostasis and during inflammatory responses (21, 29). Follow up studies will aim to further investigate the underlying molecular pathways in *in vitro* and *in vivo* as a lead for future therapy choices to attenuate activation of microvascular endothelial cells in the organs of critically ill patients with sepsis.

ETHICS STATEMENT

This study was carried out in accordance with the recommendations of the animal ethics committee of the University of Groningen.

AUTHOR CONTRIBUTIONS

JM and GM shared the conceptualization. JM, GM, and ED designed the study. ED, JP, BE, and JM performed the experiments and analyzed the data. MM provided valuable input on the statistical analysis. ED, JM, and GM wrote and edited the manuscript. All authors critically revised the manuscript and approved the submitted version.

FUNDING

This work was supported by the Skim Latihan Akademik Bumiputera (SLAB) and UNIMAS fellowship program (to ED), Ministry of Higher Education, Malaysia, and the research foundation of the Department of Critical Care, UMCG.

ACKNOWLEDGMENTS

We would like to thank Henk Moorlag from the UMCG Endothelial Cell Facility and Wayel Abdulahad, Theo Bijma, Johan Teunis, and Geert Mesander from the UMCG Central Flow Cytometry Unit for providing excellent technical support.

SUPPLEMENTARY MATERIAL

The Supplementary Material for this article can be found online at: https://www.frontiersin.org/articles/10.3389/fimmu.2019.01169/full#supplementary-material

REFERENCES

1. Singer M, Deutschman CS, Seymour C, Shankar-Hari M, Annane D, Bauer M, et al. The third international consensus definitions for sepsis and septic shock (sepsis-3). *JAMA*. (2016) 315:801–10. doi: 10.1001/jama.2016.0287
2. Fleischmann C, Scherag A, Adhikari NKJ, Hartog CS, Tsaganos T, Schlattmann P, et al. Assessment of global incidence and mortality of hospital-treated sepsis current estimates and limitations. *Am J Respir Crit Care Med*. (2016) 193:259–72. doi: 10.1164/rccm.201504-0781OC
3. Dauphinee SM, Karsan A. Lipopolysaccharide signaling in endothelial cells. *Lab Investig*. (2006) 86:9–22. doi: 10.1038/labinvest.3700366
4. Mai J, Virtue A, Shen J, Wang H, Yang XF. An evolving new paradigm: endothelial cells - conditional innate immune cells. *J Hematol Oncol*. (2013) 6:61. doi: 10.1186/1756-8722-6-61
5. Pober JS, Sessa WC. Evolving functions of endothelial cells in inflammation. *Nat Rev Immunol*. (2007) 7:803–15. doi: 10.1038/nri2171
6. van Meurs M, Kurniati NF, Wulfert FM, Asgeirsdottir SA, de Graaf IA, Satchell SC, et al. Shock-induced stress induces loss of microvascular endothelial Tie2 in the kidney which is not associated with reduced glomerular barrier function. *AJP Ren Physiol*. (2009) 297:F272–81. doi: 10.1152/ajprenal.00137.2009
7. Asgeirsdottir SA, van Solingen C, Kurniati NF, Zwiers PJ, Heeringa P, van Meurs M, et al. MicroRNA-126 contributes to renal microvascular heterogeneity of VCAM-1 protein expression in acute inflammation. *AJP Ren Physiol*. (2012) 302:F1630–9. doi: 10.1152/ajprenal.00400.2011
8. Kowalski PS, Zwiers PJ, Morselt HWM, Kuldo JM, Leus NGJ, Ruiters MHJ, et al. Anti-VCAM-1 SAINT-O-Somes enable endothelial-specific delivery of siRNA and downregulation of inflammatory genes in activated endothelium *in vivo*. *J Control Release*. (2014) 176:64–75. doi: 10.1016/j.jconrel.2013.12.029
9. Faure E, Equils O, Sieling P, Thomas L, Zhang F, Kirschning C, et al. Bacterial Lipopolysaccharide activates NF-kappa B through Toll-like receptor 4 (TLR-4) in cultured human dermal endothelial cells. *J Biol Chem*. (2000) 275:11058–63. doi: 10.1074/jbc.275.15.11058
10. Moser J, Heeringa P, Jongman RM, Zwiers PJ, Niemarkt AE, Yan R, et al. Intracellular RIG-I signaling regulates TLR4-independent endothelial inflammatory responses to endotoxin. *J Immunol*. (2016) 196:4681–91. doi: 10.4049/jimmunol.1501819

11. Jersmann HPA, Hii CST, Ferrante JV, Ferrante A. Bacterial lipopolysaccharide and tumor necrosis factor alpha synergistically increase expression of human endothelial adhesion molecules through activation of NF-κB and p38 mitogen-activated protein kinase signaling pathways. *Infect Immun*. (2001) 69:1273–9. doi: 10.1128/IAI.69.3.1273-1279.2001
12. Makó V, Czúcz J, Weiszhár Z, Herczenik E, Matkó J, Prohászka Z, et al. Proinflammatory activation pattern of human umbilical vein endothelial cells induced by IL-1β, TNF-α, and LPS. *Cytometry A*. (2010) 77:962–70. doi: 10.1002/cyto.a.20952
13. Yan W, Zhao K, Jiang Y, Huang Q, Wang J, Kan W, et al. Role of p38 MAPK in ICAM-1 expression of vascular endothelial cells induced by lipopolysaccharide. *Shock*. (2002) 17:433–8. doi: 10.1097/00024382-200205000-00016
14. Jou-Valencia D, Molema G, Popa E, Aslan A, van Dijk F, Mencke R, et al. Renal klotho is reduced in septic patients and pretreatment with recombinant klotho attenuates organ injury in lipopolysaccharide-challenged mice. *Crit Care Med*. (2018) 46:e1196–203. doi: 10.1097/CCM.0000000000003427
15. Yan R, Van Meurs M, Popa ER, Jongman RM, Zwiers PJ, Niemarkt AE, et al. Endothelial interferon regulatory factor 1 regulates lipopolysaccharide-induced VCAM-1 expression independent of NFκB. *J Innate Immun*. (2017) 9:546–50. doi: 10.1159/000477211
16. van Meurs M, Wulfert FM, Knol AJ, De Haes A, Houwertjes M, Aarts LPHJ, et al. Early organ-specific endothelial activation during hemorrhagic shock and resuscitation. *Shock*. (2007) 29:291–9. doi: 10.1097/SHK.0b013e318145a7c1
17. Ankers JM, Awais R, Jones NA, Boyd J, Ryan S, Adamson AD, et al. Dynamic NF-κb and E2F interactions control the priority and timing of inflammatory signalling and cell proliferation. *Elife*. (2016) 5:e10473. doi: 10.7554/eLife.10473
18. Dunzendorfer S, Lee H-K, Soldau K, Tobias PS. Toll-like receptor 4 functions intracellularly in human coronary artery endothelial cells: roles of LBP and sCD14 in mediating LPS-responses. *FASEB J*. (2004) 18:1117–9. doi: 10.1096/fj.03-1263fje
19. Schumann RR, Pfeil D, Lamping N, Kirschning C, Scherzinger G, Schlag P, et al. Lipopolysaccharide induces the rapid tyrosine phosphorylation of the mitogen-activated protein kinases erk-1 and p38 in cultured human vascular endothelial cells requiring the presence of soluble CD14. *Blood*. (1996) 87:2805–14. doi: 10.1115/1.2194911
20. Arditi M, Zhou J, Torres M, Durden DL, Stins M, Kim KS. Lipopolysaccharide stimulates the tyrosine phosphorylation of mitogen-activated protein kinases p44, p42, and p41 in vascular endothelial cells in a soluble CD14-dependent manner. Role of protein tyrosine phosphorylation in lipopolysaccharide-induced stimulation of endothelial cells. *J Immunol*. (1995) 155:3994–4003.
21. Aird WC. Phenotypic heterogeneity of the endothelium: I. structure, function, and mechanisms. *Circ Res*. (2007) 100:158–73. doi: 10.1161/01.RES.0000255691.76142.4a
22. Saubaméa B, Cochois-Guégan V, Cisternino S, Scherrmann JM. Heterogeneity in the rat brain vasculature revealed by quantitative confocal analysis of endothelial barrier antigen and P-glycoprotein expression. *J Cereb Blood Flow Metab*. (2012) 32:81–92. doi: 10.1038/jcbfm.2011.109
23. Fathers KE, Stone CM, Minhas K, Marriott JJA, Greenwood JD, Dumont DJ, et al. Heterogeneity of Tie2 expression in tumor microcirculation: Influence of cancer type, implantation site, and response to therapy. *Am J Pathol*. (2005) 167: 1753–62. doi: 10.1016/S0002-9440(10)61256-4
24. Beck GC, Rafat N, Brinkkoetter P, Hanusch C, Schulte J, Haak M, et al. Heterogeneity in Lipopolysaccharide responsiveness of endothelial cells identified by gene expression profiling: role of transcription factors. *Clin Exp Immunol*. (2006) 143:523–33. doi: 10.1111/j.1365-2249.2006.03005.x
25. Bischoff J, Brasel C, Kräling B, Vranovska K. E-selectin is upregulated in proliferating endothelial cells *in vitro*. *Microcirculation*. (1997) 4:279–87. doi: 10.3109/10739689709146791
26. Kräling BM, Razon MJ, Boon LM, Zurakowski D, Seachord C, Darveau RP, et al. E-selectin is present in proliferating endothelial cells in human hemangiomas. *Am J Pathol*. (1996) 148:1181–91.
27. Ruland J. Return to homeostasis: downregulation of NF-κB responses. *Nat Immunol*. (2011) 12:709–14. doi: 10.1038/ni.2055
28. Watson C, Whittaker S, Smith N, Vora AJ, Dumonde DC, Brown KA. IL-6 acts on endothelial cells to preferentially increase their adherence for lymphocytes. *Clin Exp Immunol*. (1996) 105:112–9. doi: 10.1046/j.1365-2249.1996.d01-717.x
29. Molema G. Heterogeneity in endothelial responsiveness to cytokines, molecular causes, and pharmacological consequences. *Semin Thromb Hemost*. (2010) 36:246–64. doi: 10.1055/s-0030-1253448

Conflict of Interest Statement: The authors declare that the research was conducted in the absence of any commercial or financial relationships that could be construed as a potential conflict of interest.

Copyright © 2019 Dayang, Plantinga, ter Ellen, van Meurs, Molema and Moser. This is an open-access article distributed under the terms of the Creative Commons Attribution License (CC BY). The use, distribution or reproduction in other forums is permitted, provided the original author(s) and the copyright owner(s) are credited and that the original publication in this journal is cited, in accordance with accepted academic practice. No use, distribution or reproduction is permitted which does not comply with these terms.

frontiers in Immunology

ORIGINAL RESEARCH
published: 26 June 2019
doi: 10.3389/fimmu.2019.01427

The Fluctuations of Leukocytes and Circulating Cytokines in Septic Humanized Mice Vary With Outcome

*Tomasz Skirecki[1], Susanne Drechsler[2], Grazyna Hoser[1], Mohammad Jafarmadar[2], Katarzyna Siennicka[3], Zygmunt Pojda[3], Jerzy Kawiak[1] and Marcin F. Osuchowski[2]**

[1] Laboratory of Flow Cytometry, Centre of Postgraduate Medical Education, Warsaw, Poland, [2] Ludwig Boltzmann Institute for Experimental and Clinical Traumatology in the AUVA Research Center, Vienna, Austria, [3] Department of Regenerative Medicine, Maria Sklodowska-Curie Institute-Oncology Center, Warsaw, Poland

Sepsis remains a major challenge in translational research given its heterogeneous pathophysiology and the lack of specific therapeutics. The use of humanized mouse chimeras with transplanted human hematopoietic cells may improve the clinical relevance of pre-clinical studies. However, knowledge of the human immuno-inflammatory response during sepsis in humanized mice is scarce; it is unclear how similar or divergent mouse and human-origin immuno-inflammatory responses in sepsis are. In this study, we evaluated the early outcome-dependent immuno-inflammatory response in humanized mice generated in the NSG strain after cecal ligation and puncture (CLP) sepsis. Mice were observed for 32 h post-CLP and were assigned to either predicted-to-die (P-DIE) or predicted-to-survive (P-SUR) groups for retrospective comparisons. Blood samples were collected at baseline, 6 and 24 h, whereas the bone marrow and spleen were collected between 24 and 32 h post-CLP. In comparison to P-SUR, P-DIE humanized mice had a 3-fold higher frequency of human splenic monocytes and their CD80 expression was reduced by 1.3-fold; there was no difference in the HLA-DR expression. Similarly, the expression of CD80 on the bone marrow monocytes from P-DIE mice was decreased by 32% ($p < 0.05$). Sepsis induced a generalized up-regulation of both human and murine plasma cytokines (TNFα, IL-6, IL-10, IL-8/KC, MCP-1); it was additionally aggravated in P-DIE vs. P-SUR. Human cytokines were strongly overridden by the murine ones (approx. ratio 1:9) but human TNFα was 7-fold higher than mouse TNFα. Interestingly, transplantation of human cells did not influence murine cytokine response in NSG mice, but humanized NSG mice were more susceptible to sepsis in comparison with NSG mice (79 vs. 33% mortality; $p < 0.05$). In conclusion, our results show that humanized mice reflect selected aspects of human immune responses in sepsis and therefore may be a feasible alternative in preclinical immunotherapy modeling.

Keywords: sepsis, humanized mouse, cecal ligation and puncture (CLP), peritonitis, outcome prediction, immunity

OPEN ACCESS

Edited by:
Christoph Thiemermann, Queen Mary University of London, United Kingdom

Reviewed by:
Craig Coopersmith, Emory University, United States
Regina Sordi, Federal University of Santa Catarina, Brazil

***Correspondence:**
Marcin F. Osuchowski
marcin.osuchowski@trauma.lbg.ac.at

Specialty section:
This article was submitted to Inflammation, a section of the journal Frontiers in Immunology

Received: *08 March 2019*
Accepted: *06 June 2019*
Published: *26 June 2019*

Citation:
Skirecki T, Drechsler S, Hoser G, Jafarmadar M, Siennicka K, Pojda Z, Kawiak J and Osuchowski MF (2019) The Fluctuations of Leukocytes and Circulating Cytokines in Septic Humanized Mice Vary With Outcome. Front. Immunol. 10:1427. doi: 10.3389/fimmu.2019.01427

INTRODUCTION

In more than 30 years of intensive research no new specific therapeutics for sepsis have been introduced into clinical care (1). Despite improved standards of care, the mortality rates of sepsis have not decreased (2). On the contrary, prevalence has been on the rise, reaching approximately 19 million sepsis cases per year worldwide (3), making sepsis a global medical burden (4).

The failure of anti-sepsis therapeutics to modulate the host response has been attributed to a large part to flawed pre-clinical studies (5–7). Currently, a vast majority of sepsis animal studies are performed in mice (8); one of the major translational obstacles in murine models of sepsis are substantial mouse-human differences in the immune system (9). The development of humanized mice is emerging as a promising platform for at least partially overcoming those disparities. Humanized mice are generated by xenotransplantation of human hematopoietic stem cells (HSCs) into immunocompromised mice which were additionally irradiated or chemoablated to empty their bone marrow niches for the xenograft (10). Currently, one of the most commonly used mouse strains for humanization is the NSG (NOD scid gamma) strain (11); NSG mice have composite immunodeficiency given that they lack not only lymphocytes, NK cells, and macrophages but also have an impaired complement system, enabling an efficient engraftment of the human cells with a relatively low risk of developing graft-vs.-host disease.

Humanized mice have already been used to model acute infectious diseases and have proven useful in both recapitulating some unique human responses as well as suggesting therapeutic solutions (12–14). On a limited scale, humanized mice were also employed in sepsis research using the cecal ligation and puncture (CLP), the gold standard model to recapitulate septic peritonitis (15–18). CLP-induced immuno-inflammatory responses vary according to the underlying pathophysiology, i.e., in a non-marginal severity CLP protocol (i.e., neither 100% mortality/survival), mice subjected to the same insult develop an individual response and progress to either survival or death without following a predefined immune "outcome pattern" from the onset of CLP (19). Outcomes in CLP mice can be predicted (e.g., mice predicted-to-survive/die) using body temperature and/or biomarker measurements as well as clinical assessment scores (19–22). Comparisons of such dynamic signaling changes between the surviving and dying phenotypes advance our understanding of mechanisms co-responsible for sepsis lethality (and recovery) better than simplistic (but uniformly statistically significant) comparisons of healthy to septic subjects (21–23). Humanized mice are an attractive platform for the investigation of human immuno-inflammatory responses (and treatments targeting these systems) in critical care diseases including sepsis. It is therefore crucial to characterize the cellular and cytokine responses, given that the complexity of the humanized sepsis mouse model is likely exacerbated by various inter-species interactions (11). The concomitant presence of cells and mediators of both human and murine origin results in multi-directional crosstalk which likely alters the immune-inflammatory dynamics of the host in severe infections. It is largely unclear what action the transplanted human immune cells exert upon the mouse host's response to septic insult and how impactful this interaction can be. Such a knowledge gap hinders the utility of humanized mice in modeling of sepsis as well as the translation of findings generated in such models.

To partially address the above unknowns, we subjected humanized NSG mice to polymicrobial abdominal sepsis and investigated two specific questions: (a) comparison of the initial cellular and humoral inflammatory response of human and murine origin and (b) characterization of those responses depending on outcome (i.e., dying vs. surviving) in the early phase of sepsis.

METHODS

Mice

Mice of the NSG strain (NOD.Cg-Prkdcscid Il2rgtm1Wjl/SzJ) and SCID strain were obtained from The Jackson Laboratories (Bar Harbour, ME, USA). Mice were bred in the animal facility of the Center of Postgraduate Medical Education (Warsaw, Poland) under pathogen-free conditions with 12/12 light cycle and fed with standard sterile diet and drinking water ad libitum. All experiments on animals were approved by the Local Ethics Committee no IV in Warsaw, Poland (92/2012) and adhered to the ARRIVE guidelines (24).

Generation of Humanized Mice

Human Stem Cell Harvesting

To generate humanized mice, we followed the previously published protocol from our lab (17). In brief, human umbilical cord blood (UCB) probes were processed in accordance with the procedures approved by the Institutional Review Board of the Maria Sklodowska-Curie Memorial Cancer Center and Institute of Oncology (Warsaw, Poland). The UCB units from healthy donor mothers were obtained with their informed consent. Then, human HSCs were isolated from Ficoll-centrifuged mononuclear cell fraction of human UCB and stored in liquid nitrogen after isolation. CD34-positive human stem and progenitor cells were purified from thawed mononuclear cells by positive immunomagnetic separation technique using a commercially available kit (EasySep, Stemcell Technologies, Vancouver, BC, Canada). Purity of isolated cells (>90%) was tested by flow cytometry using anti-CD34 PE/anti-CD45 FITC antibodies (BD Bioscience, San Jose, CA, USA).

Transplantation

Three- to four-week-old NSG female mice were pretreated with i.p. injections of busulfan (25 mg/kg) (Sigma-Aldrich) for 2 consecutive days before stem cell transplantation. Female mice were chosen as they are known to present a higher engraftment rate (25). Twenty-four hours after the last busulfan dose, mice were given a tail vein injection of 10^5 purified human UCB CD34+ cells. Seven weeks after transplantation, 20 μl of blood was obtained via facial vein puncture (23G needle). For the flow cytometry evaluation of human chimerism, the blood samples were stained with anti-human CD45 FITC (BD) antibody. A total of 33 mice were deemed as humanized (blood chimerism over 5%) and were enrolled in the CLP study.

CLP Sepsis Model

Surgery and Treatment

In order to reproduce human peritonitis-derived sepsis, we performed the CLP surgery in 33 humanized mice according to the original protocol from Wichterman et al. (26) with modifications (22, 27). In brief, all mice received analgesia (i.e., buprenorphine, 0.05 mg/kg in 1 ml of 0.9% saline) 20 min

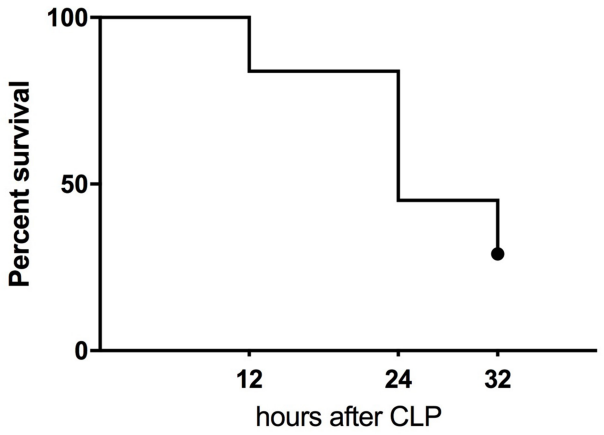

FIGURE 1 | Kaplan-Meier survival curve of humanized NSG mice subjected to CLP. The combined mortality of CLP induced by double puncture with 25G needle ($n = 19$) and 27G ($n = 14$).

prior to CLP and the abdomen was shaved and disinfected with alcohol. After midline laparotomy, the cecum was exposed, ligated underneath the ileocecal valve, and a needle puncture (through-and-through) was applied. After repositioning of the cecum, the abdomen was closed with single button sutures and Histoacryl® tissue adhesive (B. Braun, Aesculap, Germany).

Two CLP runs were performed in humanized mice: (a) with a 25G needle ($n = 19$) and (b) with a 27G needle ($n = 14$). A single CLP run with a 25G needle was performed in NSG ($n = 10$) and SCID ($n = 10$) mice. Humanized mice from both runs were combined for data shown in **Figures 1–5** (i.e., outcome-based comparisons). Two mice that died within 6 h of CLP were excluded as death was deemed to be due to the fact that they did not recover from the anesthesia/surgical intervention itself (and not sepsis). For the comparison of NSG to SCID in **Figure 6** (i.e., comparison of sensitivity to an identical insult), humanized mice from the first run (25G needle) only were used. Based on our previous CLP protocols (21, 28), we used two needle sizes in order to introduce more longitudinal outcome variability into the study. In the current study, both sizes produced similar overall outcomes at 32 h (**Supplementary Figure 1**). The more divergent variability is advantageous given that our study focused on the outcome-based differences (i.e., surviving vs. moribund phenotype) and not a CLP phenotype produced by a specific needle size. A similar (2-needle) approach was recently used by Kim et al. (29) in testing a hydrocortisone/ascorbic acid/thiamine treatment in mouse CLP.

From 2 h post-CLP on, all mice received subcutaneous broad spectrum antibiotic therapy (25 mg/kg imipenem, Zienam®; MSD, Lucerne, Switzerland) and fluid resuscitation (1 ml Ringer's solution) with analgesia (0.05 mg/kg buprenorphine, Bupaq®; Richter Pharma, Austria) twice daily (approximately every 12 h) for 5 consecutive days post-CLP.

Monitoring and Prediction of Outcome

All CLP mice were not maintained in a large animal facility but were kept in a small animal room to enable close observation for implementation of the humane endpoints and to allow allocation of individual mice into either predicted-to-die (P-DIE) or predicted-to-survive (P-SUR) group. All mice were monitored for clinical signs of illness and their status was evaluated using a modified mouse clinical assessment scoring system [M-CASS; e.g., fur, posture, mobility, alertness, startle, and righting reflex (22)] starting 12 h post-CLP. Also, rectal temperature was monitored (Fluke Series II thermometer, Fluke USA) at least twice daily (or more often whenever a mouse deteriorated). Mice were deemed moribund and assigned as P-DIE whenever the righting reflex was absent or/and M-CASS score $\geq$8 and immediately euthanized. Following the previously used protocol (21, 30), two P-SUR mice were randomly selected and euthanized at 24 h to serve as a time-matched comparison for moribund mice sacrificed as P-DIE at 24 h post-CLP. Body temperature recordings served as a supportive measure in the general health assessment and euthanasia decision-making scheme (and the P-DIE vs. P-SUR allocation) given that the body temperature fluctuations were not previously validated to serve as a predictor of outcome in any humanized mice disease model. Two mice (out of 33) died of post-surgical complications within 5 h of CLP and were excluded from data analysis.

Flow Cytometry

Flow cytometry was used for phenotyping of engrafted human cells. Probes of blood or re-suspended cells retrieved from solid organs were incubated with inactivated mouse serum to block unspecific Fc receptors. Then, mixtures of monoclonal antibodies against human antigens were added and cells were incubated for 30 min at room temperature. The following antibodies were used: anti-CD45 AmCyan, anti-CD14 PE, anti-CD3 Pacific Blue, anti-CD4 APC, anti-CD8 PE, anti-CD33 PeCy5.5, anti-HLA-DR PE.CY7, (BD Bioscience), anti-CD80 Alexa Fluor 488 (Biolegend, San Diego, USA). After staining, erythrocytes were lysed with BD Pharm Lyse solution (BD Biosciences) for 10 min, washed with PBS with 2% Newborn Calf Serum (NCS), and re-suspended in 0.5% paraformaldehyde in PBS. Cells were acquired using the FACS Canto II flow cytometer and Diva software (BD Bioscience, San Jose, CA). Analysis of immunophenotype was carried out applying the FlowJo 10 software (TreeStar, Inc., now part of FlowJo LLC, Ashland, OR, USA). The applied anti-human antibodies were verified for cross-reactivity with cells of non-transplanted mice and no staining was present.

Cytokine Measurements

Facial vein blood samples were obtained at baseline, 6 and 24 h after CLP as described (31). Samples were stored at −86°C until analysis. Plasma concentration of human and murine cytokines (IL-6, IL-8/KC, IL-10, TNF, MCP-1) was measured using Luminex Multiplex Immunoassay (Invitrogen, Thermo Fisher Scientific, Vienna, Austria) according to the manufacturer's protocol. The cross-reactivity rates provided by the supplier (expressed as % recovery of either human or mouse protein) for mouse targets are as follows: IL-6: 0.1%; TNFα: 0.0%; MCP-1: 0.5%; IL-10: 0.2% Gro alpha KC: 0.1%. For human targets: IL-10: 0.0%; IL-6: 0.0%; IL-8: n.a.; Gro alpha: 0.0%; MCP-1: not checked; TNFα: 0.0%. Two P-SUR mice were also sacrificed

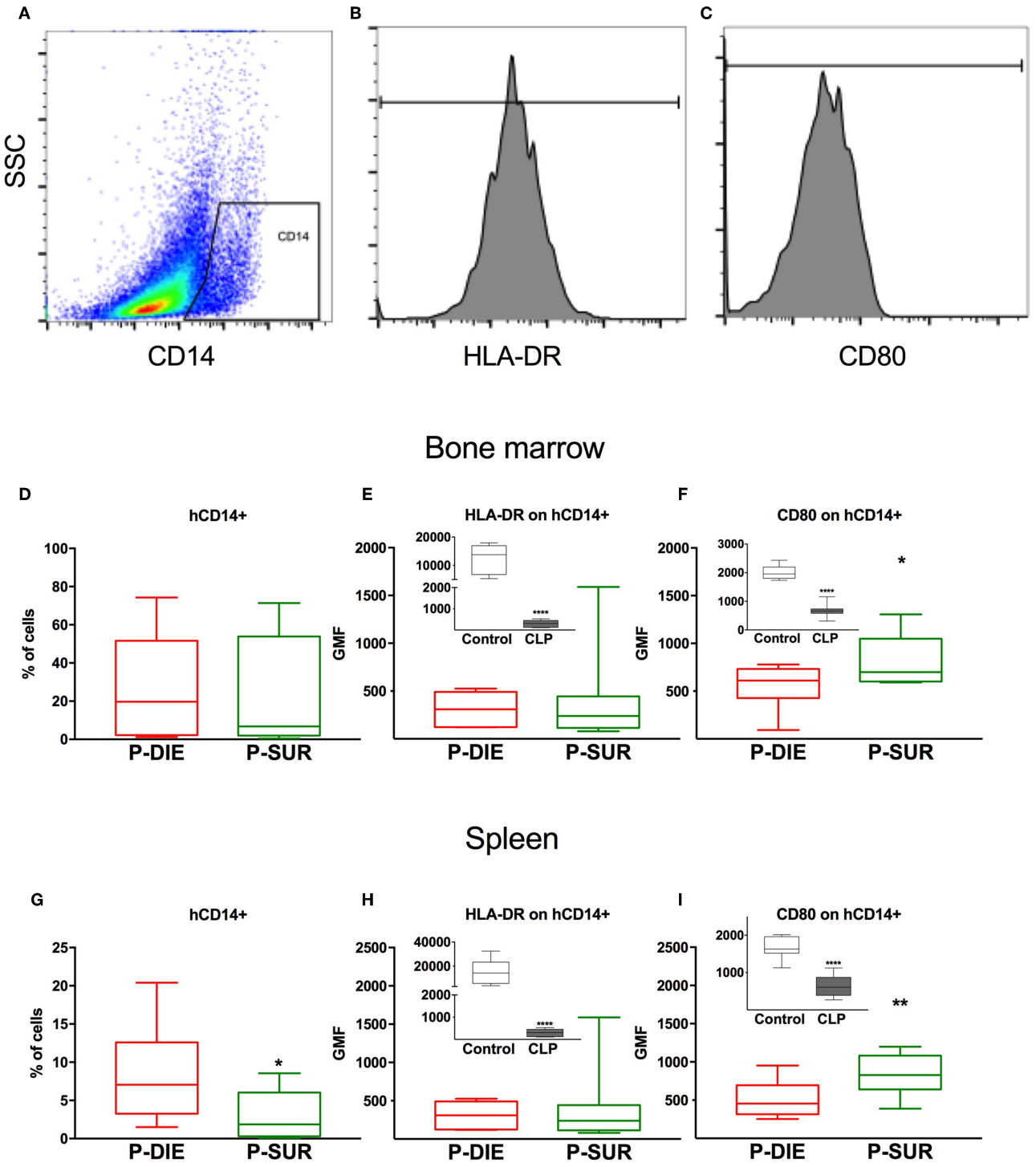

FIGURE 2 | Human monocyte response regarding sepsis outcome. **(A)** Representative cytograms and histograms of the flow cytometry analysis of human CD14+ monocytes in the spleen and their **(B)** HLA-DR and **(C)** CD80 expression. Results of the analysis of bone marrow cells: **(D)** Frequency of human CD14+ monocytes. **(E)** Geometric mean fluorescence (GMF) of anti-HLA-DR staining of human monocytes. **(F)** GMF of anti-CD80 staining of human monocytes. Analysis of splenic cells: **(G)** Frequency of human monocytes. **(H)** GMF of anti-HLA-DR staining and **(I)** GMF of anti-CD80 staining of human monocytes. Insets present a comparison of healthy ($n = 7$) vs. all septic mice ($n = 20$; irrespective of outcome). Groups were compared using t-test. $^{*}p < 0.05$; $^{**}p < 0.01$; $^{****}p < 0.0001$.

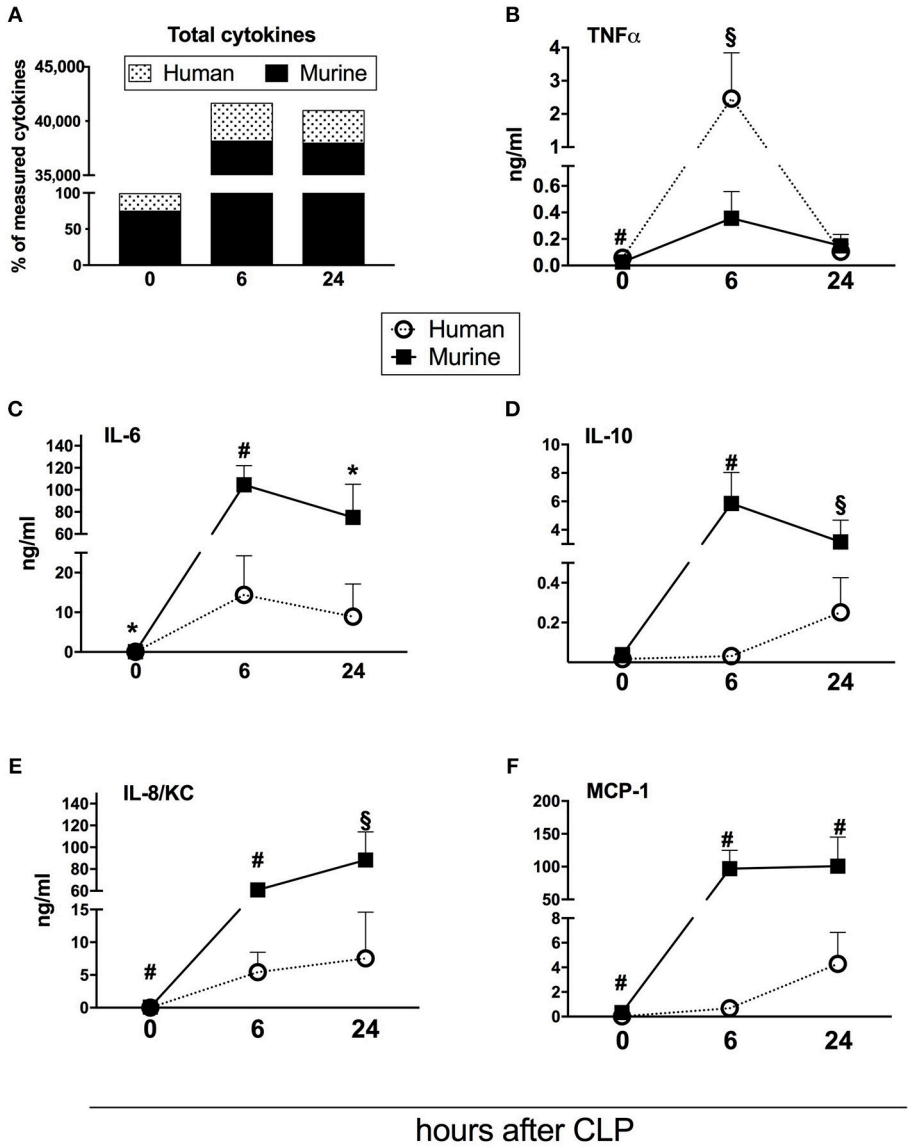

FIGURE 3 | Dynamics of human and murine cytokine responses after CLP regardless of outcome. Graphs present concentration of cytokines from 31 humanized NSG mice subjected to CLP. Dynamics of: **(A)** combined murine and human cytokines (the sum of both measured at baseline counted as 100%); **(B)** TNF; **(C)** IL-6; **(D)** IL-10; **(E)** IL-8/KC; **(F)** MCP-1. BL, baseline. Concentration of human and murine cytokines were compared using Mann-Whitney test at each time-point separately (T0,T6h n = 31, T24 n = 19). *$p < 0.05$; §$p < 0.01$; #$p < 0.001$.

at 24 h to serve as comparisons to P-DIE that were sacrificed at the same time-point. Additionally, in **Figures 2**, **6**, the individual cytokine values measured at 24 and 32 h post-CLP were merged (for P-DIE and P-SUR, respectively) and presented as the 24 h time-point only. This was justified by an overlapping cytokine expression (in all cytokines) between those two time-points (i.e., $p > 0.1$ for 24 vs. 32 h difference; data not shown).

Statistical Analysis

Normality of all data sets was assessed using the Shapiro-Wilk test and log-transformed to eliminate skewness and/or non-parametric distribution whenever present. Data are expressed as means and 95% confidence intervals (CI) if not otherwise stated. Comparisons between P-DIE and P-SUR group were performed by *t*-test (with Welch correction for unequal variances if needed) given that the P-DIE group did not meet assumptions (non-random deaths) for repeated measures testing. The correlation strength between the variables was assessed using the Pearson's rank correlation coefficient. Receiver operator curves (ROC) were calculated for the evaluation of predictive utility of selected variables. Cut-off values were chosen using the Youden's index. The areas under the curves (AUC) with CIs were calculated for assessment of the accuracy of the test. Sensitivity and specificity were calculated for the selected cut-off values of the variables.

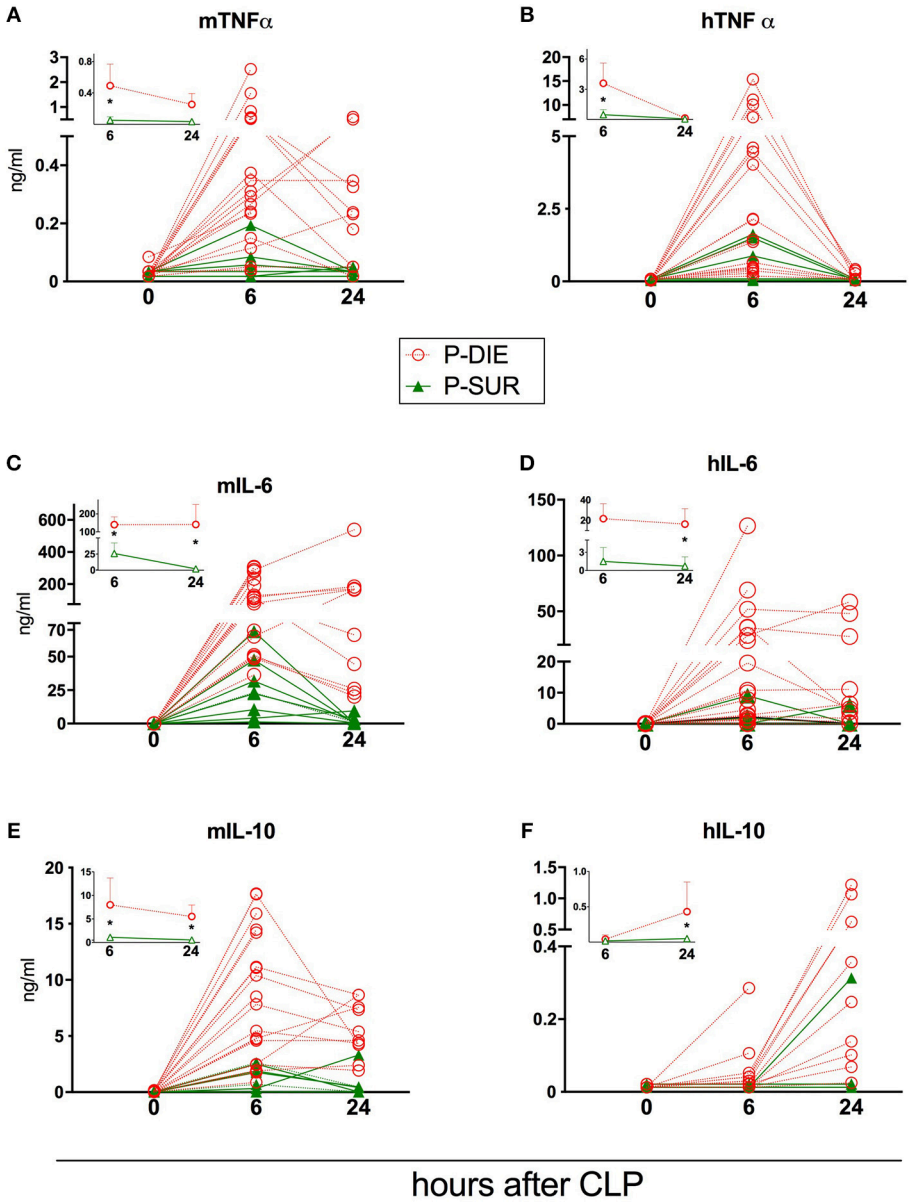

FIGURE 4 | Comparison of human and murine cytokines depending on the post-CLP outcome in humanized mice. **(A)** murine TNF; **(B)** human TNF; **(C)** murine IL-6; **(D)** human IL-6; **(E)** murine IL-10; **(F)** human IL-10. (P-Die $n = 23$, P-Sur $n = 8$). Insets present a comparison of P-DIE ($n = 22$) vs. P-SUR mice ($n = 9$). Data are presented as mean values and 95% confidence interval bars. Concentrations of cytokines of P-SUR and P-DIE mice were compared by the *t*-test at each time-point separately. *$p < 0.05$.

The Kaplan-Meier survival curves were compared using the log-rank test. $p < 0.05$ was considered significant. Statistica 12 (StatSoft, Inc., USA) and GraphPad Prism 5 (GraphPad, Inc., USA) softwares were used for evaluating the statistical significance and/or graphical depiction of the data.

RESULTS

Development of Humanized Mice

Humanized NSG mice were generated based on our previously used protocol (17). The busulfan myeloablation regimen was proven to be efficient and safe without any clinical pathology in the recipient mice. Development of human granulocytes, monocytes, and B and T cells was confirmed to be similar to our previously reported readouts in the spleen, bone marrow, and peripheral blood (17) (**Supplementary Table 1**).

Among circulating human CD45+ cells, CD20+ B cells, and CD33+ myeloid cells were the most frequent. Analysis of the thymus revealed the development of human CD3+ cells in the mouse host (data not shown). Chimerism of human CD45+ (hCD45+) cells in the peripheral blood was confirmed in all transplanted mice 1 week before the CLP

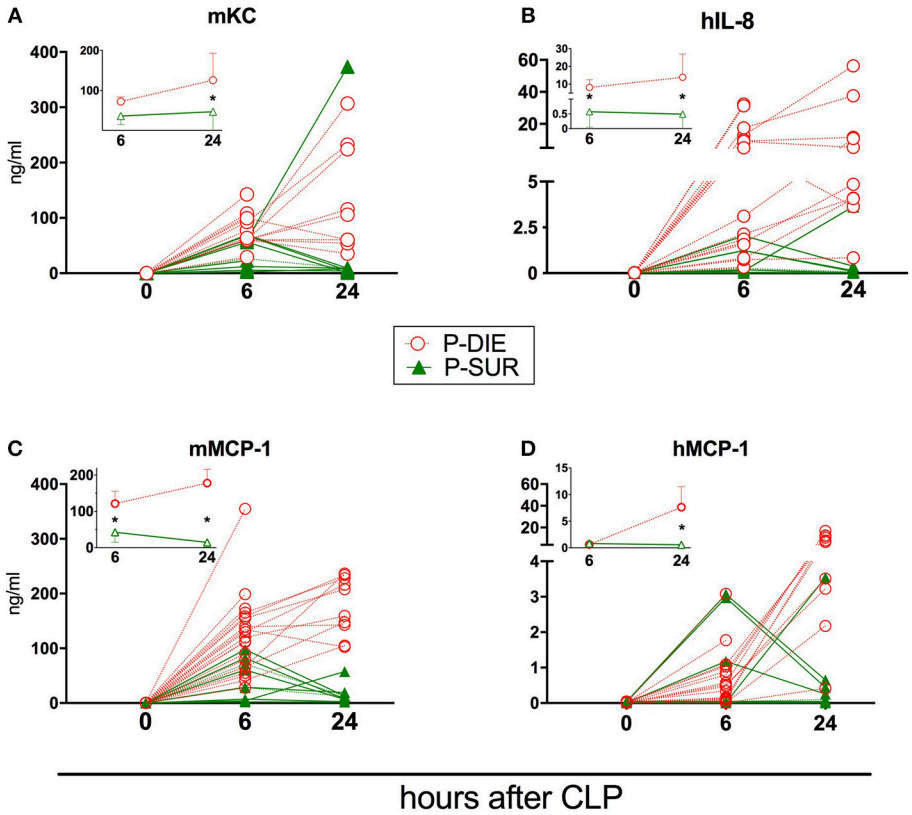

FIGURE 5 | Comparison of human and murine chemokines depending on the post-CLP outcome in humanized mice. Insets present data as mean values and 95% confidence interval bars. **(A)** murine KC; **(B)** human IL-8; **(C)** murine MCP-1; **(D)** human MCP-1. (P-DIE $n = 22$, P-SUR $n = 9$). Concentrations of chemokines between P-SUR and P-DIE mice were compared by the *t*-test at each time-point separately. $^*p < 0.05$.

experiments [mean 19.6% 95CI (11.3–27.1)]. Furthermore, all humanized mice enrolled in the study had >18% of hCD45+ cells in the bone marrow (retrospective post-CLP verification; **Supplementary Table 2**).

Humanized Septic Mice: Prediction of Outcome

CLP surgery in humanized mice resulted in 55% mortality at 24 h and 71% at 32 h (the experiment termination time-point) (**Figure 1**). At the 32 h time-point, all remaining mice were assigned either to the predicted-to-die (P-DIE; $n = 22$) or predicted-to-survive (P-SUR; $n = 9$) group based on the clinical assessment and body temperature readouts (see Methods) for further retrospective comparisons of the measured parameters.

We also performed a retrospective ROC analysis using body temperature recordings only (taken at 6 h post-CLP) to assess whether a prediction of (short term) outcome is possible in humanized septic mice. This analysis combined all CLP mice and the outcome was based on our clinical P-DIE/P-SUR allocation. The area under the curve reached 0.99 (95CI: 0.98–1.00) with the cut-off set at 33.2°C (i.e., 100% sensitivity, 95% specificity for the next 32 h). Of note, all P-SUR mice (i.e., allocated at 32 h post-CLP) had body temperature of at least 33.2°C or higher (**Supplementary Figure 2**).

Humanized Septic Mice: Outcome-Based Characterization of Human Monocytes From the Bone Marrow and Spleen

To investigate the cellular response of humanized mice to abdominal sepsis, we analyzed CLP-induced leukocyte changes in two compartments: (a) the bone marrow and (b) spleen. Leukocytes from P-DIE mice were harvested between 24 and 32 h after CLP ($n = 11$) in order to also harvest cells from mice that became moribund prior to the end of the study. Leukocytes from remaining P-SUR mice were collected at the termination of the experiment (i.e., 32 h post-CLP; $n = 9$).

There was a similar percentage frequency of hCD45+ leukocytes in both compartments: 34% P-DIE vs. 45% P-SUR in the bone marrow and 18 vs. 26% in the spleen (**Table 1**). In the bone marrow, hCD14+ monocytes (**Figures 2A,D**) were similar regardless of outcome. In contrast, the splenic hCD14+ monocytes were 3-fold higher in P-DIE compared to P-SUR mice (**Figure 2G**).

We also evaluated the geometric median fluorescence (GMF) of anti-HLA-DR and anti-hCD80 antibodies on human

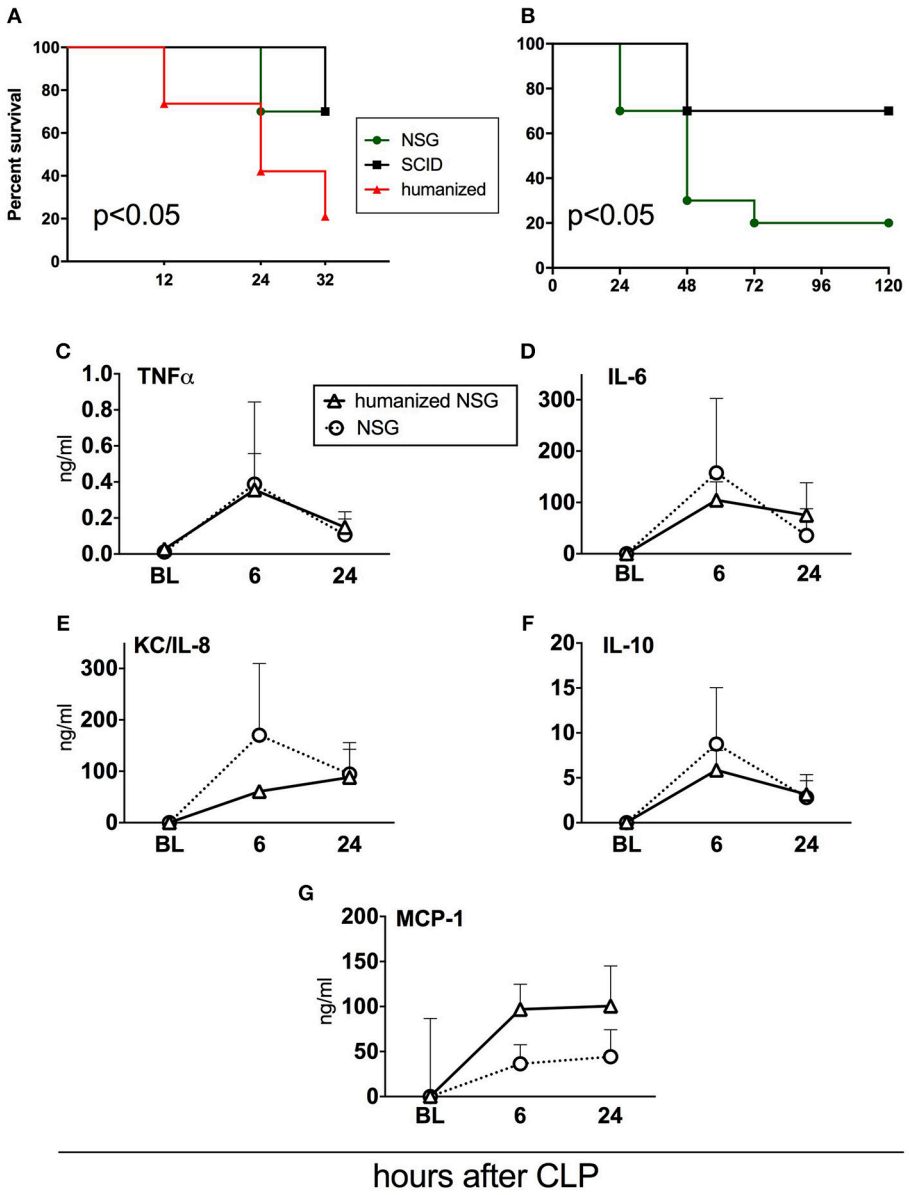

FIGURE 6 | Survival and cytokine responses in humanized NSG vs. naïve NSG and SCID mice. All mice were subjected to CLP with 25G needle size. **(A)** Acute survival curves of hNSG ($n = 19$), naïve NSG ($n = 10$), and SCID ($n = 10$). Humanized NSG mice were terminated at 32 h post-CLP for tissue collection and analysis. Survival curves were compared by Log-rank test, $p < 0.05$ for hNSG vs. NSG and vs SCID. **(B)** Long-term survival curve of NSG and SCID mice from the same experiment. (NSG $n = 10$, SCID $n = 10$, hNSG $n = 19$). Survival curves were compared by Log-rank test, $p < 0.05$. Murine cytokine responses in NSG ($n = 10$) and hNSG ($n = 19$) G: **(C)** TNF; **(D)** IL-6; **(E)** KC/IL-8; **(F)** IL-10; **(G)** MCP-1. Murine cytokine levels in humanized vs. NSG mice were compared by the paired *t*-test at each time-point separately.

monocytes (**Figures 2B,C**). The HLA-DR GMF on the bone marrow monocytes was similar, irrespective of outcome (**Figure 2E**). In contrast, the GMF of CD80 was decreased by 32% on the human monocytes from P-DIE (vs. P-SUR) mice (**Figure 2F**).

The intensity of anti-HLA-DR staining of the splenic monocytes did not differ between the groups (**Figure 2H**), however, the GMF of anti-hCD80 was 1.3-fold higher in the P-SUR compared to P-DIE mice (**Figure 2I**). Of note, the frequency of the hCD3+ T cells appeared to be (4-fold) higher in the spleen of P-SUR than P-DIE mice but this difference was not statistically significant (high individual variability).

Pearson's rank correlation coefficient revealed a moderate, but significant correlation between the frequency of hCD3+

TABLE 1 | Human immune cells in the humanized mice based on the CLP outcome.

Cell type	P-SUR ($n = 9$)	P-DIE ($n = 11$)	p
BONE MARROW			
hCD45+ [%]	45.14 (27.39–62.88)	34.82 (20.26–49.38)	>0.05
hCD14+ [%]	21.16 (−4.16–46.47)	27.30 (9.29–45.31)	>0.05
hCD14+HLA-DR [GMF]	406 (−12.00–824.30)	321.60 (213.40–429.90)	>0.05
hCD14+CD80 [GMF]	797.00 (566.90–1027.00)	546.40 (394.70–698.20)	**<0.05**
SPLEEN			
hCD45+ [%]	26.23 (6.05–46.41)	17.57 (7.95–27.19)	>0.05
hCD14+ [%]	2.91 (−0.06–5.87)	8.48 (4.27–12.69)	**<0.05**
hCD14+HLA-DR [GMF]	406.20 (−12.00–824.30)	321.60 (213.40–429.90)	>0.05
hCD14+CD80 [GMF]	835.40 (612.90–1058.00)	492.60 (337.60–647.70)	**<0.01**

Statistically significant values are bolded.

TABLE 2 | Prognostic accuracy of human and murine cytokines 6 h post-CLP for 24 h death prediction.

Cytokine	AUC (95CI) for murine	AUC (95 CI) for human
TNF	0.93 (0.85–1.00)	0.84 (0.68–1.00)
IL-6	0.97 (0.90–1.00)	0.85 (0.70–1.00)
IL-10	0.92 (0.81–1.00)	0.72 (0.54–0.90)
IL-8/KC	0.80 (0.60–1.00)	0.93 (0.83–1.00)
MCP-1	0.85 (0.70–0.99)	0.61 (0.34–0.88)

AUC, area under the curve; CI, confidence interval.

T cells in the spleen and the hCD80 GMF on hCD14+ monocytes ($r = 0.62$, $p < 0.01$).

Humanized Septic Mice: Comparison of the Human vs. Murine Circulating Cytokines

Repetitive small-volume blood sampling enabled us to sequentially evaluate the concentration of cytokines in septic mice without sacrificing them. First, we compared the combined kinetics of all measured circulating cytokines and chemokines of murine and human origin. Irrespective of outcome, the analyzed mediators typically peaked at 6 h and decreased at 24 h post-CLP (**Figure 3**).

Next, we assessed the total content of circulating cytokines of human and murine origin. The combined human mediators reached 24% of all measured cytokines in healthy mice, 8% at 6 h and 7% at 24 h post-CLP in septic mice (**Figure 3A**). Accordingly, the post-CLP concentration of individual human mediators was, in most cases, an order of magnitude lower than of their murine counterparts. Interestingly, human TNFα was the only cytokine whose early post-CLP peak (i.e., 6 h) was higher (by 7-fold) than the murine TNFα (**Figure 3B**).

While the post-CLP response dynamics of human and murine TNFα, IL-6, and IL-8/KC were similar (**Figures 3B,C,E**), circulating human IL-10 and MCP-1 showed a delayed increase in comparison to the murine mediators (**Figures 3D,F**).

There was a significant negative correlation between expression of CD80 on splenic human monocytes and the concentration of human systemic pro-inflammatory cytokines, while no correlation with IL-10 was observed 6 h after CLP (**Supplementary Figure 3**).

Humanized Septic Mice: Comparison of Humanized and Murine Circulating Cytokines Based on Outcome

Regardless of the origin species, the concentration of all circulating cytokines (except murine KC, human IL-10, and MCP-1) was typically higher in P-DIE compared to P-SUR mice at 6 h post-CLP (**Figures 4**, **5**). At 24 h, this outcome difference remained (or appeared) in IL-6, IL-8, IL-10, and MCP-1 (both origins) and disappeared in TNFα (both origins) and KC (i.e., mouse only).

Furthermore, the different species-dependent IL-10 and MCP-1 dynamic (observed in **Figures 3D,F**) was predominantly due to the changes in the P-DIE mice (IL-10: **Figures 4E,F**; MCP-1: **Figures 5C,D**); the release of human mediators was delayed to 24 h post-CLP compared to the immediate rise of the mouse cytokines at 6 h.

We also performed the ROC analysis to assess the prognostic outcome accuracy of the mediators measured at 6 h post-CLP. For murine cytokines, TNFα and IL-6 had the highest AUC of 0.93 and 0.97 (**Table 2**). Of note, AUC for human IL-8 reached 0.93, indicating a strong discriminative value for this human chemokine.

Humanized vs. Immunodeficient Mice: Outcome

To verify how human immune cells transplanted to immunocompromised NSG mice influence sepsis phenotype, we simultaneously performed CLP in naïve NSG and SCID mice (**Figure 6**). We also included SCID mice as this strain is less immunodeficient than NSG; its adaptive (but not innate) immunity is impaired (32). Using the same CLP protocol, we observed that the mortality of both non-humanized strains was lower by 46% compared to the humanized NSG mice (33 vs. 79%;

$p < 0.05$) at 32 h after CLP (**Figure 6A**). Given that we did not collect tissues from the non-humanized mice, NSG and SCID animals were followed up until day 5. Compared to SCID, NSG mice were more vulnerable to the identical CLP insult (30 vs. 80% mortality; $p < 0.05$; **Figure 6B**).

Humanized vs. Immunodeficient Mice: Circulating Cytokines

To further evaluate the impact of the human cells on murine humoral inflammatory response itself, we compared the concentrations of circulating murine cytokines after an identical CLP insult in the naïve and humanized NSG mice. The pattern of the post-CLP cytokine release was generally similar regardless of the xenotransplantation of the human immune cells (**Figures 6C–G**). The trend for an enhanced MCP-1 release (**Figure 6G**) after humanization did not reach statistical significance.

DISCUSSION

The development of humanized mice provides a unique opportunity to study responses of human immunocompetent cells residing in different tissues in a controlled setting in sepsis, however, such a model requires an extensive characterization of human and murine immuno-inflammatory components. In our study, we used clinically-relevant CLP sepsis (26) followed by antibiotic-, fluid-, and analgesic treatment to recapitulate septic patient care. The findings show for the first time that both human and murine cytokine responses have similar dynamics with regard to acute (early) post-CLP outcome. Moreover, we demonstrated that an early release of human TNFα exceeded by 10-fold the release of its murine counterpart. We also observed that the cytokine response correlated with human monocyte changes, suggesting dynamic interactions in the human immune compartment. Importantly, we revealed that the applied protocol of human HSC transplantation did not impair the ability of murine cells to mount an inflammatory response to sepsis.

We chose to focus on the response of human monocytes in the spleen and bone marrow as these are sites of robust immune processes during infection. The high frequency of monocytes among human cells in the bone marrow likely resulted from selective mobilization of other cell types to the circulation. The number of human monocytes in the spleen of P-SUR was diminished compared to P-DIE mice. CLP sepsis evokes apoptosis of human cells in the humanized mice similar to the phenomenon observed in septic patients (15, 16). Different responses of monocytes at these two sites can be attributed to the local tissue microenvironment and local production of monocytes in the bone marrow (33). We observed a significant drop of HLA-DR and CD80 expression on monocytes from humanized mice post-CLP but no difference in HLA-DR expression was apparent between P-DIE and P-SUR mice. The lack of difference in HLA-DR expression between groups of opposing outcome was surprising; HLA-DR decrease was shown to be a marker of immunosuppression and it correlated with the magnitude of inflammatory response (34). In line with our findings, however, it has been demonstrated that changes in the HLA-DR expression did not constitute an accurate marker of mortality in septic shock patients (35, 36).

CD80 is one of the co-stimulatory molecules required for T-cell activation by antigen-presenting cells. Nolan et al (29) demonstrated an increased CD80 expression on the circulating monocytes in septic patients and peritoneal macrophages from septic mice (37). Moreover, $CD80^{-/-}$ mice had improved survival after CLP (38) and in another study, CLP mice lacking CD80 displayed lower circulating IL-6 levels (38). The above was contrasted by our data: (a) Monocytes from P-DIE humanized mice showed a greater reduction of CD80 expression in comparison to their P-SUR littermates and (b) we observed a negative correlation between the CD80 expression and circulating cytokine concentration. There are several possible reasons for these discrepancies. First, we analyzed CD80 expression on the bone marrow and splenic monocytes, while the other studies focused on the circulating and peritoneal cells. The choice of sampling sites seems to be of vital importance as the immune response in sepsis appears to be highly compartmentalized (39, 40). Second, monocytes from humanized mice were shown to be partly immature, therefore their response to infection can differ from the mature cells (41). Notably, Gille et al. did not find expression of CD80 on monocytes from humanized mice developed on newborn NSG mice transplanted with UCB cells (41). Third, our humanized mice showed a low frequency of human T cells which interacted with monocytes, therefore, the mutual activation of these cells may differ from the normal human setting. Finally, the interspecies interactions in humanized mice are not known and it cannot be ruled out that the murine microenvironment modulates selected responses of human cells. It would be of interest to examine the expression of the interleukin-1 receptor-associated kinase-M in the monocytes of post-CLP humanized mice as this molecule is a master-regulator of CD80 surface expression (38).

We applied small-volume repetitive sampling (31) to monitor the changes of human and murine cytokines in early sepsis. Previously we have demonstrated a simultaneous release of pro-and anti-inflammatory cytokines in the early post-CLP phase (19). Both at baseline and post-CLP, the concentration of measured murine cytokines outbalanced human cytokines. Both human and murine cytokines were upregulated 6 h post-CLP, yet, it was apparent that murine circulating cytokines predominate (concentration-wise) over the human mediators in an approximate 9:1 ratio. This has never been reported before but such a magnitude of discrepancy is not surprising given that the only source of human circulating cytokines in these mice were hematopoietic cells. In contrast, despite humanization, mice maintain several other murine-origin cell types known to secrete cytokines (e.g., endothelium, hepatocytes, myocytes). Most murine cytokines are not active on human cells while some human cytokines are not species-specific (42). The negative correlation between expression of CD80 on human monocytes and concentration of human cytokines suggests that humanized mice recapitulate systemic interactions between humoral and cellular elements of human immunity. Interestingly, there was a

robust early peak of human TNFα which markedly outbalanced murine TNFα. As human TNFα cross-reacts with murine receptors (43), it can be speculated that the combined high TNFα load contributes to the increased mortality of humanized mice. The RIP3-mediated induction of necroptosis was shown by Duprez et al. (44) to contribute significantly to early deaths after CLP. We hypothesize that this mechanism was responsible for a greater sensitivity to CLP of humanized mice compared to naïve NSG or SCID mice to CLP. Similarly to our results, humanized mice were shown to be more sensitive to *S. aureus* infection and CLP than NSG or wild-type mice (16, 45). Ye et al. (16) showed that the high mortality of humanized mice after CLP was related to the production of HMGB-1 by human myeloid cells. It cannot be ruled out that the process of xenotransplantation impairs the murine granulocytic response in humanized mice that is otherwise efficient in the naïve NSG mice. Additionally, it is apparent that humanization did not change the general profile of post-CLP cytokine response in NSG mice. Therefore, the tissues/organs were subjected to the murine inflammatory response, preserving the ability of the host to develop organ dysfunction (recapitulating clinical sequelae).

Next, we examined whether the disease severity modulated the human/murine cytokine response. The relatively high severity (i.e., 71% by 32 h post-CLP) that we employed in our study was dictated by two elements: (a) we sought to provoke robust enough post-CLP changes in both compartments (i.e., human and murine) to enable their effective comparison and (b) a naturally high sensitivity of humanized mice to infection/injury. As early as 6 h post-CLP, all human and murine cytokines (except for human IL-10 and MCP-1) were markedly elevated in the P-DIE mice compared to P-SUR. At 24 h, only the concentration of human/murine TNFα dropped to a similarly low level regardless of outcome. Clinical sepsis data regarding the relationship between TNFα concentration and sepsis mortality are conflicting. However, several studies, in line with our own observations, demonstrated that early TNFα release (i.e., measured close to the onset of sepsis) correlates with mortality (46–48). Importantly, in septic patients, the kinetics of the TNFα response largely vary depending on patient characteristics (47); our CLP model (by default) is much more controlled, and features a relatively steady response. As revealed by the ROC analysis, human cytokines that showed the best predictive value for mortality were IL-8 and IL-6, which is in line with the clinical data (49). However, murine IL-6 and TNFα were characterized by even higher AUC values. This is rational as these cytokines are also produced by non-hematopoietic cells which constitute the majority of tissues in humanized mice.

This study has several limitations. First, our humanized mice show a (human) chimeric heterogeneity. This is unavoidable as chimerism largely depends on the donor (50). However, the heterogeneity of donors partly recapitulates the genetic variability that is present in the clinical scenario. Second, we did not further investigate human monocytes to explain the post-CLP discrepancy in CD80 expression. Third, our model included only a single gender and was characterized by a relatively high CLP severity; the current study should be repeated in males and in a low-severity sepsis scenario. Also, a study in aged humanized mice should be performed as a next step to mimic demographic characteristics of septic patients. Additionally, our study failed to characterize the fluctuations beyond day 2 post-CLP; an assessment of cellular and humoral inflammatory changes in the chronic CLP phase should be attempted. Finally, the body temperature-based prediction of early CLP outcome needs to be verified prospectively given that our assessment used retrospective readouts.

Summarizing, this study characterizes for the first time an outcome-dependent evolution of cellular (i.e., bone marrow and splenic monocytes) and circulating cytokine responses in humanized mice. We demonstrate that humanized mice subjected to CLP recapitulate important inflammatory features of clinical sepsis supporting the notion that this model can be utilized in preclinical sepsis research to maximize its translation potential.

DATA AVAILABILITY

The raw data supporting the conclusions of this manuscript will be made available by the authors, without undue reservation, to any qualified researcher.

ETHICS STATEMENT

This study was carried out in accordance with the recommendations of ARRIVE guidelines. The protocol was approved by the Local Ethic Committee no IV in Warsaw, Poland.

AUTHOR CONTRIBUTIONS

TS: design, performing experiment, analysis of the study, and writing manuscript. SD: study design, performing experiment, and correction of manuscript. GH: study design and performing experiments. MJ: sample analysis. KS: cord blood preparation. ZP: cord blood preparation and correction of manuscript. JK: study design and correction of manuscript. MO: study design, performing experiments, data analysis/interpretation, and writing manuscript.

FUNDING

Study funded by Polish National Science Centre grant no UMO-2016/23/D/NZ6/02554.

ACKNOWLEDGMENTS

The authors would like to thank Danuta Wasilewska for animal care and James Ferguson for proofreading the manuscript.

SUPPLEMENTARY MATERIAL

The Supplementary Material for this article can be found online at: https://www.frontiersin.org/articles/10.3389/fimmu.2019.01427/full#supplementary-material

REFERENCES

1. Marshall JC. Why have clinical trials in sepsis failed? *Trends Mol Med*. (2014) 20:195–203. doi: 10.1016/j.molmed.2014.01.007
2. Rhee C, Dantes R, Epstein L, Murphy DJ, Seymour CW, Iwashyna TJ, et al. Incidence and trends of sepsis in US hospitals using clinical vs claims data, 2009–2014. *JAMA*. (2017) 318:1241–9. doi: 10.1001/jama.2017.13836
3. Fleischmann C, Scherag A, Adhikari NK, Hartog CS, Tsaganos T, Schlattmann P, et al. Assessment of global incidence and mortality of hospital-treated sepsis. Current estimates and limitations. *Am J Respir Crit Care Med*. (2016) 193:259–72. doi: 10.1164/rccm.201504-0781OC
4. Rudd KE, Kissoon N, Limmathurotsakul D, Bory S, Mutahunga B, Seymour CW, et al. The global burden of sepsis: barriers and potential solutions. *Crit Care*. (2018) 22:232. doi: 10.1186/s13054-018-2157-z
5. Osuchowski MF, Ayala A, Bahrami S, Bauer M, Boros M, Cavaillon JM, et al. Minimum Quality Threshold in Pre-Clinical Sepsis Studies (MQTiPSS): an international expert consensus initiative for improvement of animal modeling in sepsis. *Shock*. (2018) 50:377–80. doi: 10.1097/SHK.0000000000001212
6. Stortz JA, Raymond SL, Mira JC, Moldawer LL, Mohr AM, Efron PA. Murine models of sepsis and trauma: can we bridge the gap? *ILAR J*. (2017) 58:90–105. doi: 10.1093/ilar/ilx007
7. Osuchowski MF, Remick DG, Lederer JA, Lang CH, Aasen AO, Aibiki M, et al. Abandon the mouse research ship? Not just yet! *Shock*. (2014) 41:463–75. doi: 10.1097/SHK.0000000000000153
8. Zingarelli B, Coopersmith CM, Drechsler S, Efron P, Marshall JC, Moldawer L, et al. Part I: Minimum Quality Threshold in Pre-Clinical Sepsis Studies (MQTiPSS) for study design and humane modeling endpoints. *Shock*. (2018) 51:10–22. doi: 10.1097/SHK.0000000000001243
9. Mestas J, Hughes CC. Of mice and not men: differences between mouse and human immunology. *J Immunol*. (2004) 172:2731–8. doi: 10.4049/jimmunol.172.5.2731
10. Walsh NC, Kenney LL, Jangalwe S, Aryee KE, Greiner DL, Brehm MA, et al. Humanized mouse models of clinical disease. *Annu Rev Pathol*. (2017) 12:187–215. doi: 10.1146/annurev-pathol-052016-100332
11. Laudanski K, Stentz M, DiMeglio M, Furey W, Steinberg T, Patel A. Potential pitfalls of the humanized mice in modeling sepsis. *Int J Inflam*. (2018) 2018:6563454. doi: 10.1155/2018/6563454
12. Mota J, Rico-Hesse R. Humanized mice show clinical signs of dengue fever according to infecting virus genotype. *J Virol*. (2009) 83:8638–45. doi: 10.1128/JVI.00581-09
13. Prince A, Wang H, Kitur K, Parker D. Humanized mice exhibit increased susceptibility to *Staphylococcus aureus* pneumonia. *J Infect Dis*. (2017) 215:1386–95. doi: 10.1093/infdis/jiw425
14. Marsden MD, Zack JA. Humanized mouse models for human immunodeficiency virus infection. *Annu Rev Virol*. (2017) 4:393–412. doi: 10.1146/annurev-virology-101416-041703
15. Unsinger J, McDonough JS, Shultz LD, Ferguson TA, Hotchkiss RS. Sepsis-induced human lymphocyte apoptosis and cytokine production in "humanized" mice. *J Leukoc Biol*. (2009) 86:219–27. doi: 10.1189/jlb.1008615
16. Ye C, Choi JG, Abraham S, Wu H, Diaz D, Terreros D, et al. Human macrophage and dendritic cell-specific silencing of high-mobility group protein B1 ameliorates sepsis in a humanized mouse model. *Proc Natl Acad Sci USA*. (2012) 109:21052–7. doi: 10.1073/pnas.1216195109
17. Skirecki T, Kawiak J, Machaj E, Pojda Z, Wasilewska D, Czubak J, et al. Early severe impairment of hematopoietic stem and progenitor cells from the bone marrow caused by CLP sepsis and endotoxemia in a humanized mice model. *Stem Cell Res Ther*. (2015) 6:142. doi: 10.1186/s13287-015-0135-9
18. Laudanski K, Lapko N, Zawadka M, Zhou BX, Danet-Desnoyers G, Worthen GS. The clinical and immunological performance of 28 days survival model of cecal ligation and puncture in humanized mice. *PLoS ONE*. (2017) 12:e0180377. doi: 10.1371/journal.pone.0180377
19. Osuchowski MF, Welch K, Siddiqui J, Remick DG. Circulating cytokine/inhibitor profiles reshape the understanding of the SIRS/CARS continuum in sepsis and predict mortality. *J Immunol*. (2006) 177:1967–74. doi: 10.4049/jimmunol.177.3.1967
20. Remick DG, Bolgos GR, Siddiqui J, Shin J, Nemzek JA. Six at six: interleukin-6 measured 6 h after the initiation of sepsis predicts mortality over 3 days. *Shock*. (2002) 17:463–7. doi: 10.1097/00024382-200206000-00004
21. Drechsler S, Weixelbaumer KM, Weidinger A, Raeven P, Khadem A, Redl H, et al. Why do they die? Comparison of selected aspects of organ injury and dysfunction in mice surviving and dying in acute abdominal sepsis. *Intensive Care Med Exp*. (2015) 3:48. doi: 10.1186/s40635-015-0048-z
22. Rademann P, Weidinger A, Drechsler S, Meszaros A, Zipperle J, Jafarmadar M, et al. Mitochondria-targeted antioxidants SkQ1 and MitoTEMPO failed to exert a long-term beneficial effect in murine polymicrobial sepsis. *Oxid Med Cell Longev*. (2017) 2017:6412682. doi: 10.1155/2017/6412682
23. Raeven P, Drechsler S, Weixelbaumer KM, Bastelica D, Peiretti F, Klotz A, et al. Systemic inhibition and liver-specific over-expression of PAI-1 failed to improve survival in all-inclusive populations or homogenous cohorts of CLP mice. *J Thromb Haemost*. (2014) 12:958–69. doi: 10.1111/jth.12565
24. Kilkenny C, Browne W, Cuthill IC, Emerson M, Altman DG, Group NCRRGW. Animal research: reporting *in vivo* experiments: the ARRIVE guidelines. *Br J Pharmacol*. (2010) 160:1577–9. doi: 10.1111/j.1476-5381.2010.00872.x
25. Notta F, Doulatov S, Dick JE. Engraftment of human hematopoietic stem cells is more efficient in female NOD/SCID/IL-2Rgc-null recipients. *Blood*. (2010) 115:3704–7. doi: 10.1182/blood-2009-10-249326
26. Wichterman KA, Baue AE, Chaudry IH. Sepsis and septic shock–a review of laboratory models and a proposal. *J Surg Res*. (1980) 29:189–201. doi: 10.1016/0022-4804(80)90037-2
27. Drechsler S, Zipperle J, Rademann P, Jafarmadar M, Klotz A, Bahrami S, et al. Splenectomy modulates early immuno-inflammatory responses to trauma-hemorrhage and protects mice against secondary sepsis. *Sci Rep*. (2018) 8:14890. doi: 10.1038/s41598-018-33232-1
28. Busch D, Kapoor A, Rademann P, Hildebrand F, Bahrami S, Thiemermann C, et al. Delayed activation of PPAR-beta/delta improves long-term survival in mouse sepsis: effects on organ inflammation and coagulation. *Innate Immun*. (2018) 24:262–73. doi: 10.1177/1753425918771748
29. Kim J, Arnaout L, Remick D. Hydrocortisone, Ascorbic Acid and Thiamine (HAT) therapy decreases oxidative stress, improves cardiovascular function and improves survival in murine sepsis. *Shock*. (2019). doi: 10.1097/SHK.0000000000001385. [Epub ahead of print].
30. Osuchowski MF, Welch K, Yang H, Siddiqui J, Remick DG. Chronic sepsis mortality characterized by an individualized inflammatory response. *J Immunol*. (2007) 179:623–30. doi: 10.4049/jimmunol.179.1.623
31. Weixelbaumer KM, Raeven P, Redl H, van Griensven M, Bahrami S, Osuchowski MF. Repetitive low-volume blood sampling method as a feasible monitoring tool in a mouse model of sepsis. *Shock*. (2010) 34:420–6. doi: 10.1097/SHK.0b013e3181dc0918
32. Yong KSM, Her Z, Chen Q. Humanized mice as unique tools for human-specific studies. *Arch Immunol Ther Exp*. (2018) 66:245–66. doi: 10.1007/s00005-018-0506-x
33. Glatman Zaretsky A, Engiles JB, Hunter CA. Infection-induced changes in hematopoiesis. *J Immunol*. (2014) 192:27–33. doi: 10.4049/jimmunol.1302061
34. Skirecki T, Borkowska-Zielinska U, Zlotorowicz M, Hoser G. Sepsis immunopathology: perspectives of monitoring and modulation of the immune disturbances. *Arch Immunol Ther Exp*. (2012) 60:123–35. doi: 10.1007/s00005-012-0166-1
35. Skirecki T, Mikaszewska-Sokolewicz M, Hoser G, Zielinska-Borkowska U. The early expression of HLA-DR and CD64 myeloid markers is specifically compartmentalized in the blood and lungs of patients with septic shock. *Mediators Inflamm*. (2016) 2016:3074902. doi: 10.1155/2016/3074902
36. Ploder M, Pelinka L, Schmuckenschlager C, Wessner B, Ankersmit HJ, Fuerst W, et al. Lipopolysaccharide-induced tumor necrosis factor alpha production and not monocyte human leukocyte antigen-DR expression is correlated with survival in septic trauma patients. *Shock*. (2006) 25:129–34. doi: 10.1097/01.shk.0000191379.62897.1d
37. Nolan A, Weiden M, Kelly A, Hoshino Y, Hoshino S, Mehta N, et al. CD40 and CD80/86 act synergistically to regulate inflammation and mortality in polymicrobial sepsis. *Am J Respir Crit Care Med*. (2008) 177:301–8. doi: 10.1164/rccm.200703-515OC
38. Nolan A, Kobayashi H, Naveed B, Kelly A, Hoshino Y, Hoshino S, et al. Differential role for CD80 and CD86 in the regulation of the innate immune response in murine polymicrobial sepsis. *PLoS ONE*. (2009) 4:e6600. doi: 10.1371/journal.pone.0006600

39. Schwacha MG, Schneider CP, Chaudry IH. Differential expression and tissue compartmentalization of the inflammatory response following thermal injury. *Cytokine*. (2002) 17:266–74. doi: 10.1006/cyto.2001.1003
40. Cavaillon JM, Annane D. Compartmentalization of the inflammatory response in sepsis and SIRS. *J Endotoxin Res*. (2006) 12:151–70. doi: 10.1179/096805106X102246
41. Gille C, Orlikowsky TW, Spring B, Hartwig UF, Wilhelm A, Wirth A, et al. Monocytes derived from humanized neonatal NOD/SCID/IL2Rgamma(null) mice are phenotypically immature and exhibit functional impairments. *Hum Immunol*. (2012) 73:346–54. doi: 10.1016/j.humimm.2012.01.006
42. Scheerlinck J-PY. Cytokine species-specificity and humanized mice. In: Poluektova LY, editor. *Humanized Mice for HIV Research*. New York, NY: Springer (2014). p. 93–108
43. Bossen C, Ingold K, Tardivel A, Bodmer JL, Gaide O, Hertig S, et al. Interactions of tumor necrosis factor (TNF) and TNF receptor family members in the mouse and human. *J Biol Chem*. (2006) 281:13964–71. doi: 10.1074/jbc.M601553200
44. Duprez L, Takahashi N, Van Hauwermeiren F, Vandendriessche B, Goossens V, Vanden Berghe T, et al. RIP kinase-dependent necrosis drives lethal systemic inflammatory response syndrome. *Immunity*. (2011) 35:908–18. doi: 10.1016/j.immuni.2011.09.020
45. Knop J, Hanses F, Leist T, Archin NM, Buchholz S, Glasner J, et al. *Staphylococcus aureus* infection in humanized mice: a new model to study pathogenicity associated with human immune response. *J Infect Dis*. (2015) 212:435–44. doi: 10.1093/infdis/jiv073
46. Terregino CA, Lopez BL, Karras DJ, Killian AJ, Arnold GK. Endogenous mediators in emergency department patients with presumed sepsis: are levels associated with progression to severe sepsis and death? *Ann Emerg Med*. (2000) 35:26–34. doi: 10.1016/S0196-0644(00)70101-6
47. Munoz C, Misset B, Fitting C, Bleriot JP, Carlet J, Cavaillon JM. Dissociation between plasma and monocyte-associated cytokines during sepsis. *Eur J Immunol*. (1991) 21:2177–84. doi: 10.1002/eji.1830210928
48. Pinsky MR, Vincent JL, Deviere J, Alegre M, Kahn RJ, Dupont E. Serum cytokine levels in human septic shock. Relation to multiple-system organ failure and mortality. *Chest*. (1993) 103:565–75. doi: 10.1378/chest.103.2.565
49. Bozza FA, Salluh JI, Japiassu AM, Soares M, Assis EF, Gomes RN, et al. Cytokine profiles as markers of disease severity in sepsis: a multiplex analysis. *Crit Care*. (2007) 11:R49. doi: 10.1186/cc5783
50. Skelton JK, Ortega-Prieto AM, Dorner M. A Hitchhiker's guide to humanized mice: new pathways to studying viral infections. *Immunology*. (2018) 154:50–61. doi: 10.1111/imm.12906

Conflict of Interest Statement: The authors declare that the research was conducted in the absence of any commercial or financial relationships that could be construed as a potential conflict of interest.

Copyright © 2019 Skirecki, Drechsler, Hoser, Jafarmadar, Siennicka, Pojda, Kawiak and Osuchowski. This is an open-access article distributed under the terms of the Creative Commons Attribution License (CC BY). The use, distribution or reproduction in other forums is permitted, provided the original author(s) and the copyright owner(s) are credited and that the original publication in this journal is cited, in accordance with accepted academic practice. No use, distribution or reproduction is permitted which does not comply with these terms.

frontiers in Immunology

ORIGINAL RESEARCH
published: 14 August 2019
doi: 10.3389/fimmu.2019.01949

Functional Annotation of Genetic Loci Associated With Sepsis Prioritizes Immune and Endothelial Cell Pathways

*Kieu T. T. Le[1], Vasiliki Matzaraki[1,2], Mihai G. Netea[2], Cisca Wijmenga[1,3], Jill Moser[4] and Vinod Kumar[1,2]**

[1] University of Groningen, University Medical Center Groningen, Genetics Department, Groningen, Netherlands, [2] Department of Internal Medicine and Radboud Centre for Infectious Diseases, Radboud University Medical Center, Nijmegen, Netherlands, [3] Department of Immunology, K.G. Jebsen Coeliac Disease Research Centre, University of Oslo, Oslo, Norway, [4] University of Groningen, University Medical Center Groningen, Department of Critical Care and Department of Pathology and Medical Biology, Groningen, Netherlands

Due to limited sepsis patient cohort size and extreme heterogeneity, only one significant locus and suggestive associations at several independent loci were implicated by three genome-wide association studies. However, genes from such suggestive loci may also provide crucial information to unravel genetic mechanisms that determine sepsis heterogeneity. Therefore, in this study, we made use of integrative approaches to prioritize genes and pathways affected by sepsis associated genetic variants. By integrating expression quantitative trait loci (eQTL) results from the largest whole-blood eQTL database, cytokine QTLs from pathogen-stimulated peripheral blood mononuclear cells (PBMCs), publicly available blood transcriptome data from pneumoniae-derived sepsis patients, and transcriptome data from pathogen-stimulated PBMCs, we identified 55 potential genes affected by 39 independent loci. By performing pathway enrichment analysis at these loci we found enrichment of genes for adherences-junction pathway. Finally, we investigated the functional role of the only one GWAS significant SNP rs4957796 on sepsis survival in altering transcription factor binding affinity in monocytes and endothelial cells. We also found that transient deficiency of *FER* and *MAN2A1* affect endothelial response to stimulation, indicating that both *FER* and *MAN2A1* could be the causal genes at this locus. Taken together, our study suggests that in addition to immune pathways, genetic variants may also affect non-immune related pathways.

Keywords: sepsis GWAS, cytokine QTLs, eQTL, functional genomics, PBMC transcriptome, endothelial response, FER locus

OPEN ACCESS

Edited by:
Lukas Martin, University Hospital RWTH Aachen, Germany

Reviewed by:
Sandra Kraemer, University Hospital RWTH Aachen, Germany
Daniel Scott-Algara, Institut Pasteur, France

***Correspondence:**
Vinod Kumar
v.kumar@umcg.nl

Specialty section:
This article was submitted to Inflammation, a section of the journal Frontiers in Immunology

Received: *14 May 2019*
Accepted: *01 August 2019*
Published: *14 August 2019*

Citation:
Le KTT, Matzaraki V, Netea MG, Wijmenga C, Moser J and Kumar V (2019) Functional Annotation of Genetic Loci Associated With Sepsis Prioritizes Immune and Endothelial Cell Pathways. Front. Immunol. 10:1949. doi: 10.3389/fimmu.2019.01949

INTRODUCTION

Sepsis is a major global health problem primarily caused by bacterial and fungal infections. It is a life-threatening organ dysfunction characterized by a dysregulated host immune response (1). The global burden of sepsis is high, with an estimated worldwide incidence of more than 30 million cases per year leading to nearly 6 million annual deaths (2). Regretfully, current strategies using a "one-size-fits-all" treatment approach for sepsis have failed because of the extreme heterogeneity in disease outcome (3). It is becoming increasingly clear that the heterogeneity is determined

by impact of multiple risk factors including host genetic variation and pathogens (2). Therefore, identifying the critical genetic factors that affect sepsis patient outcome will help us to unravel genetic mechanisms that determine sepsis heterogeneity.

Up to now, three genome-wide association studies (GWAS) have been conducted to identify risk genes for sepsis. Two GWAS were conducted to identify associations between single nucleotide polymorphisms (SNPs) and 28 day sepsis mortality (4, 5). Another GWAS was conducted in a cohort of extremely premature infants to identify genetic loci associated with sepsis onset (6). However, only one study identified a genome-wide significant association at non-coding SNPs in the intron of Fps/Fes related tyrosine kinase (*FER*) gene in patients with 28 day survival of sepsis due to pneumonia (4). Although, these studies identified associations with several common polymorphisms, it is unclear how these SNPs affect sepsis outcome. Moreover, which genes and pathways in these loci affect sepsis survival remains to be studied. Identifying these specific genes and pathways is crucial to better understand the molecular mechanisms underlying sepsis heterogeneity.

System genetic approaches have been very effective for many complex human diseases, to translate genetic associations into functional understanding (7). By integrating multiple molecular phenotypes such as gene expression, protein levels, metabolites etc. with SNPs that were associated with human diseases, studies have shown that it is possible to prioritize potential causal genes affected by GWAS SNPs and obtain insights into functional pathways that affect human disease (8). Given the polygenic nature of many complex phenotypes, SNPs that are associated with suggestive significance also provide crucial biological insights. Moreover, as GWAS SNPs function in cell-type and context-dependent manner (9), integrating such context-specific molecular data with sepsis-associated SNPs may be more effective to obtain mechanistic insights into sepsis heterogeneity.

Therefore, in this study, we used pathogen- and cell-type specific gene expression levels, cytokine responses, and genotype data from population-based cohorts to integrate molecular responses with sepsis associated SNPs. We show that about 35% of the SNPs affect gene expression (eQTLs) in blood and <30% of sepsis associated SNPs affect cytokine production by peripheral blood mononuclear cells (PBMCs) in response to pathogens. Next, we show that the genome-wide significant SNP rs4957796 in the *FER* locus affects transcription factor binding efficiency in both monocytes and endothelial cells, and *FER* and (Mannosidase Alpha Class 2A Member 1 *(MAN2A1)* *MAN2A1* could be the causal genes in this locus via regulating endothelial function.

Taken together, our study provides evidence for genetically determined variability in endothelial pathways, in addition to leukocyte responses, as one of the important factors to explain sepsis heterogeneity. Therefore, more studies on the effect of the SNPs on different pathways such as barrier function or endothelial function are needed.

MATERIALS AND METHODS

Identification of Proxy SNPs

Two hundred eighteen proxy SNPs from 39 independent loci were extracted from Haploreg using $D' = 1$, $R^2 \geq 0.95$ using 1,000 Genome CEU as a reference population.

Integration of Suggestive GWAS Loci With eQTL Data and Cytokine QTL Data

We made use of published eQTL data from eQTLgen (http://www.eqtlgen.org) and in house-cytokine QTL from 500 FG (10). We extracted only genome-wide significant eQTL signals from eQTLgen. Briefly, cis-eQTL analysis was performed in 31,684 blood samples. Significant cis-eQTLs were defined as eQTLs that show FDR corrected *P*-value of <0.05 ($P < 1{,}829 \times 10^{-5}$) (11). For cytokine QTLs from the 500 FG cohort study (cytokine QTLs were performed on 392 individuals), we extracted reported *P*-value for each SNP (10) and applied Bonferroni correction to define significant *P*-value threshold. As we tested 39 independent loci, the *P*-value threshold is 0.0012.

PBMC Transcriptome

We made use of in house PBMC transcriptome data (12). Briefly, PBMCs were freshly isolated from peripheral venous blood withdrawn from healthy volunteers, according to work permission on whole blood (Ethical Committee of Radboud University Nijmegen (nr 42561.091.12). PBMC were freshly isolated with Ficoll-Paque (Pharmacia Biotech), counted (BioRad cell counter), and adjusted to 5 million cells/ml in RPMI 1640 (Gibco, ThermoFisher Scientific), supplemented gentamicin 10 mg/ml, L-glutamine 10 mM, and pyruvate 10 mM. Cells were seeded into wells to settle overnight before stimulation. PBMC were stimulated with 100 μl of *Streptococcus pneumonia* (ATCC 49619, serotype 19F) (1 million cells/ml), *Candida albicans* (ATCC MYA-3573, UC 820) (1 million cells/ml), *and Pseudomonas aeruginosa* (1 million cells/ml). PBMCs were also stimulated with RPMI a negative control. RNA was isolated at 4 and 24 h after stimulation. RNA sequencing was performed in a Nextseq 500 platform, single-end, read length 50 bp. Reads were mapped to the human genome hg19 using STAR (version 2.3.0), Ht-seq count was used to quantify read counts and DEseq2 was used to perform statistics analysis (FDR $P \leq 0.05$ and fold change ≥2) (12).

Gene Expression in Pneumoniae-Derived Sepsis Patients

To further validate our prioritized genes, we checked their expression levels in pneumoniae-derived sepsis patient transcriptome ($N = 265$ patients) (13). Briefly, we extracted only genome-wide significant differentially expressed genes (FC>1,5, and FDR correct *P*-value of 0.05) reported in either the discovery cohort or the validation cohort (13).

Electrophoresis Mobility Shift Assay (EMSA)

EMSA were performed using LightShift Chemiluminescent EMSA Kit (Thermo Scientific) according to the manual

instruction. In brief, the protocols contain three main parts, including: probe biotination, nuclei extraction, and mobility shift assay on polyacrylamide gel. Probe biotination. Probes containing nucleotide sequence of 30 bp around the SNP were designed carrying either T allele or C allele at the SNP position. The probes were then labeled with biotin at the 3′ end using Pierce Biotin 3′ End DNA labeling kit (Thermo Scientific). After labeled, probes were annealed to make double stranded DNA probes. Labeling efficiency was evaluated following the recommended protocol. Nuclei extraction. Ten million cells were used to isolate the nuclei. Cells were suspended in lysis buffer (10 mM Tris-Cl pH8.0, 300 mM sucrose, 10 mM NaCl, 2 mM MgAc2, 6 mM CaCl2, and 0.2% of NP-40 (Igepal) for 5 min. Nuclei pellets were harvested and resuspended in 100 μl of Nuclear Extract Buffer (20 mM Tris-Cl (pH8.0), 420 mM NaCl, 1.5 mM MgCl2, 0.2 mMEDTA, 25% glycerol, 1 mM DTT and 1X protease inhibitor cocktail) for 10 min on ice. After centrifugation at 14.000 rpm for 15 min, supernatant containing nuclear extract was collected and protein concentration was determined using Bradford assay. Gel mobility assay. Mobility assay was performed according to the instruction. Briefly, 5–10 μg of total proteins from the nuclei extract was used with 20 fmol of Biotin End-labeled target DNA. Unlabeled target DNA was also used as a binding competition in the presence or absence of protein from nuclei extract. Images were obtained using BioRad system.

Cell Culture

To mimic the context of sepsis in which inflammation involves the role of endothelial cells and blood cells, we used Primary Human Umbilical Vein Endothelial cells (HUVEC) (Lonza, The Netherlands) as endothelial cells and THP-1 (ATCC, The Netherlands) as monocytes. Pooled donor-HUVEC were purchased from Lonza (C2519A, The Netherlands). Cells were cultured in EBM-2TM medium (Lonza) supplemented with EGM-2 MV SingleQuot Kit Supplements & Growth Factors (Cat. No. 3202, Lonza) and antibiotics 100 IU/ml of penicillin (Astellas Pharma, The Netherlands) and 50 μg/ml of Streptomycin (Rotexmedica GmbH, Germany). Cells were used from passage 3–7 and cultured at 37°C, 5% CO2 and saturating humidity. THP-1 cells (ATCC, The Netherlands) were cultured in Gibco TM RPMI 1640 containing L-glutamine +/HEPES + (Cat. No. 1640 52400-025) supplemented with 10% (v/v) heat-inactivated FBS (Gibco), 1%(v/v) Pen/Strep 10.000 U/ml (Gibco). THP-1 cells were kept at 37°C, 5% CO2 and saturating humidity. Cells were freshly passed twice a week to keep a density of 200.000–800.000 cells/ml and used up to passage 28.

Knock Down Experiment in HUVEC

HUVEC were seeded to reach the confluency of 70% before transfection. siFER and siMAN2A1 were delivered into HUVEC by Lipofectamine 2000 (Invitrogen). 20 pmol of siRNA sequence was transfected into one million cells according to instructed protocol. After transfection, cells were rested for 48 h before subsequent stimulation with LPS derived from *Escherichia coli*, serotype O26:B6 (15,000 endotoxin units/g) (Sigma-Aldrich, St.Louis) (1 μg/ml) (14). Cells were lysed in Trizol (Ambion, ThermoFisher) and kept at −80°C until RNA isolation.

Gene Expression by RT-qPCR

Gene expression levels were measured by RT-qPCR (reverse transcriptase-quantitative PCR) using Sybrgreen platform. Briefly, total RNA was isolated by Trizol according to the instructed protocol. RNA concentration was measured by Nanodrop. RNA quality was controlled in random samples by measuring RNA Integrity Score (Agilent). 100–5,000 ng of total RNA was loaded for cDNA synthesis using ReverAid H Minus First Strand cDNA synthesis kit (ThermoScientific). Primers (refer to **Table 1**) were designed with primer3 and conditions were optimized for each primer set. Melting curves were used to access the specificity of each reaction. GAPDH was used as a housekeeping gene. qPCR was performed in a ViiA7 real-time PCR (Applied Biosystems) following the standard protocol: 15 min at 95°C and 40 cycles of two steps: amplification (60°C for 60 s) and denaturation (95°C for 15 s). Gene expression levels were calculated based on the comparison of CT values between target gene(s) and the housekeeping gene (ΔCT). Average messenger RNA levels relative to GAPDH from the duplicate were calculated by $2^{-\Delta CT}$ Data were shown as mean ± SD. One-way ANOVA test was used to compare between conditions and control: $P \leq 0.05$ (*); $P \leq 0.01$ (**); $P \leq 0.001$ (***); $P \leq 0.0001$ (****). GraphPad Prism software (version 6.0) was used to make graphs and determine significant differences.

RESULTS

Annotation of 39 Independent Loci From Three Sepsis GWAS

Two genetic studies were conducted to identify SNPs associated with sepsis survival in adult patients (28-day mortality) and one study on sepsis onset in extremely premature infants. We extracted 25 SNPs that are associated with sepsis survival with evidence for suggestive association ($P < 10^{-5}$), which includes 11 SNPs from Rautanen et al., and 14 SNPs from Scherag et al. study (4, 5). Using the same criteria we extracted 30 SNPs that are associated with sepsis onset in infants from Srinivasan et al. study [(6); **Table S1**]. Among these 55 SNPs, we filtered by locus position, for loci located within 1 Mb from each other, and selected a SNP with the lowest P-value as the representative. As a result, we found 39 independent loci from the three GWAS. We then extracted 218 proxy SNPs ($R^2 \geq 0.95$, $D' = 1$) for these 39 independent SNPs using 1000 Genome CEU as a reference population (**Table S1**). As previously reported, none of these loci were shared between the three studies. Although, this may be because of the insufficient study power, it also emphasizes the clinical heterogeneity among patients between cohorts, which could be partly determined by genetic variations. Therefore, we followed up these independent loci to prioritize potential causal candidate genes and pathways affected by them.

TABLE 1 | Primer sequences.

Primer	Sequence (5′-3′)
MAN2A1_forward	CGCAGAAAATGATACACACGG
MAN2A1_reverse	CGTGGCTCTTTCCTAAACAGG
GAPDH_forward	CTGCATTTCATTCCAGTTCAGG
GAPDH_reverse	TCTGTCCAGTGATTCAGCCA
FER_forward	CAAATCAGCAAGCAAGAGAGC
FER_reverse	TGAACTTAGGGCGATTTTCAGG
ICAM1_forward	GGCCGGCCAGCTTATACAC
ICAM1_reverse	TAGACACTTGAGCTCGGGCA
VCAM1_forward	TCAGATTGGAGACTCAGTCATGT
VCAM1_reverse	ACTCCTCACCTTCCCGCTC
Eselectin_forward	CCCGAAGGGTTTGGTGAG
Eselectin_reverse	TAAAGCCCTCATTGCATTGA
IL8_forward	TCTGCAGCTCTGTGTGAAGG
IL8_reverse	ACTTCTCCACAACCCTCTGC
Probe_Sense (T)	CAAAATTTATAAATAT**T**ACATCATTGAAATTAT
Probe_Antisense (T)	ATAATTTCAATGATGT**A**ATATTTATAAATTTTG
Probe_Sense (C)	CAAAATTTATAAATAT**C**ACATCATTGAAATTAT
Probe_Antisense (C)	ATAATTTCAATGATGT**G**ATATTTATAAATTTTG

Expression QTL Mapping and Differential Expression Analyses Prioritized Potential Causal Pathways for Sepsis

To identify potential causal genes affected by sepsis-associated SNPs, we made use of expression-QTL (eQTL) analysis. For this we extracted results from the largest eQTL study (eQTLGen) that included nearly 35,000 blood samples (11). We found significant association of SNPs from 13 independent loci with expression levels of 45 unique genes (**Table 2**). Interestingly, three loci that were associated with sepsis onset in extremely premature infants affected the most number of nearby genes (**Table 2**). In particular, SNPs rs12490944, rs41461846, and rs3844280 affected 14, 10, and 5 genes, respectively.

Moreover, it is shown that differentially expressed genes in response to infectious agents are more likely to be associated with susceptibility to infectious diseases (15) and more than 90% of the lead SNPs that have eQTL effects are located within 100 kb of the eQTL genes (11). Therefore, as a second strategy to prioritize potential causal genes at sepsis-associated loci, we tested the expression levels of all genes located within a 200 kb window of all 39 loci with suggestive association ($P < 9.99 \times 10^{-5}$) in stimulated peripheral blood mononuclear cells (PBMCs) transcriptome. For this, we used RNAseq data from PBMCs that were stimulated with *Pseudomonas aeruginosa* (*P. aeruginosa*), *Streptococcus pneumoniae* (*S. pneumoniae*) or *Candida albicans* (*C. albicans*) for 4 or 24 h. We found that 12 out of 45 *cis*-eQTL genes (26,67%) were also differentially expressed in at least 1 condition (**Figure 1A**). In addition, we also found another 10 *cis*-genes, which were not implicated by eQTL mapping as causal genes, to be differentially expressed in at least one of the stimulations in PBMC (**Figure 1B**). In the end, by combining these two strategies, we prioritized 55 potential causal genes for sepsis.

Subsets of Prioritized Genes Are Also Associated With Severity of Sepsis

Next, we tested whether some of the prioritized sepsis-associated genes show any correlation with the severity of sepsis. To perform this analysis, we made use of publicly available blood transcriptome data from pneumoniae-derived sepsis patients (13). Out of 55 prioritized genes, we found seven genes that are differentially expressed between severe and mild sepsis patients (**Figure 2**). Among them, expression of *CSGALNACT1* is increased in severe patient group whereas *KLHDC8B*, *BCS1L,* and *NAT6* expression levels were decreased. Interestingly, except *CSGALNACT1*, all the other six genes were eQTL genes for SNPs associated with sepsis onset. This observation suggests that some of the genes associated with disease onset could also be involved in determining disease severity.

There was no evidence for enrichment of these six genes for particular pathways; however, *CYP27A1* and *SLC11A1* are known to be involved in sepsis. CYP27A1 is one of the key enzymes involved in synthesizing bile acid in the liver. Studies have shown that CYP27A1 down regulation in sepsis reduce the amount of circulating bile acid, which may be beneficial for sepsis patients (16, 17). *SLC11A1* encodes for iron channel, involved in cation metabolism and host resistance to infection. SLC11A1 was shown to be associated with active tuberculosis (18–20). It remains to be tested how these genes contribute to sepsis severity.

Around 23% of the Loci Affect Cytokine Production by Leukocytes in Response to Sepsis Causing Pathogens

In addition to a global screening for the effect of 39 suggestive loci on transcriptome response, we also tested their effects in regulating inflammatory cytokine responses, a prominent phenotype in sepsis. We tested if SNPs that are associated with sepsis survival or sepsis onset affect production of cytokines by leukocytes upon stimulation by intersecting our 218 SNPs with cytokine QTL from stimulated PBMCs (10). We found that 9 independent loci affect the production and secretion of six different cytokines in the context of Gram-negative bacteria, Gram- positive bacteria and fungi (**Table 2** and **Figure 3**), albeit with nominal statistical significance ($P < 0.05$). Only two loci, among these 9 loci, are found to be significantly associated with cytokine production in PBMCs after correcting for multiple testing ($P < 0.0012$) (**Table 1**). In particular, SNP rs2237499 affected IL-1β levels upon LPS (Gram-negative bacterial infection), whereas SNP rs13380717 altered IFN-γ levels in response to *C. albicans* hyphae infection. In summary, only around 23% of the sepsis-associated variants affected cytokine production. These results suggest that the other non-cytokine processes are also important for explaining sepsis heterogeneity.

TABLE 2 | Summary table of genes and cytokines of which the expression levels are associated with genetic variations at 39 GWAS suggestive loci. 13/39 loci could alter RNA expression level of 45 nearby genes (cis-eQTL).

Study	Independent loci	cis-eQTL (blood)	eQTL-P value	Cytokine QTL	cQTL-P value
Rautanen A	rs2709532	No		No	
	rs72661895	No		No	
	rs4957796	No		No	
	rs79423885	No		No	
	rs76881522	No		No	
	rs12114790	CSGALNACT1[a]	9.50E-66	IL1b_C.albicansconidia_PBMC_24h	0.010228723
		INTS10	3.27E-09	IL6_C.albicanshyphae_PBMC_24h	0.026800224
				TNFA_C.albicansconidia_PBMC_24h	0.040662939
	rs9566343	No		IL22_C.albicansconidia_PBMC_7days	0.009406105
				IL6_LPS100ng_PBMC_24h	0.022034182
	rs6501341	No		No	
	rs2096460	URB1[a]	6.89E-152	No	
		C21orf119	1.57E-21		
Scherag A	rs382422	WLS[b]	8.66E-12	IFNy_C.albicansconidia_PBMC_7days	0.006355623
	rs150811371	No		No	
	rs945177	No		No	
	rs9529561	No		No	
	rs2641697	CRISPLD2[a,b]	1.18E-08	IL6_S.aureus_PBMC_24h	0.029215619
		KIAA0513[b]	6.31E-07		
	rs7211184	No		No	
	rs58764888	No		No	
	rs72862231	No		No	
	rs150062338	No		No	
	rs10933728	No		No	
	rs115550031	DGKQ[a]	5.95E-06	No	No
	rs62369989	No		IL17_C.albicansconidia_PBMC_7days	0.011402725
	rs117983287	No		No	
	rs409443	No		No	
Srinivasan L	rs3100127	PTPN7	3.48E-91	No	
		LGR6[b]	6.01E-16		
	rs41461846	CYP27A1[b]	3,2717E-310	No	
		RQCD1	3,2717E-310		
		VIL1[a]	4.3769E-101		
		TTLL4[a]	1.3023E-79		
		STK36	9.0469E-76		
		USP37[a]	4.9084E-71		
		SLC11A1[a,b]	3.4111E-61		
		ZNF142	2.6409E-55		
		PRKAG3[b]	6.0805E-38		
		BCS1L	1.8409E-37		
	rs72998754	No		No	
	rs3844280	BRK1[a]	1.83E-180	No	
		LINC00852	6.43E-19		
		FANCD2[a]	8.65E-12		
		IRAK2[a,b]	6.97E-11		
		CRELD1	5.51E-06		
	rs12490944	RBM6[a]	2.01E-195	No	
		HYAL3[b]	2.98E-98		
		MON1A[a]	1.56E-79		

(Continued)

TABLE 2 | Continued

Study	Independent loci	cis-eQTL (blood)	eQTL-P value	Cytokine QTL	cQTL-P value
		UBA7[b]	5.21E-59		
		APEH	5.64E-27		
		AMT	3.54E-21		
		NICN1	2.61E-20		
		IFRD2	4.12E-10		
		NAT6	2.39E-08		
		KLHDC8B[b]	4.60E-08		
		QRICH1	2.34E-07		
		TCTA	1.42E-05		
		MST1[b]	1.57E-05		
		FAM212A	1.74E-05		
	rs17599816	No		No	
	rs6462728	AOAH	1.65E-26	IL17_C.albicansconidia_PBMC_7days	0.010838542
				IL6_C.albicansconidia_PBMC_24h	0.020869368
	rs2237499	LINC00265	4.59E-91	IL1b_LPS100ng_PBMC_24h	0.000626831
		RALA[a]	5.32E-18	TNFA_C.albicansconidia_PBMC_24h	0.012141737
		CDK13	7.48E-14	IL6_LPS100ng_PBMC_24h	0.017978737
				IL1b_E.Coli_PBMC_24h	0.033518435
	rs4730486	IMMP2L	3,2717E-310	No	
	rs513793	No		No	
	rs11597285	No		No	
	rs74487835	No		No	
	rs16913666	No		No	
	rs11840143	No		IL22_C.albicansconidia_PBMC_7days	0.021643788
				IFNy_C.albicansconidia_PBMC_7days	0.049325944
	rs13380717	No		IFNy_C.albicanshyphae_PBMC_7days	2.51E-06
				IL22_C.albicanshyphae_PBMC_7days	0.003182544
				TNFA_E.Coli_PBMC_24h	0.032629607
				IL1b_E.Coli_PBMC_24h	0.043946978
	rs645505	NAPG	5.33E-06	No	

[a] *Gene locates within 200 kb window surrounding the suggestive GWAS loci.*

[b] *eQTL genes of which RNA expression levels are differentially expressed in stimulated PBMCs. 9/39 loci could alter cytokine levels upon stimulation (cytokine-QTL).*

Sepsis Associated Genes Are Enriched for Adherence Junction Pathway

To test if genes affected by sepsis survival associated SNPs are enriched for particular biological pathways, we made use of Pascal pathway prioritization tool (21). Based on the SNP location, and the *P*-value of each SNP, the Pascal software will calculate gene score of nearby genes, and the probability of each gene in involving in any signaling pathways. We initially performed gene prioritization and pathway enrichment analyses for each study separately. However, because of less number of loci from each study, we were unable to see strong enrichment of any pathways. We, therefore, combined all 39 independent loci from three studies and performed enrichment analysis. Interestingly, the enrichment analysis showed significant enrichment of genes for adherences-junction pathway (**Figure 4**).

Particularly, the enrichment analysis was based on 36 genes located within 100 kb of 39 independent SNPs. Among those, there are 17 genes that overlapped with the 55 prioritized genes above (data not shown). These findings strengthen the common notion that disruption in barrier, especially vascular wall leakage is a critical process, which lead to organ dysfunction and mortality in sepsis.

Regulatory Function of GWAS SNP rs4957796 at FER Locus in Endothelial Cells

We showed that many of the sepsis associated SNPs affect gene expression or alter cytokine levels in response to infections in blood. However, we didn't find any association with expression or with cytokine responses for SNP rs4957796, which is the only genome-wide significant SNP from a GWAS, at FER locus (**Table 2**). This SNP is associated with the survival of pneumonia-derived septic patients. However, how the SNP contributes to the disease severity or which genes are affected by this SNP is not clearly established. Therefore, we conducted experiments in both

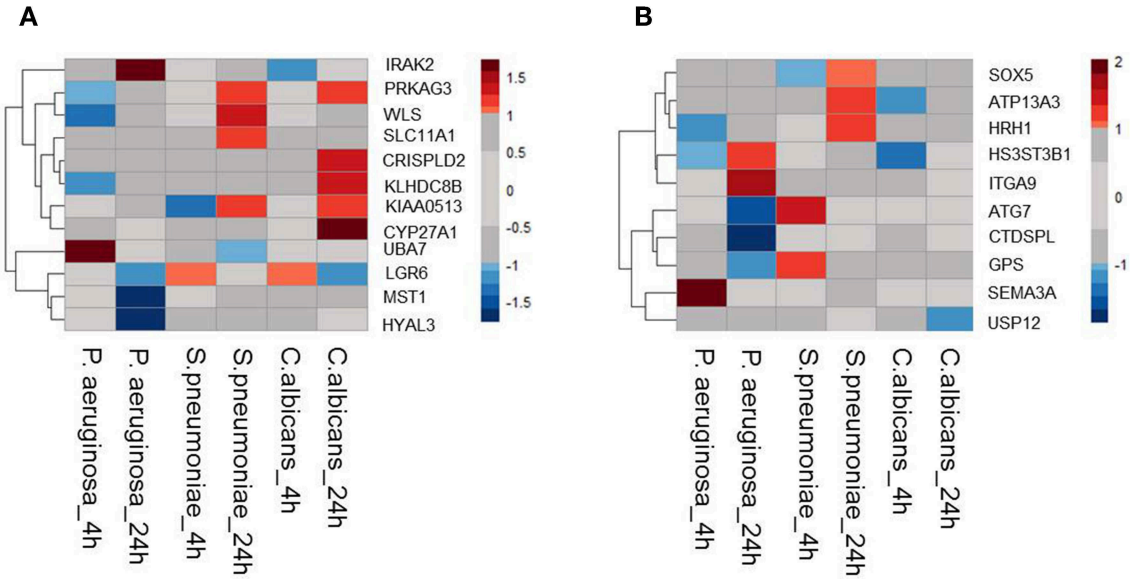

FIGURE 1 | Expression QTL mapping and differential expression analyses prioritized potential genes. **(A)** Among 45eQTL genes, there are 12 genes that are differentially expressed in at least one condition in stimulated PBMCs. **(B)** Expression levels of cis genes that have not eQTL effect in blood, but differentially expressed upon stimulation in PBMC. Heatmap was plotted based on log2 (Fold-change) of RNA expression levels in *P.aeruginosa*, *S.pneumoniae,* and *C.albicans*-stimulated PBMCs. RNA expression levels were measured after 4 or 24 h of stimulation. Colors represent the RNA expression levels, red, significantly induced genes; blue, significantly suppressed genes; gray, not significantly different between stimulated and non-stimulated PBMCs.

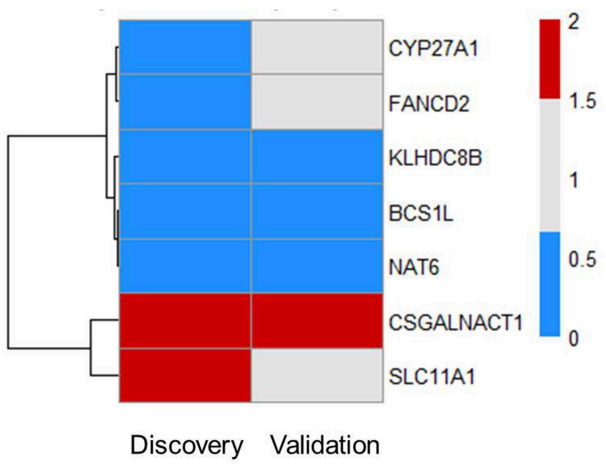

FIGURE 2 | Subsets of prioritized genes are also associated with severity of sepsis. Among 55 genes, there are seven genes that are DE in patients (FC > 1.5 and FDR ≤ 0.05). Heat map shows RNA expression levels of seven genes in both discovery and validation cohort. Colors represent expression levels by fold-change between two groups: severe patients SR1 vs. mild patients SR2. Blue, significantly lowly expressed in the severe group; red, significantly highly expressed in the severe group; white, non-significantly different between the severe and mild groups (13).

immune cells and endothelial cells (HUVEC), which play central roles in sepsis pathogenesis (22).

To gain further insight into the function of this SNP, we tested if the SNP could alter the binding site of transcription factors. The alteration of nucleotide composition can lead to changes in the binding of these transcription factors, hence, affecting expression levels of genes. Based on weight matrix prediction (23) this SNP is located in the binding motif of several transcription factors (**Figure S1**). Next, we tested the expression of these transcription factors both in stimulated PBMCs and endothelial cells. We found that ARID5A, E4BP4, HLF, Jundm2, and Ncx_2 differentially expressed in PBMCs upon stimulation. On the other hand, these transcription factors (ARID5A, BBX, E4BP4, FOXL1, Jundm2, Mef2, TBP, and p300) were expressed in endothelial cells, yet the expression levels were not altered by stimulation of IL1β, TNFα, or LPS. Next, we performed electrophoresis molecular shift assay (EMSA) to validate if the SNP can alter binding affinities of transcription factors in endothelial cells (HUVEC) and monocytes (THP-1). We found that the alteration of T (the risk allele) to C allele (the alternative allele) resulted in changes in the competition of at least two transcription factors in binding to the locus (**Figure 5A**). The effects were shared between both cell types. These findings indicated that the genome-wide significant SNP at FER locus could alter the binding of transcription factors in endothelial cells as well as in monocytes to influence the expression of *cis*-genes. Therefore, future studies should generate large scale endothelial cell gene expression data upon relevant stimulations to establish the link between sepsis associated SNPs and cis-genes.

Both FER and MAN2A1 Alter Endothelial Cell Responses to Stimulation

Previous studies have speculated that *FER* could be a potential causal gene at this locus (4). However, the expression levels

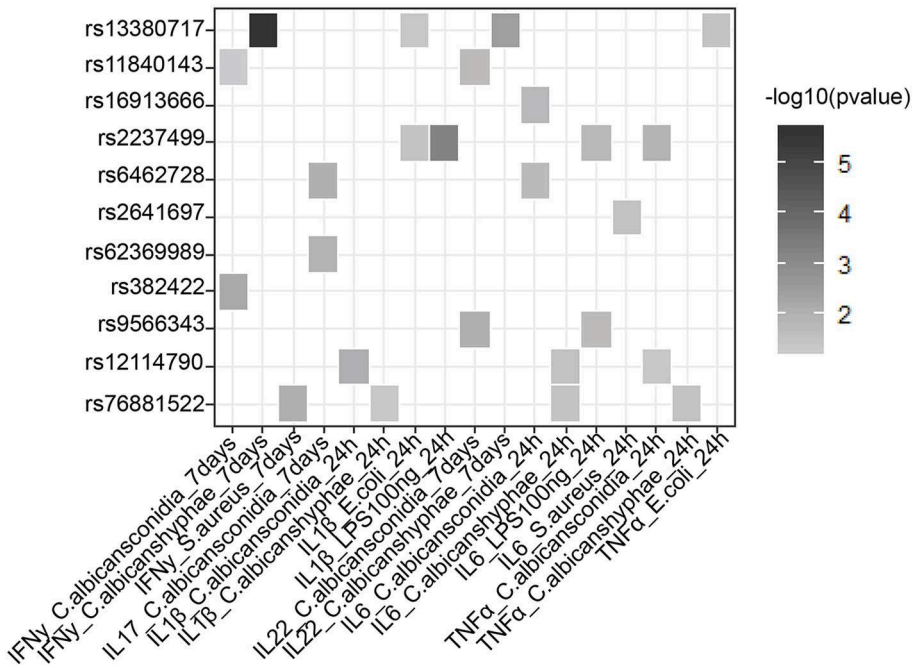

FIGURE 3 | Suggestive GWAS loci could influence the production of cytokines from PBMC in response to infection. Heat map shows cytokine- QTL (cQTL) effect of the suggestive SNPs (*P*-value ≤0.05), based on 500 FG cytokine QTL data (10). Empty boxes indicate no cQTL relationship between the SNPs and cytokine production. Color darkness was scaled base on –log10 (*P*-value).

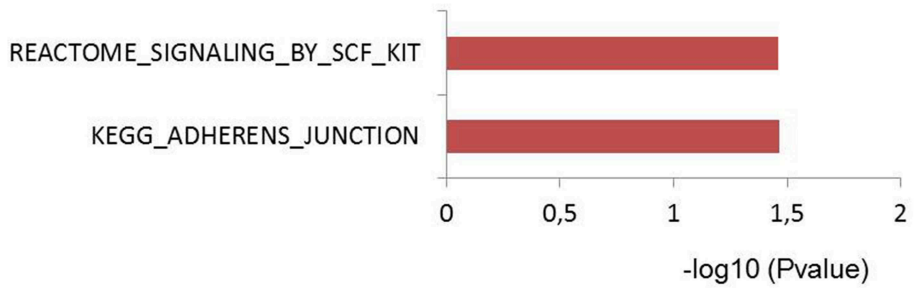

FIGURE 4 | Pascal pathway enrichment for 39 independent suggestive-GWAS loci (21). Y axis: pathways enriched by Reactome and KEGG database. X axis: –log(10) of *q*-value.

of this gene in blood of sepsis patients did not show any correlation with the severity of sepsis (13). As SNPs can alter expression levels of multiple *cis*-genes, we tested if the expression of other nearby genes are associated with the disease severity using the data from Davenport et al. (13) and found *MAN2A1* to be differentially expressed between the two patient groups. We first stimulated endothelial cells with different infectious agents representative of Gram-negative bacterial antigen (LPS), Gram-positive bacteria (*Streptococcus pneumoniae*), and Fungus (*Candida albicans*). We observed strong activation of endothelial cells by LPS but not by other stimuli (**Figure S2**). We therefore focused only on LPS stimulation for knockdown experiments. We then performed transient knockdown experiments on both *FER* and *MAN2A1* genes in endothelial cells using gene-specific siRNAs. Interestingly, both *FER* and *MAN2A1* deficiency in HUVEC altered the cell response to LPS stimulation. We found that the knockdown of *MAN2A1* showed stronger effect on the expression of both adhesion molecules (E-selectin and ICAM-1) and cytokine genes (IL-8) (**Figure 5B**). Although, it is still needed to establish the connection between SNP and these two genes, these preliminary results highlight the role of more than one causal gene at this locus.

DISCUSSION

Host genetic variation is an important factor in explaining susceptibility to infectious diseases in general, and sepsis heterogeneity in particular. Up to now, three genome-wide association studies on sepsis have been conducted. However, due to limited sepsis patient cohort size and extreme heterogeneity,

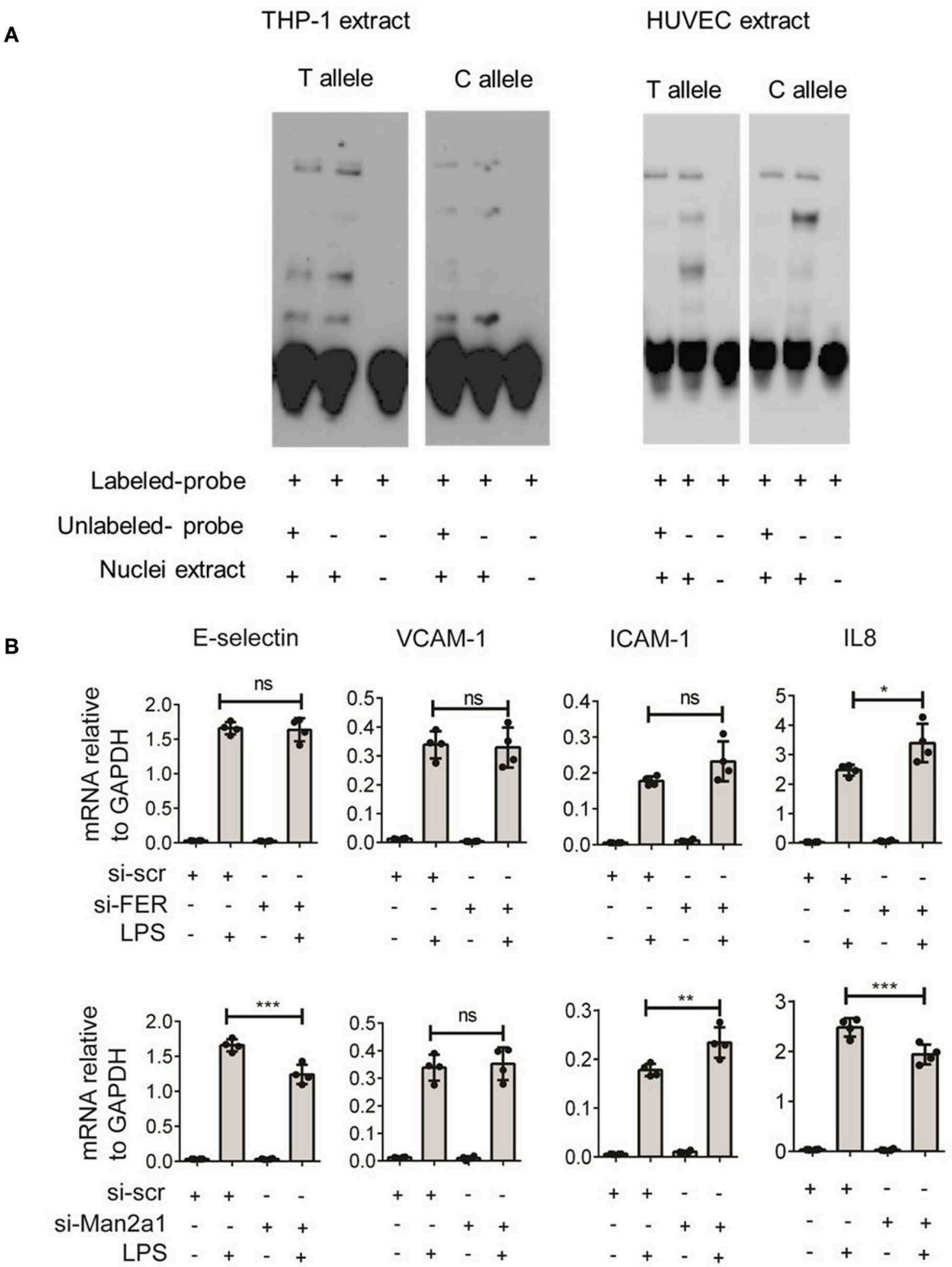

FIGURE 5 | Validation of rs4957796 SNP. **(A)** EMSA (electrophoresis molecular shift assay) of oligos resembling the sequence of 30 nts surrounding the top SNP: rs4957796, containing either T or C allele. The shift in the position of the probe carrying T or C allele indicated the effect of nucleotide alteration at rs4957796 in changing the binding affinity of transcription factor. **(B)** Effect of *FER* or *MAN2A1* deficiency in HUVEC on the expression of adhesion molecules and cytokines. RNA expression levels of E-selectin, VCAM-1, ICAM-1, and IL-8 in HUVEC after 4 h of stimulation were measured by RT-qPCR. Each dot represents one sample. Data represent for three replications.

only one significant locus was identified by a GWAS. Nevertheless, the suggestive associations implicated by these three studies may provide novel insight into genes and pathways that are relevant for understanding sepsis heterogeneity.

In this study, we took advantage of existing molecular data and integrative functional genomics approach to reveal potential causal genes and pathways associated with sepsis heterogeneity. Firstly, we show that <30% of the sepsis associated loci affect cytokine production in response to pathogens. Some of these cytokine-affecting SNPs may be regulated via their effect on expression levels of its nearby genes (eQTL genes). For example, a *WLS* gene is located in cis-region of a SNP that affects IFN-γ production in PBMCs in response to Candida conidia (**Table 1**). In NK T cells, it is shown that the *WLS* gene can activate IFN-γ production independent of Wnt/B-catenin pathway (24). Another SNP that is associated with IL17 and IL6 levels upon Candida albicans conidida stimulation in PBMCs is close to *AOAH* gene (**Table 2**). *AOAH* codes for acyloxyacyl hydrolase that can deacylates and inactivate LPS, a toxin presented on Gram-negative bacteria wall. Studies have shown that *AOAH* can drive TH17 T cell differentiation via secreting IL-6 in mice (25). Therefore, it is likely that some of these genes may affect sepsis via regulating cytokine levels in response to infections.

On the other hand, it is possible that because of the lack of sufficient statistical power in these studies, some of these associations could be false positive findings. Nevertheless, it is interesting to observe that more than 70% of the loci were not correlated with cytokine levels suggesting the role of other functional pathways in sepsis. In concordance with this we also show that, by applying PASCAL gene prioritization tool, *cis*-genes are enriched for adherens junction pathway. However, pathway enrichment analysis on only eQTL genes did not reveal any pathways. It may be due to the fact that genetic effects on gene expression can be very tissue and stimulation specific (7). Therefore, the expression quantitative trait analysis in healthy blood samples may not reflect the effect of sepsis-associated genetic variants. More studies are needed to investigate the effect of genetic variants on different pathways such as coagulation, blood pressure, barrier dysfunction, and vascular leakage that are pivotal for sepsis pathogenesis. Our EMSA assays on a SNP located within FER locus also suggested that some of these sepsis associated SNPs may affect more than one causal genes. Therefore, these factors need to be taken into account when we establish causal genes from association studies. Nevertheless, eQTL mapping shows that 33% suggestive sepsis-associated loci can affect expression levels of 55 potential causal genes and some of these genes are differentially regulated in patients with severe sepsis compared to mild sepsis patient group. These genes are of interest to perform further functional studies to understand their role in sepsis onset and survival.

Our study also has several limitations. When we compared the sepsis associated SNPs from all three GWAS, we found that none of the SNPs were replicated in each other's study. This could be either due to the limited sample size and/or the extreme heterogeneity among sepsis patients caused by several factors including age of patients, type of infectious agents, clinical treatments etc. Therefore, in the future, a large-scale meta-analysis on stratified groups of sepsis patients should be done to identify genetic variations determining sepsis onset, sepsis severity or sepsis mortality. Moreover, to overcome the heterogeneity of sepsis, GWAS on sepsis-associated phenotypes such as vascular leakage, hypertension, organ damage will also be informative to gain further insights into sepsis endo-phenotypes. Secondly, eQTL mapping results were extracted only from whole blood of healthy individuals in this study. Given the prominent role of endothelial and other cell types in sepsis, future studies should focus on generating tissue and context-specific gene expression data to reveal causal genes for sepsis.

To conclude, our approach in this study provides evidence for genetically determined variability in endothelial pathways, in addition to leucocyte responses, as one of the important factors to explain sepsis heterogeneity. Future challenge is therefore to exploit the impact of genetic variation on endothelial cell related processes using both experimental and clinical studies, to develop new treatment options for sepsis.

DATA AVAILABILITY

Publicly available datasets were analyzed in this study. This data can be found here: 500 FG cytokine: https://hfgp.bbmri.nl/, eQTL: http://www.eqtlgen.org/.

AUTHOR CONTRIBUTIONS

VK is accredited to the study conceptualization. KL, JM, and VK designed the study. KL performed experiments. KL and VM analyzed the data. MN, JM, and CW provided reagents, protocols, and facilities to conduct experiments. KL and VK prepared the manuscript. MN, CW, JM, and VK interpreted results and critically assessed the manuscript.

FUNDING

This work was supported by the Ph.D. fellowship by the Graduate School of Medical Science, UMC Groningen to KL, Radboud UMC Hypatia Tenure Track Grant and a Research Grant [2017] of the European Society of Clinical Microbiology and Infectious Diseases (ESCMID) to VK and NOCI grant from NWO gravitation grant to CW and Spinoza grant of the Netherlands Organization for Scientific Research to MN.

ACKNOWLEDGMENTS

We thank all the volunteers for donating PBMC for this study. We are grateful to authors of previous studies of whose the dataset were publically available and facilitate our studies. We thank our colleagues within the Genetics department and the EBVDT group for fruitful discussion.

SUPPLEMENTARY MATERIAL

The Supplementary Material for this article can be found online at: https://www.frontiersin.org/articles/10.3389/fimmu.2019.01949/full#supplementary-material

REFERENCES

1. Singer M, Deutschman CS, Seymour C, Shankar-Hari M, Annane D, Bauer M, et al. The third international consensus definitions for sepsis and septic shock (sepsis-3). *JAMA*. (2016) 315:801–10. doi: 10.1001/jama.2016.0287
2. Fleischmann-Struzek C, Goldfarb DM, Schlattmann P, Schlapbach LJ, Reinhart K, Kissoon N. The global burden of paediatric and neonatal sepsis: a systematic review. *Lancet Respir Med.* (2018) 6:223–30. doi: 10.1016/S2213-2600(18)30063-8
3. Vandervelden S, Malbrain ML. Initial resuscitation from severe sepsis: one size does not fit all. *Anaesthesiol Intensive Ther.* (2015) 47:Spec No:s44-55. doi: 10.5603/AIT.a2015.0075
4. Rautanen A, Mills TC, Gordon AC, Hutton P, Steffens M, Nuamah R, et al. Genome-wide association study of survival from sepsis due to pneumonia: an observational cohort study. *Lancet Respir Med.* (2015) 3:53–60. doi: 10.1016/S2213-2600(14)70290-5
5. Scherag A, Schoneweck F, Kesselmeier M, Taudien S, Platzer M, Felder M, et al. Genetic factors of the disease course after sepsis: a genome-wide study for 28 day mortality. *EBioMedicine.* (2016) 12:239–46. doi: 10.1016/j.ebiom.2016.08.043
6. Srinivasan L, Page G, Kirpalani H, Murray JC, Das A, Higgins RD, et al. Genome-wide association study of sepsis in extremely premature infants. *Arch Dis Childhood*. (2017) 102:F439–45. doi: 10.1136/archdischild-2016-311545
7. Gallagher MD, Chen-Plotkin A. The post-GWAS era: from association to function. *Am J Hum Genet.* (2018) 102:717–30. doi: 10.1016/j.ajhg.2018.04.002
8. Matzaraki V, Gresnigt MS, Jaeger M, Ricano-Ponce I, Johnson MD, Oosting M, et al. An integrative genomics approach identifies novel pathways that influence candidaemia susceptibility. *PLoS ONE.* (2017) 12:e0180824. doi: 10.1371/journal.pone.0180824
9. Tak YG, Farnham PJ. Making sense of GWAS: using epigenomics and genome engineering to understand the functional relevance of SNPs in non-coding regions of the human genome. *Epigenet Chrom.* (2015) 8:57. doi: 10.1186/s13072-015-0050-4
10. Li Y, Oosting M, Smeeken SP, Jaeger M, Aguirre-Gamboa R, Le KTT, et al. A functional genomics approach to understand variation in cytokine production in humans. *Cell.* (2016) 167:1099–110. doi: 10.1016/j.cell.2016.10.017
11. Võsa U, Claringbould A, Westra H, Jan Bonder M, Deelen P, Zeng B, et al. Unraveling the polygenic architecture of complex traits using blood eQTL meta-analysis. *bioRxiv*. (2018) 18:10–10. doi: 10.1101/447367
12. Li Y, Oosting M, Deelen P, Ricano-Ponce I, Smeekens S, Jaeger M, et al. Inter-individual variability and genetic influences on cytokine responses to bacteria and fungi. *Nat Med.* (2016) 22:952–60. doi: 10.1038/nm.4139
13. Davenport EE, Burnham KL, Radhakrishnan J, Humburg P, Hutton P, Mills TC, et al. Genomic landscape of the individual host response and outcomes in sepsis: a prospective cohort study. *Lancet Respir Med.* (2016) 4:259–71. doi: 10.1016/S2213-2600(16)00046-1
14. Moser J, Heeringa P, Jongman RM, Zwiers PJ, Niemarkt AE, Yan R, et al. Intracellular RIG-I signaling regulates TLR4-Independent endothelial inflammatory responses to endotoxin. *J Immunol.* (2016) 196:4681–91. doi: 10.4049/jimmunol.1501819
15. Chen R, Morgan AA, Dudley J, Deshpande T, Li L, Kodama K, et al. FitSNPs: highly differentially expressed genes are more likely to have variants associated with disease. *Genome Biol.* (2008) 9:R170. doi: 10.1186/gb-2008-9-12-r170
16. Matsuzaki Y, Bouscarel B, Ikegami T, Honda A, Doy M, Ceryak S, et al. Selective inhibition of CYP27A1 and of chenodeoxycholic acid synthesis in cholestatic hamster liver. *Biochim Biophys Acta*. (2002) 1588:139–48. doi: 10.1016/S0925-4439(02)00157-6
17. Bhogal HK, Sanyal AJ. The molecular pathogenesis of cholestasis in sepsis. *Front Biosci.* (2013) 5:87–96. doi: 10.2741/E598
18. Bellamy R, Ruwende C, Corrah T, McAdam PWJK, Whittle CH, Hill VSA, et al. Variations in the Nramp1 gene and susceptibility to tuberculosis. *N Engl J Med.* (1998) 338:640–4. doi: 10.1056/NEJM199803053381002
19. Velez DR, Hulme WF, Myers JL, Stryjewski ME, Abbate E, Estevan R, et al. Association of SLC11A1 with tuberculosis and interactions with NOS2A and TLR2 in African-Americans and Caucasians. *Int J Tuberculosis Lung Dis.* (2009) 13:1068–76.
20. Li XW, Yang Y, Zhou F, Zhang Y, Lu H, Jin Q, et al. SLC11A1 (NRAMP1) polymorphisms and tuberculosis susceptibility: updated systematic review and meta-analysis. *PLoS ONE.* (2011) 6:2–9. doi: 10.1371/journal.pone.0015831
21. Lamparter D, Marbach D, Rueedi R, Kutalik Z, Bergmann S. Fast and rigorous computation of gene and pathway scores from SNP-based summary statistics. *PLoS Comput Biol.* (2016) 12:1–20. doi: 10.1371/journal.pcbi.1004714
22. Van Der Poll T, Van De Veerdonk FL, Scicluna BP, Netea MG. The immunopathology of sepsis and potential therapeutic targets. *Nat Rev Immunol.* (2017) 17:407–20. doi: 10.1038/nri.2017.36
23. Kheradpour P, Ernst J, Melnikov A, Rogov P, Wang L, Zhang X, et al. Systematic dissection of regulatory motifs in 2000 predicted human enhancers using a massively parallel reporter assay. *Genome Res.* (2013) 23:800–11. doi: 10.1101/gr.144899.112
24. Kling JC, Jordan MA, Pitt LA, Meiners J, Thanh-Tran T, Tran LS, et al. Temporal regulation of natural killer T cell interferon gamma responses by β-catenin-dependent and-independent wnt signaling. *Front Immunol.* (2018) 9:483. doi: 10.3389/fimmu.2018.00483
25. Janelsins BM, Lu M, Datta SK. Altered inactivation of commensal LPS due to acyloxyacyl hydrolase deficiency in colonic dendritic cells impairs mucosal Th17 immunity. *Proc Natl Acad Sci USA.* (2013) 111:373–8. doi: 10.1073/pnas.1311987111

Conflict of Interest Statement: The authors declare that the research was conducted in the absence of any commercial or financial relationships that could be construed as a potential conflict of interest.

Copyright © 2019 Le, Matzaraki, Netea, Wijmenga, Moser and Kumar. This is an open-access article distributed under the terms of the Creative Commons Attribution License (CC BY). The use, distribution or reproduction in other forums is permitted, provided the original author(s) and the copyright owner(s) are credited and that the original publication in this journal is cited, in accordance with accepted academic practice. No use, distribution or reproduction is permitted which does not comply with these terms.

frontiers in Immunology

ORIGINAL RESEARCH
published: 21 August 2019
doi: 10.3389/fimmu.2019.01920

Midkine Is Elevated After Multiple Trauma and Acts Directly on Human Cardiomyocytes by Altering Their Functionality and Metabolism

Ina Lackner[1], Birte Weber[1], Meike Baur[1], Melanie Haffner-Luntzer[2], Tim Eiseler[3], Giorgio Fois[4], Florian Gebhard[1], Borna Relja[5], Ingo Marzi[5], Roman Pfeifer[6], Sascha Halvachizadeh[6], Miriam Lipiski[7], Nikola Cesarovic[7], Hans-Christoph Pape[6], Miriam Kalbitz[1] and TREAT Research Group*

[1] Department of Traumatology, Hand, Plastic, and Reconstructive Surgery, Center of Surgery, University of Ulm, Ulm, Germany, [2] Institute of Orthopedic Research and Biomechanics, University of Ulm, Ulm, Germany, [3] Department of Internal Medicine I, University of Ulm, Ulm, Germany, [4] Institute of General Physiology, University of Ulm, Ulm, Germany, [5] Department of Trauma, Hand and Reconstructive Surgery, Goethe University Frankfurt, Frankfurt, Germany, [6] Department of Trauma, University Hospital of Zurich, Zurich, Switzerland, [7] Department of Surgical Research, University Hospital of Zurich, Zurich, Switzerland

OPEN ACCESS

Edited by:
Lukas Martin,
University Hospital RWTH Aachen, Germany

Reviewed by:
Juerg Hamacher,
Lindenhofspital, Switzerland
Sergio Iván Valdés-Ferrer,
Instituto Nacional de Ciencias Médicas y Nutrición Salvador Zubirán (INCMNSZ), Mexico
Sandra Kraemer,
University Hospital RWTH Aachen, Germany

***Correspondence:**
Miriam Kalbitz
miriam.kalbitz@uniklinik-ulm.de

Specialty section:
This article was submitted to Inflammation, a section of the journal Frontiers in Immunology

Received: 29 April 2019
Accepted: 29 July 2019
Published: 21 August 2019

Citation:
Lackner I, Weber B, Baur M, Haffner-Luntzer M, Eiseler T, Fois G, Gebhard F, Relja B, Marzi I, Pfeifer R, Halvachizadeh S, Lipiski M, Cesarovic N, Pape H-C, Kalbitz M and TREAT Research Group (2019) Midkine Is Elevated After Multiple Trauma and Acts Directly on Human Cardiomyocytes by Altering Their Functionality and Metabolism. Front. Immunol. 10:1920. doi: 10.3389/fimmu.2019.01920

Background and Purpose: Post-traumatic cardiac dysfunction often occurs in multiply injured patients (ISS $\geq$ 16). Next to direct cardiac injury, post-traumatic cardiac dysfunction is mostly induced by the release of inflammatory biomarkers. One of these is the heparin-binding factor Midkine, which is elevated in humans after fracture, burn injury and traumatic spinal cord injury. Midkine is associated with cardiac pathologies but the exact role of Midkine in the development of those diseases is ambiguous. The systemic profile of Midkine after multiple trauma, its effects on cardiomyocytes and the association with post-traumatic cardiac dysfunction, remain unknown.

Experimental Approach: Midkine levels were investigated in blood plasma of multiply injured humans and pigs. Furthermore, human cardiomyocytes (iPS) were cultured in presence/absence of Midkine and analyzed regarding viability, apoptosis, calcium handling, metabolic alterations, and oxidative stress. Finally, the Midkine filtration capacity of the therapeutic blood absorption column CytoSorb ®300 was tested with recombinant Midkine or plasma from multiply injured patients.

Key Results: Midkine levels were significantly increased in blood plasma of multiply injured humans and pigs. Midkine acts on human cardiomyocytes, altering their mitochondrial respiration and calcium handling *in vitro*. CytoSorb®300 filtration reduced Midkine concentration *ex vivo* and *in vitro* depending on the dosage.

Conclusion and Implications: Midkine is elevated in human and porcine plasma after multiple trauma, affecting the functionality and metabolism of human cardiomyocytes *in vitro*. Further examinations are required to determine whether the application of CytoSorb®300 filtration in patients after multiple trauma is a promising therapeutic approach to prevent post-traumatic cardiac disfunction.

Keywords: polytrauma, cardiac dysfunction, fracture treatment, damage associated molecular pattern, toll-like receptor, toll-like receptor signaling, prevention cardiac injury, CytoSorb® 300

INTRODUCTION

According to the World Health Organization (WHO), trauma accounts for 10% of deaths and 16% of disabilities worldwide (1). Multiple trauma in humans (Injury Severity Score, ISS $\geq$ 16) are characterized by a massive release of different inflammatory biomarkers, such as cytokines, and damage associated molecular patterns (DAMPs). This damage affects different organs of the body and can trigger whole-body inflammation after trauma (2, 3). A substantial release of these trauma-dependent molecules is associated with the development of the so-called systemic inflammatory response syndrome (SIRS) and the multiple organ dysfunction syndrome (MODS), which are both associated with an increased mortality (4, 5). Many of the released inflammatory cytokines and DAMPs were recently shown to be cardio-depressive by acting on cardiomyocytes (CMs), altering their calcium handling, redox balance, signaling transduction, and finally resulting in post-traumatic cardiac dysfunction (6, 7). One inflammatory cytokine is the heparin-binding growth- and differentiation factor Midkine (Mdk). Increased Mdk expression is associated with different traumatic conditions such as bone fracture, burn injury, traumatic spinal cord injury, and sepsis (8–11). Increased Mdk in human blood can persist for overall 42 days after fracture (11). Furthermore, Mdk impairs fracture healing by reducing bone formation and increasing neutrophil infiltration during the fracture healing process (12, 13). However, the trauma-dependent elevation of Mdk in multiply injured patients as well as the exact impact of Mdk on the heart after trauma remains unclear. In patients with chronic heart failure, circulating Mdk increases significantly and is regarded as a novel marker, predicting different cardiac events (14, 15). Moreover, Mdk plays a role in ischemic heart injury, myocardial infarction and cardiac hypertrophy (16–18). Nevertheless, the function of Mdk in these different pathologies is still controversial, because in some cases such as ischemic heart injury, chronic heart failure and myocardial infarct, Mdk has positive effects by improving cell survival and cardiac function, inducing angiogenesis and reducing detrimental remodeling (17, 19, 20). In contrast, Mdk reduces cellular survival and induces pathological remodeling as well as fibrosis in patients with cardiac hypertrophy (18). Consequently, the exact effect of Mdk on the heart is ambiguous since Mdk can have beneficial and detrimental effects in cardiac pathology. The function of Mdk as an inflammatory cytokine on the heart during trauma especially requires clarification. After all, Mdk might be a potential therapeutic option in cardiac diseases as well as in the treatment and prevention of post-traumatic cardiac injury (21, 22). Mdk has been shown to play an important role in active myocarditis in patients and in experimental autoimmune myocarditis in mice (23). In these instances, Mdk promotes the recruitment of polymorphonuclear neutrophils (PMNs) and the production of neutrophil extracellular traps (NETs) in cardiac tissues, resulting in impaired systolic function (23). Increased activation and recruitment of neutrophils in cardiac tissue were also observed in humans after trauma and in experimental blunt chest trauma models in rats. In addition, it is linked to increased systemic levels of extracellular histones by NETosis, leading to cardiac dysfunction (24, 25).

In this study, we investigate the Mdk elevation in blood circulation after multiple trauma in pigs and humans. We further aim to thoroughly examine the effects of Mdk on human CMs. With regards to therapeutic options for posttraumatic cardiac dysfunction, the study aims to investigate the usage of CytoSorb® 300 hemadsorption. In clinical settings, CytoSorb® 300 hemadsorption improved the outcome of patients with endotoxemia, necrotizing fasciitis, septic shock, and cardiac surgery (26–29). Furthermore, CytoSorb® hemadsorption resulted in immediate hemodynamic stabilization and increased survival rates in patients with multiple organ failure (30). CytoSorb® 300 consists of highly porous (styrene-co-divinylbenzene) hemadsorbent polymer beads, which can remove substances within 10–60 kDa of molecular weight, such as complement factor 5a, cytokines DAMPs and pathogen associated molecular patterns (PAMPs), from circulating blood (26, 31). Similarly, the high-mobility group box 1 protein (HMGB1) can be removed from blood in a time dependent manner (31). Lastly, the study examines the capacity of CytoSorb® 300 to filtrate Mdk, which may be used as a therapeutic approach for preventing and handling post-traumatic cardiac dysfunction.

MATERIALS AND METHODS

Human Blood Samples

Human plasma from 11 multiply injured patients with a history of acute blunt or penetrating trauma and an ISS $\geq$ 16 was collected after hospital admission in the University Hospital of the Goethe-University Frankfurt with institutional ethics committee approval (312/10), in accordance with the Declaration of Helsinki and following the Strengthening the Reporting of Observational studies in Epidemiology (STROBE)-guidelines (32). All enrolled patients either signed the written informed consent form or written informed consent was obtained from the nominated legally authorized representative of the participants in accordance with ethical standards. Exclusion criteria were the patients being younger than 18 or older than 80 years, presenting severe burn injury, acute myocardial stroke, cancer or chemotherapy, immunosuppressive drug therapy, HIV, infectious Hepatitis, acute CMV infection, and/or thromboembolic events. Control blood samples were collected from healthy volunteers ($n = 6$, 50:50 female male, no comorbidities). Randomization of the groups was not possible during the sample collection. Blood samples were withdrawn in ethylenediaminetetraacetic acid (EDTA) tubes (Sarstedt, Nürmbrecht, Germany) directly after admission. The samples were kept on ice until centrifugation at 2,100 g for 15 min. Then, the supernatant was collected and stored at $-80°$C until assay.

Animals

This study presents partial results obtained from a large animal porcine multiple trauma model, conducted by the TREAT research group.

The animal housing and experimental protocols were approved by the Cantonal Veterinary Department, Zurich, Switzerland, under license no. ZH 138/2017, and were in accordance with Swiss Animal Protection Law. Housing and experimental procedures also conformed to the European Directive 2010/63/EU of the European Parliament and of the Council on the Protection of vertebrate animals used for scientific purposes (Council of Europe no. 123, Strasbourg 1985) and to the Guide for the Care and Use of Laboratory Animals (Institute of Laboratory Animal Resources, National Research Council, National Academy of Sciences, 2011). Twenty-five male pigs weighting 50 ± 5 kg (*Sus scrofa domestica*) were included in the study (mean height, snout-tail length: 123,6 cm). Animals were held in a controlled environment with 21 ± 3°C room temperature (50% humidity), with a light/dark cycle of 12 h. Water was available for animals *ad libitum*. General instrumentation, anesthesia and trauma induction were described previously by Horst et al. (33).

Analgesia and Anesthesia

For premedication, pigs received an intramuscular injection with ketamine (20 mg/kg body weight), azaperone (1–2 mg/kg body weight) and atropine (0.1–0.2 mg/kg body weight). Anesthesia was performed by intravenous application of propofol (2,6-diisopropylphenol) (1–2 mg/kg body weight). Anesthesia was maintained during the study period with propofol (5–10 mg/kg/h). Pain medication was ensured by sufentanyl (1 μg/kg/h) perfusion over the whole observation period.

Multiple Trauma in Pigs

Analgesia and Anesthesia of the animals was maintained during the whole procedure.

Pigs underwent either multiple trauma ($n = 20$) or sham-procedure ($n = 5$). Multiple trauma includes a combination of a penetrating thorax trauma, laparotomy, liver laceration, femur fracture, and hemorrhagic shock (ISS ≥ 27). Control animals underwent sham-procedure ($n = 5$). Femur fracture was induced by a bolt gun (Blitz-Kernen, turbocut JOBB GmbH, Germany), positioned on the mid third of the left femur. The gun was loaded with cattle-killing cartridges (9 x 17; DynamitNobel AG, Troisdorf, Germany). For introduction of blunt chest trauma, a pair of panels (steel 0.8 cm, lead 1.0 cm thickness) was placed on the right dorsal lower chest. A shock wave was induced by a bolt shot (Blitz-Kerner, turbocut JOBB GmbH, Germany), which was applied onto the panel using cattle-killing cartridges as previously described (34, 35). Midline-laparotomy was performed by exploring the right upper liver lobe. Penetrating hepatic injury was induced by cross-like incision halfway through the liver tissue. After a short period of uncontrolled bleeding (30 s), liver package was performed. Directly after the hepatic package, pressure-controlled and volume-limited hemorrhagic shock was induced by withdrawing blood until a mean arterial pressure (MAP) of 30 ± 5 mm Hg was reached. Maximal withdrawal amounts to 45% of total blood volume. The reached MAP was maintained for 60 min. At the end of the shock period, animals were resuscitated according to established trauma guidelines (ATLS®, AWMF-S3 guideline on Treatment of Patients with Severe and Multiple Injuries®) by adjusting FiO_2 and an initial substitution of the withdrawn blood volume with Ringerfundin, fluid maintenance was performed by continuous infusing additional fluids (Ringerfundin, 2 ml/kg body weight/h). Moreover, pigs were rewarmed until normothermia (38.7–39.8°C) was reached. Sham procedure ($n = 5$) included instrumentation and anesthesia but without trauma or hemorrhage. The multiple trauma group ($n = 20$) was randomized in four therapy arms: pigs received either femoral nailing without reaming ($n = 5$), standard reaming ($n = 5$), reamed irrigation and aspiration (RIA I) ($n = 5$) or reamed irrigation and aspiration with reduced diameter and improved control of irrigation and suction (RIA II) ($n = 5$). In all groups a shortened conventional tibia nail was introduced.

Follow-Up and Euthanasia

Hemodynamic parameters were continuously monitored for 6 h. Pigs were euthanized under deep general anesthesia with intravenous Na-Pentobarbital.

This animal model represents a clinically relevant porcine model of severe multiple trauma (pulmonary contusion, extremity injury, liver laceration) with post-traumatic observation period under ICU conditions (33).

Sample Collection

Serum and plasma samples were collected at baseline, 4 and 6 h after multiple trauma and kept on ice. After centrifugation (1,500 g for 12 min at 4°C), serum and EDTA-plasma were removed and stored at −80°C until analysis. Heart tissue samples were obtained 6 h after resuscitation. Tissue of the superficial and the luminal left ventricle was fixed with 4% formalin, followed by embedding in paraffin. Furthermore, tissue was quick-frozen in liquid nitrogen, followed by storage at −80°C until analysis.

Midkine ELISA

For determination of Midkine in human and porcine plasma, as well as for the CytoSorb® 300 experiments, the human Midkine ELISA (R&D Systems, McKinley, MN, USA) was used. All procedures were performed according to manufacturers' instructions. Midkine ELISA was performed by a blinded investigator. Human plasma samples were diluted 1:4 and porcine plasma samples were diluted 1:2.

ips-Cardiomyocyte Cell Culture

Human cardiomyocytes (iPS) (Cellular Dynamics, Madison, WI, USA) were cultured for 10 days in maintenance medium at 37°C and in an atmosphere of 7% CO_2, according to manufacturers' recommendations.

Binding Analysis of FITC-Labeled Midkine

Fluorescein isothiocyanate (FITC) (Sigma Aldrich, St. Louis, MO, USA) was dissolved in DMSO. Two mg/ml Midkine (Dianova, Hamburg, Germany), dissolved in 0.1 M $NaHCO_3$ were added to 3 mg/ml fluorescein isothiocyanate (FITC) (Sigma Aldrich, St. Louis, MO, USA) solution and were incubated for 1 h at RT while continuously shaking. Unbound FITC was removed

by using SnakeSkin® dialysis tube (ThermoScientific, Waltham, MA, USA). For dialysis, 1X phosphate buffered saline was used. Human CMs were seeded at a density of 6.3×10^4 cells/cm^2 on ibidi 12-well chamber slides (ibidi, Germany). Afterwards, cells were incubated for 30 and 60 min with 100 ng/ml FITC-labeled Midkine. Cells were washed, fixed with 4% formalin and cell nuclei were counterstained using Hoechst (Sigma Aldrich, St. Louis, MO, USA). Cells were mounted with ProLong® Gold Antifade Mountant (ThermoScientific, Waltham, MA, USA). Cells were analyzed by blinded investigator by using Axio Imager M.2 microscope (Zeiss, Jena, Germany) and the Zeiss ZEN 2.3 software (Zeiss, Jena, Germany). Images were performed with 40x magnification (N.A. 0.75).

Cell Viability Assay

Cell viability was analyzed using Cell Titer-Glo® Luminescent Cell Viability Assay (Promega, Madison, WI, USA). Cells were seeded with a density of 6.3×10^4 cells/cm^2 on a 96-well plate and treated with different Midkine concentrations (0.05, 0.1, 1 μg/ml) for 3 h, or with 1 μg/ml for different incubation times (0.5, 1, or 3 h). All procedures were performed according to manufacturers' instructions. For all experiments $n = 6$.

Troponin I ELISA

Human CMs were seeded with a density of 6.3×10^4 cells/cm^2 on a 24-well plate and treated for 6 h with 100 ng/ml Midkine at 37°C and 7% CO_2. Supernatant was collected and troponin I in supernatant was determined by using Human Cardiac Troponin I ELISA (Abcam, Cambridge, UK). All procedures were performed according to manufacturers' instructions. For all experiments $n = 6$.

Caspase-3/7 Assay

Human cardiomyocytes were seeded with a density of 6.3×10^4 cells/cm^2 on a 96-well plate and treated with 100 ng/ml Midkine for 6 h at 37°C. Caspase-3/7 activity in human cardiomyocytes was examined by using Caspase-Glo® 3/7 Assay (Promega, Madison, WI, USA). All procedures were performed according to manufacturers' instructions. For all experiments $n = 6$.

Live Cell Imaging

Live cell imaging was performed using Leica Microscope SP8 and LAS X software (Leica, Wetzlar, Germany). Cells were seeded with a density of 6.3×10^4 cells/cm^2 on a 96-well plate and were pre-loaded with 5 μM calcium indicator Fluo-3AM (Life Technologies, Carlsbad, CA, USA) and were incubated for 30 min at 37°C and 7% CO_2. After incubation with Fluo-3AM, cells were analyzed immediately. For measurements, cells were placed in special live cell imaging chamber, adjusted at 37°C and 7% CO_2. Cells were incubated with 100 ng/ml Mdk for 30 min and calcium signals were recorded and evaluated by using LAS X software. Cell culture medium was used during measurements. Live cell imaging was performed with 63x magnification (N.A. 1.2, water). Calcium peaks were determined and compared to baseline values. For all experiments $n = 6$.

Calcium Measurements

For calcium measurements, human cardiomyocytes (iPS) were seeded with a density of 6.3×10^4 cells/cm^2 on ibidi 8-well chambers (ibidi, Germany). Before the measurements, cells were incubated with 100 ng/ml Midkine 60 min before the start of the experiments, as well as for the duration of the experiment. For measurement of changes in intracellular Ca^{2+} concentration, cells were loaded with 5 μM Fura-2 (ThermoScientific, Waltham, MA, USA) for 30 min (in presence of pharmacological compounds if needed). After incubation, cells were washed twice with bath solution (in mM: 140 NaCl; 5.4 KCl; $MgCl_2$; 1.8 $CaCl_2$; 5.5 Glucose; 5 Hepes; pH = 7.4). Fluorescence imaging was performed on a Cell Observer inverse microscope (Zeiss, Jena, Germany). Cells were illuminated for 90 min at a rate of 2 Hz at each excitation wavelength (340 and 380 nm). Images were acquired using MetaFluor (Molecular Devices, Ismaning, Germany). Cells were measured in bath solution using 40x magnification (N.A. 1.3) at room temperature. Fura-2 ratios were calculated with ImageJ and the data obtained were analyzed with the Matlab script PeakCaller (36). For all experiments $n = 6$.

RNA Isolation

For qPCR experiments, human CMs were seeded at a density of 6.3×10^4 cells/cm^2 on a 24-well plate and were treated with 100 ng/ml Midkine for 6 h at 37°C and 7% CO_2. Cells were lysed with RLY lysis buffer (Meridian Bioscience, Cincinnati, OH, USA), containing 10 μl/ml β-mercaptoethanol (Sigma Aldrich, St. Louis, MO, USA). RNA isolation from cell lysates was performed by using ISOLATE II RNA Mini Kit (Meridian Bioscience, Cincinnati, OH, USA). Remaining DNA was digested by DNase I (Meridian Bioscience, Cincinnati, OH, USA) for 15 min at RT as recommended by the manufacturer.

Reverse Transcribed Quantitative Polymerase Chain Reaction (RT-qPCR)

The respective RNA samples were reverse transcribed in cDNA using SuperScript® IV VILO® MasterMix (Life Technologies, Carlsbad, CA, USA). For cDNA transcription, 1–5 ng/ml mRNA were used, and experiment was performed according to manufacturer's instructions. For quantitative PCR, the PowerUp® SYBR® Green Master Mix (Applied Biosystems, Waltham, MA, USA) was used. All procedures were performed according to the manufacturers' instructions. For qPCR, the QuantStudio3 (Applied Biosystems, Waltham, MA, USA) system was utilized. Five-hundred to seven-hundred ng/ml cDNA were used for quantitative PCR. Quantitative mRNA expression of human *troponin I* (for: 5′-CCTCCAACTACCGCGCGCTTAT-3′, rev: 5′-CTGCAATTTTCTCGAGGCGG-3′), *sarco/endoplasmic reticulum Ca^{2+}-ATPase (SERCA2a)* (for: 5′-CTCCTTGCCCGT GATTCTCA-3′, rev: 5′-CCAGTATTGCAGGTTCCAGGT-3′), *ryanodine receptor 1 (RyR1)* (for: 5′-GGGTTCCTGCCC GACATGAG-3′, rev: 5′-GCACAGGTAGCGGTTCACG-3′), Na^+/Ca^{2+} exchanger (NCX) (for: 5′-GCCTGGTGGAGATGAG TGAG-3′, rev: 5′-ACAGGTTGGCCAAACAGGTA-3′), *toll-like receptor 4 (TLR4)* (for: 5′-CCTGCGTGGAGGTGTGAAAT-3′, rev: 5′-CTGGATGGGGTTTCCTGTCAA-3′), *toll-like receptor 9 (TLR9)* (for: 5′-AGACCTGAGGGTGGAAGTGT-3′, rev:

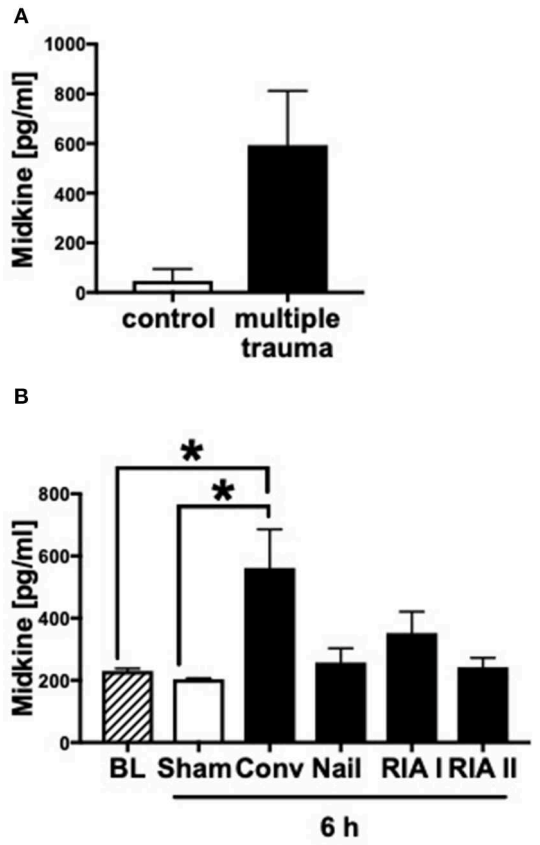

FIGURE 1 | Midkine levels in blood plasma of multiply injured humans and pigs. Midkine levels (pg/ml) in shock room blood plasma from multiply injured patients compared to healthy control group ($n = 10$) **(A)**. Midkine levels (pg/ml) in blood plasma of multiply injured pigs **(B)**. The pigs' femur fracture was either treated with femoral nailing (nailing, $n = 5$), conventional (conv, $n = 5$), or with reamer irrigator aspirator 1 or 2 (RIA I or RIA II, each $n = 5$). Control animals received sham-procedure ($n = 5$). Evaluation of blood plasma at baseline (BL) and 6 h after trauma. Results are presented as mean ± SEM. Data were analyzed by one-way ANOVA followed by Dunnett's or Tukey's multiple comparison test. Results are significant $^*p < 0.05$.

5′-CTGGATAGCACCAGTAGCGG-3′) and *purigenic receptor subtype 7 (P2X7)* (for: 5′-CACACCAAGGTGAAGGGGAT-3′, rev: 5′-GGTGTAGTCTGCGGTGTCAA-3′) was examined and calculated by the cycle threshold method ΔΔCt. Respective genes were normalized to expression of the housekeeping gene *glutaraldehyde-phosphate dehydrogenase (GAPDH)* (forward: 5′-TCTCTGCTCCTCCTGTTCGAC-3′, reverse: 5′-CCAA TACGACCAAATCCGTTGA-3′) in order to exclude variations. Quantitative mRNA expression was determined by the double-threshold method (ΔΔCT). Results are presented as mean fold change. For all experiments $n = 6$.

Reactive Oxygen Species (ROS)

For analysis of cellular ROS, human CMs were seeded at a density of 6.3×10^4 cells/cm^2 on ibidi 12-well slides (ibidi, Germany). Human CMs were treated with 100 ng/ml Midkine for 6 h at 37°C and 7% CO_2. After treatment, cells were incubated for another 30 min with 5 μM CellROX® Deep Red Reagent (Life Technologies, Carlsbad, CA, USA) at 37°C and 7% CO_2. Afterwards, cells were fixed with 4% formaldehyde and cell nuclei were stained with Hoechst. Cell were mounted with ProLong® Gold Antifade Mountant. Cells were investigated by blinded investigator by fluorescence microscopy using Axio Imager M.2 microscope and the Zeiss ZEN 2.3 software. Imaging was performed by using 20x magnification (N.A. 0.5). Relative amount of reactive oxygen species was determined by Zeiss ZEN 2.3 software in order to exclude variations. For all experiments $n = 6$.

Mitochondrial Respiration With Seahorse XF Analyzer

Mitochondrial respiration was analyzed by using the Seahorse XFe96 Analyzer (Agilent Technologies, Santa Clara, CA, USA). This extracellular flux analyzer makes it possible to perform highly accurate real-time measurements of cellular metabolism in living cells by simultaneously quantifying the rates of extracellular acidification (ECAR) and oxygen consumption (OCR), and measuring the glycolysis and the mitochondrial respiration of the cells. For the analysis of mitochondrial respiration, the Seahorse XF Cell Mito Stress Test Kit (Agilent Technologies, Santa Clara, CA, USA) was used. The Seahorse XF Cell Mito Stress Test Kit is an optimized solution for assessing mitochondrial function. During the experiment, the ECAR and the OCR were continuously measured, gaining the parameter for the basal (baseline) respiration of the mitochondria. Afterwards, 2 μM oligomycin, 1 μM carbonyl cyanide 4-(trifluoromethoxy) phenylhydrazone (FCCP), and 0.5 μM antimycin A and rotenone were pneumatically injected into the media of the cells. After automatically and gently mixing, the OCR and the ECAR were measured at multiple times after each injection. After the experiment, cells were fixed with 4% formalin at 4°C overnight. Then, cells were stained with 0.3% Janus-Green solution (Sigma Aldrich, St. Louis, MO, USA), washed and resolved with 0.5 M hydrochloric acid. Optical density was measured at 630 nm and OCR values were normalized to OD 630 nm values to exclude variations. Results were evaluated using Seahorse Wave 2.4 software (Agilent Technologies, Santa Clara, CA, USA), gaining the parameter for spare respiratory capacity of the mitochondria. For the analysis of mitochondrial respiration, cells were seeded with a density of 5×10^5 cells/cm^2 on Seahorse XFe96 analyzer cell culture plates (Agilent Technologies, Santa Clara, CA, USA) and incubated for 6 h with 100 ng/ml Midkine and the above- mentioned procedure was performed. For all experiments $n = 6$.

CytoSorb® 300 Experiments

For the therapeutic experiments, the CytoSorb® 300 was used (CytosorbensInc., MonmouthJunction, NJ, USA). Therefore, small columns were prepared. An excess of CytoSorb® 300 at the ratio 2:1 (CytoSorb® 300 to plasma samples) was added on the column as recommended by the manufacturers. Human shock room blood plasma samples were added on the columns and were

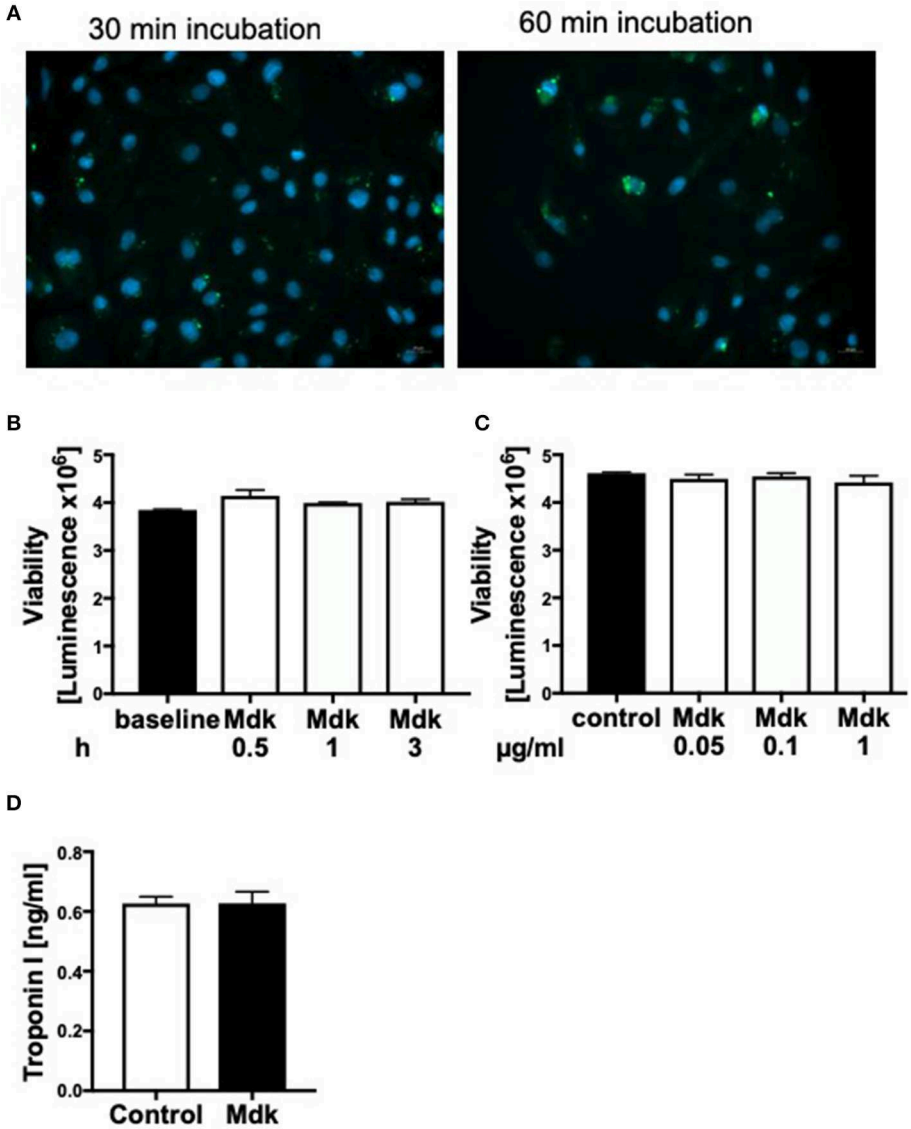

FIGURE 2 | Effects of Midkine on human cardiomyocytes. Immunofluorescence staining of human cardiomyocytes **(A)**. Human cardiomyocytes were treated for 30 and 60 min with 100 ng/ml fluorescein isothiocyanate (FITC)-labeled Midkine (green). Cell nuclei were counterstained with Hoechst (blue). Cell viability of human cardiomyocytes (Luminescence in counts/sec) treated for 0.5, 1, and 3 h with 100 ng/ml Midkine **(B)**. Cell viability of human cardiomyocytes (Luminescence in counts/sec) treated for 3 h with 0.05, 0.1, and 1 μg/ml Midkine **(C)**. Troponin I (ng/ml) in supernatant of human cardiomyocytes, treated for 6 h with 100 ng/ml Midkine **(D)**. Results are presented as mean ± SEM. For all experiments $n = 6$. Data were analyzed by two-tailed, unpaired students *t*-test.

incubated for 6 or 3 h at RT while continuously shaking. For time-doses experiments, different Midkine concentrations (10,000, 5,000, 2,500, 2,000, 1,500, 1,000, 500, 1,000 pg/ml) diluted in PBS with 1% BSA were added on the columns and were also incubated for 6 and 3 h at RT, while continuously shaking. For all experiments $n = 6$.

Statistical Analysis

All values were expressed as means ± SEM. Data were analyzed by one-way ANOVA followed by Dunnett's or Tukey's multiple comparison test. For the statistical analysis of two groups, unpaired two-tailed students *t*-test was used. $p \leq 0.05$ was considered statistically significant. GraphPad Prism 7.0 software was used for statistical analysis (GraphPad Software, Incorporated, San Diego, CA, USA).

RESULTS

Midkine Plasma Levels in Multiply Injured Humans and Pigs

In humans as well as in pigs, the blood plasma concentrations of Midkine increased after multiple trauma compared to the healthy controls (**Figures 1A,B**). Animals submitted to

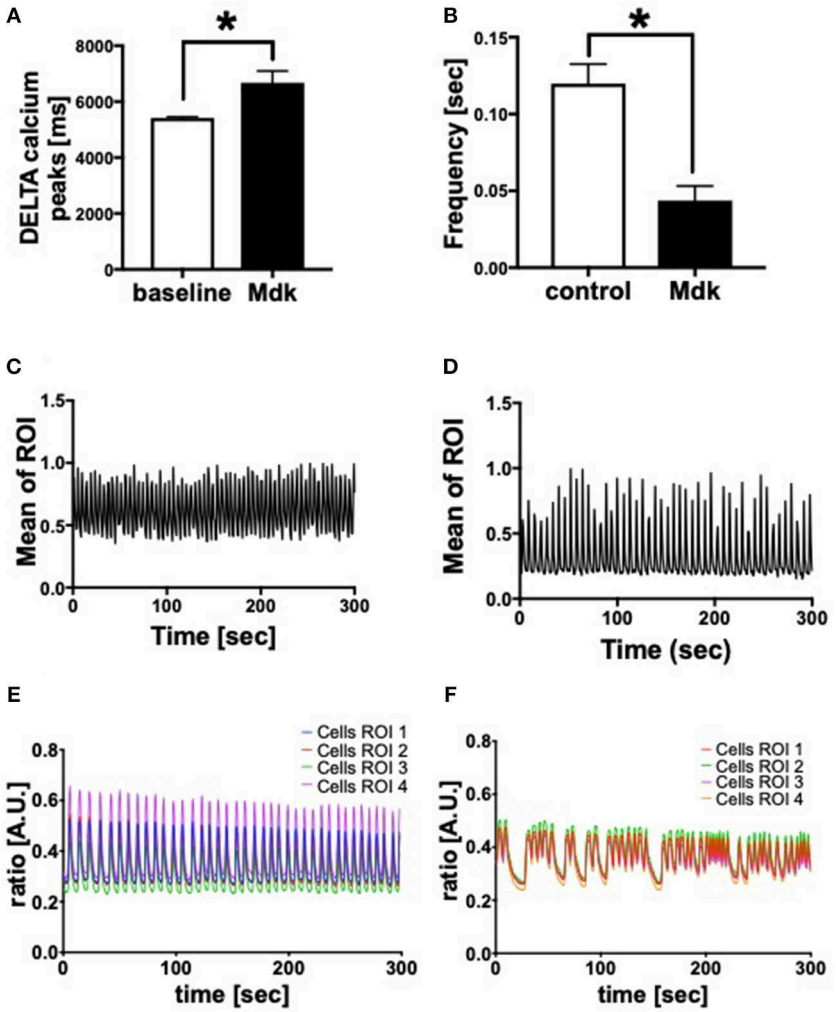

FIGURE 3 | Calcium handling of human cardiomyocytes. Delta calcium peaks (msec) of human cardiomyocytes treated for 30 min with 100 ng/ml Midkine **(A)**. Frequency of calcium signals (sec) of human cardiomyocytes treated for 60 min with 100 ng/ml Midkine **(B)**. Traces of calcium signals of human cardiomyocytes (Mean Calcium peaks of ration of interest (ROI) vs. time in sec) **(C,D)**. Traces of calcium signals of human cardiomyocytes (Ratio of Fura-2 signals in A.U. vs. time in sec) **(E,F)**. Different colors for selected ROI of calcium signals of the cells. For all experiments $n = 6$. Results are presented as mean ± SEM. Data were analyzed by one-way ANOVA followed by Dunnett's or Tukey's multiple comparison test. Results are significant $^*p < 0.05$.

reamed femoral nailing showed significantly higher Mdk levels when compared with pigs treated with conventional femoral nailing or with reamer irrigator aspirator treatment (RIA I/II; **Figure 1B**). This indicates that Mdk levels correlate with the invasiveness of the reaming method. In multiply injured pigs, plasma Mdk levels increased significantly after 6 h in the group with conventional reaming of the fracture compared to the control group.

Since plasma Mdk levels increased after multiple trauma, we investigated whether Mdk affects human cardiomyocytes (CMs). After 30 and 60 min the Mdk was actively absorbed into the human CMs and was primarily located around their nucleus *in vitro* (**Figure 2A**).

Cell Viability, Cell Damage, and Calcium Handling of Human Cardiomyocytes

Given that Mdk is actively taken into the cells, we examined whether it then affects the cell viability of the human CMs. The cell viability of the human CMs was neither affected by different Mdk concentrations nor by different incubation times (**Figures 2B,C**). Furthermore, there were no differences in troponin I concentrations in supernatant of the humans CMs treated with Mdk compared to control cells after 6 h (**Figure 2D**). However, the calcium handling of the human CMs was altered after Mdk treatment, which is exemplified by the significant increase in their delta calcium peaks (**Figure 3A**), meaning the cells beat slower in presence of Mdk. Moreover, the frequency of calcium signals

in human CMs decreased significantly in presence of Mdk, developing bradycardic conditions (**Figure 3B**), which is also demonstrated the traces of the calcium signals of the cells (**Figures 3C–F**).

Gene Expression of Human Cardiomyocytes

We showed that Mdk alters the calcium handling in human CMs. Next, we investigated the gene expression of specific cardiac calcium pumps as well as the expression of different receptors, which might be involved in Mdk signaling. In human CMs, the mRNA expression of *SERCA2a*, *NCX*, *TLR4*, *TLR9,* and *P2X7* increased significantly in presence of Mdk compared to control (**Figures 4A,C–F**), indicating for direct effects of Mdk on gene expression of calcium handling proteins. Moreover, the effects of Mdk might be mediated via TLR-P2X7 signaling. The mRNA expression of *RyR1* was unaffected (**Figure 4B**).

Mitochondrial Respiration of Human Cardiomyocytes

In addition, we analyzed the effects of Mdk on the mitochondrial respiration of CMs **Figure 5A**. The basal respiration as well as the spare respiratory capacity of the human CMs decreased significantly after the Mdk treatment (**Figures 5B,C**), indicating detrimental effects of Mdk on mitochondrial respiration.

Intracellular Reactive Oxygen Species (ROS) and Caspase3/7 Activity

As Mdk alters mitochondrial respiration and ATP production of the cells, we next investigated whether Mdk also affects the redox balance of the human CMs. The amount of ROS did not change in human CMs after being treated with Mdk compared to control cells (**Figure 5D**). Although Caspase3/7 activity increased significantly in human CMs in presence of Mdk (**Figure 5E**), indicating for enhanced apoptosis in the cells.

Filtration of Midkine by CytoSorb® 300

Because Mdk is elevated in plasma of multiply injured humans and pigs and acts on human CMs, we examined the potential of a therapeutic approach: the absorption capacity of Mdk from human blood by CytoSorb® 300. After incubation of different Mdk concentrations with CytoSorb® 300, the Mdk levels decreased between 45 and 95% within 6 h (**Figure 6A**). Especially high Mdk concentrations (10,000 pg/ml) were significantly reduced up to 95% after filtration with CytoSorb® 300 after 6 h compared to the 3 h incubation (**Figure 6A**). Moreover, Mdk levels in plasma from multiply injured patients were significantly reduced after incubation with CytoSorb® 300 (**Figure 6B**).

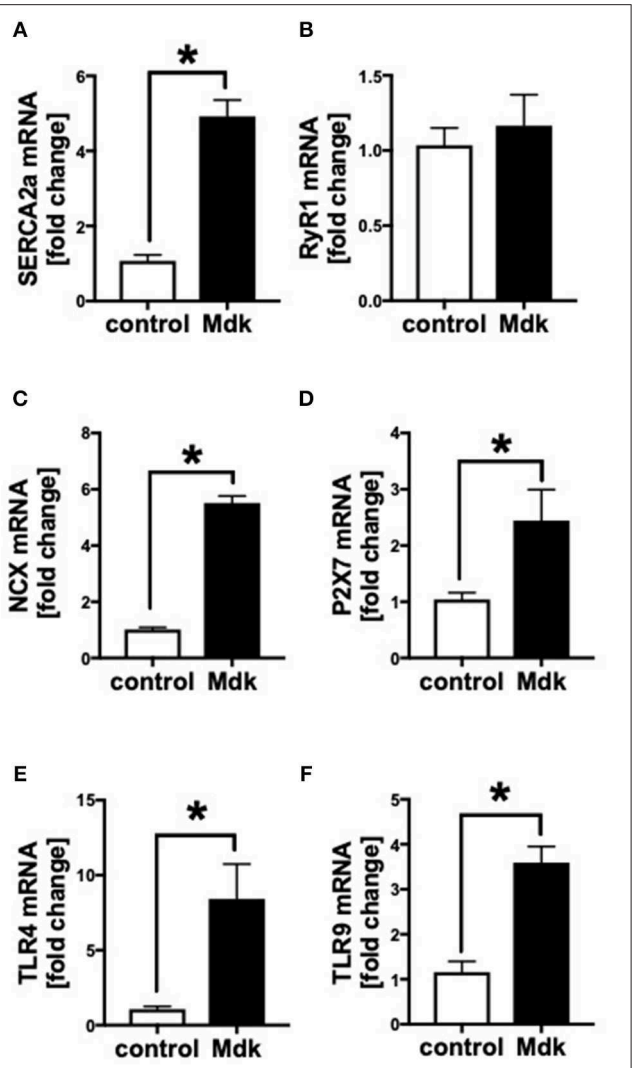

FIGURE 4 | Gene expression of human cardiomyocytes treated for 6 h with 100 ng/ml Midkine. mRNA expression (in fold change) of *sarco/endoplasmatic reticulum* Ca^{2+}*-ATPase* (*SERCA2a*) **(A)**, *ryanodine receptor-1 (RyR1)* **(B)**, *sodium-calcium exchanger (NCX)* **(C)**, *purigenic P2X receptor subtype 7 (P2X7)* **(D)**, *toll-like receptor 4 (TLR4)* **(E)**, *toll-like receptor 9 (TLR9)* **(F)**. Results are presented as mean ± SEM. Data were analyzed by two-tailed, unpaired students *t*-test. For all experiments $n = 6$. Results are significant $^*p < 0.05$.

DISCUSSION

Our study shows for the first time that Mdk is elevated in blood circulation after multiple trauma. This elevation is similar to other traumatic injuries, suggesting that circulating Mdk may act as a novel inflammatory marker for polytrauma (8, 9, 11). Furthermore, we demonstrated that Mdk acts directly on human cardiomyocytes *in vitro* and is actively taken up by these cells, altering their functionality without affecting their viability. We found that Mdk affects the functionality of the human CMs by altering their calcium handling. The delta calcium peaks of the human CMs increased significantly after Mdk treatment, meaning the cells became bradycardic. Moreover, the frequency of the calcium signals in human CMs decreased significantly after Mdk treatment, confirming the bradycardic effect of Mdk. The mRNA expression of the specific cardiac calcium pumps *SERCA2a* and *NCX* also increased significantly after Mdk treatment, suggesting direct effects of Mdk on calcium handling in the cells. The location of Mdk around the cell nucleus

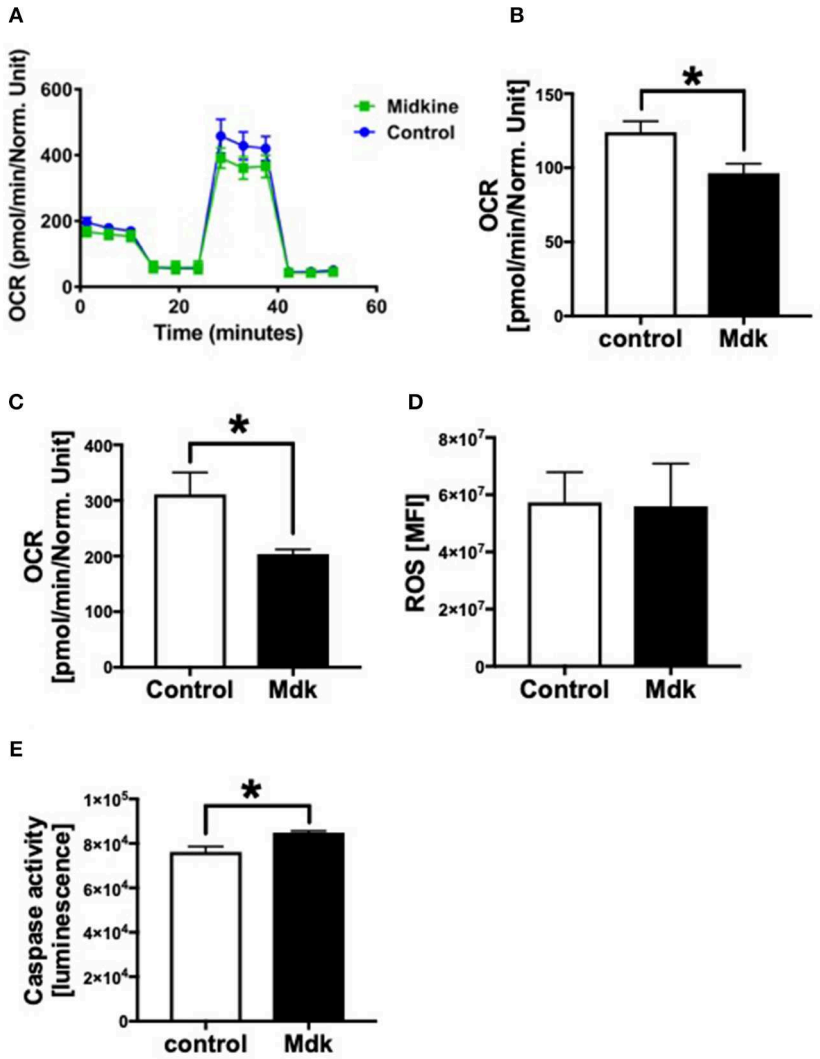

FIGURE 5 | Mitochondrial respiration, cellular reactive oxygen species (ROS) and Caspase 3/7 activity of human cardiomyocytes treated for 6 h with 100 ng/ml Midkine. Oxygen consumption rate (OCR) of human cardiomyocytes (Control, Midkine) during Seahorse MitoStress Assay (OCR in pmol/min/E630 vs. time in min) **(A)**. Basal respiration of human cardiomyocytes (OCR in pmol/min/E630) **(B)**. Spare respiratory capacity of human cardiomyocytes (OCR in pmol/min/E630) **(C)**. Amount of reactive oxygen species (mean fluorescence intensity, MFI) **(D)**. Caspase 3/7 activity (Luminescence in counts/sec) **(E)**. Results are presented as mean ± SEM. For all experiments $n = 6$. Data were analyzed by two-tailed, unpaired students *t*-test. Results are significant $^*p < 0.05$.

of the human CMs confirmed the regulatory effects on cellular gene expression of the calcium handling proteins. Alterations in calcium signals as well as in mRNA expression of *SERCA2a* and *NCX* were also described previously in presence of other trauma-related inflammatory biomarkers and DAMPs as well as in different trauma models and during sepsis, nominating Mdk as a powerful cardio-depressive mediator after trauma and during sepsis (25, 37–42). However, cardiac overexpression of SERCA2a in rodents improved cardiac contractility and relaxation, which might also indicate potential protective effects of Mdk in the heart, which would require to be investigated in future studies (43, 44). We also novelly showed that the basal respiration as well as the spare respiratory capacity of the mitochondria of the human CMs decreased significantly, indicating detrimental effects of Mdk on cellular mitochondrial respiration and energy production. Nevertheless, the amount of cytosolic reactive oxygen species (ROS) was not altered in the human CMs in presence of Mdk. Mitochondrial dysfunction was also depicted previously for other trauma-related biomarkers (7, 45, 46). The detrimental and cardio-depressive effects of Mdk on the human CMs might be mediated *via* the toll-like receptor (TLR) 4, TLR9, and the pyrogenic receptor subtype 7 (P2X7) since the mRNA expression of these receptors was significantly upregulated. All of these receptors have been demonstrated to be involved in the DAMP-associated cardiac signaling pathways in different trauma models (47, 48). The activation of the TLRs results in increased cardiac inflammation, mediated via the nuclear factor κ B (NFκB) (47). This TLR-mediated cardiac

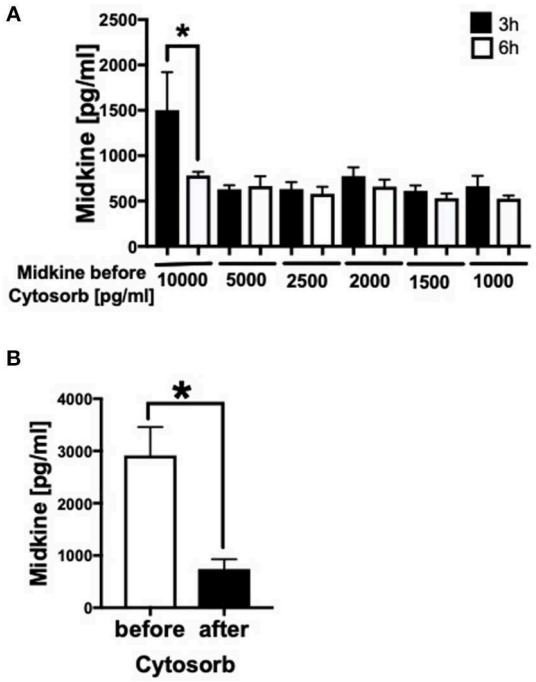

FIGURE 6 | Filtration of Midkine by CytoSorb® 300. Filtration of different Midkine concentrations (10,000, 5,000, 2,500, 2,000, 1,500, 1,000 pg/ml) ($n = 6$) with CytoSorb® 300 after 3 h (black bars) and 6 h (white bars) **(A)**. Midkine concentration before and after filtration with CytoSorb® 300 on the x-axis in pg/ml. Midkine levels (pg/ml) in human shock room blood plasma of multiply injured patients before and after filtration with CytoSorb® 300 ($n = 11$) **(B)**. Results are presented as mean ± SEM. Data were analyzed by one-way ANOVA followed by Dunnett's or Tukey's multiple comparison test. Results are significant $^*p < 0.05$.

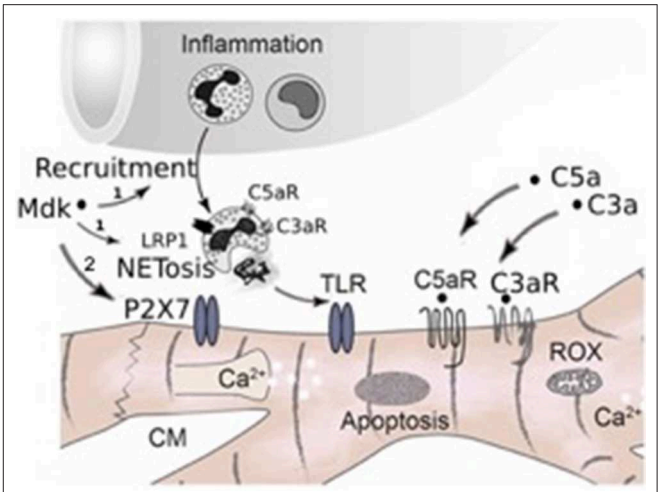

FIGURE 7 | Schematic representation of systemic inflammation after trauma and during sepsis. After trauma Midkine is released systemically. Midkine recruits polymorphonuclear neutrophils (PMNs) and induces the release of extracellular traps (NETosis) via the receptor-related protein 1 (LRP1) on the neutrophils, which was demonstrated by Weckbach et al. (23), (1). The neutrophil extracellular traps (NETs) include extracellular histones, which act via toll-like receptors (TLRs) on the surface of cardiomyocytes, inducing cardiac dysfunction and cardiac damage. Furthermore, Midkine is able to act detrimental on human cardiomyocytes by direct interactions via TLR4, TLR9, and pyrogenic receptor subtype 7 (P2X7), inducing enhanced apoptosis, disturbing calcium signaling and impairing mitochondrial respiration (2, Hypothesis of this manuscript). Additionally, after trauma and during sepsis the complement factors C5a and C3a are released systemically. Both act directly via their receptors (C5aR, C3aR) on cardiomyocytes, leading to cardiac dysfunction. Moreover, the complement factors also induce NETosis of neutrophils via their receptors.

inflammation leads to cardiac injury and finally results in cardiac contractile dysfunction (47–49). Since the mRNA expression of the TLRs was upregulated, the protein expression of these receptors might be increased after Mdk treatment. This might lead to sensitization of the CMs for other systemic circulating DAMPs, such as HMGB1 and extracellular histones, which were elevated after polytrauma, leading to cardiomyocyte dysfunction (7, 24, 50). The P2X7 receptor was also shown to be involved in cardiac contractile dysfunction (51). Interestingly, the Caspase 3/7 activity increased in human CMs after treatment with Mdk, which was demonstrated previously in cardiac tissue *in vivo* in an experimental polytrauma model in pigs (41). So far, Mdk was described as an anti-apoptotic factor by decreasing caspase activity in other cells, such as neurons and HepG2 cells, which is in accordance to unaffected cell viability in the present study (52, 53). The effects of Mdk on cellular apoptosis of human CMs has not been described, so far. In contrast to other cells, human CMs seem to follow different cellular processes and various signal cascades might be involved in Caspase-3/7 activation and activity when these cells were treated with Mdk. Moreover, this phenomenon could also be time-dependent as we solely investigated the Caspase-3/7 activity after 6 h of Mdk exposure. This observation should be the subject of future studies in order to understand the specific effects of Mdk on apoptosis of human CMs.

Therapeutic approaches treating post-traumatic cardiac dysfunction are still limited. In this study, we clearly showed that Mdk is elevated in plasma after multiple trauma and is predominantly detrimental on human CMs, causing the development of post-traumatic cardiac dysfunction. As a consequence, we investigated the efficiency of CytoSorb® 300 in filtering Mdk from human blood plasma. CytoSorb® 300 is an absorption column, composed of porous polymer beads, which is normally used in the intensive care unit (ICU) for septic patients or for patients with SIRS. The filtration potential of CytoSorb® 300 for various trauma-associated cytokines and DAMPs was already demonstrated by others (31, 54). Here, we showed for the first time that CytoSorb® 300 is able to absorb Mdk dose-dependently, filtering high Mdk concentrations (10,000 pg/ml) up to 95%. Moreover, CytoSorb® 300 filtered Mdk from human plasma obtained on admission to the emergency room, making it a very promising therapeutic approach for treatment and prevention of post-traumatic cardiac dysfunction. One huge benefit of using CytoSorb® 300 instead of single antibodies for therapy is that CytoSorb® 300 is able to filter a high amount of many miscellaneous damage- and inflammation

molecules after trauma and not only a single molecule, which is the case of antibody treatment. Furthermore, filtration of Mdk by CytoSorb® 300 might limit other negative effects of Mdk on polytrauma patients, since it was shown that Mdk acts as an inhibitor of fracture healing and that high Mdk serum levels were associated with poor outcome in septic patients. Finally, we found that systemic Mdk is higher after conventional reaming, compared to nailing without reaming and to RIA I/II. Consequently, treatment of the fracture with RIA I/II might be better for fracture outcome as well as for fracture healing after trauma (55). In addition, conventional reaming of the fracture might have other negative effects after trauma (e.g., pulmonary embolism).

One limitation of the study might be the small sample size ($n = 6$) to investigate different treatment approaches for the femur fracture. Consequently, more experiments are needed to find the best and the least invasive treatment approach. The same applies for a possible correlation between fracture treatment approaches and systemic Mdk levels. Because investigated groups were heterogenous, a bigger number of samples might be helpful to extrapolate the results to a clinical population. Another limitation might be that we only used small columns with Cytosorb® 300 polymer beads in our study, trying to mimic the clinical application in ICU. However, as our study was only an experimental approach, clinical studies should be performed, including more patients and larger application approaches of Cytosorb® 300. This may help to- confirm the therapeutic potential of Cytosorb® 300 for the prevention of post-traumatic cardiac dysfunction by filtering Mdk from human blood *in vivo*. Furthermore, it is not possible to mimic *in vitro* the real *in vivo* inflammatory conditions, which occur after trauma. The presence of many different inflammatory mediators and DAMPs and the activation of different signal cascades in the cells lead to post-traumatic cardiac dysfunction. Consequently, it is not possible to specify these detrimental effects on one single mediator like Mdk.

Taken together, in our study we observed for the first time that Mdk is elevated systemically after multiple trauma in humans and pigs, acting cardio-depressive on human CMs by impairing their calcium handling and mitochondrial respiration capacity *in vitro*. PlX27/TLR might be involved in mediating these detrimental effects of MdK (**Figure 7**). In the clinical setting, the hemadsorption filter Cytosorb® 300 might be a powerful tool to remove cardio-depressive mediators from patients' circulation and therefore help to improve cardiac function.

DATA AVAILABILITY

All datasets generated for this study are included in the manuscript and/or the supplementary files.

ETHICS STATEMENT

Human plasma from 11 multiply injured patients with a history of acute blunt or penetrating trauma and an ISS ≥ 16 was collected after hospital admission in the University Hospital of the Goethe-University Frankfurt with institutional ethics committee approval (312/10), in accordance with the Declaration of Helsinki and following the Strengthening the Reporting of Observational studies in Epidemiology (STROBE)-guidelines (32). All enrolled patients signed the written informed consent form themselves or written informed consent was obtained from the nominated legally authorized representative on the behalf of participants in accordance with ethical standards.

The animal housing and experimental protocols were approved by the Cantonal Veterinary Department, Zurich, Switzerland, under license no. ZH 138/2017, and were in accordance with Swiss Animal Protection Law. Housing and experimental procedures also conformed to the European Directive 2010/63/EU of the European Parliament and of the Council on the Protection of vertebrate animals used for scientific purposes (Council of Europe no. 123, Strasbourg 1985) and to the Guide for the Care and Use of Laboratory Animals (Institute of Laboratory Animal Resources, National Research Council, National Academy of Sciences, 2011).

AUTHOR CONTRIBUTIONS

IL, BW, MB, TE, GF, SH, ML, and NC performed the experiments including animal studies, cell culture experiments, microscopic studies, and ELISAs. IL primarily wrote the paper. MH-L, FG, BR, IM, RP, H-CP, and MK contributed to experimental design and data analysis and coordinated the study and supervised financial support for the studies. All authors made substantial contributions to conception and design of the study, participated in drafting the article, and gave final approval of the version to be published.

FUNDING

This work was conducted in the framework of the CRC 1149 funded by the Deutsche Forschungsgemeinschaft (DFG, German Research Foundation)—Project number 251293561. This work was also funded by the AO Grant S-16-133T: Effects of standard reaming and RIA techniques on local soft tissue and systemic homeostasis in a porcine trauma model.

ACKNOWLEDGMENTS

We kindly acknowledge the Department of Children and Adolescent Medicine, Division of Pediatric Endocrinology and Diabetes for the provision of the Agilent Seahorse XFe96 analyzer. Thanks to all members of the TREAT research group.

TREAT RESEARCH GROUP

Auner B, Stormann P, Simon TP, Marx G, Haug A, Egerer L, Giensven MV, Huber-Lang M, Tolba R, Reiss K, Uhlig S, Horst K, Teuben M, Almahoud K, Kalbas Y, Luken H, Almahoud K, and Hildebrand F.

REFERENCES

1. WHO. *Global Health Estimates 2015 Summary Tables: Deaths by Cause, Age and Sex, 2000–2015* [Online]. Available online at: http://www.who.int/healthinfo/global_burden_disease?GHE2015_Deaths_Global_2000_2015.xls?ua=1 (2016) (accessed October 1, 2017).
2. Sapan HB, Paturusi I, Jusuf I, Patellongi I, Massi MN, Pusponegoro AD, et al. Pattern of cytokine (IL-6 and IL-10) level as inflammation and anti-inflammation mediator of multiple organ dysfunction syndrome (MODS) in polytrauma. *Int J Burns Trauma.* (2016) 6:37–43.
3. Timmermans K, Kox M, Scheffer GJ, Pickkers P. Danger in the intensive care unit: damps in critically ill patients. *Shock.* (2016) 45:108–16. doi: 10.1097/SHK.0000000000000506
4. Dewar D, Moore FA, Moore EE, Balogh Z. Postinjury multiple organ failure. *Injury.* (2009) 40:912–8. doi: 10.1016/j.injury.2009.05.024
5. Guisasola MC, Alonso B, Bravo B, Vaquero J, Chana F. An overview of cytokines and heat shock response in polytraumatized patients. *Cell Stress Chaperones.* (2018) 23:483–9. doi: 10.1007/s12192-017-0859-9
6. Kumar A, Thota V, Dee L, Olson J, Uretz E, Parrillo JE. Tumor necrosis factor alpha and interleukin 1beta are responsible for *in vitro* myocardial cell depression induced by human septic shock serum. *J Exp Med.* (1996) 183:949–58. doi: 10.1084/jem.183.3.949
7. Kalbitz M, Grailer JJ, Fattahi F, Jajou L, Herron TJ, Campbell KF, et al. Role of extracellular histones in the cardiomyopathy of sepsis. *FASEB J.* (2015) 29:2185–93. doi: 10.1096/fj.14-268730
8. Iwashita N, Muramatsu H, Toriyama K, Torii S, Muramatsu T. Expression of midkine in normal and burn sites of rat skin. *Burns.* (1999) 25:119–24. doi: 10.1016/S0305-4179(98)00120-X
9. Sakakima H, Yoshida Y, Muramatsu T, Yone K, Goto M, Ijiri K, et al. Traumatic injury-induced midkine expression in the adult rat spinal cord during the early stage. *J Neurotrauma.* (2004) 21:471–7. doi: 10.1089/089771504323004610
10. Krzystek-Korpacka M, Mierzchala M, Neubauer K, Durek G, Gamian A. Midkine, a multifunctional cytokine, in patients with severe sepsis and septic shock: a pilot study. *Shock.* (2011) 35:471–7. doi: 10.1097/SHK.0b013e3182086001
11. Fischer V, Kalbitz M, Muller-Graf F, Gebhard F, Ignatius A, Liedert A, et al. Influence of menopause on inflammatory cytokines during murine and human bone fracture healing. *Int J Mol Sci.* (2018) 19:2070. doi: 10.3390/ijms19072070
12. Haffner-Luntzer M, Heilmann A, Rapp AE, Roessler R, Schinke T, Amling M, et al. Antagonizing midkine accelerates fracture healing in mice by enhanced bone formation in the fracture callus. *Br J Pharmacol.* (2016) 173:2237–49. doi: 10.1111/bph.13503
13. Haffner-Luntzer M, Kemmler J, Heidler V, Prystaz K, Schinke T, Amling M, et al. Inhibition of midkine augments osteoporotic fracture healing. *PLoS ONE.* (2016) 11:e0159278. doi: 10.1371/journal.pone.0159278
14. Kitahara T, Shishido T, Suzuki S, Katoh S, Sasaki T, Ishino M, et al. Serum midkine as a predictor of cardiac events in patients with chronic heart failure. *J Card Fail.* (2010) 16:308–13. doi: 10.1016/j.cardfail.2009.12.014
15. Przybylowski P, Malyszko J, Malyszko JS. Serum midkine is related to NYHA class and cystatin C in heart transplant recipients. *Transplant Proc.* (2010) 42:3704–7. doi: 10.1016/j.transproceed.2010.08.026
16. Reynolds PR, Mucenski ML, Le Cras TD, Nichols WC, Whitsett JA. Midkine is regulated by hypoxia and causes pulmonary vascular remodeling. *J Biol Chem.* (2004) 279:37124–32. doi: 10.1074/jbc.M405254200
17. Fukui S, Kitagawa-Sakakida S, Kawamata S, Matsumiya G, Kawaguchi N, Matsuura N, et al. Therapeutic effect of midkine on cardiac remodeling in infarcted rat hearts. *Ann Thorac Surg.* (2008) 85:562–70. doi: 10.1016/j.athoracsur.2007.06.002
18. Netsu S, Shishido T, Kitahara T, Honda Y, Funayama A, Narumi T, et al. Midkine exacerbates pressure overload-induced cardiac remodeling. *Biochem Biophys Res Commun.* (2014) 443:205–10. doi: 10.1016/j.bbrc.2013.11.083
19. Horiba M, Kadomatsu K, Yasui K, Lee JK, Takenaka H, Sumida A, et al. Midkine plays a protective role against cardiac ischemia/reperfusion injury through a reduction of apoptotic reaction. *Circulation.* (2006) 114:1713–20. doi: 10.1161/CIRCULATIONAHA.106.632273
20. Sumida A, Horiba M, Ishiguro H, Takenaka H, Ueda N, Ooboshi H, et al. Midkine gene transfer after myocardial infarction in rats prevents remodelling and ameliorates cardiac dysfunction. *Cardiovasc Res.* (2010) 86:113–21. doi: 10.1093/cvr/cvp386
21. Kadomatsu K, Bencsik P, Gorbe A, Csonka C, Sakamoto K, Kishida S, et al. Therapeutic potential of midkine in cardiovascular disease. *Br J Pharmacol.* (2014) 171:936–44. doi: 10.1111/bph.12537
22. Badila E, Daraban AM, Tintea E, Bartos D, Alexandru N, Georgescu A. Midkine proteins in cardio-vascular disease. Where do we come from and where are we heading to? *Eur J Pharmacol.* (2015) 762:464–71. doi: 10.1016/j.ejphar.2015.06.040
23. Weckbach LT, Grabmaier U, Uhl A, Gess S, Boehm F, Zehrer A, et al. Midkine drives cardiac inflammation by promoting neutrophil trafficking and NETosis in myocarditis. *J Exp Med.* (2019) 216:350–68. doi: 10.1084/jem.20181102
24. Abrams ST, Zhang N, Manson J, Liu T, Dart C, Baluwa F, et al. Circulating histones are mediators of trauma-associated lung injury. *Am J Respir Crit Care Med.* (2013) 187:160–9. doi: 10.1164/rccm.201206-1037OC
25. Kalbitz M, Amann EM, Bosch B, Palmer A, Schultze A, Pressmar J, et al. Experimental blunt chest trauma-induced myocardial inflammation and alteration of gap-junction protein connexin 43. *PLoS ONE.* (2017) 12:e0187270. doi: 10.1371/journal.pone.0187270
26. Kellum JA, Song M, Venkataraman R. Hemoadsorption removes tumor necrosis factor, interleukin-6, and interleukin-10, reduces nuclear factor-κB DNA binding, and improves short-term survival in lethal endotoxemia. *Crit Care Med.* (2004) 32:801–5. doi: 10.1097/01.CCM.0000114997.39857.69
27. Born F, Pichmaeier M, Peter S. Systemic inflammatory response syndrome in heart surgery: new possibilities for treatment through the use of a cytokine adsorber during ECC? *Kardiotechnik.* (2014) 14:1–10.
28. Hetz H, Berger R, Recknagel P, Steltzer H. Septic shock secondary to beta-hemolytic streptococcus-induced necrotizing fasciitis treated with a novel cytokine adsorption therapy. *Int J Artif Organs.* (2014) 37:422–6. doi: 10.5301/ijao.5000315
29. Hinz B, Jauch O, Noky T, Friesecke S, Abel P, Kaiser R. CytoSorb, a novel therapeutic approach for patients with septic shock: a case report. *Int J Artif Organs.* (2015) 38:461–4. doi: 10.5301/ijao.5000429
30. Kogelmann K, Drüner M, Jarczak D. Case study of 8 patients with multiple organ failure treated additionally with CytoSorbents haemadsorption as adjunctive therapy in septic shock and severe SIRS in cardiac failure. *Germany Infect.* (2015) 43:1–73.
31. Gruda MC, Ruggeberg KG, O'Sullivan P, Guliashvili T, Scheirer AR, Golobish TD, et al. Broad adsorption of sepsis-related PAMP and DAMP molecules, mycotoxins, and cytokines from whole blood using CytoSorb(R) sorbent porous polymer beads. *PLoS ONE.* (2018) 13:e0191676. doi: 10.1371/journal.pone.0191676
32. von Elm E, Altman DG, Egger M, Pocock SJ, Gotzsche PC, Vandenbroucke JP. The Strengthening the Reporting of Observational Studies in Epidemiology (STROBE) statement: guidelines for reporting observational studies. *J Clin Epidemiol.* (2008) 61:344–9. doi: 10.1016/j.jclinepi.2007.11.008
33. Horst K, Simon TP, Pfeifer R, Teuben M, Almahmoud K, Zhi Q, et al. Characterization of blunt chest trauma in a long-term porcine model of severe multiple trauma. *Sci Rep.* (2016) 6:39659. doi: 10.1038/srep39659
34. Eschbach D, Steinfeldt T, Hildebrand F, Frink M, Scholler K, Sassen M, et al. A porcine polytrauma model with two different degrees of hemorrhagic shock: outcome related to trauma within the first 48 h. *Eur J Med Res.* (2015) 20:73. doi: 10.1186/s40001-015-0162-0
35. Horst K, Eschbach D, Pfeifer R, Hubenthal S, Sassen M, Steinfeldt T, et al. Local inflammation in fracture hematoma: results from a combined trauma model in pigs. *Mediators Inflamm.* (2015) 2015:126060. doi: 10.1155/2015/126060
36. Artimovich E, Jackson RK, Kilander MBC, Lin YC, Nestor MW. PeakCaller: an automated graphical interface for the quantification of intracellular calcium obtained by high-content screening. *BMC Neurosci.* (2017) 18:72. doi: 10.1186/s12868-017-0391-y
37. Ballard-Croft C, Carlson D, Maass DL, Horton JW. Burn trauma alters calcium transporter protein expression in the heart. *J Appl Physiol.* (2004) 97:1470–6. doi: 10.1152/japplphysiol.01149.2003
38. Tanaka T, Kanda T, Takahashi T, Saegusa S, Moriya J, Kurabayashi M. Interleukin-6-induced reciprocal expression of SERCA and natriuretic

peptides mRNA in cultured rat ventricular myocytes. *J Int Med Res.* (2004) 32:57–61. doi: 10.1177/147323000403200109

39. Duncan DJ, Yang Z, Hopkins PM, Steele DS, Harrison SM. TNF-α and IL-1β increase Ca^{2+} leak from the sarcoplasmic reticulum and susceptibility to arrhythmia in rat ventricular myocytes. *Cell Calcium.* (2010) 47:378–86. doi: 10.1016/j.ceca.2010.02.002
40. Zhang C, Mo M, Ding W, Liu W, Yan D, Deng J, et al. High-mobility group box 1 (HMGB1) impaired cardiac excitation-contraction coupling by enhancing the sarcoplasmic reticulum (SR) Ca(2+) leak through TLR4-ROS signaling in cardiomyocytes. *J Mol Cell Cardiol.* (2014) 74:260–73. doi: 10.1016/j.yjmcc.2014.06.003
41. Kalbitz M, Schwarz S, Weber B, Bosch B, Pressmar J, Hoenes FM, et al. Cardiac depression in pigs after multiple trauma - characterization of posttraumatic structural and functional alterations. *Sci Rep.* (2017) 7:17861. doi: 10.1038/s41598-017-18088-1
42. Fattahi F, Frydrych LM, Bian G, Kalbitz M, Herron TJ, Malan EA, et al. Role of complement C5a and histones in septic cardiomyopathy. *Mol Immunol.* (2018) 102:32–41. doi: 10.1016/j.molimm.2018.06.006
43. He H, Giordano FJ, Hilal-Dandan R, Choi DJ, Rockman HA, McDonough PM, et al. Overexpression of the rat sarcoplasmic reticulum Ca^{2+} ATPase gene in the heart of transgenic mice accelerates calcium transients and cardiac relaxation. *J Clin Invest.* (1997) 100:380–9. doi: 10.1172/JCI119544
44. Vetter R, Rehfeld U, Reissfelder C, Weiss W, Wagner KD, Gunther J, et al. Transgenic overexpression of the sarcoplasmic reticulum Ca^{2+} ATPase improves reticular Ca^{2+} handling in normal and diabetic rat hearts. *FASEB J.* (2002) 16:1657–9. doi: 10.1096/fj.01-1019fje
45. Tatsumi T, Matoba S, Kawahara A, Keira N, Shiraishi J, Akashi K, et al. Cytokine-induced nitric oxide production inhibits mitochondrial energy production and impairs contractile function in rat cardiac myocytes. *J Am Coll Cardiol.* (2000) 35:1338–46. doi: 10.1016/S0735-1097(00)00526-X
46. Shen YL, Shi YZ, Chen GG, Wang LL, Zheng MZ, Jin HF, et al. TNF-α induces Drp1-mediated mitochondrial fragmentation during inflammatory cardiomyocyte injury. *Int J Mol Med.* (2018) 41:2317–27. doi: 10.3892/ijmm.2018.3385
47. Boyd JH, Mathur S, Wang Y, Bateman RM, Walley KR. Toll-like receptor stimulation in cardiomyoctes decreases contractility and initiates an NF-κB dependent inflammatory response. *Cardiovasc Res.* (2006) 72:384–93. doi: 10.1016/j.cardiores.2006.09.011
48. Bruns B, Maass D, Barber R, Horton J, Carlson D. Alterations in the cardiac inflammatory response to burn trauma in micelacking a functional Toll-like receptor 4 gene. *Shock.* (2008) 30:740–6. doi: 10.1097/SHK.0b013e318173f329
49. Avlas O, Fallach R, Shainberg A, Porat E, Hochhauser E. Toll-like receptor 4 stimulation initiates an inflammatory response that decreases cardiomyocyte contractility. *Antioxid Redox Signal.* (2011) 15:1895–909. doi: 10.1089/ars.2010.3728
50. Darrabie MD, Cheeseman J, Limkakeng AT, Borawski J, Sullenger BA, Elster EA, et al. Toll-like receptor activation as a biomarker in traumatically injured patients. *J Surg Res.* (2018) 231:270–7. doi: 10.1016/j.jss.2018.05.059
51. Gao H, Yin J, Shi Y, Hu H, Li X, Xue M, et al. Targeted P2X7 R shRNA delivery attenuates sympathetic nerve sprouting and ameliorates cardiac dysfunction in rats with myocardial infarction. *Cardiovasc Ther.* (2017) 35. doi: 10.1111/1755-5922.12245
52. Owada K, Sanjo N, Kobayashi T, Mizusawa H, Muramatsu H, Muramatsu T, et al. Midkine inhibits caspase-dependent apoptosis via the activation of mitogen-activated protein kinase and phosphatidylinositol 3-kinase in cultured neurons. *J Neurochem.* (1999) 73:2084–92. doi: 10.1046/j.1471-4159.1999.02084.x
53. Ohuchida T, Okamoto K, Akahane K, Higure A, Todoroki H, Abe Y, et al. Midkine protects hepatocellular carcinoma cells against TRAIL-mediated apoptosis through down-regulation of caspase-3 activity. *Cancer.* (2004) 100:2430–6. doi: 10.1002/cncr.20266
54. Housch yar KS, Pyles MN, Rein S, Nietzschmann I, Duscher D, Maan ZN, et al. Continuous hemoadsorption with a cytokine adsorber during sepsis - a review of the literature. *Int J Artif Organs.* (2017) 40:205–11. doi: 10.5301/ijao.5000591
55. Haffner-Luntzer M, Fischer V, Prystaz K, Liedert A, Ignatius A. The inflammatory phase of fracture healing is influenced by oestrogen status in mice. *Eur J Med Res.* (2017) 22:23. doi: 10.1186/s40001-017-0264-y

Conflict of Interest Statement: The authors declare that the research was conducted in the absence of any commercial or financial relationships that could be construed as a potential conflict of interest.

Copyright © 2019 Lackner, Weber, Baur, Haffner-Luntzer, Eiseler, Fois, Gebhard, Relja, Marzi, Pfeifer, Halvachizadeh, Lipiski, Cesarovic, Pape, Kalbitz and TREAT Research Group. This is an open-access article distributed under the terms of the Creative Commons Attribution License (CC BY). The use, distribution or reproduction in other forums is permitted, provided the original author(s) and the copyright owner(s) are credited and that the original publication in this journal is cited, in accordance with accepted academic practice. No use, distribution or reproduction is permitted which does not comply with these terms.

frontiers in Immunology

MINI REVIEW
published: 22 August 2019
doi: 10.3389/fimmu.2019.01982

IL-17, IL-27, and IL-33: A Novel Axis Linked to Immunological Dysfunction During Sepsis

Kristen N. Morrow[1,2], *Craig M. Coopersmith*[2,3] *and Mandy L. Ford*[2,4]*

[1] *Immunology and Molecular Pathogenesis Program, Laney Graduate School, Emory University, Atlanta, GA, United States,* [2] *Department of Surgery, Emory University School of Medicine, Atlanta, GA, United States,* [3] *Emory Critical Care Center, Emory University School of Medicine, Atlanta, GA, United States,* [4] *Emory Transplant Center, Emory University School of Medicine, Atlanta, GA, United States*

Sepsis is a major cause of morbidity and mortality worldwide despite numerous attempts to identify effective therapeutics. While some sepsis deaths are attributable to tissue damage caused by inflammation, most mortality is the result of prolonged immunosuppression. *Ex vivo*, immunosuppression during sepsis is evidenced by a sharp decrease in the production of pro-inflammatory cytokines by T cells and other leukocytes and increased lymphocyte apoptosis. This allows suppressive cytokines to exert a greater inhibitory effect on lymphocytes upon antigen exposure. While some pre-clinical and clinical trials have demonstrated utility in targeting cytokines that promote lymphocyte survival, this has not led to the approval of any therapies for clinical use. As cytokines with a more global impact on the immune system are also altered by sepsis, they represent novel and potentially valuable therapeutic targets. Recent evidence links interleukin (IL)-17, IL-27, and IL-33 to alterations in the immune response during sepsis using patient serum and murine models of peritonitis and pneumonia. Elevated levels of IL-17 and IL-27 are found in the serum of pediatric and adult septic patients early after sepsis onset and have been proposed as diagnostic biomarkers. In contrast, IL-33 levels increase in patient serum during the immunosuppressive stage of sepsis and remain high for more than 5 months after recovery. All three cytokines contribute to immunological dysfunction during sepsis by disrupting the balance between type 1, 2, and 17 immune responses. This review will describe how IL-17, IL-27, and IL-33 exert these effects during sepsis and their potential as therapeutic targets.

Keywords: sepsis, IL-17, IL-33, critical illness, cytokine, immunological dysfunction, IL-27

OPEN ACCESS

Edited by:
Christoph Thiemermann, Queen Mary University of London, United Kingdom

Reviewed by:
Sian M. Henson, Queen Mary University of London, United Kingdom
Marcin Filip Osuchowski, Ludwig Boltzmann Institute for Experimental and Clinical Traumatology, Austria

***Correspondence:**
Mandy L. Ford
mandy.ford@emory.edu

Specialty section:
This article was submitted to Inflammation, a section of the journal Frontiers in Immunology

Received: *15 June 2019*
Accepted: *05 August 2019*
Published: *22 August 2019*

Citation:
Morrow KN, Coopersmith CM and Ford ML (2019) IL-17, IL-27, and IL-33: A Novel Axis Linked to Immunological Dysfunction During Sepsis. Front. Immunol. 10:1982. doi: 10.3389/fimmu.2019.01982

INTRODUCTION TO SEPSIS AND THE IL-17/IL-27/IL-33 AXIS

Although it was first described centuries ago, sepsis remains a leading cause of morbidity and mortality. While the infectious agent and the organ system(s) impacted can vary between patients, sepsis is characterized by immune dysfunction linked to alterations in systemic cytokine levels and lymphocyte apoptosis (1). The immune response during sepsis was originally thought to proceed through two distinct phases through which an initially hyper-inflammatory immune response shifted toward profound immunosuppression caused by lymphocyte impairment (2). However, this only reflects the phenotype of circulating lymphocytes in some immunocompetent patients (3–6) and does not reflect the immune response in immunocompromised patients (7).

In addition, evidence now exists that both pro- and anti-inflammatory cytokines are released shortly after sepsis onset (8, 9) and continue to be released in tandem throughout the course of the illness (10–12).

While there have been many positive animal studies demonstrating the beneficial effect of targeting cytokines during sepsis, this has not translated into improvements in clinical treatment; no clinical trials so far have led to an approved therapeutic. The reasons behind this are multifactorial and partially stem from a failure to consider the interaction between individual cytokines and the larger cytokine milieu. In addition, the cytokine milieu varies between septic patients, making it difficult to distinguish any benefit in large studies of heterogenous patients. Although the failure of cytokine-based therapy in septic patients has been disappointing, recent phase I clinical trials (such as IL-7 infusion) have demonstrated the potential benefit of immunomodulation (13). However, before additional cytokines can be considered as therapeutic targets for sepsis, further work needs to be done to define the alterations that occur across the cytokine milieu during sepsis and distinguish how individual cytokines interact and modulate the effects of one another.

Recent work on the cytokines IL-17, IL-27, and IL-33 suggest the presence of a novel cytokine axis during sepsis. IL-17 primarily acts to promote the inflammatory response in mucosal tissue. In humans, serum levels of IL-17 are predictive of the development of sepsis and mortality in poly-trauma patients (14) and mutations in the IL-17A gene are associated with increased susceptibility to infection caused by gram positive bacteria and mortality (15). The immunosuppressive cytokine IL-27 increases in the plasma of many septic patients (16–27) and has been shown to inhibit the differentiation of Th17 cells (16, 18, 19, 28–33). These results have been recapitulated in diverse models of sepsis in mice (34–38). The blockade of the p28 subunit of IL-27 (38) or depletion of IL-27 using a soluble and recombinant IL-27Rα (34) significantly reduces mortality in the cecal ligation and puncture (CLP) model of sepsis and is associated with reduced bacterial burden in the tissues and blood. IL-33 is a member of the IL-1 family of cytokines that modulates Th2 responses and decreases the differentiation of T cells into Th17 cells (39). IL-33 signals through the cytokine receptor ST2 and plays an anti-inflammatory role during sepsis, improving survival during the early stages of sepsis but ultimately leading to long lasting immunosuppression through the induction of regulatory T cells (Tregs) (40–42). In addition to its interactions with IL-17, IL-33 has also been reported to interact with IL-27, with both modulating the activity of ILC2 cells (43–46). As the importance of ILC2 cells during sepsis has recently been described (47–49), these interactions may become increasingly significant for the development of effective therapeutics.

In this review, we will further discuss the individual and combined roles of IL-17, IL-27, and IL-33 during sepsis and how this axis might be therapeutically targeted.

The Role of IL-17 in Sepsis Pathophysiology

The IL-17 family of cytokines is composed of the structurally similar IL-17A-F. Apart from IL-17A (classically referred to as IL-17) and IL-17F, all the cytokines in this family are encoded separately, although they share conserved sequences. The earliest studies addressing the role of IL-17A during sepsis in animal models reported that they induced significant pathology and that eliminating IL-17A resulted in significantly improved survival (50, 51). However, subsequent studies using mice deficient in the IL-17 receptor found opposite results (52), and the literature now contains numerous studies demonstrating the mixed effects of IL-17A blockade in sepsis.

In 2012, Ogiku et al. reported that mice lacking IL-17A had significantly increased mortality following CLP that correlated with higher bacteremia at 12 h (53). Similarly, a more recent paper using the CLP model concluded that IL-17 has a partially protective role during sepsis: wild type mice had significantly increased survival and IgA production after CLP when compared to IL-17$^{-/-}$ mice (54). Interestingly, this study found that non-canonical signaling through NF-κB was responsible for much of the IL-17A production, as mice lacking RANKL and NF-κB inducing kinase (NIK) signaling in their intestinal epithelium cells had significantly reduced IL-17A and mortality similar to IL-17$^{-/-}$ mice (54).

Other studies have found that the impact of IL-17A on sepsis mortality depends on the microbe that initiated the infection. Using a bacterial pneumonia model, Ritchie et al. found that the role of IL-17A in sepsis is highly dependent on the encapsulation status of the infecting bacterium (55). IL-17A was beneficial during infections caused by minimally encapsulated bacteria, but significantly increased lung pathology and mortality if the infectious organism was heavily encapsulated (55). The authors concluded that this was due to the accumulation of neutrophils unable to phagocytose the bacteria (55). In conjunction with IL-23 signaling, IL-17A increases the recruitment of neutrophils and their accumulation in the lung following CLP, partially explaining the inflammation seen in the lung following polymicrobial sepsis originating in other tissues (56). IL-17 has also been linked to the development of acute kidney injury in septic patients and animal models (57). Given these findings, it is not surprising that multiple groups have reported that the neutralization of IL-17A or IL-17F improves survival (58, 59).

As the results of these sepsis studies conflict, it is important to note that IL-17A can induce the production of other IL-17 family cytokines, especially IL-17C (60). Although it is a distinct cytokine, it plays a similar role in neutrophil recruitment and the inflammatory process to IL-17A (60). In a mouse model of pneumonia induced by *Pseudomonas aeruginosa*, mice lacking IL-17C had 100% survival at 48 h, whereas wild type mice had only 25% survival at this time point (60). In contrast, another recent paper reported that IL-17C induction provides protection against LPS-induced endotoxemia (61). As IL-17C has been reported promote the production of IL-17A by Th17 lymphocytes in inflammatory conditions (such as autoimmune disease) (62), the authors concluded that these effects may be due more to the promotion of IL-17A than to IL-17C alone.

The Role of IL-27 in Sepsis Pathophysiology

Originally thought to be pro-inflammatory, there is now consensus that IL-27 is a potent immunosuppressant. It is composed of an alpha subunit (IL-27p28, also known as IL-30)

and EBI3 (shared with IL-35) (63). IL-27 binds to the IL-27 receptor alpha (IL-27Rα, also known as WSX-1) and gp130 and is primarily produced by dendritic cells (DCs), monocytes and macrophages (63). The lymphocyte populations that respond to the presence of IL-27 or one of its subunits are T cells, natural killer (NK) cells, natural killer T (NKT) cells, and DCs (64–69). This allows IL-27 to have wide ranging effects on cells of both the innate and adaptive immune response in addition to autocrine effects.

In septic patients and in murine models of sepsis, the plasma concentration of IL-27 significantly increases (34, 35, 70, 71), briefly causing it to be considered as a potential diagnostic biomarker in adults (22–24) and children (20, 26). However, these results have not been consistently replicated in humans, limiting its current therapeutic potential. In mice, the results are more consistent and indicate a clear role for IL-27 in the pathology of sepsis and critical illness. When the p28 subunit is neutralized or the IL-27Rα is blocked, mortality is significantly decreased in both CLP and endotoxemia (34, 37, 38).

In a study by Cao et al., mice lacking the IL-27Rα were resistant to a secondary bacterial infection caused by *Pseudomonas aeruginosa* following CLP in a manner dependent on alveolar macrophages and neutrophils (37). Specifically, the neutrophils and alveolar macrophages in these mice had a significantly improved ability to kill *P. aeruginosa* upon phagocytosis (37). Similarly, Bosmann et al. observed that the oxidative burst of macrophages was improved upon the elimination of IL-27 signaling, and determined that IL-10 limits the production of IL-27p28 *in vivo* following CLP (38). In addition, this study found that the cells primarily responsible for the production of IL-27p28 in the CLP model of sepsis are splenic macrophages (38). However, a more recent study has found conflicting evidence that indicates a protective role for p28 during sepsis (72). In this study, the administration of the p28 subunit or its overproduction through genetic therapy led to a reduction in mortality during sepsis directly linked to the reduction in NKT cell production of inflammatory cytokines (72).

In addition to its modulation of innate cells, IL-27 has a significant impact on T cells. IL-27 can promote the differentiation of Th1 cells and it is also a potent inducer of type 1 Treg (Tr1) cells (73). While Tr1 cells produce IFN-γ, they also produce large quantities of IL-10 and have potent suppressive functions (74). In addition to the induction of this cell population, IL-27 signaling leads to an increase in co-inhibitory molecule expression on T cells following chronic antigen exposure and during cancer (75). As T cell dysfunction and exhaustion is associated with the development of immunosuppression during sepsis and ultimately worsened survival (76–79), IL-27 could be an effective therapeutic target. However, mice can produce IL-27p28 in the absence of EBI3, so it is unclear if the reported effects of IL-27 during sepsis are actually due to the full heterodimeric cytokine or merely to its alpha subunit. A group has recently reported the development of transgenic B57L/6J mice in which the IL-27p28 subunit cannot be produced independently of EBI3 (80). This animal model will be necessary to truly distinguish the effects of IL-27p28 from those of IL-27.

The Role of IL-33 in Sepsis Pathophysiology

ST2 was an orphan receptor until 2005, when Schmitz et al. reported their discovery of IL-33 (81). A member of the IL-1 family, IL-33 is constitutively expressed by endothelial and epithelial cells in barrier tissues and is also found at high levels under inflammatory conditions in other tissues (82, 83). When T cells, mast cells, eosinophils, and ILC2s receive IL-33 signaling, the immune response shifts toward a type 2 response (81, 84).

The first paper to describe the role of IL-33 (rather than its receptor ST2) in sepsis was published by Alves-Filho et al. (40). The authors found that survival significantly increased when IL-33 was administered to mice following CLP (40). Another 2010 study found that IL-33 is protective against LPS induced endotoxemia (85). The ability of IL-33 to improve survival during sepsis is linked to the rescue of neutrophil migration to the site of infection (40), to improvements in bacterial clearance, and to a reduction in lymphocyte apoptosis (41). IL-33 also suppresses the inflammatory response by a variety of innate lymphocytes (86) and modulates the activity of ILC2 cells (47–49). In addition to direct effects on other lymphocytes, IL-33 impacts the activity of other cytokines, including IL-17 (41, 87). While IL-33 can bind to a soluble form of ST2 (sST2), the effects of IL-33 during sepsis appear to be dependent on signaling through membrane bound ST2; in one study, patients who had did not survive sepsis had higher levels of sST2 than patients that went on to survive their infections (40).

Despite being linked to improvements in survival early after sepsis onset, IL-33 signaling may not always be beneficial. IL-33 is implicated in the induction and maintenance of immunosuppression during sepsis through the induction of Tregs (42). Nascimento et al. found that this occurs through the production of IL-4 and IL-13 by ILC2s that receive IL-33 signaling (42). The IL-4 and IL-13 then drives the proliferation of IL-10 producing macrophages and ultimately an expansion in Treg numbers (42). When they examined the blood of a small number of patients who had been diagnosed with sepsis 5–10 months prior, they found that sepsis survivors had significantly higher concentrations of both IL-10 and IL-33 and higher circulating Treg numbers compared to previously healthy patients (42). While these findings need to be replicated, they suggest that the impact of IL-33 signaling may depend on the stage of disease.

INTERACTIONS BETWEEN IL-17, IL-27, AND IL-33

The ability for lymphocytes to recognize and respond to slight changes in their environment makes the immune system very adaptable and ensures that the balance between inflammatory and immunosuppressive responses is fine-tuned. While the ability of lymphocytes to respond so readily to their surroundings is beneficial from an evolutionary point of view, it makes it significantly harder to elucidate the role of individual cytokines. The individual and combined actions of the cytokines in the IL-17, IL-27, and IL-33 axis are summarized in **Figure 1**.

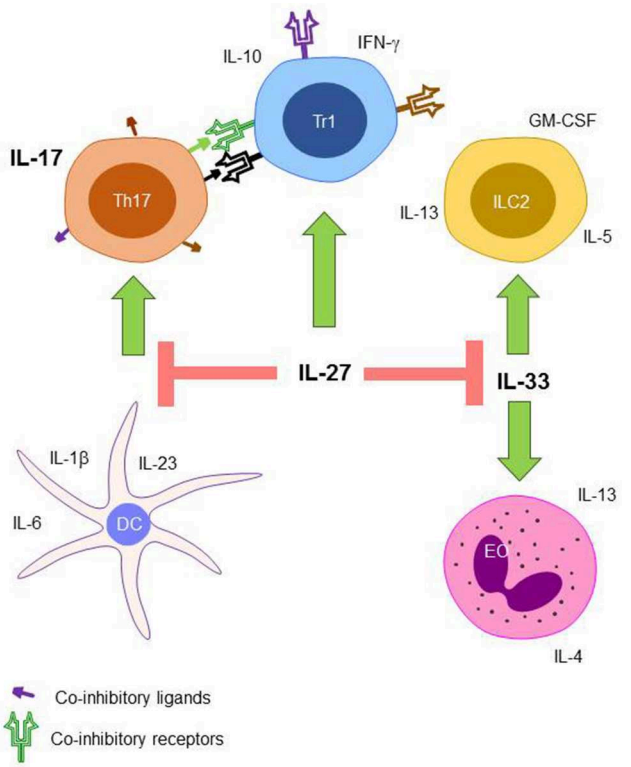

FIGURE 1 | The proposed role of the IL-17, IL-27, and IL-33 axis during sepsis. Th17 cells that receive co-inhibitory signaling from IL-27 induced Tr1 cells have inhibited production of IL-17. Differentiation of naïve T cells into Th17 cells is also inhibited by IL-27 through the modulation of DC cytokine production. ILC2 cells and EOs expansion are also inhibited through the action of IL-27 signaling on IL-33. Th17, T helper type 17 cell; Tr1, T regulatory type 1 cell; ILC2, innate lymphocyte type 2 cell; DC, dendritic cell; EO, eosinophil.

IL-17 and IL-27

IL-17 plays a harmful role in many autoimmune diseases, particularly experimental autoimmune encephalomyelitis (EAE) and rheumatoid arthritis (RA). By limiting the differentiation of naïve $CD4^+$ T cells into Th17 cells, IL-27 is able to attenuate these diseases (16, 19, 28, 31, 32, 88). Similarly, IL-27 signaling prevents the development of neurological damage during chronic *Toxoplasma gondii* infection (18) and reduces tissue damage during RSV infection (89). Further research has shown that STAT1 signaling (which IL-27 induces) inhibits the expression of the transcription factor RORγt, necessary for Th17 differentiation, while promoting the induction of the protein suppressor of cytokine signaling 1 (SOCS1) (16, 19, 30, 90). This leads to the suppression of IL-22 production by Th17 cells, impairing antimicrobial defenses in the epithelium (30, 33). In addition to its direct effects on T cells, IL-27 can also inhibit Th17 differentiation by inhibiting the production of the Th17-polarizing cytokines IL-1β, IL-6, and IL-23 by DCs (29). In contrast, T cells that have already committed to the Th17 lineage are not directly inhibited by IL-27 signaling (28, 91). Instead, inhibition occurs indirectly through the induction of Tr1 (29) and the expression of co-inhibitory receptors and their ligands (32, 88).

IL-17 and IL-33

Similar to IL-27, IL-33 has been reported to attenuate EAE through the suppression of Th17 responses (92). While IL-33 attenuates sepsis mortality, it is less clear if this is due to any effect on the Th17 response. One group reported that the administration of IL-33 actually enhanced the production of IL-17 while decreasing the levels of IL-6, IL-10, and IFNγ following CLP (41). Similarly, another group found that the deletion of the IL-33 receptor ST2 led to a reduction in the frequency and number of IL-17 producing NK cells after CLP (86). However, a recent study of human patients with *Staphylococcus aureus* bacteremia revealed that a higher ratio of Th17 to Th1 cytokines early after sepsis onset was associated with increased mortality (49). As there was a trend toward increased Th2 cells in surviving patients, the authors did a follow up study using a mouse model of *S. aureus* bacteremia (49). IL-33 provided a survival benefit in this model that was dependent on functional ILC2s and EOs, suggesting that IL-33 is protective in part because it re-balances type 1, 2, and 17 responses during sepsis (49).

IL-27 and IL-33

While IL-27 signaling promotes type 1 immune responses and directly limits type 17 immunity, it also serves as a negative regulator of type 2 responses by interfering with IL-33 signaling. The first paper to describe this phenomenon utilized *in vitro* experiments which showed that IL-27 reduced type 2 cytokine production in bone marrow cells exposed to IL-33, including IL-5, IL-13, and GM-CSF (43). For IL-5, this effect was dependent on STAT1 signaling, as STAT1 knockout bone marrow cells were not impacted by the presence of IL-27 (43). Moro et al. confirmed these findings *in vivo* using STAT1 knockout mice, and revealed that while IL-27 reduces type 2 cytokine production by ILC2 cells, it does not affect cytokine production in Th2 cells (44). Another recent study reported that the administration of IL-27 limits IL-33 induced ILC2 accumulation and activation in the lungs, liver, spleen, and mesenteric lymph node *in vivo* (45). The administration of IL-27 also led to the overrepresentation of IL-27Rα$^{-/-}$ cells in chimeric mice (45). While not specifically addressing IL-27, another murine study found that STAT1 signaling induced by infection with respiratory syncytial virus is sufficient to reduce the production of IL-33 (46). These studies collectively show that a major function of IL-27 is to negatively regulate the type 2 immune response, specifically ILC2 cells, in a manner that is dependent on STAT1 signaling.

EXPLOITING THE IL-17, IL-27, AND IL-33 AXIS DURING SEPSIS

While many reviews have discussed the therapeutic potential for targeting IL-17, IL-27, and IL-33 during sepsis (93–95), none have considered the effect that treatment targeting only one of these cytokines may have on the others. In addition, the compartmentalization of the immune response during sepsis means that cytokine therapies that

restore the function of circulating lymphocytes could cause excessive stimulation and ultimately programmed cell death in the more normally responsive tissue lymphocytes. To aid the specificity of these therapies, binding should be targeted to cells expressing the circulatory chemokine receptor molecule CCR7 or the integrin CD62L (required for lymphocyte extravasation into the lymphatic system).

As IL-17 can have either beneficial or detrimental roles during sepsis depending on the murine model used, it is currently unclear what course of action would be most beneficial for human patients. However, anything that significantly increases IL-17 levels for a long period of time raises the risk of auto-immune disease formation and increased tissue damage. It seems more tenable to target IL-27 and IL-33, with an eye to keeping a balance between these cytokines and IL-17.

Neutralizing IL-27 seems likely to provide a survival benefit in septic patients if administered early after disease onset. IL-27 signaling shifts the balance too far toward a type 1 regulatory response, but its neutralization would balance type 1 and type 2 responses through the increase in activity of the type 2 promoting cytokine IL-33. IL-33 signaling has been shown to improve sepsis survival in the short term in murine models, although one report suggests that IL-33 is linked to the development of immunosuppression during sepsis (42). In this study, mice lacking the IL-33 receptor had attenuated immunosuppression associated with a reduction in type 2 cytokines, ILC2 cells, and Tregs (42). It is currently unknown how much IL-33 signaling changes during sepsis in the absence of IL-27 signaling and therefore might lower the efficacy of IL-27 blockade in improving long term survival in sepsis patients who receive no further interventions.

Ultimately, targeting any of these cytokines in an indiscriminate fashion is unlikely to be clinically beneficial. However, understanding the complex interplay between IL-17, IL-27, and IL-33—including the timing in which cytokine augmentation or blockade may potentially be beneficial—suggests this axis may potentially be manipulatable for therapeutic gain as part of a precision medicine approach toward sepsis treatment.

AUTHOR CONTRIBUTIONS

KM wrote the initial draft of the manuscript. The final manuscript includes equal contribution from MF and CC.

FUNDING

This work was supported by funding from the National Institutes of Health (GM113228, GM104323, AA027396, GM072808).

REFERENCES

1. Gogos C, Kotsaki A, Pelekanou A, Giannikopoulos G, Vaki I, Maravitsa P, et al. Early alterations of the innate and adaptive immune statuses in sepsis according to the type of underlying infection. *Crit Care*. (2010) 14:R96. doi: 10.1186/cc9031
2. Oberholzer A, Oberholzer C, Moldawer LL. Sepsis syndromes: understanding the role of innate and acquired immunity. *Shock*. (2001) 16:83–96. doi: 10.1097/00024382-200116020-00001
3. Cavaillon JM, Adib-Conquy M, Cloez-Tayarani I, Fitting C. Immunodepression in sepsis and SIRS assessed by *ex vivo* cytokine production is not a generalized phenomenon: a review. *J Endotoxin Res*. (2001) 7:85–93. doi: 10.1177/09680519010070020201
4. Ayala A, Herdon CD, Lehman DL, Ayala CA, Chaudry IH. Differential induction of apoptosis in lymphoid tissues during sepsis: variation in onset, frequency, and the nature of the mediators. *Blood*. (1996) 87: 4261–75.
5. Cavaillon JM, Annane D. Compartmentalization of the inflammatory response in sepsis and SIRS. *J Endotoxin Res*. (2006) 12:151–70. doi: 10.1179/096805106X102246
6. Cavaillon JM, Adib-Conquy M. Determining the degree of immunodysregulation in sepsis. *Contrib Nephrol*. (2007) 156:101–11. doi: 10.1159/000102075
7. Kalil AC, Opal SM. Sepsis in the severely immunocompromised patient. *Curr Infect Dis Rep*. (2015) 17:487. doi: 10.1007/s11908-015-0487-4
8. Tamayo E, Fernandez A, Almansa R, Carrasco E, Heredia M, Lajo C, et al. Pro- and anti-inflammatory responses are regulated simultaneously from the first moments of septic shock. *Eur Cytokine Netw*. (2011) 22:82–7. doi: 10.1684/ecn.2011.0281
9. Cazalis MA, Lepape A, Venet F, Frager F, Mougin B, Vallin H, et al. Early and dynamic changes in gene expression in septic shock patients: a genome-wide approach. *Intensive Care Med Exp*. (2014) 2:20. doi: 10.1186/s40635-014-0020-3
10. Frencken JF, van Vught LA, Peelen LM, Ong DSY, Klein Klouwenberg PMC, Horn J, et al. An unbalanced inflammatory cytokine response is not associated with mortality following sepsis: a prospective cohort study. *Crit Care Med*. (2017) 45:e493–e9. doi: 10.1097/CCM.0000000000002292
11. Osuchowski MF, Craciun F, Weixelbaumer KM, Duffy ER, Remick DG. Sepsis chronically in MARS: systemic cytokine responses are always mixed regardless of the outcome, magnitude, or phase of sepsis. *J Immunol*. (2012) 189:4648–56. doi: 10.4049/jimmunol.1201806
12. Andaluz-Ojeda D, Bobillo F, Iglesias V, Almansa R, Rico L, Gandia F, et al. A combined score of pro- and anti-inflammatory interleukins improves mortality prediction in severe sepsis. *Cytokine*. (2012) 57:332–6. doi: 10.1016/j.cyto.2011.12.002
13. Francois B, Jeannet R, Daix T, Walton AH, Shotwell MS, Unsinger J, et al. Interleukin-7 restores lymphocytes in septic shock: the IRIS-7 randomized clinical trial. *JCI Insight*. (2018) 3:98960. doi: 10.1172/jci.insight.98960
14. Ahmed Ali M, Mikhael ES, Abdelkader A, Mansour L, El Essawy R, El Sayed R, et al. Interleukin-17 as a predictor of sepsis in polytrauma patients: a prospective cohort study. *Eur J Trauma Emerg Surg*. (2018) 44:621–6. doi: 10.1007/s00068-017-0841-3
15. Nakada TA, Russell JA, Boyd JH, Walley KR. IL17A genetic variation is associated with altered susceptibility to Gram-positive infection and mortality of severe sepsis. *Crit Care*. (2011) 15:R254. doi: 10.1186/cc10515
16. Diveu C, McGeachy MJ, Boniface K, Stumhofer JS, Sathe M, Joyce-Shaikh B, et al. IL-27 blocks RORc expression to inhibit lineage commitment of Th17 cells. *J Immunol*. (2009) 182:5748–56. doi: 10.4049/jimmunol.0801162
17. Colgan J, Rothman P. All in the family: IL-27 suppression of T(H)-17 cells. *Nat Immunol*. (2006) 7:899–901. doi: 10.1038/ni0906-899
18. Stumhofer JS, Laurence A, Wilson EH, Huang E, Tato CM, Johnson LM, et al. Interleukin 27 negatively regulates the development of interleukin 17-producing T helper cells during chronic inflammation of the central nervous system. *Nat Immunol*. (2006) 7:937–45. doi: 10.1038/ni1376
19. Batten M, Li J, Yi S, Kljavin NM, Danilenko DM, Lucas S, et al. Interleukin 27 limits autoimmune encephalomyelitis by suppressing the development of interleukin 17-producing T cells. *Nat Immunol*. (2006) 7:929–36. doi: 10.1038/ni1375

20. Wong HR, Cvijanovich NZ, Hall M, Allen GL, Thomas NJ, Freishtat RJ, et al. Interleukin-27 is a novel candidate diagnostic biomarker for bacterial infection in critically ill children. *Crit Care*. (2012) 16:R213. doi: 10.1186/cc11847
21. Scicluna BP, van der Poll T. Interleukin-27: a potential new sepsis biomarker exposed through genome-wide transcriptional profiling. *Crit Care*. (2012) 16:188. doi: 10.1186/cc11893
22. Wong HR, Lindsell CJ, Lahni P, Hart KW, Gibot S. Interleukin 27 as a sepsis diagnostic biomarker in critically ill adults. *Shock*. (2013) 40:382–6. doi: 10.1097/SHK.0b013e3182a67632
23. Wong HR, Liu KD, Kangelaris KN, Lahni P, Calfee CS. Performance of interleukin-27 as a sepsis diagnostic biomarker in critically ill adults. *J Crit Care*. (2014) 29:718–22. doi: 10.1016/j.jcrc.2014.04.004
24. Hanna WJ, Berrens Z, Langner T, Lahni P, Wong HR. Interleukin-27: a novel biomarker in predicting bacterial infection among the critically ill. *Crit Care*. (2015) 19:378. doi: 10.1186/s13054-015-1095-2
25. Gao F, Yang YZ, Feng XY, Fan TT, Jiang L, Guo R, et al. Interleukin-27 is elevated in sepsis-induced myocardial dysfunction and mediates inflammation. *Cytokine*. (2016) 88:1–11. doi: 10.1016/j.cyto.2016.08.006
26. He Y, Du WX, Jiang HY, Ai Q, Feng J, Liu Z, et al. Multiplex cytokine profiling identifies interleukin-27 as a novel biomarker for neonatal early onset sepsis. *Shock*. (2017) 47:140–7. doi: 10.1097/SHK.0000000000000753
27. He J, Zhang Q, Zhang W, Chen F, Zhao T, Lin Y, et al. The interleukin-27−964A>G polymorphism enhances sepsis-induced inflammatory responses and confers susceptibility to the development of sepsis. *Crit Care*. (2018) 22:248. doi: 10.1186/s13054-018-2180-0
28. El-behi M, Ciric B, Yu S, Zhang GX, Fitzgerald DC, Rostami A. Differential effect of IL-27 on developing versus committed Th17 cells. *J Immunol*. (2009) 183:4957–67. doi: 10.4049/jimmunol.0900735
29. Murugaiyan G, Mittal A, Lopez-Diego R, Maier LM, Anderson DE, Weiner HL. IL-27 is a key regulator of IL-10 and IL-17 production by human CD4+ T cells. *J Immunol*. (2009) 183:2435–43. doi: 10.4049/jimmunol.0900568
30. Liu H, Rohowsky-Kochan C. Interleukin-27-mediated suppression of human Th17 cells is associated with activation of STAT1 and suppressor of cytokine signaling protein 1. *J Interferon Cytokine Res*. (2011) 31:459–69. doi: 10.1089/jir.2010.0115
31. Fitzgerald DC, Fonseca-Kelly Z, Cullimore ML, Safabakhsh P, Saris CJ, Zhang GX, et al. Independent and interdependent immunoregulatory effects of IL-27, IFN-beta, and IL-10 in the suppression of human Th17 cells and murine experimental autoimmune encephalomyelitis. *J Immunol*. (2013) 190:3225–34. doi: 10.4049/jimmunol.1200141
32. Moon SJ, Park JS, Heo YJ, Kang CM, Kim EK, Lim MA, et al. *In vivo* action of IL-27: reciprocal regulation of Th17 and Treg cells in collagen-induced arthritis. *Exp Mol Med*. (2013) 45:e46. doi: 10.1038/emm.2013.89
33. Wang H, Li Z, Yang B, Yu S, Wu C. IL-27 suppresses the production of IL-22 in human CD4(+) T cells by inducing the expression of SOCS1. *Immunol Lett*. (2013) 152:96–103. doi: 10.1016/j.imlet.2013.05.001
34. Wirtz S, Tubbe I, Galle PR, Schild HJ, Birkenbach M, Blumberg RS, et al. Protection from lethal septic peritonitis by neutralizing the biological function of interleukin 27. *J Exp Med*. (2006) 203:1875–81. doi: 10.1084/jem.20060471
35. Nelson DA, Tolbert MD, Clemens MG, Bost KL. Interleukin-27 expression following infection with the murine gammaherpesvirus 68. *Cytokine*. (2010) 51:184–94. doi: 10.1016/j.cyto.2010.04.015
36. Gwyer Findlay E, Villegas-Mendez A, O'Regan N, de Souza JB, Grady LM, Saris CJ, et al. IL-27 receptor signaling regulates memory CD4+ T cell populations and suppresses rapid inflammatory responses during secondary malaria infection. *Infect Immun*. (2014) 82:10–20. doi: 10.1128/IAI.01091-13
37. Cao J, Xu F, Lin S, Song Z, Zhang L, Luo P, et al. IL-27 controls sepsis-induced impairment of lung antibacterial host defence. *Thorax*. (2014) 69:926–37. doi: 10.1136/thoraxjnl-2014-205777
38. Bosmann M, Russkamp NF, Strobl B, Roewe J, Balouzian L, Pache F, et al. Interruption of macrophage-derived IL-27(p28) production by IL-10 during sepsis requires STAT3 but not SOCS3. *J Immunol*. (2014) 193:5668–77. doi: 10.4049/jimmunol.1302280
39. Liew FY. IL-33: a Janus cytokine. *Ann Rheum Dis*. (2012) 71 (Suppl. 2):i101–4. doi: 10.1136/annrheumdis-2011-200589
40. Alves-Filho JC, Sonego F, Souto FO, Freitas A, Verri WA Jr, Auxiliadora-Martins M, et al. Interleukin-33 attenuates sepsis by enhancing neutrophil influx to the site of infection. *Nat Med*. (2010) 16:708–12. doi: 10.1038/nm.2156
41. Li S, Zhu FX, Zhao XJ, An YZ. The immunoprotective activity of interleukin-33 in mouse model of cecal ligation and puncture-induced sepsis. *Immunol Lett*. (2016) 169:1–7. doi: 10.1016/j.imlet.2015.11.009
42. Nascimento DC, Melo PH, Pineros AR, Ferreira RG, Colon DF, Donate PB, et al. IL-33 contributes to sepsis-induced long-term immunosuppression by expanding the regulatory T cell population. *Nat Commun*. (2017) 8:14919. doi: 10.1038/ncomms14919
43. Duerr CU, McCarthy CD, Mindt BC, Rubio M, Meli AP, Pothlichet J, et al. Type I interferon restricts type 2 immunopathology through the regulation of group 2 innate lymphoid cells. *Nat Immunol*. (2016) 17:65–75. doi: 10.1038/ni.3308
44. Moro K, Kabata H, Tanabe M, Koga S, Takeno N, Mochizuki M, et al. Interferon and IL-27 antagonize the function of group 2 innate lymphoid cells and type 2 innate immune responses. *Nat Immunol*. (2016) 17:76–86. doi: 10.1038/ni.3309
45. McHedlidze T, Kindermann M, Neves AT, Voehringer D, Neurath MF, Wirtz S. IL-27 suppresses type 2 immune responses *in vivo* via direct effects on group 2 innate lymphoid cells. *Mucosal Immunol*. (2016) 9:1384–94. doi: 10.1038/mi.2016.20
46. Stier MT, Goleniewska K, Cephus JY, Newcomb DC, Sherrill TP, Boyd KL, et al. STAT1 represses cytokine-producing group 2 and group 3 innate lymphoid cells during viral infection. *J Immunol*. (2017) 199:510–9. doi: 10.4049/jimmunol.1601984
47. Xu H, Xu J, Xu L, Jin S, Turnquist HR, Hoffman R, et al. Interleukin-33 contributes to ILC2 activation and early inflammation-associated lung injury during abdominal sepsis. *Immunol Cell Biol*. (2018) 96:935–47. doi: 10.1111/imcb.12159
48. Chun TT, Chung CS, Fallon EA, Hutchins NA, Clarke E, Rossi AL, et al. Group 2 innate lymphoid cells (ILC2s) are key mediators of the inflammatory response in polymicrobial sepsis. *Am J Pathol*. (2018) 188:2097–108. doi: 10.1016/j.ajpath.2018.05.009
49. Krishack PA, Louviere TJ, Decker TS, Kuzel TG, Greenberg JA, Camacho DF, et al. Protection against *Staphylococcus aureus* bacteremia-induced mortality depends on ILC2s and eosinophils. *JCI Insight*. (2019) 4:e124168. doi: 10.1172/jci.insight.124168
50. Chung DR, Kasper DL, Panzo RJ, Chitnis T, Grusby MJ, Sayegh MH, et al. CD4+ T cells mediate abscess formation in intra-abdominal sepsis by an IL-17-dependent mechanism. *J Immunol*. (2003) 170:1958–63. doi: 10.4049/jimmunol.170.4.1958
51. Flierl MA, Rittirsch D, Gao H, Hoesel LM, Nadeau BA, Day DE, et al. Adverse functions of IL-17A in experimental sepsis. *FASEB J*. (2008) 22:2198–205. doi: 10.1096/fj.07-105221
52. Freitas A, Alves-Filho JC, Victoni T, Secher T, Lemos HP, Sonego F, et al. IL-17 receptor signaling is required to control polymicrobial sepsis. *J Immunol*. (2009) 182:7846–54. doi: 10.4049/jimmunol.0803039
53. Ogiku M, Kono H, Hara M, Tsuchiya M, Fujii H. Interleukin-17A plays a pivotal role in polymicrobial sepsis according to studies using IL-17A knockout mice. *J Surg Res*. (2012) 174:142–9. doi: 10.1016/j.jss.2010.11.901
54. Ramakrishnan SK, Zhang H, Ma X, Jung I, Schwartz AJ, Triner D, et al. Intestinal non-canonical NFkappaB signaling shapes the local and systemic immune response. *Nat Commun*. (2019) 10:660. doi: 10.1038/s41467-019-08581-8
55. Ritchie ND, Ritchie R, Bayes HK, Mitchell TJ, Evans TJ. IL-17 can be protective or deleterious in murine pneumococcal pneumonia. *PLoS Pathog*. (2018) 14:e1007099. doi: 10.1371/journal.ppat.1007099
56. Cauvi DM, Williams MR, Bermudez JA, Armijo G, De Maio A. Elevated expression of IL-23/IL-17 pathway-related mediators correlates with exacerbation of pulmonary inflammation during polymicrobial sepsis. *Shock*. (2014) 42:246–55. doi: 10.1097/SHK.0000000000000207
57. Maravitsa P, Adamopoulou M, Pistiki A, Netea MG, Louis K, Giamarellos-Bourboulis EJ. Systemic over-release of interleukin-17 in acute kidney injury after septic shock: clinical and experimental evidence. *Immunol Lett*. (2016) 178:68–76. doi: 10.1016/j.imlet.2016.08.002

58. Li J, Zhang Y, Lou J, Zhu J, He M, Deng X, et al. Neutralisation of peritoneal IL-17A markedly improves the prognosis of severe septic mice by decreasing neutrophil infiltration and proinflammatory cytokines. *PLoS ONE*. (2012) 7:e46506. doi: 10.1371/journal.pone.0046506
59. Wynn JL, Wilson CS, Hawiger J, Scumpia PO, Marshall AF, Liu JH, et al. Targeting IL-17A attenuates neonatal sepsis mortality induced by IL-18. *Proc Natl Acad Sci USA*. (2016) 113:E2627–35. doi: 10.1073/pnas.1515793113
60. Wolf L, Sapich S, Honecker A, Jungnickel C, Seiler F, Bischoff M, et al. IL-17A-mediated expression of epithelial IL-17C promotes inflammation during acute *Pseudomonas aeruginosa* pneumonia. *Am J Physiol Lung Cell Mol Physiol*. (2016) 311:L1015–L22. doi: 10.1152/ajplung.00158.2016
61. Yamaguchi S, Nambu A, Numata T, Yoshizaki T, Narushima S, Shimura E, et al. The roles of IL-17C in T cell-dependent and -independent inflammatory diseases. *Sci Rep*. (2018) 8:15750. doi: 10.1038/s41598-018-34054-x
62. Chang SH, Reynolds JM, Pappu BP, Chen G, Martinez GJ, Dong C. Interleukin-17C promotes Th17 cell responses and autoimmune disease via interleukin-17 receptor E. *Immunity*. (2011) 35:611–21. doi: 10.1016/j.immuni.2011.09.010
63. Pflanz S, Timans JC, Cheung J, Rosales R, Kanzler H, Gilbert J, et al. IL-27, a heterodimeric cytokine composed of EBI3 and p28 protein, induces proliferation of naive CD4+ T cells. *Immunity*. (2002) 16:779–90. doi: 10.1016/S1074-7613(02)00324-2
64. Villarino AV, Larkin J III, Saris CJ, Caton AJ, Lucas S, Wong T, et al. Positive and negative regulation of the IL-27 receptor during lymphoid cell activation. *J Immunol*. (2005) 174:7684–91. doi: 10.4049/jimmunol.174.12.7684
65. Matta BM, Raimondi G, Rosborough BR, Sumpter TL, Thomson AW. IL-27 production and STAT3-dependent upregulation of B7-H1 mediate immune regulatory functions of liver plasmacytoid dendritic cells. *J Immunol*. (2012) 188:5227–37. doi: 10.4049/jimmunol.1103382
66. Mascanfroni ID, Yeste A, Vieira SM, Burns EJ, Patel B, Sloma I, et al. IL-27 acts on DCs to suppress the T cell response and autoimmunity by inducing expression of the immunoregulatory molecule CD39. *Nat Immunol*. (2013) 14:1054–63. doi: 10.1038/ni.2695
67. Sowrirajan B, Saito Y, Poudyal D, Chen Q, Sui H, DeRavin SS, et al. Interleukin-27 enhances the potential of reactive oxygen species generation from monocyte-derived macrophages and dendritic cells by induction of p47(phox). *Sci Rep*. (2017) 7:43441. doi: 10.1038/srep43441
68. Harker JA, Wong KA, Dallari S, Bao P, Dolgoter A, Jo Y, et al. Interleukin-27R signaling mediates early viral containment and impacts innate and adaptive immunity after chronic lymphocytic choriomeningitis virus infection. *J Virol*. (2018) 92:e02196-17. doi: 10.1128/JVI.02196-17
69. Wehrens EJ, Wong KA, Gupta A, Khan A, Benedict CA, Zuniga EI. IL-27 regulates the number, function and cytotoxic program of antiviral CD4 T cells and promotes cytomegalovirus persistence. *PLoS ONE*. (2018) 13:e0201249. doi: 10.1371/journal.pone.0201249
70. O'Dwyer MJ, Mankan AK, White M, Lawless MW, Stordeur P, O'Connell B, et al. The human response to infection is associated with distinct patterns of interleukin 23 and interleukin 27 expression. *Intensive Care Med*. (2008) 34:683–91. doi: 10.1007/s00134-007-0968-5
71. Rinchai D, Khaenam P, Kewcharoenwong C, Buddhisa S, Pankla R, Chaussabel D, et al. Production of interleukin-27 by human neutrophils regulates their function during bacterial infection. *Eur J Immunol*. (2012) 42:3280–90. doi: 10.1002/eji.201242526
72. Yan J, Mitra A, Hu J, Cutrera JJ, Xia X, Doetschman T, et al. Interleukin-30 (IL27p28) alleviates experimental sepsis by modulating cytokine profile in NKT cells. *J Hepatol*. (2016) 64:1128–36. doi: 10.1016/j.jhep.2015.12.020
73. Awasthi A, Carrier Y, Peron JP, Bettelli E, Kamanaka M, Flavell RA, et al. A dominant function for interleukin 27 in generating interleukin 10-producing anti-inflammatory T cells. *Nat Immunol*. (2007) 8:1380–9. doi: 10.1038/ni1541
74. Battaglia M, Gregori S, Bacchetta R, Roncarolo MG. Tr1 cells: from discovery to their clinical application. *Semin Immunol*. (2006) 18:120–7. doi: 10.1016/j.smim.2006.01.007
75. Chihara N, Madi A, Kondo T, Zhang H, Acharya N, Singer M, et al. Induction and transcriptional regulation of the co-inhibitory gene module in T cells. *Nature*. (2018) 558:454–9. doi: 10.1038/s41586-018-0206-z
76. Xie J, Crepeau RL, Chen CW, Zhang W, Otani S, Coopersmith CM, et al. Sepsis erodes CD8(+) memory T cell-protective immunity against an EBV homolog in a 2B4-dependent manner. *J Leukoc Biol*. (2019) 105:565–75. doi: 10.1002/JLB.4A0718-292R
77. Ammer-Herrmenau C, Kulkarni U, Andreas N, Ungelenk M, Ravens S, Hubner C, et al. Sepsis induces long-lasting impairments in CD4+ T-cell responses despite rapid numerical recovery of T-lymphocyte populations. *PLoS ONE*. (2019) 14:e0211716. doi: 10.1371/journal.pone.0211716
78. Thampy LK, Remy KE, Walton AH, Hong Z, Liu K, Liu R, et al. Restoration of T cell function in multi-drug resistant bacterial sepsis after interleukin-7, anti-PD-L1, and OX-40 administration. *PLoS ONE*. (2018) 13:e0199497. doi: 10.1371/journal.pone.0199497
79. Jensen IJ, Sjaastad FV, Griffith TS, Badovinac VP. Sepsis-Induced T cell immunoparalysis: the ins and outs of impaired T cell immunity. *J Immunol*. (2018) 200:1543–53. doi: 10.4049/jimmunol.1701618
80. Muller SI, Friedl A, Aschenbrenner I, Esser-von Bieren J, Zacharias M, Devergne O, et al. A folding switch regulates interleukin 27 biogenesis and secretion of its alpha-subunit as a cytokine. *Proc Natl Acad Sci USA*. (2019) 116:1585–90. doi: 10.1073/pnas.1816698116
81. Schmitz J, Owyang A, Oldham E, Song Y, Murphy E, McClanahan TK, et al. IL-33, an interleukin-1-like cytokine that signals via the IL-1 receptor-related protein ST2 and induces T helper type 2-associated cytokines. *Immunity*. (2005) 23:479–90. doi: 10.1016/j.immuni.2005.09.015
82. Moussion C, Ortega N, Girard JP. The IL-1-like cytokine IL-33 is constitutively expressed in the nucleus of endothelial cells and epithelial cells *in vivo*: a novel 'alarmin'? *PLoS ONE*. (2008) 3:e3331. doi: 10.1371/journal.pone.0003331
83. Pichery M, Mirey E, Mercier P, Lefrancais E, Dujardin A, Ortega N, et al. Endogenous IL-33 is highly expressed in mouse epithelial barrier tissues, lymphoid organs, brain, embryos, and inflamed tissues: *in situ* analysis using a novel Il-33-LacZ gene trap reporter strain. *J Immunol*. (2012) 188:3488–95. doi: 10.4049/jimmunol.1101977
84. Louten J, Rankin AL, Li Y, Murphy EE, Beaumont M, Moon C, et al. Endogenous IL-33 enhances Th2 cytokine production and T-cell responses during allergic airway inflammation. *Int Immunol*. (2011) 23:307–15. doi: 10.1093/intimm/dxr006
85. Oboki K, Ohno T, Kajiwara N, Arae K, Morita H, Ishii A, et al. IL-33 is a crucial amplifier of innate rather than acquired immunity. *Proc Natl Acad Sci USA*. (2010) 107:18581–6. doi: 10.1073/pnas.1003059107
86. Babic ZM, Zunic FZ, Pantic JM, Radosavljevic GD, Jovanovic IP, Arsenijevic NN, et al. IL-33 receptor (ST2) deficiency downregulates myeloid precursors, inflammatory NK and dendritic cells in early phase of sepsis. *J Biomed Sci*. (2018) 25:56. doi: 10.1186/s12929-018-0455-z
87. Lv R, Zhao J, Lei M, Xiao D, Yu Y, Xie J. IL-33 attenuates sepsis by inhibiting IL-17 receptor signaling through upregulation of SOCS3. *Cell Physiol Biochem*. (2017) 42:1961–72. doi: 10.1159/000479836
88. Hirahara K, Ghoreschi K, Yang XP, Takahashi H, Laurence A, Vahedi G, et al. Interleukin-27 priming of T cells controls IL-17 production in trans via induction of the ligand PD-L1. *Immunity*. (2012) 36:1017–30. doi: 10.1016/j.immuni.2012.03.024
89. de Almeida Nagata DE, Demoor T, Ptaschinski C, Ting HA, Jang S, Reed M, et al. IL-27R-mediated regulation of IL-17 controls the development of respiratory syncytial virus-associated pathogenesis. *Am J Pathol*. (2014) 184:1807–18. doi: 10.1016/j.ajpath.2014.02.004
90. Peters A, Fowler KD, Chalmin F, Merkler D, Kuchroo VK, Pot C. IL-27 induces Th17 differentiation in the absence of STAT1 signaling. *J Immunol*. (2015) 195:4144–53. doi: 10.4049/jimmunol.1302246
91. El-Behi M, Dai H, Magalhaes JG, Hwang D, Zhang GX, Rostami A, et al. Committed Tc17 cells are phenotypically and functionally resistant to the effects of IL-27. *Eur J Immunol*. (2014) 44:3003–14. doi: 10.1002/eji.201344360
92. Jiang HR, Milovanovic M, Allan D, Niedbala W, Besnard AG, Fukada SY, et al. IL-33 attenuates EAE by suppressing IL-17 and IFN-gamma production and inducing alternatively activated macrophages. *Eur J Immunol*. (2012) 42:1804–14. doi: 10.1002/eji.201141947

93. Neurath MF. New therapies for sepsis: focus on the interleukin (IL)12 family member IL27. *Ann Rheum Dis.* (2007) 66 (Suppl. 3):iii29–31. doi: 10.1136/ard.2007.078337
94. Bosmann M, Ward PA. Therapeutic potential of targeting IL-17 and IL-23 in sepsis. *Clin Transl Med.* (2012) 1:4. doi: 10.1186/2001-1326-1-4
95. Rostan O, Arshad MI, Piquet-Pellorce C, Robert-Gangneux F, Gangneux JP, Samson M. Crucial and diverse role of the interleukin-33/ST2 axis in infectious diseases. *Infect Immun.* (2015) 83:1738–48. doi: 10.1128/IAI.02908-14

Conflict of Interest Statement: The authors declare that the research was conducted in the absence of any commercial or financial relationships that could be construed as a potential conflict of interest.

Copyright © 2019 Morrow, Coopersmith and Ford. This is an open-access article distributed under the terms of the Creative Commons Attribution License (CC BY). The use, distribution or reproduction in other forums is permitted, provided the original author(s) and the copyright owner(s) are credited and that the original publication in this journal is cited, in accordance with accepted academic practice. No use, distribution or reproduction is permitted which does not comply with these terms.

frontiers in Immunology

ORIGINAL RESEARCH
published: 06 September 2019
doi: 10.3389/fimmu.2019.02129

Bruton's Tyrosine Kinase Inhibition Attenuates the Cardiac Dysfunction Caused by Cecal Ligation and Puncture in Mice

Caroline E. O'Riordan[1], Gareth S. D. Purvis[1], Debora Collotta[2], Fausto Chiazza[2], Bianka Wissuwa[3,4], Sura Al Zoubi[1], Lara Stiehler[1,5], Lukas Martin[1,5], Sina M. Coldewey[3,4], Massimo Collino[2] and Christoph Thiemermann[1]**

[1] William Harvey Research Institute, Barts and the London School of Medicine and Dentistry, Queen Mary University of London, London, United Kingdom, [2] Department of Drug Science and Technology, University of Turin, Turin, Italy, [3] Department of Anesthesiology and Intensive Care Medicine, Jena University Hospital, Jena, Germany, [4] Septomics Research Center, Jena University Hospital, Jena, Germany, [5] Department of Operative Intensive Care and Intermediate Care, RWTH University Hospital Aachen, Aachen, Germany

OPEN ACCESS

Edited by:
Rudolf Lucas,
Augusta University, United States

Reviewed by:
Basilia Zingarelli,
Cincinnati Children's Hospital Medical Center, United States
Helder Mota-Filipe,
University of Lisbon, Portugal

***Correspondence:**
Caroline E. O'Riordan
c.e.oriordan@qmul.ac.uk
Christoph Thiemermann
c.thiemermann@qmul.ac.uk

Specialty section:
This article was submitted to Inflammation, a section of the journal Frontiers in Immunology

Received: 10 April 2019
Accepted: 23 August 2019
Published: 06 September 2019

Citation:
O'Riordan CE, Purvis GSD, Collotta D, Chiazza F, Wissuwa B, Al Zoubi S, Stiehler L, Martin L, Coldewey SM, Collino M and Thiemermann C (2019) Bruton's Tyrosine Kinase Inhibition Attenuates the Cardiac Dysfunction Caused by Cecal Ligation and Puncture in Mice. Front. Immunol. 10:2129. doi: 10.3389/fimmu.2019.02129

Sepsis is one of the most prevalent diseases in the world. The development of cardiac dysfunction in sepsis results in an increase of mortality. It is known that Bruton's tyrosine kinase (BTK) plays a role in toll-like receptor signaling and NLRP3 inflammasome activation, two key components in the pathophysiology of sepsis and sepsis-associated cardiac dysfunction. In this study we investigated whether pharmacological inhibition of BTK (ibrutinib 30 mg/kg and acalabrutinib 3 mg/kg) attenuates sepsis associated cardiac dysfunction in mice. 10-week old male C57BL/6 mice underwent CLP or sham surgery. One hour after surgery mice received either vehicle (5% DMSO + 30% cyclodextrin i.v.), ibrutinib (30 mg/kg i.v.), or acalabrutinib (3 mg/kg i.v.). Mice also received antibiotics and an analgesic at 6 and 18 h. After 24 h, cardiac function was assessed by echocardiography *in vivo*. Cardiac tissue underwent western blot analysis to determine the activation of BTK, NLRP3 inflammasome and NF-κB pathway. Serum analysis of 33 cytokines was conducted by a multiplex assay. When compared to sham-operated animals, mice subjected to CLP demonstrated a significant reduction in ejection fraction (EF), fractional shortening (FS), and fractional area change (FAC). The cardiac tissue from CLP mice showed significant increases of BTK, NF-κB, and NLRP3 inflammasome activation. CLP animals resulted in a significant increase of serum cytokines and chemokines (TNF-α, IL-6, IFN-γ, KC, eotaxin-1, eotaxin-2, IL-10, IL-4, CXCL10, and CXCL11). Delayed administration of ibrutinib and acalabrutinib attenuated the decline of EF, FS, and FAC caused by CLP and also reduced the activation of BTK, NF-κB, and NLRP3 inflammasome. Both ibrutinib and acalabrutinib significantly suppressed the release of cytokines and chemokines. Our study revealed that delayed intravenous administration of ibrutinib or acalabrutinib attenuated the cardiac dysfunction associated with sepsis by inhibiting BTK, reducing NF-κB activation and the activation

of the inflammasome. Cytokines associated with sepsis were significantly reduced by both BTK inhibitors. Acalabrutinib is found to be more potent than ibrutinib and could potentially prove to be a novel therapeutic in sepsis. Thus, the FDA-approved BTK inhibitors ibrutinib and acalabrutinib may be repurposed for the use in sepsis.

Keywords: Bruton's tyrosine kinase (BTK), sepsis, cardiac dysfunction, ibrutinib, acalabrutinib, NLRP3, NF-κB, mice

INTRODUCTION

Sepsis is a life-threatening organ dysfunction caused by a dysregulated host response to an infection (1), which affects approximately 30 million people worldwide (2). In the UK, sepsis is the second leading cause of death with 36,000–64,000 patients dying each year (3) costing the NHS £2.5 billion annually (4). The development of cardiac dysfunction affects 40% of septic patients (5) and is associated with an increased mortality rate of 70–90% in comparison to 20% mortality in patients who do not present with cardiac dysfunction (6). However, the mechanisms that underlie this cardiac dysfunction are not well-known. Evidence suggests that multiple factors contribute to the pathophysiology of the cardiac dysfunction associated with sepsis. These include the activation of NF-κB and NLRP3 leading to excessive formation of e.g., IL-1 and TNF-α (7, 8). There are currently no drugs for the specific treatment of the cardiac dysfunction (or indeed the multiple organ dysfunction) associated with sepsis that specifically target NF-κB and the NLRP3 inflammasome.

Bruton's tyrosine kinase (BTK) plays a role in innate immunity and is a critical component in the development of B cells (9). The FDA has approved the use of the irreversible BTK inhibitors ibrutinib (first generation) in chronic lymphatic leukemia (CLL), mantle cell lymphoma (MCL), Waldenstrom macroglobulinemia (WM), and graft vs. host disease (10) and acalabrutinib (more selective, second generation) in MCL (11). Ibrutinib is also approved by the EMA for the treatment of CLL, MCL, and WM (12), whereas acalabrutinib has received an orphan designation for CCL, MCL, and lymphoplasmacytic lymphoma (13–15). During sepsis, bacterial LPS stimulates TLR4 and BTK is directly involved in the activation of this signaling pathway. Specifically, BTK binds to the TIR domain of TLR4 and its adaptor molecules (also found in other TLR's) MyD88 and Mal, and results in downstream activation of NF-κB and the generation of proinflammatory cytokines (16). BTK also regulates the assembly and, hence, activation of the NLRP3 inflammasome by binding to the ASC component (17, 18). Inhibition of BTK by BTK inhibitors reduces NF-κB activation and the formation of NF-κB-dependent cytokines in murine models of arthritis (19).

Given the importance of TLRs and NLRP3 in the pathophysiology of sepsis, we hypothesized that BTK inhibitors, such as ibrutinib or acalabrutinib, may attenuate the cardiac dysfunction in a murine model of polymicrobial sepsis. Additionally, we set out to investigate the potential effects of BTK inhibition on (a) the activation of NF-κB and NLRP3 in the heart, and (b) the serum levels of key, pro- and anti-inflammatory cytokines and chemokines.

METHODS

Ethical Statement

The Animal Welfare Ethics Review Board of Queen Mary University of London approved all experiments in accordance with the Home Office guidance on the operation of Animals (Scientific Procedure Act, 1986) published by Her Majesty's Stationary Office, and the Guide for the Care and Use of Laboratory Animals of the National Research Council. Work was conducted under U.K. home office project license number PC5F29685. All *in vivo* experiments are reported in accordance to ARRIVE guidelines (20).

Animals

This study was carried out on 40 10-week-old male C57BL/6 mice (Charles River Laboratories UK Ltd., Kent, UK) weighing 25–30 g and kept under standard laboratory conditions. Six mice were housed together (in each cage) with access to a chow diet and water *ad libitum*. They were subjected to a 12-h light and dark cycle with a temperature maintained at 19–23°C.

Drugs

Ibrutinib and acalabrutinib were purchased from Selleck Chemicals. Stock solutions were made in DMSO 5% and cyclodextrin 30% (vehicle).

Murine Model of Polymicrobial Sepsis Caused by Cecum Ligation and Puncture (CLP)

Mice were randomized to undergo either sham operation, CLP + vehicle (5% DMSO + 30% cyclodextrin), CLP + ibrutinib (30 mg/kg), or CLP + acalabrutinib (3 mg/kg). Before surgery, mice were injected with buprenorphine (0.05 mg/kg, i.p.). Mice were initially anesthetized by isoflurane (3 L/min) and oxygen (1 L/min) in an anesthetic chamber and maintained with isoflurane (2 L/min) and oxygen (1 L/min) via a face mask. Temperature was monitored via a rectal probe and kept at 37°C by a homeothermic mat. Veet® hair removal cream was used to remove the fur from the abdomen of the mouse and skin was then cleaned with 70% ethanol. The abdomen was opened with a 1.5 cm midline incision to expose the cecum. The cecum was fully ligated below the ileocecal valve, and a G-18 needle was used to puncture two holes in the top and bottom of the cecum. A small amount of feces was then squeezed out. The cecum was returned to the abdomen in its

anatomical position and 5 ml/kg of saline was administered into the abdomen before its closure. Saline (10 ml/kg s.c.) was administered directly after surgery. One hour after CLP, vehicle (5% DMSO + 30% cyclodextrin), ibrutinib (30 mg/kg), or acalabrutinib (3 mg/kg) was administered intravenously. At 6 and 18 h after surgery, antibiotics (imipenem/cilastatin; 20 mg/kg dissolved in saline s.c.) and an analgesic (buprenorphine; 0.05 mg/kg i.p.) were administered. After 24 h, cardiac function was assessed by echocardiography *in vivo*. Mice that underwent sham surgery were not subjected to ligation or perforation of the cecum but were otherwise treated the same way, 1 h after surgery sham animals were treated with vehicle (5% DMSO + 30% cyclodextrin).

Renal Dysfunction Analysis

Renal dysfunction was analyzed in all mice. The mice were anesthetized with isoflurane (3 L/min) and oxygen (1 L/min) before being sacrificed. Cardiac puncture was performed with a G25 needle and non-heparinized syringes to obtain approximately 0.7 ml of blood. The blood was immediately decanted into 1.3 ml serum gel tubes (Sarstedt, Nürnbrecht, Germany). The heart and lungs were then removed. The blood samples were centrifuged for 3 min at 9,000 RPM to separate the serum, where 100 μL of serum was pipetted into an aliquot and snap frozen in liquid nitrogen and stored at −80°C for further analysis. The serum was then sent to an independent veterinary testing laboratory (MRC Harwell Institute, Oxford, UK) to blindly quantify serum urea and creatinine known markers of renal dysfunction.

Echocardiography

At 24 h after CLP, cardiac function was assessed with a Vevo 3100 imaging system (VisualSonics, Toronto, Ontario, Canada). Mice were fully sedated in an anesthetic chamber with isoflurane (3 L/min) and oxygen (1 L/min) and were then transferred to the thermoregulatory platform in the supine position, where their paws were taped on to the EKG leads. Anesthetic was maintained throughout the entire procedure via a nosecone with isoflurane (0.5–2.0 L/min) and oxygen (1 L/min). The fur on the chest was removed by Veet® hair removal cream and pre-warmed echo gel was placed onto the shaven chest. The heart was then imaged with the MX550D imaging probe. To measure the left ventricle in B-mode the probe was placed along the long axis of the left ventricle, and directed toward the right of the mouse, here we measured percentage fractional area change (FAC%). The probe was then rotated 90° to visualize the short axis in the M-mode where the following parameters were measured: the percentage ejection fraction (EF%) and fractional shortening (FS%).

Western Blot Analysis

Immunoblot analyses of cardiac tissue samples were carried out using a semi-quantitative western blotting analysis. The antibody used were: 1:1,000 rabbit anti-$Ser^{176/180}$-IKKα/β, 1:1,000 rabbit anti-total IKKα/β, 1:1,000 mouse anti-$Ser^{32/36}$-IκBα, 1:1,000 mouse anti-total IκBα, 1:1,000 rabbit anti-NF-κB, 1:1,000 rabbit anti-total BTK, 1:1,000 rabbit anti-Tyr^{1217} PLCγ, 1:1,000 rabbit anti-total PLCγ (from Cell Signaling), 1:1,000 rabbit anti-Tyr^{223}-BTK, 1:5,000 rabbit anti NLRP3 inflammasome (from Abcam), 1:1,000 mouse anti-caspase 1 (p20) (from Adipogen). The apex of the heart was taken and homogenized in 1:10 of homogenization buffer at 4°C. Nuclear and cytosolic proteins were then extracted as previously described (21) and concentrations were quantified by bicinchoninic acid (BCA) protein assay (Thermo Fisher Scientific Rockford, IL). Proteins were separated by 8% sodium dodecyl sulfate (SDS)-PAGE and transferred to polyvinyldenedifluoride membranes. Membranes were blocked in 10% milk solution with TBS-Tween and then incubated with the primary antibody overnight at 4°C. The next day the secondary antibody was added for 30 min at room temperature and visualized using the ECL detection system. Tubulin and histone 3 were used as loading control. The immunoreactive bands were analyzed by the Bio-Rad Image Lab Software™ 6.0.1 and results were normalized to the sham bands.

Multiplex Flow Immunoassay

The principle of multiplex flow immunoassay technology has been reviewed previously (22, 23). Cytokines, chemokines and a growth factor were determined in serum by Bio-Plex Pro Mouse Chemokine 33-plex panel assay (Bio-Rad, Kabelsketal, Germany). The cytokines IL-1ß,−2,−4,−6,−10,−16, CCL1,−2,−3,−4,−5,−7,−11,−12,−17,−19,−20,−22,−24,−25, −27, IFN-γ, TNF-α and the chemokines CX3CL1, CXCL1,−2,−5,−10,−11,−12,−13,−16 and the growth factor GM-CSF were measured according to the manufacturer's instructions. The assays were performed in one batch, with samples randomly distributed. The lower detection limit was 3.2 pg/ml for all the analytes. Data were collected and analyzed using a Bio-Plex® 200 instrument equipped with Bio-Plex Manager software (Bio-Rad).

Statistical Analysis

All data in text and figures are expressed as mean ± standard error mean (SEM) of *n* observations. Measurements obtained from the intervention, control and sham were analyzed by one-way ANOVA followed by a Bonferroni's *post-hoc* test on GraphPad Prism 6.0 (GraphPad Software, Inc., La Jolla, CA, USA). Correlations coefficients were determined by Pearson's correlation with *P*-values based on two-tailed tests. Differences were considered to be statistically significant when $P < 0.05$.

RESULTS

Ibrutinib or Acalabrutinib Attenuate the Cardiac Dysfunction Caused by CLP-sepsis

When compared to sham-operated animals, mice subjected to CLP for 24 h (**Figure 1A**) demonstrated a significant reduction in EF, FS, and FAC ($P < 0.0001$; **Figures 1B–E**) indicating the development of systolic cardiac dysfunction. The observed reduction in EF also negatively correlated with the rise of the chemokines CXCL10 and CXCL11, both of which are well-known biomarkers of left ventricular dysfunction (**Figures 1F–I**).

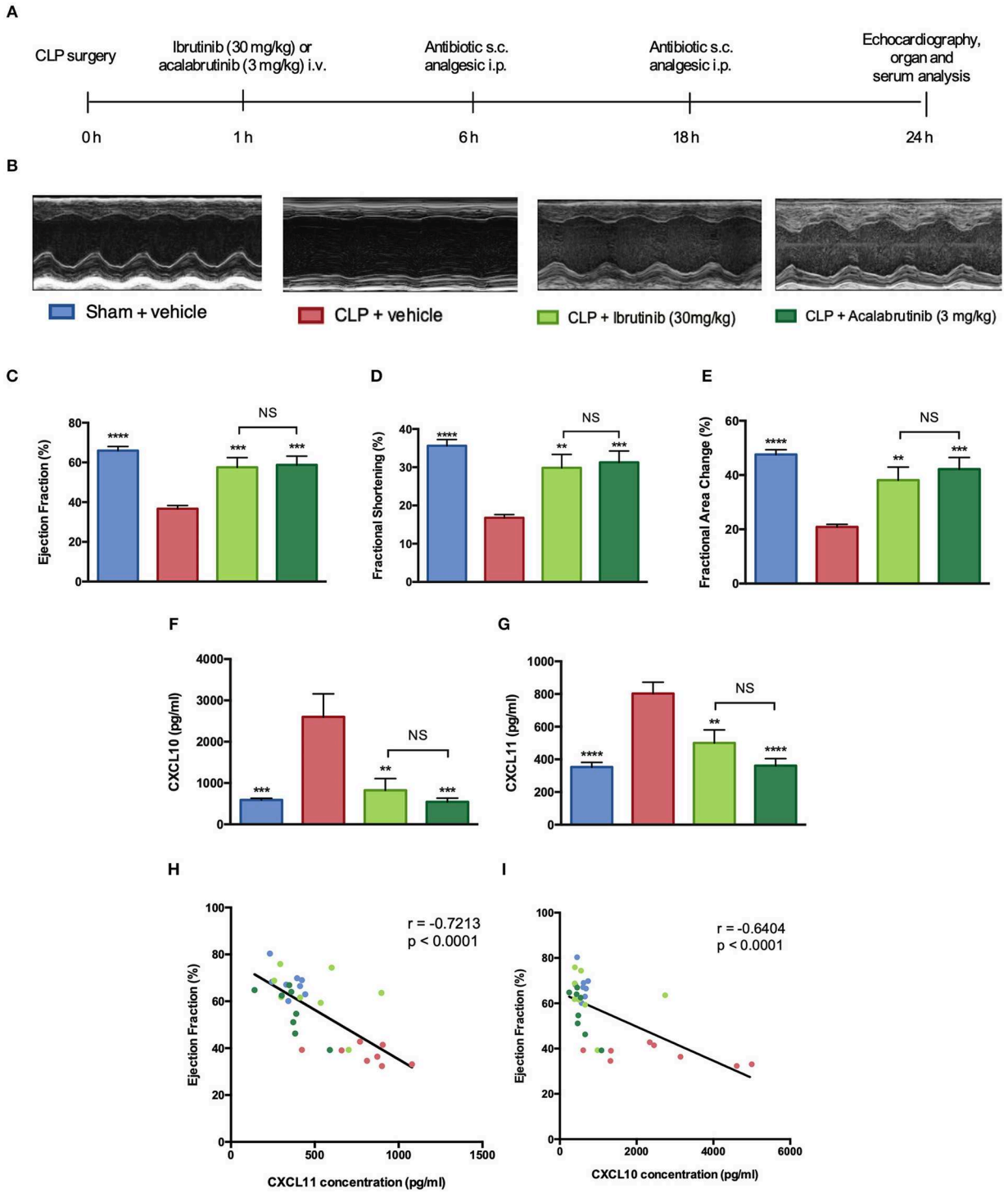

FIGURE 1 | Ibrutinib or acalabrutinib attenuate the cardiac dysfunction caused by CLP-sepsis. Mice were randomly assigned to undergo CLP or sham surgery (n = 10). One hour later, mice were treated with ibrutinib (30 mg/kg i.v.), acalabrutinib (3 mg/kg i.v.), or vehicle (5% DMSO + 30% cyclodextrin i.v.). Cardiac function was assessed 24 h after CLP surgery (n = 10 per group). **(A)** Illustration of the timelines of the CLP model. **(B)** Representative M-mode echocardiograms. **(C)** Ejection fraction (%). **(D)** Fractional shortening (%). **(E)** Fractional area change (%). **(F)** CXCL10 serum concentration (pg/ml). **(G)** CXCL11 serum concentration (pg/ml). **(H)** correlation of ejection fraction and CXCL10 serum concentration. **(I)** Correlation of ejection fraction and CXCL11 serum concentration. All data are expressed as mean ± SEM for n number of observations. A value of $^{****}P < 0.0001$, $^{***}P < 0.001$, $^{**}P < 0.01$ was considered to be statistically significant when compared to the control by one-way ANOVA followed by a Bonferroni's *post-hoc* test. Correlations coefficients were determined by Pearson's correlation with P-values based on two-tailed tests.

When compared to CLP mice treated with vehicle (control), the administration of ibrutinib (30 mg/kg) or acalabrutinib (3 mg/kg) at 1 h after CLP significantly attenuated the decline in EF, FS and FAC caused by CLP ($P < 0.01$; **Figures 1B–E**). The rise in the serum levels of the chemokines CXCL10 and CXCL11 caused by CLP were also significantly reduced by either ibrutinib or acalabrutinib ($P < 0.05$; **Figures 1F–I**). No significant differences were observed in any of the cardiac parameters or cytokines measured in CLP animals treated with either ibrutinib or acalabrutinib ($P > 0.05$; **Figures 1B–I**). To gain a better insight into the mechanism by which the two BTK-inhibitors reduce the cardiac dysfunction associated with sepsis, we investigated the effects of ibrutinib and acalabrutinib on (a) BTK-activation and signaling, (b) NF-κB activation, and (c) NLRP3 inflammasome assembly and activation (see below).

Ibrutinib or Acalabrutinib Attenuate the Renal Dysfunction Caused by CLP-sepsis

Urea and creatinine were measured to study the effect of CLP (in the absence and presence of BTK inhibitors) on kidney function. When compared to sham, mice subjected to CLP and treated with vehicle had a significant increase of urea and creatinine, indicating kidney dysfunction ($P < 0.0001$; **Figure 2**). Administration of ibrutinib (30 mg/kg) or acalabrutinib (3 mg/kg) to CLP mice significantly attenuated the rise in urea and creatinine when compared to CLP mice treated with vehicle (*P*

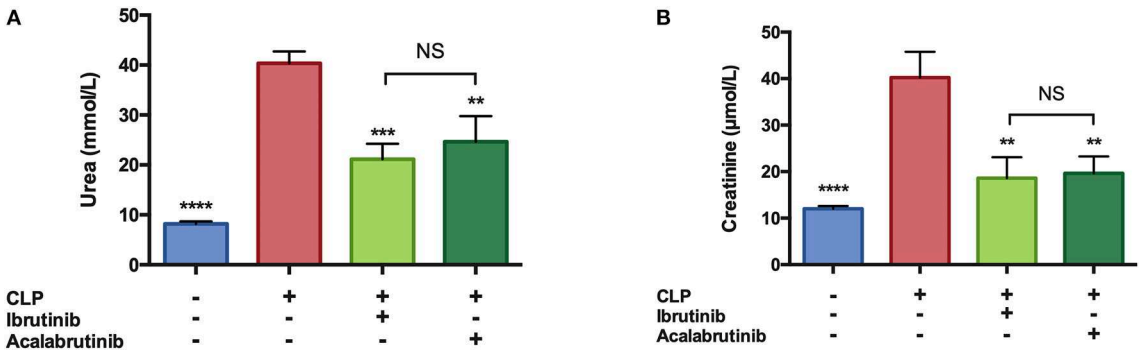

FIGURE 2 | Ibrutinib or acalabrutinib attenuate the renal dysfunction caused by CLP-sepsis. Mice were randomly assigned to undergo CLP or sham surgery ($n = 10$). One hour later, mice were treated with ibrutinib (30 mg/kg i.v.), acalabrutinib (3 mg/kg i.v.), or vehicle (5% DMSO + 30% cyclodextrin i.v.). At 24 h after CLP, blood samples were collected for analyses (n = 10 per group). **(A)** Serum urea (mmol/L). **(B)** Serum creatinine (μmol/L). All data are expressed as mean ± SEM for *n* number of observations. A value of $^{****}P < 0.0001$, $^{***}P < 0.001$, $^{**}P < 0.01$ was considered to be statistically significant when compared to the control by one-way ANOVA followed by a Bonferroni's *post-hoc* test.

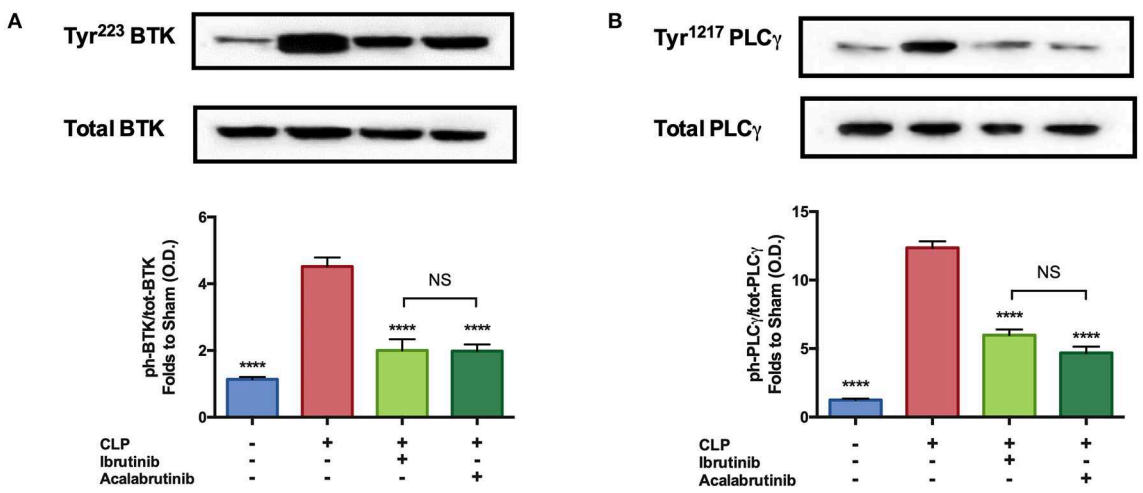

FIGURE 3 | Cardiac BTK is activated in CLP mice and reduced by ibrutinib or acalabrutinib. Mice were randomly assigned to undergo CLP or sham surgery. One hour later, mice were treated with ibrutinib (30 mg/kg i.v.), acalabrutinib (3 mg/kg i.v.), or vehicle (5% DMSO + 30% cyclodextrin i.v.). At 24 h after CLP surgery, the activation of BTK in the heart was analyzed by western blot analysis ($n = 5$ per group). Specifically, densitometric analysis of the bands is expressed as relative OD of **(A)** phosphorylation of BTK at Tyr^{223} corrected for the corresponding total BTK and normalized using the related sham band. **(B)** Phosphorylation of PLCγ at Tyr^{1217} corrected for the corresponding total PLCγ. All data are expressed as mean ± SEM for *n* number of observations. A value of $^{****}P < 0.0001$ was considered to be statistically significant when compared to the control by one-way ANOVA followed by a Bonferroni's *post-hoc* test.

< 0.01; **Figure 2**), without any significant difference between the two treatment.

Cardiac BTK Is Activated in CLP Mice and Reduced by Ibrutinib or Acalabrutinib

Using Western blot analysis, we investigated whether CLP-sepsis leads to an activation of BTK in the heart. The activation of BTK and the subsequent activation of BTK-signaling involves (a) phosphorylation of BTK at Tyr^{223} and (b) the phosphorylation of PLCγ at Tyr^{1217} by phosphorylated (activated) BTK as the first step in the BTK-signaling cascade. When compared to sham operated mice, CLP mice treated with vehicle demonstrated significant increases in the phosphorylation of cardiac BTK at Tyr^{223} and the phosphorylation of PLCγ at Tyr^{1217}, indicating that BTK is activated in septic hearts ($P < 0.0001$; **Figure 3A**). Administration of ibrutinib (30 mg/kg) or acalabrutinib (3 mg/kg) in CLP mice resulted in a significant decrease in the phosphorylation of cardiac BTK at Tyr^{223} and the phosphorylation of PLCγ at Tyr^{1217} when compared to CLP mice treated with vehicle ($P < 0.0001$; **Figure 3B**) demonstrating that the doses of the two BTK inhibitors used in our study caused a significant inhibition of BTK-signaling in the heart. No significant differences were observed in the degree of phosphorylation of cardiac BTK at Tyr^{223} and the phosphorylation of PLCγ at Tyr^{1217} in CLP-animals treated with either ibrutinib or acalabrutinib ($P > 0.05$; **Figures 3A,B**).

Cardiac NF-κB Activation in CLP Mice Is Reduced by Ibrutinib or Acalabrutinib

To understand the signaling mechanism associated with the observed cardiac dysfunction, we investigated the effect of BTK inhibition on the activation of key signaling pathways of inflammation including pathways leading to the activation of NF-κB. When compared to sham operated mice, CLP mice treated with vehicle had significant increases in the phosphorylation of IKKα/β at $Ser^{176/180}$, the phosphorylation of IκBα at $Ser^{32/36}$ and the translocation of p65 to the nucleus ($P < 0.001$; **Figures 4A–C**). When compared with CLP mice treated with vehicle, treatment of CLP mice with ibrutinib (30 mg/kg) or acalabrutinib (3 mg/kg) significantly attenuated the increases in cardiac phosphorylation of IKKα/β at $Ser^{176/180}$ and Iκ Bα at $Ser^{32/36}$ and the nuclear translocation of p65 ($P < 0.0001$; **Figures 4A–C**). No significant differences were observed in the degree of phosphorylation of IKKα/β at $Ser^{176/180}$, the phosphorylation of IκBα at $Ser^{32/36}$ and the translocation of p65 to the nucleus in CLP animals treated with either ibrutinib or acalabrutinib ($P > 0.05$; **Figures 4A–C**).

Cardiac NLRP3 Activation in CLP Mice Is Reduced by Ibrutinib or Acalabrutinib

We next assessed the potential involvement of NLRP3 in the cardiac dysfunction of CLP mice. When compared to sham operated mice, CLP-sepsis (vehicle-treatment) resulted in the increased expression of the NLRP3 inflammasome and cleavage of pro-caspase-1 to caspase-1 in the heart and a rise in serum IL-1β ($P < 0.0001$; **Figures 5A–C**). When compared to CLP mice treated with vehicle, treatment of CLP mice with ibrutinib or acalabrutinib significantly inhibited the expression of NLRP3, cleavage of pro-caspase-1 to caspase-1 and the rise in IL-1β ($P < 0.01$; **Figures 5A–C**), without any significant difference between the two drug treatments.

Relationship Between BTK Activation and Cardiac Dysfunction in CLP-sepsis

To address the question whether the degree of activation of BTK correlates with alterations in cardiac function, we correlated the degree of phosphorylation of BTK at Tyr^{223} (**Figure 6A**)

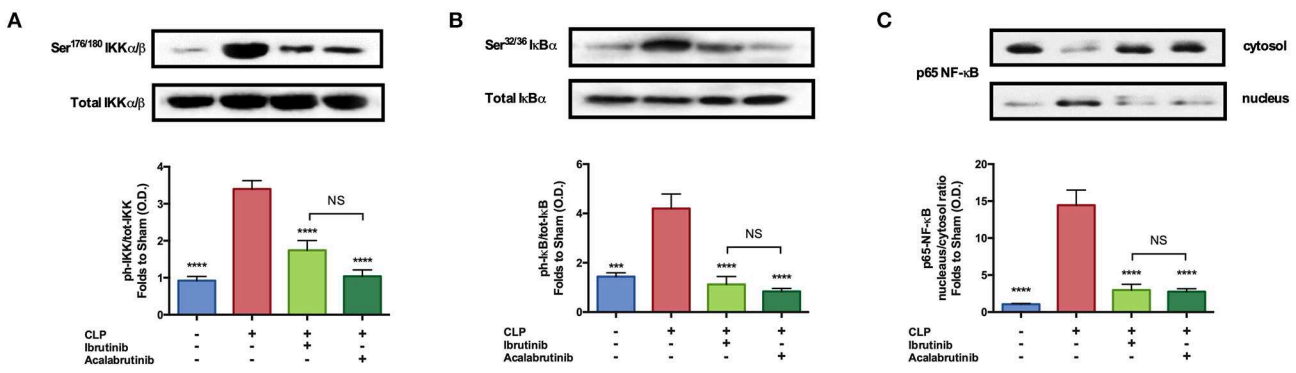

FIGURE 4 | Cardiac NF-κB activation in CLP mice is reduced by ibrutinib or acalabrutinib. Mice were randomly assigned to undergo CLP or sham surgery. One hour later, mice were treated with ibrutinib (30 mg/kg i.v.), acalabrutinib (3 mg/kg i.v.), or vehicle (5% DMSO + 30% cyclodextrin i.v.). At 24 h cardiac tissue was collected and signaling was assessed ($n = 5$ per group). Densitometric analysis of the bands is expressed as relative OD of **(A)** phosphorylation of IKKα/β at $Ser^{176/180}$ corrected for the corresponding total IKKα/β and normalized using the related sham band. **(B)** Phosphorylation of IκBα at $Ser^{32/36}$ corrected for the corresponding total IκBα and normalized using the related sham band. **(C)** NF-κB p65 in both nucleus and cytosol and expressed as a ratio, normalized using the sham related bands. All data are expressed as mean ± SEM for *n* number of observations. A value of $^{****}P < 0.0001$ was considered to be statistically significant when compared to the control by one-way ANOVA followed by a Bonferroni's *post-hoc* test.

and the phosphorylation of PLCγ at Tyr^{1217} (**Figure 6B**) with EF. We found a highly significant negative correlation between the degree of BTK and PLCγ activation and the decline in EF, strongly suggesting that BTK activation drives or precedes the cardiac dysfunction associated with sepsis. To address the question whether the degree of activation of BTK also correlates with alterations in the activation of NF-κB, we correlated the degree of phosphorylation of BTK at Tyr^{223} with the translocation of p65 (**Figure 6C**) and the phosphorylation of IKKα/β at $Ser^{176/180}$ (**Figure 6D**). We found a highly significant positive correlation between the degree of BTK activation and the activation of NF-κB when measured as either the translocation of p65 (**Figure 6C**) and the phosphorylation of IKKα/β at $Ser^{176/180}$ (**Figure 6D**). To address the question whether the degree of activation of BTK also correlates with alterations in the assembly and activation of the inflammasome, we correlated the degree of phosphorylation of BTK at Tyr^{223} with either NLRP3 assembly (**Figure 6E**) or the activation of caspase-1 (**Figure 6F**). We found a highly significant positive correlation between the degree of BTK activation and the NLRP3 (**Figure 6E**) increased expression and the activation of caspase-1 (**Figure 6F**).

Systemic Inflammation in CLP Mice Is Reduced by Ibrutinib or Acalabrutinib

We also studied the effect of CLP (in the absence and presence of BTK inhibitors) on the systemic synthesis of pro-inflammatory cytokines, anti-inflammatory cytokines and pro-inflammatory chemokines. When compared to sham operated mice, CLP (vehicle) resulted in a significant rise in the serum levels of (a) the pro-inflammatory cytokines TNF-α, IFN-γ, IL-6; (b) the anti-inflammatory cytokines IL-4 and IL-10, and (c) the pro-inflammatory chemokines KC/CXCL1, eotaxin-1/CCL11, eotaxin-2/CCL24 ($P < 0.05$; **Figures 7A–H**). The sepsis-induced increase in these cytokines and chemokines was significantly attenuated by both BTK inhibitors, the only exception being IL-6, which was not significantly reduced by ibrutinib but a

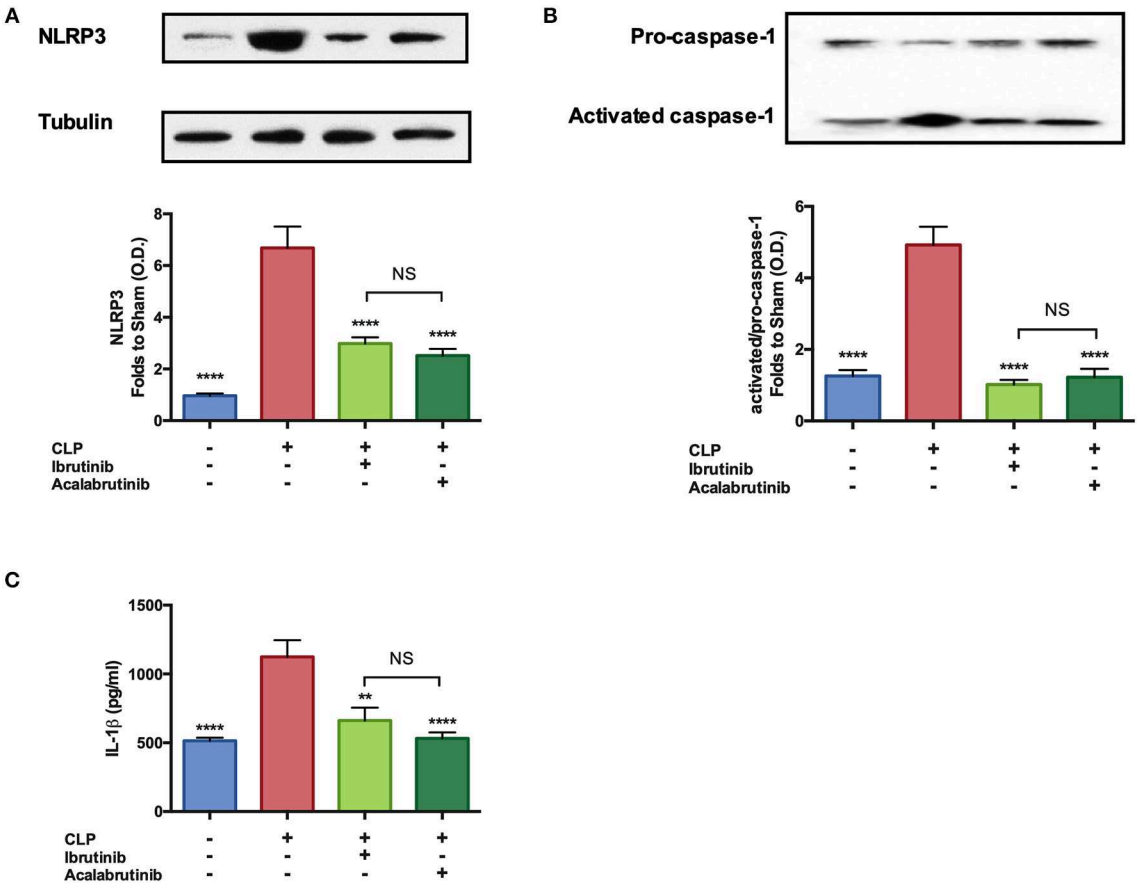

FIGURE 5 | Cardiac NLRP3 activation in CLP mice is reduced by ibrutinib or acalabrutinib. Mice were randomly assigned to undergo CLP or sham surgery. One hour later, mice were treated with ibrutinib (30 mg/kg i.v.), acalabrutinib (3 mg/kg i.v.), or vehicle (5% DMSO + 30% cyclodextrin i.v.). At 24 h after CLP surgery, the assembly and activation of NLRP3 in the heart was analyzed by western blot analysis ($n = 5$ per group). Specifically, densitometric analysis of the bands is expressed as relative OD of **(A)** NLRP3 activation, corrected against tubulin and normalized using the sham related bands. **(B)** Pro-caspase-1 against activated caspase-1 and normalized using the sham related bands. **(C)** IL-1β serum concentration analyzed by multiplex assay ($n = 8$). All data are expressed as mean ± SEM for n number of observations. A value of $^{****}P < 0.0001$, $^{**}P < 0.01$ was considered to be statistically significant when compared to the control by one-way ANOVA followed by a Bonferroni's *post-hoc* test.

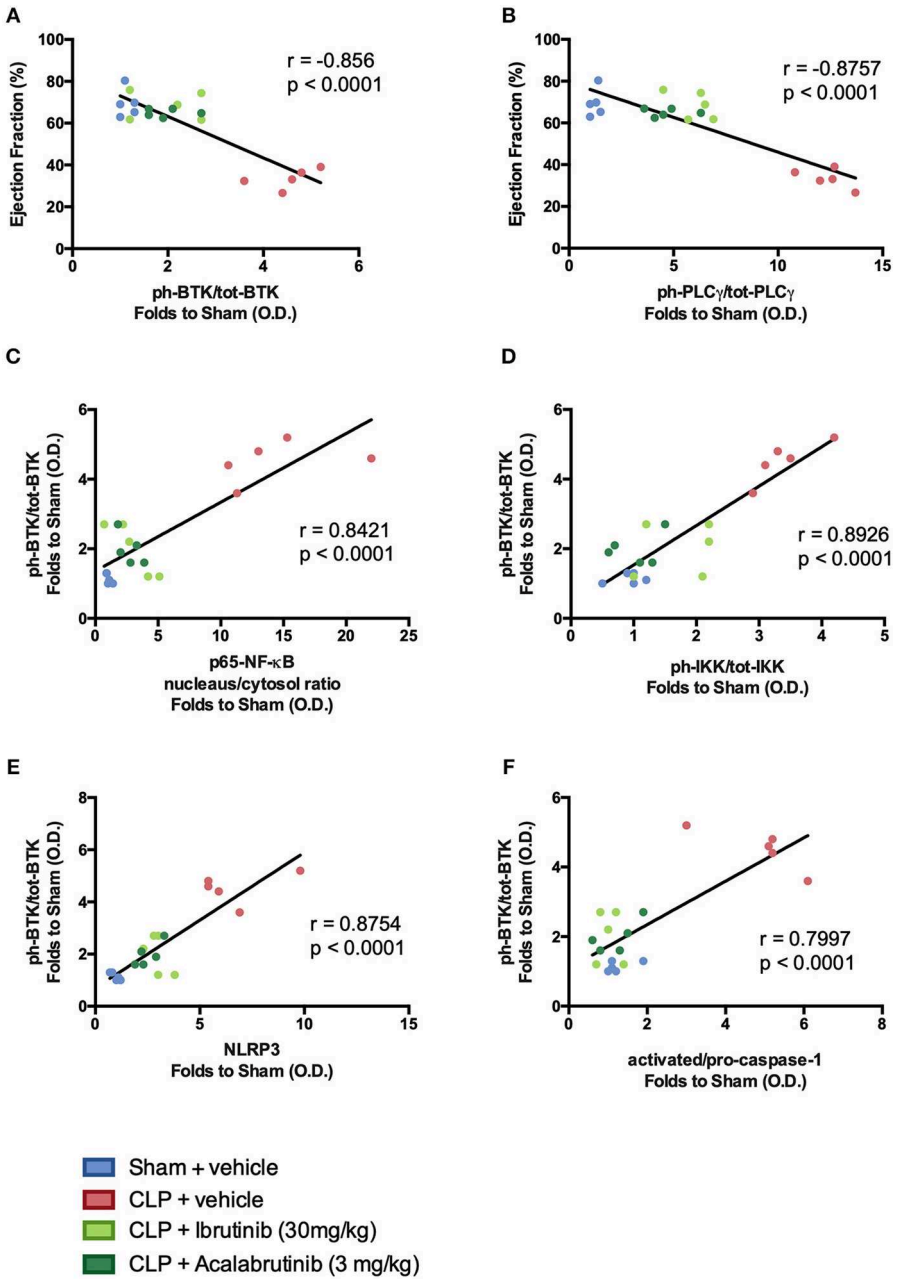

FIGURE 6 | Relationship between BTK activation and cardiac dysfunction in CLP-sepsis. Correlation data to show **(A)** ejection fraction (%) vs. phosphorylation of BTK at Tyr^{223}. **(B)** ejection fraction (%) vs. of PLCγ at Tyr^{1217}. **(C)** Phosphorylation of BTK at Tyr^{223} vs. NF-κB p65. **(D)** Phosphorylation of BTK at Tyr^{223} vs. phosphorylation of IKKα/β $atSer^{176/180}$. **(E)** Phosphorylation of BTK at Tyr^{223} vs. NLRP3. **(F)** Phosphorylation of BTK at Tyr^{223} vs. activated/pro-caspase-1. Data was analyzed by the Pearson correlation coefficient test to calculate the r value and a two tailed *T*-test for significance.

trend in reduction was observed. No significant differences were observed in the levels of cytokines or chemokines in CLP animals treated with either ibrutinib or acalabrutinib ($P > 0.05$; **Figures 7A–H**).

The data of all other cytokines/chemokines/growth factors that we measured in all groups are provided in **Supplementary Figure 1**.

DISCUSSION

We show here, for the first time, that administration of two structurally different BTK inhibitors (ibrutinib and acalabrutinib) both ameliorate the cardiac dysfunction (measured as decline in EF, FS, or FAC by echocardiography) caused by CLP-sepsis. The observed decline in EF also

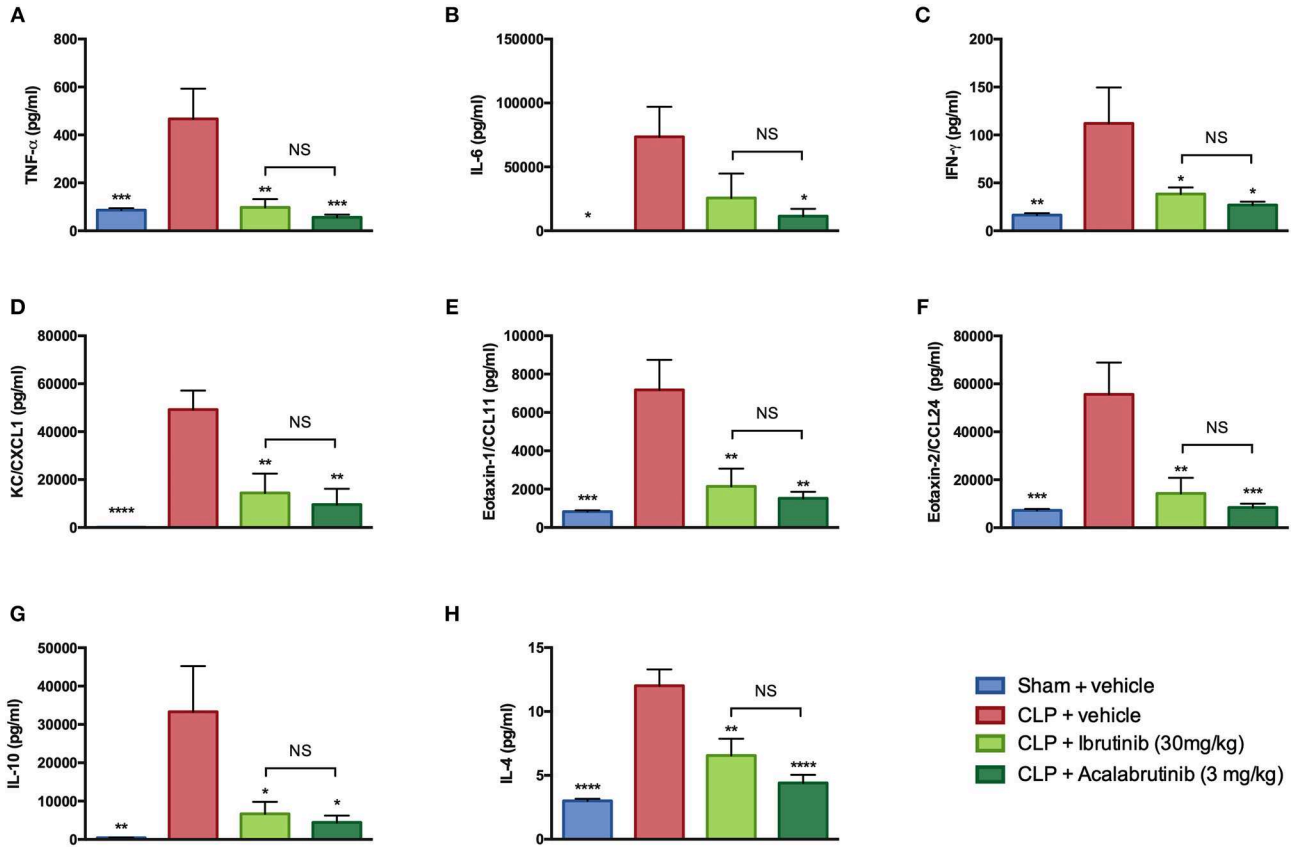

FIGURE 7 | Systemic inflammation in CLP mice is reduced by ibrutinib or acalabrutinib. Mice were randomly assigned to undergo CLP or sham surgery. One hour later, mice were treated with ibrutinib (30 mg/kg i.v.), acalabrutinib (3 mg/kg i.v.), or vehicle (5% DMSO + 30% cyclodextrin i.v.). At 24 h after CLP, blood samples were collected, and the serum concentration of cytokines and chemokines were measured by a multiplex assay ($n = 8$ per group). **(A)** TNF-α serum concentration (pg/ml). **(B)** IL-6 serum concentration (pg/ml). **(C)** IFN-γ serum concentration (pg/ml). **(D)** KC/CXCL1 serum concentration (pg/ml). **(E)** Eotaxin-1/CCL11 serum concentration (pg/ml). **(F)** Eotaxin-2/CCL24 serum concentration (pg/ml). **(G)** IL-10 serum concentration (pg/ml). **(H)** IL-4 serum concentration (pg/ml). All data are expressed as mean ± SEM for *n* number of observations. Correlations coefficients were determined by Pearson's correlation with *P*-values based on two-tailed tests a value of $^{****}P < 0.0001$, $^{***}P < 0.001$, $^{**}P < 0.01$, $^{*}P < 0.05$ was considered to be statistically significant.

was associated with a significant increase in the serum levels of two, well-known biomarkers of left ventricular dysfunction, namely CXCL10 and CXCL11 (24–26). Most notably, ibrutinib or acalabrutinib also attenuated the rises in CXCL10 and CXCL11 caused by CLP-sepsis. In addition, ibrutinib or acalabrutinib also reduced the renal dysfunction (measured as increase in serum urea or creatinine) caused by CLP-sepsis. Thus, both BTK inhibitors reduced the cardiac and renal dysfunction caused by sepsis.

What, then, is the mechanism by which ibrutinib or acalabrutinib reduce the cardiac (renal) dysfunction caused by sepsis? Ibrutinib is a potent BTK inhibitor, but not very specific (as it also inhibits a multitude of other kinases), which is approved by the FDA and the EMA for the use in CLL, MCL, and WM. Acalabrutinib is a potent, but highly specific BTK inhibitor: At a (relatively high) concentration of 1 μM, acalabrutinib strongly inhibited only the following 5 kinases: BTK, Bmx, ErbB4, RIPK2, and TEC, while the same concentration of ibrutinib inhibited 35 kinases. It should be noted that the doses of acalabrutinib and ibrutinib that we used in our study in the mouse resulted in a similar, ∼70%, inhibition of BTK activity in septic hearts. We, therefore, propose that inhibition of BTK activity explains the observed beneficial effects of ibrutinib or acalabrutinib in sepsis. The activation of BTK and the subsequent activation of BTK signaling involves (a) phosphorylation of BTK at Tyr^{223} and (b) the phosphorylation of PLCγ at Tyr^{1217} by phosphorylated (activated) BTK as the first step in the BTK signaling cascade (27). We report here that sepsis results in significant increases in the phosphorylation of cardiac BTK at Tyr^{223} and the phosphorylation of PLCγ at Tyr^{1217}, indicating that BTK is activated in septic hearts. Most notably, the activation of BTK negatively correlated with EF indicating that activation of BTK is associated with the cardiac dysfunction in sepsis. Indeed, inhibition of BTK activity with ibrutinib or acalabrutinib in the heart of septic animals reduces the cardiac dysfunction in sepsis suggesting that activation of BTK plays a pivotal role in the pathophysiology of the cardiac dysfunction in sepsis.

What are the mechanisms by which the activation of BTK (in the heart) leads to cardiac dysfunction in sepsis? There is good evidence that (a) the activation of BTK precedes the activation of NF-κB (16), and (b) the activation of NF-κB plays an important role in the cardiac dysfunction in sepsis (28, 29). Specifically, inhibition of the activity of NF-κB attenuates the cardiac dysfunction in sepsis (30, 31). We report here, for the first time, that (a) activation of BTK is associated activation of NF-κB in septic hearts, and (b) inhibition of BTK activity with ibrutinib or acalabrutinib reduces both the activation of NF-κB in septic hearts and the cardiac dysfunction caused by sepsis. Thus, we propose that inhibition of the activation of NF-κB contributes to the observed beneficial effects of the BTK inhibitors ibrutinib and acalabrutinib in sepsis. When challenging BTK KO-mice with LPS, Gabhann and colleagues observed reduced (i) activation of NF-κB p65, (ii) Akt phosphorylation, and (iii) M1 polarization of macrophages (32).

Activation of NF-κB drives the formation of a number of pro- and anti-inflammatory cytokines and chemokines. We report here that CLP-sepsis leads to a significant increase in the serum levels of the pro-inflammatory cytokines TNF-α, IL-6, IFN-γ, anti-inflammatory cytokines IL-10, IL-4 and the chemokines KC/CXCL1, eotaxin-1/CCL11, eotaxin-2/CCL24, all of which importantly contribute to the local and systemic inflammation and organ injury associated with sepsis (33). Most notably, we see the powerful pro-inflammatory cytokine TNF-α to be ameliorated by both BTK inhibitors. TNF-α has been implicated in murine models of sepsis and in humans with sepsis. TNF-α acts in an autocrine and paracrine manner leading to macrophage production and activation, resulting in the release of other proinflammatory cytokines such as IL-6 and IL-8 (34, 35).

Similarly, there is also good evidence that activation of BTK plays a crucial role in the assembly and activation of the NLRP3 inflammasome (17, 18). The activation of the NLRP3 inflammasome has been suggested to play a role in the cardiac dysfunction (36) and the pathophysiology of sepsis (37). Others have reported that inhibition of the assembly and activation of NLRP3 inflammasome protects against microbial sepsis (37). We report here for the first time that (a) activation of BTK is associated with the activation of the NLRP3 inflammasome in septic hearts, and (b) inhibition of BTK activity with ibrutinib and acalabrutinib reduces both the assembly and subsequent activation of the NLRP3 inflammasome in septic hearts (and the cardiac dysfunction caused by sepsis). Thus, we propose that inhibition of the activation of the NLRP3 inflammasome may also contribute to the observed beneficial effects of the BTK inhibitors ibrutinib and acalabrutinib in sepsis.

Activation of the NLRP3 inflammasome drives the formation of IL-1β and IL-18, both of which play an important role in the systemic inflammation and/or organ dysfunction in sepsis (38). Specifically, inhibition of caspase-1 results in an inhibition of IL-18 and IL-1β secretion, which, in turn, attenuated the cardiac dysfunction caused by myocardial ischemia (39). The role of the inflammasome in the pathophysiology of sepsis, however, is still controversial: For example, survival was similar in wild-type and caspase-1/11 knockout mice with sepsis, while the neutralization of IL-1 and IL-18 reduced mortality in endotoxemia (38). Here we show that BTK inhibition results in reduced serum levels of IL-1β, and this was associated with an improvement of cardiac function.

The evaluation of the efficacy of the BTK inhibitors used in our study depends on the assumption that the development of organ dysfunction (and specifically cardiac and renal dysfunction) correlates with outcome. There is good evidence that the occurrence of cardiac and/or renal dysfunction correlates positively with an increase in mortality in patients with sepsis (6). We have, however, not investigated the effects of BTK inhibition on survival in animals with sepsis due to ethical reasons. It would be useful to confirm whether inhibition of BTK activity does, indeed, improve survival in longer models of sepsis (rather than the very acute model employed here).

In addition to inhibiting BTK, ibrutinib and acalabrutinib also strongly inhibit four other kinases. To ensure that inhibition of BTK, indeed, accounts for the inhibition of NF-kB and the inflammasome and ultimately the observed beneficial effects in sepsis, it would be useful to repeat our study in BTK knockout mice. Interestingly, of the kinases which are strongly inhibited by ibrutinib and acalabrutinib, expression of ErbB4 (rather than its activation) may play a role in the cardiac dysfunction and cognitive impairment associated with sepsis (40). In contrast, RIP2 kinase is unlikely to play a significant role in sepsis, as the CLP-induced septic peritonitis was similar in RIP2 knockout mice and their wild-type litter mates (41).

CONCLUSIONS

There are currently no specific treatments, which reduce the cardiac dysfunction or, indeed, mortality in sepsis. Our data shows for the first time that two commercially available BTK inhibitors, ibrutinib or acalabrutinib, attenuate the CLP-induced cardiac dysfunction through inhibition of the activation of BTK/NF-κB and/or the NLRP3 inflammasome, which in turn reduces the formation of a number of chemokines and cytokines including TNF-α. Notably, no significant qualitative or quantitative differences were found with two, chemically distinct BTK-inhibitors suggesting that the observed beneficial effects of both compounds in experimental sepsis are likely to be a drug class related effect. Thus, BTK inhibitors are FDA-approved drugs that maybe repurposed for the use in sepsis, but also for other diseases associated with either local or systemic inflammation.

DATA AVAILABILITY

All datasets generated for this study are included in the manuscript and/or the **Supplementary Files**.

ETHICS STATEMENT

This study was carried out in accordance with the recommendations of Home Office guidance on the operation of Animals (Scientific Procedure Act, 1986) published by Her Majesty's Stationary Office, the Guide for the Care and Use

of Laboratory Animals of the National Research Council and the ARRIVE guidelines. The protocol was approved by The Animal Welfare Ethics Review Board of Queen Mary University of London and conducted under U.K. home office license number PC5F29685.

AUTHOR CONTRIBUTIONS

CO'R, GP, SC, MC, and CT conceived and designed the experiment. CO'R, GP, DC, FC, BW, SA, and LS performed the experiments. CO'R, MC, SC, BW, LM, and CT analyzed the data. CO'R, and CT contributed to the writing of the manuscript. MC, FC, SC, BW, LM, and SA contributed to the revision prior to submission.

FUNDING

CO'R was sponsored by Barts and The London School of Medicine and Dentistry, Queen Mary University of London. This work was, in part, supported by William Harvey Research Limited and the William Harvey Research Foundation, the British Heart Foundation (Award number: FS/13/58/30648 to GP), the Federal Ministry of Education and Research, Germany (Grant 03Z22JN12 to SC, Research Group Translational Septomics, Center for Innovation Competence Septomics), and the German Research Foundation DFG (MA 7082/3-1).

ACKNOWLEDGMENTS

We would like to thank Jacqueline Fischer for technical assistance.

SUPPLEMENTARY MATERIAL

The Supplementary Material for this article can be found online at: https://www.frontiersin.org/articles/10.3389/fimmu.2019.02129/full#supplementary-material

Supplementary Figure 1 | Systemic inflammation in CLP mice is reduced by ibrutinib or acalabrutinib. Mice were randomly assigned to undergo CLP or sham surgery. One hour later, mice were treated with ibrutinib (30 mg/kg i.v.), acalabrutinib (3 mg/kg i.v.), or vehicle (5% DMSO + 30% cyclodextrin i.v.). At 24 h after CLP, blood samples were collected, and the serum concentration of cytokines and chemokines were measured by a multiplex assay ($n = 8$ per group). All data are expressed as mean ± SEM for n number of observations. A value of $^{****}P < 0.0001$, $^{***}P < 0.001$, $^{**}P < 0.01$, $^{*}P < 0.05$ was considered to be statistically significant when compared to the control by one-way ANOVA followed by a Bonferroni's *post-hoc* test. A value of $^{\$\$\$\$}P < 0.0001$, $^{\$\$}P < 0.01$ was considered to be statistically significant when compared to the sham by one-way ANOVA followed by a Bonferroni's *post-hoc* test.

REFERENCES

1. Singer M, Deutschman CS, Seymour CW, Shankar-Hari M, Annane D, Bauer M, et al. The third international consensus definitions for sepsis and septic shock (Sepsis-3). *JAMA*. (2016) 315:801–10. doi: 10.1001/jama.2016.0287
2. Fleischmann C, Scherag A, Adhikari NKJ, Hartog CS, Tsaganos T, Schlattmann P, et al. Assessment of global incidence and mortality of hospital-treated sepsis. Current estimates and limitations. *Am J Respir Crit Care Med*. (2016) 193:259–72. doi: 10.1164/rccm.201504-0781OC
3. Daniels R. Surviving the first hours in sepsis: getting the basics right (an intensivist's perspective). *J Antimicrob Chemother*. (2011) 66:ii11–23. doi: 10.1093/jac/dkq515
4. Richards M. *Sepsis Management as an NHS Clinical Priority*. UK Sepsis Group (2014). Available online at: http://www.england.nhs.uk/wp-content/uploads/2013/12/sepsis-brief.pdf (accessed March 1, 2019).
5. Hunter JD, Doddi M. Sepsis and the heart. *Br J Anaesth*. (2010) 104:3–11. doi: 10.1093/bja/aep339
6. Parrillo JE, Parker MM, Natanson C, Suffredini AF, Danner RL, Cunnion RE, et al. Septic shock in humans. *Ann Intern Med*. (1990) 113:227. doi: 10.7326/0003-4819-113-3-227
7. Kumar A, Thota V, Dee L, Olson J, Uretz E, Parrillo JE. Tumor necrosis factor alpha and interleukin 1beta are responsible for *in vitro* myocardial cell depression induced by human septic shock serum. *J Exp Med*. (1996) 183:949–58. doi: 10.1016/S0300-9572(96)90072-6
8. Martin L, Derwall M, Al Zoubi S, Zechendorf E, Reuter DA, Thiemermann C, et al. The septic heart: current understanding of molecular mechanisms and clinical implications. *Chest*. (2019) 155:427–37. doi: 10.1016/j.chest.2018.08.1037
9. Tsukada S, Saffran DC, Rawlings DJ, Parolini O, Allen RC, Klisak I, et al. Deficient expression of a B cell cytoplasmic tyrosine kinase in human X-linked agammaglobulinemia. *Cell*. (1993) 72:279–90. doi: 10.1016/0092-8674(93)90667-F
10. Sanford DS, Wierda WG, Burger JA, Keating MJ, O'Brien SM. Three newly approved drugs for chronic lymphocytic leukemia: incorporating ibrutinib, idelalisib, and obinutuzumab into clinical practice. *Clin Lymphoma Myeloma Leuk*. (2015) 15:385–91. doi: 10.1016/j.clml.2015.02.019
11. Markham A, Dhillon S. Acalabrutinib: first global approval. *Drugs*. (2018) 78:139–45. doi: 10.1007/s40265-017-0852-8
12. European Medicines Agency. *Imbruvica*. (2019). Available online at: https://www.ema.europa.eu/en/medicines/human/EPAR/imbruvica (accessed August 21, 2019).
13. European Medicines Agency. *Orphan designation: Acalabrutinib for: Treatment of Chronic Lymphocytic Leukaemia/Small Lymphocytic Lymphoma*. (2016). Available online at: https://www.ema.europa.eu/en/medicines/human/orphan-designations/eu3161626 (accessed August 21, 2019).
14. European Medicines Agency. *Orphan Designation: Acalabrutinib for: Treatment of Lymphoplasmacytic Lymphoma*. (2016). Available online at: https://www.ema.europa.eu/en/medicines/human/orphan-designations/eu3161626 (accessed August 21, 2019).
15. European Medicines Agency. *Orphan Designation: Acalabrutinib for: Treatment of Mantle Cell Lymphoma*. (2016). Available online at: https://www.ema.europa.eu/en/medicines/human/orphan-designations/eu3161625 (accessed August 21, 2019).
16. Jefferies CA, Doyle S, Brunner C, Dunne A, Brint E, Wietek C, et al. Bruton's tyrosine kinase is a Toll/interleukin-1 receptor domain-binding protein that participates in nuclear factor kappaB activation by Toll-like receptor 4. *J Biol Chem*. (2003) 278:26258–64. doi: 10.1074/jbc.M301484200
17. Liu X, Pichulik T, Wolz OO, Dang TM, Stutz A, Dillen C, et al. Human NACHT, LRR, and PYD domain–containing protein 3 (NLRP3) inflammasome activity is regulated by and potentially targetable through Bruton tyrosine kinase. *J Allergy Clin Immunol*. (2017) 140:1054–67.e10. doi: 10.1016/j.jaci.2017.01.017
18. Ito M, Shichita T, Okada M, Komine R, Noguchi Y, Yoshimura A, et al. Bruton's tyrosine kinase is essential for NLRP3 inflammasome activation and contributes to ischaemic brain injury. *Nat Commun*. (2015) 6:7360. doi: 10.1038/ncomms8360
19. Wu H, Huang Q, Qi Z, Chen Y, Wang A, Chen C, et al. Irreversible inhibition of BTK kinase by a novel highly selective inhibitor CHMFL-BTK-11 suppresses inflammatory response in rheumatoid arthritis model. *Sci Rep*. (2017) 7:466. doi: 10.1038/s41598-017-00482-4
20. Kilkenny C, Browne WJ, Cuthill IC, Emerson M, Altman DG. Improving bioscience research reporting: the ARRIVE guidelines for reporting

animal research. *PLoS Biol.* (2010) 8:e1000412. doi: 10.1371/journal.pbio.1000412
21. Collino M, Pini A, Mugelli N, Mastroianni R, Bani D, Fantozzi R, et al. Beneficial effect of prolonged heme oxygenase 1 activation in a rat model of chronic heart failure. *Dis Model Mech.* (2013) 6:1012–20. doi: 10.1242/dmm.011528
22. Morgan E, Varro R, Sepulveda H, Ember JA, Apgar J, Wilson J, et al. Cytometric bead array: a multiplexed assay platform with applications in various areas of biology. *Clin Immunol.* (2004) 110:252–66. doi: 10.1016/j.clim.2003.11.017
23. Varro R, Chen R, Sepulveda H, Apgar J. Bead-based multianalyte flow immunoassays. In: *Methods in Molecular Biology* (Clifton, NJ: Humana Press). p. 125–52.
24. Altara R, Mallat Z, Booz GW, Zouein FA. The CXCL10/CXCR3 axis and cardiac inflammation: implications for immunotherapy to treat infectious and noninfectious diseases of the heart. *J Immunol Res.* (2016) 2016:4396368. doi: 10.1155/2016/4396368
25. Altara R, Manca M, Hessel MH, Gu Y, van Vark LC, Akkerhuis KM, et al. CXCL10 is a circulating inflammatory marker in patients with advanced heart failure: a pilot study. *J Cardiovasc Transl Res.* (2016) 9:302–14. doi: 10.1007/s12265-016-9703-3
26. Altara R, Gu YM, Struijker-Boudier HAJ, Thijs L, Staessen JA, Blankesteijn WM. Left ventricular dysfunction and CXCR3 ligands in hypertension: from animal experiments to a population-based pilot study. *PLoS ONE.* (2015) 10:e0141394. doi: 10.1371/journal.pone.0141394
27. Kurosaki T, Maeda A, Ishiai M, Hashimoto A, Inabe K, Takata M. Regulation of the phospholipase C-gamma2 pathway in B cells. *Immunol Rev.* (2000) 176:19–29. doi: 10.1034/j.1600-065X.2000.00605.x
28. Pritts TA, Moon MR, Wang Q, Hungness ES, Salzman AL, Fischer JE, et al. Activation of NF-kappaB varies in different regions of the gastrointestinal tract during endotoxemia. *Shock.* (2000) 14:118–22. doi: 10.1097/00024382-200014020-00007
29. Liu SF, Ye X, Malik AB. Pyrrolidine dithiocarbamate prevents I-kappaB degradation and reduces microvascular injury induced by lipopolysaccharide in multiple organs. *Mol Pharmacol.* (1999) 55:658–67.
30. Al Zoubi S, Chen J, Murphy C, Martin L, Chiazza F, Collotta D, et al. Linagliptin attenuates the cardiac dysfunction associated with experimental sepsis in mice with Pre-existing Type 2 diabetes by inhibiting NF-κB. *Front Immunol.* (2018) 9:2996. doi: 10.3389/fimmu.2018.02996
31. Chen J, Kieswich JE, Chiazza F, Moyes AJ, Gobbetti T, Purvis GSD, et al. IκB Kinase inhibitor attenuates sepsis-induced cardiac dysfunction in CKD. *J Am Soc Nephrol.* (2017) 28:94–105. doi: 10.1681/ASN.2015060670
32. Ní Gabhann J, Hams E, Smith S, Wynne C, Byrne JC, Brennan K, et al. Btk regulates macrophage polarization in response to lipopolysaccharide. *PLoS ONE.* (2014) 9:e85834. doi: 10.1371/journal.pone.0085834
33. Chaudhry H, Zhou J, Zhong Y, Ali MM, McGuire F, Nagarkatti PS, et al. Role of cytokines as a double-edged sword in sepsis. *In Vivo.* (2013) 27:669–84.
34. Fong Y, Tracey KJ, Moldawer LL, Hesse DG, Manogue KB, Kenney JS, et al. Antibodies to cachectin/tumor necrosis factor reduce interleukin 1 beta and interleukin 6 appearance during lethal bacteremia. *J Exp Med.* (1989) 170:1627–33. doi: 10.1084/jem.170.5.1627
35. Cohen J. The immunopathogenesis of sepsis. *Nature.* (2002) 420:885–91. doi: 10.1038/nature01326
36. Zhang W, Xu X, Kao R, Mele T, Kvietys P, Martin CM, et al. Cardiac fibroblasts contribute to myocardial dysfunction in mice with sepsis: the role of NLRP3 inflammasome activation. *PLoS ONE.* (2014) 9:e107639. doi: 10.1371/journal.pone.0107639
37. Lee S, Nakahira K, Dalli J, Siempos II, Norris PC, Colas RA, et al. NLRP3 Inflammasome deficiency protects against microbial sepsis via increased Lipoxin B_4 synthesis. *Am J Respir Crit Care Med.* (2017) 196:713–26. doi: 10.1164/rccm.201604-0892OC
38. Berghe TV, Demon D, Bogaert P, Vandendriessche B, Goethals A, Depuydt B, et al. Simultaneous targeting of IL-1 and IL-18 is required for protection against inflammatory and septic shock. *Am J Respir Crit Care Med.* (2014) 189:282–91. doi: 10.1164/rccm.201308-1535OC
39. Pomerantz BJ, Reznikov LL, Harken AH, Dinarello CA. Inhibition of caspase 1 reduces human myocardial ischemic dysfunction via inhibition of IL-18 and IL-1beta. *Proc Natl Acad Sci USA.* (2001) 98:2871–6. doi: 10.1073/pnas.041611398
40. An R, Feng J, Xi C, Xu J, Sun L. miR-146a attenuates sepsis-induced myocardial dysfunction by suppressing IRAK1 and TRAF6 via targeting ErbB4 expression. *Oxid Med Cell Longev.* (2018) 2018:1–9. doi: 10.1155/2018/7163057
41. Sônego F, Castanheira FVS, Czaikoski PG, Kanashiro A, Souto FO, França RO, et al. MyD88-, but not Nod1- and/or Nod2-deficient mice, show increased susceptibility to polymicrobial sepsis due to impaired local inflammatory response. *PLoS ONE.* (2014) 9:e103734. doi: 10.1371/journal.pone.0103734

Conflict of Interest Statement: The authors declare that the research was conducted in the absence of any commercial or financial relationships that could be construed as a potential conflict of interest.

Copyright © 2019 O'Riordan, Purvis, Collotta, Chiazza, Wissuwa, Al Zoubi, Stiehler, Martin, Coldewey, Collino and Thiemermann. This is an open-access article distributed under the terms of the Creative Commons Attribution License (CC BY). The use, distribution or reproduction in other forums is permitted, provided the original author(s) and the copyright owner(s) are credited and that the original publication in this journal is cited, in accordance with accepted academic practice. No use, distribution or reproduction is permitted which does not comply with these terms.

frontiers in Immunology

ORIGINAL RESEARCH
published: 01 October 2019
doi: 10.3389/fimmu.2019.02276

Endogenous Uteroglobin as Intrinsic Anti-inflammatory Signal Modulates Monocyte and Macrophage Subsets Distribution Upon Sepsis Induced Lung Injury

Andrea Janicova[1,2,3], Nils Becker[1], Baolin Xu[1], Sebastian Wutzler[4], Jan Tilmann Vollrath[1], Frank Hildebrand[5], Sabrina Ehnert[6], Ingo Marzi[1], Philipp Störmann[1†] and Borna Relja[1†]*

[1] Department of Trauma, Hand and Reconstructive Surgery, Goethe University, Frankfurt, Germany, [2] Department of Aquatic Ecotoxicology, Goethe University, Frankfurt, Germany, [3] Department of Radiology and Nuclear Medicine, Experimental Radiology, Otto-von-Guericke University, Magdeburg, Germany, [4] Orthopedic and Trauma Surgery, Helios Horst Schmidt Clinic, Wiesbaden, Germany, [5] Department of Trauma Surgery, RWTH University, Aachen, Germany, [6] Department of Trauma and Reconstructive Surgery, Siegfried Weller Research Institute, BG Trauma Center Tuebingen, Eberhard Karls University Tuebingen, Tuebingen, Germany

OPEN ACCESS

Edited by:
Christoph Thiemermann, Queen Mary University of London, United Kingdom

Reviewed by:
Hugo Caire Castro-Faria-Neto, Oswaldo Cruz Foundation (Fiocruz), Brazil
Xin Zhou, Tianjin Medical University General Hospital, China
Christoph Emontzpohl, University Hospital RWTH Aachen, Germany

***Correspondence:**
Borna Relja
info@bornarelja.com

† These authors have contributed equally to this work

Specialty section:
This article was submitted to Inflammation, a section of the journal Frontiers in Immunology

Received: *14 June 2019*
Accepted: *09 September 2019*
Published: *01 October 2019*

Citation:
Janicova A, Becker N, Xu B, Wutzler S, Vollrath JT, Hildebrand F, Ehnert S, Marzi I, Störmann P and Relja B (2019) Endogenous Uteroglobin as Intrinsic Anti-inflammatory Signal Modulates Monocyte and Macrophage Subsets Distribution Upon Sepsis Induced Lung Injury. Front. Immunol. 10:2276. doi: 10.3389/fimmu.2019.02276

Sepsis is a serious clinical condition which can cause life-threatening organ dysfunction, and has limited therapeutic options. The paradigm of limiting excessive inflammation and promoting anti-inflammatory responses is a simplified concept. Yet, the absence of intrinsic anti-inflammatory signaling at the early stage of an infection can lead to an exaggerated activation of immune cells, including monocytes and macrophages. There is emerging evidence that endogenous molecules control those mechanisms. Here we aimed to identify and describe the dynamic changes in monocyte and macrophage subsets and lung damage in CL57BL/6N mice undergoing blunt chest trauma with subsequent cecal ligation and puncture. We showed that early an increase in systemic and activated $Ly6C^{+}CD11b^{+}CD45^{+}Ly6G^{-}$ monocytes was paralleled by their increased emigration into lungs. The ratio of pro-inflammatory $Ly6C^{high}CD11b^{+}CD45^{+}Ly6G^{-}$ to patrolling $Ly6C^{low}CD11b^{+}CD45^{+}Ly6G^{-}$ monocytes significantly increased in blood, lungs and bronchoalveolar lavage fluid (BALF) suggesting an early transition to inflammatory phenotypes during early sepsis development. Similar to monocytes, the level of pro-inflammatory $Ly6C^{high}CD45^{+}F4/80^{+}$ macrophages increased in lungs and BALF, while tissue repairing $Ly6C^{low}CD45^{+}F4/80^{+}$ macrophages declined in BALF. Levels of inflammatory mediators TNF-α and MCP-1 in blood and RAGE in lungs and BALF were elevated, and besides their boosting of inflammation via the recruitment of cells, they may promote monocyte and macrophage polarization, respectively, toward the pro-inflammatory phenotype. Neutralization of uteroglobin increased pro-inflammatory cytokine levels, activation of inflammatory phenotypes and their recruitment to lungs; concurrent with increased pulmonary damage in septic mice. In *in vitro* experiments, the influence of uteroglobin on monocyte functions including migratory behavior, TGF-β1 expression, cytotoxicity and viability were proven. These results highlight an important role of endogenous uteroglobin as intrinsic anti-inflammatory signal upon sepsis-induced early lung injury, which modules the early monocyte/macrophages driven inflammation.

SHORT SUMMARY

Blunt chest injury is the third largest cause of death following major trauma, and ongoing excessive pro-inflammatory immune response entails high risk for the development of secondary complications, such as sepsis, with limited therapeutic options. In murine double hit trauma consisting of thoracic trauma and subsequent cecal ligation and puncture, we investigated the cytokine profile, pulmonary epithelial integrity and phenotypic shift of patrolling Ly6C^{low}CD11b^{+}CD45^{+}Ly6G^{-} monocytes and Ly6C^{low}CD45^{+}F4/80^{+} macrophages to pro-inflammatory Ly6C^{high}CD11b^{+}CD45^{+}Ly6G^{-} monocytes and Ly6C^{high}CD45^{+}F4/80^{+} cells in blood, lungs and bronchoalveolar lavage fluid (BALF). Pro-inflammatory mediators and phenotypes were elevated and uteroglobin neutralization led to further increase. Enhanced total protein levels in BALF suggests leakage of respiratory epithelium. *In vitro*, uteroglobin inhibited the migratory capacity of monocytes and the TGF-β1 expression without affecting the viability. These results highlight an important role of endogenous uteroglobin as an intrinsic anti-inflammatory signal upon sepsis-induced early lung injury, which modulates the early monocyte/macrophages driven inflammation.

Keywords: uteroglobin, CC16, chest injury, acute lung injury, CLP, sepsis, monocytes, macrophages

INTRODUCTION

Trauma is one of leading causes of death worldwide (1). Twenty to twenty-five percent of patients with multiple injuries suffer from severe lung contusion, whereas thoracic trauma represents the third most frequent cause of death after major trauma (2, 3). Thoracic injury contributes significantly to the development of acute respiratory distress syndrome (ARDS) (4), while infectious complications such as e.g., sepsis constitute a serious risk factors for up to 50% of mortalities occurring upon ARDS (5). Thus, the development of secondary complications is still a major contributing factor in trauma-associated mortality (6–8).

In general, traumatic injury-related tissue damage induces a release of endogenous damage-associated molecular patterns to initiate the resolution of non-pathogenic and pathogenic inflammation with subsequent tissue repair (9). This systemic inflammatory response syndrome triggers an excessive release of pro-inflammatory cytokines such as tumor necrosis factor (TNF)-α (9), interleukin (IL)-6 (9) and chemokines, such as monocyte chemoattractant protein (MCP)-1 (10, 11), which is a potent factor for monocyte and macrophage migration and infiltration (12).

Monocytes play a pivotal role in pathogen recognition and killing, and although their functional and phenotypic alterations provide a good base for prediction of complications after trauma or of poor prognosis in septic patients, exact pathophysiologic mechanisms and solid biomarkers still remain to be elucidated (13–17). Murine monocytes expressing high levels of lymphocyte antigen (Ly)6C have pro-inflammatory and anti-microbial features and have been shown to be precursors for patrolling monocytes, which survey the vasculature and contribute to the early response of inflammation and tissue repair, and which are characterized by a low expression of Ly6C (18, 19). Next to monocytes, resident alveolar macrophages initiate the inflammatory cascade and secrete pro-inflammatory mediators during acute lung injury (ALI) (20–22). While the pro-inflammatory M1 macrophages release e.g., nitric oxide, TNF-α, interferon-γ and IL-12 and critically contribute to pathogen clearance, their apoptosis during the process of pathogen clearance simultaneously contributes to downregulation of the pro-inflammatory phase and transition of M1 to tissue-repairing M2 macrophages (23). With regards to specific roles of monocytes/macrophages during lung injury and/or sepsis, both beneficial or detrimental effects of each cell type have been reported. While an early depletion of circulating monocytes before lipopolysaccharide (LPS) administration deteriorated lung injury (24), later monocyte depletion ameliorated lung injury (25, 26). Furthermore, macrophage polarization into M1 phenotype improved organ dysfunction and reduced mortality in lethal sepsis (27), while an intratracheal administration of M2 macrophages after CLP reduced mortality (28). These results indicate that an early balance of the pro-inflammatory and the anti-inflammatory response is required for ameliorating lung injury.

Uteroglobin (club cell protein (CC)16), is a 15.8 kDa protein secreted primarily by non-ciliated club cells along the tracheobronchial epithelium, especially in distal respiratory and terminal bronchioles (29, 30). Next to its biomarker character to indicate the development of secondary pulmonary complications after trauma, CC16 exerts anti-inflammatory and immunosuppressive properties (31–33). Its anti-inflammatory

Abbreviations: Ab, antibody; ALI, acute lung injury; ARDS, acute respiratory distress syndrome; BALF, bronchoalveolar lavage fluid; CC, club cell protein; CLP, cecal ligation and puncture; HV, healthy volunteers; ISS, injury severity score; LPS, lipopolysaccharide; Ly, lymphocyte antigen; MCP, monocyte chemoattractant protein; MPP, matrix metalloproteinase; RAGE, receptor for advanced glycation endproducts; TNF, tumor necrosis factor; TP, trauma patient; TxT, thoracic trauma.

biology has been confirmed in tracheal epithelial cells, isolated human mononuclear cells and murine macrophages (34–36). Due to this, CC16 has been described as being protective in the development of chronic obstructive pulmonary disease in human (37) and mouse (33).

Considering that functional and phenotypic alterations of monocytes/macrophages play an important role in sepsis development and due to the potent anti-inflammatory biology of CC16, we hypothesize that an early upregulation of the pro-inflammatory response by local CC16 neutralization will deteriorate the dynamic changes in monocyte and macrophage subsets and early lung damage in a murine trauma model of sepsis after blunt chest trauma.

MATERIALS AND METHODS

Ethics

The *in vitro* study was performed in the University Hospital Frankfurt, Goethe-University, Germany, with the institutional ethical committee approval (312/10) in accordance with the Declaration of Helsinki and following STROBE-guidelines (38). In this experimental trial, twenty severely injured trauma patients (TP) with a history of acute blunt or penetrating trauma with an injury severity score (ISS) of $\geq$ 16 were enrolled, along with and 8 healthy volunteers. All individuals who were <18 or >80 years of age, suffering from a severe burn injury, acute myocardial infarction, cancer or chemotherapy, HIV, infectious hepatitis, acute CMV infection and/or thromboembolic events, or receiving immunosuppressive drug therapy were excluded. The ISS was calculated according to the abbreviated injury scale (39) upon arrival to the emergency department. The signed written informed consent form was obtained from all patients or their legally authorized representatives, as well as from all included healthy volunteers (HV).

Animal experiments were conducted at the Zentrale Forschungseinrichtung of the University Hospital Frankfurt in accordance with the German Federal Law in regard of protection of animals with the approval of the responsible government authority, the Veterinary Department of the Regional Council in Darmstadt, Germany (Regierungspräsidium Darmstadt, Hessen, Germany; AZ: FK 1068). All experiments were performed in accordance with the ARRIVE Guidelines (40).

Animals and Experimental Model

Forty male CL57BL/6N mice (25 ± 5 g, 6–8 weeks old) were included (Janvier Labs, France) (41). Before and after experimental procedures, all animals had access to water and food *ad libidum*. Blunt chest trauma was performed under general mask anesthesia as described before (41). Briefly, the animals were placed in a supine position and a blunt bilateral thoracic trauma (TxT) was induced by a standardized pressure wave provided directly to the chest (41). After 24 h, a median laparotomy with moderate cecal ligation and puncture (CLP) followed as described before (41). Eight animals underwent only TxT. Twenty-four animals underwent the double hit consisting of TxT and CLP. Eight animals in the sham control group underwent anesthesia without performing any surgical procedures. After 6 h, euthanasia was done to facilitate sampling.

Group Allocation Based on the Administration of CC16 Neutralizing Antibody

Animals were randomly assigned to different experimental groups for local antibody (Ab) application to the lungs. Administration of Uteroglobin/SCGB1A1 (CC16 Ab, 10 μg/mL, LS Biosciences) or IgG Control (IgG) Antibody (10 μg/mL, R&D Systems) was performed immediately after the induction of thoracic trauma. For this procedure, mice were placed in a supine position and the tongue was thoroughly kept aside. A buttoned cannula was placed at the beginning of the trachea and 50 μL of the Ab solution were carefully administered. Then, mice were kept in a reverse trendelenburg position for 30 s to ensure the Ab distribution inside the lungs.

Sampling and Quantification of Protein Expression Levels in Lungs, Plasma, and BALF

The *vena cava* was punctured by a heparinized syringe for blood withdrawal at 6 h after CLP. After centrifugation at 1,164 g for 15 min at 4°C, the plasma was stored at –80°C for the subsequent measurements of pro-inflammatory mediators. MCP-1 and TNF-α were measured in plasma with the CBA Mouse Inflammation Kit (BD Bioscience, San Jose, CA, USA) according to the manufacturer's instructions. Briefly, 50 μL of the Capture Beads were added into polystyrene FACS tubes (BD Pharmingen™) to 50 μL of plasma. To each FACS tube, 50 μL of the Mouse Inflammation PE Detection Reagent were added and incubated at room temperature in the dark for 2 h. Subsequently, samples were washed with 1 mL of Wash Buffer and centrifuged at 200 g for 5 min. Supernatant was discarded and pellet resuspended in 300 μL of Wash buffer. Analysis was performed using a BD FACS Canto 2™ and FCAP Array™Software (BD).

After blood withdrawal, the trachea was punctured, intubated and the lungs were flushed with 1.2 mL phosphate buffered saline (PBS) to gain the bronchoalveolar lavage fluid (BALF) for analysis. BALF samples were centrifuged at 1,164 g at 4°C for 5 min and the supernatant was used for the detection of the receptor for advanced glycation endproducts (RAGE DuoSet® ELISA Kit; R&D Systems, Minneapollis, US). Quickly, a microplate (Sarstedt, Nümbrecht, Germany) was coated with 100 μL Capture Antibody overnight at room temperature. Following a washing step, 300 μL of Reagent Diluent was added for 1 h to block the microplate. After another washing step, samples were loaded and incubated for 2 h at room temperature. Subsequently, the microplate was washed again and incubated with 100 μL Detection Antibody for 2 h. Microplate was washed again and incubated with 100 μL Streptavidin-HRP solution for 20 min in the dark at room temperature. Following the last washing step, 100 μL Substrate Solution was added to the wells and incubated in the dark at room temperature until a color reaction occurred. Subsequently, the reaction was stopped by adding 50 μL Stop Solution. The optical density was measured with the Infinite M200 microplate reader (Tecan, Männedorf, Switzerland, 450 nm absorbance, 570 nm reference wavelength; software Magellan).

The cell pellets from BALF were resuspended in 100 μL PBS supplemented with 0.5% bovine serum albumin (FACS buffer), and 40 μL were transferred into polystyrene FACS tubes (BD Pharmingen™) for subsequent cell staining as described below.

Then the animals were perfused with 20 mL PBS via the caudal *vena cava*, and, subsequently, the lungs were removed. One lung lobe was snap-frozen using liquid nitrogen for later protein isolation, and the other one was used for flow cytometric analyses. For protein isolation, lung tissue was homogenized in protein lysis buffer at 4°C, followed by centrifugation for 30 min at 4°C at 20,000 g. Supernatants were stored at −80°C for later analysis. Protein concentrations of pulmonary RAGE were determined using a mouse RAGE DuoSet® ELISA Kit (R&D Systems) as described above.

Analysis of Monocyte and Macrophage Subsets by Flow Cytometry

Lung tissue was processed as described in the Minute Single Cell Isolation protocol (Invent Biotechnologies, Minnesota, US). Briefly, 25 mg of fresh lung tissue were placed into a filter cartridge where 100 μL ice-cold Buffer A were subsequently added. The tissue was grinded with a plastic rod for 50–60 times. After adding further 400 μL Buffer A, sample was mixed by inverting the closed filter cartridge and centrifuged at 1,200 g and 4°C for 5 min. The pellet was resuspended and centrifuged again at 400 g and 4°C for 5 min. Subsequently, supernatant was discarded and pellet was resuspended in 100 μL FACS buffer. Forty microliter were transferred into each polystyrene FACS tubes (BD Pharmingen™) and stained for flow cytometry analysis as described below.

Thirty microliters of whole blood was transferred into each polystyrene FACS tubes (BD Pharmingen™) and stained for flow cytometry analysis as described below.

The cell pellets from BALF were resuspended in 100 μL of FACS buffer, and 40 μL was transferred into polystyrene FACS tubes (BD Pharmingen™).

Then, the samples were incubated with Pacific Blue-conjugated anti-mouse Ly-6G/Ly6C antibody (Ab) (Clone RB6-8C5; BioLegend, San Diego, California, US), APC/Fire 750 conjugated anti-mouse CD45 Ab (Clone 30-F11; BioLegend), Alexa Fluor 647-conjugated anti-mouse CD11b Ab (Clone M1/70; BioLegend), Brilliant Violett 510-conjugated anti-mouse F4/80 Ab (Clone BM8; BioLegend), and Phycoerythrin-Cyanine7-conjugated anti-mouse Ly6C Ab (Clone RB6-8C5; BioLegend). Control stainings with the corresponding isotype antibodies were applied for the settings. After 30 min on ice, 5 μL of 7-AAD (BD Biosciences, Franklin Lakes, USA) were added, and samples were incubated for further 15 min. Then, the samples were washed with 2 mL FACS buffer [7 min at room temperature (RT) and 423 g]. Supernatants were removed and cell pellets were homogenized in 1 mL of BD FACS Lysing Solution for an additional 10 min (RT). Then, samples were centrifuged at 400 g for 7 min and washed twice with 2 mL of FACS buffer. After removal of supernatants, cells were diluted in 80 μL FACS buffer and stored on ice until measurement. Each cell population was defined by gating the corresponding forward and side scatter scan as well as the viable cells by applying 7-AAD for gating. From each sample a minimum of 3.0 x 10^4 cells was measured, which were subsequently analyzed. The percentage of $Ly6C^+$ out of $CD11b^+Ly6G^-CD45^+$ and $F4/80^+CD45^+$ viable cells was assessed by flow cytometric analyses using a BD FACS Canto 2™ and FACS DIVA™ software (BD). The gating is shown in **Figure 2**.

Quantification of Uteroglobin in Sera From Healthy Volunteers and Trauma Patients

Collected sera from healthy volunteers and trauma patients were analyzed using human Uteroglobin Quantikine ELISA Kit (R&D Systems, Minneapolis, US) according to the manufacturer's instructions. Briefly, 100 μL of Assay Diluent were added to each well with subsequent addition of 50 μL of each sample and incubated at room temperature for 2 h. Then, each well was washed with 400 μL Wash Buffer. Subsequently, wells were incubated with 200 μl of Human Uteroglobin Conjugate for 2 h. After the next washing step, 200 μL of Substrate Solution were added into the wells for 30 min. The reaction was stopped by addition of 50 μl of Stop Solution to each well. The optical density was measured with the Infinite M200 microplate reader (Tecan, Männedorf, Switzerland, 450 nm absorbance, 570 nm reference wavelength; software Magellan).

Isolation of $CD14^+$ Monocytes

Isolation of peripheral blood mononuclear cells was performed by a density-gradient centrifugation (Bicoll separating solution, Biochrom, Berlin, Germany) according to manufacturer's instructions. Briefly, 25 mL of Bicoll separating solution (density: 1.077 g/mL) was carefully overlaid with an equal volume of heparinized whole blood from HV and centrifuged at 800 g for 30 min. Interphase containing peripheral blood mononuclear cells was transferred to another tube and washed with PBS w/o Ca^{2+} and Mg^{2+} (Invitrogen, Carlsbad, California, US). The remaining red blood cells were lysed by lysis buffer (0.155 M NH_4Cl, 0.01 M $KHCO_3$, 0.1 mM EDTA) and washed with MACS buffer (0.5% BSA, 2 mM EDTA). For CD14 labeling, cell pellet was resuspended in 75 μL of MACS buffer and incubated with 25 μL magnetic CD14 microbeads (Miltenyi Biotec, Bergisch Gladbach, Germany) for 15 min. After washing, $CD14^+$ monocytes were isolated by magnetic isolation with LS columns (Miltenyi Biotec) according to the manufacturer's protocol. Cell number and cell viability were determined by Türk's solution exclusion assay (Merck, Darmstadt, Germany). Only cell cultures with a purity of ≥95% were used for further experiments. The cells were cultured in RPMI 1640 medium (Seromed, Berlin, Germany), supplemented with 10% heat-inactivated fetal calf serum (Gibco, Karlsruhe, Germany), 100 IU/mL penicillin (Gibco), 10 μg/mL streptomycin (Gibco) and 20 mM HEPES buffer (Sigma) at 37°C and 5% CO_2.

Monocyte Treatment

Ex vivo, $CD14^+$ monocytes isolated from HV were treated with sera from HV and TP that were obtained at the admission to the emergency department. Prior to the experiment, the sera were incubated with or without anti-CC16-antibody (1 μg/mL;

R&D Systems) for CC16 neutralization or corresponding isotype control antibody (1 μg/mL; R&D Systems), respectively, for 1 h at 37°C and 5% CO_2, slightly slewing every 15 min. For monocyte stimulation, cell culture media was supplemented with 20% sera for 2 h at 37°C and 5% CO_2 and used for further analysis.

Migration Assay

Alterations in migratory capacity were determined by CytoSelect™ Cell Migration Assay (3 μm pores; Cell Biolabs, San Diego, US). 100,000 cells were plated in the upper chamber and treated as described in the Monocyte treatment section. MCP-1 (10 ng/mL; R&D Systems) was added to the lower chamber. After 3 h at 37°C and 5% CO_2, the upper chamber was removed and cells in the lower chamber were lysed and quantified using CyQuant® GR Fluorescent Dye (Cell Biolabs, San Diego, US) according to the manufacturer's instructions. Briefly, the cells containing supernatant from the feeder tray was transferred into a black-walled, clear bottom microplate. CyQuant® GR Dye was diluted 1:75 in 4x Lysis Buffer and subsequently added to each well to reach a 1x concentration. Samples were incubated at RT for 20 min. Fluorescence intensity was measured by Twinkle LB 970 Microplate Fluorometer (490 nm excitation/520 nm emission; software MikroWin 2000).

Measurement of TGF-β1 Expression in Monocytes by Flow Cytometry

100,000 cells per polystyrene FACS tube (BD Pharmingen™) were treated according to the Monocyte treatment section with slight change. After 1 h of treatment with sera, Brefeldin A (Invitrogen) was added to each tube to 1x concentration and monocytes were incubated for further 2 h at 37°C and 5% CO_2. Subsequently, monocytes were incubated with Phycoerythrin-conjugated anti-human CD14 antibody (2 μL; Clone M5E2; BioLegend) and fixable yellow dead cell stain (2 μL; Invitrogen, Carlsbad, California, US). After 30 min at RT, cells were washed with FACS buffer and centrifuged at 400 g for 5 min. Supernatant was removed and monocytes were fixed with Fix and Perm Medium A at room temperature for 15 min. After further washing step, cells were permeabilized with Fix and Perm Medium B (both Invitrogen, Carlsbad, California, US) and incubated with PerCP/Cyanine5.5-conjugated anti-human TGF-β1 antibody (2 μL; Clone TW4-2F8; BioLegend) at room temperature for 30 min. Following the washing step, monocytes were resuspended in 50 μL FACS buffer and analyzed using BD FACS Canto 2™ and FACD DIVA™ software (BD). Monocytes were gated by the corresponding forward and side scatter scan and as shown in **Figures 5A,B**. The percentage of TGF-β1 expression of viable $CD14^+$ monocytes was analyzed.

Quantification of IL-6 and TNF-α Levels in Monocyte Supernatants

100,000 cells were seeded in flat-bottom 96-well plate (Sarstedt) and treated as described in the Monocyte treatment section. The supernatants were collected to detect the IL-6 (Diaclone, Besançon cedex, France) or TNF-α (R&D Systems, Minneapollis, US) levels using ELISA kits according to the provider's instructions. For a brief IL-6 protocol, see equivalent RAGE measurement protocol in the Sampling and quantification of protein expression levels in lungs, plasma and BALF section. The protocol for TNF-α is equivalent to the Uteroglobin Quantikine ELISA Kit described in the section Quantification of uteroglobin in sera from healthy volunteers and trauma patients.

Cell Viability Assay

100,000 cells per well were plated in a clear bottom, black-walled 96-well plate (BD Biosciences) and left to adhere for 30 min at 37°C and 5% CO_2. Subsequently, monocytes were treated as described in the Monocyte treatment section. For cell viability measurement, Calcein AM reagent (1 μg/mL; Cayman Chemical, Michigan, US) was added to the cells and incubated at 37°C and 5% CO_2 for 30 min. Fluorescence intensity was measured by Twinkle LB 970 Microplate Fluorometer (490 nm excitation/520 nm emission; software MikroWin 2000).

LDH Assay

100,000 cells per well were plated in a flat bottom 96-well plate (Sarstedt) and let to adhere at 37°C and 5% CO_2 for 30 min. Subsequently, media was replaced with phenol-free RPMI 1640 medium, supplemented with 10% heat-inactivated fetal calf serum, 100 IU/mL penicillin, 10 μg/mL streptomycin and 20 mM HEPES buffer and monocytes were treated as described in Monocyte treatment section.

For cell cytotoxicity detection, 100 μL of monocyte supernatant was transferred to a fresh 96-well plate and incubated with LDH reaction mixture (Cytotoxicity Detection Kit, Roche, Mannheim, Germany) according to the manufacturer's instructions in dark at RT for 30 min. Absorbance was measured by Infinite M200 microplate reader (490 nm absorbance, 600 nm reference wavelength; software Magellan).

Statistical Analysis

GraphPad Prism 6 (GraphPad Software Inc., San Diego, CA) was used to perform the statistical analyses. Normality of all data was analyzed by the D'Agostino-Pearson normality test. Differences between the groups were determined by non-parametric Kruskal-Wallis test which does not assume a normal distribution of the residuals followed by Dunn's *post hoc* test for the correction of multiple comparisons. A p-value below 0.05 was considered significant. Data are given as box-whisker plot and min to max.

RESULTS

Pro-inflammatory Mediators and Lung Damage Significantly Increase in the Early Phase of Sepsis

TxT in mice increased TNF-α and MCP-1 levels in plasma, whereby the TxT+CLP group showed a significant increase compared to the control group ($p < 0.05$, data not shown). RAGE protein levels were significantly higher in TxT+CLP compared to control, both in BALF and lungs ($p < 0.05$, data not shown). Following TxT and TxT+CLP, the total protein content in bronchoalveolar lavage which is associated with the extent of

lung damage significantly increased compared to control ($p < 0.05$, data not shown).

The Ratio of Inflammatory and Patrolling Monocytes Increases in Blood, Lungs, and BALF in the Early Phase of Sepsis

For detailed examination of monocyte and macrophage subset distributions, the constituent phenotypes were characterized by their specific surface protein markers. In blood, TxT alone slightly increased levels of activated $Ly6C^+CD11b^+Ly6G^-CD45^+$ monocytes, whereas TxT+CLP resulted in a significant elevation compared to control ($p < 0.05$, data not shown). Regarding the subset distribution, inflammatory $Ly6C^{hi}CD11b^+Ly6G^-CD45^+$ monocyte subset expanded significantly in TxT+CLP animals ($p < 0.05$, data not shown), and, in parallel, patrolling $Ly6C^{lo}CD11b^+Ly6G^-CD45^+$ monocytes showed an equivalent decrease vs. control ($p < 0.05$, data not shown). Thus, a significant increase in the ratio between inflammatory and patrolling monocytes was observed in early phase of sepsis ($p < 0.05$, data not shown).

Similarly, activated $Ly6C^+CD11b^+Ly6G^-CD45^+$ monocytes were markedly more abundant in lungs following TxT+CLP compared to control lungs ($p < 0.05$, data not shown). Whereas a significant increase of the inflammatory $Ly6C^{hi}CD11b^+Ly6G^-CD45^+$ phenotype was observed in TxT+CLP group compared to control group ($p < 0.05$, data not shown), the number of patrolling $Ly6C^{lo}CD11b^+Ly6G^-CD45^+$ monocytes was equally reduced ($p < 0.05$, data not shown). Therefore, comparable to systemic monocytes, the ratio of inflammatory to patrolling monocytes increased markedly in TxT+CLP vs. control ($p < 0.05$, data not shown).

Furthermore, significantly higher emigration rates of activated $Ly6C^+CD11b^+Ly6G^-CD45^+$ monocytes to BALF were found in TxT and TxT+CLP compared to control ($p < 0.05$, data not shown). Regarding the inflammatory phenotypes in BALF, the inflammatory $Ly6C^{hi}CD11b^+Ly6G^-CD45^+$ monocyte subset increased in TxT and TxT+CLP compared to control ($p < 0.05$, data not shown), whereas the patrolling $Ly6C^{lo}CD11b^+Ly6G^-CD45^+$ monocyte population was reduced ($p < 0.05$, data not shown). Concurrent with this data, an increased ratio between pro-inflammatory and patrolling monocytes was found in both, TxT and TxT+CLP groups, vs. control group ($p < 0.05$, data not shown).

The Number of Pro-inflammatory Macrophages Increases in Lungs and BALF

No significant systemic changes in $Ly6C^+F4/80^+CD45^+$ cell counts were found after TxT and TxT+CLP compared to control (data not shown). The pro-inflammatory $Ly6C^{hi}F4/80^+CD45^+$ phenotype slightly increased in TxT with further expansion in TxT+CLP vs. control but both without significance (data not shown). A decline of patrolling $Ly6C^{lo}F4/80^+CD45^+$ phenotype was observed in TxT and TxT+CLP vs. control (data not shown).

Whereas, no differences in total macrophage counts were shown in the lungs of TxT and TxT+CLP, a significant increase of pro-inflammatory $Ly6C^{hi}F4/80^+CD45^+$ macrophages compared to control was detected ($p < 0.05$, data not shown). The cell number of tissue repairing $Ly6C^{lo}F4/80^+CD45^+$ macrophages in lungs did not change after TxT and TxT+CLP vs. control (data not shown).

Following TxT, mice displayed a slight increase of $Ly6C^+F4/80^+CD45^+$ macrophage counts in BALF, whereas TxT with subsequent CLP did not markedly affect the cell numbers compared to control (data not shown). The inflammatory $Ly6C^{hi}F4/80^+CD45^+$ phenotype expanded significantly in both, TxT and TxT+CLP group in comparison to control group ($p < 0.05$), while a significant decline of tissue repairing $Ly6C^{lo}F4/80^+CD45^+$ macrophages was observed in BALF of TxT and TxT+CLP compared to control ($p < 0.05$, data not shown).

CC16 Neutralization Is Associated With an Increase of Inflammatory Markers and Lung Damage

To investigate the impact of CC16 on inflammatory changes and lung injury, CC16 was neutralized (CC16 Ab) in mice undergoing TxT and subsequent CLP. TxT+CLP induced a significant systemic increase of pro-inflammatory TNF-α and MCP-1 levels compared to control ($p < 0.05$) with a trend to a further increase in animals that underwent CC16 neutralization (**Figures 1A,B**). Whereas, protein concentrations of RAGE in both lungs (C) and BALF (D) were significantly increased after TxT+CLP vs. control, CC16 neutralization significantly increased RAGE in the lungs after TxT+CLP ($p < 0.05$, **Figures 1C,D**). With regards to lung tissue damage, total protein content, that was measured in the BALF, and was significantly increased after TxT+CLP vs. control, with a further significant increase in the TxT+CLP group after CC16 neutralization vs. reference TxT+CLP group ($p < 0.05$, **Figure 1E**).

CC16 Modulates Phenotypic Distribution of Monocytes and Macrophages

The effect of CC16 on the subset distribution of monocytes and macrophages was analyzed. The representative gating for the data analyses is shown in **Figure 2**. Total counts of activated $Ly6C^+CD11b^+Ly6G^-CD45^+$ monocytes in blood increased significantly after TxT+CLP compared to control, while CC16 neutralization did not show any significant impact on this increase compared with the TxT+CLP group ($p < 0.05$, **Figure 3A**). Similarly, although inflammatory $Ly6C^{hi}CD11b^+Ly6G^-CD45^+$ monocytes became significantly more abundant, and the patrolling $Ly6C^{lo}CD11b^+Ly6G^-CD45^+$ monocytes displayed a significant decline in TxT+CLP animals vs. control, CC16 neutralization did not affect this subset distribution ($p < 0.05$, **Figures 3B,C**). The ratio of pro-inflammatory to patrolling monocytes was significantly increased in both TxT+CLP groups vs. control ($p < 0.05$, **Figure 3D**).

TxT+CLP induced a significantly increased migration of $Ly6C^+CD11b^+Ly6G^-CD45^+$ monocytes to the lungs ($p < 0.05$, **Figure 3E**). CC16 neutralization markedly reinforced this effect, and significantly enhanced the presence of

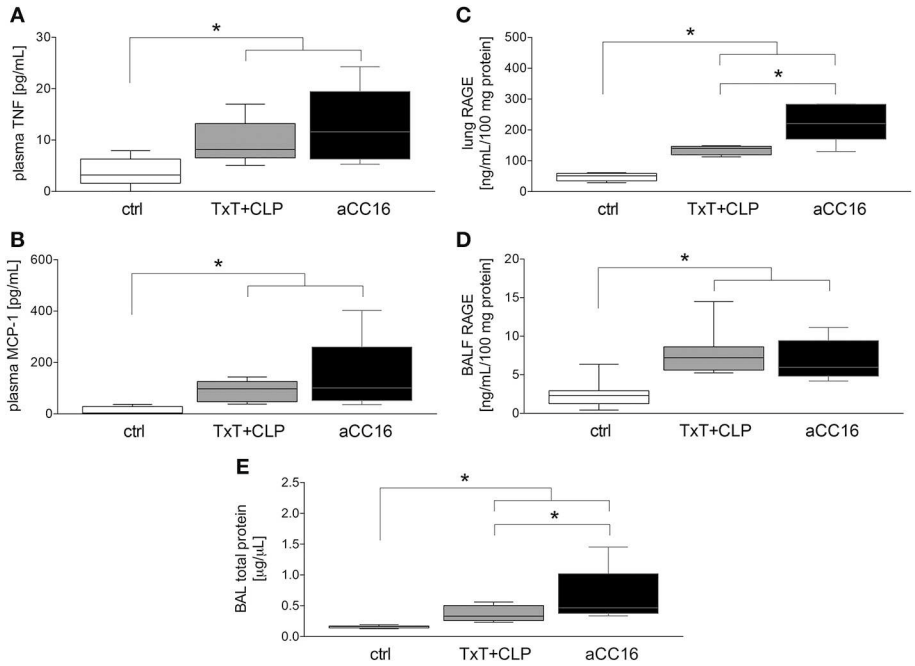

FIGURE 1 | Impact of CC16 neutralization on expression levels of pro-inflammatory mediators **(A–D)** and the total pulmonary protein amount **(E)** following thoracic trauma (TxT) with cecal ligation and puncture (CLP). Plasma levels of TNF **(A)** and MCP-1 **(B)**, and RAGE protein levels in lungs **(C)** and BALF **(D)** were measured. Total protein amount was determined in BALF. Data are represented as box-whisker plot and min to max, $*p < 0.05$ vs. control.

$Ly6C^+CD11b^+Ly6G^-CD45^+$ monocytes in the lungs after TxT+CLP compared to the TxT+CLP reference group ($p < 0.05$, **Figure 3E**). However, compared to control, the significant increase of pro-inflammatory $Ly6C^{hi}CD11b^+Ly6G^-CD45^+$ and a respective decrease of patrolling $Ly6C^{lo}CD11b^+Ly6G^-CD45^+$ monocytes were not significantly modulated by CC16 neutralization after TxT+CLP ($p < 0.05$, **Figures 3F,G**). Thus, the ratio between $Ly6C^{hi}CD11b^+Ly6G^-CD45^+$ to $Ly6C^{lo}CD11b^+Ly6G^-CD45^+$ monocytes was significantly increased in both TxT+CLP and the TxT+CLP group undergoing CC16 neutralization compared to the control (**Figure 3H**).

In BALF, a significant expansion of activated $Ly6C^+CD11b^+Ly6G^-CD45^+$ monocytes after TxT+CLP was detected ($p < 0.05$, **Figure 3I**). CC16 neutralization after TxT+CLP did not change this increase compared to control ($p < 0.05$, **Figure 3I**). The pro-inflammatory $Ly6C^{hi}CD11b^+Ly6G^-CD45^+$ phenotype was significantly more abundant in TxT+CLP vs. control ($p < 0.05$, **Figure 3J**), while CC16 neutralization further enhanced the migration of inflammatory monocytes into the BALF showing a significant increase compared with the TxT+CLP group ($p < 0.05$, **Figure 3J**). The counts of patrolling $Ly6C^{lo}CD11b^+Ly6G^-CD45^+$ monocytes significantly declined in TxT+CLP vs. control, while CC16 neutralization did not significantly further impact this monocyte subset decrease after TxT+CLP ($p < 0.05$, **Figure 3K**). TxT+CLP induced a significant increase on the ratio of pro-inflammatory to patrolling monocytes compared to control ($p < 0.05$, **Figure 3L**), while a further significant increase after CC16 neutralization vs. TxT+CLP reference group was detected ($p < 0.05$, **Figure 3L**).

Systemic $Ly6C^+F4/80^+CD45^+$ cells were not markedly changed after TxT+CLP or intervention with aCC16 (**Figure 4A**). Neither the pro-inflammatory $Ly6C^{hi}F4/80^+CD45^+$ phenotype (**Figure 4B**) nor the patrolling $Ly6C^{lo}F4/80^+CD45^+$ phenotype (**Figure 4C**) were changed.

With regards to local influence of CC16 after TxT+CLP, in lungs, $Ly6C^+F4/80^+CD45^+$ macrophage levels remained stable in TxT+CLP compared to control (**Figure 4D**). However, the inflammatory macrophage subset expanded significantly after TxT+CLP vs. control ($p < 0.05$, **Figure 4E**), whereas the anti-inflammatory phenotype decreased significantly after TxT+CLP ($p < 0.05$, **Figure 4F**). CC16 neutralization did not have a significant impact on macrophage subset redistribution after TxT+CLP in lungs (**Figures 4D–F**).

Total macrophage counts in BALF did not change after TxT+CLP, neither did CC16 neutralization change their levels (**Figure 4G**). However, pro-inflammatory $Ly6C^{hi}F4/80^+CD45^+$ macrophages elevated significantly, while patrolling $Ly6C^{lo}F4/80^+CD45^+$ macrophages declined significantly in TxT+CLP or TxT+CLP with CC16 neutralization compared to control ($p < 0.05$, **Figures 4H,I**). CC16 neutralization significantly increased the percentage of pro-inflammatory macrophages and reduced significantly the percentage of patrolling macrophages after TxT+CLP compared to the TxT+CLP reference group ($p < 0.05$, **Figures 4H,I**).

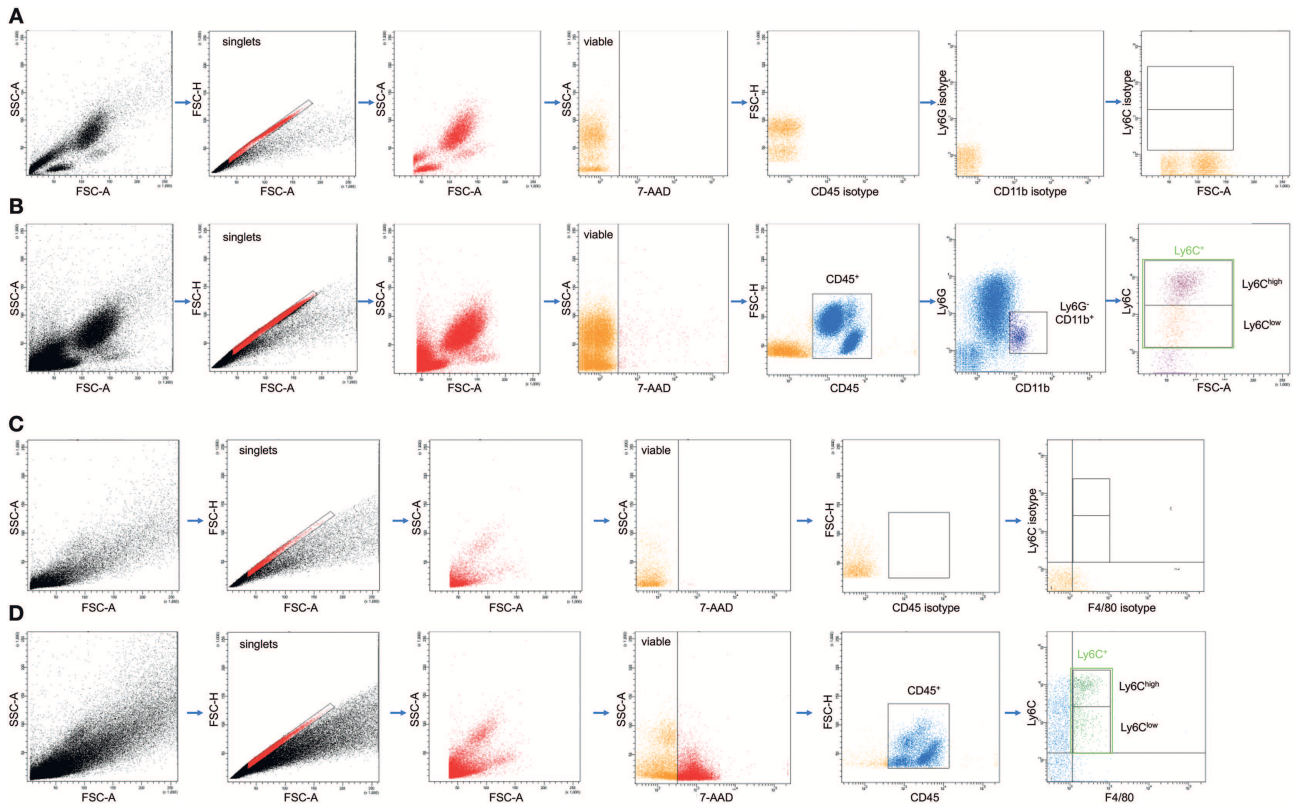

FIGURE 2 | Representative gating strategy for the flow cytometric analyses and evaluation of different monocyte subsets in whole blood **(A,B)** and macrophage subsets in lungs **(C,D)** as dot plot analyses is shown. **(A,C)** are showing the gating upon staining with isotype control antibodies, while **(B,D)** show results from the staining with specific antibodies as described in the material and method section.

CC16 Inhibits Migratory Capacity and TGF-β1 Expression in CD14$^+$ Monocytes *ex vivo*

To examine the impact of CC16 on monocytes under septic conditions, systemic monocytes were isolated from healthy volunteers and subsequently stimulated with sera from HV or TP (with as well as without septic complications), since the last are known to contain higher levels of CC16 compared to control or trauma patients without complications (42). We have determined CC16 concentrations in samples of trauma patients and healthy volunteers. We found that CC16 was significantly increased in sera obtained from traumatized patients compared to those obtained from healthy volunteers (28.09 ± 4.60 vs. 15.18 ± 1.25 ng/mL, $p < 0.05$; data not shown). Regarding the migratory rate, stimulation of CD14$^+$ monocytes with sera from HV did not show any changes compared to control and the neutralization of CC16 or application of isotype antibody in these sera did not affect the migration either (**Figure 5C**). Although the migration of CD14$^+$ monocytes treated with sera from TP remained unchanged vs. control and HV, CC16 neutralization resulted in significantly higher migration rates toward MCP-1 compared to control, stimulation with sera alone or with IgG ($p < 0.05$, **Figure 5C**). Intracellular TGF-β1 expression showed no significant changes following treatment with sera from HV vs. control (**Figure 5D**). Stimulation of monocytes with sera from TP significantly declined TGF-β1 expression, and administration of CC16 neutralizing antibodies recovered TGF-β1 level to the baseline ($p < 0.05$, **Figure 5D**). Furthermore, TNF-α and IL-6 levels in the supernatants obtained from human monocytes that were treated with sera were determined. Stimulation of CD14$^+$ monocytes with sera obtained from HV and TP did not induce any significant impact on TNF-α nor IL-6 levels (data not shown). TNF-α concentration of the control was 30.06 ± 4.60 pg/mL. Following treatment with sera from HV, TNF-α level was comparable at 32.42 ± 6.90 pg/mL, whereas CC16 neutralization in those sera did not lead to a significant decrease (24.70 ± 5.306 pg/mL). Supernatants from cells that were stimulated with TP sera have shown comparable concentrations of TNF-α to those obtained after incubation with TP sera upon CC16 neutralization (22.01 ± 3.20 vs. 30.18 ± 3.66 pg/mL). Control IL-6 concentration was 46.96 ± 12.31 pg/mL. Treatment with sera from HV did not change the IL-6 level, which was 50.13 ± 19.57 pg/mL and which also stayed stable after CC16 neutralization (40.48 ± 13.14 pg/mL). Comparable results were found in supernatants from TP samples (40.97 ± 6.436 pg/mL) and the corresponding CC16 neutralized sample also (45.84 ± 6.66 pg/mL). Further, we examined the cytotoxic potential of CC16 analyzing the release of LDH. Here, the stimulation

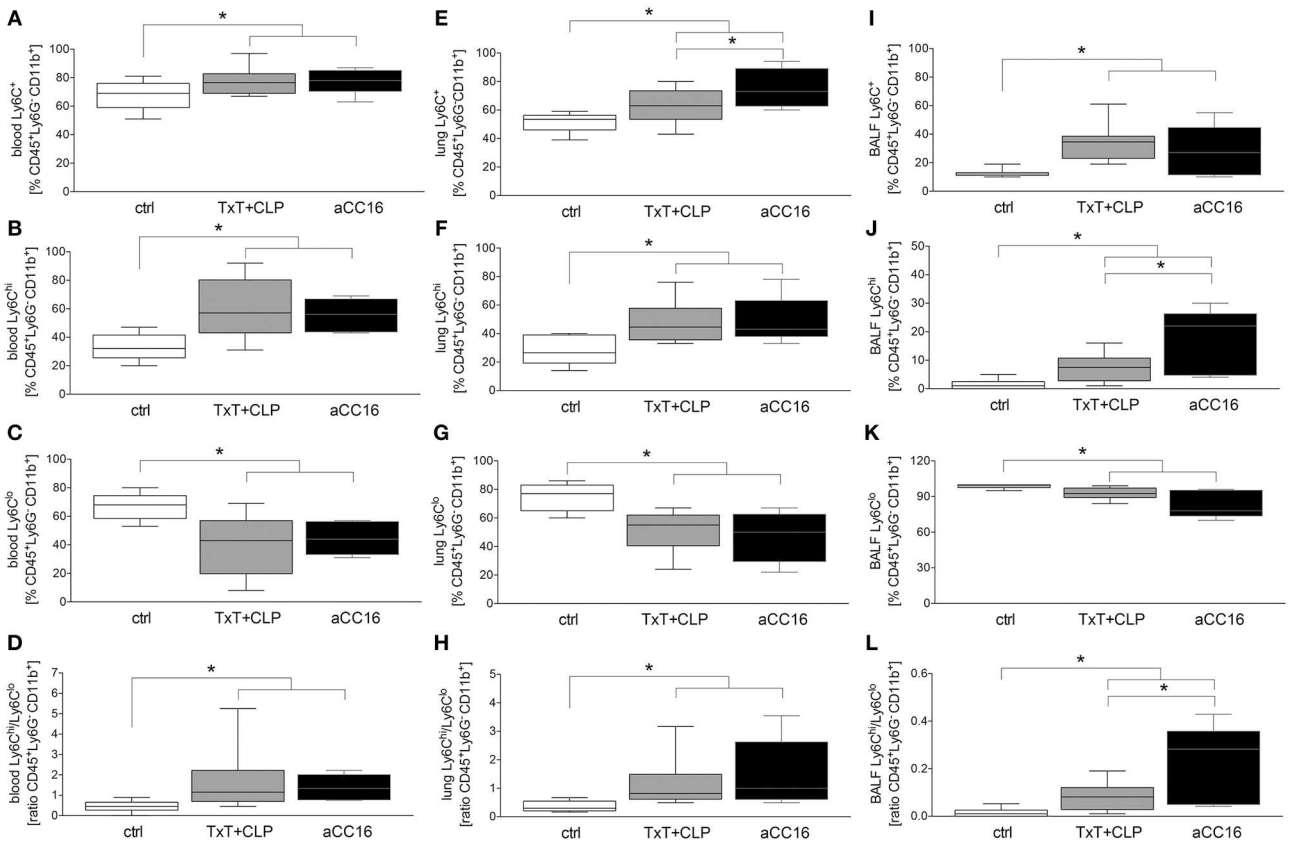

FIGURE 3 | Impact of CC16 neutralization on distribution of monocyte subsets following thoracic trauma (TxT) with cecal ligation and puncture (CLP). Activated monocyte count (Ly6C^{+}) as well the pro-inflammatory (Ly6C^{hi}) and patrolling (Ly6C^{lo}) subsets and the ratio between them were assessed in blood **(A–D)**, lungs **(E–H)** and BALF **(I–L)** by flow cytometry. Data are represented as box-whisker plot and min to max, *$p < 0.05$ vs. control.

with neither sera from HV nor TP changed the LDH release compared to untreated control (**Figure 5E**). Finally, treatment with both sera and sera with neutralized CC16 or IgG did not show significant changes in the viability of CD14^{+} monocytes (**Figure 5F**).

DISCUSSION

Since blunt chest injury with ongoing excessive pro-inflammatory immune response entails high risk for the development of secondary complications with limited therapeutic options, the unveiling of underlying mechanisms is necessary (43, 44). Here, we discuss the dynamic changes in monocyte and macrophage subsets and uncover the potentially protective role of the anti-inflammatory endogenous CC16 in the very early phase of sepsis development following thoracic injury. We confirmed the anti-inflammatory potential of CC16 in the early phase of sepsis-induced ALI following blunt chest injury. Its local neutralization after thoracic trauma increased the immigration of pro-inflammatory cell phenotypes to the lungs, and was accompanied by increased total protein levels in BALF, indicating the loss of epithelial lung integrity, and thus lung damage. Concurrently, systemic elevation of humoral pro-inflammatory mediators was observed. This is in line with our recent study, where early increased lung infiltration with neutrophils and lung injury in this model was shown (45). However, in that study, 24 h post-CLP, the lung injury was ameliorated and the lungs have exhibited no further increase in neutrophilic infiltration after CC16 neutralization (45). Thus, CC16 may first reduce a necessary early pro-inflammatory immune response for tissue repair, and at a later time point, may contribute to the amelioration of the lung injury. Although the mechanism is still not clear, the observed lung injury could be caused by the paralleled enhanced lung infiltration with neutrophils. This assumption is supported by Lerman et al. where neutrophil extravasation and tissue infiltration in murine CLP-induced sepsis were inhibited by blocking or deletion of α3β1 and paralleled by significantly reduced mortality (46).

Following infectious or non-infectious stimuli, alveolar macrophages are, among other cells, the first to be involved in the early immune response, initiating the inflammatory cascade and secretion of pro-inflammatory mediators (20–23). We have shown that thoracic injury followed by CLP increased systemic levels of TNF-α; which is an important indicator of sepsis development (47). Neutralization of endogenous CC16 forced further increase of TNF-α, indicating anti-inflammatory capacity

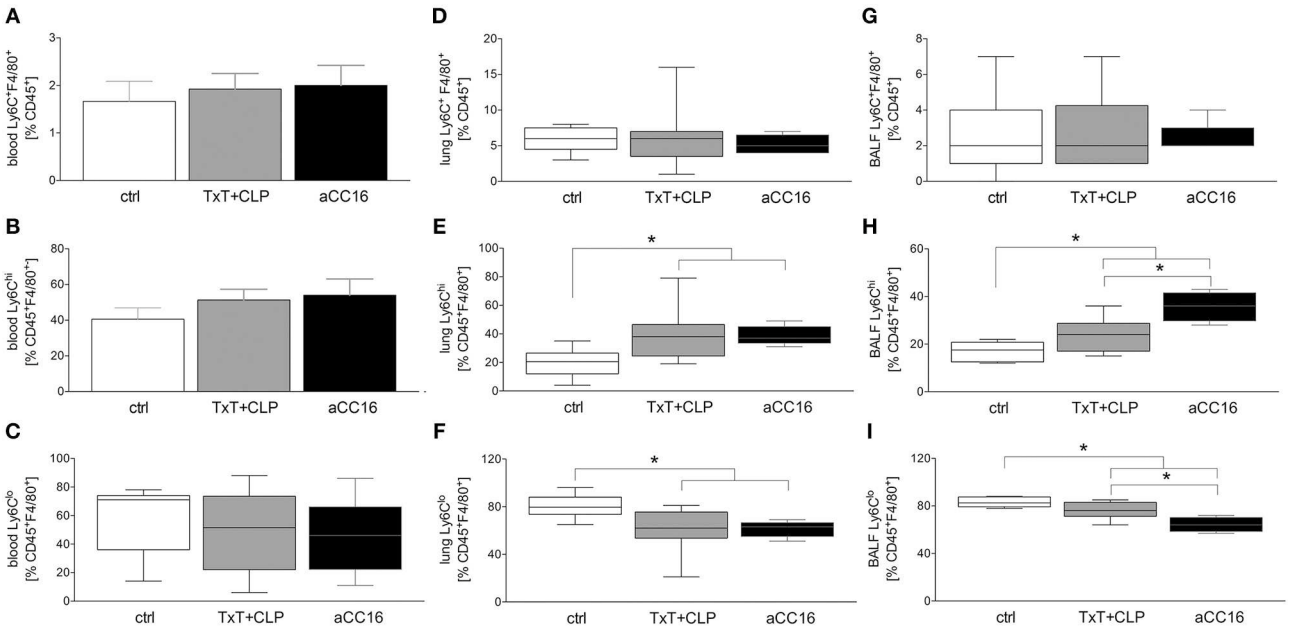

FIGURE 4 | Impact of CC16 neutralization on distribution of macrophage subsets following thoracic trauma (TxT) with cecal ligation and puncture (CLP). Amount of macrophages ($Ly6C^{+}F4/80^{+}$) as well as of the pro-inflammatory ($Ly6C^{hi}$) and patrolling ($Ly6C^{lo}$) subsets was assessed in blood **(A–C)**, lungs **(D–F)** and BALF **(G–I)** by flow cytometry. Data are represented as box-whisker plot and min to max, $^{*}p < 0.05$ vs. control.

of CC16 in the present model, and confirming in general its anti-inflammatory character. In turn, elevated TNF-α level is also one of the factors inducing MCP-1 expression by a variety of cell types (48). Consistent with literature, we have shown that TNF-α increase after thoracic trauma and CLP was paralleled by a systemic MCP-1 increase. CC16 neutralization led similarly to TNF-α to a further systemic increase of MCP-1. Whether this further MPC-1 increase is caused directly by CC16 or indirectly by an increase of TNF-α or other factors still remains to be elucidated in future studies.

Further, we have shown that expression of RAGE significantly increased in lungs and BALF of septic mice, whereas CC16 neutralization led to further significant increase in the lungs. In a clinical study, both CC16 and RAGE were identified as plausible biomarkers for ARDS in patients with severe sepsis (49), but whether RAGE positively or negatively regulates the immune response seems to differ according to the inflammatory mechanism (50, 51). Moreover, we have shown that blunt chest injury itself increased the protein levels in BALF and subsequent CLP did not cause a further increase after 6 h. This does not mean that sepsis did not have an impact on lung epithelial integrity, but lungs are at this time point affected by thorax trauma directly and abdominal-induced sepsis may take longer to affect the lung epithelial integrity than could be seen in the observation period. Upon CC16 neutralization, total protein level in BALF further increased, suggesting a positive impact of CC16 in lung epithelial injury.

Following sepsis-induced ALI after blunt chest trauma, a significant increase of monocyte counts was observed in blood and lungs, as well as in the BALF. The characterization of monocytes has uncovered significantly more pro-inflammatory monocytes compared to a marked decline of the patrolling phenotype. Since MCP-1 is the pivotal regulator of monocyte recruitment to the site of injury (12), the observed elevated MCP-1 levels in septic mice may be the key factor for the excessive infiltration of lungs with pro-inflammatory monocytes, whereby the disrupted lung epithelial integrity may contribute to the higher monocyte content in BALF as well. Upon CC16 neutralization, increased monocyte emigration to the lungs was observed, indicating the anti-migratory potential of CC16. To substantiate our assumption, we isolated monocytes from healthy volunteers and stimulated them with sera obtained from healthy volunteers or from trauma patients, since we have shown in previous studies that increased systemic concentrations of CC16 correlate with the development of secondary respiratory complications following traumatic injury in patients and is lowered in healthy individuals (31, 42, 52). CC16 neutralization in patient's sera before monocyte stimulation led to a significant increase of monocyte chemotaxis toward MCP-1 but the mechanism still remains to be elucidated. However, although CC16 was neutralized, monocytes from TP+aCC16 display elevated migration compared to controls. Serum from trauma patients contains other mediators beside CC16, which may change the migratory behavior of monocytes, thus further mediators such as IL-6 or RANTES that potentially increase the migratory capacity of monocytes are probably concurrently present in the blood from trauma patients (53–56). In a further *ex vivo* experiment, we have shown unaffected viability of isolated monocytes and their release of lactate dehydrogenase following treatment with sera, suggesting no cytotoxic effects of CC16.

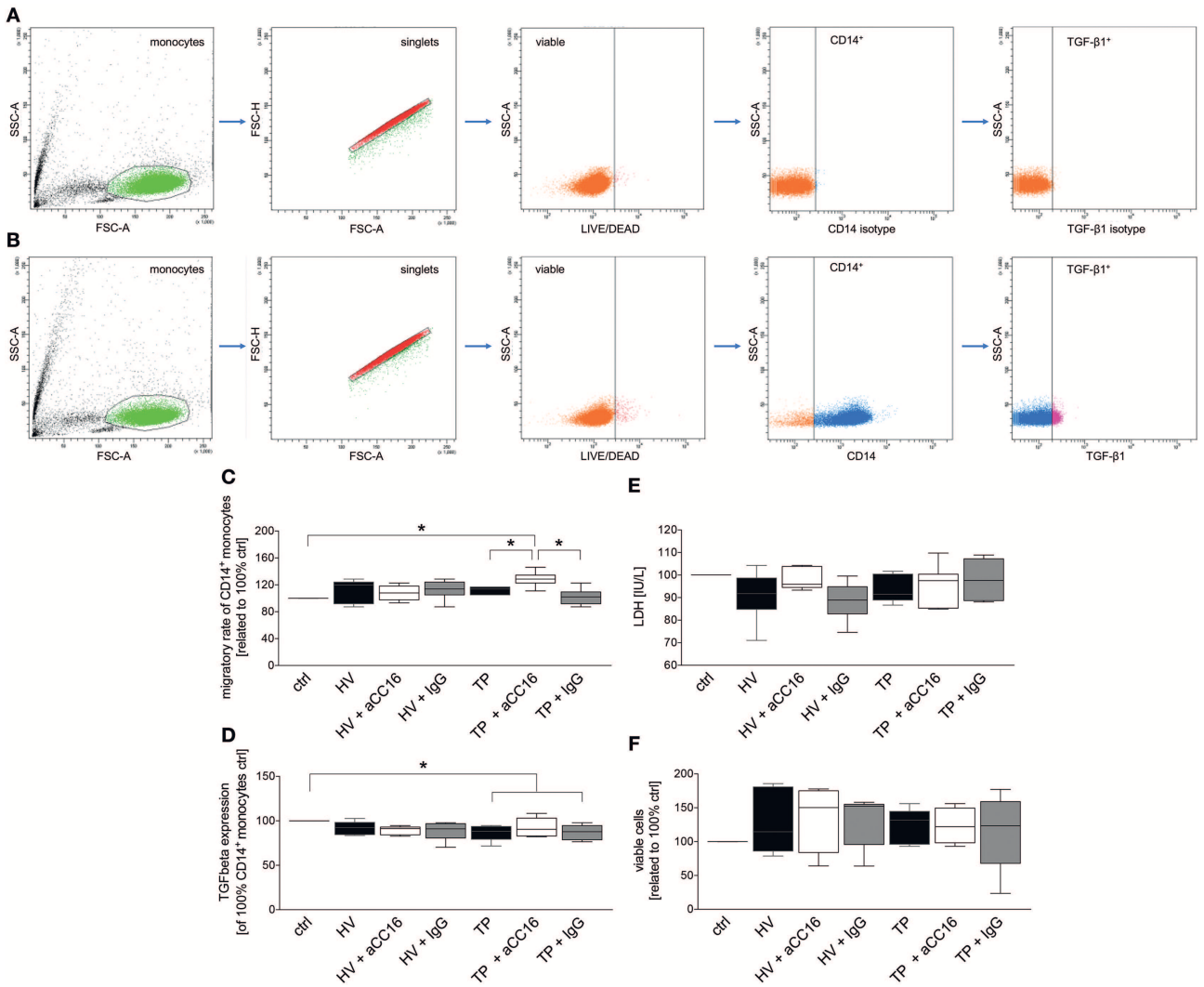

FIGURE 5 | Representative gating strategy for the flow cytometric analysis and evaluation of isolated CD14$^+$ monocytes with regard to their TGF-β1 expression as dot plot analysis is shown. **(A)** is showing representative isotype staining controls, while **(B)** shows representative gating after staining with specific antibodies. **(C–F)** show effects of serum samples obtained from healthy volunteers (HV) or trauma patients (TP) and CC16 on CD14$^+$ monocytes behavior. CD14$^+$ monocytes isolated from HV were incubated with sera obtained from HV or TP. Cell culture medium was applied alone (control) or with/without prior intervention/neutralization with either CC16 antibody (aCC16) or IgG control antibody (IgG) in sera from HV or TP. Migratory capacity toward MCP-1 **(C)**, TGF-β1 expression **(D)**, and the impact of sera on monocyte cytotoxicity **(E)** and viability **(F)** were evaluated. Data are represented as box-whisker plot and min to max, $^*p < 0.05$ vs. indicated.

Interestingly, stimulation of isolated human monocytes with sera obtained from trauma patients led to a significant decrease of TGF-β1 expression, whereas neutralization of CC16 recovered the levels to the baseline. Although this was unexpected, it was already reported in rodent models of lung fibrosis that CC16 contributes to diminished TGF-β1 levels, however, the mechanism still remains elusive (37, 57). Here, some studies indicate that CC16 suppresses TGF-β1 expression via MPP-9 inhibition (34, 58).

Regarding macrophage distribution, we observed elevated levels of pro-inflammatory macrophages paralleled by decline of anti-inflammatory phenotype in lungs and BALF. CC16 neutralization reinforced the observed changes, whereas lung infiltration remained unaffected. Since resident alveolar macrophages have been described to have anti-inflammatory properties in steady state and, upon infection or injury, they display a phenotypic shift and gain pro-inflammatory features (18), we hypothesized that CC16 neutralization may contribute to macrophage polarization toward the pro-inflammatory phenotype. Whether CC16 in fact suppresses an exaggerated transition to pro-inflammatory macrophages remains to be further elucidated by future studies.

LIMITATIONS

Showing an isolated CLP group with performed interventions would further increase the relevance of our results. However,

since the scope of the present study was to elaborate the role of CC16 in the underlying double-hit model, this approach was not considered. In humans, it is well-known that secondary stimuli (e.g., surgeries and infections) following chest trauma contribute to the development of secondary pulmonary complications, including ALI and ARDS (44). In mice, it was already shown that pulmonary contusion primes the systemic innate immune response to the LPS challenge, increasing inflammation and worsening lung injury compared to injury or LPS application alone (59). Moreover, recently we have shown that isolated blunt chest trauma in mice was not enough to mimic human conditions since the ongoing pro-inflammatory response decreased to baseline within 24 h, and that combining blunt chest trauma with CLP led to pulmonary changes that were characteristic for ALI (41). However, the mechanism is still unknown, and it remains to be elucidated whether either direct local tissue injury and the subsequent pro-inflammatory response, or the second hit with excessive pro-inflammatory response and remote organ damage contribute more to the ALI development (41, 60). However, literature indicates that the combination of both hits contributes to the increased pro-inflammatory response following double-hit trauma (61–64). Thus, the question of whether CC16 neutralization would affect the isolated CLP animals in the same way as in the TxT+CLP group remains unanswered. Furthermore, showing CC16 levels in all experimental groups at the timing of therapy would support our findings. Yet, due to ethical reasons with regard to animal protection, such analyses were not possible. Following the principle of 3Rs (Replacement, Reduction, Refinement) the number of animals per each group was limited to 8. Following severe thoracic injury, human trauma patients mostly require mechanical ventilation, whereas mice were spontaneously breathing in our experimental settings. Thus, the impact of mechanical ventilation following chest injury could not be considered. Moreover, although mouse models are key tools for studying different pathophysiologies, the immune response between mouse and human differs and the applied treatment cannot be directly translated into human settings. We could not show the impact of CLP on lung integrity, and we consider the short observation period as a further limitation that could lead to negative results. Similarly, monocytes and recruited and resident alveolar macrophages seem to have specific functions in a time-dependent manner. Thus, the right time frame for the examination of monocyte and macrophage function is essential and has to be examined further. In flow cytometric analysis, the chosen markers did not distinguish between recruited and resident alveolar macrophages and this has to be examined in future studies also. Furthermore, although CC16 neutralization increased pro-inflammatory monocyte and macrophages phenotypes, whether CC16 directly contributes to exaggerated transition to pro-inflammatory macrophages still remains to be elucidated. A longer observation period of up to 7 days would bring clarity to the beneficial or negative effects of CC16. Additionally, the distribution of neutrophil and monocyte/macrophage subsets should be evaluated as well. Comparing this with the extent of the lung injury would clarify whether CC16 has either a negative or positive effect on outcomes. It would be interesting to know whether in case of positive effects, CC16 would improve only the lung injury and pro-inflammatory immune response or whether the survival would be improved as well. To confirm the above-discussed potential results, recombinant CC16 therapy should be applied as well. In *in vitro* studies, we pooled sera from only ten trauma patients without secondary complications and 10 trauma patients who developed sepsis in a later course, and thus, a larger sample size may clarify the results. Although CC16 is known to have anti-inflammatory properties, we have shown recovered TGF-β1 protein expression levels in $CD14^+$ monocytes following treatment with a trauma patient's sera. It is possible that TGF-β1 expression is inhibited indirectly by another mechanism and this has to be evaluated in further studies as well.

DATA AVAILABILITY STATEMENT

All relevant datasets for this study are contained in the manuscript.

ETHICS STATEMENT

This studies involving human participants were reviewed and approved by Institutional Ethical Committee of the University Hospital Frankfurt, Goethe-University, Germany. The patients/participants provided their written informed consent to participate in this study. The animal study was reviewed and approved by Veterinary Department of the Regional Council in Darmstadt, Germany (Regierungspräsidium Darmstadt, Hessen.

AUTHOR CONTRIBUTIONS

BR: conceptualization, supervision, and project administration. AJ, PS, NB, BX, and BR: methodology. AJ: validation, data curation, and writing—original draft preparation. BR and AJ: formal analysis. AJ, PS, NB, and BX: investigation. BR, SW, FH, and IM: resources. AJ, JV, SE, and BR: writing—review and editing. AJ and BR: visualization. BR, FH, and SW: funding acquisition.

FUNDING

This work was supported by grants from the DFG WU 820/2-1, HI 820/5-1, and RE 3304/8-1.

ACKNOWLEDGMENTS

We thank Katrin Jurida and Kerstin Kontradowitz for outstanding technical assistance.

REFERENCES

1. Sakran JV, Greer SE, Werlin E, McCunn M. Care of the injured worldwide: trauma still the neglected disease of modern society. *Scand J Trauma Resusc Emerg Med*. (2012) 20:64. doi: 10.1186/1757-7241-20-64
2. Chrysou K, Halat G, Hoksch B, Schmid RA, Kocher GJ. Lessons from a large trauma center: impact of blunt chest trauma in polytrauma patients-still a relevant problem? *Scand J Trauma Resusc Emerg Med*. (2017) 25:42. doi: 10.1186/s13049-017-0384-y
3. Leenen LP. Focus on chest trauma. *Eur J Trauma Emerg Surg*. (2017) 43:153–4. doi: 10.1007/s00068-017-0780-z
4. Tignanelli CJ, Hemmila MR, Rogers MAM, Raghavendran K. Nationwide cohort study of independent risk factors for acute respiratory distress syndrome after trauma. *Trauma Surg Acute Care Open*. (2019) 4:e000249. doi: 10.1136/tsaco-2018-000249
5. Brun-Buisson C, Minelli C, Bertolini G, Brazzi L, Pimentel J, Lewandowski K, et al. Epidemiology and outcome of acute lung injury in European intensive care units. Results from the ALIVE study. *Intensive Care Med*. (2004) 30:51–61. doi: 10.1007/s00134-003-2022-6
6. Prin M, Li G. Complications and in-hospital mortality in trauma patients treated in intensive care units in the United States, 2013. *Inj Epidemiol*. (2016) 3:18. doi: 10.1186/s40621-016-0084-5
7. Pfeifer R, Tarkin IS, Rocos B, Pape HC. Patterns of mortality and causes of death in polytrauma patients–has anything changed? *Injury*. (2009) 40:907–11. doi: 10.1016/j.injury.2009.05.006
8. Osborn TM, Tracy JK, Dunne JR, Pasquale M, Napolitano LM. Epidemiology of sepsis in patients with traumatic injury. *Crit Care Med*. (2004) 32:2234–40. doi: 10.1097/01.CCM.0000145586.23276.0F
9. Rani M, Nicholson SE, Zhang Q, Schwacha MG. Damage-associated molecular patterns (DAMPs) released after burn are associated with inflammation and monocyte activation. *Burns*. (2017) 43:297–303. doi: 10.1016/j.burns.2016.10.001
10. Ziraldo C, Vodovotz Y, Namas RA, Almahmoud K, Tapias V, Mi Q, et al. Central role for MCP-1/CCL2 in injury-induced inflammation revealed by in vitro, in silico, and clinical studies. *PLoS ONE*. (2013) 8:e79804. doi: 10.1371/journal.pone.0079804
11. Tesch GH, Schwarting A, Kinoshita K, Lan HY, Rollins BJ, Kelley VR. Monocyte chemoattractant protein-1 promotes macrophage-mediated tubular injury, but not glomerular injury, in nephrotoxic serum nephritis. *J Clin Invest*. (1999) 103:73–80. doi: 10.1172/JCI4876
12. Lu B, Rutledge BJ, Gu L, Fiorillo J, Lukacs NW, Kunkel SL, et al. Abnormalities in monocyte recruitment and cytokine expression in monocyte chemoattractant protein 1-deficient mice. *J Exp Med*. (1998) 187:601–8. doi: 10.1084/jem.187.4.601
13. De AK, Laudanski K, Miller-Graziano CL. Failure of monocytes of trauma patients to convert to immature dendritic cells is related to preferential macrophage-colony-stimulating factor-driven macrophage differentiation. *J Immunol*. (2003) 170:6355–62. doi: 10.4049/jimmunol.170.12.6355
14. Winkler MS, Rissiek A, Priefler M, Schwedhelm E, Robbe L, Bauer A, et al. Human leucocyte antigen (HLA-DR) gene expression is reduced in sepsis and correlates with impaired TNFalpha response: a diagnostic tool for immunosuppression? *PLoS ONE*. (2017) 12:e0182427. doi: 10.1371/journal.pone.0182427
15. Cheron A, Floccard B, Allaouchiche B, Guignant C, Poitevin F, Malcus C, et al. Lack of recovery in monocyte human leukocyte antigen-DR expression is independently associated with the development of sepsis after major trauma. *Crit Care*. (2010) 14:R208. doi: 10.1186/cc9331
16. Relja B, Horstmann JP, Kontradowitz K, Jurida K, Schaible A, Neunaber C, et al. Nlrp1 inflammasome is downregulated in trauma patients. *J Mol Med*. (2015) 93:1391–400. doi: 10.1007/s00109-015-1320-0
17. Santos SS, Carmo AM, Brunialti MK, Machado FR, Azevedo LC, Assuncao M, et al. Modulation of monocytes in septic patients: preserved phagocytic activity, increased ROS and NO generation, and decreased production of inflammatory cytokines. *Intensive Care Med Exp*. (2016) 4:5. doi: 10.1186/s40635-016-0078-1
18. Kratofil RM, Kubes P, Deniset JF. Monocyte conversion during inflammation and injury. *Arterioscler Thromb Vasc Biol*. (2017) 37:35–42. doi: 10.1161/ATVBAHA.116.308198
19. Yona S, Kim KW, Wolf Y, Mildner A, Varol D, Breker M, et al. Fate mapping reveals origins and dynamics of monocytes and tissue macrophages under homeostasis. *Immunity*. (2013) 38:79–91. doi: 10.1016/j.immuni.2012.12.001
20. Naidu BV, Krishnadasan B, Farivar AS, Woolley SM, Thomas R, Van Rooijen N, et al. Early activation of the alveolar macrophage is critical to the development of lung ischemia-reperfusion injury. *J Thorac Cardiovasc Surg*. (2003) 126:200–7. doi: 10.1016/S0022-5223(03)00390-8
21. Niesler U, Palmer A, Froba JS, Braumuller ST, Zhou S, Gebhard F, et al. Role of alveolar macrophages in the regulation of local and systemic inflammation after lung contusion. *J Trauma Acute Care Surg*. (2014) 76:386–93. doi: 10.1097/TA.0b013e3182aaa499
22. Pribul PK, Harker J, Wang B, Wang H, Tregoning JS, Schwarze J, et al. Alveolar macrophages are a major determinant of early responses to viral lung infection but do not influence subsequent disease development. *J Virol*. (2008) 82:4441–8. doi: 10.1128/JVI.02541-07
23. Herold S, Mayer K, Lohmeyer J. Acute lung injury: how macrophages orchestrate resolution of inflammation and tissue repair. *Front Immunol*. (2011) 2:65. doi: 10.3389/fimmu.2011.00065
24. Herold S, Tabar TS, Janssen H, Hoegner K, Cabanski M, Lewe-Schlosser P, et al. Exudate macrophages attenuate lung injury by the release of IL-1 receptor antagonist in gram-negative pneumonia. *Am J Respir Crit Care Med*. (2011) 183:1380–90. doi: 10.1164/rccm.201009-1431OC
25. Jiang Z, Zhou Q, Gu C, Li D, Zhu L. Depletion of circulating monocytes suppresses IL-17 and HMGB1 expression in mice with LPS-induced acute lung injury. *Am J Physiol Lung Cell Mol Physiol*. (2017) 312:L231–42. doi: 10.1152/ajplung.00389.2016
26. Dhaliwal K, Scholefield E, Ferenbach D, Gibbons M, Duffin R, Dorward DA, et al. Monocytes control second-phase neutrophil emigration in established lipopolysaccharide-induced murine lung injury. *Am J Respir Crit Care Med*. (2012) 186:514–24. doi: 10.1164/rccm.201112-2132OC
27. Yang X, Yin Y, Yan X, Yu Z, Liu Y, Cao J. Flagellin attenuates experimental sepsis in a macrophage-dependent manner. *Crit Care*. (2019) 23:106. doi: 10.1186/s13054-019-2408-7
28. Shen Y, Song J, Wang Y, Chen Z, Zhang L, Yu J, et al. M2 macrophages promote pulmonary endothelial cells regeneration in sepsis-induced acute lung injury. *Ann Trans Med*. (2019) 7:142. doi: 10.21037/atm.2019.02.47
29. Hermans C, Bernard A. Lung epithelium-specific proteins: characteristics and potential applications as markers. *Am J Respir Crit Care Med*. (1999) 159:646–78. doi: 10.1164/ajrccm.159.2.9806064
30. Broeckaert F, Clippe A, Knoops B, Hermans C, Bernard A. Clara cell secretory protein (CC16): features as a peripheral lung biomarker. *Ann N Y Acad Sci*. (2000) 923:68–77. doi: 10.1111/j.1749-6632.2000.tb05520.x
31. Wutzler S, Backhaus L, Henrich D, Geiger E, Barker J, Marzi I, et al. Clara cell protein 16: a biomarker for detecting secondary respiratory complications in patients with multiple injuries. *J Trauma Acute Care Surg*. (2012) 73:838–42. doi: 10.1097/TA.0b013e31825ac394
32. Dierynck I, Bernard A, Roels H, De Ley M. The human Clara cell protein: biochemical and biological characterisation of a natural immunosuppressor. *Mult Scler*. (1996) 1:385–7. doi: 10.1177/135245859600100621
33. Pang M, Liu HY, Li T, Wang D, Hu XY, Zhang XR, et al. Recombinant club cell protein 16 (CC16) ameliorates cigarette smokeinduced lung inflammation in a murine disease model of COPD. *Mol Med Rep*. (2018) 18:2198–206. doi: 10.3892/mmr.2018.9216
34. Pang M, Wang H, Bai JZ, Cao D, Jiang Y, Zhang C, et al. Recombinant rat CC16 protein inhibits LPS-induced MMP-9 expression via NF-kappaB pathway in rat tracheal epithelial cells. *Exp Biol Med*. (2015) 240:1266–78. doi: 10.1177/1535370215570202
35. Pang M, Yuan Y, Wang D, Li T, Wang D, Shi X, et al. Recombinant CC16 protein inhibits the production of pro-inflammatory cytokines via NF-kappaB and p38 MAPK pathways in LPS-activated RAW264.7 macrophages. *Acta Biochim Biophys Sin*. (2017) 49:435–43. doi: 10.1093/abbs/gmx020
36. Dierynck I, Bernard A, Roels H, De Ley M. Potent inhibition of both human interferon-gamma production and biologic activity by the Clara cell protein CC16. *Am J Respir Cell Mol Biol*. (1995) 12:205–10. doi: 10.1165/ajrcmb.12.2.7865218
37. Laucho-Contreras ME, Polverino F, Gupta K, Taylor KL, Kelly E, Pinto-Plata V, et al. Protective role for club cell secretory protein-16

(CC16) in the development of COPD. *Eur Respir J*. (2015) 45:1544–56. doi: 10.1183/09031936.00134214
38. von Elm E, Altman DG, Egger M, Pocock SJ, Gotzsche PC, Vandenbroucke JP, et al. The Strengthening the Reporting of Observational Studies in Epidemiology (STROBE) statement: guidelines for reporting observational studies. *J Clin Epidemiol*. (2008) 61:344–9. doi: 10.1016/j.jclinepi.2007.11.008
39. JAMA. Rating the severity of tissue damage. I. The abbreviated scale. *JAMA*. (1971) 215:277–80. doi: 10.1001/jama.215.2.277
40. Kilkenny C, Browne WJ, Cuthill IC, Emerson M, Altman DG. Improving bioscience research reporting: the ARRIVE guidelines for reporting animal research. *PLoS Biol*. (2010) 8:e1000412. doi: 10.1371/journal.pbio.1000412
41. Stormann P, Becker N, Kunnemeyer L, Wutzler S, Vollrath JT, Lustenberger T, et al. Contributing factors in the development of acute lung injury in a murine double hit model. *Eur J Trauma Emerg Surg*. (2019) 8:896. doi: 10.1007/s00068-019-01121-5
42. Lin J, Zhang W, Wang L, Tian F. Diagnostic and prognostic values of Club cell protein 16 (CC16) in critical care patients with acute respiratory distress syndrome. *J Clin Lab Anal*. (2018) 32:e22262. doi: 10.1002/jcla.22262
43. Dennis BM, Bellister SA, Guillamondegui OD. Thoracic trauma. *Surg Clin North Am*. (2017) 97:1047–64. doi: 10.1016/j.suc.2017.06.009
44. Wutzler S, Wafaisade A, Maegele M, Laurer H, Geiger EV, Walcher F, et al. Lung Organ Failure Score (LOFS): probability of severe pulmonary organ failure after multiple injuries including chest trauma. *Injury*. (2012) 43:1507–12. doi: 10.1016/j.injury.2010.12.029
45. Stormann P, Becker N, Vollrath JT, Kohler K, Janicova A, Wutzler S, et al. Early local inhibition of club cell protein 16 following chest trauma reduces late sepsis-induced acute lung injury. *J Clin Med*. (2019) 8:E896. doi: 10.3390/jcm8060896
46. Lerman YV, Lim K, Hyun YM, Falkner KL, Yang H, Pietropaoli AP, et al. Sepsis lethality via exacerbated tissue infiltration and TLR-induced cytokine production by neutrophils is integrin alpha3beta1-dependent. *Blood*. (2014) 124:3515–23. doi: 10.1182/blood-2014-01-552943
47. Tracey KJ, Beutler B, Lowry SF, Merryweather J, Wolpe S, Milsark IW, et al. Shock and tissue injury induced by recombinant human cachectin. *Science*. (1986) 234:470–4. doi: 10.1126/science.3764421
48. Murao K, Ohyama T, Imachi H, Ishida T, Cao WM, Namihira H, et al. TNF-alpha stimulation of MCP-1 expression is mediated by the Akt/PKB signal transduction pathway in vascular endothelial cells. *Biochem Biophys Res Commun*. (2000) 276:791–6. doi: 10.1006/bbrc.2000.3497
49. Ware LB, Koyama T, Zhao Z, Janz DR, Wickersham N, Bernard GR, et al. Biomarkers of lung epithelial injury and inflammation distinguish severe sepsis patients with acute respiratory distress syndrome. *Crit Care*. (2013) 17:R253. doi: 10.1186/cc13080
50. Noto MJ, Becker KW, Boyd KL, Schmidt AM, Skaar EP. RAGE-mediated suppression of interleukin-10 results in enhanced mortality in a murine model of *Acinetobacter baumannii* sepsis. *Infect Immun*. (2017) 85:e00954–16. doi: 10.1128/IAI.00954-16
51. Ramsgaard L, Englert JM, Manni ML, Milutinovic PS, Gefter J, Tobolewski J, et al. Lack of the receptor for advanced glycation end-products attenuates E. coli pneumonia in mice. *PLoS ONE*. (2011) 6:e20132. doi: 10.1371/journal.pone.0020132
52. Wutzler S, Lehnert T, Laurer H, Lehnert M, Becker M, Henrich D, et al. Circulating levels of Clara cell protein 16 but not surfactant protein D identify and quantify lung damage in patients with multiple injuries. *J Trauma*. (2011) 71:E31–6. doi: 10.1097/TA.0b013e3181f6f0b4
53. Clahsen T, Schaper F. Interleukin-6 acts in the fashion of a classical chemokine on monocytic cells by inducing integrin activation, cell adhesion, actin polymerization, chemotaxis, and transmigration. *J Leukoc Biol*. (2008) 84:1521–9. doi: 10.1189/jlb.0308178
54. Okeny PK, Ongom P, Kituuka O. Serum interleukin-6 level as an early marker of injury severity in trauma patients in an urban low-income setting: a cross-sectional study. *BMC Emerg Med*. (2015) 15:22. doi: 10.1186/s12873-015-0048-z
55. Volin MV, Shah MR, Tokuhira M, Haines GK, Woods JM, Koch AE. RANTES expression and contribution to monocyte chemotaxis in arthritis. *Clin Immunol Immunopathol*. (1998) 89:44–53. doi: 10.1006/clin.1998.4590
56. Albert V, Subramanian A, Agrawal D, Bhoi SK, Pallavi P, Mukhopadhayay AK. RANTES levels in peripheral blood, CSF and contused brain tissue as a marker for outcome in traumatic brain injury (TBI) patients. *BMC Res Notes*. (2017) 10:139. doi: 10.1186/s13104-017-2459-2
57. Cai Y, Kimura S. Secretoglobin 3A2 exhibits anti-fibrotic activity in bleomycin-induced pulmonary fibrosis model mice. *PLoS ONE*. (2015) 10:e0142497. doi: 10.1371/journal.pone.0142497
58. Yu Q, Stamenkovic I. Cell surface-localized matrix metalloproteinase-9 proteolytically activates TGF-beta and promotes tumor invasion and angiogenesis. *Genes Dev*. (2000) 14:163–76. doi: 10.1101/gad.14.2.163
59. Hoth JJ, Martin RS, Yoza BK, Wells JD, Meredith JW, McCall CE. Pulmonary contusion primes systemic innate immunity responses. *J Trauma*. (2009) 67:14–21. doi: 10.1097/TA.0b013e31819ea600
60. Stormann P, Wagner N, Kohler K, Auner B, Simon TP, Pfeifer R, et al. Monotrauma is associated with enhanced remote inflammatory response and organ damage, while polytrauma intensifies both in porcine trauma model. *Eur J Trauma Emerg Surg*. (2019). doi: 10.1007/s00068-019-01098-1. [Epub ahead of print].
61. Orman MA, Ierapetritou MG, Berthiaume F, Androulakis IP. The dynamics of the early inflammatory response in double-hit burn and sepsis animal models. *Cytokine*. (2011) 56:494–502. doi: 10.1016/j.cyto.2011.07.001
62. Orman MA, Ierapetritou MG, Berthiaume F, Androulakis IP. Long-term dynamic profiling of inflammatory mediators in double-hit burn and sepsis animal models. *Cytokine*. (2012) 58:307–15. doi: 10.1016/j.cyto.2012.01.017
63. Orman MA, Nguyen TT, Ierapetritou MG, Berthiaume F, Androulakis IP. Comparison of the cytokine and chemokine dynamics of the early inflammatory response in models of burn injury and infection. *Cytokine*. (2011) 55:362–71. doi: 10.1016/j.cyto.2011.05.010
64. Rao R, Orman MA, Berthiaume F, Androulakis IP. Dynamics of hepatic gene expression and serum cytokine profiles in single and double-hit burn and sepsis animal models. *Data Brief*. (2015) 3:229–33. doi: 10.1016/j.dib.2015.02.018

Conflict of Interest: The authors declare that the research was conducted in the absence of any commercial or financial relationships that could be construed as a potential conflict of interest.

The reviewer CE declared a shared affiliation, with no collaboration, with one of the authors, FH, to the handling editor.

Copyright © 2019 Janicova, Becker, Xu, Wutzler, Vollrath, Hildebrand, Ehnert, Marzi, Störmann and Relja. This is an open-access article distributed under the terms of the Creative Commons Attribution License (CC BY). The use, distribution or reproduction in other forums is permitted, provided the original author(s) and the copyright owner(s) are credited and that the original publication in this journal is cited, in accordance with accepted academic practice. No use, distribution or reproduction is permitted which does not comply with these terms.

frontiers in Immunology

ORIGINAL RESEARCH
published: 25 October 2019
doi: 10.3389/fimmu.2019.02508

Leukocyte-Released Mediators in Response to Both Bacterial and Fungal Infections Trigger IFN Pathways, Independent of IL-1 and TNF-α, in Endothelial Cells

Kieu T. T. Le[1], Xiaojing Chu[1], Martin Jaeger[2], Josée A. Plantinga[3], Vasiliki Matzaraki[1], Sebo Withoff[1], Leo A. B. Joosten[2], Mihai G. Netea[2], Cisca Wijmenga[1,4], Yang Li[1†], Jill Moser[3,5†] and Vinod Kumar[1,2*†]*

[1] Department of Genetics, University Medical Center Groningen, University of Groningen, Groningen, Netherlands, [2] Department of Internal Medicine and Radboud Centre for Infectious Diseases (RCI), Radboud University Medical Center, Nijmegen, Netherlands, [3] Department of Pathology and Medical Biology, Medical Biology Section, University Medical Center Groningen, University of Groningen, Groningen, Netherlands, [4] Department of Immunology, K.G. Jebsen Coeliac Disease Research Centre, University of Oslo, Oslo, Norway, [5] Department of Critical Care, University Medical Center Groningen, University of Groningen, Groningen, Netherlands

OPEN ACCESS

Edited by:
Pietro Ghezzi,
Brighton and Sussex Medical School,
United Kingdom

Reviewed by:
Toshiyuki Murai,
Osaka University, Japan
Selinda Jane Orr,
Cardiff University, United Kingdom

***Correspondence:**
Jill Moser
j.moser@umcg.nl
Vinod Kumar
v.kumar@umcg.nl

†Last authorship

Specialty section:
This article was submitted to Inflammation, a section of the journal Frontiers in Immunology

Received: 04 August 2019
Accepted: 07 October 2019
Published: 25 October 2019

Citation:
Le KTT, Chu X, Jaeger M, Plantinga JA, Matzaraki V, Withoff S, Joosten LAB, Netea MG, Wijmenga C, Li Y, Moser J and Kumar V (2019) Leukocyte-Released Mediators in Response to Both Bacterial and Fungal Infections Trigger IFN Pathways, Independent of IL-1 and TNF-α, in Endothelial Cells. Front. Immunol. 10:2508. doi: 10.3389/fimmu.2019.02508

In sepsis, dysregulated immune responses to infections cause damage to the host. Previous studies have attempted to capture pathogen-induced leukocyte responses. However, the impact of mediators released after pathogen-leukocyte interaction on endothelial cells, and how endothelial cell responses vary depending on the pathogen-type is lacking. Here, we comprehensively characterized the transcriptomic responses of human leukocytes and endothelial cells to Gram negative-bacteria, Gram positive-bacteria, and fungi. We showed that whole pathogen lysates induced strong activation of leukocytes but not endothelial cells. Interestingly, the common response of leukocytes to various pathogens converges on endothelial activation. By exposing endothelial cells to leukocyte-released mediators, we observed a strong activation of endothelial cells at both transcription and protein levels. By adding IL-1RA and TNF-α antibody in leukocyte-released mediators before exposing to endothelial cells, we identified specific roles for IL-1 and TNF-α in driving the most, but not all, endothelial activation. We also showed for the first time, activation of interferon response by endothelial cells in response to leukocyte-released mediators, independently from IL-1 and TNF-α pathways. Our study therefore, not only provides pathogen-dependent transcriptional changes in leukocytes and endothelial cells during infections, but also reveals a role for IFN, together with IL1 and TNFα signaling, in mediating leukocyte-endothelial interaction in infections.

Keywords: leukocyte-endothelial interaction, sepsis, bacterial infection, fungal infection, leukocyte transcriptomes, endothelial transcriptomes, interferon pathways

INTRODUCTION

Sepsis is a life-threatening organ dysfunction caused by a dysregulated host response to infection (1). Despite advances in early recognition, sepsis affects around 30 million people worldwide every year and has a mortality rate of 20–40% (2). Sepsis is known to be a heterogeneous syndrome with various outcomes that depend on pathogenic characteristics as well as on host susceptibility. Despite decades of research, sepsis pathophysiology remains poorly understood. However, it is known that an interaction between innate immune cells and endothelial cells is central for the pathogenesis of sepsis, with recognition of infectious pathogens as a first step toward full activation of inflammation. The activated cells interact with different blood compartments and organ cell types such as platelets, adaptive immune leukocytes, and parenchymal cells (3). Failure in properly regulating these cellular responses and interactions often leads to multiple organ failure, and even mortality in sepsis patients.

Recent studies have employed transcriptomic approaches to characterize the global response of immune cells, particularly peripheral blood mononuclear cells (PBMCs) to various pathogens. After microbial recognition, innate immune cells are prone to inflammatory and stress responses while reducing apoptosis signaling, resulting in the release of cytokines, chemokines, and damage-associated molecular pattern factors into the circulation (4). Gene expression profiles of whole blood from human volunteers challenged with a low dose of endotoxin also showed a reduction in integrin-α and integrin-β chain expression, indicating changes in the host immune system in adherence to and interaction with other cell types (5). Nevertheless, we still know relatively little about the impact of these transcriptomic alterations of immune cells on its interaction with other cell types, specifically on endothelial cells.

Endothelial cells are a monolayer of cells lining the blood vessel that is actively involved in homeostasis as well as interacting with immune cells to regulate inflammation (6). The endothelium is activated not only by inflammatory cytokines such as IL-1β and TNF-α (7), but also by endotoxins such as lipopolysaccharides (LPS) via the Toll like receptor-4 (TLR4) and RIG-I pathways (8, 9). Upon activation, the endothelium secretes cytokines (IL-6 and IL-8) and expresses adhesion molecules (E-selectin, VCAM-1, and ICAM-1) to facilitate leukocyte extravasation. The increased influx of neutrophils and monocytes into the tissue during sepsis could then indirectly lead to tissue damage by secreting exaggerated amounts of inflammatory mediators and reactive molecules (10). In the context of sepsis, the endothelium can be exposed to different types of infectious pathogens such as bacteria (*Streptococcus pneumoniae*) or fungi (*Candida albicans*). However, the impact of these pathogens on endothelial activation has not been studied systematically.

Given the ability of endothelial cells to respond to pathogens and interact with immune cells, it is important to characterize endothelial responses upon exposure to the mixture of various cytokines, chemokines and proteins secreted by activated immune cells, as well as to different types of infectious pathogens. Therefore, in this study, we applied a two-step *in vitro* stimulation model to comprehensively characterize: (1) the transcriptomic responses and inflammatory proteins secreted by PBMCs in response to a variety of stimulating pathogens, including Gram-negative bacteria, Gram-positive bacteria, and fungi; and (2) the transcriptomic responses of endothelial cells exposed to humoral signals from activated PBMCs that were exposed to various pathogens. Through this work, we were able to identify the role of IL-1 and TNF-α in driving most, but not all, endothelial activation. We show that, independent of IL-1 and TNF-α, interferon (IFN) pathways in endothelial cells are strongly induced by humoral signals from activated leukocytes.

Our study provides crucial insights into the role of pathways mediating leukocyte-endothelial interactions, including IL-1, TNF-α, and IFN pathways. Further studies are required to validate the function of IFN pathways in endothelial function and IFN's role in determining sepsis progression.

MATERIALS AND METHODS

PBMC Isolation

Venous blood samples were collected from healthy volunteers. All donors provided written informed consent. Ethical permission for this study was approved by the Ethical Committee of Radboud University Nijmegen (nr 42561.091.12). Blood was collected in EDTA tubes (BD vacutainer). PBMCs were quickly isolated within 3 h of collection. Blood was diluted with 1 volume of DPBS (Gibco, ThermoFisher Scientific) before adding to Ficoll-Paque (Pharmacia Biotech). Gradient centrifugation was performed for 30 min at 400 g, using no brake. After centrifugation, the layer containing PBMCs was collected using a Pasteur pipette. PBMCs were washed twice with PBS, counted (BioRad cell counter), and adjusted to reach the final concentration of 2 million cells/ml in RPMI 1640 (Gibco, ThermoFisher Scientific), supplemented with 10% heat-inactivated Fetal Cow Serum (Gibco, ThermoFisher Scientific), gentamicin 10 mg/ml, L-glutamine 10 mM, and pyruvate 10 mM. Cells were seeded into wells to settle overnight before stimulation.

PBMC Stimulation

To study PBMC transcriptomes upon five types of heat-killed pathogens, PBMCs were stimulated with various pathogens, including heat-killed *Streptococcus pneumonia* (ATCC 49619, serotype 19F) at 1 million cells/ml, heat-killed *C. albicans* (ATCC MYA-3573, UC 820) at 1 million cells/ml, heat-killed *Aspergillus fumigatus* (V05-27) at 1 million cells/ml, *Mycobacterium tuberculosis* (H37Rv) at 1 million cells/ml, and heat-killed *Pseudomonas aeruginosa* at 1 million cells/ml (11). Cells were also incubated with RPMI 1640 only as a negative control. RNA was isolated from PBMCs at 4 and 24 h after stimulation.

Endothelial Cell Culture and Direct Stimulation

Primary Human Umbilical Vein Endothelial Cells (HUVECs) were used to study the response of endothelial cells upon infection. Pooled donor HUVECs were purchased (Lonza,

Breda, the Netherlands) and cultured in EBM-2™ medium (Lonza) supplemented with EGM-2 MV SingleQuot Kit Supplements & Growth Factors (Lonza) at 37°C, 5% CO_2 and saturating humidity. Passage 3–5, confluent cells were used for all experiments.

For direct stimulation, HUVECs were stimulated with either heat-killed *Streptococcus pneumonia (*ATCC 49619, serotype 19F) at the concentration of 1 million cells/ml, heat-killed *C. albicans (*ATCC MYA-3573, UC 820) at 1 million cells/ml, LPS (*Escherichia coli* serotype O26:B6, Sigma, St. Louis, MO, USA) at 1,000 ng/ml, IL-1β (Biosource Netherlands, Etten-Leur, The Netherlands) at 10 ng/ml, TNF-α (Biosource Netherlands) at 10 ng/ml for 6 or 24 h.

Leukocyte-Endothelial Cell Interaction

To study the effect of soluble factors released by activated PBMCs on endothelial cells, PBMCs were diluted to 2 million cells/ml and stimulated with three different types of pathogens at the ratio of 2 cells:1 pathogen heat-killed *Streptococcus pneumonia,* heat-killed *C. albicans* and LPS (10 ng/ml). RPMI medium was used as the negative control. Supernatants were collected after 24 h of stimulation, aliquoted, filtered (0.45 μm filter) and kept at −20°C before either exposing to HUVECs or measuring cytokine levels with OLINK and ELISA.

The supernatants from activated PBMCs were thawed overnight at 4°C and warmed up shortly to 37°C. Polymyxin B (InvivoGen, Toulouse, France) was added to the supernatants at a final concentration of 100 μg/ml to neutralize residual LPS (9). The supernatants were then added to HUVECs. To study the effect of IL-1 and TNF-α secreted by activated PBMCs on endothelial cells, LEAF-purified TNF-α Antibody (BioLegend, San Diego, CA, USA) and/or IL-1RA (Anakinra) were added to the supernatants at the final concentration of 4 and 300 ng/ml, respectively, incubated at 37°C for 1 h before adding to HUVECs (https://patents.google.com/patent/US7227003). HUVECs were incubated with the supernatants from stimulated PBMCs for 6 and 24 h. At the time of harvesting, conditioned medium, and cells were collected for ELISA, RNA isolation and flow cytometry.

RNA Isolation

Cells were harvested and lysed in lysis buffer from the MirVanva MagMax RNA isolation kit Applied Biosystems Nieuwerkerk aan den IJssel, The Netherlands. RNA was isolated according to the manufactures instructions. RNA concentration was measured based on Optical density (OD260) using the Nanodrop machine (NanoDrop Technologies, Rockland, ME, USA). RNA integrity was determined using the Bioanalyzer (Agilent D2000). All samples had RIN score > 9.

RNA Sequencing and Pathway Enrichment Analysis

For PBMC sequencing, 1,000 ng of total RNA (RIN score ≥ 9) were submitted for RNA library preparation using the NEXTflex TM Rapid Directional RNA-seq kit, BioScientific. NGS libraries were enriched for polyA tail RNA. Samples were sequenced using the Illumina NextSeq 500 platform, single-end read. Samples were randomly assigned into different flows and sequenced to reach 12–15 million reads per sample. Sequencing reads were then mapped to the human genome using STAR (version 2.3.0) with a reference to Ensembl GRCh37.71. Read counts per gene was quantified by Htseq-count, Python package HTseq (version 0.5.4p3) using the default union-counting mode (*The HTSeq package, http://htseq.readthedocs.io/).* For endothelial RNA sequencing. 500 ng of total RNA (RIN score ≥ 9) were sent to GenomeScan, Leiden, The Netherlands for analysis. mRNA (polyA) enriched libraries were constructed, and sequenced with the NextSeq 500 platform, single end, 75 bp with 15–20 million reads/ sample. Fragments were aligned using Hisat2. Raw counts were calculated with String Tie. Pathway analysis was performed using gene set enrichment analysis on differential expressed genes using the default setting from ConsensusPathDB-human database (http://cpdb.molgen.mpg.de).

Flow Cytometry

To determine the protein expression of adhesion molecules on the HUVEC membrane, cells were washed with PBS, detached using trypsin, washed with PBS, and re-suspended in ice-cold FACS buffer (PBS supplemented with 5% FCS). The cells were divided equally into separate FACS tubes. The cells were stained using the following antibodies: PE-conjugated anti-human E-selectin (CD62E) (Biolegend), APC-anti human VCAM-1 (CD106) (Biolegend), FITC- anti human ICAM-1 (CD54) (Biolegend), and IgG isotope controls (IgG isotope controls, Biolegend) for 30 min on ice. The cells were washed once and resuspended in FACS buffer. Samples were analyzed using a MACSQuant Analyzer 10 system (Miltenyi Biotech, San Diego, CA, USA). Multi-color compensation was calibrated using positive control cell population (LPS activated HUVECs). Data were presented as the Geometric Mean of Fluorescence Intensity (MFI).

ELISA

Cytokine levels secreted by PBMCs and/or HUVECs were determined using the ELISA Duo kits, IL-6 (R&D), IL-1β (R&D), IL-1α (R&D), TNF-α (R&D) and IL-8 (R&D), according to the manufacturer's instructions. Data were presented as pg/ml.

OLINK

To further quantify the levels of other secreted proteins upon various stimulations, supernatant samples were analyzed by proximity extension assay provided commercially by Proseek Multiplex analysis (Olink Bioscience, Uppsala, Sweden) using their inflammation panel (https://www.olink.com/products/inflammation). In brief, for each marker, a pair of nucleotide probe-conjugated antibodies was incubated with the sample. Only when binding to target antigen presented in the sample, the pair of probes are in proximity, enabling the probes to anneal and amplify during Realtime PCR. Internal control was used to minimize variation within runs. The output data is an arbitrary unit of normalized $\log_2$ expression scale (NPX- normalized protein expression). The NPX value is different for each protein due to the sensitivity of each of the probes. The range and estimated inversion from NPX value to absolute amount (ng/μl) can be found in Olink website. Data were shown as NPX value.

Statistical Methods

For RNAsequencing data, differentially expressed genes were identified by statistical analysis using the DESeq2 package from Bioconductor. A statistically significant threshold (FDR P $\leq$ 0.05 and fold change $\geq$ 2) was applied. For pathway analysis, significant threshold (FDR <= 0.05) was used to identify significant pathways. For FACS and ELISA, graphs and statistical tests were performed using GraphPad Prism software v.6 (GraphPad Prism Software Inc., San Diego, CA, USA). Differences were considered significant when $p < 0.05$. ELISA and FACS data were checked for normality distribution with Omnibus K2 test. One-way ANOVA with Turkey multiple comparison tests were performed to identify significant differences between conditions and control for direct stimulation.

RESULTS

Pathogen-Dependent Early and Late Transcriptional Responses of PBMCs

To identify pathogen-dependent transcriptional responses in leukocytes, we first studied the global transcriptional changes of human PBMCs upon various stimuli. PBMCs were isolated from eight healthy individuals and stimulated by five types of pathogens: *Pseudomonas aeruginosa* (*P. aeruginosa*), *Streptococcus pneumoniae* (*S. pneumonia*), *Mycobacterium tuberculosis* (*M. tuberculosis*), *Candida albicans* (*C. albicans*), and *Aspergilus Fumigatus* (*A. fumigatus*) for 4 and 24 h. We performed RNA sequencing followed by differential expression analysis to identify differentially expressed (DE) genes between stimulated and un-stimulated samples (RPMI control). This identified 4,189 protein-coding genes that were significantly differentially regulated in response to at least one of the stimulations (Adjusted $P \leq 0.05$, FC $\geq$ 2-fold). Among those DE protein-coding genes, we observed both common genes, which respond to all pathogens, and pathogen-specific genes at 4 h (**Figure 1A**) and 24 h of stimulation (**Figure 1B**). We observed that the Gram-negative bacteria *P. aeruginosa* altered the expression levels of more than 2,000 genes at 4 h. In contrast, we found fewer genes to be differently regulated in response to *C. albicans* (666 genes) and Gram-positive bacteria (956 genes) at 4 h (**Supplemental Figure S1A**). At 24 h, we found more genes being differentially regulated by different pathogens. This indicates that *P. aeruginosa* is one of the stronger inducers of early responses in leukocytes (**Supplemental Figure S1B**). In contrast, *C. albicans* induced three times more genes, indicating it is a strong immune stimulator at later time points.

Next we performed pathway enrichment analyses on pathogen-specific DE genes (**Supplemental Table S1**). Pathway enrichment analysis of *P. aeruginosa*-specific genes at 4 h showed significant enrichment of DE genes for several immune pathways, including cytokine responses, IFN signaling, TNF signaling, IL-1 signaling, apoptosis, and inflammasome activation. Interestingly, *S. pneumonia*-specific DE genes are enriched for the suppression of inflammatory pathways and TCR signaling at both 4 and 24 h. In contrast, *C. albicans* specific pathways are enriched for antigen presentation and initiating inflammatory responses (**Supplemental Table S1**). Overall, the distinct pathways enriched with DE genes by each pathogen highlight the induction of different inflammatory responses in PBMCs: TNF signaling, IL-1 signaling, and IFN signaling. The transcriptome response, thus reflects complex cytokine responses of PBMCs that are needed to interact with different cell types, depending on the type of infectious pathogens.

Common Responses of PBMCs to a Variety of Pathogens Converge on Endothelial Cells

Next we tested whether common genes that are differentially regulated in response to all pathogens are enriched for particular pathways. At 4 h of stimulation, there were 123 genes that responded to all five pathogens (**Figure 1C**). Of note, some of the pathways that were activated at the early time point (4 h) also remained active at 24 h. Among 123 common genes that are either induced or repressed at 4 h, 50% show consistent differences at 24 h. Interestingly, chemokine genes such as *CCL2*, *CCL3*, *CCL7*, *CXCL8* (IL-8), and IL-10 are more strongly induced at 24 h, indicating the role of chemokine signaling in communicating with different cell types at later time points (**Supplemental Figure S2**). Pathway enrichment of the 123 common genes showed the enrichment of genes involved in initiating chemokine responses as well as in arranging cell-cell interaction, and assembly of cell junctions. Interestingly, expression levels of the cadherin genes *CDH5* and *CDH6* are reduced, suggesting a repression of adherens junction interactions (**Figure 1D**). At 24 h, we found 236 DE genes shared between all pathogens (**Figure 1E**). The up-regulated genes were enriched for the interaction of immune cells with the extracellular matrix and vascular cell wall, as well as for regulation of trafficking through gap junction (**Figure 1F**). These results show that the common pathways induced in leukocytes in response to different sepsis-causing pathogens are also involved in regulating the interaction of immune cells with the cellular matrix and in interaction with endothelial cells at the vasculature. Endothelial cells are known as a non-classical innate immune cell type that recognize and respond to bacterial lipopeptides via Toll-like receptor signaling. Endothelial responses to infection produce cytokines and chemokines, alter leukocyte migration, facilitate coagulation and, ultimately, contribute to controlling infection (12). Therefore, based on the complexity of cytokine signals released by leukocytes to different types of infection and their convergent effect on endothelial cells, it is crucial to understand the impact of leukocyte humoral signals on endothelial cells and their coordination to fight against infections.

Minimal Impact of Heat-Killed Pathogens on Endothelial Inflammatory Responses

In sepsis, endothelial barrier disruption is commonly observed in septic shock where organ function fails (13). However, not much is known about whether different types of pathogens can activate vascular endothelial cells directly. We therefore investigated if HUVECs can respond to direct stimulation by LPS, heat-killed *S. pneumoniae* or heat-killed *C. albicans*. Transcriptome profiles of HUVECs after 6 h direct stimulation

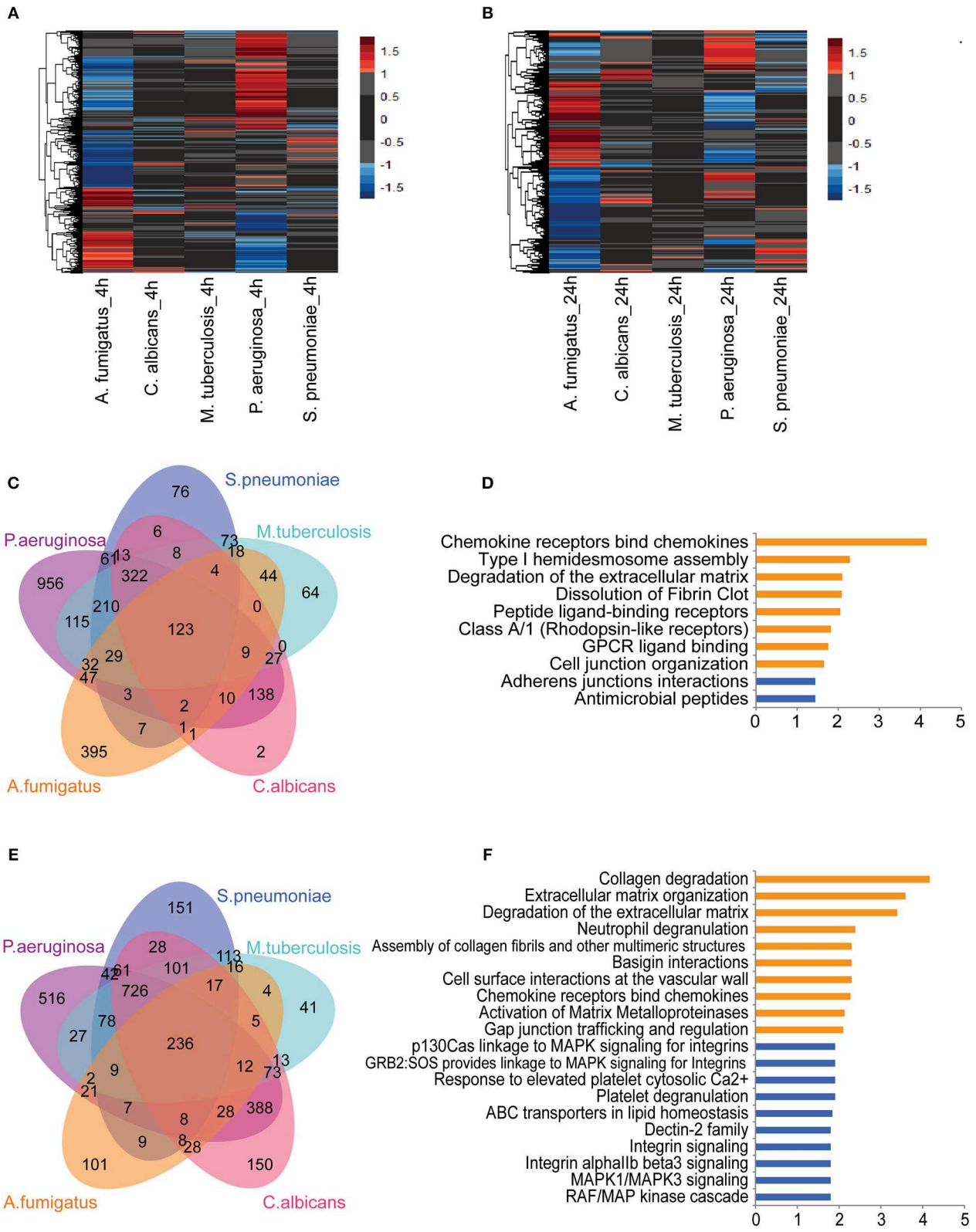

FIGURE 1 | Core transcriptional responses of PBMC to different stimulations affect EC. The expression levels (log_2-fold change) of differentially expressed (DE) genes in PBMC upon stimulation at **(A)** 4 h and **(B)** 24 h. Color represents log_2-fold change value. Number of shared and specific DE genes at **(C)** 4 h and **(E)** 24 h. Pathways enriched for common DE genes at **(D)** 4 h and top-10 pathways enriched at **(F)** 24 h. Orange and blue indicate pathways enriched by upregulated and suppressed genes, respectively. Data are represented as **(A,B)** mean expression levels from PBMC isolated from eight individuals **(D,F)** $-log_{10}$ *q*-value.

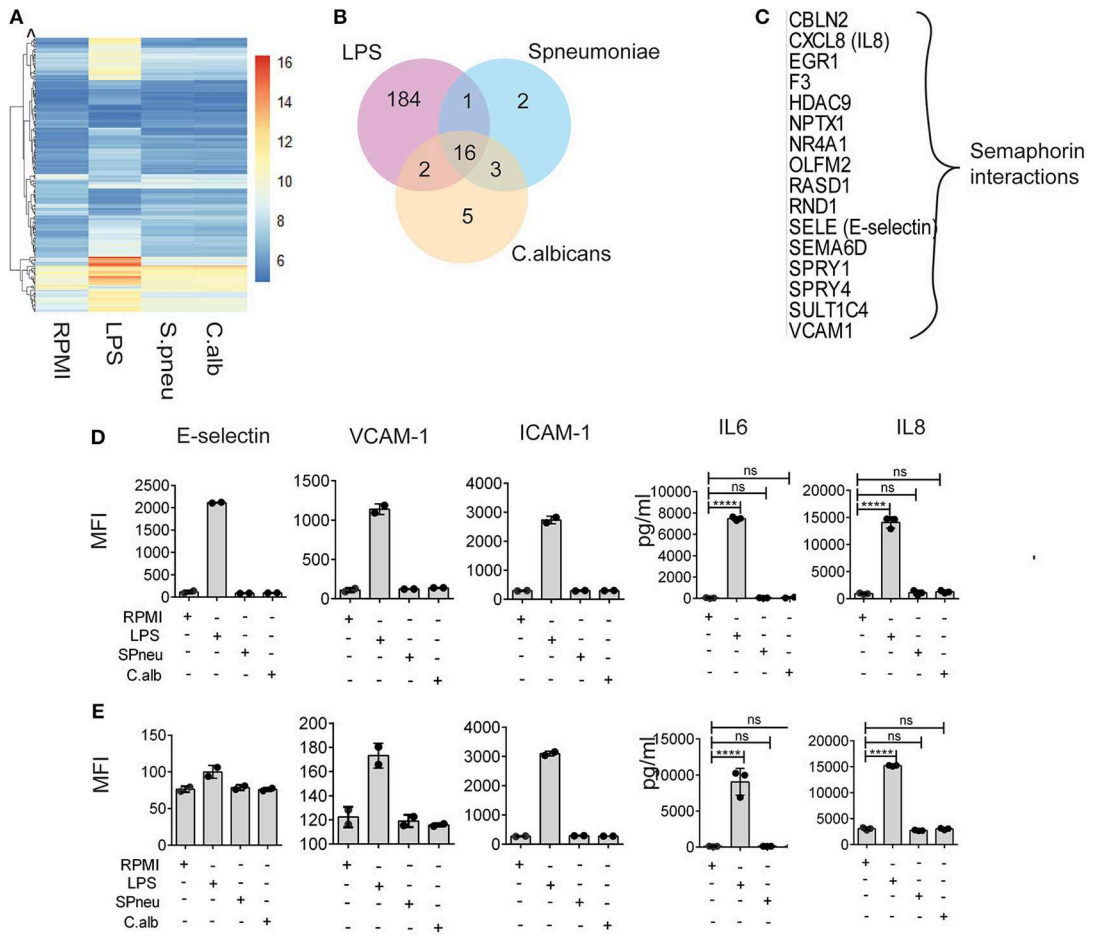

FIGURE 2 | Heat-killed pathogens do not directly induce EC activation. **(A)** Mean RNA expression level (VST) of 213 DE genes responding to either LPS, *S. pneumoniae* or *C. albicans* on EC. Color scales by VST value, ranging from weak to strong expression (6–16). Data are represented as mean of three replications. **(B)** Number of shared and unique genes induced in EC upon stimulation. **(C)** List of 16 common DE genes (with protein names), and their pathway enriched by Reactome. **(D,E)** Protein expression levels of E-selectin, VCAM-1, ICAM-1, IL-6, and IL-8 in EC at 6 and 24 h after stimulation with LPS, *S. pneumoniae (SPneu)* and *C. albicans (C.alb)*, respectively. E-selectin, VCAM-1 and ICAM-1 were measured by flow cytometry, data were presented as Geometric Mean Florescence Intensity (MFI). IL-6 and IL-8 were measured by ELISA, data were presented as pg/ml. Data are shown as mean (*SD*), representative for three independent experiments. ****$p < 0.0001$.

showed strong response of HUVECs to LPS in contrast to heat-killed pathogens (**Figures 2A,B**). We found 203 genes that significantly responded to LPS, whereas only 22 and 26 genes were induced by *S. pneumoniae* and *C. albicans*, respectively (**Figure 2B**). There were 16 genes in HUVECs that responded to all stimulations (**Figure 2C**), and these were enriched for alterations in semaphorin interaction. RNAseq data also showed significant differences in the expression levels upon stimulation of the inflammatory markers: IL-8 (*CXCL8*), E-selectin (*SELE*), and VCAM-1 (*VCAM1*). However, the small changes in RNA levels of these markers upon *S. pneumonie and C.albicans* stimulation did not significantly alter protein levels (**Figures 2D,E**). Therefore, direct activation of endothelial cells by pathogens has minimal effect on inducing endothelial cell inflammatory responses. We therefore hypothesized that in response to pathogens, the leukocytes produce mediators that activate endothelial cells much more strongly than direct pathogen stimulation.

Leukocyte-Released Mediators Significantly Induce Endothelial Cell Activation

During bloodstream infection, endothelial cells are in contact with both infectious pathogens and immune cells. RNAseq data from activated PBMCs indicated up-regulation of several cytokine pathways upon stimulation with different types of pathogens. We therefore investigated the effect of cytokines from stimulated immune cells on endothelial cells. To mimic the humoral interaction between immune cells and endothelial cells, we first stimulated PBMCs with either LPS, *S. pneumoniae* or *C. albicans* for 24 h, then harvested the supernatant,

neutralized the LPS-trace by polymyxin B (9), and exposed HUVECs to the supernatant containing cytokine signals from the activated PBMCs. After 6 h of exposure, we measured the expression levels of inflammatory markers on endothelial cells. We observed strong activation of endothelial cells at protein level. Interestingly, whereas direct exposure of HUVECs to heat-killed pathogens did not induce endothelial activation, the exposure to supernatants from *S. pneumonia*-stimulated PBMCs (Spneu_Sup) and *C. albicans*-stimulated PBMCs (C.alb_Sup) significantly induced the expression levels of adhesion molecules (E-selectin, VCAM-1, and ICAM-1) and cytokines (IL-6 and IL-8) (**Figures 3A–C**). Endothelial cells, together with PBMCs, are the main source of IL-6. We conclude that endothelial cells become activated by heat-killed pathogens via cytokines and other inflammatory mediators released from activated PBMCs.

To further characterize the genes and pathways activated in HUVECs outside the conventional markers, we performed RNAseq to look at the transcriptome of endothelial cells exposed to PBMC supernatants (**Figures 3D,E**). We found 72 genes induced by LPS_Sup, 180 genes induced by Spneu_Sup and 222 genes induced by Calb_Sup. Among these, 65 genes are shared between all supernatants, which is 90% of the LPS_Sup responding genes, 36% of Spneu_Sup responding genes, and 29% of Calb_Sup responding genes (**Figure 3E**). Among the 65 shared genes, 60 are uniquely induced by supernatant and five are also commonly induced by direct stimulation (*CXCL8*, *F3*, *RND1*, *SELE*, *VCAM1*). Pathway enrichment for the 60 unique genes shows a strong enrichment for cytokine signaling, IFN signaling, IL-1 signaling and TNF signaling (**Figure 3F** and **Supplemental Figure S3**). Since LPS, hence LPS_Sup, cannot represent the complexity of PBMC responses to bacteria, we also looked at the genes shared between Spneu_Sup and Calb_Sup. Interestingly, here we found 85 commonly responding genes, which is 47% of the S.pneu_Sup and 38% of the Calb_Sup responding genes. Pathway enrichment for these genes also indicated strong enrichment for cytokine signaling, particularly for interleukins, IFN, and IL-1 (**Figures 3G–I**). Altogether, this evidence suggests that the activation of endothelial cells by mediators released from PBMCs is mostly shared and independent of the type of infectious pathogens.

IL-1 and TNF-α Are Major Mediators, Yet There Are Contributions From Other Cytokines Secreted by PBMCs on EC Activation

Although blocking of IL-1 or TNF-α has resulted in inconsistent results due to study design, recent clinical trials in stratified patients have shown IL-1- or TNF-blocking therapy to be effective in improving sepsis survival (14–16). Since endothelial cells express receptors for IL-1 (17, 18) and TNF-α (19), we were intrigued to investigate the effect of IL-1 and TNF-α present in the PBMC-supernatant on inducing endothelial activation, and if other PBMC secreted-mediators play a role. Before adding the supernatants to HUVECs, we either neutralized TNF-α in the supernatants with a TNF-α blocking antibody or blocked the effect of IL-1α and IL-1β by adding IL-1RA (Anakinra), or both. The blocking dose efficiency was 100% for IL-1 and approximately 75% for TNF-α (**Supplemental Figure S3**). We found that TNF-α secreted by activated PBMCs was the main mediator for endothelial expression of adhesion molecules (E-selectin, VCAM-1, and ICAM-1). However, it was not the sole mediator. IL-1α and/or IL-1β also activated the expression of E-selectin, but not VCAM-1 and ICAM-1 (**Figures 4A–C**). Moreover, neutralization of both TNF-α and IL-1 in the supernatant secreted by activated PBMCs almost completely inhibited endothelial activation, indicating an additive effect of TNF-α and IL-1 on endothelial cell activation (**Figures 4A–C**). On the other hand, TNF-α had no effect on the induction of IL-6 secretion by endothelial cells. This is in contrast to IL-1 blockage, which inhibited endothelial IL-6 secretion. However, the extent to which IL-1 regulates IL-6 expression on endothelial cells depends on other mediators that are co-secreted by PBMCs in response to a specific pathogen. Neutralization of IL-1 in the PBMC supernatant reduced the amount of IL-6 secretion only in the case of *C. albicans*. Of note, cytokine levels secreted by endothelial cells do not completely return to baseline levels even after blocking TNF-a and IL-1, which suggests that other pathways may be involved in producing endothelial cytokines at a marginal level.

Up-Regulation of IFN Pathways in Endothelial Cells by Humoral Mediators From PBMCs Is Independent of IL-1 and TNF-α

As IL-1 and TNF-α are the major mediators that induce a strong response in endothelial cells, we tested the effect of blocking IL-1 and TNF-α on endothelial transcriptional responses (**Figures 4D–F**). Comparison of DE genes in HUVECs exposed to supernatants before and after TNF-α Ab and IL-1RA treatment revealed differential expression of 15, 47, and 81 genes in the context of LPS, *S. pneumoniae* and *C. albicans*, respectively (**Figure 4E**). Interestingly, these genes were shared between different supernatants and are enriched for IFN-α/β and IFN-γ pathways (**Figure 4F**). The enrichment was much stronger in the case of *C. albicans* stimulation suggesting *C. albicans* is one of the strong stimulators of IFN-inducing mediators. Notably, in the context of *S. pneumoniae* and *C. albicans*, we found the differential expression both IFN-induced genes and the upstream genes, including *DDX58* (RIG-I), *NLRC5,* and *TLR3*. We also found the expression of IFN receptor genes in HUVECs at RNA levels (**Supplemental Figure S4A**). These results suggest that the IFN-α/β and IFN-γ pathways are up-regulated in endothelial cells by mediators released by leukocytes in response to sepsis-causing pathogens, and are independent on IL-1 and TNF-α.

Validation of an IL-1- and TNF-α-Independent Effect of IFN-α/β/γ on Endothelial Response

In view of the above data, to test if IL-1- and TNF-α-independent effect on endothelial cells was mainly driven by IFN-α/β/γ, we made use of previously published microarray gene expression data (20). We compared whether the genes induced by direct

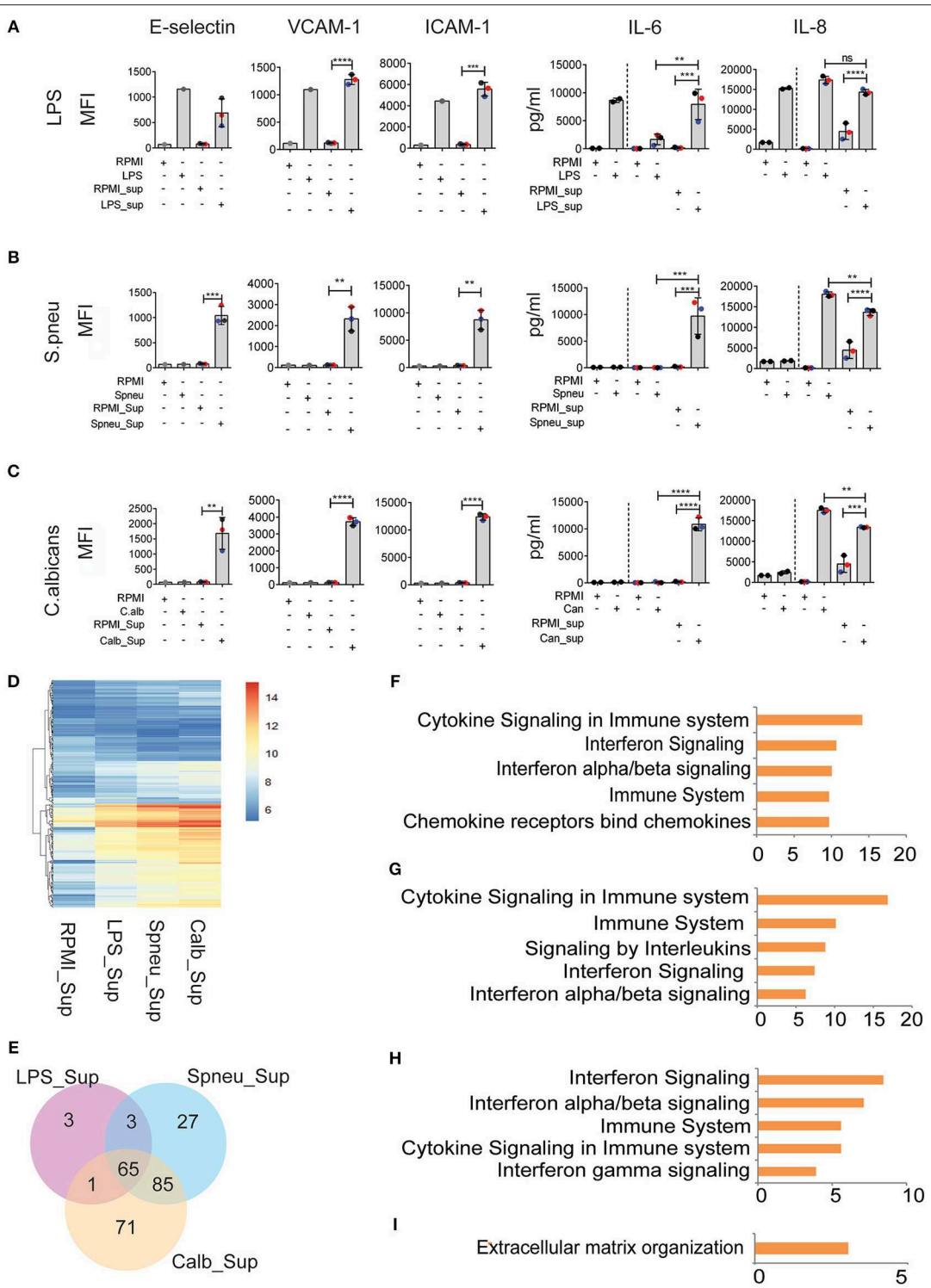

FIGURE 3 | Leukocyte-mediators significantly induce EC activation. **(A–C)** Protein levels of E-selectin, VCAM-1, and ICAM-1 measured by flow cytometry, and secreted IL-6 and IL-8 measured by ELISA on EC after 6 h exposed to direct stimulation (first 2 columns) and to PBMC medium (other columns). Data were presented as Mean florescence Intensity (MFI) for E-selectin, VCAM-1 and ICAM-1 and pg/ml for IL-6 and IL-8. For IL-6 and IL-8, the amount of cytokines presented in PBMC medium before adding to EC were plotted in the 3rd and 4th column, whereas the amount of total cytokines after exposure to EC were plotted in the 5th and 6th column. Colors represent three different individuals of whom PBMC were isolated. **(D)** RNA expression levels (VST) of 255 DE genes in EC induced by PBMC medium. **(E)** The number of shared and unique DE genes between various conditions. **(F)** Top five pathways enriched by 60 common genes induced by all PBMC medium. **(G–I)** Top 5 pathways enriched by genes responded to **(G)** Spneu_Sup and Calb_Sup, **(H)** only Calb_Sup, and **(I)** only Spneu_Sup. Data are shown as **(A–C)** representative of three independent experiments (mean and *SD*) **(D,E)** mean from three biological replications **(F–I)**, $-\log_{10}$ of *q*-value. $^{**}p < 0.01$, $^{***}p < 0.001$, $^{****}p < 0.0001$.

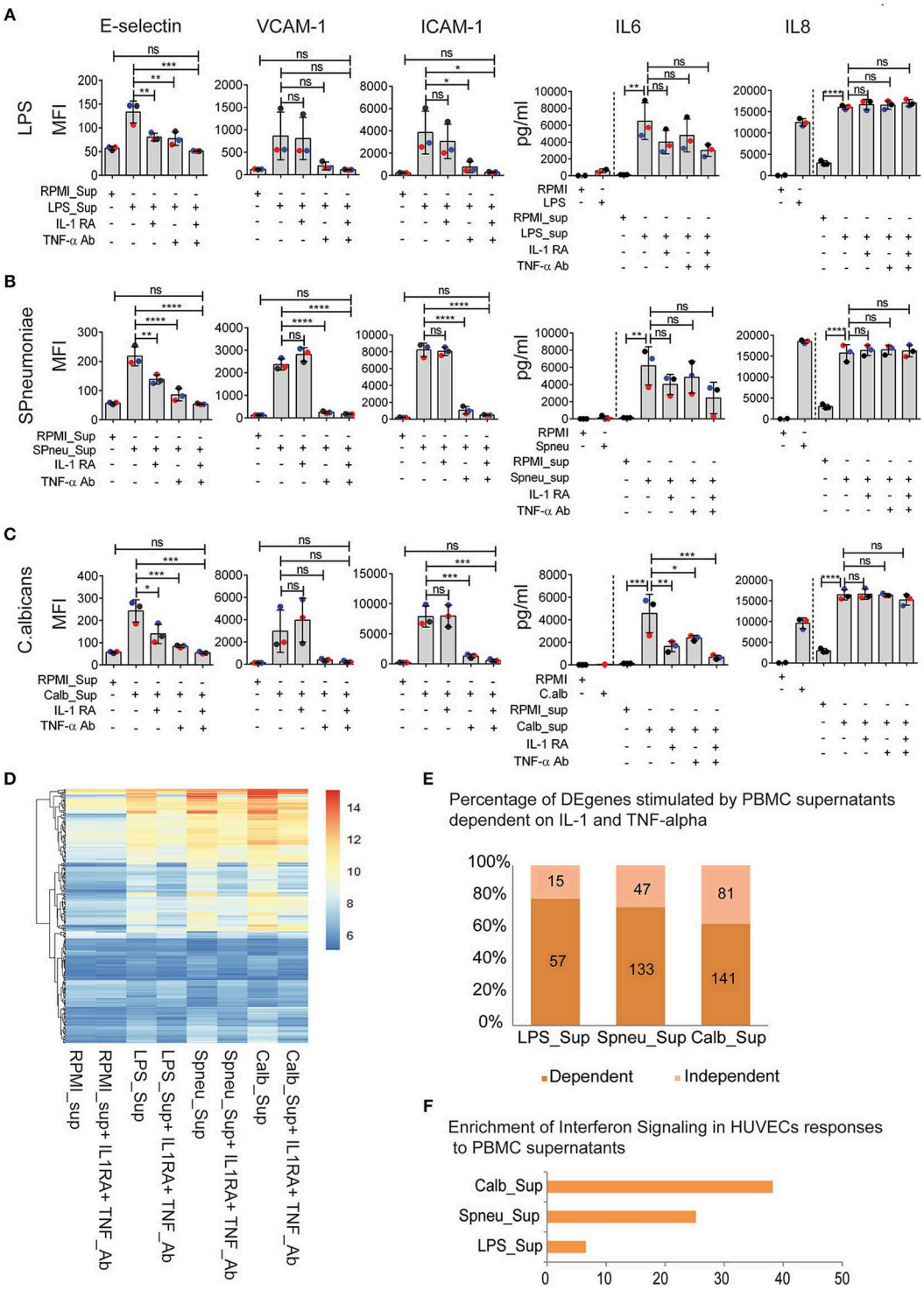

FIGURE 4 | IFN pathways remain active in EC after neutralization of IL1 and TNFα in leukocyte-mediators. **(A–C)** Protein abundance on EC after exposure to **(A)** LPS-activated PBMC medium **(B)**, *S. pneumonia*-activated PBMC medium **(C)**, *C. albicans*-activated PBMC medium with, or without IL-1RA and TNF-α Ab for 6 h. For cytokines, the amount of cytokines presented in PBMC medium before adding to HUVECs were plotted before the dash line whereas that after 6 h exposed to HUVECs were plotted behind the dash line. Colors of dots indicate different PBMC donors. **(D)** RNA expression levels (VST) of 255 DE genes activated in EC by PBMC medium with or without blocking. **(E)** Percentage of genes independent from IL-1 and TNF-α. Number of genes that are dependent (dark shade) and independent (light shade) of IL1 and TNF α. **(F)** Genes expressed independent of IL-1 and TNF-α are strongly enriched for IFN signaling. Data are shown as **(A–C)** mean (*SD*), representative of three independent experiments **(D)**, mean expression value of 3 biological replications **(F)**, $-\log_{10}$ of *q*-value. $^{*}p < 0.05$, $^{**}p < 0.01$, $^{***}p < 0.001$, $^{****}p < 0.0001$.

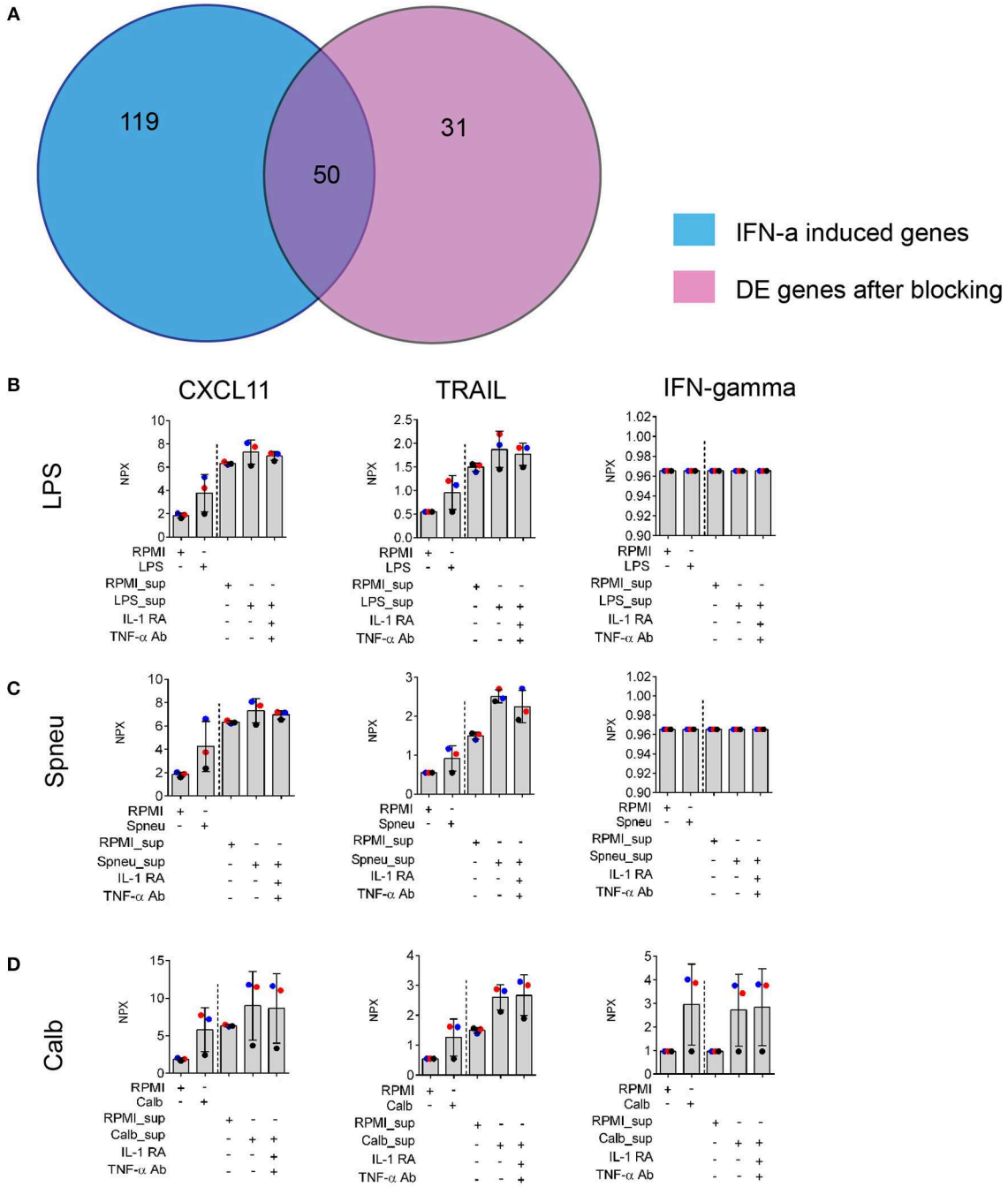

FIGURE 5 | Validation of IFNs effect on EC. **(A)** Number share and unique genes induced by IFN-α on ECs (20) and leukocyte- mediators after blocking of both IL-1 and TNF-α on ECs. **(B–D)** Protein levels of IFN-α downstream genes: CXCL11 and TRAIL, and IFN-gamma produced by stimulated leukocytes (before the dash line) and EC (after the dash line) in the supernatants, measured by Olink®. Data are shown as mean (SD), represented for two independent experiments. Colors correlate to three donors of whom PBMCs were isolated.

activation of HUVEC by IFN-α/β/γ are also induced in our experiment after blocking IL-1 and TNF-α. We found that 62% of genes induced in HUVECs after exposure to *Candida*-induced supernatant with IL-1 and TNF-α blocking agents are also present in the list of differential expressed genes induced by IFN-α (**Figure 5A**). We also found expression of IFN-β and IFN-ϒ in PBMCs in response to stimulation at RNA levels (**Supplemental Figure S4B**). Altogether, it suggests the presence of IFN-α in the mediators released by leukocytes. We also found high levels of circulatory IFN-γ in the supernatants from

Candida-stimulated leukocytes (**Figure 5D**). In addition, we also confirmed the up-regulation chemokines such as CXCL11 and TRAIL which is known to be present at higher levels in the endothelium following treatment with IFN-α (20). Of notice, protein levels of these proteins are not dependent on IL-1 and TNF-α (**Figures 5B–D**).

DISCUSSION

Sepsis is not a homogeneous disease, but rather life-threatening organ dysfunction syndrome caused by a dysregulation of host response to infection (1). Given the heterogeneity of sepsis patients, many clinical trials targeting the hyper-inflammatory response in sepsis, including corticosteroids, and anti-cytokine therapies (e.g., anti-IL1 and anti TNF-α) have yielded disappointing results (21, 22). Understanding the impact of the complex interactions between causal cell types in a pathogen-specific manner is therefore crucial to delineate the molecular basis of heterogeneity in sepsis outcome. In the present study, we applied an integrative genomics approach to not only characterize the global transcriptional response of leukocytes and endothelial cells to many sepsis-causing pathogens, but to also identify important molecular pathways induced during leukocyte-endothelium cross-talk in regulating overall immune response in sepsis.

First, to identify leukocyte responses to three classes of infectious pathogens (Gram-negative bacteria, Gram-positive bacteria, and fungi) we assessed the transcriptional response of PBMCs to *P. aeruginosa*, *S. pneumoniae*, *M. tuberculosis*, *C. albicans,* and *A. fumigatus*. This allowed us to identify several pathways that were induced in a pathogen-specific manner. The *S. pneumoniae*-specific transcriptome revealed the repression of genes involved in IFN signaling and antigen presentation, while *P. aeruginosa*-specific genes were enriched for the TNF-α and cytokine signaling pathways. These findings suggest that pathogen-specific responses in leukocytes could influence pathophysiology found sepsis patients, partly underlying the heterogeneity observed in sepsis. However, our analysis also identified core pathways that were induced in PBMCs in response to all pathogens as reported before (4). This suggests that the common genes that correspond to core pathways such as antigen presentation, cell-cell signaling, immune regulatory pathways, are absolutely necessary to fight against all types of bacterial or fungal infections. Importantly, we found a strong enrichment of genes involved in leukocyte interaction with endothelial cells and cellular matrix. This finding suggests that the core leukocyte response to pathogens converges on endothelial cells. Interestingly, as suggested by our previous study (23), genes located nearby genetic variants that are associated with sepsis are enriched for immune and endothelial pathways. Therefore, studying leukocyte-endothelium cross-talk is critical in the context of sepsis and potentially can explain sepsis heterogeneity.

Second, by characterizing the global transcriptional response of endothelial cells to sepsis causing pathogens, we emphasize the role of leukocyte-endothelial cross-talk during infections. Although endothelial cells are not considered classical immune cells, HUVECs have been shown to express TLR4 and RIG-I, pattern recognition receptors for LPS-mediating responses to regulate cytokine responses and endothelial activation (8, 9). We indeed observed very strong activation of endothelial transcriptional pathways in response to LPS in comparison to direct stimulation of endothelial cells using other bacterial and fungal pathogens. These findings are in line with the observation of Filler et al. who showed that heat-killed *C. albicans* were not sufficient to induce strong expression of cytokines and adhesion molecules in endothelial cells in comparison to live and germinating *C. albicans* (24). Our study mapped the whole transcriptomic response to various pathogens including heat-killed *S. pneumoniae* and heat-killed *C. albicans*, which to our understanding, has not been reported before. Moreover, we showed that endothelial responses to Gram-positive bacteria and fungi are strongly affected by inflammatory signals from activated leukocytes. More than 66% of responding genes in HUVECs stimulated by PBMC humoral signals are shared across all stimuli. Although we expected to find activation of endothelial cells in response to circulatory mediators released by leukocytes, it was interesting to find a strong induction of IFN pathways together with IL-1 and TNF-α pathways. Whereas, IL-1 and TNF-α pathways have been investigated as a strategy to improve sepsis outcome, by studying the impact of humoral signals from leukocytes on endothelial cells, we observed a stronger enrichment of IFN-α/β and IFN-γ signaling than IL-1 and TNF-α signaling in endothelial cells. This suggests that, together with IL-1 and TNF-α, IFN pathways can result in aberrant responses within endothelial cells. Moreover, by neutralizing IL-1 with Anakinra and TNF-α with TNF-α blocking antibody in leukocyte humoral signals, we confirmed that IL-1 and TNF-α are the major mediators involved in activating endothelial cells. Intriguingly, we also identified different downstream mechanisms regulating endothelial adhesion molecules such as E-selectin, VCAM-1, and ICAM-1. E-selectin is strongly regulated by IL-1 and TNF-α, whereas ICAM-1 and VCAM-1 are driven more by TNF-α. We also found that activated endothelial cells are a major source of IL-6 production, corroborating a previous study (25).

Interestingly, even after blocking IL-1 and TNF-α, we were able to identify strong activation of IFN-α/β and IFN-γ pathways in endothelial cells. Several studies have already identified IFN-α/β pathway in leukocytes in response to bacteria (26) and fungi (27). In endothelial cells, although, IFN-α/β has been shown to promote endothelial proliferation *in vitro* (28), and reduce intracellular NO generation and impair fibrinolysis of HUVECs *in vitro* (29), the precise impact of IFN-α/β on endothelial function in the context of bloodstream infection or sepsis is not clear. Since NO production from the endothelium maintains blood pressure and blood flow (30) and reduced NO bioactivity is associated with sepsis severity (31), it will be relevant to study the effect of neutralizing IFNs to improve sepsis outcomes. In fact, it is currently being discussed whether IFN-β should be neutralized during the hyper-inflammatory phase in sepsis patients due to its contribution to pro-inflammation and/or whether it needs to be supplemented while patients are in the hypo-inflammatory phase given its ability to restore and reverse immunosuppression (32).

Further studies should investigate which inflammatory mediator(s) from activated leukocytes induced IFN-α and IFN-β signaling in endothelial cells. We observed the mRNA expression of IFN-α/β receptors (*IFNAR1*, *IFNAR2*) in endothelial cells

across all the stimulatory pathogens we studied, but could not detect IFN-α or IFN-β in the medium of activated leukocytes (data not shown). Nevertheless, we observed a high amount of IFN- γ released by leukocytes in response to *C. albicans* and also increased RNA expression of IFN- γ receptor (*IFNGR1*) in endothelial cells. We also observed that *C. albicans*-stimulated leukocytes secrete the most potent mix of mediators for inducing endothelial activation, which suggests that *C. albicans* could be a good model to represent the broad impact of leukocyte signals on endothelial cells. One could use it, for example, as a model to study the interaction of leukocytes and endothelial cells with more functional assays to study the biological effect of IFN-activation on endothelial function.

Interestingly, we also observed that *TLR3* (TLR-3), *DDX58* (RIG-I), and *NLRC5*, together with *IRF-1, -2, -3,* and *-7* were highly expressed in endothelial cells exposed exclusively to *C. albicans*- and *S. pneumoniae*-derived supernatants. RIG-I and IRF-1 are important mediators of endothelial activation in response to LPS and TNF-α as described previously (9, 33, 34). Nevertheless, what regulates the expression of these upstream molecules, either cytosolic DNA or other mediators present in the supernatants, remains elusive.

One of the limitation of our study is the use of heat-killed pathogens, which mounts, to some extent, differences in the host response to pathogens due to the exposure of ligands and the lack of dynamic interactions between the pathogens and the host cells. It has been shown that heat-killed pathogens (such as *Bordetella pertussis*) induce consistently high RNA expression of inflammatory cytokines (such as TNF-α, MIP-1β, IL1-α, and IL-1β) over time, whereas live bacteria induce a transient increase of those genes that was followed by gene suppression (35). Live bacteria, on the other hand, can induce inflammasome activation, altering the amount of secreted IL-1β in macrophages and dendritic cells whereas heat-killed pathogens cannot (36). In our study, although each heat-killed pathogen induced the responses in PBMCs (at RNA levels), which match with the typically known pathogenic toxins and ligands, to what extent the differences between the heat-killed and live pathogens affect the interaction between leukocytes and endothelial cells remains to be further investigated.

Future studies, if possible, should also investigate the host response to live attenuated pathogens or heat-killed pathogen lysate supplemented with bacterial RNA (36). Secondly, although we characterized the global transcription and protein expression levels during leukocyte and endothelial cells cross-talk, follow-up studies are needed to understand the consequences of up-regulated IFN signaling in endothelial cells during sepsis. In addition, it will be important to also study the impact of interaction between neutrophils together with leukocytes and endothelial cells in human-relevant model systems. In conclusion, our work suggests that activation of IFN pathways in endothelial cells plays an important role in the context of sepsis.

DATA AVAILABILITY STATEMENT

The sequencing data generated by this study was deposited to GEO, access number: GSE131590.

ETHICS STATEMENT

Ethical permission for this study was approved by the Ethical Committee of Radboud University Nijmegen (nr 42561.091.12). The patients/participants provided written informed consent to participate in this study.

AUTHOR CONTRIBUTIONS

YL, VK, and JM shared the conceptualization. KL, JM, and VK designed the study and prepared the manuscript. KL, MJ, and JP performed experiments. XC, VM, and YL analyzed the transcriptome data. LJ, MN, SW, and CW provided reagents, protocols, and facilities to conduct stimulation/blocking experiments. LJ, MN, CW, YL, JM, and VK interpreted results and critically assessed the manuscript.

FUNDING

This work was supported by the Ph.D. fellowship from the Graduate School of Medical Science, University Medical Center Groningen to KL, a Radboud University Medical Center Hypatia Tenure Track Grant, and a Research Grant (2017) from the European Society of Clinical Microbiology and Infectious Diseases (ESCMID) to VK and a NWO Gravitation Netherlands Organ-on-Chip Initiative (024.003.001) grant to CW. MN was supported by a Spinoza grant of the Netherlands Organization for Scientific Research.

ACKNOWLEDGMENTS

We thank all the volunteers for donating PBMCs for this study. We are grateful to K. McIntyre for editing the manuscript and our colleagues within the Genetics department and the EBVDT-SHOCK Research group for fruitful discussion.

SUPPLEMENTARY MATERIAL

The Supplementary Material for this article can be found online at: https://www.frontiersin.org/articles/10.3389/fimmu.2019.02508/full#supplementary-material

REFERENCES

1. Singer M, Deutschman CS, Seymour CW, Shankar-Hari M, Annane D, Bauer M, et al. The third international consensus definitions for sepsis and septic shock (sepsis-3). *JAMA*. (2016) 315:801–10. doi: 10.1001/jama.2016.0287

2. Fleischmann C, Scherag A, Adhikari NK, Hartog CS, Tsaganos T, Schlattmann P, et al. Assessment of global incidence and mortality of hospital-treated sepsis current estimates and limitations. *Am J Respir Crit Care Med.* (2016) 193:259–72. doi: 10.1164/rccm.201504-0781OC

3. van der Poll T, van de Veerdonk FL, Scicluna BP, Netea MG. The immunopathology of sepsis and potential therapeutic targets. *Nat Rev Immunol.*(2017) 17:407–20. doi: 10.1038/nri.2017.36
4. Jenner RG, Young RA. Insights into host responses against pathogens from transcriptional profiling. *Nat Rev Microbiol.* (2005) 3:281–94. doi: 10.1038/nrmicro1126
5. Calvano SE, Xiao W, Richards DR, Felciano RM, Baker HV, Cho RJ, et al. A network-based analysis of systemic inflammation in humans. *Nature.* (2005) 437:1032–7. doi: 10.1038/nature03985
6. Pober JS, Sessa WC. Evolving functions of endothelial cells in inflammation. *Nat Rev Immunol.* (2007) 7:803–15. doi: 10.1038/nri2171
7. Molema G. Heterogeneity in endothelial responsiveness to cytokines, molecular causes, and pharmacological consequences. *Semin Thromb Hemost.* (2010) 36:246–64. doi: 10.1055/s-0030-1253448
8. Faure E, Equils O, Sieling PA, Thomas L, Zhang FX, Kirschning CJ, et al. Bacterial lipopolysaccharide activates NF-kappaB through toll-like receptor 4 (TLR-4) in cultured human dermal endothelial cells. Differential expression of TLR-4 and TLR-2 in endothelial cells. *J Biol Chem.* (2000) 275:11058–63. doi: 10.1074/jbc.275.15.11058
9. Moser J, Heeringa P, Jongman RM, Zwiers PJ, Niemarkt AE, Yan R, et al. Intracellular RIG-I signaling regulates TLR4-independent endothelial inflammatory responses to endotoxin. *J Immunol.* (2016) 196:4681–91. doi: 10.4049/jimmunol.1501819
10. Ince C, Mayeux PR, Nguyen T, Gomez H, Kellum JA, Ospina-Tascon GA, et al. The endothelium in sepsis. *Shock.* (2016) 45:259–70. doi: 10.1097/SHK.0000000000000473
11. Li Y, Marije O, Patrick D, Isis Ricaño-Ponce, Sanne S, Martin J, et al. Inter-individual variability and genetic influences on cytokine responses to bacteria and fungi. *Nat Med.* (2016) 22:952–60. doi: 10.1038/nm.4139
12. Khakpour S, Wilhelmsen K, Hellman J. Vascular endothelial cell toll-like receptor pathways in sepsis. *Innate Immun.* (2015) 21:827–46. doi: 10.1177/1753425915606525
13. Opal SM, van der Poll T. Endothelial barrier dysfunction in septic shock. *J Intern Med.* (2015) 277:277–93. doi: 10.1111/joim.12331
14. Qiu P, Cui X, Barochia A, Li Y, Natanson C, Eichacker PQ. The evolving experience with therapeutic TNF inhibition in sepsis: considering the potential influence of risk of death. *Expert Opin Investig Drugs.* (2011) 20:1555–64. doi: 10.1517/13543784.2011.623125
15. Panacek EA, Marshall JC, Albertson TE, Johnson DH, Johnson S, MacArthur RD, et al. Efficacy and safety of the monoclonal anti-tumor necrosis factor antibody F(ab')2 fragment afelimomab in patients with severe sepsis and elevated interleukin-6 levels. *Crit Care Med.* (2004) 32:2173–82. doi: 10.1097/01.CCM.0000145229.59014.6C
16. Rajasekaran S, Kruse K, Kovey K, Davis AT, Hassan NE, Ndika AN, et al. Therapeutic role of anakinra, an interleukin-1 receptor antagonist, in the management of secondary hemophagocytic lymphohistiocytosis/sepsis/multiple organ dysfunction/macrophage activating syndrome in critically ill children*. *Pediatr Crit Care Med.* (2014) 15:401–8. doi: 10.1097/PCC.0000000000000078
17. Boraschi D, Rambaldi A, Sica A, Ghiara P, Colotta F, Wang JM, et al. Endothelial cells express the interleukin-1 receptor type I. *Blood.* (1991) 78:1262–7.
18. Kuldo JM, Westra J, Asgeirsdóttir SA, Kok RJ, Oosterhuis K, Rots MG, et al. Differential effects of NF-{kappa}B and p38 MAPK inhibitors and combinations thereof on TNF-{alpha}- and IL-1{beta}-induced proinflammatory status of endothelial cells *in vitro*. *Am J Physiol Cell Physiol.* (2005) 289:C1229–39. doi: 10.1152/ajpcell.00620.2004
19. Gaeta ML, Johnson DR, Kluger MS, Pober JS. The death domain of tumor necrosis factor receptor 1 is necessary but not sufficient for golgi retention of the receptor and mediates receptor desensitization. *Lab Invest.* (2000) 80:1185–94. doi: 10.1038/labinvest.3780126
20. Indraccolo S, Pfeffer U, Minuzzo S, Esposito G, Roni V, Mandruzzato S, et al. Identification of genes selectively regulated by IFNs in endothelial cells. *J Immunol.* (2007) 178:1122–35. doi: 10.4049/jimmunol.178.2.1122
21. Opal SM, Fisher CJ, Dhainaut JF, Vincent JL, Brase R, Lowry SF, et al. Confirmatory interleukin-1 receptor antagonist trial in severe sepsis: a phase III, randomized, double-blind, placebo-controlled, multicenter trial. the interleukin-1 receptor antagonist sepsis investigator group. *Crit Care Med.* (1997) 25:1115–24. doi: 10.1097/00003246-199707000-00010
22. Lv S, Han M, Yi R, Kwon S, Dai C, Wang R. Anti-TNF-alpha therapy for patients with sepsis: a systematic meta-analysis. *Int J Clin Pract.* (2014) 6:520–8. doi: 10.1111/ijcp.12382
23. Le KTT, Matzaraki V, Netea MG, Wijmenga C, Moser J, Kumar V. Functional annotation of genetic loci associated with sepsis prioritizes immune and endothelial cell pathways. *Front Immunol.* (2019) 10:1949. doi: 10.3389/fimmu.2019.01949
24. Filler SG, Pfunder AS, Spellberg BJ, Spellberg JP, Edwards JE. *Candida albicans* stimulates cytokine production and leukocyte adhesion molecule expression by endothelial *Cells*. (1996) 64:2609–17.
25. Podor TJ, Jirik FR, Loskutoff DJ, Carson DA, Lotz M. Human endothelial cells produce IL-6. lack of responses to exogenous IL-6. *Ann NY Acad Sci.* (1989) 557:374–86. doi: 10.1111/j.1749-6632.1989.tb24030.x
26. Boxx GM, Cheng G. The roles of type I interferon in bacterial infection. *Cell Host Microbe.* (2016) 19:760–9. doi: 10.1016/j.chom.2016.05.016
27. Smeekens SP, Ng A, Kumar V, Johnson MD, Plantinga TS, van Diemen C, et al. Functional genomics identifies type I interferon pathway as central for host defense against *Candida albicans*. *Nat Commun.* (2013) 4:1342. doi: 10.1038/ncomms2343
28. Gomez D, Reich NC. Stimulation of primary human endothelial cell proliferation by IFN. *J Immunol.* (2003) 170:5373–81. doi: 10.4049/jimmunol.170.11.5373
29. Jia H, Thelwell C, Dilger P, Bird C, Daniels S, Wadhwa M. Endothelial cell functions impaired by interferon in vitro: Insights into the molecular mechanism of thrombotic microangiopathy associated with interferon therapy. *Thromb Res.* (2018) 163:105–16. doi: 10.1016/j.thromres.2018.01.039
30. Gamboa A, Shibao C, Diedrich A, Choi L, Pohar B, Jordan J, et al. Contribution of endothelial nitric oxide to blood pressure in humans. *Hypertension.* (2007) 49:170–7. doi: 10.1161/01.HYP.0000252425.06216.26
31. Winkler MS, Kluge S, Holzmann M, Moritz E, Robbe L, Bauer A, et al. Markers of nitric oxide are associated with sepsis severity: An observational study. *Critical Care.* (2017) 21:189. doi: 10.1186/s13054-017-1782-2
32. Rackov G, Shokri R, De Mon MÁ, Martínez-AC, Balomenos D. The role of IFN-beta during the course of sepsis progression and its therapeutic potential. *Front Immunol.* (2017) 8:493. doi: 10.3389/fimmu.2017.00493
33. Yan R, van Meurs M, Popa ER, Jongman RM, Zwiers PJ, Niemarkt AE, et al. Endothelial interferon regulatory factor 1 regulates lipopolysaccharide-induced VCAM-1 expression independent of NFkappaB. *J Innate Immun.* (2017) 9:546–60. doi: 10.1159/000477211
34. Venkatesh D, Ernandez T, Rosetti F, Batal I, Cullere X, Luscinskas FW, et al. Endothelial TNF receptor 2 induces IRF1 transcription factor-dependent interferon-beta autocrine signaling to promote monocyte recruitment. *Immunity.* (2013) 38:1025–37. doi: 10.1016/j.immuni.2013.01.012
35. Boldrick JC, Alizadeh AA, Diehn M, Dudoit S, Liu CL, Belcher CE, et al. Stereotyped and specific gene expression programs in human innate immune responses to bacteria. *Proc Natl Acad Sci USA.* (2002) 99:972–7. doi: 10.1073/pnas.231625398
36. Sander LE, Davis MJ, Boekschoten MV, Amsen D, Dascher CC, Ryffel B, et al. Detection of prokaryotic mRNA signifies microbial viability and promotes immunity. *Nature.* (2011) 474:385–9. doi: 10.1038/nature10072

Conflict of Interest: The authors declare that the research was conducted in the absence of any commercial or financial relationships that could be construed as a potential conflict of interest.

Copyright © 2019 Le, Chu, Jaeger, Plantinga, Matzaraki, Withoff, Joosten, Netea, Wijmenga, Li, Moser and Kumar. This is an open-access article distributed under the terms of the Creative Commons Attribution License (CC BY). The use, distribution or reproduction in other forums is permitted, provided the original author(s) and the copyright owner(s) are credited and that the original publication in this journal is cited, in accordance with accepted academic practice. No use, distribution or reproduction is permitted which does not comply with these terms.

frontiers in Immunology

REVIEW
published: 30 October 2019
doi: 10.3389/fimmu.2019.02536

DAMPs and NETs in Sepsis

Naomi-Liza Denning[1,2,3], *Monowar Aziz*[1,2]*, *Steven D. Gurien*[1,3] *and Ping Wang*[1,2,3,4]*

[1] Center for Immunology and Inflammation, Feinstein Institutes for Medical Research, Manhasset, NY, United States, [2] Elmezzi Graduate School of Molecular Medicine, Manhasset, NY, United States, [3] Department of Surgery, Donald and Barbara Zucker School of Medicine at Hofstra/Northwell, Manhasset, NY, United States, [4] Department of Molecular Medicine, Donald and Barbara Zucker School of Medicine at Hofstra/Northwell, Manhasset, NY, United States

Sepsis is a deadly inflammatory syndrome caused by an exaggerated immune response to infection. Much has been focused on host response to pathogens mediated through the interaction of pathogen-associated molecular patterns (PAMPs) and pattern recognition receptors (PRRs). PRRs are also activated by host nuclear, mitochondrial, and cytosolic proteins, known as damage-associated molecular patterns (DAMPs) that are released from cells during sepsis. Some well described members of the DAMP family are extracellular cold-inducible RNA-binding protein (eCIRP), high mobility group box 1 (HMGB1), histones, and adenosine triphosphate (ATP). DAMPs are released from the cell through inflammasome activation or passively following cell death. Similarly, neutrophil extracellular traps (NETs) are released from neutrophils during inflammation. NETs are webs of extracellular DNA decorated with histones, myeloperoxidase, and elastase. Although NETs contribute to pathogen clearance, excessive NET formation promotes inflammation and tissue damage in sepsis. Here, we review DAMPs and NETs and their crosstalk in sepsis with respect to their sources, activation, release, and function. A clear grasp of DAMPs, NETs and their interaction is crucial for the understanding of the pathophysiology of sepsis and for the development of novel sepsis therapeutics.

Keywords: DAMPs (damage-associated molecular patterns), NETs (neutrophil extracellular traps), sepsis, HMGB1 (high-mobility group box 1), CIRP, cold-inducible RNA-binding protein, histone, neutrophils

OPEN ACCESS

Edited by:
Timothy Robert Billiar, University of Pittsburgh, United States

Reviewed by:
Markus Bosmann, Boston University, United States
Michael Thomas Lotze, University of Pittsburgh Cancer Institute, United States

***Correspondence:**
Monowar Aziz
maziz1@northwell.edu
Ping Wang
pwang@northwell.edu

Specialty section:
This article was submitted to Inflammation, a section of the journal Frontiers in Immunology

Received: *14 May 2019*
Accepted: *11 October 2019*
Published: *30 October 2019*

Citation:
Denning N-L, Aziz M, Gurien SD and Wang P (2019) DAMPs and NETs in Sepsis. Front. Immunol. 10:2536. doi: 10.3389/fimmu.2019.02536

INTRODUCTION

Sepsis is common and deadly; 30–50% of patients suffering an in-hospital mortality have sepsis. In the United States, sepsis affects 1.7 million adults annually resulting in more than 250,000 deaths (1, 2). It is estimated that, worldwide, sepsis impacts 30 million people per year and leads to 6 million deaths (3). Until recently, sepsis was defined as the systemic inflammatory response syndrome (SIRS)—hypo or hyperthermia (>38°C or <36°C), increased heart rate and respiratory rate and increased or decreased white blood cell count- in the presence of an infection. Sepsis with organ dysfunction was severe sepsis and fluid-refractory hypotension was septic shock (2). New guidelines, called Sepsis-3, established new definitions of sepsis, defining sepsis as "life threatening organ dysfunction caused by dysregulated host response to infection" (2). Organ dysfunction, as recommended by Sepsis-3, is defined clinically as changes of 2 points or more on the Sequential [Sepsis-related] Organ Failure Assessment (SOFA). The most severe subset of sepsis—septic shock- is defined as "sepsis in which underlying circulatory and cellular metabolism abnormalities are profound enough to substantially increase mortality" (2).

Sepsis arises from the body's exaggerated immune response to infection (4). Based on the "germ theory" of disease (5), it was initially thought that the inflammation, organ injury, and death that follows an infection were solely due to the body's response to microbial products,

such as pathogen-associated molecular patterns (PAMPs) (6). PAMPs are recognized by pattern recognizing receptors (PRRs) expressed on immune-reactive cells (7). Numerous studies have been published to demonstrate the role of PAMPs and PRRs in activating the immune system in sepsis (4, 6). During the last several decades, subsequent studies have identified damage-associated molecular patterns (DAMPs). DAMPs are host nuclear or cytoplasmic non-microbial molecules which, when released from the cell following tissue injury, serve as potent activators of the immune system initiating and perpetuating a non-infectious inflammatory response to cause systemic inflammation, organ injury, and death (8–10). Like PAMPs, DAMPs are also recognized by PRRs and utilize the same signal transduction machinery to activate the immune system (6, 11). Clinically, sepsis severity has been shown to correlate with DAMPs; studies have shown that increased serum levels of DAMPs including high mobility group box 1 (HMGB1), extracellular cold-inducible RNA-binding protein (eCIRP), and H3 correspond with increased with disease severity (12–14). This review describes several well-known DAMPs, details the mechanisms of their release and actions, and describes therapeutic strategies that target DAMPs in sepsis.

Neutrophils are the most abundant leukocytes in the body and serve as the first line of defense against infection (15). The effector function of neutrophils is mediated through phagocytosis, reactive oxygen species (ROS), and protease dependent killing of ingested pathogens. In addition, activated neutrophils release neutrophil extracellular traps (NETs)—webs of DNA and anti-microbial proteins designed to kill pathogens (16, 17). The discovery of NETs provided new insights into neutrophil effector function. However, numerous studies have also revealed the detrimental role of NETs in sepsis (18). Homeostasis in regards to NETs requires the interplay between their beneficial bactericidal properties and the hyperstimulation of immune cells by the DNA and proteins contained within NETs that results in inflammation and tissue injury in sepsis.

A number of review articles have been published demonstrating the individual role of DAMPs or NETs in sepsis (6, 19, 20). In sepsis, DAMP mediated signaling fuels pro-inflammatory cytokine and chemokine production by macrophages and other immune cells. This, in turn, leads to excessive neutrophil infiltration into the tissue. Activated neutrophils produce reactive oxygen species (ROS), inducible nitric oxide synthase (iNOS), and NETs which contain noxious molecules, leading to tissue inflammation and injury in sepsis. In this review, we focus on DAMPs, NETs, and explore their interplay during sepsis (**Figure 1**). We also discuss some of the therapeutic interventions targeting both DAMPs and NETs in experimental sepsis (**Table 1**).

DAMPs

DAMPs were first proposed as part of the "Danger Theory" by Polly Matzinger in the mid 1990's as an initial explanation for the robust inflammatory response elicited in response to sterile inflammation, which could not be explained solely by the self vs. non-self-hypothesis of the time (8). Intracellularly, DAMPs are hidden from view of the innate immune system. After tissue injury, caused by either sterile or infectious insults, they are released extracellularly to activate the immune system and resultant pro-inflammatory cascades (34). As discussed above, DAMPs are thus defined as endogenous molecules that can initiate and potentiate a non-infectious inflammatory response (8). In addition to their role in sepsis, as is discussed in the rest of this article, the release of DAMPs is critical to the development of sterile inflammation including inflammation that occurs secondary to organ ischemia and reperfusion injuries (35–37), non-infectious inflammatory liver diseases such as non-alcoholic fatty liver disease (38), or the sterile inflammation associated with aging (39).

Allowing the evolution of the Danger Theory from an abstract concept to a concrete entity, probably the first DAMP identified was HMGB1 (40, 41). Other DAMPs include histones, ATP, uric acid, DNA, mitochondrial DNA, and IL-33 (42). Recently, eCIRP has been identified as a newly discovered DAMP (43, 44). Although numerous endogenous molecules have been identified as inflammation-causing DAMPs, here we briefly review a selective group of DAMPs which have been strongly implicated in sepsis.

HMGB1

HMGB1 is a highly conserved protein expressed in all mammalian cells (21). HMGB1 as a DAMP causing sterile inflammation was discovered in 1999 (41). HMGB1 can be released actively via cytoplasmic vesicles or passively from necrotic cells. Active release is mediated by several pathways; JAK/STAT-1 mediated acetylation is responsible for the initial HMGB1 translocation from the nucleus to the cytoplasm, while extracellular release is partially mediated by double-stranded RNA-activated protein kinase R (PKR)/inflammasome-mediated pyroptosis (45). While passive release after necrotic cell death is rapid, active HMGB1 release is much slower. HMGB1 levels reach a plateau approximately 16–32 h after the onset of endotoxemia (46). HMGB1 related signaling is modulated by the redox state of its three cysteines (numbers 23, 45, and 106) (47, 48). Once released into the extracellular space, HMGB1 activates innate immune cells to propagate pro-inflammatory signaling cascades (49). HMGB1 induces recruitment of neutrophils to the site of tissue injury (50). HMGB1 binds to other PAMPs, including DNA (51), LPS (52), and lipoteichoic acid (53), potentiating their inflammatory responses. HMGB1 has been shown to bind to numerous cell surface receptors, including but not limited to receptor for advanced glycation end products (RAGE), TLR2, TLR4, TLR9, and triggering receptor expressed in myeloid cells 1 (TREM-1) (49, 54). After binding to these receptors, it activates macrophages and endothelial cells, stimulating the production of proinflammatory chemokines, cytokines, and endothelial adhesion molecules (49). HMGB1 is elevated in patients with sepsis (12, 55), and dozens of studies have demonstrated that targeting HMBG1 improves outcomes in sepsis (24, 25, 56, 57).

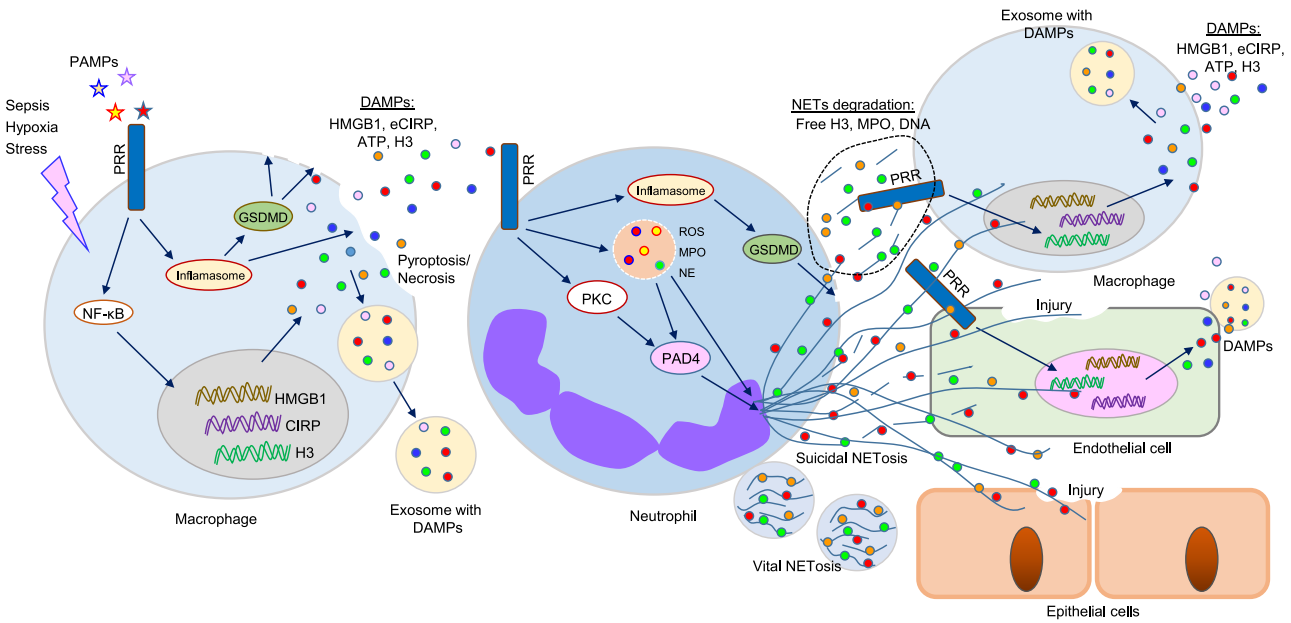

FIGURE 1 | Cross talks between DAMPs and NETs in sepsis. Sepsis or hypoxia activates immune reactive cells, including macrophages, and neutrophils. In bacterial sepsis, PAMPs interact with PRR on macrophages to activate NF-κB, leading to increased expression of DAMPs (HMGB1, CIRP, H3) at transcriptional and translational levels. These intracellular DAMPs are then released extracellularly through different mechanisms, such as inflammasome-mediated GSDMD activation, which causes increased membrane pore formation to release intracellular DAMPs, or pyroptosis-, necroptosis-, or exosome-mediated pathways. These DAMPs can in turn recognize PRR on surrounding neutrophils and activate PAD4, GSDMD to promote NET formation. NETs components such as H3, MPO, or DNA can further activate immune cells and endothelial cells to release increased levels of DAMPs to augment the inflammatory cascade. In epithelial cells, extracellular histones derived from NETs promote cell/tissue injury, resulting in increased severity of ALI. DAMPs, damage-associated molecular patterns (DAMPs); NETs, neutrophil extracellular traps; PAMPs, pathogen-associated molecular patterns; PRR, pattern recognizing receptors; GSDMD, gasdermin D; HMGB1, high mobility group box 1; CIRP, cold-inducible RNA-binding protein; PAD4, peptidoglycan arginine deiminase 4; ALI, acute lung injury.

eCIRP

Extracellular CIRP is an 172-amino acid RNA chaperone protein (26, 58–60) that was previously identified as a DAMP in 2013 (43). It is a cold shock protein, originally recognized as a protein that suppresses mitosis and promotes cell differentiation in the setting of hypothermia (61). It is upregulated by hypothermia, hypoxia, and oxidative stress, such as UV irradiation. In addition to passive release during necrotic cell death, in times of cellular stress (like the aforementioned hypothermia, hypoxia, or oxidative stress), CIRP can translocate from the nucleus to cytoplasmic stress granules; from these, it is released to the extracellular space (62). After eCIRP binding to its receptor, the TLR4-myeloid differentiation factor 2 (MD2) receptor complex (43), activation proceeds through the TLR4/MyD88/NF-κB pathway (63) to stimulate the release of pro-inflammatory cytokines TNF-α and HMGB1 from macrophages (43). Furthermore, during sepsis, hemorrhage or ischemia-reperfusion (I/R) injury, CIRP is released extracellularly and leads to organ injury (36, 43). Elevated plasma levels of eCIRP have been independently correlated with a poor prognosis in patients with sepsis (13).

eCIRP as a DAMP has been demonstrated in several cell types including macrophages, lymphocytes, and neutrophils in the context of cellular activation, cytokine and chemokine production and neutrophil extracellular trap (NET) formation (44). eCIRP has also been shown to stimulate the Nlrp3 inflammasome, cause endoplasmic reticulum (ER) stress, and induce pyroptosis in lung endothelial cells (EC) (64, 65). eCIRP is associated with acute lung injury (ALI). Healthy mice injected with recombinant murine (rm) CIRP develop ALI via macrophage, neutrophil, and EC activation, and cytokine production in the lungs (65). Beneficial outcomes have been seen in CIRP$^{-/-}$ mice or CIRP inhibition in murine models of renal, intestinal, and hepatic I/R injury (36, 66, 67). CIRP$^{-/-}$ mice are protected from sepsis and ALI (64, 65). In an animal models of adult or neonatal sepsis, treatment with a polyclonal anti-CIRP antibody or a CIRP-derived inhibitory peptide prolonged survival and attenuated organ injury (43, 68, 69).

HISTONES

Histones are highly basic proteins that are located mainly in the nucleus. In humans, histone H2A, H2B, H3, and H4 form a complex with DNA, called a nucleosome. The nucleosome regulates gene transcription and facilitates efficient higher-order chromatin compaction (22). However, histones

TABLE 1 | Therapeutic outcomes by targeting DAMPs and NETs in sepsis.

DAMPs/NETs	Strategies	Outcomes	References
eCIRP	CIRP$^{-/-}$ mice; Anti-CIRP Ab; C23	Decreased organ injury markers (AST, ALT, LDH), decreased cytokines and chemokines, protected from lung injury including decreased MPO levels, neutrophil infiltration, and cellular apoptosis in lungs.	(4)[ab], (43)[a,b], (68)[a], (69)[a]
HMGB1	Anti-HMGB1 Ab; Zingerone; HMGB1-antagonsits interacting with RAGE; small molecule inhibitors of HMGB1; sodium sulfonate derivative of tanshinone IIA (TSNIIA-SS); synthetic molecules including nafamostat mesylate and gabexate mesylate; peptide inhibitors including vasoactive intestinal peptide, pituitary adenylate cyclase-activating polypeptide (PACAP), and urocortin	Increased survival after endotoxemia and CLP, improved cytokine profile after CLP sepsis, inhibited LPS-induced HMGB1 secretion, reduced vascular permeability, reduced expression of cellular adhesion molecules, reduced sepsis-mediated liver injury, reduced LPS-mediated cytokine release and lung injury.	(56)[a,b], (57)[a], (25)[ab]
Histone	Anti-histone ab; Activated Protein C	Increased survival in LPS, TNF-α, and CLP sepsis, rescued from lethality in E. coli infusion, attenuated cardiac injury and dysfunction in sepsis.	(71)[c], (73)[b]
ATP	P2X7 receptor blockade $^{+/-}$ adenosine A_{2A} receptor stimulation; ATP hydrolase (apyrase)	Prevented tissue damage, apoptosis, and cytokine production in the liver of mice after CLP, reduced cytokines, prevented mitochondrial damage, reduced apoptosis, reduced intestinal barrier disruption, increased survival.	(89)[a], (90)[a]
NETs	DNAse I; PAD4$^{+/-}$ mice; CL-Amidine; Anti-citrullinated histone 3 Ab	Reduced lung injury and increased survival in a pneumonia model, reduced NETs and improved survival in CLP sepsis.	(135)[ab], (180)[a], (185)[a]

[a]*Rodent,* [b]*Human,* [c]*Non-human primates.*

play proinflammatory functions upon their release from the nucleus into the extracellular environment (23). Histone release from cells can occur passively after cellular necrosis or as part of an active process such via NETosis (70). In 2009, Xu et al. demonstrated that histones were cytotoxic when added to cultured endothelial cells (71). *In vivo,* intravenous injection of histones in mice was lethal, whilst anti-histone antibodies were found to reduce mortality in murine models of LPS endotoxemia, TNF-α, or cecal ligation, and puncture experimental models of murine sepsis (71). Xu subsequently demonstrated that the injection of sublethal doses of histones resulted in high levels of the cytokines TNF-α, IL-6, and IL-10, a phenomenon which did not occur when TLR4$^{-/-}$ mice were used. Conversely, TLR2$^{-/-}$ mice maintained their hyperinflammatory profiles after histone injection (72). However, using specific TLR-transfected HEK cells, histones signaling was transduced via both TLR4 and TLR2 (72). Histones have also been shown to bind to TLRs in cardiomyocytes where they alter levels of regulatory proteins and potentiate sepsis-induced cardiomyopathy (27). The impact of histones has also been investigated in human sepsis. *Ex-vivo* administration of serum from septic patients directly induced cardiomyocyte death; this effect was abolished by anti-histone antibody (73). Histone levels in septic patients are significantly increased and, like in murine models, appear to cause cellular injury in a TLR4 dependent method (14).

CELL FREE DNA

In the extracellular space, deoxyribonucleic acid (DNA) can serve as a DAMP. Apoptosis, necroptosis, NETosis, and pyroptosis can all contribute to the release of nuclear contents into the extracellular space (74). Cell free DNA in plasma is elevated in patients with severe sepsis or septic shock when compared to patients without these diagnoses (28), and increased levels of cell free DNA in the plasma of septic patients has been linked to increased mortality during sepsis (75).

Viral, bacterial, and even host cell free DNA can all function as a DAMP and initiate pro-inflammatory cascades (74, 76). Additionally, mitochondrial DNA (mtDNA) has been proven to be a DAMP; it is released into the circulation during trauma or sepsis (77, 78). mtDNA has been shown to cause TNF-α secretion by mouse splenocytes and IL-1β release from bone marrow-derived macrophages (79). In addition to promoting the release of proinflammatory cytokines, DNA has been shown to prolong the lifespan of neutrophils. Neutrophils stimulated with either purified bacterial or mitochondrial DNA demonstrated increased viability compared to controls (78). Excessive neutrophil accumulation in tissues has been associated with poor outcomes in sepsis (80).

Viral, bacteria, host cell free DNA, and mtDNA can all act via the TLR9 receptor (74), which is located intracellularly in endosomes (81). It is important to recognize the spatial relationship of DNA that acts as an immunomodulatory molecule and the TLR9 receptor. TLR9's intracellular location requires that nuclear DNA molecules that are released into the extracellular space by NETosis, apoptosis and other forms of cell death need to be translocated intracellularly in recipient cells in order to activate the TLR9 receptor (74). Besides TLR9, intracellular DNA can trigger other alarmin sensors such as cyclic guanosine monophosphate-adenosine monophosphate synthase (cGAS), absent in melanoma 2 (AIM2), interferon-inducible protein 16

(IFI16), and stimulator of interferon genes (STING), all of which lead to the initiation of immune responses (74).

ATP

ATP is a nucleotide that, in times of homeostasis, is generated mainly within mitochondria during the tricarboxylic acid cycle and from the respiratory chain. ATP is also produced in the cytoplasm during glycolysis (82). ATP is released actively from dying cells during apoptosis, and passively during necroptosis and cellular necrosis (38, 83). Although some extracellular ATP is beneficial, as it functions as a chemoattractant recruiting phagocytic cells to the site of tissue damage, extracellular ATP is also detrimental, binding to ionotropic P2X receptors (P2XR) (84). P2XR channel opening results in increases in intracellular calcium, which activates the p38 MAPK pathway, activating the inflammasome with the associated caspase-1 activation and release of pro-inflammatory cytokines IL-1β and IL-18 (84–86). Elevated ATP levels in the plasma of septic patients interfere with neutrophil function and signaling, resulting in an excessive and uncoordinated neutrophil activation (87). Excessive extracellular ATP has also been associated with T cell suppression in sepsis (88). Reduction in the extracellular levels of ATP has proven to be an effective method of attenuating sepsis severity in some murine models of sepsis. Removal of extracellular ATP to decrease activation of the P2X7 receptor by CD39 has been shown to attenuate sepsis-induced liver injury (89). Treatment with apyrase, an ATP hydrolase that removed extracellular ATP, protected mice against a lethal LPS challenge and resulted in a reduction of serum cytokines (90).

MOLECULES THAT MAY OR MAY NOT BE DAMPs

Several endogenous molecules located intracellularly or on the cell surface are released into the circulation and serve as diagnostic and prognostic markers in various inflammatory diseases (4, 29). These molecules include components of the extracellular matrix (ECM) like collagen, fibrinogen, and laminin and shredded cell surface receptors, such as soluble ST-2(30), a member of the interleukin 1 receptor family, sMD2(91), sTREM-1(92), microRNAs (93), exosomes (94), and vesicles (95). However, it is not clear whether these and similar molecules should be classified as DAMPs (**Figure 2**). DAMPs are frequently released from cells following necrosis, pyroptosis or apoptosis, however the ECM, shredded receptors, exosomes, micro-vesicles are released into the extracellular environment without cell lysis. Conversely, mtDNA and cell-free DNA are classified as DAMPs and are released in both suicidal and vital NETosis, meaning a molecule can be classified as a DAMP without cell lysis first occurring. Many DAMPs undergo structural modification (96, 97) e.g., oxidation, reduction, acetylation, phosphorylation, or cleavage after release into the circulation. Conversely, it is not known whether the shredded receptors or exosomal molecules undergo post release modification in the extracellular milieu. Extracellularly, DAMPs play largely pro-inflammatory roles, while the secreted proteins, cleaved receptors, exosomes and vesicles are not always pro-inflammatory and are not necessarily responsible for excessive inflammation (98). Cell surface proteins that are shed have diverse functions and include chemokines, cytokines, adhesion molecules, growth factors, and their receptors (99).

The shedding process of these proteins regulates the density of cell surface receptors, the release of factors that serve as agonists, and the release of soluble receptors that can function as antagonists (100). Cleaved receptors such as sTREM-1 acts as a decoy receptor, sequestering TREM-1-ligands and dampening TREM-1 activation (101, 102). Soluble ST-2 serves as an antagonist for IL-33 to control excessive innate immune response (103). Exosomes, macrovesicles, and microparticles are enriched in pro- and anti-inflammatory molecules, therefore they may play dual roles in sepsis. LPS-challenged macrophages have been shown to release histone-coated microvesicles to cause inflammation (104). Exosomes released from alveolar macrophages during hemorrhagic shock have been shown to promote necroptosis (105). By contrast, exosomes filled with anti-inflammatory molecule milk fat globule-EGF-factor-8 (MFG-E8) were shown to be beneficial in reducing markers of inflammation in sepsis and improving survival (106). Cleaved receptors or exosomes often directly serve as chemoattractants (107), but the ability of DAMPs to directly serve as a chemokine are not as well studied.

Excess production and release of ECMs may cause tissue fibrosis, abnormal cell proliferation, migration and inflammation (108). Receptor protein cleavage occurs due to the actions of matrix metalloproteinases (MMPs), disintegrins, and metalloproteinases (ADAMs) which are upregulated during inflammation (109). The exosomes and microvesicles are released from the cells through pore formation in the plasma membrane by caspase-mediated GSDMD or by a budding out process (110). The release of excess amount of exosomes and microvesicles are correlated with an increased release of DAMPs, allowing the possibility that exosomes and microvesicles may be a mechanism of DAMP release in sepsis (111). Exosomes and microvesicles may also serve as a means to maintain cell to cell communication; they have the ability to enter into adjacent cells and modulate function. Extracellular microRNAs levels are increased in various inflammatory conditions and may serve as diagnostic markers (112). Studies have shown that extracellular microRNA plays a pro-inflammatory role following its re-entry into macrophages and activation of the endosomal TLR7 receptor to produce TNF-α and IL-6 (113).

More studies on these molecules will help elucidate their pathophysiological role in sepsis and other inflammatory conditions. This information will aid in clarification of these molecules as DAMPs or non-DAMPs.

NETs

Neutrophils are phagocytic cells; they predominantly defend against pathogens either by engulfing the offending cell and destroying it via oxidant- or protease-dependent mechanisms

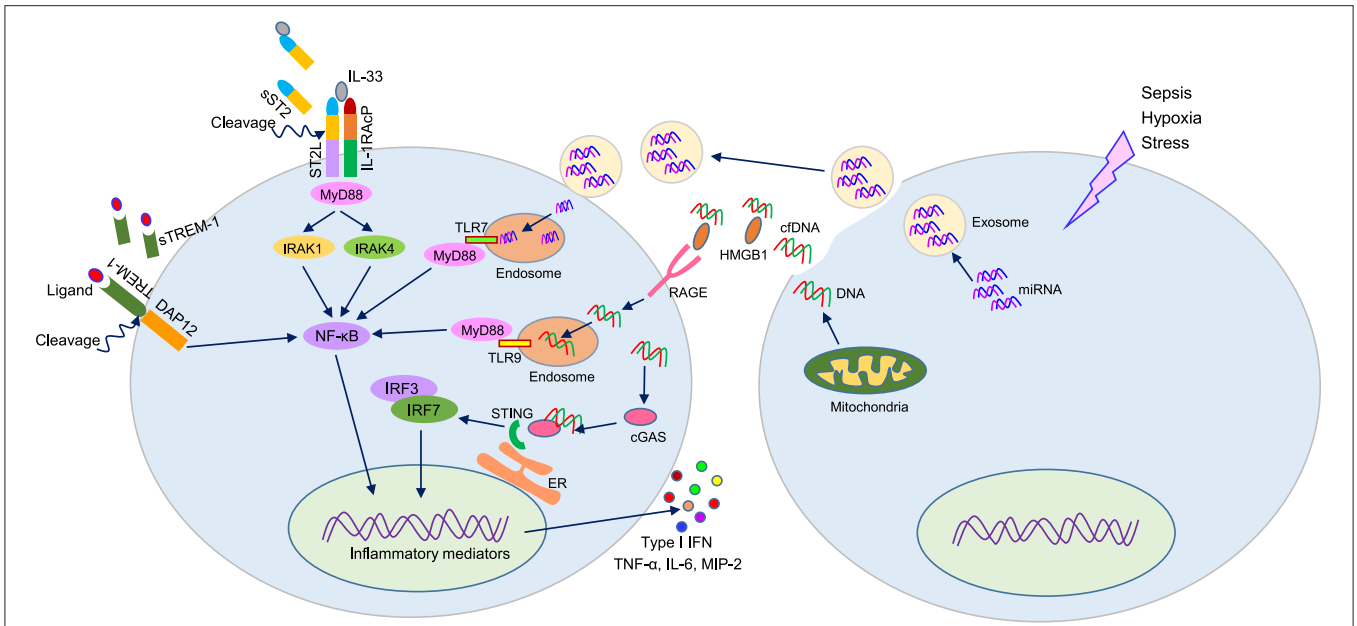

FIGURE 2 | DAMPs or not DAMPs? In sepsis, extracellular motifs of several receptors like TREM-1, ST2 are cleaved by matrix metalloproteinases, leading to increased accumulation of truncated receptors in the blood. These soluble receptors serve as decoy molecules to recognize their ligands, thereby modulating respective intracellular signal transduction. During sepsis, cells release miRNA or cfDNA through exosomes or passively. Extracellular miRNAs can enter into adjacent cells and recognize endosomal TLR7 to induce inflammation. cfDNA can recognize HMGB1, and this protein-DNA complex is then recognized by the RAGE receptor and become internalized. Intracellular cfDNA then can activates endosomal TLR9 or STING to activate the production of pro-inflammatory mediators. DAMPs, damage-associated molecular patterns (DAMPs); TREM-1, triggering receptor expressed on myeloid cells-1; HMGB1, high mobility group box 1; cfDNA, cell-free DNA; STING, stimulator of interferon genes.

or by the secretion of anti-microbial peptides (114). This classical understanding of neutrophil function was found to be incomplete after the discovery of a third effector function of neutrophils in 2004, the release of NETs (17). NETs are web-like chromatin based structures that are released into the extracellular environment to aid in pathogen clearance, but they have also been implicated in excessive inflammation with resultant tissue damage, potentiation of autoimmunity, and promotion of vascular thrombosis (16). NETosis is a form of cellular death in which neutrophils decondense their nuclear chromatin and DNA into the cytoplasm. Chromatin and DNA mix with granule-derived antimicrobial peptides and are extruded into the extracellular space (115). NETosis can be induced in many ways; one of the most well-described is phorbol myristate acetate (PMA), a protein kinase C (PKC) activator (116).

NETs contain proteins from azurophilic granules e.g., neutrophil elastase (NE), myeloperoxidase (MPO) and cathepsin G; proteins from secondary and tertiary granules e.g., lactoferrin, and gelatinase; and nuclear proteins e.g., histones H1, H2A, H2B, H3, and H4 (117). Detection of NETs has proved challenging due their fragile structure, timing of NET formation and turnover, and ubiquitous presence of DNase I. Several tools to assay NETosis have been reported: these include microscopy (118), flow cytometry (119, 120), ImageStream® (121), and ELISA (122). The ability to detect NETs precisely is paramount to studying the disease pathophysiology associated with NETosis.

MECHANISM OF NET FORMATION

The first reported descriptions of NETs demonstrated that neutrophils stimulated with PMA, IL-8 or LPS released NETs (17). Subsequent studies have revealed a wide range of stimuli including bacteria, virus, fungi, yeast, parasites, and concanavalin A are capable of inducing NET formation (20). In addition, NETs are upregulated in various cancers, including pancreatic cancer, through receptor for advanced glycation end products (RAGE)-dependent and neutrophil autophagy mediated pathways (123). The induction of NETosis by various DAMPs will be discussed in the later part of this article.

Two forms of NETosis have been described: suicidal NETosis, in which NET formation only occurs via neutrophil cell death and was described above, and vital NETosis where NETs are released without cell death (124). In suicidal NETosis, NADPH-dependent ROS production is a prerequisite. This leads to increased calcium influx and peptidyl arginine deaminase 4 (PAD4) activation, leading to chromatin decondensation. Elastase and MPO are also transported from the granules to the nucleus to cleave linker histone H1 and modify the core histones. MPO also intensifies chromatin decondensation, through the synthesis of hypochlorous acid. Finally, chromatin is released outside the cell through membrane pores and cellular lysis through the activation of a pore forming protein GSDMD (125, 126).

First described in 2012, vital NETosis results in the release of NETs without a loss in the integrity of the nuclear or plasma membrane (127). As such, neutrophils are able to survive the process and are still capable of normal neutrophil functions including phagocytosis. Unlike suicidal NETosis, vital NETosis does not require generation of ROS or activation of the Raf/MERK/ERK pathway (126). In contrast to the several hour time frame required for stimulation of suicidal NETosis, vital NETosis occurs quickly, usually within 5 to 60 min after neutrophil are stimulated (128). In vital NETosis, after neutrophil stimulation, typically via TLR or complement receptor for C3 protein ligand binding, the nuclear membrane morphology changes to allow vesicle budding. These vesicles, containing nuclear DNA, move through the cytoplasm to coalesce with the plasma membrane and are released extracellularly (118, 124, 126).

Besides the aforementioned types of NETosis, in 2009 it was reported that neutrophils are able to undergo vital NETosis using mitochondrial DNA (129). GM-CSF primed neutrophils, when activated via TLR-4 or complement factor 5a receptor stimulation, generated NETs containing solely mitochondrial DNA. NETosis facilitated release of mitochondrial DNA seems to be ROS-mediated (129). *In vivo*, NETs containing mitochondrial DNA have been found in the serum of individuals after trauma (130) and associated orthopedic surgery (131).

Several other mechanisms of NET formation have been reported. Carestia et al. demonstrated that activated platelets are able to amplify the amount of NETs released from neutrophils (132). This process seemed to depend on interaction between glycoprotein Ib (CD42) in platelets with β2 integrin (CD18) in neutrophils, as well as the release of von Willebrand Factor. Platelet triggered NETosis did not rely on NADPH oxidase or ROS generation, but was reduced when inhibitors of ERK, PI3K, or Src kinases were used (132). NET formation has been shown to depend on the activation of cell-cycle proteins CDK4/6; $Cdk6^{-/-}$ neutrophils and mice showed impaired NET formation to several stimuli including PMA and C. albicans (133). The lipoxin pathway has been shown to reduce lung inflammation and acute lung injury after both infectious and sterile inflammation (134). Lefrancais et al. demonstrated that this pathway, through Fpr2 receptor signaling, is a potent modulator of NET formation. After intratracheal injection of methicillin-resistant Staphylococcus aureus (MRSA), $Fpr2^{-/-}$ mice produced excessive NETs compared to wild type mice (135). Additional studies are needed focusing on the pathways behind these types of NET formation to determine the type of NETosis-suicidal or vital.

PHENOTYPIC AND FUNCTION DIVERSITIES OF NEUTROPHILS AND NET FORMATION

Neutrophils exhibit phenotypic and functional heterogeneity (136). Neutrophil heterogeneity has tremendous impact on NET formation. Neutrophils from diabetic patients are more likely to undergo NETosis than neutrophils from euglycemic patients (31). Neutrophils from pediatric patients with systemic lupus erythematosus also undergo increased NETosis as compared to their healthy counterparts (137). ICAM-1 (CD54) is mainly expressed on the endothelial cell surface (138). Following simulation of neutrophils with PAMPs or DAMPs, ICAM-1 expression in the neutrophils is dramatically increased (139–141). The ICAM-1^{+} neutrophils produce higher levels of NETs, probably because of increased ROS (140). However, the involvement of ICAM-1 or its ligand Mac-1 in the increased levels of NETs in these cells has not been elucidated. The relationship seems to be circular, with NETs inducing ICAM-1 in neutrophils and ICAM-1^{+} neutrophils producing increased quantities of NETs (142). ICAM-1^{+} neutrophils are found in increased concentrations in blood and lungs of humans and mice under inflammatory conditions (143–146).

It is still not clearly known which type of neutrophils-circulating or tissue resident-produce increased levels of NETs. Using density gradient centrifugation, circulating neutrophils can be separated into two layers- high density neutrophils (HDN) and low-density neutrophils (LDN) which co-localize with peripheral blood mononuclear cells (147). LDN are a heterogeneous population containing both immature and mature neutrophils and their functions differ depending on the inflammatory stimulus (148, 149). Interestingly, it has been demonstrated that LDNs have an increased proinflammatory profile as compared to other neutrophils with increased secretion of proinflammatory cytokines (150, 151) and an increased capacity to generate NETs (149, 152, 153).

Since the ROS pathway is essential for suicidal NETosis (125), it is logical that neutrophils that produce increased levels of ROS may produce excessive NETs. Although evidence is conflicting (154), Zhang et al. found that aged neutrophils (CXCR4^{+}) produced both increased levels of ROS and increased amounts of NETs (155). It is also evident that human neutrophils are more prone to produce NETs compared to murine neutrophils (156, 157), indicating the role of specific surface markers in NETs production between these species. Overall, neutrophil heterogeneity may play a pivotal role in NET formation.

INCREASED NET FORMATION IN SEPSIS

NETs are vital to pathogen clearance, but simultaneously NETs induce collateral damage to host tissues in sepsis (16). In 2007, Clark et al. described an interaction between platelets and neutrophils in sepsis, resulting in NET formation and enhanced bacterial trapping in blood vessels (158). Activation of TLR4 receptors on platelets lead to the binding of the platelets to neutrophils in the blood. These neutrophils were then activated and produced NETs. These results were recapitulated using the plasma from severely septic patients (158).

Sepsis often results in acute lung injury (ALI) (159). Lefrancais et al. demonstrated abundant NET formation in both murine models of severe bacterial pneumonia and ALI (135). Furthermore, when comparing NET levels in samples from critically ill human subjects they found higher levels of NETs in subjects with infectious etiology of acute respiratory

distress syndrome (ARDS) as opposed to patients with cardiac-induced respiratory dysfunction. In addition, among patients with microbiologically confirmed pneumonia, plasma NET levels were higher in patients with ARDS than in patients without. Finally, there was a correlation between the severity of ARDS, mortality, and the serum level of NETs (135).

In a clinical study, the levels of neutrophil-derived circulating free DNA (cf-DNA/NETs) have been shown to directly correlate with multiple organ dysfunction score, sepsis-related organ failure assessment, leukocyte counts, and MPO levels (160). A 2018 study of 55 critically ill patients demonstrated rapid and sustained increases in the circulating levels of MPO-DNA complex in the serum, indicating NET formation in the early stages of sepsis. In this study, MPO-DNA complex levels were also correlated with the severity of organ dysfunction and 28-day mortality rates (161).

In opposition to these findings, impaired NET formation in neonates has been associated with relative immunodeficiency of human newborns (162). Czaikoski et al. found increased bacterial burden in the blood and decreased survival in a murine model of CLP in mice treated with DNase to prevent NET formation, however these effects were ameliorated by treatment with DNase plus antibiotics (163). Given that there are both hyper and hypodynamic phases of sepsis, the levels of NETosis at various stages in sepsis may impact the outcomes. This idea is supported by work done by Mai et al. (164). They found that when given early after induction of sepsis by CLP, DNase increased pro-inflammatory cytokines and worsened renal and pulmonary damage. However, when given at a later timepoint after CLP, DNase administration reduced IL-6 levels, increased levels of anti-inflammatory IL-10, and reduced organ damage and bacterial dissemination. It also increased survival after CLP (164).

Several studies have demonstrated that severe sepsis alters the neutrophil phenotype and hinders NETosis *ex vivo* (165, 166). However, it is not clear from these studies whether *in vivo* NET formation is impaired during sepsis. Further investigation will need to be done in this area.

DETRIMENTAL EFFECTS OF NETs IN SEPSIS

During sepsis, neutrophil-endothelial interaction is increased to promote neutrophil infiltration into tissues (167). Neutrophil-endothelial cell (EC) interaction leads to increased NET formation; this increased NET formation is partially dependent on IL-8 released from activated EC (168). Prolonged co-culture of neutrophils with EC resulted in EC damage; this damage is attributed to NETs as co-incubation with either NAPDH oxidase inhibitors or DNase ameliorated this damage (168).

Recent studies demonstrated the crucial role of NETs in the pathogenesis of disseminated intravascular coagulation and intravascular thrombosis, both of which increase morbidity and mortality in sepsis (169–173). McDonald et al. found profound platelet aggregation, thrombin activation, and fibrin clot formation within NETs, implicating the NET–platelet–thrombin axis in the promotion of intravascular coagulation in sepsis. Inhibition of NETs during sepsis by DNase infusion reduced intravascular coagulation, improved microvascular perfusion, and reduced organ damage (172).

NETs have been detected in bronchoalveolar lavage samples from septic humans or canines with ARDS, indicating that, even after transmigration, neutrophils are capable of undergoing NETosis (174, 175). A recent study utilizing samples from different models of ALI in mice and from patients with ALI revealed increased levels of NETs and histones H3 and H4 in the bronchoalveolar lavage fluids (BALF) (176). Administration of the extracellular histones contained in NETs resulted in damage to alveolar epithelial cells and increased severity of ALI (176).

In addition to the damage inflicted by the DNA released during NETosis, enzymes released during NETosis also have a detrimental effect on the surrounding tissues. Neutrophil elastase, a key component of chromatin degranulation, has been show to increase permeability of alveolar epithelial cells by altering the actin cytoskeleton (177) and its inhibition has been demonstrated to be beneficial in animal models of inflammation and associated ALI (178, 179). Serine proteases released during NETosis have been shown to degrade surfactants which are vital in the clearance of inflammatory cells and residual inflammation after ALI (18). These findings clearly demonstrate that excessive NETs play detrimental role in sepsis.

THERAPEUTIC STRATEGIES TARGETING NETs IN SEPSIS

Therapeutic strategies aimed at NETs primarily target the DNA component- DNase is the most frequent treatment modality. DNase treatment reduced NETs, improving lung injury and survival in a murine model of pneumonia (135). Cl-Amidine, a PAD4 inhibitor, had no effect on the level of neutrophil-DNA complexes or the degree of lung inflammation in a murine pneumonia model (135) but Biron et al. found that Cl-Amidine prevented H3 citrullination, NET formation, and improved survival in a murine model of CLP-induced polymicrobial sepsis (180). Similarly, $PAD4^{-/-}$ mice demonstrated decreased NETs and lung injury in the pneumonia model (135). However, these benefits were offset by an increased bacterial load and increased systemic inflammation. Therefore, Lefrancais et al. developed a mouse with a partial PAD4 deficiency ($PAD4^{+/-}$) which demonstrated an improved survival curve (135). These findings support the notion that a there is a thin line for the amount of NETosis required to both prevent lung injury and maintain microbial control.

Chloroquine has also been effective as an early upstream inhibitor of NETs, decreasing NETosis and the associated hypercoagubility and improving survival in murine models of pancreatic adenocarcinoma (181) and acute pancreatitis (32). Activated protein C (APC) is a multifunctional protease with anti-inflammatory, anticoagulant, and cytoprotective properties (182). A recent study demonstrated that APC binds human leukocytes and prevents activated platelet supernatant or PMA from inducing NETosis. Additionally, they found that pretreatment of neutrophils with APC prior to induction of

NETosis inhibited platelet adhesion to NETs (182). It should be noted however, that activated protein C has failed to have any impact on survival in large scale human clinical trials of patients with severe sepsis (183, 184). Li et al. demonstrated that antibodies neutralizing serum citrullinated Histone 3 could improve survival after a murine CLP model (185). These studies demonstrate that abrogating excessive NET formation can lead to beneficial outcomes in sepsis.

The early inhibitors of NETs such as chloroquine, PAD4 inhibitors, and APC are specifically targeted for controlling NET formation. By contrast, late inhibitors of NETs, such as DNase and anti-histone antibodies, can target extracellular DNA or histones regardless of their source. These molecules are also considered as DAMPs and can be released by a number of immune cells, in addition to their release from neutrophils. Therefore, the molecules/drugs that specifically control intracellular NET formation could be used as a more specific therapeutic regimen against NETs.

CROSSTALK BETWEEN DAMPs AND NETs IN SEPSIS AND INFLAMMATION

Although the extracellular release of DAMPs and NET formation are both a byproduct of sepsis, there is increasing evidence of linkage between the two. The major components of NETs, i.e., DNA, histones, and granule proteins- are recognized as DAMPs that can trigger inflammation, inducing cell death and organ failure. Extracellular histones are elevated in patients with coagulopathy and multiple organ failure (186) and are believed to be a major mediator of death in sepsis (71). Cell free DNA has been shown to be cytotoxic and results in coagulopathy and disseminated intravascular coagulation (DIC) (33) Additionally, inhibition of NETosis via PAD4 deficiency or inhibition results in a reduction in the release of DNA and improves outcomes in sepsis (187–189).

Concomitantly, various DAMPs have been shown to induce NETosis. Tadie et al. demonstrated that HMGB-1 is able to induce NETosis via TLR4 signaling (190). Incubation of neutrophils with HMGB-1 resulted in increased extracellular DNA, histone 3, and histone 3 citrullination. Exposure of neutrophils isolated from wild type and RAGE KO mice to HMGB1 resulted in significant NET formation, whereas neutrophils from TLR4 KO mice demonstrated a diminished ability to form NETs. Finally, HMGB1 acted synergistically with LPS, as neutrophils from the bronchoalveolar lavage (BAL) of mice exposed to both LPS and HMGB1 displayed greater ability to produced NETs compared to neutrophils isolated from the BALs of mice that received LPS alone. This increase was hindered by a neutralizing antibody to HMGB1 (190).

eCIRP has also been shown to activate NETosis through a TLR4/NF-κβ dependent mechanism (140). Mice subjected to polymicrobial sepsis via cecal ligation and puncture demonstrated increased levels of ICAM-1^+ neutrophils in both the blood and the lungs. In contrast, mice genetically deficient in CIRP displayed diminished levels of ICAM-1^+ neutrophils. *In vitro,* treatment of neutrophils with recombinant murine CIRP (rmCIRP) increased levels of ICAM-1^+ neutrophils, and this increase was inhibited by both a neutralizing antibody to TLR4 or an NF-κβ inhibitor. ICAM-1^+ neutrophils displayed increased levels of NETosis (140).

Unlike eCIRP and HMGB1, mitochondrial DNA (mtDNA) seems to generate NETosis through a TLR9 dependent pathway. mtDNA induced NADPH oxidase-independent NET formation in polymorphonuclear neutrophils of healthy volunteers. NETosis was completely inhibited by treatment with a TLR9 inhibitor (130). Liu et al. further identified that mtDNA also activates NETosis via the STING pathway (191). Neutrophils treated with mtDNA demonstrated increased NETosis in a manner which displayed significant increases of AKT and ERK1/2 phosphorylation and increased expression of Rac2 and PAD4. They further confirmed that both TLR9 and STING pathways are important in mtDA-induced NETosis via examination of the lungs of mice intravenously injected with mtDNA (191). Lungs displayed decreased NET formation in TLR9 KO and STING KO mice compared to wild type mice. Additionally, *in vitro* stimulation of BMDN from TLR$9^{-/-}$ and STING$^{-/-}$ mice displayed decreased percentages of NETs after treatment with mtDNA as compared to WT mice (191). Further confirming that mtDNA-induced NETosis proceeds through the Raf/MEK/ERK and p38 MAPK pathways, TLR$9^{-/-}$ and STING$^{-/-}$ neutrophils exhibited decreased phosphorylation of ERK 1/2 and p38 MAPK, as well as decreased levels of PAD4 and Rac2 after stimulation with mtDNA than WT neutrophils did. Inhibitors of these downstream mediators resulted in decreased mtDNA-induced NET formation in WT neutrophils (191).

Oxidized low-density lipoproteins (oxLDL) are upregulated in sepsis and intestinal inflammation (192) and have been recognized as a DAMP (193). *In vitro* treatment of PMNs with oxLDL resulted in increased NET formation in a dose dependent manner. oxLDL stimulation of NETosis seems to depend on TLR2 and 6; blocking of neutrophils with a TLR4 antibody had no effect on NET formation, while blocking with anti-TLR2 or TLR6 antibodies modestly reduced NETosis. However, the combination of anti-TRL2 and anti-TLR6 antibody treatment of PMNs prior to oxLDL stimulation resulted in a significant reduction in the formation of NETs (194). Additionally, confirming the role of the PKC pathway in oxLDL-induced NETOsis, inhibition of PKC or IRAK was able to reduce NET formation in normal neutrophils. Inhibition of downstream mediators in the pathway, ERK1/2 and p38 MAPK, also reduced oxLDL-induced NET formation (194).

FUTURE DIRECTIONS AND CONCLUSIONS

In this review article, we discussed DAMPs and NETs in sepsis, with a focus on their interaction and therapeutic strategies for amelioration of sepsis-associated morbidity and mortality.

Future studies on the interaction between the two entities would add value to the study of innate immunology and could be expanded to other inflammatory conditions in addition to sepsis. Moreover, future emphasize should also be focused on pinpointing the relationship between PAMPs and NETs and developing new therapeutic tools to target their interplay. DAMPs are released by several cell types, while NETs are specific to neutrophils. Recently, extracellular traps (ETosis) has been described in macrophages (195) and eosinophils (196). Future studies on DAMPs and ETosis would be interesting. Immune cells in sepsis are very plastic with several phenotypic polarizations—more investigation is needed into the role of immune cell plasticity on DAMP release. Similarly, future studies on how DAMPs skew immune cell polarization and the subsequent impact on sepsis would be revealing. In conclusion, we have provided a literature review of the role of DAMPs, NETs, and their interaction in sepsis to increase and update our understanding in this area of research.

AUTHOR CONTRIBUTIONS

N-LD and MA did literature review and wrote the manuscript. SG helped in writing the extracellular DNA section and reviewing the manuscript. N-LD prepared the table and MA prepared the figures. PW reviewed, edited the manuscript, and conceived the original idea of the project.

FUNDING

This study was supported by the National Institutes of Health (NIH) grant R35GM118337 (PW) and R01GM129633 (MA).

REFERENCES

1. Rhee C, Jones TM, Hamad Y, Pande A, Varon J, O'Brien C, et al. Prevalence, underlying causes, and preventability of sepsis-associated mortality in US acute care hospitals. *JAMA Netw Open*. (2019) 2:e187571. doi: 10.1001/jamanetworkopen.2018.7571
2. Singer M, Deutschman CS, Seymour CW, Shankar-Hari M, Annane D, Bauer M, et al. The third international consensus definitions for sepsis and septic shock (Sepsis-3). *JAMA*. (2016) 315:801–10. doi: 10.1001/jama.2016.0287
3. Fleischmann C, Scherag A, Adhikari NK, Hartog CS, Tsaganos T, Schlattmann P, et al. Assessment of global incidence and mortality of hospital-treated sepsis. current estimates and limitations. *Am J Respir Crit Care Med*. (2016) 193:259–72. doi: 10.1164/rccm.201504-0781OC
4. Aziz M, Jacob A, Yang WL, Matsuda A, Wang P. Current trends in inflammatory and immunomodulatory mediators in sepsis. *J Leukoc Biol*. (2013) 93:329–42. doi: 10.1189/jlb.0912437
5. Cabrera-Perez J, Badovinac VP, Griffith TS. Enteric immunity, the gut microbiome, and sepsis, Rethinking the germ theory of disease. *Exp Biol Med*. (2017) 242:127–39. doi: 10.1177/1535370216669610
6. Gentile LF, Moldawer LL. DAMPS, PAMPS and the origins of SIRS in bacterial sepsis. *Shock*. (2013) 39:113–4. doi: 10.1097/SHK.0b013e318277109c
7. Takeuchi O, Akira, S. Pattern recognition receptors and inflammation. *Cell*. (2010) 140:805–20. doi: 10.1016/j.cell.2010.01.022
8. Matzinger P. Tolerance, danger, and the extended family. *Annu Rev Immunol*. (1994) 12:991–1045. doi: 10.1146/annurev.iy.12.040194.005015
9. Seong SY, Matzinger P. Hydrophobicity: an ancient damage-associated molecular pattern that initiates innate immune responses. *Nat Rev Immunol*. (2004) 4:469–78. doi: 10.1038/nri1372
10. Rubartelli A, Lotze MT. Inside, outside, upside down: damage-associated molecular-pattern molecules (DAMPs) and redox. *Trends Immunol*. (2007) 28:429–36. doi: 10.1016/j.it.2007.08.004
11. McCarthy G, Goulopoulou S, Wenceslau CF, Spitler K, Matsumoto T, Webb RC. Toll-like receptors and damage-associated molecular patterns: novel links between inflammation and hypertension. *Am J Physiol Heart Circ Physiol*. (2014) 306:H184–96. doi: 10.1152/ajpheart.00328.2013
12. Sunden-Cullberg J, Norrby-Teglund A, Rouhiainen A, Rauvala H, Herman G, Tracey KJ, et al. Persistent elevation of high mobility group box-1 protein (HMGB1) in patients with severe sepsis and septic shock. *Crit Care Med*. (2005) 33:564–73. doi: 10.1097/01.CCM.0000155991.88802.4D
13. Zhou Y, Dong H, Zhong Y, Huang J, Lv J, Li J. The Cold-Inducible RNA-Binding Protein (CIRP) level in peripheral blood predicts sepsis outcome. *PLoS ONE*. (2015) 10:e0137721. doi: 10.1371/journal.pone.0137721
14. Ekaney ML, Otto GP, Sossdorf M, Sponholz C, Boehringer M, Loesche W, et al. Impact of plasma histones in human sepsis and their contribution to cellular injury and inflammation. *Crit Care*. (2014) 18:543. doi: 10.1186/s13054-014-0543-8
15. Kolaczkowska E, Kubes P. Neutrophil recruitment and function in health and inflammation. *Nat Rev Immunol*. (2013) 13:159–75. doi: 10.1038/nri3399
16. Papayannopoulos V. Neutrophil extracellular traps in immunity and disease. *Nat Rev Immunol*. (2018) 18:134–47. doi: 10.1038/nri.2017.105
17. Brinkmann V, Reichard U, Goosmann C, Fauler B, Uhlemann Y, Weiss DS, et al. Neutrophil extracellular traps kill bacteria. *Science*. (2004) 303:1532–5. doi: 10.1126/science.1092385
18. Li RHL, Tablin F. A comparative review of neutrophil extracellular traps in sepsis. *Front Vet Sci*. (2018) 5:291. doi: 10.3389/fvets.2018.00291
19. Schaefer L. Complexity of danger: the diverse nature of damage-associated molecular patterns. *J Biol Chem*. (2014) 289:35237–45. doi: 10.1074/jbc.R114.619304
20. Brinkmann V. Neutrophil extracellular traps in the second decade. *J Innate Immun*. (2018) 10:414–21. doi: 10.1159/000489829
21. Sessa L, Bianchi ME. The evolution of High Mobility Group Box (HMGB) chromatin proteins in multicellular animals. *Gene*. (2007) 387:133–40. doi: 10.1016/j.gene.2006.08.034
22. Venkatesh SJL. Workman. Histone exchange, chromatin structure and the regulation of transcription. *Nat Rev Mol Cell Biol*. (2015) 16:178–89. doi: 10.1038/nrm3941
23. Marsman G, Zeerleder S, Luken BM. Extracellular histones, cell-free DNA, or nucleosomes: differences in immunostimulation. *Cell Death Dis*. (2016) 7:e2518. doi: 10.1038/cddis.2016.410
24. Lee W, Yuseok O, Yang S, Lee BS, Lee JH, Park EK, et al. JH-4 reduces HMGB1-mediated septic responses and improves survival rate in septic mice. *J Cell Biochem*. (2019) 120:6277–89. doi: 10.1002/jcb.27914
25. Musumeci D, Roviello GN, Montesarchio D. An overview on HMGB1 inhibitors as potential therapeutic agents in HMGB1-related pathologies. *Pharmacol Ther*. (2014) 141:347–57. doi: 10.1016/j.pharmthera.2013.11.001
26. Wellmann S, Buhrer C, Moderegger E, Zelmer A, Kirschner R, Koehne P, et al. Oxygen-regulated expression of the RNA-binding proteins RBM3 and CIRP by a HIF-1-independent mechanism. *J Cell Sci*. (2004) 117(Pt 9):1785–94. doi: 10.1242/jcs.01026
27. Ward PA, Fattahi F. New strategies for treatment of infectious sepsis. *J Leukoc Biol*. (2019) 106:187–92. doi: 10.1002/JLB.4MIR1118-425R
28. Rhodes A, Wort SJ, Thomas H, Collinson P, Bennett ED. Plasma DNA concentration as a predictor of mortality and sepsis in critically ill patients. *Crit Care*. (2006) 10:R60. doi: 10.1186/cc4894
29. Rios-Toro JJ, Marquez-Coello M, Garcia-Alvarez JM, Martin-Aspas A, Rivera-Fernandez R, Saez de Benito A, Giron-Gonzalez JA. Soluble membrane receptors, interleukin 6, procalcitonin and C reactive protein as prognostic markers in patients with severe sepsis and septic shock. *PLoS ONE*. (2017) 12:e0175254. doi: 10.1371/journal.pone.0175254

30. Hoogerwerf JJ, Tanck MWT, van Zoelen MAD, Wittebole X, Laterre PF, van der Poll T. Soluble ST2 plasma concentrations predict mortality in severe sepsis. *Intensive Care Med*. (2010) 36:630–7. doi: 10.1007/s00134-010-1773-0
31. Wong SL, Demers M, Martinod K, Gallant M, Wang Y, Goldfine AB, et al. Diabetes primes neutrophils to undergo NETosis, which impairs wound healing. *Nat Med*. (2015) 21:815–9. doi: 10.1038/nm.3887
32. Murthy P, Singhi AD, Ross MA, Loughran P, Paragomi P, Papachristou GI, et al. Enhanced neutrophil extracellular trap formation in acute pancreatitis contributes to disease severity and is reduced by chloroquine. *Front Immunol*. (2019) 10:28. doi: 10.3389/fimmu.2019.00028
33. Liaw PC, Ito T, Iba T, Thachil J, Zeerleder S. DAMP and DIC: the role of extracellular DNA and DNA-binding proteins in the pathogenesis of DIC. *Blood Rev*. (2016) 30:257–61. doi: 10.1016/j.blre.2015.12.004
34. Martin SJ. Cell death and inflammation: the case for IL-1 family cytokines as the canonical DAMPs of the immune system. *FEBS J*. (2016) 283:2599–615. doi: 10.1111/febs.13775
35. van Golen RF, Reiniers MJ, Marsman G, Alles LK, van Rooyen DM, Petri BVA, et al. The damage-associated molecular pattern HMGB1 is released early after clinical hepatic ischemia/reperfusion. *Biochim Biophys Acta Mol Basis Dis*. (2019) 1865:1192–200. doi: 10.1016/j.bbadis.2019.01.014
36. McGinn JT, Aziz M, Zhang F, Yang WL, Nicastro JM, Coppa GF, et al. Cold-inducible RNA-binding protein-derived peptide C23 attenuates inflammation and tissue injury in a murine model of intestinal ischemia-reperfusion. *Surgery*. (2018) 164:1191–7. doi: 10.1016/j.surg.2018.06.048
37. Tian Y, Charles EJ, Yan Z, Wu D, French BA, Kron IL, et al. The myocardial infarct-exacerbating effect of cell-free DNA is mediated by the high-mobility group box 1-receptor for advanced glycation end products-Toll-like receptor 9 pathway. *J Thorac Cardiovasc Surg*. (2018) 15:2256–69.e3. doi: 10.1016/j.jtcvs.2018.09.043
38. Mihm S. Danger-Associated Molecular Patterns (DAMPs): molecular triggers for sterile inflammation in the liver. *Int J Mol Sci*. (2018) 19:E3104. doi: 10.3390/ijms19103104
39. Feldman N, Rotter-Maskowitz A, Okun E. DAMPs as mediators of sterile inflammation in aging-related pathologies. *Ageing Res Rev*. (2015) 24(Pt. A):29–39. doi: 10.1016/j.arr.2015.01.003
40. Scaffidi P, Misteli T, Bianchi ME. Release of chromatin protein HMGB1 by necrotic cells triggers inflammation. *Nature*. (2002) 418:191–5. doi: 10.1038/nature00858
41. Wang H, Bloom O, Zhang M, Vishnubhakat JM, Ombrellino M, Che J, et al. HMG-1 as a late mediator of endotoxin lethality in mice. *Science*. (1999) 285:248–51. doi: 10.1126/science.285.5425.248
42. Roh JS, Sohn DH. Damage-associated molecular patterns in inflammatory diseases. *Immune Netw*. (2018) 18:e27. doi: 10.4110/in.2018.18.e27
43. Qiang X, Yang WL, Wu R, Zhou M, Jacob A, Dong W, et al. Cold-inducible RNA-binding protein (CIRP) triggers inflammatory responses in hemorrhagic shock and sepsis. *Nat Med*. (2013) 19:1489–95. doi: 10.1038/nm.3368
44. Aziz M, Brenner M, Wang P. Extracellular CIRP (eCIRP) and inflammation. *J Leukoc Biol*. (2019) 106:133–46. doi: 10.1002/JLB.3MIR1118-443R
45. Lu B, Wang C, Wang M, Li W, Chen F, Tracey KJ, Wang H. Molecular mechanism and therapeutic modulation of hmgb1 release and action: an updated review. *Expert Rev Clin Immunol*. (2014) 10:713–27. doi: 10.1586/1744666X.2014.909730
46. Andersson U, Yang H, Harris H. Extracellular HMGB1 as a therapeutic target in inflammatory diseases. *Expert Opin Ther Targets*. (2018) 22:263–77. doi: 10.1080/14728222.2018.1439924
47. Janko C, Filipovic M, Munoz LE, Schorn C, Schett G, Ivanovic-Burmazovic I, et al. Redox modulation of HMGB1-related signaling. *Antioxid Redox Signal*. (2014) 20:1075–85. doi: 10.1089/ars.2013.5179
48. Abdulmahdi W, Patel D, Rabadi MM, Azar T, Jules E, Lipphardt M, et al. HMGB1 redox during sepsis. *Redox Biol*. (2017) 13:600–7. doi: 10.1016/j.redox.2017.08.001
49. Wang H, Ward MF, Sama AE. Targeting HMGB1 in the treatment of sepsis. *Expert Opin Ther Targets*. (2014) 18:257–68. doi: 10.1517/14728222.2014.863876
50. Abraham E, Arcaroli J, Carmody A, Wang H, Tracey KJ. HMG-1 as a mediator of acute lung inflammation. *J Immunol*. (2000) 165:2950–4. doi: 10.4049/jimmunol.165.6.2950
51. Anggayasti WL, Mancera RL, Bottomley S, Helmerhorst E. The self-association of HMGB1 and its possible role in the binding to DNA and cell membrane receptors. *FEBS Lett*. (2017) 591:282–94. doi: 10.1002/1873-3468.12545
52. Youn JH, Oh YJ, Kim ES, Choi JE, Shin JS. High mobility group box 1 protein binding to lipopolysaccharide facilitates transfer of lipopolysaccharide to CD14 and enhances lipopolysaccharide-mediated TNF-alpha production in human monocytes. *J Immunol*. (2008) 180:5067–74. doi: 10.4049/jimmunol.180.7.5067
53. Kwak MS, Lim M, Lee YJ, Lee HS, Kim YH, Youn JH, et al. HMGB1 binds to lipoteichoic acid and enhances TNF-alpha and IL-6 production through HMGB1-mediated transfer of lipoteichoic acid to CD14 and TLR2. *J Innate Immun*. (2015) 7:405–16. doi: 10.1159/000369972
54. Wu J, Li J, Salcedo R, Mivechi NF, Trinchieri G, Horuzsko A. The proinflammatory myeloid cell receptor TREM-1 controls Kupffer cell activation and development of hepatocellular carcinoma. *Cancer Res*. (2012) 72:3977–86. doi: 10.1158/0008-5472.CAN-12-0938
55. Angus DC, Yang L, Kong L, Kellum JA, Delude RL, Tracey KJ, et al. Circulating high-mobility group box 1 (HMGB1) concentrations are elevated in both uncomplicated pneumonia and pneumonia with severe sepsis. *Crit Care Med*. (2007) 35:1061–7. doi: 10.1097/01.CCM.0000259534.68873.2A
56. Stevens NE, Chapman MJ, Fraser CK, Kuchel TR, Hayball JD, Diener KR. Therapeutic targeting of HMGB1 during experimental sepsis modulates the inflammatory cytokine profile to one associated with improved clinical outcomes. *Sci Rep*. (2017) 7:5850. doi: 10.1038/s41598-017-06205-z
57. Lee W, Ku SK, Bae JS. Zingerone reduces HMGB1-mediated septic responses and improves survival in septic mice. *Toxicol Appl Pharmacol*. (2017) 329:202–11. doi: 10.1016/j.taap.2017.06.006
58. De Leeuw F, Zhang T, Wauquier C, Huez G, Kruys V, Gueydan C. The cold-inducible RNA-binding protein migrates from the nucleus to cytoplasmic stress granules by a methylation-dependent mechanism and acts as a translational repressor. *Exp Cell Res*. (2007) 313:4130–44. doi: 10.1016/j.yexcr.2007.09.017
59. Xue JH, Nonoguchi K, Fukumoto M, Sato T, Nishiyama H, Higashitsuji H, et al. Effects of ischemia and H2O2 on the cold stress protein CIRP expression in rat neuronal cells. *Free Radic Biol Med*. (1999) 27:1238–44. doi: 10.1016/S0891-5849(99)00158-6
60. Sheikh MS, Carrier F, Papathanasiou MA, Hollander MC, Zhan Q, Yu K, et al. Identification of several human homologs of hamster DNA damage-inducible transcripts. Cloning and characterization of a novel UV-inducible cDNA that codes for a putative RNA-binding protein. *J Biol Chem*. (1997) 272:26720–6. doi: 10.1074/jbc.272.42.26720
61. Ward PA. An endogenous factor mediates shock-induced injury. *Nat Med*. (2013) 19:1368–9. doi: 10.1038/nm.3387
62. Zhu X, Bührer C, Wellmann S. Cold-inducible proteins CIRP and RBM3, a unique couple with activities far beyond the cold. *Cell Mol Life Sci*. (2016) 73:3839–59. doi: 10.1007/s00018-016-2253-7
63. Li Z, Fan EK, Liu J, Scott MJ, Li Y, Li S, et al. Cold-inducible RNA-binding protein through TLR4 signaling induces mitochondrial DNA fragmentation and regulates macrophage cell death after trauma. *Cell Death Dis*. (2017) 8:e2775. doi: 10.1038/cddis.2017.187
64. Khan MM, Yang WL, Brenner M, Bolognese AC, Wang P. Cold-inducible RNA-binding protein (CIRP) causes sepsis-associated acute lung injury via induction of endoplasmic reticulum stress. *Sci Rep*. (2017) 7:41363. doi: 10.1038/srep41363
65. Yang WL, Sharma A, Wang Z, Li Z, Fan J, Wang P. Cold-inducible RNA-binding protein causes endothelial dysfunction via activation of Nlrp3 inflammasome. *Sci Rep*. (2016) 6:26571. doi: 10.1038/srep26571
66. McGinn J, Zhang F, Aziz M, Yang WL, Nicastro J, Coppa GF, et al. The protective effect of a short peptide derived from cold-inducible RNA-binding protein in renal ischemia-reperfusion injury. *Shock*. (2018) 49:269–76. doi: 10.1097/SHK.0000000000000988

67. Godwin A, Yang WL, Sharma A, Khader A, Wang Z, Zhang F,et al. Blocking cold-inducible RNA-binding protein protects liver from ischemia-reperfusion injury. *Shock*. (2015) 43:24–30. doi: 10.1097/SHK.0000000000000251
68. Zhang F, Brenner M, Yang WL, Wang P. A cold-inducible RNA-binding protein (CIRP)-derived peptide attenuates inflammation and organ injury in septic mice. *Sci Rep*. (2018) 8:3052. doi: 10.1038/s41598-017-13139-z
69. Denning NL, Yang WL, Hansen L, Prince J, Wang P. C23, an oligopeptide derived from cold-inducible RNA-binding protein, suppresses inflammation and reduces lung injury in neonatal sepsis. *J Pediatr Surg*. (2019). doi: 10.1016/j.jpedsurg.2018.12.020. [Epub ahead of print].
70. Szatmary P, Huang W, Criddle D, Tepikin A, Sutton R. Biology, role and therapeutic potential of circulating histones in acute inflammatory disorders. *J Cell Mol Med*. (2018) 22:4617–29. doi: 10.1111/jcmm.13797
71. Xu J, Zhang X, Pelayo R, Monestier M, Ammollo CT, Semeraro F, et al. Extracellular histones are major mediators of death in sepsis. *Nat Med*. (2009) 15:1318–21. doi: 10.1038/nm.2053
72. Xu J, Zhang X, Monestier M, Esmon NL, Esmon CT. Extracellular histones are mediators of death through TLR2 and TLR4 in mouse fatal liver injury. *J Immunol*. (2011) 187:2626–31. doi: 10.4049/jimmunol.1003930
73. Alhamdi Y, Abrams ST, Cheng Z, Jing S, Su D, Liu Z, et al. Circulating histones are major mediators of cardiac injury in patients with sepsis. *Crit Care Med*. (2015) 43:2094–103. doi: 10.1097/CCM.0000000000001162
74. Magna M, Pisetsky DS. The alarmin properties of DNA and DNA-associated Nuclear Proteins. *Clin Ther*. (2016) 38:1029–41. doi: 10.1016/j.clinthera.2016.02.029
75. Dwivedi DJ, Toltl LJ, Swystun LL, Pogue J, Liaw KL, Weitz JI, et al. Prognostic utility and characterization of cell-free DNA in patients with severe sepsis. *Crit Care*. (2012) 16:R151. doi: 10.1186/cc11466
76. Li Y, Berke IC, Modis Y. DNA binding to proteolytically activated TLR9 is sequence-independent and enhanced by DNA curvature. *Embo J*. (2012) 31:919–31. doi: 10.1038/emboj.2011.441
77. Zhang Q, Raoof M, Chen Y, Sumi Y, Sursal T, Junger W, et al. Circulating mitochondrial DAMPs cause inflammatory responses to injury. *Nature*. (2010) 464:104–7. doi: 10.1038/nature08780
78. Bhagirath VC, Dwivedi DJ, Liaw PC. Comparison of the proinflammatory and procoagulant properties of nuclear, mitochondrial, and bacterial DNA. *Shock*. (2015) 44:265–71. doi: 10.1097/SHK.0000000000000397
79. Collins LV, Hajizadeh S, Holme E, Jonsson IM, Tarkowski A. Endogenously oxidized mitochondrial DNA induces *in vivo* and *in vitro* inflammatory responses. *J Leukoc Biol*. (2004) 75:995–1000. doi: 10.1189/jlb.0703328
80. Brown KA, Brain SD, Pearson JD, Edgeworth JD, Lewis SM, Treacher DF. Neutrophils in development of multiple organ failure in sepsis. *Lancet*. (2006) 368:157–69. doi: 10.1016/S0140-6736(06)69005-3
81. Blasius L, Beutler B. Intracellular toll-like receptors. *Immunity*. (2010) 32:305–15. doi: 10.1016/j.immuni.2010.03.012
82. Bonora M, Patergnani S, Rimessi A, De Marchi E, Suski JM, Bononi A, et al. ATP synthesis and storage. *Purinergic Signal*. (2012) 8:343–57. doi: 10.1007/s11302-012-9305-8
83. Kaczmarek A, Vandenabeele P, Krysko DV. Necroptosis: the release of damage-associated molecular patterns and its physiological relevance. *Immunity*. (2013) 38:209–23. doi: 10.1016/j.immuni.2013.02.003
84. Vénéreau E, Ceriotti C, Bianchi ME. DAMPs from cell death to new life. *Front Immunol*. (2015) 6:422. doi: 10.3389/fimmu.2015.00422
85. Zha QB, Wei HX, Li CG, Liang YD, Xu LH, Bai WJ, et al. ATP-induced inflammasome activation and pyroptosis is regulated by AMP-activated protein kinase in macrophages. *Front Immunol*. (2016) 7:597. doi: 10.3389/fimmu.2016.00597
86. Gombault A, Baron L, Couillin I. ATP release and purinergic signaling in NLRP3 inflammasome activation. *Front Immunol*. (2012) 3:414. doi: 10.3389/fimmu.2012.00414
87. Ledderose A, Bao Y, Kondo Y, Fakhari M, Slubowski C, Zhang J, Junger WG. Purinergic signaling and immune responses in sepsis. *Clin Ther*. (2016) 38:1054–65. doi: 10.1016/j.clinthera.2016.04.002
88. Sueyoshi K, Ledderose C, Shen Y, Lee AH, Shapiro NI, Junger WG. Lipopolysaccharide suppresses T cells by generating extracellular ATP that impairs their mitochondrial function via P2Y11 receptors. *J Biol Chem*. (2019) 294:6283–93. doi: 10.1074/jbc.RA118.007188
89. Savio LEB, de Andrade Mello P, Figliuolo VR, de Avelar Almeida TF, Santana PT, Oliveira SDS, et al. Coutinho-Silva. CD39 limits P2X7 receptor inflammatory signaling and attenuates sepsis-induced liver injury. *J Hepatol*. (2017) 67:716–26. doi: 10.1016/j.jhep.2017.05.021
90. Cauwels, Rogge E, Vandendriessche B, Shiva S, Brouckaert P. Extracellular ATP drives systemic inflammation, tissue damage and mortality. *Cell Death Dis*. (2014) 5:e1102. doi: 10.1038/cddis.2014.70
91. Pugin J, Stern-Voeffray S, Daubeuf B, Matthay MA, Elson G, Dunn-Siegrist I. Soluble MD-2 activity in plasma from patients with severe sepsis and septic shock. *Blood*. (2004) 104:4071–9. doi: 10.1182/blood-2003-04-1290
92. Gibot S, Kolopp-Sarda MN, Bene MC, Bollaert PE, Lozniewski A, Mory F, et al. A soluble form of the triggering receptor expressed on myeloid cells-1 modulates the inflammatory response in murine sepsis. *J Exp Med*. (2004) 200:1419–26. doi: 10.1084/jem.20040708
93. Benz F, Roy S, Trautwein C, Roderburg C, Luedde T. Circulating MicroRNAs as biomarkers for sepsis. *Int J Mol Sci*. (2016) 17:E78. doi: 10.3390/ijms17010078
94. Real JM, Ferreira LRP, Esteves GH, Koyama FC, Dias MVS, Bezerra-Neto JE, et al. Exosomes from patients with septic shock convey miRNAs related to inflammation and cell cycle regulation: new signaling pathways in sepsis? *Crit Care*. (2018) 22:68. doi: 10.1186/s13054-018-2003-3
95. Xu J, Feng Y, Jeyaram A, Jay SM, Zou L, Chao W. Circulating plasma extracellular vesicles from septic mice induce inflammation via MicroRNA- and TLR7-dependent mechanisms. *J Immunol*. (2018) 2018:ji1801008. doi: 10.4049/jimmunol.1801008
96. Rider P, Voronov E, Dinarello CA, Apte RN, Cohen I. Alarmins: feel the stress. *J Immunol*. (2017) 198:1395–402. doi: 10.4049/jimmunol.1601342
97. Yu Y, Tang D, Kang R. Oxidative stress-mediated HMGB1 biology. *Front Physiol*. (2015) 6:93. doi: 10.3389/fphys.2015.00093
98. Sanjabi S, Zenewicz LA, Kamanaka M, Flavell RA. Anti-inflammatory and pro-inflammatory roles of TGF-beta, IL-10, and IL-22 in immunity and autoimmunity. *Curr Opin Pharmacol*. (2009) 9:447–53. doi: 10.1016/j.coph.2009.04.008
99. Scheller J, Chalaris A, Schmidt-Arras D, Rose-John S. The pro- and anti-inflammatory properties of the cytokine interleukin-6. *Biochim Biophys Acta*. (2011) 1813:878–88. doi: 10.1016/j.bbamcr.2011.01.034
100. Mishra HK, Ma J, Walcheck B. Ectodomain shedding by ADAM17: its role in neutrophil recruitment and the impairment of this process during sepsis. *Front Cell Infect Microbiol*. (2017) 7:138. doi: 10.3389/fcimb.2017.00138
101. Bouchon, Facchetti F, Weigand MA, Colonna M. TREM-1 amplifies inflammation and is a crucial mediator of septic shock. *Nature*. (2001) 410:1103–7. doi: 10.1038/35074114
102. Haselmayer P, Grosse-Hovest L, von Landenberg P, Schild H, Radsak MP. TREM-1 ligand expression on platelets enhances neutrophil activation. *Blood*. (2007) 110:1029–35. doi: 10.1182/blood-2007-01-069195
103. Xi H, Katschke KJ Jr, Li Y, Truong T, Lee WP, Diehl L, et al. IL-33 amplifies an innate immune response in the degenerating retina. *J Exp Med*. (2016) 213:189–207. doi: 10.1084/jem.20150894
104. Nair RR, Mazza D, Brambilla F, Gorzanelli A, Agresti A, Bianchi ME. LPS-challenged macrophages release microvesicles coated with histones. *Front Immunol*. (2018) 9:1463. doi: 10.3389/fimmu.2018.01463
105. Jiao Y, Li Z, Loughran PA, Fan EK, Scott MJ, Li Y, et al. Frontline Science: Macrophage-derived exosomes promote neutrophil necroptosis following hemorrhagic shock. *J Leukoc Biol*. (2018) 103:175–83. doi: 10.1189/jlb.3HI0517-173R
106. Miksa M, Wu R, Dong W, Das P, Yang D, Wang P. Dendritic cell-derived exosomes containing milk fat globule epidermal growth factor-factor VIII attenuate proinflammatory responses in sepsis. *Shock*. (2006) 25:586–93. doi: 10.1097/01.shk.0000209533.22941.d0
107. Szatmary C, Nossal R, Parent CA, Majumdar R. Modeling neutrophil migration in dynamic chemoattractant gradients: assessing the role of exosomes during signal relay. *Mol Biol Cell*. (2017) 28:3457–70. doi: 10.1091/mbc.e17-05-0298
108. Wynn T. Cellular and molecular mechanisms of fibrosis. *J Pathol*. (2008) 214:199–210. doi: 10.1002/path.2277

109. Klein T, Bischoff R. Physiology and pathophysiology of matrix metalloproteases. *Amino Acids*. (2011) 41:271–90. doi: 10.1007/s00726-010-0689-x
110. Raposo G, Stoorvogel W. Extracellular vesicles: exosomes, microvesicles, friends. *J Cell Biol*. (2013) 200:373–83. doi: 10.1083/jcb.201211138
111. Collett GP, Redman CW, Sargent IL, Vatish M. Endoplasmic reticulum stress stimulates the release of extracellular vesicles carrying danger-associated molecular pattern (DAMP) molecules. *Oncotarget*. (2018) 9(6):6707–17. doi: 10.18632/oncotarget.24158
112. Etheridge A, Lee I, Hood L, Galas D, Wang K. Extracellular microRNA: a new source of biomarkers. *Mutat Res*. (2011) 717:85–90. doi: 10.1016/j.mrfmmm.2011.03.004
113. Feng Y, Zou L, Yan D, Chen H, Xu G, Jian W, et al. Extracellular MicroRNAs induce potent innate immune responses via TLR7/MyD88-dependent mechanisms. *J Immunol*. (2017) 199:2106–17. doi: 10.4049/jimmunol.1700730
114. Mayadas TN, Cullere X, Lowell CA. The multifaceted functions of neutrophils. *Annu Rev Pathol*. (2014) 9:181–218. doi: 10.1146/annurev-pathol-020712-164023
115. Cooper PR, Palmer LJ, Chapple IL. Neutrophil extracellular traps as a new paradigm in innate immunity: friend or foe? *Periodontol 2000*. (2013) 63:165–97. doi: 10.1111/prd.12025
116. Carmona-Rivera C, Kaplan MJ. Induction and quantification of NETosis. *Curr Protoc Immunol*. (2016) 115:14.41.1–14. doi: 10.1002/cpim.16
117. Chapman EA, Lyon M, Simpson D, Mason D, Beynon RJ, Moots RJ, et al. Caught in a Trap? proteomic analysis of neutrophil extracellular traps in rheumatoid arthritis and systemic lupus erythematosus. *Front Immunol*. (2019) 10:423. doi: 10.3389/fimmu.2019.00423
118. de Buhr N, von Köckritz-Blickwede M. How neutrophil extracellular traps become visible. *J Immunol Res*. (2016) 2016:4604713. doi: 10.1155/2016/4604713
119. Zharkova O, Tay SH, Lee HY, Shubhita T, Ong WY, Lateef A, et al. A flow cytometry-based assay for high-throughput detection and quantification of neutrophil extracellular traps in mixed cell populations. *Cytometry A*. (2019) 95:268–78. doi: 10.1002/cyto.a.23672
120. Gavillet M, Martinod K, Renella R, Harris C, Shapiro NI, Wagner DD, et al. Flow cytometric assay for direct quantification of neutrophil extracellular traps in blood samples. *Am J Hematol*. (2015) 90:1155–8. doi: 10.1002/ajh.24185
121. Ginley BG, Emmons T, Lutnick B, Urban CF, Segal BH, Sarder P. Computational detection and quantification of human and mouse neutrophil extracellular traps in flow cytometry and confocal microscopy. *Sci Rep*. (2017) 7:17755. doi: 10.1038/s41598-017-18099-y
122. Thålin C, Daleskog M, Göransson SP, Schatzberg D, Lasselin J, Laska AC, et al. Validation of an enzyme-linked immunosorbent assay for the quantification of citrullinated histone H3 as a marker for neutrophil extracellular traps in human plasma. *Immunol Res*. (2017) 65:706–12. doi: 10.1007/s12026-017-8905-3
123. Boone BA, Orlichenko L, Schapiro NE, Loughran P, Gianfrate GC, Ellis JT, et al. The receptor for advanced glycation end products (RAGE) enhances autophagy and neutrophil extracellular traps in pancreatic cancer. *Cancer Gene Ther*. (2015) 22:326–34. doi: 10.1038/cgt.2015.21
124. Yipp BG, Kubes P. NETosis: how vital is it? *Blood*. (2013) 122:2784–94. doi: 10.1182/blood-2013-04-457671
125. Yang H, Biermann MH, Brauner JM, Liu Y, Zhao Y, Herrmann M. New insights into neutrophil extracellular traps: mechanisms of formation and role in inflammation. *Front Immunol*. (2016) 7:302. doi: 10.3389/fimmu.2016.00302
126. Delgado-Rizo V, Martinez-Guzman MA, Iniguez-Gutierrez L, Garcia-Orozco A, Alvarado-Navarro A, Fafutis-Morris M. Neutrophil extracellular traps and its implications in inflammation: an overview. *Front Immunol*. (2017) 8:81. doi: 10.3389/fimmu.2017.00081
127. Yipp BG, Petri B, Salina D, Jenne CN, Scott BN, Zbytnuik LD, et al. Infection-induced NETosis is a dynamic process involving neutrophil multitasking *in vivo*. *Nat Med*. (2012) 18:1386–93. doi: 10.1038/nm.2847
128. Manda, Pruchniak MP, Arazna M, Demkow UA. Neutrophil extracellular traps in physiology and pathology. *Cent Eur J Immunol*. (2014) 39:116–21. doi: 10.5114/ceji.2014.42136
129. Yousefi S, Mihalache C, Kozlowski E, Schmid I, Simon HU. Viable neutrophils release mitochondrial DNA to form neutrophil extracellular traps. *Cell Death Differ*. (2009) 16:1438–44. doi: 10.1038/cdd.2009.96
130. Itagaki K, Kaczmarek E, Lee YT, Tang IT, Isal B, Adibnia Y, et al. Mitochondrial DNA released by trauma induces neutrophil extracellular traps. *PLoS ONE*. (2015) 10:e0120549. doi: 10.1371/journal.pone.0120549
131. McIlroy DJ, Jarnicki AG, Au GG, Lott N, Smith DW, Hansbro PM, et al. Mitochondrial DNA neutrophil extracellular traps are formed after trauma and subsequent surgery. *J Crit Care*. (2014) 29:1133.e1–5. doi: 10.1016/j.jcrc.2014.07.013
132. Carestia A, Kaufman T, Rivadeneyra L, Landoni VI, Pozner RG, Negrotto S, et al. Mediators and molecular pathways involved in the regulation of neutrophil extracellular trap formation mediated by activated platelets. *J Leukoc Biol*. (2016) 99:153–62. doi: 10.1189/jlb.3A0415-161R
133. Amulic A, Knackstedt SL, Abu Abed U, Deigendesch N, Harbort CJ, Caffrey BE, et al. Cell-cycle proteins control production of neutrophil extracellular traps. *Dev Cell*. (2017) 43:449–62.e5. doi: 10.1016/j.devcel.2017.10.013
134. Ortiz-Munoz G, Mallavia B, Bins A, Headley M, Krummel MF, Looney MR. Aspirin-triggered 15-epi-lipoxin A4 regulates neutrophil-platelet aggregation and attenuates acute lung injury in mice. *Blood*. (2014) 124:2625–34. doi: 10.1182/blood-2014-03-562876
135. Lefrancais E, Mallavia B, Zhuo H, Calfee CS, Looney MR. Maladaptive role of neutrophil extracellular traps in pathogen-induced lung injury. *JCI Insight*. (2018) 3:98178. doi: 10.1172/jci.insight.98178
136. Silvestre-Roig C, Hidalgo A, Soehnlein O. Neutrophil heterogeneity: implications for homeostasis and pathogenesis. *Blood*. (2016) 127:2173–81. doi: 10.1182/blood-2016-01-688887
137. Garcia-Romo GS, Caielli S, Vega B, Connolly J, Allantaz F, Xu Z, et al. Netting neutrophils are major inducers of type I IFN production in pediatric systemic lupus erythematosus. *Sci Transl Med*. (2011) 3:73ra20. doi: 10.1126/scitranslmed.3001201
138. Lehmann JC, Jablonski-Westrich D, Haubold U, Gutierrez-Ramos JC, Springer T, Hamann A. Overlapping and selective roles of endothelial intercellular adhesion molecule-1 (ICAM-1) and ICAM-2 in lymphocyte trafficking. *J Immunol*. (2003) 171:2588–93. doi: 10.4049/jimmunol.171.5.2588
139. Woodfin A, Beyrau M, Voisin MB, Ma B, Whiteford JR, Hordijk PL, et al. ICAM-1-expressing neutrophils exhibit enhanced effector functions in murine models of endotoxemia. *Blood*. (2016) 127:898–907. doi: 10.1182/blood-2015-08-664995
140. Ode Y, Aziz M, Wang P. CIRP increases ICAM-1(+) phenotype of neutrophils exhibiting elevated iNOS and NETs in sepsis. *J Leukoc Biol*. (2018) 103:693–707. doi: 10.1002/JLB.3A0817-327RR
141. Alarcon P, Manosalva C, Conejeros I, Carretta MD, Munoz-Caro T, Silva LM R,et al. d (-) lactic acid-induced adhesion of bovine neutrophils onto endothelial cells is dependent on neutrophils extracellular traps formation and CD11b expression. *Front Immunol*. (2017) 8:975. doi: 10.3389/fimmu.2017.00975
142. Folco EJ, Mawson TL, Vromman A, Bernardes-Souza B, Franck G, Persson O, et al. Neutrophil extracellular traps induce endothelial cell activation and tissue factor production through interleukin-1alpha and cathepsin G. *Arterioscler Thromb Vasc Biol*. (2018) 38:1901–12. doi: 10.1161/ATVBAHA.118.311150
143. Elsner J, Sach M, Knopf HP, Norgauer J, Kapp A, Schollmeyer P, et al. Synthesis and surface expression of ICAM-1 in polymorphonuclear neutrophilic leukocytes in normal subjects and during inflammatory disease. *Immunobiology*. (1995) 193:456–64. doi: 10.1016/S0171-2985(11)80430-4
144. Wang SZ, Smith PK, Lovejoy M, Bowden JJ, Alpers JH, Forsyth KD. Shedding of L-selectin and PECAM-1 and upregulation of Mac-1 and ICAM-1 on neutrophils in RSV bronchiolitis. *Am J Physiol*. (1998) 275:L983–9. doi: 10.1152/ajplung.1998.275.5.L983
145. Fortunati E, Kazemier KM, Grutters JC, Koenderman L, Van den Boschv J. Human neutrophils switch to an activated phenotype after homing to

the lung irrespective of inflammatory disease. *Clin Exp Immunol*. (2009) 155:559–66. doi: 10.1111/j.1365-2249.2008.03791.x
146. Zhao Y, Yi W, Wan X, Wang J, Tao T, Li J, et al. Blockade of ICAM-1 improves the outcome of polymicrobial sepsis via modulating neutrophil migration and reversing immunosuppression. *Mediators Inflamm*. (2014) 2014:195290. doi: 10.1155/2014/195290
147. Sagiv JY, Voels S, Granot Z. Isolation and characterization of low- vs. high-density neutrophils in cancer. *Methods Mol Biol*. (2016) 1458:179–93. doi: 10.1007/978-1-4939-3801-8_13
148. Rosales C. Neutrophil: a cell with many roles in inflammation or several cell types? *Front Physiol*. (2018) 9:113. doi: 10.3389/fphys.2018.00113
149. Kanamaru R, Ohzawa H, Miyato H, Matsumoto S, Haruta H, Kurashina K, et al. Low density neutrophils (LDN) in postoperative abdominal cavity assist the peritoneal recurrence through the production of neutrophil extracellular traps (NETs). *Sci Rep*. (2018) 8:632 doi: 10.1038/s41598-017-19091-2
150. Denny MF, Yalavarthi S, Zhao W, Thacker SG, Anderson M, Sandy AR, et al. A distinct subset of proinflammatory neutrophils isolated from patients with systemic lupus erythematosus induces vascular damage and synthesizes type I IFNs. *J Immunol*. (2010) 184:3284–97. doi: 10.4049/jimmunol.0902199
151. Li Y, Li H, Wang H, Pan H, Zhao H, Jin H, et al. The proportion, origin and pro-inflammation roles of low density neutrophils in SFTS disease. *BMC Infect Dis*. (2019) 19:109. doi: 10.1186/s12879-019-3701-4
152. Herteman N, Vargas A, Lavoie JP. Characterization of circulating low-density neutrophils intrinsic properties in healthy and asthmatic horses. *Sci Rep*. (2017) 7:7743. doi: 10.1038/s41598-017-08089-5
153. Villanueva E, Yalavarthi S, Berthier CC, Hodgin JB, Khandpur R, Lin AM, et al. Netting neutrophils induce endothelial damage, infiltrate tissues, expose immunostimulatory molecules in systemic lupus erythematosus. *J Immunol*. (2011) 187:538–52. doi: 10.4049/jimmunol.1100450
154. Uhl B, Vadlau Y, Zuchtriegel G, Nekolla K, Sharaf K, Gaertner F, et al. Aged neutrophils contribute to the first line of defense in the acute inflammatory response. *Blood*. (2016) 128:2327–37. doi: 10.1182/blood-2016-05-718999
155. Zhang D, Chen G, Manwani D, Mortha A, Xu C, Faith JJ, et al. Neutrophil ageing is regulated by the microbiome. *Nature*. (2015) 525:528–32. doi: 10.1038/nature15367
156. Ermert D, Urban CF, Laube B, Goosmann C, Zychlinsky A, Brinkmann V. Mouse neutrophil extracellular traps in microbial infections. *J Innate Immun*. (2009) 1:181–93. doi: 10.1159/000205281
157. Kaplan MJ, Radic M. Neutrophil extracellular traps: double-edged swords of innate immunity. *J Immunol*. (2012) 189:2689–95. doi: 10.4049/jimmunol.1201719
158. Clark SR, Ma AC, Tavener SA, McDonald B, Goodarzi Z, Kelly MM, et al. Platelet TLR4 activates neutrophil extracellular traps to ensnare bacteria in septic blood. *Nat Med*. (2007) 13:463–9. doi: 10.1038/nm1565
159. Grommes J, Soehnlein O. Contribution of neutrophils to acute lung injury. *Mol Med*. (2011) 17:293–307. doi: 10.2119/molmed.2010.00138
160. Margraf S, Logters T, Reipen J, Altrichter J, Scholz M, Windolf J. Neutrophil-derived circulating free DNA (cf-DNA/NETs): a potential prognostic marker for posttraumatic development of inflammatory second hit and sepsis. *Shock*. (2008) 30:352–8. doi: 10.1097/SHK.0b013e31816a6bb1
161. Maruchi Y, Tsuda M, Mori H, Takenaka N, Gocho T, Huq MA, et al. Plasma myeloperoxidase-conjugated DNA level predicts outcomes and organ dysfunction in patients with septic shock. *Crit Care*. (2018) 22:176. doi: 10.1186/s13054-018-2109-7
162. Yost CC, Cody MJ, Harris ES, Thornton NL, McInturff AM, Martinez ML, et al. Impaired neutrophil extracellular trap (NET) formation: a novel innate immune deficiency of human neonates. *Blood*. (2009) 113:6419–27. doi: 10.1182/blood-2008-07-171629
163. Czaikoski PG, Mota J, Nascimento DC, Sônego F, Castanheira FS, Melo PH, et al. Neutrophil extracellular traps induce organ damage during experimental and clinical sepsis. *PLoS ONE*. (2016) 11: e0148142. doi: 10.1371/journal.pone.0148142
164. Mai SH, Khan M, Dwivedi DJ, Ross CA, Zhou J, Gould TJ, et al. Delayed but not early treatment with dnase reduces organ damage and improves outcome in a murine model of sepsis. *Shock*. (2015) 44:166–72. doi: 10.1097/SHK.0000000000000396
165. Patel JM, Sapey E, Parekh D, Scott A, Dosanjh D, Gao F, et al. Sepsis induces a dysregulated neutrophil phenotype that is associated with increased mortality. *Mediators Inflamm*. (2018) 2018:4065362. doi: 10.1155/2018/4065362
166. Hashiba M, Huq A, Tomino A, Hirakawa A, Hattori T, Miyabe H, et al. Neutrophil extracellular traps in patients with sepsis. *J Surg Res*. (2015) 194:248–54. doi: 10.1016/j.jss.2014.09.033
167. Lerman YV, Kim M. Neutrophil Migration under normal and sepsis conditions. *Cardiovasc Hematol Disord Drug Targets*. (2015) 15:19–28. doi: 10.2174/1871529X15666150108113236
168. Gupta K, Joshi MB, Philippova M, Erne P, Hasler P, Hahn S, Resink TJ. Activated endothelial cells induce neutrophil extracellular traps and are susceptible to NETosis-mediated cell death. *FEBS Lett*. (2010) 584:3193–7. doi: 10.1016/j.febslet.2010.06.006
169. Kimball S, Obi AT, Diaz JA, Henke PK. The emerging role of NETs in venous thrombosis and immunothrombosis. *Front Immunol*. (2016) 7:236. doi: 10.3389/fimmu.2016.00236
170. Martinod K, Wagner DD. Thrombosis: tangled up in NETs. *Blood*. (2014) 123:2768–76. doi: 10.1182/blood-2013-10-463646
171. Delabranche X, Stiel L, Severac F, Galoisy AC, Mauvieux L, Zobairi F, et al. Evidence of netosis in septic shock-induced disseminated intravascular coagulation. *Shock*. (2017) 47:313–17. doi: 10.1097/SHK.0000000000000719
172. McDonald A, Davis RP, Kim SJ, Tse M, Esmon CT, Kolaczkowska E, et al. Platelets and neutrophil extracellular traps collaborate to promote intravascular coagulation during sepsis in mice. *Blood*. (2017) 129:1357–67. doi: 10.1182/blood-2016-09-741298
173. Yang S, Qi H, Kan K, Chen J, Xie H, Guo X, et al. Neutrophil extracellular traps promote hypercoagulability in patients with sepsis. *Shock*. (2017) 47:132–9. doi: 10.1097/SHK.0000000000000741
174. Mikacenic A, Moore R, Dmyterko V, West TE, Altemeier WA, Liles WC, et al. Neutrophil extracellular traps (NETs) are increased in the alveolar spaces of patients with ventilator-associated pneumonia. *Crit Care*. (2018) 22:358. doi: 10.1186/s13054-018-2290-8
175. Li RH L, Johnson LR, Kohen C, Tablin F. A novel approach to identifying and quantifying neutrophil extracellular trap formation in septic dogs using immunofluorescence microscopy. *BMC Vet Res*. (2018) 14:210. doi: 10.1186/s12917-018-1523-z
176. Bosmann M, Grailer JJ, Ruemmler R, Russkamp NF, Zetoune FS, Sarma JV, et al. Extracellular histones are essential effectors of C5aR- and C5L2-mediated tissue damage and inflammation in acute lung injury. *FASEB J*. (2013) 27:5010–21. doi: 10.1096/fj.13-236380
177. Peterson MW, Walter ME, Nygaard SD. Effect of neutrophil mediators on epithelial permeability. *Am J Respir Cell Mol Biol*. (1995) 13:719–27. doi: 10.1165/ajrcmb.13.6.7576710
178. Ishii T, Doi K, Okamoto K, Imamura M, Dohi M, Yamamoto K, et al. Neutrophil elastase contributes to acute lung injury induced by bilateral nephrectomy. *Am J Pathol*. (2010) 177:1665–73. doi: 10.2353/ajpath.2010.090793
179. Tsai YF, Yu HP, Chang WY, Liu FC, Huang ZC, Hwang TL. Sirtinol inhibits neutrophil elastase activity and attenuates lipopolysaccharide-mediated acute lung injury in mice. *Sci Rep*. (2015) 5:8347. doi: 10.1038/srep08347
180. Biron BM, Chung CS, O'Brien XM, Chen Y, Reichner JS, Ayala A. Cl-amidine prevents histone 3 citrullination, net formation, and improves survival in a murine sepsis model. *J Innate Immun*. (2017) 9:22–32. doi: 10.1159/000448808
181. Boone BA, Murthy P, Miller-Ocuin J, Doerfler WR, Ellis JT, Liang X, et al. Chloroquine reduces hypercoagulability in pancreatic cancer through inhibition of neutrophil extracellular traps. *BMC Cancer*. (2018) 18:678. doi: 10.1186/s12885-018-4584-2
182. Healy LD, Puy C, Fernandez JA, Mitrugno A, Keshari RS, Taku NA, et al. Activated protein C inhibits neutrophil extracellular trap formation *in vitro* and activation *in vivo*. *J Biol Chem*. (2017) 292:8616–29. doi: 10.1074/jbc.M116.768309
183. Alaniz C. An update on activated protein C (Xigris) in the management of sepsis. *P T*. (2010) 35:504–8, 29.
184. Marti-Carvajal J, Sola I, Gluud C, Lathyris D, Cardona AF. Human recombinant protein C for severe sepsis and septic shock in adult and paediatric patients. *Cochrane Database Syst Rev*. (2012) 12:Cd004388. doi: 10.1002/14651858.CD004388.pub6

185. Li Y, Liu Z, Liu B, Zhao T, Chong W, Wang Y, et al. Citrullinated histone H3 – a novel target for treatment of sepsis. *Surgery*. (2014) 156:229–34. doi: 10.1016/j.surg.2014.04.009
186. Yokoyama Y, Ito T, Yasuda T, Furubeppu H, Kamikokuryo C, Yamada S, et al. Circulating histone H3 levels in septic patients are associated with coagulopathy, multiple organ failure, and death: a single-center observational study. *Thromb J*. (2019) 17:1. doi: 10.1186/s12959-018-0190-4
187. Martinod K, Fuchs TA, Zitomersky NL, Wong SL, Demers M, Gallant M, et al. PAD4-deficiency does not affect bacteremia in polymicrobial sepsis and ameliorates endotoxemic shock. *Blood*. (2015) 125:1948–56. doi: 10.1182/blood-2014-07-587709
188. Biron BM, Chung CS, Chen Y, Wilson Z, Fallon EA, Reichner JS, et al. PAD4 deficiency leads to decreased organ dysfunction and improved survival in a dual insult model of hemorrhagic shock and sepsis. *J Immunol*. (2018) 200:1817–28. doi: 10.4049/jimmunol.1700639
189. Lewis HD, Liddle J, Coote JE, Atkinson SJ, Barker MD, Bax BD, et al. Inhibition of PAD4 activity is sufficient to disrupt mouse and human NET formation. *Nat Chem Biol*. (2015) 11:189–91. doi: 10.1038/nchembio.1735
190. Tadie JM, Bae HB, Jiang S, Park DW, Bell CP, Yang H, et al. HMGB1 promotes neutrophil extracellular trap formation through interactions with Toll-like receptor 4. *Am J Physiol Lung Cell Mol Physiol*. (2013) 304:L342–9. doi: 10.1152/ajplung.00151.2012
191. Liu L, Mao Y, Xu B, Zhang X, Fang C, Ma Y, et al. Induction of neutrophil extracellular traps during tissue injury: involvement of STING and Toll-like receptor 9 pathways. *Cell Prolif*. (2019) 52:e12579. doi: 10.1111/cpr.12579
192. Al-Banna N, Lehmann C. Oxidized LDL and LOX-1 in experimental sepsis. *Mediators Inflamm*. (2013) 2013:761789. doi: 10.1155/2013/761789
193. Miller YI, Choi SH, Wiesner P, Fang L, Harkewicz R, Hartvigsen K, et al. Oxidation-specific epitopes are danger-associated molecular patterns recognized by pattern recognition receptors of innate immunity. *Circ Res*. (2011) 108:235–48. doi: 10.1161/CIRCRESAHA.110.223875
194. Awasthi A, Nagarkoti S, Kumar A, Dubey M, Singh AK, Pathak P, et al. Oxidized LDL induced extracellular trap formation in human neutrophils via TLR-PKC-IRAK-MAPK and NADPH-oxidase activation. *Free Radic Biol Med*. (2016) 93:190–203. doi: 10.1016/j.freeradbiomed.2016.01.004
195. Boe DM, Curtis BJ, Chen MM, Ippolito JA, Kovacs EJ. Extracellular traps and macrophages: new roles for the versatile phagocyte. *J Leukoc Biol*. (2015) 97:1023–35. doi: 10.1189/jlb.4RI1014-521R
196. Ueki S, Tokunaga T, Fujieda S, Honda K, Hirokawa M, Spencer LA, et al. Eosinophil ETosis and DNA Traps: a New Look at Eosinophilic Inflammation. *Curr Allergy Asthma Rep*. (2016) 16:54. doi: 10.1007/s11882-016-0634-5

Conflict of Interest: The authors declare that the research was conducted in the absence of any commercial or financial relationships that could be construed as a potential conflict of interest.

Copyright © 2019 Denning, Aziz, Gurien and Wang. This is an open-access article distributed under the terms of the Creative Commons Attribution License (CC BY). The use, distribution or reproduction in other forums is permitted, provided the original author(s) and the copyright owner(s) are credited and that the original publication in this journal is cited, in accordance with accepted academic practice. No use, distribution or reproduction is permitted which does not comply with these terms.

frontiers in Immunology

ORIGINAL RESEARCH
published: 19 November 2019
doi: 10.3389/fimmu.2019.02675

Orthopedic Surgery Triggers Attention Deficits in a Delirium-Like Mouse Model

Ravikanth Velagapudi[1†], Saraswathi Subramaniyan[1†], Chao Xiong[1†‡], Fiona Porkka[2], Ramona M. Rodriguiz[2], William C. Wetsel[2,3] and Niccolò Terrando[1]*

[1] Department of Anesthesiology, Center for Translational Pain Medicine, Duke University Medical Center, Durham, NC, United States, [2] Department of Psychiatry and Behavioral Sciences, Mouse Behavioral and Neuroendocrine Analysis Core Facility, Duke University Medical Center, Durham, NC, United States, [3] Departments of Neurobiology and Cell Biology, Duke University Medical Center, Durham, NC, United States

OPEN ACCESS

Edited by:
Massimo Gadina,
National Institute of Arthritis and Musculoskeletal and Skin Diseases (NIAMS), United States

Reviewed by:
Paul S. Garcia,
Columbia University, United States
Pietro Ghezzi,
Brighton and Sussex Medical School, United Kingdom

***Correspondence:**
Niccolò Terrando
niccolo.terrando@duke.edu

[†]These authors share first authorship

[‡]**Present address:**
Chao Xiong,
State Key Laboratory of Cardiovascular Disease, Department of Anesthesiology, National Center for Cardiovascular Disease, Fuwai Hospital, Chinese Academy of Medical Sciences, Peking Union Medical College, Beijing, China

Specialty section:
This article was submitted to Inflammation, a section of the journal Frontiers in Immunology

Received: 20 March 2019
Accepted: 30 October 2019
Published: 19 November 2019

Citation:
Velagapudi R, Subramaniyan S, Xiong C, Porkka F, Rodriguiz RM, Wetsel WC and Terrando N (2019) Orthopedic Surgery Triggers Attention Deficits in a Delirium-Like Mouse Model. Front. Immunol. 10:2675. doi: 10.3389/fimmu.2019.02675

Postoperative delirium is a frequent and debilitating complication, especially amongst high risk procedures such as orthopedic surgery, and its pathogenesis remains unclear. Inattention is often reported in the clinical diagnosis of delirium, however limited attempts have been made to study this cognitive domain in preclinical models. Here we implemented the 5-choice serial reaction time task (5-CSRTT) to evaluate attention in a clinically relevant mouse model following orthopedic surgery. The 5-CSRTT showed a time-dependent impairment in the number of responses made by the mice acutely after orthopedic surgery, with maximum impairment at 24 h and returning to pre-surgical performance by day 5. Similarly, the latency to the response was also delayed during this time period but returned to pre-surgical levels within several days. While correct responses decreased following surgery, the accuracy of the response (e.g., selection of the correct nose-poke) remained relatively unchanged. In a separate cohort we evaluated neuroinflammation and blood-brain barrier (BBB) dysfunction using clarified brain tissue with light-sheet microscopy. CLARITY revealed significant changes in microglial morphology and impaired astrocytic-tight junction interactions using high-resolution 3D reconstructions of the neurovascular unit. Deposition of IgG, fibrinogen, and autophagy markers (TFEB and LAMP1) were also altered in the hippocampus 24 h after surgery. Together, these results provide translational evidence for the role of peripheral surgery contributing to delirium-like behavior and disrupted neuroimmunity in adult mice.

Keywords: attention, delirium, blood-brain barrier, microglia, neuroinflammation, surgery

INTRODUCTION

Postoperative delirium is a common complication characterized by acute cognitive impairments featuring disorganized thinking, fluctuating levels of consciousness, altered arousal levels, and inattention (1). A diagnosis of delirium consistently correlates with a poor prognosis (i.e., a 5-fold increased risk for mortality at 6 months), persistent functional decline, increased nursing staff time per patient, increased hospital stays, and higher rates of nursing home placement (2, 3). This condition contributes to escalating healthcare costs previously estimated >$150 billion each year (4). Delirium is frequently seen in medical, intensive, emergency, nursing, and palliative care settings amongst any age group; however, it is the most common surgical complication in older adults (5).

Orthopedic surgery is a common intervention across every age group that can frequently contribute to cognitive impairments, emotional disturbances, and pain in a significant proportion of patients (6). As many as 50% of patients suffer from postoperative delirium after orthopedic surgery (7) and delirium is a well-appreciated predictor for mortality and adverse outcomes in patients with underlying dementia (8, 9). We have developed a mouse model of tibial fracture and repair to study the impact of orthopedic surgery on the central nervous system (CNS) and to interrogate the pathogenesis of perioperative neurocognitive disorders (10). We and others have described some of the behavioral changes affecting the hippocampus and other brain areas after surgery, although no formal evaluation of attention has been conducted to translate preclinical findings to human delirium assessment. The 5-choice serial reaction time task (5-CSRTT) is a well-established attention paradigm used to assess various aspects of attentional control in rodents, including selective, divided, and sustained attention or vigilance (11). The 5-CSRTT has been commonly used to elucidate attention impairments in several neuropsychiatric conditions including attention deficit/hyperactivity disorder (ADHD) and schizophrenia (12).

Neuroinflammation has emerged as an active driver in the pathogenesis of multiple neurological conditions, including neuropsychiatric, neurodegenerative, and perioperative disorders (13, 14). Following surgical procedures such as orthopedic surgery, pro-inflammatory cytokines have been detected in the cerebrospinal fluid of patients developing postoperative delirium (15, 16). The exact roles of these cellular processes in postoperative delirium remains elusive and their active involvement after anesthesia and surgery is generating significant interest. Recent advances in tissue clarification techniques have enabled complex 3D features in intact specimens to be observed, especially in brain (17, 18). CLARITY provides a unique approach to preserve cellular integrity through the formation of a tissue-hydrogel mesh that enables deeper optical imaging. This technology can elucidate complex 3D structures and cellular architectures of relevance to both tissue physiology and pathology, including the diagnosis of clinical conditions (19–21).

In the present study, we hypothesized that orthopedic surgery may acutely impair attention processes as assessed with the 5-CSRTT, and this delirium-like behavior may correlate with CNS inflammation assessed by microglial morphology, glial fibrillary acidic protein (GFAP) expression, and blood-brain barrier (BBB) permeability. We also implemented a CLARITY protocol combined with light sheet microscopy to enable visualization and 3D rendering of pathological features associated with postoperative complications focusing on neuroinflammation and endothelial dysfunction.

MATERIALS AND METHODS

Animals

A total of 61 inbred C57BL6 (male, 12 weeks old) were purchased from The Jackson Laboratory (Bar Harbor, ME) and housed in the Mouse Behavioral and Neuroendocrine Analysis Core Facility. Animals were matched for weight and housed 3–5 per under controlled temperature and humidity with a 14:10 h light:dark cycle (lights on at 0600 h). Mice were fed standard rodent chow (Prolab RMH3500, Autoclavable; LabDiet, St. Louis, MO) and had access *ad libitum* access to food and water. Thirty animals were used for histological evaluation. Open field motor activity was assessed in 16 mice and was performed 24 h following fracture surgery (8 sham controls and 8 fracture animals). The remaining 15 mice were assigned to the 5-CSRTT study. One week before beginning the 5-CSRTT testing, animals were handled daily and food-restricted to achieve and be maintained at 85–90% normal body weight. Food restriction continued through the duration of the study. Once 5-CSRTT begun, mice were always fed 2–3 h following completion of training or testing. All experiments were conducted under an approved protocol from the Institutional Animal Care and Use Committee at Duke University Medical Center and under the guidelines described in the National Science Foundation "Guide for the Care and Use of Laboratory Animals" (2011). Duke University is an AAALAC certified institution.

Surgery

Tibial facture was performed as described (10) with minor modifications. Mice were anesthetized with isoflurane using the SomnoSuite apparatus, a low-flow digital anesthesia system (Kent Scientific Corporation, Torrington, CT). Heart rate, blood oxygen saturation, and core body temperature (36.5 $\pm$ 0.6°C) were monitored throughout the procedure using pulse oximetry and a homeothermic pad system (Kent Scientific Corporation). Muscles were disassociated following an incision on the left hind-paw. A 0.38-mm stainless steel pin was inserted into the tibia intramedullary canal, followed by osteotomy, and the incision was sutured with 6-0 Prolene.

Open Field Assessment of Activity Following Tibial Fracture Surgery

Motor activity was assessed in a 5-min open field test within 24 h of surgery for animals subjected to tibia fracture with sham controls matched for age and weight. Testing began when mice were singly placed into a 60 $\times$ 40 $\times$ 24 cm polyfoam box indirectly illuminated at 375 lux with a single camera suspended overhead interfaced to a computer running Ethovision 11.5 software (Noldus Information Technology Inc., Leesburg, VA). Activity of the mice was assessed with 3-point tracking and the total distance moved (cm) was scored for each animal.

5-Choice Serial Reaction Time Task (5-CSRTT)

Testing occurred in 5-CSRTT chambers (24 $\times$ 18.5 cm; MedAssociates, St. Albans, VT). Each operant chamber had five 1.24 cm^2 nose-poke apertures, illuminated with LED lights, with infrared diodes to register nose pokes into the aperture. A single food magazine with an LED light and infrared diodes was positioned on the opposite wall. The food magazine dispersed single food rewards (20 mg chocolate Rodent Purified Diet pellets; BioServ, Flemington, NJ). After surgery, perforated plastic mesh canvas (Darice Inc., Strongsville, OH) with 0.01 cm^2

openings were placed on bottoms of each test chamber to ensure animal mobility. Mice were trained and tested in the same chamber during 1,000 and 1,500 h. Animals were trained with a modified procedure (11, 22). For the first week of training (phase 1), all nose poke apertures were illuminated. If mouse poked into any hole, the food magazine was illuminated and a food reward dispensed. The mice had 5 s to retrieve and consume the food reward. After a 5 s inter-trial interval (ITI) the next trial began with the illumination of the nose poke apertures. This procedure was repeated until 20 rewards were earned or a maximum of 1 h had elapsed. Once mice earned 20 rewards and showed consistent performance for 3 days, the next phase was initiated. In phase 2, a single nose poke aperture was lit for a 5 s stimulus duration (SD). Animals could respond during the 5 s illuminated period or during the 5 s limited hold (LH) period which followed if the mouse didn't make an immediate selection while the aperture was lit. If the mouse selected the correct aperture during the SD or LH periods, the food magazine was illuminated and a food reward dispensed. Mice were given 5 s to retrieve the pellet. If a mouse failed to respond during the SD or LH periods or poked into an incorrect hole, the trial was immediately terminated and a 5 s time-out (TO) was initiated before proceeding to the next ITI. Mice were trained daily with the 5 s SD and 5 s LH until the animal achieved correct responses on at least 80 percent of the trials (i.e., 32 trials of 40 total trials/day) over 3-consecutive days. Of the 15 mice which began the study, 14 were capable of being trained to nose poke for food reward in phase 1 of training. Upon meeting criterion, the SD was decreased by 0.5 s each day. If the animal was successful in achieving 80% correct responses at that presentation time, the SD was reduced the following day by 0.5 s until the mouse reached a 2 s SD. In all cases, the LH was set to 5 s. When the mice exhibited at least 80% correct responses out of 40 trials for 3 consecutive days at the 2s SD, the animals were subjected to tibial fracture surgery within 24 h. Of the 14 mice that begun training with decreased SD, only 8 animals were capable of reaching the criterion for tibial fracture surgery. Surgery was done between 0700 and 1,200 h. Animals were given ∼25–28 h to recover following surgery before 5-CSRTT testing and this proceeded on day 1 post-surgery between 1,300 and 1,600 h. Testing continued daily with 40 trials per day with the 2 s SD and 5 s LH for 7 days until animals reached pre-surgical performance levels.

For all phases of training and testing, task performance was assessed by three primary measures. Correct responses were defined as the number of trials in which the mice nose-poked into the correct aperture during the SD or LH divided by the total number of trials administered (40 trials) and expressed as a percentage. The accuracy rate was calculated as the total number of trials in which the mouse made a correct response divided by the number of trials in which the animal made a nose-poke response and was expressed as a percentage. Finally, the omission rate was calculated as the number of trials in which the mouse failed to respond divided by the total number of trials (40 trials) and expressed as a percentage. In addition, the latency to nose-poke (s) was recorded for each trial. On trials when a mouse failed to nose-poke, a maximum latency of 7 s was recorded (2 s SD + 5 s LH).

Tissue Collection for Brain Samples

Under isoflurane anesthesia, mice were perfused transcardially with 30–50 mL PBS (Gibco, #10010-023), followed by 20–30 mL 4% paraformaldehyde (PFA) (#158127, Sigma-Aldrich, St. Louis, MO) in PBS, pH 7.4. Brains were harvested and post-fixed in 4% PFA at 4°C for 24 h. Brains were sliced into 1 mm thick coronal slices according to specific stereotaxic coordinates (Bregma 1.4 to 0.4; −1.2 to −2.2; −2.2 to −3.2 mm) with a vibratome. Slices were incubated in 1x PBS at 4°C for 24 h before beginning polymerization.

Tissue Polymerization and Active Tissue Clearing

Each 1 mm thick slice was incubated in 1 mL X-CLARITY™ Hydrogel Solution (#C1310X; Logos Biosystems, Annandale, VA) at 4°C for 24 h. After incubation, polymerization was performed using the X-CLARITY™ Polymerization System (Logos Biosystems) at 37°C for 3 h. Active tissue clearing occurred using the X-CLARITY™ Tissue Clearing System (Logos Biosystems) and electrophoretic tissue clearing (ETC) solution (#C13001; Logos Biosystems) with the following setting: 0.9 A, 37°C, for 3 h. After clearing, slices were washed 3x with PBS- 0.2% Triton™-X100 (#T8787; Sigma-Aldrich) solution overnight on a shaker at room temperature.

Tissue Labeling

After tissue clearing, each slice was incubated with primary antibody diluted in 1 mL blocking buffer (10% normal donkey serum in PBS-0.2% Triton™-X100 solution) at 4°C for 3 days. Slices were washed 3x in PBS-0.1% Triton™-X100 solution at 4°C overnight. Slices were incubated in secondary antibody and DAPI diluted in 1 mL blocking buffer at 4°C for 3 days. Slices were washed 3x in blocking buffer at 4°C overnight and were stored in PBS at 4°C before mounting. Details of the primary and secondary antibodies can be found in **Table 1**.

Imaging Setup

Slices were embedded with 1% agarose (#BP160-100, ThermoFisher Scientific, Waltham, MA) and placed in 1 mL syringes (#300013; BD Biosciences, San Jose, CA) without

TABLE 1 | Antibodies used for immunostaining on clarified tissues.

Antibody	Company	Catalog#	Species	Dilution
Iba-1	Waco	019-19741	Rabbit	1:500
GFAP	Dako	Z0334	Rabbit	1:500
Claudin 5	ThermoScientific	352588	Mouse	1:200
CD31	R&D systems	AF3628	Goat	1:200
TFEB	Invitrogen	PA5-96632	Rabbit	1:500
LAMP1	DSHB	AB528127	Mouse	1:200
AQP4	Mllipore	AB3594	Rabbit	1:500
Fibrinogen	Dako	A0080	Rabbit	1:200
Alexa Fluor Cy3 anti-Rabbit IgG (H+L)	JacksonImmuno	711-165-152	Donkey	1:200
DAPI	Sigma	D9542	–	1:1,000

tips and incubated with mounting solution (#C13101; Logos Biosystems) at 4°C overnight followed by 1 h incubation at room temperature before imaging. Slices were imaged with a light sheet fluorescence microscope (LSFM, Z1; Zeiss, Germany) at the Duke University Light Microscopy Core Facility. During imaging, slices were immersed with mounting solution in a CLARITY optimized sample chamber. Slices were rotated to be parallel with the glass of the detection lens. All z-stacks and tile scans were acquired with 16-bit depth and 1,920 × 1,920 pixels using 5x or 20x objectives. Refractive index of the detection objective was set as 1.46. For laser excitations, the 405/488/561/640 filter set was used. Laser intensities were set between 0.5 and 2%. The exposure time for each frame was 29.97 ms. The step interval between frames was 0.659 μm.

Image Analyses

Tile scans were stitched together and presented as high resolution 3D rendering and corresponding movies using Arivis 4D viewer (Washington, DC). The 3D rendering of single z-stack was performed with Imaris software 8.21 (Bitplane USA, Concord, MA). Immunoreactivity intensity for each channel was calculated automatically with Imaris. For automated detection of glia cells the "surface" function of Imaris was used. Volume size of each glial cell was automatically calculated after removing those segmented at the edges of the image frame. The 3D algorithm-based surface rendering and quantification of fluorescence intensity for Iba-1, IgG, GFAP, and claudin-5 were performed with Imaris at 100% rendering quality. Each channel was analyzed separately. 3D surface rendering detected immunostained cells and their processes. The channel mean intensity filter was applied and minimum thresholds were used for all the experimental groups. Voxel-based surface rendering was applied to each channel. The preset parameters remained constant throughout the subsequent analysis of Iba-1, IgG, GFAP, and claudin-5 immunoreactivities. The quantification of microglia and astrocyte number (GFAP co-labeled with DAPI) was facilitated using the Spot tools of Imaris module. All the adjustments during image processing in Imaris and Arivis were performed under identical conditions for the surgical and control groups.

Dextran Imaging Studies to Detect Blood-Brain Barrier (BBB) Permeability

Mice were deeply anesthetized with isoflurane followed by transcardial infusion of TMR (Tetramethyl Rhodamine) 70kD dextran tracer (ThermoFischer Scientific) that was diluted in sterile PBS into 2 mM stocks and stored from light at −20°C. After 5 min, mice were perfused using 20 mL of 0.1 M PBS. The brains were harvested immediately and embedded in optimal cutting temperature (OCT) compound on dry ice (Tissue-Tek, USA). The blocks were cut into 10 μm sections using a cryostat (Microm HM550; Thermo Scientific, Waltham, MA) and the sections transferred to slides placed at room temperature. Once dried they were stored at −80°C. On the day of staining, the slides were thawed at RT for 10 min and the sections fixed with 4% PFA for 10 min at room temperature followed by washing in PBS for 5 min. Subsequently, sections were blocked using blocking buffer made of 10% normal donkey serum (#D9663; Sigma-Aldrich) with 0.3% Triton X-100 in PBS for 1 h at RT. The slides were then incubated overnight at 4°C with CD31 primary antibody (1:200, Goat CD31, R&D Systems, USA), diluted in the blocking buffer. The next day, the slides were washed with blocking buffer for 15 min followed by secondary antibody incubation in the above buffer for 1 h at room temperature. For CD31 immunostaining, donkey anti-goat Alexa 633 was used at a dilution of 1:500 (ThermoFischer Scientific). For staining of nuclei, DAPI (4,6-diamidino-2-phenylindole dihydrochloride, 1:1,000; Sigma-Aldrich) in PBS was incubated for 20 min. The sections were mounted, dehydrated and cover-slipped. Images were acquired using Zeiss 880 inverted confocal Airy scan. For the quantification, z-stack images were imported into Imaris x64 (version 9, Bitplane AG, Zurich, Switzerland) for 3D surface rendering and volumetric analysis. After display adjustment, the DAPI filter was removed to view the images in blend mode with rendering quality set to 100%. A volume filter was then applied to remove non-specific staining and minimum thresholds were used for both control and surgery groups. To quantify dextran volume, a "Filament Trace" was created from a masked surface channel of CD31. Later, by removing the CD31 filter the dextran volume was quantified using same threshold parameters for both control and surgery groups.

Statistics

The data were expressed as mean ± S.E.M and sample sizes (n) are provided in the figure legends. The behavioral data were analyzed with SPSS 25 (IBM SPSS Statistics, Chicago, IL) using repeated measures ANOVA (RMANOVA) where test day was used as the within-subject variable for 5-CSRTT. For open field testing, a comparison of distance moved for surgical animals compared to shams was examined with an independent samples t-test. Statistical analyses for the imaging data were made using Prism GraphPad 8.0 (GraphPad Software, San Diego, CA). Bonferroni corrected pair-wise comparisons were used for *post-hoc* analyses. In all cases, a $P < 0.05$ was considered statistically significant.

RESULTS

5-CSRTT

Attention impairment is a salient component of delirium (1). Here, we assessed attention using the 5-CSRTT task before and following orthopedic surgery (**Figure 1A**). Several measures of performance were evaluated, including the percent correct responses, accuracy, omitted responses, and the latency for the correct responses. A RMANOVA for the percent correct responses revealed a significant effect across days [$F_{(7,49)} = 21.716$, $p < 0.001$; **Figure 1B**]. Mice were significantly impaired over the first 3 days post-tibial fracture ($p \leq 0.043$–0.001). For percent accuracy the RMANOVA revealed a significant time effect [$F_{(7,49)} = 4.612$, $p < 0.001$; **Figure 1C**], however, Bonferroni corrected *post-hoc* comparisons failed to find a significant reduction in accuracy on the first day following surgery compared to baseline ($p = 0.346$). Interestingly,

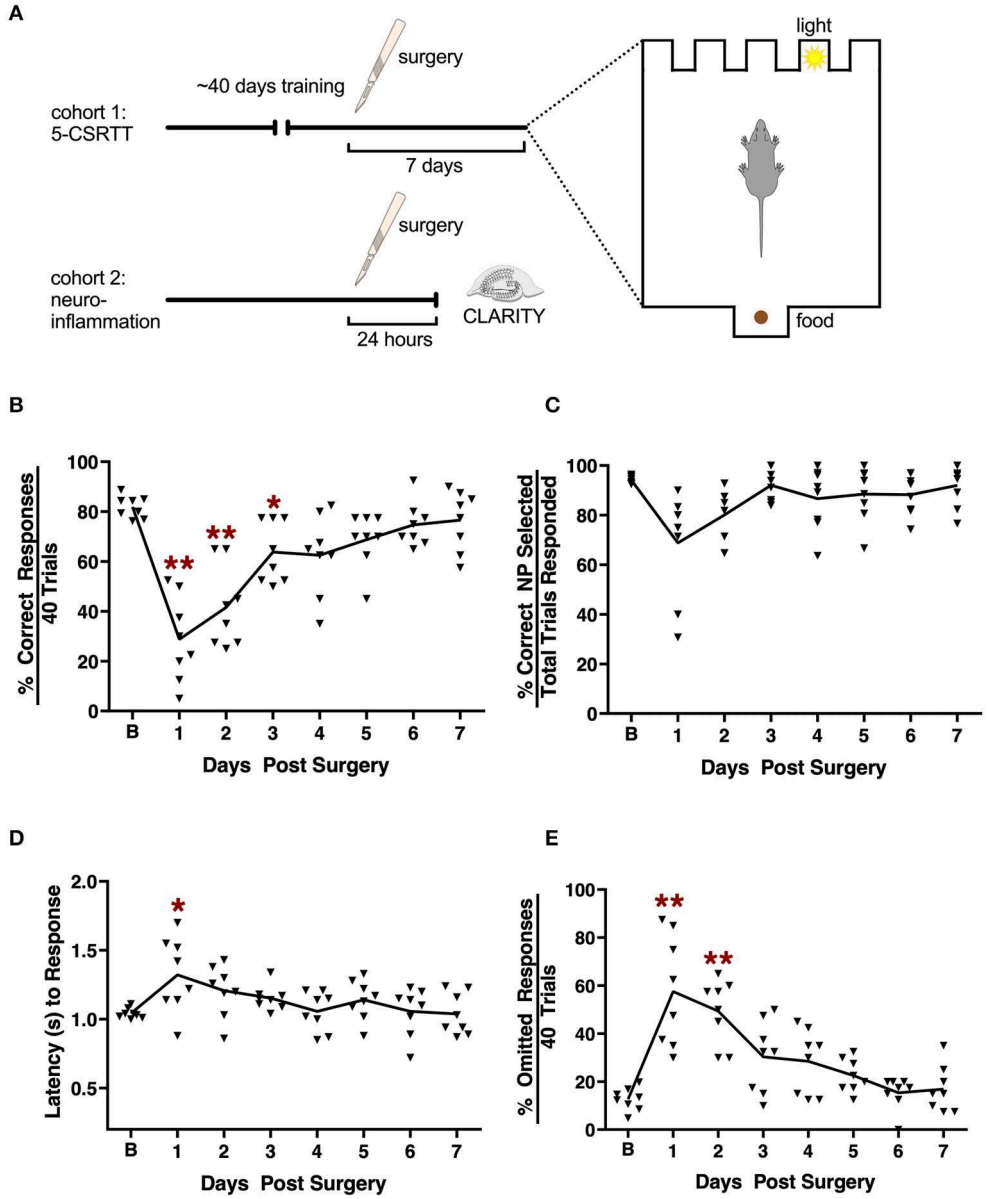

FIGURE 1 | Effects of tibial fracture on attention processes using the 5-choice serial reaction time task. **(A)** Schematic of the experimental design. **(B)** Tibial fracture significantly impaired overall performance over the first 3 days post-surgery as assessed by the percent correct responses out of a total of 40 trials/day. Percent accuracy **(C)** showed small but non-significant changes following surgery. Latency (s) to correct responding **(D)** was prolonged on day 1 post-surgery compared to baseline prior to surgery. **(E)** The percent omission errors increased significantly for 2 days post-surgery before returning to baseline. Baseline 5-CSRTT performance represents the mean performance on the last 4 prior to surgery. $n = 8$ mice; results are presented as means ± SEMs; **(A–C)** $^{*}p < 0.05$, $^{**}p < 0.01$ Bonferroni *post hoc* for post-surgical time point compared to pre-surgical "baseline".

the mean overall latency to respond to the correct nose-poke aperture (**Figure 1D**) was highly significant [$F_{(7,49)} = 4.164$, $p < 0.001$]. Despite this small, albeit significant delay across test days, the Bonferroni comparisons failed to find a significant difference between day 1 post-surgery compared to baseline ($p = 0.599$). Tibial fracture was sufficient to induce an increase in omission errors [$F_{(7,49)} = 16.932$, $p < 0.001$; **Figure 1E**] over the first 2 days post-surgery. Bonferroni analyses revealed significant increases in omission errors on days 1 and 2 post-surgery compared to the baseline omission rate ($p \leq 0.026$–0.001). As a control, we evaluated general locomotor activity 1 day after surgery and found no significant differences, including changes in body weight or food intake, that may have confounded the 5-CSRTT results (**Supplementary Figure 1**). Taken together, these results indicate that attention processes as evaluated with the 5-CSRTT

task are significantly impaired at least on the first day post-surgery, and this deficiency is not the result of any motor impairment.

Surgery Alters Microglial Morphology in Clarified Hippocampus

Next we evaluated postoperative neuroinflammation using CLARITY. One mm thick brain slices were processed and cleared using electrophoresis (active clearing). Ortho-image and 3D reconstruction of the whole 1,000 μm z-stack was performed to test imaging depth and antibody penetration, and it was found to be homogeneous across clarified slices (**Supplementary Figure 2**, **Supplementary Video 1**). Orthopedic surgery activates microglial cells in the hippocampus, with morphological changes observed at 24 h post-surgery by standard histology (23, 24). Thus, we have focused our analyses at this time point using CLARITY. Surgery significantly affected microglial morphology, with an overall reduction in their ramifications (**Figure 2A**). Retraction of thin-ramified processes is associated with microglial activation in response to changes in the CNS microenvironment, such as pro-inflammatory cytokines and infiltrating immune cells (25). Larger, more complex cells indicative of a surveillance state, were clearly identifiable in control slices but were absent 24 h after surgery. Using surface area 3D reconstruction in Imaris we confirmed the decrease in the average volume of microglial cells, with a significant overall loss of area coverage following surgery ($p < 0.05$, **Figure 2B**). Further studies in surgery group failed to reveal any gross changes in the number of microglia compared to control (**Figures 2C,D**). Consistent with altered microglial morphology in the surgery group, we observed an increased translocation of transcription factor EB (TFEB), a master regulator of the autophagy-lysosome system along with the LAMP-1 expression that coordinates autophagy and lysosomal biogenesis ($p < 0.001$, **Figures 2E,F**). These results suggest that higher activity of lysosomal biogenesis in activated microglia is closely linked to the inflammation in the CNS.

Time-Dependent BBB Opening After Surgery

BBB disruption is a key hallmark of many neurodegenerative conditions and it often correlates with disease progression (26). Here we used CLARITY to evaluate IgG deposition in whole hippocampal tissue 24 h after surgery ($p < 0.001$, **Figures 3A,B**). Surgery increased IgG deposition as compared to naive control mice (**Supplementary Video 2**). We confirmed these results using another marker for BBB disruption, fibrinogen, which was also up-regulated in the vessels of operated mice ($p < 0.001$, **Figures 3C,D**). Parenthetically, fibrinogen is a blood coagulation protein deposited in the brain during neurodegeneration that drives microglial activation (via CD11b receptor binding) and cognitive dysfunction (27). Interestingly, experiments using the 70 kD dextran tracer perfused at 24 h after surgery revealed no BBB leakage compared to control (**Figures 3E,F**), suggesting the barrier opens transiently within the first 24 h after surgery.

Astrocytic and Endothelial Dysfunction After Surgery

Astrocytes are critical to the formation and maintenance of the BBB (28). At 24 h after surgery we found that orthopedic surgery induced significant changes in the expression of the intermediate filament GFAP in clarified hippocampal slices (**Figure 4A**). We evaluated this increase by using surface rendering in Imaris, which revealed changes both in the number of GFAP-positive astrocytes ($p < 0.05$, **Figure 4B**) as well as coverage area of these enlarged cells ($p < 0.001$, **Figure 4C**). Next, we focused on the expression of aquaporin-4 (AQP4), a water channel that is highly localized in the end feet of astrocytes that are in contact with BBB. Alterations in the expression of AQP4 has been linked to neurodegenerative diseases (29). AQP4 levels were reduced in the hippocampus of surgical mice compared to naïve controls ($p < 0.001$, **Figures 4D,E**). Finally, using CLARITY we measured alterations in claudin-5 (cld-5), one of several intracellular tight junction proteins that form BBB (**Figures 4F,G**). Surgery caused a significant disruption of cld-5 compared to control 24 h after surgery. Interestingly, the loss of cld-5 coverage was especially notable in the granular cell layer, as well as other areas of the hippocampus. Collectively, these results suggest that orthopedic surgery triggers astrogliosis and endothelial impairments in the hippocampus.

DISCUSSION

This study provides new evidence for the impact of peripheral surgery on a cognitive domain of major relevance to postoperative delirium. We also explored the contribution of postoperative neuroinflammation and endothelial dysfunction using CLARITY in this clinically-relevant model of orthopedic surgery.

Inattention is one of the core features of delirium and a mandatory component for diagnosis in compliance with DSM-5 criteria (30). However, delirium is a very heterogeneous syndrome characterized by multiple features and subtypes, which often make its characterization challenging and under diagnosed in hospital settings (31). Other cardinal features of delirium include an acute onset with fluctuating course, disorganized thinking, and altered level of consciousness, which can be difficult to define both in humans and preclinical models. In rodents, we and others have previously reported on different behavioral deficits affected by orthopedic surgery. These include changes in fear conditioning (23, 24, 32, 33), novel object recognition memory/open field (33, 34), zero maze (35), Y-maze (32, 36), and Morris water maze (37). While spatial and working memory tasks have overlapping mechanisms with attention (38), the 5-CSRTT allowed us to examine and manipulate more discrete aspects of attention. The 5-CSRTT is an appetitive task and is one of the most robust assays to study visuospatial attention in rodents, which is analogous the commonly used continuous performance task used measure of attention in both clinical and research settings (39). Our results using the 5-CSRTT after surgery demonstrate the most profound impairment occurs

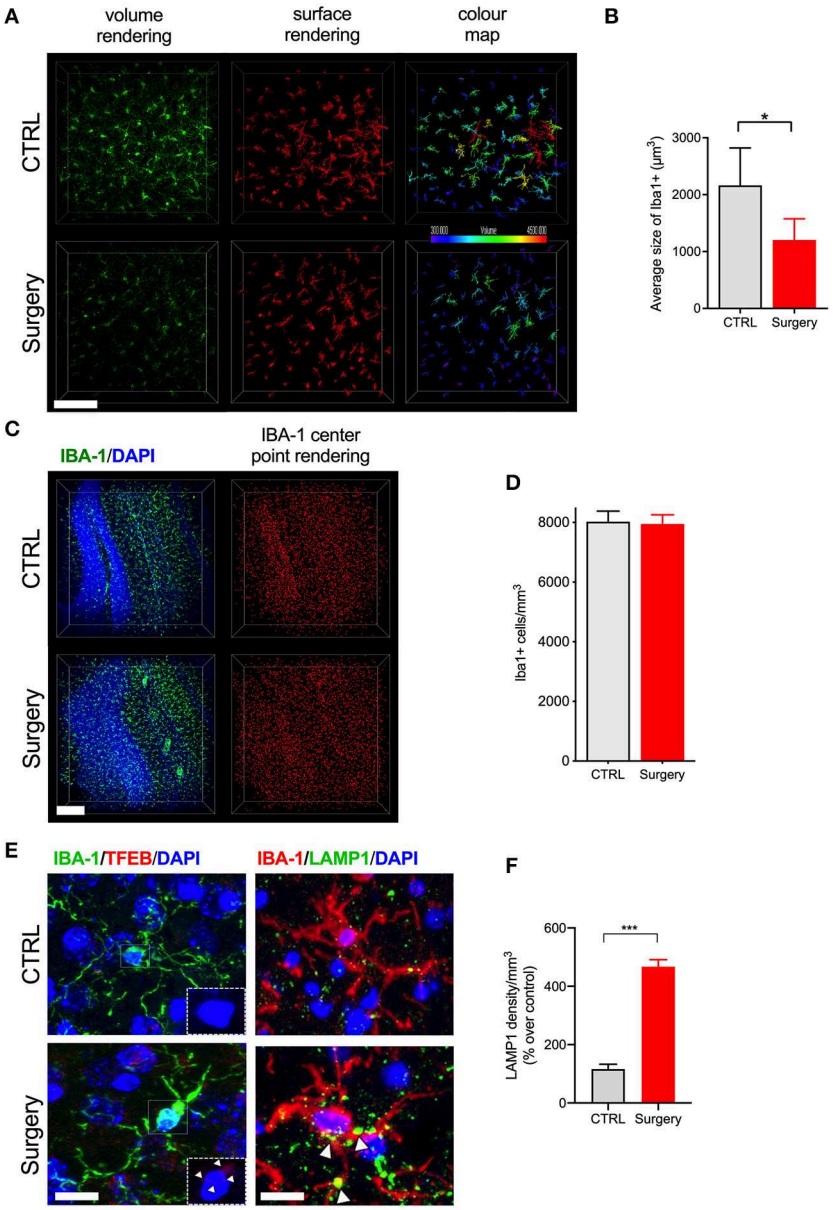

FIGURE 2 | Tibial fracture alters microglial morphology and increases TFEB and LAMP1 expression. **(A)** Iba-1 staining was used to detect cytoskeletal alterations as morphological changes in microglia. Surgery significantly reduced larger, ramified, microglia. A 3D reconstruction of cell morphometry in the hippocampus is shown in the color map, with a greater loss of larger cells (green to red spectrum) in mice after tibial fracture. Scale bar: 150 µm. **(B)** Imaris-based quantification demonstrates a significant reduction in the average size of cells 24 h after surgery. $n = 4$ (CTRL) and 5 (surgery). **(C)** Iba-1 positive cell numbers were measured using center-point rendering. Scale bar: 150 µm. **(D)** Imaris-based quantification revealed no change in the Iba-1 positive cell numbers between the control and surgery groups. **(E)** Double immunostaining of Iba1 (green), TFEB (red), and Iba1 (red), LAMP1 (green) in the DG region of hippocampus. Scale bar: 2 µm. **(F)** Quantification of LAMP1 in the microglia in control and surgery groups. Tibial fracture increased the expression of both LAMP1 and TFEB puncta in the microglia. The results are presented as means ± SEMs, $^{*}p < 0.05$, $^{***}p < 0.001$ Student's *t*-test ($n = 3$ for autophagy markers).

24 h after surgery with full recovery by day 5 post-procedure. This time-course is very similar to the clinical manifestation of delirium and it provides a valid endpoint to test possible interventions. Notably, discrete aspects of 5-CSRTT performance are centrally mediated by cholinergic and other transmitter manipulations (40). Acetylcholine (ACh) has been strongly linked to selective attention processing across species, including humans (41), and cholinergic dysfunction has been proposed as a key feature of delirium (42, 43). Recent data from elective surgical patients suggest that acetylcholinesterase activity, the enzyme responsible for degrading ACh, is higher in patients with delirium compared to non-delirious controls, supporting

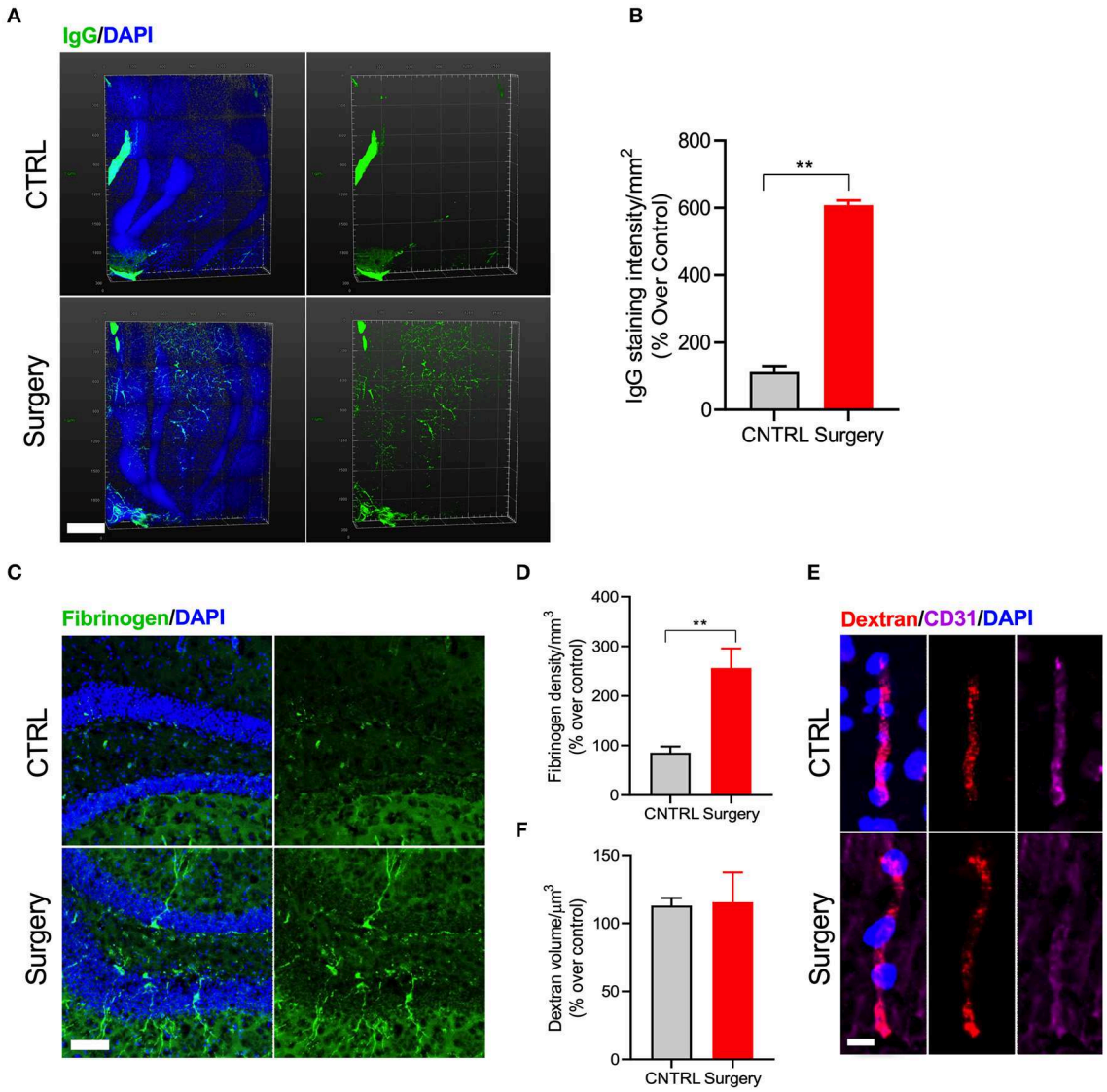

FIGURE 3 | Surgery increased IgG and fibrinogen deposition. **(A)** Double staining with IgG and DAPI-nuclear stain using CLARITY. **(B)** Quantification of the IgG deposition in both control and surgery groups. Higher levels of IgG deposition are observed in the DG region of the hippocampus 24 h after orthopedic surgery. Scale bar: 500 µm. **(C)** Representative images of fibrinogen with DAPI in the DG region of the hippocampus 24 h after tibial fracture. **(D)** Quantification shows an increased fibrinogen deposition in the surgery group compared to control. Scale bar: 20 µm. **(E)** Representative images showing immunofluorescence staining for dextran tracer along with CD31 to assess brain permeability changes in mice after surgery. Scale bar: 20 µm. **(F)** Quantification of the dextran volume in the vessel. No leakage of tracer from vessels was observed, confirming that equal volume of dextran was present in both groups. The results are presented as means ± SEMs, $^{**}p < 0.01$ Student's *t*-test ($n = 4$).

the cholinergic hypothesis for postoperative delirium (44). Similar findings in rodents suggest that cholinergic depletion predisposes to acute cognitive impairments and microgliosis after systemic LPS challenge (45). Here, we described changes in the expression of autophagy markers in microglia, which may relate to the systemic inflammatory response and monocytic infiltration following orthopedic surgery (46–48). Whether autophagy is induced by this peripheral response or centrally as a protective mechanism for microglia to resolve neuroinflammation needs further elucidation. Gliosis and endothelial dysfunction have been recently observed in critically ill patients with delirium (49). Using CLARITY we have implemented a staining protocol to improve quantification of these changes from standard immunofluorescence and are now better able to evaluate morphological changes in these highly complex structures. Vascular patterns of BBB disruption can be observed in the hippocampus at 24 h. Interestingly, injection of 70 kDa dextran at this time point revealed no significant parenchymal leak,

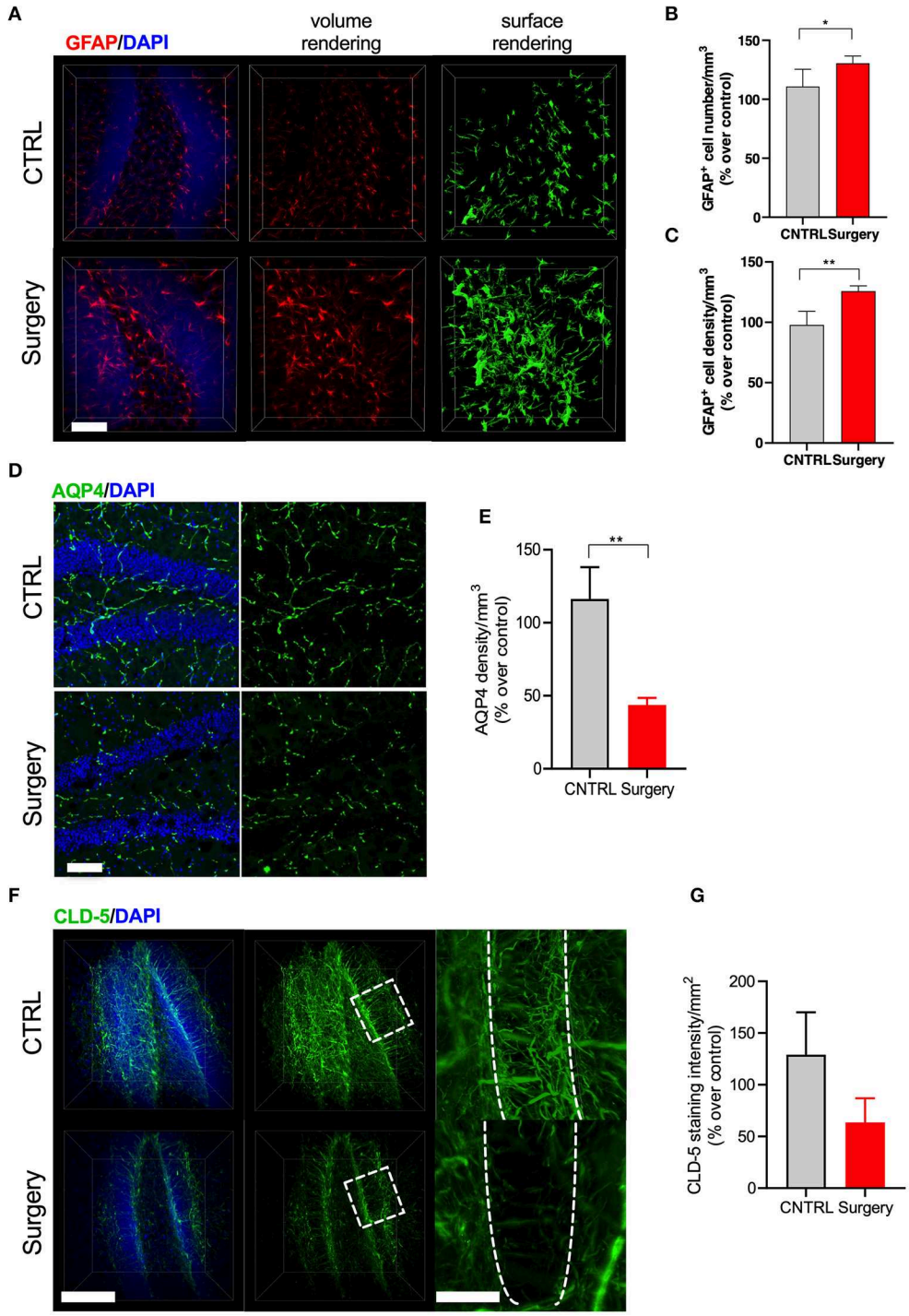

FIGURE 4 | Surgery-induced astrogliosis and endothelial dysfunction. **(A)** GFAP staining and 3D reconstruction of astrocytes 24 h after surgery in clarified tissues. **(B)** Quantification revealed that surgery induces astrogliosis by modifying both cellular process and **(C)** numbers of GFAP-positive cells in the DG. **(D)** Representative image of AQP4 from the DG region of hippocampus across control and surgery groups. $N = 4$ (CTRL) and 5 (surgery). Scale bars: 20 μm. **(E)** Quantification of the percent area of AQP4 in the DG area between control and surgery groups. **(F)** 3D surface and volume rendered reconstruction of tight junction marker claudin-5 staining 24 h after surgery. $N = 2$ for CLD-5. Scale bars: 50 and 20 μm (insets). **(G)** Quantification revealed that control mice show increased CLD-5 expression while surgery significantly reduced it. The results are presented as means ± SEMs, $^{*}p < 0.05$, $^{**}p < 0.01$ Student's *t*-test.

suggesting the barrier opens transiently. These changes can be detected using other markers, such as IgG and fibrinogen. This is consistent with other work where laparotomy triggered changes in selective tight junctions, including claudin-1, occluding, ZO-1, and 10 kDa dextran but not 70 kDa (50). Thus, it is possible for peripheral cytokines to enter the CNS and trigger delirium-like behaviors after surgery. Circulating plasma proteins, including pro-inflammatory makers like C-reactive protein and IL-6, have been recently correlated with patients developing delirium after non-cardiac surgery (51). Importantly, we previously found IL-6 to be upregulated both in the periphery as well as in the CNS (23), and administration of a selective monoclonal antibody was shown to prevent postoperative neuroinflammation and cognitive decline in this model (52). Selective blockade of pro-inflammatory cytokines may have translational implication for delirium treatment, although side effects associated with excessive immunosuppression and/or impaired wound healing will need to be evaluated carefully. Since, pro-inflammatory cytokines are detected in the cerebrospinal fluid (CSF) of patients with delirium (15, 53), blocking these mediators in the CSF without affecting the peripheral immune response may reveal alternative approaches to prevent surgery-induced neuroinflammation. Finally, many of these cytokines are already upregulated at baseline in patients at-risk for delirium. In fact, aging and chronic stress elevates IL-6 amongst other mediators (54, 55) and these cytokines can further prime microglia cells and possibly impair neuro-immune circuits of relevance to delirium-like behavior. Indeed surgery also triggers acute plasma cortisol, which was found elevated in patients with delirium after cardiac surgery (56). However, recent trials using steroids have not shown significant effects on delirium outcomes after surgery and critical illness (57, 58). In this context, delirium may be considered a surrogate marker for neuroinflammation in *selective* brain areas that may contribute to the different clinical manifestations of this disorder (59), thus requiring more selective disease-modifying therapies to treat and possibly prevent.

Preclinical models to study postoperative delirium have been notably limited. Systemic infective challenges (e.g., lipopolysaccharide or LPS) have been used to examine certain aspects of behavioral change. Culley et al. (60) have evaluated the effects of LPS using the attention set-shifting task (AST) and found selective impairments in attention/executive function in aged rats for up to 72 h post-surgery. Parenthetically, AST involves a series of discriminations based on stimulus dimensions such as digging medium or shape cue in a task analogous to the Wisconsin Card Sorting Task. Without affecting initial discrimination learning, LPS impaired reversal-learning at 24 but not at 48 h and extra-dimensional shift discrimination at 72 h. Transient changes in working memory have been similarly described in other delirium models of neurodegeneration after LPS exposure using the Y maze, T maze alternation tasks, and novel object recognition memory (61). Peng et al. (62) have evaluated certain aspects of delirium in a mouse model of abdominal surgery using composite Z scores from a battery of tests including the buried food test, open field test and Y maze. They found that anesthesia and surgery impaired both natural and learned behavior of the mice with acute onset and fluctuating course, modeling one of the cardinal features of delirium. Further, other studies have described behavioral changes after anesthesia exposures that can affect neuronal circuits related to recognition memory, arousal, and motoric behaviors (63, 64). In this study we have not included an anesthesia exposure group for several reasons. First, we previously reported that isoflurane exposure in this exact model does not trigger significant neuroinflammation, or behavioral deficits (23). We have confirmed this by assessing sham and surgical mice in the open field without observing significant deficits. Second, recent work by Hambrecht-Wiedbusch et al. showed no effects of general anesthesia (including ketamine exposure) focusing on attention in healthy rats using the 5-CSRTT (65). Last, we allowed the mice to have a full 24 h recovery before resuming testing 25 h later in order to avoid any possible effects of isoflurane exposure on food intake or nausea; although studies have shown that a single exposure of isoflurane in C57BL/6 mice does not have significant effects on food intake for up to 9 days post exposure (66).

This study presents limitations and challenges to this emerging field of preclinical research. Inattention is one of many features of delirium; in fact, its fluctuating course was not addressed by these experiments and may require other correlates, such as electrophysiology, to fully ascertain in rodents. Further, not all patients experience delirium. However, our data indicate that mice have different degrees of attentional impairment so this may provide opportunities to identify resiliency traits that may impact on perioperative cognitive outcomes. Finally, we have not addressed the contribution of advanced age and other risk factors into this model, which will be objective of future work as well as more mechanistic experiments to further identify the contribution of neuroinflammation and endothelial dysfunction as key drivers of delirium pathogenesis. Defining more specific targets at the neurovascular unit may provide much needed therapies to resolve neuroinflammation and inform future clinical trials.

In conclusion we have provided translational evidence using a well-established surgical model to study attention processes and features relevant to the pathophysiology of postoperative delirium. The utility of these endpoints can be translated into trials evaluating biomarkers of neuro-glia and endothelial dysfunction after surgery, which may contribute to a better understanding on the genesis of postoperative delirium.

DATA AVAILABILITY STATEMENT

The raw data supporting the conclusions of this manuscript will be made available by the authors, without undue reservation, to any qualified researcher.

AUTHOR CONTRIBUTIONS

CX optimized the CLARITY protocol. RV, CX, and SS analyzed light-sheet images. RV performed dextran

experiments and immunostainings. FP and RR conducted and analyzed behavioral experiments. RR, WW, and NT designed research and provided new analytical tools. NT drafted the manuscript. All authors read and approved the final manuscript.

FUNDING

This study was supported by NIH grants R01AG057525, and R21AG055877-01A1, the Duke Institute for Brain Sciences, and a DREAM Innovation Grant from Duke Anesthesiology to purchase the X-CLARITY setup (to NT). Some of the behavioral experiments were conducted with equipment and software funded with a North Carolina Biotechnology Center grant (to WW). The Zeiss light sheet was purchased with an NIH S10 grant 1S10OD020010-01A1 (PI Lisa Cameron).

ACKNOWLEDGMENTS

NT attended the hands-on CLARITY training workshops managed and developed by Kristin Overton, Ph.D. and Karl Deisseroth, M.D., Ph.D. at Stanford University. We thank Ping Wang, Ph.D. (Terrando lab, Duke University) for providing the image of the agar mount; Benjamin Carlson, Ph.D. (Light Microscopy Core Facility, Duke University) for excellent technical support with the light sheet imaging; and Christopher Means (Behavioral Core Facility at Duke University) for assistance in behavioral testing.

SUPPLEMENTARY MATERIAL

The Supplementary Material for this article can be found online at: https://www.frontiersin.org/articles/10.3389/fimmu.2019.02675/full#supplementary-material

Supplementary Figure 1 | Schema for 5-choice serial reaction time task at the time of tibial fracture. **(A)** A trial is initiated once a mouse is placed into a darkened 5-CSRTT chamber. Testing begins when one of the five nose-poke apertures is randomly illuminated. The nose poke aperture is lit for 2 s and the mouse has 5 s to respond after the light is extinguished. If the mouse responds with a nose-poke in the lit aperture ("correct response"), the food magazine is immediately illuminated and a 20 mg chocolate food pellet ("reward") is dispensed. The mouse has 5 s to consume the food reward, followed by a 5 s inter-trial interval (ITI) before the commencing of the next trial. If the mouse responds with a nose-poke into an unlit aperture ("incorrect response") or fails to respond at all ("omission"), the mouse is given a 5 s time-out (TO), where all lights are extinguished, and the 5 s ITI. **(B)** Open field activity in mice 24-h following tibial fracture. No significant differences were found between sham ($n = 10$) and mice subjected to tibia fracture ($n = 10$) for distance (cm) traveled during a 5 min open field tested 24 h post-surgery. **(C,D)** represent body weight and food intake in the mice exposed to the 5-CSRTT task. No significant changes were observed throughout the duration of the study. Results are presented as means ± S.E.M.

Supplementary Figure 2 | Schema of the clearing process and transparency of 1 mm coronal brain slices. **(A)** The transparency and agar mount for 1 mm mouse brain slice after tissue clearing. **(B)** Imaging depth was verified using Iba-1 (green)/DAPI (blue) immunostaining and **(C)** staining quality evaluated at every 200 μm z-stack intervals up to 1,000 μm (20X objective, stack size 1 mm). $n = 5$ slices. Scale bars: 4 mm **(A)**, 200 μm **(B)**, 100 μm **(C)**.

Supplementary Video 1 | Iba1+ microglia in the hippocampus. Cleared brain slices were stained with Iba1 (Green) and DAPI (Blue). The video was generated using Arivis 4D viewer.

Supplementary Video 2 | IgG deposition in the hippocampus 24 h after surgery. Endothelial permeability was assessed by IgG staining (Green) followed by DAPI counterstain (Blue). The video was generated using Arivis 4D viewer.

REFERENCES

1. Marcantonio ER. Delirium in hospitalized older adults. *N Engl J Med*. (2017) 377:1456–66. doi: 10.1056/NEJMcp1605501
2. Inouye SK, Marcantonio ER, Kosar CM, Tommet D, Schmitt EM, Travison TG, et al. The short-term and long-term relationship between delirium and cognitive trajectory in older surgical patients. *Alzheimers Dement*. (2016) 12:766–75. doi: 10.1016/j.jalz.2016.03.005
3. Girard TD, Jackson JC, Pandharipande PP, Pun BT, Thompson JL, Shintani AK, et al. Delirium as a predictor of long-term cognitive impairment in survivors of critical illness. *Crit Care Med*. (2010) 38:1513–20. doi: 10.1097/CCM.0b013e3181e47be1
4. Leslie DL, Marcantonio ER, Zhang Y, Leo-Summers L, Inouye SK. One-year health care costs associated with delirium in the elderly population. *Arch Intern Med*. (2008) 168:27–32. doi: 10.1001/archinternmed.2007.4
5. AGS/NIA Delirium Conference Writing Group, Planning Committee and Faculty. The American Geriatrics Society/National Institute on aging bedside-to-bench conference: research agenda on delirium in older adults. *J Am Geriatr Soc*. (2015) 63:843–52. doi: 10.1111/jgs.13406
6. Geisser ME, Kratz AL. Cognitive dysfunction and pain: considerations for future research. *Pain*. (2018) 159:189–90. doi: 10.1097/j.pain.0000000000001093
7. Inouye SK, Westendorp RG, Saczynski JS. Delirium in elderly people. *Lancet*. (2014) 383:911–22. doi: 10.1016/S0140-6736(13)60688-1
8. Lee HB, Oldham MA, Sieber FE, Oh ES. Impact of delirium after hip fracture surgery on one-year mortality in patients with or without dementia: a case of effect modification. *Am J Geriatr Psychiatry*. (2016) 25:308–15. doi: 10.1016/j.jagp.2016.10.008
9. Mosk CA, Mus M, Vroemen JP, van der Ploeg T, Vos DI, Elmans LH, et al. Dementia and delirium, the outcomes in elderly hip fracture patients. *Clin Interv Aging*. (2017) 12:421–30. doi: 10.2147/CIA.S115945
10. Xiong C, Zhang Z, Baht GS, Terrando N. A mouse model of orthopedic surgery to study postoperative cognitive dysfunction and tissue regeneration. *J Vis Exp*. (2018). doi: 10.3791/56701
11. Patel S, Stolerman IP, Asherson P, Sluyter F. Attentional performance of C57BL/6 and DBA/2 mice in the 5-choice serial reaction time task. *Behav Brain Res*. (2006) 170:197–203. doi: 10.1016/j.bbr.2006.02.019
12. Robbins TW. The 5-choice serial reaction time task: behavioural pharmacology and functional neurochemistry. *Psychopharmacology*. (2002) 163:362–80. doi: 10.1007/s00213-002-1154-7
13. Heneka MT, Carson MJ, El Khoury J, Landreth GE, Brosseron F, Feinstein DL, et al. Neuroinflammation in Alzheimer's disease. *Lancet Neurol*. (2015) 14:388–405. doi: 10.1016/S1474-4422(15)70016-5
14. Subramaniyan S, Terrando N. Neuroinflammation and perioperative neurocognitive disorders. *Anesth Analg*. (2019) 128:781–8. doi: 10.1213/ANE.0000000000004053
15. Hirsch J, Vacas S, Terrando N, Yuan M, Sands LP, Kramer J, et al. Perioperative cerebrospinal fluid and plasma inflammatory markers after orthopedic surgery. *J Neuroinflammation*. (2016) 13:211. doi: 10.1186/s12974-016-0681-9
16. Neerland BE, Hall RJ, Seljeflot I, Frihagen F, MacLullich AM, Raeder J, et al. Associations between delirium and preoperative cerebrospinal fluid C-Reactive Protein, Interleukin-6, and Interleukin-6 receptor in individuals with acute hip fracture. *J Am Geriatr Soc*. (2016) 64:1456–63. doi: 10.1111/jgs.14238

17. Chung K, Wallace J, Kim SY, Kalyanasundaram S, Andalman AS, Davidson TJ, et al. Structural and molecular interrogation of intact biological systems. Nature. (2013) 497:332–7. doi: 10.1038/nature12107
18. Chung K, Deisseroth K. CLARITY for mapping the nervous system. *Nat Methods*. (2013) 10:508–13. doi: 10.1038/nmeth.2481
19. Hsueh B, Burns VM, Pauerstein P, Holzem K, Ye L, Engberg K, et al. Pathways to clinical CLARITY: volumetric analysis of irregular, soft, and heterogeneous tissues in development and disease. *Sci Rep*. (2017) 7:5899. doi: 10.1038/s41598-017-05614-4
20. Epp JR, Niibori Y, Liz Hsiang HL, Mercaldo V, Deisseroth K, Josselyn SA, et al. Optimization of CLARITY for Clearing Whole-Brain and Other Intact Organs(1,2,3). *eNeuro*. (2015) 2:ENEURO.0022-15.2015. doi: 10.1523/ENEURO.0022-15.2015
21. Yang B, Treweek JB, Kulkarni RP, Deverman BE, Chen CK, Lubeck E, et al. Single-cell phenotyping within transparent intact tissue through whole-body clearing. *Cell*. (2014) 158:945–58. doi: 10.1016/j.cell.2014.07.017
22. Bari A, Dalley JW, Robbins TW. The application of the 5-choice serial reaction time task for the assessment of visual attentional processes and impulse control in rats. *Nat Protoc*. (2008) 3:759–67. doi: 10.1038/nprot.2008.41
23. Cibelli M, Fidalgo AR, Terrando N, Ma D, Monaco C, Feldmann M, et al. Role of interleukin-1beta in postoperative cognitive dysfunction. *Ann Neurol*. (2010) 68:360–8. doi: 10.1002/ana.22082
24. Terrando N, Monaco C, Ma D, Foxwell BM, Feldmann M, Maze M. Tumor necrosis factor-alpha triggers a cytokine cascade yielding postoperative cognitive decline. *Proc Natl Acad Sci USA*. (2010) 107:20518–22. doi: 10.1073/pnas.1014557107
25. Hanisch UK, Kettenmann H. Microglia: active sensor and versatile effector cells in the normal and pathologic brain. *Nat Neurosci*. (2007) 10:1387–94. doi: 10.1038/nn1997
26. Daneman R. The blood-brain barrier in health and disease. *Ann Neurol*. (2012) 72:648–72. doi: 10.1002/ana.23648
27. Merlini M, Rafalski VA, Rios Coronado PE, Gill TM, Ellisman M, Muthukumar G, et al. Fibrinogen induces microglia-mediated spine elimination and cognitive impairment in an Alzheimer's disease model. *Neuron*. (2019) 101:1099–108.e6. doi: 10.1016/j.neuron.2019.01.014
28. Alvarez JI, Katayama T, Prat A. Glial influence on the blood brain barrier. *Glia*. (2013) 61:1939–58. doi: 10.1002/glia.22575
29. Ikeshima-Kataoka H. Neuroimmunological implications of AQP4 in astrocytes. *Int J Mol Sci*. (2016) 17:1306. doi: 10.3390/ijms17081306
30. Inouye SK. Delirium in older persons. *N Engl J Med*. (2006) 354:1157–65. doi: 10.1056/NEJMra052321
31. Safavynia SA, Arora S, Pryor KO, García PS. An update on postoperative delirium: clinical features, neuropathogenesis, and perioperative management. *Curr Anesthesiol Rep*. (2018) 8:252–62. doi: 10.1007/s40140-018-0282-5
32. Xu J, Dong H, Qian Q, Zhang X, Wang Y, Jin W, et al. Astrocyte-derived CCL2 participates in surgery-induced cognitive dysfunction and neuroinflammation via evoking microglia activation. *Behav Brain Res*. (2017) 332:145–53. doi: 10.1016/j.bbr.2017.05.066
33. Sun L, Dong R, Xu X, Yang X, Peng M. Activation of cannabinoid receptor type 2 attenuates surgery-induced cognitive impairment in mice through anti-inflammatory activity. *J Neuroinflammation*. (2017) 14:138. doi: 10.1186/s12974-017-0913-7
34. Netto MB, de Oliveira Junior AN, Goldim M, Mathias K, Fileti ME, da Rosa N, et al. Oxidative stress and mitochondrial dysfunction contributes to postoperative cognitive dysfunction in elderly rats. *Brain Behav Immun*. (2018) 73:661–9. doi: 10.1016/j.bbi.2018.07.016
35. Shi X, Guo TZ, Li W, Sahbaie P, Rice KC, Sulima A, et al. Exercise reverses nociceptive sensitization, upregulated neuropeptide signaling, inflammatory changes, anxiety, and memory impairment in a mouse tibia fracture model. *Anesthesiology*. (2018) 129:557–75. doi: 10.1097/ALN.0000000000002332
36. Zhang X, Dong H, Li N, Zhang S, Sun J, Zhang S, et al. Activated brain mast cells contribute to postoperative cognitive dysfunction by evoking microglia activation and neuronal apoptosis. *J Neuroinflammation*. (2016) 13:127. doi: 10.1186/s12974-016-0592-9
37. Feng X, Degos V, Koch LG, Britton SL, Zhu Y, Vacas S, et al. Surgery results in exaggerated and persistent cognitive decline in a rat model of the Metabolic Syndrome. *Anesthesiology*. (2013) 118:1098–105. doi: 10.1097/ALN.0b013e318286d0c9
38. Awh E, Jonides J. Overlapping mechanisms of attention and spatial working memory. *Trends Cogn Sci*. (2001) 5:119–26. doi: 10.1016/S1364-6613(00)01593-X
39. Riccio CA, Reynolds CR, Lowe P, Moore JJ. The continuous performance test: a window on the neural substrates for attention? *Arch Clin Neuropsychol*. (2002) 17:235–72. doi: 10.1016/S0887-6177(01)00111-1
40. Humby T, Laird FM, Davies W, Wilkinson LS. Visuospatial attentional functioning in mice: interactions between cholinergic manipulations and genotype. *Eur J Neurosci*. (1999) 11:2813–23. doi: 10.1046/j.1460-9568.1999.00701.x
41. Noudoost B, Moore T. The role of neuromodulators in selective attention. *Trends Cogn Sci*. (2011) 15:585–91. doi: 10.1016/j.tics.2011.10.006
42. Hshieh TT, Fong TG, Marcantonio ER, Inouye SK. Cholinergic deficiency hypothesis in delirium: a synthesis of current evidence. *J Gerontol A Biol Sci Med Sci*. (2008) 63:764–72. doi: 10.1093/gerona/63.7.764
43. van Gool WA, van de Beek D, Eikelenboom P. Systemic infection and delirium: when cytokines and acetylcholine collide. *Lancet*. (2010) 375:773–5. doi: 10.1016/S0140-6736(09)61158-2
44. Müller A, Olbert M, Heymann A, Zahn PK, Plaschke K, von Dossow V, et al. Relevance of peripheral cholinesterase activity on postoperative delirium in adult surgical patients (CESARO): a prospective observational cohort study. *Eur J Anaesthesiol*. (2019) 36:114–22. doi: 10.1097/EJA.0000000000000888
45. Field RH, Gossen A, Cunningham C. Prior pathology in the basal forebrain cholinergic system predisposes to inflammation-induced working memory deficits: reconciling inflammatory and cholinergic hypotheses of delirium. *J Neurosci*. (2012) 32:6288–94. doi: 10.1523/JNEUROSCI.4673-11.2012
46. Terrando N, Eriksson LI, Ryu JK, Yang T, Monaco C, Feldmann M, et al. Resolving postoperative neuroinflammation and cognitive decline. *Ann Neurol*. (2011) 70:986–95. doi: 10.1002/ana.22664
47. Shibutani ST, Saitoh T, Nowag H, Münz C, Yoshimori T. Autophagy and autophagy-related proteins in the immune system. *Nat Immunol*. (2015) 16:1014–24. doi: 10.1038/ni.3273
48. Yang T, Xu G, Newton PT, Chagin AS, Mkrtchian S, Carlström M, et al. Maresin 1 attenuates neuroinflammation in a mouse model of perioperative neurocognitive disorders. *Br J Anaesth*. (2019) 122:350–60. doi: 10.1016/j.bja.2018.10.062
49. Hughes CG, Pandharipande PP, Thompson JL, Chandrasekhar R, Ware LB, Ely EW, et al. Endothelial activation and blood-brain barrier injury as risk factors for delirium in critically Ill patients. *Crit Care Med*. (2016) 44:e809–17. doi: 10.1097/CCM.0000000000001739
50. Yang S, Gu C, Mandeville ET, Dong Y, Esposito E, Zhang Y, et al. Anesthesia and surgery impair blood-brain barrier and cognitive function in mice. *Front Immunol*. (2017) 8:902. doi: 10.3389/fimmu.2017.00902
51. Fong TG, Chan NY, Dillon ST, Zhou W, Tripp B, Ngo LH, et al. Identification of plasma proteome signatures associated with surgery using SOMAscan. *Ann Surg*. (2019). doi: 10.1097/SLA.0000000000003283 [Epub ahead of print].
52. Hu J, Feng X, Valdearcos M, Lutrin D, Uchida Y, Koliwad SK, et al. Interleukin-6 is both necessary and sufficient to produce perioperative neurocognitive disorder in mice. *Br J Anaesth*. (2018) 120:537–45. doi: 10.1016/j.bja.2017.11.096
53. Hall RJ, Watne LO, Cunningham E, Zetterberg H, Shenkin SD, Wyller TB, et al. CSF biomarkers in delirium: a systematic review. *Int J Geriatr Psychiatry*. (2018) 33:1479–500. doi: 10.1002/gps.4720
54. Kiecolt-Glaser JK, Preacher KJ, MacCallum RC, Atkinson C, Malarkey WB, Glaser R. Chronic stress and age-related increases in the proinflammatory cytokine IL-6. *Proc Natl Acad Sci USA*. (2003) 100:9090–5. doi: 10.1073/pnas.1531903100
55. Steptoe A, Hamer M, Chida Y. The effects of acute psychological stress on circulating inflammatory factors in humans: a review and meta-analysis. *Brain Behav Immun*. (2007) 21:901–12. doi: 10.1016/j.bbi.2007.03.011
56. Kazmierski J, Banys A, Latek J, Bourke J, Jaszewski R. Cortisol levels and neuropsychiatric diagnosis as markers of postoperative delirium: a prospective cohort study. *Crit Care*. (2013) 17:R38. doi: 10.1186/cc12548
57. Royse CF, Saager L, Whitlock R, Ou-Young J, Royse A, Vincent J, et al. Impact of methylprednisolone on postoperative quality of recovery

and delirium in the steroids in cardiac surgery trial: a randomized, double-blind, placebo-controlled substudy. *Anesthesiology*. (2017) 126:223–33. doi: 10.1097/ALN.0000000000001433
58. Wolters AE, Veldhuijzen DS, Zaal IJ, Peelen LM, van Dijk D, Devlin JW, et al. Systemic corticosteroids and transition to delirium in critically Ill patients. *Crit Care Med*. (2015) 43:e585–8. doi: 10.1097/CCM.0000000000001094
59. Robinson TN, Raeburn CD, Tran ZV, Brenner LA, Moss M. Motor subtypes of postoperative delirium in older adults. *Arch Surg*. (2011) 146:295–300. doi: 10.1001/archsurg.2011.14
60. Culley DJ, Snayd M, Baxter MG, Xie Z, Lee IH, Rudolph J, et al. Systemic inflammation impairs attention and cognitive flexibility but not associative learning in aged rats: possible implications for delirium. *Front Aging Neurosci*. (2014) 6:107. doi: 10.3389/fnagi.2014.00107
61. Murray C, Sanderson DJ, Barkus C, Deacon RM, Rawlins JN, Bannerman DM, et al. Systemic inflammation induces acute working memory deficits in the primed brain: relevance for delirium. *Neurobiol Aging*. (2012) 33:603–16.e3. doi: 10.1016/j.neurobiolaging.2010.04.002
62. Peng M, Zhang C, Dong Y, Zhang Y, Nakazawa H, Kaneki M, et al. Battery of behavioral tests in mice to study postoperative delirium. *Sci Rep*. (2016) 6:29874. doi: 10.1038/srep29874
63. Mees L, Fidler J, Kreuzer M, Fu J, Pardue MT, García PS. Faster emergence behavior from ketamine/xylazine anesthesia with atipamezole versus yohimbine. *PLoS ONE*. (2018) 13:e0199087. doi: 10.1371/journal.pone.0199087
64. Zurek AA, Bridgwater EM, Orser BA. Inhibition of alpha5 gamma-Aminobutyric acid type A receptors restores recognition memory after general anesthesia. *Anesth Analg*. (2012) 114:845–55. doi: 10.1213/ANE.0b013e31824720da
65. Hambrecht-Wiedbusch VS, LaTendresse KA, Avidan MS, Nelson AG, Phyle M, Ajluni RE, et al. General anesthesia does not have persistent effects on attention in rodents. *Front Behav Neurosci*. (2019) 13:76. doi: 10.3389/fnbeh.2019.00076
66. Hohlbaum K, Bert B, Dietze S, Palme R, Fink H, Thöne-Reineke C. Severity classification of repeated isoflurane anesthesia in C57BL/6JRj mice-Assessing the degree of distress. *PLoS ONE*. (2017) 12:e0179588. doi: 10.1371/journal.pone.0179588

Conflict of Interest: The authors declare that the research was conducted in the absence of any commercial or financial relationships that could be construed as a potential conflict of interest.

Copyright © 2019 Velagapudi, Subramaniyan, Xiong, Porkka, Rodriguiz, Wetsel and Terrando. This is an open-access article distributed under the terms of the Creative Commons Attribution License (CC BY). The use, distribution or reproduction in other forums is permitted, provided the original author(s) and the copyright owner(s) are credited and that the original publication in this journal is cited, in accordance with accepted academic practice. No use, distribution or reproduction is permitted which does not comply with these terms.

frontiers in Immunology

ORIGINAL RESEARCH
published: 20 November 2019
doi: 10.3389/fimmu.2019.02699

Diurnal Variation in Systemic Acute Inflammation and Clinical Outcomes Following Severe Blunt Trauma

Akram M. Zaaqoq[1,2†], Rami A. Namas[1,3†], Othman Abdul-Malak[1], Khalid Almahmoud[1], Derek Barclay[1], Jinling Yin[1], Ruben Zamora[1,3], Matthew R. Rosengart[1,2], Timothy R. Billiar[1,3] and Yoram Vodovotz[1,3]*

[1] Department of Surgery, University of Pittsburgh, Pittsburgh, PA, United States, [2] Department of Critical Care Medicine, MedStar Washington Hospital Center, Washington, DC, United States, [3] Center for Inflammation and Regeneration Modeling, McGowan Institute for Regenerative Medicine, University of Pittsburgh, Pittsburgh, PA, United States

OPEN ACCESS

Edited by:
Valentin A. Pavlov,
Northwell Health, United States

Reviewed by:
Ioannis P. Androulakis,
Rutgers, The State University of New Jersey, United States
Charles Wade,
University of Texas Health Science Center at Houston, United States

***Correspondence:**
Yoram Vodovotz
vodovotzy@upmc.edu

[†]These authors have contributed equally to this work

Specialty section:
This article was submitted to Inflammation, a section of the journal Frontiers in Immunology

Received: 13 September 2019
Accepted: 04 November 2019
Published: 20 November 2019

Citation:
Zaaqoq AM, Namas RA, Abdul-Malak O, Almahmoud K, Barclay D, Yin J, Zamora R, Rosengart MR, Billiar TR and Vodovotz Y (2019) Diurnal Variation in Systemic Acute Inflammation and Clinical Outcomes Following Severe Blunt Trauma. Front. Immunol. 10:2699. doi: 10.3389/fimmu.2019.02699

Animal studies suggest that the time of day is a determinant of the immunological response to both injury and infection. We hypothesized that due to this diurnal variation, time of injury could affect the systemic inflammatory response and outcomes post-trauma and tested this hypothesis by examining the dynamics of circulating inflammatory mediators in blunt trauma patients injured during daytime vs. nighttime. From a cohort of 472 blunt trauma survivors, two stringently matched sub-cohorts of moderately/severely injured patients [injury severity score (ISS) >20] were identified. Fifteen propensity-matched, daytime-inured ("mDay") patients (age 43.6 ± 5.2, M/F 11/4, ISS 22.9 ± 0.7) presented during the shortest local annual period (8:00 am−5:00 pm), and 15 propensity-matched "mNight" patients (age 43 ± 4.3, M/F 11/4, ISS 24.5 ± 2.5) presented during the shortest night period (10:00 pm−5:00 am). Serial blood samples were obtained (3 samples within the first 24 h and daily from days 1–7) from all patients. Thirty-two plasma inflammatory mediators were assayed. Two-way Analysis of Variance (ANOVA) was used to compare groups. Dynamic Network Analysis (DyNA) and Dynamic Bayesian Network (DyBN) inference were utilized to infer dynamic interrelationships among inflammatory mediators. Both total hospital and intensive care unit length of stay were significantly prolonged in the mNight group. Circulating IL-17A was elevated significantly in the mNight group from 24 h to 7 days post-injury. Circulating MIP-1α, IL-7, IL-15, GM-CSF, and sST2 were elevated in the mDay group. DyNA demonstrated elevated network complexity in the mNight vs. the mDay group. DyBN suggested that cortisol and sST2 were central nodes upstream of TGF-β1, chemokines, and Th17/protective mediators in both groups, with IL-6 being an additional downstream node in the mNight group only. Our results suggest that time of injury affects clinical outcomes in severely injured patients in a manner associated with an altered systemic inflammation program, possibly implying a role for diurnal or circadian variation in the response to traumatic injury.

Keywords: circadian rhythm, blunt trauma, chemokines, nervous system, acute inflammation

INTRODUCTION

Despite advances in critical care over the past 40 years, severe blunt trauma is still associated with significant long-term morbidity and mortality (1, 2). Systemic acute inflammation is thought to be a key driver of post-injury critical illness (3). Although properly regulated inflammation is crucial for promoting adequate tissue healing and recovery, an overly exuberant or insufficient response may result in immune dysregulation as well as secondary tissue and organ damage that can be complicated by prolonged hospitalization (4–6).

The timing of the light-dark cycle results in a shift of the circadian rhythms, functioning to synchronize and coordinate organ systems in response to environmental light dynamics (7, 8). The immune system is under direct circadian control by systemic cues and molecular clocks within immune cells (9). These oscillations may also help to promote tissue recovery and the clearance of potentially harmful cellular elements from the circulation (8, 9). The suprachiasmatic nucleus (SCN) of the anterior hypothalamus contains specialized neurons that receive photo input through the retinohypothalamic tract (RHT) and non-photo cues by disparate neural inputs (9, 10). Subsequently, the nervous system regulates the inflammatory response through neuronal and neuroendocrine pathways (7).

At the molecular level, there are multiple sets of transcription factors that result in autoregulatory transcription-translation feedback loops of core clock genes, such as BMAL1 and CLOCK, which in turn control the output of circadian physiology and behavior (11). Recent studies have suggested that this complex system impacts inflammatory responses in the context of sepsis (12–14).

To address whether the time of injury alters trauma-induced systemic inflammation and, thereby, trauma-related outcomes, we retrospectively analyzed data from a large cohort of blunt trauma patients who survived up to discharge. A granular, temporal sampling of the early systemic inflammatory response of both the overall cohort as well as in propensity-matched sub-cohorts of patients injured during the day vs. the nighttime, combined with data-driven computational methods, allowed us to define differential dynamic inflammation networks as a function of time of injury. Our analyses revealed that early, persistent changes in post-injury inflammation manifest in unique biomarker patterns associated with the time of injury. Also, these patterns, which are independent of the mechanism of injury, injury severity, age, or gender suggest a diurnal, and perhaps also circadian, control of post-trauma inflammation that impacts clinical outcomes.

MATERIALS AND METHODS

The study protocol was reviewed and approved by the University of Pittsburgh Institutional Review Board (IRB), and has been detailed previously (15, 16). Written informed consent was taken from each patient or the next of kin in line with our locally agreed protocols with Institutional Review Board regulations. Patients eligible for enrollment in the study were at least 18 years of age, admitted to the intensive care unit (ICU) within 24 h of injury, and, per the treating physician, were expected to live more than 24 h. Reasons for ineligibility were isolated head injury, penetrating trauma (due to our focus on blunt trauma), and pregnancy. Blunt trauma patients were enrolled in the study from 2004 to 2012. Laboratory results and basic demographic data were recorded in the database directly from the electronic medical record. Three plasma samples, starting with the initial blood draw upon arrival to the emergency department (ED), were assayed within the first 24 h following trauma and then daily between 4:00 and 5:00 a.m. from days 1 to 7 post-injury. The blood samples were centrifuged, and plasma aliquots were stored in cryoprecipitate tubes at −80°C for subsequent analysis of inflammatory mediators.

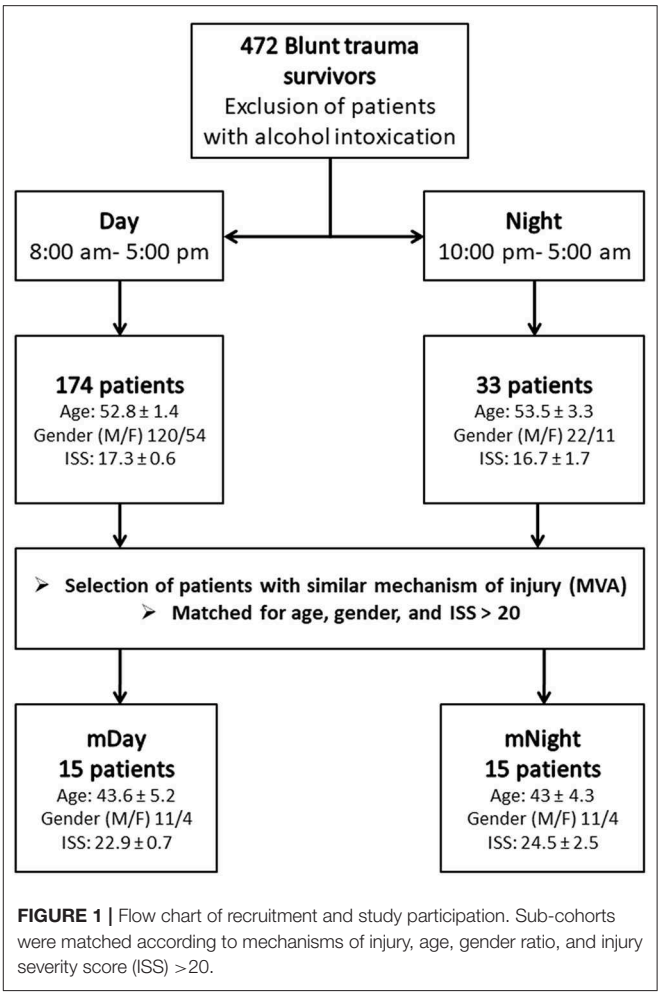

FIGURE 1 | Flow chart of recruitment and study participation. Sub-cohorts were matched according to mechanisms of injury, age, gender ratio, and injury severity score (ISS) >20.

Study Design

A retrospective study involving a cohort of 472 blunt trauma survivors (330 males and 142 females, age 48.4 ± 0.9, ISS 19.6 ± 0.5) who were admitted to the emergency department of the Presbyterian University Hospital (Level 1 trauma center) (16) (**Figure 1**). Exclusion criteria included patients with evidence of alcohol intoxication upon admission due to the potential impact of alcohol on systemic inflammation. From this cohort, "Day"

TABLE 1 | Demographics, mechanism of injury, co-morbid conditions, and clinical outcomes of the total trauma cohort compared to the Day and Night cohorts.

Variables	Total cohort *n* = 472	Day cohort *n* = 174	Night cohort *n* = 33	*P*
DEMOGRAPHICS				
Age, yr	48.4 ± 0.9	52.8 ± 1.4	53.5 ± 3.3	0.9
Sex, male/female	330/142	120/54	22/11	0.8
Injury severity score (ISS)	19.6 ± 0.5	17.3 ± 0.6	16.7 ± 1.7	0.5
ABBREVIATED INJURY SCALE (AIS)				
Head and Neck	1.4 ± 0.08	0.89 ± 0.1	1.69 ± 0.3	0.003
Face	0.39 ± 0.04	0.31 ± 0.05	0.27 ± 0.1	0.9
Chest	2.02 ± 0.07	1.95 ± 0.1	2.06 ± 0.3	0.7
Abdomen	1.16 ± 0.06	1.04 ± 0.09	0.94 ± 0.2	0.6
Extremities	1.5 ± 0.06	1.5 ± 0.09	1 ± 0.2	0.017
External	0.67 ± 0.02	0.66 ± 0.04	0.61 ± 0.09	0.6
MECHANISM OF INJURY				
Motor vehicle accident (MVA), *n* (%)	269 (57%)	106 (60.9%)	19 (57.5)	0.7
Fall, *n* (%)	102 (21.6%)	36 (20.7%)	10 (30.3%)	0.2
Motorcycle, *n* (%)	65 (13.8%)	20 (11.5%)	2 (6.1%)	0.4
Other, *n* (%)	36 (7.6%)	12 (6.9%)	2 (6.1%)	0.9
CO-MORBID CONDITIONS				
Hypertension, *n* (%)	143 (30.3%)	68 (39.1%)	8 (24.2%)	0.1
Diabetes, *n* (%)	58 (12.3%)	29 (16.7%)	5 (15.2%)	0.8
Psychiatric conditions, *n* (%)	58 (12.3%)	27 (15.5%)	5 (15.2%)	0.9
Thyroid diseases, *n* (%)	26 (5.5%)	12 (6.9%)	4 (12.1%)	0.3
Bronchial asthma, *n* (%)	28 (5.9%)	28 (16.1%)	4 (12.1%)	0.8
None, *n* (%)	154 (32.6%)	55 (31.6%)	12 (36.4%)	0.8
OUTCOME				
Mechanical ventilation, days	3.1 ± 0.3	2.7 ± 0.5	2.2 ± 0.7	0.7
Intensive Care Unit length of stay, days	7.01 ± 0.36	5.9 ± 0.5	6.7 ± 1.3	0.8
Total hospital length of stay, days	12.72 ± 0.44	11.6 ± 0.7	12.1 ± 1.7	0.7

Values are expressed as mean ± SEM. One-Way ANOVA or Fisher exact test were used as appropriate with statistical significance set at $P < 0.05$.

patients were identified based on the time of presentation to Presbyterian University Hospital during the shortest daylight in Pittsburgh, PA, USA throughout the year (8:00 a.m.−5:00 p.m.) and "Night" patients presented during the shortest night period (10:00 p.m.−5:00 a.m.) (**Figure 1**). The overall demographics, mechanism of injury, clinical data, and co-morbidities of the 174 (121 males and 53 females, age 52.8 ± 1.4, ISS 17.3 ± 0.6) patients in the Day group vs. 33 (22 males and 11 females, age 53.3 ± 3.3, ISS 16.7 ± 1.7) patients in the Night group are shown in **Table 1**. Initially, we sought to avoid the confounding impact related to the type of mechanism of injury by selecting patients based on the predominant mechanism of injury in both cohorts, i.e., motor vehicle accidents (MVA). Given that the Night group exhibited statistically significantly higher rates of head and extremity injuries when compared to the Day group (see **Table 1**) as revealed by the abbreviated injury scale (AIS), we next performed a one-to-one propensity matching based on age, sex, and ISS > 20, which yielded two sub-cohorts of 15 Day patients (mDay) matched to 15 Night patients (mNight) (**Figure 1**).

Clinical Data Collection

Clinical data, including injury severity score (ISS), abbreviated injury scale (AIS) score, Marshall Multiple Organ Dysfunction (MOD) score, ICU LOS, hospital LOS, and days on mechanical ventilation were collected from the hospital inpatient electronic and trauma registry database. ISS (17) and AIS scores (18) were calculated for each patient by a single trauma surgeon after attending radiology evaluations were finalized. The ISS is based on an anatomical scoring system that provides an overall score for patients with multiple injuries (17). Each injury is assigned an AIS score, allocated to one of six body regions: head, face, chest, abdomen, extremities (including pelvis), and external. We focused our studies on trauma patients with ISS > 20, which would be considered moderate/severe (19).

As an index of organ dysfunction, the MOD score (20) (ranging from 0 to 24) was calculated. In brief, six variables were obtained from the electronic trauma data registry including (a) the respiratory system (PO_2/FIO_2 ratio); (b) the renal system (serum creatinine concentration); (c) the hepatic system (serum bilirubin concentration); (d) the hematologic system (platelet count); (e) the central nervous system (Glasgow Coma Scale); and (f) the cardiovascular system- the pressure-adjusted heart rate (PAR).

Analysis of Inflammatory Mediators

Blood samples were collected into citrated tubes via indwelling catheters within 24 h of admission and daily for 7 days post-injury. The blood samples were centrifuged, and plasma aliquots were stored in cryoprecipitate tubes at −80°C for subsequent analysis of inflammatory mediators. The human inflammatory MILLIPLEX™ MAP Human Cytokine/Chemokine Panel-Premixed 26 Plex (Millipore Corporation, Billerica, MA) and Luminex™ 100 IS (Luminex, Austin, TX) was used to measure plasma levels of interleukin (IL)-1β, IL-1 receptor antagonist (IL-1Ra), IL-2, soluble IL-2 receptor-α (sIL-2Rα), IL-4, IL-5, IL-6, IL-7, IL-8, IL-10, IL-13, IL-15, IL-17A, interferon (IFN)-γ, IFN-γ inducible protein (IP)-10 (CXCL10), monokine induced by gamma interferon (MIG; CXCL9), macrophage inflammatory protein (MIP)-1α (CCL3), MIP-1β (CCL4), monocyte chemotactic protein (MCP)-1 (CCL2), granulocyte-macrophage colony stimulating factor (GM-CSF), Eotaxin, and tumor necrosis factor-alpha (TNF-α). The human Th17 MILLIPLEX Panel kit (Millipore Corporation, Billerica, MA) was used to measure IL-9, IL-21, IL-22, IL-23, IL-17E/25, and

IL-33. The Luminex™ system was used in accordance to the manufacturer's instructions. Soluble ST2 (sST2) was measured by a sandwich ELISA assay (R&D Systems, Minneapolis, MN). NO_2^-/NO_3^- was measured using the nitrate reductase/Griess assay (Cayman Chemical Co., Ann Arbor, MI). Serum cortisol and transforming growth factor (TGF)-β1 were assayed using commercially available enzyme-linked immunosorbent assays (ELISA) kits (R&D Systems, Minneapolis, MN) according to the manufacturer's instructions. In brief, active vs. latent TGF-β1 were assayed as follows: To collect platelet-poor plasma, plasma was collected on ice using EDTA as an anticoagulant and centrifuged for 15 min at 1,000 × g within 30 min of collection followed by an additional centrifugation step of the plasma at 10,000 × g for 10 min at 2–8°C for complete platelet removal. To activate latent TGF-β1 to immunoreactive TGF-β1 detectable by the Quantikine® TGF-β1 immunoassay, 20 μL of 1 N HCl was added to each 40 μL of plasma, mixed and incubated for 10 min at room temperature. Next, the acidified samples were neutralized by adding 20 μL of 1.2 N NaOH/0.5 M HEPES, mixed and then diluted with calibrator diluent prior to the assay. To perform the assay, 50 μL of diluent RD1-73 were added to each well-followed by addition of 50 μL of recombinant human TGF-β1 standard, control, or activated sample per well and incubated for 2 h at room temperature. Following 4 aspirations/wash steps, 100 μL of TGF-β1 conjugate was added to each well and incubated for an additional 2 h at room temperature, washed, and then 100 μL substrate solution was added to each well and incubated for 30 min at room temperature. Finally, 100 μL of stop solution was added to each well and the optical density (wavelength set at 450 nm) was determined.

Statistical Analysis

All data are expressed as mean ± SEM. Group-time interaction of plasma inflammatory mediators' levels was determined by Two-way analysis of variance (ANOVA) which was confirmed by non-parametric Mann-Whitney U test to compare the *P*-values generated by the Two-way ANOVA in the case where values were not normally distributed, all using SigmaPlot™ 11 software (Systat Software, Inc., San Jose, CA). Fisher's exact test was performed for categorical data using Graphpad PRISM (GraphPad Software, Inc., La Jolla, CA). The correlation between different inflammatory mediators was determined by Spearman's correlation using the actual values of these inflammatory mediators. $P < 0.05$ was considered statistically significant for all analyses.

Dynamic Bayesian Network Inference

Dynamic Bayesian Network (DyBN) inference was carried out to define the most likely single-network structure that best characterizes the dynamic interactions among systemic inflammatory mediators across time, in the process suggesting likely feedback structures that define central nodes. The networks might also suggest possible mechanisms by which the progression of the inflammatory response differs within a given experimental group. This analysis was carried out using MATLAB™ (The MathWorks, Inc., Natick, MA), using an algorithm adapted from Grzegorczyk and Husmeier (21) and revised by our group (22). In this analysis, inflammatory mediators were represented at multiple time points within the same network structure. In this approach, time was modeled discretely as in a discrete Markov chain. Each mediator was given a time index subscript indicating the time slice to which it belonged. Additional temporal dependencies were represented in a DyBN by edges between time slices. Each node in the network was associated with a conditional probability distribution of a variable that is conditioned upon its parents (upstream nodes). This particular network structure was used to assess the dominant inflammatory mediators and the probable interaction among various mediators, including possible feedback (21).

Data-Driven Modeling: Dynamic Network Analysis (DyNA)

DyNA was carried out as described previously (15, 23, 24). The goal of this analysis was to gain insights into dynamic changes in network connectivity of the post-traumatic inflammatory response for both day and night over time. The mathematical formation of this method is essential to calculate the correlation between the variables by which we can examine their dependence. To do so, inflammatory mediator networks were created in adjacent 8-h time periods (0–8, 8–16, and 16–24 h) using MATLAB® (The MathWorks, Inc., Natick, MA). Connections in the network were created if the correlation coefficient between two nodes (inflammatory mediators) was greater or equal to a threshold of 0.7. For the network density calculation, to account for network sizes (number of significantly altered nodes) in the adjacent 8-h time periods detailed above, we utilized the following formula: [a minor revision of the one reported by Assenov et al. (25)].

$$\frac{\text{Total number of edges} * \text{Number of total nodes}}{\text{Maximum possible edges among total nodes}}$$

RESULTS

Overview of Demographics and Outcomes in a Large Cohort of Blunt Trauma Patients

Over the 8-year study period, 472 blunt trauma patients admitted to the ICU were enrolled in the study, as previously described (15, 16). The majority of the 472 trauma patients were males (70.6 %), with a mean age of 48.4 ± 0.9 years and a mean ISS of 19.6 ± 0.5. These patients sustained blunt trauma in the form of MVA (57%), falls (21.6%), motorcycle accidents (13.8%), and others (7.6%). The AIS analysis revealed that the Night cohort exhibited statistically significantly higher rates of head (1.69 ± 0.3 vs. 0.89 ± 0.1; $P < 0.003$) and extremity (1 ± 0.2 vs. 1.5 ± 0.09; $P = 0.017$) injuries when compared to the day group (**Table 1**). The average ICU LOS was 7.01 ± 0.36 d, the mean hospital LOS was 12.7 ± 0.4

d, and the mean number of days on a mechanical ventilator was 3.1 ± 0.3 d.

Characteristics of Day and Night Injury Cohorts: Demographics, Outcomes, and Propensity Matching

A total of 174 patients met our definition of being injured during the day and 33 patients injured during the night as defined in the *Materials and Methods* (**Table 1**). Overall, males were predominant in both the Day and Night cohorts (68.9 and 66.7%, respectively), with no statistical difference in mean age (52.8 ± 1.4 vs. 53.5 ± 3.3; $P = 0.9$) between the two cohorts. Also, there was no statistically significant difference in ISS (17.3 ± 0.6 vs. 16.7 ± 1.7; $P = 0.5$), ICU LOS (5.9 ± 0.5 vs. 6.7 ± 1.3; $P = 0.8$), hospital LOS (11.6 ± 0.7 vs. 12.1 ± 1.7; $P = 0.7$), days on mechanical ventilation (2.7 ± 0.5 vs. 2.2 ± 0.7; $P = 0.7$), the prevalence of nosocomial infection (NI: 39/173 [22.5%] vs. 8/33 [24.2%]; $P = 0.8$), or the average Marshall MOD score across days 1 to 7 (1.3 vs. 1.6; $P = 0.9$) between the two cohorts.

A total of 15 patients in the Night cohort (matched Night [mNight]) were matched with 15 patients in Day cohort (matched Day [mDay]), according to age, gender, and ISS >20. Overall, males were predominant in both mDay and mNight sub-cohorts (73.3% in both sub-cohorts), with no statistical difference in mean age (43.6 ± 5.2 vs. 43 ± 4.3; $P = 0.9$; respectively) between the two sub-cohorts. Moreover, ISS was not statistically significantly different between both groups (22.9 ± 0.7 vs. 24.5 ± 2.5; $P = 0.9$; respectively; **Figure 2A**). Importantly, there were no statistically significant differences in any of the body regions between both sub-cohorts based on AIS body regions (the components of the ISS; *see Materials and Methods*) (**Figure 2B**).

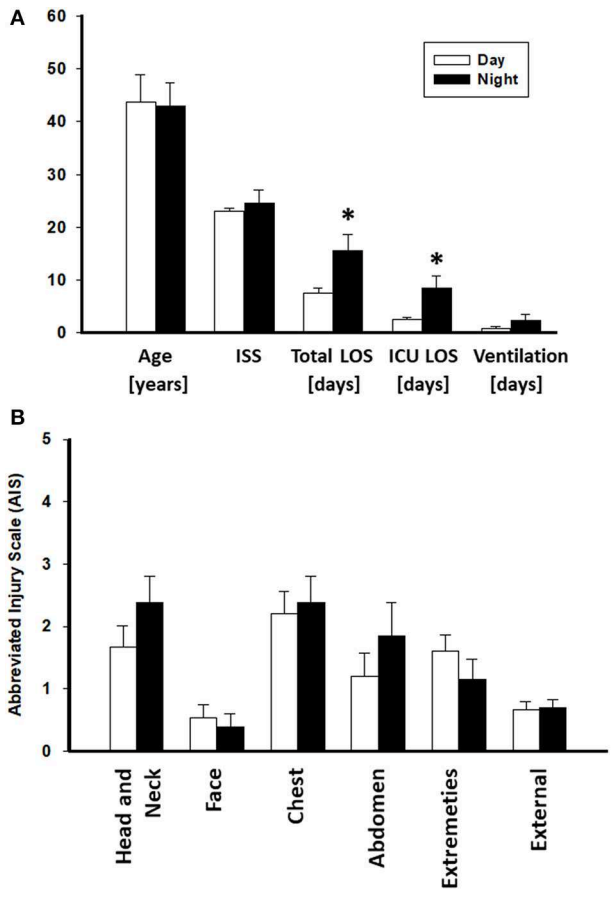

FIGURE 2 | Abbreviated Injury Scale (AIS) values of the Day ($n = 174$) and Night ($n = 33$) cohorts. No statistically significant difference was found between both groups. *$P < 0.05$ by Student's *t*-test.

TABLE 2 | Demographics, mechanism of injury, co-morbid conditions, and clinical outcomes of the stringently matched (m)Day and mNight sub-cohorts.

Variables	mDay $n = 15$	mNight $n = 15$	*P*
DEMOGRAPHICS			
Age, yr	43.6 ± 5.2	43 ± 4.3	0.9
Sex, male/female	11/4	11/4	0.9
Injury severity score (ISS)	22.9 ± 0.7	24.5 ± 2.5	0.9
MECHANISM OF INJURY			
Motor vehicle accident (MVA), *n* (%)	11 (73.3%)	12 (80%)	0.7
Motorcycle, *n* (%)	3 (20%)	1 (6.7%)	0.3
Other, *n* (%)	1 (6.7%)	2 (13.3%)	0.5
ABBREVIATED INJURY SCALE (AIS)			
Head and Neck	1.3 ± 1.6	2.4 ± 1.5	0.09
Face	0.5 ± 0.8	0.4 ± 0.8	0.6
Chest	2.2 ± 1.4	2.4 ± 1.5	0.7
Abdomen	0.7 ± 1	1.8 ± 1.9	0.14
Extremities	1.6 ± 1	1.2 ± 1.1	0.3
External	0.67 ± 0.5	0.69 ± 0.5	0.9
CO-MORBID CONDITIONS			
Hypertension, *n* (%)	5 (33.3%)	3 (20%)	0.4
Diabetes, *n* (%)	4 (26.7%)	1 (6.7%)	0.14
Psychiatric conditions, *n* (%)	2 (13.3%)	3 (20%)	0.6
Thyroid diseases, *n* (%)	1 (6.7%)	1 (6.7%)	1
Bronchial asthma, *n* (%)	2 (13.3%)	1 (6.7%)	0.5
None, *n* (%)	6 (40%)	8 (53.3%)	0.5
OUTCOME			
Mechanical ventilation, days	0.8 ± 0.3	2.3 ± 1.1	0.9
Intensive Care Unit length of stay, days	2.6 ± 0.3	8.5 ± 2.3	0.043
Total hospital length of stay, days	7.6 ± 0.9	15.5 ± 3	0.02

Values are expressed as mean ± SEM. One-Way ANOVA or Fisher exact test were used as appropriate with statistical significance set at $P < 0.05$.

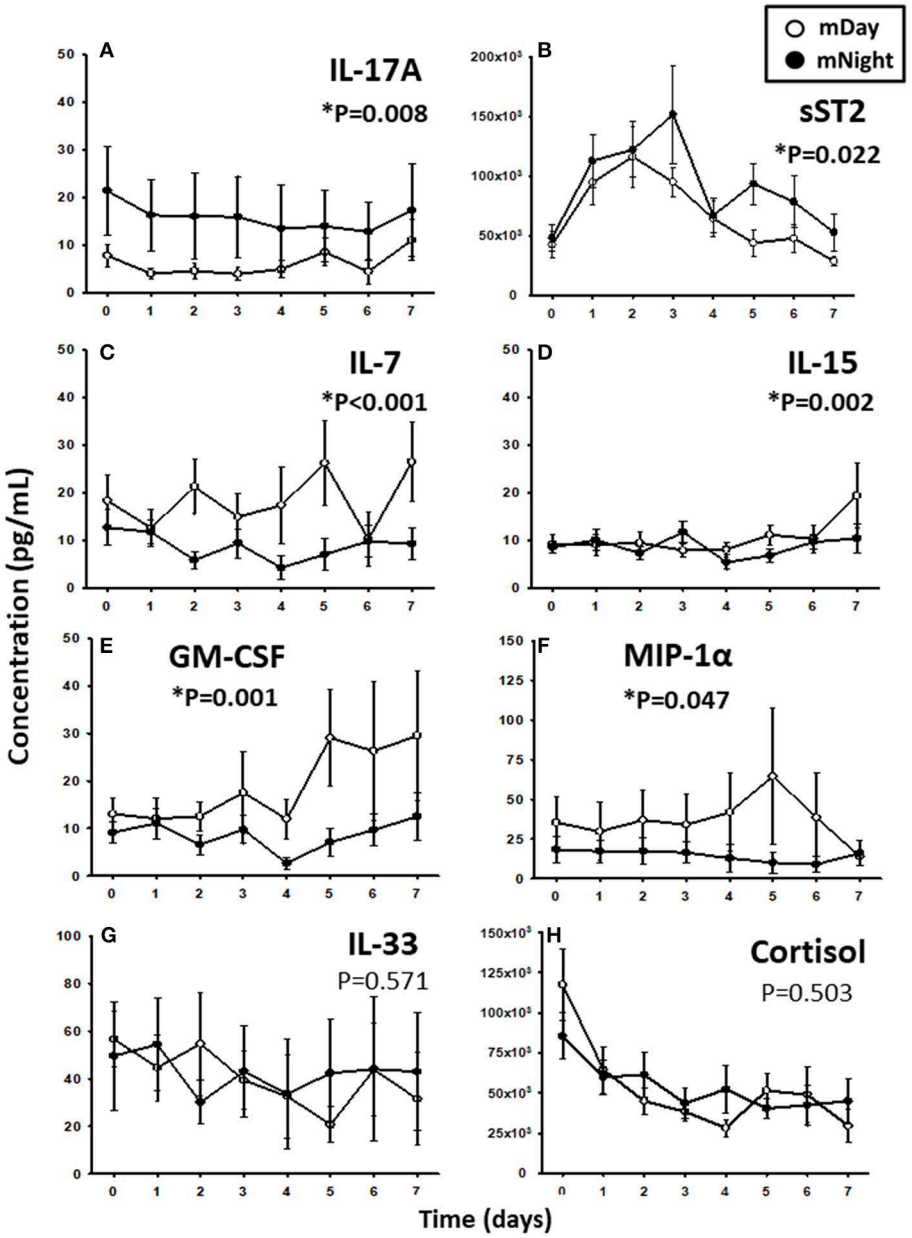

FIGURE 3 | Time course analysis of inflammatory mediators in the matched (m)Day sub-cohort ($n = 15$) vs. the mNight sub-cohort ($n = 15$). **(A)** Time course of IL-17A. **(B)** Time course of sST2. **(C)** Time course of IL-7. **(D)** Time course of IL-15. **(E)** Time course of GM-CSF. **(F)** Time course of MIP-1α. **(G)** Time course of IL-33. **(H)** Time course of cortisol. The indicated inflammatory mediators were assessed in serial plasma samples obtained at the indicated time points. Values are mean ± SEM (pg/mL). *$P < 0.05$ by Two-Way ANOVA (also indicated in bold).

Greater Requirement for Surgical Interventions Needed for Trauma Management, as Well as Worse Clinical Outcomes, in Stringently Matched Night vs. Day Sub-cohorts

The mNight group required more surgical interventions than the mDay group. These interventions were mainly either reductions/fixations for simple or compound fractures: 5/15 (33.3%) of the mNight patients had orthopedic intervention vs. 2/15 (13.3%) in the mDay sub-cohort ($P = 0.02$). There was no difference in the rate of exploratory laparotomies between the sub-cohorts. In addition, there was no statistically significant difference in the rates of NI (5/15 [33.3%] vs. 2/15 [13.3%]; $P = 0.2$) and average Marshall MOD score (1.3 vs. 0.9; $P = 0.4$) between the two sub-cohorts. Interestingly, though there was no statistically significant difference in the requirement for mechanical ventilation (0.8 ± 0.3, 2.3 ± 1.1; $P = 0.9$), there was

a statistically significantly longer ICU LOS (2.6 ± 0.3 vs. 8.5 ± 2.3; $P = 0.04$) and total hospital LOS (7.6 ± 0.9 vs. 15.5 ± 3; $P = 0.02$) in mNight sub-cohort when compared to the mDay group (**Table 2**).

Divergent Systemic Inflammatory Responses in Stringently Matched Day vs. Night vs. Sub-cohorts

Since trauma and subsequent organ dysfunction elicit a systemic inflammatory response which is regulated in part by diurnal and circadian rhythms, we hypothesized that the dynamics of inflammatory mediators could differ according to the time of injury and day/night cycle. We observed that IL-17A ($P = 0.008$; **Figure 3A**) and sST2 ($P = 0.022$; **Figure 3B**) were significantly higher in the mNight sub-cohort compared to the mDay sub-cohort. In contrast, IL-7 ($P < 0.001$; **Figure 3C**), IL-15 ($P = 0.002$; **Figure 3D**), GM-CSF ($P = 0.001$; **Figure 3E**), and MIP-1α ($P = 0.047$; **Figure 3F**) were significantly lower in the mNight sub-cohort. Notably, the circulating levels of the ligand for ST-2, IL-33 (26, 27), which we previously reported as being elevated in trauma patients (28), were not significantly different in the mDay vs. mNight cohorts (**Figure 3G**). Though cortisol is a key mediator whose levels vary with time of day in healthy individuals (29, 30), no differences in circulating cortisol levels were observed between mDay and mNight patients (**Figure 3H**). Also, there was no statistically significant difference in active, latent, and total TGF-β1 (**Figure 4**) between the mDay and mNight sub-cohorts.

Different Dynamic Inflammatory Networks Inferred in Day vs. Night Patients

We next sought to gain insights into the systemic inflammatory programs present in mDay and mNight sub-cohorts by examining dynamic network connectivity among inflammatory mediators using Dynamic Network Analysis (DyNA) (15, 23, 24). In addition to determining which networks were present at specific time intervals, we also assessed the total degree of connectivity at each of these intervals. **Figure 5** shows the detailed DyNA results for Day and Night in three different time periods following presentation (0–8, 8–16, and 16–24 h). We focused especially on DyNA connectivity among nodes with ≥ 4 connections. In the mDay group, these highly connected sub-networks initially involved MCP-1/IL-10/sIL-2Rα/IL-5/IL-7/IFN-γ/IL-6, and IL-1RA (0–8 h), and then MCP-1/IL-1β/IL-2/IL-5/IL-13/IL-10/IL-15/IFN-γ over the period of 8–16 h (**Figure 5**).

In contrast, network analysis of the mNight sub-cohort data revealed interactions among IL-4/IL-5/IL-6/IL-8/IL-13/IL-17A/sIL-2Rα/IL-1Rα/MIP-1α over the first 0–8 h. During the 8–16 h time period, the network interactions included sIL-1Rα/IL-8/IL-6/Eotaxin and IL-10/IP-10/MCP-1/MIP-1β. The overall degree of network complexity was lower in the mDay group over the first 0–8 h period, and then increased over time approaching the degree of inflammatory network complexity of mNight patients by 16–24 h (**Figure 6**).

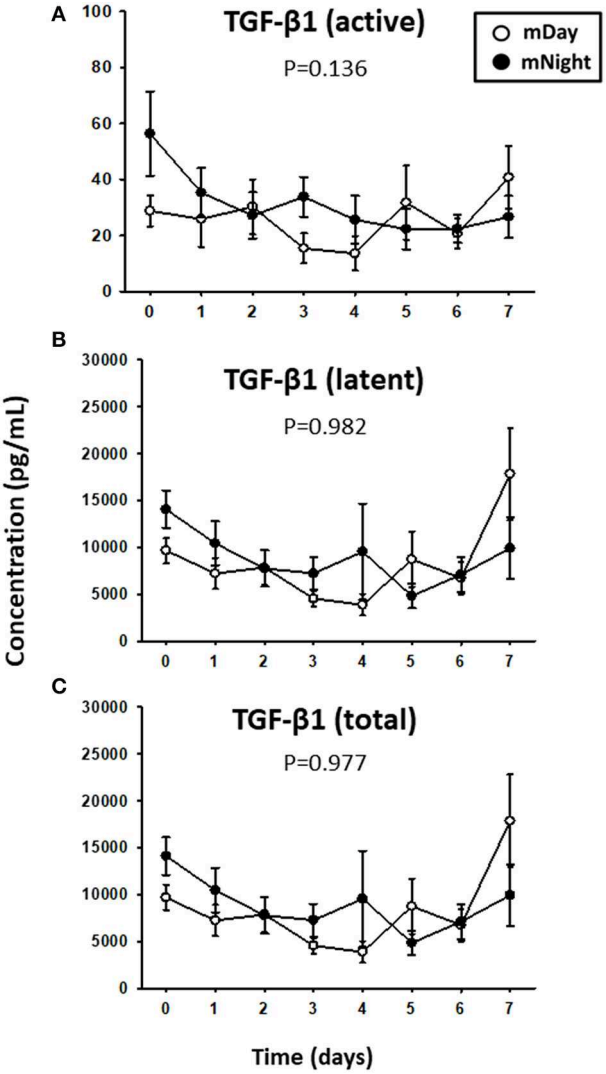

FIGURE 4 | Time course analysis of active, latent, and total TGF-β1 in the matched (m)Day group ($n = 15$) vs. the mNight group ($n = 15$). **(A)** Time course of active TGF-β1. **(B)** Time course of latent TGF-β1. **(C)** Time course of total (latent + active) TGF-β1. Mean circulating levels of TGF-β1 in both the mDay ($n = 15$) and mNight ($n = 15$) sub-cohorts. The indicated inflammatory mediators were assessed in serial plasma samples obtained at the indicated time points. Values are mean ± SEM (pg/ml). None of the levels were significantly different between mDay and mNight patients.

Finally, we sought to define potential feedback structures in the dynamic networks of inflammation associated with the first 24 h post-injury during the day vs. night, and to this end, we employed DyBN inference as in previous studies (31, 32). Based on this analysis, we inferred a central motif involving dynamic interactions between cortisol and sST2 in both sub-cohorts, affecting the levels of MIG/CXCL9, IP-10/CXCL10, MCP-1/CCL2, TGF-β1 latent, TGF-β1 total, IL-22, IL-23, and IL-17E/IL-25 (**Figure 7**). Notably,

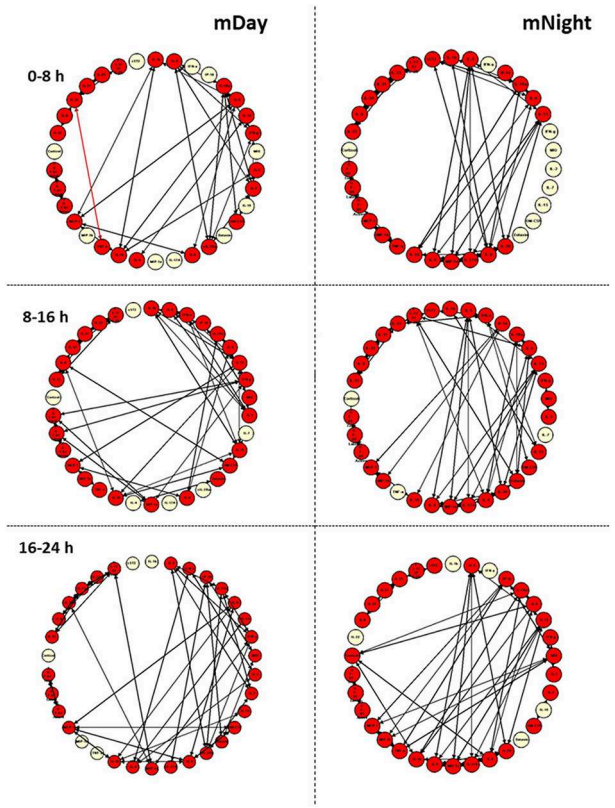

FIGURE 5 | Dynamic network analysis (DyNA) of inflammatory mediators in the matched (m)Day and mNight sub-cohorts ($n = 15$ each). DyNA was carried out using data on all inflammatory mediators assessed, as described in the *Materials and Methods*. This analysis suggested a higher dynamic network complexity/connectivity in the mNight as compared to the mDay group.

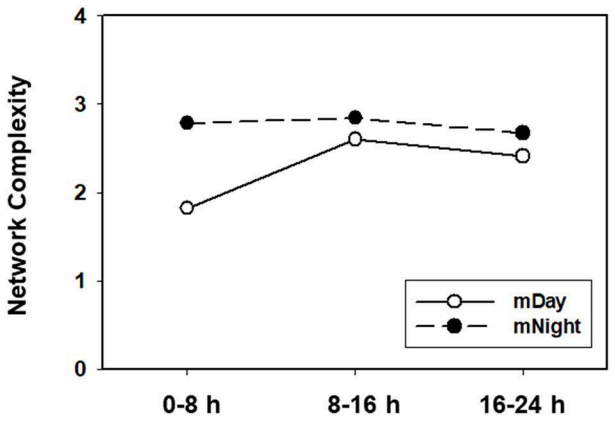

FIGURE 6 | Quantification of dynamic network complexity in the mDay and mNight sub-cohorts. The mNight group exhibited relatively a higher network density at 0–8 h time point which decreased over time but remained higher than the mDay group.

the only differentiating feature in these networks was the presence of IL-6 as a downstream node in mNight but not mDay patients.

DISCUSSION

The interactions of earth's rotation, sleep-wake cycle, the individual suprachiasmatic nucleus of the hypothalamus, and cellular core clock genes led to the evolution of daily circadian rhythms. Numerous physiological systems are under that circadian control, including inflammatory and immune responses (8, 33–35). Previous animal studies confirmed that murine responses to various pathogens as well as pro-inflammatory cytokines are under circadian control (36–40). Moreover, a recent study demonstrated that circadian rhythm was disrupted in trauma patients who went on to become septic (41). However, our study is the first to test directly for an association between diurnal variability and blunt trauma-induced clinical outcomes and systemic inflammatory responses in human subjects. In this study, we found worse clinical outcomes and more complex dynamic networks of systemic inflammation in trauma patients injured during the night as compared to during the day.

Trauma triggers a robust inflammatory response, which is important for an effective resolution of injury (16, 24, 42). However, the dysregulated immune response can impair recovery and complicate the clinical outcome (43, 44). In parallel, key components of the immune system exhibit circadian rhythmicity, which is dependent on the rest-activity diurnal phase (45). Indeed, diurnal variation was demonstrated previously in circulating levels of human peripheral blood mononuclear cell (PBMC) subsets and serum cytokine and cytokine receptors including IL-2, IL-10, GM-CSF, IL-1β, IL-6, TNF-α, MCP-1/JE, CCR2/CD192, IFN-γ, and IFN receptors (46–48). Thus, we hypothesized that the timing of the insult relative to the circadian oscillation of the immune system would trigger differential immune/inflammatory response associated with divergent clinical outcomes.

In the present study, we focused on the potential role of time of injury in propensity-matched, moderately/severely injured patients. A key observation was the association between nighttime injury and adverse clinical outcomes, namely longer intensive care unit and hospital length of stay. While controversial factors related to the quality of medical care during nighttime (49–51) or other variables such as hospital volume and socioeconomic factors cannot be ruled out in our study, our data suggest that patients injured during the night require additional and more extensive procedures rather than experiencing worse outcomes with the same degree of intervention. Moreover, the use of stringent propensity matching further reduces the likelihood of artifactual reasons underlying our findings.

Our dynamic network analyses suggest potential mechanisms underlying the differential inflammatory responses in daytime- vs. nighttime-injured patients. While neither cortisol levels nor levels of TGF-β1 and several other mediators were statistically significantly different in mDay vs. mNight, several other pathways were inferred to be activated differentially in patients injured at night vs. during the day. The lack of statistically significant differences in circulating cortisol levels in mNight vs. mDay patients suggests that trauma induces derangements in the known diurnal variation of this mediator. Indeed, cortisol

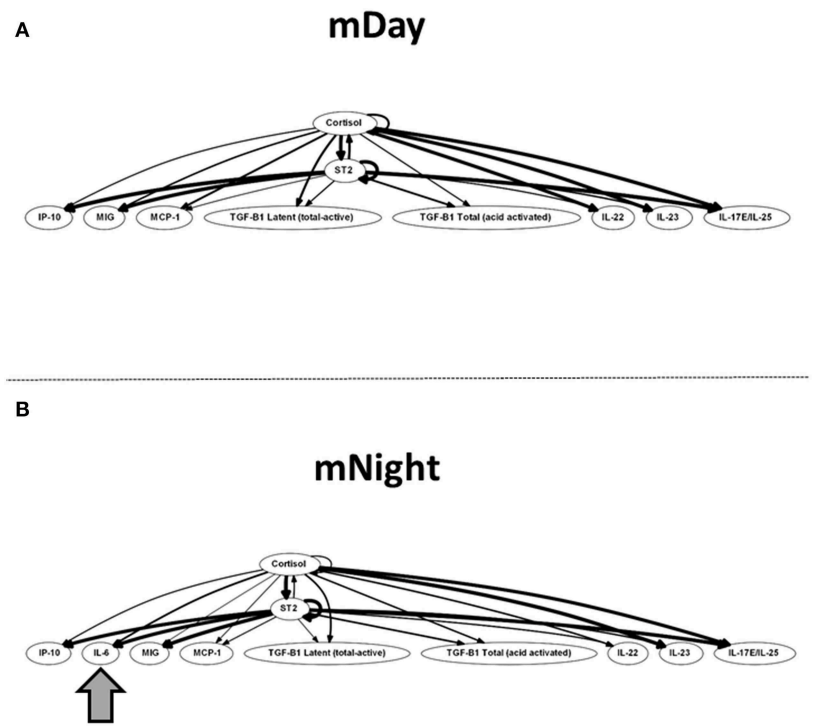

FIGURE 7 | Dynamic Bayesian Network (DyBN) of inflammation biomarkers in matched **(A)** (m)Day and **(B)** mNight sub-cohorts. DyBN suggested that both cortisol and sST2 affects the production of MIG/CXCL9, IP-10, MCP-1, TGF-β1 latent, TGF-β1 total, IL-22, IL-23, and IL-17E/IL-25 production in the first 24 h post-injury in both groups.

dysregulation and the role of adrenal insufficiency have been appreciated as key aspects of trauma-induced critical illness (52, 53). Importantly, cortisol is a key regulator of systemic inflammation, and we observed differences in circulating levels of multiple cytokines and chemokines. Within the panoply of inflammatory and immune pathways known to be by a traumatic injury (54, 55), there has been a recent focus on type 17 immunity (56). Notably, circulating IL-17A levels were higher in mNight patients as compared to mDay patients, suggesting the possibility that a dysregulated IL-17A response may in part underlie the worse clinical outcomes in mNight patients. Moreover, circadian rhythms are known to impact Th17 development and function (57). We have previously utilized correlation analyses (IL-17A vs. GM-CSF and IL-17A vs. IL-10 to suggest the presence of pathogenic and non-pathogenic Th17 cells) (15). In a similar analysis of the mDay vs. mNight cohorts, no significant correlations were observed (**Supplementary Figure 1**). However, there was a trend suggesting the possible prevalence of non-pathogenic Th17 cells in the mDay sub-cohort ($r = 0.19$, $P = 0.06$; **Supplementary Figure 1B**) and a similar trend suggesting the prevalence of pathogenic Th17 cells in the mNight sub-cohort ($r = 0.19$, $P = 0.051$; **Supplementary Figure 1C**). Further studies with larger cohorts may thus be warranted to define the role, if any, of circadian alterations on Th17 (and other IL-17A-producing) cells.

We gleaned additional information by examining the dynamic evolution of networks of systemic inflammation using two different algorithms: DyNA (23) and DyBN (22). DyNA suggested a generally higher degree of inflammatory activation in mNight patients as compared to mDay patients suggesting an early activation of immune pathways compared to the mDay group. Moreover, the inflammatory responses of mDay patients were more "Th2-like" (involving IL-5, IL-10, and IL-13 early on), whereas the networks of mNight patients involved both Th2 responses (involving IL-4, IL-5, and IL-13) as well as Th17 responses (IL-17A and also IL-6, though the latter is involved in multiple other pathways). As discussed above, we speculate that the presence of type 17 immunity in the mNight group may indicate the presence of overly exuberant inflammation. We further speculate that the presence of Th2 responses in both mDay and mNight patients may underlie the absence of significant differences in nosocomial infections in patients injured at night vs. the day, though this may be a function of the limited data set in propensity-matched patients (see below).

We recognize that there are several limitations to the current study. First, this is a single-center study and thus may not be generalizable to other centers that adopt alternative management practices or challenged by different demographics or injury characteristics. These issues warrant multi-centric studies to validate the results suggested by the current one. Moreover, the number of inflammatory biomarkers analyzed was limited to the number of analytes we could measure using commercially available Luminex^{TM} bead sets. Further future studies examining a larger panel of inflammatory

biomarkers are suggested. Finally, we note that DyNA lacks mechanistic insight; however, it can be used to understand abstract key features and interactions of the trauma-induced inflammatory response.

In conclusion, we report for the first time on a potential impact of time of injury on blunt trauma outcomes and the dynamics of systemic inflammation in humans. Our findings may have larger implications for a growing body of evidence implicating the need to consider the time of day when designing therapeutic approaches, especially in the context of diseases that are strongly impacted by immune/inflammatory interactions (12, 58–60). The present study adds to this field by demonstrating that clinical outcomes of trauma patients are likewise impacted by time of injury along with other factors such as injury severity, genotype, and the character of systemic inflammation and immune dysregulation that ensues following severe injury. Given the complexity of the intertwined inflammatory, immune, and physiologic interactions in the context of circadian rhythms, it is likely that systems and computational biology approaches (59, 61) will be necessary to help define novel therapeutic control points in the context of traumatic injury (54).

DATA AVAILABILITY STATEMENT

All datasets generated for this study are included in the article/**Supplementary Material**.

ETHICS STATEMENT

The studies involving human participants were reviewed and approved by University of Pittsburgh Institutional Review Board (IRB). The patients/participants provided their written informed consent to participate in this study.

AUTHOR'S NOTE

This work was presented in part at the 37th Annual Conference on Shock.

AUTHOR CONTRIBUTIONS

AZ and RN participated in study design, data collection and interpretation, and writing. OA-M and KA participated in data collection. DB and JY participated in analysis of inflammatory mediators. RZ participated in computational and statistical analysis, data interpretation, and writing. MR and TB participated in data interpretation and writing. YV participated in study design, data interpretation, and writing.

FUNDING

This work was supported by the Office of the Assistant Secretary of Defense for Health Affairs, through the Defense Medical Research and Development Program under Award Nos. W81XWH-18-2-0051 and W81XWH-15-PRORP-OCRCA.

SUPPLEMENTARY MATERIAL

The Supplementary Material for this article can be found online at: https://www.frontiersin.org/articles/10.3389/fimmu.2019.02699/full#supplementary-material

Supplementary Figure 1 | Correlation analyses aimed at defining Th17 cell subsets computationally. Spearman correlations were carried out on mDay vs. mNight patient cytokine data to suggest the presence of pathogenic (IL-17A vs. GM-CSF; **A,C**) and non-pathogenic (IL-17A vs. IL-10; **B,D**) Th17 cells. This analysis suggested the possible predominance of pathogenic Th17 cells in the mNight group and non-pathogenic Th17 cells in the mDay.

REFERENCES

1. Ciesla DJ, Moore EE, Johnson JL, Burch JM, Cothren CC, Sauaia A. A 12-year prospective study of postinjury multiple organ failure: has anything changed? *Arch Surg.* (2005) 140:432–8. doi: 10.1001/archsurg.140.5.432
2. Boomer JS, To K, Chang KC, Takasu O, Osborne DF, Walton AH, et al. Immunosuppression in patients who die of sepsis and multiple organ failure. *JAMA.* (2011) 306:2594–605. doi: 10.1001/jama.2011.1829
3. Hawkins RB, Raymond SL, Stortz JA, Horiguchi H, Brakenridge SC, Gardner A, et al. Chronic critical illness and the persistent inflammation, immunosuppression, and catabolism syndrome. *Front Immunol.* (2018) 9:1511. doi: 10.3389/fimmu.2018.01511
4. Mclellan BA, Vingilis E, Larkin E, Stoduto G, Macartney-Filgate M, Sharkey PW. Psychosocial characteristics and follow-up of drinking and non-drinking drivers in motor vehicle crashes. *J Trauma.* (1993) 35:245–50. doi: 10.1097/00005373-199308000-00012
5. Adrie C, Pinsky MR. The inflammatory balance in human sepsis. *Intensive Care Med.* (2000) 26:364–75. doi: 10.1007/s001340051169
6. Nathan C. Points of control in inflammation. *Nature.* (2002) 420:846–52. doi: 10.1038/nature01320
7. Castro R, Angus DC, Rosengart MR. The effect of light on critical illness. *Crit Care.* (2011) 15:218. doi: 10.1186/cc10000
8. Scheiermann C, Kunisaki Y, Frenette PS. Circadian control of the immune system. *Nat Rev Immunol.* (2013) 13:190–8. doi: 10.1038/nri3386
9. Logan RW, Sarkar DK. Circadian nature of immune function. *Mol Cell Endocrinol.* (2012) 349:82–90. doi: 10.1016/j.mce.2011.06.039
10. Rosenwasser AM. Functional neuroanatomy of sleep and circadian rhythms. *Brain Res Rev.* (2009) 61:281–306. doi: 10.1016/j.brainresrev.2009.08.001
11. Takahashi JS, Hong HK, Ko CH, Mcdearmon EL. The genetics of mammalian circadian order and disorder: implications for physiology and disease. *Nat Rev Genet.* (2008) 9:764–75. doi: 10.1038/nrg2430
12. Kizaki T, Sato S, Shirato K, Sakurai T, Ogasawara J, Izawa T, et al. Effect of circadian rhythm on clinical and pathophysiological conditions and inflammation. *Crit Rev Immunol.* (2015) 35:261–75. doi: 10.1615/CritRevImmunol.2015014925
13. Acuna-Castroviejo D, Rahim I, Acuna-Fernandez C, Fernandez-Ortiz M, Solera-Marin J, Sayed RKA, et al. Melatonin, clock genes and mitochondria in sepsis. *Cell Mol Life Sci.* (2017) 74:3965–87. doi: 10.1007/s00018-017-2610-1
14. Lewis AJ, Zhang X, Griepentrog JE, Yuan D, Collage RD, Waltz PK, et al. Blue light enhances bacterial clearance and reduces organ injury during sepsis. *Crit Care Med.* (2018) 46:e779–87. doi: 10.1097/CCM.0000000000003190
15. Abboud A, Namas RA, Ramadan M, Mi Q, Almahmoud K, Abdul-Malak O, et al. Computational analysis supports an early, type 17 cell-associated divergence of blunt trauma survival and mortality. *Crit Care Med.* (2016) 44:e1074–81. doi: 10.1097/CCM.0000000000001951
16. Namas RA, Vodovotz Y, Almahmoud K, Abdul-Malak O, Zaaqoq A, Namas R, et al. Temporal patterns of circulating inflammation biomarker networks differentiate susceptibility to nosocomial infection following blunt trauma in humans. *Ann Surg.* (2016) 263:191–8. doi: 10.1097/SLA.0000000000001001

17. Baker SP, O'neill B, Haddon W Jr, Long WB. The injury severity score: a method for describing patients with multiple injuries and evaluating emergency care. *J Trauma.* (1974) 14:187–96. doi: 10.1097/00005373-197403000-00001
18. Gennarelli TA, Wodzin E. AIS 2005: a contemporary injury scale. *Injury.* (2006) 37:1083–91. doi: 10.1016/j.injury.2006.07.009
19. Cottington EM, Young JC, Shufflebarger CM, Kyes F, Peterson FV Jr, Diamond DL. The utility of physiological status, injury site, and injury mechanism in identifying patients with major trauma. *J Trauma.* (1988) 28:305–11. doi: 10.1097/00005373-198803000-00005
20. Marshall JC, Cook DJ, Christou NV, Bernard GR, Sprung CL, Sibbald WJ. Multiple organ dysfunction score: a reliable descriptor of a complex clinical outcome. *Crit Care Med.* (1995) 23:1638–52. doi: 10.1097/00003246-199510000-00007
21. Grzegorczyk M, Husmeier D. Improvements in the reconstruction of time-varying gene regulatory networks: dynamic programming and regularization by information sharing among genes. *Bioinformatics.* (2011) 27:693–9. doi: 10.1093/bioinformatics/btq711
22. Azhar N, Ziraldo C, Barclay D, Rudnick D, Squires R, Vodovotz Y. Analysis of serum inflammatory mediators identifies unique dynamic networks associated with death and spontaneous survival in pediatric acute liver failure. *PLoS ONE.* (2013) 8:e78202. doi: 10.1371/journal.pone.0078202
23. Mi Q, Constantine G, Ziraldo C, Solovyev A, Torres A, Namas R, et al. A dynamic view of trauma/hemorrhage-induced inflammation in mice: principal drivers and networks. *PLoS ONE.* (2011) 6:e19424. doi: 10.1371/journal.pone.0019424
24. Abdul-Malak O, Vodovotz Y, Zaaqoq A, Guardado J, Almahmoud K, Yin J, et al. Elevated admission base deficit is associated with a complex dynamic network of systemic inflammation which drives clinical trajectories in blunt trauma patients. *Mediat Inflamm.* (2016) 2016:7950374. doi: 10.1155/2016/7950374
25. Assenov Y, Ramirez F, Schelhorn SE, Lengauer T, Albrecht M. Computing topological parameters of biological networks. *Bioinformatics.* (2008) 24:282–4. doi: 10.1093/bioinformatics/btm554
26. Griesenauer B, Paczesny S. The ST2/IL-33 axis in immune cells during inflammatory diseases. *Front Immunol.* (2017) 8:475. doi: 10.3389/fimmu.2017.00475
27. Cayrol C, Girard JP. Interleukin-33 (IL-33): a nuclear cytokine from the IL-1 family. *Immunol Rev.* (2018) 281:154–68. doi: 10.1111/imr.12619
28. Xu J, Guardado J, Hoffman R, Xu H, Namas R, Vodovotz Y, et al. IL33-mediated ILC2 activation and neutrophil IL5 production in the lung response after severe trauma: a reverse translation study from a human cohort to a mouse trauma model. *PLoS Med.* (2017) 14:e1002365. doi: 10.1371/journal.pmed.1002365
29. Daly JR, Evans JI. Daily rhythms of steroid and associated pituitary hormones in man and their relationship to sleep. *Adv Steroid Biochem Pharmacol.* (1974) 4:61–110. doi: 10.1016/B978-0-12-037504-2.50005-5
30. Weitzman ED. Circadian rhythms and episodic hormone secretion in man. *Annu Rev Med.* (1976) 27:225–43. doi: 10.1146/annurev.me.27.020176.001301
31. Zaaqoq AM, Namas R, Almahmoud K, Azhar N, Mi Q, Zamora R, et al. Inducible protein-10, a potential driver of neurally controlled interleukin-10 and morbidity in human blunt trauma. *Crit Care Med.* (2014) 42:1487–97. doi: 10.1097/CCM.0000000000000248
32. Almahmoud K, Namas RA, Zaaqoq AM, Abdul-Malak O, Namas R, Zamora R, et al. Prehospital hypotension is associated with altered inflammation dynamics and worse outcomes following blunt trauma in humans. *Crit Care Med.* (2015) 43:1395–404. doi: 10.1097/CCM.0000000000000964
33. Bass J, Takahashi JS. Circadian integration of metabolism and energetics. *Science.* (2010) 330:1349–54. doi: 10.1126/science.1195027
34. Mohawk JA, Green CB, Takahashi JS. Central and peripheral circadian clocks in mammals. *Annu Rev Neurosci.* (2012) 35:445–62. doi: 10.1146/annurev-neuro-060909-153128
35. Curtis AM, Bellet MM, Sassone-Corsi P, O'neill LA. Circadian clock proteins and immunity. *Immunity.* (2014) 40:178–86. doi: 10.1016/j.immuni.2014.02.002
36. Shackelford PG, Feigin RD. Periodicity of susceptibility to pneumococcal infection: influence of light and adrenocortical secretions. *Science.* (1973) 182:285–7. doi: 10.1126/science.182.4109.285
37. Hrushesky WJ, Langevin T, Kim YJ, Wood PA. Circadian dynamics of tumor necrosis factor alpha (cachectin) lethality. *J Exp Med.* (1994) 180:1059–65. doi: 10.1084/jem.180.3.1059
38. House SD, Ruch S, Koscienski WF III, Rocholl CW, Moldow RL. Effects of the circadian rhythm of corticosteroids on leukocyte-endothelium interactions in the AM and PM. *Life Sci.* (1997) 60:2023–34. doi: 10.1016/S0024-3205(97)00167-7
39. Silver AC, Arjona A, Walker WE, Fikrig E. The circadian clock controls toll-like receptor 9-mediated innate and adaptive immunity. *Immunity.* (2012) 36:251–61. doi: 10.1016/j.immuni.2011.12.017
40. Heipertz EL, Harper J, Lopez CA, Fikrig E, Hughes ME, Walker WE. Circadian rhythms influence the severity of sepsis in mice via a TLR2-dependent, leukocyte-intrinsic mechanism. *J Immunol.* (2018) 201:193–201. doi: 10.4049/jimmunol.1701677
41. Coiffard B, Diallo AB, Culver A, Mezouar S, Hammad E, Vigne C, et al. Circadian rhythm disruption and sepsis in severe trauma patients. *Shock.* (2019) 52:29–36. doi: 10.1097/SHK.0000000000001241
42. Maier B, Lefering R, Lehnert M, Laurer HL, Steudel WI, Neugebauer EA, et al. Early versus late onset of multiple organ failure is associated with differing patterns of plasma cytokine biomarker expression and outcome after severe trauma. *Shock.* (2007) 28:668–74. doi: 10.1097/shk.0b013e318123e64e
43. Namas R, Ghuma A, Torres A, Polanco P, Gomez H, Barclay D, et al. An adequately robust early TNF-alpha response is a hallmark of survival following trauma/hemorrhage. *PLoS ONE.* (2009) 4:e8406. doi: 10.1371/journal.pone.0008406
44. Neunaber C, Zeckey C, Andruszkow H, Frink M, Mommsen P, Krettek C, et al. Immunomodulation in polytrauma and polymicrobial sepsis - where do we stand? *Recent Pat Inflamm Allergy Drug Discov.* (2011) 5:17–25. doi: 10.2174/187221311794474892
45. Haus E, Smolensky MH. Biologic rhythms in the immune system. *Chronobiol Int.* (1999) 16:581–622. doi: 10.3109/07420529908998730
46. Born J, Lange T, Hansen K, Molle M, Fehm HL. Effects of sleep and circadian rhythm on human circulating immune cells. *J Immunol.* (1997) 158:4454–64.
47. Takane H, Ohdo S, Baba R, Koyanagi S, Yukawa E, Higuchi S. Relationship between 24-hour rhythm in antiviral effect of interferon-beta and interferon-alpha/beta receptor expression in mice. *Jpn J Pharmacol.* (2002) 90:304–12. doi: 10.1254/jjp.90.304
48. Hayashi M, Shimba S, Tezuka M. Characterization of the molecular clock in mouse peritoneal macrophages. *Biol Pharm Bull.* (2007) 30:621–6. doi: 10.1248/bpb.30.621
49. Medicine IO. *Resident Duty Hours: Enhancing Sleep, Supervision, and Safety.* Washington, DC: The National Academies Press (2009).
50. Yaghoubian A, Kaji AH, Ishaque B, Park J, Rosing DK, Lee S, et al. Acute care surgery performed by sleep deprived residents: are outcomes affected? *J Surg Res.* (2010) 163:192–6. doi: 10.1016/j.jss.2010.04.011
51. Yaghoubian A, Kaji AH, Putnam B, De Virgilio C. Trauma surgery performed by "sleep deprived" residents: are outcomes affected? *J Surg Educ.* (2010) 67:449–51. doi: 10.1016/j.jsurg.2010.09.003
52. Reichgott MJ, Melmon KL. Should corticosteroids be used in shock? *Med Clin North Am.* (1973) 57:1211–23. doi: 10.1016/S0025-7125(16)32223-4
53. Rushing GD, Britt RC, Collins JN, Cole FJ, Weireter LJ, Britt LD. Adrenal insufficiency in hemorrhagic shock. *Am Surg.* (2006) 72:552–4.
54. Namas R, Mi Q, Namas R, Almahmoud K, Zaaqoq A, Abdul Malak O, et al. Insights into the role of chemokines, damage-associated molecular patterns, and lymphocyte-derived mediators from computational models of trauma-induced inflammation. *Antiox Redox Signal.* (2015) 10:1370–87. doi: 10.1089/ars.2015.6398
55. Lamparello AJ, Namas RA, Constantine G, Mckinley TO, Elster E, Vodovotz Y, et al. A conceptual time window-based model for the early stratification of trauma patients. *J Intern. Med.* (2019) 286:2–15. doi: 10.1111/joim.12874
56. Almahmoud K, Abboud A, Namas RA, Zamora R, Sperry J, Peitzman AB, et al. Computational evidence for an early, amplified systemic inflammation program in polytrauma patients with severe extremity injuries. *PLoS ONE.* (2019) 14:e0217577. doi: 10.1371/journal.pone.0217577

57. Yu X, Rollins D, Ruhn KA, Stubblefield JJ, Green CB, Kashiwada M, et al. TH17 cell differentiation is regulated by the circadian clock. *Science.* (2013) 342:727–30. doi: 10.1126/science.1243884
58. Arjona A, Silver AC, Walker WE, Fikrig E. Immunity's fourth dimension: approaching the circadian-immune connection. *Trends Immunol.* (2012) 33:607–12. doi: 10.1016/j.it.2012.08.007
59. Ballesta A, Innominato PF, Dallmann R, Rand DA, Levi FA. Systems chronotherapeutics. *Pharmacol Rev.* (2017) 69:161–99. doi: 10.1124/pr.116.013441
60. Cederroth CR, Albrecht U, Bass J, Brown SA, Dyhrfjeld-Johnsen J, Gachon F, et al. Medicine in the fourth dimension. *Cell Metab.* (2019) 30:238–50. doi: 10.1016/j.cmet.2019.06.019
61. Rao R, Androulakis IP. The physiological significance of the circadian dynamics of the HPA axis: interplay between circadian rhythms, allostasis and stress resilience. *Horm Behav.* (2019) 110:77–89. doi: 10.1016/j.yhbeh.2019.02.018

Disclaimer: Opinions, interpretations, conclusions, and recommendations are those of the authors and not necessarily endorsed by the Department of Defense.

Conflict of Interest: The authors declare that the research was conducted in the absence of any commercial or financial relationships that could be construed as a potential conflict of interest.

Copyright © 2019 Zaaqoq, Namas, Abdul-Malak, Almahmoud, Barclay, Yin, Zamora, Rosengart, Billiar and Vodovotz. This is an open-access article distributed under the terms of the Creative Commons Attribution License (CC BY). The use, distribution or reproduction in other forums is permitted, provided the original author(s) and the copyright owner(s) are credited and that the original publication in this journal is cited, in accordance with accepted academic practice. No use, distribution or reproduction is permitted which does not comply with these terms.

frontiers in Immunology

ORIGINAL RESEARCH
published: 06 December 2019
doi: 10.3389/fimmu.2019.02774

Modeling Cardiac Dysfunction Following Traumatic Hemorrhage Injury: Impact on Myocardial Integrity

Johanna Wall[1†], Sriveena Naganathar[1†], Banjerd Praditsuktavorn[1], Oscar F. Bugg[1], Simon McArthur[2], Christoph Thiemermann[1,3], Jordi L. Tremoleda[1] and Karim Brohi[1]*

[1] Centre for Trauma Sciences, Neuroscience, Surgery and Trauma, Blizard Institute, Queen Mary University of London, London, United Kingdom, [2] Centre for Oral Immunobiology & Regenerative Medicine, Institute of Dentistry, Queen Mary University of London, London, United Kingdom, [3] Department of Translational Medicine and Therapeutics, William Harvey Research Institute, Queen Mary University of London, London, United Kingdom

OPEN ACCESS

Edited by:
Guochang Hu,
University of Illinois at Chicago,
United States

Reviewed by:
David N. Naumann,
University of Birmingham,
United Kingdom
Neil Herring,
University of Oxford, United Kingdom

***Correspondence:**
Jordi L. Tremoleda
j.lopez-tremoleda@qmul.ac.uk

[†]These authors have contributed equally to this work

Specialty section:
This article was submitted to Inflammation, a section of the journal Frontiers in Immunology

Received: 12 September 2019
Accepted: 12 November 2019
Published: 06 December 2019

Citation:
Wall J, Naganathar S, Praditsuktavorn B, Bugg OF, McArthur S, Thiemermann C, Tremoleda JL and Brohi K (2019) Modeling Cardiac Dysfunction Following Traumatic Hemorrhage Injury: Impact on Myocardial Integrity. Front. Immunol. 10:2774. doi: 10.3389/fimmu.2019.02774

Cardiac dysfunction (CD) importantly contributes to mortality in trauma patients, who survive their initial injuries following successful hemostatic resuscitation. This poor outcome has been correlated with elevated biomarkers of myocardial injury, but the pathophysiology triggering this CD remains unknown. We investigated the pathophysiology of acute CD after trauma using a mouse model of trauma hemorrhage shock (THS)-induced CD with echocardiographic guidance of fluid resuscitation, to assess the THS impact on myocardial integrity and function. Mice were subjected to trauma (soft tissue and bone fracture) and different degrees of hemorrhage severity (pressure controlled ~MABP < 35 mmHg or <65 mmHg) for 1 h, to characterize the acute impact on cardiac function. In a second study, mice were subjected to trauma and hemorrhage (MABP < 35 mmHg) for 1 h, then underwent two echocardiographic-guided resuscitations to baseline stroke volume at 60 and 120 min, and were monitored up to 180 min to study the longer impact of THS following resuscitation. Naïve and sham animals were used as controls. At 60 min post-THS injury, animals showed a lower cardiac output (CO) and stroke volume (SV) and an early rise of heart fatty acid-binding protein (H-FABP = 167 ± 38 ng/ml; 90% increase from shams, 3.54 ± 3.06 ng/ml), when subjected to severe hemorrhage and injury. Despite resuscitation, these animals maintained lower CO (6 ml/min vs. 23 ml/min), lower SV (10 μl vs. 46 μl; both ~75% decreased), and higher H-FABP (levels (340 ± 115 ng/ml vs. 10.3 ± 0.2 ng/ml; all THS vs. shams, $P < 0.001$) at 180 min post-THS injury. Histopathological and flow-cytometry analysis of the heart confirmed an influx of circulatory leukocytes, compared to non-injured hearts. Myocardial injury was supported by an increase of troponin I and h-FABP and the widespread ultrastructural disorganization of the morphology of sarcomeres and mitochondria. DNA fragmentation and chromatin condensation driven by leakage of apoptosis-inducing factor (AIF) may suggest a mitochondria-driven progressive cell death. THS modeling in the mouse results in cardiomyocyte damage and reduced

myocardial function, which mimics the cardiac dysfunction seen in trauma patients. This CD model may, therefore, provide further understanding to the mechanisms underlying CD and act as a tool for developing cardioprotective therapeutics to improve survival after injury.

Keywords: trauma, cardiac dysfunction, myocardial damage, haemorrhagic injury, murine models

INTRODUCTION

Trauma is a large and growing problem worldwide, accounting for 10.1% of the global burden of disease (1), with half of all trauma deaths being due to excessive bleeding and the subsequent severe shock (2, 3). New paradigms of hemostatic resuscitation to manage coagulopathy have led to large decreases in mortality worldwide (4, 5). With more patients surviving the initial bleeding episode, cardiac dysfunction is increasingly common and an important determinant of outcome. Over half of all critically injured trauma patients admitted to intensive care develop cardiovascular dysfunction within the first 48 h, of which 20% will die (6). Identifying these patients early in their care and rescuing them from this downward trajectory would have a dramatic impact on trauma mortality.

Cardiac dysfunction in trauma patients is initially difficult to recognize, as it develops within the context of hypovolemia and a widespread inflammatory response (7). Patients often initially show a normal cardiac response with a high cardiac output, but over a relatively short period they experience a dramatic fall in SV and CO, despite inotrope and vasopressor support. We have previously shown that trauma patients have elevated levels of biomarkers of myocardial damage within the first 2 h of injury, and this is associated with increased risks of adverse cardiac events and mortality (8, 9). Cardiac histopathology in non-survivors has shown multiple pathological identifiers of indirect or secondary cardiac injury (10, 11). The pathophysiology and mechanisms of secondary cardiac dysfunction are unknown, with most critical care studies limited to sepsis (12). There is some pre-clinical evidence for the development of cardiac injury and dysfunction arising as an indirect consequence of trauma and hemorrhage in pigs (13) and in rodents (14–16), suggesting a local cardiac inflammatory response as the main driver of cardiomyocyte structural and functional damage.

Our overall aim for this study was to investigate the pathophysiology of cardiac dysfunction after trauma by implementing a clinically relevant murine model of post trauma hemorrhage cardiac dysfunction. Specifically, our objectives were to: (1) determine the nature and extent of myocardial damage and cardiac dysfunction in an un-resuscitated model of trauma hemorrhage; (2) determine the progression of cardiac dysfunction over time in a resuscitated model of trauma hemorrhage; and (3) explore the inflammatory myocardial response and ultrastructural integrity, to elucidate possible mechanistic pathways for cardiomyocyte cell damage.

MATERIALS AND METHODS

Ethical Statement

All animal procedures were carried out under a Project License (PC5F29685) approved by the Animal Welfare and Ethical Review Body at Queen Mary University of London and the UK Home Office, in accordance with the EU Directive 2010/63/EU. All animal facilities and suppliers have been approved by the UK Home Office Licensing Authority and meet all current regulations and standards for the UK. A total of 98 mice were used for the work described in this study (details in **Supplementary Table 1**).

For this study we used $n = 6$–10 animals per group, to provide a valuable discriminatory power of 90% with a significance level of $\alpha = 0.05$ to detect up to 15–20% relative differences in primary outcomes (lactate levels, cardiac function, cardiac injury biomarkers). Experimental planning for data randomization and blinded data acquisition and analysis was carried out following the ARRIVE guidelines (17).

Animal Housing and Husbandry

Adult male C57Bl/6 mice (weight range 25–30 g; 9–11 weeks old) were obtained from Charles River Laboratories (Margate, UK). Health screens provided by the official vendor indicated that animals were free of known pathogens in accordance with FELASA guidelines for health monitoring of rodent colonies (18). Animals were housed in groups of 4–6 per individually ventilated cage (IVC; Allentown Europe, UK), in a 12 h light dark cycle (06:30–18:30 light; 18:30–06:30 dark), with controlled room temperature (21 ± 1°C) and relative humidity (40–60%). Animals were allocated to cages on arrival and remained in the same social group throughout the study, including a 7 day acclimatization phase prior to any study, with *ad libitum* access to standard diet and water.

Induction of Hemorrhagic Traumatic Injury

Animals were anesthetized (Isoflurane: 4–5% induction, 0.5–1.5% for maintenance in 0.8–1 lt/min 100% medical O_2). Anesthesia depth was controlled clinically and by hemodynamic monitoring (Mean Arterial Blood Pressure; MABP). Core temperature was maintained at 36± 1°C throughout the study with a homoeothermic blanket (Harvard Apparatus Ltd., UK) and heat lamps. All experiments were carried out under terminal anesthesia with no recovery, and all animals were humanely culled at the end of the experiment.

A 1 cm incision was made in the middle of the cervical skin and the left jugular vein was cannulated [polyethylene tubing pre-flushed with heparinized saline (25 IU/mL); Portex. Smith's

Medical Int. Ltd. Kent, UK] The right carotid artery was then cannulated in the same fashion and connected to a pressure transducer (Capto SP 844, AD Instruments, UK) attached to a PowerLab 8/30 (ML870, AD Instruments Ltd, Oxford, UK) to monitor MABP using the LabChart software (ADInstruments Ltd, UK). The neck incision was covered and regularly checked for evidence of line displacement and/or bleeding. If either of these developed, the animal was euthanized and removed from the study.

A 2 cm midline laparotomy was then performed, and the rectus muscle was crushed using forceps in a systematic fashion in each animal. The abdominal area was examined to exclude inadvertent iatrogenic injury and/or bleeding, and then the incision was closed using 5.0-prolene suture material (Ethicon, UK). Immediately thereafter, animals were subjected to a bilateral hind limb fracture. Fractures were performed using a closed, manual 3-point bending technique. Following 5 min' stabilization after traumatic injury, a "baseline" MABP was recorded. Then, a pressure-controlled hemorrhage via the carotid cannula was induced to achieve a target MABP of 30–40 mmHg to reach a traumatic hemorrhagic shock state (THS). Animals underwent a 60 min observation period, during which the target blood pressure (30–40 mmHg) was maintained with removal of blood as required via the carotid cannula. Shed blood was kept warm in a heparinized 1 mL syringe (25 IU/mL), which was occasionally agitated to prevent thrombus formation. In-dwelling vascular catheters were intermittently flushed with small volumes of heparinized saline and wound sites checked for signs of hemorrhage. All volumes of heparinized saline were taken into account when recording volumes of shed and reinfused blood.

Sham controls underwent cannulation of the carotid artery for invasive MABP monitoring only, without trauma, hemorrhage or fluid resuscitation.

Echocardiography of the left ventricle (LV) was performed at baseline (prior to any traumatic hemorrhagic intervention), and at defined time-points after injury to assess the impact of THS injury at 60 (T60), 120 (T120), and 180 (T180) min post THS, using the Vevo 770 high-resolution system (Visualsonics Inc. Toronto, Canada). M-mode short axis measurements were used to calculate stroke volume (SV), left ventricular end-diastolic volume (LVEDV), and cardiac output (CO). Measurements were carried out in triplicate.

The acute impact of THS in cardiac function was studied in animals subjected to sham, trauma only, THS to 60–70 mmHg MABP or THS to 30–40 mmHg MABP procedures ($n = 6$/group) following 1 h post-intervention, without any resuscitation. At 60 min post THS (T60), cardiac function and shock status were assessed and animals were culled via terminal exsanguination and blood samples processed for further analysis (**Figure 1A**).

To investigate the CD associated with THS, the THS model with a 30–40 mmHg MABP was extended up to 3 h through 2 resuscitation phases at T60 and T120 (THS and sham, $n = 10$/group) and terminated at T180. Echocardiography was carried out at T60, T120, and T180 to assess cardiac function and also to guide the resuscitation volume requirements to restore the SV to baseline levels during each resuscitation at T60 and T120 (**Figure 2A**).

For the first resuscitation (RESUS 1 at T60), the whole shed blood was transfused as a bolus over 5 min *via* the jugular catheter, and boluses of warmed Hartmann's solution (Vetivex11. Dechra Veterinary Products, Shrewsbury, UK) were then administered to reach SV baseline. In the second resuscitation phase (RESUS 2 at T120), a bolus of Hartmann's alone was administered over 5–10 min. At each resuscitation, animals received volume resuscitation to restore left ventricular stroke volume to baseline. During the second resuscitation, if the target SV was not reached and yet there was no incremental response to further fluid boluses (and in the confirmed absence of bleeding from wound sites), this was deemed to represent the completion of the resuscitation phase. All studies were terminated at T180, through controlled exsanguination via carotid line and confirmation of death via HR and MABP.

At the end of the experiment, sham animals were culled *via* terminal exsanguination and blood samples and tissue taken.

Assessment of Shock Status

MAPB and heart rate were measured throughout hemorrhage and resuscitation. Blood lactate was measured and used as an index of shock and tissue perfusion. Arterial lactate concentrations (mmol/L) were assessed using the Accutrend Lactate monitor (Roche, Mannheim, Germany). Echocardiography measured at T60 and T120 before and after resuscitation, and at T180 was carried out to assess cardiac function (left ventricle SV). Hematocrit (Hct; %) and hemoglobin (Hb; g/dL) were measured with a ProCyte Dx Hematology Analyzer (IDEXX Europe B.V, Hoofddorp, The Netherlands).

Terminal Blood Sampling and Tissue Storage

Terminal exsanguination was performed via the carotid catheter only and processed for serum separation (Z-Gel microtube, Starstedt. Westphalia, Germany). Serum samples were stored at −80°C. The hearts were removed immediately after the end of the experiment and processed accordingly to further test specifics.

Cardiac Biomarker Assessment

Serum heart fatty acid-binding protein (H-FABP) levels were assayed using commercially available mouse specific enzyme-linked immunosorbent assay (ELISA Cat. No. HFABP-1) kit (supplied by Life Diagnostics Inc., West Chester, PA, USA.). ELISAs were performed in accordance with the manufacturer's instructions. Standard curves for all ELISAs were plotted and dilution-corrected sample concentrations were interpolated from the standard curve.

Immunohistochemistry Analysis

At 3 h THS, a subset of animal ($n = 3$ naïve, $n = 5$ THS) were terminally anesthetized and cardiac tissue was immediately fixated (10% NBF). Naïve animals were housed together under the same conditions but did not have any surgical intervention, trauma, hemorrhage or fluid resuscitation. Cardiac tissue was paraffin-fixed for histology and immunohistochemistry (IHC).

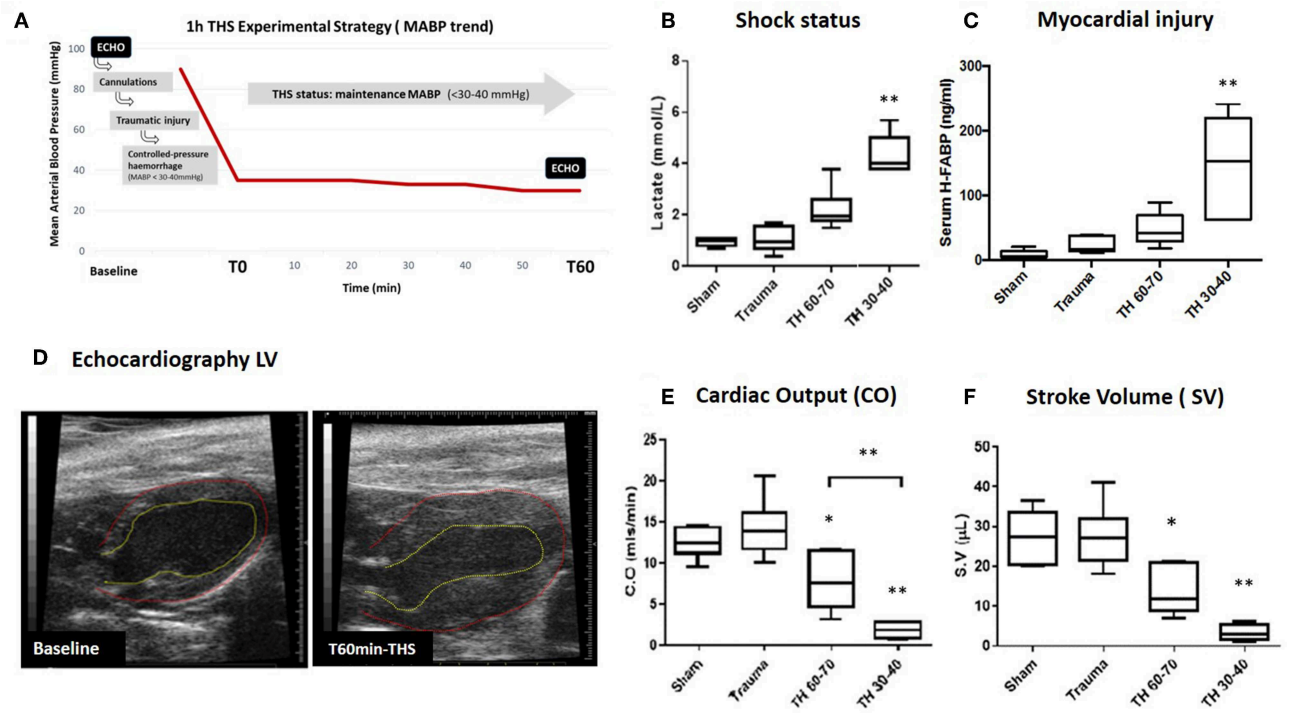

FIGURE 1 | Characterization of the shock status and cardiac dysfunction at 60 min post traumatic hemorrhagic shock injury (1 h post-THS). **(A)** Modeling strategy describing the experimental set up with vessel cannulations, traumatic soft and hard tissue injury and pressure-controlled hemorrhage. **(B)** Median values, interquartile range and range of arterial blood lactate levels at 60 min post-THS between the experimental groups (S, sham with only vessel cannulation only; T, Traumatic injury alone; TH 60–70, THS with 60–70 mmHg; MABP and TH 30–40, THS with 30–40 mmHg MABP). $^{**}P < 0.001$ between TH 30–40 and S, T, and TH 60–70. **(C)** Serum H-FABP levels as a myocardial injury biomarker at 60 min post-THS between the S, T, and THS 60–70 and 30–40 mmHg groups, showing a significant difference in the THS-30–40 group vs. the others ($^{**}P < 0.001$). **(D)** Representative echocardiographic images across the longitudinal heart axis showing the collapsed LV in THS animals at 60 min post-injury, in comparison with baseline non-no injured heart; yellow line depicts the endocardium; red line depicts epicardium. **(E)** Cardiac outcome (CO; ml/min) at 60 min post-injury, showing the impact of pre-load effects on the THS 60–70 and the THS 30–40 groups compared to S and T groups ($^{*}P < 0.05$, $^{**}P < 0.001$ between groups; $^{**}P < 0.01$ TH 60–70 vs. TH 30–40). **(F)** Stroke volume (SV; µL) at 60 min post-injury, showing the impact of pre-load effects on the THS 60–70 and the THS 30–40 groups ($^{*}P < 0.05$, $^{**}P < 0.001$ between groups).

Sections (7 µm) were deparaffinized and hydrated through xylene and ethanol baths. Sections were subjected to antigen retrieval (10 mM of citrate buffer, pH 6.0, 10 min in microwave) and then cooled at room temperature. Tissue was permeabilized with 10% Triton-X in PBS for 15 min and then blocked with 10% goat or donkey serum, 1% bovine serum albumin (BSA) in PBS for an hour, at room temperature (RT). The following primary antibodies diluted in blocking solution were used (overnight incubation in a humid chamber at 4°C): goat anti-ionized calcium binding adaptor molecule 1 (Iba-1; for macrophages and monocytes 1:500; Wako Chemicals USA, Inc., Richmond, VA; Cat#ab109497), rat anti-Lymphocyte antigen 6 complex, locus G (Ly6G-clone 1A8; for neutrophils 1:200; BioLegend, London, IK; Cat# 127602); rabbit anti-mouse cleaved caspase-8 1:200 (Asp387; Cell Signaling Tec.; Cat#8592); rabbit anti-mouse MTCO2 (1:125; Abcam plc, Cambridge, UK; Cat#ab110258); or rabbit polyclonal anti-AIF (1:100; Abcam, UK; Cat#ab2086). The secondary antibodies were donkey anti-goat IgG 568, goat anti-rat 594 IgG, goat anti-rabbit IgG 488 or goat anti-mouse IgG 594 (Molecular Probes, Leiden, the Netherlands; 1:400 in PBS). Sudan black (0.3% w/v in 70% ethanol) was used to reduce autofluorescence and Hoescht 33342 stain (Sigma-Aldrich, Gillingham UK; 1 µg/ml of PBS) was used to visualize nuclei. Slides were mounted and cover-slipped using Vectashield mounting medium (H-1000, Vector Laboratories, Burlingame, CA).

For calculations, 2 slides per animal with at least 18 fields were captured across the short-axis LV myocardium stained section. Images were viewed (x400) and photographed using a Zeiss Axioskop 2 microscope (Carl Zeiss, Jena, Germany) with a Hamamatsu camera (C4742-95; Hamamatsu Photonics K.K., Hamamatsu, Japan). Analysis was done using the ImageJ analysis software for counting the number of positively stained cells. Total nuclei count was measured to normalize percentage of positive stained cells across fields. All imaging acquisition and analysis were carried out blinded to the experimental interventions, and data were only allocated to the specific experimental group at the end of the analysis.

Flow Cytometry Full Heart Analysis

At 3 h post-study, a subset of animals ($n = 6$ naïve, $n = 5$ sham-subjected to vessel cannulation and terminal anesthesia only, n

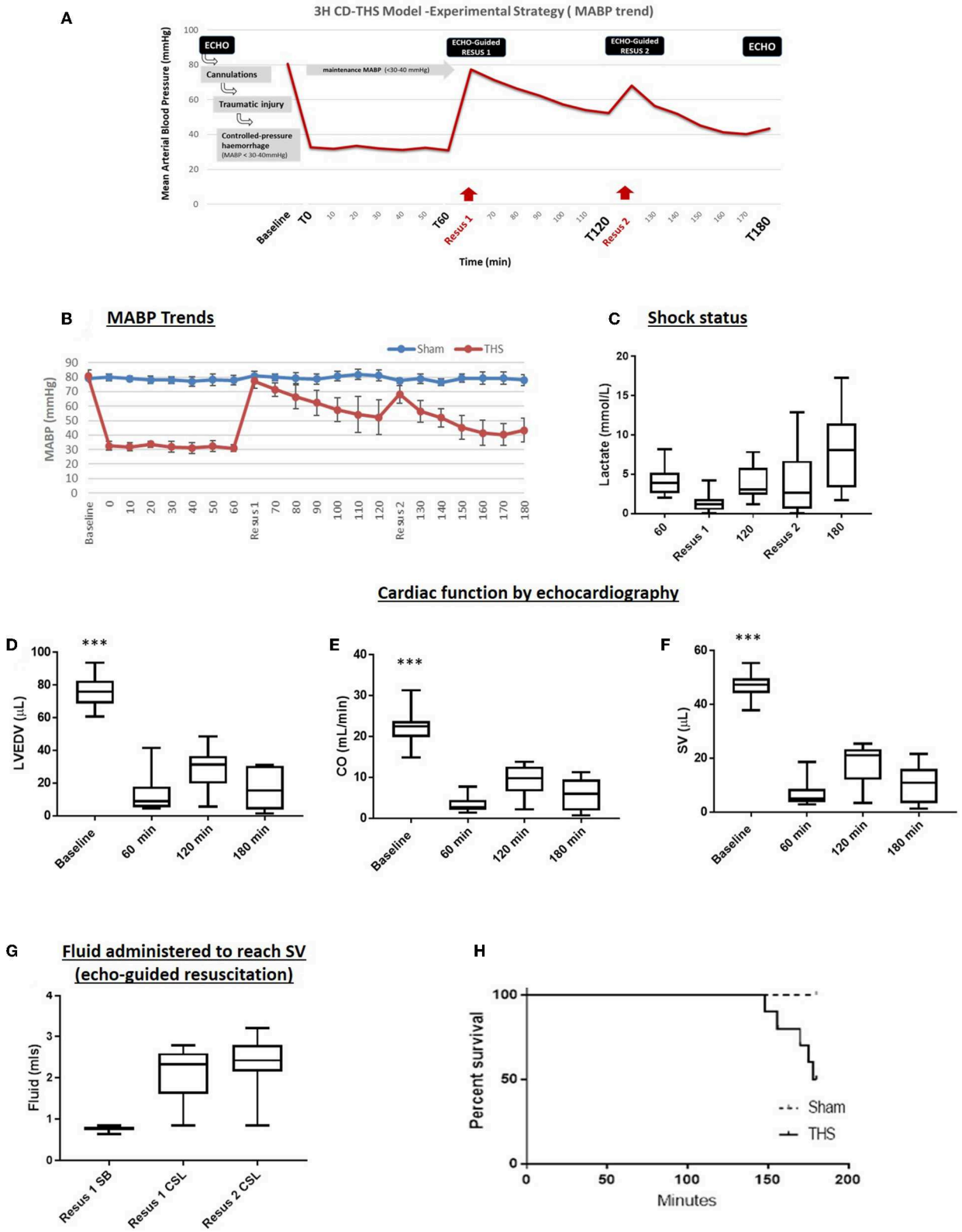

FIGURE 2 | Characterization of the 3 h THS cardiac dysfunction (CD) model. **(A)** Modeling strategy: mice subjected to trauma hemorrhage are held at a MAP of 30–40 mmHg for an hour and then resuscitated with shed blood & crystalloid (Resus1) to their original stroke volume (SV). Mice are then left for a further hour and

(Continued)

FIGURE 2 | resuscitated again (Resus 2) and then left to complete a 3 h experiment. Animals undergo two echocardiographic-guided resuscitations at 60 and 120 min to baseline SV. **(B)** Progressive decrease of MABP despite pre-load resuscitation fluids. **(C)** Serum lactate levels increase steadily after the 1st resus (3.93 ± 0.93 mmol/L) to T180 post-THS (7.9 ± 5.19 mmoL). **(D)** Left ventricular end-diastolic volume (LVEDV) does not regain baseline levels despite resuscitation pre-loads (Baseline: 76.17 ± 10.15 vs. 180 min 16.40 ± 12.98 at T180 post-THS; ***$P < 0.0001$ *vs.* all other groups, one-way ANOVA). **(E)** Cardiac Output (CO; ml/min; ***$P < 0.0001$ *vs.* all other groups, one-way ANOVA) and **(F)** SV (μL) indicate the progressive loss of LV function despite pre-load resuscitation (***$P < 0.0001$ *vs*. all other groups, one-way ANOVA). This is observed already following the 1st resus after T60 THS insult, despite temporary increases in CO and SV immediately following resuscitations (at T60 and T120; see **Supplementary Table 4**). **(G)** Following the initial dosing of shed blood (SB) during the 1st resus at T 60 min, the crystalloid fluid require to reach baseline SV is steadily increased during the 1st and 2nd resuscitation (THS60 min and THs 120 min, respectively). **(H)** Impact of CD in the median survival, with 50% decrease survival at THS 180 min.

= 5 THS) were intracardially perfused with heparinized saline under terminal anesthesia. The hearts were then immediately isolated, cut into 1 mm^3 pieces and dissociated by incubation with papain (Merck, UK) and DNAse I (ThermoFisher Scientific, UK) for 30 min at 37°C. Following lysis of residual red blood cells (RBC Lysis Buffer, Biolegend, UK), cell suspensions were incubated with CD16/CD32-block (Biolegend, UK) for 30 min at 4°C, followed by incubation for 30 min at 4°C with PE-conjugated anti-CD45 to define immune cell populations, and FITC-conjugated anti-Ly6C/G (clone RB6-8C5) and APC-conjugated anti-F4/80 (all ThermoFisher Scientific, UK) to differentiate neutrophils (F4/80Neg, Ly6C/GHi) from pro-inflammatory (F4/80Pos, Ly6C/GInt) and anti-inflammatory (F4/80Pos, Ly6C/GLow) monocytes/macrophages (19, 20). Cells were then analyzed by flow cytometry using a BD FACSCanto II instrument (BD Biosciences) and FlowJo 8.8.1 software (TreeStar Inc., FL, USA). In all cases, 20,000 singlet CD45Pos events were analyzed per sample; positive staining was defined by inclusion of fluorescence-minus-one controls for all antigens.

Transmission Electron Microscopy (TEM)

TEM was used to study micro-structural changes associated to specific cell injury and death in the cardiomyocyte following THS. In a subset cohort of THS and sham animals from the 3 h studies, the animals were humanely killed by overdose of anesthesia and the heart tissue immediately dissected, cut into smaller tissue specimen (∼1 mm^3), and fixed in 2% glutaraldehyde. Fixed tissue was washed three times in cacodylate buffer 0.1 M pH 7.4 and then incubated in 1% osmium tetroxide in ddH2O for 2 h at 4°C. After 3 washes in ddH_2O, specimens were dehydrated (progressive incubation from 25 to 100% acetone) following by impregnation in an increasing concentration of the epoxy resin Araldite 502 (from 25 to 100% of araldite in acetone) used as the embedding medium for TEM. Samples were stored in fresh araldite for up to 72 h and then stored at 60°C for 48 h until the block was hard.

Protein Expression in the Heart

Western blotting (WB) was used to study biochemical changes associated to cardiomyocyte injury (troponin I, H-FABP) and cell death pathways (Caspase 8 and Apoptosis Inducing Factor-AIF) following THS. Tissue from THS ($n = 6$) and sham ($n = 6$) animals was used. At 3 h post-study, animals were deeply anesthetized and heart tissue was immediately dissected, weighted and immersed in RIPA buffer [0.1 g/1 ml w/v; 50 mM TrisHCl (pH 7.4), 150 mM NaCl, 1% Triton X-100, 0.5% sodium deoxylcholate, 0.1 % SDS, 1 mM EDTA, 10 mM NaF in ddH2O] with a cocktail of protease inhibitor and phosphatase inhibitor tablets (Pierce™ Protease and Phosphatase Inhibitor Mini Tablets Cat no. 88668, Sigma-Aldrich, UK). The tissue was minced in RIPA on a cooling slide on dry ice and mash in Dounce homogenizer. The sample was then sonicated (50 pulses in rounds of 10 s with 10 s rest). Samples were spun (@13,000 rpm in cooling centrifuge for 20 min) and the supernatant protein sample was collected. Protein concentrations were determined by Bradford assay. Equal amounts of protein sample were mixed with NuPAGE® MOPS SDS Running Buffer. 20X)-NP0001 was made up and a tank filled. Bolt™ 4–12%, 10-well NW04122BOX) Bis-Tris Plus Gel was inserted into the tank; 10 μl of samples were loaded with protein ladder (RPN800E-GE health care) into 10 well NuPage Bis-Tris Mini gel. Optical density was determine using ImageJ software (NIH). A cardiac tissue specific, mouse monoclonal troponin I antibody (Ab10231, Abcam, UK; 24 kDa) was used for the labeling of troponin. Caspase-8 (rabbit monoclonal anti-cleaved caspase 8; 8592S; Cell Signaling, UK; 41 kDa) expression was used as a marker of activation of death receptor initiated cell death pathway. AIF (rabbit polyclonal anti-AIF; Ab2086; Abcam, UK; 67 kDa) expression and location was assessed by WB analysis, with the tissue homogenates being processed for differential centrifugation to assess the sub-cellular compartmentation, removing the large organelles nuclei, cellular debris and intact cells, and allowing for selective extraction of the cytosol and mitochondria using Cytosol and Mitochondrial Extraction Buffer Mix containing DTT and Protease Inhibitors. MTCO2 (Anti-MTCO2; Ab198286; Abcam, UK; 1/150–25 kDa) and GAPDH (Anti-GAPDH antibody; Ab8245; Abcam, UK) were used as a mitochondrial and cytosol markers, respectively.

Statistical Analysis

Lactate levels (mmol/L), MABP measurements (mmHg), resuscitation fluids (ml), echocardiographic LV data (CO = ml/min; SV = μl; LDEDV = μl), % of inflammatory cells (neutrophils/monocytes/macrophages) and H-FABP serums levels = ng/ml) were expressed using mean values, with standard deviation (SD). Statistical analysis was performed using GraphPad Prism 8 (GraphPad Software, San Diego, USA). Normally distributed data was analyzed using Student's two-tailed *t*-test or one-way ANOVA, followed by Tukey's multiple comparison test. Non-normally distributed data was analyzed with Kruskall-Wallis and Mann-Whitney U test analysis. $P < 0.05$ was taken to represent significance. All analysis was performed blinded to the experimental interventions (Further details in **Supplementary Table 2**).

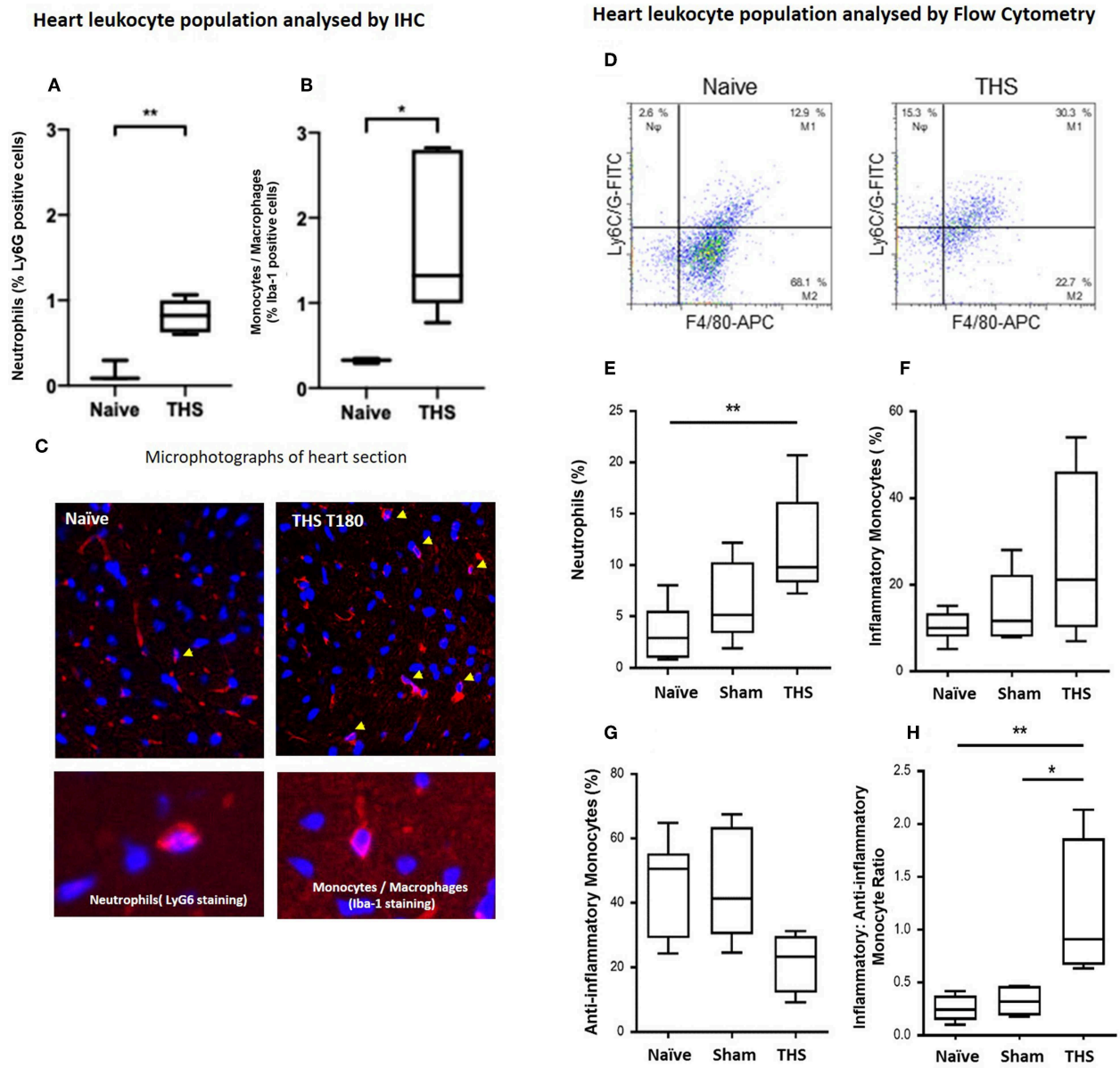

FIGURE 3 | Characterization of acute cardiac inflammation response in the Trauma Hemorrhage induced CD murine model (THS). Immunohistochemistry (IHC) myocardial analysis shows **(A)** a significant increase in neutrophils (% Ly6G cells) and **(B)** Monocytes/Macrophages (% Iba-1 cells) in the THS model (T180 min) compared to naïve (**$p < 0.001$, *$p = 0.02$; two-tailed unpaired *t*-test). Data is presented as means ± SD. **(C)** Representative IHC microphotographs in heart section in a THA and naïve animal (x400) and zoom insets of the LY6G and Iba-1 staining (red) for the neutrophils and monocyte/macrophage, respectively, with the nuclei Hoechst staining (blue) in a THS model. **(D–H)** Flow cytometry assessment of heart-infiltrating leukocytes. **(D)** Representative forward scatter/side scatter profile and a live cell gate. Following a CD45/side scatter plot to obtain the CD45+ leukocyte2, Ly6G Hi, or low expression with F4/80 plots was used to derived percentages of pro-inflammatory monocytes (Ly6GHi, F4/80+: M1 phenotype) and anti-inflammatory monocytes/macrophages (Ly6GLow, F4/80+: M2 phenotype). The heart from THS animals showed a significant increase in the M1:M2 phenotype ratio, compared to the naïve animals. **(E)** A significant presence of neutrophils (% Ly6G+ F4/80- cells) and a high ratio of inflammatory monocytes (**F–H**; Higher ratio of Ly6GHi, F4/80+ inflammatory monocytes vs. F4/80+: M2 anti-inflammatory macrophages/monocytes; **$p < 0.001$, *$p = 0.02$; one-way ANOVA with *post-hoc* analysis). Data all presented as means ± SD.

RESULTS

Myocardial Injury After Trauma and Hemorrhage

The trauma hemorrhage model demonstrated progressive myocardial damage and cardiac dysfunction following an hour of trauma and hemorrhage without resuscitation (**Figure 1**). We examined cardiac effects of trauma alone, trauma and hemorrhage to target MABP of 60–70 mmHg (THS 60–70); and to a target an MABP of 30–40 mmHg (THS 30–40), achieving different depths of shock severity (**Figure 1A**; **Supplementary Table 3**) Myocardial damage, as measured by

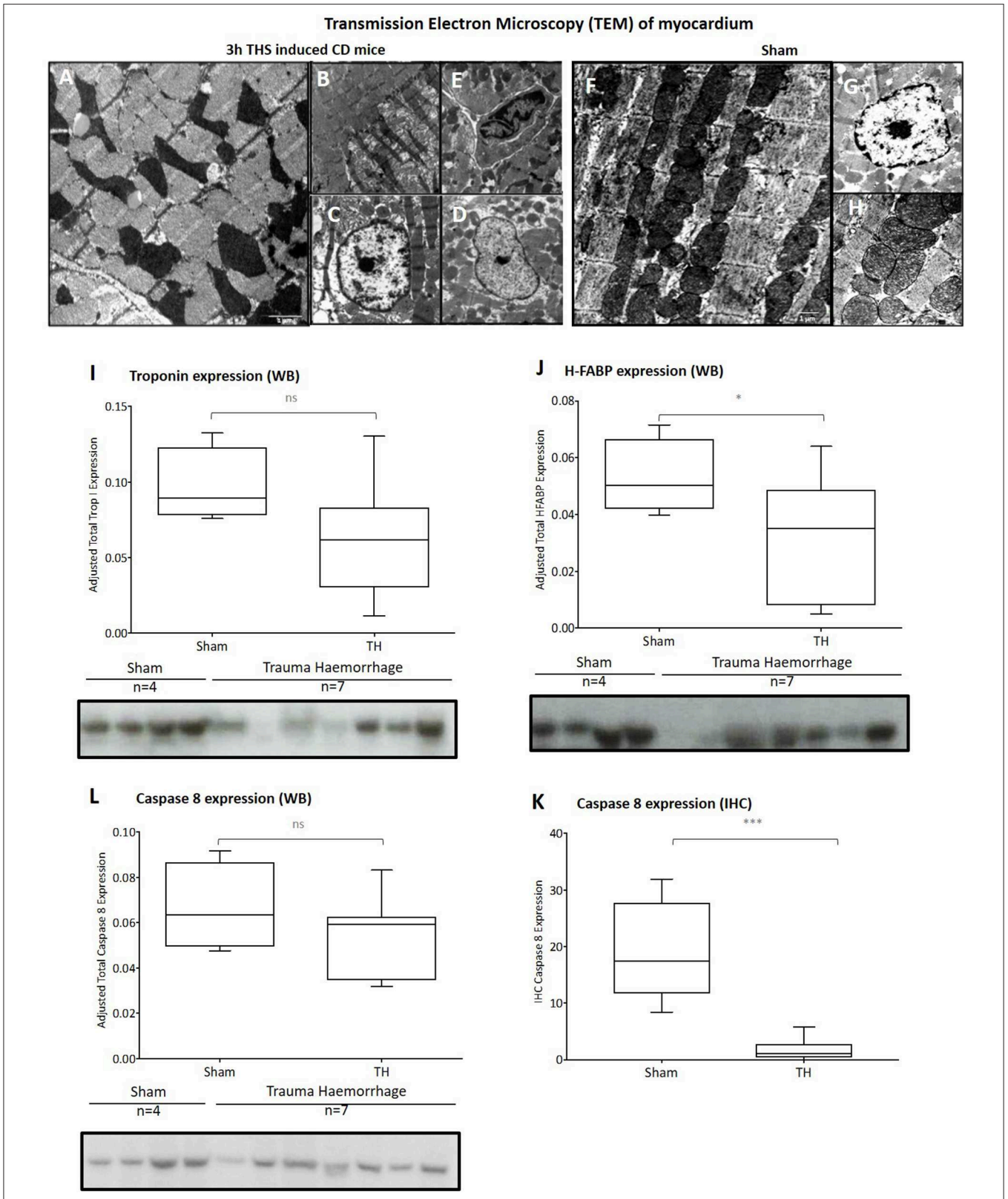

FIGURE 4 | Myocardial injury in the trauma hemorrhage induced CD murine model. TEM shows severe myocardial injury in the heart of THS mice, with interstitial oedema, widespread disorganization of the myoc ardium with relaxation of the sarcomere and poorly circumscribed mitochondria distributed in a disorderly fashion

(Continued)

FIGURE 4 | (A). Significant amounts of mitochondrial oedema **(B)** Nuclei shows margination of chromatin, rarefaction of the nucleoplasm **(C)** and glycogen depletion **(D)**; and some cardiomyocytes dead cells with margination of chromatin **(E)**. TEM of sham mice heart tissue shows a well-organized myofibrils, with mitochondria evenly organized along the cristae sarcomere **(F)** with intact nucleus **(G)** and mitochondria **(H)**. WB analysis of Troponin-I (cTnI) **(I)** and H-FABP **(J)** expression shows elevated levels in the myocardium of THS mice ($p = 0.06$ NS; $^{*}p = 0.04$, respectively; two-tailed unpaired *t*-test; means ± SD). **(K,L)** Low caspase 8 expression is observed in heart of THS mice (IHC $^{***}p < 0.0001$; WB $p > 0.05$ compared to sham animals).

serum H-FABP concentrations, increased with increasing model severity, and were significantly elevated for the most severe THS group (THS 30–40 = 166.69 ± 38.64 ng/ml), compared to sham, trauma only and 60–70 mmHg THS group ($p < 0.01$, **Figure 1C**). At end-experiment, stroke volume and cardiac output were significantly decreased from baseline in all groups (**Figures 1D–F**). In the THS 30–40 group, with over 30% blood loss, cardiac output was 87% lower than baseline (**Figure 1E**) at 1 h post trauma compared to sham and trauma-only groups ($p < 0.001$, **Figure 1E**).

Cardiac Dysfunction Following Myocardial Damage

In order to determine the functional effects of myocardial damage, we extended our TH 30–40 mmHg model for 3 h to include two resuscitation phases at 60 and 120 min post-hemorrhage (**Figures 2A,B**). Shock severity worsened over time despite the two resuscitation steps (**Figures 2B,C**), with serum lactate reaching a median of 7.9 ± 5.2 mmol/L at 180 min (from 1.4 ± 0.37 mmol/l at baseline $p = 0.004$, **Supplementary Table 4**). MABP increased immediately after resuscitation, but then progressively declined, despite transient increases with volume resuscitation. End-experiment MABP was 44% lower than post Resus-1 levels (43.3 ± 8 vs. 77.4 ± 5 mmHg **Figure 2B**; **Supplementary Table 4**). Hb concentration and Hct were not significantly different between the THS group and sham, at 3 h (Hb 14.5 ± 1.6 vs. 13.2 ± 1.4 and Hct 47.5 ± 8.7 vs. 43.1 ± 5.4, in sham and THS groups, respectively, **Supplementary Figure 1**).

On functional echocardiographic assessment, volume resuscitation to normalize stroke volume did not maintain LVEDV, stroke volume, or cardiac output. Mean LVEDV was only 23% of baseline at end-experiment (16.40 μl vs. 76.17 μl; $p < 0.0001$); stroke volume was 22% of baseline (10.5 μl vs. 47.1 μl, $p < 0.0001$) and total cardiac output was 30% from baseline (5.8 μl vs. 22.4 μl, $p < 0.0001$, **Figures 2D–G**; **Supplementary Table 4**). In line with these findings, H-FABP concentrations continued to increase from T60 min post-THS, rising to a mean of 340 ng/ml at end-experiment compared to 116.7 ng/ml at T60 ($p = 0.003$) and 10.3 ng/ml compared to sham animals at end-experiment, $p < 0.001$, **Supplementary Table 4**). Despite resuscitation, 50% of animals had died by 3 h post-hemorrhage (**Figure 2H**).

Myocardial Inflammation and Structural Damaged Following THS Impacts on Cardiomyocyte Survival

From our *in situ* IHC-analysis in the myocardium, a significantly higher % of neutrophils (Ly6G stained cells) was identified in the heart of the THS group compared to naïve animals (0.15 ± 0.07 vs. 0.8 ± 0.1% of positive LyG66G cells, respectively; $P = 0.02$, **Figures 3A,C**); a high presence of macrophages and monocytes were also identified in the THS group (1.7 ± 0.01 vs. 0.3 ± 0.01% positive Iba-1 cells in THS vs. naïve, respectively; $P = 0.001$, **Figures 3B,C**).

From the flow cytometry analysis carried out following *ex vivo* heart cells disaggregation, a significantly higher number of neutrophils were identified in THS group compared to naïve non-injured animals (11.7 ± 5.2 vs. 3.4 ± 2.7% F4/80Neg, Ly6C/GHi cells; one way ANOVA with Tukey's multiple Comparison $P = 0.01$) (**Figures 3D,E**). Sham animals did not differ from naïve or THS (6.4 ± 3.9% F4/80Neg, Ly6C/GHi cells). When investigating monocyte cell population, we identified a statistically higher ratio of pro-inflammatory (F4/80Pos, Ly6C/GInt) vs. anti-inflammatory (F4/80Pos, Ly6C/GLow) monocytes in the THS group compared to the naïve and sham animals (1.14 ± 0.8 for THS group vs. 0.25 ± 0.1 for naïve group and 0.32 ± 0.1 for sham group; $P = 0.006$ and $P = 0.01$, respectively, **Figures 3F–H**). There was also a trend to shift the presence of pro vs. anti-inflammatory monocytes in the hearts of THS animals, compared to that for the naïve and sham groups; but these data did not reach the threshold for statistical significance (**Figures 3F,G**).

TEM analysis demonstrated significant morphological changes within the myocardium, with interstitial oedema and widespread disorganization of the cardiac myofibrillar ultrastructure, and a relaxation of the sarcomere in the cardiomyocytes (**Figure 4A**). We identified the presence of poorly circumscribed mitochondria distributed in a disorderly fashion across cardiac muscle fibers, with significant structural changes. In THS animals, 33% of the mitochondria contained amorphous dense bodies, in comparison to 23% in the sham animals ($p = 0.006$). Mitochondrial swelling, with loss of electron dense material from the matrix and breakdown of the cristae and vacuolation, was also observed in THS animals (**Figure 4B**). The nuclei of this THS group also exhibited signs of irreversible structural changes, such as margination of chromatin, associated with surrounding oedema, chromatin condensation, and rarefaction of the nucleoplasm, where there is loss of the chromatin (**Figures 4C–E**), compare to sham animals (**Figures 4F–H**). Most of these lesions are consistent with presence of myocardial ischemia injury the THS hearts (**Figure 4**).

Myocardial damaged was confirmed by the reduced levels of H-FABP in the myocardium of the THS hearts ($p = 0.06$ NS; $^{*}p = 0.04$, respectively; two-tailed unpaired *t*-test; means ± SD), indicating the loss /release of these proteins, attributable to myocardial injury (**Figures 4I,J**).

A significant decrease in caspase 8 expression in THS was seen on IHC (**Figure 4K**) is suggestive that the cardiomyocte

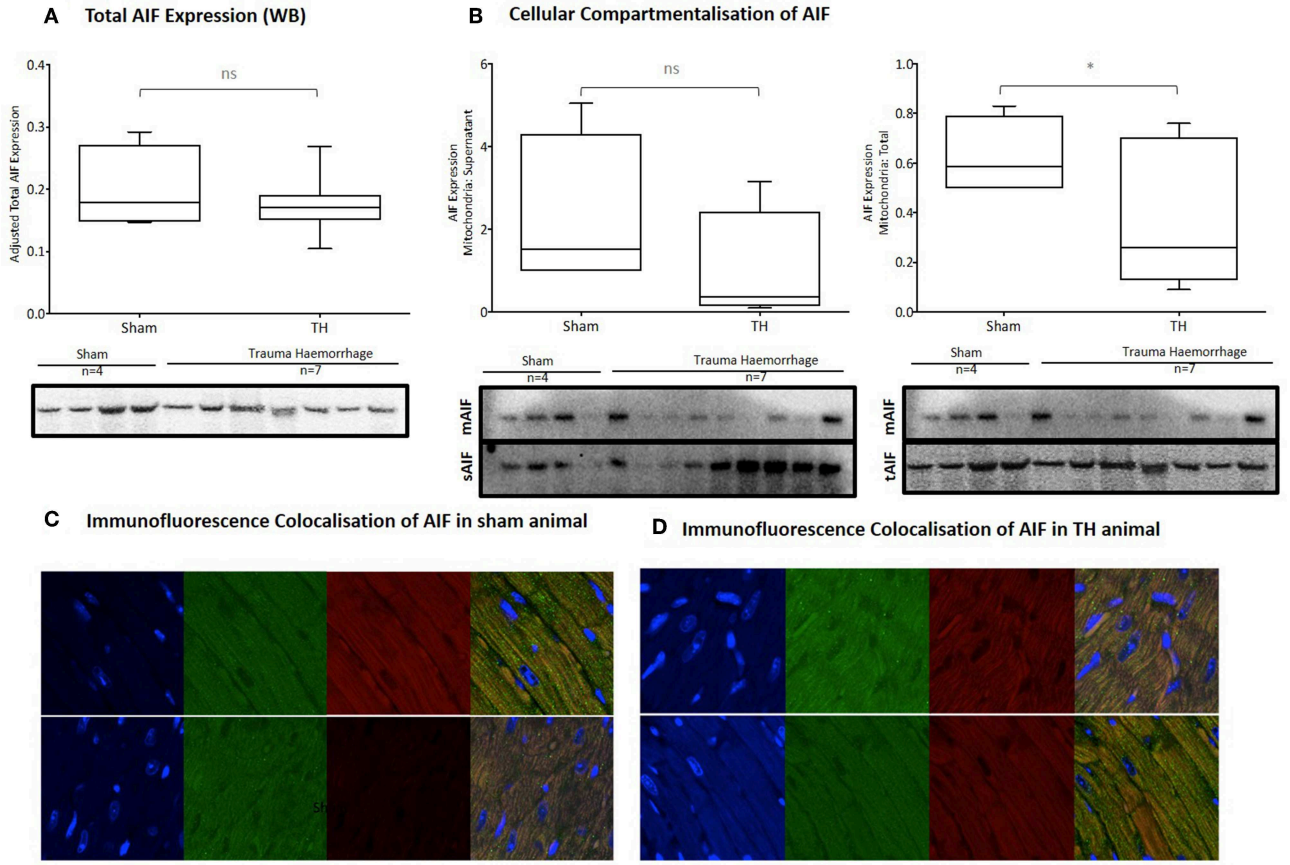

FIGURE 5 | AIF localization in the trauma hemorrhage induced CD murine model. **(A)** AIF expression as demonstrated by western blot analysis. The total AIF expression is similar in the Sham and THS models (0.20 vs. 0.17, respectively). **(B)** Cellular compartmentalization of AIF as demonstrated by WB analysis. A higher proportion of AIF is found outside the mitochondria in the THS models. The mean ratio of mitochondrial AIF (mAIF) to supernatant AIF (sAIF) is 1.5 in sham compared to 0.4 in THS group, $p = 0.16$. When comparing total AIF which includes the nucleus, a lower proportion is still found in the mitochondria. Ratio of mitochondrial AIF (mAIF) to total AIF (tAIF) in sham group is 0.6 compared to 0.3 in THS animals, $^*p = 0.04$. This is suggestive of its translocation of the AIF out of the mitochondrion, potentially to the nucleus, triggering initiation of cells death. IHC sections from TH animals, DAPI (blue), AIF (green), MTCO2 (red), and combined images. In the combined images, localization of AIF in the nucleus can be seen in the THS **(D)** which in absent in the sham animals **(C)**.

damage seen is not dependent upon death receptor initiated or protease dependent apoptosis. The difference in caspase 8 on WB although downward trending was not statistically significant (**Figure 4L**). The total AIF expression was similar between Sham and THS models (0.20 vs. 0.17 respectively, NS, **Figure 5A**), but a compartmentalization of AIF outside the mitochondria was observed in the TH models. The decrease in the mitochondrial AIF in comparison to cytosolic AIF in the THS hearts (mitochondria vs. total cell $P = 0.04$ and mitochondria vs. supernatant/cytosol $P = 0.04$, **Figure 5B**) suggests a leakage of the mitochondrial AIF into the cytosol, with the potential activation of a mitochondrial driven cell death pathway (**Figures 5A–D**).

DISCUSSION

Our study confirms that the preclinical modeling approach that we have developed physiologically and biochemically mirrors the cardiac dysfunction seen in bleeding trauma patients. Traumatic injury and controlled hemorrhage induced significant acute cardiac damage despite subsequent echocardiography-guided volume resuscitation. These changes were associated with demonstrable myocardial cell death and inflammation leading to reduced survival.

In our unresuscitated model, we identified cardiac functional changes and myocardial damage with comparable elevations in the cardiomyocyte damage molecule H-FABP (21) to those reported in clinical studies (8, 22). The associated functional decreases in cardiac output were at least in part related to the loss of stroke volume. However, our resuscitated model, with confirmed restoration of volume preload, demonstrated a persistent and progressive loss of cardiac function associated with increasing myocardial injury indicated by further elevations in H-FABP. Catecholamine release with increased inotropy will undoubtedly compensate for some degree of cardiomyocyte loss. However in our model, volume resuscitation to baseline LVEDV was not able to restore cardiac function to pre-shock levels. This resultant cardiac dysfunction is increasingly recognized as a key

determinant of critical care utilization and survival in trauma patients (10, 23, 24).

Cardiac dysfunction is well-known in sepsis (12, 25), but the etiology of trauma induced myocardial injury likely has different underlying pathophysiology (1–16, 26). We observed an acute cardiac inflammatory response, with an increase in monocytes/macrophages and neutrophils infiltration in the heart is identified following THS injury. This may be driven by the systemic inflammatory response to trauma (15, 26), or may be a direct response of the immune system to cardiomyocyte cell death. The acute recruitment of monocytes and neutrophils from circulation into the myocardium has also been reported in cardiac stress ischemic conditions (27). The persistence of this myocardial inflammation response may lead to further endogenous cytokine production and leukocyte recruitment and infiltration, increasing oxidative stress, cell damage and cardiac dysfunction (28).

We observed severe cardiomyocyte ultrastructural and organelle dysfunctional damage by 3 h post trauma, with myofibrillary disarray, relaxation of sarcomeric proteins, mitochondrial vacuole formation, membrane disruption and chromatin features consistent with irreversible damage. Such cellular stress features, augurs of cell death, have been described in rodent cardiomyocytes following ischemia-reperfusion (29). Furthermore, the increased translocation of mitochondrial AIF into the cytosol, and then into the nucleus, confirms the activation of cell death pathways associated with cell death. This presence of AIF leakage in addition to the reduced expression of caspase 8, may indicate the involvement of the alternate cell death pathway of necroptosis as a principle mode of cardiomyocyte cell death in trauma (30, 31). Many alarmins released following trauma (ATP, DNA, histones, HMGB-1, HSP70) have been associated with necroptosis signaling (32), and such necroptosis has already been identified as central to other sterile inflammation conditions such as acute pancreatitis (33) and organ injury (34). Our data raises the possibility of mitochondrial mediated necroptosis triggered by specific extracellular alarmins as the underlying cardiomyocyte cell death pathways, leading to cardiac dysfunction in trauma patients. However, the role of AIF and necroptosis is still poorly understood in the realm of organ injury and unexamined in the context of trauma. Therefore, it is pertinent to conduct further studies to modulate AIF translocation and examine its effect on necroptosis, cell survival and therefore cardiac dysfunction in models prior to translation to humans. Our modeling approach will support further mechanistic studies on the role of inflammatory mediators in driving specific tissue/organ dysfunction after trauma, particularly allowing for the use of transgenic animals for inflammatory pathways.

There are several limitations to this study. We limited our model to 3 h, and longer durations will be required to examine the longer term impacts of injury on cardiac function. The implementation of serial echocardiography to guide resuscitation is unique in trauma models and delivers a new *in-vivo* understanding of cardiac dysfunction in trauma hemorrhage. However, it was difficult to assess myocardial contractility with ultrasound and further advanced imaging approaches such as speckle tracking or MRI tagging could be used to explore this, as well as *ex-vivo* isolated heart techniques. Monitoring of other clinically relevant resuscitation parameters like urine output, arterial blood gas, or central venous pressure could also have been explored, but their implementation in this echo-guided trauma mouse model remain challenging due to low blood volumes and technical limitations. Our inflammatory and biochemical analyses identified cardiomyocyte cell death suggesting, but not definitive of, activation of necroptosis pathways. Further work will be required, to fully characterize the cell death mechanism and its relationship with the sterile inflammatory response.

Cardiac dysfunction is now a major mode of trauma hemorrhage death after admission. We have identified the development of severe and irreversible myocardial damage, despite fluid resuscitation, leading to cardiac dysfunction and death. We pose AIF-driven necroptosis as a possible underlying mechanistic pathway for the cell death. Myocardial protection through novel management strategies and therapeutic approaches represents a major opportunity for improving survival after major trauma.

DATA AVAILABILITY STATEMENT

The datasets generated for this study are available on request to the corresponding author.

ETHICS STATEMENT

This study was carried out in accordance with the recommendations of Home Office guidance on the operation of Animals (Scientific Procedure Act, 1986) in accordance with the EU Directive 2010/63/EU and the Guide for the Care and Use of Laboratory Animals of the National Research Council. The protocols were approved by the Animal Welfare and Ethics Review Board of Queen Mary University of London and conducted under the UK home office license number PC5F29685. Experimental planning and design was performed in accordance with the ARRIVE guidelines for data randomization, blinding for results analysis and sample size calculation. All studies were carried out under non-recovery terminal anesthesia. Animals never regained conscious state, been constantly monitored (MABP, HR, Resp. rate, body temperature) throughout the study. Survival state is defined as the animal's ability to maintain a MAP $>$ 15 mmHg with measurable respiratory and cardiac function. Once any animal reaches any physiological state below the survival threshold, the animals is humanely killed by exsanguination to collect terminal tissue/blood samples.

AUTHOR CONTRIBUTIONS

KB, JW, SN, and JT designed the overall study and experimental programme, together with CT. JW, SN, BP, OB, SM, and JT performed the experiments including animal studies, cell sorting experiments, microscopic studies, and ELISAs. JW, SN, BP, JT, and KB contributed to experimental design and data analysis and coordinated the study and supervised financial support for the

studies. JW, SN, and JT produced initial drafts of the manuscript. CT is the project license holder for the animal work carried out. All authors contributed and revised the drafting of the article and gave final approval of the version to be published.

ACKNOWLEDGMENTS

We acknowledge the support from the Biological Services at QMUL during all the animal studies, from Prof. Adrian Hobbs and his team for their advice on heart IHC and all the members from the Centre for Trauma Sciences for their advice.

SUPPLEMENTARY MATERIAL

The Supplementary Material for this article can be found online at: https://www.frontiersin.org/articles/10.3389/fimmu.2019.02774/full#supplementary-material

REFERENCES

1. Haagsma JA, Graetz N, Bolliger I, Naghavi M, Higashi H, Mullany EC, et al. The global burden of injury: incidence, mortality, disability-adjusted life years and time trends from the Global Burden of Disease study. *Inj Prev*. (2013) 22:3–18. doi: 10.1136/injuryprev-2015-041616
2. Drake SA, Holcomb JB, Yang Y, Thetford C, Myers L, Brock M, et al. Establishing a regional trauma preventable/potentially preventable death rate. *Ann Surg*. (2018) doi: 10.1097/SLA.0000000000002999. [Epub ahead of print].
3. Gunst M, Ghaemmaghami V, Gruszecki A, Urban J, Frankel H, Shafi S. Changing epidemiology of trauma deaths leads to a bimodal distribution. *Proceedings*. (2010) 23:349–54. doi: 10.1080/08998280.2010.11928649
4. Holcomb JB, Jenkins D, Rhee P, Johannigman J, Mahoney P, Mehta S, et al. Damage control resuscitation: directly addressing the early coagulopathy of trauma. *J Trauma*. (2007) 62:307–10. doi: 10.1097/TA.0b013e3180324124
5. Tieu BH, Holcomb JB, Schreiber MA. Coagulopathy: its pathophysiology and treatment in the injured patient. *World J Surg*. (2007) 31:1055–64. doi: 10.1007/s00268-006-0653-9
6. Probst C, Zelle BA, Sittaro NA, Lohse R, Krettek C, Pape HC. Late death after multiple severe trauma: when does it occur and what are the causes? *J Trauma*. (2009) 66:1212–17. doi: 10.1097/TA.0b013e318197b97c
7. Cryer HG, Leong K, McArthur DL, Demetriades D, Bongard FS, Fleming AW, et al. Multiple organ failure: by the time you predict it, it's already there. *J Trauma*. (1999) 46:597–604. doi: 10.1097/00005373-199904000-00007
8. De'Ath HD, Rourke C, davenport R, Manson J, Renfrew I, Uppal R, et al. Clinical and biomarker profile of trauma-induced secondary cardiac injury. *Br J Surg*. (2012) 99:789–97. doi: 10.1002/bjs.8728
9. Naganathar S, De'Ath HD, Wall J, Brohi K. Admission biomarkers of trauma-induced secondary cardiac injury predict adverse cardiac events and are associated with plasma catecholamine levels. *J Trauma Acute Care Surg*. (2015) 79:71–7. doi: 10.1097/TA.0000000000000694
10. Gawande NB, Tumrum NK, Dongre AP. Cardiac changes in hospitalized patients of trauma. *Shock*. (2014) 42:211–17. doi: 10.1097/SHK.0000000000000194
11. Cebelin MS, Hirsch CS. Human stress cardiomyopathy. Myocardial lesions in victims of homicidal assaults without internal injuries. *Hum Pathol*. (1980) 11:123–32. doi: 10.1016/S0046-8177(80)80129-8
12. Fenton KE, Parker MM. Cardiac function and dysfunction in sepsis. *Clin Chest Med*. (2016) 37:289–98. doi: 10.1016/j.ccm.2016.01.014
13. Kalbitz M, Schwarz S, Weber B, Bosch B, Pressmar J, Hoenes FM et al. TREAT Research Group. cardiac depression in pigs after multiple trauma – characterisation of posttraumatic structural and functional alterations. *Sci Rep*. (2017) 7:17861. doi: 10.1038/s41598-017-18088-1
14. Yang S, Zheng R, Hu S, Ma Y, Choudhry MA, Messina JL, et al. Mechanisms of cardiac depression after trauma-hemorrhage: increased cardiomyocyte IL-6 and effect of sex steroids on IL-6 regulation and cardiac function. *Am J Physiol Heart Circ Physiol*. (2006) 287:H2183–91. doi: 10.1152/ajpheart.00624.2003
15. Zhang X, Lu C, Gao M, Cao X, Ha T, Kalbfleisch JH, et al. Toll-like receptor 4 plays a central role in cardiac dysfunction during trauma hemorrhage shock. *Shock*. (2014) 42:31–7. doi: 10.1097/SHK.0000000000000155
16. Zhang X, Gao M, Ha T, Kalbfleisch JH, Williams DL, Li C, Kao RL. The toll-like receptor 9 agonist, CpG-oligodeoxynucleotide 1826, ameliorates cardiac dysfunction after trauma-hemorrhage. *Shock*. (2012) 38:146–52. doi: 10.1097/SHK.0b013e31825ce0de
17. Kilkenny C, Browne WJ, Cuthill IC, Emerson M, Altman DG. Improving bioscience research reporting: the ARRIVE guidelines for reporting animal research. *PLoS Biol*. (2010) 8:e1000412. doi: 10.1371/journal.pbio.1000412
18. Mahler M, Berard M, Feinstein R, Gallagher A, Illgen-Wilcke B, Pritchett-Corning K, et al. FELASA recommendations for the health monitoring of mouse, rat, hamster, guinea pig and rabbit colonies in breeding and experimental units. Working party report. *Lab Anim*. (2014) 48:178–92. doi: 10.1177/0023677213516312
19. Varga T, Mounier R, Patsalos A, Gogolák P, Peloquin M, Horvath A, et al. Macrophage PPARγ, a lipid activated transcription factor controls the growth factor GDF3 and skeletal muscle regeneration. *Immunity*. (2016) 45:1038–51. doi: 10.1016/j.immuni.2016.10.016
20. McArthur S, Gobbetti T, Gaëtan J, Desgeorges T, Theret M, Gondin J, et al. Annexin A1 drives macrophage skewing towards a resolving phenotype to accelerate the regeneration of muscle injury through AMPK activation. *BioRxiv*. (2018) 375709. doi: 10.1101/375709
21. Wall J, Tremoleda J, Brohi K. Heart Fatty Acid Binding Protein (H-FABP) is a biomarker of trauma-induced secondary cardiac injury in a pre-clinical model of trauma-haemorrhage. *Shock*. (2015) 44:21–2. doi: 10.1097/01.shk.0000472071.00900.4e
22. Montazer SH, Jahanian F, Khatir IG, Bozorgi F, Assadi T, Pashaei SM, et al. Prognostic value of cardiac troponin I and T on admission in mortality of multiple trauma patients admitted to the emergency department: a prospective follow-up study. *Med Arch*. (2019) 73:11–14. doi: 10.5455/medarh.2019.73.11-14
23. Bland RD, Shoemaker WC, Abraham E, Cobo JC. Hemodynamic and oxygen transport patterns in surviving and nonsurviving postoperative patients. *Crit Care Med*. (1985) 13:85–90. doi: 10.1097/00003246-198502000-00006
24. Sauaia A, Moore FA, Moore EE, Moser KS, Brennan R, Read RA, et al. Epidemiology of trauma deaths: a reassessment. *J Trauma*. (1995) 38:185–19. doi: 10.1097/00005373-199502000-00006
25. Frencken JF, Donker DW, Spitoni C, Koster-Brouwer ME, Soliman IW, Ong DSY, et al. Myocardial injury in patients with sepsis and its association with long-term outcome. *Circ Cardiovasc Qual Outcomes*. (2018) 11:e004040. doi: 10.1161/CIRCOUTCOMES.117.004040
26. De'Ath H, Manson J, Davenport R, Glasgow S, Renfrew I, Davies L, et al. Trauma-induced secondary cardiac injury is associated with hyperacute elevations in inflammatory cytokines. *Shock*. (2013) 39:415–20. doi: 10.1097/SHK.0b013e31828ded41
27. Swirski FK, Nahrendorf M, Etzrodt M, Wildgruber M, Cortez-Retamozo V, Panizzi P, et al. Identification of splenic reservoir monocytes and their deployment to inflammatory sites. *Science*. (2009) 325:612–6. doi: 10.1126/science.1175202
28. Liu J, Wang H, Li J. Inflammation and inflammatory cells in myocardial infarction and reperfusion injury: a double-edged sword. *Clin Med Insights Cardiol*. (2016) 10:79–84. doi: 10.4137/CMC.S33164
29. Feng Y, Liu Y, Wang D, Zhang X, Liu W, Fu F, et al. Insulin alleviates post trauma cardiac dysfunction by inhibiting tumor necrosis factor-alpha-mediated reactive oxygen species production. *Crit Care Med*. (2013) 41:e74–84. doi: 10.1097/CCM.0b013e318278b6e7
30. Tummers B, Green DR. Caspase-8: regulating life and death. *Immunol Rev*. (2017) 277:76–89. doi: 10.1111/imr.12541
31. Baritaud M, Cabon L, Delavallée L, Galán-Malo P, Gilles ME, Brunelle-Navas MN, et al. AIF-mediated caspase-independent necroptosis requires ATM and

DNA-PK-induced histone H2AX Ser139 phosphorylation. *Cell Death Dis*. (2012) 3:e390. doi: 10.1038/cddis.2012.120
32. Davidovich P, Kearney CJ, Martin SJ. Inflammatory outcomes of apoptosis, necrosis and necroptosis. *Biol Chem*. (2014) 395:1163–71. doi: 10.1515/hsz-2014-0164
33. Wang G, Qu FZ, Li L, Lv JC, Sun B. Necroptosis: a potential, promising target and switch in acute pancreatitis. *Apoptosis*. (2016) 21:121–9. doi: 10.1007/s10495-015-1192-3
34. Zhao H, Jaffer T, Eguchi S, Wang Z, Linkermann A, Ma D. Role of necroptosis in the pathogenesis of solid organ injury. *Cell Death Dis*. (2015) 6:e1975. doi: 10.1038/cddis.2015.316

Conflict of Interest: The authors declare that the research was conducted in the absence of any commercial or financial relationships that could be construed as a potential conflict of interest.

Copyright © 2019 Wall, Naganathar, Praditsuktavorn, Bugg, McArthur, Thiemermann, Tremoleda and Brohi. This is an open-access article distributed under the terms of the Creative Commons Attribution License (CC BY). The use, distribution or reproduction in other forums is permitted, provided the original author(s) and the copyright owner(s) are credited and that the original publication in this journal is cited, in accordance with accepted academic practice. No use, distribution or reproduction is permitted which does not comply with these terms.

frontiers in Immunology

ORIGINAL RESEARCH
published: 09 January 2020
doi: 10.3389/fimmu.2019.03028

Trauma Severity and Its Impact on Local Inflammation in Extremity Injury—Insights From a Combined Trauma Model in Pigs

Klemens Horst[1,2], Johannes Greven[1,2], Hannah Lüken[1], Qiao Zhi[2], Roman Pfeifer[3], Tim P. Simon[4], Borna Relja[5,6], Ingo Marzi[5], Hans-Christoph Pape[3] and Frank Hildebrand[1]*

[1] Department of Orthopedic Trauma, University Hospital Aachen, Aachen, Germany, [2] Orthopedic Trauma Research Laboratory, University Hospital Aachen, Aachen, Germany, [3] Department of Orthopaedic Trauma Surgery, University Hospital Zurich, Zurich, Switzerland, [4] Department of Intensive Care and Intermediate Care, RWTH Aachen University, Aachen, Germany, [5] Department of Trauma-, Hand- and Reconstructive Surgery, University Hospital Frankfurt, Frankfurt, Germany, [6] Experimental Radiology, Department of Radiology and Nuclear Medicine, Otto von Guericke University Magdeburg, Magdeburg, Germany

OPEN ACCESS

Edited by:
Christoph Thiemermann, Queen Mary University of London, United Kingdom

Reviewed by:
Greg Gaski, Indiana University, United States
Jordi Lopez Tremoleda, Queen Mary University of London, United Kingdom
Martijn van Griensven, cBITE, MERLN Institute, Maastricht University, Netherlands

***Correspondence:**
Klemens Horst
khorst@ukaachen.de

Specialty section:
This article was submitted to Inflammation, a section of the journal Frontiers in Immunology

Received: *28 November 2018*
Accepted: *10 December 2019*
Published: *09 January 2020*

Citation:
Horst K, Greven J, Lüken H, Zhi Q, Pfeifer R, Simon TP, Relja B, Marzi I, Pape H-C and Hildebrand F (2020) Trauma Severity and Its Impact on Local Inflammation in Extremity Injury—Insights From a Combined Trauma Model in Pigs. Front. Immunol. 10:3028. doi: 10.3389/fimmu.2019.03028

Background: Extremity fracture is frequently seen in multiple traumatized patients. Local post-traumatic inflammatory reactions as well as local and systemic interactions have been described in previous studies. However, trauma severity and its impact on the local immunologic reaction remains unclear. Therefore, fracture-associated local inflammation was investigated in a porcine model of isolated and combined trauma to gain information about the early inflammatory stages.

Material and Methods: Polytrauma (PT) consisted of lung contusion, liver laceration, femur fracture, and controlled hemorrhage. Monotrauma (MT) consisted of femur fracture only. The fracture was operatively stabilized and animals were monitored under ICU-standard for 72 h. Blood, fracture hematoma (FH) as well as muscle samples were collected throughout the experimental period. Levels of local and systemic pro- and anti-inflammatory as well as angiogenetic cytokines were measured by ELISA.

Results: Both groups showed a significant decrease in pro-inflammatory IL-6 in FH over time. However, concentrations in MT were significantly higher than in PT. The IL-8 concentrations initially decreased in FH, but recovered by the end of the observation period. These dynamics were only statistically significant in MT. Furthermore, concentrations measured in muscle tissue showed inverse kinetics compared to those in FH. The IL-10 did not present statistical resilient dynamics over time, although a slight increase in FH was seen by the end of the observation time in the MT group.

Conclusions: Time-dependent dynamics of the local inflammatory response were observed. Trauma severity showed a significant impact, with lower values in pro- as well as angiogenetic mediators. Fracture repair could be altered by these trauma-related changes of the local immunologic milieu, which might serve as a possible explanation for the higher rates of delayed or non-union bone repair in polytraumatised patients.

Keywords: polytrauma, pigs, local inflammation, extremity, hematoma, muscle, fixation

INTRODUCTION

Trauma severity directly affects the pattern of injuries. Beside injuries to the head, thorax and abdomen, extremity injuries are common, and present in the majority of multiple traumatized patients (1, 2). However, fracture incidence also increased in the non-polytraumatised patient population during the past decade (3). The severity of extremity injury and its negative impacts on long-term outcome are well-documented (4–6). While pain and limited range of motion are frequently seen in isolated trauma (4, 5), previous clinical and experimental studies linked multiple trauma to significantly longer fracture healing times and higher incidences of non-unions in comparison to isolated fractures (7–9). Overwhelming local and systemic inflammatory responses with an associated negative influence on downstream processes of bone repair are a potential pathomechanism for this impaired fracture healing (10–13). Despite knowledge about the connectivity between the systemic and local inflammatory responses, information on the impact of trauma severity on systemic and local immunologic interactions and responses is scarce (14). Against this background, the purpose of this study was to investigate and compare systemic and local inflammatory responses in isolated and combined trauma. Within an established long-term porcine model of combined trauma (femur fracture, chest-, and abdominal injury, and hemorrhagic shock) (15), post-traumatic immunologic responses were analyzed and compared to those gained from a group with isolated femur fracture. Early kinetics of systemic and local (fracture hematoma and surrounding muscle tissue) immunologic response around the fracture zone were investigated during a 72 h clinically realistic study period.

MATERIALS AND METHODS

Animal Care

Official permission to perform the study was granted from the governmental animal care and use office (Landesamt für Natur, Umwelt und Verbraucherschutz Nordrhein-Westfalen, Recklinghausen, Germany, AZ: 84.02.04.2014A265). All experimental protocols were approved by the governmental animal care and use office and performed in accordance with the German legislation governing animal studies, following The *Principles of Laboratory Animal Care* (16). The data presented in this paper were collected in the context of a larger study (15) for the benefit of the principles of the 3Rs (Replacement, Refinement, and Reduction) (17).

In total 24 male pigs (German Landrace, *Sus scrofa*) weighing 30 ± 5 kg, aged 3 months were used. After arrival from a disease-free barrier breeding facility all animals underwent clinical examination by a veterinarian. Thereafter all animals were housed for 7 days before experiments started. Polytrauma (PT) was induced to 12 animals while 12 animals received isolated femur fracture and were defined as monotrauma (MT). Animals were housed in ventilated rooms and allowed to acclimatize to their surroundings for a minimum of 7 days before start of the experiment. All sections of this report adhere to the ARRIVE Guidelines for reporting animal research (18).

Sample Size and Power Calculation

A sample size calculation was performed for the primary study (15). The chosen sample sizes of 12 in the two groups (MT, PT) show comparable effect sizes as observed in a previous published study on hypothermia in a porcine trauma model (19) and will provide at least 80% power at a significance level of 5%. As all physiological, morphological and inflammatory outcomes characterizing the long-term evolution of severe multiple trauma are equally important to describe the intermodal animal model, no distinction between primary, and secondary outcome was made.

General Instrumentation and Anesthesia

The model was previously described in detail elsewhere (15). In brief: premedication was induced by an intramuscular injection of azaperone (4 mg kg^{-1}). During the 12-h fasting period animals had free access to water. Anesthesia was induced by propofol (3 mg kg^{-1}), followed by orotracheal intubation. Volume-controlled, lung protective mechanical ventilation was applied, and vital parameters were continuously monitored and documented as previously described (20).

During the entire study period, general anesthesia was maintained with propofol and sufentanil (40–90 $\mu g\ Kg^{-1}$/h). Continuous crystalloid infusion (Sterofundin ISO®; 2 ml/kg BW/h) preserved animals from dehydration (15).

Administration of fluids and anesthesia was done by a central venous catheter which was placed in the external jugular vein. Furthermore, this was used to monitor the central venous pressure. The right femoral vein was instrumented via a three-lumen haemodialysis catheter to perform hemorrhage. Continuous monitoring of blood pressure, e.g., mean arterial pressure (MAP) was performed via an arterial line, that was placed in the femoral artery. Reference for intravascular pressure measurements was the mid-chest level and at end of expiration. Suprapubic catheter was applied. Finally, random allocation to either the PT group or the MT group was performed (15).

Induction of Multiple Trauma and Hemorrhage

Trauma was induced as previously described (15) and after achieving stable baseline conditions (at least 120 min after instrumentation). During the 90-min period of shock animals were not prevented from hypothermia to simulate the clinical situation (in humans) after trauma and transport to the hospital.

A bolt gun machine (Blitz-Kerner, turbocut JOBB GmbH, Germany) was used to induce femur fracture in mono- as well as multiple trauma. Therefore the bolt hit a custom-made punch positioned on the mid third of the femur. Cattle-killing cartridges (9×17; DynamitNobel AG, Troisdorf, Germany) were used. The PT group received blunt chest trauma, induced by a bolt shot fired on a pair of panels that was placed on the right dorsal, lower chest (20, 21). Lungs were inflated when the bolt shot was applied. Moreover, a midline-laparotomy was performed and the right upper liver lobe was explored in PT. A penetrating hepatic injury was induced by a crosswise incision (4.5 x 4.5 cm) halfway through the liver tissue (22, 23). Liver packing was carried out with five sterile packs of 10×10-cm gauze after a short period of

uncontrolled bleeding (30 s). Thereafter, hemorrhagic shock was induced by withdrawal of blood until a MAP of 40 ± 5 mm Hg was reached, with a maximum withdrawal of 45% of the total blood volume. The MAP was maintained for 90 min. The ISS (Injury Severity Score) was calculated as 27 points in PT. One investigator (KH) induced trauma, and the period of shock was monitored by two experienced clinicians (KH, TPS) (15).

Animals were resuscitated at the end of the shock period in accordance with established trauma guidelines (ATLS®, AWMF-S3 guideline on Treatment of Patients with Severe and Multiple Injuries®) by adjusting FiO_2 to baseline values and re-infusing the withdrawn blood and additional fluids (Sterofundin ISO®; 2 ml kg/BW/h) in PT (24). Furthermore, animals were rewarmed until normothermia (38.7–39.8°C) was reached using a forced-air warming system (24).

According to established trauma guidelines, operative stabilization of the femur fracture was performed after surgical disinfection and sterile draping at the end of the resuscitation (25). Fluoroscopy (Ziehm Vision, ZiehmImaging, Germany) was used to guide reduction and operation of the femur fracture. According to the clinical situation were internal as well as external stabilization is used for fracture treatment, an intramedullary nail (T2 System, Stryker) was applied to six animals in each group while the remaining six animals received external fixation (Radiolucent Fixator, Orthofix). Surgery was performed by one experienced trauma surgeon. Before surgery and then every 24 h until the end of the experiment antibiotics (Ceftriaxon® 2 g, i.v.) were administered (15).

Data Collection

Following parameters were measured every 30 min by blood gas analysis (BGA) for a period of 5.5 h after trauma: pH, lactate (LAC), pCO_2, pO_2, hemoglobin (Hb), and base excess (BE). From then on, BGA was performed every 6 h until observation period came to an end. Time points of whole blood sampling are paralleled by data on physiologic responses (MAP and heart rate; HR) as well as BGA results. Results demonstrating severe signs of shock were published earlier (15).

Blood samples used in this study were obtained after resuscitation and operative treatment (3.5 h) and after 24, 48, and 72 h (15). Samples were kept on ice. Subsequently, after centrifugation at 2,000 × g for 15 min at 4°C, serum samples were stored at −80°C until analysis of IL-6, IL-8, and IL-10 concentrations (Quantikine® porcine ELISA kit; R&D systems, USA), according to the manufacturer's instructions. Muscle tissue was obtained by biopsy after resuscitation and operative treatment (3.5 h) and after 24, 48, and 72 h; samples were frozen in liquid nitrogen. For protein analysis, 100 mg of frozen muscle tissue were thawed in 300 µL of lysis and extraction buffer and immediately homogenized in an Eppendorf tube on ice with a T10 basic ULTRA-TURRAX® (IKA, Germany). Protein concentrations were measured with commercially available ELISA kits. Fracture hematoma was extracted under sterile conditions by puncturing the fracture zone at 3,5, 24, 48, and 72 h. Hematoma was collected in an EDTA monovette® (SARSTEDT AG & Co, Germany) and diluted with Sterofundin® 1:1. After centrifugation, serum was removed and stored at −80°C for further analysis. Referring to higher concentrations, all fracture hematoma samples were diluted once more (IL-6 1:10, IL-8: 1:4, IL-10: 1:4).

Statistical Analysis

Statistics were performed with SPSS (Version 21.0.0.0) using Mann-Whitney-U, Wilcoxon rank sum and Friedman tests (including Chi^2-Test) [illustrated as mean (SEM)]. For all comparisons, the significance level was set at 5%. Graphics were created using SPSS.

RESULTS

Physiological Response

In contrast to previously reported data from the PT group (15), MT did not present with comparable shock parameters. The mean arterial pressure (MAP) was significantly higher ($p < 0.001$) in MT (69 ± 2.3 mmHg) than in PT (43 ± 1.9 mmHg) 90 min after trauma induction. Additionally, heart rate was significantly lower ($p < 0.001$) in MT (85 ± 7b/min) compared to PT (170 ± 11b/min) at this time. Furthermore pH (MT 7.51 ± 0.01 vs. PT 7.43 ± 0.01, $p < 0.001$), Lactate (MT 1.2 ± 0.2 mmol vs. PT 4.4 ± 0.4 mmol, $p < 0.001$), Base Excess (MT 4.8 ± 0.5 mmol vs. PT 0.4 ± 0.6 mmol, $p < 0.001$) did prove severe haemorrhagic shock only in the PT group. In regard to the reported time points during further clinical course only Lactate was slightly increased after 3.5 h (MT 1.01 ± 0.12 mmol vs. PT 1.38 ± 0.11 mmol). Otherwise there were no statistically significant differences found between the groups. Due to interrupted warming during the trauma phase body temperature was 36.7 ± 0.3°C in MT and 36.7 ± 0.2°C in PT after 90 min. These values were not statistically significant ($p = 0.887$). After rewarming, animals presented with physiological body temperature (MT 3.5 h: 38.2 ± 0.2°C; D1: 38.7 ± 0.1°C; D2: 38.7 ± 0.3°C and D3: 38.8 ± 0.1°C, $p < 0.001$ resp. PT 3.5 h: 37.9 ± 0.1°C; D1: 38.7 ± 0.1°C; D2: 38.8 ± 0.1°C and D3: 38.9 ± 0.1°C, $p < 0.001$). Although temperature changed statistically significant during the clinical course in both groups, there were no differences between the groups.

Interleukin-6

According to the post-traumatic phase, a decrease in serum concentrations was observed in PT, while concentrations in MT remained stable on a low level (**Table 1**). In both groups, a statistically significant decrease in local IL-6 concentrations in muscle tissue as well as fracture haematoma were observed over time (**Table 1** and **Figure 1**). Although fracture haematoma concentrations were higher compared to serum concentrations in both groups, local concentrations of IL-6 in fracture haematoma were significantly lower in PT than in MT (**Table 1**). In contrast to PT, haematoma concentrations in MT showed statistically significantly higher levels compared to muscle tissue concentrations (**Table 1**).

Interleukin-8

Serum IL-8 showed a slight increase over time in PT, while in MT, there was a decrease in systemic concentrations. However,

TABLE 1 | Systemic and local concentrations of IL-6 pg/ml; [a]$p < 0.05$ compared to serum concentrations, [b]$p < 0.05$ compared to muscle concentrations, [c]$p < 0.05$ compared to PT.

Time (h)	Polytrauma (PT)			Monotrauma (MT)		
	Serum	Muscle	Haematoma	Serum	Muscle	Haematoma
3.5[W]	154 (24)	1,803 (535)	3,387 (927)[a]	65 (16)[c]	2,665 (377)[a]	6,286 (1,158)[a,b]
24[W]	81 (11)	1,244 (222)[a]	2,483 (463)[a]	56 (18)	1,347 (230)[a]	4,940 (932)[a,b,c]
48[W]	77 (19)	348 (42)[a]	671 (95)[a]	49 (24)	492 (120)[a]	2,228 (560)[a,b,c]
72[W]	63 (16)	170 (25)	485 (133)[a]	58 (20)	160 (54)	945 (318)[a,b]
p-value[F]	0.002	0.011	<0.001	0.858	0.001	<0.001

Values are given in mean (SEM), [F] Friedman-Test and Chi²-Test, [W] Wilcoxon-Test.

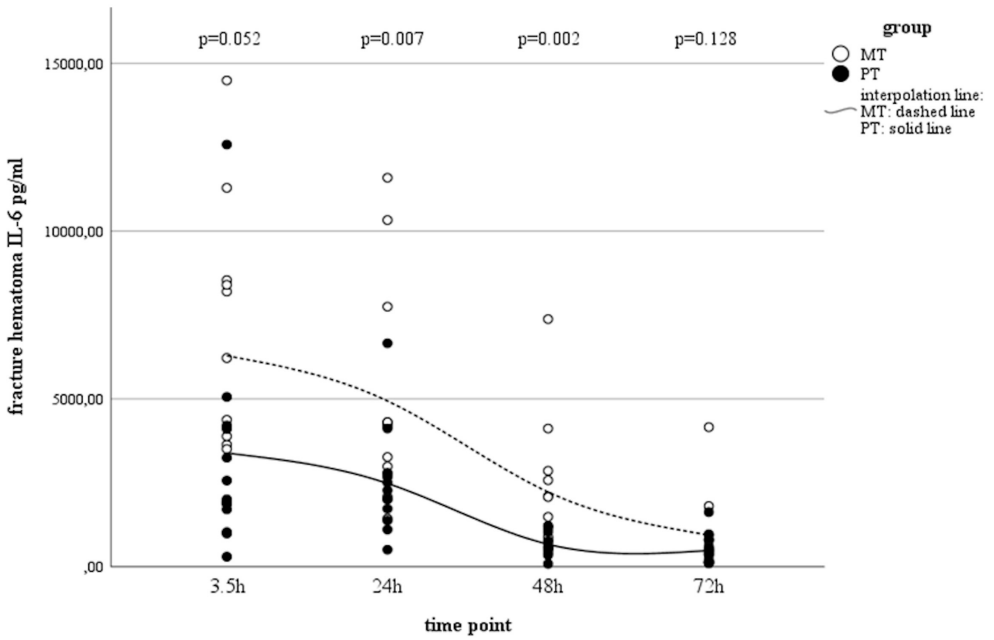

FIGURE 1 | IL-6 concentrations in fracture hematoma between groups and different time points (PT, Polytrauma; MT, Monotrauma; pg/ml, picogram per milliliter; h, hours).

this finding in MT was statistically not significant (**Table 2**). Interestingly, concentrations in muscle tissue showed opposite trends compared to the systemic ones. Initially increasing concentrations decreased by the end of the observation time (**Table 2**). In contrast, concentrations measured in fracture haematoma presented with inverse dynamics compared to those seen in muscle tissue. IL-8 dynamics in haematoma described a v-shaped curve, which was statistically significant in MT (**Table 2** and **Figure 2**). At all measured time points, IL-8 concentrations in fracture haematoma of MT were higher compared to those in PT (**Table 2**).

Interleukin-10

While serum concentrations of IL-10 in PT slightly decreased over time (**Table 3**), values in MT did not present statistically significant changes over time. Although local concentrations measured in muscle tissue and fracture hematoma remained uneventful and were detectable only on a very low level, haematoma concentrations in MT showed an increase by the end of the observation period (**Table 3** and **Figure 3**). However, this finding was not statistically significant.

DISCUSSION

Fracture healing is significantly influenced by the local inflammatory response after trauma (26–29). The impact of trauma severity may lead to a different post-traumatic response, which potentially influences the onset of fracture healing (30, 31). However, information about local inflammatory reactions regarding fracture repair are mostly gained from small animal models with either limited observation time or conditions that do not closely mimic a clinically realistic situation (32–36). As pigs respond to trauma similar to humans, we used an established long-term porcine model of isolated and multiple

TABLE 2 | Systemic and local concentrations of IL-8 pg/ml; [a]$p < 0.05$ compared to serum concentrations, [b]$p < 0.05$ compared to muscle concentrations, [c]$p < 0.05$ compared to PT.

Time (h)	Polytrauma (PT)			Monotrauma (MT)		
	Serum	Muscle	Haematoma	Serum	Muscle	Haematoma
3.5[W]	4 (1)	2,172 (400)[a]	405 (163)[a]	25 (11)	5,947 (2,116)[a]	1,582 (566)[a,b,c]
24[W]	11 (6)	8,115 (1,517)	127 (24)[a]	13 (5)	10,656 (2,116)[a]	448 (88)[a,b,c]
48[W]	12 (4)	6,704 (2,895)[a]	163 (30)[a,b]	12 (7)	9183 (2,711)[a]	471 (111)[a,b,c]
72[W]	13 (5)	1,782 (1,386)[a]	270 (86)[a]	15 (7)	555 (174)[a]	1,123 (658)[a]
p-value[F]	0.01	0.026	0.05	0.514	0.011	0.022

Values are given in mean (SEM), [F] Friedman-Test and Chi²-Test, [W] Wilcoxon-Test.

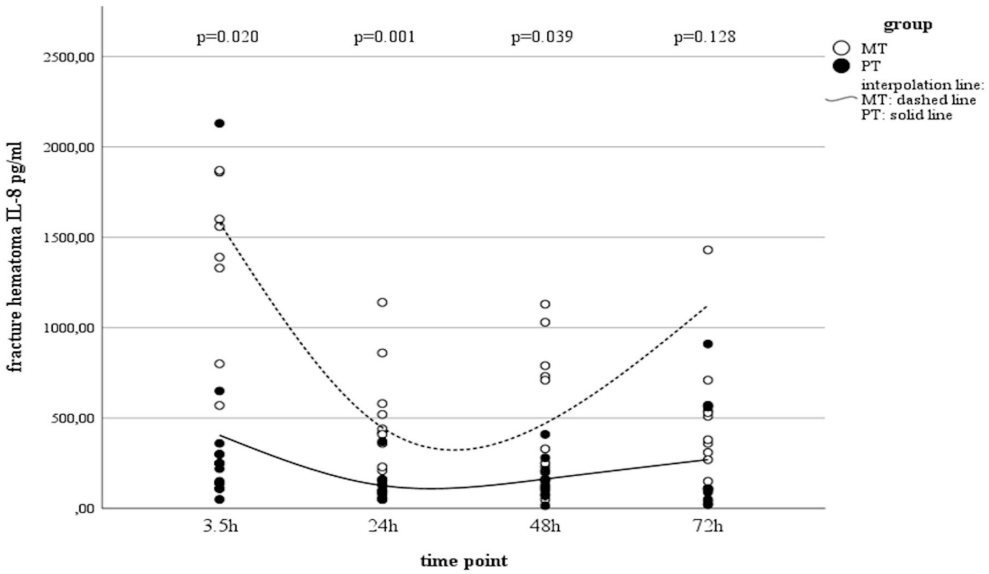

FIGURE 2 | IL-8 concentrations in fracture haematoma between groups and different time points (PT, Polytrauma; MT, Monotrauma; pg/ml, picogram per milliliter; h, hours).

trauma to investigate the local and systemic inflammatory responses in regard to extremity injury and trauma impact (37, 38).

The main results might be summarized as follows:

- Local fracture haematoma concentrations of pro-inflammatory IL-6 and angiogenetic IL-8, but not of anti-inflammatory IL-10, exceeded the systemic values. Fracture haematoma concentrations of IL-6 and IL-8 were higher in MT compared to those in PT.
- In both groups, IL-8 concentrations in muscle tissue showed contrary dynamics compared to those seen in fracture haematoma. Concentrations in muscle tissue exceeded haematoma concentrations. Dynamics of haematoma concentrations described a v-shaped curve, implying a temporary decrease before recovery. This trend was statistically significant only in MT.
- Anti-inflammatory IL-10 presented increasing concentrations in fracture haematoma of MT, but not in PT by the end of the observation period, demonstrating a shift toward an inflammatory milieu. However, this finding was not statistically significant.

The Pro-inflammatory Phase

The early post-traumatic immunologic milieu of fracture hematoma is characterized by inflammation and hypoxia (28). During this early period of acute inflammation, pro-inflammatory mediators such as IL-6 recruit cells needed for tissue regeneration (39). As previously reported and confirmed by others, IL-6 in fracture haematoma increases during the initial post-traumatic phase, followed by a continuous decrease during the further clinical course (20, 40, 41). While its early peak is discussed to maintain the onset of bone healing, persistent high values negatively influence osteogenic differentiation from stem cells (42–44). In regard to multiple trauma commonly associated with an advanced post-traumatic inflammatory response (45), Recknagel et al. revealed that concomitant thoracic trauma considerably enhanced the number of PMN, decreased the number of macrophages and slightly increased IL-6 expression

TABLE 3 | Systemic and local concentrations of IL-10 pg/ml; [a]$p < 0.05$ compared to serum concentrations, [b]$p < 0.05$ compared to muscle concentrations, [c]$p < 0.05$ compared to PT.

Time (h)	Polytrauma (PT)			Monotrauma (MT)		
	Serum	Muscle	Haematoma	Serum	Muscle	Haematoma
3.5[W]	48 (25)	0 (0)[a]	38 (14)	85 (47)	5 (5)	37 (11)[b]
24[W]	39 (26)	18 (7)	38 (17)	92 (50)	15 (10)	28 (9)
48[W]	33 (30)	12 (7)	32 (14)	145 (86)	25 (20)	33 (11)
72[W]	25 (21)	0 (0)	38 (18)	86 (45)	0 (0)	72 (44)[b]
p-value[F]	0.027	0.101	0.972	0.260	0.392	0.779

Values are given in mean (SEM), [F] Friedman-Test and Chi²-Test, [W] Wilcoxon-Test.

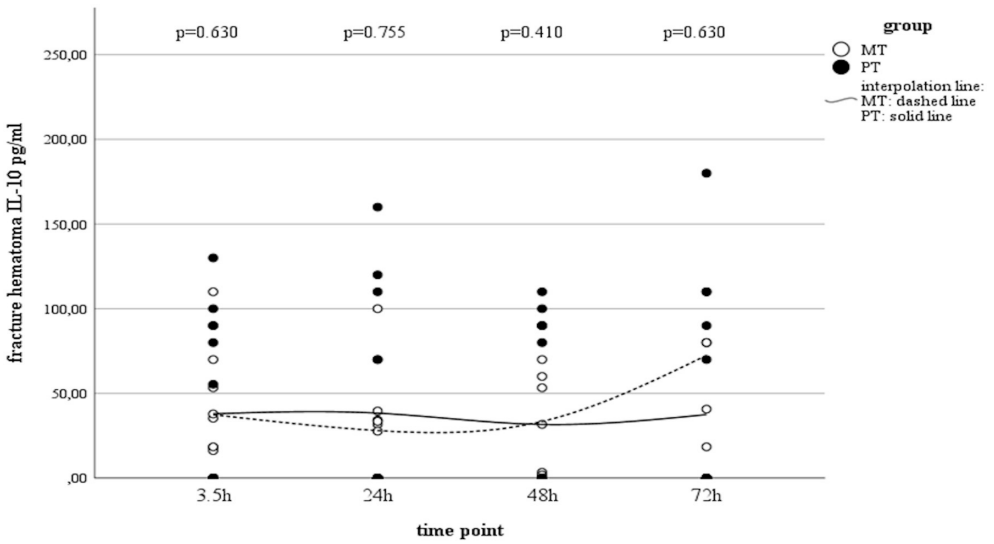

FIGURE 3 | IL-10 concentrations in fracture haematoma between groups and different time points (PT, Polytrauma; MT, Monotrauma; pg/ml, picogram per milliliter; h, hours).

locally at the fracture site, suggesting that post-traumatic systemic inflammation altered the finely tuned inflammatory balance during the early healing phase, leading to impaired bone healing (31, 46). Accordingly, De Benedetti et al. showed that overexpression of IL-6 resulted in severe osteopenia with reduced osteoblast and increased osteoclast numbers and activity (47). Thus, the observed time-dependent decrease in IL-6 concentrations seems to be a consistent step in the sequence of fracture repair. Heiner et al. suggested IL-6-induced up-regulation of the suppressor of cytokine signaling-3 (SOCS-3) as a possible mechanism for the reduction of local IL-6 concentrations (40).

Although we found this decrease in both groups, significant differences between concentrations of IL-6 in MT and PT were observed, with higher values in MT. This dichotomy is interesting as excessive trauma is known to increase systemic cytokine concentrations (14). However, in contrast to lung contusion or haemorrhagic shock, fracture associated soft tissue trauma was found not to be the driving force leading to significant increase of cytokine concentrations (36, 48, 49). Moreover, haemorrhagic shock was discussed to reduce supply in the fracture zone (50), which might explain the observed lower cytokine concentrations in PT fracture hematoma compared to MT ones. Altered immunologic reactions after bone injury with hemorrhage compared to isolated bone injury were previously described and support our findings (51–53). An altered immunologic milieu in the early fracture hematoma also support the findings reported by Lichte et al. who demonstrated impaired bone healing and a significantly decreased number of osteoclasts, a decrease in bone quality and more cartilage islands after hemorrhagic shock in mice (53). Additionally, Wichmann et al. reported on a murine model comparing isolated tibia fracture with tibia fracture and combined hemorrhagic shock (51). The authors concluded that severe hemorrhage after closed bone fracture depresses osteoblast activity and increases osteocyte necrosis, which should compromise fracture healing under those conditions (51). In line with others, the authors discussed decreased blood supply to the fracture zone to negatively influence fracture repair (51–53). Thus, our observation of lower pro-inflammatory concentrations in the PT group suggests the absence of important

pro-inflammatory pacemakers in the very early phase of fracture repair, leading to a delay in skeletogenic mesenchymal stem cell differentiation, with consecutive non- or delayed bone healing (54–56). This finding could serve as one possible explanation why polytraumatised patients suffer from bony non-union more often than patients with isolated injury (9, 30, 57). Against this background, the value of traumatic hemorrhage and its influence on the local immunologic milieu in fracture healing must not be underestimated. Comparable to the benefit of typical shock organs (58), it seems likely, that early resuscitation would also improve the perfusion at the site of the fracture zone supporting recovery to a physiological and immunological state (59, 60). In this context, Augat et al. found that a transient hemorrhagic shock situation followed by isovolumetric blood volume resuscitation resulted in improved fracture healing. The authors concluded that the positive healing response might be associated with improved revascularization of the soft callus adjacent to the fracture site (59, 60). Accordingly, Melnyk et al. described that soft tissue damage without destruction of the bone-soft tissue interface is likely to have only a limited effect on fracture healing (61).

Beside its pro-inflammatory properties, IL-8 is well-known for its angiogenetic characteristics. Accordingly, high local levels were found in fracture haematoma in a previous clinical study, which underlines the importance of IL-8 in the process of bone healing (28). Our data revealed that IL-8 kinetics in muscle tissue showed opposite trends to those seen in fracture haematoma. While concentrations in muscle tissue increased initially and decreased during the clinical course, haematoma concentrations initially decreased and recovered during the later clinical course. Comparable to the observations made in IL-6, the dynamics of IL-8 in fracture haematoma may be explained by reduced blood flow due to haemorrhagic shock in PT (62). Accordingly, Heppenstall et al. report on a rabbit model with an inhibition of fracture healing in hypovolaemia, which was attributed to impaired delivery of oxygen to the fracture site (63). According to our divergent findings in muscle tissue and fracture haematoma, Schmidt-Bleek et al. reported differences in the immunologic milieus of muscle haematoma and fracture haematoma in a sheep model (64). The authors indicate that the inflammatory processes differ due to a unique immune cell composition (64). Although the authors report on a different animal model of isolated trauma, investigating cell migration, our data also reveal differences in the immunologic post-traumatic milieus of muscle tissue and fracture haematoma within the MT, but not the PT group. In regard to the concentrations measured in muscle tissue, our findings are supported by Dragu et al. who proved alterations in the gene expression level in human muscle free flaps after ischaemia and reperfusion (65). The authors report on IL8 as one of four genes that were significantly upregulated after reperfusion of ischemic muscle tissue (65). Accordingly, Huda et al. showed that a significantly elevated concentration was measurable in blood plasma after 3–4 h of reperfusion (66). Furthermore, Kukielka et al. investigated IL-8 expression after ischemia and reperfusion in canine myocardium. The authors found that IL-8 mRNA peaked in the first 3 h of reperfusion and persisted at high levels beyond 24 h (67). Based on these findings, Kukielka et al. speculated that surface-bound chemoattractants may represent an effective mechanism of chemotactic agent presentation and neutrophil activation wherever a reduced blood flow prevents the establishment of a stable soluble chemotactic gradient (67). The observation of increased IL-8 levels are in line with our results from muscle tissue analysis. Both groups showed increased IL-8 concentrations 24 and 48 h after trauma. While values in MT were doubled, concentrations in PT increased even four times compared to initial values. As PT received haemorrhagic shock, this finding might support Kukielka's speculation on the effect of surface-bound chemoattractants in tissue with reduced blood flow. Thus, cell composition as well as interaction of immunologic key players in the early local inflammatory response after multiple trauma must be the focus of further studies.

The Anti-inflammatory Phase

Interleukin-10 is known as an anti-inflammatory mediator that also plays a central role in the fracture healing process (28). It influences bone resorption and enhanced bone healing (35, 68, 69), and a deficit results in osteopenia, mechanical fragility of bones, and defects in their formation (70). While some authors report increased IL-10 concentrations in fracture haematoma during the early post-traumatic phase (71, 72), we could not prove significant kinetics over time. Baker et al. compared different trauma models and proofed that polytrauma plus hemorrhage did not induce the systemic release of IL-10 (49). The authors showed that an additional hemorrhage component appears to attenuate the systemic release of IL-10 after polytrauma (49). In line with Baker et al. and Wichmann et al. proofed that a bone injury, coupled with haemorrhagic shock, produces a more severe depression of immune functions than a haemorrhagic shock alone (73). The authors concluded that bone injury appears to play a contributory role in further depressing immune functions in trauma patients who experienced major blood loss (73). These observations may further reflect that the combined insult leads to the induction of a state of immune paralysis, which also affects IL-10 concentrations within the fracture haematoma (49, 74). In contrast, Hauser et al. found significantly increased IL-10 levels in fracture haematomas in the early phase after trauma, whereas lower levels were observed in the later period (>24 h) (71). However, the authors reported on isolated injures with very heterogeneous entity and severity, which might not realistically reflect the polytraumatised situation. Additionally, Hoff et al. also reported elevated IL-10 concentrations in fracture haematoma (72). However, these values were compared to IL-10 concentrations gained from non-traumatic osteotomy in hip replacement. Thus, the expressiveness of this early "increase" might be also questioned against the background of traumatic injuries. Delayed migration of IL-10-producing cells into fracture haematoma, proved by Schmidt-Bleek et al. may be another cause for time-dependent kinetics in local IL-10 concentrations (44). This might allow a careful speculation about the observed IL-10 increase in fracture haematoma of the MT group, but not the

PT group after 72 h, representing a possible shift from a pro-inflammatory immunologic milieu toward an anti-inflammatory and angiogenic one (28, 44, 75). Yet, literature about local concentrations of IL-10 remains sparse, and further research is warranted. However, the absence of IL-10 in the haematoma of polytraumatised patients might be another explanation for impaired bone regeneration in this patient cohort.

Limitations

The purpose of our study was to gain knowledge about trauma impact and its effect on local inflammatory response around the fracture zone in a clinically relevant, large animal model of isolated vs. multiple trauma. Unfortunately, molecular mechanisms that regulate local or systemic inflammatory response could not be derived. Also, interaction of local inflammatory response to osteo- and chondrogenesis remain unlighted. Furthermore, testing of a relatively small sample size yielded relatively large standard errors for each parameter. Additionally, it would have been interesting to analyse individual immunologic responses as well as financial restrictions led to measurement of only three mediators which is regrettable in the context of a vast immunologic system whereby dozens of inflammatory mediators dynamically interact resulting in a plethora of possible phenotypes. However, research regarding this field is ongoing, and follow-up studies that concentrate on cell migration, but also on bone healing, are in preparation.

CONCLUSIONS

To the best of our knowledge, this is the first study that characterizes and compares chronologic data of locally active inflammatory mediators in regard to femur fracture and trauma impact. Although inference of systemically circulating mediators cannot be drawn from this study, it might be suggested that concomitant injuries, such as haemorrhagic shock, significantly influence local post-traumatic reactions in fracture/soft-tissue haematomas. Combined trauma (or "severe trauma") may cause perturbations in local and/or systemic cytokines and chemokine levels intimately involved in the early phases fracture healing, which may influence adverse outcomes such as fracture non-union. Based on the results of this study, further studies of our group will focus on the role of inflammatory mediators in the repairing process of injured tissue and their role in the systemic process of responding to trauma.

ADVANCES IN KNOWLEDGE

To our knowledge, this is the first study comparing and discussing local (fracture haematoma and muscle tissue) inflammatory response in a large animal model of isolated (MT) and combined (PT) trauma, giving chronological data of locally active inflammatory mediators in regard to extremity fracture during early post-traumatic stages up to 72 h.

ETHICS STATEMENT

This study was carried out in accordance with the recommendations of the German legislation governing animal studies, following The Principles of Laboratory Animal Care (16). Official permission was granted from the governmental animal care and use office (Landesamt für Natur, Umwelt und Verbraucherschutz Nordrhein-Westfalen, Recklinghausen, Germany, AZ: 84.02.04.2014A265). The protocol was approved by the governmental animal care and use office (Landesamt für Natur, Umwelt und Verbraucherschutz Nordrhein-Westfalen, Recklinghausen, Germany, AZ: 84.02.04.2014A265).

AUTHOR CONTRIBUTIONS

KH and FH conceived the study, set up its design and coordinated the experimental and analytic phase. KH, JG, HL, QZ, and TS carried out the experiments and performed the analysis. RP participated in its design and coordination. BR, IM, and H-CP conceived the study, participated in its design and coordination, and helped to draft the manuscript. All authors listed have made a substantial, direct and intellectual contribution to the work, read and approved the final manuscript.

FUNDING

Project no. S-14–14P was supported by the AO Foundation.

ACKNOWLEDGMENTS

The authors thank Yannik Kalbas, Rafael Serve, Lukas Schimunek, Birte Weber, Lukas Egerer, Felix Hönes, and Simona Klee for their assistance in conducting the experiments. We also thank Thaddeus Stopinski for his considerable support during the entire study. Finally, we would like to thank the RWTH Aachen, Faculty of Medicine, for supporting the project via the scientific rotation program for young researchers.

REFERENCES

1. Banerjee M, Bouillon B, Shafizadeh S, Paffrath T, Lefering R, Wafaisade A. Epidemiology of extremity injuries in multiple trauma patients. *Injury.* (2013) 44:1015–21. doi: 10.1016/j.injury.2012.12.007
2. Lefering R. *TraumaRegister DGU®—Annual Report 2017*. German Trauma Society (2017). Available online at: http://www.traumaregister-dgu.de/fileadmin/user_upload/traumaregister-dgu.de/docs/Downloads/TR-DGU-Jahresbericht_2017.pdf (accessed November 04, 2019).
3. Beerekamp MSH, de Muinck Keizer RJO, Schep NWL, Ubbink DT, Panneman MJM, Goslings JC. Epidemiology of extremity fractures in the Netherlands. *Injury.* (2017) 48:1355–62. doi: 10.1016/j.injury.2017.04.047
4. Ferguson M, Brand C, Lowe A, Gabbe B, Dowrick A, Hart M, et al. Outcomes of isolated tibial shaft fractures treated at level 1 trauma centres. *Injury.* (2008) 39:187–95. doi: 10.1016/j.injury.2007.03.012
5. Sanders DW, MacLeod M, Charyk-Stewart T, Lydestad J, Domonkos A, Tieszer C. Functional outcome and persistent disability after isolated fracture

of the femur. *Can J Surg.* (2008) 51:366–70. Available online at: http://canjsurg.ca/wp-content/uploads/2014/03/51-5-366.pdf
6. Steel J, Youssef M, Pfeifer R, Ramirez JM, Probst C, Sellei R, et al. Health-related quality of life in patients with multiple injuries and traumatic brain injury 10+ years postinjury. *J Trauma.* (2010) 69:523–30. doi: 10.1097/TA.0b013e3181e90c24
7. Balogh ZJ, Reumann MK, Gruen RL, Mayer-Kuckuk P, Schuetz MA, Harris IA, et al. Advances and future directions for management of trauma patients with musculoskeletal injuries. *Lancet.* (2012) 380:1109–19. doi: 10.1016/S0140-6736(12)60991-X
8. Hildebrand F, van Griensven M, Huber-Lang M, Flohe SB, Andruszkow H, Marzi I, et al. Is there an impact of concomitant injuries and timing of fixation of major fractures on fracture healing? a focused review of clinical and experimental evidence. *J Orthop Trauma.* (2016) 30:104–12. doi: 10.1097/BOT.0000000000000489
9. Zura R, Watson JT, Einhorn T, Mehta S, Della Rocca GJ, Xiong Z, et al. An inception cohort analysis to predict nonunion in tibia and 17 other fracture locations. *Injury.* (2017) 48:1194–203. doi: 10.1016/j.injury.2017.03.036
10. Park SH, Silva M, Bahk WJ, McKellop H, Lieberman JR. Effect of repeated irrigation and debridement on fracture healing in an animal model. *J Orthop Res.* (2002) 20:1197–204. doi: 10.1016/S0736-0266(02)00072-4
11. Bunn RJ, Burke G, Conelly C, Li G, Marsh D. Inflammation—a double edged sowrd in high-energy fractures? *J Bone Joint Surg Br.* (2005) 87:265–6. Available online at: https://online.boneandjoint.org.uk/doi/abs/10.1302/0301-620X.87BSUPP_III.0870265c
12. Bastian O, Pillay J, Alblas J, Leenen L, Koenderman L, Blokhuis T. Systemic inflammation and fracture healing. *J Leukoc Biol.* (2011) 89:669–73. doi: 10.1189/jlb.0810446
13. Hoff P, Gaber T, Strehl C, Jakstadt M, Hoff H, Schmidt-Bleek K, et al. A Pronounced inflammatory activity characterizes the early fracture healing phase in immunologically restricted patients. *Int J Mol Sci.* (2017) 18:583–96. doi: 10.3390/ijms18030583
14. Almahmoud K, Namas RA, Abdul-Malak O, Zaaqoq AM, Zamora R, Zuckerbraun BS, et al. Impact of injury severity on dynamic inflammation networks following blunt trauma. *Shock.* (2015) 44:101–9. doi: 10.1097/SHK.0000000000000395
15. Horst K, Simon TP, Pfeifer R, Teuben M, Almahmoud K, Zhi Q, et al. Characterization of blunt chest trauma in a long-term porcine model of severe multiple trauma. *Sci Rep.* (2016) 6:39659. doi: 10.1038/srep39659
16. National Research Council (US) Committee for the Update of the Guide for the Care and Use of Laboratory Animals. *Guide for the Care and Use of Laboratory Animals*. 8th ed. Washington, DC: National Academies Press (2011).
17. Russell W, and Burch R. *The Principles of Humane Experimental Technique*. Wheathampstead: Universities Federation for Animal Welfare (1959).
18. Kilkenny C, Browne WJ, Cuthill IC, Emerson M, Altman DG. Improving bioscience research reporting: the ARRIVE guidelines for reporting animal research. *PLoS Biol.* (2010) 8:e1000412. doi: 10.1371/journal.pbio.1000412
19. Horst K, Eschbach D, Pfeifer R, Relja B, Sassen M, Steinfeldt T, et al. Long-term effects of induced hypothermia on local and systemic inflammation - results from a porcine long-term trauma model. *PLoS ONE.* (2016) 11:e0154788. doi: 10.1371/journal.pone.0154788
20. Horst K, Eschbach D, Pfeifer R, Hubenthal S, Sassen M, Steinfeldt T, et al. Local inflammation in fracture hematoma: results from a combined trauma model in pigs. *Mediators Inflamm.* (2015) 2015:126060. doi: 10.1155/2015/126060
21. Eschbach D, Steinfeldt T, Hildebrand F, Frink M, Scholler K, Sassen M, et al. A porcine polytrauma model with two different degrees of hemorrhagic shock: outcome related to trauma within the first 48 h. *Eur J Med Res.* (2015) 20:73. doi: 10.1186/s40001-015-0162-0
22. Holcomb JB, Pusateri AE, Harris RA, Charles NC, Gomez RR, Cole JP, et al. Effect of dry fibrin sealant dressings versus gauze packing on blood loss in grade V liver injuries in resuscitated swine. *J Trauma.* (1999) 46:49–57. doi: 10.1097/00005373-199901000-00009
23. Wong YC, Lai YY, Tan MH, Tan CS, Wu J, Zeng LZ, et al. Potential biomarker panel for predicting organ dysfunction and acute coagulopathy in a polytrauma porcine model. *Shock.* (2015) 43:157–65. doi: 10.1097/SHK.0000000000000279
24. Majde JA. Animal models for hemorrhage and resuscitation research. *J Trauma.* (2003) 54:S100–5. doi: 10.1097/01.TA.0000064503.24416.F4
25. German-Trauma-Society. *S3—Guideline on Treatment of Patients with Severe and Multiple Injuries*. (2016). Available online at: https://www.awmf.org/uploads/tx_szleitlinien/012-019l_S3_Polytrauma_Schwerverletzten-Behandlung_2017-08.pdf (accessed July 1, 2016).
26. Timlin M, Toomey D, Condron C, Power C, Street J, Murray P, et al. Fracture hematoma is a potent proinflammatory mediator of neutrophil function. *J Trauma.* (2005) 58:1223–9. doi: 10.1097/01.TA.0000169866.88781.F1
27. Mountziaris PM, Mikos AG. Modulation of the inflammatory response for enhanced bone tissue regeneration. *Tissue Eng Part B Rev.* (2008) 14:179–86. doi: 10.1089/ten.teb.2008.0038
28. Kolar P, Gaber T, Perka C, Duda GN, Buttgereit F. Human early fracture hematoma is characterized by inflammation and hypoxia. *Clin Orthop Relat Res.* (2011) 469:3118–26. doi: 10.1007/s11999-011-1865-3
29. Walters G, Pountos I, Giannoudis PV. The cytokines and micro-environment of fracture haematoma: current evidence. *J Tissue Eng Regen Med.* (2017) 12:e1662–77. doi: 10.1002/term.2593
30. Calori GM, Albisetti W, Agus A, Iori S, Tagliabue L. Risk factors contributing to fracture non-unions. *Injury.* (2007) 38(Suppl. 2), S11–8. doi: 10.1016/S0020-1383(07)80004-0
31. Recknagel S, Bindl R, Kurz J, Wehner T, Ehrnthaller C, Knoferl MW, et al. Experimental blunt chest trauma impairs fracture healing in rats. *J Orthop Res.* (2011) 29:734–9. doi: 10.1002/jor.21299
32. Levy RM, Prince JM, Yang R, Mollen KP, Liao H, Watson GA, et al. Systemic inflammation and remote organ damage following bilateral femur fracture requires Toll-like receptor 4. *Am J Physiol Regul Integr Comp Physiol.* (2006) 291:R970–6. doi: 10.1152/ajpregu.00793.2005
33. Levy RM, Mollen KP, Prince JM, Kaczorowski DJ, Vallabhaneni R, Liu S, et al. Systemic inflammation and remote organ injury following trauma require HMGB1. *Am J Physiol Regul Integr Comp Physiol.* (2007) 293:R1538–44. doi: 10.1152/ajpregu.00272.2007
34. Kobbe P, Kaczorowski DJ, Vodovotz Y, Tzioupis CH, Mollen KP, Billiar TR, et al. Local exposure of bone components to injured soft tissue induces Toll-like receptor 4-dependent systemic inflammation with acute lung injury. *Shock.* (2008) 30:686–91. doi: 10.1097/SHK.0b013e31816f257e
35. Toben D, Schroeder I, El Khassawna T, Mehta M, Hoffmann JE, Frisch JT, et al. Fracture healing is accelerated in the absence of the adaptive immune system. *J Bone Miner Res.* (2011) 26:113–24. doi: 10.1002/jbmr.185
36. Pfeifer R, Darwiche S, Kohut L, Billiar TR, Pape HC. Cumulative effects of bone and soft tissue injury on systemic inflammation: a pilot study. *Clin Orthop Relat Res.* (2013) 471:2815–21. doi: 10.1007/s11999-013-2908-8
37. Gentile LF, Nacionales DC, Lopez MC, Vanzant E, Cuenca A, Cuenca AG, et al. A better understanding of why murine models of trauma do not recapitulate the human syndrome. *Crit Care Med.* (2014) 42:1406–13. doi: 10.1097/CCM.0000000000000222
38. Mair KH, Sedlak C, Kaser T, Pasternak A, Levast B, Gerner W, et al. The porcine innate immune system: an update. *Dev Comp Immunol.* (2014) 45:321–43. doi: 10.1016/j.dci.2014.03.022
39. Einhorn TA, Gerstenfeld LC. Fracture healing: mechanisms and interventions. *Nat Rev Rheumatol.* (2015) 11:45–54. doi: 10.1038/nrrheum.2014.164
40. Heiner DE, Meyer MH, Frick SL, Kellam JF, Fiechtl J, Meyer RA Jr. Gene expression during fracture healing in rats comparing intramedullary fixation to plate fixation by DNA microarray. *J Orthop Trauma.* (2006) 20:27–38. doi: 10.1097/01.bot.0000184143.90448.aa
41. Currie HN, Loos MS, Vrana JA, Dragan K, Boyd JW. Spatial cytokine distribution following traumatic injury. *Cytokine.* (2014) 66:112–8. doi: 10.1016/j.cyto.2014.01.001
42. Lacey DC, Simmons PJ, Graves SE, Hamilton JA. Proinflammatory cytokines inhibit osteogenic differentiation from stem cells: implications for bone repair during inflammation. *Osteoarthr Cartil.* (2009) 17:735–42. doi: 10.1016/j.joca.2008.11.011
43. Schmidt-Bleek K, Schell H, Schulz N, Hoff P, Perka C, Buttgereit F, et al. Inflammatory phase of bone healing initiates the regenerative healing cascade. *Cell Tissue Res.* (2012) 347:567–73. doi: 10.1007/s00441-011-1205-7
44. Schmidt-Bleek K, Schell H, Lienau J, Schulz N, Hoff P, Pfaff M, et al. Initial immune reaction and angiogenesis in bone healing. *J Tissue Eng Regen Med.* (2014) 8:120–30. doi: 10.1002/term.1505

45. Gebhard F, Pfetsch H, Steinbach G, Strecker W, Kinzl L, Bruckner U. B. Is interleukin 6 an early marker of injury severity following major trauma in humans? *Arch Surg.* (2000) 135:291–5. doi: 10.1001/archsurg.135.3.291
46. Recknagel S, Bindl R, Brochhausen C, Gockelmann M, Wehner T, Schoengraf P, et al. Systemic inflammation induced by a thoracic trauma alters the cellular composition of the early fracture callus. *J Trauma Acute Care Surg.* (2013) 74:531–7. doi: 10.1097/TA.0b013e318278956d
47. De Benedetti F, Rucci N, Del Fattore A, Peruzzi B, Paro R, Longo M, et al. Impaired skeletal development in interleukin-6-transgenic mice: a model for the impact of chronic inflammation on the growing skeletal system. *Arthritis Rheum.* (2006) 54:3551–63. doi: 10.1002/art.22175
48. Perl M, Gebhard F, Knoferl MW, Bachem M, Gross HJ, Kinzl L, et al. The pattern of preformed cytokines in tissues frequently affected by blunt trauma. *Shock.* (2003) 19:299–304. doi: 10.1097/00024382-200304000-00001
49. Baker TA, Romero J, Bach HHt, Strom JA, Gamelli RL, Majetschak M. Systemic release of cytokines and heat shock proteins in porcine models of polytrauma and hemorrhage. *Crit Care Med.* (2012) 40:876–85. doi: 10.1097/CCM.0b013e318232e314
50. Pfeifer R, Tarkin IS, Rocos B, Pape HC. Patterns of mortality and causes of death in polytrauma patients–has anything changed? *Injury.* (2009) 40:907–11. doi: 10.1016/j.injury.2009.05.006
51. Wichmann MW, Arnoczky SP, DeMaso CM, Ayala A, Chaudry IH. Depressed osteoblast activity and increased osteocyte necrosis after closed bone fracture and hemorrhagic shock. *J Trauma.* (1996) 41:628–33. doi: 10.1097/00005373-199610000-00006
52. Neunaber C, Yesilkaya P, Putz C, Krettek C, Hildebrand F. Differentiation of osteoprogenitor cells is affected by trauma-haemorrhage. *Injury.* (2013) 44:1279–84. doi: 10.1016/j.injury.2013.05.011
53. Lichte P, Kobbe P, Pfeifer R, Campbell GC, Beckmann R, Tohidnezhad M, et al. Impaired fracture healing after hemorrhagic shock. *Mediators Inflamm.* (2015) 2015:132451. doi: 10.1155/2015/132451
54. Gerstenfeld LC, Cho TJ, Kon T, Aizawa T, Tsay A, Fitch J, et al. Impaired fracture healing in the absence of TNF-alpha signaling: the role of TNF-alpha in endochondral cartilage resorption. *J Bone Miner Res.* (2003) 18:1584–92. doi: 10.1359/jbmr.2003.18.9.1584
55. Yang X, Ricciardi BF, Hernandez-Soria A, Shi Y, Pleshko Camacho N, Bostrom MP. Callus mineralization and maturation are delayed during fracture healing in interleukin-6 knockout mice. *Bone.* (2007) 41:928–36. doi: 10.1016/j.bone.2007.07.022
56. Wallace A, Cooney TE, Englund R, Lubahn JD. Effects of interleukin-6 ablation on fracture healing in mice. *J Orthop Res.* (2011) 29:1437–42. doi: 10.1002/jor.21367
57. Copuroglu C, Calori GM, Giannoudis PV. Fracture non-union: who is at risk? *Injury.* (2013) 44:1379–82. doi: 10.1016/j.injury.2013.08.003
58. Santry HP, Alam HB. Fluid resuscitation: past present and the future. *Shock.* (2010) 33:229–41. doi: 10.1097/SHK.0b013e3181c30f0c
59. Bumann M, Henke T, Gerngross H, Claes L, Augat P. Influence of haemorrhagic shock on fracture healing. *Langenbecks Arch Surg.* (2003) 388:331–8. doi: 10.1007/s00423-003-0405-3
60. Augat P, Bumann M, Henke T, Gerngross H, Claes L. Resuscitation regimens after hemorrhagic shock influence fracture healing outcome. In: *50th Annual Meeting of the Orthopaedic Research Society*. (2004). Available online at: https://www.ors.org/Transactions/50/0481.pdf (accessed November 04, 2019).
61. Melnyk M, Henke T, Claes L, Augat P. Revascularisation during fracture healing with soft tissue injury. *Arch Orthop Trauma Surg.* (2008) 128:1159–65. doi: 10.1007/s00402-007-0543-0
62. Gaston MS, Simpson AH. Inhibition of fracture healing. *J Bone Joint Surg Br.* (2007) 89:1553–60. doi: 10.1302/0301-620X.89B12.19671
63. Heppenstall RB, Brighton CT. Fracture healing in the presence of anemia. *Clin Orthop Relat Res.* (1977) 123:253–8. doi: 10.1097/00003086-197703000-00067
64. Schmidt-Bleek K, Schell H, Kolar P, Pfaff M, Perka C, Buttgereit F, et al. Cellular composition of the initial fracture hematoma compared to a muscle hematoma: a study in sheep. *J Orthop Res.* (2009) 27:1147–51. doi: 10.1002/jor.20901
65. Dragu A, Schnurer S, Surmann-Schmitt C, von der Mark K, Sturzl M, Unglaub F, et al. Gene expression analysis of ischaemia and reperfusion in human microsurgical free muscle tissue transfer. *J Cell Mol Med.* (2011) 15:983–93. doi: 10.1111/j.1582-4934.2010.01061.x
66. Huda R, Solanki DR, Mathru M. Inflammatory and redox responses to ischaemia/reperfusion in human skeletal muscle. *Clin Sci.* (2004) 107:497–503. doi: 10.1042/CS20040179
67. Kukielka GL, Smith CW, LaRosa GJ, Manning AM, Mendoza LH, Daly TJ, et al. Interleukin-8 gene induction in the myocardium after ischemia and reperfusion *in vivo*. *J Clin Invest.* (1995) 95:89–103. doi: 10.1172/JCI117680
68. Sasaki H, Hou L, Belani A, Wang CY, Uchiyama T, Muller R, et al. IL-10, but not IL-4, suppresses infection-stimulated bone resorption *in vivo*. *J Immunol.* (2000) 165:3626–30. doi: 10.4049/jimmunol.165.7.3626
69. Liu D, Yao S, Wise GE. Effect of interleukin-10 on gene expression of osteoclastogenic regulatory molecules in the rat dental follicle. *Eur J Oral Sci.* (2006) 114:42–9. doi: 10.1111/j.1600-0722.2006.00283.x
70. Dresner-Pollak R, Gelb N, Rachmilewitz D, Karmeli F, Weinreb M. Interleukin 10-deficient mice develop osteopenia decreased bone formation and mechanical fragility of long bones. *Gastroenterology.* (2004) 127:792–801. doi: 10.1053/j.gastro.2004.06.013
71. Hauser CJ, Joshi P, Zhou X, Kregor P, Hardy KJ, Devidas M, et al. Production of interleukin-10 in human fracture soft-tissue hematomas. *Shock.* (1996) 6:3–6. doi: 10.1097/00024382-199607000-00002
72. Hoff P, Gaber T, Strehl C, Schmidt-Bleek K, Lang A, Huscher D, et al. Immunological characterization of the early human fracture hematoma. *Immunol Res.* (2016) 64:1195–206. doi: 10.1007/s12026-016-8868-9
73. Wichmann MW, Zellweger R, DeMaso CM, Ayala A, Williams C, Chaudry IH. Immune function is more compromised after closed bone fracture and hemorrhagic shock than hemorrhage alone. *Arch Surg.* (1996) 131:995–1000. doi: 10.1001/archsurg.1996.01430210093021
74. Hotchkiss RS, Karl IE. The pathophysiology and treatment of sepsis. *N Engl J Med.* (2003) 348:138–50. doi: 10.1056/NEJMra021333
75. Loi F, Cordova LA, Pajarinen J, Lin TH, Yao Z, Goodman SB. Inflammation, fracture and bone repair. *Bone.* (2016) 86:119–30. doi: 10.1016/j.bone.2016.02.020

Conflict of Interest: The authors declare that the research was conducted in the absence of any commercial or financial relationships that could be construed as a potential conflict of interest.

Copyright © 2020 Horst, Greven, Lüken, Zhi, Pfeifer, Simon, Relja, Marzi, Pape and Hildebrand. This is an open-access article distributed under the terms of the Creative Commons Attribution License (CC BY). The use, distribution or reproduction in other forums is permitted, provided the original author(s) and the copyright owner(s) are credited and that the original publication in this journal is cited, in accordance with accepted academic practice. No use, distribution or reproduction is permitted which does not comply with these terms.

frontiers in Immunology

ORIGINAL RESEARCH
published: 09 January 2020
doi: 10.3389/fimmu.2019.02957

Citrullinated Histone H3 as a Therapeutic Target for Endotoxic Shock in Mice

Qiufang Deng[1,2†], Baihong Pan[1,2†], Hasan B. Alam[2], Yingjian Liang[2,3], Zhenyu Wu[1,2], Baoling Liu[2], Nirit Mor-Vaknin[4], Xiuzhen Duan[5], Aaron M. Williams[2], Yuzi Tian[1,2], Justin Zhang[2] and Yongqing Li[2*]*

[1] Xiangya Hospital, Central South University, Changsha, China, [2] Department of Surgery, University of Michigan, Ann Arbor, MI, United States, [3] The First Hospital, China Medical University, Shenyang, China, [4] Division of Infectious Diseases, Department of Internal Medicine, University of Michigan, Ann Arbor, MI, United States, [5] Department of Pathology, Loyola University Medical Center, Maywood, IL, United States

OPEN ACCESS

Edited by:
Patrizia Rovere Querini, Vita-Salute San Raffaele University, Italy

Reviewed by:
Kimberly Martinod, KU Leuven, Belgium
Claudia Farias Benjamim, Federal University of Rio de Janeiro, Brazil

***Correspondence:**
Hasan B. Alam
alamh@med.umich.edu
Yongqing Li
yqli@med.umich.edu

[†] These authors have contributed equally to this work

Specialty section:
This article was submitted to Inflammation, a section of the journal Frontiers in Immunology

Received: 06 June 2019
Accepted: 02 December 2019
Published: 09 January 2020

Citation:
Deng Q, Pan B, Alam HB, Liang Y, Wu Z, Liu B, Mor-Vaknin N, Duan X, Williams AM, Tian Y, Zhang J and Li Y (2020) Citrullinated Histone H3 as a Therapeutic Target for Endotoxic Shock in Mice. Front. Immunol. 10:2957. doi: 10.3389/fimmu.2019.02957

Sepsis results in millions of deaths every year, with acute lung injury (ALI) being one of the leading causes of mortality in septic patients. As neutrophil extracellular traps (NETs) are abundant in sepsis, neutralizing components of NETs may be a useful strategy to improve outcomes of sepsis. Citrullinated histone H3 (CitH3) has been recently shown to be involved in the NET formation. In this study, we demonstrate that CitH3 damages human umbilical vein endothelial cells (HUVECs) and potentiates NET formation through a positive feedback mechanism. We developed a novel CitH3 monoclonal antibody to target peptidylarginine deiminase (PAD) 2 and PAD 4 generated CitH3. In a mouse model of lethal lipopolysaccharide (LPS) induced shock, neutralizing CitH3 with the newly developed anti-CitH3 monoclonal antibody attenuates inflammatory responses, ameliorates ALI, and improves survival. Our study suggests that effectively blocking circulating CitH3 might be a potential therapeutic method for the treatment of endotoxemia.

Keywords: citrullinated histone H3, endotoxic shock, neutrophil extracellular traps, new anti-CitH3 antibody, inflammation, acute lung injury, survival

INTRODUCTION

Sepsis is defined as a life-threatening organ dysfunction caused by the dysregulation of host response secondary to infection (1). Acute lung injury (ALI) develops in nearly 40% of the septic patients and is one of the leading causes of death (2).

Excessive neutrophil extracellular traps (NETs) have been detected in sepsis and are associated with significant organ injury (3). NETs are stranded, decondensed DNA (deoxyribonucleic acid) fibers accompanied by intracellular proteins, including histones, neutrophil elastase (NE), myeloperoxidase (MPO), and other proteins coming from various neutrophil organelles (4, 5). Histone citrullination/deimination induced by peptidyl arginine deiminases (PADs) is an important posttranslational modification that facilitates chromatin decondensation during NET formation (6). Moreover, citrullinated histones are found in the extracellular space of neutrophils along with DNA as components of NETs (7).

NETs are generally regarded as a double-edged sword (8). NETs can immobilize and kill a broad range of pathogens: gram-positive and -negative bacteria, fungi, viruses, and protozoa (4, 9–14).

However, they also promote tissue damage, increase thrombosis, and cause disruption of the autoimmune system (15). Strategies targeting NET formation or NET components have proven therapeutic in animal models of sepsis. PAD inhibitors, which can disrupt NET formation, have been shown to protect animals from endotoxic shock or septic shock. Administration of a pan-PAD Inhibitor, Cl-amidine, improves survival in both lethal and sub-lethal models of murine sepsis, increases bacterial clearance, and ameliorates thymus and bone marrow atrophy (16, 17). YW3-56, another pan-PAD inhibitor, has been shown to increase survival in mice with lipopolysaccharide (LPS)-induced endotoxic shock (18). Administration of DNase has been demonstrated to markedly reduce cell-free DNA and improve outcomes in both *Escherichia coli*-induced and CLP-induced sepsis (19, 20). Neutralization of histone H4, a NET component, has been shown to significantly reduce the mortality in mouse models of cecal ligation and puncture (CLP) (21).

Citrullinated histone H3 (CitH3) has been shown to be highly involved in the process of NETosis (4, 6, 18, 22). As such, CitH3 is considered a good biomarker for the diagnosis of endotoxic shock due to its early appearance (as early as 30 min) in the blood, long half-life, high specificity, and response to treatment (23). However, the physio-pathologic role of CitH3 in sepsis has not been well-defined. Furthermore, it is unknown whether CitH3 could be considered a therapeutic target. In this study, we investigated the adverse effects of CitH3 and developed a new anti- histone H3 (citrullinated R2+R8+R17+R26) monoclonal antibody [CitH3 mAb (4 Cit)] utilizing CitH3 with four citrullines (4 Cit) as the antigen. We then evaluated this novel antibody in a murine model of endotoxic shock to explore the therapeutic value of neutralizing the circulating CitH3 protein.

MATERIALS AND METHODS

Generation of CitH3 mAb (4 Cit)

CitH3 peptide with four citrulline residues [A(Cit)TKQTA(Cit) KSTGGKAP(Cit) KQLATKAA(Cit)KSAP], referred to as CitH3 (R2+R8+R17+R26) peptide, was chemically synthesized by New England Peptide, Inc. (Gardner, MA, USA) and utilized to generate the 4 Cit monoclonal antibody in ProMab Biotechnologies, Inc. (Richmond, CA, USA) using the company-approved animal protocol. Balb/c mice were immunized with the CitH3 (R2+R8+R17+R26) peptide. Antibody titers were then determined by enzyme-linked immunosorbent assay (ELISA). Splenocytes from the mouse with the highest antibody titer were fused with myeloma cells (SP2/0) to generate hybridomas. Anti-CitH3 (R2+R8+R17+R26) peptide-specific hybridomas were identified using ELISA against the CitH3 (R2+R8+R17+R26) peptide. One to two million viable hybridoma cells were injected into a mouse peritoneal cavity to produce ascites, which was harvested, and particles were removed through centrifugation. Protein G purification was performed to get the final CitH3 mAb (4 Cit).

Abbreviations: CitH3 mAb (4 Cit), anti-histone H3 (citrullinated R2+R8+R17+R26) monoclonal antibody; CitH3 mAb (3 Cit), anti-histone H3 (citrullinated R2+R8+R17) monoclonal antibody.

Cell Culture and Treatment

Human umbilical vein endothelial cells (HUVECs) (Lonza, Walkersville, MD, USA) were cultured using endothelial cell growth medium (EGM) BulletKit (Lonza, Walkersville, MD, USA). HUVECs (5×10^5 cells/ml) were grown on 12-mm Transwells with 0.4 μm pore polyester membrane inserts (Corning Life Sciences, Corning, NY, USA) for 3 days to develop a confluent (90%) monolayer. HUVECs were then treated for 16 h with 5 μg/ml histone H3 peptide (ARTKQTARKSTGGKAP RKQLATKAARKSAP) or CitH3 peptide [A(Cit)TKQTA(Cit) KSTGGKAP(Cit)KQLATKAA(Cit)KSAP]. Chambers were then incubated in the presence of 1 mg/ml 10-kDa FITC-dextran (Thermo Scientific, Rockford, IL, USA). The fluorescence of media in the lower chambers was measured by a GloMax-multi detection system (Promega, Madison, WI, USA).

Mice

Male C57BL/6 mice (7–8 weeks) were purchased from The Jackson Laboratory (Bar Harbor, ME, USA) and housed for at least 3 days with food and water *ad libitum* before the experiment. All experiments were performed in compliance with the animal welfare and research regulations. The animal protocol for this study was approved by the University of Michigan Institutional Animal Care and Use Committee.

Lethal Endotoxic Shock and Antibody Treatment

LPS was injected intraperitoneally (20 mg/kg), inducing lethal endotoxic shock in the mice. Either CitH3 mAb (4 Cit) (about 20 mg/kg) or the same amount of anti-histone H3 [(citrullinated R2+R8+R17) monoclonal antibody (CitH3 mAb (3 Cit), Item number 9003062 with Batch numbers 0515031-1, 0513766-1, and 0516044-1; Cayman Chemical, Ann Arbor, MI, USA)] was administered via tail vein injection. Mouse receiving immunoglobulin G (IgG) only (20 mg/kg) or LPS followed by IgG served as controls ($n = 9$/group). Survival was monitored for 10 days. Kaplan–Meier curves were used to compare the survival rates.

In another cohort, mice were also randomly divided into four groups: (1) IgG only (20 mg/kg), (2) LPS (20 mg/kg) + IgG (20 mg/kg), (3) LPS + CitH3 mAb (4 Cit) (20 mg/kg), and (4) LPS + CitH3 mAb (3 Cit) (20 mg/kg) ($n = 3$/group). Animals were sacrificed 12 h after treatment ($n = 3$), and organs were collected and stored in −80°C for further use. Blood samples were at room temperature (RT) for 1 h to allow for clotting and separation of serum. Serum was collected by centrifugation of the clotted blood at 3,000 × *g* at 4°C for 20 min, and then stored immediately at −80°C.

Western Blotting for Antibody Validation

One-half microgram of five different peptides [H3, AceH3, CitH3 (R2+R8+R17+R26), CitH3 (R26), and MetH3] or 3 ng of CitH3 protein was subjected to SDS-polyacrylamide gel electrophoresis and was transferred onto a nitrocellulose membrane. Membranes were then probed with the same concentration (2 μg/ml) of CitH3 mAb (4 Cit) or CitH3 mAb (3 Cit). Donkey anti-mouse 800 CW antibodies (LI-COR, Lincoln, NE, USA) were

used as the secondary detection antibodies (1: 5,000 dilution). Finally, the membranes were exposed to 800 channel Odyssey Imaging System (LI-COR, Lincoln, NE, USA). Immunoblot signal intensity was analyzed using Image Studio Lite (LI-COR, Lincoln, NE, USA).

CitH3 ELISA

A "sandwich" ELISA, which has been developed by our laboratory and described previously (23), was used. In brief, 0.5 μg/well CitH3 mAb (4 Cit) or CitH3 mAb (3 Cit) was coated in 96-well plates (Corning Life Sciences, Corning, NY, USA) at 4°C overnight and then blocked with 100 μl of protein-free blocking buffer (Thermo Scientific, Rockford, IL, USA) at 4°C overnight. The wells were then incubated with CitH3 (R2+R8+R17+R26) peptide or mouse serum (1:1 diluted in blocking buffer) at RT for 2 h, followed by rabbit anti-CitH3 polyclonal antibody (1:3,000 diluted, Abcam, Cambridge, MA, USA) incubation for 2 h at RT. Next, 96-well plates were probed with donkey anti-rabbit horseradish peroxidase (HRP) conjugate IgG (1:50,000 diluted, Jackson ImmunoResearch, West Grove, PA, USA). 3,3′,5,5′-Tetramethylbenzidine (TMB, Thermo Fisher Scientific, Waltham, MA, USA) was utilized to develop the plate for 30 min at RT in the dark before adding stop solution (R&D Systems Inc., Minneapolis, MN, USA). Absorbance was measured at 450 nm.

Cytokines

Levels of pro-inflammatory cytokines in the serum or lung homogenates were measured by ELISA. IL-1β was measured using the Mouse IL-1β/IL-1F2 DuoSet ELISA (R&D Systems, Minneapolis, MN, USA) and TNF-α was detected using Mouse TNF-α DuoSet ELISA (R&D Systems, Minneapolis, MN, USA). The ELISA was performed blindly by an independent researcher.

Histopathology

Twelve hours after treatment, lung samples were collected and fixed with 4% paraformaldehyde, and then dehydrated in 70% ethanol. The lung tissues were embedded in paraffin and cut into 5-μm sections. Hematoxylin–eosin staining was performed by a blinded researcher. Histological analysis of ALI was also graded by a blinded pathologist with a scale from 0 to 3 among the following domains: (1) septal mononuclear cell/lymphocyte infiltration, (2) septal hemorrhage and congestion, (3) neutrophils, (4) alveolar macrophages, (5) alveolar hemorrhage, and (6) alveolar edema (0: "absent," 1: "mild," 2: "moderate," and 3: "severe"). The total injury score was calculated by adding up the scores for all parameters.

Human Neutrophil Isolation and Treatment

Collection of blood samples from a healthy human volunteer was approved by the Institutional Review Board (IRB) of the University of Michigan (HUM00048623). Neutrophil isolation has been described previously (24). Briefly, human whole blood up to 60 ml was placed in 7 ml 0.25 M citrate solution and 10 ml 6% dextran solution in PBS. After incubation for 30 min, the upper phase was collected and layered on 15 ml of Histopaque-1077 (Sigma, St. Louis, MO, USA), and separated through centrifugation for 30 min at 800 × *g* at RT. The pellet was resuspended with 3 ml of cold PBS and layered on 12 ml of Histopaque-1119 (Sigma, St. Louis, MO, USA) and centrifuged again for 30 min at 800 × *g* at RT. The neutrophil layer was then transferred to a 50-ml tube and 40 ml of PBS was added. After 10 min centrifugation at 500 × *g*, 4°C, the supernatant was disposed and the neutrophil fraction was suspended in RPMI 1640 supplemented with 2% BSA to make the final neutrophil concentration at 500,000 cells/ml. One milliliter cell solution was added to each 22 × 22, 1.5/2.5 glass coverslip that has been treated with 0.001% poly-L-lysine (Sigma, St. Louis, MO, USA). After cell adherence, neutrophils were treated for 2 h with 5 μg/ml CitH3 peptide [A(Cit)TKQTA(Cit) KSTGGKAP(Cit)KQLATKAA(Cit)KSAP] or H3 peptide (ARTKQTARKSTGGKAPRKQLATKAARKSAP) as control. Media was removed before immunocytochemistry.

Immunocytochemistry

Cells were washed before fixation in 3.7% paraformaldehyde/PBS for 10 min at RT. After three washes with PBS for 5 min each, cells were blocked in 2% BSA/PBS overnight at 4°C. Neutrophils were then probed overnight at 4°C with anti-CitH3 monoclonal antibody (Cayman Chemical, Ann Arbor, Michigan, USA) at a dilution of 1: 1,000 and anti-MPO polyclonal antibody (Abcam, Cambridge, MA, USA) at the dilution of 1:100 in 10% normal donkey serum. Cells were washed with PBS three times for 5 min each. Next, cells were incubated at RT for 1 h with FITC-conjugated donkey anti-rabbit and TRITC-conjugated donkey anti-mouse IgG (Jackson ImmunoResearch Laboratories, West Grove, PA, USA) at a dilution of 1:300 in 10% normal donkey serum. Following another three washes with PBS, the coverslips were mounted with anti-fade reagent with DAPI (Thermo Fisher Scientific, Waltham, MA, USA). Eight fields each group were selected randomly for further quantification of NETs formation. Fluorescence microscopy images were analyzed with Image J software to count the number of NETs induced by peptides per 100 neutrophils.

Measurement of Serum Levels of dsDNA

The PicoGreen assay kit (Invitrogen, San Diego, CA, USA) was used to detect circulating dsDNA per manufacturer's instruction.

Statistical Analysis

Analyses were performed with GraphPad Prism 7 (GraphPad Software Inc., La Jolla, CA, USA). Data are presented as mean ± standard error of mean (SEM). Log-rank test was used to analyze the survival curve. One-way analysis of variance (ANOVA) followed by Bonferroni's multiple comparison test was used for comparisons between three or more groups. Mann–Whitney *U* test (non-parametric test) was performed for comparisons between two groups. A $p < 0.05$ was considered statistically significant. $^{*}p < 0.05$; $^{**}p < 0.01$; $^{***}p < 0.001$; $^{****}p < 0.0001$.

RESULTS

CitH3 Increases HUVEC Permeability and Induces NET Formation

CitH3 is undetectable in the serum and peritoneal fluid under normal physiologic conditions in mice; however, it is elevated in the samples obtained from endotoxic or septic mice (17, 23).

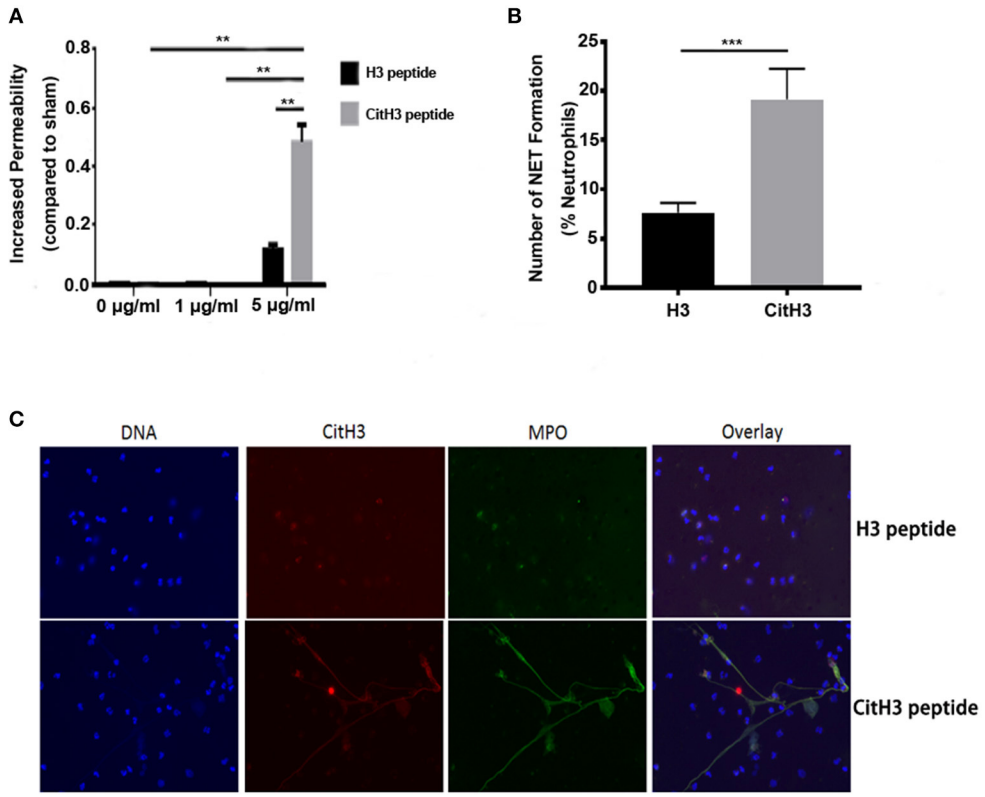

FIGURE 1 | CitH3 induces vascular leakage and formation of NETs. **(A)** HUVECs were treated with 1 μg/ml or 5 μg/ml of H3 peptide or CitH3 peptide for 16 h after forming a confluent (90%) monolayer on Transwells. Chambers were then incubated in 1 mg/ml 10-kDa FITC-dextran. The fluorescence of media in the lower chambers were presented as means ± SEM ($n = 5$/group). **(B,C)** Human neutrophils were purified from the peripheral blood of a healthy volunteer. After 2 h treatment with 5 μg/ml CitH3 peptide, or H3 peptide as a control ($n = 3$/group), neutrophils were stained with DAPI (blue), mouse anti-CitH3 (red), and rabbit anti-MPO (green) antibodies. Neutrophils stimulated with CitH3 peptide formed NETs, whereas those treated with H3 peptide did not. Fluorescence microscopy images were analyzed with Image J software to count the number of NETs induced by peptides per 100 neutrophils. $^{**}p < 0.01$; $^{***}p < 0.001$.

The function of CitH3 remains largely unknown. It was recently reported that human recombinant CitH3 protein could disrupt endothelial barrier *in vivo*, probably through opening cell–cell adheres junctions and reorganizing the actin cytoskeleton (25). This conclusion needs further evaluation since the recombinant CitH3 protein was catalyzed by PAD4 purified from *E. coli*, and endotoxin contamination can compromise the validity of the experimental results (26, 27).

In the present study, synthesized CitH3 peptide was used. It was found that the synthesized CitH3 peptide (5 μg/ml) significantly increased ($p < 0.01$) dextran leakage from HUVECs compared to sham control or 1 μg/ml CitH3 treatment (**Figure 1A**). HUVECs treated with 5 μg/ml H3 peptide had increased dextran leakage compared to sham; however, it was significantly lower ($p < 0.01$) compared to CitH3 at the same concentration (5 μg/ml). The result suggests that CitH3 might be more toxic to HUVECs than H3, implicating the adverse effect of CitH3 in sepsis. Since CitH3 could induce prominent leakage from endothelial cells, neutralizing CitH3 may be beneficial in endotoxic shock or sepsis.

Human neutrophils incubated with CitH3 peptide also produced NETs after a short incubation period of 2 h. To visualize NETs, cells were co-stained with MPO, CitH3, and DNA. As shown in **Figure 1C**, there were no NETs detected in neutrophils treated with H3 peptide; however, NET structures were observed following CitH3 treatment, including stretched DNA filaments along with MPO and CitH3. As such, CitH3 increases HUVEC permeability and can induce NET formation *ex vivo*.

The CitH3 mAb (4 Cit) Recognizes Histone H3 Citrullinated R26 and Has Higher Binding Capacity Compared to the Antibody Against Histone H3 [Citrullinated R2+R8+R17 (CitH3 mAb (3 Cit))]

Although there are some commercially available antibodies that bind to citrulline residues in histones, their efficacy has been found to be inconsistent (28), and there is a need for more reliable anti-CitH3 antibodies. In addition, the commercially available anti-CitH3 mAb only recognizes histone H3 citrullinated R2+R8+R17 [CitH3 mAb (3 Cit)], for which PAD4 is responsible (29). However, histone H3 R26 can also be citrullinated, by PAD2 but not PAD4 (30). Therefore, utilizing the CitH3 peptide with four citrulline residues at histone 2+8+17+26, we developed

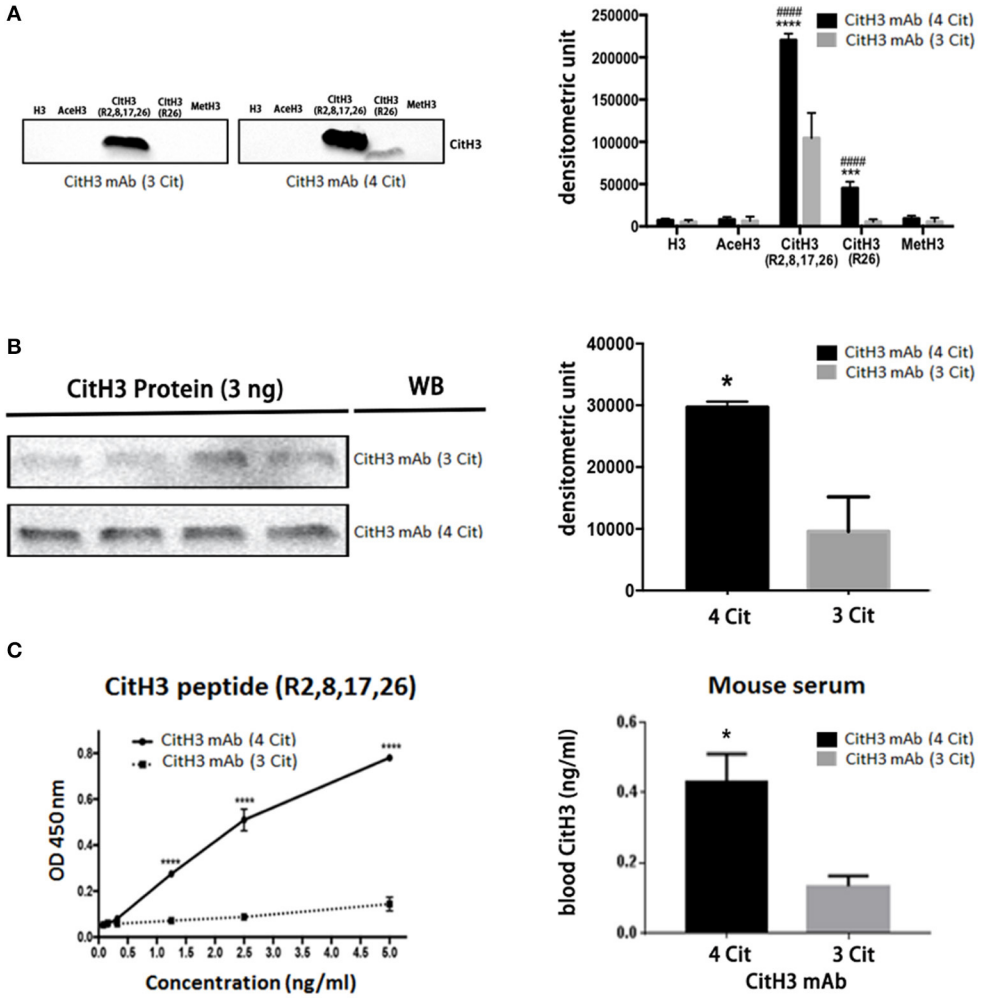

FIGURE 2 | The newly developed anti-CitH3 mAb (4 Cit) recognizes histone H3 citrullinated R2+R8+R17+R26 with higher binding capability than the commercially available anti-CitH3 monoclonal antibody [CitH3 mAb (3 Cit)]. **(A)** Half microgram of five different peptides [H3, AceH3, CitH3 (R2,8,17,26), CitH3 (R26), and MetH3] or **(B)** 3 ng CitH3 protein were submitted to SDS-polyacrylamide gel electrophoresis and transferred onto a nitrocellulose membrane. Then, membranes were probed with the same concentration of CitH3 mAb (4 Cit) or CitH3 mAb (3 Cit) (2 μg/ml). Other immunoblotting conditions were kept the same. Signal intensity was analyzed using Image Studio Lite and presented as mean ± SEM ($n = 4$/group). **(C)** Half microgram of CitH3 mAb (4 Cit) or CitH3 mAb (3 Cit) was coated per well in 96-well plates and incubated for 2 h at room temperature (RT) with CitH3 peptide (left panel), and or serum (1:1 diluted, right panel) from endotoxic mice, followed by anti-CitH3 polyclonal antibody incubation and then donkey anti-rabbit HRP-conjugated IgG. 3,3′,5,5′-Tetramethylbenzidine was utilized to develop the plate for 30 min at RT in the dark before adding stop solution. Absorbance was measured at 450 nm and presented as mean ± SEM ($n = 3$/group). $^{*}p < 0.05$ compared to CitH3 mAb (3 Cit); $^{***}p < 0.001$ compared to CitH3 mAb (3 Cit); $^{****}p < 0.0001$ compared to CitH3 mAb (3 Cit); $^{\#\#\#\#}p < 0.0001$ compared to H3 incubated with CitH3 mAb (4 Cit). WB, Western blot.

the new mouse anti-CitH3 monoclonal antibody, referred to as CitH3 mAb (4 Cit), with the intention to completely block the CitH3 catalyzed by both PAD2 and PAD4.

To ensure the quality of the CitH3 mAb (4 Cit), we performed both immunoblotting and ELISA to test its specificity and capability for CitH3 recognition, compared with a commercial CitH3 mAb (3 Cit) (**Figure 2**). Immunoblotting was performed under the same experimental conditions, including concentration of antibodies, incubation time, and same-time exposure. As shown in **Figure 2A**, both CitH3 mAb (4 Cit) and CitH3 mAb (3 Cit) had a high specificity for CitH3. However, no band was detected for H3 (non-modified H3), AceH3 (acetylated H3), or MetH3 (methylated H3). For CitH3 detection, CitH3 mAb (3 Cit) only showed staining for CitH3 (R2+R8+R17+R26) peptide; however, no signal was found for CitH3 (R26) peptide. The CitH3 mAb (4 Cit) specifically detected histone H3 citrullinated R26, in accordance with our expectation. Furthermore, using CitH3 mAb (4 Cit), a stronger blot signal appeared for the CitH3 (R2+R8+R17+R26) peptide [densitometry unit, CitH3 mAb (4 Cit) vs. CitH3 mAb (3 Cit): 220,413.7 ± 4,444.8 vs. 104,416.3 ± 17,285.4; $p < 0.0001$]. Consistent with the peptide immunoblotting results, CitH3 mAb (4 Cit) gave a higher signal (three-fold) for the CitH3 protein [**Figure 2B**, densitometry unit, CitH3 mAb (4 Cit) vs. CitH3

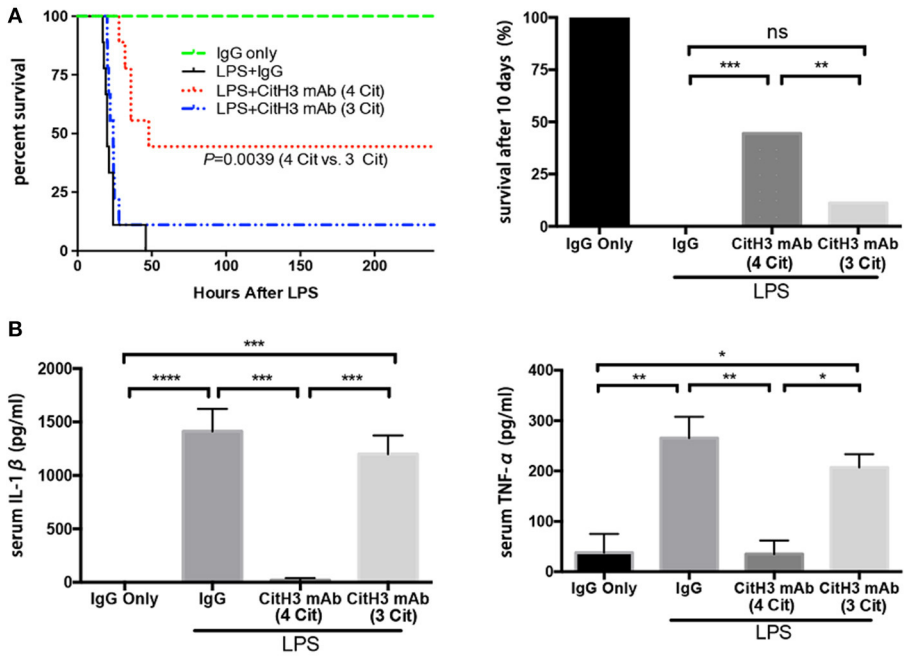

FIGURE 3 | The CitH3 mAb (4 Cit) improves survival and attenuates serum cytokines compared to the CitH3 mAb (3 Cit) in a mouse model of lethal endotoxic shock. C57BL/6J mice were randomized to injection: (1) IgG only (20 mg/kg), (2) LPS (20 mg/kg) + mouse IgG (20 mg/kg), LPS + CitH3 mAb (4 Cit) (~20 mg/kg), LPS + CitH3 mAb (3 Cit) (~20 mg/kg). **(A)** Survival was monitored for 10 days ($n = 9$/group). Kaplan–Meier curves were used for survival rate analysis. The CitH3 mAb (4 Cit) significantly improved mouse survival compared to the LPS + mouse IgG group ($p = 0.0004$) and to the LPS + CitH3 mAb (3 Cit) group ($p = 0.0039$). There was no survival difference between the LPS + IgG group and the LPS + CitH3 mAb (3 Cit) group. **(B)** In another cohort ($n = 3$/group), blood and organs were harvested at 12 h after LPS injection. Serum levels of IL-1β and TNF-α were measured using ELISA. Data are presented as mean ± SEM ($n = 3$/group). $^*p < 0.05$; $^{**}p < 0.01$; $^{***}p < 0.001$; $^{****}p < 0.0001$. ns, non significance.

mAb (3 Cit): 29,689 ± 919.8 vs. 9,596 ± 5,598; $p < 0.05$]. Since the experimental conditions of immunoblotting can only be roughly controlled, ELISA was used to further confirm the superiority of CitH3 mAb (4 Cit) in comparison with CitH3 mAb (3 Cit). As shown in **Figure 2C**, CitH3 mAb (4 Cit) showed significantly higher optical density (OD) than the CitH3 mAb (3 Cit) in detecting CitH3 peptide at various concentrations. Most importantly, a higher concentration of CitH3 was detected using CitH3 mAb (4 Cit) compared to the CitH3 mAb (3 Cit) in a mouse model of endotoxic shock (the right panel of **Figure 2C**).

Taken together, these findings suggest that CitH3 mAb (4 Cit) not only has specificity comparable to CitH3 mAb (3 Cit) but also possesses higher binding capabilities and recognizes more citrulline residues such as histone H3 citrullinated R2+R8+R17.

The CitH3 mAb (4 Cit) Improves Survival Compared to CitH3 mAb (3 Cit) Following LPS-Induced Endotoxic Shock

After validation of the CitH3 mAb (4 Cit), we evaluated whether the new antibody could improve survival in a mouse model of LPS-induced endotoxic shock. It has been shown previously that CitH3 appears within 30 min of endotoxic shock (18, 23). In the present study, mice were intravenously administrated anti-CitH3 mAb immediately after LPS injection. The potential non-specific therapeutic effects of immunoglobulin were controlled in a parallel cohort by giving mouse IgG treatment. Survival was monitored for 10 days (**Figure 3A**). The CitH3 mAb (4 Cit) treatment significantly improved the survival rate of endotoxic mice compared to either LPS + IgG (44.44 vs. 0%; $p = 0.0004$) or LPS + CitH3 mAb (3 Cit) group (44.44 vs. 11.11%; $p = 0.0039$). In addition, a significant decrease was observed in the serum IL-1β and TNF-α levels with CitH3 mAb (4 Cit) treatment at the 12-h time point, compared to either the LPS + IgG group ($p < 0.001$ and $p < 0.01$, respectively) or the LPS + CitH3 mAb (3 Cit) group ($p < 0.01$ and $p < 0.05$, respectively) (**Figure 3B**).

These data revealed that the new CitH3 mAb (4 Cit) could effectively protect the mice from lethal endotoxic shock, and significantly ameliorate the pro-inflammatory effects caused by LPS administration, in comparison with CitH3 mAb (3 Cit) and mouse IgG.

The CitH3 mAb (4 Cit) Protects Against LPS-Induced ALI

Sepsis causes end-organ dysfunction, and septic patients are particularly at the risk of developing ALI (31). Moreover, ALI is one of the leading causes of mortality in septic patients (32). Therefore, we examined pathological changes in the lung 12 h after LPS insult, using H&E staining. As shown in the left panel of **Figure 4A**, IgG injected control animals showed normal histology, while the lungs from the LPS + IgG group displayed obvious inflammatory changes: inflammatory infiltrates, pulmonary congestion, edema, alveolar hemorrhage,

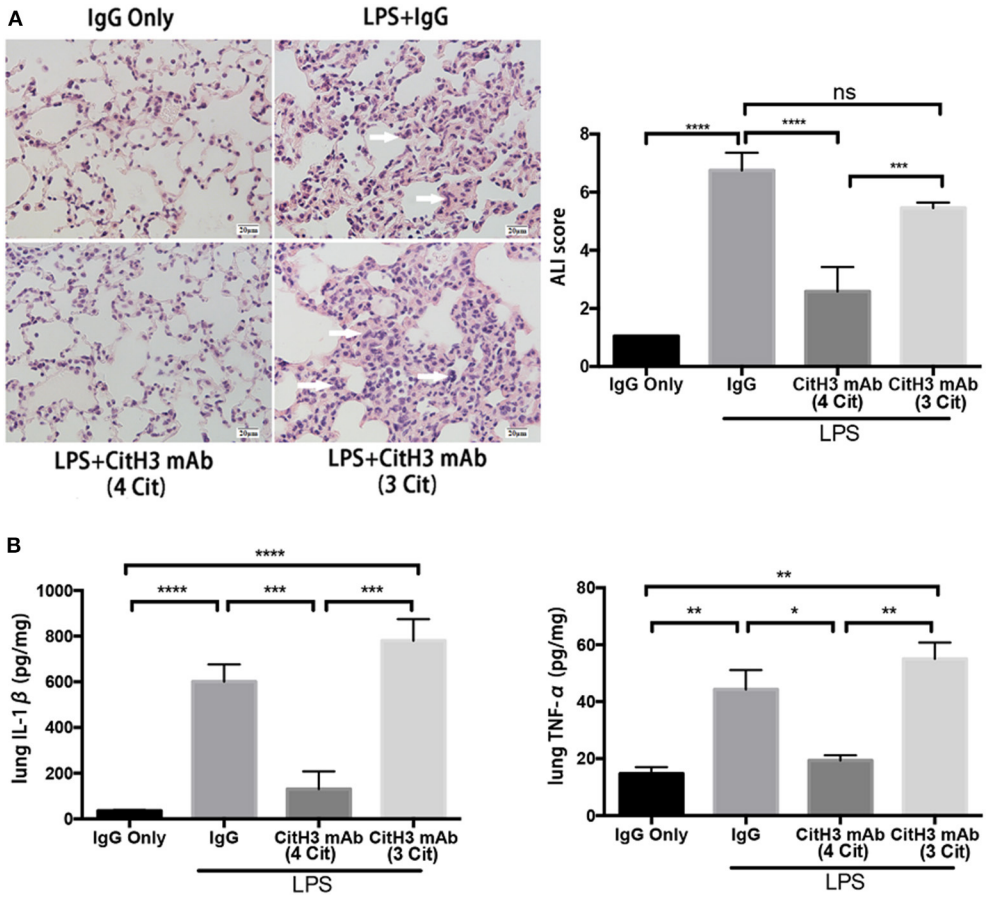

FIGURE 4 | The CitH3 mAb (4 Cit) ameliorates acute lung injury in lethal endotoxic shock. Mice were randomly divided into four groups: (1) IgG only (20 mg/kg), (2) LPS (20 mg/kg) + IgG (20 mg/kg), (3) LPS + CitH3 mAb (4 Cit) (20 mg/kg), and (4) LPS + CitH3 mAb (3 Cit) (20 mg/kg) (n = 3/group). Blood and organs were harvested at 12 h after LPS injection. **(A)** Representative hematoxylin and eosin staining of mouse lung sections is shown, and histological analysis of acute lung injury (ALI) was graded by a blinded pathologist and presented as ALI score (mean ± SEM, n = 3/group). White arrows indicate inflammatory changes. **(B)** IL-1β and TNF-α of lung homogenates were determined by ELISA. Cytokine levels were normalized by protein concentration and were significantly lower in CitH3 mAb (4 Cit)-treated mice (mean ± SEM, n = 3/group). *$p < 0.05$; **$p < 0.01$; ***$p < 0.001$; ****$p < 0.0001$. ns, non significance.

and thickening of the alveolar wall. The CitH3 mAb (4 Cit) administration markedly ameliorated the histopathology changes induced by LPS. On the contrary, the CitH3 mAb (3 Cit) treatment was unable to protect the lungs against ALI.

The severity of lung injury was further quantitatively evaluated by a pathologist, blinded to the group allocation of the samples, by calculating the ALI score (**Figure 4A**). Lung septal mononuclear cell/lymphocyte, septal hemorrhage and congestion, neutrophils, alveolar macrophages, alveolar hemorrhage, and alveolar edema were assessed (see Materials and Methods). The ALI score was significantly increased after LPS insult (LPS + IgG vs. IgG: 6.750 ± 0.351 vs. 1.050 ± 0.000; $p < 0.0001$); however, the score was markedly reduced more than two-fold in the CitH3 mAb (4 Cit) treatment group [LPS + CitH3 mAb (4 Cit) vs. LPS + IgG: 2.583 ± 0.483 vs. 6.750 ± 0.3512; $p < 0.0001$]. The effects of CitH3 mAb (3 Cit) were not as strong as the CitH3 mAb (4 Cit). Even though the mean ALI score value of the LPS + CitH3 mAb (3 Cit) group was slightly lower than the LPS + IgG group, there were no statistical difference between the groups [LPS + CitH3 mAb (3 Cit) vs. LPS + IgG: 5.457 ± 0.107 vs. 6.750 ± 0.3512; $p < 0.0001$].

We also measured the levels of IL-1β and TNF-α in the lung homogenate. A significant decrease in lung IL-1β [LPS + CitH3 mAb (4 Cit) vs. LPS + IgG: 130.7 ± 44.67 vs. 601.0 ± 43.47 pg/mg; $p < 0.001$] and TNF-α [LPS + CitH3 mAb (4 Cit) vs. LPS + IgG: 19.33 ± 1.856 vs. 44.33 ± 6.741 pg/mg; $p < 0.01$] after CitH3 mAb (4 Cit) treatment was observed, in accordance with the serum IL-1β and TNF-α changes. However, the CitH3 mAb (3 Cit) could not effectively decrease IL-1β [LPS + CitH3 mAb (3 Cit) vs. LPS + IgG: 780 ± 54.5 vs. 601.0 ± 43.47 pg/mg; ns] or TNF-α [LPS + CitH3 mAb (3 Cit) vs. LPS + IgG: 55.00 ± 5.774 vs. 44.33 ± 6.741 pg/mg; ns]. In these experiments, the sample size may seem low (n = 3/group) but the results reach significant difference ($p < 0.05$) based on our statistical analysis.

Taken together, administration of CitH3 mAb (4 Cit), but not CitH3 mAb (3 Cit), was found to protect against LPS-induced ALI and attenuate the inflammatory cytokines.

Administration of CitH3 mAb (4 Cit) Decreases Serum Levels of dsDNA

Since CitH3 is generally considered a component of NETs, the binding of the anti-CitH3 antibody and the antigen might affect NETs in the circulation.

dsDNA levels were significantly decreased after the CitH3 mAb (4 Cit) treatment [LPS + IgG vs. LPS + CitH3 mAb (4 Cit): 9.047 ± 0.816 vs. 2.537 ± 0.3767 μg/ml; $p < 0.001$]. However, this was not observed with the CitH3 mAb (3 Cit) [LPS + IgG vs. LPS + CitH3 mAb (3 Cit): 9.047 ± 0.816 vs. 10.72 ± 0.68 μg/ml; ns]. Moreover, the CitH3 mAb (4 Cit) treatment group had less dsDNA compared with the 3 Cit mAb [LPS + CitH3 mAb (4 Cit) vs. LPS + 3 Cit mAb: 2.537 ± 0.3767 vs. 10.72 ± 0.68 μg/ml; $p < 0.0001$].

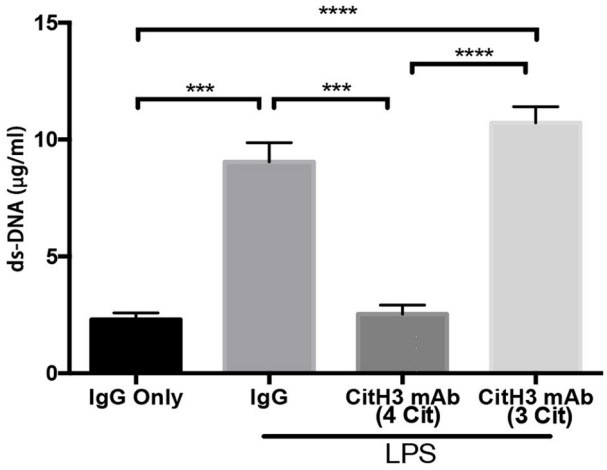

FIGURE 5 | The CitH3 mAb (4 Cit) decreases serum dsDNA. Mice were randomly divided into four groups: (1) IgG only (20 mg/kg), (2) LPS (20 mg/kg) + IgG (20 mg/kg), (3) LPS + 4 CitH3 mAb (20 mg/kg), and (4) LPS + CitH3 mAb (3 Cit) (20 mg/kg) ($n = 3$/group). Blood was harvested at 12 h after LPS injection. dsDNA was measured using PicoGreen assay kit and expressed as mean ± SEM ($n = 3$/group). ***$p < 0.001$; ****$p < 0.0001$.

DISCUSSION

In the current study, we have demonstrated that exposure to CitH3 can increase endothelial cell leakage and induce the formation of NETs through a positive feedback system. We neutralized the circulating CitH3 with a newly developed CitH3 mAb (4 Cit) that strongly binds to four citrulline sites on CitH3, in comparison with the commercial CitH3 mAb (3 Cit) that binds to only three citrulline sites. We found that injection of CitH3 mAb (4 Cit) markedly improves survival following LPS-induced lethal endotoxic shock and attenuates pro-inflammatory responses, ALI, as well as NET formation. Our antibody fills the gap in the field of citrullinated histone that was reported by Neeli and Radic, "current challenges and limitations in antibody-based detection of citrullinated histones," in *Frontiers in Immunology* (28). In addition, we believe that CitH3 can be a potential target for directed therapies in endotoxic patients in the future.

Neutrophils are the most abundant innate immune cells in humans, and their functions include phagocytosis of pathogens, release of multiple inflammatory mediators, and induction of NET formation. Release of NETs by neutrophils was first discovered by Brinkman et al. (4), and has attracted significant interest in recent years. NETs have been found to play key roles in various diseases including sepsis, tumors, systemic lupus erythematosus (SLE), rheumatoid arthritis (RA), gout, and others (15). NETs also play a key role in sepsis. NETs are able to trap microbes and keep them in a restricted area with high concentrations of anti-microbial agents, which are released as components of NETs (33). DNA itself has been reported to possess anti-microbial activities (34). Histones and histone-like proteins also function as microbial-combating reagents in a variety of species (35). However, unless carefully controlled, excessive NETs and components of NETs can be detrimental in sepsis. Histones and citrullinated histones are both components of NETs and have been found to be elevated in sepsis. Histones bind to endothelial cells, cause an increase in endothelial cell permeability and Ca^{2+} influx, eventually leading to cell death (36). Histones also promote thrombosis through impairing thrombomodulin-dependent protein C activation (37, 38). In addition, extracellular histones have been found to mediate liver injury through toll-like receptor 2 (TLR2) and TLR4 (39). Unlike histones, the role of citrullinated histones in diseases remains largely unknown. CitH3 release has been detected in blood and peritoneal fluid in sepsis (17, 18, 23); however, the effects of CitH3 production and its pathophysiologic roles in sepsis are unclear.

There are multiple ways to induce septic response in animals: (1) LPS, bacterial, or cecal slurry injection; (2) endogenic protection barrier model, such as CLP and colon ascendens stent peritonitis (CASP); and (3) extra-abdominal models of sepsis: pneumonia and urosepsis (40). Due to its stability, repeatability, and long track record (41), we selected LPS-induced endotoxic shock as a starting model to test the therapeutic efficacy of the CitH3 mAb (4 Cit). The commercial anti-CitH3 mAb (3 Cit) detected H3 citrullinated R2+R8+R16 and served as a control. Improved survival was observed in the CitH3 mAb (4 Cit)-treated mice compared to the CitH3 mAb (3 Cit) or IgG-treated endotoxic mice (**Figure 3A**). Several reasons might contribute to the better outcome after CitH3 mAb (4 Cit) administration: (1) less endothelial leakage (**Figure 1A**); (2) inhibited inflammatory responses (**Figure 3B**, **Figure 4B**); (3) attenuated ALI (**Figure 4A**); and (4) decreased formation of NETs (**Figure 5**).

Endothelial dysfunction is the main reason for multiple organ failure in sepsis, since it causes tissue edema, disarrangement of hemostasis, and vasomotor control, eventually leading to death (42). In this study, the CitH3 peptide was shown to increase permeability of HUVECs *in vitro* (**Figure 1A**). In addition, infusion of CitH3 protein has been shown to induce an extravasation of fluorescent-labeled albumin across mouse mesenteric micro vessels without cell death (25). These observations suggest that CitH3 might be one of the causes for vascular leakage and organ edema in sepsis.

Release of cytokines, for example, IL-1β and TNF-α, can activate and recruit effector inflammatory cells to the site of infection. However, excessive or deregulated cytokine profile is a common occurrence in sepsis, exerting harmful effects

both systemically and locally. The level of TNF-α in septic patients correlates with fatal outcome (43). Persistent elevation of cytokine concentrations in patient plasma, including TNF-α and IL-1β, is associated with poor prognosis in septic patients with acute respiratory distress syndrome (ARDS) (44). The fact that CitH3 mAb (4 Cit) can decrease the levels of circulating IL-1β and TNF-α (**Figure 3B**) could attenuate the adverse effects that result from excessive cytokine release.

ALI is one of the most frequent complications to develop in septic patients and among the leading causes of deaths in these patients (32). In our experimental LPS model, survival correlated strongly with reduced lung injury. Endotoxic mice treated with the CitH3 mAb (4 Cit) had better lung histology (lower ALI score) as well as much less pro-inflammatory cytokines in lung, compared to the mice treated with IgG or the CitH3 mAb (3 Cit) (**Figure 4A**). The alleviated ALI might be one of the mechanisms responsible for the significantly better survival in the CitH3 mAb (4 Cit)-treated mice. Endotoxin/sepsis-induced inflammatory responses are important defense mechanisms in disease conditions; however, they can also contribute to the development of ALI. Endothelial cells, epithelial cells, resident alveolar macrophages, and neutrophils secrete cytokines and chemokines, leading to an increase in tissue inflammation and subsequent cellular damage. Among the cytokines, IL-1β and TNF-α are major cytokines released into the alveolar spaces of patients with ARDS (45). In our study, we also found elevated levels of IL-1β and TNF-α in lung homogenates (**Figure 4B**). IL-1β and TNF-α are known to exaggerate the inflammatory responses initiated by endotoxin, which could result in adverse consequences. We have shown that administration of CitH3 mAb (4 Cit) significantly attenuated the local concentrations of IL-1β and TNF-α in the lung, which could be protective against development of ALI.

Our results (**Figure 1C**) also suggest that CitH3 can induce NET formation through a positive feedback mechanism. There is plenty of evidence showing the detrimental role of NETs (15). NETs can damage epithelium, endothelium, and various tissues including liver and lung (36, 46–48); moreover, NETs promote thrombosis, leading to vasculature occlusion (49–52). The level of circulating dsDNA has been shown to correlate with disseminated intravascular coagulation (DIC) score and predicts DIC independently (53). In this study, the CitH3 mAb (4 Cit) efficiently inhibited this positive feedback loop, leading to less formation of CitH3/NETs (**Figure 5**). The underlying mechanism may be that the mAb (4 Cit) binds to CitH3 and forms immune complex, which are further cleared by immune system (54, 55). The DNA backbone and associated proteins may also be eliminated along with the ICs. Therefore, neutralizing CitH3 directly decreased free CitH3 in circulation, as well as blocking the positive feedback to inhibit CitH3 self-amplification, thus preventing the endothelial dysfunction caused by CitH3.

The major difference between the CitH3 mAb (4 Cit) and the CitH3 mAb (3 Cit) is thought to be secondary to their relative abilities to neutralize the CitH3 protein. The newly developed CitH3 mAb (4 Cit) recognizes four citrulline sites: H3 citrullinated R2+R8+R17+R26, while the CitH3 mAb (3 Cit) is only designed for three citrulline spots: H3 citrullinated R2+R8+R17. As demonstrated by immunoblotting and ELISA (**Figure 2**), the CitH3 mAb (4 Cit) specifically recognized H3 R26 citrullination and had a stronger capability to bind CitH3. In addition, different citrullination may correspond to different PADs. Among the five PAD isoforms that have been discovered, only PAD2 and PAD4 have been demonstrated by several lines of evidence to translocate from cytosol to nucleus and citrullinate histone H3. We reasoned that CitH3 in sepsis originated from PAD2 or PAD4 pathways, or both. It has been reported that H3 R26 is a valid target for PAD2, but not PAD4 (30). Therefore, the CitH3 mAb (4 Cit) is suspected to bind and neutralize more circulating CitH3. The one citrulline difference partly contributes to the binding ability discrepancy between these two antibodies.

Wang et al. have demonstrated in *Science* that PAD4 deiminates three arginine residues on H3 at Arg 2, Arg 8, and Arg 17 *in vitro*, and two arginine residues on H3 at Arg 8 and Arg 17 *in vivo* (29). It is not clear what causes the different citrullinations. Basically, an enzyme's active site binds substrates and plays a role in catalysis. It is conceivable that some proteins might bind to histone H3 in the *in vivo* condition and therefore prevent H3 from citrullination by PAD4.

Our interpretations regarding differential PAD2/PAD4 involvement in CitH3 production is supposed not only by the data from this study but also by previous reports by other investigators (29). These findings will need additional verification in the future, and more mechanistic experiments will have to be performed to fully understand this complex process.

In this study, we decided to use the histone H3 peptide for several reasons. *First*, the N-terminal tail (N-tail) of histone H3, which protrudes beyond the nucleosome DNA (56), is regulated by multiple posttranslational modifications (PTMs) (57). Focusing on citrullination of the N-tail, we synthesized N-terminal CitH3 peptide, instead of CitH3 protein, to ensure that histone H3 is citrullinated at the N-terminus of four arginine residues. *Second*, the commercial CitH3 (citrulline R2+R8+R17) (58, 59) antibodies, including Item 9003062 (Cayman Chemical, Ann Arbor, MI) and ab5103 (abcam, Cambridge, MA), are generated with CitH3 N-tail peptide. To compare our CitH3 mAb (4 Cit) to the commercial CitH3 mAb (3 Cit), it is more appropriate to use the N-terminal CitH3 peptide as an antigen. *Third*, histone H3 (citrullinated or non-citrullinated) epitope(s) can be cleaved off at the N-terminus of H3 (60). To determine the effect of the N-tail of H3 and CitH3 *in vitro*, it is logical to use the N-terminal H3/CitH3 peptide as the stimulus.

There are several limitations to this study. We only used a murine endotoxic shock model to test the therapeutic effects of the CitH3 mAb (4 Cit); however, further evaluation is required in different models of bacterial and polymicrobial infections. In addition, more mechanism studies are needed. For example, further exploration of CitH3 in diverse cell signaling pathways is helpful to better explain how the CitH3 mAb (4 Cit) improves outcomes in endotoxic shock.

In conclusion, we have demonstrated that CitH3 can increase endothelial cell leakage and self-amplify through positive feedback. Neutralizing circulating CitH3 with the CitH3 mAb (4 Cit) markedly increases mouse survival from LPS-induced

lethal endotoxic shock, likely secondary to the CitH3 mAb (4 Cit) binding to CitH3 and specifically recognizing H3 R26 citrullination. The CitH3 mAb (4 Cit) also attenuates pro-inflammatory responses, ALI, as well as NET formation, compared to the CitH3 mAb (3 Cit). Overall, these results suggest that sufficient neutralization of CitH3 might be a promising therapeutic strategy for endotoxic shock.

DATA AVAILABILITY STATEMENT

All datasets generated for this study are included in the article.

ETHICS STATEMENT

The protocol for the animal experiments was approved by the University of Michigan Institutional Animal Care and Use Committee (PRO00008861). All experiments complied with animal welfare and research regulations.

AUTHOR CONTRIBUTIONS

YLi and HA designed this study. QD, BP, and YLia performed the experiments and collected and analyzed data. BL, YT, AW, and JZ provided experimental support. XD pathologically examined the lung tissues. QD wrote the manuscript, which was critically reviewed and revised by YLi, HA, NM-V, ZW, and AW. All authors read and approved the final manuscript.

FUNDING

This work was funded by grants from Mcubed U049657 and Kickstart N022142 to YLi, SIS to AW, and UMHS-PUHSC Joint Institute U050150 to HA.

REFERENCES

1. Singer M, Deutschman CS, Seymour CW, Shankar-Hari M, Annane D, Bauer M, et al. The third international consensus definitions for sepsis and septic shock (Sepsis-3). *JAMA*. (2016) 315:801–10. doi: 10.1001/jama.2016.0287
2. Hudson LD, Milberg JA, Anardi D, Maunder RJ. Clinical risks for development of the acute respiratory distress syndrome. *Am J Respir Crit Care Med.* (1995) 151:293–301. doi: 10.1164/ajrccm.151.2.7842182
3. Shen XF, Cao K, Jiang JP, Guan WX, Du JF. Neutrophil dysregulation during sepsis: an overview and update. *J Cell Mol Med.* (2017) 21:1687–97. doi: 10.1111/jcmm.13112
4. Brinkmann V, Reichard U, Goosmann C, Fauler B, Uhlemann Y, Weiss DS, et al. Neutrophil extracellular traps kill bacteria. *Science.* (2004) 303:1532–5. doi: 10.1126/science.1092385
5. Dabrowska D, Jablonska E, Garley M, Ratajczak-Wrona W, Iwaniuk, A. New aspects of the biology of neutrophil extracellular traps. *Scand J Immunol.* (2016) 84:317–22. doi: 10.1111/sji.12494
6. Wang Y, Li M, Stadler S, Correll S, Li P, Wang D, et al. Histone hypercitrullination mediates chromatin decondensation and neutrophil extracellular trap formation. *J Cell Biol.* (2009) 184:205–13. doi: 10.1083/jcb.200806072
7. Obermayer A, Stoiber W, Krautgartner WD, Klappacher M, Kofler B, Steinbacher P, et al. New aspects on the structure of neutrophil extracellular traps from chronic obstructive pulmonary disease and *in vitro* generation. *PLoS ONE.* (2014) 9:e97784. doi: 10.1371/journal.pone.0097784
8. Kaplan MJ, Radic, M. Neutrophil extracellular traps: double-edged swords of innate immunity. *J Immunol.* (2012) 189:2689–95. doi: 10.4049/jimmunol.1201719
9. Guimaraes-Costa AB, Nascimento MT, Froment GS, Soares RP, Morgado FN, Conceicao-Silva F, et al. Leishmania amazonensis promastigotes induce and are killed by neutrophil extracellular traps. *Proc Natl Acad Sci USA*. (2009) 106:6748–53. doi: 10.1073/pnas.0900226106
10. Baker VS, Imade GE, Molta NB, Tawde P, Pam SD, Obadofin MO, et al. Cytokine-associated neutrophil extracellular traps and antinuclear antibodies in *Plasmodium falciparum* infected children under six years of age. *Malar J.* (2008) 7:41. doi: 10.1186/1475-2875-7-41
11. Beiter K, Wartha F, Albiger B, Normark S, Zychlinsky A, Henriques-Normark B. An endonuclease allows *Streptococcus pneumoniae* to escape from neutrophil extracellular traps. *Curr Biol.* (2006) 16:401–7. doi: 10.1016/j.cub.2006.01.056
12. Buchanan JT, Simpson AJ, Aziz RK, Liu GY, Kristian SA, Kotb M, et al. DNase expression allows the pathogen group A Streptococcus to escape killing in neutrophil extracellular traps. *Curr Biol.* (2006) 16:396–400. doi: 10.1016/j.cub.2005.12.039
13. Saitoh T, Komano J, Saitoh Y, Misawa T, Takahama M, Kozaki T, et al. Neutrophil extracellular traps mediate a host defense response to human immunodeficiency virus-1. *Cell Host Microbe.* (2012) 12:109–16. doi: 10.1016/j.chom.2012.05.015
14. Urban CF, Reichard U, Brinkmann V, Zychlinsky A. Neutrophil extracellular traps capture and kill *Candida albicans* yeast and hyphal forms. *Cell Microbiol.* (2006) 8:668–76. doi: 10.1111/j.1462-5822.2005.00659.x
15. Papayannopoulos V. Neutrophil extracellular traps in immunity and disease. *Nat Rev Immunol.* (2018) 18:134–47. doi: 10.1038/nri.2017.105
16. Zhao T, Pan B, Alam HB, Liu B, Bronson RT, Deng Q, et al. Protective effect of Cl-amidine against CLP-induced lethal septic shock in mice. *Sci Rep.* (2016) 6:36696. doi: 10.1038/srep36696
17. Biron BM, Chung CS, O'Brien XM, Chen Y, Reichner JS, Ayala A. Cl-amidine prevents histone 3 citrullination and neutrophil extracellular trap formation, and improves survival in a murine sepsis model. *J Innate Immun.* (2017) 9:22–32. doi: 10.1159/000448808
18. Liang Y, Pan B, Alam HB, Deng Q, Wang Y, Chen E, et al. Inhibition of peptidylarginine deiminase alleviates LPS-induced pulmonary dysfunction and improves survival in a mouse model of lethal endotoxemia. *Eur J Pharmacol.* (2018) 833:432–40. doi: 10.1016/j.ejphar.2018.07.005
19. Laukova L, Konecna B, Babickova J, Wagnerova A, Meliskova V, Vlkova B, et al. Exogenous deoxyribonuclease has a protective effect in a mouse model of sepsis. *Biomed Pharmacother.* (2017) 93:8–16. doi: 10.1016/j.biopha.2017.06.009
20. Mai SH, Khan M, Dwivedi DJ, Ross CA, Zhou J, Gould TJ, et al. Delayed but not early treatment with DNase reduces organ damage and improves outcome in a murine model of sepsis. *Shock.* (2015) 44:166–72. doi: 10.1097/SHK.0000000000000396
21. Xu J, Zhang X, Pelayo R, Monestier M, Ammollo CT, Semeraro F, et al. Extracellular histones are major mediators of death in sepsis. *Nat Med.* (2009) 15:1318–21. doi: 10.1038/nm.2053
22. Kraaij T, Tengstrom FC, Kamerling SW, Pusey CD, Scherer HU, Toes RE, et al. A novel method for high-throughput detection and quantification of neutrophil extracellular traps reveals ROS-independent NET release with immune complexes. *Autoimmun Rev.* (2016) 15:577–84. doi: 10.1016/j.autrev.2016.02.018
23. Pan B, Alam HB, Chong W, Mobley J, Liu B, Deng Q, et al. CitH3: a reliable blood biomarker for diagnosis and treatment of endotoxic shock. *Sci Rep.* (2017) 7:8972. doi: 10.1038/s41598-017-09337-4
24. Mor-Vaknin N, Saha A, Legendre M, Carmona-Rivera C, Amin MA, Rabquer BJ, et al. DEK-targeting DNA aptamers as therapeutics for inflammatory arthritis. *Nat Commun.* (2017) 8:14252. doi: 10.1038/ncomms14252

25. Meegan JE, Yang X, Beard RS Jr, Jannaway M, Chatterjee V, Taylor-Clark TE, et al. Citrullinated histone 3 causes endothelial barrier dysfunction. *Biochem Biophys Res Commun.* (2018) 503:1498–502. doi: 10.1016/j.bbrc.2018.07.069
26. Mamat U, Wilke K, Bramhill D, Schromm AB, Lindner B, Kohl TA, et al. Detoxifying *Escherichia coli* for endotoxin-free production of recombinant proteins. *Microb Cell Fact.* (2015) 14:57. doi: 10.1186/s12934-015-0241-5
27. Schwarz H, Schmittner M, Duschl A, Horejs-Hoeck J. Residual endotoxin contaminations in recombinant proteins are sufficient to activate human CD1c+ dendritic cells. *PLoS ONE.* (2014) 9:e113840. doi: 10.1371/journal.pone.0113840
28. Neeli I, Radic M. Current challenges and limitations in antibody-based detection of citrullinated histones. *Front Immunol.* (2016) 7:528. doi: 10.3389/fimmu.2016.00528
29. Wang Y, Wysocka J, Sayegh J, Lee YH, Perlin JR, Leonelli L, et al. Human PAD4 regulates histone arginine methylation levels via demethylimination. *Science.* (2004) 306:279–83. doi: 10.1126/science.1101400
30. Zhang X, Bolt M, Guertin MJ, Chen W, Zhang S, Cherrington BD, et al. Peptidylarginine deiminase 2-catalyzed histone H3 arginine 26 citrullination facilitates estrogen receptor alpha target gene activation. *Proc Natl Acad Sci USA.* (2012) 109:13331–6. doi: 10.1073/pnas.1203280109
31. Martin GS, Mannino DM, Eaton S, Moss M. The epidemiology of sepsis in the United States from 1979 through 2000. *N Engl J Med.* (2003) 348:1546–54. doi: 10.1056/NEJMoa022139
32. Varisco BM. The pharmacology of acute lung injury in sepsis. *Adv Pharmacol Sci.* (2011) 2011:254619. doi: 10.1155/2011/254619
33. Nauseef WM. How human neutrophils kill and degrade microbes: an integrated view. *Immunol Rev.* (2007) 219:88–102. doi: 10.1111/j.1600-065X.2007.00550.x
34. Halverson TW, Wilton M, Poon KK, Petri B, Lewenza S. DNA is an antimicrobial component of neutrophil extracellular traps. *PLoS Pathog.* (2015) 11:e1004593. doi: 10.1371/journal.ppat.1004593
35. Hoeksema M, van Eijk M, Haagsman HP, Hartshorn KL. Histones as mediators of host defense, inflammation and thrombosis. *Future Microbiol.* (2016) 11:441–53. doi: 10.2217/fmb.15.151
36. Saffarzadeh M, Juenemann C, Queisser MA, Lochnit G, Barreto G, Galuska SP, et al. Neutrophil extracellular traps directly induce epithelial and endothelial cell death: a predominant role of histones. *PLoS ONE.* (2012) 7:e32366. doi: 10.1371/journal.pone.0032366
37. Ammollo CT, Semeraro F, Xu J, Esmon NL, Esmon CT. Extracellular histones increase plasma thrombin generation by impairing thrombomodulin-dependent protein C activation. *J Thromb Haemost.* (2011) 9:1795–803. doi: 10.1111/j.1538-7836.2011.04422.x
38. Semeraro F, Ammollo CT, Morrissey JH, Dale GL, Friese P, Esmon NL, et al. Extracellular histones promote thrombin generation through platelet-dependent mechanisms: involvement of platelet TLR2 and TLR4. *Blood.* (2011) 118:1952–61. doi: 10.1182/blood-2011-03-343061
39. Xu J, Zhang X, Monestier M, Esmon NL, Esmon CT. Extracellular histones are mediators of death through TLR2 and TLR4 in mouse fatal liver injury. *J Immunol.* (2011) 187:2626–31. doi: 10.4049/jimmunol.1003930
40. Lewis AJ, Seymour CW, Rosengart MR. Current murine models of sepsis. *Surg Infect.* (2016) 17:385–93. doi: 10.1089/sur.2016.021
41. Remick DG, Ward PA. Evaluation of endotoxin models for the study of sepsis. *Shock.* (2005) 24:7–11. doi: 10.1097/01.shk.0000191384.34066.85
42. Ince C, Mayeux PR, Nguyen T, Gomez H, Kellum JA, Ospina-Tascon GA, et al. The endothelium in sepsis. *Shock.* (2016) 45:259–70. doi: 10.1097/SHK.0000000000000473
43. Martin C, Boisson C, Haccoun M, Thomachot L, Mege JL. Patterns of cytokine evolution (tumor necrosis factor-alpha and interleukin-6) after septic shock, hemorrhagic shock, and severe trauma. *Crit Care Med.* (1997) 25:1813–9. doi: 10.1097/00003246-199711000-00018
44. Meduri GU, Headley S, Kohler G, Stentz F, Tolley E, Umberger R, et al. Persistent elevation of inflammatory cytokines predicts a poor outcome in ARDS. *Chest.* (1995) 107:1062–73. doi: 10.1378/chest.107.4.1062
45. Meduri GU, Kohler G, Headley S, Tolley E, Stentz F, Postlethwaite A. Inflammatory cytokines in the BAL of patients with ARDS. Persistent elevation over time predicts poor outcome. *Chest.* (1995) 108:1303–14. doi: 10.1378/chest.108.5.1303
46. Villanueva E, Yalavarthi S, Berthier CC, Hodgin JB, Khandpur R, Lin AM, et al. Netting neutrophils induce endothelial damage, infiltrate tissues, and expose immunostimulatory molecules in systemic lupus erythematosus. *J Immunol.* (2011) 187:538–52. doi: 10.4049/jimmunol.1100450
47. Huang H, Tohme S, Al-Khafaji AB, Tai S, Loughran P, Chen L, et al. Damage-associated molecular pattern-activated neutrophil extracellular trap exacerbates sterile inflammatory liver injury. *Hepatology.* (2015) 62:600–14. doi: 10.1002/hep.27841
48. Narasaraju T, Yang E, Samy RP, Ng HH, Poh WP, Liew A-A, et al. Excessive neutrophils and neutrophil extracellular traps contribute to acute lung injury of influenza pneumonitis. *Am J Pathol.* (2011) 179:199–210. doi: 10.1016/j.ajpath.2011.03.013
49. Fuchs TA, Brill A, Duerschmied D, Schatzberg D, Monestier M, Myers DD Jr, et al. Extracellular DNA traps promote thrombosis. *Proc Natl Acad Sci USA.* (2010) 107:15880–5. doi: 10.1073/pnas.1005743107
50. Martinod K, Demers M, Fuchs TA, Wong SL, Brill A, Gallant M, et al. Neutrophil histone modification by peptidylarginine deiminase 4 is critical for deep vein thrombosis in mice. *Proc Natl Acad Sci USA.* (2013) 110:8674–9. doi: 10.1073/pnas.1301059110
51. Jiménez-Alcázar M, Napirei M, Panda R, Köhler EC, Kremer Hovinga JA, Mannherz HG, et al. Impaired DNase1-mediated degradation of neutrophil extracellular traps is associated with acute thrombotic microangiopathies. *J Thromb Haemost.* (2015) 13:732–42. doi: 10.1111/jth.12796
52. Brill A, Fuchs TA, Savchenko AS, Thomas GM, Martinod K, De Meyer SF, et al. Neutrophil extracellular traps promote deep vein thrombosis in mice. *J Thromb Haemost.* (2012) 10:136–44. doi: 10.1111/j.1538-7836.2011.04544.x
53. Kim JE, Lee N, Gu JY, Yoo HJ, Kim HK. Circulating levels of DNA-histone complex and dsDNA are independent prognostic factors of disseminated intravascular coagulation. *Thromb Res.* (2015) 135:1064–9. doi: 10.1016/j.thromres.2015.03.014
54. Rojko JL, Evans MG, Price SA, Han B, Waine G, DeWitte M, et al. Formation, clearance, deposition, pathogenicity, and identification of biopharmaceutical-related immune complexes: review and case studies. *Toxicol Pathol.* (2014) 42:725–64. doi: 10.1177/0192623314526475
55. Wootla B, Denic A, Rodriguez, M. Polyclonal and monoclonal antibodies in clinic. *Methods Mol Biol.* (2014) 1060:79–110. doi: 10.1007/978-1-62703-586-6_5
56. Lowe BR, Maxham LA, Hamey JJ, Wilkins MR, Partridge JF. Histone H3 mutations: an updated view of their role in chromatin deregulation and cancer. *Cancers.* (2019) 11:E660. doi: 10.3390/cancers11050660
57. Shen J, Xiang X, Chen L, Wang H, Wu L, Sun Y, et al. JMJD5 cleaves monomethylated histone H3 N-tail under DNA damaging stress. *EMBO Rep.* (2017) 18:2131–2143. doi: 10.15252/embr.201743892
58. El Shikh MEM, El Sayed R, Nerviani A, Goldmann K, John CR, Hands R, et al. Extracellular traps and PAD4 released by macrophages induce citrullination and auto-antibody production in autoimmune arthritis. *J Autoimmun.* (2019) 105:102297. doi: 10.1016/j.jaut.2019.06.008
59. Horibata S, Coonrod SA, Cherrington BD. Role for peptidylarginine deiminase enzymes in disease and female reproduction. *J Reprod Dev.* (2012) 58:274–82. doi: 10.1262/jrd.2011-040
60. Zhou P, Wu E, Alam HB, Li Y. Histone cleavage as a mechanism for epigenetic regulation: current insights and perspectives. *Curr Mol Med.* (2014) 14:1164–72. doi: 10.2174/1566524014666141015155630

Conflict of Interest: YLi and HA are inventors on a patent application related to the CitH3 mAb (4Cit).

The remaining authors declare that the research was conducted in the absence of any commercial or financial relationships that could be construed as a potential conflict of interest.

Copyright © 2020 Deng, Pan, Alam, Liang, Wu, Liu, Mor-Vaknin, Duan, Williams, Tian, Zhang and Li. This is an open-access article distributed under the terms of the Creative Commons Attribution License (CC BY). The use, distribution or reproduction in other forums is permitted, provided the original author(s) and the copyright owner(s) are credited and that the original publication in this journal is cited, in accordance with accepted academic practice. No use, distribution or reproduction is permitted which does not comply with these terms.

frontiers in Immunology

ORIGINAL RESEARCH
published: 23 January 2020
doi: 10.3389/fimmu.2019.03152

Impaired Glucocorticoid Receptor Dimerization Aggravates LPS-Induced Circulatory and Pulmonary Dysfunction

Martin Wepler[1,2†], Jonathan M. Preuss[3†], Tamara Merz[1], Clair Hartmann[1,2], Ulrich Wachter[1], Oscar McCook[1], Josef Vogt[1], Sandra Kress[1], Michael Gröger[1], Marina Fink[1], Angelika Scheuerle[4], Peter Möller[4], Enrico Calzia[1], Ute Burret[3], Peter Radermacher[1], Jan P. Tuckermann[3] and Sabine Vettorazzi[3*]*

[1] Institute for Anesthesiologic Pathophysiology and Process Engineering, Ulm University, Ulm, Germany, [2] Department of Anesthesiology, University Hospital, Ulm, Germany, [3] Institute of Comparative Molecular Endocrinology (CME), Ulm University, Ulm, Germany, [4] Institute of Pathology, University Hospital, Ulm, Germany

OPEN ACCESS

Edited by:
Guochang Hu,
University of Illinois at Chicago,
United States

Reviewed by:
Monowar Aziz,
Feinstein Institute for Medical Research, United States
Claude Libert,
Flanders Institute for Biotechnology, Belgium

***Correspondence:**
Martin Wepler
martin.wepler@uni-ulm.de
Sabine Vettorazzi
sabine.vettorazzi@uni-ulm.de

†These authors have contributed equally to this work

Specialty section:
This article was submitted to Inflammation, a section of the journal Frontiers in Immunology

Received: 12 September 2019
Accepted: 30 December 2019
Published: 23 January 2020

Citation:
Wepler M, Preuss JM, Merz T, Hartmann C, Wachter U, McCook O, Vogt J, Kress S, Gröger M, Fink M, Scheuerle A, Möller P, Calzia E, Burret U, Radermacher P, Tuckermann JP and Vettorazzi S (2020) Impaired Glucocorticoid Receptor Dimerization Aggravates LPS-Induced Circulatory and Pulmonary Dysfunction. Front. Immunol. 10:3152. doi: 10.3389/fimmu.2019.03152

Background: Sepsis, that can be modeled by LPS injections, as an acute systemic inflammation syndrome is the most common cause for acute lung injury (ALI). ALI induces acute respiratory failure leading to hypoxemia, which is often associated with multiple organ failure (MOF). During systemic inflammation, the hypothalamus-pituitary-adrenal axis (HPA) is activated and anti-inflammatory acting glucocorticoids (GCs) are released to overcome the inflammation. GCs activate the GC receptor (GR), which mediates its effects via a GR monomer or GR dimer. The detailed molecular mechanism of the GR in different inflammatory models and target genes that might be crucial for resolving inflammation is not completely identified. We previously observed that mice with attenuated GR dimerization ($GR^{dim/dim}$) had a higher mortality in a non-resuscitated lipopolysaccharide (LPS)- and cecal ligation and puncture (CLP)-induced inflammation model and are refractory to exogenous GCs to ameliorate ALI during inflammation. Therefore, we hypothesized that impaired murine GR dimerization ($GR^{dim/dim}$) would further impair organ function in LPS-induced systemic inflammation under human like intensive care management and investigated genes that are crucial for lung function in this setup.

Methods: Anesthetized $GR^{dim/dim}$ and wildtype ($GR^{+/+}$) mice were challenged with LPS (10 mg·kg^{-1}, intraperitoneal) and underwent intensive care management ("lung-protective" mechanical ventilation, crystalloids, and norepinephrine) for 6 h. Lung mechanics and gas exchange were assessed together with systemic hemodynamics, acid-base status, and mitochondrial oxygen consumption (JO_2). Western blots, immunohistochemistry, and real time quantitative polymerase chain reaction were performed to analyze lung tissue and inflammatory mediators were analyzed in plasma and lung tissue.

Results: When animals were challenged with LPS and subsequently resuscitated under intensive care treatment, $GR^{dim/dim}$ mice had a higher mortality compared to $GR^{+/+}$ mice, induced by an increased need of norepinephrine to achieve hemodynamic targets.

After challenge with LPS, GR$^{dim/dim}$ mice also displayed an aggravated ALI shown by a more pronounced impairment of gas exchange, lung mechanics and increased osteopontin (Opn) expression in lung tissue.

Conclusion: Impairment of GR dimerization aggravates systemic hypotension and impairs lung function during LPS-induced endotoxic shock in mice. We demonstrate that the GR dimer is an important mediator of hemodynamic stability and lung function, possibly through regulation of Opn, during LPS-induced systemic inflammation.

Keywords: glucocorticoid receptor, lung function, endotoxic shock, inflammation, osteopontin

INTRODUCTION

Anti-inflammatory acting glucocorticoids (GCs) mediate their effects through the glucocorticoid receptor (GR). The GR is an intracellular, ligand-activated transcription factor, which regulates gene transcription as a protein dimer or monomer in several mechanisms: as a protein dimer it can bind palindromic DNA sequences (glucocorticoid response elements—GRE) or DNA half sites as a monomeric protein [GR monomer, (1)]. Further GR monomers potentially inhibit the activity of pro-inflammatory transcription factors, e.g., NF-κB (2–5), AP-1 (6–8), or IRF-3 (9–11). This trans-repression is one major mechanism of GCs anti-inflammatory effects (12). However, it was recently shown that GC mediated anti-inflammatory responses also crucially require gene activation during inflammation (13). Indeed, mice with a point mutation in the GR DNA-binding domain (GR^{dim}) exhibit less transactivation of GC-induced genes *in vivo* (1, 14) and fail to resolve inflammation in allergic (15), autoimmune (rheumatoid arthritis) (16), and systemic inflammation (17, 18).

Previously, we identified a novel mechanism by which GCs interfere with the pathogenesis of murine ALI, involving increased sphingosine kinase 1 (SphK1) gene expression and sphingosine-1-phosphate (S1P) production. The SphK1–S1P axis is recognized as an important regulator of endothelial barrier integrity that prevents lung inflammation (19, 20). In our previous study, we showed that the induction of SphK1 was GR dimerization dependent and therefore mice with an impaired GR dimerization (GR$^{dim/dim}$) had an impaired lung barrier function during systemic lipopolysaccharides (LPS)-induced inflammation and GC treatment (13).

However, all studies described so far were lacking simultaneous control of temperature, as well as hemodynamic, and respiratory support, which is standard in intensive care treatment. Moreover, if potential beneficial effects of GCs in the treatment of lung injury occur, it is yet not clear which mechanisms are involved. Therefore, we tested the effects of an impairment of the GR in a murine model of LPS-induced systemic inflammation when factors like temperature, hemodynamics, and respiration are controlled (intensive care management including measurements of hemodynamics, infusion of crystalloids and norepinephrine to achieve hemodynamic targets, lung-protective mechanical ventilation, determination of gas exchange) in the present study. During intensive care management additional information about metabolic and hemodynamic parameters are observed that were missing in the former studies. We report that a congenital deficiency of the GR dimer aggravates hypotension, impairs lung function, and increases mortality in LPS-challenged mice.

MATERIALS AND METHODS

This study was approved by the federal authorities for animal research of the Regierungspräsidium Tübingen, Baden-Wuerttemberg, Germany, and performed in adherence with the National Institutes of Health Guidelines on the Use of Laboratory Animals and the European Union "Directive 2010/63 EU on the protection of animals used for scientific purposes". GR$^{dim/dim}$ mice (Nr3c1^{tm3Gsc}) (21) were bred in a mixed background (129/SvEv × C57BL/6) and housed in the animal facility at University Ulm. GR$^{+/+}$ littermate controls were used as wild-type mice. Animals were kept under standardized conditions and were equally distributed in terms of age and body weight.

Implementation of General Anesthesia and Surgery

Surgery for all animals included induction of anesthesia with sevoflurane (2.5%; sevoflurane, Abbott, Wiesbaden, HE, Germany) as described previously (22, 23), followed by intraperitoneal injection (ip) of ketamine (120 $\mu g \cdot g^{-1}$; Ketanest-S, Pfizer, New York City, NY), midazolam (1.25 $\mu g \cdot g^{-1}$; Midazolam-ratiopharm, Ratiopharm, Ulm, BW, Germany), and fentanyl (0.25 $\mu g \cdot g^{-1}$; Fentanyl-hameln, Hameln Pharma Plus GmbH, Hameln, NI, Germany). Afterwards, animals were placed on a closed-loop-system for body temperature control (22, 23). Lung-protective mechanical ventilation using a small animal ventilator (FlexiVent, Scireq, MO, Canada) was performed via a tracheostomy (22, 23). Surgical instrumentation comprised catheters in the jugular vein, the carotid artery, and the bladder (22, 23). General anesthesia was titrated to guarantee complete tolerance against noxious stimuli and was sustained by continuous intravenous administration of ketamine, midazolam, and fentanyl to reach deep sedation. Animals were mechanically ventilated with ventilator settings being FiO_2 0.21%, respiratory rate 150·min^{-1}, tidal volume of 6 mL·kg^{-1}, and inspiratory/expiratory time ratio 1:2. Ventilation was modified to maintain an arterial $PaCO_2$ between 30 and

45 mmHg, and positive end-expiratory pressure (PEEP) was adjusted according to the arterial PaO_2 (PaO_2/FiO_2-ratio > 300 mmHg: PEEP = 3 cmH_2O; PaO_2/FiO_2-ratio < 300 mmHg: PEEP = 5 cmH_2O; PaO_2/FiO_2-ratio < 200 mmHg: PEEP = 8 cmH_2O) (22, 23). Recruitment maneuvers (5 s hold at 18 cm H_2O) were repeated hourly to avoid any impairment of thoraco-pulmonary compliance due to anesthesia- and/or supine position-induced atelectasis.

Induction of Systemic Inflammation

After surgical instrumentation, systemic inflammation was induced by intraperitoneal (i.p.) injection of lipopolysaccharides (LPS=lipopolysaccharide from *Escherichia coli* [055:B5], L2880 Sigma, 10 $mg \cdot kg^{-1}$, dissolved in 10 $\mu l \cdot g^{-1}$ phosphate buffered saline [PBS]). Mice were then resuscitated with crystalloids (30 $\mu l \cdot g^{-1} \cdot h^{-1}$, Jonosteril, Braun Medical, Melsungen, HE, Germany). As soon as the mean arterial blood pressure (MAP) dropped below 55 mmHg, infusion of norepinephrine was started to reach a MAP >55 mmHg during the 6 h of resuscitation (maximum infusion rate 1.5 $\mu g \cdot h^{-1}$). If blood pressure declined despite increasing doses of norepinephrine, the experiment was terminated. $GR^{+/+}$ mice, which received vehicle (10 $\mu l \cdot g^{-1}$ PBS) with subsequent resuscitation, served as controls.

Parameters of Lung Mechanics, Hemodynamics, Gas Exchange, and Metabolism

Systemic hemodynamics, body temperature, and static thoraco-pulmonary compliance were recorded hourly. Blood gas tensions, acid-base status, glycaemia, and lactatemia were assessed at the end of the resuscitation period via aterial blood gas analysis (ABL800 Felx; Radiometer, Krefeld, Germany) (22, 23). At the end of the experiment, animals were exsanguinated, blood and lung tissue were taken immediately thereafter, and prepared for further analyses (22, 23). All lung tissue was utilized due to organ size. The left lung was harvested for histology and IHC, whereas the right lung served for immunoblotting, expression analysis, and cytokine and chemokine evaluation.

Histological Analysis of Lung Tissue

Histological analysis of lung tissue was independently performed by two experienced pathologists (AS and PM) blinded for group assignment. Similar to previous studies (23), analyzed criteria comprised thickening of alveolar membranes, dystelectasis, emphysema, and inflammatory cell (lymphocytes) infiltration. These parameters were scored from 0 (absent), 1 (hardly detectable), 2 (rare), 3 (minor), 4 (moderate), to 5 (extensive).

Mitochondrial Respiration

Mitochondrial respiratory capacity was determined via high-resolution respirometry with a clark-electrode-based system (Oxygraph 2k, OROBOROS Instruments Corp., Innsbruck, Austria) as described previously (22). Post-mortem heart, muscle, liver, and brain biopsies were mechanically homogenized in Mir05 (respiration medium). Mir05 is composed of 0.5 mM EGTA, 3 mM $MgCl_2 \cdot 6H_2O$, 60 mM Lactobionic acid, 20 mM Taurine, 10 mM KH_2PO_4, 20 mM HEPES, 110 mM Sucrose, 1 $g \cdot L^{-1}$ bovine serum albumin). 1.5–2 mg of tissue (1.5 mg: heart, 2 mg tissue: muscle, liver, and brain) were added to the Oxygraph chamber. By addition of a defined sequence of substrates and inhibitors, various states of mitochondrial function could be assessed. Complex I activity was determined after addition of 10 mM pyruvate, 10 mM glutamate, 5 mM malate, and 5 mM ADP. Ten micrometers cytochrome c was added to check for mitochondrial integrity. Maximum oxidative phosphorylation (OxPhos) was evaluated after subsequent addition of 1 mM octanoyl-carnitine and 10 mM succinate. Leak compensation was assessed after inhibition of the ATP-synthase by 2.5 µM oligomycin, followed by stepwise titration of the uncoupling agent Carbonyl cyanide-4-(trifluoromethoxy)-phenylhydrazone (FCCP, final concentration 1.5 µM) to reach maximum respiratory activity of the electron transfer system in the uncoupled state (ETS).

Western Blot

The lung was dissected at the end of the experiment and frozen on dry ice. The tissue was homogenized in EDTA-free lysis buffer with tissue homogenisator (Precellys®). Total protein concentration was determined using Pierce® BCA Protein Assay Kit (23225). Proteins were separated by SDS-PAGE and blotted on nitrocellulose membrane using the Trans-Blot Turbo system (BioRad). Osteopontin was detected with anti-osteopontin primary antibody (mouse anti-mouse, LFMb-14, Santa Cruz Biotechnology Inc., sc-73631) diluted 1:500. Vincullin was detected as loading control using anti-vincullin primary antibody (mouse anti-mouse, Santa Cruz Biotechnology Inc., sc-73614) diluted 1:1.000. Primary antibody incubation was done overnight at 4°C. Secondary antibody (rabbit anti-mouse, HRP coupled polyclonal Ig, Dako, P0161) was diluted 1:10.000 and incubated 1 h at room temperature. Membrane blocking and dilutions were done with 5% BSA. Except for the last washing step which was done with 1x TBS, 0.1% TBST was used. Blots were developed using immobilion forte WBLUF0500 (Merck Millipore) and ImageLab software (version 5.2). Osteopontin abundancy was quantified using ImageJ (version 1.52a) by determination of mean signal intensity of osteopontin normalized to mean intensity of vincullin.

Immunohistochemistry

The left lung was formalin-fixed and embedded in paraffin for immunohistochemistry analysis. Immunohistochemistry (IHC) for extravascular albumin content (anti-albumin rabbit polyclonal #16475-1-AP, Proteintech, USA) was performed as described previously (24). Primary antibodies were detected by secondary anti-rabbit antibody conjugated to AP (Alkaline Phosphatase-conjugated antibody; Jackson, ImmunoResearch, West Grove, Pa) and visualized with a red chromogen (Darko REAL Detection System Chromogen Red), and Mayers hematoxylin (Sigma, Taufkirchen, Germany). Visualization was performed using the Zeiss Axio Imager A1 microscope (Zeiss, Jena, TH, Germany). Four distinct 800.000 mm^2 regions were quantified for intensity of signal by using the Axio Vision 4.8 software. Results are presented as mean densitometric sum red (24, 25).

Cell Culture

The primary bone marrow-derived macrophages (BMDMs) were isolated from humerus, femur and tibia of 8–13 weeks old GR$^{+/+}$ and GR$^{dim/dim}$ mice as described previously (18). Briefly, cells were cultured until day 7 in DMEM (D5671, sigma) supplemented with 10% fetal bovine serum (FBS, F7524, sigma), 30% L929-cell conditioned medium, 1% Penicillin / Streptomycin (P0781, sigma), 1% L-Glutamine (G7513, sigma), 1% Sodium Pyruvate (S8636, sigma) at 37°C and 5% CO_2. All BMDMs were treated with PBS as control and LPS (100 ng/ml, L6529, sigma) for the indicated time points. Osteopontin Elisa (R&D System) was performed with the supernatant of GR$^{+/+}$ and GR$^{dim/dim}$ BMDMs.

Analysis of Relative mRNA Levels

For quantitative real-time PCR analysis (qRT-PCR), RNA was extracted from lungs by homogenization with tissue homogenisator (Precellys®) in Trizol (invitrogen) following the manufacturer's instructions. RNA quality was checked using the nanodrop (thermofisher). DNaseI-treated RNA (1 μg) was used to generate cDNA by oligo(dT) priming. qRT-PCR was performed with the ViiA™ 7 Realtime PCR System (Life technologies) using a Platinum SYBR Green (Invitrogen) and analyzed with the QuantStudio Realtime-PCR software using the ΔΔCT method. *β-Actin* and *Ribosomal protein L (Rpl)* served as housekeeping genes. The specific primers were obtained from Sigma with the sequences listed in **Table 1**.

Measurements of Cytokine and Chemokine Concentrations

Bio-Plex Pro Mouse Cytokine 23-plex Assay (Group I) (Biorad) was used to measure 23 cytokines, chemokines and growth factors simultaneously in the plasma. The Bio-Plex Assay was conducted according to the manufacturer's protocol. The assay was performed with Bio-Plex 200 machine (Biorad) and analyzed with the Bio-Plex Manager TM 6.1 software (Biorad).

Statistical Analysis

Unless stated otherwise, all data are presented as median (25th and 75th percentile). Data sets were analyzed using non-parametric statistics, i.e., Mann–Whitney *U*-test (one factor, two independent samples) or Kruskal–Wallis test with *post-hoc* Dunn's comparison testing (one factor, four independent samples). $P < 0.05$ were considered statistically significant. Quantitative graphical presentations and statistical analyses were accomplished by using GraphPad Prism 7 (GraphPad Software Inc., La Jolla, Calif).

TABLE 1 | Specific primers for quantitative real-time PCR analysis (qRT-PCR).

Gene	Forward primer	Reverse primer
β-Actin	GCACCAGGGTGTGATGGTG	CCAGATCTTCTCCATGTCGTCC
Il1-β	GGCTGTGGAGAAGCTGTGGCA	GGGTCCGACAGCACGAGGCT
Il-6	AAACCGCTATGAAGTTCCTCTCTGC	AGCCTCCGACTTGTGAAGTGGT
Il-10	CAGAGCCACATGCTCCTAGA	TGTCCAGCTGGTCCTTTGTT
Rpl	CCTGCTGCTCTCAAGGTT	TGGCTGTCACTGCCTGGTACTT
Tnfα	AGGGGCCACCACGCTCTTCT	TGAGTGTGAGGGTCTGGGCCAT
Sphkl	CCAAGTGCACCCAAACTACC	GCCCCACCTTCTAGCTTTCT

RESULTS

GR Dimerization Mediates Stability of Hemodynamics, Acid-Base Status, and Mitochondrial Respiration After LPS Challenge

To examine the effects of an impaired GR dimerization during resuscitation in LPS-induced systemic inflammation, hemodynamics, metabolic parameters, and mitochondrial respiration were investigated. Hemodynamic stability was defined as MAP >55 mmHg and preserved via infusion of crystalloids and, if necessary, norepinephrine (maximum infusion rate 1.5 $\mu g \cdot h^{-1}$). Therefore, in some mice (GR$^{+/+}$ PBS $n = 0$, GR$^{dim/dim}$ PBS $n = 1$, GR$^{+/+}$ LPS $n = 1$, GR$^{dim/dim}$ LPS $n = 5$), the experiment had to be terminated due to hemodynamic instability despite increasing norepinephrine doses, which lead to MAP values below 55 mmHg. After LPS-challenge, GR$^{dim/dim}$ mice had a trend toward a lower MAP when compared to GR$^{+/+}$ mice (**Table 2**). In line with the compromised systemic hemodynamics, norepinephrine requirements in GR$^{dim/dim}$ mice challenged with LPS were significantly higher when compared to LPS-challenged GR$^{+/+}$ animals (**Figure 1** and **Table 2**). In GR$^{dim/dim}$ mice, a challenge with LPS led to an increase of lactate levels at the end of the resuscitation phase, and, consequently, to a more pronounced decrease in base excess (BE) compared to GR$^{+/+}$ mice, suggesting an aggravation of metabolic acidosis (**Table 2**). Because hyperlactatemia may be linked to disturbances in mitochondrial respiration (26, 27), important metabolic organs like muscle, heart, liver and brain were investigated for mitochondrial respiration in the current study. In LPS-challenged GR$^{dim/dim}$ mice, oxygen flux during maximal coupled mitochondrial respiration (OxPhos) was decreased in heart tissue when compared to vehicle treated GR$^{dim/dim}$ mice, whereas in GR$^{+/+}$ animals OxPhos was not changed between PBS and LPS-challenge (**Figure 2A**), suggesting a disturbed mitochondrial function in the heart of GR$^{dim/dim}$ animals. In the liver tissue, oxygen flux during maximal mitochondrial respiration and during inhibited ATP synthase in the coupled state (LEAK) was higher in LPS-challenged than in vehicle challenged GR$^{+/+}$ mice (**Figure 2B**), suggesting an increased mitochondrial respiratory capacity in these animals. However, in the muscle and brain mitochondrial respiration was not changed neither in GR$^{dim/dim}$ nor in GR$^{+/+}$ animals during PBS- or LPS-challenge under resuscitation (**Figures 2C,D**). In summary, the impaired dimerization of the GR results in higher noradrenaline requirements and therefore compromised systemic hemodynamics as well as a more pronounced lactic acidosis and altered mitochondrial respiration during LPS-challenge.

TABLE 2 | Hemodynamic and metabolic measurements as well as parameters of lung function in GR$^{dim/dim}$ and GR$^{+/+}$ mice intraperitoneally challenged with lipopolysaccharide (LPS) or vehicle (phosphate buffered saline, PBS) at the end of the experiment.

Parameters	Resuscitation (IV crystalloids and norepinephrine)			
	GR$^{+/+}$ + Vehicle (n = 8)	GR$^{dim/dim}$ + Vehicle (n = 7)	GR$^{+/+}$ + LPS (n = 9)	GR$^{dim/dim}$ + LPS (n = 11)
Bodyweight [g]	26.7 (23.0; 31.6)	24.6 (20.6; 32.7)	29.0 (26.6; 31.1)	24.0 (22.7; 28.2)
Heart rate [beats·min^{-1}]	478 (335; 518)	551 (520; 558)	529 (471; 557)	523 (460; 580)
Mean arterial pressure [mmHg]	61 (56; 65)	54 (52; 61)	56 (49; 58)	49 (43; 51)
$PaCO_2$ [mmHg]	37 (30; 45)	41 (39; 44)	34 (33; 47)	43 (40; 46)
Minute ventilation [mL·kg^{-1}·min^{-1}]	905 (838; 1,058)	1,000 (980; 1,080)	1,000 (960; 1,040)	1,060 (980; 1,170)
Horovitz-Index [mmHg]	465 (409; 498)	363 (342; 371)	349 (302; 463)	327 (291; 352)
Glucose [mg·dL^{-1}]	129 (121; 147)	139 (136; 176)	78 (60; 89)	94 (80; 183)
Arterial pH	7.28 (7.26; 7.34)	7.23 (7.19; 7.28)	7.14 (7.12; 7.32)	7.12 (6.99;7.20)
Arterial base excess [mmol·L^{-1}]	−8.4 (−11.3; −5.6)	−7.9 (−10.5; −7.4)	−11.0 (−13.2; −10.2)	**−14.5 (−19.9; −12.0)#**
Lactate [mmol·L^{-1}]	1.1 (0.8; 1.6)	1.5 (1.2; 2.1)	2.8 (2.1; 3.1)	**5.3 (3.9; 6.6)#**
Hemoglobin [g·dL^{-1}]	8.7 (8.3; 10.6)	9.0 (8.6; 11.4)	8.2 (7.3; 10.1)	9.0 (8.0; 9.7)
Urinary output [μL]	1,796 (997; 2,413)	2,309 (1,494; 3,628)	881 (646; 1,906)	**969 (514; 1,060)#**

#P < 0.05 vs. GR^{dim} PBS. PBS = phosphate buffered saline (vehicle), 10 μl·g^{-1}. LPS = Lipopolysaccharide from Escherichia coli (055:B5), 10 mg·kg^{-1}. Data is shown as median (25th and 75th percentile).

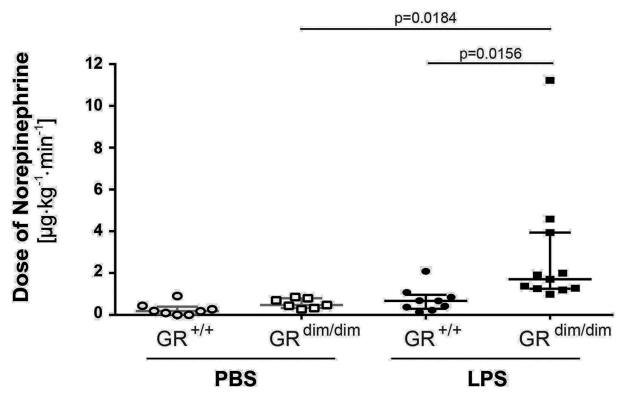

FIGURE 1 | Doses of norepinephrine in mechanically ventilated GR$^{dim/dim}$ and GR$^{+/+}$ mice intraperitoneally challenged with lipopolysaccharides (LPS) or vehicle (PBS) and resuscitated (crystalloids, norepinephrine) for 6 h. Norepinephrine was titrated intravenously during resuscitation to keep systemic mean arterial blood pressure above 55 mmHg. LPS = lipopolysaccharide from *Escherichia coli* [055:B5], 10 mg·kg^{-1}, dissolved in 10 μl·g^{-1} phosphate buffered saline (PBS). GR$^{+/+}$ mice challenged with PBS: n = 8, GR$^{dim/dim}$ mice challenged with PBS: n = 7, GR$^{+/+}$ mice challenged with LPS: n = 9, GR$^{dim/dim}$ mice challenged with LPS: n = 11. Data is presented as median (25th and 75th percentile and minimum/maximum).

GR$^{dim/dim}$ Mice Have Higher Mortality After LPS Challenge With Subsequent Resuscitation

In LPS-challenged mice with subsequent resuscitation for a maximum of 6 h (lung-protective mechanical ventilation, hemodynamic measurements, crystalloid and norepinephrine infusion to keep hemodynamic stability), mortality was significantly higher in GR$^{dim/dim}$ mice when compared to GR$^{+/+}$ animals (**Supplementary Figure 1**).

No Differences in Most Plasma Cytokines 6 h After LPS Challenge and Resuscitation

After LPS-challenge, the concentration of Il-1α in plasma increased in GR$^{dim/dim}$, but not in GR$^{+/+}$ mice. In contrast, concentrations of Il-2, Eotaxin, and Ifnγ only increased in GR$^{+/+}$ mice, but not in GR$^{dim/dim}$ mice, however, all are expressed on a low level (**Table 3**). Pro-inflammatory plasma cytokines like Il1-β (**Figure 3A**), Il-6 (**Figure 3B**), and Tnfα (**Figure 3C**) were significantly induced in both genotypes after LPS challenge, demonstrating that the intensive care management and resuscitation does not increase basal level of these inflammatory cytokines.

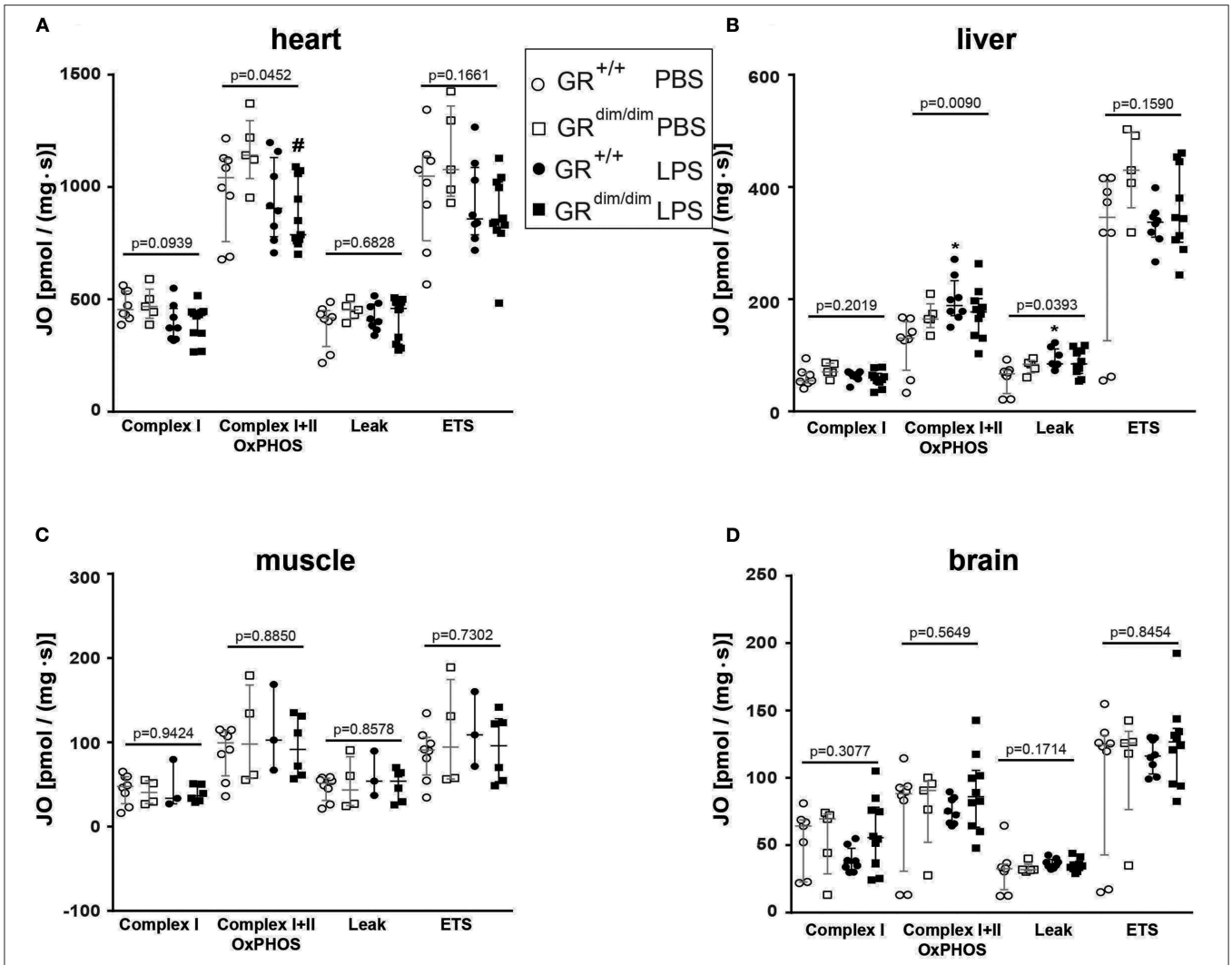

FIGURE 2 | Mitochondrial respiration (JO_2) in tissue from heart **(A)**, liver **(B)**, muscle **(C)**, and brain **(D)** in GR$^{dim/dim}$ and GR$^{+/+}$ mice intraperitoneal challenged with lipopolysaccharide (LPS) or vehicle (PBS). *$p < 0.05$ vs. GR$^{+/+}$ PBS. #$p < 0.05$ vs. GR$^{dim/dim}$ PBS. Overall p-values from Kruskal–Wallis-Test are shown above accordingly. LPS = lipopolysaccharide from *Escherichia coli* [055:B5], 10 mg·kg^{-1}, dissolved in 10 µl·g^{-1} phosphate buffered saline [PBS]. GR$^{+/+}$ mice challenged with PBS: $n = 7$–8, GR$^{dim/dim}$ mice challenged with PBS: $n = 4$–5, GR$^{+/+}$ mice challenged with LPS: $n = 3$–8, GR$^{dim/dim}$ mice challenged with LPS: $n = 6$–11. Data is presented as median (25th and 75th percentile and minimum/maximum).

Lung Function Is Impaired in GR$^{dim/dim}$ Mice During Intensive Care Treatment

Lung compliance as a marker for lung mechanics was reduced in PBS-treated GR$^{dim/dim}$ mice in comparison to PBS-treated GR$^{+/+}$ animals (**Figure 4A**). A significantly lower lung compliance was observed in GR$^{dim/dim}$ mice compared to GR$^{+/+}$ controls during LPS-challenge (**Figure 4A**). In line with a lower lung compliance, GR$^{dim/dim}$ mice had a reduced Horovitz-Index (partial pressure of oxygen in the arterial blood, divided by the inspiratory concentration of oxygen) as a marker for systemic oxygenation (**Table 2**). However, GR$^{+/+}$ animals did not show any significant changes in lung compliance or Horovitz-Index after LPS-challenge in comparison to PBS-challenged GR$^{+/+}$ animals (**Figure 4A** and **Table 2**), suggesting a more severe lung dysfunction in response to LPS-challenge in GR dimerization impaired mice. The histological evaluation of lung tissue revealed no significant differences in the total score between the corresponding groups, however the GR$^{dim/dim}$ animals had a slight elevated total score (**Table 4**). Immunohistochemistry (IHC) for albumin extravasation showed a higher expression in lung tissue after LPS-challenge in GR$^{dim/dim}$ mice compared to GR$^{+/+}$ mice, whereas no difference was observed in extravascular albumin expression between GR$^{dim/dim}$ and GR$^{+/+}$ mice after vehicle treatment (**Figure 4B**). In previous studies, increased albumin extravasation and vascular leakage was accompanied by a reduced expression of *Sphk1* dependent on the GR dimerization during inflammation (13). In the present study, LPS-challenged GR$^{+/+}$ mice showed increased *Sphk1* expression

TABLE 3 | Concentrations of cytokines in plasma of GR$^{dim/dim}$ and GR$^{+/+}$ mice intrapoeritoneal challenged with lipopolysaccharide (LPS) or vehicle (phosphate buffered saline, PBS) measured at the end of the experiment.

Parameters	Resuscitation (IV crystalloids and norepinephrine)			
	GR$^{+/+}$ + Vehicle (n = 7–8)	**GR$^{dim/dim}$ + Vehicle (n = 6–7)**	**GR$^{+/+}$ + LPS (n = 7–8)**	**GR$^{dim/dim}$ + LPS (n = 10–11)**
Il-1 alpha [pg·ml^{-1}]	27 (12; 65)	19 (10; 22)	67 (55; 70)	**67 (22; 68)$^{\#}$**
Il-2 [pg·ml^{-1}]	3.5 (1.1; 6.4)	2.9 (1.6; 6.6)	**16.2 (14.0; 19.2)***	13.7 (7,5; 17.3)
Il-3 [pg·ml^{-1}]	1.4 (0.8; 2.0)	1.1 (0.2; 1.6)	**13.1 (12.4; 14.0)***	**12.7 (5.4; 13.7)$^{\#}$**
Il-5 [pg·ml^{-1}]	15.9 (7.6; 27.9)	12.8 (6.7; 28.0)	23.5 (19.2; 31.1)	29.5 (18.1; 48.0)
Il-10 [pg·ml^{-1}]	27 (20; 48)	22 (16; 52)	**336 (301; 487)***	**1,017 (428; 1,416)$^{\#}$**
Eotaxin [pg·ml^{-1}]	602 (517; 736)	857 (775; 1,292)	**1,756 (1,263; 1,992)***	1,365 (1,000; 1,779)
KC [pg·ml^{-1}]	30 (24; 38)	26 (19; 32)	**2,318 (1,454; 2,698)***	**1,358 (266; 2,268)$^{\#}$**
Mcp-1 [pg·ml^{-1}]	289 (239; 349)	239 (194; 398)	**51,720 (30,400; 96,096)***	**78,358 (4,385; 164,779)$^{\#}$**
Rantes [mg·dL^{-1}]	72 (70; 80)	51 (33; 59)	**4,252 (2,936; 6,277)***	**3,457 (583; 4,424)$^{\#}$**
Ifn gamma [pg·ml^{-1}]	6 (3; 10)	13 (6; 26)	**90 (45; 195)***	107 (16; 152)

*$P < 0.05$ vs. GR$^{+/+}$ PBS. $^{\#}P < 0.05$ vs. GR^{dim} PBS. PBS = phosphate buffered saline (vehicle), 10 $\mu l \cdot g^{-1}$. LPS = Lipopolysaccharide from Escherichia coli (055:B5), 10 mg·kg^{-1}. Data is shown as median (25th and 75th percentile). Bold values indicate significant differences.

that correlated with lower albumin expression compared to GR$^{dim/dim}$ challenged LPS mice having increased extravascular albumin expression and significantly reduced *Sphk1* expression (**Figures 4B,C**). Taken together, lung function was impaired in GR$^{dim/dim}$ mice upon LPS-challenge during intensive care treatment. In PBS-treated animals a so far not described slight basal difference in lung function was observed in GR$^{dim/dim}$ mice. These data revealed that the dimerization of the GR is crucial for the lung compliance in an inflammatory setting under intensive care management.

Increased Osteopontin in GR$^{dim/dim}$ Mice Might Contribute to Disturbed Lung Function

Inflammatory cytokine mRNA expression of *Il1-β* (**Figure 5A**), *Il-6* (**Figure 5B**), *Tnfα* (**Figure 5C**), and *Il-10* (**Figure 5D**) in the lung revealed no significant differences between GR$^{dim/dim}$ and GR$^{+/+}$ mice after challenge with LPS under intensive care management. Therefore, the reduced lung compliance is most likely not a result of the aforementioned inflammatory mediators. Next to the expression of *Sphk1*, which was identified as an important regulator of lung barrier integrity, we now also aimed at other potential regulators of lung injury. Osteopontin (Opn, secreted phosphoprotein 1–Spp1) is a crucial mediator for inflammatory responses and a regulator of inflammation, especially lung inflammation. Opn neutralizing antibody could protect mice against ALI during sepsis (28). In our setting (intensive care management) Opn protein expression was significantly enhanced in lungs of GR$^{dim/dim}$ compared to GR$^{+/+}$ mice, both under PBS-treatment and LPS-challenge (**Figures 6A,B**). Opn was shown to have an impact on type-1 immunity to bacterial infections as OPN deficient mice have increased Il-10 production (29). In accordance with this, GR$^{dim/dim}$ mice with increased levels of Opn showed a trend toward reduced *Il-10* mRNA expression in the lung compared to GR$^{+/+}$ mice during PBS and LPS-challenge (**Figure 5D**). This suggests that increased Opn expression in the lung of GR$^{dim/dim}$ mice might have an impact on *Il-10* mRNA expression. However, in the plasma of GR$^{+/+}$ and GR$^{dim/dim}$ PBS- and LPS-challenged animals only a trend to induced Opn expression was observed, due to high variations in the groups (**Supplementary Figure 2A**). To assess the effect of impaired GR dimerization in macrophages and their contribution to Opn expression and inflammatory cytokines bone marrow-derived macrophages (BMDM) from GR$^{+/+}$ and GR$^{dim/dim}$ animals were stimulated with LPS. LPS stimulation increased the inflammatory cytokine expression in GR$^{+/+}$ and GR$^{dim/dim}$ BMDMs, however, no genotype difference for the upregulation of *Il-6* expression (**Supplementary Figure 2B**), *Tnfα* expression (**Supplementary Figure 2C**), and *iNos* expression (**Supplementary Figure 2D**) could be detected after LPS

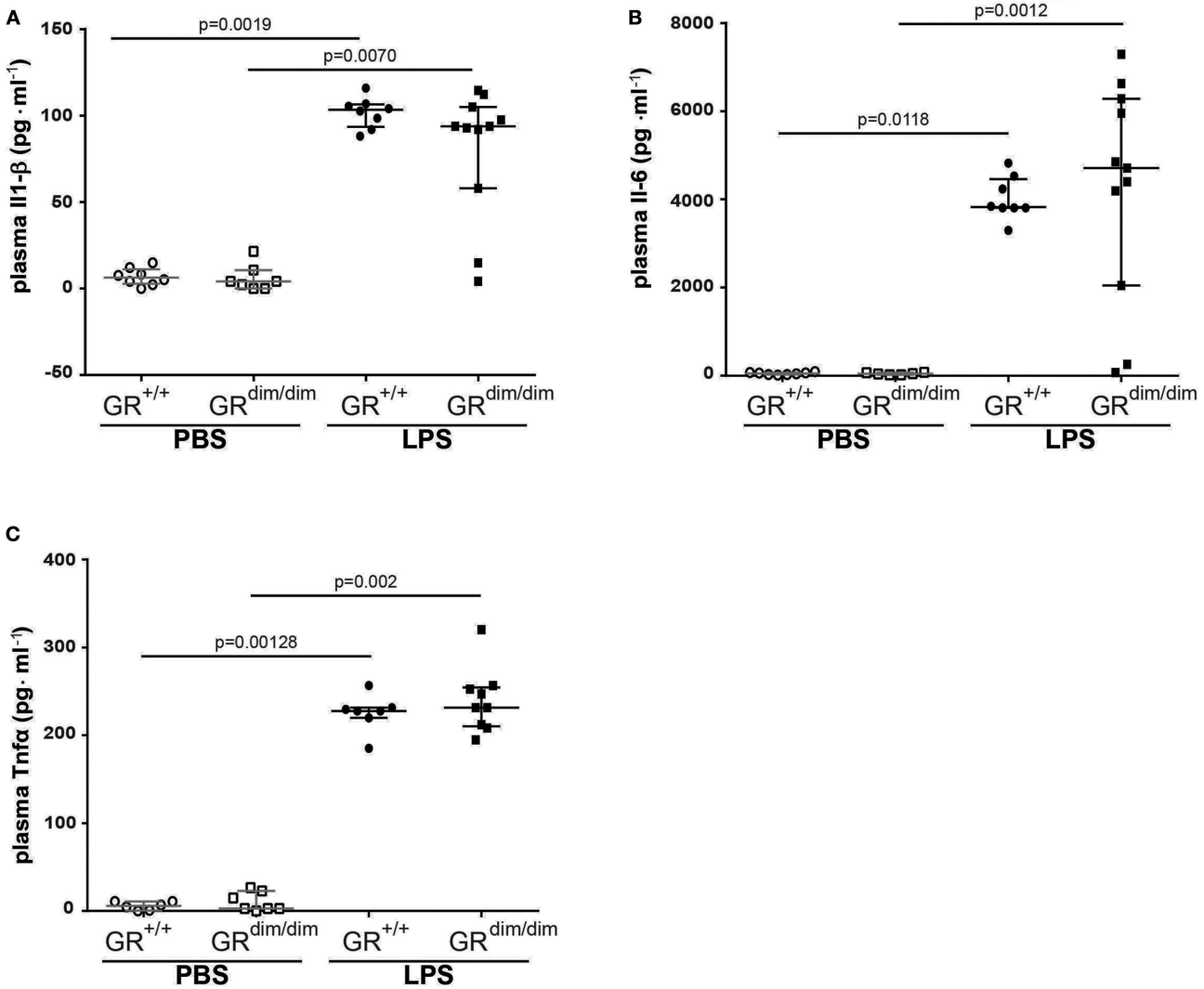

FIGURE 3 | Level of inflammatory cytokines in the plasma. Concentration of **(A)** interleukin 6 (Il-6), **(B)** interleukin 1 β (Il-1β), and **(C)** tumor necrosis factor α (Tnfα) in the plasma of GR$^{dim/dim}$ and GR$^{+/+}$ mice after an intraperitoneally challenge with lipopolysaccharides (LPS) or treatment with PBS. LPS = lipopolysaccharide from *Escherichia coli* [055:B5], 10 mg·kg^{-1}, dissolved in 10 µl·g^{-1} phosphate buffered saline (PBS). GR$^{+/+}$ mice challenged with PBS: $n = 6$–8, GR$^{dim/dim}$ mice challenged with PBS: $n = 6$–7, GR$^{+/+}$ mice challenged with LPS: $n = 7$–8, GR$^{dim/dim}$ mice challenged with LPS: $n = 9$–11. Data is presented as median (25th and 75th percentile and minimum/maximum).

treatment. *Opn* expression was not different, however a slight, but not significant, increase could be detected after LPS treatment in GR$^{+/+}$ and GR$^{dim/dim}$ BMDMs with a more pronounced trend in the GR$^{dim/dim}$ BMDMs (**Supplementary Figure 2E**). This observation is supported by the Opn levels in the supernatant of the LPS-treated GR$^{dim/dim}$ BMDMs, that showed a trend to induced Opn compared to GR$^{+/+}$, however, not significantly different (**Supplementary Figure 2F**). This suggests that macrophages are not the main source of GR$^{dim/dim}$ dependent regulation of Opn, but they contribute to the Opn induction. Moreover, these data suggest that GR dimerization dependent regulation of Opn *in vivo* might depend on other cells.

In summary, there is possibly a correlation between increased Opn expression in the lung of the GR$^{dim/dim}$ mice that renders them more sensitive during inflammation and therefore, Opn may be a target for the reduced lung compliance.

DISCUSSION

In the present study, we tested the hypothesis if an impaired glucocorticoid receptor (GR) function, presented as an impaired GR dimerization (GR^{dim}), would impair organ function in lipopolysaccharide (LPS)-induced systemic inflammation in mice undergoing intensive care treatment to compensate for LPS-induced cardiovascular depression. We found that GR$^{dim/dim}$ mice challenged with LPS had a significantly increased need of norepinephrine to achieve hemodynamic targets and a more

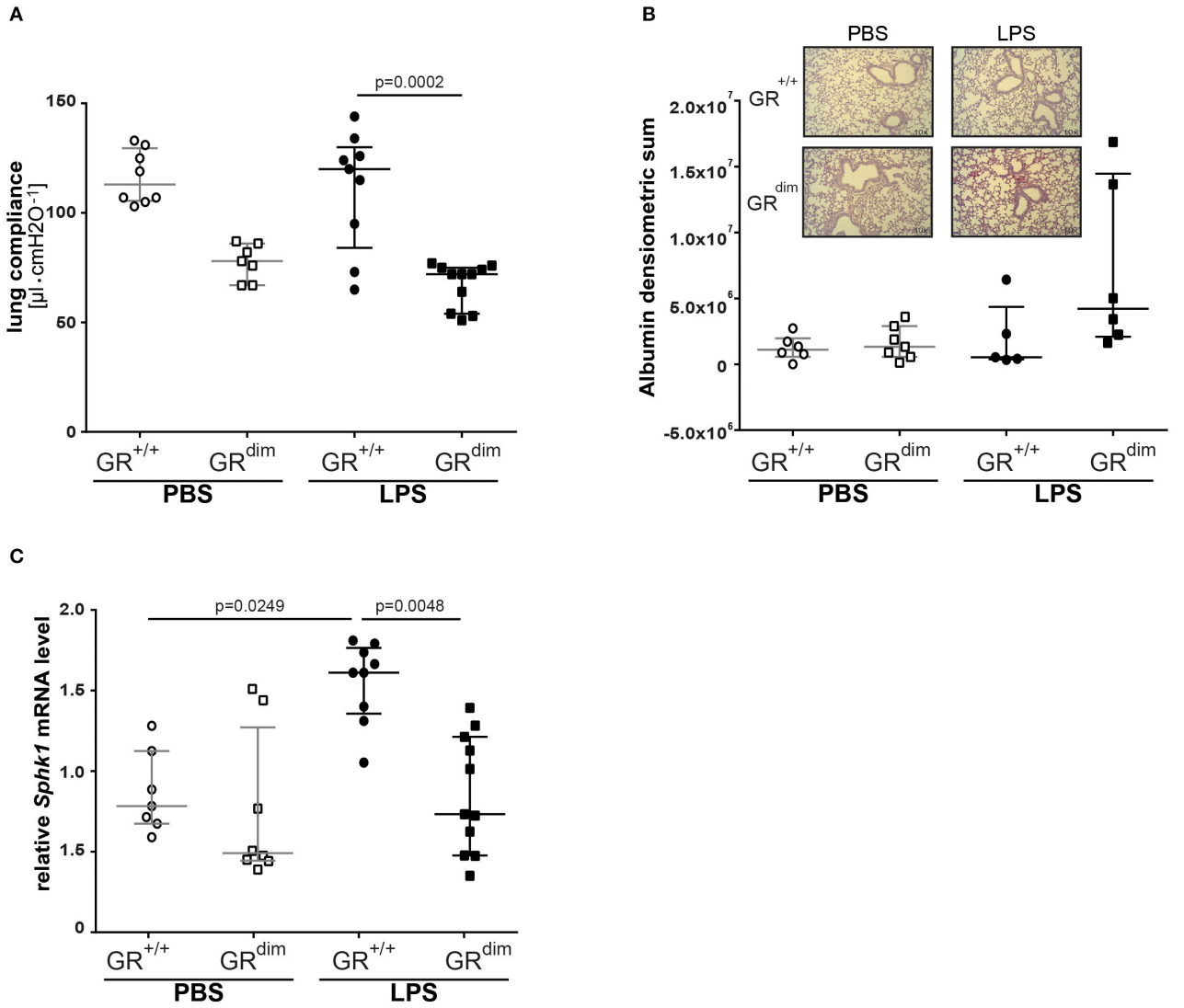

FIGURE 4 | Lung function and mRNA expression of glucocorticoid receptor associated genes in mechanically ventilated GR$^{dim/dim}$ and GR$^{+/+}$ mice intraperitoneally challenged with lipopolysaccharides (LPS) or vehicle (PBS). **(A)** Lung compliance: $p = 0.0735$ for GR$^{+/+}$ vs. GR$^{dim/dim}$ mice treated with PBS for Kruskal–Wallis-Test with multiple comparisons and *post-hoc* Dunn's Test. LPS = lipopolysaccharide from *Escherichia coli* [055:B5], 10 mg·kg^{-1}, dissolved in 10 µl·g^{-1} phosphate buffered saline (PBS). GR$^{+/+}$ mice challenged with PBS: $n = 8$, GR$^{dim/dim}$ mice challenged with PBS: $n = 7$, GR$^{+/+}$ mice challenged with LPS: $n = 9$, GR$^{dim/dim}$ mice challenged with LPS: $n = 11$. Data is presented as median (25th and 75th percentile and minimum/maximum). **(B)** Immunohistochemical (IHC) analysis of extravascular albumin expression in lung tissue of GR$^{dim/dim}$ and GR$^{+/+}$ mice challenged with lipopolysaccharide (LPS) or vehicle (PBS) and example pictures of albumin extravasation in lung tissue in GR$^{+/+}$ and GR$^{dim/dim}$ mice (lower picture). Albumin was detected with a secondary Alkaline Phosphatase-conjugated antibody and visualized with a red chromogen and regions were quantified for signal. GR$^{+/+}$ mice challenged with PBS: $n = 6$, GR$^{dim/dim}$ mice challenged with PBS: $n = 7$, GR$^{+/+}$ mice challenged with LPS: $n = 5$, GR$^{dim/dim}$ mice challenged with LPS: $n = 6$. Data is presented as median (25th and 75th percentile and minimum/maximum). **(C)** Measurements of relative mRNA level of sphingosine kinase 1 (*Sphk1*) in lung tissue of GR$^{dim/dim}$ and GR$^{+/+}$ mice challenged with lipopolysaccharide (LPS) or vehicle (PBS). GR$^{+/+}$ mice challenged with PBS: $n = 7$, GR$^{dim/dim}$ mice challenged with PBS: $n = 8$, GR$^{+/+}$ mice challenged with LPS: $n = 9$, GR$^{dim/dim}$ mice challenged with LPS: $n = 11$. Data is presented as median (25th and 75th percentile and minimum/maximum).

pronounced lactic acidosis during resuscitation measures ("lung-protective" ventilation, fluid resuscitation, and norepinephrine treatment) compared to LPS-challenged GR$^{+/+}$ mice. Most interestingly, GR$^{dim/dim}$ mice challenged with LPS presented with aggravated ALI, shown by a more pronounced impairment of lung mechanics when compared to LPS-challenged GR$^{+/+}$ mice. According to the results of the present study, the impaired lung function in GR$^{dim/dim}$ mice was most likely mediated via an increased endothelial barrier dysfunction, indicated via a reduced expression of sphingosine kinase 1 (*Sphk1*), which was associated with a higher albumin extravasation in lung tissue. Furthermore, the lung injury in GR$^{dim/dim}$ mice was accompanied by an increase in Osteopontin (Opn) levels in lung tissue, which indicated Opn as a marker of lung injury. The impaired lung

TABLE 4 | Quantification of lung histology analysis in GR$^{dim/dim}$ and GR$^{+/+}$ mice that underwent an intraperitoneally challenge with lipopolysaccharide (LPS) or vehicle (phosphate buffered saline, PBS) and were resuscitated for 6 h thereafter.

Parameters	Resuscitation (IV crystalloids and norepinephrine)			
	GR$^{+/+}$ + Vehicle ($n = 8$)	GR$^{dim/dim}$ + Vehicle ($n = 7$)	GR$^{+/+}$ + LPS ($n = 5$)	GR$^{dim/dim}$ + LPS ($n = 6$)
Alveolar membrane thickening	1.0 (0.9; 1.0)	1.5 (1.0; 2.0)	1.0 (1.0; 2.0)	1.5 (1.0; 2.0)
Dystelectasis	0.5 (0.0; 0.5)	0.5 (0.0; 1.0)	0.0 (0.0; 0.0)	0.3 (0.0; 0.5)
Emphysema	2.0 (2.0; 2.0)	2.0 (1.8; 2.0)	2.5 (2.5; 2.5)	2.5 (2.0; 3.0)
Lymphocytes	1.0 (1.0; 1.3)	**2.0 (2.0; 2.5)***	1.0 (1.0; 2.0)	2.0 (1.3; 2.0)
Total score	4.5 (4.0; 5.0)	6.0 (5.8; 7.0)	4.5 (4.5; 6.5)	5.8 (5.1; 6.8)

*For detailed description of the score for histological tissue analysis see Methods section. *$P < 0.05$ vs. GR$^{+/+}$ vehicle. PBS = phosphate buffered saline (vehicle), LPS = Lipopolysaccharide from Escherichia coli (055:B5), 10 mg·kg^{-1}. Data is shown as median (interquartile range).*

function in GR$^{dim/dim}$ mice after LPS-challenge was not mediated via the systemic inflammatory response, because we found no differences in cytokine levels between the genotypes, neither in lung tissue (**Figure 3**) nor in plasma (**Table 3**).

We previously showed that GR$^{dim/dim}$ mice present a higher mortality in LPS-and cecal ligation and puncture (CLP)-induced systemic inflammation without any resuscitation procedures (18). In the present study, after LPS-challenge GR$^{dim/dim}$ mice had (i) an increased hemodynamic instability indicated by a significantly increased need of norepinephrine, (ii) more pronounced lactic acidosis, and (iii) a reduced lung compliance, which altogether lead to an increased mortality rate despite resuscitative measures. The increased mortality of GR$^{dim/dim}$ mice in the current study (**Supplementary Figure 1**) confirms that the GR dimer is of importance for survival after challenge with LPS, even when animals receive fluid resuscitation and norepinephrine treatment to achieve target hemodynamics as well as "lung-protective" mechanical ventilation (22, 23).

i) ***Hemodynamic instability***: In the present study, GR$^{dim/dim}$ mice presented with an aggravated hemodynamic instability after LPS-challenge, reflected by a significantly increased need of norepinephrine to reach hemodynamic targets (**Figure 1**). Aggravated hemodynamic instability after LPS-challenge, which also led to increased mortality, has also been reported in mice with an endothelial-specific GR deletion (GR^{ECKO}) (30). The increased hemodynamic instability in these mice was accompanied by an increased expression of inducible (iNOS) and endothelial (eNOS) nitric oxide synthase (NOS), which resulted in increased levels of nitric oxide (NO) following LPS-challenge, thus contributing to arterial hypotension. Interestingly, corticosterone levels increased after challenge with LPS, but did not differ between GR^{ECKO} and control mice (30). While an endothelial GR dysfunction induces hypotension, in other studies it is reported that a stimulation of an intact GR via GCs leads to hypertension. In addition, this GC-induced hypertension was reported to be mediated via downregulation of eNOS in rats (31). Therefore, endothelial GR dysfunction leads to NO-induced hypotension, whereas GR stimulation via GCs leads to downregulation of NO synthases, which induces hypertension. Although we did not examine any vascular specific effects of an ubiquitous impairment of GR dimerization, it is likely that the increased hemodynamic instability in GR$^{dim/dim}$ mice has been, at least in part, meditated via a NO-induced vasodilation after LPS-challenge in the present study as reported previously (30). The anesthesia and surgery represent a trauma for the animals and this is most likely the reason for the slight increased mortality of the GR$^{dim/dim}$ mice compared to GR$^{+/+}$ challenged with PBS. We can only speculate about the reasons for this increased instability. Due to the decreased blood pressure in the GR$^{dim/dim}$ mice during the ICU management, it is most likely that either the systemic vascular resistance or the cardiac output is affected. A decreased hemodynamic instability has already been described for mice with an endothelial glucocorticoid receptor knockout (30).

ii) ***Lactic acidosis***: Additionally, GR$^{dim/dim}$ mice developed lactic acidosis until the end of the LPS-challenge (**Table 2**). In the present study, GR$^{+/+}$ mice showed an increase in mitochondrial respiration in the liver, which was lacking in GR$^{dim/dim}$ mice (**Figure 2**). Moreover, GR$^{dim/dim}$ mice presented with a more severe shock and lactic acidosis under highest norepinephrine requirements to counteract arterial hypotension. While shock-induced hypotension causes increased norepinephrine needs to achieve hemodynamic targets, shock-related lactic acidosis originates from disturbed microcirculatory perfusion and/or impaired cellular O_2 utilization, the later possibly resulting from mitochondrial dysfunction. Moreover, catecholamines *per se* can aggravate both, impaired microcirculatory perfusion and mitochondrial dysfunction, the latter as a result of increased radical formation. Therefore, the lacking increase in mitochondrial respiration in LPS-challenged GR$^{dim/dim}$ mice in the liver and the more pronounced lactic acidosis might be explained by a mitochondrial dysfunction *per se* and/or due to higher norepinephrine doses.

iii) ***Lung compliance***: The importance of the GR for lung function already becomes apparent during lung maturation *in utero*. Here, GR signaling mediates downsizing of the interstitial mesenchymal tissue compartment. This in turn brings the underlying vasculature into close proximity with the future alveolar airspaces, and enables oxygenation of the blood, therefore allowing survival after birth *ex utero* (32). The importance of the GR for survival after birth becomes apparent even more when studying GR deficient mice. At birth, these GR$^{-/-}$ mice die within a few hours due to respiratory distress, which seems to be mediated through severe lung atelectasis (33). Interestingly, in these GR$^{-/-}$ mice, severe lung atelectasis could not be linked to an impaired surfactant homeostasis. In the present study, we studied mice with

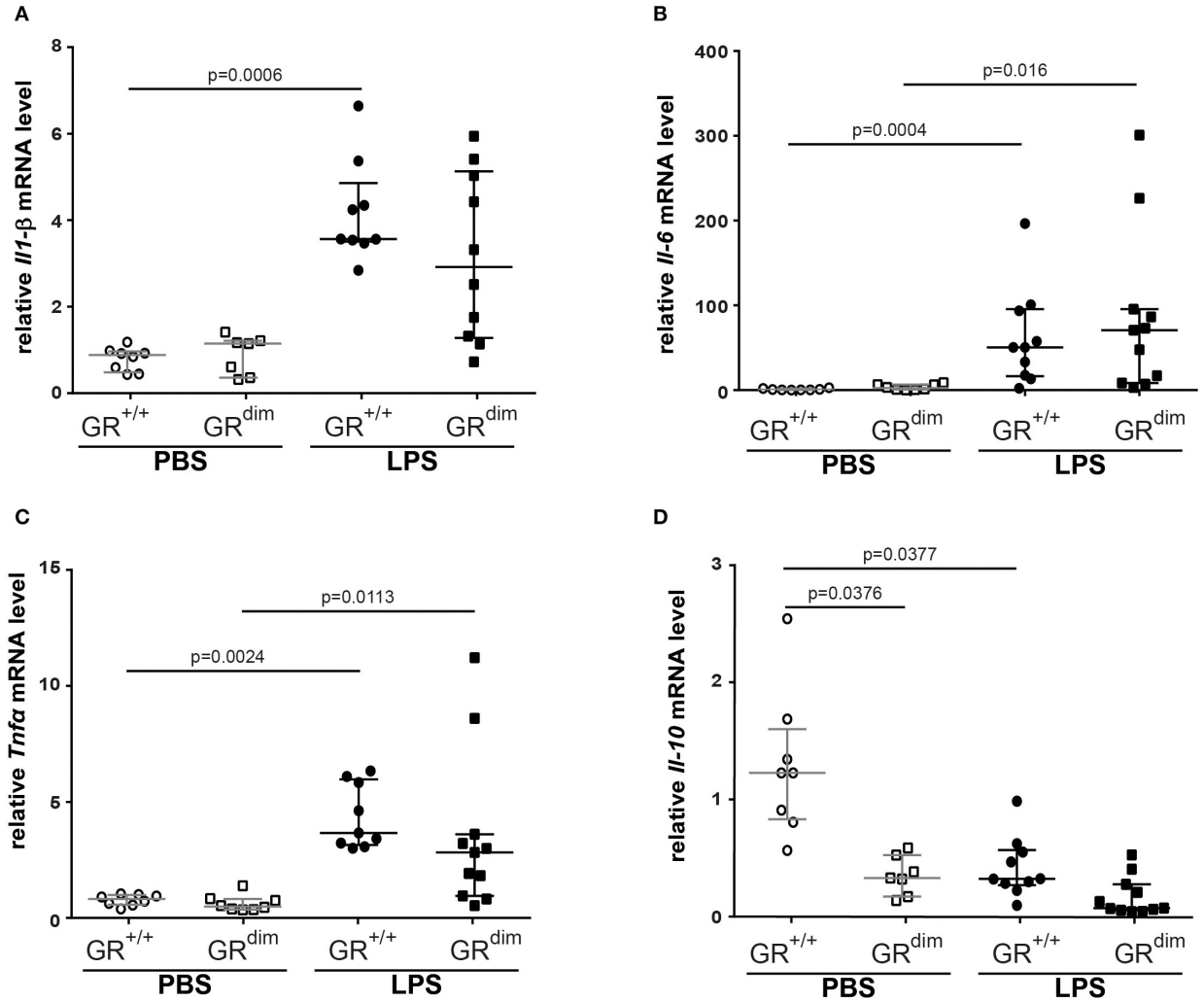

FIGURE 5 | Measurements of relative mRNA level of cytokines in lung tissue. Relative mRNA level of **(A)** interleukin 1β (*Il-1β*), **(B)** interleukin 6 (*Il-6*), **(C)** tumor necrosis factor α (*Tnfα*), and **(D)** interleukin 10 (*Il-10*) in lung tissue of GR$^{dim/dim}$ and GR$^{+/+}$ mice intraperitoneally challenged with lipopolysaccharide (LPS) or vehicle (PBS). LPS = lipopolysaccharide from *Escherichia coli* [055:B5], 10 mg·kg^{-1}, dissolved in 10 µl·g^{-1} phosphate buffered saline (PBS). GR$^{+/+}$ mice challenged with PBS: n = 8, GR$^{dim/dim}$ mice challenged with PBS: n = 7–8, GR$^{+/+}$ mice challenged with LPS: n = 9–10, GR$^{dim/dim}$ mice challenged with LPS: n = 10–11. Data is presented as median (25th and 75th percentile and minimum/maximum).

an attenuated GR dimerization (GR$^{dim/dim}$), which leads to only partial GR impairment; therefore these mice survive after birth. However, in our model of systemic inflammation via LPS-challenge, GR$^{dim/dim}$ mice presented with impaired lung function, here indicated by a reduced lung compliance (**Figure 4A**). This reduced lung compliance was accompanied by a clear trend toward an increased albumin extravasation in GR$^{dim/dim}$ mice after LPS-challenge (**Figure 4B**), indicating an impaired lung barrier function. Independent of the presence or absence of ICU treatment, we (13) and others (34–36) reported an impaired lung barrier function after LPS-challenge in previous studies. A major mediator of endothelial barrier function in the lung is sphingosine kinase 1 (SphK1). The impaired lung barrier function in our previous study could be linked to a GR dimerization-dependent SphK1 expression in myeloid cells, particularly macrophages, because ablation of the SphK1 gene in the myeloid lineage abolished GC effects on vascular leakage and inflammation (13). In addition, mice with a complete deletion of SphK1 (SphK1$^{-/-}$) are highly susceptible to LPS-induced ALI and exhibit increased lung vascular leakage (37). In the current study, reduced lung compliance after LPS-challenge was accompanied by a significantly lower *Sphk1* expression in GR$^{dim/dim}$ mice (**Figure 4C**), highlighting the contribution of *Sphk1* expression to mediate a physiological lung function. In addition, there was no change in lung compliance in GR$^{+/+}$ mice despite LPS-challenge but a significant increase of lung *Sphk1* expression compared to PBS-treated GR$^{+/+}$ mice, which also might suggest a beneficial impact of SphK1

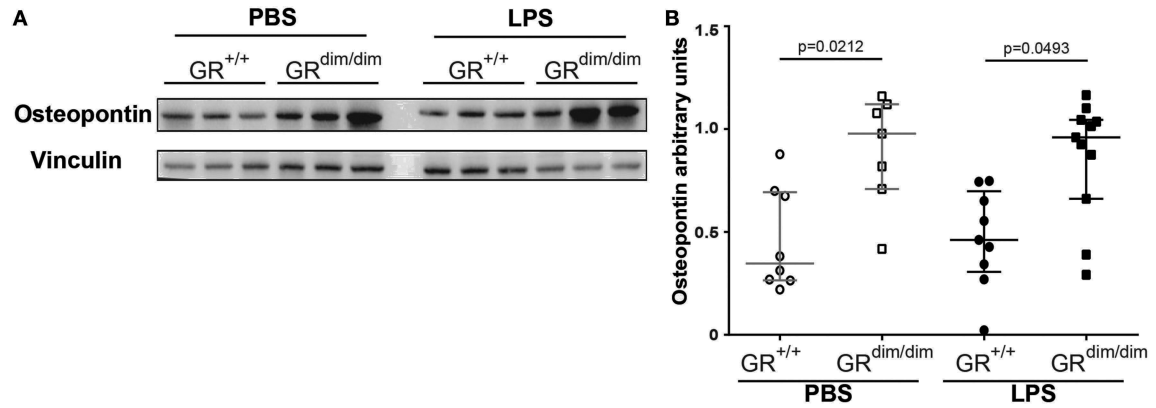

FIGURE 6 | Analysis of Osteopontin (Opn) levels in lung tissue. **(A)** Representative western blot analysis and **(B)** arbitrary units of Opn, in lung tissue of GR$^{dim/dim}$ and GR$^{+/+}$ mice intraperitoneally challenged with lipopolysaccharide (LPS) or vehicle (PBS). LPS = lipopolysaccharide from *Escherichia coli* [055:B5], 10 mg·kg^{-1}, dissolved in 10 μl·g^{-1} phosphate buffered saline (PBS). GR$^{+/+}$ mice challenged with PBS: $n = 8$, GR$^{dim/dim}$ mice challenged with PBS: $n = 7$, GR$^{+/+}$ mice challenged with LPS: $n = 9$, GR$^{dim/dim}$ mice challenged with LPS: $n = 11$. Data is presented as median (25th and 75th percentile and minimum/maximum).

in lung function. However, PBS-treated GR$^{dim/dim}$ mice revealed a trend toward a reduced lung *Sphk1* expression, which correlates with the trend, however, not significant, to reduced lung compliance in GR$^{dim/dim}$ animals.

The glucocorticoid receptor is involved in modulating the host response to inflammatory stimuli; therefore, we assessed cytokine mRNA levels in lung tissue (**Figure 5**) as well as cytokine concentrations in the plasma (**Figure 3** and **Table 3**). Interestingly, we did not find any significant genotype difference in systemic inflammatory mediators in the plasma and lung mRNA expression after LPS-challenge. However, in our previous LPS-induced endotoxic shock model without intensive care management we already described that GR$^{dim/dim}$ mice present increased levels of inflammatory mediators at later time points (18). This could explain the difference to our present findings, where mice were observed for only 6 h after LPS-induced endotoxic shock under intensive care management.

Another inflammatory mediator involved in the pathogenesis of inflammatory diseases is osteopontin (Opn) (38, 39), especially in the lung, as patients with various pulmonary diseases revealed increased lung Opn expression (40–45). Furthermore, in experimental models of lung diseases (asthma, lung injury, lung fibrosis), Opn has a detrimental and functional role (40, 46–50), and, moreover, Opn neutralizing antibody could protect mice against ALI during sepsis (28). We showed that mice with an impaired GR dimerization have elevated Opn protein expression in the lung, the same animals that had a significant decrease in lung compliance after LPS-induced endotoxic shock. The finding that Opn might be a critical regulator of lung compliance is supported by Opn knockout mice showing an increased lung compliance (51). Here we describe, for the first time, that Opn expression in the lung is linked with GR dimerization. Mice lacking GR dimerization had increased Opn expression in the lung, which was accompanied by impaired lung mechanics.

Il-10 is described to be negatively regulated by Opn in LPS-stimulated macrophages, higher Il-10 levels were observed during infections in Opn knockout mice (29). Our data showed a trend to reduced *Il-10* expression in the lung of PBS-treated GR$^{dim/dim}$ mice (**Figure 5**), and this effect was enhanced in the inflammatory setting. In addition, GR$^{+/+}$ animals revealed a trend to reduced *Il-10* expression in the lung upon inflammation, independent of Opn, suggesting an alternative regulation of *Il-10* that might be mis-regulated in GR$^{dim/dim}$ animals. Possibly, the duration of the GR$^{dim/dim}$ mice in the intensive care management during systemic inflammation was too short to detect more pronounced effects concerning inflammatory cytokines, because our previous results during systemic inflammation (without intensive care management) revealed significant differences at later time points only (18).

In conclusion, impairment of GR dimerization aggravates systemic hypotension and impairs lung function during LPS-induced endotoxic shock in mice. We now demonstrate that the GR dimer is an important mediator of hemodynamic stability and lung function during LPS-induced systemic inflammation. Further studies are warranted to examine if selective activation of the GR dimer may be able to attenuate lung injury during systemic inflammation.

DATA AVAILABILITY STATEMENT

All datasets generated for this study are included in the article/**Supplementary Material**.

ETHICS STATEMENT

The animal study was reviewed and approved by the federal authorities for animal research of the Regierungspräsidium Tübingen, Baden-Wuerttemberg, Germany.

AUTHOR CONTRIBUTIONS

SV, MW, EC, PR, and JT conceived and designed the study. SV, MW, JP, TM, CH, UW, OM, JV, SK, MG, MF, EC, and UB performed the experiments and organ analysis. AS and PM examined the histology. SV, MW, JP, TM, UW, and OM analyzed the data and interpreted the results. SV, JP, and MW prepared the figures. SV and MW wrote the manuscript. PR and JT revised the manuscript.

FUNDING

PR and JT were supported by the Deutsche Forschungsgemeinschaft (Collaborative Research Center 1149, DFG Tu 220/13-1 to JT). MW was supported by the GEROK program of the Deutsche Forschungsgemeinschaft (Collaborative Research Center 1149), and the University Hospital Ulm. CH was supported by the Hertha-Nathorff-Fellowship of the Medical Faculty of Ulm University. SV was supported by the Deutsche Forschungsgemeinschaft (Collaborative Research Center 1149), Pulmosens GRK 2203, and the University Hospital Ulm.

ACKNOWLEDGMENTS

We are grateful to the staff of the animal facilities of the University of Ulm, our animal welfare officer Dr. Sibylle Ott and in particular to Birgit Widmann.

SUPPLEMENTARY MATERIAL

The Supplementary Material for this article can be found online at: https://www.frontiersin.org/articles/10.3389/fimmu.2019.03152/full#supplementary-material

REFERENCES

1. Lim H-W, Uhlenhaut NH, Rauch A, Weiner J, Hübner S, Hübner N, et al. Genomic redistribution of GR monomers and dimers mediates transcriptional response to exogenous glucocorticoid *in vivo*. *Genome Res.* (2015) 25:836–44. doi: 10.1101/gr.188581.114
2. Reichardt HM, Tuckermann JP, Göttlicher M, Vujic M, Weih F, Angel P, et al. Repression of inflammatory responses in the absence of DNA binding by the glucocorticoid receptor. *EMBO J.* (2001) 20:7168–73. doi: 10.1093/emboj/20.24.7168
3. Tuckermann JP, Reichardt HM, Arribas R, Richter KH, Schütz G, Angel P. The DNA binding-independent function of the glucocorticoid receptor mediates repression of AP-1-dependent genes in skin. *J Cell Biol.* (1999) 147:1365–70. doi: 10.1083/jcb.147.7.1365
4. de Bosscher K, Schmitz ML, Vanden Berghe W, Plaisance S, Fiers W, Haegeman G. Glucocorticoid-mediated repression of nuclear factor-κB-dependent transcription involves direct interference with transactivation. *Proc Natl Acad Sci USA.* (1997) 94:13504–9. doi: 10.1073/pnas.94.25.13504
5. Heck S, Bender K, Kullmann M, Göttlicher M, Herrlich P, Cato AC. IκBα-independent downregulation of NF-κB activity by glucocorticoid receptor. *EMBO J.* (1997) 16:4698–707. doi: 10.1093/emboj/16.15.4698
6. Jonat C, Rahmsdorf HJ, Park KK, Cato AC, Gebel S, Ponta H, et al. Antitumor promotion and antiinflammation: down-modulation of AP-1 (Fos/Jun) activity by glucocorticoid hormone. *Cell.* (1990) 62:1189–204. doi: 10.1016/0092-8674(90)90395-U
7. Yang-Yen HF, Chambard JC, Sun YL, Smeal T, Schmidt TJ, Drouin J, et al. Transcriptional interference between c-Jun and the glucocorticoid receptor: mutual inhibition of DNA binding due to direct protein-protein interaction. *Cell.* (1990) 62:1205–15. doi: 10.1016/0092-8674(90)90396-V
8. Schüle R, Rangarajan P, Kliewer S, Ransone LJ, Bolado J, Yang N, et al. Functional antagonism between oncoprotein c-Jun and the glucocorticoid receptor. *Cell.* (1990) 62:1217–26. doi: 10.1016/0092-8674(90)90397-W
9. Ogawa S, Lozach J, Benner C, Pascual G, Tangirala RK, Westin S, et al. Molecular determinants of crosstalk between nuclear receptors and toll-like receptors. *Cell.* (2005) 122:707–21. doi: 10.1016/j.cell.2005.06.029
10. Reily MM, Pantoja C, Hu X, Chinenov Y, Rogatsky I. The GRIP1:IRF3 interaction as a target for glucocorticoid receptor-mediated immunosuppression. *EMBO J.* (2006) 25:108–17. doi: 10.1038/sj.emboj.7600919
11. Flammer JR, Dobrovolna J, Kennedy MA, Chinenov Y, Glass CK, Ivashkiv LB, et al. The type I interferon signaling pathway is a target for glucocorticoid inhibition. *Mol Cell Biol.* (2010) 30:4564–74. doi: 10.1128/MCB.00146-10
12. Hübner S, Dejager L, Libert C, Tuckermann JP. The glucocorticoid receptor in inflammatory processes: transrepression is not enough. *Biol Chem.* (2015) 396:1223–31. doi: 10.1515/hsz-2015-0106
13. Vettorazzi S, Bode C, Dejager L, Frappart L, Shelest E, Klaßen C, et al. Glucocorticoids limit acute lung inflammation in concert with inflammatory stimuli by induction of SphK1. *Nat Commun.* (2015) 6:7796. doi: 10.1038/ncomms8796
14. Frijters R, Fleuren W, Toonen, Erik J M, Tuckermann JP, Reichardt HM, et al. Prednisolone-induced differential gene expression in mouse liver carrying wild type or a dimerization-defective glucocorticoid receptor. *BMC Genomics.* (2010) 11:359. doi: 10.1186/1471-2164-11-359
15. Tuckermann JP, Kleiman A, Moriggl R, Spanbroek R, Neumann A, Illing A, et al. Macrophages and neutrophils are the targets for immune suppression by glucocorticoids in contact allergy. *J Clin Invest.* (2007) 117:1381–90. doi: 10.1172/JCI28034
16. Baschant U, Frappart L, Rauchhaus U, Bruns L, Reichardt HM, Kamradt T, et al. Glucocorticoid therapy of antigen-induced arthritis depends on the dimerized glucocorticoid receptor in T cells. *Proc Natl Acad Sci USA.* (2011) 108:19317–22. doi: 10.1073/pnas.1105857108
17. Vandevyver S, Dejager L, van Bogaert T, Kleyman A, Liu Y, Tuckermann J, et al. Glucocorticoid receptor dimerization induces MKP1 to protect against TNF-induced inflammation. *J Clin Invest.* (2012) 122:2130–40. doi: 10.1172/JCI60006
18. Kleiman A, Hübner S, Rodriguez Parkitna JM, Neumann A, Hofer S, Weigand MA, et al. Glucocorticoid receptor dimerization is required for survival in septic shock via suppression of interleukin-1 in macrophages. *FASEB J.* (2012) 26:722–9. doi: 10.1096/fj.11-192112
19. Blé F-X, Cannet C, Zurbruegg S, Gérard C, Frossard N, Beckmann N, et al. Activation of the lung S1P(1) receptor reduces allergen-induced plasma leakage in mice. *Br J Pharmacol.* (2009) 158:1295–301. doi: 10.1111/j.1476-5381.2009.00391.x
20. Zhao Y, Gorshkova IA, Berdyshev E, He D, Fu P, Ma W, et al. Protection of LPS-induced murine acute lung injury by sphingosine-1-phosphate lyase suppression. *Am J Respir Cell Mol Biol.* (2011) 45:426–35. doi: 10.1165/rcmb.2010-0422OC
21. Reichardt HM, Kaestner KH, Tuckermann J, Kretz O, Wessely O, Bock R, et al. DNA binding of the glucocorticoid receptor is not essential for survival. *Cell.* (1998) 93:531–41. doi: 10.1016/S0092-8674(00)81183-6
22. Gröger M, Wepler M, Wachter U, Merz T, McCook O, Kress S, et al. The effects of genetic 3-mercaptopyruvate sulfurtransferase deficiency in murine traumatic-hemorrhagic shock. *Shock.* (2019) 51:472–8. doi: 10.1097/SHK.0000000000001165

23. Hartmann C, Gröger M, Noirhomme J-P, Scheuerle A, Möller P, Wachter U, et al. In-depth characterization of the effects of cigarette smoke exposure on the acute trauma response and hemorrhage in mice. *Shock.* (2018) 51:68–77. doi: 10.1097/SHK.0000000000001115
24. Wagner K, Gröger M, McCook O, Scheuerle A, Asfar P, Stahl B, et al. Blunt chest trauma in mice after cigarette smoke-exposure: effects of mechanical ventilation with 100% O_2. *PLoS ONE.* (2015) 107:e0132810. doi: 10.1371/journal.pone.0132810
25. Wagner F, Scheuerle A, Weber S, Stahl B, McCook O, Knöferl MW, et al. Cardiopulmonary, histologic, and inflammatory effects of intravenous Na2S after blunt chest trauma-induced lung contusion in mice. *J Trauma.* (2011) 71:1659–67. doi: 10.1097/TA.0b013e318228842e
26. Barth E, Albuszies G, Baumgart K, Matejovic M, Wachter U, Vogt J, et al. Glucose metabolism and catecholamines. *Crit Care Med.* (2007) 35(9 Suppl.):S508–18. doi: 10.1097/01.CCM.0000278047.06965.20
27. Vogt JA, Wachter U, Wagner K, Calzia E, Gröger M, Weber S, et al. Effects of glycemic control on glucose utilization and mitochondrial respiration during resuscitated murine septic shock. *Intensive Care Med Exp.* (2014) 21:19. doi: 10.1186/2197-425X-2-19
28. Hirano Y, Aziz M, Yang W-L, Wang Z, Zhou M, Ochani M, et al. Neutralization of osteopontin attenuates neutrophil migration in sepsis-induced acute lung injury. *Crit Care.* (2015) 19:53. doi: 10.1186/s13054-015-0782-3
29. Ashkar S, Weber GF, Panoutsakopoulou V, Sanchirico ME, Jansson M, Zawaideh S, et al. Eta-1 (osteopontin): an early component of type-1 (cell-mediated) immunity. *Science.* (2000) 287:860–4. doi: 10.1126/science.287.5454.860
30. Goodwin JE, Feng Y, Velazquez H, Sessa WC. Endothelial glucocorticoid receptor is required for protection against sepsis. *Proc Natl Acad Sci USA.* (2013) 110:306–11. doi: 10.1073/pnas.1210200110
31. Wallerath T, Witte K, Schäfer SC, Schwarz PM, Prellwitz W, Wohlfart P, et al. Down-regulation of the expression of endothelial NO synthase is likely to contribute to glucocorticoid-mediated hypertension. *Proc Natl Acad Sci USA.* (1999) 96:13357–62. doi: 10.1073/pnas.96.23.13357
32. Bird AD, McDougall ARA, Seow B, Hooper SB, Cole TJ. Glucocorticoid regulation of lung development: lessons learned from conditional GR knockout mice. *Mol Endocrinol.* (2015) 29:158–71. doi: 10.1210/me.2014-1362
33. Cole TJ, Blendy JA, Monaghan AP, Krieglstein K, Schmid W, Aguzzi A, et al. Targeted disruption of the glucocorticoid receptor gene blocks adrenergic chromaffin cell development and severely retards lung maturation. *Genes Dev.* (1995) 9:1608–21. doi: 10.1101/gad.9.13.1608
34. Kreil EA, Greene E, Fitzgibbon C, Robinson DR, Zapol WM. Effects of recombinant human tumor necrosis factor alpha, lymphotoxin, and *Escherichia coli* lipopolysaccharide on hemodynamics, lung microvascular permeability, and eicosanoid synthesis in anesthetized sheep. *Circ Res.* (1989) 65:502–14. doi: 10.1161/01.RES.65.2.502
35. Petersen B, Bloch KD, Ichinose F, Shin H-S, Shigematsu M, Bagchi A, et al. Activation of Toll-like receptor 2 impairs hypoxic pulmonary vasoconstriction in mice. *Am J Physiol Lung Cell Mol Physiol.* (2008) 294:L300–8. doi: 10.1152/ajplung.00243.2007
36. Ichinose F, Zapol WM, Sapirstein A, Ullrich R, Tager AM, Coggins K, et al. Attenuation of hypoxic pulmonary vasoconstriction by endotoxemia requires 5-lipoxygenase in mice. *Circ Res.* (2001) 88:832–8. doi: 10.1161/hh0801.089177
37. Wadgaonkar R, Patel V, Grinkina N, Romano C, Liu J, Zhao Y, et al. Differential regulation of sphingosine kinases 1 and 2 in lung injury. *Am J Physiol Lung Cell Mol Physiol.* (2009) 296:L603–13. doi: 10.1152/ajplung.90357.2008
38. Lamort A-S, Giopanou I, Psallidas I, Stathopoulos GT. Osteopontin as a link between inflammation and cancer: the thorax in the spotlight. *Cells.* (2019) 8:815. doi: 10.3390/cells8080815
39. Rittling SR, Singh R. Osteopontin in immune-mediated diseases. *J Dent Res.* (2015) 94:1638–45. doi: 10.1177/0022034515605270
40. Takahashi F, Takahashi K, Shimizu K, Cui R, Tada N, Takahashi H, et al. Osteopontin is strongly expressed by alveolar macrophages in the lungs of acute respiratory distress syndrome. *Lung.* (2004) 182:173–85. doi: 10.1007/s00408-004-0309-1
41. Nau GJ, Guilfoile P, Chupp GL, Berman JS, Kim SJ, Kornfeld H, et al. A chemoattractant cytokine associated with granulomas in tuberculosis and silicosis. *Proc Natl Acad Sci USA.* (1997) 94:6414–9. doi: 10.1073/pnas.94.12.6414
42. O'Regan AW, Chupp GL, Lowry JA, Goetschkes M, Mulligan N, Berman JS. Osteopontin is associated with T cells in sarcoid granulomas and has T cell adhesive and cytokine-like properties *in vitro*. *J Immunol.* (1999) 162:1024–31.
43. Kelly MM, Leigh R, Gilpin SE, Cheng E, Martin GEM, Radford K, et al. Cell-specific gene expression in patients with usual interstitial pneumonia. *Am J Respir Crit Care Med.* (2006) 174:557–65. doi: 10.1164/rccm.200510-1648OC
44. Carlson I, Tognazzi K, Manseau EJ, Dvorak HF, Brown LF. Osteopontin is strongly expressed by histiocytes in granulomas of diverse etiology. *Lab Invest.* (1997) 77:103–8.
45. van der Windt GJW, Hoogendijk AJ, Schouten M, Hommes TJ, Vos AF de, Florquin S, et al. Osteopontin impairs host defense during pneumococcal pneumonia. *J Infect Dis.* (2011) 203:1850–8. doi: 10.1093/infdis/jir185
46. Simoes DCM, Xanthou G, Petrochilou K, Panoutsakopoulou V, Roussos C, Gratziou C. Osteopontin deficiency protects against airway remodeling and hyperresponsiveness in chronic asthma. *Am J Respir Crit Care Med.* (2009) 179:894–902. doi: 10.1164/rccm.200807-1081OC
47. Xanthou G, Alissafi T, Semitekolou M, Simoes DCM, Economidou E, Gaga M, et al. Osteopontin has a crucial role in allergic airway disease through regulation of dendritic cell subsets. *Nat Med.* (2007) 13:570–8. doi: 10.1038/nm1580
48. Kohan M, Breuer R, Berkman N. Osteopontin induces airway remodeling and lung fibroblast activation in a murine model of asthma. *Am J Respir Cell Mol Biol.* (2009) 41:290–6. doi: 10.1165/rcmb.2008-0307OC
49. Berman JS, Serlin D, Li X, Whitley G, Hayes J, Rishikof DC, et al. Altered bleomycin-induced lung fibrosis in osteopontin-deficient mice. *Am J Physiol Lung Cell Mol Physiol.* (2004) 286:L1311–8. doi: 10.1152/ajplung.00394.2003
50. Takahashi F, Takahashi K, Okazaki T, Maeda K, Ienaga H, Maeda M, et al. Role of osteopontin in the pathogenesis of bleomycin-induced pulmonary fibrosis. *Am J Respir Cell Mol Biol.* (2001) 24:264–71. doi: 10.1165/ajrcmb.24.3.4293
51. Ganguly K, Martin TM, Concel VJ, Upadhyay S, Bein K, Brant KA, et al. Secreted phosphoprotein 1 is a determinant of lung function development in mice. *Am J Respir Cell Mol Biol.* (2014) 51:637–51. doi: 10.1165/rcmb.2013-0471OC

Conflict of Interest: The authors declare that the research was conducted in the absence of any commercial or financial relationships that could be construed as a potential conflict of interest.

Copyright © 2020 Wepler, Preuss, Merz, Hartmann, Wachter, McCook, Vogt, Kress, Gröger, Fink, Scheuerle, Möller, Calzia, Burret, Radermacher, Tuckermann and Vettorazzi. This is an open-access article distributed under the terms of the Creative Commons Attribution License (CC BY). The use, distribution or reproduction in other forums is permitted, provided the original author(s) and the copyright owner(s) are credited and that the original publication in this journal is cited, in accordance with accepted academic practice. No use, distribution or reproduction is permitted which does not comply with these terms.

frontiers in Immunology

ORIGINAL RESEARCH
published: 03 February 2020
doi: 10.3389/fimmu.2020.00053

Short-Chain Alcohols Upregulate GILZ Gene Expression and Attenuate LPS-Induced Septic Immune Response

Hang Pong Ng[1], *Scott Jennings*[1], *Steve Nelson*[2] *and Guoshun Wang*[1,2]*

[1] Department of Microbiology, Immunology and Parasitology, Louisiana State University Health Sciences Center, New Orleans, LA, United States, [2] Department of Medicine, Louisiana State University Health Sciences Center, New Orleans, LA, United States

Alcohol differentially affects human health, depending on the pattern of exposure. Moderate intake provides beneficial mood modulation and an anti-inflammatory effect, while excessive consumption leads to immunosuppression and various alcohol use disorders. The mechanism underlying this bi-phasic action mode of alcohol has not been clearly defined. Our previous publication demonstrated that ethanol, in the absence of glucocorticoids (GCs), induces expression of Glucocorticoid-Induced Leucine Zipper (GILZ), a key molecule that transduces GC anti-inflammatory effect through a non-canonical activation of glucocorticoid receptor (1). Here we report that similar short-chain alcohols, such as ethanol, propanol and isopropanol, share the same property of upregulating GILZ gene expression, and blunt cell inflammatory response *in vitro*. When mice were exposed to these alcohols, GILZ gene expression in immune cells was augmented in a dose-dependent manner. Monocytes and neutrophils were most affected. The short-chain alcohols suppressed host inflammatory response to lipopolysaccharide (LPS) and significantly reduced LPS-induced mortality. Intriguingly, propanol and isopropanol displayed more potent protection than ethanol at the same dose. Inhibition of ethanol metabolism enhanced the ethanol protective effect, suggesting that it is ethanol, not its derivatives or metabolites, that induces immune suppression. Taken together, short-chain alcohols *per se* upregulate GILZ gene expression and provide immune protection against LPS toxicity, suggesting a potential measure to counter LPS septic shock in a resource limited situation.

Keywords: ethanol, propanol, isopropanol, anti-inflammation, immunosuppression, GILZ, LPS, septic shock

OPEN ACCESS

Edited by:
Lukas Martin,
University Hospital RWTH Aachen, Germany

Reviewed by:
Babak Baban,
Augusta University, United States
Carlo Riccardi,
University of Perugia, Italy
Borna Relja,
Otto von Guericke University, Germany
Emira Ayroldi,
University of Perugia, Italy

***Correspondence:**
Guoshun Wang
gwang@lsuhsc.edu

Specialty section:
This article was submitted to Inflammation, a section of the journal Frontiers in Immunology

Received: *08 July 2019*
Accepted: *09 January 2020*
Published: *03 February 2020*

Citation:
Ng HP, Jennings S, Nelson S and Wang G (2020) Short-Chain Alcohols Upregulate GILZ Gene Expression and Attenuate LPS-Induced Septic Immune Response. Front. Immunol. 11:53. doi: 10.3389/fimmu.2020.00053

INTRODUCTION

An alcohol is any organic compound in which a hydroxyl group (−OH) is bound to a carbon atom of an alkyl or substituted alkyl group. In daily life, alcohol usually refers to ethanol, also known as grain alcohol or spirits of wine. Because of its mood modulation property, ethanol is one of the most consumed recreational substances, which often leads to abuse. In medicine, ethanol and its similar short-chain alcohols (propanol and isopropanol) are commonly used as antiseptics and disinfectants. Ethanol has long been known to be anti-inflammatory

and immunosuppressive. Moderate ethanol intake is associated with reductions in many adverse health conditions, including coronary artery disease, diabetes, hypertension, congestive heart failure, stroke, arthritis, and dementia (2–4). However, excessive ethanol intake has been clearly linked to organ and tissue damage (4–6) and life-threatening medical disorders (7, 8). Alcohol abuse predisposes individuals to infections by bacteria, fungi, and viruses (4, 9–12) and leads to specific defects in innate and adaptive immunity (7, 13). Acute ethanol exposure, *in vitro* as well as *in vivo*, inhibits the production of pro-inflammatory mediators, including TNF-α, IL-1, IL-6, IL-8, and MCP-1 (14), and enhances the production of anti-inflammatory mediators, such as IL-10 (15). Additionally, acute ethanol exposure reduces lipopolysaccharide (LPS)-induced inflammatory response *in vivo* (16, 17) and protects mice against staphylococcal enterotoxin B (18, 19). Multiple inflammatory networks, including AP-1 and NF-κB, are reported to be involved in alcohol tempering host response to LPS and SEB (20). However, the upstream signaling pathways underlying this alcohol immunosuppressive effect have not been clearly defined.

Sepsis is defined as a life-threatening organ dysfunction caused by a dysregulated host response to infection (21, 22), which frequently manifests an initial hyper-inflammatory phase, reflected by fever, shock, and respiratory failure (23). If patients survive the initial phase and sepsis persists, they enter a phase of immunosuppression (22, 24, 25). Septic shock, a subset of sepsis marked by severe circulatory, cellular, and metabolic abnormalities, is associated with a greater risk of mortality than sepsis alone (21). Septic shock caused by LPS, the major component of the cell wall of Gram-negative bacteria, is a common condition encountered clinically (26). To study the disease process, an animal model often employed is the peritoneal challenge of mice with LPS. Strikingly, there are natural mouse strains that are exceptionally resistant to LPS. For example, SPRET/Ei mice are highly resistant to LPS and Gram-negative bacterial infection (27), while C3H/HeJ and C57BL10/ScCr mouse strains are resistant to LPS, but susceptible to bacterial infection (28). Genetic analyses of both have revealed that the C3H/HeJ and C57BL10/ScCr mice are deficient in Toll-like receptor 4 (TLR4) function. In contrast, the SPRET/Ei mice highly express Glucocorticoid-Induced Leucine Zipper (GILZ), a member of the transforming growth factor-beta (TGF-β)-stimulated clone-22 (TSC22) family (29) from the gene located on the X-chromosome (30). GILZ, ubiquitously expressed, is primarily regulated by glucocorticoid receptor (GR) signaling to transduce glucocorticoid (GC) effects (31–34). GILZ is known to regulate cell apoptosis, proliferation and differentiation, and to modulate host immunity and inflammation (35–39). More evidence suggesting the crucial role of GILZ in LPS resistance comes from mice receiving recombinant cell-permeable GILZ protein. The GILZ protein administration leads to increased resistance to LPS and reduced LPS-induced mortality (40). Moreover, overexpression of GILZ protects mice against lethal septic peritonitis (41). Directly related to the current alcohol study, our and others' research indicated that ethanol activates GR signaling in the absence of GCs (42, 43). This activation is through ethanol interplay with the cytoplasmic GR complex, releasing GR without GC coupling. The bare GR enters the nuclei to activate its downstream responsive genes, including GILZ (1), which contributes to ethanol inflammosuppression and immunosuppression.

In the current study, we hypothesized that if ethanol indeed prompts GR-GILZ signaling non-canonically, other short-chain alcohols should share the same effect. To test this hypothesis, we compared ethanol, propanol and isopropanol in their modulation of GILZ expression and their effect on host protection against LPS septic immune response.

MATERIALS AND METHODS

Reagents

Dexamethasone, mifepristone, fomepizole, and common reagents were purchased from Sigma-Aldrich. Lipopolysaccharide (*E. coli*, serotype O111:B4 L2630) was from List Biological Laboratories (Campbell, CA) or from Sigma-Aldrich. Pure anhydrous ethyl alcohol or ethanol (200 proof/100%, Koptec), propanol (Sigma-Aldrich), and isopropanol (2-propanol, Sigma-Aldrich) were obtained commercially.

Cell Culture and Treatments

Human Mono-Mac-6 (MM6) cells were cultured in advanced RPMI-1640 (Invitrogen, Carlsbad, CA) supplemented with 10% fetal bovine serum (FBS) (HyClone, Logan, Utah), 2 mM GlutaMax (Gibco), 100 U/ml penicillin, 100 μg/ml streptomycin, 0.25 μg/ml amphotericin B, OPI media supplement, and non-essential amino acids. The cells were incubated in 5% CO_2 at 37°C. When alcohol and/or LPS were applied, freshly cultured MM6 cells were exposed to ethanol, propanol, or isopropanol at the level of 50 mM for 24 h in a respective alcohol presaturated incubator. LPS (1 μg/ml) was added 1 h after alcohol addition, and kept in the system until cell harvest. Cells were pelleted and supernatants were collected for cytokine measurements.

Real-Time Quantitative PCR (RT-qPCR) and Immunofluorescent Staining to Measure GILZ Gene Expression in MM6 Cells

RT-qPCR of GILZ mRNA

MM6 cells (1.5×10^6) were exposed to one of the short-chain alcohols (ethanol, propanol or isopropanol) at a 50-mM concentration or 1 μM dexamethasone (Dex) for 24 h in the presence or absence of 5 μM mifepristone. The cells were harvested and washed twice with 1x PBS. Total RNAs were extracted using the Qiagen RNeasy Kit. The cDNAs were synthesized using the Quantitect Reverse Transcriptase Kit (Qiagen). Human GILZ primers (GILZ-F: 5′-CATGGAGGTGGCGGTCTATC-3′ and GILZ-R: 5′-CACCTCCTCTCTCACAGCGT-3′) and Glyceraldehyde 3-phosphate dehydrogenase (GAPDH) primers (GAPDH-F: 5′-AAGGTCGGAGTCAACGGATTTGGT-3′ and GAPDH-R: 5′- ACAAAGTGGTCGTTGAGGGCAATG-3′) were used at a final concentration of 500 nM, as published previously (1). The final reaction for each sample was brought to a total volume

of 20 μl with RT SYBR green qPCR mastermix (Qiagen). All reactions were carried out in duplicate on a CFX96 system (Bio-Rad Laboratories, Hercules, CA) for quantitative real-time PCR (qPCR) detection. The qPCR data were analyzed by the comparative Ct (ΔΔCT) method. The expression of GILZ of each treated group was compared to that of GAPDH, and normalized to the non-treatment group.

Immunofluorescence Staining of GILZ Protein in MM6 Cells

MM6 cells (1.5×10^6) were exposed to ethanol, propanol or isopropanol at a final concentration of 50 mM or dexamethasone (Dex, 1 μM) for 24 h. The cells were then fixed with 4% paraformaldehyde for 1 h at room temperature. The fixed cells were permeabilized with 0.5% Triton X-100/PBS for 1 h, washed with PBS, and blocked with Blocking Buffer [PBS containing 0.1% Triton X-100, 2% donkey serum and 1% bovine serum albumin (BSA)], for 1 h. GILZ expression was detected by staining with a rabbit anti-GILZ antibody (5 μg/ml; Santa Cruz Biotechnology, Dallas, Texas) for 1 h. PE-conjugated $F(ab)_2$ donkey anti-rabbit IgG (5 μg/ml; Jackson ImmunoResearch Laboratories, Inc., West Grove, PA) was used as the secondary antibody. The stained cells were analyzed by flow cytometry.

ELISA Measurements of Human Cytokines From MM6 Cells

MM6 cells were exposed to 50 mM ethanol, propanol, or isopropanol for 24 h. LPS (1 μg/ml) was added 1 h after alcohol addition, and was kept in the system until cell harvest. After centrifuging to pellet cells, the supernatants were collected for TNF-α and IL-6 production measurement using ELISA (R & D Systems, Minneapolis, MN).

Animal Experiments

This animal research was approved by the LSUHSC Institutional Animal Care and Use Committee (IACUC #3578). Adult C57BL/6 mice (7–12 weeks old, mixed sex) were either purchased from The Jackson Laboratory or produced from our breeding colony.

Alcohol Exposure and LPS Challenge

Mice were exposed to ethanol (2 or 4 g/kg), propanol (2 g/kg), isopropanol (2 g/kg) or PBS via intraperitoneal injection. One hour later, a lethal dose of LPS (10 mg/kg, i.p.) was injected. Animals were monitored every 2 h for 36 h post LPS injection. Then, the surviving animals were continuously observed once a day for one more week before termination of the experiment. For experiments where alcohol dehydrogenase inhibitor was applied, fomepizole (10 mg/ml) was injected with the alcohol solutions. For serum cytokine measurements, a separate set of animals that received a similar procedure was reserved. The assigned animals at the indicated time points were anesthetized and bled via cardiac puncture. Serum from each animal was obtained and stored at −20°C until use.

Assessment of Alcohol Influence of GILZ Expression in Peripheral Blood Leukocytes

Mice were intraperitoneally injected with dose-escalating ethanol, propanol, or isopropanol at 0, 2, and 4 g/kg, respectively. Peripheral blood was collected 16 h post-injection. After red blood cell lysis, peripheral blood leukocytes were fixed in 4% paraformaldehyde, followed by permeabilization with 0.5% Triton X-100 in PBS for 1 h. After washing with PBS, the cells were blocked with Blocking Buffer (PBS containing 0.1% Triton X-100, 2% donkey serum and 1% BSA) for 1 h. GILZ expression was detected by staining with a rabbit anti-GILZ antibody (5 μg/ml; Santa Cruz Biotechnology, Dallas, Texas) for 1 h. PE-conjugated $F(ab)_2$ donkey anti-rabbit IgG (0.25 mg/ml; Jackson ImmunoResearch Laboratories, Inc., West Grove, PA) was used as the secondary antibody. The stained samples were analyzed by flow cytometry.

To examine alcohol influence of GILZ expression in different types of leukocytes, we selected ethanol as the representative alcohol. Mice were administered (i.p.) with PBS or 4 g/kg ethanol for 8 or 16 h. Under CO_2 anesthesia, blood from each animal was collected via cardiac puncture. After centrifugation, the cell pellet was resuspended in Qiagen red blood cell lysis buffer, and white blood cells (WBCs) were obtained. Next, the WBCs were blocked with TruStain FcTMXPLUS (2.5 μg/ml; BioLegend), and subjected to immunostaining with antibodies against CD11b-FITC (5 μg/ml; Invitrogen), Ly6G-APC (4 μg/ml; BD Pharmingen), CD3e-Alexa 700 (10 μg/ml; BD Pharmingen), CD8-Pacific Blue (5 μg/ml; BioLegend), CD4-PE-Cy5 (10 μg/ml; BD Pharmingen), and CD19-PerCP Cy5.5 (10 μg/ml; BD Pharmingen), Next, the cells were permeabilized and fixed using BD Cytofix/Cytoperm™ Fixation/Permeabilization Kit. Then, the cells were intracellularly stained with GILZ-PE antibody (5 μg/ml; Invitrogen), followed by flow cytometry analysis.

Assessment of Phospho-IκB Levels in Peripheral Blood Leukocytes

Adult C57BL/6 mice were exposed to LPS (10 mg/kg) alone or combined with 4 g/kg ethanol for 16 h. Under CO_2 anesthesia, cardiac puncture was performed to obtain blood. After plasma and cell separation, the cell component was resuspended in Qiagen red blood cell lysis buffer, and the consequent white blood cells were isolated. Next, the cells were blocked with TruStain FcTMXPLUS (0.25 μg/ml; BioLegend), and subjected to immunostaining with the following surface marker antibodies: CD11b-FITC (5 μg/ml; Invitrogen), Ly6G-APC (4 μg/ml; BD Pharmingen), CD3e-Alexa 700 (10 μg/ml; BD Pharmingen), CD8-Pacific Blue (5 μg/ml; BioLegend), CD4-PE-Cy5 (10 μg/ml; BD Pharmingen), and CD19-PerCP Cy5.5 (10 μg/ml; BD Pharmingen). Next, the cells were permeabilized and fixed using the BD Cytofix/Cytoperm™ Fixation/Permeabilization Kit. Then, the cells were intracellularly stained with phospho-IκB-PE antibody (1.25 μg/ml; Invitrogen), followed by flow cytometry analysis.

ELISA Measurement of Mouse Cytokines

The collected plasma were diluted appropriately and ELISA was performed to measure the serum level of IL-6, an indicator septic

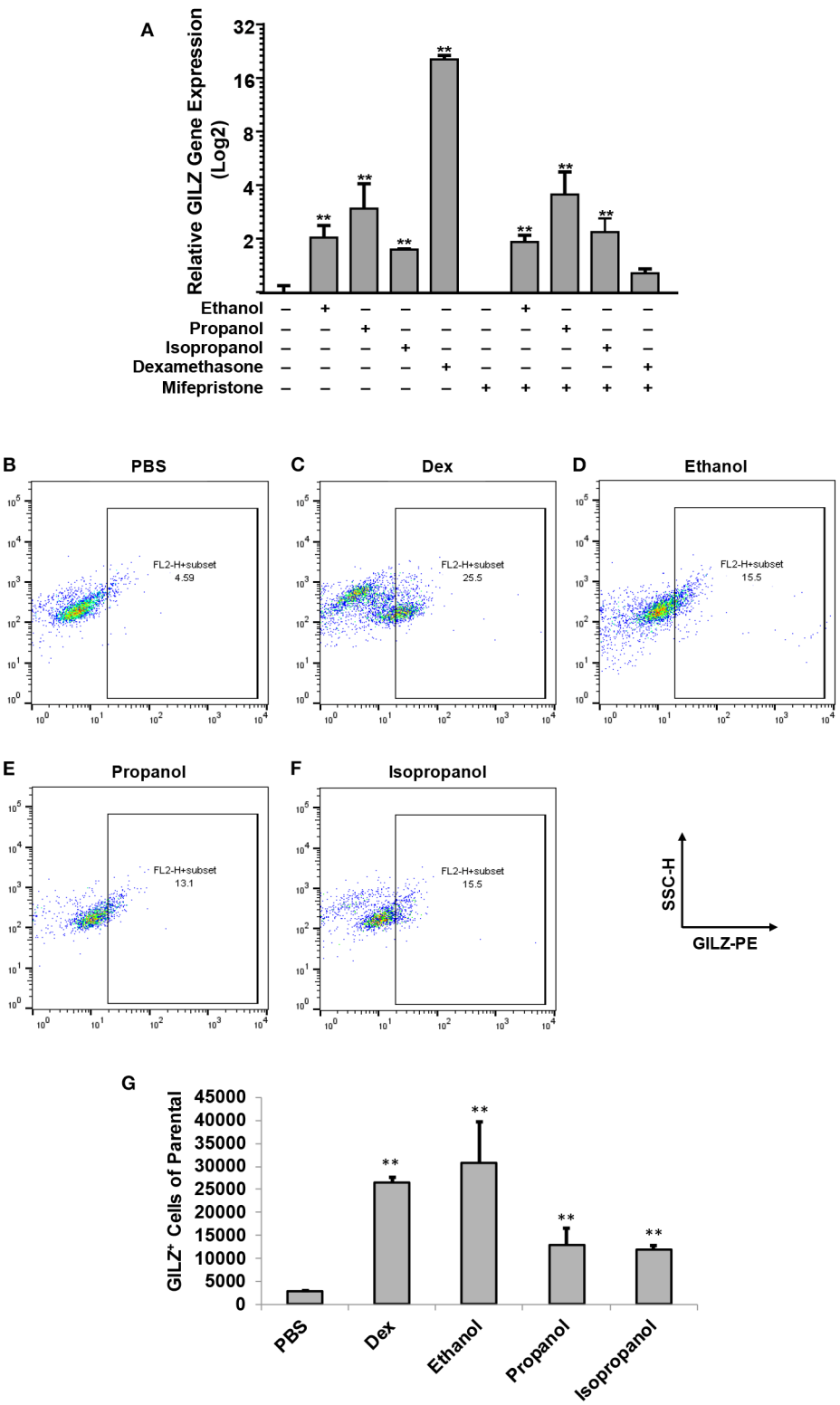

FIGURE 1 | Short-chain alcohols upregulate GILZ expression *in vitro*. **(A)** RT-qPCR to measure GILZ transcription. MM6 cells were exposed to ethanol, propanol, or isopropanol at 50 mM for 24 h. A PBS-control group of MM6 cells was similarly set. GILZ mRNA levels were determined by RT-qPCR. **(B–F)** Flow cytometry. The alcohol-exposed MM6 cells were immunostained for GILZ protein and analyzed by flow cytometry. Representative dot-plot data from each condition are shown. X-axis measures GILZ-PE staining, and Y-axis indicates sidescatter property. **(G)** Statistical data. Total 50,000 cells were acquired for each condition. GILZ-positive cells of the parental were expressed. Asterisks denote significant difference as compared to the respective control by Student's *t*-test ($P < 0.01$, $n = 3$ per condition).

cytokine, using the mouse Duoset ELISA kits (R & D Systems, Minneapolis, MN).

Statistics

Data were statistically analyzed by Student's *t*-test for differences between two comparing groups. The animal survival data were compared by Log-Rank test. Results were expressed as mean ±SD. Differences with *P*-values smaller than or equal to 0.05 were considered statistically significant.

RESULTS

Short-Chain Alcohols Upregulate GILZ Expression in MM6 Cells

Our previous studies demonstrated that ethanol upregulates GILZ gene expression and suppresses LPS-elicited inflammatory response in human airway epithelial cells and MM6 cells (1, 42). As ethanol, propanol, and isopropanol are all short-chain alcohols with a similar molecular structure, we predicted that they share the same property in regulating GILZ expression and cell inflammatory response. To test this prediction, we exposed MM6 cells to the three alcohols, separately, at 50 mM for 24 h. As GILZ is a glucocorticoid- (GC-) responsive gene, we also stimulated the control group of cells with dexamethasone (Dex, 1 μM). Furthermore, we previously found that ethanol activates the GILZ gene via a GC-independent non-canonical mechanism (1). A parallel experiment was set with addition of mifepristone (5 μM) to block GR. RT-qPCR was performed to measure the GILZ mRNA levels. The results (**Figure 1A**) demonstrate that the three short-chain alcohols significantly enhanced GILZ gene expression, and mifepristone did little to blunt such an effect. In contrast, the Dex-activated GILZ expression was abolished by mifepristone, suggesting that Dex and the short-chain alcohols exploit different mechanisms to activate *GILZ*. To validate this finding at the protein level, we performed GILZ immunofluorescence staining and flow cytometric analysis. The results (**Figures 1B–G**) show that ethanol, propanol, and isopropanol significantly elevated GILZ protein expression in the exposed cells, compared to the no alcohol control cells. Taken together, these results indicate that short-chain alcohols are capable of upregulating GILZ expression at both transcriptional and translational levels.

Short-Chain Alcohols Suppress LPS-Stimulated Inflammatory Response *in vitro*

To examine if propanol and isopropanol behave like ethanol in suppressing cell inflammatory response to LPS, we exposed MM6 cells to 50 mM ethanol, propanol, or isopropanol, followed by LPS (1 μg/ml) stimulation. Levels of TNF-α and IL-6, the two major proinflammatory cytokines in cell response to LPS, in the supernatant of each treatment were determined by ELISA. As shown in **Figure 2**, the LPS-stimulated cells produced high levels of TNF-α and IL-6, which were significantly reduced by each alcohol.

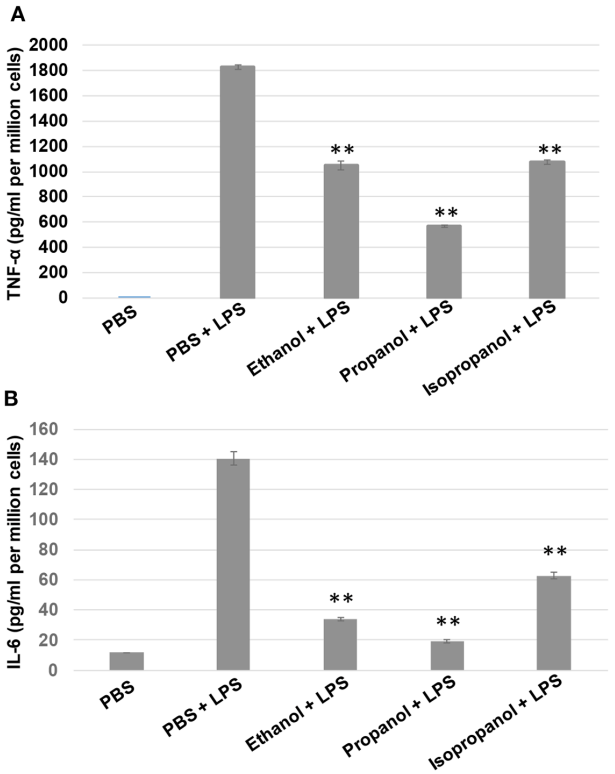

FIGURE 2 | Short-chain alcohols reduce LPS-stimulated TNF-α and IL-6 production by MM6 cells. MM6 cells (1×10^6) were exposed to 50 mM ethanol, propanol, or isopropanol for 24 hours. LPS exposure (1 μg/ml) was added 1 h after the addition of alcohol. A PBS control group of MM6 cells was similarly set and stimulated. Culture media were collected. TNF-α **(A)** and IL-6 **(B)** levels were measured by ELISA, and are expressed here as picogram per milliliter per million cells. Asterisks denote statistically significant difference by student's *t*-test ($p < 0.01$, $n = 4$ per condition).

Short-Chain Alcohols Enhance GILZ Expression *in vivo*

Short-chain alcohols (ethanol, propanol, or isopropanol) at an escalating dose for each (0, 2, or 4 g/kg) were intraperitoneally administered to adult C57BL/6 mice. Sixteen hours later, white blood cells (WBCs) from each animal were isolated, intracellularly stained for GILZ, and analyzed by flow cytometry. The data (**Figures 3A–H**) demonstrate that GILZ expression in the cells responded to each of the applied alcohols in a dose-dependent manner, and was significantly higher than that of the non-alcohol treated control.

To determine which types of immune cells were altered by alcohol in GILZ expression, we similarly exposed a separate set of mice to ethanol (4 g/kg), a representative alcohol, for 8 or 16 h. Cell-surface staining with antibodies against CD11b, Ly6G, CD19, CD3, CD4, and CD8, in combination with intracellular staining of GILZ was performed. Flow cytometry using the gating strategy (**Figure S1**) revealed that GILZ expression in monocytes ($CD11b^+Ly6G^-$) was significantly reduced after ethanol exposure for 8 h. However, neutrophils ($CD11b^+Ly6G^+$)

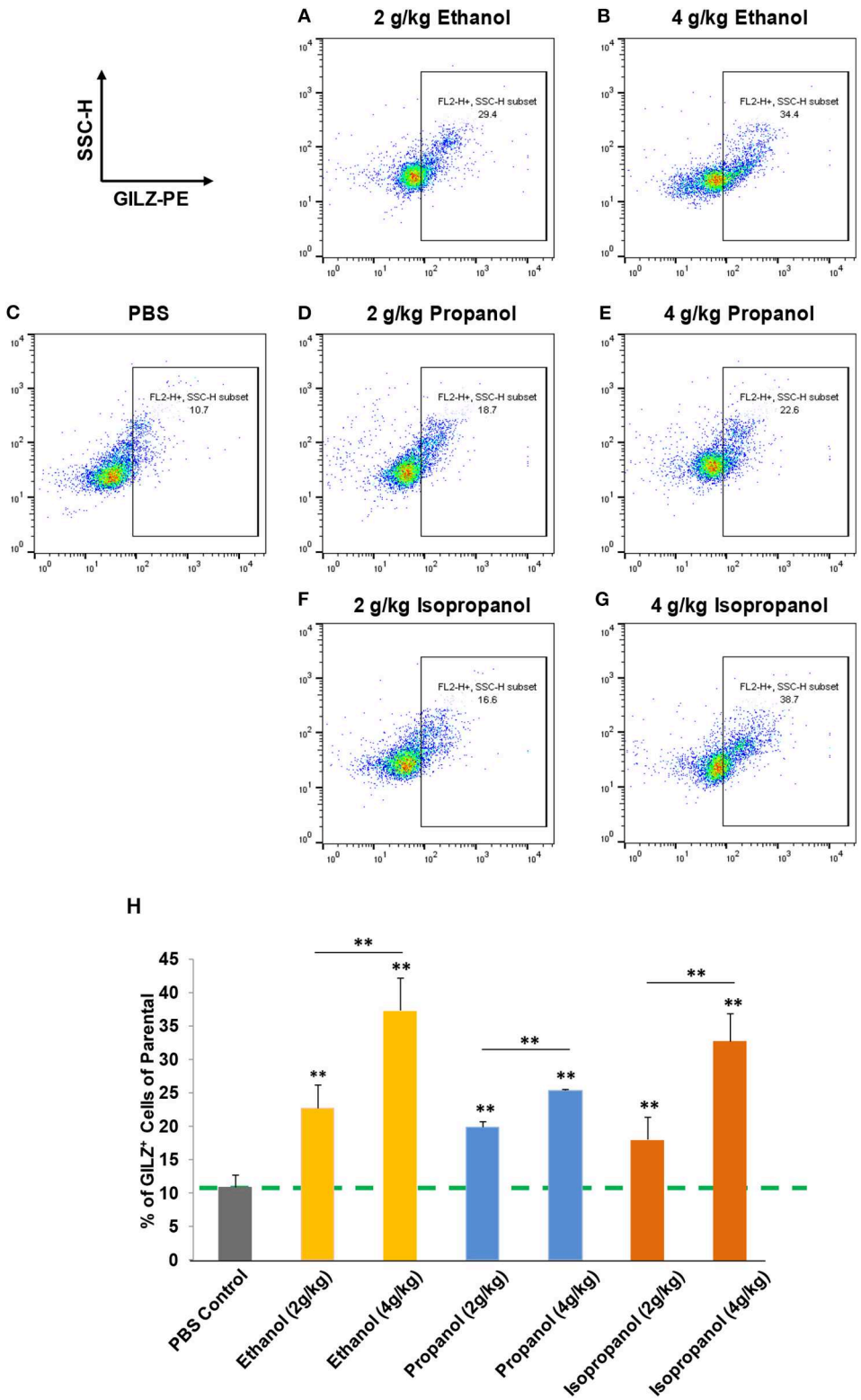

FIGURE 3 | Short-chain alcohols enhance GILZ gene expression *in vivo*. **(A–G)** Dot plot of flow cytometry. Mice were administered (i.p.) with 0, 2, or 4 g/kg of ethanol, propanol, or isopropanol. After 24 h, peripheral blood from each animal was collected, and white blood cells (WBCs) were isolated and subjected to immunostaining for GILZ, followed by flow cytometry. Representative data from each treatment are shown. **(H)** Statistical data. GILZ expression from each condition was compared to that of the PBS control (dashed line). Data are expressed by percent of GILZ-positive cells in each sample. Asterisks denote statistically significant difference in each comparison by Student's *t*-test ($p < 0.01$, $n = 4$ per group).

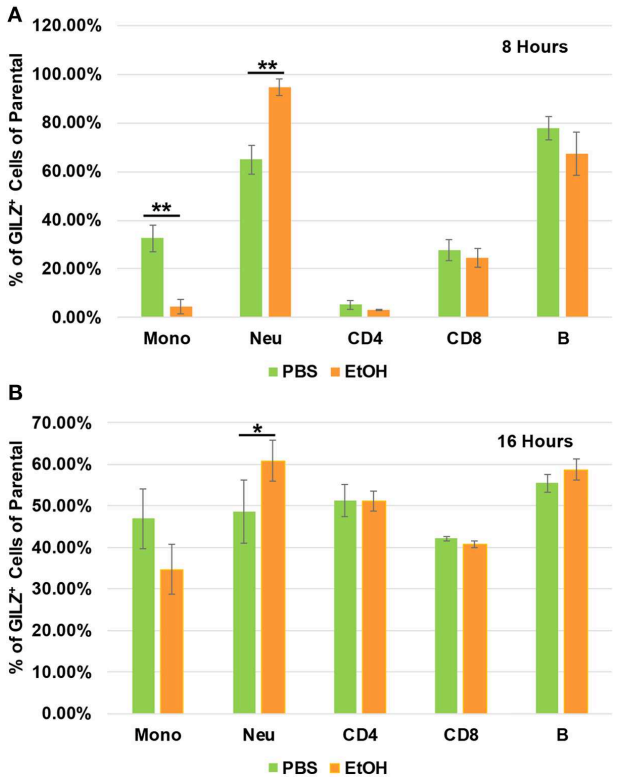

FIGURE 4 | GILZ expression in different types of immune cells. Peripheral blood WBCs from mice that had been exposed to 4 g/kg ethanol or PBS for 8 h **(A)** or 16 h **(B)** were isolated. Immunostainings for cell surface markers (CD11b, Ly6G, CD19, CD3, CD4, and CD8) and GILZ were performed. Monocytes ($CD11b^+Ly6G^-$), neutrophils ($CD11b^+Ly6G^+$), B lymphocytes ($CD19^+$), CD4 lymphocytes ($CD3^+CD4^+$), and CD8 lymphocytes ($CD3^+CD8^+$) were categorized. GILZ-positive cells in each cell type of the parental were compared between the ethanol and control groups. Asterisks indicate statistically significant difference by student's *t*-test ($n \geq 3$ per group). Mono (Monocytes); Neu (Neutrophils). $^*P \leq 0.05$, and $^{**}P \leq 0.01$.

had significantly higher GILZ expression (**Figure 4A**). Moreover, 16 h ethanol exposure led to significantly higher expression of GILZ in neutrophils (**Figure 4B**). These data suggest that neutrophils are a major cell type in alcohol upregulation of GILZ expression in the current experimental setting.

Short-Chain Alcohols Protect Mice From LPS Septic Shock

Administration of a lethal dose of LPS elicits an overwhelming inflammatory response that leads to multiple organ failure, shock, and death. As short-chain alcohols effectively suppress inflammatory response to LPS *in vitro*, we predicted that they should attenuate LPS-induced septic shock *in vivo*. To test this hypothesis, we administered adult C57BL/7 mice with ethanol (4 g/kg), propanol (2 g/kg), isopropanol (2 g/kg), or PBS control. The reason for selection of a higher dose of ethanol is that our pilot experiments indicated that ethanol at a 2 g/kg dose provided little protection against lethal LPS. One hour after alcohol exposure, the animals were challenged with a lethal dose of LPS (10 mg/kg). A survival curve for each condition was traced, and compared with that of the non-alcohol control (**Figure 5A**). The results show that without alcohol administration, almost all animals died within the time frame of 16–36 h after LPS challenge, while the short-chain alcohol exposures significantly protected the mice from LPS-induced septic shock. No further casualties were observed after 36 h until termination of the experiment a week later.

LPS-induced septic shock in mice is a well-studied and widely used model, which mimics almost all the pathological consequences that occur during sepsis (44). Mortality caused by sepsis or septic shock is associated with overproduction of inflammatory cytokines, also referred to as cytokine storm (45). IL-6, IL-1β and TNF-α are among the major cytokines responsible for sepsis disease pathogenesis. To delineate the potential mechanism underlying the alcohol LPS protection, we measured the serum level of IL-6, a representative cytokine to indicate the severity of sepsis. Adult mice were exposed to the short-chain alcohols similarly, as previously stated, and challenged with the lethal dose of LPS. Sixteen hours post LPS challenge, all live animals were bled to collect their sera for IL-6 cytokine measurement. Data (**Figure 5B**) demonstrate that ethanol (4 g/kg), propanol (2 g/kg) and isopropanol (2 g/kg) significantly reduced IL-6 serum levels. However, ethanol at the 2 g/kg dose had no significant impact on LPS-induced inflammation.

One crucial mechanism for ethanol to attenuate LPS toxicity is through suppression of NF-κB signaling (46, 47). To investigate whether this mechanism was involved in the observed alcohol-protection against LPS in our experimental model, we examined the levels of IκB phosphorylation in WBCs from the animals that had been exposed to ethanol (4 g/kg) and LPS. Cell surface marker and phospho-IκB double-immunostaining was performed, followed by flow cytometry analysis using the gating strategy (**Figure S2**). As compared to the non-alcohol treated cohort, neutrophils and CD4 cells from the alcohol-treated animals had significantly lower phospho-IκB levels (**Figure 5C**), suggesting that the observed alcohol protection against LPS septic shock is, at least partially, through the suppression of NF-κB signaling.

Ethanol Instead of Its Derivatives Confers LPS Protection

It was unexpected that ethanol at the 2 g/kg dose failed to suppress LPS inflammation and protect mice from lethal LPS challenge, while the same dose of propanol and isopropanol were effective. We hypothesized that this may result from a greater or faster metabolic rate of ethanol. If this hypothesis is correct, inhibition of ethanol metabolism may enhance ethanol LPS protection. Three groups of adult C57BL/6 mice were assigned, with one group administered with PBS and the alcohol dehydrogenase inhibitor fomepizole (10 mg/kg), another administered with ethanol (2 g/kg) alone, and the third group with ethanol (2 g/kg) and fomepizole (10 mg/kg) together. One hour later, all animals were challenged with the lethal dose of LPS (10 mg/kg). A Kaplan-Meier survival curve for each condition was traced (**Figure 6A**) and statistically compared by

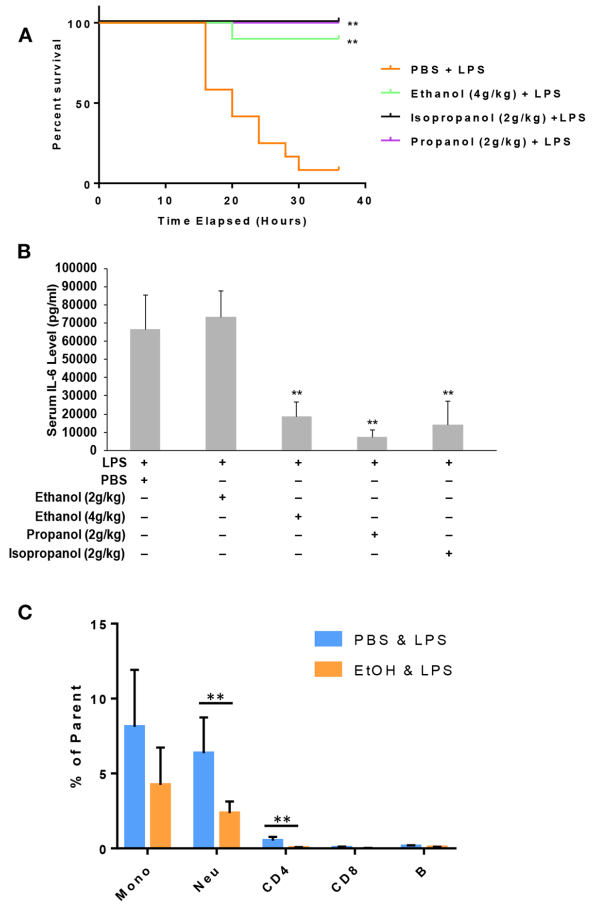

FIGURE 5 | Short-chain alcohol protection against LPS septic shock. **(A)** Survival curves. C57BL/6 mice were i.p. injected with ethanol (4 g/kg), isopropanol (2 g/kg), propanol (2 g/kg), or PBS. One hour later, the animals were challenged with a lethal dose of LPS (10 mg/kg). The animals were observed for 36 h. The Kaplan-Meier survival curve for each group of animals was traced, and statistical comparisons were performed by Log-rank test. Asterisks denote significant difference in each comparison with PBS group or indicated group ($n = 10$ per group, $p < 0.01$). **(B)** Short-chain alcohols attenuate host inflammatory response to LPS. C57BL/6 mice were i.p. injected with ethanol (2 g/kg or 4 g/kg), isopropanol (2 g/kg), propanol (2 g/kg), or PBS. One hour later, the animals were challenged with LPS (10 mg/kg). Sixteen hours after LPS challenge, the animals were bled. Serum from each animal was obtained and measured for IL-6 levels. Asterisks denote significant difference in each comparison ($n = 4$ per group, $p < 0.01$). **(C)** Ethanol exposure significantly affects cellular Phospho-IκB levels in monocytes and neutrophils. Peripheral blood WBCs were isolated from the mice that had been exposed to 4 g/kg ethanol and LPS (10 mg/kg) or the control mice that had been exposed to PBS and LPS (10 mg/kg). Immunostainings for cell surface markers (CD11b, Ly6G, CD19, CD3, CD4, and CD8) and phospho-IκB were performed. Monocytes ($CD11b^+Ly6G^-$), neutrophils ($CD11b^+Ly6G^+$), B lymphocytes ($CD19^+$), CD4 lymphocytes ($CD3^+CD4^+$), and CD8 lymphocytes ($CD3^+CD8^+$) were categorized. Percentage of the phospho-IκB-positive cells in each cell type of the gated population were compared between the ethanol and control groups. Asterisks denote statistically significant difference by student's *t*-test ($p < 0.01$, $n \geq 3$ per group).

Log-Rank test. The results demonstrate that without fomepizole, 2 g/kg ethanol had no protective effect on LPS septic shock. However, fomepizole significantly improved the protection efficacy of ethanol at the otherwise non-protective concentration. To further investigate whether fomepizole enhances ethanol suppression of host inflammatory response to LPS, we performed a parallel experiment with the same design. Sixteen hours later after LPS challenge, the serum obtained from each animal was measured to determine the indicator cytokine IL-6 level. As displayed in **Figure 6B**, fomepizole significantly reduced the serum IL-6 levels, indicating enhancement of ethanol suppression of the host inflammatory response to LPS. Taken together, the data indicate that inhibiting ethanol metabolism facilitates ethanol protection against LPS septic shock, strongly suggesting that it is the molecular ethanol instead of its derivatives or metabolites that engenders the protective effect against LPS-induced septic immune response.

DISCUSSIONS

The legal blood ethanol concentration limit for driving in the United States is 0.08%, which is equivalent to 17.36 mM. However, blood ethanol levels can reach to over 87 mM in patients with acute alcohol intoxication (48, 49). A previous study from our group (50) documented that acute alcohol intoxication in mice by intraperitoneal (i.p.) injection of 20% alcohol in pyrogen-free saline at a dose of 5 g/kg gave rise to blood alcohol levels of 119.7 ± 1.3, 106.3 ± 1.5, 87.7 ± 3.6, and 48.4 ± 3.5 mM, respectively, at 45 min, 90 min, 3 h, and 6 h post alcohol administration. In the current study, the highest dose of ethanol used *in vivo* was 4 g/kg. Thus, the blood ethanol level should be lower than the levels referenced. Isopropanol is widely used in household applications. Deliberate or accidental ingestion of isopropanol ranks second as a cause of alcohol poisoning clinically (51). Blood isopropanol concentrations have been reported as high as 560 mg/dl (93 mM) (52). In the current paper, we used 2 g/kg isopropanol for i.p. administration. A previous publication reported that injection of mice with 2 g/kg isopropanol generates a blood alcohol concentration of 200 mg/dl (33 mM) after 30 min (19). Thus, the alcohol doses used in this study should be relevant to clinically encounterable alcohol levels.

Glucocorticoids (GCs) are steroid hormones produced by the adrenal cortex under control of the hypothalamic–pituitary–adrenal (HPA) axis in response to internal circadian clock and external stress challenge (53, 54). GCs are the most prescribed anti-inflammatory drugs. The profound effectiveness of GCs provides the rationale for their use in a wide range of autoimmune, inflammatory, and allergic diseases, such as rheumatoid arthritis, lupus erythematosus, inflammatory bowel disease, transplant rejection and asthma (55, 56). However, long-term application of these steroids results in detrimental side effects, including diabetes, immunosuppression, osteoporosis and increased risk of cardiovascular events, all of which are closely associated with the alteration of physiological metabolism by GCs (57). Thus, new anti-inflammatory drugs are urgently needed, ideally ones that maintain the effectiveness of GCs while avoiding the GC-associated detrimental effects. Bypassing GCs to activate GILZ represents a novel strategy to achieve

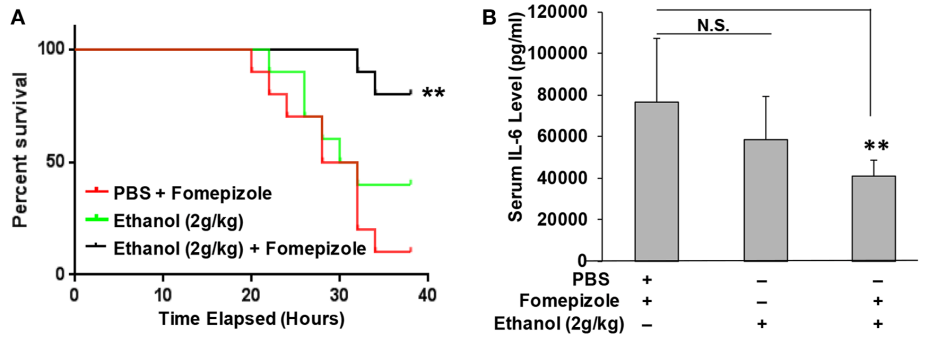

FIGURE 6 | Alcohol dehydrogenase inhibitor fomepizole enhances ethanol suppression of host inflammatory response to LPS and reduces LPS septic shock mortality. **(A)** C57BL/6 mice were i.p. injected with ethanol (2 g/kg) with or without fomepizole (10 mg/kg). One hour later, a lethal dose of LPS (10 mg/kg) was used to challenge the animals. Control mice were injected with PBS and fomepizole. The Kaplan-Meier survival curve for each group of animals was traced, and statistical comparisons were performed by Log-rank test. Asterisks denote significant difference in each comparison ($n = 10$ per group, $p < 0.01$). **(B)** Serum IL-6 levels of the mice with similar ethanol and LPS applications in the absence or presence of fomepizole. Asterisks denote significant difference in the comparison ($n = 4$ per group, $p < 0.01$). N.S. indicates no significance.

anti-inflammation. In the current study, we found that short-chain alcohols (ethanol, propanol and isopropanol) upregulate GILZ without GCs, which deserves further investigation to explore if the alcohols can serve as prototype compounds to search for new anti-inflammatory agents.

Our previous genome-wide gene expression analysis on human airway epithelial cells that were exposed to dose-escalating ethanol (42) revealed that a cluster of glucocorticoid-targeting genes, including TSC22D3 (GILZ), ALOX15B, SYNPO2, and PTEN, responded in a dose-dependent manner. GILZ was the most affected, upregulated 2-fold by 50 mM ethanol and 3-fold by 100 mM ethanol (42). Importantly, GILZ is an essential molecule to convey the alcohol anti-inflammatory effect, as knockdown of GILZ diminishes alcohol suppression of LPS-induced inflammatory response (1). Our further research revealed that ethanol activation of the GILZ gene is through a non-canonical activation of the GR signaling pathway, which is independent of GCs (1). In the current study, we found that other similar short-chain alcohols (propanol and isopropanol) share the same property of modulating GILZ expression *in vitro* and *in vivo*, validating the novel alcohol-GR interaction. It is well studied that ethanol modulates the immune function of T cells, monocytes, macrophages, dendritic cells and neutrophils (4, 58–60), and the specific effects depend on the pattern of ethanol exposure (acute or chronic) (61). Acute ethanol decreases TLR responses and attenuates pro-inflammatory cytokine production (62, 63). However, chronic ethanol exposure renders monocytes and macrophages more responsive to LPS stimulation. Mechanistic studies demonstrate that the ethanol-induced LPS tolerance or sensitization is mediated through modulation of IRAK-M, IRAK1/4, Bcl-3, and NF-κB (14, 47). In contrast, the isopropanol-induced effect is conveyed through the regulation of discrete members of the NFAT family of transcription factors and AP-1 family of transcription factors (18, 19). In the current study, we demonstrate that short-chain alcohols modulate GILZ gene expression and suppress IκB phosphorylation, which adds another layer of regulation to the known mechanisms. Even though GILZ is known to interact with the key inflammatory signaling mediators NF-κB and AP-1 (32, 64, 65), the finding that short-chain alcohols exploit this mechanism for inflammosuppression and immunosuppression is novel. A recent publication reported that ethanol and other short-chain alcohols inhibit NLRP3 inflammasome activation through protein tyrosine phosphatase stimulation (66). It is noteworthy that stimulation of a functional inflammasome requires two steps. The first step is priming during which activation of NF-κB is essential to induction of several components of the inflammasome. Our data have shown that short-chain alcohols suppress IκB phosphorylation, which inevitably undermines the priming and the downstream activation of the inflammasome. It will be very interesting to investigate whether alcohol-induced protein tyrosine phosphatase stimulation subdues phospho-IκB production in future studies.

Despite intensive research, sepsis continues to be a major health problem world-wide. The incidence of sepsis in the past two decades has annually increased by 9%, to reach 240 per 100,000 people in the US (67, 68). This rate of occurrence translates into ∼750,000 cases and over 250,000 deaths each year (68). When septic shock develops, the mortality rate of patients is substantially increased. At present, there is no specific treatment for sepsis and septic shock. Clinical management basically focuses on infection containment and organ function support (69). Alcohol attenuation of LPS-induced septic shock, as we demonstrated in this report, may be employed as an emergency measure to save lives under the circumstance of no medical care available. With regard to potential use of alcohol for therapy, recent studies have proposed to use ethanol to treat traumatic brain injury in humans (51, 52). Acute ethanol gavage attenuates hemorrhage/resuscitation-induced injury (70). Thus, alcohol, the oldest drug in medicine, may find new applications, as long as the molecular mechanism for its action is clearly understood.

While this is related to but beyond the scope of the current research, alcohol activation of GR signaling and upregulation of GILZ expression may be important in explaining alcohol-associated psycho-behavioral problems. Alcohol is

long known to be an emotion regulatory agent. Moderate intake relieves stresses and produces pleasure, while heavy drinking induces mood and psychological abnormalities, such as depression. GILZ over-expression is found to be associated with depression (71, 72). Our data clearly demonstrated that short-chain alcohols upregulate GILZ, which may serve as a critical mechanism for alcohol mood regulation and alcohol-precipitated depression.

There are several limitations associated with this research. First, only acute and one-dose application of alcohols was tested. Multiple doses may have a stronger potency in immunosuppression against LPS. Second, this study was to prove the principle. Alcohols were applied prior to LPS challenge. However, in a clinical setting LPS septic shock typically occurs first. Future studies will test the clinically relevant mode. Third, in this report alcohols were administered intraperitoneally. Alternatively, gavage through a feeding tube is another clinically applicable way to deliver alcohols, which will be tested in the future.

In summary, this report demonstrated that short-chain alcohols upregulate GILZ expression, suppress host immune response to LPS, and attenuate LPS-triggered septic shock. This finding implies that short-chain alcohols can be used to alleviate LPS sepsis as an emergency measure if no other medicines are available.

DATA AVAILABILITY STATEMENT

All datasets generated for this study are included in the article/**Supplementary Material**.

ETHICS STATEMENT

The animal study was reviewed and approved by the Institutional Animal Care and Use Committee of Louisiana State University Health Sciences Center with IACUC #3578.

AUTHOR CONTRIBUTIONS

HN and SJ performed experiments and data analyses. SN contributed to the original concept and design of the work. GW designed and conducted experiments, performed data analyses, and did manuscript writing.

FUNDING

This work was supported by the research grant to GW from the National Institutes of Health (AA024549).

ACKNOWLEDGMENTS

The authors would like to thank Connie Porretta at LSUHSC Flow Cytometry Core Facility for her technical assistance in flow cytometry analyses. We also would like to thank Dianne Wellems for her critical reading of this manuscript.

SUPPLEMENTARY MATERIAL

The Supplementary Material for this article can be found online at: https://www.frontiersin.org/articles/10.3389/fimmu.2020.00053/full#supplementary-material

REFERENCES

1. Ng HP, Jennings S, Wang J, Molina PE, Nelson S, Wang G. Non-canonical glucocorticoid receptor transactivation of gilz by alcohol suppresses cell inflammatory response. *Front Immunol*. (2017) 8:661. doi: 10.3389/fimmu.2017.00661
2. Kloner RA, Rezkalla SH. To drink or not to drink? That is the question. *Circulation*. (2007) 116:1306–17. doi: 10.1161/CIRCULATIONAHA.106.678375
3. O'Keefe JH, Bybee KA, Lavie CJ. Alcohol and cardiovascular health: the razor-sharp double-edged sword. *J Am Coll Cardiol*. (2007) 50:1009–14. doi: 10.1016/j.jacc.2007.04.089
4. Goral J, Karavitis J, Kovacs EJ. Exposure-dependent effects of ethanol on the innate immune system. *Alcohol*. (2008) 42:237–47. doi: 10.1016/j.alcohol.2008.02.003
5. Zakhari S, Li TK. Determinants of alcohol use and abuse: impact of quantity and frequency patterns on liver disease. *Hepatology*. (2007) 46:2032–9. doi: 10.1002/hep.22010
6. Presti RL, Carollo C, Caimi G. Wine consumption and renal diseases: new perspectives. *Nutrition*. (2007) 23:598–602. doi: 10.1016/j.nut.2007.04.012
7. Nelson S, Kolls JK. Alcohol, host defence and society. *Nat Rev Immunol*. (2002) 2:205–9. doi: 10.1038/nri744
8. Moss M, Burnham EL. Chronic alcohol abuse, acute respiratory distress syndrome, and multiple organ dysfunction. *Crit Care Med*. (2003) 31:S207–12. doi: 10.1097/01.CCM.0000055389.64497.11
9. Ruiz M, Ewig S, Marcos MA, Martinez JA, Arancibia F, Mensa J, et al. Etiology of community-acquired pneumonia: impact of age, comorbidity, and severity. *Am J Respir Crit Care Med*. (1999) 160:397–405. doi: 10.1164/ajrccm.160.2.9808045
10. Zisman DA, Strieter RM, Kunkel SL, Tsai WC, Wilkowski JM, Bucknell KA, et al. Ethanol feeding impairs innate immunity and alters the expression of Th1- and Th2-phenotype cytokines in murine Klebsiella pneumonia. *Alcohol Clin Exp Res*. (1998) 22:621–7. doi: 10.1111/j.1530-0277.1998.tb04303.x
11. Szabo G, Dolganiuc A, Dai Q, Pruett SB. TLR4, ethanol, and lipid rafts: a new mechanism of ethanol action with implications for other receptor-mediated effects. *J Immunol*. (2007) 178:1243–9. doi: 10.4049/jimmunol.178.3.1243
12. Zhang P, Bagby GJ, Happel KI, Summer WR, Nelson S. Pulmonary host defenses and alcohol. *Front Biosci*. (2002) 7:d1314–30. doi: 10.2741/A842
13. Zhang P, Bagby GJ, Happel KI, Raasch CE, Nelson S. Alcohol abuse, immunosuppression, and pulmonary infection. *Curr Drug Abuse Rev*. (2008) 1:56–67. doi: 10.2174/1874473710801010056
14. Szabo G, Mandrekar P. A recent perspective on alcohol, immunity, and host defense. *Alcohol Clin Exp Res*. (2009) 33:220–32. doi: 10.1111/j.1530-0277.2008.00842.x
15. Mandrekar P, Catalano D, White B, Szabo G. Moderate alcohol intake in humans attenuates monocyte inflammatory responses: inhibition of nuclear regulatory factor kappa B and induction of interleukin 10. *Alcohol Clin Exp Res*. (2006) 30:135–9. doi: 10.1111/j.1530-0277.2006.00012.x
16. Ajisaka H, Okajima M, Goto Y, Taniguchi T, Inaba H. Effects of acute low-dose ethanol on inflammatory reactions to endotoxin-induced shock in rats. *J Toxicol Sci*. (2012) 37:649–54. doi: 10.2131/jts.37.649
17. Zhang P, Bagby GJ, Boe DM, Zhong Q, Schwarzenberger P, Kolls JK, et al. Acute alcohol intoxication suppresses the CXC chemokine response during endotoxemia. *Alcohol Clin Exp Res*. (2002) 26:65–73. doi: 10.1111/j.1530-0277.2002.tb02433.x
18. Desy O, Carignan D, Caruso M, de Campos-Lima PO. Immunosuppressive effect of isopropanol: down-regulation of cytokine production results from

the alteration of discrete transcriptional pathways in activated lymphocytes. *J Immunol*. (2008) 181:2348–55. doi: 10.4049/jimmunol.181.4.2348
19. Carignan D, Desy O, de Campos-Lima PO. The dysregulation of the monocyte/macrophage effector function induced by isopropanol is mediated by the defective activation of distinct members of the AP-1 family of transcription factors. *Toxicol Sci*. (2012) 125:14456. doi: 10.1093/toxsci/kfr283
20. Desy O, Carignan D, de Campos-Lima PO. Short-term immunological effects of nonethanolic short-chain alcohols. *Toxicol Lett*. (2012) 210:44–52. doi: 10.1016/j.toxlet.2012.01.005
21. Armstrong BA, Betzold RD, May AK. Sepsis and septic shock strategies. *Surg Clin North Am*. (2017) 97:1339–79. doi: 10.1016/j.suc.2017.07.003
22. Minasyan H. Sepsis and septic shock: pathogenesis and treatment perspectives. *J Crit Care*. (2017) 40:229–42. doi: 10.1016/j.jcrc.2017.04.015
23. Russell JA, Rush B, Boyd J. Pathophysiology of septic shock. *Crit Care Clin*. (2018) 34:43–61. doi: 10.1016/j.ccc.2017.08.005
24. Hotchkiss RS, Coopersmith CM, McDunn JE, Ferguson TA. The sepsis seesaw: tilting toward immunosuppression. *Nat Med*. (2009) 15:496–7. doi: 10.1038/nm0509-496
25. Angus DC, van der Poll T. Severe sepsis and septic shock. *N Engl J Med*. (2013) 369:2063. doi: 10.1056/NEJMra1208623
26. Ramachandran G. Gram-positive and gram-negative bacterial toxins in sepsis: a brief review. *Virulence*. (2014) 5:213–8. doi: 10.4161/viru.27024
27. Mahieu T, Park JM, Revets H, Pasche B, Lengeling A, Staelens J, et al. The wild-derived inbred mouse strain SPRET/Ei is resistant to LPS and defective in IFN-beta production. *Proc Natl Acad Sci USA*. (2006) 103:2292–7. doi: 10.1073/pnas.0510874103
28. Verghese MW, Snyderman R. Differential anti-inflammatory effects of LPS in susceptible and resistant mouse strains. *J Immunol*. (1981) 127:288–93.
29. D'Adamio F, Zollo O, Moraca R, Ayroldi E, Bruscoli S, Bartoli A, et al. A new dexamethasone-induced gene of the leucine zipper family protects T lymphocytes from TCR/CD3-activated cell death. *Immunity*. (1997) 7:803–12. doi: 10.1016/S1074-7613(00)80398-2
30. Pinheiro I, Dejager L, Petta I, Vandevyver S, Puimege L, Mahieu T, et al. LPS resistance of SPRET/Ei mice is mediated by Gilz, encoded by the Tsc22d3 gene on the X chromosome. *EMBO Mol Med*. (2013) 5:45670. doi: 10.1002/emmm.201201683
31. Cannarile L, Delfino DV, Adorisio S, Riccardi C, Ayroldi E. Implicating the Role of GILZ in Glucocorticoid Modulation of T-Cell Activation. *Front Immunol*. (2019) 10:1823. doi: 10.3389/fimmu.2019.01823
32. Ayroldi E, Riccardi C. Glucocorticoid-induced leucine zipper (GILZ): a new important mediator of glucocorticoid action. *FASEB J*. (2009) 23:3649–58. doi: 10.1096/fj.09-134684
33. Ayroldi E, Macchiarulo A, Riccardi C. Targeting glucocorticoid side effects: selective glucocorticoid receptor modulator or glucocorticoid-induced leucine zipper? A perspective. *FASEB J*. (2014) 28:5055–70. doi: 10.1096/fj.14-254755
34. Ronchetti S, Migliorati G, Riccardi C. GILZ as a mediator of the anti-inflammatory effects of glucocorticoids. *Front Endocrinol*. (2015) 6:170. doi: 10.3389/fendo.2015.00170
35. Beaulieu E, Morand EF. Role of GILZ in immune regulation, glucocorticoid actions and rheumatoid arthritis. *Nat Rev Rheumatol*. (2011) 7:340–8. doi: 10.1038/nrrheum.2011.59
36. Bruscoli S, Sorcini D, Flamini S, Gagliardi A, Adamo F, Ronchetti S, et al. Glucocorticoid-induced leucine zipper inhibits interferongamma production in B cells and suppresses colitis in mice. *Front Immunol*. (2018) 9:1720. doi: 10.3389/fimmu.2018.01720
37. Bereshchenko O, Migliorati G, Bruscoli S, Riccardi C. Glucocorticoid-induced leucine zipper: a novel anti-inflammatory molecule. *Front Pharmacol*. (2019) 10:308. doi: 10.3389/fphar.2019.00308
38. Soundararajan R, Wang J, Melters D, Pearce D. Differential activities of glucocorticoid-induced leucine zipper protein isoforms. *J Biol Chem*. (2007) 282:36303–13. doi: 10.1074/jbc.M707287200
39. Dragotto J, Canterini S, Del Porto P, Bevilacqua A, Fiorenza MT. The interplay between TGF-beta-stimulated TSC22 domain family proteins regulates cell-cycle dynamics in medulloblastoma cells. *J Cell Physiol*. (2019) 234:18349–60. doi: 10.1002/jcp.28468
40. Vago JP, Tavares LP, Garcia CC, Lima KM, Perucci LO, Vieira EL, et al. The role and effects of glucocorticoid-induced leucine zipper in the context of inflammation resolution. *J Immunol*. (2015) 194:4940–50. doi: 10.4049/jimmunol.1401722
41. Ballegeer M, Vandewalle J, Eggermont M, Van Isterdael G, Dejager L, De Bus L, et al. Overexpression of gilz protects mice against lethal septic peritonitis. *Shock*. (2019) 52:208–14. doi: 10.1097/SHK.0000000000001252
42. Gomez M, Raju SV, Viswanathan A, Painter RG, Bonvillain R, Byrne P, et al. Ethanol upregulates glucocorticoid-induced leucine zipper expression and modulates cellular inflammatory responses in lung epithelial cells. *J Immunol*. (2010) 184:5715–22. doi: 10.4049/jimmunol.0903521
43. Mandrekar P, Bellerose G, Szabo G. Inhibition of NF-kappa B binding correlates with increased nuclear glucocorticoid receptor levels in acute alcohol-treated human monocytes. *Alcohol Clin Exp Res*. (2002) 26:1872–9. doi: 10.1097/00000374-200212000-00015
44. Remick DG, Newcomb DE, Bolgos GL, Call DR. Comparison of the mortality and inflammatory response of two models of sepsis: lipopolysaccharide vs. cecal ligation and puncture. *Shock*. (2000) 13:110–6. doi: 10.1097/00024382-200013020-00004
45. Chousterman BG, Swirski FK, Weber GF. Cytokine storm and sepsis disease pathogenesis. *Sem Immunopathol*. (2017) 39:517–28. doi: 10.1007/s00281-017-0639-8
46. Mandrekar P, Jeliazkova V, Catalano D, Szabo G. Acute alcohol exposure exerts antiinflammatory effects by inhibiting IkappaB kinase activity and p65 phosphorylation in human monocytes. *J Immunol*. (2007) 178:7686–93. doi: 10.4049/jimmunol.178.12.7686
47. Mandrekar P, Szabo G. Signalling pathways in alcohol-induced liver inflammation. *J Hepatol*. (2009) 50:1258–66. doi: 10.1016/j.jhep.2009.03.007
48. Majori S, Ricci G, Marchiori F, Bocchi M, Zannoni M. Prevalence of acute alcohol intoxication in Borgo Trento Hospital Emergency Department (Verona). *J Prev Med Hyg*. (2015) 56:E196–202.
49. Bendtsen P, Hultberg J, Carlsson M, Jones AW. Monitoring ethanol exposure in a clinical setting by analysis of blood, breath, saliva, and urine. *Alcohol Clin Exp Res*. (1999) 23:1446–51. doi: 10.1111/j.1530-0277.1999.tb04665.x
50. Zhang P, Welsh DA, Siggins RW II, Bagby GJ, Raasch CE, Happel KI, Nelson S. Acute alcohol intoxication inhibits the lineage- c-kit+ Sca-1+ cell response to *Escherichia coli* bacteremia. *J Immunol*. (2009) 182:1568–76. doi: 10.4049/jimmunol.182.3.1568
51. Brennan JH, Bernard S, Cameron PA, Rosenfeld JV, Mitra B. Ethanol and isolated traumatic brain injury. *J Clin Neurosci*. (2015) 22:1375–81. doi: 10.1016/j.jocn.2015.02.030
52. Talving P, Plurad D, Barmparas G, Dubose J, Inaba K, Lam L, et al. Isolated severe traumatic brain injuries: association of blood alcohol levels with the severity of injuries and outcomes. *J Trauma*. (2010) 68:357–62. doi: 10.1097/TA.0b013e3181bb80bf
53. Zanchi NE, Filho MA, Felitti V, Nicastro H, Lorenzeti FM, Lancha AH Jr. Glucocorticoids: extensive physiological actions modulated through multiple mechanisms of gene regulation. *J Cell Physiol*. (2010) 224:311–5. doi: 10.1002/jcp.22141
54. Suarez-Bregua P, Guerreiro PM, Rotllant J. Stress, glucocorticoids and bone: a review from mammals and fish. *Front Endocrinol*. (2018) 9:526. doi: 10.3389/fendo.2018.00526
55. Kadmiel M, Cidlowski JA. Glucocorticoid receptor signaling in health and disease. *Trends Pharmacol Sci*. (2013) 34:518–30. doi: 10.1016/j.tips.2013.07.003
56. Vandewalle J, Luypaert A, De Bosscher K, Libert C. Therapeutic mechanisms of glucocorticoids. *Trends Endocrinol Metab*. (2018) 29:42–54. doi: 10.1016/j.tem.2017.10.010
57. Rhen T, Cidlowski JA. Antiinflammatory action of glucocorticoids–new mechanisms for old drugs. *N Engl J Med*. (2005) 353:1711–23. doi: 10.1056/NEJMra050541
58. Cannon AR, Morris NL, Hammer AM, Curtis B, Remick DG, Yeligar SM, et al. Alcohol and inflammatory responses: highlights of the 2015 Alcohol and Immunology Research Interest Group (AIRIG) meeting. *Alcohol*. (2016) 54:73–7. doi: 10.1016/j.alcohol.2016.06.005
59. Szabo G, Saha B. Alcohol's effect on host defense. *Alcohol Res*. (2015) 37:159–70.

60. Saeed RW, Varma S, Peng T, Tracey KJ, Sherry B, Metz CN. Ethanol blocks leukocyte recruitment and endothelial cell activation *in vivo* and *in vitro*. *J Immunol*. (2004) 173:637683. doi: 10.4049/jimmunol.173.10.6376
61. Molina PE, Happel KI, Zhang P, Kolls JK, Nelson S. Focus on: alcohol and the immune system. *Alcohol Res Health*. (2010) 33:97–108.
62. Mandrekar P, Bala S, Catalano D, Kodys K, Szabo G. The opposite effects of acute and chronic alcohol on lipopolysaccharide-induced inflammation are linked to IRAK-M in human monocytes. *J Immunol*. (2009) 183:1320–7. doi: 10.4049/jimmunol.0803206
63. Bala S, Tang A, Catalano D, Petrasek J, Taha O, Kodys K, et al. Induction of Bcl3 by acute binge alcohol results in toll-like receptor 4/LPS tolerance. *J Leukoc Biol*. (2012) 92:611–20. doi: 10.1189/jlb.0112050
64. Ayroldi E, Migliorati G, Bruscoli S, Marchetti C, Zollo O, Cannarile L, et al. Modulation of T-cell activation by the glucocorticoid-induced leucine zipper factor via inhibition of nuclear factor kappaB. *Blood*. (2001) 98:743–53. doi: 10.1182/blood.V98.3.743
65. Mittelstadt PR, Ashwell JD. Inhibition of AP-1 by the glucocorticoid-inducible protein GILZ. *J Biol Chem*. (2001) 276:29603–10. doi: 10.1074/jbc.M101522200
66. Hoyt LR, Ather JL, Randall MJ, DePuccio DP, Landry CC, Wewers MD, et al. Ethanol and other short-chain alcohols inhibit NLRP3 inflammasome activation through protein tyrosine phosphatase stimulation. *J Immunol*. (2016) 197:1322–34. doi: 10.4049/jimmunol.1600406
67. Angus DC, Linde-Zwirble WT, Lidicker J, Clermont G, Carcillo J, Pinsky MR. Epidemiology of severe sepsis in the United States: analysis of incidence, outcome, and associated costs of care. *Crit Care Med*. (2001) 29:1303–10. doi: 10.1097/00003246-200107000-00002
68. Martin GS, Mannino DM, Eaton S, Moss M. The epidemiology of sepsis in the United States from 1979 through 2000. *N Engl J Med*. (2003) 348:1546–54. doi: 10.1056/NEJMoa022139
69. Riedemann NC, Guo RF, Ward PA. Novel strategies for the treatment of sepsis. *Nat Med*. (2003) 9:517–24. doi: 10.1038/nm0503-517
70. Relja B, Wilhelm K, Wang M, Henrich D, Marzi I, Lehnert M. Acute ethanol gavage attenuates hemorrhage/resuscitation-induced hepatic oxidative stress in rats. *Oxid Med Cell Longev*. (2012) 2012:983427. doi: 10.1155/2012/983427
71. Thiagarajah AS, Eades LE, Thomas PR, Guymer EK, Morand EF, Clarke DM, et al. GILZ: Glitzing up our understanding of the glucocorticoid receptor in psychopathology. *Brain Res*. (2014) 1574:60–9. doi: 10.1016/j.brainres.2014.06.008
72. Ryan KM, McLoughlin DM. Peripheral blood GILZ mRNA levels in depression and following electroconvulsive therapy. *Psychoneuroendocrinology*. (2019) 101:304–10. doi: 10.1016/j.psyneuen.2018.12.234

Conflict of Interest: The authors declare that the research was conducted in the absence of any commercial or financial relationships that could be construed as a potential conflict of interest.

Copyright © 2020 Ng, Jennings, Nelson and Wang. This is an open-access article distributed under the terms of the Creative Commons Attribution License (CC BY). The use, distribution or reproduction in other forums is permitted, provided the original author(s) and the copyright owner(s) are credited and that the original publication in this journal is cited, in accordance with accepted academic practice. No use, distribution or reproduction is permitted which does not comply with these terms.

frontiers in Immunology

ORIGINAL RESEARCH
published: 13 February 2020
doi: 10.3389/fimmu.2020.00210

Hepatocyte-Specific Deletion of AMPKα1 Results in Worse Outcomes in Mice Subjected to Sepsis in a Sex-Specific Manner

Satoshi Kikuchi[1], *Giovanna Piraino*[2], *Michael O'Connor*[2], *Vivian Wolfe*[2], *Kiana Ridings*[2], *Patrick Lahni*[2] *and Basilia Zingarelli*[2,3]*

[1] Department of Emergency Medicine, Ehime University, Toon, Japan, [2] Division of Critical Care Medicine, Cincinnati Children's Hospital Medical Center, Cincinnati, OH, United States, [3] Department of Pediatrics, College of Medicine, University of Cincinnati, Cincinnati, OH, United States

Alterations in the energy homeostasis contribute to sepsis-mediated multiple organ failure. The liver plays a central role in metabolism and participates to the innate immune and inflammatory responses of sepsis. Several clinical and experimental studies have suggested that females are less susceptible to the adverse outcome of sepsis. However, underlying mechanisms of organ damage in sepsis remain largely undefined. AMP-activated protein kinase (AMPK) is an important regulator of mitochondrial quality control. The AMPK catalytic α1 isoform is abundantly expressed in the liver. Here, we determined the role of hepatocyte AMPKα1 in sepsis by using hepatocyte-specific AMPKα1 knockout mice (H-AMPKα1 KO) generated with Cre-recombinase expression under the control of the albumin promoter. Using a clinically relevant model of polymicrobial sepsis by cecal ligation and puncture (CLP), we observed that male H-AMPKα1 KO mice had higher plasma levels of tumor necrosis factor-α and interleukin-6 and exhibited a more severe liver and lung injury than male H-AMPKα1 WT mice, as evaluated by histology and neutrophil infiltration at 18 h after CLP. Plasma levels of interleukin-10 and the keratinocyte-derived chemokine were similarly elevated in both KO and WT male mice. At transmission electron microscopy analysis, male H-AMPKα1 KO mice exhibited higher liver mitochondrial damage, which was associated with a significant decrease in liver ATP levels when compared to WT mice at 18 h after sepsis. Mortality rate was significantly higher in the male H-AMPKα1 KO group (91%) when compared to WT mice (60%) at 7 days after CLP. Female H-AMPKα1 WT mice exhibited a similar degree of histological liver and lung injury, but significantly milder liver mitochondrial damage and higher autophagy when compared to male WT mice after CLP. Interestingly, H-AMPKα1 KO female mice had lower organ neutrophil infiltration, lower liver mitochondrial damage and lower levels of cytokines than WT female mice. There was no significant difference in survival rate between WT and KO mice in the female group. In conclusion, our study demonstrates that AMPKα1 is a crucial hepatoprotective enzyme during sepsis. Furthermore, our results suggest that AMPK-dependent liver metabolic functions may influence the susceptibility to multiple organ injury in a sex-dependent manner.

Keywords: AMPKα1, Cre-lox, cecal ligation and puncture, mitochondria, lung injury, liver injury, female sex

OPEN ACCESS

Edited by:
Valentin A. Pavlov,
Northwell Health, United States

Reviewed by:
Charles E. McCall,
Wake Forest Baptist Medical Center, United States
Qun Sophia Zang,
UT Southwestern Medical Center, United States

***Correspondence:**
Basilia Zingarelli
basilia.zingarelli@cchmc.org

Specialty section:
This article was submitted to Inflammation, a section of the journal Frontiers in Immunology

Received: *11 November 2019*
Accepted: *27 January 2020*
Published: *13 February 2020*

Citation:
Kikuchi S, Piraino G, O'Connor M, Wolfe V, Ridings K, Lahni P and Zingarelli B (2020) Hepatocyte-Specific Deletion of AMPKα1 Results in Worse Outcomes in Mice Subjected to Sepsis in a Sex-Specific Manner. Front. Immunol. 11:210. doi: 10.3389/fimmu.2020.00210

INTRODUCTION

Sepsis is a life-threating organ dysfunction caused by dysregulated host responses to infection (1). Sepsis is the most common cause of patient mortality in intensive care units, with a global incidence of ∼18 million cases per year and a mortality rate of 28–40% (2). Although co-morbidities contribute to the clinical variability, numerous experimental and clinical studies indicate that sex-specific differences influence the susceptibility to sepsis and the subsequent multiple organ dysfunction syndrome (MODS) and mortality (3–5).

The liver plays a central role in metabolic and immunological homeostasis (6). Clinical studies have shown that liver dysfunction and failure are serious complication in sepsis and directly contributes to disease progression and death (6, 7).

Mitochondrial dysfunction has been proposed as an important cause of sepsis-related organ failure in sepsis (8, 9). AMP-activated protein kinase (AMPK) is a crucial sensor of energy status and contributes to several metabolic processes for energy homeostasis. This kinase consists of a catalytic α-subunit (α1 and α2) and two β and γ regulating subunits, which are allosterically activated by low levels of adenosine triphosphate (ATP) and high levels of adenosine monophosphate (AMP) (10–12). A key component of the metabolic effects of AMPK is the activation of mitochondrial biogenesis leading to improved cellular energy utilization (10). AMPK also contributes to activation of autophagy, a highly conserved catabolic process that degrades and recycles dysfunctional cytoplasmic constituents, including damaged mitochondria, thus ensuring a proper process of mitochondrial turnover (10, 13).

We have recently demonstrated that specific pharmacological activators of AMPK exert beneficial effects in sepsis and reduce hepatic, cardiac and pulmonary injury in experimental models using male mice (14–16). Specifically, in the liver, these beneficial effects are associated with amelioration of mitochondrial biogenesis and function (14).

Given the potential benefit for AMPK activators to attenuate sepsis-induced liver injury, further investigation is merited to determine the biologic role of AMPK within the liver. As AMPKα1 is abundantly expressed in the liver of rodents and the predominant isoform in human hepatocytes (11, 12, 17), we sought to investigate the role of the hepatocyte AMPKα1 on sepsis-induced liver injury and mortality by employing hepatocyte-specific AMPKα1 knockout (H-AMPKα1 KO) young male mice (18). In order to characterize the sexual dimorphism of liver injury, we also used young H-AMPKα1 KO female mice. In these loss-of function studies, we demonstrated that specific AMPKα1 gene deletion in hepatocytes was associated with increased susceptibility to sepsis-induced liver and lung injury and increased mortality in male mice only. On the contrary, hepatocyte-specific AMPKα1 deletion in female mice had a surprising protective effect in liver mitochondrial structure, lung injury and systemic inflammatory response. Thus, our data suggest that hepatocyte AMPKα1 is an important modulator of the metabolic response in sepsis; however, its function is sex-dependent.

MATERIALS AND METHODS

Murine Model of Polymicrobial Sepsis

The investigation conformed to the National Institutes of Health Guide for the Care and Use of Laboratory Animals (Eighth Edition, 2011) and was approved by the Institutional Animal Care and Use Committee of the Cincinnati Children's Hospital Medical Center. Specific deletion of AMPKα1 in hepatocyte was achieved by using Cre-lox technology. Mice expressing Cre recombinase under the control of the albumin promoter [B6.Cg-Tg(Alb-cre)21Mgn/J] and AMPKα1flox/flox mice (Prkaa1tm1.1Sjm/J), both on C57BL/6 genetic background, were obtained from Jackson Laboratories (Bar Harbor, Maine) and were crossed to generate hepatocyte-specific AMPKα1 (H-AMPKα1) KO mice. Mice were housed in pathogen-free conditions under a 10 h light/14 h dark cycle with free access to food and water. Both male and female mice were used at 8–12 weeks of age. Mice were anesthetized with 2.0% isoflurane in 50% oxygen and polymicrobial sepsis was induced by cecal ligation and puncture (CLP) (19). A midline laparotomy was performed. After opening the abdomen, the cecum was exteriorized, ligated and punctured twice with a 23-G needle. The cecum was then returned into the peritoneal cavity and the abdominal incision was closed. Mice were resuscitated subcutaneously with 35 ml/kg 5% dextrose solution immediately after and at 3 h after the surgical procedure. Control mice did not undergo any surgical procedure. Mice were then sacrificed at 18 h after CLP. Blood, liver, and lungs were collected for biochemical assays.

Survival Study

In a separate study, another cohort of mice (n = 20–23) was subjected to a milder model of CLP by puncture with 25-G needle and was used for assessing survival rate. Mice received fluid resuscitation (35 ml/kg normal saline with 5% dextrose subcutaneously) immediately after, at 3 h and every 24 h after the CLP procedure up to 72 h. To minimize pain at the surgical incision site, lidocaine hydrochloride (1%, 4 mg/kg total dose) was applied locally immediately after the procedure and every 12 h up to 48 h. Survival was monitored for 7 days.

Myeloperoxidase Activity

Myeloperoxidase (MPO) activity was measured as an indicator of neutrophil infiltration in lung and liver tissue (20). Tissues were homogenized in a solution containing 0.5% hexa-decyl-trimethyl-ammonium bromide dissolved in 10 mM potassium phosphate buffer (pH 7.0) and centrifuged for 30 min at 4,000 × g at 4°C. An aliquot of the supernatant was allowed to react with a solution of tetra-methyl-benzidine (1.6 mM) and hydrogen peroxide (0.1 mM). The rate of change in absorbance was measured by spectrophotometry at 650 nm. MPO activity was defined as the quantity of enzyme degrading 1 μmol of hydrogen peroxide/min at 37°C and expressed in units per 100 mg weight of tissue.

Histopathologic Analysis

Frozen liver sections and paraffin-embedded lung sections were stained with hematoxylin and eosin, and evaluated by two independent observers blinded to the treatment groups. Liver

injury was evaluated on the presence of necrosis, sinusoid congestion and infiltration of red blood and inflammatory cells. Lung injury was evaluated on the presence of alveolar capillary congestion, infiltration of red blood cells and inflammatory cells into the airspace, alveolar wall thickness, and hyaline membrane formation.

Plasma Alanine Aminotransferase (ALT)

Plasma levels of ALT was evaluated as index of liver function by an enzymatic assay kit (Sekisui Diagnostics, Charlottetown, Canada) using the protocols recommended by the manufacturer.

Measurement of ATP Levels

Mitochondrial function in the liver was assessed by measuring ATP levels. Homogenates were obtained from fresh livers and were deproteinized with perchloric acid using a Deproteinization Sample Preparation Kit (BioVision, San Francisco, CA). Liver ATP levels were measured using an ATP Fluorometric Assay Kit (BioVision, San Francisco, CA). ATP levels were expressed as nmol/g tissue weight.

Transmission Electron Microscopy

Liver samples were fixed in 3% glutaraldehyde, postfixed in 1% osmium tetroxide in sodium phosphate buffer, and cut with ultramicrotome. Samples were stained with 2% uranyl acetate and lead citrate. The sections were viewed and photographed on Hitachi H-7650 transmission electron microscope at 120 kV. The total number of mitochondria and autophagosomes, and the presence of abnormal or enlarged mitochondria with loose matrix, fragmented cristae and membranes were determined in 9 consecutive cells in four different sections for each animal by using NIH ImageJ analysis (21).

Cytosol Extraction and Western Blot Analysis

Livers were homogenized in a buffer containing 0.32 M sucrose, 10 mM Tris-HCl (pH 7.4), 1 mM EGTA, 2 mM EDTA, 5 mM NaN3, 10 mM β-mercaptoethanol, 20 μM leupeptin, 0.15 μM pepstatin A, 0.2 mM phenylmethanesulfonyl fluoride, 50 mM NaF, 1 mM sodium orthovanadate, and 0.4 nM microcystin. Samples were centrifuged at 1,000 × g for 10 min at 4°C and the supernatants collected as cytosol extracts. Cytosol content of the light-chain (LC)3B-I and LC3B-II was determined by immunoblot analyses. Extracts were boiled in equal volumes of NuPAGE® LDS Sample Buffer (4X) and 40 μg of protein loaded per lane on a 16% Tris-glycine gradient gel. Proteins were separated electrophoretically and transferred to nitrocellulose membranes. For immunoblotting, membranes were blocked with 5% non-fat dried milk in Tris-buffered saline (TBS) for 1 h and incubated with primary antibodies for 24 h. Membranes were washed in TBS with 0.1% Tween 20 and incubated with secondary peroxidase-conjugated antibody; the immunoreaction was visualized by chemiluminescence and x-ray. Membranes were also re-probed with primary antibody against GADPH to ensure equal loading for cytosol proteins. Densitometric analysis of blots was performed using Quantity One (Bio-Rad Laboratories, Des Plaines, IL, USA).

Plasma Levels of Cytokines

Plasma levels of tumor necrosis factor-α (TNFα), interleukin-10 (IL-10), interleukin-6 (IL-6), and keratinocyte-derived chemokine (KC) were evaluated by a commercially available multiplex array system (Milliplex, Millipore Corporation, Billerica, MA) using the protocols recommended by the manufacturer.

Materials

The primary antibodies directed at LC3B-I and LC3B-II were obtained from Cell Signaling (Beverly, MA); the primary antibody directed at GADPH was obtained from Abcam (Cambridge, MA); the secondary antibodies were obtained from Santa Cruz Biotechnology (Santa Cruz, CA). Unless otherwise stated, all other chemicals were obtained from Sigma-Aldrich (St. Louis, MO).

Statistical Analysis

Statistical analysis was performed using SigmaPlot 13.0 (Systat Software, San Jose, CA, USA). Data in figures and text are expressed means ± SEM of n observations (n = 4–8 animals for each group). The results were examined by analysis of variance followed by the Student-Newman-Keuls's correction *post hoc* *t*-test. The Gehan-Breslow and log-rank tests were used to compare differences in survival rates (n = 20–23 animals for each group). A value of $P < 0.05$ was considered significant.

RESULTS

Hepatocyte-Specific Deficiency of AMPKα1 Results in Liver Damage After Sepsis in a Sex-Independent Manner

At 18 h after CLP, both male and female WT mice exhibited liver damage with modest areas of necrosis and sinusoid congestion at histological examination. However, H-AMPKα1 KO mice of both sexes showed more prominent liver damage with significant necrosis, edema and infiltration of inflammatory cells (**Figures 1A–H**). To confirm the histological findings of liver neutrophil infiltration in KO mice after sepsis we measured the activity of MPO, a neutrophil lysosomal enzyme. At 18 h after CLP, there was no increase in liver MPO activity in male or female WT mice. However, both male and female KO mice exhibited a significant elevation of MPO after sepsis when compared to sex-matched WT septic mice (**Figure 1I**). To further quantify liver injury, we measured plasma levels of ALT. Both male and female WT mice exhibited a similar degree of plasma ALT levels at 18 h after CLP. However, male and female KO mice had significant higher levels of ALT after sepsis when compared to sex-matched WT septic mice, thus confirming a more severe liver injury in a sex-independent manner (**Figure 1J**).

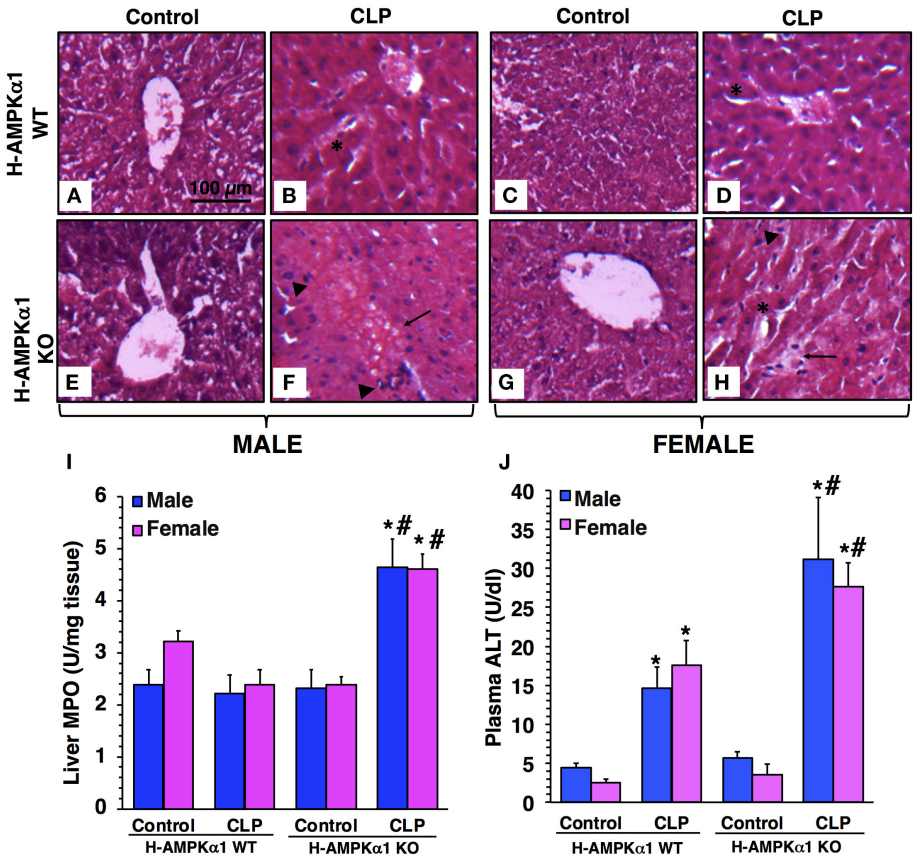

FIGURE 1 | Representative histology photomicrographs of liver sections of hepatocyte-specific (H-AMPKα1) wild-type (WT) and knock-out (KO) mice at basal control condition and at 18 h after cecal ligation and puncture (CLP). Normal liver architecture in control male WT **(A)** and male KO **(E)**, and in control female WT **(C)** and female KO **(G)** mice. Liver damage in male **(B)** and female **(D)** H-AMPKα1 WT mice with modest areas of sinusoid congestion (asterisks). Liver damage in male **(F)** and female **(H)** H-AMPKα1 KO mice with necrosis (arrows) and infiltration of inflammatory cells (arrowheads). Magnification ×100; scale bar = 100 μm. A similar pattern was seen in $n = 4$–8 different tissue sections in each experimental group. Liver myeloperoxidase (MPO) activity **(I)**, plasma ALT levels **(J)** in male and female H-AMPKα1 WT and KO mice at 18 h after CLP. Data represents the mean ± SEM of 4–8 mice for each group. $^{*}P < 0.05$ vs. sex-matched control mice; $^{\#}P < 0.05$ vs. sex-matched WT mice.

Hepatocyte-Specific Deficiency of AMPKα1 Results in Liver Mitochondrial Damage After Sepsis in a Sex-Dependent Manner

At electron microscopic analysis, mild mitochondria damage was evident in both male and female H-AMPKα1 WT mice at 18 h after CLP and was characterized by a few swollen mitochondria (**Figure 2**). H-AMPKα1 WT mice of both sexes also exhibited an increased number of autophagosomes and autolysosomes with sequestrated materials when compared to basal levels of control mice. There was also a significant increase of elongated mitochondrial morphology in H-AMPKα1 WT mice of both sexes after CLP. On the contrary, male H-AMPKα1 KO mice exhibited a significantly higher structural damage of mitochondria at 18 h after CLP when compared to male WT mice. Structural damage was characterized by the presence of swollen organelles with distorted cristae, translucent matrix and disrupted membrane. Interestingly, mitochondrial damage was significantly lower in KO female mice when compared to WT female mice and KO male mice after CLP; whereas there was no difference in the number of elongated organelles between WT and KO mice of both sexes. H-AMPKα1 WT and KO mice also exhibited an increased number of autophagosomes and autolysosomes with sequestrated materials when compared to basal levels of control mice. However, WT female mice had a higher number of autophagosomes and autolysosomes when compared to WT male mice after sepsis. Interestingly, number of autophagosomes was significantly lower in female KO mice when compared to sex-matched WT mice and to male KO mice after sepsis. To determine whether hepatocyte-specific deficiency of AMPKα1 might affect energy homeostasis, we measured ATP levels in the liver. There was no change in ATP levels after sepsis in male or female WT mice when compared to baseline conditions of WT sex-matched control animals (**Figure 2L**). However, male KO experienced a significant decrease in ATP levels at 18 h after CLP when compared to baseline conditions of KO control animals. Interestingly, there were no changes in

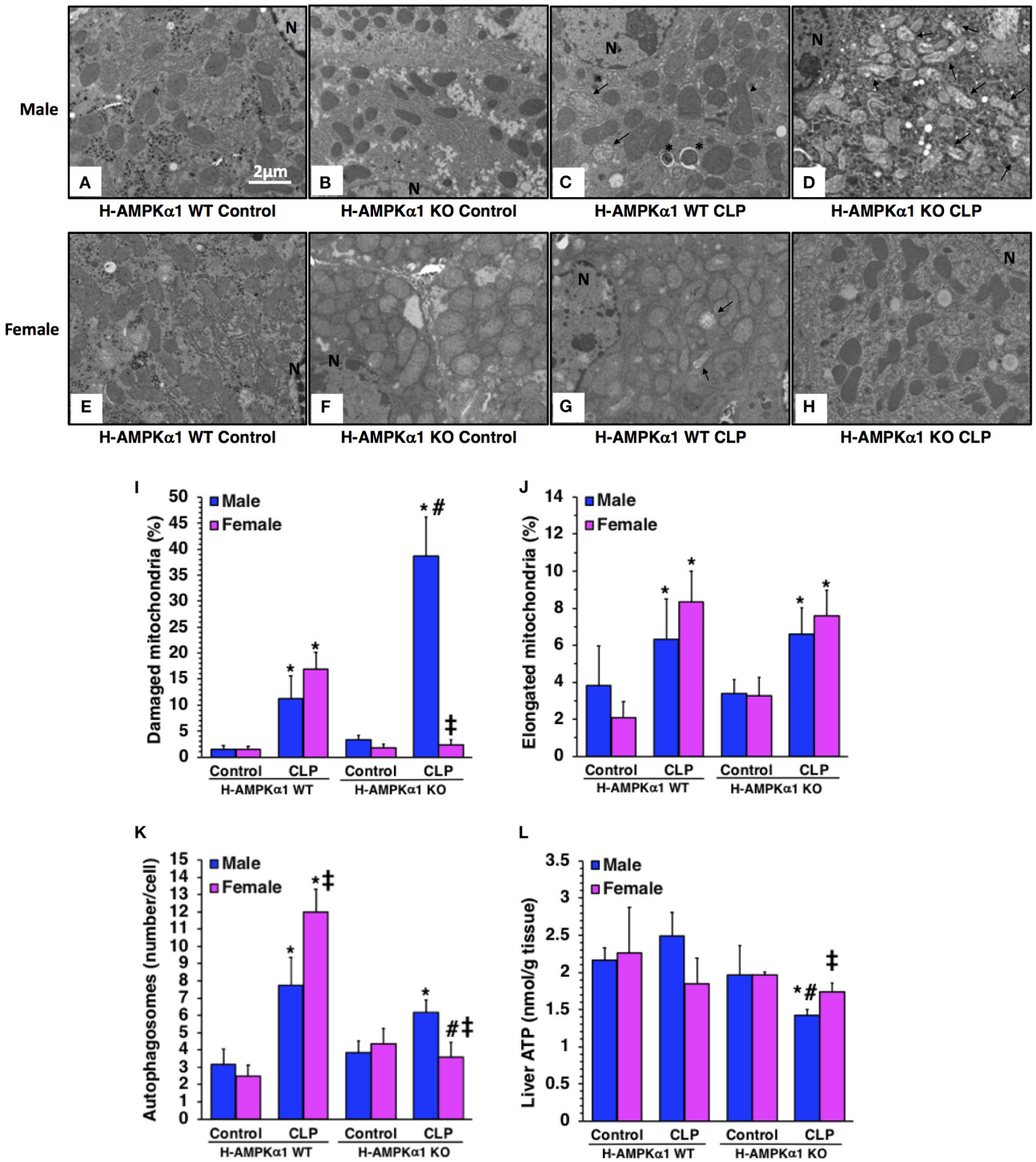

FIGURE 2 | Transmission electron microscopy of hepatocytes in hepatocyte-specific (H-AMPKα1) wild-type (WT) and knock-out (KO) male **(A–D)** and female **(E–H)** mice at basal control condition or 18 h after cecal ligation and puncture (CLP). Arrows, damaged mitochondria presenting translucent matrix, disrupted membrane and cristae; arrow heads, elongated mitochondria; asterisk, autophagic vescicles packed with mitochondria; N, nucleus. Quantification of damaged mitochondria **(I)**, elongated mitochondria **(J)**, and autophagosomes **(K)** of hepatocytes of hepatocyte-specific (H- AMPKα1) wild-type (WT) and knock-out (KO) mice at 18 h after cecal ligation and puncture (CLP). Liver sections were examined at transmission electron microscopy. Damaged, elongated mitochondria and autophagosomes were determined by using the NIH Image J software and expressed as percentage of total number of mitochondria in nine consecutive cells. Data are means ± SEM of 3–4 mice for each group. Liver ATP content **(L)** of hepatocyte-specific (H-AMPKα1) wild-type (WT) and knock-out (KO) mice at 18 h after cecal ligation and puncture (CLP). Data represents the mean ± SEM of 4–6 mice for each group. $^{*}P < 0.05$ vs. sex-matched control mice; $^{\#}P < 0.05$ vs. sex-matched WT mice; $^{\ddagger}P < 0.05$ vs. male group of the same genotype.

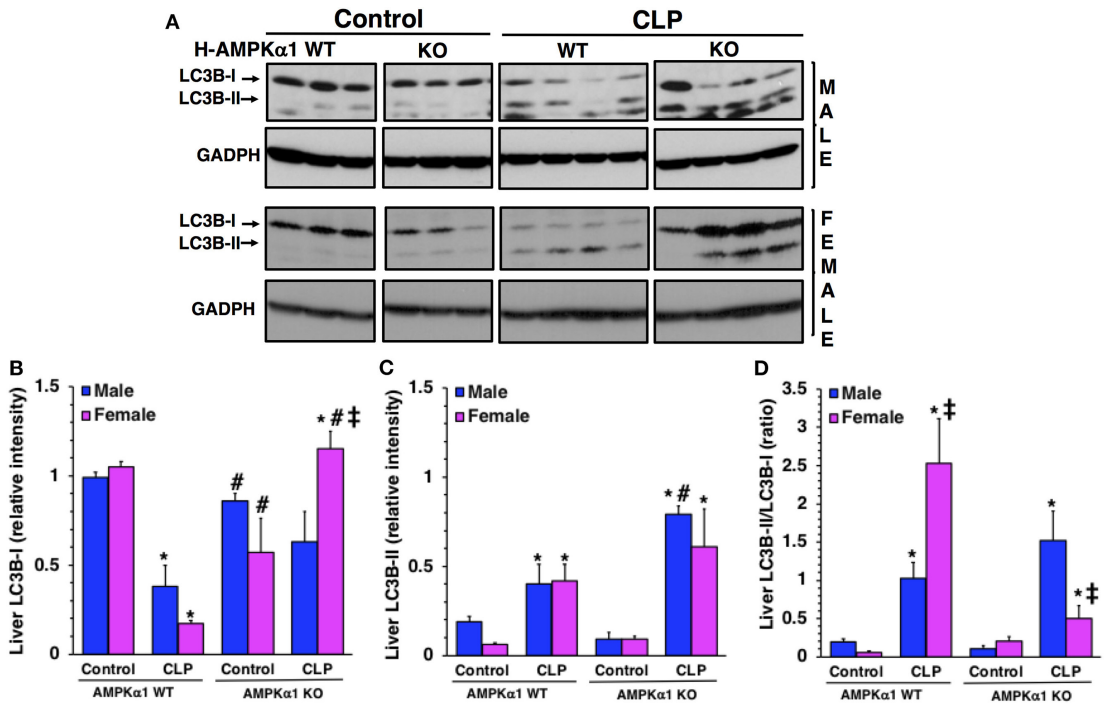

FIGURE 3 | Representative Western blots of protein expression of LC3B-I and LC3B-II in liver cytosol extracts; GADPH was used as loading control protein **(A)**. Image analyses of cytosol relative intensity of LC3B-I **(B)**, LC3 B-II **(C)** and LC3B-II/LC3B-I **(D)** as determined by densitometry. Each data represents the mean ± SEM of 3–4 animals for each group. $^{*}P < 0.05$ vs. sex-matched control mice; $^{\#}P < 0.05$ vs. sex-matched WT mice; $^{\ddagger}P < 0.05$ vs. male group of the same genotype.

ATP content after sepsis in female KO mice. Thus, hepatocyte-specific AMPKα1 deficiency promotes mitochondrial damage in a sex-dependent manner.

Hepatocyte-Specific Deficiency of AMPKα1 Influences Liver Autophagy After Sepsis in a Sex-Dependent Manner

To confirm the number of autophagosomes observed at electron microscopy, we further quantified the process of autophagy in the liver by evaluating the expression of the light chain 3B protein (LC3B) (**Figure 3**). The protein is converted from a cytosolic LC3B-I form to a conjugated LC3B-II form in the autophagosomal membrane and correlates with autophagic vesicle formation (22). At 18 h after CLP, LC3B-II/LC3B-I ratio significantly increased in both male and female WT mice when compared to baseline content of sex-matched control mice. However, WT female mice had a higher ratio when compared to WT male mice after sepsis, further confirming the higher number of autophagosomes seen at electron microscopy. Interestingly, female KO mice exhibited a higher expression of LC3BI when compared to male KO mice after sepsis. Consequently, LC3B-II/LC3B-I ratio was significantly lower in female KO mice when compared to sex-matched WT mice and to male KO mice after sepsis. There was no difference in LC3B-II/LC3B-I ratio between WT and KO mice in the male group. Thus, hepatocyte-specific AMPKα1 deficiency influences autophagy in a sex-dependent manner.

Hepatocyte-Specific Deficiency of AMPKα1 Results in Lung Injury After Sepsis in a Sex- Dependent Manner

To obtain insight into the role of hepatocyte AMPKα1 in the development of multiple organ failure we also evaluated lung injury by histology. At 18 h after CLP, both male and female H-AMPKα1 WT mice exhibited similar lung damage with modest infiltration of inflammatory cells and reduced alveolar space (**Figure 4**). However, male H-AMPKα1 KO mice exhibited marked lung injury characterized by reduced alveolar space, alveolar and bronchial congestion and accumulation of red and inflammatory cells when compared to male WT mice (**Figures 4A–D**). Male KO mice also exhibited higher lung MPO when compared to WT male mice (**Figure 4I**). Interestingly, the H-AMPKα1 KO female mice had lower MPO levels than WT female mice after CLP. Also, lung injury was milder (**Figures 4E–H**) and tissue MPO (**Figure 4I**) levels were significantly lower in KO female mice when compared to KO male mice after CLP. Thus, hepatocyte-specific AMPKα1 deficiency influenced the inflammatory response in the lung in a sex-dependent manner.

Hepatocyte-Specific Deficiency of AMPKα1 Influences Systemic Production of Cytokines in a Sex-Dependent Manner

To determine whether hepatocyte AMPKα1 influenced the systemic production of cytokines during sepsis, plasma levels

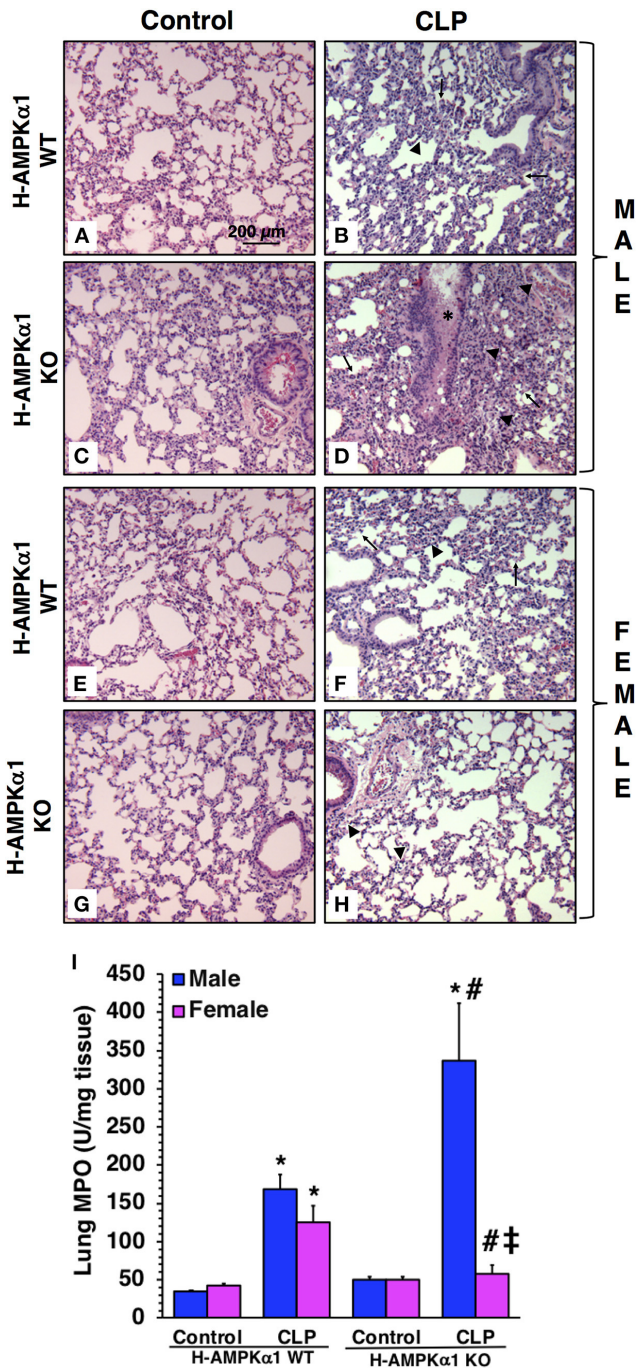

FIGURE 4 | Representative histology photomicrographs of lung sections of hepatocyte-specific (H-AMPKα1) wild-type (WT) and knock-out (KO) male **(A–D)** and female **(E–H)** mice at baseline conditions (Control) or 18 h after cecal ligation and puncture (CLP). Lung damage in H-AMPKα1 WT male **(B)** and female **(F)** mice with modest infiltration of inflammatory cells (*arrow heads*) and reduced alveolar space (*arrows*). Lung damage in H- AMPKα1 KO male mice **(D)** with reduced alveolar space, bronchial congestion (*asterisk*) and accumulation of red and inflammatory cells. Mild lung damage in H-AMPKα1 KO female mice **(H)** with mild infiltration of inflammatory cells only.

(Continued)

FIGURE 4 | Magnification ×100; scale bar = 200 μm. A similar pattern was seen in $n = 4$–8 different tissue sections in each experimental group. Lung myeloperoxidase (MPO) activity **(I)** in male and female H- AMPKα1 WT and KO mice at 18 h after CLP. Data represents the mean ± SEM of 4–8 mice for each group. $^{*}P < 0.05$ vs. sex-matched control mice; $^{\#}P < 0.05$ vs. sex-matched WT mice; $^{\ddagger}P < 0.05$ vs. male group of the same genotype.

of TNFα, IL-6, IL-10, and KC were measured. At 18 h after CLP, both male and female WT mice exhibited a significant elevation in plasma levels of all cytokines compared with sex-matched control mice. However, male KO mice had significantly higher levels of TNFα and IL-6 after sepsis when compared to male WT septic mice (**Figures 5A,B**), while levels of IL-10 and KC were similar in both WT and KO male mice (**Figures 5C,D**). Interestingly, plasma levels of cytokines were significantly lower in KO female mice when compared to WT female mice and KO male mice after CLP (**Figure 5**). Thus, hepatocyte-specific AMPKα1 deficiency influenced the systemic inflammatory response in a sex-dependent manner.

Hepatocyte-Specific Deficiency of AMPKα1 Exacerbates Sepsis-Induced Mortality in Male Mice Only

To confirm the protective role of hepatocyte AMPKα1 in long-term outcomes of sepsis, we performed a model of CLP with low mortality at 48 h after CLP (<20% mortality) but delayed high mortality between 3 and 7 days after CLP. Male H-AMPKα1 KO mice experienced higher mortality (91%) than WT mice (60%, $P < 0.05$) at 7 days after CLP. However, this effect was not observed in female H-AMPKα1 KO mice, which had similar mortality rate as female WT mice (67% in KO mice and 76% in WT mice) (**Figure 6**).

DISCUSSION

Being responsible of important physiological functions, such as detoxification, energy production, hormonal and immune balance, and coagulation, the liver is a critical organ for host survival following severe injury, including sepsis (6). Among sepsis patients, liver dysfunction or failure is associated with mortality rates ranging from 54 to 68%, higher than the mortality rates of sepsis patients with respiratory system dysfunction or failure (23–25). Despite these data of poor prognosis, the pathophysiology of liver dysfunction and its potential role in influencing multiple organ failure remain unclear. In the present study we have demonstrated that hepatocyte AMPKα1 is a key regulator of liver metabolic and innate immune function. Specifically, we have provided evidence that hepatocyte-specific AMPKα1 deletion worsened liver and lung injury and exacerbated the lethal effects of sepsis in young male mice. The underlying cellular mechanisms of this excessive vulnerability to injury related to increased neutrophil infiltration in liver and lung and increased systemic production

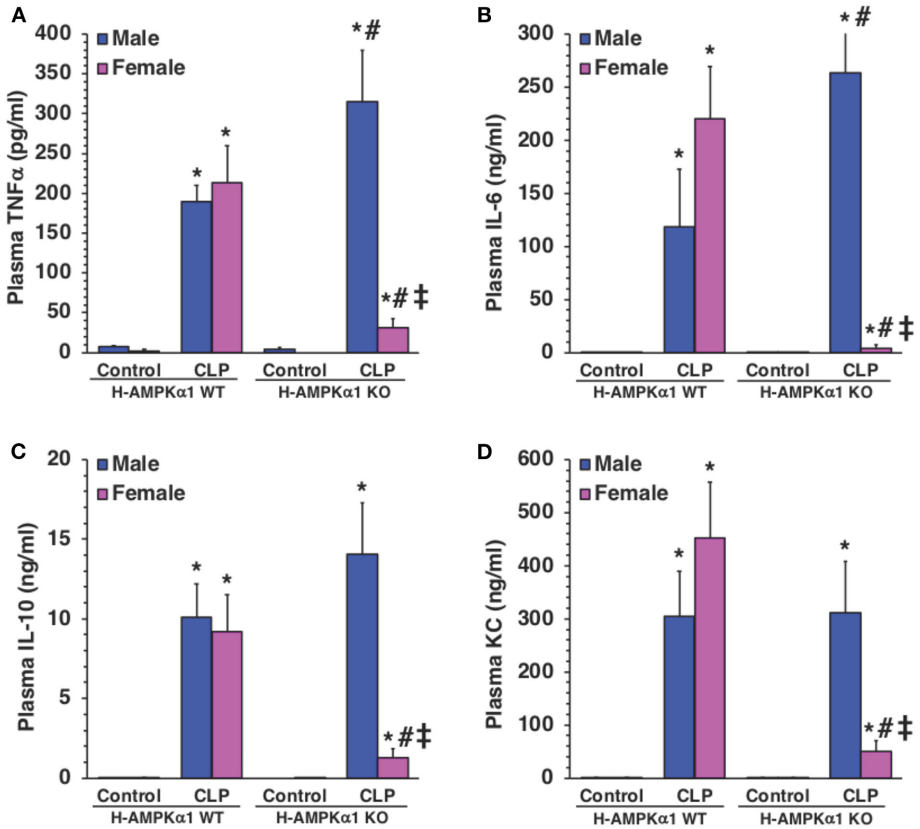

FIGURE 5 | Plasma levels of TNFα **(A)**, IL-6 **(B)**, IL-10 **(C)**, and KC **(D)**. Data represents the mean ± SEM of 4–8 mice for each group. $^{*}P < 0.05$ vs. sex-matched control mice; $^{\#}P < 0.05$ vs. sex-matched WT mice; $^{\ddagger}P < 0.05$ vs. male group of the same genotype.

of TNFα and IL-6. However, the most intriguing observation made here was that, in young female mice with hepatocyte-specific AMPKα1 deletion, the signs of liver injury did not coincide with worsening of sepsis. On the contrary, hepatocyte-specific AMPKα1 deficiency in female mice was associated with protective effects in the lung and reduced systemic inflammatory response without affecting survival. Thus, our data demonstrate that AMPKα1 modulates the metabolic and inflammatory responses in the liver in a sex-dependent manner.

AMPK is the master regulator of diverse metabolic events to maintain energy homeostasis. The protein consists of a catalytic α-subunit and two regulatory β- and γ-subunits. Two isoforms have been identified of the α-subunit (1 and 2) and β-subunit (1 and 2) and three isoforms of the γ-subunit (1, 2, and 3). Both AMPKα1 and α2-containing complexes are present in the liver in equal distribution in rodent models (11, 12, 18), but AMPKα1 is the predominant form in human hepatocytes (17). In previous studies, we have demonstrated that pharmacological activation of AMPK ameliorated liver injury in young and mature male animals subjected to CLP by regulating autophagy and gene transcription of mitochondrial structural and transport proteins, and metabolic enzymes (14). In this current study, despite sharing some histological and biomarkers similarities of liver injury, male and female H-AMPKα1 KO mice exhibited quite different liver mitochondrial features, as KO female mice did not exhibit ultrastructural damage compared with WT littermates. On the contrary, H-AMPKα1 KO female mice had the least mitochondrial damage and maintained normal ATP production among all groups of septic mice. In regard to this discrepancy between histological injury and changes in mitochondrial damage, it must be noted that such conflicting results have also been reported in clinical studies. Autopsy studies revealed a discordance between histologic findings and the degree of organ dysfunction of patients who died of sepsis (26). Cell death in the heart, kidney, liver, and lung was relatively minor and did not reflect the clinical evidence of more profound organ dysfunction (26). Furthermore, examination of *post mortem* organs from septic patients identified abnormalities of mitochondrial structures in cardiomyocytes, but cardiomyocyte cell death was rarely observed despite the magnitude of organ dysfunction (27). Taken together, our data suggest that maintenance of metabolic stability is associated with resilience to deleterious effects of sepsis and further confirm that mitochondrial damage is the major pathophysiologic characteristic of organ failure as seen in human sepsis.

Clinical studies have reported increased autophagy in multiple organs and tissues in sepsis (28). AMPK induces autophagy

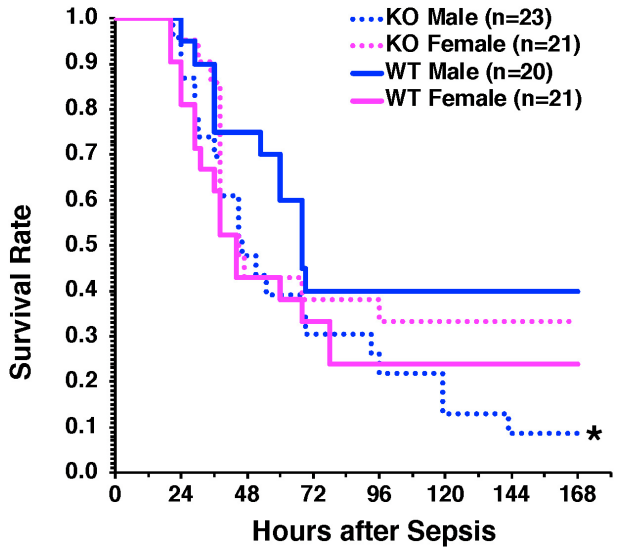

FIGURE 6 | Survival rate of hepatocyte-specific (H- AMPKα1) wild-type (WT) and knock-out (KO) mice at 7 days after cecal ligation and puncture (CLP). Mice were subjected to CLP and received fluid resuscitation (35 ml/kg normal saline with 5% dextrose subcutaneously) immediately after, at 3 h and every 24 h after the CLP procedure up to 72 h. *$P < 0.05$ of KO males vs. WT males as determined by Gehan-Breslow analysis.

by inhibiting the mammalian target of rapamycin pathway (10, 13). Autophagy is a critical step in maintaining mitochondrial quality control by selective removal of damaged organelles (13). There is experimental evidence that disruption of autophagy is associated with organ dysfunction. For example, using a young rat model, Chien et al. demonstrated that liver autophagy occurred early during sepsis, but it declined at later time points, when it was associated with liver dysfunction (29). On the contrary, AMPK-mediated autophagy has been shown to attenuate mitochondrial dysfunction in endotoxin stimulated hepatocytes (30). Mitochondrial morphology is also an adaptive response to cellular metabolic demands and an elongated pattern of mitochondria has been associated to mechanisms of fission/fusion to maximize ATP production (31). However, male H-AMPKα1 WT had less autophagosomes than WT female mice. At examination of molecular events, the conversion of LC3B from its free form (LC3B-I) to its phosphatidyl-ethanol-amine-conjugated form (LC3B-II) is a required step in autophagosome formation. Therefore, the LC3B-II/LC3B-I can be considered as a reliable marker to quantify autophagy (22). In our study, the LC3B-II/LC3B-I ratio was higher after sepsis in the liver of H-AMPKα1 WT female mice, thus suggesting a better capability to mount an autophagic event in response to cellular stress. Interestingly, female KO mice exhibited a reduction of autophagosomes when compared to WT littermates after sepsis. This event was also consistent with lower number of altered mitochondria in female KO mice when compared to male KO mice, thus suggesting that mitochondrial damage is an important requisite for upregulation of autophagy. Therefore, our data further suggest that AMPKα1 influences organ function in a sex-dependent manner also through finely tuning of autophagy according to the degree of mitochondrial impairment.

In concert with Kupffer cells, other immune competent and non-hematopoietic resident cells, hepatocytes produce a complex cytokine milieu of both pro-inflammatory and anti-inflammatory cytokines, which contribute to the initiation and amplification of the systemic acute phase response (32, 33). In our study, we observed that AMPKα1 deficiency in male mice enhanced systemic production of TNFα and IL-6, thus suggesting that AMPKα1 modulates the acute phase response. Consistent with our observation, it has been demonstrated that pharmacological activation of AMPK suppressed immune stimulated inflammation in mouse and human hepatocytes (34). Interestingly, in our study the specific inactivation of AMPKα1 in the liver in male mice led to an exacerbation of lung injury, thus suggesting that liver metabolic disturbance affects distant organ function. Therefore, the results presented here, employing a mouse model for genetic specific inactivation of AMPKα1 in hepatocytes, further extend the evidence for the liver as a key driver of immune and inflammatory responses during sepsis and strongly validate AMPK as a potential therapeutic target.

Paradoxically, specific deficiency of AMPKα1 in hepatocytes in female mice led to a remarkable reduction in the systemic inflammatory response and protected against sepsis-induced lung injury. Because AMPKα1 deficiency was not accompanied with liver metabolic defects in female mice, these sex-dependent differences point to other liver compensatory mechanisms independent by AMPKα1 in young female. In this regard, it is possible that estrogen may exert a compensatory effect for AMPKα1 deletion. For example, previous studies reported that double global genetic deficiency of AMPKα1 and AMPKα2 in female mice did not affect the inflammatory process of osteoarthritis; whereas estrogen prevented articular cartilage destruction (35, 36). Since in our study male and female H-AMPKα1 WT mice exhibited similar organ injury and outcomes after sepsis, we speculate that the differential hormonal milieu between male and female may, indeed, result in a diversification of mitochondria quality control during acute stress only in condition of dysregulation of AMPKα1 and the level of expression *per se* of this enzyme is most likely a key element for sex-dependent switch of metabolic regulation. Further comprehensive studies and elucidations of mitochondrial bioenergetics are required to better understand the signaling pathways and molecules involved in this switch.

CONCLUSIONS AND LIMITATION

Our findings are based on cross-sectional data comparing young age-matched male and female mice, future longitudinal studies are needed to disentangle age and sexual maturation effects, including the impact of ovariectomy and orchiectomy, steroid hormonal levels and the hepatoprotective effects of estrogen during sepsis. We used male and female mice at the age of 8–12 weeks old, which are in their peak reproductive age

(37). Therefore, their comparison with older groups of mice is necessary to establish association with levels of estrogens and decline of sexual maturation. Furthermore, a broad investigation of bioenergetic and biosynthetic mitochondrial functionalities by omics technologies should be included to identify novel sex-related mitochondrial pathomechanisms. Nevertheless, by means of cell type-specific gene knockout technology, the current study provides conclusive data that AMPKα1 expression in hepatocytes functions as a protective factor against sepsis in young male mice. However, paradoxically findings of our study point out that sex-dependent differences exist in the susceptibility to sepsis in the context of AMPKα1 deficiency. As AMPK activators, such as metformin, are widely used for diabetes type II in the clinical arena (38), further insight into the exact biological mechanism of AMPK may help to provide better clarity as to the potential pharmacological targeting of AMPK in sepsis.

DATA AVAILABILITY STATEMENT

The datasets generated for this study are available on request to the corresponding author.

ETHICS STATEMENT

The animal study was reviewed and approved by the Institutional Animal Care and Use Committee of the Cincinnati Children's Hospital Medical Center.

AUTHOR CONTRIBUTIONS

SK and BZ conceived and designed the projects. SK and VW performed the animal experiments. SK, GP, PL, and MO'C performed the biochemical assays. SK, GP, and KR performed the electron microscopy analysis. SK, GP, and BZ analyzed the data and prepared graphics. SK and BZ wrote the draft of the manuscript. All authors reviewed and approved the final manuscript.

FUNDING

This work was supported by the National Institutes of Health grants R01 GM-067202 and GM-115973 to BZ, and in part by grant P30 DK-078392 of the Digestive Research Core Center (Integrative Morphology Core).

REFERENCES

1. Singer M, Deutschman CS, Seymour CW, Shankar-Hari M, Annane D, Bauer M, et al. The third international consensus definitions for sepsis and septic shock (Sepsis-3). *JAMA*. (2016) 315:801–10. doi: 10.1001/jama.2016.0287
2. Hajj J, Blaine N, Salavaci J, Jacoby D. The "centrality of sepsis": a review on incidence, mortality, and cost of care. *Healthcare*. (2018) 6:E90. doi: 10.3390/healthcare6030090
3. Mahmood K, Eldeirawi K, Wahidi MM. Association of gender with outcomes in critically ill patients. *Crit Care*. (2012) 16:R92. doi: 10.1186/CC11355
4. Sakr Y, Elia C, Mascia L, Barberis B, Cardellino S, Livigni S, et al. The influence of gender on the epidemiology of and outcome from severe sepsis. *Crit Care*. (2013) 17:R50. doi: 10.1186/cc12570
5. Angele MK, Pratschke S, Hubbard WJ, Chaudry IH. Gender differences in sepsis: cardiovascular and immunological aspects. *Virulence*. (2014) 5:12–9. doi: 10.4161/viru.26982
6. Yan J, Li S, Li S. The role of the liver in sepsis. *Int Rev Immunol*. (2014) 33:498–510. doi: 10.3109/08830185.2014.889129
7. Canabal JM, Kramer DJ. Management of sepsis in patients with liver failure. *Curr Opin Crit Care*. (2008) 14:189–97. doi: 10.1097/MCC.0b013e3282f6a435
8. Brealey D, Brand M, Hargreaves I, Heales S, Land J, Smolenski R, et al. Association between mitochondrial dysfunction and severity and outcome of septic shock. *Lancet*. (2002) 360:219–23. doi: 10.1016/S0140-6736(02)09459-X
9. Arulkumaran N, Deutschman CS, Pinsky MR, Zuckerbraun B, Schumacker PT, Gomez H, et al. Mitochondrial function in sepsis. *Shock*. (2016) 45:271–81. doi: 10.1097/SHK.0000000000000463
10. Carling D, Viollet B. Beyond energy homeostasis: the expanding role of AMP-activated protein kinase in regulating metabolism. *Cell Metab*. (2015) 21:799–804. doi: 10.1016/j.cmet.2015.05.005
11. Stapleton D, Mitchelhill KI, Gao G, Widmer J, Michell BJ, Teh T, et al. Mammalian AMP-activated protein kinase subfamily. *J Biol Chem*. (1996) 271:611–14. doi: 10.1074/jbc.271.2.611
12. Stapleton D, Woollatt E, Mitchelhill KI, Nicholl JK, Fernandez CS, Michell BJ, et al. AMP-activated protein kinase isoenzyme family: subunit structure and chromosomal location. *FEBS Lett*. (1997) 409:452–56. doi: 10.1016/S0014-5793(97)00569-3
13. Mihaylova MM, Shaw RJ. The AMPK signalling pathway coordinates cell growth, autophagy and metabolism. *Nat Cell Biol*. (2011) 13:1016–23. doi: 10.1038/ncb2329
14. Inata Y, Kikuchi S, Samraj RS, Hake PW, O'Connor M, Ledford JR, et al. Autophagy and mitochondrial biogenesis impairment contributes to age-dependent liver injury in experimental sepsis: dysregulation of AMP-activated protein kinase pathway. *FASEB J*. (2018) 32:728–41. doi: 10.1096/fj.201700576R
15. Inata Y, Piraino G, Hake PW, O'Connor M, Lahni P, Wolfe V, et al. Age-dependent cardiac function during experimental sepsis: effect of pharmacological activation of AMP-activated protein kinase by AICAR. *Am J Physiol Heart Circ Physiol*. (2018) 315:H826–37. doi: 10.1152/ajpheart.00052.2018
16. Kitzmiller L, Ledford JR, Hake PW, O'Connor M, Piraino G, Zingarelli B. Activation of AMP-Activated Protein Kinase by A769662 ameliorates sepsis-induced acute lung injury in adult mice. *Shock*. (2019) 52:540–49. doi: 10.1097/SHK.0000000000001303
17. Stephenne X, Foretz M, Taleux N, van der Zon GC, Sokal E, Hue L, et al. Metformin activates AMP-activated protein kinase in primary human hepatocytes by decreasing cellular energy status. *Diabetologia*. (2011) 54:3101–10. doi: 10.1007/s00125-011-2311-5
18. Viollet B, Athea Y, Mounier R, Guigas B, Zarrinpashneh E, Horman S, et al. AMPK: lessons from transgenic and knockout animals. *Front Biosci*. (2009) 14:19–44. doi: 10.2741/3229
19. Hubbard WJ, Choudhry M, Schwacha MG, Kerby JD, Rue LW III, Bland KI, et al. Cecal ligation and puncture. *Shock*. (2005) 24(Suppl. 1):52–7. doi: 10.1097/01.shk.0000191414.94461.7e
20. Mullane KM, Kraemer R, Smith B. Myeloperoxidase activity as a quantitative assessment of neutrophil infiltration into ischemic myocardium. *J Pharmacol Methods*. (1985) 14:157–67. doi: 10.1016/0160-5402(85)90029-4
21. Schneider CA, Rasband WS, Eliceiri KW. NIH Image to ImageJ: 25 years of image analysis. *Nat Methods*. (2012) 9:671–75. doi: 10.1038/nmeth.2089
22. Ryter SW, Choi AM. Autophagy in lung disease pathogenesis and therapeutics. *Redox Biol*. (2015) 4:215–25. doi: 10.1016/j.redox.2014.12.010
23. Cheng B, Xie G, Yao S, Wu X, Guo Q, Gu M, et al. Epidemiology of severe sepsis in critically ill surgical patients in ten university hospitals in China. *Crit Care Med*. (2007) 35:2538–46. doi: 10.1097/01.CCM.0000284492.30800.00

24. Brun-Buisson C, Meshaka P, Pinton P, Vallet B. EPISEPSIS: a reappraisal of the epidemiology and outcome of severe sepsis in French intensive care units. *Intensive Care Med.* (2004) 30:580–8. doi: 10.1007/s00134-003-2136-x
25. Blanco J, Muriel-Bombin A, Sagredo V, Taboada F, Gandia F, Tamayo L, et al. Incidence, organ dysfunction and mortality in severe sepsis: a Spanish multicentre study. *Crit Care.* (2008) 12:R158. doi: 10.1186/cc7157
26. Hotchkiss RS, Karl IE. The pathophysiology and treatment of sepsis. *N Engl J Med.* (2003) 348:138–50. doi: 10.1056/NEJMra021333
27. Takasu O, Gaut JP, Watanabe E, To K, Fagley RE, Sato B, et al. Mechanisms of cardiac and renal dysfunction in patients dying of sepsis. *Am J Respir Crit Care Med.* (2013) 187: 509–17. doi: 10.1164/rccm.201211-1983OC
28. Watanabe E, Muenzer JT, Hawkins WG, Davis CG, Dixon DJ, McDunn JE, et al. Sepsis induces extensive autophagic vacuolization in hepatocytes: a clinical and laboratory-based study. *Lab Invest.* (2009) 89:549–61. doi: 10.1038/labinvest.2009.8
29. Chien WS, Chen YH, Chiang PC, Hsiao HW, Chuang SM, Lue SI, et al. Suppression of autophagy in rat liver at late stage of polymicrobial sepsis. *Shock.* (2011) 35:506–11. doi: 10.1097/SHK.0b013e31820b2f05
30. Xing W, Yang L, Peng Y, Wang Q, Gao M, Yang M, et al. Ginsenoside Rg3 attenuates sepsis-induced injury and mitochondrial dysfunction in liver via AMPK-mediated autophagy flux. *Biosci Rep.* (2017) 37:BSR20170934. doi: 10.1042/BSR20170934
31. Gomes LC, Di Benedetto G, Scorrano L. During autophagy mitochondria elongate, are spared from degradation and sustain cell viability. *Nat Cell Biol.* (2011) 13:589–98. doi: 10.1038/ncb2220
32. Moshage H. Cytokines and the hepatic acute phase response. *J Pathol.* (1997) 181:257–66. doi: 10.1002/(SICI)1096-9896(199703)181:3<257::AID-PATH756>3.0.CO;2-U
33. Gabay C, Kushner I. Acute-phase proteins and other systemic responses to inflammation. *N Engl J Med.* (1999) 340:448–54. doi: 10.1056/NEJM199902113400607
34. Nerstedt A, Cansby E, Amrutkar M, Smith U, Mahlapuu M. Pharmacological activation of AMPK suppresses inflammatory response evoked by IL-6 signalling in mouse liver and in human hepatocytes. *Mol Cell Endocrinol.* (2013) 375:68–78. doi: 10.1016/j.mce.2013.05.013
35. Zhou S, Lu W, Chen L, Ge Q, Chen D, Xu Z, et al. AMPK deficiency in chondrocytes accelerated the progression of instability-induced and ageing-associated osteoarthritis in adult mice. *Sci Rep.* (2017) 7:43245. doi: 10.1038/srep43245
36. Ge Y, Zhou S, Li Y, Wang Z, Chen S, Xia T, et al. Estrogen prevents articular cartilage destruction in a mouse model of AMPK deficiency via ERK-mTOR pathway. *Ann Transl Med.* (2019) 7:336. doi: 10.21037/atm.2019.06.77
37. Königsberg M, López-Diazguerrero NE, Rivera-Martinez LP, González-Puertos VY, González-Vieira R, Gutiérrez-Ruiz MC, et al. Physiological deterioration associated with breeding in female mice: a model for the study of senescence and aging. *Comp Biochem Physiol A Mol Integr Physiol.* (2007) 146:695–701. doi: 10.1016/j.cbpa.2006.05.005
38. Viollet B, Guigas B, Sanz Garcia N, Leclerc J, Foretz M, Andreelli F. Cellular and molecular mechanisms of metformin: an overview. *Clin Sci.* (2012) 122:253–70. doi: 10.1042/CS20110386

Disclaimer: The content is solely the responsibility of the authors and does not necessarily represent the official views of the National Institutes of Health.

Conflict of Interest: The authors declare that the research was conducted in the absence of any commercial or financial relationships that could be construed as a potential conflict of interest.

Copyright © 2020 Kikuchi, Piraino, O'Connor, Wolfe, Ridings, Lahni and Zingarelli. This is an open-access article distributed under the terms of the Creative Commons Attribution License (CC BY). The use, distribution or reproduction in other forums is permitted, provided the original author(s) and the copyright owner(s) are credited and that the original publication in this journal is cited, in accordance with accepted academic practice. No use, distribution or reproduction is permitted which does not comply with these terms.

frontiers in Immunology

ORIGINAL RESEARCH
published: 25 February 2020
doi: 10.3389/fimmu.2020.00285

Mangiferin Attenuates LPS/D-GalN-Induced Acute Liver Injury by Promoting HO-1 in Kupffer Cells

Sen Yang[1†], Ge Kuang[1†], Liangke Zhang[1], Shengwang Wu[2], Zizuo Zhao[3], Bin Wang[3], Xinru Yin[4], Xia Gong[2] and Jingyuan Wan[1*]*

[1] Chongqing Key Laboratory of Biochemistry and Molecular Pharmacology, Chongqing Medical University, Chongqing, China, [2] Department of Anatomy, Chongqing Medical University, Chongqing, China, [3] Department of Anesthesiology, The First Affiliated Hospital of Chongqing Medical University, Chongqing, China, [4] Department of Gastroenterology, Institute of Surgery Research, Daping Hospital, Third Military Medical University, Chongqing, China

OPEN ACCESS

Edited by:
Christoph Thiemermann,
Queen Mary University of London,
United Kingdom

Reviewed by:
Yongsheng Li,
Army Medical University, China
Enrico Calzia,
University of Ulm, Germany

***Correspondence:**
Xia Gong
xiagong@cqmu.edu.cn
Jingyuan Wan
jywan@cqmu.edu.cn

[†]These authors have contributed equally to this work

Specialty section:
This article was submitted to Inflammation, a section of the journal Frontiers in Immunology

Received: 05 June 2019
Accepted: 04 February 2020
Published: 25 February 2020

Citation:
Yang S, Kuang G, Zhang L, Wu S, Zhao Z, Wang B, Yin X, Gong X and Wan J (2020) Mangiferin Attenuates LPS/D-GalN-Induced Acute Liver Injury by Promoting HO-1 in Kupffer Cells. Front. Immunol. 11:285. doi: 10.3389/fimmu.2020.00285

Acute liver injury and its terminal phase, hepatic failure, trigger a series of complications, including hepatic encephalopathy, systematic inflammatory response syndrome, and multiorgan failure, with relatively high morbidity and mortality. Liver transplantation is the ultimate intervention, but the shortage of donor organs has limited clinical success. Mangiferin (MF), a xanthone glucoside, has been reported to have excellent anti-inflammatory efficacy. Here, a lipopolysaccharide (LPS)/D-galactosamine (D-GalN)-induced acute liver injury mouse model was established to investigate the protective role of MF and the underlying mechanisms of action. Pretreatment with MF improved survival, decreased serum aminotransferase activities, and inhibited hepatic TNF-α production in LPS/D-GalN-challenged mice. Through Kupffer cell (KC) deletion by $GdCl_3$ and KC adoptive transfer, KCs were confirmed to be involved in these beneficial effects of MF. MF reduced LPS-mediated TNF-α production via the suppression of the TLR4/NF-κB signaling pathway *in vitro*. MF promoted HO-1 expression, but the knockdown of HO-1 prevented TNF-α inhibition, suggesting that the damage-resistance effects of HO-1 occurred via the suppression of TNF-α synthesis. When HO-1-silenced KCs were transferred to the liver with KC deletion, the protective effect of MF against LPS/D-GalN-induced acute liver injury was reduced, illustrating the role of KC-derived HO-1 in the anti-injury effects of MF. Collectively, MF attenuated acute liver injury induced by LPS/D-GalN via the inhibition of TNF-α production by promoting KCs to upregulate HO-1 expression.

Keywords: mangiferin, heme oxygenase-1 (HO-1), acute liver injury, lipopolysaccharide/D-galactosamine (LPS/D-GalN), TNF-α

INTRODUCTION

The liver is the most important metabolic organ and plays a pivotal role in the host's defensive response owing to its ability to scavenge pathogenic microorganisms and toxins (1). However, the liver is also the main victim of such attacks, resulting in the activation of host immune cells, which incites inflammation (2). The dysregulated inflammatory response not only impairs the defensive

function of liver but also induces massive necrosis of hepatocytes, triggering acute liver injury and, ultimately, provoking fulminant hepatic failure (FHF) (3, 4). As the incidence of FHF is associated with high mortality and there is no recognized treatment, the terminal stage of FHF should be prevented. Thus, there is an urgent need for new therapeutic agents for the clinical treatment of acute liver injury (5).

Lipopolysaccharide, a component of Gram-negative bacteria, can induce acute liver injury with high lethality in D-galactosamine (D-GalN)-sensitized mice (6). This well-established experimental murine model, developed by Galanos et al. (7), is distinguished by a dramatic activation of Kupffer cells (KCs), the resident macrophages of the liver tissue (8), which can produce many pro-inflammatory mediators in the liver (9). Among these mediators, TNF-α, the terminal effector in the pathogenesis of acute liver injury, initiates extensive hepatocyte apoptosis and massive hepatocyte necrosis, prompting the explosion of inflammation. Considering that the model exactly resembles the pathogenesis of human clinical FHF, it is employed widely as an experimental animal model to investigate the underlying mechanism of clinical FHF and develop effective therapeutic strategies for endotoxin challenge (10).

Heme oxygenase-1 (HO-1), a cellular stress protein belonging to the heme oxygenase enzyme system, is part of the rate-limiting step in the degradation of heme to carbon monoxide (CO), iron, and biliverdin-IXa (BV); all of these are involved in various pathophysiological processes (11). It has manifold biological activities, such as anti-oxidative stress, anti-inflammatory, and anti-apoptosis activity (12, 13). HO-1, a downstream molecule in multiple signaling pathways, is induced and responds to pathological challenges from various diverse stimuli (14). Recent studies have demonstrated that expression of HO-1 is upregulated in acute liver injury and that the increase in HO-1 activity alleviated the toxic action of LPS in the liver (15). In particular, the stimulation of macrophage-derived HO-1 appears to significantly attenuate liver injury, which has caused researchers to recognize its critical role (16).

Mangiferin, a xanthone glucoside, exhibits a broad spectrum of pharmacological properties, including antioxidant, antiviral, antitumor, anti-inflammatory, and gene-regulatory effects (17, 18). A growing number of studies have reported that MF exerts potent anti-oxidative and anti-inflammatory effects against the acute inflammation of multiple organs, such as the lung and kidney and the cardiovascular system (19–21). The attenuation of liver injury by MF via multiple pathways has been previously reported, illustrating its prominent role in hepatic inflammation (22, 23). With respect to the signaling pathways concerning anti-inflammation, Nrf2/HO-1 exerts its defense against injury by abating oxidative stress, mitigating the inflammatory response, and preventing cell death (24). Pan et al. (25) reported that MF alleviated LPS/D-GalN-induced acute liver injury, coupled with the activation of the Nrf2 signaling pathway. The evidence encouraged us to explore whether the underlying target of MF is closely associated with KC-derived HO-1 in LPS-D-GalN-mediated fulminant hepatic damage. Overall, the study aimed to search for effective molecule targets of MF against FHF, to elucidate the protective mechanism of MF, and to demonstrate the involvement of HO-1. The study has screened for a potential antidote to LPS/D-GalN-induced acute liver injury and has provided novel insights into the target and mechanisms of MF.

MATERIALS AND METHODS

Animals

BALB/c mice, weighing 18–22 g, were obtained from the Experimental Animal Center of Chongqing Medical University. The animals were kept in individual wire-bottomed cages. All animals were fed a standard laboratory diet and water *ad libitum* and maintained in a controlled environment (20–25°C, 50% ± 5% relative humidity, 12 h dark/light cycle). The animals were acclimatized to the experimental conditions for at least l week before use in experiments. All experimental procedures involving animals were approved by the Animal Care and Use Committee of Chongqing Medical University.

Reagents

MF ($C_{19}H_{18}O_{11}$, FW = 422.34, purity ≥ 95%) was purchased from Nanjing ZeLang Medical Technology Co. Ltd. (Nanjing, China). LPS (*Escherichia coli*, 0111: B4), D-GalN, and ZnPP IX were obtained from Sigma (St. Louis, MO, USA). ALT and AST detection kits were purchased from Nanjing Jiancheng Bioengineering Institute (Nanjing, China). The bicinchoninic acid (BCA) protein assay kit was purchased from Pierce (Rockford, IL, USA). Trizol reagent was purchased from Invitrogen (Grand Island, NY, USA). AMV transcriptase, RNasin, SYBR green PCR Master Mix, and the Dual-Luciferase Reporter Assay kit were obtained from Promega (Madison, WI, USA). The tumor necrosis factor (TNF)-α ELISA kit was obtained from Bender MedSystems (Vienna, Austria). Rabbit HO-1 antibody was obtained from Abcam (Cambridge, MA, UK), rabbit β-actin antibody was purchased from Cell Signaling Technology (Boston, MA, USA), and the rat anti-mouse TLR4/MD-2 complex and rat IgG2a isotype control PE were obtained from eBioscience (San Diego, CA, USA). Lipofectamine 2000 was obtained from Invitrogen (Carlsbad, CA, USA).

Kupffer Cell Isolation and Culture

Liver-resident Kupffer cells were isolated from mice. Briefly, liver samples were perfused with calcium (Ca^{2+})- and magnesium (Mg^{2+})-free Hanks' balanced salt solution (HBSS) containing 0.5 mM EGTA, 10 mM HEPES, and 4.2 mM $NaHCO_3$, Type I collagenase (0.05%), and trypsin inhibitor (50 μg/mL) for 10–20 min. The liver samples were removed from the solution and transferred into a sterile tube, minced into small pieces by using scissors, and placed in RPMI 1640 medium supplemented with 5% fetal bovine serum (FBS) and 0.5 mg/mL collagenase at 37°C for 15 min. Then, the liver cell suspensions were filtered through a sterile nylon mesh and placed into fresh, calcium-free medium and subsequently centrifuged at 250 rpm for 15 min. The supernatant was discarded, and the cell pellets were resuspended in RPMI with 5% FBS and separated by centrifugation on a 25–50% Percoll gradient. The Kupffer cells in the interface

were seeded in RPMI 1640 containing 10% FBS, 100 μM β-mercaptoethanol, 10 μg/mL insulin, 100 μg/mL streptomycin, and 100 U/mL penicillin at 37°C in an atmosphere of 5% CO_2.

Experimental Protocols

FHF was induced in mice by the injection of LPS (10 μg/kg) and D-GalN (700 mg/kg). The mice were gavaged orally with PBS (Control) or MF (30, 100, or 150 mg/kg, respectively) twice, at 1 and 7 h prior to LPS/D-GalN injection. ZnPP IX (45 mg/kg) was administered intraperitoneally (i.p.) 30 min before LPS/D-GalN. The survival rate was evaluated for up to 48 h after LPS/D-GalN administration. The serum and liver were collected at the indicated time point for the analysis. For KC depletion, 25 mg/kg $GdCl_3$ was intravenously (i.v.) injected into mice at 24 h before challenge or cell transfer. In the adoptive transfer experiment, 2×10^6 donor KCs were i.v.-infused into the tail vein of the recipient mouse in the 24 h before LPS challenge.

In the experiment with KCs, primary KCs were cultured in FBS-free RMPI 1640 and pretreated with PBS or MF (10^{-5} M) for 30 min, and then PBS or LPS (100 ng/mL) was added. The supernatants and cells were collected at 30 min or 3 h after LPS for the subsequent analyses.

ALT and AST Measurement

Blood was collected from the retro-orbital vein of the eye of mice 6 h after the LPS/D-GalN injection. The blood samples were centrifuged at 3,000 rpm for 10 min. The serum was separated, transferred to other tubes, and frozen at −20°C. ALT and AST activities were assayed by using commercially available kits in accordance with the manufacturer's recommendations.

Cytokine Analysis

Hepatic tissues and cell supernatants were assayed for TNF-α level by ELISA in accordance with the manufacturer's protocol. Briefly, samples or standards were pipetted into a microplate pre-coated with a monoclonal antibody specific for mouse TNF-α. After any unbound substances had been washed away, an enzyme-linked polyclonal antibody specific for mouse TNF-α was added to each well. After any unbound antibody-enzyme reagent had been washed away, a substrate solution was added to the wells. The enzyme reaction yielded a blue product that turned yellow when the stop solution was added. The intensity of the color was in proportion to the amount of mouse TNF-α bound in the initial step, and the concentration of the sample values were then read from the standard curve.

Histopathology Analysis

The liver tissue samples from mice were excised and fixed in 10% formaldehyde at 25°C and then embedded in paraffin. Serial paraffin sections (4 μm) were stained with hematoxylin-eosin for conventional morphological evaluation by using a light microscope (Olympus, Tokyo, Japan).

Reverse Transcription-Quantitative Polymerase Chain Reaction (RT-qPCR)

Total RNA was isolated from the liver and cell samples by using Trizol reagent in accordance with the manufacturer's protocol. First-strand complementary DNA (cDNA) was synthesized. The cDNA samples were then incubated at 90°C for 7 min to stop the reaction. Quantitative PCR was performed with SYBR Green PCR Master Mix in accordance with the protocol. The primers were used to amplify TNF-α cDNA (sense, 5′-TTC TCA TTC CTG CTT GTG GC-3; antisense, 5′-GTT TGC TAC GAC GTG GGC TA-3′), HO-1 cDNA (sense, 5′-GAG ATA GAG CGC AAC AAG CAG-3′; antisense, 5′-CTT GAC CTC AGG TGT CAT CTC-3′), GAPDH cDNA (sense, 5′-CCT GCA CCA CCA ACT GCT TA-3′; antisense, 5′-TCA TGA GCC CTT CCA CAA TG-3′). The generation of specific PCR products was confirmed by melting curve analysis. Relative HO-1 mRNA expression was normalized to GAPDH expression. Data were calculated by using the $2^{-\Delta\Delta Ct}$ method as described by the manufacturer and were expressed as fold increase over the indicated controls.

Western Blotting Analysis

The protein contents of liver and cell samples were prepared by using a Protein Extraction Kit (20 mM Tris, 150 mM NaCl, 1 mM EDTA, 1 mM EGTA, 1% Triton X-100, 2.5 mM sodium pyrophosphate, 1 mM Na_3VO_4, 1 mM β-glycerophosphate, 1 μg/mL leupeptin, and aprotinin). Protein concentrations were determined by using the BCA protein assay kit. Protein extracts (40 μg) were fractionated on 12% polyacrylamide-sodium dodecyl sulfate (SDS) gel and then transferred to nitrocellulose membranes. Non-specific binding to the membrane was blocked by incubation in 5% (w/v) fat-free milk in Tris-buffered saline (TBS) containing 0.05% Tween-20, followed by incubation with a rabbit primary polyclonal antibody at 4°C overnight. The membrane was then treated with horseradish peroxidase-conjugated goat anti-rabbit secondary antibody. Antibody binding was visualized by using a chemiluminescence system and brief exposure of the membrane to X-ray film (Kodak, Japan).

Flow Cytometry Analysis

KCs were collected, washed with fluorescence-activated cell sorting (FACS) buffer, and blocked with the anti-FcR antibody for 15 min. The cells were then stained by using rat anti-mouse TLR4/MD-2 complex PE or rat IgG2a isotype control PE in the dark at room temperature. Cells were incubated for 30 min, washed twice, and resuspended in 0.5 mL FACS buffer. Fluorescence was measured by flow cytometry and analyzed by using FlowJo software (Tree Star, Inc., Ashland, OR).

Transfection of Reporter Plasmids and Small Interference RNA (siRNA)

KCs were seeded at 1×10^6 cells per well in 24-well plates and allowed to rest for 1 day before transfection. Cells were transiently transfected with pAP1-Luc or pNF-κB-Luc and the pRL-TK *Renilla* plasmid by using Lipofectamine 2000. The activities of both firefly and *Renilla* luciferases were measured by using the Dual-Luciferase Reporter Assay System according to the manufacturer's instructions. To silence murine HO-1 in primary KCs, pre-confirmed HO-1 specific siRNA and non-targeting control siRNAs were transfected into freshly isolated primary KCs by using Lipofectamine 2000. At 24 h after transfection, the cells were used for subsequent experiments.

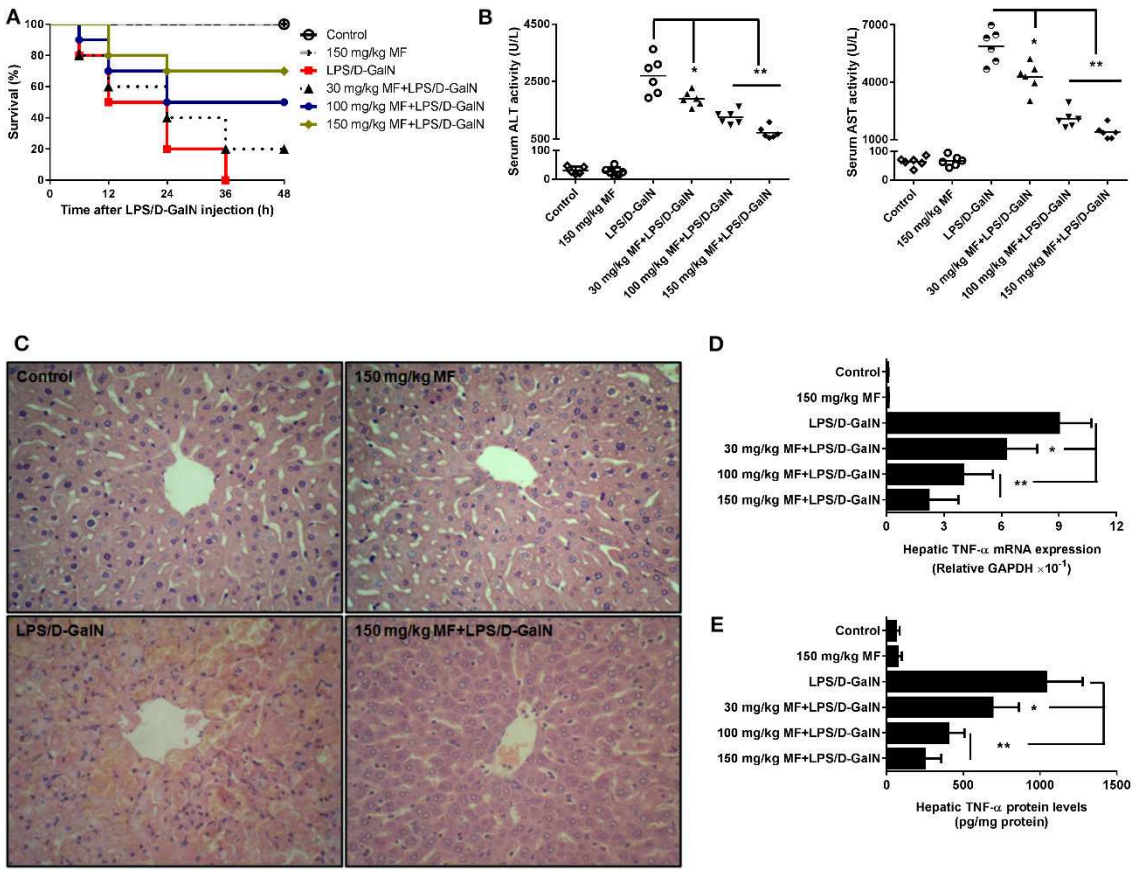

FIGURE 1 | MF improved survival and pathological liver injury induced by LPS/D-GalN. Mice were pretreated orally with vehicle (PBS) or MF (30, 100, or 150 mg/kg, respectively) at 1 and 7 h prior to LPS/D-GalN challenge. Survival rates of mice **(A)** were monitored for 48 h after LPS/D-GalN challenge. Serum ALT and AST activities **(B)** and hepatic tissue pathological changes **(C)** were assessed at 6 h after LPS/D-GalN challenge. Hepatic TNF-α mRNA **(D)** and protein **(E)** were determined by RT-qPCR and ELISA at 1.5 h after LPS/D-GalN challenge. Data are presented as mean ± SD. $n = 10$ (for survival rate analysis) or 6; $^{*}P < 0.05$ and $^{**}P < 0.01$.

HO-1 Activity Assay

HO enzymatic activity was measured by bilirubin generation, as described previously (26). Briefly, frozen hepatic and cell samples were homogenized in lysis buffer (250 mM Tris·HCl, pH 7.4; 150 mM NaCl; 250 mM sucrose; 0.5 mM PMSF; 1 μg/μL leupeptin; 1 μg/μL aprotinin). The microsomal fraction was obtained by successive centrifugation and washing with 0.15 M KCl, followed by centrifugation (105,000 × *g* for 30 min). The pellet was solubilized in 0.1 M potassium phosphate by sonication and stored at −80°C. The reaction was performed in a mixture containing 2–3 mg/mL protein microsomal fraction, 1 mM glucose-6-phosphate, 0.2 units/mL glucose-6-phosphate dehydrogenase, 0.8 mM NADPH, and 0.025 mg/mL hemin at 37°C for 45 min. After chloroform extraction, the amount of extracted bilirubin was calculated by the difference in absorbance at 464 and 530 nm.

Statistical Analysis

The study data were expressed as mean ± standard deviation (S.D.). The differences between two groups were calculated by Student's *t*-test, and comparisons of multiple groups were evaluated by one-way analysis of variance (ANOVA), followed by the Tukey *post hoc* test. The survival rates were determined using Kaplan-Meier curves with log-rank tests. $P < 0.05$ were considered to be statistically significant.

RESULTS

MF Improved Survival and Pathological Liver Injury Induced by LPS/D-GalN in Mice

First, we examined the survival rates induced by LPS/D-GalN in MF-treated and untreated mice. As expected, LPS/D-GalN resulted in high lethality, with 100% mortality occurring within 36 h. Pre-treatment of mice with MF improved survival rates in a dose-dependent manner; 70% of the mice survived to the end of the 48-h observation period in the 150 mg/kg MF-treated group (**Figure 1A**). With regard to the association of lethality with hepatic damage, we analyzed the liver enzymes and pathological changes in the serum aminotransferases and tissue sections. Serum concentrations of ALT/AST, which are released into the blood upon damage to liver cells by LPS/D-GalN, were markedly lower in MF-treated mice (**Figure 1B**). Similarly, there were clear

improvements in the pathology of the liver after MF treatment (**Figure 1C**). These results indicated that MF exerts protective activity against LPS/D-GalN-induced mortality and liver injury.

MF Alleviated Hepatic Expression of TNF-α mRNA and Protein Induced by LPS/D-GalN in Mice

After confirmation of the critical role of TNF-α in endotoxin-induced acute liver injury, we attempted to determine whether MF affected LPS-induced TNF-α production. As shown, the expressions of hepatic TNF-α mRNA and protein was sharply increased in LPS/D-GalN-stimulated mice compared to in control mice; in contrast, the increased expression of TNF-α was dose-dependently decreased by MF treatment (**Figures 1D,E**, $p < 0.05$), suggesting that MF could inhibit the expression increases of TNF-α mRNA and protein induced by LPS/D-GalN.

MF Promoted Hepatic HO-1 Expression and Activity in LPS/D-GalN-Challenged Mice

HO-1 is an inducible heat shock protein that participates in cytoprotection. It has been shown that HO-1 exerts a protective effect against LPS/D-GalN-induced FHF. Therefore, we examined whether MF could modify the expression and activity of HO-1. Intriguingly, the expression and activity of HO-1 in hepatic tissues were significantly upregulated by MF treatment compared to those in LPS/D-GalN-treated mice (**Figures 2A–C**).

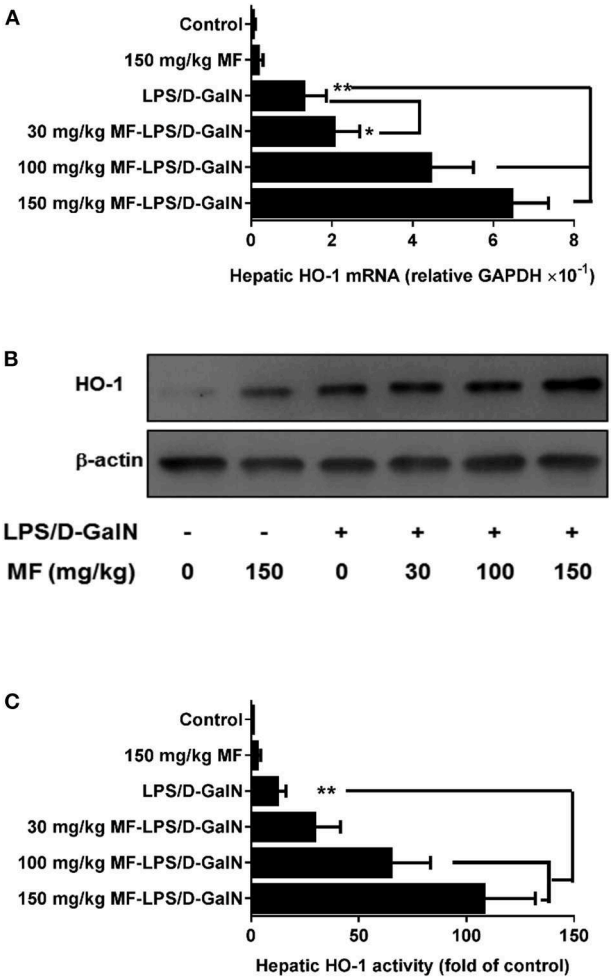

FIGURE 2 | MF upregulated HO-1 expression and activity in LPS/D-GalN-challenged mice. Mice were pretreated orally with vehicle (PBS) or MF (30, 100, or 150 mg/kg, respectively) at 1 and 7 h prior to LPS/D-GalN challenge. Hepatic tissue HO-1 mRNA **(A)** and protein **(B)** expression and activity **(C)** were determined at 6 h after LPS/D-GalN challenge. Data are presented as mean ± SD. $n = 6$, $^{*}P < 0.05$, and $^{**}P < 0.01$.

HO-1 Is Responsible for the Effect of MF on LPS/D-GalN-Induced Liver Injury in Mice

ZnPP-IX, a widely used HO-1 inhibitor, could suppress HO-1 activity via the competitive conjugation with the porphyrin ring structure owing to its similarity to heme (27, 28). Hence, LPS/D-GalN-treated mice treated with or without MF were exposed to ZnPP-IX. As shown in **Figure 3A**, ZnPP-IX markedly blunted the improved survival of MF in LPS/D-GalN-treated mice. Likewise, ZnPP-IX blocked the effects of MF on the LPS/D-GalN-induced increases in ALT/AST activities and TNF-α production (**Figures 3B–D**).

KCs Are Involved in the Protective Effect of MF on LPS-Mediated Acute Liver Injury in D-GalN-Sensitized Mice

As hepatic TNF-α is produced mainly in inflammatory cells, especially in KCs, we then investigated whether KCs contributed to these effects. We injected mice with $GdCl_3$ to selectively deplete KCs in accordance with the previous study (29) and found that this almost completely abrogated LPS/D-GalN-induced mortality and hepatic damage, as indicated by improved survival and decreased serum liver enzymes (**Figures 4A,B**). Meanwhile, hepatic TNF-α mRNA and protein expression were also sharply diminished (**Figures 4C,D**). In contrast, adoptive transfer of KCs to $GdCl_3$-treated mice restored these effects of the depletion of KCs, suggesting that KCs are required for LPS/D-GalN-induced acute liver injury and TNF-α production. In keeping with those findings, KC depletion could also abolish the protection of MF on LPS/D-GalN-mediated acute liver injury; adoptive transfer of KCs restored the protective effect of MF on LPS/D-GalN-mediated acute liver injury and TNF-α production (**Figure 4**). Collectively, these data provided compelling evidence that KCs were involved not only in LPS/D-GalN-induced acute liver injury but also in the protective effects of MF on FHF induced by LPS/D-GalN.

KCs Are Involved in MF-Mediated HO-1 Upregulation in LPS-D-GalN-Treated Mice

To assess whether HO-1 upregulation of MF was involved in KCs, we first used $GdCl_3$ to remove KCs in MF-treated LPS-D-GalN-induced mice. As expected, in **Figure 5**, $GdCl_3$ can be seen to have markedly abrogated MF-upregulated HO-1

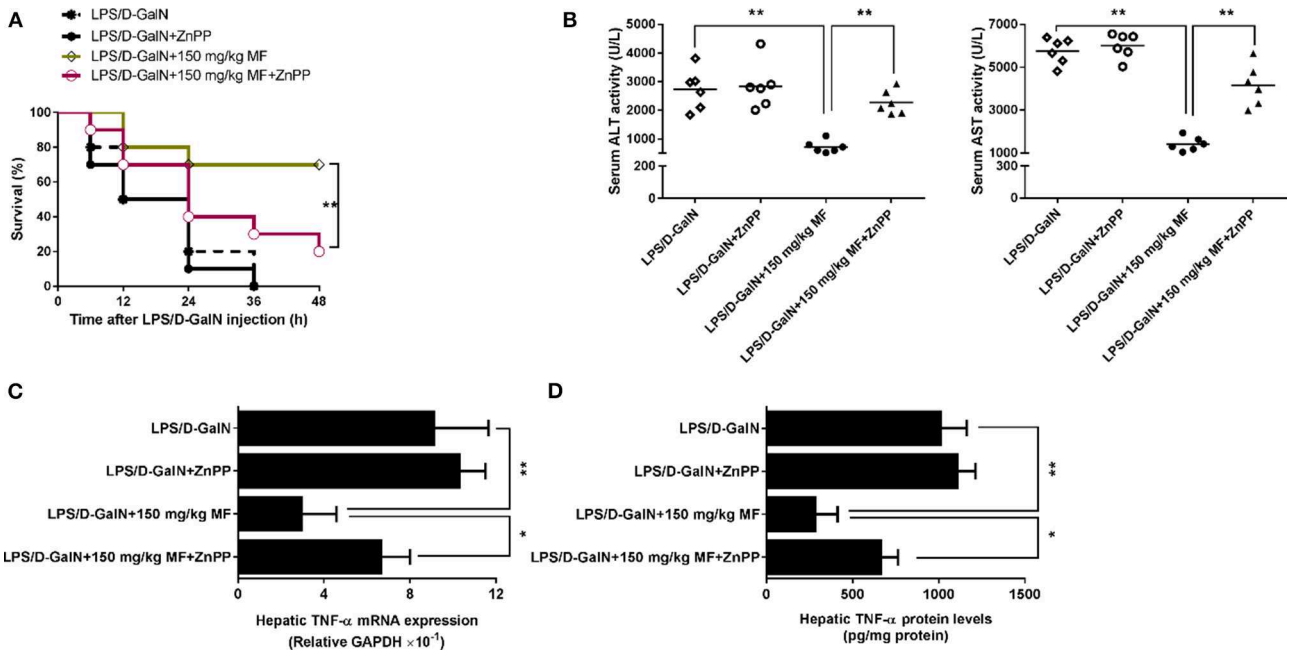

FIGURE 3 | Inhibition of HO-1 removed the protective effect of MF against LPS/D-GalN-induced acute liver injury. Mice were pretreated orally with MF (150 mg/kg) at 1 and 7 h with or without ZnPP IX (40 mg/kg) i.p. 30 min prior to LPS/D-GalN challenge. **(A)** Survival rates of mice were monitored for 48 h after LPS/D-GalN challenge. **(B)** Serum ALT and AST activity were assessed at 6 h after LPS/D-GalN challenge. Hepatic TNF-α mRNA **(C)** and protein **(D)** expression were determined by RT-qPCR and western blotting, respectively, at 1.5 h after LPS/D-GalN. Data were presented as mean ± SD. $n = 6$, $^{*}P < 0.05$, $^{**}P < 0.01$.

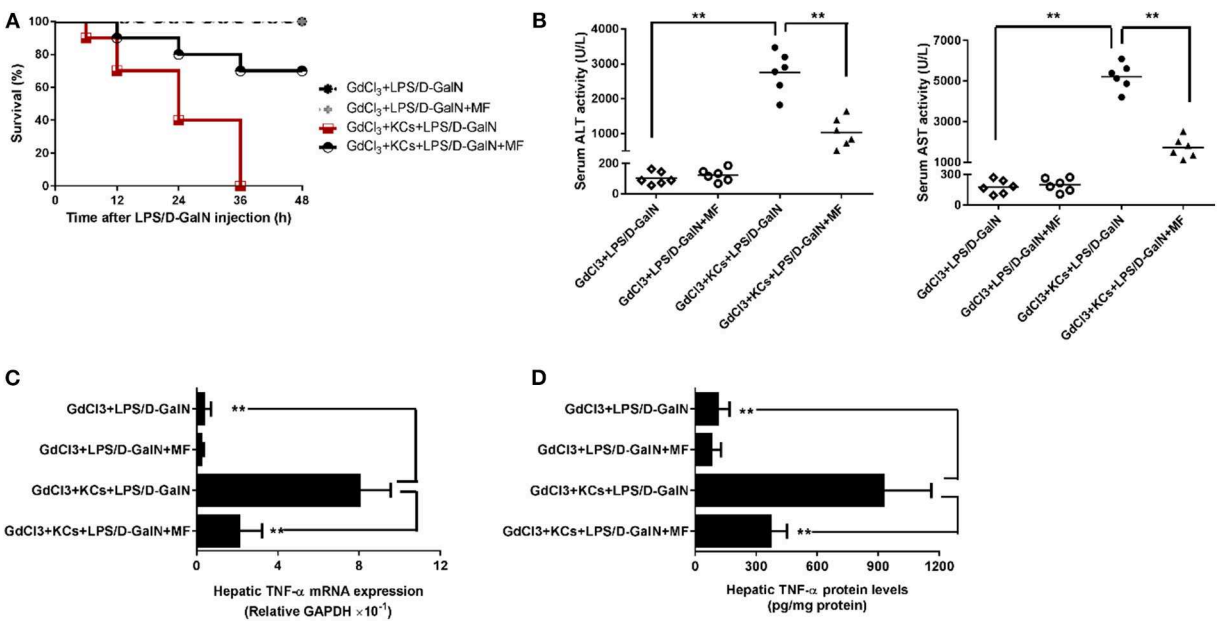

FIGURE 4 | KCs are involved in the protective effect of MF on LPS-mediated acute liver injury in D-GalN-sensitized mice. Mice were injected i.p. with $GdCl_3$ 2 days before LPS/D-GalN challenge, KCs were i.v.-infused into mice at 24 h prior to LPS/D-GalN challenge, and MF pretreatment was given orally at 1 and 7 h prior to LPS/D-GalN challenge. **(A)** Survival rates of mice were monitored for 48 h after LPS/D-GalN challenge. **(B)** Serum ALT and AST activities were assessed at 6 h after LPS/D-GalN challenge. Hepatic TNF-α mRNA **(C)** and protein **(D)** expression were determined by RT-qPCR and ELISA, respectively, at 1.5 h after LPS/D-GalN challenge. Data are presented as mean ± SD. $n = 6$, $^{**}P < 0.01$.

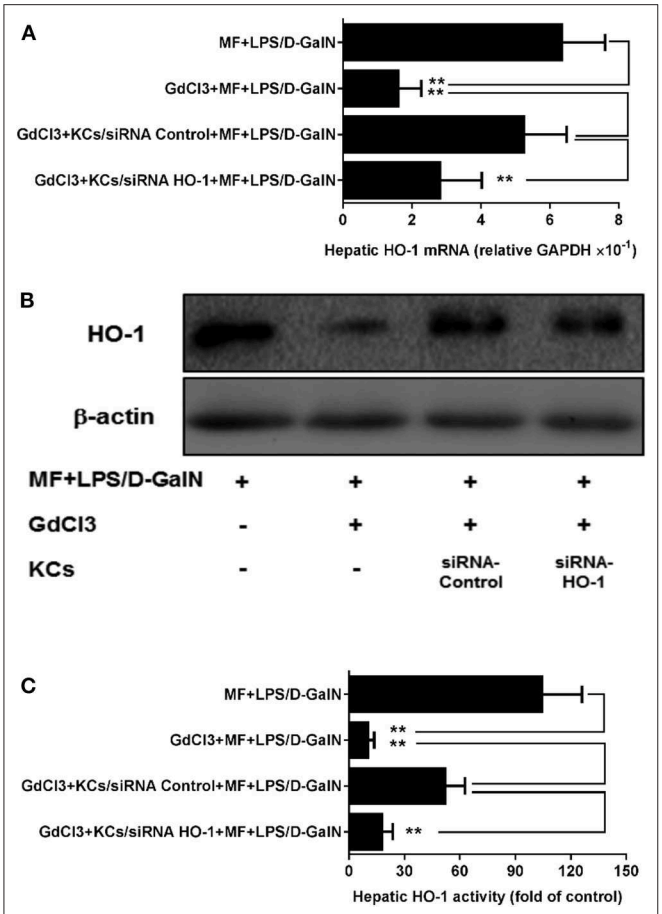

FIGURE 5 | KCs are involved in MF-mediated upregulation of HO-1 in LPS-D-GalN-treated mice. Mice were injected i.p. with $GdCl_3$ 2 days before LPS/D-GalN challenge, KCs were i.v.-infused into mice at 24 h prior to LPS/D-GalN challenge, and MF pretreatment was given orally at 1 and 7 h prior to LPS/D-GalN challenge. Hepatic tissues HO-1 mRNA **(A)** and protein **(B)** expression and activity **(C)** were determined at 6 h after LPS/D-GalN challenge. Data are presented as mean ± SD. $n = 6$, $^{**}P < 0.01$.

expression and activity in LPS-D-GalN-treated mice. Further, the adoptive transfer of KCs with control siRNA restored MF-mediated upregulation of HO-1. However, adoptive transfer of KCs with HO-1 siRNA showed an inhibitory effect on HO-1 expression and activity (**Figure 5**, $p < 0.01$).

KC-Derived HO-1 Is Key for the Effect of MF in Mice in Response to LPS/D-GalN

Finally, we investigated whether KC-derived HO-1 participated in the protective effects of MF on LPS/D-GalN-mediated acute liver injury in mice. To test this hypothesis, the HO-1 siRNA- or control siRNA-transfected KCs were transferred separately into mice with KC depletion. As shown in **Figure 6**, transferral of HO-1 siRNA- or control siRNA-transfected KCs into MF alone-pretreated mice with KC depletion did not affect mouse survival rate, ALT/AST activities, or TNF-α production. However, in HO-1 siRNA-knockdown KCs, the protective effects of MF on LPS/D-GalN-induced FHF were reduced compared with those in HO-1 positive KCs, as indicated by the increased death rate, elevated ALT/AST activities, and enhanced TNF-α production (**Figures 6A–D**, $p < 0.01$). Overall, these results indicated that KC-derived HO-1 was crucial for the effects of MF on LPS/D-GalN-induced FHF.

MF Inhibited LPS-Activated TLR4 Signaling and TNF-α Production in KCs

The observations above suggested that KCs might be a target of the effects of MF in response to LPS. To further verify this hypothesis, we isolated KCs from mice and examined whether MF also has an anti-inflammatory effect on the TNF-α production from KCs stimulated by LPS. Triggering of TLR4 by LPS leads to the activation of transcript factors AP-1 and NF-κB, which promote the expression of TNF-α. The analysis of ELISA and RT-qPCR results revealed that MF remarkably inhibited LPS-induced expression of mRNA and protein TNF-α (**Figures 7A,B**). Further, the assay of reporter genes showed that MF significantly decreased LPS-induced AP-1 and NF-κB activities (**Figure 7C**). In parallel with these results, flow cytometry analysis indicated that MF also downregulated LPS-enhanced TLR4 expression on the surface of KCs (**Figure 7D**). All these data supported the conclusion that MF could effectively suppress TLR4 signaling and TNF-α production triggered by LPS in KCs.

HO-1 Mediated the Suppression of MF on LPS-Triggered Inflammatory Responses in KCs

Given that the inhibitory role of MF in TLR signaling occurs through the HO-1 pathway in KCs, we first assessed the role of MF in the expression and activity of HO-1. Consistent with the above results observed in the animal experiment, the expression and activity of HO-1 were greater in MF-treated KCs than in untreated LPS-stimulated KCs (**Figures 7E–G**, $p < 0.01$). Further, knockdown of HO-1 with a specific HO-1 small interfering RNA markedly downregulated the HO-1 expression and activity induced by MF in LPS-stimulated KCs (**Figures 8A–C**). In line with these results, knockdown of HO-1 also abolished the beneficial role of MF on the TLR4 expression and TNF-α production induced by LPS (**Figures 8D–F**). These data indicated that HO-1 may mediate the anti-inflammatory effect of MF in KCs by downregulating the TLR4 signaling pathway.

DISCUSSION

Fulminant liver failure is one of the most lethal clinical syndromes and is characterized by rapid deterioration of liver function, which leads to hepatic encephalopathy, systemic inflammatory response syndrome, and even multiorgan failure, which pose severe threats to a patient (4). Liver transplantation remains the only effective therapeutic strategy, but patient recovery is currently constrained by the limitations of organ donation (30). Accordingly, there is an urgent need to find effective drugs to ameliorate FHF and avoid severe secondary

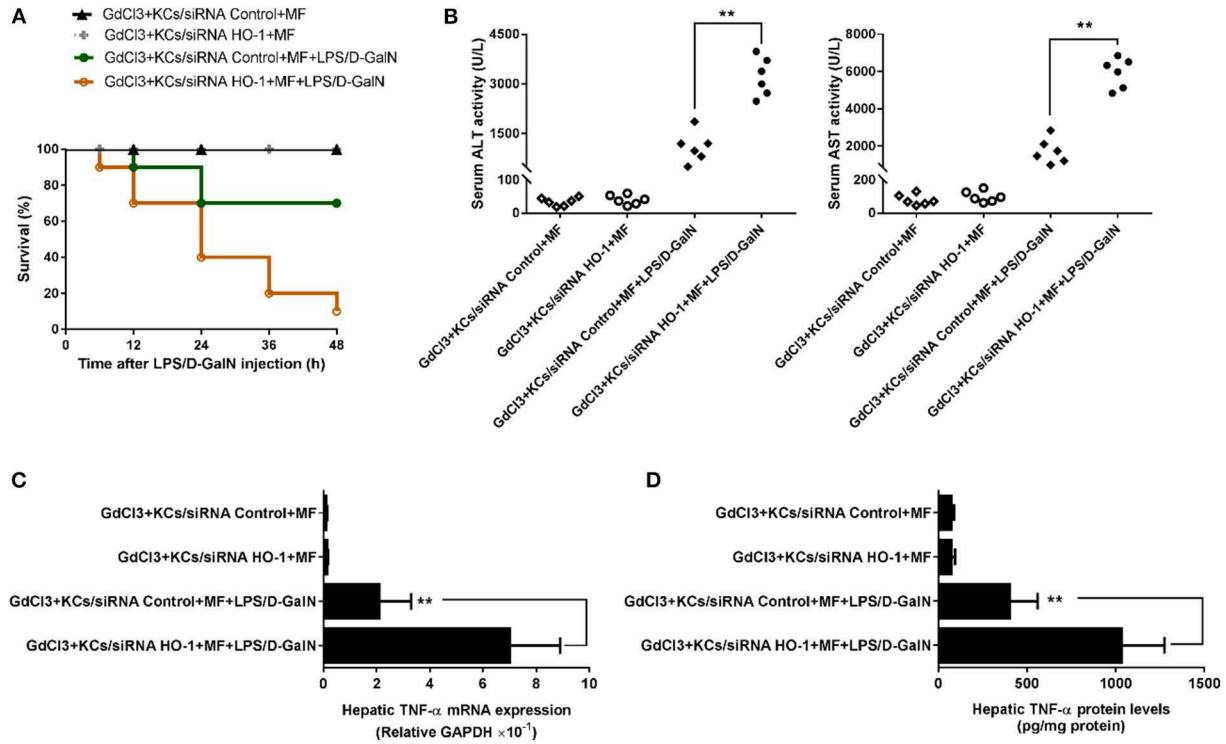

FIGURE 6 | KC-derived HO-1 is critical for the effect of MF against LPS/D-GalN-induced acute liver injury in mice. KCs transfected with HO-1-specific siRNA or non-targeting control were i.v.-infused into mice with KC deletion by $GdCl_3$ at 24 h prior to LPS/D-GalN challenge. Mice were pretreated with MF orally at 1 and 7 h prior to LPS/D-GalN challenge. Survival rates **(A)** were evaluated for 48 h following LPS/D-GalN challenge. Serum ALT and AST activities **(B)** were determined at 6 h after LPS/D-GalN challenge. mRNA **(C)** and protein **(D)** expression of TNF-α were measured by RT-qPCR and ELISA. Data are presented as mean ± SD. $n = 6$, $^{**}P < 0.01$.

complications. In this study, the protective role of MF and the underlying mechanism of action were explored in an LPS/D-GalN-induced mouse model of FHF. Pretreatment with MF significantly enhanced the survival of FHF mice, decreased the activities of ALT and AST in serum, and attenuated liver injury induced by LPS/D-GalN. MF administration not only reduced LPS-mediated TNF-α production but also inhibited KC activation by suppressing the TLR4/NF-κB signaling pathway. Furthermore, the inhibition of TNF-α by MF was indeed associated with the upregulation of HO-1 in KCs.

TNF-α is recognized as a critical inflammatory mediator in the pathogenesis of inflammation and infection-related diseases; moreover, its toxicity may directly damage hepatocytes (31). High amounts of circulating pro-inflammatory TNF-α, the characteristic manifestation of FHF, ultimately induce multiple organ failure (32). TNF-α, via binding TNF receptor on the surface of hepatocytes as an exocellular death signal, can stimulate inner oxidative stress and initiate the apoptotic pathway, which triggers more extensive hepatocyte death and a serious inflammatory response (33). The administration of TNF-α was shown to accelerate liver injury in this model by neutralizing antibodies against TNF-α or inhibitors of TNF-α production; knock-out of TNF-α or TNF-α receptors completely abrogated LPS/D-GalN-induced FHF (34–36). In addition, the production and liberation of TNF-α are predominantly regulated by the TLR4/NF-κB signaling pathway during liver inflammation (37). Accordingly, the inhibition of the TLR4/NF-κB signaling pathway can decrease TNF-α production, which is an effective strategy for FHF alleviation (38, 39). In our study, MF suppressed TNF-α synthesis transcriptionally and translationally, as shown by the decrease in mRNA and protein of TNF-α after MF pretreatment in both mice and KCs. As shown by the reporter gene in KCs, the TLR4 signaling pathway was significantly inhibited by MF, suggesting that MF could reduce TNF-α production via inhibition of TLR4/NF-κB signaling. The abrogation of TNF-α by MF pretreatment significantly retarded the progression of fulminant hepatic damage, which was a critical contribution to the mechanism of MF against acute liver injury.

Although various cell types in the liver are capable of producing TNF-α, KCs are acknowledged as the main source (40). KC-derived TNF-α is majorly involved in the development of FHF (41). Indeed, the liver injury in LPS/D-GalN-induced FHF is associated with activated KCs. The deletion of KCs by $GdCl_3$ not only completely blocked this disease but also inhibited TNF-α production (42). In contrast, the infusion of KCs restored the diseased state (43). Given these results, we hypothesized that the beneficial effect of MF on LPS/D-GalN-induced FHF was through the inhibition of KCs to produce TNF-α. To confirm

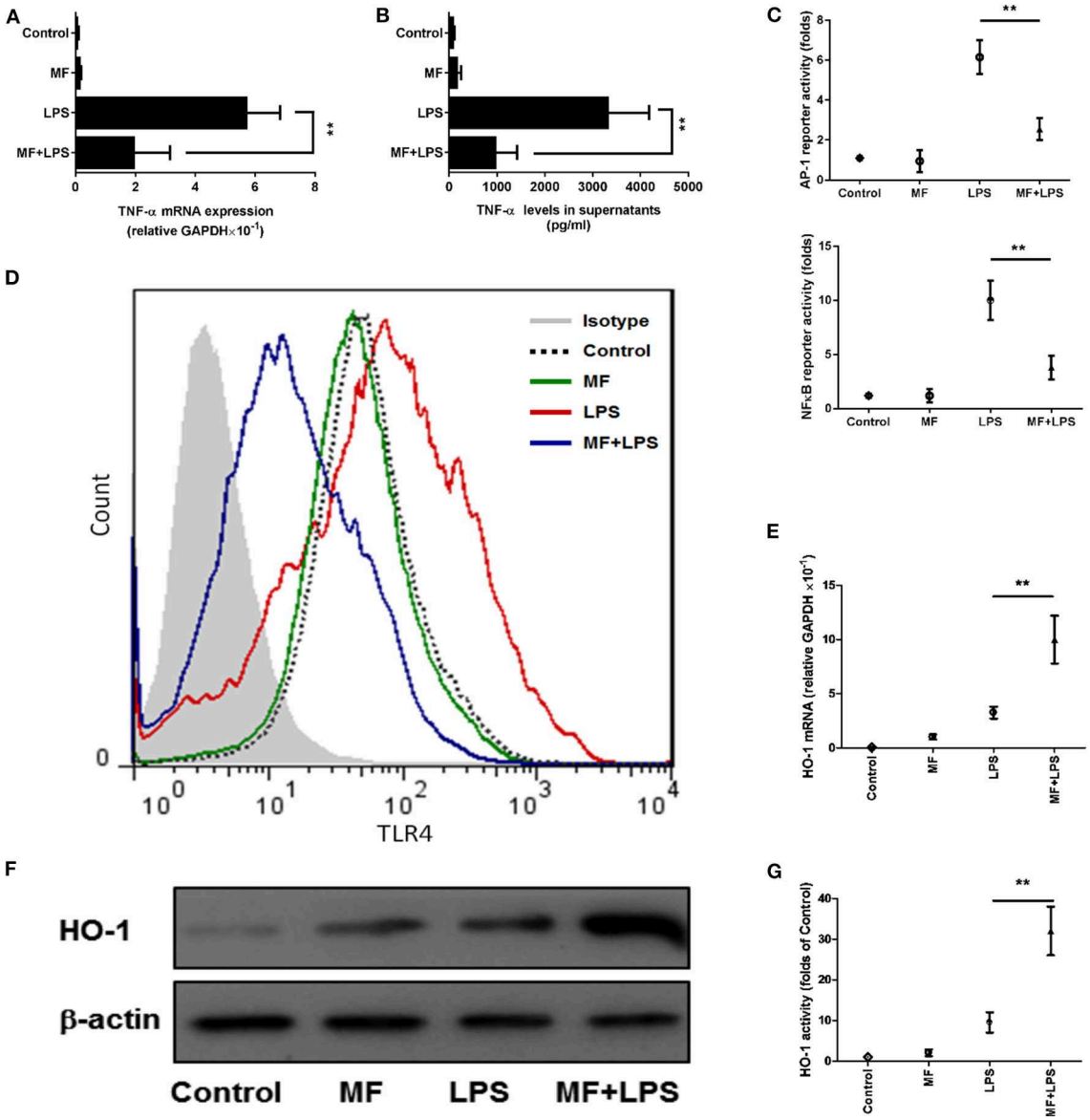

FIGURE 7 | MF inhibited LPS-activated TLR4 signaling and HO-1 upregulation in KCs. KCs were transfected with both pAP1-Luc or pNF-κB-Luc and the pRL-TK *Renilla* plasmid for 24 h, pretreated with PBS or MF (10^{-5} M) 30 min prior to PBS or LPS challenge (100 ng/mL). **(A)** RNA was extracted from KCs at 3 h after LPS challenge and TNF-α mRNA was assayed by real-time RT-PCR. **(B)** Cell culture supernatant was obtained 3 h after LPS stimulation to determine TNF-α levels by using ELISA. **(C)** AP1 and NF-κB activities were measured at 30 min after LPS challenge. **(D)** The expression of TLR4 on the surface of KCs was analyzed at 3 h after LPS by using flow cytometry. HO-1 mRNA **(E)** and protein **(F)** expression and activity **(G)** were determined at 3 h after LPS challenge. Data are presented as mean ± SD. $n = 6$, $^{**}P < 0.01$.

this, we utilized $GdCl_3$ to delete primary KCs and subsequently treated LPS/D-GalN-treated mice with MF. KC deletion indeed ameliorated the inflammatory response following LPS/D-GalN administration, although the activities of ALT and AST and the expression of TNF-α were not remarkably different in the mice with or without MF pretreatment. Moreover, after transferring KCs to the KC-deleted mice, the severe hepatic inflammation was restored, and the protective effect of MF was again observed, indicating the key role of KCs in the protection of MF against LPS/D-GalN-induced FHF.

HO-1, a member of the cellular defense system, fulfills a significant function in the elimination of oxidative stress products and the suppression of inflammatory response through multiple pathways. HO-1 exerts a protective effect by catalyzing the oxidative degradation of heme to carbon monoxide (CO), iron, and biliverdin-IXα, which scavenges endogenous injury factors to protect hepatocytes (11). Several studies have reported that HO-1 has a positive protective role in hepatitis and that the downregulation of HO-1 expression aggravated the severity of hepatic injury (44, 45). Consistent with this, it was observed that

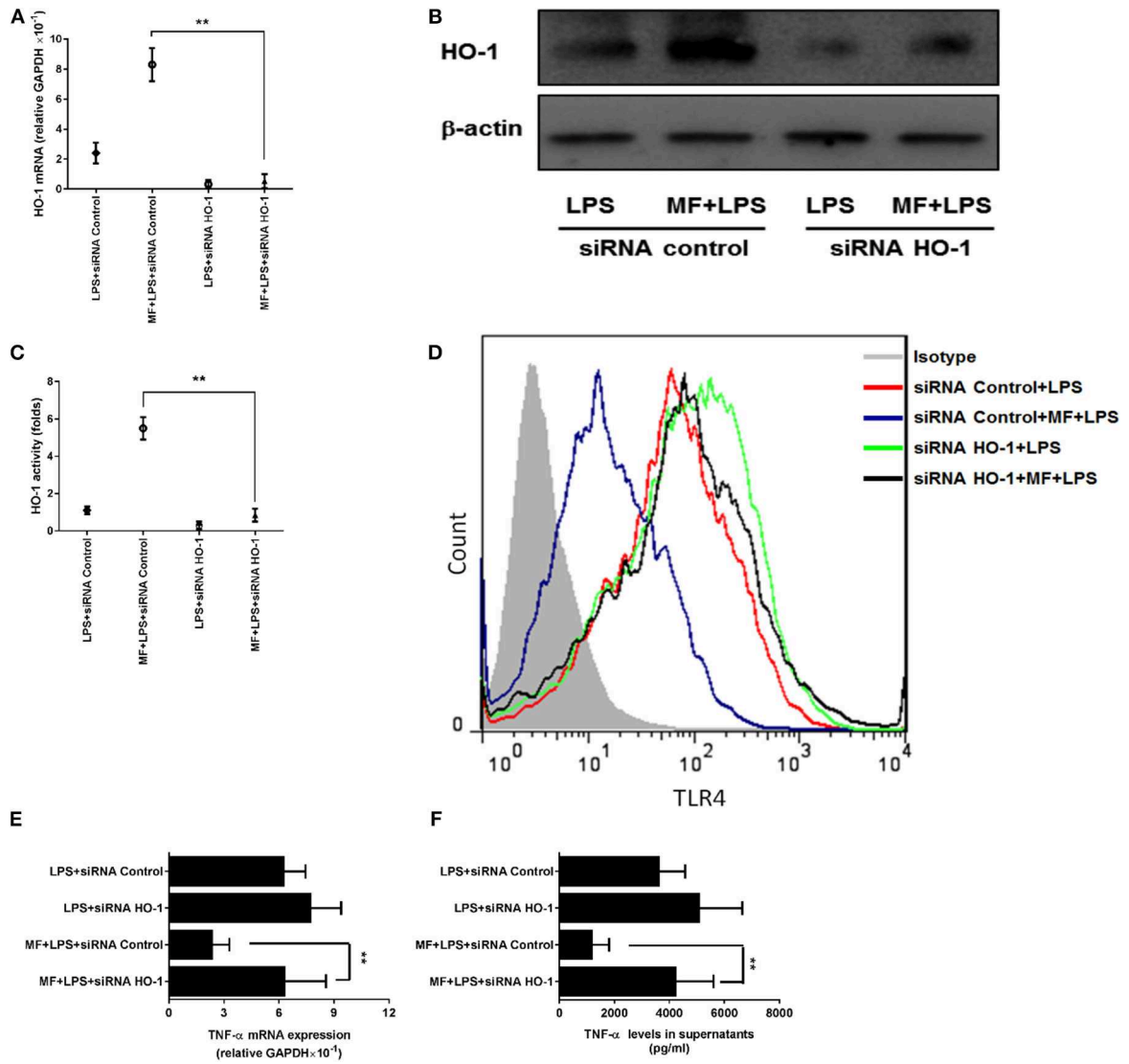

FIGURE 8 | HO-1 mediated the suppression of MF on the LPS-induced inflammatory responses in KCs. HO-1 specific siRNA and non-targeting control siRNA were transfected into freshly isolated primary KCs for 24 h. After transfection, the cells were pretreated PBS or MF (10^{-5} M) 30 min prior to PBS or LPS challenge (100 ng/mL). HO-1 mRNA **(A)** and protein **(B)** expression and activity **(C)** were determined at 3 h after LPS challenge. Total RNA was extracted from KCs at 3 h after LPS challenge and TNF-α mRNA expression was assayed by real-time RT-PCR **(D)**. Cell culture supernatant was obtained at 3 h after LPS challenge and TNF-α protein expression was determined by ELISA **(E)**. The expressions of TLR4 on the surface of KCs was analyzed at 3 h after LPS challenge by flow cytometry **(F)**. Data are presented as mean ± SD. $n = 6$, $^{**}P < 0.01$.

the expression and activity of HO-1 were elevated by MF in the LPS/D-GalN-treated mice, but the protective role of MF was not observed after the use of an HO-1 inhibitor (ZnPP-IX), which showed that the upregulation of HO-1 was a potential target for preventing the deterioration of hepatic injury. However, HO-1 exhibits distinctive regulatory states in different types of cells in the liver, and not every cell can be a therapeutic target for MF against FHF. Hepatic inflammation develops through cascade amplification (46). Thus, the restrictions of the target cell and the superior inflammatory response can fundamentally block the development of liver injury from the source. Activation of KCs has a clear link with the development of hepatic inflammation (47). To confirm this, KCs were examined, and the role of HO-1 in KCs was also investigated. MF pretreatment promoted the expression and activity of HO-1 in KCs, but the protection of MF was equally abated when KC-derived HO-1 expression was silenced by siRNA. Furthermore, when KCs with HO-1 or control siRNA were transferred to primary KC-deleted mice that were subjected to LPS/D-GalN challenge, the survival rate and the activities of transaminases were not improved, and meanwhile the high level of TNF-α. These data more comprehensively illuminated that the upregulation of KC-derived HO-1 was imperative for the attenuation of acute liver injury by MF.

In conclusion, these data revealed that MF exhibited significant protection against LPS/D-GalN-induced acute liver injury and alleviated TNF-α production through the inhibition of the TLR4/NF-κB signaling pathway. The abrogation of TNF-α was correlated with the upregulation of HO-1 expression. Furthermore, KCs played a key role in the protection of MF against acute liver injury and the promotion of KC-derived HO-1 was involved in the protective effects of MF. Collectively, MF attenuated acute liver injury induced by LPS/D-GalN through a reduction in TNF-α production by promoting KCs to upregulate HO-1 expression. This study has demonstrated a potential prophylactic agent with a novel mechanism of action against LPS/D-GalN-induced acute liver injury.

DATA AVAILABILITY STATEMENT

The raw data supporting the conclusions of this article will be made available by the authors, without undue reservation, to any qualified researcher.

ETHICS STATEMENT

The animal study was reviewed and approved by the Animal Care and Use Committee of Chongqing Medical University. Written informed consent was obtained from the owners for the participation of their animals in this study.

AUTHOR CONTRIBUTIONS

SY and GK performed experiments, analyzed data, and wrote the manuscript. SW, ZZ, and XY performed experiments and analyzed data. LZ and BW provided guidance and suggestions for the study. XG and JW conceived and supervised the study, designed experiments, analyzed and interpreted data, and wrote the manuscript.

FUNDING

This study was supported by the National Natural Science Foundation of China (81774124) and Chongqing Yuzhong District Science and Technology Project (20170104).

ACKNOWLEDGMENTS

The authors thank Ms. Rong Jiang for providing professional technical support for tissue section and analysis.

REFERENCES

1. Knolle PA, Wohlleber D. Immunological functions of liver sinusoidal endothelial cells. *Cell Mol Immunol*. (2016) 13:347–53. doi: 10.1038/cmi.2016.5
2. McDonald B, Kubes P. Innate immune cell trafficking and function during sterile inflammation of the liver. *Gastroenterology*. (2016) 151:1087–95. doi: 10.1053/j.gastro.2016.09.048
3. Yin X, Gong X, Zhang L, Jiang R, Kuang G, Wang B, et al. Glycyrrhetinic acid attenuates lipopolysaccharide-induced fulminant hepatic failure in d-galactosamine-sensitized mice by up-regulating expression of interleukin-1 receptor-associated kinase-M. *Toxicol Appl Pharmacol*. (2017) 320:8–16. doi: 10.1016/j.taap.2017.02.011
4. Bernal W, Wendon J. Acute liver failure. *New Engl J Med*. (2013) 369:2525–34. doi: 10.1056/NEJMra1208937
5. Kodali S, McGuire BM. Diagnosis and management of hepatic encephalopathy in fulminant hepatic failure. *Clin Liver Dis*. (2015) 19:565–76. doi: 10.1016/j.cld.2015.04.006
6. Plociennikowska A, Hromada-Judycka A, Borzecka K, Kwiatkowska K. Co-operation of TLR4 and raft proteins in LPS-induced pro-inflammatory signaling. *Cell Mol Life Sci*. (2015) 72:557–81. doi: 10.1007/s00018-014-1762-5
7. Galanos C, Freudenberg MA, Reutter W. Galactosamine-induced sensitization to the lethal effects of endotoxin. *Proc Natl Acad Sci USA*. (1979) 76:5939–43. doi: 10.1073/pnas.76.11.5939
8. Silverstein R. D-galactosamine lethality model: scope and limitations. *J Endotoxin Res*. (2004) 10:147–62. doi: 10.1179/096805104225004879
9. Tsutsui H, Nishiguchi S. Importance of Kupffer cells in the development of acute liver injuries in mice. *Int J Mol Sci*. (2014) 15:7711–30. doi: 10.3390/ijms15057711
10. Wang JB, Wang DL, Wang HT, Wang ZH, Wen Y, Sun CM, et al. Tumor necrosis factor-alpha-induced reduction of glomerular filtration rate in rats with fulminant hepatic failure. *Lab Invest*. (2014) 94:740–51. doi: 10.1038/labinvest.2014.71
11. Ryter SW, Choi AM. Targeting heme oxygenase-1 and carbon monoxide for therapeutic modulation of inflammation. *Transl Res*. (2016) 167:7–34. doi: 10.1016/j.trsl.2015.06.011
12. Mahmoud AM, Zaki AR, Hassan ME, Mostafa-Hedeab G. Commiphora molmol resin attenuates diethylnitrosamine/phenobarbital-induced hepatocarcinogenesis by modulating oxidative stress, inflammation, angiogenesis and Nrf2/ARE/HO-1 signaling. *Chem Biol Interact*. (2017) 270:41–50. doi: 10.1016/j.cbi.2017.04.012
13. Zhao X, Dong W, Gao Y, Shin DS, Ye Q, Su L, et al. Novel indolyl-chalcone derivatives inhibit A549 lung cancer cell growth through activating Nrf-2/HO-1 and inducing apoptosis *in vitro* and *in vivo*. *Sci Rep*. (2017) 7:3919. doi: 10.1038/s41598-017-04411-3
14. Loboda A, Damulewicz M, Pyza E, Jozkowicz A, Dulak J. Role of Nrf2/HO-1 system in development, oxidative stress response and diseases: an evolutionarily conserved mechanism. *Cell Mol Life Sci*. (2016) 73:3221–47. doi: 10.1007/s00018-016-2223-0
15. Tian Y, Li Z, Shen B, Zhang Q, Feng H. Protective effects of morin on lipopolysaccharide/d-galactosamine-induced acute liver injury by inhibiting TLR4/NF-kappaB and activating Nrf2/HO-1 signaling pathways. *Int Immunopharmacol*. (2017) 45:148–55. doi: 10.1016/j.intimp.2017.02.010
16. Nakamura K, Zhang M, Kageyama S, Ke B, Fujii T, Sosa RA, et al. Macrophage heme oxygenase-1-SIRT1-p53 axis regulates sterile inflammation in liver ischemia-reperfusion injury. *J Hepatol*. (2017) 67:1232–42. doi: 10.1016/j.jhep.2017.08.010
17. Gold-Smith F, Fernandez A, Bishop K. Mangiferin and cancer: mechanisms of action. *Nutrients*. (2016) 8:396. doi: 10.3390/nu8070396
18. Khare P, Shanker K. Mangiferin: a review of sources and interventions for biological activities. *Biofactors*. (2016) 42:504–14. doi: 10.1002/biof.1308
19. Sadhukhan P, Saha S, Dutta S, Sil PC. Mangiferin ameliorates cisplatin induced acute kidney injury by upregulating nrf-2 via the activation of pi3k and exhibits synergistic anticancer activity with cisplatin. *Front Pharmacol*. (2018) 9:638. doi: 10.3389/fphar.2018.00638
20. Mahalanobish S, Saha S, Dutta S, Sil PC. Mangiferin alleviates arsenic induced oxidative lung injury via upregulation of the Nrf2-HO1 axis. *Food Chem Toxicol*. (2019) 126:41–55. doi: 10.1016/j.fct.2019.02.022
21. Choy KW, Murugan D, Mustafa MR. Natural products targeting ER stress pathway for the treatment of cardiovascular diseases. *Pharm Res*. (2018) 132:119–29. doi: 10.1016/j.phrs.2018.04.013

22. Das J, Ghosh J, Roy A, Sil PC. Mangiferin exerts hepatoprotective activity against D-galactosamine induced acute toxicity and oxidative/nitrosative stress via Nrf2-NFkappaB pathways. *Toxicol Appl Pharmacol*. (2012) 260:35–47. doi: 10.1016/j.taap.2012.01.015
23. El-Sayyad SM, Soubh AA, Awad AS, El-Abhar HS. Mangiferin protects against intestinal ischemia/reperfusion-induced liver injury: involvement of PPAR-gamma, GSK-3beta and Wnt/beta-catenin pathway. *Eur J Pharmacol*. (2017) 809:80–6. doi: 10.1016/j.ejphar.2017.05.021
24. Wang Z, Guo S, Wang J, Shen Y, Zhang J, Wu Q. Nrf2/HO-1 mediates the neuroprotective effect of mangiferin on early brain injury after subarachnoid hemorrhage by attenuating mitochondria-related apoptosis and neuroinflammation. *Sci Rep*. (2017) 7:11883. doi: 10.1038/s41598-017-12160-6
25. Pan CW, Pan ZZ, Hu JJ, Chen WL, Zhou GY, Lin W, et al. Mangiferin alleviates lipopolysaccharide and D-galactosamine-induced acute liver injury by activating the Nrf2 pathway and inhibiting NLRP3 inflammasome activation. *Eur J Pharmacol*. (2016) 770:85–91. doi: 10.1016/j.ejphar.2015.12.006
26. Morita T, Perrella MA, Lee ME, Kourembanas S. Smooth muscle cell-derived carbon monoxide is a regulator of vascular cGMP. *Proc Natl Acad Sci USA*. (1995) 92:1475–9. doi: 10.1073/pnas.92.5.1475
27. Li Q, Xiang Y, Chen Y, Tang Y, Zhang Y. Ginsenoside Rg1 protects cardiomyocytes against hypoxia/reoxygenation injury via activation of Nrf2/HO-1 signaling and inhibition of JNK. *Cell Physiol Biochem*. (2017) 44:21–37. doi: 10.1159/000484578
28. Mylroie H, Dumont O, Bauer A, Thornton CC, Mackey J, Calay D, et al. PKCepsilon-CREB-Nrf2 signalling induces HO-1 in the vascular endothelium and enhances resistance to inflammation and apoptosis. *Cardiovasc Res*. (2015) 106:509–19. doi: 10.1093/cvr/cvv131
29. Przybocki JM, Reuhl KR, Thurman RG, Kauffman FC. Involvement of nonparenchymal cells in oxygen-dependent hepatic injury by allyl alcohol. *Toxicol Appl Pharmacol*. (1992) 115:57–63. doi: 10.1016/0041-008X(92)90367-2
30. Gotthardt D, Riediger C, Weiss KH, Encke J, Schemmer P, Schmidt J, et al. Fulminant hepatic failure: etiology and indications for liver transplantation. *Nephrol Dial Transplant*. (2007) 22(Suppl. 8):viii5–8. doi: 10.1093/ndt/gfm650
31. Filliol A, Piquet-Pellorce C, Le Seyec J, Farooq M, Genet V, Lucas-Clerc C, et al. RIPK1 protects from TNF-alpha-mediated liver damage during hepatitis. *Cell Death Dis*. (2016) 7:e2462. doi: 10.1038/cddis.2016.362
32. Perego J, Bourbon C, Chasson L, Laprie C, Spinelli L, Camosseto V, et al. Guanabenz prevents d-galactosamine/lipopolysaccharide-induced liver damage and mortality. *Front Immunol*. (2017) 8:679. doi: 10.3389/fimmu.2017.00679
33. Brenner C, Galluzzi L, Kepp O, Kroemer G. Decoding cell death signals in liver inflammation. *J Hepatol*. (2013) 59:583–94. doi: 10.1016/j.jhep.2013.03.033
34. Liu Y, Zhu L, Liang S, Yao S, Li R, Liu S, et al. Galactose protects hepatocytes against TNF-alpha-induced apoptosis by promoting activation of the NF-kappaB signaling pathway in acute liver failure. *Lab Invest*. (2015) 95:504–14. doi: 10.1038/labinvest.2015.34
35. Zhang W, Zhou Y, Li X, Xu X, Chen Y, Zhu R, et al. Macrophage-targeting and reactive oxygen species (ROS)-responsive nanopolyplexes mediate anti-inflammatory siRNA delivery against acute liver failure (ALF). *Biomater Sci*. (2018) 6:1986–93. doi: 10.1039/C8BM00389K
36. Wang W, Sun L, Deng Y, Tang J. Synergistic effects of antibodies against high-mobility group box 1 and tumor necrosis factor-alpha antibodies on D-(+)-galactosamine hydrochloride/lipopolysaccharide-induced acute liver failure. *FEBS J*. (2013) 280:1409–19. doi: 10.1111/febs.12132
37. Nakamoto N, Kanai T. Role of toll-like receptors in immune activation and tolerance in the liver. *Front Immunol*. (2014) 5:221. doi: 10.3389/fimmu.2014.00221
38. Tao YC, Wang ML, Wu DB, Luo C, Tang H, Chen EQ. Apolipoprotein A5 alleviates LPS/D-GalN-induced fulminant liver failure in mice by inhibiting TLR4-mediated NF-kappaB pathway. *J Transl Med*. (2019) 17:151. doi: 10.1186/s12967-019-1900-9
39. Luo J, Zhang P, Zhao T, Jia M, Yin P, Li W, et al. Golgi apparatus-targeted chondroitin-modified nanomicelles suppress hepatic stellate cell activation for the management of liver fibrosis. *ACS Nano*. (2019) 13:3910–23. doi: 10.1021/acsnano.8b06924
40. Filliol A, Piquet-Pellorce C, Raguenes-Nicol C, Dion S, Farooq M, Lucas-Clerc C, et al. RIPK1 protects hepatocytes from Kupffer cells-mediated TNF-induced apoptosis in mouse models of PAMP-induced hepatitis. *J Hepatol*. (2017) 66:1205–13. doi: 10.1016/j.jhep.2017.01.005
41. Wu Z, Kong X, Zhang T, Ye J, Fang Z, Yang X. Pseudoephedrine/ephedrine shows potent anti-inflammatory activity against TNF-alpha-mediated acute liver failure induced by lipopolysaccharide/D-galactosamine. *Eur J Pharmacol*. (2014) 724:112–21. doi: 10.1016/j.ejphar.2013.11.032
42. Kono H, Fujii H, Asakawa M, Yamamoto M, Maki A, Matsuda M, et al. Functional heterogeneity of the kupffer cell population is involved in the mechanism of gadolinium chloride in rats administered endotoxin. *J Surg Res*. (2002) 106:179–87. doi: 10.1006/jsre.2002.6434
43. Yang P, Zhou W, Li C, Zhang M, Jiang Y, Jiang R, et al. Kupffer-cell-expressed transmembrane TNF-alpha is a major contributor to lipopolysaccharide and D-galactosamine-induced liver injury. *Cell Tissue Res*. (2016) 363:371–83. doi: 10.1007/s00441-015-2252-2
44. Zhao M, Chen J, Zhu P, Fujino M, Takahara T, Toyama S, et al. Dihydroquercetin (DHQ) ameliorated concanavalin A-induced mouse experimental fulminant hepatitis and enhanced HO-1 expression through MAPK/Nrf2 antioxidant pathway in RAW cells. *Int Immunopharmacol*. (2015) 28:938–44. doi: 10.1016/j.intimp.2015.04.032
45. Tseng CK, Hsu SP, Lin CK, Wu YH, Lee JC, Young KC. Celastrol inhibits hepatitis C virus replication by upregulating heme oxygenase-1 via the JNK MAPK/Nrf2 pathway in human hepatoma cells. *Antivir Res*. (2017) 146:191–200. doi: 10.1016/j.antiviral.2017.09.010
46. Kubes P, Mehal WZ. Sterile inflammation in the liver. *Gastroenterology*. (2012) 143:1158–72. doi: 10.1053/j.gastro.2012.09.008
47. Tian L, Li W, Yang L, Chang N, Fan X, Ji X, et al. Cannabinoid receptor 1 participates in liver inflammation by promoting M1 macrophage polarization via RhoA/NF-kappaB p65 and ERK1/2 pathways, respectively, in mouse liver fibrogenesis. *Front Immunol*. (2017) 8:1214. doi: 10.3389/fimmu.2017.01214

Conflict of Interest: The authors declare that the research was conducted in the absence of any commercial or financial relationships that could be construed as a potential conflict of interest.

Copyright © 2020 Yang, Kuang, Zhang, Wu, Zhao, Wang, Yin, Gong and Wan. This is an open-access article distributed under the terms of the Creative Commons Attribution License (CC BY). The use, distribution or reproduction in other forums is permitted, provided the original author(s) and the copyright owner(s) are credited and that the original publication in this journal is cited, in accordance with accepted academic practice. No use, distribution or reproduction is permitted which does not comply with these terms.

frontiers in Immunology

MINI REVIEW
published: 21 April 2020
doi: 10.3389/fimmu.2020.00647

Mesenchymal Stem Cell-Derived Extracellular Vesicles: A Novel Cell-Free Therapy for Sepsis

Yanwei Cheng[1†], *Xue Cao*[2†] *and Lijie Qin*[1*]

[1] Department of Emergency, Henan Provincial People's Hospital, People's Hospital of Zhengzhou University, People's Hospital of Henan University, Zhengzhou, China, [2] Department of Rheumatology and Immunology, Henan Provincial People's Hospital, People's Hospital of Zhengzhou University, People's Hospital of Henan University, Zhengzhou, China

Sepsis remains a serious and life-threatening disease with high morbidity and mortality. Due to the unique immunomodulatory, anti-inflammatory, anti-apoptotic, anti-microbial, anti-oxidative, and reparative properties, mesenchymal stem cells (MSCs) have been extensively used in preclinical and clinical trials for diverse diseases and have shown great therapeutic potential in sepsis. However, concerns remain regarding whether MSCs can become tumorigenic or have other side effects. Extracellular vesicles (EVs) are a heterogeneous group of membrane-enclosed particles released from almost any cell and perform an important role in intercellular communication. Recently, it has emerged that EVs derived from MSCs (MSC-EVs) appear to exert a therapeutic benefit similar to MSCs in protecting against sepsis-induced organ dysfunction by delivering a cargo that includes RNAs and proteins to target cells. More importantly, compared to their parent cells, MSC-EVs have a superior safety profile, can be safely stored without losing function, and possess other advantages. Hence, MSC-EVs may be used as a novel alternative to MSC-based therapy in sepsis. Here, we summarize the properties and applications of MSC-EVs in sepsis.

Keywords: mesenchymal stem cell-derived extracellular vesicles (MSC-EVs), sepsis-induced acute lung injury, sepsis-induced acute kidney injury, sepsis-associated cardiovascular disorder, sepsis-induced liver injury

OPEN ACCESS

Edited by:
Lukas Martin,
University Hospital RWTH Aachen, Germany

Reviewed by:
Sebastian Wendt,
University Hospital RWTH Aachen, Germany
Yasser Mohamed El-Sherbiny,
Nottingham Trent University, United Kingdom

***Correspondence:**
Lijie Qin
qinlijie1819@163.com

[†] *These authors share first authorship*

Specialty section:
This article was submitted to Inflammation, a section of the journal Frontiers in Immunology

Received: *12 January 2020*
Accepted: *23 March 2020*
Published: *21 April 2020*

Citation:
Cheng Y, Cao X and Qin L (2020) Mesenchymal Stem Cell-Derived Extracellular Vesicles: A Novel Cell-Free Therapy for Sepsis. Front. Immunol. 11:647. doi: 10.3389/fimmu.2020.00647

INTRODUCTION

In the recent "sepsis-3.0" consensus (1), sepsis is defined as a life-threatening, multiorgan dysfunction caused by a dysregulated host response to infection. In view of the high morbidity and mortality, sepsis has been described as the quintessential medical disorder of the 21st century. Despite continuous progress in the development of therapeutic strategies, sepsis is still a major clinical problem and remains the leading cause of death (2, 3) in the critically ill patient population, due to uncontrolled inflammation together with immunosuppression. In such a context, an investigation into novel therapies to ameliorate sepsis would be urgently needed.

With the emergence of stem cells as potential therapeutic agents for diverse diseases, attempts to use stem cells, especially mesenchymal stem cells (MSCs), to ameliorate sepsis in animal models have increased exponentially. Growing preclinical data have suggested that MSCs can directly modify pathophysiology and underlying injury mechanisms in sepsis through the immunomodulatory, anti-bacterial, anti-inflammatory, anti-oxidative, anti-apoptotic, and reparative properties. It is worth noting that MSCs have also been confirmed as having a therapeutic effect on sepsis in two clinical trials (4, 5). Even then, the utilization of MSCs as therapeutic

agents for sepsis has raised several concerns over the past decade, including senescence-induced genetic instability, the heterogeneity of MSCs populations, quality assurance challenges of MSCs, and finding optimal MSCs tissue sources. Most crucially, the significant hurdles that potential therapeutics face in the future are MSCs safety concerns. It has been reported that MSCs play a dual role in immune regulation; on the one hand, MSCs exhibit immunosuppressive function (6), while on the other hand, MSCs may act as antigen-presenting cells, inducing an immune response (7). In addition, MSCs can potentially become tumorigenic either by direct malignant transformation of MSCs or indirectly by facilitating the growth of other tumor cells (8). So far MSCs have been found in several tumor types, including gastric adenocarcinoma (9), lipoma (10), and osteosarcoma (11), strongly indicating their involvement in tumor development. In light of this fact, the probability of the risks must be cautiously weighed against the potential benefits to every patient.

Recently, special attention has been paid to the extracellular vesicles (EVs) derived from MSCs (MSCs-EVs), which can function as shuttles for the delivery of a cargo that includes RNAs and proteins from parental to target cells and are as biologically active as the parent cells themselves (12–15). Hence, it is conceivable that the protective effect of MSCs on sepsis is at least partly due to the release of EVs.

CHARACTERIZATION OF MSC-EVS (FIGURE 1)

EVs are a heterogeneous group of membrane-enclosed particles that can be released from almost any cell. Based on the current knowledge of their size and biogenesis, EVs can be classified into three broad groups: exosomes (Exos), microvesicles (MVs), and apoptotic bodies. Exos (40–150 nm) bud from the endosomal system, whereas MVs (100–1,000 nm) are shed directly from the plasma membrane, and apoptotic bodies (1,000–5,000 nm) originate from apoptotic cells (16–18). In general, apoptotic bodies can be removed by the commonly used isolation method of ultracentrifugation (19). It should be noted that each individual cell can release both Exos and MVs simultaneously. However, so far it is impossible to unanimously distinguish MVs and Exos. In addition, most studies have not clearly defined the origin of EVs under study. Therefore, we here use EVs as an umbrella term to include both MVs and Exos.

MSC-EVs are released from resting MSCs and can be markedly increased during cellular activation or cell stress (12, 20, 21). They contain a trove of bioactive substances such as proteins, lipids, and most importantly, nucleic acids, thereby playing an important role in immune modulation, pro-angiogenesis, anti-apoptosis, and tissue regeneration. Up to now, over 5,000 species of MSC-EVs proteins have been characterized, including mediators controlling self-renewal, differentiation, signal transduction, and additional MSCs antigens affecting the migration of MSCs (19, 22). In addition, MSC-EVs contain a number of adhesion molecules such as CD44, CD29, alpha 4-integrin, and alpha 5-integrin etc., which contribute to the identification of MSC-EVs (22). Accumulating evidence has demonstrated that MSC-EVs modulate immune response by producing cytokines, growth factors, and tolerogenic molecules, such as IL-10, IL-6, IL-37, and lipocalin-2 and transforming growth factor (TGF)-β, programmed death ligand-1(PD-L1), galectin-1, etc. (20, 23, 24). Other than proteins, MSC-EVs are enriched with nucleic acids, including mRNA, microRNA (miRNA), and DNA (25). It has been demonstrated that the transfer of miRNAs from MSC-EVs to target cells may be the underlying mechanism in alleviating injury of the kidney (26, 27), heart (28), liver (29), and brain (30). In recent years, more than 150 miRNAs have been identified in the cargo of MSC-EVs. These miRNAs are usually related to apoptosis, tumorigenesis, immune responses, angiogenesis, and organism development, such as miR-221, miR-23b, miR-125b, miR-451, miR-31, miR-24, miR-214, miR-122, miR-16, miR-150, and miR133b, etc. (19, 31–34). All the internal components in MSC-EVs are surrounded by a bilayer of lipids that play an important role in protecting them. Compared to their parent cells, EVs are enriched with some specific lipids (cholesterol, glycosphingolipids, and phosphatidylserine) (35–38), making them more functional. Our previous study (21) also showed that sphingosine-1-phosphate enriched within MSC-EVs could enhance the repair effect of MSCs for articular cartilage.

THERAPEUTIC APPLICATIONS OF MSC-EVS IN SEPSIS

Through delivering proteins and nucleic acids, MSC-EVs seem to hold many functions of the MSCs themselves and are described as a new mechanism of intercellular communication (39). Nowadays, increasing studies have clearly confirmed that EVs alone are responsible for the therapeutic effects of MSCs in sepsis-induced organ dysfunction, including sepsis-induced acute lung injury, sepsis-induced acute kidney injury, sepsis-associated cardiovascular disorder, and sepsis-induced liver injury (40). Accordingly, MSCs-EVs may be an alternative therapy to MSCs and will be the next-generation therapeutic route for sepsis.

MSC-EVs and Sepsis-Induced Actue Lung Injury

Acute lung injury (ALI) is the most common organ injury in septic patients and leads to a greater mortality. In the past few years, the beneficial effects of MSCs on sepsis-induced ALI have been shown to be attributed to the release of EVs. Using LPS-induced ALI in an *ex vivo* perfused human lung, Park et al. (41) reported that MSC-EVs significantly increased alveolar fluid clearance and reduced protein permeability and numerically lowered the bacterial load in the injured alveolus. In a mouse model of *E. coli* endotoxin-induced ALI, Zhu et al. (42) also confirmed the similar beneficial effects of human MSC-EVs and further demonstrated that the protection was in part due to the delivery of keratinocyte growth factor (KGF) mRNA from MSC-EVs to the injured alveolar epithelium and lung endothelium. This falls in good accordance with Monsel's study (43) that MSC-EVs improved survival in ALI from *E. coli* pneumonia via a

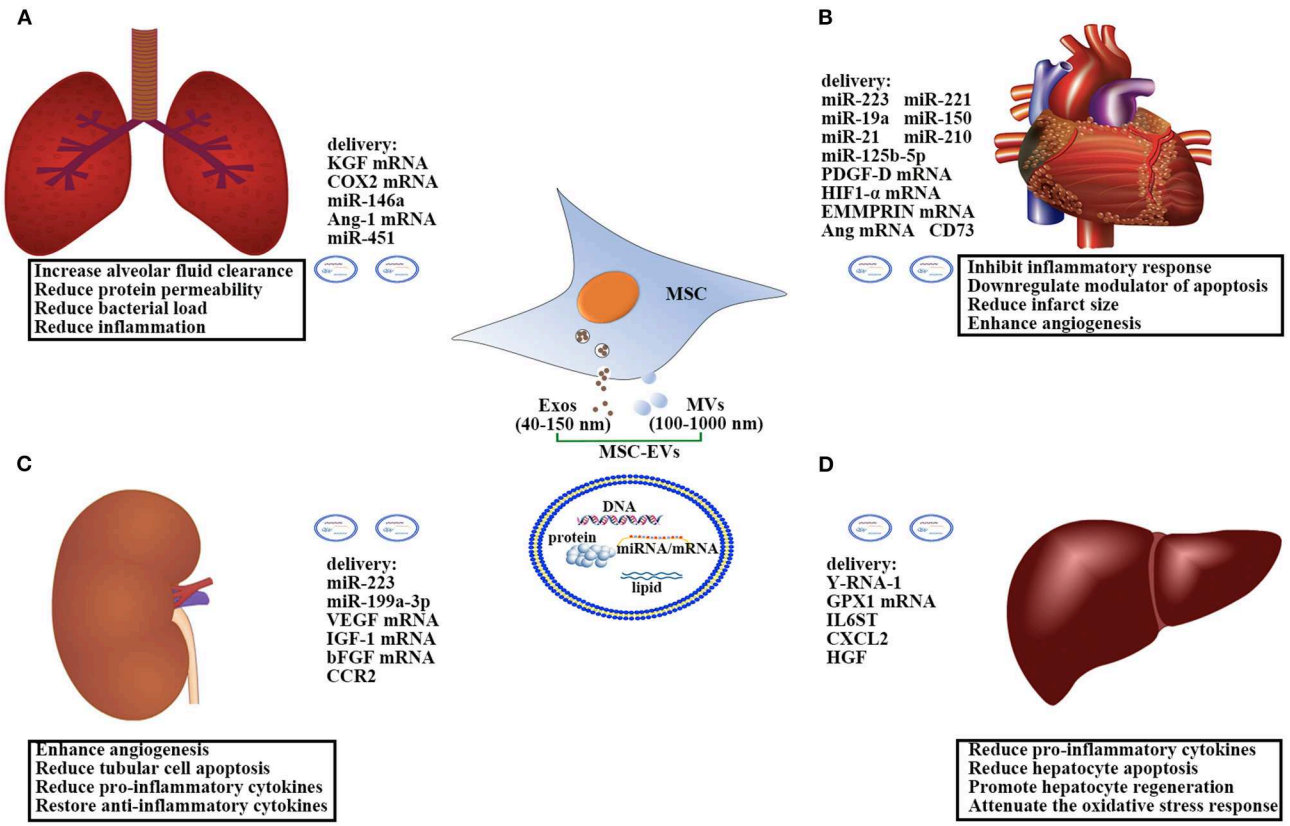

FIGURE 1 | Therapeutic effects and mechanisms of the action of MSC-EVs in: **(A)** sepsis-induced acute lung injury; **(B)** sepsis-induced acute kidney injury; **(C)** sepsis-associated cardiovascular disorder; **(D)** sepsis-induced liver injury. EVs comprise a heterogeneous population of membrane vesicles of various origins. Here we use EVs as an umbrella term to include both MVs and Exos. MSC-EVs can shuttle various cargoes, including proteins, lipids, and nucleic acids, to the recipient cells to protect against sepsis-induced organ dysfunction. Ang, Angiopoietin; bFGF, Basic fibroblast growth factor; COX2, cyclooxygenase 2; CCR2, C-C motif chemokine receptor-2; CXCL2, Chemokine Ligand 2; EVs, Extracellular vesicles; Exos, Exosomes; EMMPRIN, Extracellular matrix metalloproteinase inducer; GPX1, Glutathione peroxidase 1; HIF1-α, Hypoxia-inducible factor 1-alpha; HGF, Hepatocyte growth factor; IL6ST, Interleukin 6 signal transducer; IGF-1, Insulin-like growth factor 1; KGF, Keratinocyte growth factor; MVs, Microvesicles; MSCs, Mesenchymal Stem Cells; miR, microRNA; PDGF-D, Platelet-derived growth factor D; VEGF, Vascular endothelial growth factor.

mechanism partially dependent on KGF secretion. The authors (43) further discovered that MSC-EVs could enhance monocyte phagocytosis of bacteria through transferring cyclooxygenase 2 (COX2) mRNA to monocytes, with a resultant increase in prostaglandin E2 (PGE2) secretion. PGE2 is essential for transforming the polarization of monocytes-macrophages M1 into M2 phenotype (44–46). In addition, Song et al. (47) showed that miR-146a promoted polarization of M2 macrophages and finally led to increased survival in septic mice. MSC-EVs also contain a substantial quantity of angiopoietin-1 (Ang-1) mRNA, which plays an essential role in vascular stabilization and resolving inflammation. In the current study, Tang et al. (48) demonstrated that the therapeutic benefit of EVs in ALI, and their immunomodulatory properties on macrophages, were partly mediated through their content of Ang-1 mRNA. Furthermore, the transfer of miR-451 and mitochondria from MSC-EVs to the alveolar epithelium and macrophages also contributed to preventing ALI (49). Altogether, these data indicate that MSC-EVs may represent a novel therapeutic option for sepsis-induced ALI.

MSC-EVs and Sepsis-Induced Actue Kidney Injury

Mounting studies have provided convincing evidence that MSCs exert their renoprotective effects by releasing EVs in several acute kidney injury (AKI) models. AKI is commonly present in more than 20% of septic patients (50). However, data about the therapeutic effects of MSC-EVs in sepsis-induced AKI are scarce. Currently, the anti-apoptosis (51), pro-angiogenesis (52), and anti-inflammatory (53) properties of MSC-EVs have been considered as the important mechanistic approaches to ameliorate AKI induced by different causes. In AKI mice models induced by ischemia-reperfusion injury, Bruno et al. (27) found that MSC-EVs induced the expression of anti-apoptotic genes (Bcl-XL, Bcl2, and BIRC8) in renal tubular epithelial cells while simultaneously down-regulating pro-apoptotic genes

(Casp1, Casp8, and LTA), thus reducing tubular cell apoptosis and conferring an anti-apoptotic phenotype necessary for tissue repair. Interestingly, the anti-apoptosis effect of MSC-EVs may be mediated in part by the transfer of miRNAs (miR-223 and miR-199a-3p) to tubular cells (54, 55). In addition, MSC-EVs can directly shuttle several pro-angiogenesis transcription factors including vascular endothelial growth factor (VEGF) (52), insulin-like growth factor 1 (IGF-1) (56), and basic fibroblast growth factor (bFGF) (57) to the damaged renal tubular epithelial cells and enhance angiogenesis, which is considered as an important step in tissue regeneration. In a mouse model of AKI induced by glycerol, Bruno (58) demonstrated that 15 μg of MSC-EVs injected intravenously activated the proliferative progress in viable tubular cells through their pro-angiogenesis effects. Importantly, the effects of MSC-EVs on the recovery of AKI were as effective as their parental MSCs. It is well known that excessive inflammation is the culprit leading to sepsis-induced AKI. MSC-EVs can modulate renal inflammation by reducing the release of several pro-inflammatory cytokines, including IL-1, IL-6, and TNF-α, while restoring the level of the anti-inflammatory cytokine IL-10 (26, 53, 59). This anti-inflammatory effect may be associated with the C-C motif chemokine receptor-2 (CCR2) contained within MSC-EVs, which can suppress macrophages function and attenuate renal injury (60). At present, MSC-EVs have been studied in patients with chronic kidney disease (61). The results showed that administration of MSC-EVs had no side effects and caused significant improvement of the kidney function. Collectively, there are good reasons to believe that MSC-EVs could be exploited as a new therapeutic approach for sepsis-induced AKI.

MSC-EVs and Sepsis-Associated Cardiovascular Disorder

Despite only a few studies having addressed potential cardioprotective effects of MSCs on sepsis-induced cardiovascular disease, the data still support that MSCs mediate their protection through the secretion of EVs. In septic mice induced by cecal ligation and puncture (CLP), MSC-EVs displayed cardioprotective benefits and enhanced survival of cardiomyocyte cells. In this research, Wang et al. (28) further proved that miR-223 enriched in MSC-EVs was critical for EVs-elicited action in sepsis. miR-223 can inhibit the expression of Sema3A and Stat3, negatively regulating the expression of many inflammatory genes, such as TNF-α, IL-6, and IL-1 (62). Another important piece of research by Tabet et al. (63) also mentioned that miR-223 was able to alleviate the inflammatory process in human coronary artery endothelial cells by downregulating intercellular adhesion molecule 1. In addition, some anti-apoptotic miRNAs contained within MSCs-EVs showed a vital role in cardioprotection. For example, miR-221 can reduce the expression of p53 upregulated modulator of apoptosis and is more highly enriched in MSC-EVs than that in their parent MSCs. Numerous studies (34, 64) have confirmed that the delivery of miR-221 contained within EVs contributed to the cardioprotection by MSC-EVs. A study by Yu et al. (65) demonstrated that MSC-EVs enriched with anti-apoptotic miR-19a also restored cardiac function and reduced infarct size in a rat model of acute myocardial infarction (AMI). In addition to miRNAs, the protein of CD73 on the surface of MSC-EVs was suggested to overcome the pro-apoptotic milieu of the perfused myocardium (66). In AMI mice models, Bian et al. (67) reported that intramyocardial injection of MSC-EVs markedly promoted angiogenesis and reduced infarct size. They further identified that MSC-EVs might be a mixture of miR-150-enriched MVs and Exos (33). Moreover, the pro-angiogenesis effect of the other cargo of MSC-EVs had been investigated *in vitro* and *in vivo* MI models, including miR-210 (66), miR-21 (68), platelet-derived growth factor D (PDGF-D) (69), hypoxia-inducible factor 1-alpha (HIF1-α) (70), and extracellular matrix metalloproteinase inducer (EMMPRIN) (71) and angiopoietin (72). Recently, Xiao et al. (73) demonstrated that the beneficial effects offered by MSCs in MI model were at least partially because of improved autophagic flux through excreted EVs containing mainly miR-125b-5p. On the basis of these studies, MSC-EVs seem to be an ideal therapeutic agent for sepsis-induced cardiovascular disease in the near future.

MSC-EVs and Sepsis-Induced Liver Injury

During sepsis, liver injury occurs frequently and contributes to the pathogenesis of multiple organ dysfunction, and has been considered as an early indicator of poor outcome in septic patients (74, 75). Studies in a range of liver disease models demonstrated that MSC-EVs could suppress inflammatory response, reduce hepatocyte apoptosis, and enhance liver regeneration. However, few applications of MSC-EVs into sepsis-induced liver injury are available. Nong et al. (76) studied the hepatoprotective effect of MSC-EVs in a mouse model of hepatic ischemia-reperfusion injury. They showed that human-induced pluripotent stem cell-derived MSC-EVs protected hepatocytes via reducing pro-inflammatory cytokine production, such as TNF-α, IL-6, and high mobility group box 1 (HMGB1). Likewise using a concanavalin-A-induced liver injury model, Tamura et al. (77) demonstrated that MSC-EVs decreased production of pro-inflammatory cytokines, while anti-inflammatory cytokine and regulatory T cell levels increased. Recently, the anti-apoptotic and anti-oxidant effects of MSC-EVs were also investigated. A study in a lethal mouse model of liver failure induced by D-galactosamine/TNF-α showed that MSC-EVs containing Y-RNA-1 activated anti-apoptotic pathways, thus mitigating hepatic injury and enhancing survival (78). In carbon tetrachloride (CCl4)-induced liver injury, Yan et al. (79) demonstrated that MSC-EVs promoted the recovery of hepatic oxidant injury through the delivery of glutathione peroxidase 1 (GPX1). Additionally, Tan et al. (80) confirmed that MSC-EVs were capable of promoting hepatocyte regeneration by inducing the IL-6/STAT3 pathway and cell cycle progression. Proteins in MSC-EVs, such as interleukin 6 signal transducer (IL6ST), chemokine Ligand 2 (CXCL2), and hepatocyte growth factor (HGF) etc., were found to be involved in the liver-regeneration process (80). However, it remains to be determined whether miRNAs or other mRNAs within MSC-EVs may have any impact on the proliferation effect of the hepatocytes. According to these studies, MSC-EVs may be considered as a novel therapeutic approach for

alleviating sepsis-induced liver injury, and correlative research should fill the gap in this field in the future.

ADVANTAGES AND CHALLENGES OF MSC-EVS THERAPY

Compared to MSC-based therapy, MSC-EVs therapy offers more advantages. First, MSC-EVs are highly stable and suitable for long-term storage without the addition of potentially toxic cryopreservatives (21, 81, 82). Second, MSC-EVs can induce stronger signaling in intercellular communication by directly transferring functional proteins and miRNAs to the recipient cells (83, 84). Third, MSC-EVs have no heterologous risk (85, 86) and no immune response after allogeneic application (87). Furthermore, a significant advantage of MSC-EVs is to circumvent the potential tumorigenicity of MSCs. So far, there is no evidence showing the oncogenic potential of MSC-EVs. A study (88) reported that MSC-EVs can inhibit tumor growth and exert an anti-tumor activity both *in vitro* and *in vivo*. Given this, MSC-EVs look to be a novel and promising therapeutic approach for sepsis.

However, there remain significant challenges that need to be addressed prior to the potential application of MSC-EVs in human sepsis. First, the protocol for isolation has to be standardized. Currently, no "gold standard protocol" for EVs isolation exists, instead different isolation methods are used to isolate different subsets of EVs even though the source is the same. Second, the suitable markers to analyze EVs at a single-vesicle level must be established. So far no consensus exists regarding the nomenclature of EVs or the markers that distinguish each type of EV once they have been secreted or shed from the cells. Third, there is a paucity of knowledge about the content within MSC-EVs. EVs contain a trove of cellular cargos, which are able to act as diverse functions and can vary widely between sources and conditions. It is unknown which effector molecules are important within EVs or which are not protective or harmful. Meanwhile, there is a critical need for exploiting possible ways to modify MSC-EVs composition and modulate their biological activities. Fourth, the therapeutic capacity of MSC-EVs derived from different sources in sepsis should be investigated. In addition, much work is needed on how to optimize the methods to produce MSC-EVs on a large scale, how to validate the dosage and half-life of MSC-EVs, and confirming the potential effects of MSC-EVs in the late stage of sepsis. Finally, the unknown negative effects of MSC-EVs have to be clarified.

CONCLUSIONS

Extracellular vesicles (EVs) are naturally released from almost any cell and participate in cell-to-cell communication in physiological as well as pathological processes by transferring their components, such as proteins, miRNA, mRNA, and even mitochondria. A study (89) considered EVs as possible culprits during the pathogenesis of sepsis, whereas EVs derived from MSCs showed striking therapeutic benefits in sepsis. In this review, we have summarized the recent knowledge related to the therapeutic applications of MSC-EVs in sepsis. These considerable preclinical data support the hypothesis that cell-free therapy with MSC-EVs could be a novel alternative MSC-based therapy in sepsis, especially in early stage sepsis. However, realizing this promising therapeutic approach of MSC-EVs would require extensive testing to validate their safety and efficacy.

AUTHOR CONTRIBUTIONS

YC and XC wrote the first draft of this article and designed the figure. LQ critically revised the manuscript for important intellectual content. All authors approved the final version.

FUNDING

The present work was supported by the 23456 Talent Project of Henan Provincial People's Hospital to LQ, Research Startup fund of Henan Provincial People's Hospital to YC and XC.

REFERENCES

1. Singer M, Deutschman CS, Seymour CW, Shankar-Hari M, Annane D, Bauer M, et al. The Third International Consensus definitions for sepsis and septic shock (sepsis-3). *JAMA.* (2016) 315:801–10. doi: 10.1001/jama.2016.0287
2. Melamed A, Sorvillo FJ. The burden of sepsis-associated mortality in the United States from 1999 to 2005: an analysis of multiple-cause-of-death data. *Crit Care.* (2009) 13:R28. doi: 10.1186/cc7733
3. Dombrovskiy VY, Martin AA, Sunderram J, Paz HL. Rapid increase in hospitalization and mortality rates for severe sepsis in the United States: a trend analysis from 1993 to 2003. *Crit Care Med.* (2007) 35:1244–50. doi: 10.1097/01.CCM.0000261890.41311.E9
4. Wilson JG, Liu KD, Zhuo H, Caballero L, McMillan M, Fang X, et al. Mesenchymal stem (stromal) cells for treatment of ARDS: a phase 1 clinical trial. *Lancet Respir Med.* (2015) 3:24–32. doi: 10.1016/S2213-2600(14)70291-7
5. Galstian GM, Parovichnikova EN, Makarova PM, Kuzmina LA, Troitskaya VV, Gemdzhian E, et al. The results of the russian clinical trial of mesenchymal stromal cells (MSCs) in severe neutropenic patients (pts) with septic shock (SS) (RUMCESS trial). *Blood.* (2015) 126:2220. doi: 10.1182/blood.V126.23.2220
6. Jarvinen L, Badri L, Wettlaufer S, Ohtsuka T, Standiford TJ, Toews GB, et al. Lung resident mesenchymal stem cells isolated from human lung allografts inhibit T cell proliferation via a soluble mediator. *J Immunol.* (2008) 181:4389–96. doi: 10.4049/jimmunol.181.6.4389
7. Stagg J, Pommey S, Eliopoulos N, Galipeau J. Interferon-gamma-stimulated marrow stromal cells: a new type of nonhematopoietic antigen-presenting cell. *Blood.* (2006) 107:2570–7. doi: 10.1182/blood-2005-07-2793
8. Rosland GV, Svendsen A, Torsvik A, Sobala E, McCormack E, Immervoll H, et al. Long-term cultures of bone marrow-derived human mesenchymal stem cells frequently undergo spontaneous malignant transformation. *Cancer Res.* (2009) 69:5331–9. doi: 10.1158/0008-5472.CAN-08-4630
9. Xu X, Zhang X, Wang S, Qian H, Zhu W, Cao H, et al. Isolation and comparison of mesenchymal stem-like cells from human gastric cancer and adjacent non-cancerous tissues. *J Cancer Res Clin Oncol.* (2011) 137:495–504. doi: 10.1007/s00432-010-0908-6

10. Lin TM, Chang HW, Wang KH, Kao AP, Chang CC, Wen CH, et al. Isolation and identification of mesenchymal stem cells from human lipoma tissue. *Biochem Biophys Res Commun.* (2007) 361:883–9. doi: 10.1016/j.bbrc.2007.07.116
11. Brune JC, Tormin A, Johansson MC, Rissler P, Brosjo O, Lofvenberg R, et al. Mesenchymal stromal cells from primary osteosarcoma are non-malignant and strikingly similar to their bone marrow counterparts. *Int J Cancer.* (2011) 129:319–30. doi: 10.1002/ijc.25697
12. Tan X, Gong YZ, Wu P, Liao DF, Zheng XL. Mesenchymal stem cell-derived microparticles: a promising therapeutic strategy. *Int J Mol Sci.* (2014) 15:14348–63. doi: 10.3390/ijms150814348
13. Carandini T, Colombo F, Finardi A, Casella G, Garzetti L, Verderio C, et al. Microvesicles: what is the role in multiple sclerosis? *Front Neurol.* (2015) 6:111. doi: 10.3389/fneur.2015.00111
14. Schneider A, Simons M. Exosomes: vesicular carriers for intercellular communication in neurodegenerative disorders. *Cell Tissue Res.* (2013) 352:33–47. doi: 10.1007/s00441-012-1428-2
15. Toh WS, Lai RC, Hui JHP, Lim SK. MSC exosome as a cell-free MSC therapy for cartilage regeneration: implications for osteoarthritis treatment. *Semin Cell Dev Biol.* (2017) 67:56–64. doi: 10.1016/j.semcdb.2016.11.008
16. Karpman D, Stahl AL, Arvidsson I. Extracellular vesicles in renal disease. *Nat Rev Nephrol.* (2017) 13:545–62. doi: 10.1038/nrneph.2017.98
17. Chaput N, Thery C. Exosomes: immune properties and potential clinical implementations. *Semin Immunopathol.* (2011) 33:419–40. doi: 10.1007/s00281-010-0233-9
18. Thery C. Exosomes: secreted vesicles and intercellular communications. *F1000 Biol Rep*. (2011) 3:15. doi: 10.3410/B3-15
19. Jafarinia M, Alsahebfosoul F, Salehi H, Eskandari N, Ganjalikhani-Hakemi M. Mesenchymal stem cell-derived extracellular vesicles: a novel cell-free therapy. *Immunol Invest.* (2020). doi: 10.1080/08820139.2020.1712416. [Epub ahead of print].
20. Mokarizadeh A, Delirezh N, Morshedi A, Mosayebi G, Farshid AA, Mardani K. Microvesicles derived from mesenchymal stem cells: potent organelles for induction of tolerogenic signaling. *Immunol Lett.* (2012) 147:47–54. doi: 10.1016/j.imlet.2012.06.001
21. Xiang C, Yang K, Liang Z, Wan Y, Cheng Y, Ma D, et al. Sphingosine-1-phosphate mediates the therapeutic effects of bone marrow mesenchymal stem cell-derived microvesicles on articular cartilage defect. *Transl Res.* (2018) 193:42–53. doi: 10.1016/j.trsl.2017.12.003
22. Kim HS, Choi DY, Yun SJ, Choi SM, Kang JW, Jung JW, et al. Proteomic analysis of microvesicles derived from human mesenchymal stem cells. *J Proteome Res.* (2012) 11:839–49. doi: 10.1021/pr200682z
23. Qiu G, Zheng G, Ge M, Wang J, Huang R, Shu Q, et al. Functional proteins of mesenchymal stem cell-derived extracellular vesicles. *Stem Cell Res Ther.* (2019) 10:359. doi: 10.1186/s13287-019-1484-6
24. Alcayaga-Miranda F, Cuenca J, Khoury M. Antimicrobial activity of mesenchymal stem cells: current status and new perspectives of antimicrobial peptide-based therapies. *Front Immunol.* (2017) 8:339. doi: 10.3389/fimmu.2017.00339
25. Wang XQ, Zhu XJ, Zou P. [Research progress of mesenchymal stem cell-derived microvesicle]. *Zhongguo Shi Yan Xue Ye Xue Za Zhi.* (2013) 21:227–30. doi: 10.7534/j.issn.1009-2137.2013.01.046
26. Collino F, Bruno S, Incarnato D, Dettori D, Neri F, Provero P, et al. AKI recovery induced by mesenchymal stromal cell-derived extracellular vesicles carrying microRNAs. *J Am Soc Nephrol.* (2015) 26:2349–60. doi: 10.1681/ASN.2014070710
27. Bruno S, Grange C, Collino F, Deregibus MC, Cantaluppi V, Biancone L, et al. Microvesicles derived from mesenchymal stem cells enhance survival in a lethal model of acute kidney injury. *PLoS ONE.* (2012) 7:e33115. doi: 10.1371/journal.pone.0033115
28. Wang X, Gu H, Qin D, Yang L, Huang W, Essandoh K, et al. Exosomal miR-223 contributes to mesenchymal stem cell-elicited cardioprotection in polymicrobial sepsis. *Sci Rep.* (2015) 5:13721. doi: 10.1038/srep13721
29. Chen L, Lu FB, Chen DZ, Wu JL, Hu ED, Xu LM, et al. BMSCs-derived miR-223-containing exosomes contribute to liver protection in experimental autoimmune hepatitis. *Mol Immunol.* (2018) 93:38–46. doi: 10.1016/j.molimm.2017.11.008
30. Xin H, Katakowski M, Wang F, Qian JY, Liu XS, Ali MM, et al. MicroRNA cluster miR-17-92 cluster in exosomes enhance neuroplasticity and functional recovery after stroke in rats. *Stroke.* (2017) 48:747–53. doi: 10.1161/STROKEAHA.116.015204
31. Fonsato V, Collino F, Herrera MB, Cavallari C, Deregibus MC, Cisterna B, et al. Human liver stem cell-derived microvesicles inhibit hepatoma growth in SCID mice by delivering antitumor microRNAs. *Stem Cells.* (2012) 30:1985–98. doi: 10.1002/stem.1161
32. Ono M, Kosaka N, Tominaga N, Yoshioka Y, Takeshita F, Takahashi RU, et al. Exosomes from bone marrow mesenchymal stem cells contain a microRNA that promotes dormancy in metastatic breast cancer cells. *Sci Signal.* (2014) 7:ra63. doi: 10.1126/scisignal.2005231
33. Li J, Zhang Y, Liu Y, Dai X, Li W, Cai X, et al. Microvesicle-mediated transfer of microRNA-150 from monocytes to endothelial cells promotes angiogenesis. *J Biol Chem.* (2013) 288:23586–96. doi: 10.1074/jbc.M113.489302
34. Yu B, Gong M, Wang Y, Millard RW, Pasha Z, Yang Y, et al. Cardiomyocyte protection by GATA-4 gene engineered mesenchymal stem cells is partially mediated by translocation of miR-221 in microvesicles. *PLoS ONE.* (2013) 8:e73304. doi: 10.1371/journal.pone.0073304
35. Haraszti RA, Didiot MC, Sapp E, Leszyk J, Shaffer SA, Rockwell HE, et al. High-resolution proteomic and lipidomic analysis of exosomes and microvesicles from different cell sources. *J Extracell Vesicles.* (2016) 5:32570. doi: 10.3402/jev.v5.32570
36. Llorente A, Skotland T, Sylvanne T, Kauhanen D, Rog T, Orlowski A, et al. Molecular lipidomics of exosomes released by PC-3 prostate cancer cells. *Biochim Biophys Acta.* (2013) 1831:1302–9. doi: 10.1016/j.bbalip.2013.04.011
37. Simbari F, McCaskill J, Coakley G, Millar M, Maizels RM, Fabrias G, et al. Plasmalogen enrichment in exosomes secreted by a nematode parasite versus those derived from its mouse host: implications for exosome stability and biology. *J Extracell Vesicles.* (2016) 5:30741. doi: 10.3402/jev.v5.30741
38. Tan KT, Lip GY. The potential role of platelet microparticles in atherosclerosis. *Thromb Haemost.* (2005) 94:488–92. doi: 10.1160/TH05-03-0201
39. Bruno S, Camussi G. Role of mesenchymal stem cell-derived microvesicles in tissue repair. *Pediatr Nephrol.* (2013) 28:2249–54. doi: 10.1007/s00467-013-2413-z
40. Alcayaga-Miranda F, Varas-Godoy M, Khoury M. Harnessing the angiogenic potential of stem cell-derived exosomes for vascular regeneration. *Stem Cells Int.* (2016) 2016:3409169. doi: 10.1155/2016/3409169
41. Park J, Kim S, Lim H, Liu A, Hu S, Lee J, et al. Therapeutic effects of human mesenchymal stem cell microvesicles in an *ex vivo* perfused human lung injured with severe *E. coli* pneumonia. *Thorax.* (2018) 74:43–50. doi: 10.1136/thoraxjnl-2018-211576
42. Zhu YG, Feng XM, Abbott J, Fang XH, Hao Q, Monsel A, et al. Human mesenchymal stem cell microvesicles for treatment of *Escherichia coli* endotoxin-induced acute lung injury in mice. *Stem Cells.* (2014) 32:116–25. doi: 10.1002/stem.1504
43. Monsel A, Zhu YG, Gennai S, Hao Q, Hu S, Rouby JJ, et al. Therapeutic effects of human mesenchymal stem cell-derived microvesicles in severe pneumonia in mice. *Am J Respir Crit Care Med.* (2015) 192:324–36. doi: 10.1164/rccm.201410-1765OC
44. Lee JW, Krasnodembskaya A, McKenna DH, Song Y, Abbott J, Matthay MA. Therapeutic effects of human mesenchymal stem cells in ex vivo human lungs injured with live bacteria. *Am J Respir Crit Care Med.* (2013) 187:751–60. doi: 10.1164/rccm.201206-0990OC
45. Krasnodembskaya A, Samarani G, Song Y, Zhuo H, Su X, Lee JW, et al. Human mesenchymal stem cells reduce mortality and bacteremia in gram-negative sepsis in mice in part by enhancing the phagocytic activity of blood monocytes. *Am J Physiol Lung Cell Mol Physiol.* (2012) 302:L1003-13. doi: 10.1152/ajplung.00180.2011
46. Wang Y, Tan L, Jin J, Sun H, Chen Z, Tan X, et al. Non-cultured dermal-derived mesenchymal cells attenuate sepsis induced by cecal ligation and puncture in mice. *Sci Rep.* (2015) 5:16973. doi: 10.1038/srep16973
47. Song Y, Dou H, Li X, Zhao X, Li Y, Liu D, et al. Exosomal miR-146a contributes to the enhanced therapeutic efficacy of interleukin-1beta-primed mesenchymal stem cells against sepsis. *Stem Cells.* (2017) 35:1208–21. doi: 10.1002/stem.2564

48. Tang XD, Shi L, Monsel A, Li XY, Zhu HL, Zhu YG, et al. Mesenchymal stem cell microvesicles attenuate acute lung injury in mice partly mediated by Ang-1 mRNA. *Stem Cells*. (2017) 35:1849–59. doi: 10.1002/stem.2619
49. Phinney DG, Di Giuseppe M, Njah J, Sala E, Shiva S, St Croix CM, et al. Mesenchymal stem cells use extracellular vesicles to outsource mitophagy and shuttle microRNAs. *Nat Commun*. (2015) 6:8472. doi: 10.1038/ncomms9472
50. Zhang Z. Biomarkers, diagnosis and management of sepsis-induced acute kidney injury: a narrative review. *Heart Lung Vessel*. (2015) 7:64–73.
51. Gatti S, Bruno S, Deregibus MC, Sordi A, Cantaluppi V, Tetta C, et al. Microvesicles derived from human adult mesenchymal stem cells protect against ischaemia-reperfusion-induced acute and chronic kidney injury. *Nephrol Dial Transplant*. (2011) 26:1474–83. doi: 10.1093/ndt/gfr015
52. Zou X, Gu D, Xing X, Cheng Z, Gong D, Zhang G, et al. Human mesenchymal stromal cell-derived extracellular vesicles alleviate renal ischemic reperfusion injury and enhance angiogenesis in rats. *Am J Transl Res*. (2016) 8:4289–99.
53. Lin KC, Yip HK, Shao PL, Wu SC, Chen KH, Chen YT, et al. Combination of adipose-derived mesenchymal stem cells (ADMSC) and ADMSC-derived exosomes for protecting kidney from acute ischemia-reperfusion injury. *Int J Cardiol*. (2016) 216:173–85. doi: 10.1016/j.ijcard.2016.04.061
54. Zhu G, Pei L, Lin F, Yin H, Li X, He W, et al. Exosomes from human-bone-marrow-derived mesenchymal stem cells protect against renal ischemia/reperfusion injury via transferring miR-199a-3p. *J Cell Physiol*. (2019) 234:23736–749. doi: 10.1002/jcp.28941
55. Yuan X, Wang X, Chen C, Zhou J, Han M. Bone mesenchymal stem cells ameliorate ischemia/reperfusion-induced damage in renal epithelial cells via microRNA-223. *Stem Cell Res Ther*. (2017) 8:146. doi: 10.1186/s13287-017-0599-x
56. Tomasoni S, Longaretti L, Rota C, Morigi M, Conti S, Gotti E, et al. Transfer of growth factor receptor mRNA via exosomes unravels the regenerative effect of mesenchymal stem cells. *Stem Cells Dev*. (2013) 22:772–80. doi: 10.1089/scd.2012.0266
57. Choi HY, Moon SJ, Ratliff BB, Ahn SH, Jung A, Lee M, et al. Microparticles from kidney-derived mesenchymal stem cells act as carriers of proangiogenic signals and contribute to recovery from acute kidney injury. *PLoS ONE*. (2014) 9:e87853. doi: 10.1371/journal.pone.0087853
58. Bruno S, Grange C, Deregibus MC, Calogero RA, Saviozzi S, Collino F, et al. Mesenchymal stem cell-derived microvesicles protect against acute tubular injury. *J Am Soc Nephrol*. (2009) 20:1053–67. doi: 10.1681/ASN.2008070798
59. Reis LA, Borges FT, Simoes MJ, Borges AA, Sinigaglia-Coimbra R, Schor N. Bone marrow-derived mesenchymal stem cells repaired but did not prevent gentamicin-induced acute kidney injury through paracrine effects in rats. *PLoS ONE*. (2012) 7:e44092. doi: 10.1371/journal.pone.0044092
60. Shen B, Liu J, Zhang F, Wang Y, Qin Y, Zhou Z, et al. CCR2 positive exosome released by mesenchymal stem cells suppresses macrophage functions and alleviates ischemia/reperfusion-induced renal injury. *Stem Cells Int*. (2016) 2016:1240301. doi: 10.1155/2016/1240301
61. Mendt M, Rezvani K, Shpall E. Mesenchymal stem cell-derived exosomes for clinical use. *Bone Marrow Transplant*. (2019) 54 (Suppl. 2):789–92. doi: 10.1038/s41409-019-0616-z
62. Wang X, Huang W, Yang Y, Wang Y, Peng T, Chang J, et al. Loss of duplexmiR-223 (5p and 3p) aggravates myocardial depression and mortality in polymicrobial sepsis. *Biochim Biophys Acta*. (2014) 1842:701–11. doi: 10.1016/j.bbadis.2014.01.012
63. Tabet F, Vickers KC, Cuesta Torres LF, Wiese CB, Shoucri BM, Lambert G, et al. HDL-transferred microRNA-223 regulates ICAM-1 expression in endothelial cells. *Nat Commun*. (2014) 5:3292. doi: 10.1038/ncomms4292
64. Feng Y, Huang W, Wani M, Yu X, Ashraf M. Ischemic preconditioning potentiates the protective effect of stem cells through secretion of exosomes by targeting Mecp2 via miR-22. *PLoS One*. (2014) 9:e88685. doi: 10.1371/journal.pone.0088685
65. Yu B, Kim HW, Gong M, Wang J, Millard RW, Wang Y, et al. Exosomes secreted from GATA-4 overexpressing mesenchymal stem cells serve as a reservoir of anti-apoptotic microRNAs for cardioprotection. *Int J Cardiol*. (2015) 182:349–60. doi: 10.1016/j.ijcard.2014.12.043
66. Lai RC, Yeo RW, Tan KH, Lim SK. Mesenchymal stem cell exosome ameliorates reperfusion injury through proteomic complementation. *Regen Med*. (2013) 8:197–209. doi: 10.2217/rme.13.4
67. Bian S, Zhang L, Duan L, Wang X, Min Y, Yu H. Extracellular vesicles derived from human bone marrow mesenchymal stem cells promote angiogenesis in a rat myocardial infarction model. *J Mol Med*. (2014) 92:387–97. doi: 10.1007/s00109-013-1110-5
68. Wang K, Jiang Z, Webster KA, Chen J, Hu H, Zhou Y, et al. Enhanced cardioprotection by human endometrium mesenchymal stem cells driven by exosomal microRNA-21. *Stem Cells Transl Med*. (2017) 6:209–22. doi: 10.5966/sctm.2015-0386
69. Ma J, Zhao Y, Sun L, Sun X, Zhao X, Sun X, et al. Exosomes derived from Akt-modified human umbilical cord mesenchymal stem cells improve cardiac regeneration and promote angiogenesis via activating platelet-derived growth factor D. *Stem Cells Transl Med*. (2017) 6:51–9. doi: 10.5966/sctm.2016-0038
70. Gonzalez-King H, Garcia NA, Ontoria-Oviedo I, Ciria M, Montero JA, Sepulveda P. Hypoxia inducible factor-1alpha potentiates jagged 1-mediated angiogenesis by mesenchymal stem cell-derived exosomes. *Stem Cells*. (2017) 35:1747–59. doi: 10.1002/stem.2618
71. Vrijsen KR, Maring JA, Chamuleau SA, Verhage V, Mol EA, Deddens JC, et al. Exosomes from cardiomyocyte progenitor cells and mesenchymal stem cells stimulate angiogenesis via EMMPRIN. *Adv Healthc Mater*. (2016) 5:2555–65. doi: 10.1002/adhm.201600308
72. Wysoczynski M, Pathan A, Moore JBT, Farid T, Kim J, Nasr M, et al. Pro-angiogenic actions of CMC-derived extracellular vesicles rely on selective packaging of angiopoietin 1 and 2, but Not FGF-2 and VEGF. *Stem Cell Rev Rep*. (2019) 15:530–42. doi: 10.1007/s12015-019-09891-6
73. Xiao C, Wang K, Xu Y, Hu H, Zhang N, Wang Y, et al. Transplanted mesenchymal stem cells reduce autophagic flux in infarcted hearts via the exosomal transfer of miR-125b. *Circ Res*. (2018) 123:564–78. doi: 10.1161/CIRCRESAHA.118.312758
74. Kramer L, Jordan B, Druml W, Bauer P, Metnitz PG. Incidence and prognosis of early hepatic dysfunction in critically ill patients–a prospective multicenter study. *Crit Care Med*. (2007) 35:1099–104. doi: 10.1097/01.CCM.0000259462.97164.A0
75. Chen G, Deng H, Song X, Lu M, Zhao L, Xia S, et al. Reactive oxygen species-responsive polymeric nanoparticles for alleviating sepsis-induced acute liver injury in mice. *Biomaterials*. (2017) 144:30–41. doi: 10.1016/j.biomaterials.2017.08.008
76. Nong K, Wang W, Niu X, Hu B, Ma C, Bai Y, et al. Hepatoprotective effect of exosomes from human-induced pluripotent stem cell-derived mesenchymal stromal cells against hepatic ischemia-reperfusion injury in rats. *Cytotherapy*. (2016) 18:1548–59. doi: 10.1016/j.jcyt.2016.08.002
77. Tamura R, Uemoto S, Tabata Y. Immunosuppressive effect of mesenchymal stem cell-derived exosomes on a concanavalin A-induced liver injury model. *Inflamm Regen*. (2016) 36:26. doi: 10.1186/s41232-016-0030-5
78. Haga H, Yan IK, Takahashi K, Matsuda A, Patel T. Extracellular vesicles from bone marrow-derived mesenchymal stem cells improve survival from lethal hepatic failure in mice. *Stem Cells Transl Med*. (2017) 6:1262–72. doi: 10.1002/sctm.16-0226
79. Yan Y, Jiang W, Tan Y, Zou S, Zhang H, Mao F, et al. hucMSC exosome-derived GPX1 is required for the recovery of hepatic oxidant injury. *Mol Ther*. (2017) 25:465–79. doi: 10.1016/j.ymthe.2016.11.019
80. Tan CY, Lai RC, Wong W, Dan YY, Lim SK, Ho HK. Mesenchymal stem cell-derived exosomes promote hepatic regeneration in drug-induced liver injury models. *Stem Cell Res Ther*. (2014) 5:76. doi: 10.1186/scrt465
81. Lai RC, Arslan F, Lee MM, Sze NS, Choo A, Chen TS, et al. Exosome secreted by MSC reduces myocardial ischemia/reperfusion injury. *Stem Cell Res*. (2010) 4:214–22. doi: 10.1016/j.scr.2009.12.003
82. Chen TS, Lai RC, Lee MM, Choo AB, Lee CN, Lim SK. Mesenchymal stem cell secretes microparticles enriched in pre-microRNAs. *Nucleic Acids Res*. (2010) 38:215–24. doi: 10.1093/nar/gkp857
83. Collino F, Deregibus MC, Bruno S, Sterpone L, Aghemo G, Viltono L, et al. Microvesicles derived from adult human bone marrow and tissue specific mesenchymal stem cells shuttle selected pattern of miRNAs. *PLoS ONE*. (2010) 5:e11803. doi: 10.1371/journal.pone.0011803

84. Farsad K. Exosomes: novel organelles implicated in immunomodulation and apoptosis. *Yale J Biol Med*. (2002) 75:95–101.
85. Zhou YF, Bosch-Marce M, Okuyama H, Krishnamachary B, Kimura H, Zhang L, et al. Spontaneous transformation of cultured mouse bone marrow-derived stromal cells. *Cancer Res.* (2006) 66:10849–54. doi: 10.1158/0008-5472.CAN-06-2146
86. Buyanovskaya OA, Kuleshov NP, Nikitina VA, Voronina ES, Katosova LD, Bochkov NP. Spontaneous aneuploidy and clone formation in adipose tissue stem cells during different periods of culturing. *Bull Exp Biol Med.* (2009) 148:109–12. doi: 10.1007/s10517-009-0647-3
87. Kordelas L, Rebmann V, Ludwig AK, Radtke S, Ruesing J, Doeppner TR, et al. MSC-derived exosomes: a novel tool to treat therapy-refractory graft-versus-host disease. *Leukemia.* (2014) 28:970–3. doi: 10.1038/leu.2014.41
88. Bruno S, Collino F, Deregibus MC, Grange C, Tetta C, Camussi G. Microvesicles derived from human bone marrow mesenchymal stem cells inhibit tumor growth. *Stem Cells Dev.* (2013) 22:758–71. doi: 10.1089/scd.2012.0304
89. Mortaza S, Martinez MC, Baron-Menguy C, Burban M, de la Bourdonnaye M, Fizanne L, et al. Detrimental hemodynamic and inflammatory effects of microparticles originating from septic rats. *Crit Care Med.* (2009) 37:2045–50. doi: 10.1097/CCM.0b013e3181a00629

Conflict of Interest: The authors declare that the research was conducted in the absence of any commercial or financial relationships that could be construed as a potential conflict of interest.

Copyright © 2020 Cheng, Cao and Qin. This is an open-access article distributed under the terms of the Creative Commons Attribution License (CC BY). The use, distribution or reproduction in other forums is permitted, provided the original author(s) and the copyright owner(s) are credited and that the original publication in this journal is cited, in accordance with accepted academic practice. No use, distribution or reproduction is permitted which does not comply with these terms.

frontiers in Immunology

ORIGINAL RESEARCH
published: 07 May 2020
doi: 10.3389/fimmu.2020.00757

Non-invasive Assessment of Mitochondrial Oxygen Metabolism in the Critically Ill Patient Using the Protoporphyrin IX-Triplet State Lifetime Technique—A Feasibility Study

Charles Neu[1,2,3†], *Philipp Baumbach*[1,2†], *Alina K. Plooij*[1,2], *Kornel Skitek*[1,2], *Juliane Götze*[1,2], *Christian von Loeffelholz*[1], *Christiane Schmidt-Winter*[1,2] *and Sina M. Coldewey*[1,2,3*]

[1] Department of Anesthesiology and Intensive Care Medicine, Jena University Hospital, Jena, Germany, [2] Septomics Research Center, Jena University Hospital, Jena, Germany, [3] Center for Sepsis Control and Care, Jena University Hospital, Jena, Germany

OPEN ACCESS

Edited by:
Pietro Ghezzi,
Brighton and Sussex Medical School, United Kingdom

Reviewed by:
Robert Campbell,
The University of Utah, United States
Sergio Iván Valdés-Ferrer,
Salvador Zubirán National Institute of Medical Sciences and Nutrition (INCMNSZ), Mexico

***Correspondence:**
Sina M. Coldewey
sina.coldewey@med.uni-jena.de

[†]These authors have contributed equally to this work

Specialty section:
This article was submitted to Inflammation, a section of the journal Frontiers in Immunology

Received: 23 December 2019
Accepted: 03 April 2020
Published: 07 May 2020

Citation:
Neu C, Baumbach P, Plooij AK, Skitek K, Götze J, von Loeffelholz C, Schmidt-Winter C and Coldewey SM (2020) Non-invasive Assessment of Mitochondrial Oxygen Metabolism in the Critically Ill Patient Using the Protoporphyrin IX-Triplet State Lifetime Technique—A Feasibility Study. Front. Immunol. 11:757. doi: 10.3389/fimmu.2020.00757

The imbalance of oxygen delivery and oxygen consumption resulting in insufficient tissue oxygenation is pathognomonic for all forms of shock. Mitochondrial function plays an important role in the cellular oxygen metabolism and has been shown to impact a variety of diseases in the intensive care setting, specifically sepsis. Clinical assessment of tissue oxygenation and mitochondrial function remains elusive. The *in vivo* protoporphyrin IX-triplet state lifetime technique (PpIX-TSLT) allows the direct, non-invasive measurement of mitochondrial oxygen tension ($mitoPO_2$) in the human skin. Our recently established measurement protocol for the Cellular Oxygen Metabolism (COMET) Monitor, a novel device employing the PpIX-TSLT, additionally allows the evaluation of oxygen consumption ($mitoVO_2$) and delivery ($mitoDO_2$). In the intensive care setting, these variables might provide new insight into mitochondrial oxygen metabolism and especially $mitoDO_2$ might be a surrogate parameter of microcirculatory function. However, the feasibility of the PpIX-TSLT in critically ill patients has not been analyzed systematically. In this interim study analysis, we evaluated PpIX-TSLT measurements of 40 patients during the acute phase of sepsis. We assessed (a) potential adverse side effects of the method, (b) the rate of analyzable measurements, (c) the stability of $mitoPO_2$, $mitoVO_2$, and $mitoDO_2$, and (d) potential covariates. Due to excessive edema in patients with sepsis, we specifically analyzed the association of patients' hydration status, assessed by bioimpedance analysis (BIA), with the aforementioned variables. We observed no side effects and acquired analyzable measurements sessions in 92.5% of patients ($n = 37/40$). Different measures of stability indicated moderate to good repeatability of the PpIX-TSLT variables within one session of multiple measurements. The determined limits of agreement and minimum detectable differences may be helpful in identifying outlier measurements. In conjunction with signal quality they mark a first step in developing a previously unavailable standardized measurement quality protocol. Notably,

higher levels of hydration were associated with lower mitochondrial oxygen tension. We conclude that COMET measurements are viable in patients with sepsis. To validate the clinical and diagnostic relevance of the PpIX-TSLT using the COMET in the intensive care setting, future studies in critically ill patients and healthy controls are needed.

Keywords: sepsis, COMET, mitochondrial dysfunction, critically ill patients, protoporphyrin IX-triplet state lifetime technique, cellular oxygen metabolism, mitochondrial oxygen metabolism, mitochondrial oxygen tension

INTRODUCTION

Sepsis is defined as a life-threatening host response toward infection resulting in organ dysfunction (1). Despite advances in the pathophysiological understanding of this condition, research has not led to significant changes in sepsis therapy. It therefore remains one of the most prevalent critical conditions worldwide with only supportive therapy. A major hallmark of sepsis and septic shock in particular is disturbed tissue oxygenation. Hitherto, surrogate parameters of tissue oxygenation have been shown to be of limited reliability. Early goal-directed therapy, focusing on central venous oxygen saturation as a surrogate parameter of tissue oxygenation, for example, has shown no overall benefit in a recent meta-analysis (2) leaving clinicians without any evidence on which to base their decisions. Therefore, there is a need for new research into the direct measurement of tissue oxygenation.

In recent years, the mitochondrion has become a focus of medical research. The mitochondrion, as "powerhouse" of the cell, is responsible for the regulation of cellular oxygen metabolism and could therefore pose a potential target for the measurement of tissue oxygenation. Studies have demonstrated a pathophysiological involvement of mitochondrial function in, among others, cancer, heart, and age-related diseases (3–5). In sepsis, studies have yielded first indications of a dysregulated mitochondrial function. Clinical trials showed increased mitochondrial protein synthesis in patients with sepsis (6, 7). Another study demonstrated a decreased mitochondrial function in biopsies from patients with sepsis (8). Thus far, clinical measurements were performed in muscle biopsies. As the analysis is *ex vivo* there may be pre-analytical confounders influencing the results. Also, the procedure is invasive and therefore unlikely to be used routinely for diagnostic purposes. Non-invasive direct measurements of mitochondrial function in patients could pose a feasible method to assess tissue oxygenation in patients with sepsis.

Mik et al. introduced the protoporphyrin IX-triplet state lifetime technique (PpIX-TSLT) for non-invasively measuring mitochondrial oxygen tension ($mitoPO_2$) (9). In brief, the method is based on the delayed fluorescence of protoporphyrin IX (PpIX), the naturally occurring precursor of the heme molecule, which can be enriched in skin cells by external application of 5-aminolevulinic acid (5-ALA). The delayed fluorescence is induced by pulses of green light and is inversely correlated with mitochondrial oxygen tension. The recent development of the CE-certified Cellular Oxygen METabolism Monitor (COMET) now enables the application of the PpIX-TSLT in the clinical setting. As this device allows the direct measurement of oxygen metabolism on the cellular level, it could be employed as a diagnostic tool for patients with sepsis. Thus far, the COMET has been employed in a pharmacological study (10) and in healthy controls (11, 12).

The primary objective of this study was to test how feasible the PpIX-TSLT measurements are in the acute phase of sepsis during the treatment at the critical care unit. The secondary objectives were to assess the distribution and the stability of PpIX-TSLT variables for single measurements and to identify potential covariates, in particular the patients' fluid status.

METHODS

Patient Sample

This study is an intermediate analysis of patients from the study *Identification of cardiovascular and molecular prognostic factors for the medium- and long-term outcomes of sepsis* (ICROS, DRKS00013347, and NCT03620409). Patients with sepsis were recruited at the intensive care units of the Jena University Hospital. The inclusion and exclusion criteria of the study are presented in **Table 1**. For PpIX-TSLT measurements, contraindications were: allergies to contents of the Alacare® plaster (photonamic, Wedel, Germany), porphyria, skin conditions aggravated by sunlight, or increased sensitivity to light. For BIA measurements contraindications were: electronic implants (e.g., pacemaker) or active prostheses. Study physicians obtained written informed consent from either the patient or the patient's legal proxy if the patient was incapacitated. The study was approved by the ethics committee of the Friedrich Schiller University Jena (5276-09/17).

PpIX-TSLT Measurements

PpIX-TSLT measurements took place within 3 ± 1 days after the onset of sepsis. A 4 cm^2 patch containing 5-ALA (Alacare®, photonamic, Wedel, Germany) was applied to the clavipectoral triangle at least 5 h before the planned measurement to ensure sufficient accumulation of PpIX. Before application, the skin was cleaned and prepared with an abrasive paste (skinPure®, Nihon Kohden, Rosbach, Germany). For 48 h after application, the skin was protected from light with an additional patch. The measurements were performed with the COMET measurement

Abbreviations: 5-ALA, 5-aminolevulinic acid; BIA, bioimpedance analysis; BIVA, bioimpedance vector analysis; COMET, Cellular Oxygen Metabolism Monitor; $mitoDO_{2\,:\,average}$, average mitochondrial oxygen delivery; $mitoDO_{2\,:\,maximum}$, maximum mitochondrial oxygen delivery; $mitoPO_{2\,:\,baseline}$, baseline mitochondrial oxygen tension; $mitoPO_{2\,:\,post}$, post-mitochondrial oxygen tension; $mitoVO_{2\,:\,average}$, average mitochondrial oxygen consumption; $mitoVO_{2\,:\,maximum}$, maximum mitochondrial oxygen consumption; PpIX, protoporphyrin IX; PpIX-TSLT, protoporphyrin IX-triplet state lifetime; SEM, standard error of measurement.

TABLE 1 | Inclusion and exclusion criteria for the study.

Inclusion criteria
Sepsis or septic shock meeting Sepsis-3 criteria (1)
Onset of first infection-caused organ dysfunction no longer than 72 h before enrolment
At least 18 years of age
Written informed consent from the patient, legal representative or proxy, or preliminary consent after consultation of an independent medical doctor
Exclusion criteria
Cardiac surgery in the last 12 months
Significant heart disease:
Endocarditis
Higher degree valve disorders (severe valvular heart disease, symptomatic aortic valve stenosis, moderate mitral regurgitation with reduced ejection fraction)
Congenital heart defect (e.g., transposition of the great arteries, tetralogy of Fallot, atrioventricular septal defect)
Hemodynamically relevant shunting heart defect
Reduced cardiac output (EF < 45% or 10% below norm*) prior to sepsis
Pulmonary arterial hypertension prior to onset of sepsis
Myocardial infarction 12 months prior to onset of sepsis
History of heart transplantation
Cardiopulmonary resuscitation 4 weeks prior to onset of sepsis
History of pneumonectomy
Child C liver cirrhosis
Contraindications for transesophageal echocardiography and insufficient quality of transthoracic echocardiography
Terminal chronic kidney disease with dialysis
Sepsis within 8 months prior to onset of sepsis
Pregnancy/breast-feeding
Therapy limitation/do-not-resuscitate order
Remaining life expectancy <6 months due to other causes than sepsis
Prior participation in this study
Participation in another interventional study

**Left ventricular ejection fraction >52% in men, >54% in women according to the American Society of Echocardiography and the European Association of Cardiovascular Imaging (13).*

system (Photonics Healthcare, Utrecht, Netherlands). Before the measurement session, the sensor was shielded from light and applied to the prepared skin. During one session multiple measurements with the following parameters were performed (see also **Figure 1**): In the first 30 s, the $mitoPO_{2:baseline}$ was measured. Thereafter, we applied pressure to the sensor for 45 s to inhibit the microcirculation of that part of the skin and to measure oxygen consumption ($mitoVO_{2:maximum}$ and $mitoVO_{2:average}$). Finally, the pressure was released to evaluate the re-oxygenation ($mitoDO_{2:maximum}$ and $mitoDO_{2:average}$) and post-re-oxygenation $mitoPO_2$ ($mitoPO_{2:post}$). A single measurement took 105 s and was performed at least three times per session. We used two complementary sigmoid functions to fit the raw PpIX-TSLT signals of each single measurement:

$$\frac{K_1}{1+e^{(-B_1\times(x-M_1))}}+\frac{K_2}{1+e^{(-B_2\times(x-M_2))}}+Z \qquad (1)$$

The estimation of these function parameters allows a direct inference of the PpIX-TSLT variables. For details please [see (12)].

We used a self-developed program (Halley) under MATLAB (MATLAB and Statistics Toolbox Release 2017a, The MathWorks, Inc., Natick, Massachusetts, United States) for data management, data preparation and PpIX-TSLT variable estimation.

Bioimpedance Vector Analysis

The patient's fluid status was evaluated using the seca medical Body Composition Analyzer 525 (seca Germany, Hamburg, Germany). For bioimpedance vector analysis (BIVA), raw impedance variables, resistance (R) and reactance (Xc), were standardized to body height ($R_{/height}$, $Xc_{/height}$) in meters (14). Two characteristics of the resulting bivariate vector were analyzed: the phase angle [arc tangent of (Xc/R) × 180°/π] as vector orientation and the vector length (square root of $Xc^2_{height} + R^2_{height}$). Especially the latter one is an indicator of the hydration status (14, 15) and has already been proven to be applicable in the critical care setting (16). Short vectors, resulting from decreased resistance, indicate high levels of hydration and can indicate the presence of edema secondary to low oncotic pressure or endothelial barrier dysfunction. Long vectors, resulting from increased resistance, are an indicator of a low hydration status, i.e., dehydration. Where feasible, body height, and weight were obtained by means of a measuring tape and the Seca bed scale 985 (Seca Germany, Hamburg, Germany), respectively. Otherwise, information from the medical history was used.

Descriptive Analysis

In descriptive analysis, means, standard deviations (SD), medians, as well as first and third quartiles (Q_1/Q_3) are reported. For categorical and dichotomous variables we report absolute and relative frequencies. The distribution of the PpIX-TSLT variables was assessed using histograms, Q-Q-plots, Shapiro-Wilk-Tests, and an estimation of kurtosis and skewness with corresponding standard errors (SE) and kurtosis excess (kurtosis – 3).

Stability of PpIX-TSLT Variables

To analyze the repeatability, i.e., stability, of PpIX-TSLT variables during one measurement session we took the following steps: First, descriptive mean differences between measurement pairs and corresponding *p*-values of the paired samples *t*-tests are reported. Second, Pearson correlation coefficients of all available measurement pairs are presented. Correlation coefficients can be interpreted in the following way: $r < 0.10$ negligible, r 0.1–0.39 weak, 0.40–0.69 moderate, 0.70–0.89 strong, 0.90–1.00 very strong (17). Third, measurement pairs were analyzed using Bland-Altman plots to assess limits of agreement (LOA) (18, 19). In detail, the mean of a measurement pair is plotted against the difference between both single measurements (LOA = mean of the differences ± 1.96 × SD of the differences). The corresponding 95% confidence intervals (95%CI) for LOA were obtained using two-sided tolerance factors (20). At population level, 95% of PpIX-TSLT variable differences between single

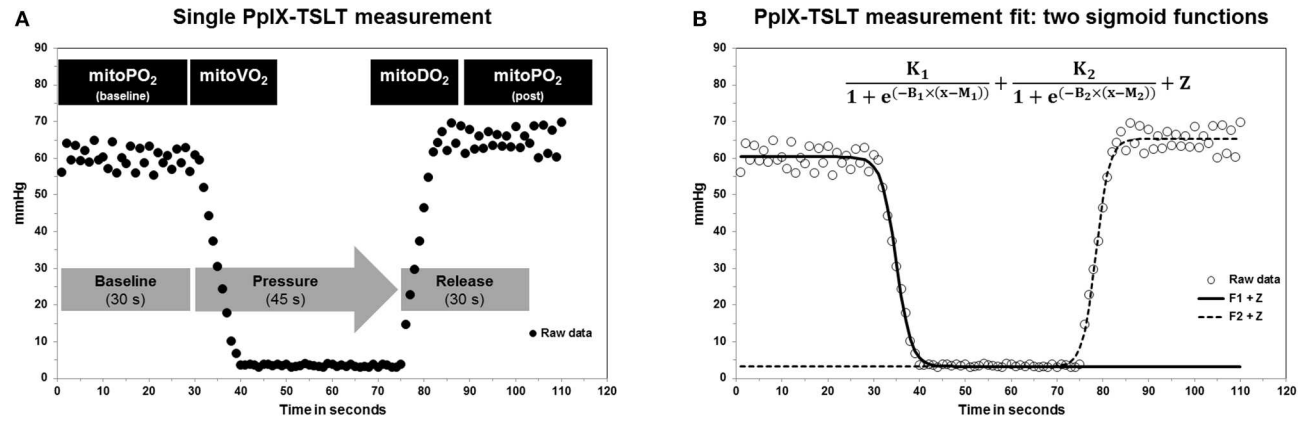

FIGURE 1 | (A) Description of a single PpIX-TSLT measurement to obtain mitochondrial oxygen tension ($mitoPO_2$), mitochondrial oxygen consumption ($mitoVO_2$), and mitochondrial oxygen delivery ($mitoDO_2$). **(B)** Illustration of the raw PpIX-TSLT data and the two sigmoid fit functions to estimate the PpIX-TSLT variables.

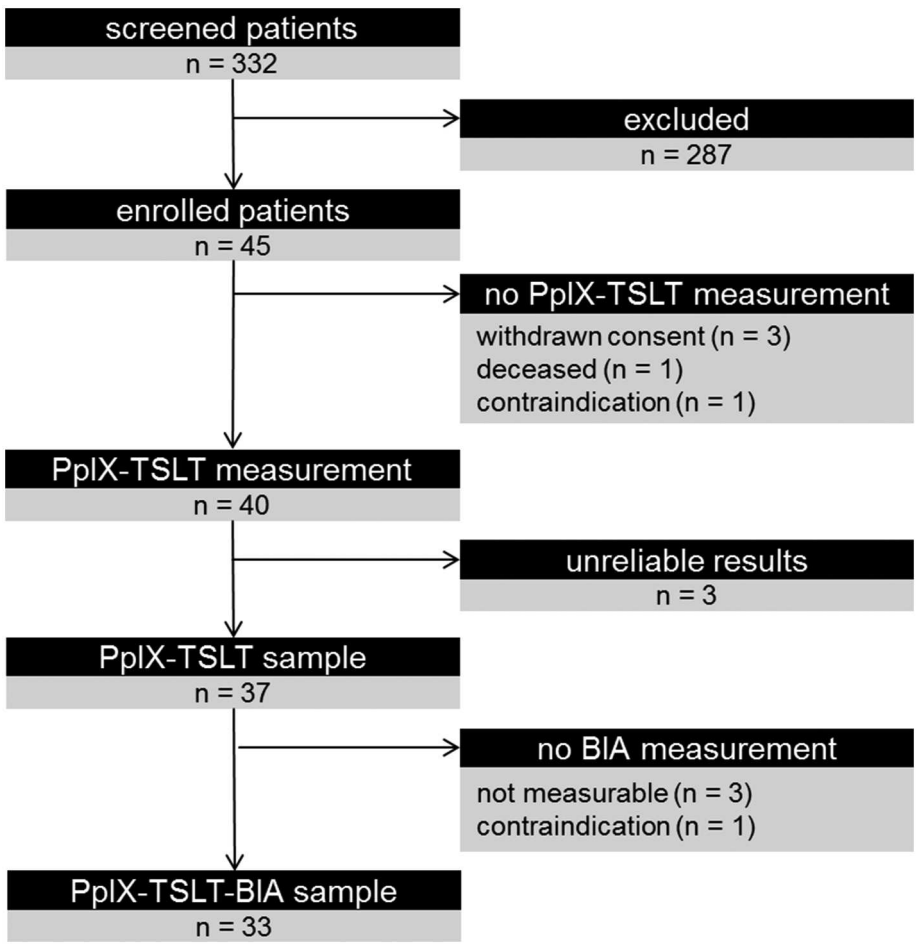

FIGURE 2 | Overview of the patient inclusion and analytical cohorts. Results for primary analysis are reported from the PpIX-TSLT sample. Results for Bioimpedance Analysis (BIA) and additional correlative analyses with PpIX-TSLT variables are reported for the PpIX-TSLT-BIA sample.

PpIX-TSLT measurements within one session, according to our protocol, should lie within these LOA. Fourth, intra-class correlation coefficients (ICC) for all available measurement pairs using the two-way mixed effects analysis of variance (ANOVA) for single measures with absolute agreement were obtained (21). ICCs and corresponding confidence intervals can be interpreted as follows: ICC $<$ 0.5 poor, 0.5 $\leq$ ICC $\leq$ 0.75 moderate, 0.75 $\leq$ ICC $\leq$ 0.90 good, and ICC $>$ 0.90 excellent reliability (21). Finally, the standard error of measurement (SEM) as the square root of the mean square error term from repeated-measures ANOVA for all available measurement pairs (22) and the Minimum Detectable Difference (MDD, SEM $\times$ 1.96 $\times$ $2^{1/2}$) are reported.

Exploratory Analysis of Potential Covariates

Potential covariates for PpIX-TSLT variables were analyzed parametrically and non-parametrically with Pearson correlation coefficients and Spearman's rank correlation coefficients, respectively. PpIX-TSLT variables from multiple single measurements were averaged before correlative analysis. Results were additionally visualized with scatterplots and regression lines from the simple linear regression models (PpIX-TSLT variables served as dependent variables). We considered the following variables: sex, age, BIVA variables (see above), PpIX-TSLT-associated variables (duration of 5-ALA application, average signal quality, room, sensor, skin, and body temperature, goodness of fit of the fitting procedure), physiological data (heart rate, systolic and diastolic blood pressure, SpO_2, hemoglobin, fluid balance), and treatment-associated data (initial SOFA score, catecholamine status, ventilation status). Treatment-related variables were obtained from electronic patient records on ICU (Copra System, Berlin, Germany).

For statistical analysis we used SPSS Statistics 24 (IBM Corporation, Armonk, NY, USA) and R [Version 3.5.1, Vienna, Austria (23)]. We applied a significance level of 5% and report two-sided *p*-values.

RESULTS

Sample Description

Figure 2 summarizes the study inclusion. Of 332 screened patients, 45 patients with sepsis were enrolled in the study. After excluding patients who withdrew consent, died before the measurement or had contraindications, PpIX-TSLT measurements were performed on 40 patients. 37 patients with reliable PpIX-TSLT measurements were included in the primary analysis. Demographic and clinical characteristics of the study sample are displayed in **Table 2**.

Primary Analysis

In 37 (92.5%) of the 40 included patients with sepsis, reliable PpIX-TSLT measurement sessions could be recorded. In the 3 patients with unreliable measurement sessions either the signal quality was too low and/or $mitoVO_2$ could not be induced consistently during multiple measurements. We did not observe any side effects of the 5-ALA application or the PpIX-TSLT measurement itself in any patient.

TABLE 2 | Demographics and clinical characteristics ($n = 37$ patients).

Variable	[Unit]	Median	Q_1	Q_3
Age	[years]	70.00	58.00	79.00
Initial SOFA increase	[points]	5.00	4.00	7.00
Body weight	[kilogram]	76.20	68.00	92.00
Body height	[meter]	1.72	1.65	1.75
BMI	[kg/m²]	27.13	23.57	31.02
Body surface	[m²]	1.89	1.66	2.04
Variable	**Category**		***n***	**%**
Sex	Female		13	35.1
	Male		24	64.9
Sepsis focus	Pneumonia		17	45.9
	Intra-abdominal/ gastrointestinal		13	35.1
	Thoracic		2	5.4
	Urogenital		3	8.1
	Bone/soft-tissue		1	2.7
	Skin		1	2.7
Ventilation[a]	Spontaneous		20	54.1
	Invasive/non-invasive		17	45.9
Catecholamines[b]	None		11	29.7
	Medium[b]		11	29.7
	High[c]		15	40.5

For continuous measures median, first and third quartile (Q_1/Q_3) are displayed. For categorical variables number (n) and percent (%) are shown.

[a] *Any duration of invasive ventilation. Non-invasive ventilation > 6 h.*

[b] *Dopamine > 5 μg/kg/min or epinephrine ≤ 0.1 μg/kg/min or norepinephrine ≤ 0.1 μg/kg/min.*

[c] *Dopamine > 15 μg/kg/min or epinephrine > 0.1 μg/kg/min or norepinephrine > 0.1 μg/kg/min.*

Secondary Objectives

Descriptive Statistics and Variable Distribution

The descriptive statistics of the PpIX-TSLT variables are displayed in **Table 3**. Additional information on variable distribution is provided in **Supplement S-1**. Shapiro-Wilk tests indicated that $mitoPO_2$ variables were normally distributed ($p > 0.05$). The *p*-values of the Shapiro-Wilk tests for the other PpIX-TSLT variables were significant ($p < 0.01$). All PpIX-TSLT parameters were positively skewed and kurtosis excess values ranged between -2.4 ($mitoPO_{2:\text{baseline}}$, platykurtic) to 3.0 ($mitoVO_{2:\text{average}}$, leptokurtic). After removing outlier values (values $>Q_3 + 1.5$ times the interquartile range, see also **Table 3**) none of the *p*-values of the Shapiro-Wilk tests reached significance ($p > 0.05$) indicating normally distributed values.

Stability of PpIX-TSLT Measurements

$MitoPO_{2:\text{baseline}}$ values showed a mean difference of 4.42 mmHg between subsequent measurements, resulting in a significant *p*-value of the corresponding paired *t*-test (**Table 4**). In addition, both $mitoDO_2$ variables differed significantly between

TABLE 3 | Descriptive statistics for PpIX-TSLT variables.

Variable	[Unit]	*n*	Mean ± SD	[95%CI]	Median	Q_1	Q_3	Threshold	
								Lower	Upper
$MitoPO_{2:baseline}$	[mmHg]	37	61.86 ± 19.97	[55.42, 68.29]	65.15	49.21	70.84	16.75	103.30
$MitoPO_{2:post}$	[mmHg]	37	55.52 ± 15.64	[50.48, 60.56]	56.75	44.18	64.38	13.88	94.68
$MitoVO_{2:maximum}$	[mmHg/s]	37	4.82 ± 2.39	[4.05, 5.59]	4.65	3.16	5.71	0.00	9.54
$MitoVO_{2:average}$	[mmHg/s]	37	3.43 ± 1.71	[2.88, 3.98]	3.31	2.25	4.07	0.00	6.80
$MitoDO_{2:maximum}$	[mmHg/s]	37	6.87 ± 4.06	[5.56, 8.18]	5.76	4.23	7.56	0.00	12.57
$MitoDO_{2:average}$	[mmHg/s]	37	4.89 ± 2.89	[3.96, 5.82]	4.11	3.01	5.39	0.00	8.95

All PpIX-TSLT variables from one measurement session were averaged before descriptive analysis.
$mitoPO_2$, mitochondrial oxygen tension; $mitoVO_2$, mitochondrial oxygen consumption; $mitoDO_2$, mitochondrial oxygen delivery.
Thresholds are defined as $Q_1 - 1.5 \times$ interquartile range and $Q_3 + 1.5 \times$ interquartile range.
SD, standard deviation; 95%CI, 95 percent confidence interval, Q_1/Q_3, first and third quartile.

TABLE 4 | Intra-session stability of the PpIX-TSLT variables ($n = 36$ patients with at least 2 reliable PpIX-TSLT measurements).

			Difference							Limits of agreement (LOA)					
Variable	[Unit]	*n*	Δmean		SD	[95%CI]	p_{ttest}	*r*	p_r	Lower	95%CI		Upper	95%CI	
$MitoPO_{2:baseline}$	[mmHg]	114	−4.42	±	13.62	[−6.92, −1.92]	**0.001**	0.75	**<0.001**	−31.12	−35.27	−28.14	22.28	19.30	26.43
$MitoPO_{2:post}$	[mmHg]	114	−0.95	±	11.24	[−3.01, 1.11]	0.369	0.72	**<0.001**	−22.99	−26.41	−20.53	21.09	18.63	24.51
$MitoVO_{2:maximum}$	[mmHg/s]	114	−0.02	±	1.54	[−0.30, 0.26]	0.901	0.81	**<0.001**	−3.03	−3.50	−2.70	3.00	2.66	3.47
$MitoVO_{2:average}$	[mmHg/s]	114	−0.01	±	1.10	[−0.22, 0.19]	0.893	0.81	**<0.001**	−2.16	−2.50	−1.92	2.14	1.90	2.47
$MitoDO_{2:maximum}$	[mmHg/s]	114	1.07	±	3.96	[0.34, 1.79]	**0.005**	0.68	**<0.001**	−6.69	−7.89	−5.82	8.82	7.96	10.03
$MitoDO_{2:average}$	[mmHg/s]	114	0.76	±	2.82	[0.24, 1.28]	**0.005**	0.68	**<0.001**	−4.76	−5.62	−4.14	6.28	5.66	7.14

Mean difference (Δmean), corresponding standard deviation (SD), and 95% confidence intervals (95%CI) for PpIX-TSLT measurement pairs are shown. Additionally, Pearson correlation coefficients (r), corresponding p-values (p_r), and p-values of the paired t-tests (p_{ttest}) for PpIX-TSLT measurement pairs are displayed. Further, limits of agreement (LOA) with corresponding 95%CI and p-values are shown. $P < 0.05$ are printed in bold.

subsequent measurements ($p < 0.01$) with a mean difference of 1.07 ($mitoDO_{2:maximum}$) and 0.76 ($mitoDO_{2:average}$), respectively. $MitoPO_{2:Post}$ and both $mitoVO_2$ variables did not differ significantly between subsequent measurements. All variables were moderately ($mitoDO_2$) to strongly (all others) correlated between subsequent measurements (**Table 4**). The limits of agreement and corresponding Bland-Altman-Plots for subsequent measurements are displayed in **Table 4** and **Supplement S-2**. The intraclass correlation coefficients for all PpIX-TSLT variables showed significant *p*-values ($p < 0.001$) and ranged between 0.652 (moderate) for $mitoDO_2$ variables and 0.805 (good) for $mitoVO_2$ variables (**Table 5**). Finally, the standard error of measurement (SEM) and Minimum Detectable Difference (MDD) of PpIX-TSLT variables are displayed in **Table 5**.

Correlative Analysis

Statistically significant associations between PpIX-TSLT variables and tested covariates are shown in **Table 6**. The descriptive statistics for BIVA-variables and potential covariates are shown in **Supplement S-3**. In summary, $mitoPO_{2:baseline}$ correlated positively with height-standardized vector length of BIVA. Maximum and average $mitoVO_2$-variables showed correlation coefficients of 1. The same applies for $mitoDO_2$ variables. For this reason, only results for $mitoVO_{2:average}$ and $mitoDO_{2:average}$ are reported. $MitoVO_2$ variables were positively correlated with the goodness of fit (R^2) of the fitting function. $MitoDO_2$ variables were negatively correlated with the duration of 5-ALA application, the average signal quality during PpIX-TSLT measurement and body height. In addition, $mitoDO_2$ variables were positively correlated with the room temperature. Finally, the mean signal quality of one measurement was positively correlated with the duration of the 5-ALA application and negatively correlated with the room temperature. All other tested covariates showed no statistically significant correlation coefficients with PpIX-TSLT variables (data not shown). $MitoPO_{2:baseline}$ tended to differ between female (median: 69.95, $Q_{1|3}$: 54.03 | 74.08) and male patients (median: 57.19, $Q_{1|3}$: 44.36 | 69.25). In addition, we found significant sex differences between $mitoDO_{2:average}$ with higher values for females (median: 5.25, $Q_{1|3}$: 3.45 | 9.98) compared to males (median: 3.73, $Q_{1|3}$: 2.55 | 5.27, $U = 84$, $p = 0.022$). Neither the ventilation status nor the catecholamine dosage was significantly associated with any of the PpIX-TSLT variables. After adjusting for multiple testing using the Bonferroni-Holm method, only the *p*-value for the association between $mitoVO_2$ variables and the goodness of fit (R^2) reached significance (adjusted *p*-values not shown).

DISCUSSION

Feasibility of PpIX-TSLT Measurements of Mitochondrial Function in Patients With Sepsis

In this study, we report for the first time direct *in vivo* assessment of mitochondrial oxygen metabolism by PpIX-TSLT measurements in a cohort of patients with sepsis. Thus

TABLE 5 | Intraclass correlation coefficients (ICC) with corresponding 95% confidence intervals, standard error of measurement (SEM), and minimum detectable difference (MDD) for PpIX-TSLT variables ($n = 36$ patients with at least 2 reliable PpIX-TSLT measurements).

					Intraclass correlation coefficients			
Variable	***n***	**SEM**	**MDD**	**[Unit]**	**ICC**	**95%CI**		***p***
$MitoPO_{2:baseline}$	114	9.63	26.70	[mmHg]	0.729	0.612	0.811	**<0.001**
$MitoPO_{2:post}$	114	7.95	22.04	[mmHg]	0.717	0.615	0.796	**<0.001**
$MitoVO_{2:maximum}$	114	1.09	3.01	[mmHg/s]	0.805	0.729	0.861	**<0.001**
$MitoVO_{2:average}$	114	0.78	2.15	[mmHg/s]	0.805	0.729	0.861	**<0.001**
$MitoDO_{2:maximum}$	114	2.80	7.75	[mmHg/s]	0.652	0.526	0.749	**<0.001**
$MitoDO_{2:average}$	114	1.99	5.52	[mmHg/s]	0.652	0.526	0.749	**<0.001**

P < 0.05 are printed in bold.
ICC < 0.5 poor, 0.5 ≤ ICC ≤ 0.75 moderate, 0.75 ≤ ICC ≤ 0.90 good, ICC > 0.90 excellent (21).

TABLE 6 | Main findings of the correlation analyses for the PpIX-TSLT variables and potential covariates.

Variable	**Covariate**	***n***	ρ	p_ρ	***r***	p_r
$MitoPO_{2:baseline}$	BIVA: vector length[†]	33	0.36	**0.042**	0.23	0.191
$MitoVO_{2:average}$	Goodness of Fit	37	0.71	**<0.001**	0.58	**<0.001**
$MitoDO_{2:average}$	Body height	37	−0.38	**0.020**	−0.32	0.051
	Duration of 5-ALA application	36	−0.37	**0.024**	−0.37	**0.026**
	Signal Quality	37	−0.34	**0.039**	−0.27	0.113
	Temperature: room	37	0.40	**0.015**	0.25	0.140
Signal quality	Duration of 5-ALA application	36	0.35	**0.038**	0.22	0.198
	Temperature: room	37	−0.34	**0.039**	−0.39	**0.016**

Spearman's rank correlation coefficient (ρ) with the corresponding p-value (p_ρ) and the Pearson correlation coefficient (r) with the corresponding p-value (p_r) are shown. P < 0.05 are printed in bold.
mitoPO$_2$, mitochondrial oxygen tension; mitoVO$_2$, mitochondrial oxygen consumption; mitoDO$_2$, mitochondrial oxygen delivery.
[†] *Obtained from height-standardized resistance and reactance values.*

far, only reports in healthy subjects or surgical patients have been published. In our cohort of 40 patients, PpIX-TSLT measurements yielded analyzable datasets in 92.5% of patients. Also, no side effects of the measurements were observed. We therefore conclude that PpIX-TSLT measurements with the COMET are feasible in patients with sepsis in the ICU setting. In our previous study, analyzable results were obtained from 75% of healthy subjects (12). We believed at the time that compliance problems concerning 5-ALA application may have contributed to this relatively low success rate. As the ICU offers a standardized environment, protocol adherence was very high. Hence, our results may confirm our assumption and stress the importance of controlling the duration of 5-ALA application. Of the three measurements that failed in this study, one was due to low signal quality. This may have been due to inadequate skin absorption of 5-ALA despite using a standardized protocol. In the other two cases, mitoVO$_2$ could not be induced. This phenomenon is not entirely understood and deserves future attention.

Distribution and Stability of PpIX-TSLT Variables

After removing outliers, all variables were normally or near-to-normally distributed. In our previous trial, PpIX-TSLT variables were also distributed near to normal (12). Therefore, we conclude both parametric and non-parametric analyses may be applicable for PpIX-TSLT variables.

All variables were moderately to highly correlated between replicate measurements. All ICCs of PpIX-TSLT variables showed significant p-values and ranged from moderate to good. Although t-tests showed significant differences in $mitoPO_{2:baseline}$ and both mitoDO$_2$ variables between iterative measurements, the corresponding effect sizes were low ($d = 0.32$, $d = 0.27$, and $d = 0.27$, respectively). Taken together, the stability of replicate measurements in one session can be seen as moderate to good. We nonetheless recommend multiple measurements in one session. Judging from the LOA and MDD, we can determine that an increase in $mitoPO_{2:baseline}$ of 35 mmHg or a decrease of 25 mmHg between measurements is probably due to incorrect measurement and the measurement should be repeated. Similarly, absolute changes of 2 mmHg/s for $mitoVO_{2:average}$ and 5 mmHg/s for $mitoDO_{2:average}$ could indicate incorrect measurements. All these results are very similar to values determined in our previous study of healthy controls (12).

Potential Covariates of PpIX-TSLT Measurements

We identified potential covariates of the PpIX-TSLT measurements. We demonstrated a positive association between $mitoPO_{2:baseline}$ and BIVA vector length, which in turn correlates negatively with hydration status (14, 16). Therefore, more hydrated patients (i.e., with edema), may show lower

$mitoPO_2$: $_{baseline}$ values. Thus, we recommend considering the presence of edema or conditions with low intravascular oncotic pressure as influence factors when employing the PpIX-TSLT in patients with sepsis. The duration of the 5-ALA plaster application was positively associated with signal quality. One should therefore perform the measurement using a standardized minimum duration of 5-ALA application. Furthermore, room temperature was associated with $mitoDO_{2:average}$ and signal quality. Signal quality could be improved by performing measurements in a cool environment if possible. The patient's sex posed another covariate. $MitoPO_{2:average}$ tended to differ between female and male patients. In addition, we found significant sex differences between $mitoDO_{2:average}$. Both variables showed higher values for females compared to males. This result could indicate the need for sex-specific normal values of PpIX-TSLT variables. Interestingly, neither the status of ventilation nor the dosage of catecholamines showed significant associations with PpIX-TSLT variables.

Limitations

The generalizability of the results for our secondary objectives are limited by the relatively small number of patients ($n = 37$) and selective exclusion criteria (i.e., exclusion of patients with pre-existing cardiac conditions). Furthermore, in correlative analysis for the identification of potential covariates we did not adjust for multiple testing. Thus, our results need to be confirmed in larger trials. Especially the potential influence of the patient's hydration status on PpIX-TSLT variables should be examined. A direct estimation of total body water using BIA may be useful but is strongly dependent on body weight and height. As measuring body weight accurately in intensive care patients is difficult, we restricted our analyses to the weight-independent BIA variables (BIVA). Due to the fluctuation of physiological variables in critically ill patients, we only analyzed the short-term stability of PpIX-TSLT variables, with iterative measurements within minutes. The long-term stability of PpIX-TSLT variables was not analyzed.

CONCLUSION

We conclude that PpIX-TSLT measurements with the COMET are feasible in the critical care setting. Despite the moderate to good stability of the PpIX-TSLT variables using our protocol, we recommend the recording of multiple measurements during one session to increase the reliability of results. The determined limits of agreement and the minimum detectable differences may help to identify potential outlier measurements and additionally improve data quality. Future studies in larger cohorts of critically ill patients are needed to determine the clinical and diagnostic relevance of the PpIX-TSLT using the COMET. Furthermore, healthy controls should be measured to generate normal values for the PpIX-TSLT variables. This study poses a first step toward an evidence-based approach in the assessment of tissue oxygenation in the intensive care unit.

DATA AVAILABILITY STATEMENT

The datasets generated for this study are available on request to the corresponding author.

ETHICS STATEMENT

The studies involving human participants were reviewed and approved by Ethics Committee of the Friedrich Schiller University Jena. The patients/participants provided their written informed consent to participate in this study.

AUTHOR CONTRIBUTIONS

SC, CN, and PB: conception and design of the study. CN, PB, AP, KS, JG, and CS-W: performance of measurements. PB, CN, AP, KS, and JG: clinical data collection. PB, KS, and AP: data analysis and statistical analysis. CN, PB, AP, KS, JG, CS-W, and SC: drafting the manuscript for important intellectual content. CN, CL, PB, and SC: revising the manuscript prior to submission. All authors carefully reviewed and approved the manuscript.

FUNDING

This study was funded by the Federal Ministry of Education and Research within the Centre for Innovation Competence Septomics (Research Group Translational Septomics, Grant 03Z22JN12 to SC). The funding source had no involvement in the study design, the collection, analysis, and interpretation of data, in the writing of the report, or in the decision to submit the article for publication.

ACKNOWLEDGMENTS

We thank the study nurse team of the department of Anesthesiology and Intensive Care Medicine of the Jena University Hospital for their support.

SUPPLEMENTARY MATERIAL

The Supplementary Material for this article can be found online at: https://www.frontiersin.org/articles/10.3389/fimmu.2020.00757/full#supplementary-material

REFERENCES

1. Singer M, Deutschman CS, Seymour CW, Shankar-Hari M, Annane D, Bauer M, et al. The third international consensus definitions for sepsis and septic shock (Sepsis-3). *JAMA*. (2016) 315:801–10. doi: 10.1001/jama.2016.0287
2. Rowan KM, Angus DC, Bailey M, Barnato AE, Bellomo R, Canter RR, et al. Early, goal-directed therapy for septic shock - a patient-level meta-analysis. *N Engl J Med*. (2017) 376:2223–34. doi: 10.1056/NEJMoa1701380
3. Lane RK, Hilsabeck T, Rea SL. The role of mitochondrial dysfunction in age-related diseases. *Biochim Biophys Acta*. (2015) 1847:1387–400. doi: 10.1016/j.bbabio.2015.05.021
4. Giampazolias E, Tait SW. Mitochondria and the hallmarks of cancer. *FEBS J*. (2016) 283:803–14. doi: 10.1111/febs.13603
5. Murphy E, Ardehali H, Balaban RS, Dilisa F, Dorn GW II, Kitsis RN, Otsu K, et al. Mitochondrial function, biology, and role in disease: a scientific

statement from the american heart association. *Circ Res.* (2016) 118:1960–91. doi: 10.1161/RES.0000000000000104
6. Fredriksson K, Tjader I, Keller P, Petrovic N, Ahlman B, Scheele C, et al. Dysregulation of mitochondrial dynamics and the muscle transcriptome in ICU patients suffering from sepsis induced multiple organ failure. *PLoS ONE*. (2008) 3:e3686. doi: 10.1371/annotation/68d951f9-a236-472f-98af-24e4cc4c1a20
7. Carre JE, Orban JC, Re L, Felsmann K, Iffert W, Bauer M, et al. Survival in critical illness is associated with early activation of mitochondrial biogenesis. *Am J Respir Crit Care Med*. (2010) 182:745–51. doi: 10.1164/rccm.201003-0326OC
8. Brealey D, Brand M, Hargreaves I, Heales S, Land J, Smolenski R, et al. Association between mitochondrial dysfunction and severity and outcome of septic shock. *Lancet*. (2002) 360:219–23. doi: 10.1016/S0140-6736(02)09459-X
9. Mik EG, Stap J, Sinaasappel M, Beek JF, Aten JA, Van Leeuwen TG, et al. Mitochondrial PO_2 measured by delayed fluorescence of endogenous protoporphyrin IX. *Nat Methods*. (2006) 3:939–45. doi: 10.1038/nmeth940
10. Van Diemen MPJ, Berends CL, Akram N, Wezel J, Teeuwisse WM, Mik BG, et al. Validation of a pharmacological model for mitochondrial dysfunction in healthy subjects using simvastatin: a randomized placebo-controlled proof-of-pharmacology study. *Eur J Pharmacol*. (2017) 815:290–7. doi: 10.1016/j.ejphar.2017.09.031
11. Harms FA, Stolker RJ, Mik EG. Cutaneous respirometry as novel technique to monitor mitochondrial function: a feasibility study in healthy volunteers. *PLoS ONE*. (2016) 11:e0159544. doi: 10.1371/journal.pone.0163399
12. Baumbach P, Neu C, Derlien S, Bauer M, Nisser M, Buder A, et al. A pilot study of exercise-induced changes in mitochondrial oxygen metabolism measured by a cellular oxygen metabolism monitor (PICOMET). *Biochim Biophys Acta Mol Basis Dis*. (2019) 1865:749–58. doi: 10.1016/j.bbadis.2018.12.003
13. Lang RM, Badano LP, Mor-Avi V, Afilalo J, Armstrong A, Ernande L, et al. Recommendations for cardiac chamber quantification by echocardiography in adults: an update from the American Society of Echocardiography and the European Association of Cardiovascular Imaging. *J Am Soc Echocardiogr*. (2015) 28:1–39.e14. doi: 10.1016/j.echo.2014.10.003
14. Piccoli A, Rossi B, Pillon L, Bucciante G. A new method for monitoring body fluid variation by bioimpedance analysis: the RXc graph. *Kidney Int*. (1994) 46:534–9. doi: 10.1038/ki.1994.305
15. Norman K, Stobaus N, Pirlich M, Bosy-Westphal A. Bioelectrical phase angle and impedance vector analysis–clinical relevance and applicability of impedance parameters. *Clin Nutr*. (2012) 31:854–61. doi: 10.1016/j.clnu.2012.05.008
16. Jones SL, Tanaka A, Eastwood GM, Young H, Peck L, Bellomo R, et al. Bioelectrical impedance vector analysis in critically ill patients: a prospective, clinician-blinded investigation. *Crit Care*. (2015) 19:290. doi: 10.1186/s13054-015-1009-3
17. Schober P, Boer C, Schwarte LA. Correlation coefficients: appropriate use and interpretation. *Anesth Analg*. (2018) 126:1763–8. doi: 10.1213/ANE.0000000000002864
18. Bland JM, Altman DG. Statistical methods for assessing agreement between two methods of clinical measurement. *Lancet*. (1986) 1:307–10. doi: 10.1016/S0140-6736(86)90837-8
19. Bland JM, Altman DG. Agreed statistics: measurement method comparison. *Anesthesiology*. (2012) 116:182–5. doi: 10.1097/ALN.0b013e31823d7784
20. Carkeet A. Exact parametric confidence intervals for Bland-Altman limits of agreement. *Optom Vis Sci*. (2015) 92:e71–80. doi: 10.1097/OPX.0000000000000513
21. Koo TK, Li MY. A guideline of selecting and reporting intraclass correlation coefficients for reliability research. *J Chiropr Med*. (2016) 15:155–63. doi: 10.1016/j.jcm.2016.02.012
22. Weir JP. Quantifying test-retest reliability using the intraclass correlation coefficient and the SEM. *J Strength Cond Res*. (2005) 19:231–40. doi: 10.1519/00124278-200502000-00038
23. R Development Core Team *R: A Language and Environment for Statistical Computing*. Vienna: R Foundation for Statistical Computing (2013).

Conflict of Interest: The authors declare that the research was conducted in the absence of any commercial or financial relationships that could be construed as a potential conflict of interest.

Copyright © 2020 Neu, Baumbach, Plooij, Skitek, Götze, von Loeffelholz, Schmidt-Winter and Coldewey. This is an open-access article distributed under the terms of the Creative Commons Attribution License (CC BY). The use, distribution or reproduction in other forums is permitted, provided the original author(s) and the copyright owner(s) are credited and that the original publication in this journal is cited, in accordance with accepted academic practice. No use, distribution or reproduction is permitted which does not comply with these terms.

frontiers in Immunology

ORIGINAL RESEARCH
published: 21 May 2020
doi: 10.3389/fimmu.2020.01001

The Effect of β_2-Adrenoceptor Agonists on Leucocyte-Endothelial Adhesion in a Rodent Model of Laparotomy and Endotoxemia

Mansoor Nawaz Bangash[1]*, *Tom E. F. Abbott*[2], *Nimesh S. A. Patel*[2], *Charles Johnston Hinds*[2], *Christoph Thiemermann*[2] and *Rupert Mark Pearse*[2]

[1] Department of Critical Care & Anaesthesia, University Hospitals Birmingham NHS Trust, Birmingham, United Kingdom, [2] Centre for Translational Medicine & Therapeutics, William Harvey Research Institute, Queen Mary University of London, London, United Kingdom

OPEN ACCESS

Edited by:
Rudolf Lucas, Medical College of Georgia - Augusta University, United States

Reviewed by:
Massimo Collino, University of Turin, Italy
Christian Lehmann, Dalhousie University, Canada

***Correspondence:**
Mansoor Nawaz Bangash
mansoor.bangash@uhb.nhs.uk

Specialty section:
This article was submitted to Inflammation, a section of the journal Frontiers in Immunology

Received: *13 January 2020*
Accepted: *27 April 2020*
Published: *21 May 2020*

Citation:
Bangash MN, Abbott TEF, Patel NSA, Hinds CJ, Thiemermann C and Pearse RM (2020) The Effect of β_2-Adrenoceptor Agonists on Leucocyte-Endothelial Adhesion in a Rodent Model of Laparotomy and Endotoxemia. Front. Immunol. 11:1001. doi: 10.3389/fimmu.2020.01001

Background: The β_2-adrenoceptor agonist dopexamine may possess anti-inflammatory actions which could reduce organ injury during endotoxemia and laparotomy. Related effects on leucocyte-endothelial adhesion remain unclear.

Methods: Thirty anesthetized Wistar rats underwent laparotomy followed by induction of endotoxemia with lipopolysaccharide and peptidoglycan ($n = 24$) or sham ($n = 6$). Animals received dopexamine at 0.5 or 1 μg kg^{-1} min^{-1} (D0.5 and D1), salbutamol at 0.1 μg kg^{-1} min^{-1}, or saline vehicle (Sham and Control) for 5 h. Intravital microscopy was performed in the ileum of the small intestine to assess leucocyteendothelial adhesion, arteriolar diameter, and functional capillary density. Global hemodynamics and biochemical indices of renal and hepatic function were also measured.

Results: Endotoxemia was associated with an increase in adherent leucocytes in post-capillary venules, intestinal arteriolar vasoconstriction as well-reduced arterial pressure and relative cardiac index, but functional capillary density in the muscularis was not significantly altered. Dopexamine and salbutamol administration were associated with reduced leucocyte-endothelial adhesion in post-capillary venules compared to control animals. Arteriolar diameter, arterial pressure and relative cardiac index all remained similar between treated animals and controls. Functional capillary density was similar for all groups. Control group creatinine was significantly increased compared to sham and higher dose dopexamine.

Conclusions: In a rodent model of laparotomy and endotoxemia, β_2-agonists were associated with reduced leucocyte-endothelial adhesion in post-capillary venules. This effect may explain some of the anti-inflammatory actions of these agents.

Keywords: adrenergic β_2 receptor agonists, dopexamine, inflammation, microcirculation, surgery

INTRODUCTION

Complications following major gastrointestinal surgery have a significant impact on both short and long-term survival (1–3). Inotropic agents may have important effects on outcomes for this patient group (4). Dopexamine is a dopamine analog with agonist activity at β_2-adrenoceptor and dopaminergic receptors. This spectrum of activity confers vasodilator actions in addition to chronotropic and mild inotropic effects (5). Dopexamine has been used to increase cardiac output and hence tissue oxygen delivery in several trials of peri-operative haemodynamic therapy (6, 7). Other cardiovascular effects of dopexamine may include improved tissue microvascular flow and oxygenation (8). Various groups have studied the effects of dopexamine in patients following major gastrointestinal surgery (6, 9), with promising results, although the findings of a recent large trial were inconclusive (7).

Investigators have previously demonstrated potent anti-inflammatory effects of β_2-adrenoceptor agonists (10–18), in particular dopexamine (19–22). However, it is unclear that β_2-adrenoceptor agonism is responsible for the dopexamine-dependent reduction of leucocyte-endothelial adhesion seen in several endotoxemia studies (19, 20). The findings of previous laboratory and clinical investigations suggest dopexamine may improve tissue microvascular flow and oxygenation (8, 19, 20, 23–26), and it is thought that these effects may account for much of the potential benefit of inotropic agents in the critically ill (27). However, in a previous laboratory study from our group, the haemodynamic actions of dopexamine infusion appeared to be less important than anti-inflammatory effects, including decreased plasma cytokine levels, modulation of neutrophil CD11b surface expression, and decreased pulmonary neutrophil infiltration (28). We sought to further clarify how leucocyte-endothelial adhesion under endotoxemia might relate to the β_2-adrenoceptor agonist effects of dopexamine, and its effects on arterial pressure, cardiac output and the microcirculation.

We therefore investigated the effects of dopexamine on leucocyte-endothelial adhesion within the microcirculation. Our hypothesis was that, in a rodent model of laparotomy and endotoxemia, dopexamine would decrease leucocyte-endothelial adhesion in intestinal post-capillary venules, through β_2-adrenoceptor mediated actions. The relative contribution of β_2-adrenoceptor agonism to these effects was assessed by using the β_2 adrenergic agonist salbutamol as a comparator.

MATERIALS AND METHODS

Thirty male Wistar rats (240–340 g) received a standard diet and water *ad libitum* before the experiments. All procedures were performed with institutional approval and in accordance with the United Kingdom Home Office Guidance on the Operation of the Animals (Scientific Procedures) Act 1986 under the project license PPL 70/6526. Anesthesia was induced by intra-peritoneal injection of thiopental (120 mg kg^{-1}) and maintained with supplementary injections administered according to regular testing for limb withdrawal to a standard stimulus. Animals were placed on a warming mat to maintain a core temperature of 37 ± 0.5°C. A tracheostomy was performed, following which a short section of polyethylene tubing (internal diameter, 1.67 mm) was inserted to maintain airway patency and to facilitate spontaneous respiration. The right carotid artery was cannulated to allow blood sampling and continuous monitoring of heart rate (HR) and mean arterial pressure (MAP). The left jugular vein was cannulated for drug and fluid administration.

A 2 cm midline incision was then made through the abdominal wall to expose the peritoneum. Following laparotomy, bowel was evacuated into a moist cotton receptacle. Blunt dissection was then performed to access the abdominal vasculature. After isolation from the vena cava, a 1.5 mm ultrasonic aortic transit time flow probe (MA1.5PRB; Transonic Systems Inc., Ithaca, USA) was placed on the infra-renal aorta to measure aortic blood flow allowing calculation of relative stroke volume and relative cardiac index. The bowel was then replaced in the abdominal cavity, except for a loop of ileum just proximal to the caecum. The exposed bowel was kept moist by the application of 0.9% saline drops through a pipette. The laparotomy incision above and below the exit of the terminal ileal loop from the abdomen was then closed with 5.0 vicryl to prevent excessive insensible fluid losses. The animal was maintained on a warming mat on an intravital microscopy platform and placed in the right lateral position so the ileal loop fell on to a raised section of the platform at the level of the laparotomy incision. The temperature of the raised section was thermostatically controlled at 37.5°C to ensure the temperature of the exposed bowel was similar to the core temperature. This position did not interfere with the ability of the ultrasonic probes to measure aortic blood flow. Subsequently the bowel was covered with Saran wrap to prevent evaporative losses from its surface and maintain bowel microvascular integrity (29). This was followed by a 5 ml kg^{-1} bolus of normal saline to replace insensible fluid losses and a 15 min stabilization period to allow microvascular flow to stabilize. A first set of arterial blood samples was then taken (see below), the volume being replaced with an equal volume of normal saline. Animals were allowed to stabilize for 15 min before being allocated randomly to one of five groups (sham, control, D0.5, D1, S).

Endotoxemia was induced over a 10 min period in four of five groups by administering 1 ml kg^{-1} of a solution containing Escherichia coli lipopolysaccharide 0111:B4 (LPS, 1 mg ml^{-1}) and peptidoglycan (PepG, 0.3 mg ml^{-1}) intravenously, the sham group received 0.9% saline vehicle alone. In all groups this was followed by an infusion of 0.9% saline at 4.3 ml kg^{-1} h^{-1} though different doses of dopexamine or salbutamol were added to the D0.5, D1, and S groups' infusion fluid. This resulted in dopexamine infusion rates of 0.5 and 1 μg kg^{-1} min^{-1} for groups D0.5 and D1, respectively, and a salbutamol infusion rate of 0.1 μg kg^{-1} min^{-1} in group S. This dose of salbutamol was selected as previous studies conducted in isolated guinea–pig tracheal preparations showed a 10-fold greater potency of salbutamol at the β_2-adrenoceptor when compared with dopexamine (30). Intravital microscopy in the intestinal ileum was performed after 150 min, midway through resuscitation. It was not possible to measure global hemodynamics during this procedure. The

experiment ended after 5 h of resuscitation when the heart and lungs were excised.

Analysis of Plasma Lactate, Base Deficit, and Renal and Hepatic Function

Two hundred microliter of blood was taken at baseline and at the end of the experiment for measurement of plasma lactate concentration (Accutrend Lactate; Roche Diagnostics, Basel, Switzerland) and base deficit (Radiometer ABL77, Copenhagen, Denmark). A 1ml blood sample was also taken at the end of the experiment for measurements of urea, creatinine, alanine aminotransferase, and aspartate aminotransferase by a commercial veterinary laboratory (IDEXX Laboratories Ltd, Sussex, UK).

MEASUREMENT OF AORTIC BLOOD FLOW

A 1.5 mm perivascular probe was applied with water-soluble sonicating gel and sited as described earlier. The probe was connected to a TS420 monitor (Transonic Systems Inc., Ithaca, USA), which was connected to a Powerlab/8SP monitoring system (AD Instruments). This allowed continuous recording of aortic blood flow and HR, and calculation of relative stroke volume and relative cardiac output (relative as infra-renal aortic blood flow is not equivalent to cardiac output). Aortic blood flow was indexed to body weight to provide a measure of changes in relative stroke volume index (SVI) and relative cardiac index (CI). Probe calibration was performed daily according to the manufacturer's instructions before experiments.

Intravital Microscopy (IVM)

Fifteen minutes before the midpoint of fluid resuscitation, 0.2 ml of 0.17 g L^{-1} rhodamine 6G (Sigma-Aldrich, Gillingham, UK) was administered intravenously to enhance the visibility of leucocytes. The animal platform was then transferred to the stage of an intravital microscope. Fluorescence microscopy was carried out using an Olympus BX61W1 microscope (Carl Zeiss Ltd.) connected to an Olympus BXUCB lamp, Uniblitz VCMD1 shutter driver and DG4-700 shutter instrument. Recordings were captured using Slidebook 5.0 software (Intelligent Imaging TTL) and saved for later offline analysis. All images were taken at x40 magnification. Leucocyte rolling and adhesion (>30 s stationary) was quantified in ileal post-capillary venules: the course of microvessels of the ileal submucosal layer was followed from collecting venules (V1) to postcapillary venules (V3), the latter being selected for analysis. Vessel length and diameter was measured and recorded. Images were recorded for a minimum of 40 s. A further 0.2 ml of 250 mg kg^{-1} ml^{-1} of FITC labeled bovine albumin (Sigma-Aldrich) was then administered intravenously in order to measure functional capillary density (FCD) and arteriolar diameters: the course of microvessels of the ileal submucosal layer was followed from supply arterioles (A1) to pre-capillary arterioles (A3), the latter being selected for analysis. Vessel diameter was measured and recorded. Capillaries were identified in the circular and longitudinal layers of the ileum and images were recorded for a minimum of 40 s. These images were later analyzed offline. The platform was then removed from the microscope stage and observations continued as before.

Recordings of intravital videos were stored electronically. These files were later analyzed offline using Slidebook 5.0 Reader [Intelligent Imaging Innovations (3i)] by an observer blinded to the experiment groups. Leucocyte adhesion was quantified and indexed to endothelial surface area (mm^2), calculated from the diameters and lengths of the vessel segments studied and assuming cylindrical vessel geometry. Firmly adherent leucocytes were defined as those that did not move or detach from the endothelial lining within an observation period of 30 s. FCD was calculated as the total length of perfused capillaries indexed to the visualized area (mm^{-1}).

Statistical Analysis

Data were presented as Mean (SEM) unless expressed otherwise and specifically. Kolmogorov-Smirnov normality testing was performed for all groups. Normally distributed data were tested using one-way analysis of variance (ANOVA) for comparison across all groups at a given time point. Post-testing was performed with Bonferroni's tests. Occasionally when ANOVA revealed significant results but post-tests did not indicate which group was responsible, *t*-tests (with or without Welch's correction depending on the variance of data) were performed to gain additional insight to the data. When data were not normally distributed in at least one group for any measurement, data were expressed as median (IQR) and the Kruskal-Wallis test was used in place of one-way ANOVA with Mann Whitney post-tests (and a Bonferroni correction). Two-tailed paired *t*-tests were used to compare hemodynamics at baseline with those at other time points for animals within the same group. Data were analyzed with PrismGraph 4.0 (GraphPad Software, San Diego, USA). Significance was set at $p < 0.05$.

RESULTS

Baseline characteristics and fluid management are described in (**Table 1** and **Supplementary Table 1**). There were no significant differences between groups regarding weight or volume of fluid received. Animals in the sham group required a slightly greater dose of thiopental to maintain anesthesia (**Supplementary Table 1**). There were no baseline differences in hemodynamics, base deficit, lactate or hematocrit. In the sham group, MAP and HR did not change significantly but CI and SVI increased progressively (**Table 1**, **Figure 1**, **Supplementary Table 1**, **Supplementary Figures 1, 2**). Compared with the sham group and baseline, controls had a significantly higher HR ($p < 0.05$) and a significantly lower SVI and CI at 5 h (**Table 1**, **Figure 1**, **Supplementary Figures 1, 2**). At this point control group plasma base deficit and lactate were increased compared with sham animals, the latter significantly ($p < 0.05$) (**Table 1**, **Supplementary Figure 3**). Compared to shams, there were more firmly adherent leucocytes (control: 703 $\pm$ 86 mm^{-2} vs. sham: 186 $\pm$ 68 mm^{-2}; $p < 0.001$), and fewer

TABLE 1 | Fluid administered, temporal changes in blood gas and haemodynamic parameters for each group ($n = 6$ all groups).

	Sham	Control	D 0.5	D1	S
Administered fluid (ml kg^{-1})	29.9 (29.2–30.5)	29.4 (29.3–29.5)	29.8 (29.4–30.5)	30.1 (29.4–30.5)	29.8 (29.4–30.4)
Baseline HR (bpm)	378 (357–421)	399 (379–417)	415 (390–420)	379 (356–441)	392 (370–423)
Baseline MAP (mmHg)	120 (7)	111 (3)	114 (5)	108 (3)	110 (6)
End experiment HR (bpm)	371 (8)***	447 (12)	465 (15)	478 (9)	445 (5)
End experiment MAP (mmHg)	114 (95–133)	93 (69–101)	81 (76–106)	94 (79–106)	78 (70–106)
End experiment lactate (mmol L^{-1})	1.7 (0.2)*	3.4 (0.5)	3.1 (0.3)	2.6 (0.4)	3.8 (0.3)
End experiment base deficit (mmol L^{-1})	−0.6 (1.0)	4.5 (1.6)	2.9 (1.5)	3.3 (1.5)	6.0 (1.0)
Mean change in SVI during experiment (ml kg^{-1})	0.044 (0.014)*	−0.036 (0.008)**	−0.050 (0.009)**	−0.054 (0.003)***	−0.020 (0.011)
Mean change in CI during experiment (ml min^{-1} kg^{-1})	15.3 (6.2)	−10.5 (3.2)*	−16.1 (4.2)*	−14.4 (2.0)***	3.0 (4.9)

There were no significant differences between groups in baseline hemodynamics or volumes of fluid administered. Over the course of the experiment in shams SVI significantly increased and CI also tended to increase, though HR and MAP did not change. In contrast HR significantly increased, while SVI and CI significantly decreased in control and dopexamine groups. MAP was significantly decreased, though this was not a consistent finding. HR also significantly increased in group S and although CI and SVI remained relatively stable MAP decreased significantly. A significantly lower lactate was seen in shams compared to controls. Data presented as mean (SEM) when all groups normally distributed, otherwise median (IQR) if ≥ 1 group not normally distributed. One-way ANOVA (post hoc Bonferroni's test, $^{*}p < 0.05$, $^{**}p < 0.01$, $^{***}p < 0.001$ vs. controls). Paired t-tests of baseline vs. end experiment for mean changes ($^{*}p < 0.05$, $^{**}p < 0.01$, $^{***}p < 0.001$).

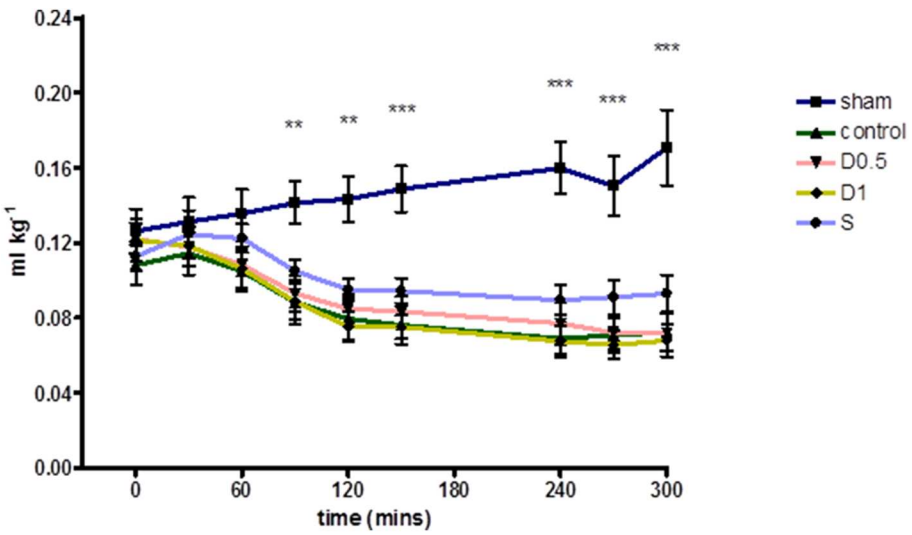

FIGURE 1 | Relative Stroke Volume Index during 5 h of laparotomy and endotoxemia recorded every 30 min. Values not plotted for t180–t210 [animals were undergoing IVM at this time and aortic flow and HR could not be measured (therefore relative SVI could not be calculated)]. Relative stroke volume index in controls differed significantly for most of the experiment and until its end when compared to shams. However, no significant differences in relative stroke volume index were observed between controls and groups treated with dopexamine or salbutamol at any time. The mean change in relative stroke volume index from baseline to end experiment was also significant in all groups except salbutamol treated animals (also see **Table 1**). Data presented as mean (SEM). One-way ANOVA at each time point (Bonferroni's post-tests, $^{**}p < 0.01$, $^{***}p < 0.001$ vs. controls).

rolling leucocytes in the post-capillary venules of control animals (**Figure 2**, **Supplementary Figure 4**). Intestinal arteriolar diameters were reduced in control animals [control: 21 ± 2 μm vs. sham: 39 ± 3 μm; $p < 0.01$; **Figure 2** (mid)] although FCD in the muscularis and its component circular and longitudinal layers did not differ significantly from shams [**Figure 2** (right), **Supplementary Figure 4**]. Endotoxemia was associated with acute kidney injury but not liver dysfunction (**Figure 3**).

Dopexamine infusion had no significant effect on any haemodynamic parameters when compared to

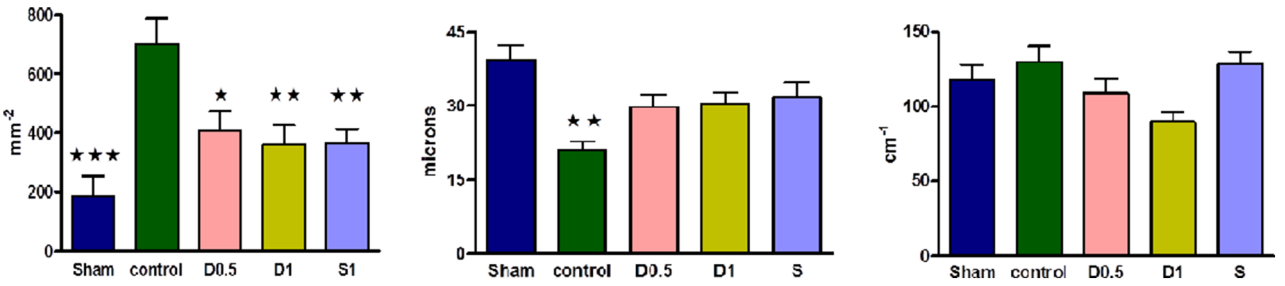

FIGURE 2 | (Left) Numbers of adherent leucocytes per square mm of endothelium in ileal post-capillary venules at 2.5 h of laparotomy and endotoxemia ($n = 6$ all groups). Numbers of vessels observed per group ranged from 8 to 18. Sham, dopexamine, and salbutamol treated groups demonstrated significantly less adhesion than controls. Data presented as mean (SEM). One-way ANOVA (Bonferroni's post-tests, $^{*}p < 0.05$, $^{**}p < 0.01$, $^{***}p < 0.001$ vs. controls). (Mid) Intestinal arteriolar diameters of the ileum at 2.5 h of laparotomy and endotoxemia ($n = 6$ all groups). Numbers of vessels measured per group ranged from 8 to 19. When compared to shams and unlike controls, ileal arteriolar diameters were not significantly reduced in dopexamine and salbutamol treated groups. Data presented as mean (SEM). One-way ANOVA (Bonferroni's post-tests, $^{**}p < 0.01$ vs. shams). (Right) Intestinal functional capillary density in longitudinal layers of the ileal muscularis at 2.5 h of laparotomy and endotoxemia ($n = 6$ all groups). Number of images per group ranged from 16 to 25. Groups were significantly different with respect to longitudinal FCD at 2.5 h. Data presented as mean (SEM). One-way ANOVA $p = 0.024$ (no groups positive in post-tests, although $p < 0.01$ when comparing control and D1 group with unpaired *t*-test with Welch's correction).

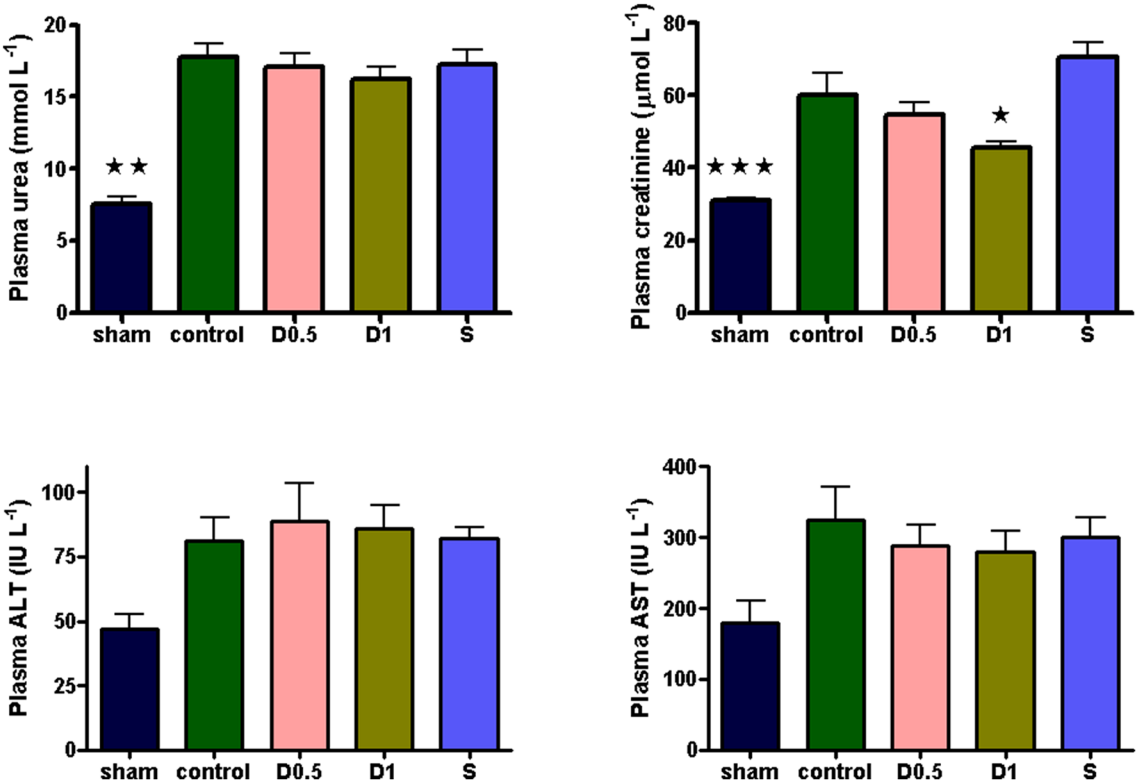

FIGURE 3 | Plasma urea, creatinine, ALT and AST sampled 5 h after laparotomy and endotoxemia ($n = 6$ all groups). 5 h of laparotomy and endotoxemia caused significant acute kidney injury in controls. The degree of injury was significantly less in the D1 group. All data presented as mean (SEM). Plasma urea and creatinine: One-way ANOVA (Bonferroni's post-tests, $^{*}p < 0.05$, $^{**}p < 0.01$, $^{***}p < 0.001$ vs. controls). ALT: One-way ANOVA, $p = 0.0246$ (no groups positive in post-tests).

controls, except for an increase in heart rate (**Table 1**, **Figure 1**, **Supplementary Table 1**, **Supplementary Figures 1, 2**). Similarly, dopexamine was not associated with any improvement in plasma lactate or base deficit in endotoxaemic animals (**Table 1**, **Supplementary Figure 3**). The major finding of this study was that at the mid-point of resuscitation dopexamine significantly reduced leucocyte adhesion in post-capillary venules when compared to controls (D0.5: 409 ± 65 mm^{-2}, $p < 0.05$ vs. control; D1: 361 ± 66 mm^{-2}, $p < 0.01$ vs. control) (**Figure 2**). Furthermore, dopexamine prevented the reduction in arteriolar diameter observed in control animals [**Figure 2** (mid)]. The effects of dopexamine on FCD were complex. There

were significant differences between groups in longitudinal muscle FCD (one-way ANOVA $p = 0.024$) [**Figure 2** (right)], but post-tests did not show which group was responsible for this difference. However, isolated *t*-tests comparing each group against controls reveal that only the D1 group had a significantly reduced longitudinal FCD compared to controls (unpaired *t*-test with Welch's correction, $p = 0.0034$). Dopexamine had no effect on FCD in the circular layer of the muscularis at any dose. When comparing total muscularis FCD for all groups, differences fell outside of the limits of statistical significance (one way ANOVA $p = 0.058$) (**Supplementary Figure 4**). Regarding organ function, renal function was improved in the D1 group compared to controls, but not the D0.5 animals (**Figure 3**).

The infusion of salbutamol was associated with a similar pattern of hemodynamics to those observed in dopexamine treated animals (**Table 1**, **Figure 1**, **Supplementary Table 1**, **Supplementary Figure 2**), and there was also no improvement in indices of tissue perfusion (**Supplementary Figure 3**). Compared to controls, salbutamol significantly reduced leucocyte-endothelial adhesion (S: 365 ± 49 mm^{-2}, $p < 0.01$ vs. control) (**Figure 2**). Salbutamol also appeared to prevent arteriolar vasoconstriction, but unlike dopexamine was not associated with any change in FCD in any layer of the muscularis [**Figure 2** (mid, right), **Supplementary Figure 4**] and had no effect on organ injury (**Figure 3**).

DISCUSSION

The principal findings of this experiment were that in a rodent model of laparotomy and endotoxemia, clinically relevant doses of dopexamine were associated with decreased leucocyte-endothelial adhesion and reduced arteriolar constriction in the intestinal microvasculature. However, with the exception of an increase in heart rate, dopexamine infusion was not associated with any systemic cardiovascular effects and in particular, relative cardiac index was not improved. In the higher dose dopexamine group an amelioration of renal dysfunction as assessed by plasma creatinine was observed. Almost all these findings were replicated by the β_2-adrenoceptor agonist salbutamol though salbutamol failed to improve renal function (28).

This study provides evidence that dopexamine modulates the inflammatory response by reducing leucocyte-endothelial adhesion. We have previously demonstrated that in addition to reducing the pro-inflammatory cytokine response, dopexamine may also reduce the expression of leucocyte surface integrins following endotoxemia. We have also previously demonstrated a reduction in neutrophil infiltration in the lung of dopexamine treated endotoxaemic rats (28). It is possible that these observations are linked, such that during endotoxemia, a dopexamine mediated reduction in surface integrin expression results in reduced leucocyte-endothelial adhesion and consequential neutrophil transmigration into the tissues. Although this experiment does not elucidate the cellular events that result in reduced leucocyte-endothelial adhesion, the similar effects of salbutamol suggest a β_2-adrenoceptor mediated mechanism. In this regard it has been shown that β_2- and non-β_2-adrenoceptor mediated elevations of cAMP reduce leucocyte adhesion (31, 32), whilst tonic activity of Protein Kinase A prevents β_2-integrin activation (33). Other factors including, but not limited to, an amelioration of pro-inflammatory cytokines or drug effects on vascular endothelium may be of equal or greater relevance to these observed changes. Furthermore, the relevance of reduced leucocyte-endothelial adhesion to the effect of dopexamine on organ function is also unclear because although salbutamol reduced leucocyte adhesion in post-capillary venules it did not ameliorate renal injury.

The reduction in arteriolar vasoconstriction by dopexamine is consistent with the preservation of arteriolar diameters in villus arterioles and hepatic sinusoids observed in previous endotoxemia studies with dopexamine. In those studies, dopexamine treated endotoxaemic animals had an associated preservation of total organ and microvascular blood flow compared to untreated groups (23, 26). However, in our previous study we observed a reduction in ileal red cell flux during endotoxemia (28). Assuming the same effect occurred in this study, then the similar muscularis FCD in control and sham animals suggests that any perfusion defect (assessed by FCD) must occur in the mucosa, as has been shown in other studies using intravital microscopy (34). The non-significant trend to reduction in longitudinal FCD in dopexamine treated animals may then indicate a dopexamine mediated re-distribution of blood from the outer layer of the ileum to the hypoxia prone mucosa. In this regard it is interesting to note that although salbutamol and dopexamine had similar effects on arteriolar diameters, salbutamol did not show any tendency to produce this effect on longitudinal layer FCD, did not improve renal function and showed no tendency to a reduced plasma lactate either. These differences, despite the similarity of effects otherwise, are notable and warrant further study.

Previous clinical studies in major surgery including those by our own group have emphasized the role of cardiovascular optimisation in enhancing tissue oxygen delivery to reduce peri-operative morbidity (7, 8). Early studies drove clinicians to suggest this approach was beneficial as it reduced potentially harmful tissue ischaemia (35). The importance of maintaining tissue perfusion is still supported by modern studies from peri-operative medicine where MAP is clamped at higher levels and shown to reduce the incidence of post-operative morbidity (36). This may also relate to improvements in microvascular perfusion (37). However, we previously showed in surgical patients kept to a narrow MAP range that peri-operative stroke-volume guided fluid management protocols with continuous 0.5 $\mu g\,kg^{-1}\,min^{-1}$ dopexamine infusion produced improvements in tissue oxygenation but without beneficial effects on markers of systemic inflammation or organ dysfunction (8). We also showed in a rodent model that dopexamine 1–2 $\mu g\,kg^{-1}\,min^{-1}$ brings about potent immunomodulatory effects that are associated with improved organ function despite MAP and microvascular flow being similar to controls (28). This suggests that under surgical conditions therapeutic benefit is achievable through modulation of the host response to tissue injury and that further increases in tissue oxygenation or blood flow when perfusion

is already guaranteed are redundant. In support of this, an analysis of surgical trials shows that patients with higher levels of baseline systemic inflammation are more likely to develop surgical complications (38). Similarly patients with impaired pre-operative microvascular function (who are known to have higher levels of inflammatory markers) are also more likely to suffer later complications (37, 39). Considering that previous studies have shown that surgical stress is associated with an upregulation of chemokines in the peritoneum and lungs, modulation of the host response to surgery becomes a potential explanation for the beneficial effects of dopexamine (40). However, the failure of salbutamol to improve renal function while producing a very similar spectrum of immune effects to dopexamine suggests that the mechanisms of renal protection with dopexamine are not necessarily only related to β_2-adrenoceptor mediated effects on leucocyte-endothelial adhesion.

Differential abilities of dopexamine and salbutamol to increase cellular cAMP may explain divergent effects on renal function (41). This might be the case if dopaminergic receptor activation by dopexamine further increased cAMP levels above that provided by β_2-adrenoceptor activation (5). The importance of increasing cAMP is that regulated cell death that causes tissue injury in acute kidney injury is inhibited by cAMP mediated-pathways, as is mitochondrial biogenesis which is required for enhanced recovery from cell stress (42, 43). On the other hand β_2-adrenoceptor activation has also been shown to alter systemic metabolism to increase tissue tolerance of injury (44). Therefore, unexpected differential effects of the drugs at β_2-adrenoceptors or in cAMP generation provide two mechanisms through which tissue damage can be minimized during the hours during and after emergency laparotomy and elective major abdominal surgery. This might also provide some explanation for the opposite findings in trials of β_2-adrenoceptor agonism in acute respiratory distress syndrome (45). In those trials a week long infusion of higher doses of salbutamol were used to try and improve outcomes through a reduction in extravascular lung water but resulted in increased mortality. On the other hand in peri-operative medicine shorter-term infusions of similar agents are used to try and minimize tissue damage and organ dysfunction that can result from major surgery—trials in this setting with dopexamine have not shown any signal to increased mortality (7).

Several findings of this study are consistent with previous investigations. The haemodynamic effects of endotoxemia with or without dopexamine were replicated here and are in keeping with other studies (20, 28). Findings of intestinal arteriolar constriction are in keeping with the intense splanchnic vasoconstriction and rapid reduction of blood flow seen following endotoxemia and shock in rodents (20, 28, 46). This study, in keeping with other studies, found arteriolar constriction could be ameliorated by dopexamine (23). Similar studies have found an increase in adherent leucocyte numbers in intestinal or mesenteric post-capillary venules that could be ameliorated by dopexamine (19, 20). A significant increase in adherent leucocytes (reduced by dopexamine) and a decrease in rolling leucocyte numbers in post-capillary venules at two and a half hours would likely have resulted in leukopenia, as found in other studies (19–23). However, some findings of the experiment reported here, such as the failure of endotoxemia to decrease longitudinal and circular muscularis functional capillary density are not consistent with previous studies (20). These inconsistencies are likely to be the result of differences in the endotoxin serotype, dose, method of administration and fluid loading conditions of each experiment. Our study also appears to contradict the findings of Schmidt et al. regarding the role of β_2-adrenoceptor agonism in leucocyte-endothelial adhesion (19). Importantly, our study design avoided the ablation of both endogenous and exogenous β_2–adrenoceptor agonism that may account for differences in findings between the two studies.

Our study has several strengths. The use of IVM gave qualitative and quantitative data that is unobtainable from laser Doppler flowmetry studies (20). The nature of endotoxemia was modified, using peptidoglycan, which increases the generalizability of these findings outside of Gram negative septicaemia alone. Although the duration and nature of endotoxemia differed from our previous study, the model behaved in a similar fashion to our previous study with respect to hemodynamics, markers of perfusion and resultant organ dysfunction. With respect to biochemical markers of tissue perfusion, it is possible that the lack of statistical significance in the D1 group where lactic acidosis and base deficit were less severe (as in our previous study) is the result of smaller sample sizes. If correct, it is notable that salbutamol neither showed any signal to an amelioration of plasma lactate nor resulted in any amelioration of renal dysfunction. This could suggest there are additional important mechanisms of action of reducing organ injury that dopexamine possesses (as discussed above).

There are also limitations to the study performed. Although there were many similarities with our previous experiments, fundamental differences in design mean that it is not possible to be certain that the models behaved in an identical fashion. Secondly, although the use of IVM permitted direct visualization of the intestinal microcirculation, expected differences in FCD were not seen between shams and controls. This may have related to the mild severity of the model (note no significant hepatic dysfunction was observed in any group), to visualizing the intestinal microcirculation too early in the course of the experiment or even to the volume of fluid administered. In this regard the inability to observe changes in the microvascular bed over the entire course of the experiment was a weakness of this study. Furthermore, although arteriolar diameters and muscularis FCD were observed, the inability to measure center-line red cell velocity, mucosal FCD and mucosal inflow arteriolar diameters prevents a complete picture of the distribution of intestinal blood flow being made. Although reductions in leucocyte-endothelial adhesion were observed, it is not possible to ascertain the relative importance of this phenomenon to the reduction in organ injury seen in this or previous experiments. Derivation of the surrogates relative stroke volume and relative cardiac index from infra-renal blood flow is recognized in the literature. Nevertheless, it should be noted that cardiac index may have differed between groups and the effects of different doses of vasoactive drugs may have led to differing organ blood flows above the level of measurement, none of which could

have been detected by an infra-renal flow probe. Regarding the use of dopexamine and salbutamol, dose equivalence was based on previous studies in isolated tracheal preparations (30). Although hemodynamics were similar between D1 and S groups suggesting the dose selection was probably correct, it is still not possible to be certain that the effect at the β_2-adrenoceptor was identical for both drugs. This may be compounded by the fact that salbutamol is a mix of two enantiomers, adding further complexity to the comparison. In this regard the use of a selective β_2-adrenoceptor antagonist to further disentangle the role of this drug effects will be useful in future studies. Finally, although the use of peptidoglycan increases the generalizability of these findings outside of Gram negative septicaemia, the choice of an endotoxin based model may still be criticized for lack of a true clinical correlate.

In summary, we present experimental evidence confirming that clinically relevant doses of dopexamine reduce leucocyte-endothelial adhesion in the intestinal microvasculature and are associated with improved renal function at clinically relevant doses. As a consequence of our experiments some avenues warrant further research. The relationship between β_2-adrenoceptor signaling and downstream effects on leucocyte CD11b expression, tissue tolerance mechanisms and inhibition of regulated cell death deserve further attention. The effect of dopexamine on microvascular recruitment and its relationship to cardiac index under differing fluid regimes and also the effect of dopexamine on the distribution of microvascular blood flows are two areas that also warrant further study given the disparity seen in results of our studies and others (8, 20, 23). Although peri-operative dopexamine use has been shown to be safe in randomized controlled trials and a Bayesian analysis of the OPTIMIZE trial suggested a high probability of superiority of treatment efficacy, a new randomized controlled trial of peri-operative optimisation using β_2-adrenoceptor agonists including dopexamine is underway and will inform clinicians definitively regarding the role of peri-operative dopexamine and haemodynamic optimisation (7, 47, 48).

DATA AVAILABILITY STATEMENT

The datasets generated for this study are available on request to the corresponding author.

ETHICS STATEMENT

The protocol was approved on 17/10/2011 under the project license number PPL 70/6526, by the AWERB (Animal Welfare and Ethical Review Body of Queen Mary University of London). All procedures were performed in accordance with the United Kingdom Home Office Guidance on the Operation of the Animals (Scientific Procedures) Act 1986.

AUTHOR CONTRIBUTIONS

MB carried out the *in vivo* studies and statistical analysis of all data. NP provided advice during *in vivo* studies and on study design. TA took offline measurements from intravital microscopy videos. CT participated in the design and coordination of the study and provided guidance throughout. RP conceived the study, participated in its design and co-ordination, and helped with statistical analysis. RP, CH, CT, and MB together drafted the manuscript. All authors read and approved the final manuscript.

FUNDING

This work was supported by research grants from a British Journal of Anaesthesia/Royal College of Anaesthetists Project Grant and an Intensive Care Society Young Investigator Award. NP was supported by a Kidney Research UK Post-Doctoral Fellowship (PDF4/2009). TA was supported by a jointly funded Medical Research Council and British Journal of Anaesthesia Clinical Research Training Fellowship. This work forms part of the research themes contributing to the translational portfolio of Barts and The London Cardiovascular Biomedical Research Unit, which was supported and funded by the National Institute of Health Research. RP is a National Institute for Health Research (UK) Research Professor.

SUPPLEMENTARY MATERIAL

The Supplementary Material for this article can be found online at: https://www.frontiersin.org/articles/10.3389/fimmu.2020.01001/full#supplementary-material

REFERENCES

1. Pearse RM, Moreno RP, Bauer P, Pelosi P, Metnitz P, Spies C, et al. Mortality after surgery in Europe: a 7 day cohort study. *Lancet*. (2012) 380:1059–65. doi: 10.1016/S0140-6736(12)61148-9
2. Khuri SF, Henderson WG, DePalma RG, Mosca C, Healey NA, Kumbhani DJ. Determinants of long-term survival after major surgery and the adverse effect of postoperative complications. *Ann Surg*. (2005) 242:326–41. doi: 10.1097/01.sla.0000179621.33268.83
3. Pearse RM, Holt PJ, Grocott MP. Managing perioperative risk in patients undergoing elective non-cardiac surgery. *BMJ*. (2011) 343:d5759. doi: 10.1136/bmj.d5759
4. Grocott MP, Dushianthan A, Hamilton MA, Mythen MG, Harrison D, Rowan K. Perioperative increase in global blood flow to explicit defined goals and outcomes after surgery: a cochrane systematic review. *Br J Anaesth*. (2013) 111:535–48. doi: 10.1002/14651858.CD004082.pub5
5. Bangash MN, Kong ML, Pearse RM. Use of inotropes and vasopressor agents in critically ill patients. *Br J Pharmacol*. (2012) 165:2015–33. doi: 10.1111/j.1476-5381.2011.01588.x
6. Pearse RM, Belsey JD, Cole JN, Bennett ED. Effect of dopexamine infusion on mortality following major surgery: individual patient data meta-regression analysis of published clinical trials. *Crit Care Med*. (2008) 36:1323–9. doi: 10.1097/CCM.0b013e31816a091b
7. Pearse RM, Harrison DA, MacDonald N, Gillies MA, Blunt M, Ackland G, et al. Effect of a perioperative, cardiac output-guided hemodynamic therapy algorithm on outcomes following major gastrointestinal surgery: a randomized clinical trial and systematic review. *JAMA*. (2014) 311:2181–90. doi: 10.1001/jama.2014.5305

8. Jhanji S, Vivian-Smith A, Lucena-Amaro S, Watson D, Hinds CJ, Pearse RM. Haemodynamic optimisation improves tissue microvascular flow and oxygenation after major surgery: a randomised controlled trial. *Crit Care*. (2010) 14:R151. doi: 10.1186/cc9220
9. Gillies MA, Shah AS, Mullenheim J, Tricklebank S, Owen T, Antonelli J, et al. Perioperative myocardial injury in patients receiving cardiac output-guided haemodynamic therapy: a substudy of the OPTIMISE Trial. *Br J Anaesth*. (2015) 115:227–33. doi: 10.1093/bja/aev137
10. Bowden JJ, Sulakvelidze I, McDonald DM. Inhibition of neutrophil and eosinophil adhesion to venules of rat trachea by beta 2-adrenergic agonist formoterol. *J Appl Physiol*. (1994) 77:397–405. doi: 10.1152/jappl.1994.77.1.397
11. Link A, Selejan S, Maack C, Lenz M, Bohm M. Phosphodiesterase 4-inhibition but not beta-adrenergic stimulation suppresses tumor necrosis factor-alpha release in peripheral blood mononuclear cells in septic shock. *Crit Care*. (2008) 12:R159. doi: 10.1186/cc7158
12. Wu CC, Liao MH, Chen SJ, Chou TC, Chen A, Yen MH. Terbutaline prevents circulatory failure and mitigates mortality in rodents with endotoxemia. *Shock*. (2000) 14:60–7. doi: 10.1097/00024382-200014010-00011
13. Wu JY, Liaw WJ, Tzao C, Chen SJ, Wang JH, Wu CC. Comparison of terbutaline and dobutamine in rats with endotoxemia. *Chin J Physiol*. (2002) 45:155–62.
14. Tsao CM, Chen SJ, Shih MC, Lue WM, Tsou MY, Chen A, et al. Effects of terbutaline on circulatory failure and organ dysfunction induced by peritonitis in rats. *Intens Care Med*. (2010) 36:1571–8. doi: 10.1007/s00134-010-1839-z
15. Liaw WJ, Tzao C, Wu JY, Chen SJ, Wang JH, Wu CC. Inhibition by terbutaline of nitric oxide and superoxide anion levels of endotoxin-induced organs injury in the anesthetized rat. *Shock*. (2003) 19:281–8. doi: 10.1097/00024382-200303000-00014
16. Nakamura A, Imaizumi A, Yanagawa Y, Kohsaka T, Johns EJ. beta(2)-Adrenoceptor activation attenuates endotoxin-induced acute renal failure. *J Am Soc Nephrol*. (2004) 15:316–25. doi: 10.1097/01.ASN.0000111247.76908.59
17. Nakamura A, Johns EJ, Imaizumi A, Yanagawa Y, Kohsaka T. beta(2)-adrenoceptor agonist suppresses renal tumour necrosis factor and enhances interleukin-6 gene expression induced by endotoxin. *Nephrol Dial Transplant*. (2000) 15:1928–34. doi: 10.1093/ndt/15.12.1928
18. Nakamura A, Niimi R, Yanagawa Y. Renal beta2-adrenoceptor blockade worsens the outcome of an induced Escherichia coli renal infection. *J Nephrol*. (2010) 23:341–9.
19. Schmidt W, Hacker A, Gebhard MM, Martin E, Schmidt H. Dopexamine attenuates endotoxin-induced microcirculatory changes in rat mesentery: role of beta2 adrenoceptors. *Crit Care Med*. (1998) 26:1639–45. doi: 10.1097/00003246-199810000-00012
20. Birnbaum J, Klotz E, Spies CD, Lorenz B, Stuebs P, Hein OV, et al. Effects of dopexamine on the intestinal microvascular blood flow and leukocyte activation in a sepsis model in rats. *Crit Care*. (2006) 10:R117. doi: 10.1186/cc5011
21. Jacinto SM, Lokhandwala MF, Jandhyala BS. Studies on the pharmacological interventions to prevent oxygen free radical (OFR)-mediated toxicity; effects of dopexamine, a DA1 receptor and beta 2 adrenoceptor agonist. *Naunyn Schmiedebergs Arch Pharmacol*. (1994) 350:277–83. doi: 10.1007/BF00175033
22. Oberbeck R, Schmitz D, Schuler M, Wilsenack K, Schedlowski M, Exton M. Dopexamine and cellular immune functions during systemic inflammation. *Immunobiology*. (2004) 208:429–38. doi: 10.1078/0171-2985-00290
23. Schmidt H, Secchi A, Wellmann R, Bach A, Bhrer H, Martin E. Dopexamine maintains intestinal villus blood flow during endotoxemia in rats. *Crit Care Med*. (1996) 24:1233–7. doi: 10.1097/00003246-199607000-00028
24. Lund N, de Asla RJ, Cladis F, Papadakos PJ, Thorborg PA. Dopexamine hydrochloride in septic shock: effects on oxygen delivery and oxygenation of gut, liver, and muscle. *J Trauma*. (1995) 38:767–75. doi: 10.1097/00005373-199505000-00016
25. Schmidt H, Weigand MA, Schmidt W, Plaschke K, Martin E, Bardenheuer HJ. Effect of dopexamine on intestinal tissue concentrations of high-energy phosphates and intestinal release of purine compounds in endotoxemic rats. *Crit Care Med*. (2000) 28:1979–84. doi: 10.1097/00003246-200006000-00049
26. Secchi A, Ortanderl JM, Schmidt W, Walther A, Gebhard MM, Martin E, et al. Effects of dobutamine and dopexamine on hepatic micro- and macrocirculation during experimental endotoxemia: an intravital microscopic study in the rat. *Crit Care Med*. (2001) 29:597–600. doi: 10.1097/00003246-200103000-00023
27. Uusaro A, Russell JA. Could anti-inflammatory actions of catecholamines explain the possible beneficial effects of supranormal oxygen delivery in critically ill surgical patients? *Intens Care Med*. (2000) 26:299–304. doi: 10.1007/s001340051153
28. Bangash MN, Patel NS, Benetti E, Collino M, Hinds CJ, Thiemermann C, et al. Dopexamine can attenuate the inflammatory response and protect against organ injury in the absence of significant effects on hemodynamics or regional microvascular flow. *Crit Care*. (2013) 17:R57. doi: 10.1186/cc12585
29. Horstick G, Kempf T, Lauterbach M, Ossendorf M, Kopacz L, Heimann A, et al. Plastic foil technique attenuates inflammation in mesenteric intravital microscopy. *J Surg Res*. (2000) 94:28–34. doi: 10.1006/jsre.2000.5990
30. Brown RA, Dixon J, Farmer JB, Hall JC, Humphries RG, Ince F, et al. Dopexamine: a novel agonist at peripheral dopamine receptors and beta 2-adrenoceptors. *Br J Pharmacol*. (1985) 85:599–608. doi: 10.1111/j.1476-5381.1985.tb10554.x
31. Bloemen PG, van den Tweel MC, Henricks PA, Engels F, Kester MH, van de Loo PG, et al. Increased cAMP levels in stimulated neutrophils inhibit their adhesion to human bronchial epithelial cells. *Am J Physiol*. (1997) 272(Pt. 1):L580–7. doi: 10.1152/ajplung.1997.272.4.L580
32. Derian CK, Santulli RJ, Rao PE, Solomon HF, Barrett JA. Inhibition of chemotactic peptide-induced neutrophil adhesion to vascular endothelium by cAMP modulators. *J Immunol*. (1995) 154:308–17.
33. Chilcoat CD, Sharief Y, Jones SL. Tonic protein kinase A activity maintains inactive beta2 integrins in unstimulated neutrophils by reducing myosin light-chain phosphorylation: role of myosin light-chain kinase and Rho kinase. *J Leukoc Biol*. (2008) 83:964–71. doi: 10.1189/jlb.0405192
34. Schmidt H, Secchi A, Wellmann R, Bach A, Bohrer H, Gebhard MM, et al. Effect of endotoxemia on intestinal villus microcirculation in rats. *J Surg Res*. (1996) 61:521–6. doi: 10.1006/jsre.1996.0157
35. Shoemaker WC. Relation of oxygen transport patterns to the pathophysiology and therapy of shock states. *Intens Care Med*. (1987) 13:230–43. doi: 10.1007/BF00265111
36. Futier E, Lefrant JY, Guinot PG, Godet T, Lorne E, Cuvillon P, et al. Effect of individualized vs standard blood pressure management strategies on postoperative organ dysfunction among high-risk patients undergoing major surgery: a randomized clinical trial. *JAMA*. (2017) 318:1346–57. doi: 10.1001/jama.2017.14172
37. Jhanji S, Stirling S, Patel N, Hinds CJ, Pearse RM. The effect of increasing doses of norepinephrine on tissue oxygenation and microvascular flow in patients with septic shock. *Crit Care Med*. (2009) 37:1961–6. doi: 10.1097/CCM.0b013e3181a00a1c
38. Ackland GL, Abbott TEF, Cain D, Edwards MR, Sultan P, Karmali SN, et al. Preoperative systemic inflammation and perioperative myocardial injury: prospective observational multicentre cohort study of patients undergoing non-cardiac surgery. *Br J Anaesth*. (2019) 122:180–7. doi: 10.1016/j.bja.2018.09.002
39. Taqueti VR, Ridker PM. Inflammation, coronary flow reserve, and microvascular dysfunction: moving beyond cardiac syndrome X. *JACC Cardiovasc Imaging*. (2013) 6:668–71. doi: 10.1016/j.jcmg.2013.02.005
40. van Till JW, van Veen SQ, den Broeder V, Bresser P, Lutter R, Out TA, et al. Compartmental apoptosis and neutrophil accumulation in severe peritonitis. *J Surg Res*. (2010) 164:321–8. doi: 10.1016/j.jss.2009.09.020
41. Brunskole Hummel I, Reinartz MT, Kalble S, Burhenne H, Schwede F, Buschauer A, et al. Dissociations in the effects of beta2-adrenergic receptor agonists on cAMP formation and superoxide production in human neutrophils: support for the concept of functional selectivity. *PLoS ONE*. (2012) 8:e64556. doi: 10.1371/journal.pone.0064556
42. Chen R, Zeng L, Zhu S, Liu J, Zeh HJ, Kroemer G, et al. cAMP metabolism controls caspase-11 inflammasome activation and pyroptosis in sepsis. *Sci Adv*. (2019) 5:eaav5562. doi: 10.1126/sciadv.aav5562
43. Arif E, Nihalani D. Beta2-adrenergic receptor in kidney biology: a current prospective. *Nephrology*. (2019) 24:497–503. doi: 10.1111/nep.13584
44. Luan HH, Wang A, Hilliard BK, Carvalho F, Rosen CE, Ahasic AM, et al. GDF15 Is an inflammation-induced central mediator of tissue tolerance. *Cell*. (2019) 178:1231–44 e11. doi: 10.1016/j.cell.2019.07.033
45. Gao Smith F, Perkins GD, Gates S, Young D, McAuley DF, Tunnicliffe W, et al. Effect of intravenous beta-2 agonist treatment

on clinical outcomes in acute respiratory distress syndrome (BALTI-2): a multicentre, randomised controlled trial. *Lancet*. (2012) 379:229–35. doi: 10.1016/S0140-6736(11)61623-1

46. Toung T, Reilly PM, Fuh KC, Ferris R, Bulkley GB. Mesenteric vasoconstriction in response to hemorrhagic shock. *Shock*. (2000) 13:267–73. doi: 10.1097/00024382-200004000-00003
47. Ryan EG, Harrison EM, Pearse RM, Gates S. Perioperative haemodynamic therapy for major gastrointestinal surgery: the effect of a Bayesian approach to interpreting the findings of a randomised controlled trial. *BMJ Open*. (2019) 9:e024256. doi: 10.1136/bmjopen-2018-024256
48. Edwards MR, Forbes G, MacDonald N, Berdunov V, Mihaylova B, Dias P, et al. Optimisation of perioperative cardiovascular management to improve surgical outcome II (OPTIMISE II) trial: study protocol for a multicentre international trial of cardiac output-guided fluid therapy with low-dose inotrope infusion compared with usual care in patients undergoing major elective gastrointestinal surgery. *BMJ Open*. (2019) 9:e023455. doi: 10.1136/bmjopen-2018-023455

Conflict of Interest: RP has received equipment loans from LiDCO Ltd and has performed consultancy work for Edwards Lifesciences and Massimo Inc. RP is a member of the associate editorial board of the British Journal of Anaesthesia. CT is CEO of William Harvey Research Limited, which is a CRO and has conducted contracted research in the area of critical care. CT is also Senior Associate Editor for the journal Shock.

The remaining authors declare that the research was conducted in the absence of any commercial or financial relationships that could be construed as a potential conflict of interest.

Copyright © 2020 Bangash, Abbott, Patel, Hinds, Thiemermann and Pearse. This is an open-access article distributed under the terms of the Creative Commons Attribution License (CC BY). The use, distribution or reproduction in other forums is permitted, provided the original author(s) and the copyright owner(s) are credited and that the original publication in this journal is cited, in accordance with accepted academic practice. No use, distribution or reproduction is permitted which does not comply with these terms.

frontiers in Immunology

ORIGINAL RESEARCH
published: 07 July 2020
doi: 10.3389/fimmu.2020.01415

Csf2 Attenuated Sepsis-Induced Acute Kidney Injury by Promoting Alternative Macrophage Transition

Yiming Li[1], *Pan Zhai*[2], *Yawen Zheng*[3], *Jing Zhang*[1], *John A. Kellum*[4] *and Zhiyong Peng*[1,4]*

[1] Department of Critical Care Medicine, Zhongnan Hospital of Wuhan University, Wuhan, China, [2] Department of Neurology, Hubei Province Hospital of Tradition Chinese Medicine, Wuhan, China, [3] Department of Urological Organ Transplantation, The Second Xiangya Hospital of Central South University, Changsha, China, [4] Center of Critical Care Nephrology, Department of Critical Care Medicine, University of Pittsburgh School of Medicine, Pittsburgh, PA, United States

OPEN ACCESS

Edited by:
Lukas Martin,
University Hospital RWTH Aachen, Germany

Reviewed by:
Basilia Zingarelli,
Cincinnati Children's Hospital Medical Center, United States
Zoltan Nemeth,
Morristown Medical Center, United States

***Correspondence:**
Zhiyong Peng
zn001590@whu.edu.cn

Specialty section:
This article was submitted to Inflammation, a section of the journal Frontiers in Immunology

Received: *22 November 2019*
Accepted: *02 June 2020*
Published: *07 July 2020*

Citation:
Li Y, Zhai P, Zheng Y, Zhang J, Kellum JA and Peng Z (2020) Csf2 Attenuated Sepsis-Induced Acute Kidney Injury by Promoting Alternative Macrophage Transition. Front. Immunol. 11:1415. doi: 10.3389/fimmu.2020.01415

Sepsis is a systemic inflammatory state that occurs in response to infection and significantly increases mortality in combination with acute kidney injury (AKI). Macrophages accumulate in the kidney after injury and undergo a transition from a proinflammatory (M1) phenotype to an alternatively activated (M2) phenotype that is required for normal repair. However, the specific signals that regulate the transition from the M1 to M2 phenotype *in vivo* are unknown. Here, we found an unexpected role of Colony stimulating factor 2 (Csf2) in controlling macrophage transition *in vitro* and in a mouse model of sepsis induced by cecal ligation and puncture (CLP). We first co-cultured human M1 macrophages with HK-2 cells and characterized cytokine/chemokine profiles via Luminex. Of the cytokines and chemokines that were overexpressed in medium from M1 macrophages cocultured with human kidney-2 (HK-2) cells compared with that from M1 macrophages cultured alone, Csf2 and IL6 showed the greatest increases. Csf2 was exclusively secreted by HK-2 cells but not by M1 macrophages. Furthermore, recombinant human Csf2 protein promoted transition of M1 macrophages to the M2 phenotype in a dose and time-dependent manner. The apoptosis and reactive oxygen species (ROS) release induced by M1 macrophages in HK-2 cells was attenuated after exposure to exogenous Csf2. In addition, the switch from the proinflammatory M1 phenotype to the M2 phenotype occurred via the p-Stat5 pathway, which was activated by Csf2. Importantly, we found that intraperitoneal injection of a Csf2-neutralizing antibody after CLP aggravated kidney injury and suppressed tubular proliferation, subsequently decreasing survival. However, administration of recombinant mouse Csf2 protein could rescue mice with sepsis. Together, our results indicate that Csf2 plays critical roles in regulating macrophage transition via activation of p-STAT5. These data form a foundation upon which new therapeutic strategies can be designed to improve the therapeutic efficacy of cytokine-based treatments for sepsis-induced AKI.

Keywords: sepsis, acute kidney injury, macrophage transition, Csf2, cytokine-based therapy

INTRODUCTION

Sepsis is a complex clinical syndrome characterized by a systemic inflammatory response to infection. Acute kidney injury (AKI) is one of the most frequent and serious complications and contributes to high mortality. Up to 60% of cases with sepsis are complicated with AKI, and approximately half of AKI cases are related to sepsis (1–3). The disease burden from AKI results in an estimated $10 billion of additional costs for the health care system in the United States (4), and severe AKI is associated with a mortality of 45–70% (2, 5–7).

Pathogen-associated molecular patterns (PAMPs) activate resident macrophages and kidney parenchymal cells, leading to the secretion of proinflammatory cytokines and chemokines that cause nonspecific tissue damage (8). An excessive inflammatory response and oxidative stress are considered to be the main mechanisms of septic AKI (9). Kidney monocytes have been implicated in pathogenesis and healing in mouse models of AKI; these cells infiltrate the injured kidney shortly after neutrophils in the early stage of injury, differentiate into macrophages, and contribute to tissue injury (10). Various experimental models suggest that extended inflammatory macrophage activation augments inflammation. Increased inflammatory cell infiltration and cytokine/chemokine release contribute to AKI (11), and many of these proinflammatory mediators can trigger cell death pathways. Furthermore, the removal of these activated cells and cytokines results in improved survival (12).

Indeed, prolonged inflammatory activity results in further tissue damage, ultimately inhibiting the reparative phase of injury resolution (13). The inflammatory milieu is reversed by the actions of reparative cells via secretion of anti-inflammatory cytokines and pro-proliferative signals. In disease states and injury, macrophages expand and play distinct but important roles in the immune response. They acquire a spectrum of phenotypes that range from highly inflammatory at the beginning of disease to highly reparative toward the resolution of injury. M1 macrophages exacerbate injury by producing proinflammatory cytokines (14), resulting in the recruitment of other inflammatory cells (15). M1 macrophages also secrete antipathogenic molecules, such as NO generated by inducible nitric oxide synthase (iNOS) and ROS, both of which can also induce mitochondrial damage and apoptosis (16). Activated M2 macrophages recognize and downregulate high levels of inflammatory proteins. M2 macrophages also promote the deposition of extracellular matrix by producing arginase, and they inhibit inflammatory immune cell activity via the secretion of resolvents, lipoxins, matrix metalloproteinases, and TGFβ, which target and cleave chemokines and chemoattractants (17). Moreover, depletion of macrophages in the reparative stages results in a significant increase in kidney injury biomarkers (18). However, these two disparate roles of macrophages, from inflammation and injury in the early stage to tissue repair and remodeling in the recovery stage, remain to be further studied. Therefore, identification of the trigger that promotes the transformation from the M1 phenotype to the M2 phenotype may provide therapeutic targets to relieve inflammation and promote tissue repair.

In this study, we showed that macrophage polarization from M1 to M2 in the kidney promotes repair and attenuates septic AKI. M1 macrophages were cocultured with human kidney cells to assess the interaction between these two cell types. Csf2 secreted by kidney tubular cells promoted the repair of tubular cell injury by inducing M0/M1-to-M2 transformation *in vitro*. To further determine how tubular cells promote M2 transformation, we examined the JAK-p-STAT5 pathway in cultured macrophages. Finally, a neutralizing Csf2 antibody and recombinant Csf2 protein were injected intraperitoneally to evaluate alternative macrophage activation and tubular cell injury during the repair stage after AKI. These findings not only address our knowledge gaps regarding the detrimental roles of M1 in AKI but also identify an unexpected role of Csf2 in regulating M1-to-M2 transformation. Modulating Csf2 signaling could improve the therapeutic efficacy of cytokine-based therapies in septic AKI.

MATERIALS AND METHODS

Cell Culture

The human kidney-2 (HK-2) and THP-1 cell lines were purchased from the Cell Bank of the Chinese Academy of Sciences. We followed the cell culture methods of Li et al. (19). Then, 10 μg/mL LPS (Sigma, L3129) was used to treat HK-2 cells for 18 h. Next, 100 nM phorbol-12-myristate-13-acetate (PMA) was applied to induce THP-1 cell differentiation into M0 macrophages. As shown in **Figure 1A**, different methods were used to promote M1 or M2 differentiation. For the coculture experiments, the LPS-treated HK-2 cells were washed with PBS and then cocultured with M1 or M0 macrophages in 5% fetal bovine serum (FBS)-containing medium for several additional days. The Transwell chambers (0.4 μm pore size) used for coculture were purchased from Thermo Fisher. HLA-DR is a marker of M1 macrophages. CD206, CD163 and IL-10 are M2 markers. CD68 is usually used to label M0 macrophages.

Cytokine and Chemokine Assays

Multiplex kits for measuring cytokines and chemokines were purchased from Bio-Rad (Austin, TX, USA). Plates were measured and analyzed with Bio-Plex Manager version 6.1 (Luminex, Austin, TX, USA), sold by Wayen Biotechnologies, Inc. (Shanghai, China). The 27-plex cytokine panel and 40-plex chemokine panel kits were used to measure the concentrations of cytokines and chemokines in the supernatant. Twelve cytokines overlapped between these two detection kits.

Cell Viability Assays

M1 macrophages were treated with recombinant human Csf2 (215-GM-050, Novus, USA). Cell viability was then tested with a Cell Counting Kit 8 (Dojindo Molecular Technologies, Japan) at 48 h after coculture. The absorbance at 450 nm was measured using a Thermo Scientific Microplate Reader.

Flow Cytometry Assay

At 48 h after coculture with M1 macrophages for 48 h, HK-2 cells were collected. The cells were fixed with 70% ethanol. The

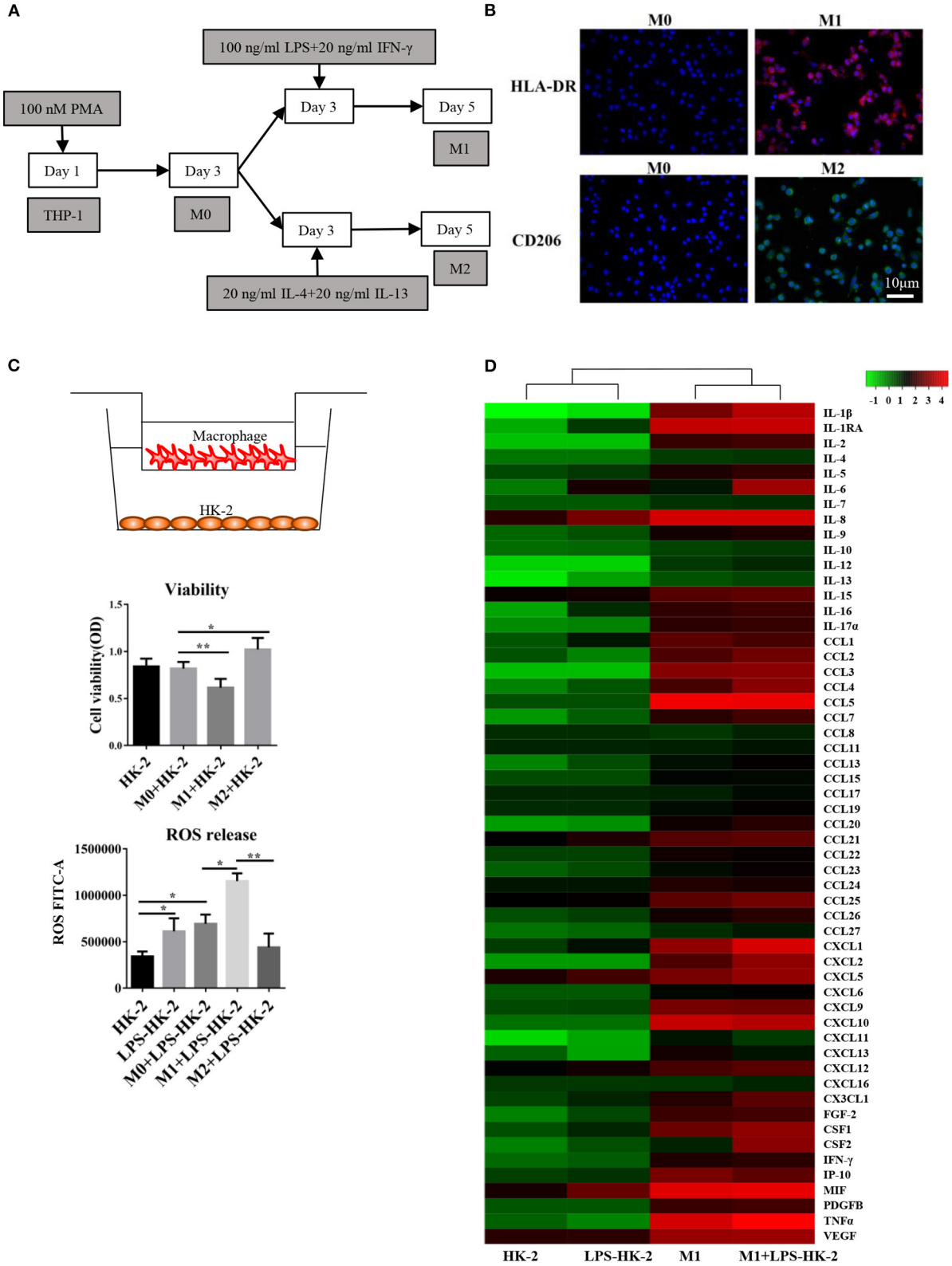

FIGURE 1 | Differentiation and cytokine profiles of M1 macrophages. **(A)** Schematic diagram showing the *in vitro* differentiation of THP-1 cells into M1 and M2 macrophages. **(B)** Images show HLA-DR (red, M1 marker) and CD206 (green, M2 marker) expression after differentiation. DAPI was used to counterstain nuclei.

(Continued)

FIGURE 1 | Slides were directly visualized using an Olympus fluorescence microscope at a 20X magnification, scale bar = 20 μm. Representative images were from two independent experiments. **(C)** M0/M1/M2 macrophages were plated on 0.4 mm Transwell inserts and grown over a 2-day period. HK-2/LPS-HK2 cells were plated in 24-wells. The HK-2 cells were subjected to a viability assay. ROS release was detected in HK-2 cells by flow cytometry. LPS-HK2 cells were pretreated with LPS. Data are represented as the mean ± SD from $n = 3$ experiments. The significance of differences was tested using Student's *t*-test. $^{*}p < 0.05$ and $^{**}p < 0.01$. **(D)** Cytokines and chemokines in the supernatant after HK-2/LPS-HK-2/M1 culture or M1+ LPS-HK-2 coculture were assessed with a 27-plex cytokine panel and a 40-plex chemokine panel. Twelve cytokines overlapped between these two detection kits. Fifty-five cytokines and chemokines are shown in the heatmap. The Z-score was used to depict the variation between different samples. The culture media were pooled from three experiments and then subjected to Luminex.

fixed cells were washed with PBS and then treated with DCFH-DA according to the Reactive Oxygen Species Assay Kit (Yeasen, Shanghai, China). In the apoptosis experiment, Annexin V-FITC/PI (Annexin V-FITC/PI Apoptosis Detection Kit, Yeasen, Shanghai, China) was used to label apoptotic cells. The stained cells were analyzed using a Becton Dickinson flow cytometer (Franklin Lakes, NJ).

Cell Migration Assays

Transwell chambers (8-μm pore size, Corning, USA) were used to perform the cell migration assays. M1 macrophages (2×10^5) were seeded in the insert of the chamber. After coculture with LPS-treated HK-2 cells for 48 h, cells that migrated to the lower surface were stained with crystal violet (Sigma-Aldrich, St. Louis, MO) and photographed.

ELISA

TIMP2 and Csf2 levels in the cell culture supernatant were measured with an ELISA kit (Bio-Swamp Life Science, Shanghai, China) according to the manufacturer's instructions. To detect IL-10 and TNF-α in kidney tissues, the kidney cortex was homogenized, and the protein concentration was determined using the Coomassie blue method. IL-10 and TNF-α levels in tissue and cell culture supernatant were measured with ELISA kits. Each sample was measured in triplicate.

RNA Extraction and qRT-PCR

Total RNA was extracted from HK-2 cells, macrophages and kidney tissues using the YPH EASY spin tissue/cell RNA quick extraction kit (YPH, Beijing, China). Furthermore, cDNA was synthesized with the ReverTra Ace Kit (Toyobo, Osaka, Japan). The SYBR Green real-time polymerase chain reaction (PCR) kit was used to detect the expression of target mRNA. The human primer sequences were as follows: Csf2 sense, 5′-TAC CTTTGTTGCAGCTGCTG−3′, and anti-sense, 5′-CACCACCC ACTGTTCGCTG−3′; CD163 sense, 5′-TTTGTCAACTTGAGT CCCTTCAC−3′, and anti-sense, 5′-TCCCGCTACACTTGTTT TCAC−3′; and IL10 sense, 5′-GACTTTAAGGGTTACCTGGG TTG−3′, and anti-sense, 5′-TCACATGCGCCTTGATGTCTG-3′. The mouse primer sequences were as follows: Csf2 sense, 5′-GGCCTTGGAAGCATGTAGAGG-3′, and anti-sense, 5′-GG AGAACTCGTTAGAGACGACTT−3′; CD163 sense, 5′-ATGG GTGGACACAGAATGGTT-3', and anti-sense, 5′-CAGGAGCG TTAGTGACAGCAG-3'; and IL10 sense, 5′-GCTCTTACTGA CTGGCATGAG-3′, and anti-sense, 5′-CGCAGCTCTAGGAG CATGTG-3′.

Western Blot Analysis

The cells or kidney tissues were lysed, and lysates were prepared. Membranes were incubated with primary Abs specific for the following proteins: Csf2 (Abcam, ab54429), CD206 (Proteintech, 18704-1-AP), ARG1 (Proteintech, 16001-1-AP), t-Stat5 (Abcam, ab227687), p-STAT5 (Cell Signaling Technology, mAb #4322), and Jak2 (Proteintech, 17670-1-AP). Anti-glyceraldehyde 3-phosphate dehydrogenase (GAPDH, Proteintech, 60004-1-Ig) was used as a loading control.

Immunofluorescence

Immunofluorescence staining of the kidney was performed using paraffin or frozen sections as previously described (19). The sections were incubated with HLA-DR and CD206 antibodies (1:100). The slides were then exposed to a Cy3-conjugated secondary antibody for HLA-DR (red) and a fluorescein isothiocyanate (FITC)-conjugated secondary antibody for CD206 (green). The sections were visualized using fluorescence microscopy (Olympus, Tokyo, Japan).

Sepsis-Induced CLP Model

C57BL/6 mice (male, 10–12 weeks old) were subjected to CLP to induce sepsis as previously described (20). Briefly, the animals were anesthetized with isoflurane. Under aseptic conditions, a 2-cm midline laparotomy was created below the diaphragm to expose the caecum. The cecum was ligated at the middle with a 5-0 silk suture and punctured twice with a 22-gauge needle. The caecum was then squeezed gently to extrude a small amount of feces through the perforation site. Animals were resuscitated with 1 ml of saline subcutaneously (s.c.) after CLP. We followed the methods of Li et al. (19). To minimize variability across experiments, the CLP procedure was always performed by the same investigator. All experiments were performed in accordance with the Animal Care and Use Committee of Wuhan University.

Csf2 Antibody and Csf2 Protein Administration to Mice

For Csf2 neutralization experiments, five doses of 300 mg of anti-mouse Csf2-neutralizing antibody (BioXcell, BE0259-5MG) (13) or rat IgG isotype control (BioXcell, BE0089-5MG) in 100 μl of PBS were injected intraperitoneally daily starting 24 h after CLP. For rescue experiments, recombinant mouse Csf2 protein (2.5 μg/mouse/d, NOVUS) (21) in 100 μl of PBS was intraperitoneally administered five times after CLP. We used the 7-day survival rate as the endpoint for our survival study.

Evaluation of Renal Function

Mice were sacrificed at 48 h following Csf2 antibody or Csf2 protein administration. Heparinized blood was centrifuged to separate the plasma. Serum creatinine (Scr) and blood urea nitrogen (BUN) were detected using commercial kit reagents (Institute of Jiancheng Bioengineering, Nanjing, China).

H&E Staining

Kidneys were fixed in a 10% buffered formaldehyde solution. The tissue was processed routinely and paraffin embedded. Paraffin blocks were cut using a microtome at a thickness of 4 μm, and the sections were deparaffinized, hydrated, and stained with hematoxylin and eosin (H&E). Photomicrographs were obtained randomly from the kidney renal cortex.

TUNEL Assay and Immunohistochemistry

Forty-eight hours following Csf2 antibody or Csf2 protein administration, kidney tissues were harvested and fixed with 4% paraformaldehyde for 30 min at room temperature. The TUNEL assay was performed using a TUNEL Apoptosis Detection Kit (Yeason, Shanghai, China) according to the manufacturer's instructions. Briefly, 4-μm kidney sections were deparaffinized and rehydrated. Then, the sections were incubated with TUNEL reagent mixture for 30 min at room temperature and washed with PBS three times for 5 min each time. 4′,6-Diamidino-2-phenylindole was used to stain nuclei. For immunohistochemistry, a Ki67 antibody (Proteintech, 27309-1-AP) was used to stain the tissue sections. The numbers of total cells and Ki67+ cells were determined.

Statistical Analysis

All tests were analyzed with SPSS version 20.0 or GraphPad Prism 8.0. Student's *t*-test was used for comparisons between the two groups. Survival data were analyzed using the log-rank test. In all comparisons, $P < 0.05$ indicated statistical significance. The data are presented as the mean and standard deviation.

RESULTS

Changes in Cytokines/Chemokines Produced by Macrophages and HK-2 in Response to LPS

An *in vitro* model based on differentiation of the THP-1 human monocyte cell line into M1 or M2 macrophages was first established. THP-1 cells grew in suspension with a rounded morphology, and they became attached to the plate in the presence of PMA. The schematic diagram shows that THP-1 cells differentiated into M1 and M2 macrophages (**Figure 1A**). Immunofluorescence staining for the macrophage markers HLA-DR (M1 marker) and CD206 (M2 marker) was used to confirm the phenotype of these macrophages. After LPS and IFN-γ treatment, the macrophages expressed high levels of HLA-DR (M1, red), while exposure to IL4 and IL13 resulted in the expression of CD206 (M2) (**Figure 1B**). Following activation, M0, M1 or M2 macrophages were cocultured with HK-2 cells pretreated with LPS for 18 h. Cell viability of HK-2 cells was significantly higher after coculture with M2 macrophages and lower after coculture with M1 macrophages. Similarly, the release of ROS was increased in the M1+ LPS-HK2 group compared to the M0+ LPS-HK2 group (**Figure 1C**).

Macrophages at various tissue sites have different cytokine profiles (22). Thus, we first measured a panel of 55 cytokines and chemokines in conditioned medium (**Figure 1D**). The absolute value of cytokines and chemokines were shown in **Supplementary Table 1**. Most proinflammatory cytokines, such as IL8 and MIF, were increased in HK-2 cells after exposure to LPS. Moreover, CXCL1, IL-1β and tumor necrosis factor (TNF) α were secreted at higher levels by M1 macrophages cocultured with HK-2 cells than by M1 macrophages cultured alone. Of the cytokines and chemokines that were overexpressed in medium from M1 + LPS-HK-2 cultures compared with medium from M1 macrophages cultured alone, IL-6 and Csf2 showed the greatest increases (147.5- and 114.3-fold, respectively, for M1 + LPS-HK-2 vs. M1). The changes in cytokine profiles between M1 macrophages cultured alone and macrophages cocultured with LPS-HK-2 cells confirmed that crosstalk existed between macrophages and HK-2 cells. These cytokine and chemokine array results also indicated that several cytokines might regulate the differentiation of macrophages. Csf2 was reported to facilitate the development of the immune system and promote defense against infections (23). These results indicate that macrophages interacted with kidney cells and that Csf2 was increased in the coculture medium.

Csf2 Was Derived Exclusively From HK-2 Cells and Decreased HK-2 Cell Apoptosis

Csf2 is considered a mediator by which T cells communicate with myeloid populations during tissue inflammation (24). To verify the specific role of Csf2 in sepsis, exogenous Csf2 was added to the medium in the M1 macrophage and HK-2 cell coculture system. The viability of HK-2 cells was decreased after exposure to M1 macrophages. However, additional Csf2 treatment rescued the viability of HK-2 cells (**Figure 2A**). The apoptosis rate was assayed to determine the antiapoptotic effect of Csf2. The total apoptosis percentage, including early apoptosis (Annexin V-positive and PI-negative) and late apoptosis (Annexin V and PI double-positive), of HK-2 cells was increased in the M1 + LPS-HK-2 group (10.49% vs. 18.18%, LPS-HK-2 vs. M1 + LPS-HK-2), but the apoptosis percentage decreased to 7.76% after exposure to additional Csf2 (**Figure 2B**). Next, the Transwell assay was performed to investigate the ability of Csf2 to attract M1 macrophages. Fewer M1 macrophages migrated toward the HK-2 cells when Csf2 was added to the medium (**Figure 2C**). Moreover, the concentration of TIMP-2, a biomarker of kidney cell stress, was also reduced (**Figure 2D**). We next measured the concentration of Csf2 in this coculture system. We found that Csf2 secretion increased significantly in a time-dependent manner (**Figure 2E**). This increased Csf2 could be derived from either HK-2 cells, M1 macrophages, or both. To determine the source of Csf2, qRT-PCR was performed to detect the relative expression of Csf2 in HK-2 cells and M1 macrophages. Interestingly, Csf2 was mainly secreted by HK-2 cells but not M1 macrophages (**Figures 2F,G**). This increase in Csf2

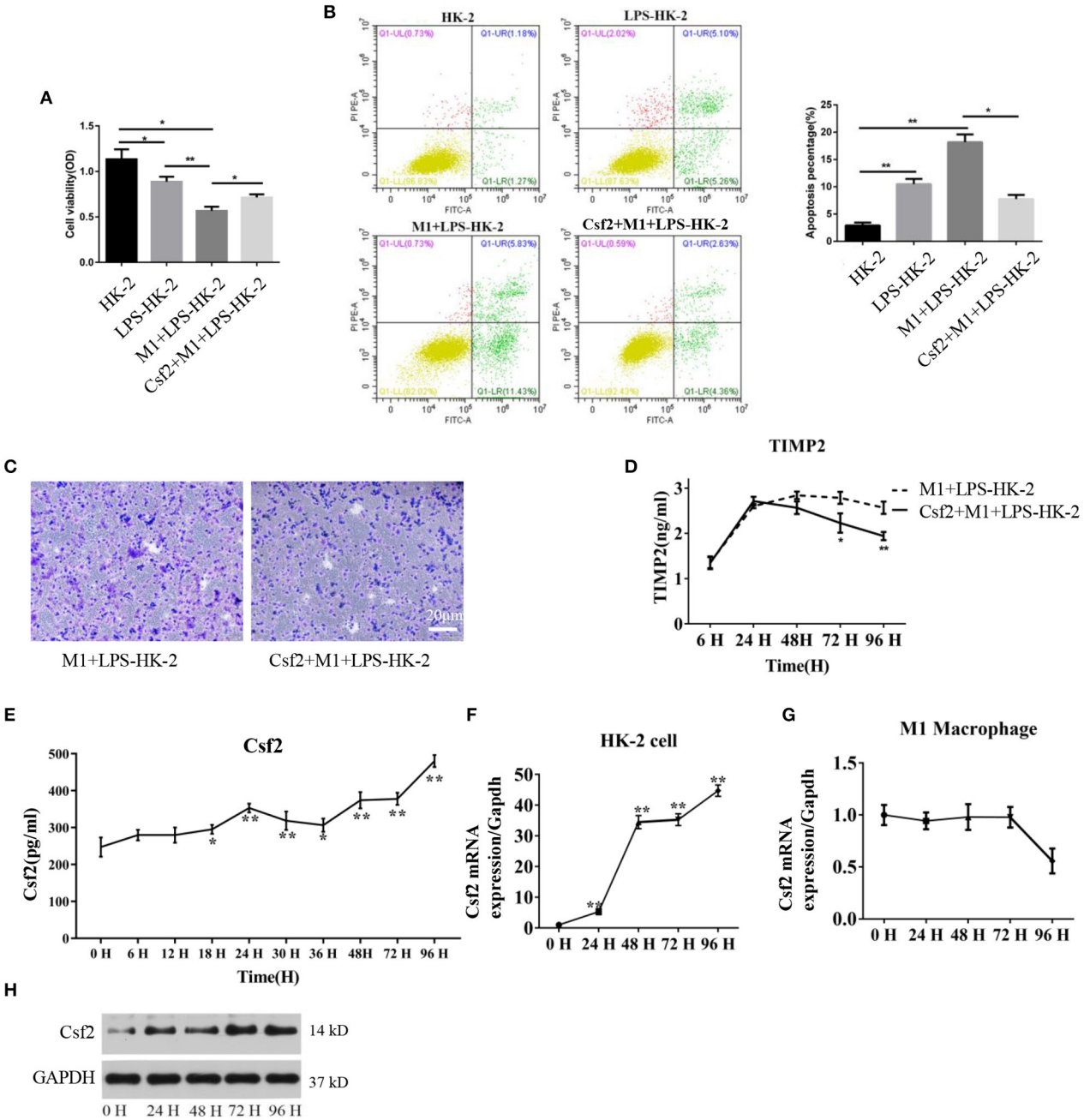

FIGURE 2 | Csf2 secreted from HK-2 cells decreases HK-2 cell apoptosis. **(A)** HK-2 cells were treated with LPS, followed by washing with PBS (LPS-HK-2). LPS-HK-2 cells were cocultured with M1 (M1 + LPS-HK-2 group) or with 25 ng/mL Csf2 (Csf2 + M1 + LPS-HK-2 group) for 18 h, followed by the cell viability test. Three independent experiments were performed. **(B)** Apoptosis of HK-2 cells treated as described above was analyzed by flow cytometry. The apoptosis percentage (Annexin V-FITC+) was shown in the right panel. Three independent experiments were performed. *$p < 0.05$ and **$p < 0.01$; Student's *t*-test. **(C)** M1 macrophages were seeded in the upper chamber. After coculture with LPS-treated HK-2 cells for 48 h, M1 macrophages that migrated to the lower chamber were stained with crystal violet. Representative photos were obtained from three independent experiments at a 200× magnification. **(D)** The concentration of TIMP2 in M1and LPS-HK-2 culture media with or without Csf2 was detected by ELISA. **(E)** The concentration of Csf2 in the medium of LPS-stimulated HK-2 cells cocultured with M1 macrophages was detected by ELISA. Three independent experiments were performed. *$p < 0.05$ and **$p < 0.01$; Student's *t*-test. **(F,G)** The mRNA of Csf2 was measured independently in HK-2 cells and M1 macrophages after coculture for the indicated times. Data are the mean ± SD of 3 separate experiments. The significance of differences was tested using Student's *t*-test. *$p<0.05$. **(H)** Western blot analysis was used to detect the content of Csf2 in HK-2 cells after coculture with M1 macrophages. Three independent experiments were performed.

expression was confirmed by Western blotting in HK-2 cells after coculture with M1 macrophages (**Figure 2H**). Taken together, these findings clearly demonstrated that Csf2 could decrease HK-2 cell apoptosis and improve cell viability and that Csf2 was derived exclusively from HK-2 cells.

Csf2 Mediated Macrophage Transition Toward an M2 Phenotype via the p-STAT5 Pathway

To study the effect of Csf2 on macrophages, M1 macrophages were treated with Csf2 for 72 h. We detected changes in the expression of HLA-DR (red, M1 macrophage) and CD206 (green, M2 macrophage). CD206 fluorescence was increased at the cell membrane of M1 macrophages (**Figure 3A**). Among the different doses of Csf2, the mRNA expression of the M2 phenotype markers CD163 and IL-10 was increased, with the highest increase at a dose of 25 ng/ml (**Figure 3B**). Additionally, immunofluorescence staining showed that the expression of CD206 on the M1 macrophage surface increased over time following coculture with HK-2 cells after Csf2 exposure (**Figure 3C**). We then wondered whether Csf2 had a similar effect on M0 macrophages. The number of CD68 (red, M0 marker) and CD206 (green, M2 macrophage) double-positive cells increased in a dose-dependent manner in response to Csf2 (from 0.5 to 25 ng/ml, **Figure 3D**). This finding indicates that M1 macrophages differentiated into M2 macrophages in the presence of Csf2.

Macrophage reprogramming is mediated by the JNK, PI3K/Akt, Notch, JAK/STAT, TGF-β, and TLR/NF-κB pathways (25). The JAK-STAT pathway plays an important role in regulating macrophage transformation (26, 27). To determine whether the JAK-STAT signaling pathway was involved in tubular cell-mediated macrophage activation, we analyzed STAT5 signaling pathways in M1 macrophages at multiple time points after Csf2 treatment. Phosphorylated STAT5 levels were much higher in macrophages after 48-72 h of Csf2 exposure (**Figure 3E**). Moreover, the M2 markers CD206 and ARG1 were also increased. These findings support the hypothesis that M1 macrophages shift toward an M2 phenotype through the STAT5 pathway when exposed to mediators such as Csf2.

Effect of Csf2 on Kidney Function and Survival Rates in a Sepsis Model

A previous study showed that CLP minimally affected survival in $Csf2^{-/-}$ mice while markedly reducing survival in wild-type mice (28). We hypothesized that the Csf2 antibody may aggravate AKI and decrease survival in a sepsis model. To test our hypothesis, a Csf2-neutralizing antibody or recombinant mouse Csf2 protein was intraperitoneally injected five times starting at 24 h after CLP. As shown in **Figure 4A**, five doses of anti-mouse Csf2-neutralizing antibody or recombinant mouse Csf2 protein were injected intraperitoneally. Serum was harvested 48 h following Csf2 antibody or Csf2 protein administration. Scr and BUN levels in the CLP group were increased compared with those in the SHAM group. Notably, intraperitoneal injection of the Csf2 antibody significantly exacerbated renal dysfunction, as evaluated by Scr and BUN levels. However, Scr and BUN levels were decreased after Csf2 injection compared with IgG isotype injection (**Figures 4B,C**). The survival rate decreased to 15.8% at 7 days after Csf2 antibody injection, compared with 36.8% after Csf2 isotype injection. Surprisingly, injection of Csf2 after CLP significantly reduced mortality (**Figure 4D**). These data revealed that blockade of Csf2 after CLP aggravated kidney injury and decreased survival and that Csf2 could rescue sepsis in mice.

Blockade of Csf2 After CLP Inhibited Kidney Macrophage Transition and Reduced Tubular Cell Proliferation

Our data indicate that Csf2 could promote the transformation from M1 to M2 macrophages *in vitro*. Therefore, we hypothesized that blocking Csf2 signaling may inhibit macrophage transition in the kidneys of septic mice. To test whether Csf2 signaling also regulates macrophage transition *in vivo*, we first tested the expression of markers of M1 and M2 macrophages in kidney tissue. Double HLA-DR/CD206 immunofluorescence staining indicated that CD206 (red, M2 marker) expression was decreased after Csf2 antibody injection (**Figure 5A**), which indicated a decline in kidney macrophage transition toward the M2 phenotype after neutralizing antibody administration. In addition, the M2 markers CD163 and IL-10 were significantly reduced in the kidney cortex following Csf2 antibody treatment compared with isotype antibody treatment (**Figures 5B,C**), whereas the mRNA expression of Csf2 remained unchanged in these two groups (**Figure 5D**). Western blotting was used to detect the expression of p-STAT5 and Jak2. p-STAT5 and Jak2 activation decreased in the kidney cortex after anti-Csf2 antibody administration (**Figure 5E**).

To better and more objectively characterize the effect of Csf2 on M2, we detected the concentrations of IL-10 and TNFα in kidney tissue. As shown in **Figures 5F,G**, we found that the concentration of TNFα was much higher in the CLP + Ab group than in the CLP + ISO group, while the concentration of IL-10 was decreased following Csf2 antibody administration. The TUNEL assay was performed to detect the apoptosis rate. Kidneys from mice treated with the Csf2-neutralizing antibody showed a marked increase in the number of TUNEL-positive tubular epithelial cells (**Figure 5H**). We then attempted to confirm the histopathological damage among the different groups. H&E staining was performed on kidney tissue slices. H&E staining showed that tubular epithelial swelling and brush border injury were even worse in the CLP + Csf2 Ab group than in the CLP + ISO group (**Figure 5I**). AKI with proximal tubule death is usually followed by a wave of tubular proliferation, peaking at 48 h after injury, to restore tubular cell mass. The surviving epithelial cells have an equivalent capacity for repair (29, 30). Ki67, a marker of proliferation, was detected to characterize the repair process. The percentage of Ki67-positive cells was significantly decreased by Csf2–neutralizing antibody injection compared with isotype antibody injection after CLP (**Figure 5J**). These findings support our hypothesis that the Csf2 antibody significantly inhibited macrophage transition toward

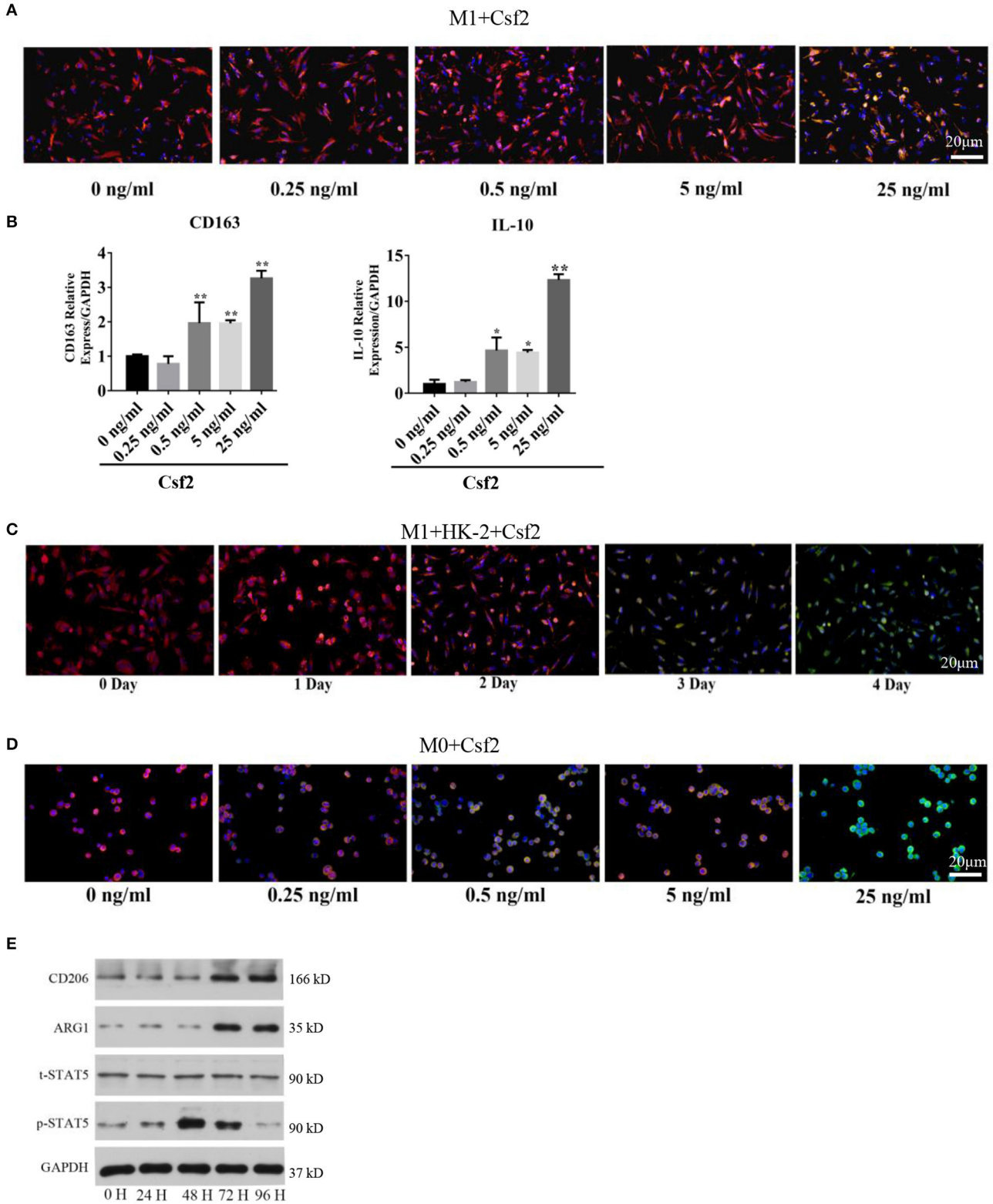

FIGURE 3 | Csf2 mediated alternative activation via the p-STAT5 pathway. **(A)** Representative immunofluorescence images of M1 macrophages showing the expression of HLA-DR (red, M1 marker) and CD206 (green, M2 marker) with Csf2 stimulation at different doses for 48 h. Slides were directly visualized using an Olympus fluorescence microscope at a 20X magnification, scale bar = 20 μm. **(B)** qRT-PCR was used to detect the mRNA levels of CD163 and IL-10 in M1

(Continued)

FIGURE 3 | macrophages exposed to different doses of Csf2. Data are the mean ± SD of three separate experiments. The significance of differences was tested using Student's *t*-test. *$p < 0.05$. **(C)** Representative immunofluorescence images of M1 macrophages showing the expression of HLA-DR (red, M1 marker) and CD206 (green, M2 marker) after coculture with LPS-HK-2 for 4 days. Slides were directly visualized using an Olympus fluorescence microscope at a 20X magnification, scale bar = 20 μm. **(D)** Representative immunofluorescence images of M0 macrophages showing the expression of CD68 (red, M0 marker) and CD206 (green, M2 marker) following Csf2 stimulation at different doses for 48 h. Slides were directly visualized using an Olympus fluorescence microscope at a 20X magnification, scale bar = 20 μm. **(E)** Western blot analysis was used to detect CD206 (M2 marker), ARG1 (M2 marker), total STAT5 and phosphorylated STAT5 in M1 macrophages at the indicated times. Three independent experiments were performed.

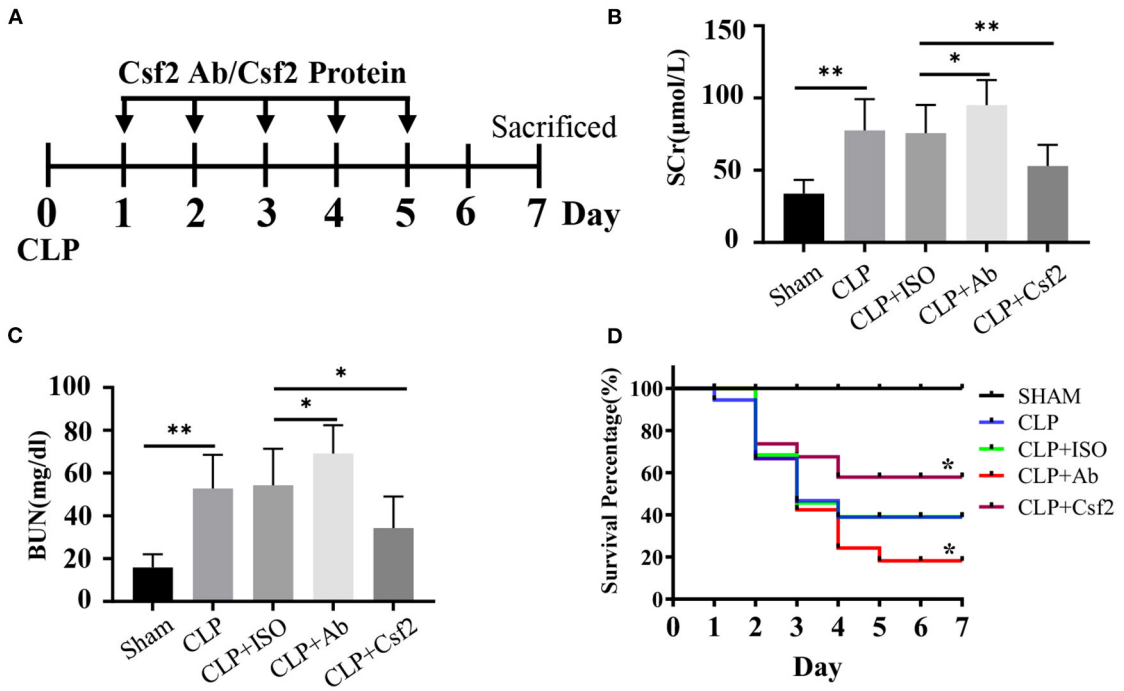

FIGURE 4 | Effect of Csf2 on kidney function and survival rates in a sepsis model. **(A)** Schematic timeline of the experiment. Mice were subjected to CLP and then injected with a neutralizing Csf2 antibody, recombinant Csf2 protein or an isotype antibody daily starting 24 h after CLP. Five doses of 300 mg/mouse/d anti-mouse Csf2-neutralizing antibody or 2.5 μg/mouse/d recombinant mouse Csf2 protein were injected intraperitoneally. **(B,C)** Mice were sacrificed at 48 h following Csf2 antibody or Csf2 protein administration. Scr and BUN levels were determined in the SHAM and CLP groups. Data are shown as the mean ± SD of 10 mice and were pooled from three independent experiments, *$p < 0.05$; **$p < 0.01$, two-tailed unpaired Student's t-test. **(D)** Seven-day survival was observed, n=20/group, *$p < 0.05$; CLP+ Ab vs. CLP + ISO; CLP + Csf2 vs. CLP + ISO. The significance of differences was tested using the log-rank test.

the M2 phenotype via the JAK2-STAT5 pathway and reduced tubular cell repair.

DISCUSSION

AKI is a global health problem with high morbidity and mortality (31). Macrophages are highly heterogeneous in terms of origin and function. Different subpopulations play various roles at different stages in the course of renal disease. Accumulating evidence has suggested that macrophages shift from an M1-like proinflammatory state during the early phase after injury to an M2-like reparative state during the tubular recovery phase. The signals that instruct macrophages to alter their gene expression profiles and promote tubular repair after septic AKI are unknown. Here, we revealed the molecular mechanism by which kidney tubular cells induce macrophage transformation. We found that Csf2 derived from tubular cells induced M0/M1-to-M2 differentiation and subsequently played a protective role in sepsis-induced AKI. Our findings suggest a novel therapeutic target for septic AKI.

Csf2 was one of the top 2 differentially expressed cytokines in the M1 + LPS-HK-2 group compared with the M1 group. Csf2 has been reported to regulate complement- and antibody-mediated phagocytosis, antigen presentation, leukocyte chemotaxis, microbicidal capacity, dendritic cell homeostasis, and adhesion (32, 33). Csf2 is produced by a variety of cells, such as fibroblasts, macrophages, endothelial cells, DCs, neutrophils, T cells, and tissue-resident cells, during inflammatory/autoimmune reactions. Additionally, Csf2 has various effects on the regulation of myeloid populations, including survival, activation, differentiation, and mobilization (34, 35). Csf2-dependent inflammatory pathways in monocytes (and macrophages) are likely to be critical for the purported

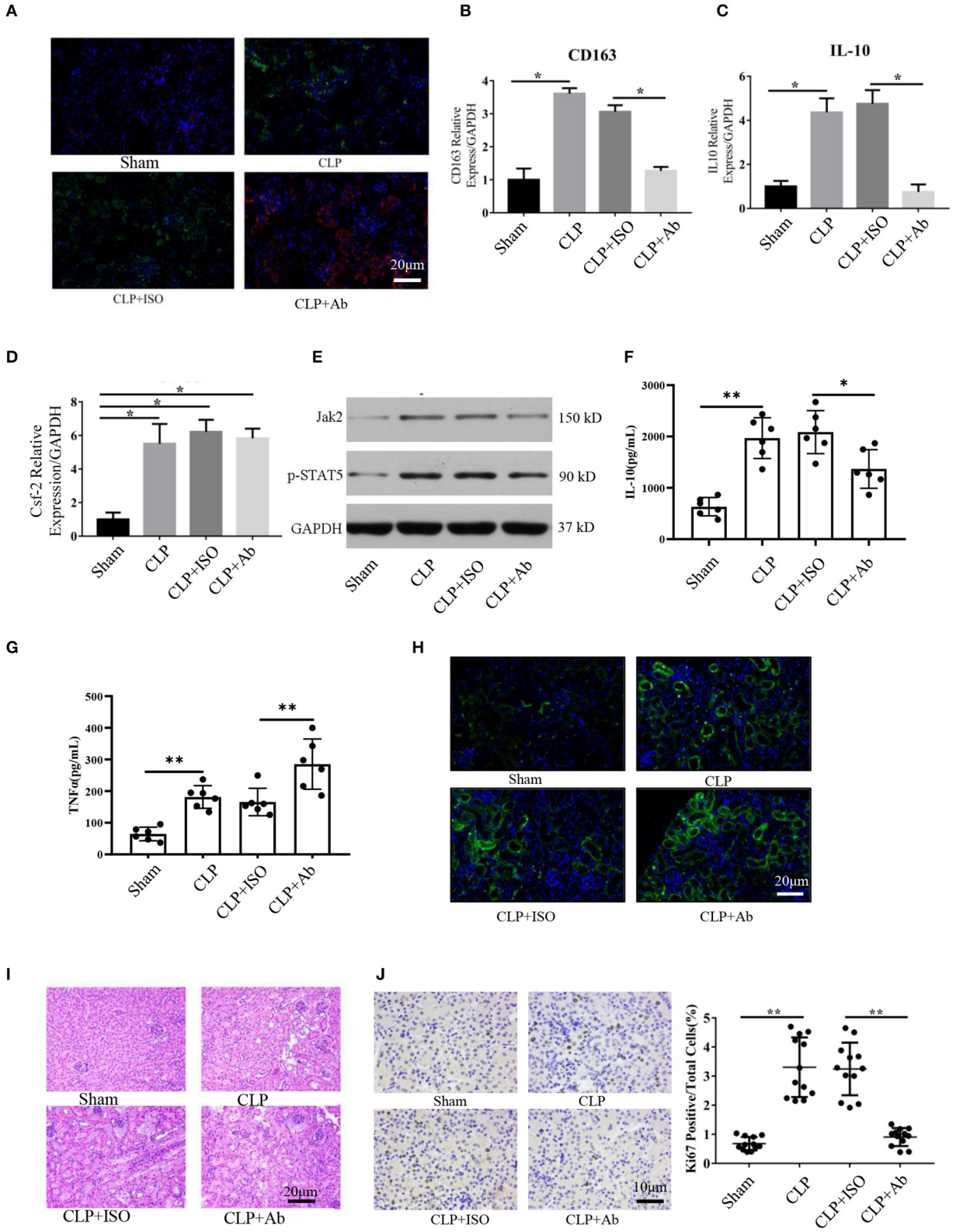

FIGURE 5 | Blockade of Csf2 after CLP attenuated kidney macrophage alternative activation and slowed reparative tubule proliferation. **(A)** Serum and kidney tissues were collected for Scr and H&E staining at day 6. Representative immunofluorescence images of kidney tissue showing the expression of HLA-DR (M1 marker, red)

(Continued)

FIGURE 5 | and CD206 (M2 marker, green) after neutralizing Csf2 antibody or isotype antibody injection. Data are shown as the mean ± SD of 6 mice per group per experiment and were pooled from two independent experiments. **(B–D)** The indicated M2 markers (CD163 and IL10) and Csf2 were assessed using qRT-PCR. Data are shown as the mean ± SD of six mice per group per experiment, and two independent experiments were performed. $^{*}p < 0.05$; two-tailed unpaired Student's *t*-test. **(E)** Western blotting was utilized to detect total STAT5 and phosphorylated STAT5 in the kidney cortex. Six mice were used per group per experiment, and two independent experiments were performed. **(F,G)** The concentrations of TNFα and IL10 in the kidney cortex were assayed by ELISA. Data are shown as the mean ± SD of 6 mice per group per experiment. **(H)** The apoptosis rate was analyzed in the kidneys of mice by TUNEL. Data are shown as the mean ± SD of 6 mice per group per experiment. **(I)** The collected kidneys from the four groups were stained with H&E. Scale bars: 20 μm. Kidney histology from CLP mice showing significant tubular epithelial swelling and brush border injury. Data are shown as the mean ± SD of six mice per group per experiment and were pooled from two independent experiments. **(J)** Photomicrograph of kidney tissue sections immunohistochemically stained for Ki67. Dense brown nuclear immunohistochemical staining indicates Ki67-positive status. Quantification of Ki67-positive tubular cells in the outer medulla. Data are shown as the mean ± SD of six mice per group per experiment and were pooled from two independent experiments, $^{**}p < 0.01$; two-tailed unpaired Student's *t*-test.

role of Csf2 in inflammation, autoimmunity and host defense (36). However, the role of Csf2 in sepsis-induced AKI remains largely unknown. We found that administration of Csf2 in the coculture system decreased the apoptosis rate of HK-2 cells. Furthermore, fewer M1 macrophages migrated to the lower chamber, and the AKI biomarker TIMP-2 was also decreased in the culture medium. These results demonstrate a protective role of Csf2 in LPS-induced kidney injury. Basal levels of Csf2 are low under homeostatic conditions but can be quickly elevated during infection or inflammation. Modulating the functional homeostasis of macrophages can be of great benefit for sepsis-induced AKI (37). Therefore, it is reasonable to speculate that Csf2 could play a central role in mitigating sepsis-induced AKI.

Surprisingly, the source of Csf2 in our model system was exclusively secretion by HK-2 cells, not macrophages. Furthermore, Csf2 induced the M2 transition in a dose-dependent manner at doses up to 25 ng/ml, and 3 days were required for M1-M2 transition after exposure to Csf2 *in vitro*. In Fleetwood et al.'s study, Csf2-dependent murine bone marrow-derived macrophages (BMM) produced significantly more TNF-α and IL-6 compared with Csf1-dependent murine BMM. Based only on increased expression of pro-inflammatory cytokines, Csf2-treated monocytes/macrophages after exposure with LPS produce more cytokines have been termed "M1-like" (38). However, Csf2 is often used to generate DCs populations in BMM (39–41), and DCs express TLR2 and TLR4 (42, 43). No wonder that Csf2-dependent BMM secreted more proinflammatory cytokines after exposure to LPS. In our study, M1 macrophages polarization was induced with THP-1 cells by incubation with LPS and IFN-γ according to routine protocol (44, 45). After stimuli macrophage expressed the typical M1 makers, and Csf2 induced the transformation from M1 to M2. These results are consistent with the pathological process, in which proinflammatory macrophages (M1) predominate during the early injury phase (first 24–48 h), when tubular apoptosis is prominent, and local macrophages begin to express M2 markers during the tubular repair phase (3–5 days), when tubular epithelial cells are growing and remodeling the damaged nephron (46, 47).

Disturbances in macrophage plasticity might compromise immune responses and lead to the development of disease conditions (25). The phenotypic changes and functions of macrophages are regulated by various signaling pathways. Transcription factors, including MAPK, JNK, and NF-κB, are involved in M1 programming (48). PPARγ-deficient macrophages are resistant to M2 polarization and promote insulin resistance (49). IRF, C/EBPβ and STAT regulate the M2 phenotype (26). The core factors that control macrophage phenotype and function in sepsis-induced AKI are still unclear. Our results showed that the Jak2-STAT5 pathway was involved in tubular cell-mediated macrophage transition. The Csf2 receptor, a dodecamer structure, was activated after Csf2 treatment, recruited Jak2 and led to downstream activation of STAT5, thus promoting the M1-to-M2 transition. The Jak2-STAT5 pathway was activated at 24 h and reached a peak at 48 h after Csf2 treatment. We identified tubule-derived Csf2 as a STAT5 activator mediating the macrophage transition from a proinflammatory to a proreparative phenotype.

Because Csf2 promotes the transition from the M1 phenotype to the M2 phenotype *in vitro*, we also examined whether a Csf2 antibody or recombinant Csf2 could contribute to macrophage differentiation in a murine sepsis model. Csf2 blockade through antibodies strongly inhibited M1 macrophage differentiation and increased mortality in CLP-induced septic kidney injury. Consistent with the data obtained in mice subjected to injection of a Csf2-neutralizing antibody, Csf2 protein administration improved the survival rate, suggesting that Csf2 signaling may promote the transition to M2 macrophages. M2 macrophages attenuate sepsis-induced AKI by upregulating IL-10 expression and suppressing TNF-α secretion. Moreover, the reparative process in kidney injury was inhibited following administration of the Csf2 antibody. Our result is also consistent with a randomized controlled trial of 39 patients with sepsis who had immune dysfunctions: Csf2 therapy in these patients was safe and effectively restored the immunocompetence of monocytes (50).

We have sufficient supporting evidence to propose that tubule cell-secreted Csf2 induces macrophage transformation and protects against AKI, although there are some limitations to our study. Previous research has reported that the production of Csf2 is induced by proinflammatory cytokines such as IL-1α, IL-1β, IL-12, and TNF and inhibited by IL-4, IFN-γ, and IL-10 (51, 52). In our study, Csf2 was increased at an early time point (18 h) in the kidney, but the stimulus resulting in Csf2 overexpression remains unknown. As Csf2 may serve as a potential therapeutic target for sepsis-induced AKI, host defense parameters, including circulating cytokines and the bacterial load, should be evaluated in a CLP model following Csf2 treatment. Moreover, whether

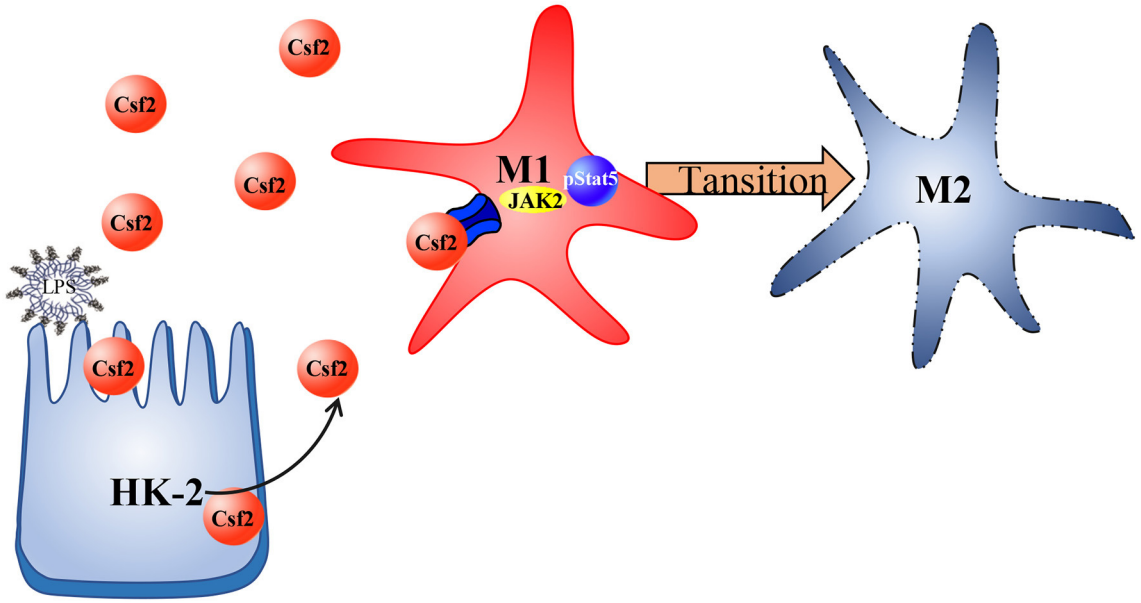

FIGURE 6 | Schematic representation of Csf2 regulation of macrophage transformation in sepsis-induced AKI. Csf2 secreted by tubular cells promotes Stat5 phosphorylation, reduces cell apoptosis, facilitates injured tubular cell repair and therefore attenuates kidney injury *in vitro* and *in vivo*.

other organs are affected by Csf2 treatment is unknown and must be further investigated.

CONCLUSIONS

In summary, we investigated the regulatory function of Csf2 in sepsis-induced AKI and found that Csf2 secreted by HK-2 cells could promote macrophage transition toward the M2 phenotype via the p-STAT5 signaling pathway. Activated proinflammatory macrophages became polarized to the M2 phenotype, which dampens the proinflammatory response. Csf2 treatment reduced tubular cell apoptosis and subsequently improved AKI and survival (**Figure 6**). Csf2-mediated macrophage transition is an important mechanism of renal epithelial cell repair after kidney injury and could provide an alternative method for the treatment of septic AKI in the future.

DATA AVAILABILITY STATEMENT

All datasets generated for this study are included in the article/**Supplementary Material**.

ETHICS STATEMENT

The animal study was reviewed and approved by Animal Care and Use Committee of Wuhan University.

AUTHOR CONTRIBUTIONS

YL: conceived the project, designed the project, extract and analyzed data, drafted the manuscript, and approved the final manuscript. YZ: drafted the part of the discussion and background of the manuscript. YL, PZ, and JZ: conducted the experiments. JK and ZP: designed the project, edited the manuscript, and approved the final version. All authors contributed to the article and approved the submitted version.

FUNDING

This work was supported by the National Natural Science Foundation of China (Nos. 81772046, 81560131), and the Health Commission of Hubei Province (No. WJ2017Z008).

SUPPLEMENTARY MATERIAL

The Supplementary Material for this article can be found online at: https://www.frontiersin.org/articles/10.3389/fimmu.2020.01415/full#supplementary-material

Supplementary Table 1 | The absolute value of cytokines and chemokines in the supernatant.

REFERENCES

1. Yegenaga I, Hoste E, Van Biesen W, Vanholder R, Benoit D, Kantarci G, et al. Clinical characteristics of patients developing ARF due to sepsis/systemic inflammatory response syndrome: results of a prospective study. *Am J Kidney Dis.* (2004) 43:817–24. doi: 10.1053/j.ajkd.2003.12.045
2. Uchino S, Kellum JA, Bellomo R, Doig GS, Morimatsu H, Morgera S, et al. Acute renal failure in critically ill patients: a multinational,

multicenter study. *JAMA*. (2005) 294:813–8. doi: 10.1001/jama.294.7.813
3. Bagshaw SM, Lapinsky S, Dial S, Arabi Y, Dodek P, Wood G, et al. Acute kidney injury in septic shock: clinical outcomes and impact of duration of hypotension prior to initiation of antimicrobial therapy. *Intensive Care Med.* (2009) 35:871–81. doi: 10.1007/s00134-008-1367-2
4. Chertow GM, Burdick E, Honour M, Bonventre JV, Bates DW. Acute kidney injury, mortality, length of stay, and costs in hospitalized patients. *J Am Soc Nephrol.* (2005) 16:3365–70. doi: 10.1681/ASN.2004090740
5. Bagshaw SM, Laupland KB, Doig CJ, Mortis G, Fick GH, Mucenski M, et al. Prognosis for long-term survival and renal recovery in critically ill patients with severe acute renal failure: a population-based study. *Crit Care.* (2005) 9:R700–9. doi: 10.1186/cc3879
6. Liangos O, Wald R, O'Bell JW, Price L, Pereira BJ, Jaber BL., et al. Epidemiology and outcomes of acute renal failure in hospitalized patients: a national survey. *Clin J Am Soc Nephrol.* (2006) 1:43–51. doi: 10.2215/CJN.00220605
7. Wald R, Quinn RR, Luo J, Li P, Scales DC, Mamdani MM, et al. Chronic dialysis and death among survivors of acute kidney injury requiring dialysis. *JAMA*. (2009) 302:1179–85. doi: 10.1001/jama.2009.1322
8. Anders HJ, Ryu M. Renal microenvironments and macrophage phenotypes determine progression or resolution of renal inflammation and fibrosis. *Kidney Int.* (2011) 80:915–25. doi: 10.1038/ki.2011.217
9. Zhang J, Ankawi G, Sun J, Digvijay K, Yin Y, Rosner MH, et al. Gut-kidney crosstalk in septic acute kidney injury. *Crit Care.* (2018) 22:117. doi: 10.1186/s13054-018-2040-y
10. Alikhan MA, Ricardo SD. Mononuclear phagocyte system in kidney disease and repair. *Nephrology.* (2013) 18:81–91. doi: 10.1111/nep.12014
11. Peng ZY, Wang HZ, Srisawat N, Wen X, Rimmele T, Bishop J, et al. Bactericidal antibiotics temporarily increase inflammation and worsen acute kidney injury in experimental sepsis. *Crit Care Med.* (2012) 40:538–43. doi: 10.1097/CCM.0b013e31822f0d2e
12. Peng ZY, Carter MJ, Kellum JA. Effects of hemoadsorption on cytokine removal and short-term survival in septic rats. *Crit Care Med.* (2008) 36:1573–7. doi: 10.1097/CCM.0b013e318170b9a7
13. Huen SC, Huynh L, Marlier A, Lee Y, Moeckel GW, Cantley LG., et al. GM-CSF promotes macrophage alternative activation after renal ischemia/reperfusion injury. *J Am Soc Nephrol.* (2015) 26:1334–45. doi: 10.1681/ASN.2014060612
14. Kinsey GR, Li L, Okusa MD. Inflammation in acute kidney injury. *Nephron Exp Nephrol.* (2008) 109:e102–7. doi: 10.1159/000142934
15. Mosser DM, Edwards JP. Exploring the full spectrum of macrophage activation. *Nat Rev Immunol.* (2008) 8:958–69. doi: 10.1038/nri2448
16. Gottlieb RA. Cell death pathways in acute ischemia/reperfusion injury. *J Cardiovasc Pharmacol Ther.* (2011) 16:233–8. doi: 10.1177/1074248411409581
17. Nourshargh S, Alon R. Leukocyte migration into inflamed tissues. *Immunity.* (2014) 41:694–707. doi: 10.1016/j.immuni.2014.10.008
18. Klinkert K, Whelan D, Clover AJP, Leblond AL, Kumar AHS, Caplice NM., et al. Selective M2 macrophage depletion leads to prolonged inflammation in surgical wounds. *Eur Surg Res.* (2017) 58:109–20. doi: 10.1159/000451078
19. Li YM, Zhang J, Su LJ, Kellum JA, Peng ZY. Downregulation of TIMP2 attenuates sepsis-induced AKI through the NF-kappab pathway. *Biochim Biophys Acta Mol Basis Dis.* (2019) 1865:558–69. doi: 10.1016/j.bbadis.2018.10.041
20. Zarjou A, Agarwal A. Sepsis and acute kidney injury. *J Am Soc Nephrol.* (2011) 22:999–1006. doi: 10.1681/ASN.2010050484
21. Fujiu K, Shibata M, Nakayama Y, Ogata F, Matsumoto S, Noshita K, et al. A heart-brain-kidney network controls adaptation to cardiac stress through tissue macrophage activation. *Nat Med.* (2017) 23:611–22. doi: 10.1038/nm.4326
22. Wynn TA, Chawla A, Pollard JW. Macrophage biology in development, homeostasis and disease. *Nature.* (2013) 496:445–55. doi: 10.1038/nature12034
23. Subramanian Vignesh K, Landero Figueroa JA, Porollo A, Caruso JA, Deepe GS Jr., et al. Granulocyte macrophage-colony stimulating factor induced Zn sequestration enhances macrophage superoxide and limits intracellular pathogen survival. *Immunity.* (2013) 39:697–710. doi: 10.1016/j.immuni.2013.09.006
24. Becher B, Tugues S, Greter M. GM-CSF: from growth factor to central mediator of tissue inflammation. *Immunity.* (2016) 45:963–73. doi: 10.1016/j.immuni.2016.10.026
25. Malyshev I, Malyshev Y. Current concept and update of the macrophage plasticity concept: intracellular mechanisms of reprogramming and M3 macrophage "switch" phenotype. *Biomed Res Int.* (2015) 2015:341308. doi: 10.1155/2015/341308
26. Lawrence T, Natoli G. Transcriptional regulation of macrophage polarization: enabling diversity with identity. *Nat Rev Immunol.* (2011) 11:750–61. doi: 10.1038/nri3088
27. Zhou D, Huang C, Lin Z, Zhan S, Kong L, Fang C, et al. Macrophage polarization and function with emphasis on the evolving roles of coordinated regulation of cellular signaling pathways. *Cell Signal.* (2014) 26:192–7. doi: 10.1016/j.cellsig.2013.11.004
28. Spight D, Trapnell B, Zhao B, Berclaz P, Shanley TP. Granulocyte-macrophage-colony-stimulating factor-dependent peritoneal macrophage responses determine survival in experimentally induced peritonitis and sepsis in mice. *Shock.* (2008) 30:434–42. doi: 10.1097/SHK.0b013e3181673543
29. Kusaba T, Lalli M, Kramann R, Kobayashi A, Humphreys BD. Differentiated kidney epithelial cells repair injured proximal tubule. *Proc Natl Acad Sci USA.* (2014) 111:1527–32. doi: 10.1073/pnas.1310653110
30. Chang-Panesso M, Humphreys BD. Cellular plasticity in kidney injury and repair. *Nat Rev Nephrol.* (2017) 13:39–46. doi: 10.1038/nrneph.2016.169
31. Linares-Linares MA, Figueroa-Tarrillo JA, Cerna Viacava R, Carreazo NY, Valdivia-Vega RP. Risk factors associated to hospital mortality in patients with acute kidney injury on hemodialysis. *Medwave.* (2017) 17:e6879. doi: 10.5867/medwave.2017.02.6879
32. Greter M, Helft J, Chow A, Hashimoto D, Mortha A, Agudo-Cantero J, et al. GM-CSF controls nonlymphoid tissue dendritic cell homeostasis but is dispensable for the differentiation of inflammatory dendritic cells. *Immunity.* (2012) 36:1031–46. doi: 10.1016/j.immuni.2012.03.027
33. Martinez FO, Gordon S. The M1 and M2 paradigm of macrophage activation: time for reassessment. *F1000Prime Rep.* (2014) 6:13. doi: 10.12703/P6-13
34. Akashi K, Traver D, Miyamoto T, Weissman IL. A clonogenic common myeloid progenitor that gives rise to all myeloid lineages. *Nature.* (2000) 404:193–7. doi: 10.1038/35004599
35. Fogg DK, Sibon C, Miled C, Jung S, Aucouturier P, Littman DR, et al. A clonogenic bone marrow progenitor specific for macrophages and dendritic cells. *Science.* (2006) 311:83–7. doi: 10.1126/science.1117729
36. Hamilton JA. GM-CSF-dependent inflammatory pathways. *Front Immunol.* (2019) 10:2055. doi: 10.3389/fimmu.2019.02055
37. Cheng Y, Marion TN, Cao X, Wang W, Cao Y. Park 7: a novel therapeutic target for macrophages in sepsis-induced immunosuppression. *Front Immunol.* (2018) 9:2632. doi: 10.3389/fimmu.2018.02632
38. Fleetwood AJ, Lawrence T, Hamilton JA, Cook AD. Granulocyte-macrophage colony-stimulating factor (CSF) and macrophage CSF-dependent macrophage phenotypes display differences in cytokine profiles and transcription factor activities: implications for CSF blockade in inflammation. *J Immunol.* (2007) 178:5245–52. doi: 10.4049/jimmunol.178.8.5245
39. Conti L, Gessani S. GM-CSF in the generation of dendritic cells from human blood monocyte precursors: recent advances. *Immunobiology.* (2008) 213:859–70. doi: 10.1016/j.imbio.2008.07.017
40. Pamir N, Liu NC, Irwin A, Becker L, Peng Y, Ronsein GE, et al. Granulocyte/macrophage colony-stimulating factor-dependent dendritic cells restrain lean adipose tissue expansion. *J Biol Chem.* (2015) 290:14656–67. doi: 10.1074/jbc.M115.645820
41. Chow KV, Delconte RB, Huntington ND, Tarlinton DM, Sutherland RM, Zhan Y, et al. Innate allorecognition results in rapid accumulation of monocyte-derived dendritic cells. *J Immunol.* (2016) 197:2000–8. doi: 10.4049/jimmunol.1600181
42. Chandran SS, Verhoeven D, Teijaro JR, Fenton MJ, Farber DL. TLR2 engagement on dendritic cells promotes high frequency effector and memory CD4 T cell responses. *J Immunol.* (2009) 183:7832–41. doi: 10.4049/jimmunol.0901683
43. Ling GS, Bennett J, Woollard KJ, Szajna M, Fossati-Jimack L, Taylor PR, et al. Integrin CD11b positively regulates TLR4-induced signalling pathways

in dendritic cells but not in macrophages. *Nat Commun.* (2014) 5:3039. doi: 10.1038/ncomms4039
44. Genin M, Clement F, Fattaccioli A, Raes M, Michiels C. M1 and M2 macrophages derived from THP-1 cells differentially modulate the response of cancer cells to etoposide. *BMC Cancer.* (2015) 15:577. doi: 10.1186/s12885-015-1546-9
45. Popena I, Abols A, Saulite L, Pleiko K, Zandberga E, Jekabsons K, et al. Effect of colorectal cancer-derived extracellular vesicles on the immunophenotype and cytokine secretion profile of monocytes and macrophages. *Cell Commun Signal.* (2018) 16:17. doi: 10.1186/s12964-018-0229-y
46. Jo SK, Sung SA, Cho WY, Go KJ, Kim HK. Macrophages contribute to the initiation of ischaemic acute renal failure in rats. *Nephrol Dial Transplant.* (2006) 21:1231–9. doi: 10.1093/ndt/gfk047
47. Lin SL, Li B, Rao S, Yeo EJ, Hudson TE, Nowlin BT, et al. Macrophage Wnt7b is critical for kidney repair and regeneration. *Proc Natl Acad Sci USA.* (2010) 107:4194–9. doi: 10.1073/pnas.0912228107
48. Han HI, Skvarca LB, Espiritu EB, Davidson AJ, Hukriede NA. The role of macrophages during acute kidney injury: destruction and repair. *Pediatr Nephrol.* (2019) 34:561–9. doi: 10.1007/s00467-017-3883-1
49. Charo IF. Macrophage polarization and insulin resistance: PPARgamma in control. *Cell Metab.* (2007) 6:96–8. doi: 10.1016/j.cmet.2007.07.006
50. Meisel C, Schefold JC, Pschowski R, Baumann T, Hetzger K, Gregor J, et al. Granulocyte-macrophage colony-stimulating factor to reverse sepsis-associated immunosuppression: a double-blind, randomized, placebo-controlled multicenter trial. *Am J Respir Crit Care Med.* (2009) 180:640–8. doi: 10.1164/rccm.200903-0363OC
51. El-Behi M, Ciric B, Dai H, Yan Y, Cullimore M, Safavi F, et al. The encephalitogenicity of T(H)17 cells is dependent on IL-1- and IL-23-induced production of the cytokine GM-CSF. *Nat Immunol.* (2011) 12:568–75. doi: 10.1038/ni.2031
52. Lukens JR, Barr MJ, Chaplin DD, Chi H, Kanneganti TD. Inflammasome-derived IL-1beta regulates the production of GM-CSF by CD4(+) T cells and gammadelta T cells. *J Immunol.* (2012) 188:3107–15. doi: 10.4049/jimmunol.1103308

Conflict of Interest: JK discloses grant support and consulting fees from Astute Medical.

The remaining authors declare that the research was conducted in the absence of any commercial or financial relationships that could be construed as a potential conflict of interest.

Copyright © 2020 Li, Zhai, Zheng, Zhang, Kellum and Peng. This is an open-access article distributed under the terms of the Creative Commons Attribution License (CC BY). The use, distribution or reproduction in other forums is permitted, provided the original author(s) and the copyright owner(s) are credited and that the original publication in this journal is cited, in accordance with accepted academic practice. No use, distribution or reproduction is permitted which does not comply with these terms.

Advantages of publishing in Frontiers

OPEN ACCESS
Articles are free to read for greatest visibility and readership

FAST PUBLICATION
Around 90 days from submission to decision

HIGH QUALITY PEER-REVIEW
Rigorous, collaborative, and constructive peer-review

TRANSPARENT PEER-REVIEW
Editors and reviewers acknowledged by name on published articles

Frontiers
Avenue du Tribunal-Fédéral 34
1005 Lausanne | Switzerland

Visit us: www.frontiersin.org
Contact us: info@frontiersin.org | +41 21 510 17 00

REPRODUCIBILITY OF RESEARCH
Support open data and methods to enhance research reproducibility

DIGITAL PUBLISHING
Articles designed for optimal readership across devices

FOLLOW US
@frontiersin

IMPACT METRICS
Advanced article metrics track visibility across digital media

EXTENSIVE PROMOTION
Marketing and promotion of impactful research

LOOP RESEARCH NETWORK
Our network increases your article's readership